

Vol. 23, No. 4, December, 2024

ISSN (Print): 0972-6268; ISSN (Online) : 2395-3454

# NATURE ENVIRONMENT & POLLUTION TECHNOLOGY

*A Multidisciplinary, International Journal  
on Diverse Aspects of Environment*



**Technoscience Publications**

website: [www.neptjournal.com](http://www.neptjournal.com)



# Technoscience Publications

A-504, Bliss Avenue, Balewadi,  
Opp. SKP Campus, Pune-411 045  
Maharashtra, India

[www.neptjournal.com](http://www.neptjournal.com)

## Nature Environment and Pollution Technology

(An International Quarterly Scientific Research Journal)

### EDITORS

**Dr. P. K. Goel (Chief Editor)**

Former Head, Deptt. of Pollution Studies  
Y. C. College of Science, Vidyanagar  
Karad-415 124, Maharashtra, India

**Dr. K. P. Sharma (Honorary Editor)**

Former Professor, Deptt. of Botany  
University of Rajasthan  
Jaipur-302 004, India

**Executive Editor** : Ms. Apurva P. Goel, C-102, Building No. 12, Swarna CGHS,  
Beverly Park, Kanakia, Mira Road (E) (Thane) Mumbai-401107,  
Maharashtra, India

**Published by** : Ms. T. P. Goel, Technoscience Publications, A-504, Bliss Avenue,  
Balewadi, Pune-411 045, Maharashtra, India

**E-mail** : [contact@neptjournal.com](mailto:contact@neptjournal.com); [operations@neptjournal.com](mailto:operations@neptjournal.com)

### INSTRUCTIONS TO AUTHORS

#### Scope of the Journal

The Journal publishes original research/review papers covering almost all aspects of environment like monitoring, control and management of air, water, soil and noise pollution; solid waste management; industrial hygiene and occupational health hazards; biomedical aspects of pollution; conservation and management of resources; environmental laws and legal aspects of pollution; toxicology; radiation and recycling, etc.

#### Format of Manuscript

- The manuscript (mss) should be typed in double space leaving wide margins on both the sides.
- First page of mss should contain only the title of the paper, name(s) of author(s) and name and address of Organization(s) where the work has been carried out along with the affiliation of the authors.

*Continued on back inner cover...*

# Nature Environment and Pollution Technology

Vol. 23, No. (4), December 2024

## CONTENTS

1. **Reynald M. Quilang**, Biodiversity and Soil Characterization of Ancestral Domain of the Tagbanua Tribe in Aborlan, Palawan, Philippines 1857-1884
2. **Anand Shankar**, Dynamic Impact-Based Heavy Rainfall Warning with Multi-classification Machine Learning Approaches 1885-1900
3. **Rodny Peñafiel, Fabián Rodrigo Morales-Fiallos, Bolivar Paredes-Beltran, Dilon Moya, Adriana Jacqueline Frias Carrion and Belén Moreano**, Heavy Metals in Water and Sediments and Their Impact on Water Quality in Andean Micro-watersheds: A Study of the Colorado and Alajua Rivers in the Ambato River Watershed, Tungurahua, Ecuador 1901-1916
4. **N. Gandhi, Y. Rama Govinda Reddy and Ch. Vijaya**, Hepatotoxic Effects of Gaseous Sulfur Dioxide (SO<sub>2</sub>), Nitrogen Dioxide (NO<sub>2</sub>), and Their Mixture on Sea Bass (*Centropristis striata*): Hematological, Biochemical and Genotoxic Studies 1917-1936
5. **M. Trad and A. Harb**, Analysis of the Lebanese Society's Behavior Regarding Electronic Waste Management 1937-1955
6. **M. V. Shah, N. M. Rathod, D. N. Prajapati, P. J. Mehta, R. R. Panchal and Vijay Upadhye**, Transforming Soil Stability: A Review on Harnessing Plant Cell Compounds and Microbial Products for Modifying Cation Exchange Capacity 1957-1971
7. **A. Khan, G. Khan, M. Minhas, S. A. Hussain Gardezi, J. Ahmed and N. Abbas**, Landslide Susceptibility Zonation Mapping Using Machine Learning Algorithms and Statistical Prediction at Hunza Watershed Basin, Pakistan 1973-1993
8. **Loveena Gaur and Poonam Poonia**, Optimization, Characterisation and Evaluation of Biochar Obtained from Biomass of Invasive Weed *Crotalaria burhia* 1995-2008
9. **S. Isworo, E. Jasmienne and P. S. Oetari**, The Waste Management System in the Parking and Traders Arrangement in the Borobudur Temple Area, Central Java, Indonesia 2009-2023
10. **Sujit Kumar Jally, Rakesh Kumar and Sibabrata Das**, Integrating Satellite Data and In-situ Observations for Trophic State Assessment of Renuka Lake, Himachal Pradesh, India 2025-2038
11. **Rijal Asnawi, Antariksa, Sukir Maryanto and Aminudin Afandhi**, Economic Feasibility of On-Grid Photovoltaic Solar Power Plants at Private Universities in Indonesia 2039-2048
12. **Aashutosh Kumar Mandwa, Atul Kumar Bhardwaj, Rajesh Kumar, K.K. Chandra, Chanchal Kumari and S. K. Padey**, Impact of Urban Xenobiotics on Mycorrhizal Associations in Urban Plants 2049-2057
13. **A. S. Nur Chairat, L. Abdullah, M. N. Maslan, M. S. M. Aras, M. H. F. Md Fauadi, R. A. Hamid and H. Batih**, Cost Assessment of Emission Mitigation Technology for the Palm Oil Sector in Indonesia 2059-2069
14. **V. Ramesh and P. Kumaresan**, Advancements in Machine Learning and Deep Learning Techniques for Crop Yield Prediction: A Comprehensive Review 2071-2086
15. **D. O. Olukanni, M. J. Kamlenga, C. N. Ojukwu and T. Mkwandwire**, Anaerobic Co-digestion of Palm Oil Sludge, Cassava Peels, Cow Dung and Ground Eggshells: Process Optimization and Biogas Generation 2087-2099
16. **Jayamala Kumar Patil and Vinay Sampatrao Mandlik**, Plant Leaf Disease Detection Using Integrated Color and Texture Features 2101-2113
17. **Manish Hassani and Kamlesh Purohit**, Optimization and Thermodynamic Analysis of CO<sub>2</sub> Refrigeration Cycle for Energy Efficiency and Environmental Control 2115-2127
18. **Farah Rania, Farou Brahim, Kouahla Zineddine and Seridi Hamid**, Enhancing Smart Grids for Sustainable Energy Transition and Emission Reduction with Advanced Forecasting Techniques 2129-2141
19. **P. Solanki, S. Jain, R. Mehrotra, P. Mago and S. Dagar**, Microplastics in Agricultural Soil and Their Impact: A Review 2143-2155
20. **Fatima M. A. Al-khafaji and Hussein A. M. Al-Zubaidi**, Numerical Modeling of Instantaneous Spills in One-dimensional River Systems 2157-2166
21. **Girish Kumar, M. M. Singh, Dheeraj Kumar Singh, Bal Krishan Choudhary, Vijay Kumar Singh Rathore and Pramod Kumar**, Assessment of Water Poverty Index (WPI) Under Changing Land Use/Land Cover in a Riverine Ecosystem of Central India 2167-2178
22. **M. S. Islam, T. M. Ekhwan, F. N. Rasli and C. T. Goh**, Assessment of Physicochemical Properties of Water and Public Perceptions of Water Quality in Tasik Chini, Pahang, Malaysia 2179-2188
23. **Ardra Suseelan and Senthil Vadivel. T.**, Environmental Monitoring and Assessment for Sustainable Construction Projects: Leveraging Lean Techniques 2189-2200
24. **V. Pushpalatha, H. N. Mahendra, A. M. Prasad, N. Sharmila, D. Mahesh Kumar, N. M. Basavaraju, G. S. Pavithra and S. Mallikarjunaswamy**, An Assessment of Land Use Land Cover Using Machine Learning Technique 2201-2209
25. **V. Pushpalatha, H. N. Mahendra, A. M. Prasad, N. Sharmila, D. Mahesh Kumar, N. M. Basavaraju, G. S. Pavithra and S. Mallikarjunaswamy**, An Assessment of Land Use Land Cover Using Machine Learning Technique 2211-2219
26. **S. Piyavadee, R. Chumaporn and V. Patipat**, Evaluating the Association Between Ambient Pollutants and Climate Conditions in Chiangmai, Thailand 2221-2229
27. **Shivani Jadhav and Asha Verma**, Environmental Awareness Toward Issues and Challenges of Sustainable Consumerism in the Indian Apparel Industry 2231-2239
28. **A. J. Dakhil, E. K. Hussain and F. F. Aziz**, Evaluation of the Drought Situation Using Remote Sensing Technology, an Applied Study on a Part of North Wasit Governorate in Iraq 2241-2249

29. **Punam Chanda, Pintu Majhi and Salina Akther**, Testing the Validity of Environmental Kuznets Curve for Carbon Emission: A Cross-Section Analysis 2251-2258
30. **D. F. Wardhani, D. Arisanty, A. Nugroho and U. B. L. Utami**, Environmental Education Model Based on Local Wisdom of the Dayak Paramasan Tribe Indonesia 2259-2272
31. **Dnyaneshwar V. Wadkar, Ganesh C. Chikute, Pravin S. Patil, Pallavi D. Wadkar and Manasi G. Chikute**, Effectiveness of Different Artificial Neural Network Models in Establishing the Suitable Dosages of Coagulant and Chlorine in Water Treatment Works 2273-2281
32. **Naresh Anguralia and Shamsher Singh**, A Comparative Study on India's Green Tax Policies Vis-a-Vis China with Reference to Environmental Justice in the Automobile Industry 2283-2290
33. **P. P. Shinde, R. J. Sayyad, S. S. Shukla, S. A. Waghmode and S. R. Gadale**, Investigations on Photodegradation and Antibacterial Activity of Mixed Oxide Nanocrystalline Materials 2291-2303
34. **I. Alouiz, M. Benhadj, D. Elmontassir, M. Sennoune, M.Y. Amarouch and D. Mazouzi**, Potential Low-cost Treatment of Tannery Effluents from Industry by Adsorption on Activated Charcoal Derived from Olive Pomace 2305-2314
35. **S. Dash and M. Kujur**, Contribution of Organic Carbon, Moisture Content, Microbial Biomass-Carbon, and Basal Soil Respiration Affecting Microbial Population in Chronosequence Manganese Mine Spoil 2315-2323
36. **G. O. Chukwurah, N. M. Aguome, M. O. Isimah, E. C. Enoguanbhor, N. E. Obi-Aso, N. U. Azani and O. C. Nnamani**, Community Perception on the Effect of Cultural Livelihoods on the Environment in Kogi State, Nigeria 2325-2334
37. **S. Sudalai, S. Prabakaran, M. G. Devanesan and A. Arumugam**, Process Optimization for *Madhuca indica* Seed Kernel Oil Extraction and Evaluation of its Potential for Biodiesel Production 2335-2345
38. **R. Krishna Kumari**, Revolutionizing Education: Harnessing Graph Machine Learning for Enhanced Problem-Solving in Environmental Science and Pollution Technology 2347-2354
39. **Syed Abdul Moeed, Bellam Surendra Babu, M. Sreevani, B. V. Devendra Rao, R. Raja Kumar and Gouse Baig Mohammed**, An Intelligent Crow Search Optimization and Bi-GRU for Forest Fire Detection System Using Internet of Things 2355-2370
40. **R. Ravikiran, G. Raghu and B. Praveen**, A Comprehensive Genetic Analysis of Mycotoxin-Producing *Penicillium expansum* Isolated from River Water Using Molecular Profiling, DNA Barcoding, and Secondary Structure Prediction 2371-2382
41. **Jamal S. Abd Al Rukabie, Salwa S. Naif and Monim H. Al-Jiboori**, Quantitative Impact of Monthly Precipitation on Urban Vegetation, Surface Water and Potential Evapotranspiration in Baghdad Under Wet and Dry Conditions 2383-2389
42. **S. Sudalai, M. G. Devanesan and A. Arumugam**, Dolomite as A Potential Source of Heterogenous Catalyst for Biodiesel Production from *Pongamia pinnata* 2391-2396
43. **Mónica Santa María Paredes-Agurto, Armando Fortunato Ugaz Cherre, José Manuel Marchena Diones and Robert Barrionuevo García**, Aquatic Macroinvertebrate Diversity and Water Quality, La Gallega-Morropón Creek, Piura, Peru 2397-2402
44. **Sugata Datta, Abhishek Chauhan, Anuj Ranjan, Abul Hasan Sardar, Hardeep Singh Tuli, Ammar Abdulrahman Jairoun, Moyad Shahwan, Ujjawal Sharma and Tanu Jindal**, Bisphenol A in Indian Take-Out Soups: Compliance, Implications and Sustainable Solutions 2403-2409
45. **Watemin, Slamet Rosyadi and Lilis Siti Badriah**, The Impact of Socio-Economic and Climate Change on Poverty in Indonesia 2411-2418
46. **W. Muslihatin, R. P. D. Wahyudi, M. Iqbal, T. B. Saputro and T. Nurhidayati**, The Influence of Gibberellins and Smoke Water as a Stimulant for Germination and Vegetative Growth of *Syzygium aromaticum* (L.) Merr. & L. M. Perry 2419-2425
47. **O. L. Rominiyi, M. A. Akintunde, E. I Bello, L. Lajide, O. M. Ikumapayi, O. T. Laseinde and B. A. Adaramola**, Characterization of the Liquid Fuel Produced from Catalytic Depolymerization of Polymeric Waste Using Batch Reactor 2427-2433
48. **Mashud Ahmed, Md Kamrul Islam and Samar Das**, Climate Change Effects on Crop Area Dynamics in the Cachar District of Assam, India: An Empirical Study 2435-2440
49. **Estabraq Mohammed Ati, Shahla Hussien Hano, Rana Fadhil abbas, Reyam Najji Ajmi and Abdalkader Saeed Latif**, Laser Induced Spectroscopy (LIBS) Technology and Environmental Risk Index (RI) to Detect Microplastics in Drinking Water in Baghdad, Iraq 2441-2446
50. **S. Ivanova, A. Vesnina, N. Fotina and A. Prosekov**, Technogenically Disturbed Lands of Coal Mines: Restoration Methods 2447-2452
51. **Bhawishya Pradhan, Banjul Bhattacharyya, N. Elakkiya and T. Gowthaman**, Fitting Probability Distributions and Statistical Trend Analysis of Rainfall of Agro-climatic Zone of West Bengal 2453-2460
52. **M. H. F. Md Fauadi, M. F. H. Mohd Zan, M. A. M Ali, L. Abdullah, S. N. Yaakop and A. Z. M. Noor**, Enhancing Driving Safety and Environmental Consciousness through Automated Road Sign Recognition Using Convolutional Neural Networks 2461-2468
53. **Mahima Chaurasia, Sanjeev Kumar Srivastava and Suraj Prakash Yadav**, Evaluating Sustainability: A Comparison of Carbon Footprint Metrics Evaluation Criteria 2469-2476
54. **Eduard Tshovrebov, Vladimir Moshkov, Irina Oltyan and Filyuz Niyazgulov**, A New Approach to Assessing the Accuracy of Forecasting of Emergencies with Environmental Consequences Based on the Theory of Fuzzy Logic 2477-2481
55. **D. Srinivasa Rao, Ch. Rajasekhar, P. M. K. Prasad and G. B. S. R. Naidu** Sustainability and Environmental Impact of Mining and Maintaining Cryptocurrencies: A Review 2483-2487
56. **A. S. Ulum, M. S. Djati, Susilo and A. I. Rozuli**, Community-Based Plastic Waste Management Model in Bangun Village, Mojokerto Regency, Indonesia 2489-2498

The Journal  
is  
Currently  
**Abstracted  
and  
Indexed**  
in:

WorldCat (OCLC)

British Library

Connect Journals (India)

Indian Science

JournalSeek

Research Bible (Japan)

SHERPA/RoMEO

Directory of Science

AGRIS (UN-FAO)

Ulrich's (Refereed) database

NAAS Rating 2024 = 5.33

CNKI Scholar (China National Knowledge Infrastructure)

Scopus Cite Score (2023) 1.2

Scopus®, SJR (2023) 0.204

Index Copernicus (2022) = 132.21

Indian Science Abstracts, New Delhi, India

Chemical Abstracts, U.S.A.

Pollution Abstracts, U.S.A.

Elsevier Bibliographic Databases

Paryavaran Abstract, New Delhi, India

Zoological Records

CAB Abstracts, U.K.

Electronic Social and Science Citation Index (ESSCI)

Indian Citation Index (ICI)

CrossRef (DOI)

EBSCO: Environment Index™

ProQuest, U.K.

Google Scholar

DOAJ

Zetoc

J-Gate

Environment Abstract, U.S.A.

Centre for Research Libraries

Elektronische Zeitschriftenbibliothek (EZB)

CSA: Environmental Sciences and Pollution Management

Access to Global Online Research in Agriculture (AGORA)

Present in UGC-CARE List (Group II)

UDL-EDGE (Malaysia) Products like i-Journals, i-Focus and i-Future

[www.neptjournal.com](http://www.neptjournal.com)

# NATURE ENVIRONMENT AND POLLUTION TECHNOLOGY

## EDITORS

### Dr. P. K. Goel (Chief Editor)

Former Head, Deptt. of Pollution Studies  
Yashwantrao Chavan College of Science  
Vidyanagar, Karad-415124  
Maharashtra, India

### Dr. K. P. Sharma (Honorary Editor)

Former Professor, Ecology Lab, Deptt. of Botany  
University of Rajasthan  
Jaipur-302004  
Rajasthan, India

**Executive Editor:** Ms. Apurva Goel (Bachelor of Engineering; Masters in Environment) C-102, Building No.12, Swarna CGHS, Beverly Park, Kanakia, Mira Road (E) (Thane) Mumbai-401107, Maharashtra, India  
(E-mail: [operations@neptjournal.com](mailto:operations@neptjournal.com))

**Business Manager:** Ms. Tara P. Goel, Technoscience Publications, A-504, Bliss Avenue, Balewadi, Pune-411045, Maharashtra, India (E-mail: [contact@neptjournal.com](mailto:contact@neptjournal.com))

## EDITORIAL ADVISORY BOARD

1. **Dr. Saikat Kumar Basu**, Deptt. of Biological Sciences, University of Lethbridge, Lethbridge AB, Alberta, Canada
2. **Dr. Elsayed Elsayed Hafez**, Plant Protection and Biomolecular Diagnosis Department, Arid Lands Cultivation Research Institute (ALCRI), Alexandria, Egypt
3. **Dr. Tri Nguyen-Quang**, Department of Engineering Agricultural Campus, Dalhousie University, Canada
4. **Dr. Sang-Bing Tsai**, Wuyi University Business School, Wuyishan, China
5. **Dr. Zawawi Bin Daud**, Faculty of Civil and Environmental Engg., Universiti Tun Hussein Onn, Malaysia, Johor, Malaysia
6. **Dr. B. Akbar John**, School of Industrial Technology, Universiti Sains Malaysia (USM), Penang, Malaysia
7. **Dr. C. Stella**, Centre for Agro Marine Research, Sethubhaskara Agricultural College and Research Foundation, Visalayankottai, Karaikudi, T.N., India
8. **Dr. G.R. Pathade**, Krishna Institute of Allied Scinces, Krishna Vishwa Vidyapeeth, Karad, Maharashtra, India
9. **Dr. Amit Arora**, Department of Chemical Engineering, National Institute of Technology (NIT), Hamirpur, H.P., India
10. **Prof. Riccardo Buccolieri**, Deptt. of Atmospheric Physics, University of Salento, Dipartimentodi Scienzee Tecnologie Biologicheed Ambientali, Laboratory of Micrometeorology, Lecce, Italy
11. **Dr. Tai-Shung Chung**, Graduate Institute of Applied Science and Technology, National Taiwan University of Science and Technology, Taipei, Taiwan
12. **Dr. Abdeltif Amrane**, Technological Institute of Rennes, University of Rennes, France
13. **Dr. Giuseppe Ciaburro**, Dept. of Architecture and Industrial Design, Universita degli Studi, Della Campania, Italy
14. **Dr. A.B. Gupta**, Dept. of Civil Engineering, Malviya National Institute of Technology (MNIT), Jaipur, India
15. **Claudio M. Amescua García**, Department of Publications Centro de Ciencias dela Atmósfera, Universidad Nacional Autónoma de México
16. **Alexander B. Ruchin**, Joint Directorate of the Mordovia State Nature Reserve and National Park, Saransk 430005, Russia
17. **Wei (Welsh) Wang**, State Key Lab of Environmental and Biological Analysis, Hong Kong Baptist University, Hong Kong



# Biodiversity and Soil Characterization of Ancestral Domain of the Tagbanua Tribe in Aborlan, Palawan, Philippines

Reynald M. Quilang†

College of Agriculture, Forestry and Environmental Science, Western Philippines University, San Juan, Aborlan, Palawan, Philippines

†Corresponding author: Reynald M. Quilang; Reymquilang3@gmail.com

Nat. Env. & Poll. Tech.  
Website: [www.neptjournal.com](http://www.neptjournal.com)

Received: 10-01-2024

Revised: 14-03-2024

Accepted: 03-04-2024

## Key Words:

Ancestral domain  
Species composition  
Diversity  
Tagbanua  
Indigenous people

## ABSTRACT

This study was conducted to determine strategies to enhance the sustainable forest management practices of the Tagbanua tribe. Specifically to describe the biodiversity and soil characteristics of the ancestral domain. The modified belt-transect method for biodiversity assessment developed by B+WISER (2014), further modified by the Department of Environment and Natural Resources (DENR) in the assessment, was used in this study. Results of soil chemical analysis showed significant variations among various land uses. The ancestral domain had at least 73 plant species belonging to 34 families and 59 genera. Four (4) taxa whose SN/families were still undetermined and another three (3) genera under families Annonaceae, Meliaceae, and Sapindaceae were unidentified. It had 12 plant species that are threatened with one critically endangered based on the list of threatened Philippine plants of the DENR. On the other hand, a total of 372 birds representing 61 species from 29 families were recorded. The high Shannon-Weiner Diversity Index ( $H' = 3.69$ ) and Shannon's Evenness ( $HE = 0.90$ ) values indicate high avifaunal diversity and equitable distribution among the detected species. Most of the conservation priority species recorded in the area are Palawan endemic species. The survival of these birds is threatened by extinction due to habitat loss. This observation emphasized the importance of the ancestral domain as a refuge for these endemic species and conservation priority areas.

## INTRODUCTION

In the Philippines, the annual forest cover loss is placed at 49,954 ha or 1.4 percent annually from 1990 to 2000, making it one of the notoriety in SE Asia and the second country with the thinnest forest cover (Aquino et al. 2014). The forest cover of the Philippines declined from 70 percent of the country's total land area of 30 million hectares (ha) in 1900 to about 18.3 percent, or just over 5 million ha of residual and old-growth natural forests, in 1999 (ESSC 1999). Official records showed that in 2010, the forest cover was 23% or about 6.8 million hectares (FMB 2019).

At present, the few remaining areas in the country with intact forests are mostly those in which indigenous forest management persists (Guiang et al. 2001). The top 3 regions that had the highest forest cover based on 2010 satellite images released by the NAMRIA are Regions 2 with 1.04 million hectares, Region 4-B, MIMAROPA with 915,664 and CAR with 773,191 (DENR 2015). The fact is, these regions are home to various indigenous peoples.

Indigenous Peoples have always played an important role in the conservation and preservation of the country's forest

areas. Among them are Tagbanua tribe in the province of Palawan who relied on the forests for their survival. They are fully dependent on forests for rice production through Kaingin farming. They also generate income from extracting forest products such as bamboo, Almaciga resins, rattan, and honey gathering.

In 2009, an ancestral domain with a total land area of 12,874.74 hectares was awarded to this tribal group. It is important to document what are the plant resources found therein for sustainable management of resources in the ancestral domain. The inventory and documentation of the indigenous plant species further aid in biodiversity conservation; the study site, being an ancestral domain, is prone to exploitation. Keeping these species protected and conserved for biodiversity may also serve as a natural gene bank of plant species in the province.

## Objectives/Statement of the Problem

The general objective of this study was to determine strategies to enhance the forest management practices of the Tagbanua in Aborlan, Palawan, Philippines. Specifically,

this was conducted in order to describe the biodiversity and soil characteristics of the ancestral domain.

## MATERIALS AND METHODS

### Location of the Study Site

The study was conducted in the ancestral domain area of the Tagbanua tribe in Barangay Cabigaan, in the municipality of Aborlan, Palawan (Fig. 1). The Certificate of Ancestral Domain Title (CADT) was awarded on July 24, 2009, with a total land area of 12,874.74 hectares covering Brgys Cabigaan, Aborlan and portion in Sitio Manaili, Brgy Dumanguena of Narra, Palawan. There are 600 IP rights holders of this ancestral domain. The area is recognizably having a portion of intact forest, particularly in the watershed area and on the highest elevation of the ancestral domain. The watershed is the primary source of irrigation water systems providing potable water in seven (7) barangays within which the majority of the tribal communities reside.

### Floral Survey

#### Establishment of woody flora diversity plots and transects:

The modified belt-transect method for biodiversity assessment developed by B+WISER (2014), further modified by DENR in the assessment of forestlands, was used in this study. As stipulated in the guidebook on Biodiversity Assessment and Monitoring System (BAMS) in September 2017, a 2 km transect was used; two (2) line transects were established in 2 sites with a measurement of 2 km per transect. Eight plots with a measurement of 20m x 20m in each two-kilometer transect were established, with a total of 16 plots in all sampling areas. The distance per plot is 250 meters.

**Plant identification:** Plant species identification was verified through herbarium records and flora (Hooker 1872-1887, Hooker 1890, Pradhan & Lachungpa 1990, Kholia 2010). The unidentified species in the field were photographed and later identified by taxonomy experts. Identification of

floral species was up to the species level. Dubious identified species, morphotype system and/or use of higher taxa (genus, family) were used to facilitate distinction.

Endemism and ecological status of the different species were assessed to determine the ecological importance of the vegetation in the area. Nomenclature of the species followed the latest Angiosperm Phylogeny Group classification (Stevens 2001).

### Avifauna Survey

The avifaunal survey was conducted using a standard transect count method described by the Biodiversity Management Bureau (BMB) of the DENR and the Deutsche Gesellschaft für Internationale Zusammenarbeit (GIZ) GmbH (BMB-DENR & GIZ, 2017). The study used a standard two-kilometer transect line that was established between the coordinates 9.44688 N 118.44363 E and 9.45959 N 118.43153 E. The survey was carried out by identifying, counting, and recording all the birds detected using visual and auditory cues while walking along the transect route. The counting of birds was repeated six times based on the species discovery curve. All bird counts were done early in the morning (6:00 am) and late in the afternoon (3:00 pm) as the bird activities peak at these periods.

### Prior Informed Consent

Before entering the community, the researcher had complied with the guidelines and important requirements such as secure Free Prior and Informed Consent (FPIC) in compliance with NCIP Administrative Order Nos. 1, Series of 2012, otherwise known as The Indigenous Knowledge System and Practices (IKSP's) and Customary laws (CLs) Research and Documentation Guidelines of 2012. Among others, the guidelines stated that the FPIC of the ICCs/IPs permission should be secured before the commencement of any undertakings, i.e., research activity that affects them.

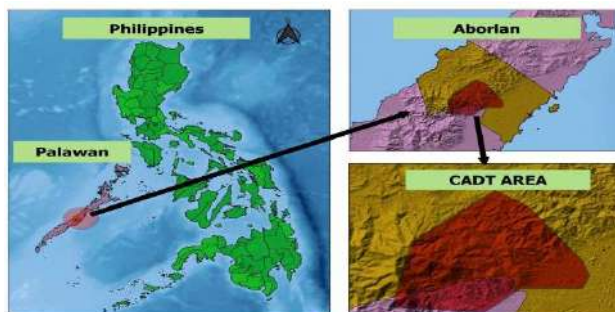
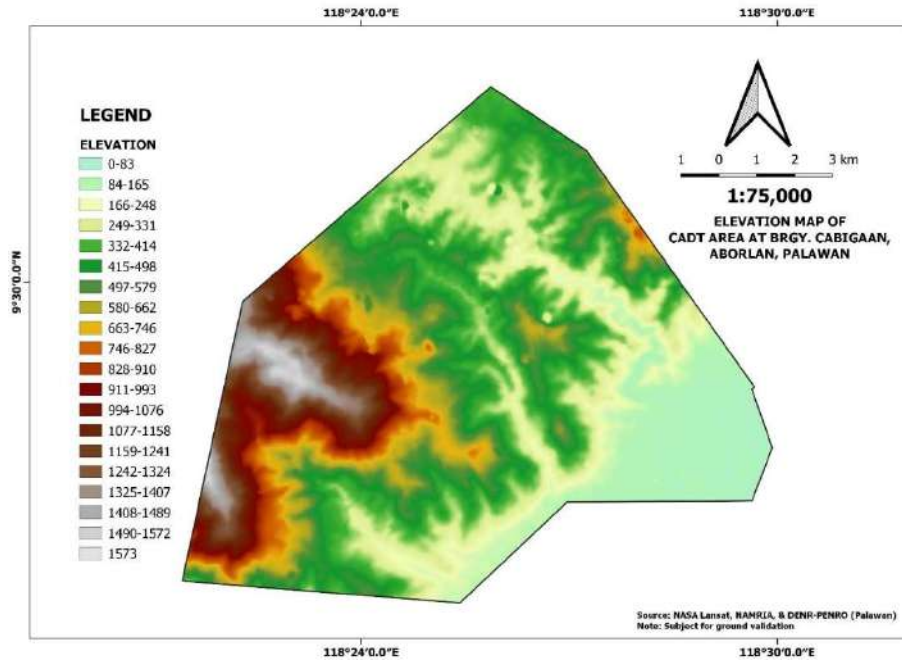


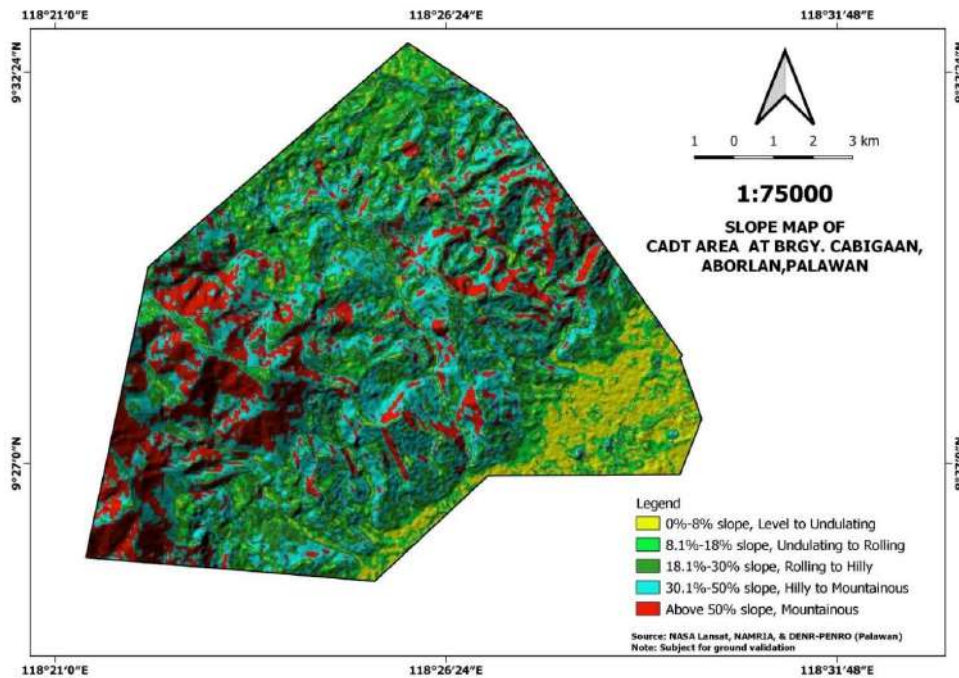
Fig. 1: Location map of the study site.





(Source: DENR-CENRO Puerto Princesa, 2020)

Fig. 2: Elevation map of the ancestral domain.



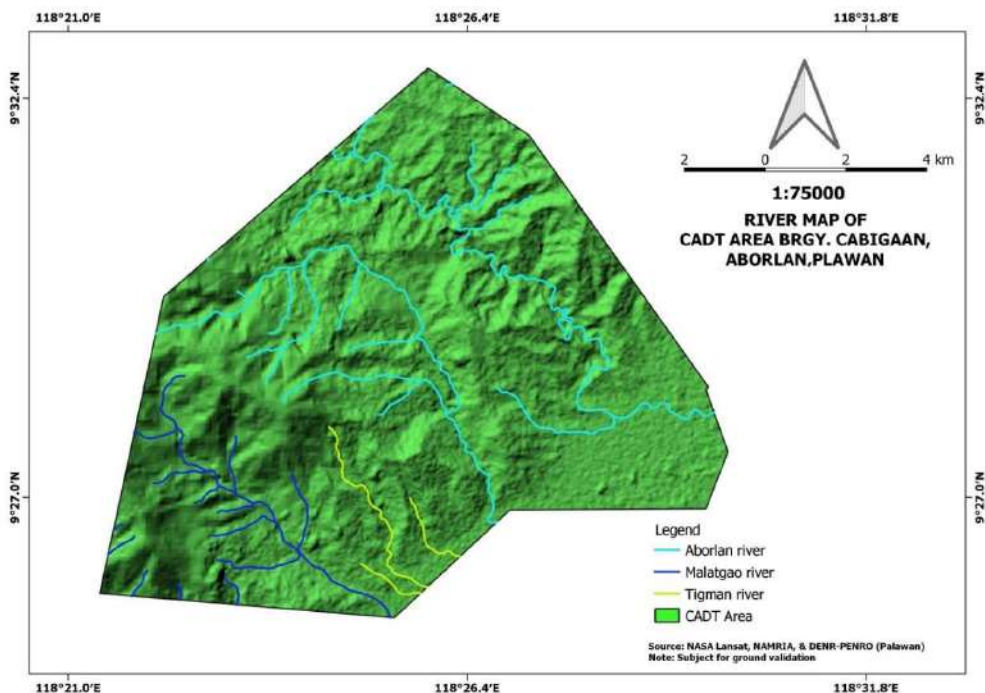
(Source: DENR-CENRO Puerto Princesa, 2020)

Fig. 3: Slope map of the ancestral domain.

## RESULTS AND DISCUSSION

### Biophysical Characteristics

**Morphology and drainage:** The topography is characterized by a flat to hilly to mountainous slope. The highest elevation is at 1,505 – 1,573 meters above sea level (masl) in the



(Source: DENR-CENRO Puerto Princesa)

Fig. 4: River system of the ancestral domain.

Culandanum area in the western portion of the municipality of Aborlan, while the lowest is at 16- 70 meters above sea level (Fig. 2), which is in Brgy. Cabigaan proper, including the portion of the Talakaigan watershed.

The ancestral domain is a part of the Victoria–Anepahan Mountain Range (VAMR), which is considered one of the 11 important bird areas in Palawan (Mallari et al. 2001). Slopes vary from 0% level to very steep (>50%) (Fig. 3). The slope 30.1% - 50% had the biggest total area of 4,340.22 hectares representing 33% of the total land area, followed by 18.1% -30% slope, (rolling to hilly) with an area of 2,932.08 hectares representing 22%. Generally, the latter is preferred by the IPs in conducting their farming activities for their convenience. On the other hand, areas above 50% cover 2,617.95 hectares, which represents 20%, a mountainous portion of the ancestral domain where the forest is relatively intact.

The 3 river systems include Aborlan, Malatgao, and Tigman. Aborlan River is considered a “lifeblood” due to its importance among the Tagbanua tribe and that of the 7 barangays (out of 19) who are the direct beneficiaries of the watershed in Talakaigan River. There is an existing dam structure that serves as a source of water for agriculture and households, mostly of Brgys Cabigaan, Iraan, Magbabadil, Barake, Apis, Sagpangan, and Mabini. (Fig. 4). The watershed is also a recreational area for residents.

In 2017, data from the Palawan Council and Sustainable

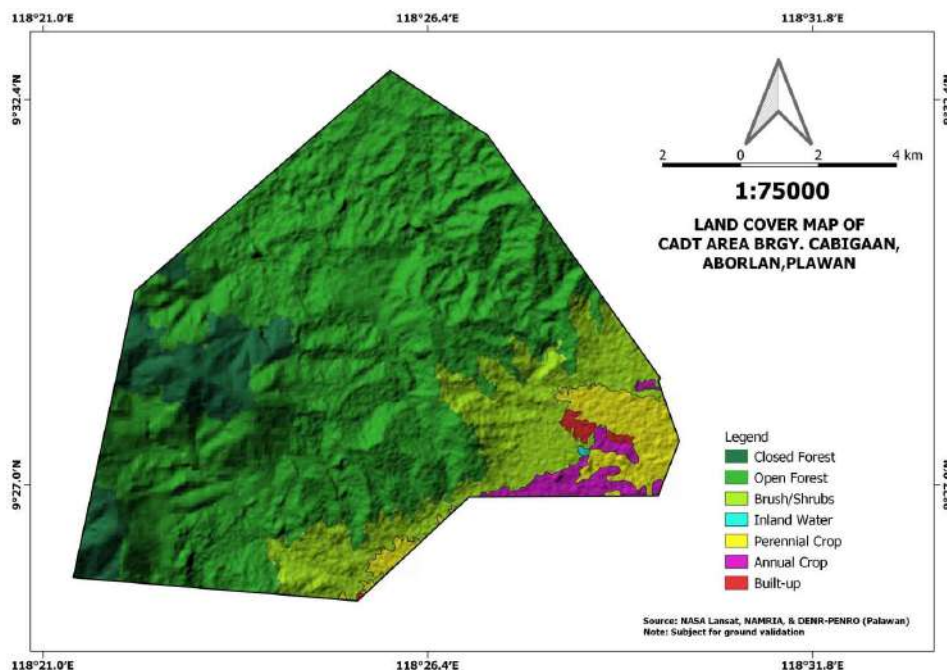
Development (PCSD) showed that the major land use of the area was as “open forests,” which comprise an area of 9,173.74 hectares or 71% of its total land area. Agricultural area for annual crops had limited coverage, with only 248.72 hectares (Table 1).

Generally, there is intact vegetation in the closed forest, which extends a portion of the Talakaigan watershed. Vegetation in the lower elevation and flat terrain is shrublands (1,795.86 has.), which serve as an ecotone between the forest and agricultural ecosystems. Other significant land uses were built-up areas (53.57 ha.) and inland waters (5.93 ha.), which cover a portion of the Talakaigan watershed forest situated in the rough terrain and higher elevations (Fig. 5).

Table 1: Land cover of the ancestral domain.

Land Cover (2014)	Area [has.]
Annual Crop	248.72
Built-up	53.57
Closed Forest	1,053.87
Inland Water	5.93
Open Forest	9,173.74
Perennial Crop	543.06
Brush/Shrubs	1,795.86
TOTAL	12,874.74

(Source: PCSD, 2017)



(Source: DENR-CENRO Puerto Princesa)

Fig. 5: Land cover map of the ancestral domain.

## Land Use

Using the Indigenous Peoples classification of land uses, below are the different land-use types in the area:

- Village (*sagpon-sagpon*). This is where clustered houses are built.
- Rivers (*danum*). Are sources of freshwater resources.
- Coconut plantation (*niogan*). Area planted to coconut.
- Swidden farm (*kaingin*). This refers to upland areas planted with rice, vegetables, root crops, and legumes.
- Pasture land (*kesgetan*). The area is designated as a communal pasture/grazing area.
- Natural Forest (*talun*). These are mountain ranges and ridges that serve as a source of community forest products such as wild fruits, mineral resources, and wild animals.

## Soil

The soil is classified as rough, mountainous, or undifferentiated (Fig. 6), which is characterized by an extensively developed slope (lateral) flow of soil moisture owing to the considerable steepness of the slopes and the high water permeability of the gravel-like rock masses. Soils are also highly diverse and can vary significantly within limited areas due to different exposures and steepness.

## Soil Chemical Characteristics of the Ancestral Domain of the Tagbanuas Soil pH

Comparison among the land uses revealed that lowland ricefield (*basakan*), vegetable production area (*gulayan*), and coconut plantation (*niyogan*) had a pH average value of 5.8, while forest soil (*talun*) and swidden (*kaingin*) had both average values of 5.4 (Table 2). Using FAO Staff (1976) as the standard range of some chemical and physical properties of soils, the area is considered acidic. Analysis of variance (Table 3) showed that pH levels were significantly different among the land-use systems.

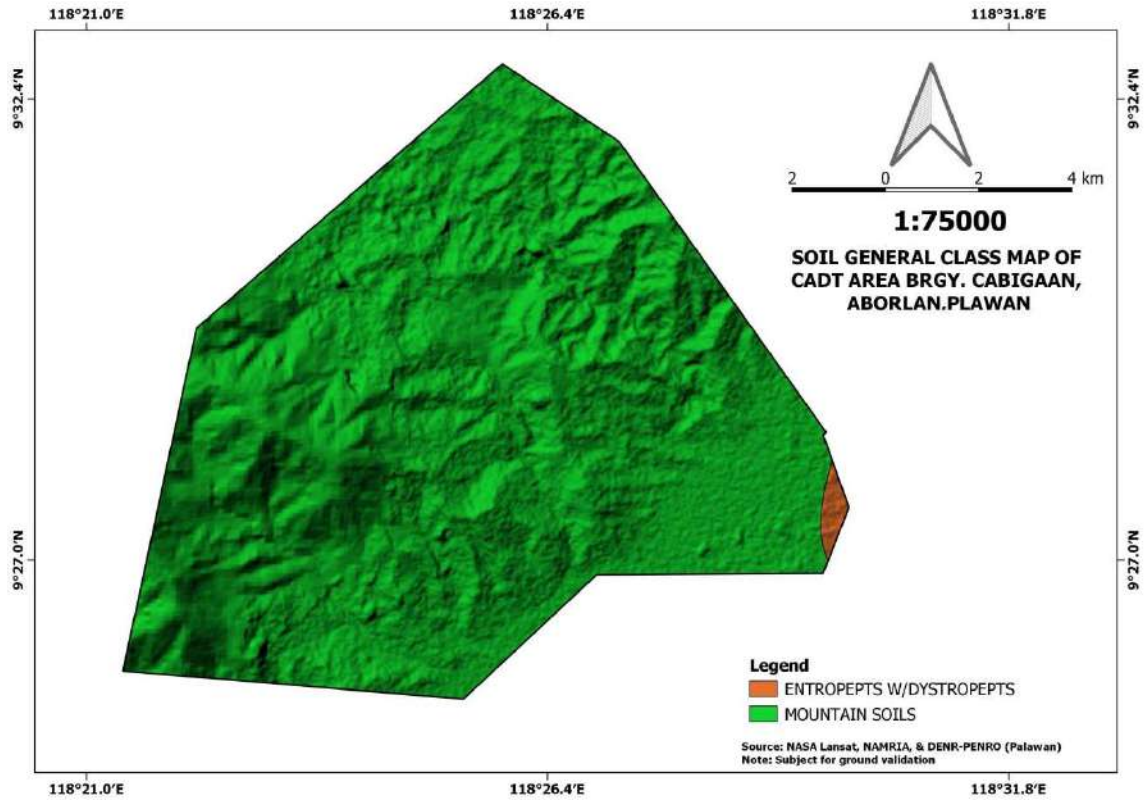
Treatments with the same subscript are not significantly different from each other at a 5% level of significance using Duncan's Multiple Response Test (DMRT)

## Total Nitrogen

The "forest soil" had the highest nitrogen level of 1.0, described as "high" using the FAO standard (FAO 1973). Analysis of variance (Table 4) showed differences in Nitrogen with *highly* significant differences in the forest soil compared to the other land uses attributed to the frequent cultivation for agricultural production purposes.

## Available Phosphorus

Analysis of variance revealed significant differences in the



(Source: DENR-CENRO, Puerto Princesa)

Fig. 6: Soil map of the ancestral domain.

Table 2: Chemical analysis of soils in the ancestral domain.

Soil Chemical Properties	Soil Samples				
	Lowland Ricefield ( <i>Basakan</i> )	Vegetable Production Area ( <i>Gulayan</i> )	Forest Soil ( <i>Talun</i> )	Coconut Farm ( <i>Niyogan</i> )	Swidden ( <i>Kaingin</i> )
pH	5.8 <sub>a</sub>	5.8 <sub>a</sub>	5.4 <sub>b</sub>	5.8 <sub>a</sub>	5.4 <sub>b</sub>
Nitrogen	0.5 <sub>b</sub>	0.5 <sub>b</sub>	1.0 <sub>a</sub>	0.5 <sub>b</sub>	0.5 <sub>b</sub>
Phosphorous (ppm)	88 <sub>b</sub>	108 <sub>a</sub>	38 <sub>e</sub>	46 <sub>d</sub>	48 <sub>c</sub>
Potassium (ppm)	44 <sub>c</sub>	60 <sub>d</sub>	122 <sub>b</sub>	248 <sub>a</sub>	80 <sub>c</sub>

Table 3: Analysis of variance for the pH value of soils.

Source of Variation	Df	Sum of Squares	Mean Square	F	p-Value	F-Crit
pH	4	0.576	0.144	14.400	0.000*	3.11
Error	10	0.100	0.010			
Total	14	0.676				

\*significant at 0.05 level of significance

phosphorus content among the indigenous forest management systems (Table 5). Phosphorus content of the IPs soil was found to be significantly different in vegetable production (*gulayan*) (108 ppm) as compared to those of the lowland rice farms (*basakan*) (88 ppm), swidden (*kaingin*) (48 ppm), coconut farm (*niyogan*) (46) and forest soil (*talun*) (38 ppm).

Based on FAO Staff (1976), the value of available P in all areas is high (25-45 ppm) to very high (> 45 ppm). The vegetable production area (*gulayan*) had the highest value due to the application of inorganic P by farmers. Using the FAO Staff standard, all other indicated uses have “high” levels of phosphorus.

Table 4: Analysis of variance for the Nitrogen value of soils.

Source of Variation	Df	Sum of Squares	Mean Square	F	p-Value	F-Crit
Nitrogen	4	0.600	0.150	15.000	0.000*	3.11
Error	10	0.100	0.010			
Total	14	0.700				

\*significant at 0.05 level of significance

Table 5: Analysis of variance for the Phosphorous value of soils.

Source of Variation	Df	Sum of Squares	Mean Square	F	p-Value	F-Crit
Phosphorus	4	11265.600	2816.400	2816.400	0.000*	3.11
Error	10	10.000	1.000			
Total	14	11275.600				

\*significant at 0.05 level of significance

Table 6: Analysis of variance for the Potassium value of soils.

Source of Variation	Df	Sum of Squares	Mean Square	F	p-Value	F-Crit
Potassium	4	80822.400	20205.600	20205.600	0.000*	3.11
Error	10	10.000	1.000			
Total	14	80832.400				

\*significant at 0.05 level of significance

### Available Potassium

The coconut farm (*niyogan*) had the highest soil potassium content (248 ppm) while “moderately low” in forest soil (*talun*) (122 ppm), “low” in swidden (*kaingin*) (80 ppm), vegetable farm (*gulayan*) (60 ppm) and lowland rice farm (*basakan*) (44 ppm). The frequent cultivation and harvest in their lowland rice farm (*basakan*) explains why it had the lowest potassium content. Based on Phosyn Chemicals Limited (1987), as cited by Palijon (1998), the guideline level for potassium is 200 ppm. In this study, only the coconut farm (*niyogan*) had the highest amount of potassium, while the rest of the land uses have low levels of K content. Analysis of variance for K revealed significant differences among the indigenous land-use management system (Table 6).

### Floral Description and Species Composition of the Ancestral Domain

Results showed that there were at least 73 plant species belonging to at least 33 families and 59 genera (Table 7). There were 4 taxa whose SN/families were still undetermined and genera under families Annonaceae (1), Meliaceae (3), and Sapindaceae (1). Voucher specimens were all kept in duplicate at the Herbarium of the Department of Forestry and Environmental Science (DFES) of the College of Agriculture, Forestry and Environmental Sciences (CAFES) at the Western Philippines University (WPU), main campus, Aborlan, Palawan, Philippines.

Most of the species are classified under families Meliaceae with 8, Moraceae represented by 6, Burseraceae (4), Euphorbiaceae (4), and Malvaceae (4). Using the diversity values for the Shannon-Weiner classification scale developed by Fernando (1998), the forest area of the ancestral domain is considered *high*, with a value of 3.42 (Table 8).

The big floral composition is due in part to its geographical location. The vegetation area is a typical tropical lowland evergreen rainforest, the most luxuriant of all plant communities (Whitmore 1984, 1990). The trees are tall, dense and with large numbers growing in groups. The vegetation had three strata or canopy layers. The top stratum is composed of emergent trees such as apitong (*Dipterocarpus grandiflorus*) and manggis (*Koompassia excelsa* (Becc.) Taub., and amugis (*Koordersiodendron pinnatum* (Blanco) Merr., growing either individually or in groups.

The main layer or the trees below the emergent trees are composed of species such as nato (*Palaquium bataanense* Merr.), bunog (*Garcinia benthami* Pierre), Kalingag/Himaraan (*Cinnamomum mercadoi*), and of Syzygium, Pometia (*Pometia pinnata* JR & G Forst.) and Symplocos (*Symplocos odoratissima* (Blume) Choisy ex Zoll).

Smaller trees such as species of *Aglaia* and *Elaeocarpus*, and saplings of the top canopy comprised the undergrowth stratum. The herbaceous vegetation on the ground is usually sparse, with few individuals of fern species. Rattan and woody lianas are also present. The ancestral domain is also a

Table 7: Checklist of identified plant species within the ancestral domain.

No.	Common/local name	Scientific name	Family name
1	Putian	<i>Alangium chinense</i> (Lour.) Rehder	Alangiaceae
2	Morangsang (Dao)	<i>Dracontamelon dao</i> (Blanco) Merr.& Rolfe	Anacardiaceae
3	Amugis	<i>Koordersiodendron pinnatum</i> (Blanco) Merr.	Anacardiaceae
4	Uway-uway (Kamiring)	<i>Semecarpus</i> sp.	Anacardiaceae
5	Samirig	----	Annonaceae
6	Lanutan	<i>Mitrephora lanotan</i> (Blanco) Merr.	Annonaceae
7	Kamanglit (dita)	<i>Alstonia scholaris</i> (L.) R.Br.	Apocynaceae
8	Palanguton	<i>Ervatamia</i> sp.	Apocynaceae
9	Malapapaya	<i>Polyscias nodosa</i>	Araliaceae
10	Banga	<i>Orania paraguayensis</i> Becc.	Arecaceae
11	Bugo	<i>Garuga floribunda</i>	Burseraceae
12	Saling	<i>Canarium</i> sp.	Burseraceae
13	Pagsahingin	<i>Canarium asperum</i> Benth.	Burseraceae
14	Magusalang/Manggusaleng	<i>Protium connarifolium</i> , cf.	Burseraceae
15	Repetek	<i>Kokoona ochracea</i> (Elmer) Merr.	Celastraceae
16	Bukbok	<i>Atuna racemosa</i> Raf.	Chrysobalanaceae
17	Bunog	<i>Garcinia benthami</i> Pierre	Clusiaceae
18	Garcinia	<i>Garcinia venulose</i>	Clusiaceae
19	Kandis	<i>Garcinia lateriflora</i> Blume	Clusiaceae
20	Binuang	<i>Octomeles sumatrana</i>	Datiaceae
21	Apitong	<i>Dipterocarpus grandiflorus</i> (Blanco)	Dipterocarpaceae
22	Kamagong	<i>Diospyros discolor</i> (Desr.) Gurke	Ebenaceae
23	Takip asin	<i>Macaranga grandifolia</i>	Euphorbiaceae
24	Bagonay	<i>Drypetes littoralis</i> (C Robinson) Merr.	Euphorbiaceae
25	Balakat gubat	<i>Sapium luzonicum</i> (Vid.) Merr.	Euphorbiaceae
26	Tangan	<i>Macaranga</i> sp.	Euphorbiaceae
27	Ipil	<i>Intsia bijuga</i> (Colebr.) Kuntze	Fabaceae
28	Manggis	<i>Koompassia excelsa</i> (Becc.) Taub.	Fabaceae
29	Pangi	<i>Pangium edule</i> Reinw. ex Blume	Flacourtiaceae
30	Bago	<i>Gnetum gnemon</i> L.	Gnetaceae
31	Lingo-lingo	<i>Viticipremna philippinensis</i> (Turcz.) H.J.Lam.	Lamiaceae
32	Bikayan (Malaikmo)	<i>Cinnamomum</i> sp.	Lauraceae
33	Himaraan (Kalingag)	<i>Cinnamomum mercadoi</i> S. Vidal	Lauraceae
34	Apalang (Palawan Putat)	<i>Barringtonia palawanensis</i> P. Chantaranothai	Lecythidaceae
35	Putat	<i>Barringtonia racemosa</i> (L.) Blume ex DC	Lecythidaceae
36	Datu	<i>Leea manillensis</i>	Leeaceae
37	Bayok	<i>Pterospermum diversifolium</i> Blume	Malvaceae
38	Durian	<i>Durio zibethinus</i>	Malvaceae
39	Taluto	<i>Pterocybium tinctorium</i> Merr.	Malvaceae
40	Grewia	<i>Astronia Grewia</i>	Malvaceae
41	Balukanag	<i>Chisocheton cumingianus</i> (C.DC.) Harms.	Meliaceae
42	Mararango	<i>Azadirachta excels</i> (Jack) Jacobs	Meliaceae

Table Cont....

No.	Common/local name	Scientific name	Family name
43	Lambunao	<i>Aglaia elliptica</i> Blume	Meliaceae
44	Bagingsado (Malasaging Elanan)	<i>Aglaia</i> sp.	Meliaceae
45	Bayuso (Malasaging Pula)	<i>Aglaia</i> sp.	Meliaceae
46	Alalandeg	<i>Dysoxylum</i> sp.	Meliaceae
47	Lipso	<i>Chisocheton</i> sp.	Meliaceae
48	Parina		Meliaceae
49	Antipolo/Malagda	<i>Artocarpus blancoi</i> (Elm.) Merr.	Moraceae
50	Kalios	<i>Streblus asper</i>	Moraceae
51	Kanapay	<i>Ficus magnoliifolia</i>	Moraceae
52	Katel/Katol	<i>Ficus glandulifera</i> (Wall. ex Miq.) King	Moraceae
53	Sisian (Tangisang bayawak)	<i>Ficus variegata</i> Blume	Moraceae
54	Kobi	<i>Artocarpus mitida</i>	Moraceae
55	Duguan/Palawan duguan	<i>Myristica guaterifolia</i> A DC	Myristicaceae
56	Tanghas	<i>Myristica elliptica</i>	Myristicaceae
57	Malabayabas/Palawan malabayabas	<i>Tristaniaopsis oblongifolia</i> (Merr.) Peter G. Wilson & Waterhouse	Myrtaceae
58	Indang/Undang	<i>Syzygium</i> sp.	Myrtaceae
59	Anuling	<i>Pisonia umbellifera</i> (Forst.) Seem.	Nyctaginaceae
60	Bananato	<i>Microdesmis casearifolia</i> Planch.	Pandaceae
61	Saog	<i>Ardisia</i> sp.	Primulaceae
62	Agtap	<i>Neonauclea</i> sp.	Rubiaceae
63	Rambutan	<i>Nephelium lappaceum</i> L.	Sapindaceae
64	Dipanga/malugai	<i>Pometia pinnata</i> JR & G Forst.	Sapindaceae
65	Balisangkad	-----	Sapindaceae
66	Benselagen	<i>Mimusops parvifolia</i>	Sapotaceae
67	Nato	<i>Palaquium bataanense</i> Merr.	Sapotaceae
68	Ulam	<i>Planchonella</i> sp.	Sapotaceae
69	Ragingding	<i>Symplocos odoratissima</i> (Blume) Choisy ex Zoll.	Symplocaceae
70	Maraapog	-----	
71	Panghasaan	-----	
72	Pupuan	-----	
73	Dampilingan	-----	

home of dipterocarp i.e., Apitong (*Dipterocarpus grandiflorus* (Blanco) Blanco). The largest and tallest tree measured was nato (*Palaquium bataanense* Merr.), with a diameter at breast height (dbh) of 118 and approximately 17 m tall.

Table 8: Diversity values for the Shannon-Weiner classification scale developed by Fernando (1998).

Relative values	H' Values
Very High	> 3.5000
High	3.0000 - 3.4999
Moderate	2.5000 - 2.9999
Low	2.0000 - 2.4999
Very Low	< 1.9999

The number of individuals by dbh group (Fig. 7) showed that a big percentage (40%) of trees had smaller diameters (dbh of 1-10 cm), which shows that the area is currently regenerating. The wide distribution of dbh ranging from 1-120 cm is indicative of an old-growth forest condition of the ancestral domain.

The most frequent species (Fig. 8) was Dipanga (*Pometia pinnata* JR & G Forst.) (41 individuals), with at least 2 individuals encountered in each of the 16 plots established, followed by Apalang (*Barringtonia palawanensis* P. Chantaranonthai) (39 individuals),

Ragingding (*Symplocos odoratissima* (Blume) Choisy ex Zoll. (29), Rambutan (*Nephelium lappaceum* L.) (28) and

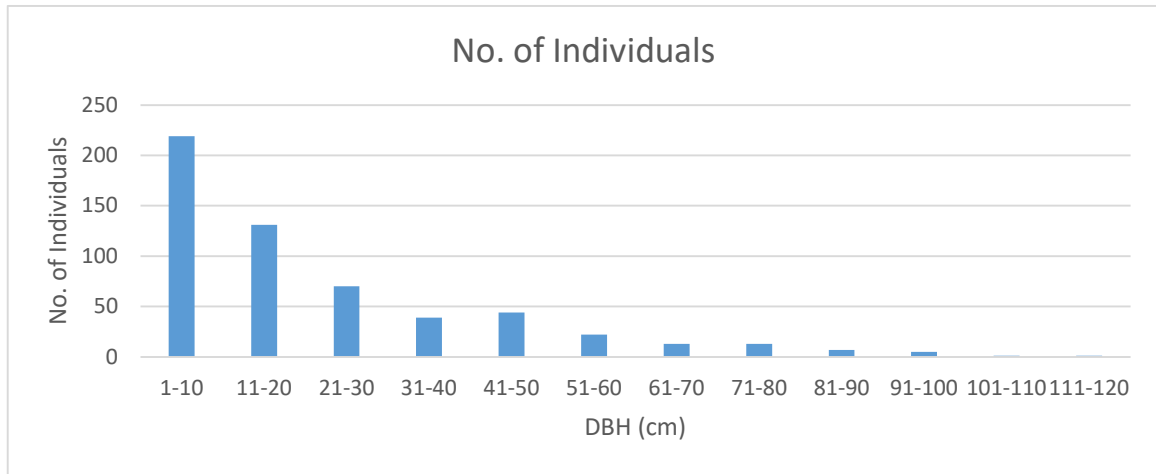


Fig. 7: Frequency histogram of 517 individuals in the ancestral domain.

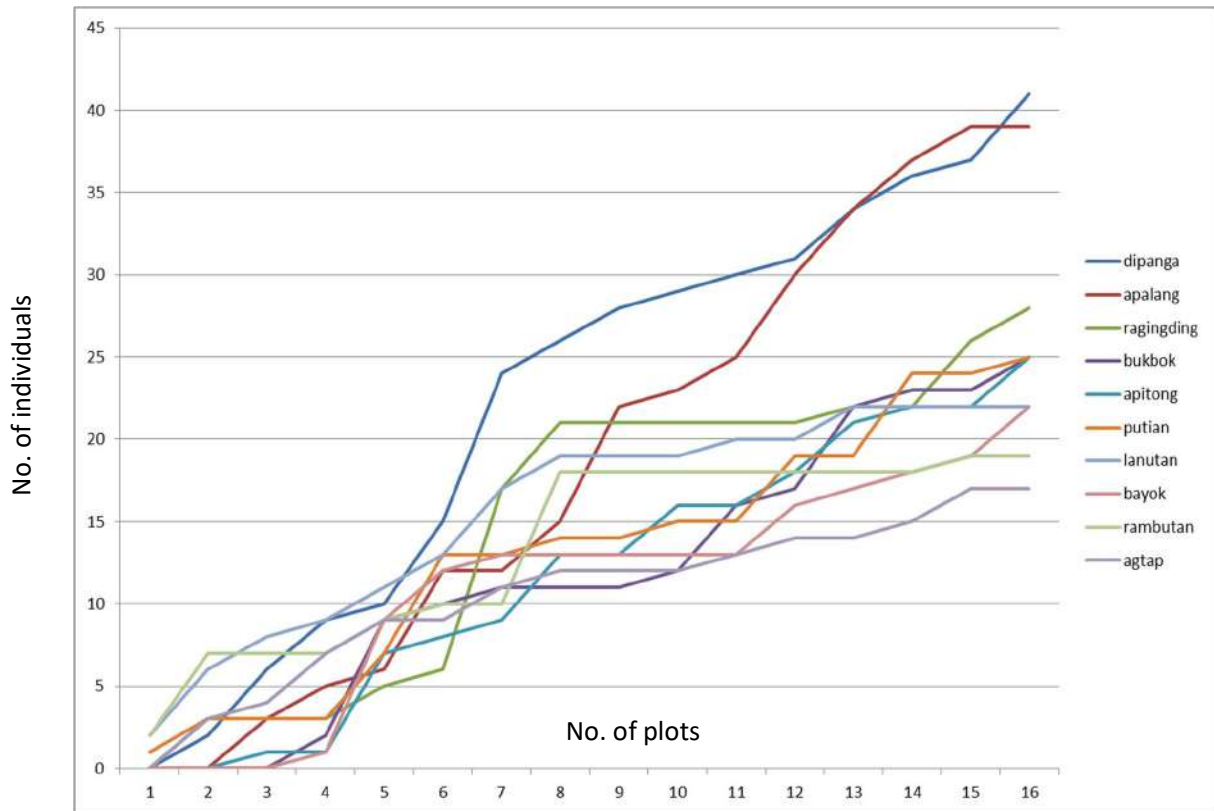


Fig. 8: Frequency Distribution of Species.

Apitong (*Dipterocarpus grandiflorus*) (Blanco) Blanco (25), Bukbuk (*Atuna racemosa* Raf.) (25) and Putian (*Alangium chinense* (Lour.) Rehder (25)). In this study, the most number of individuals, basal area, and volume belong to the families under Sapindaceae, Lecythidaceae, Malvaceae, Annonaceae, and Meliaceae (Figs. 8, 9, and 10).

**Conservation Status**

There were 12 plant species recorded that are categorized as either critically endangered, threatened and vulnerable, or other threatened species (Table 9) based on the updated national list of threatened Philippine plants of the Department



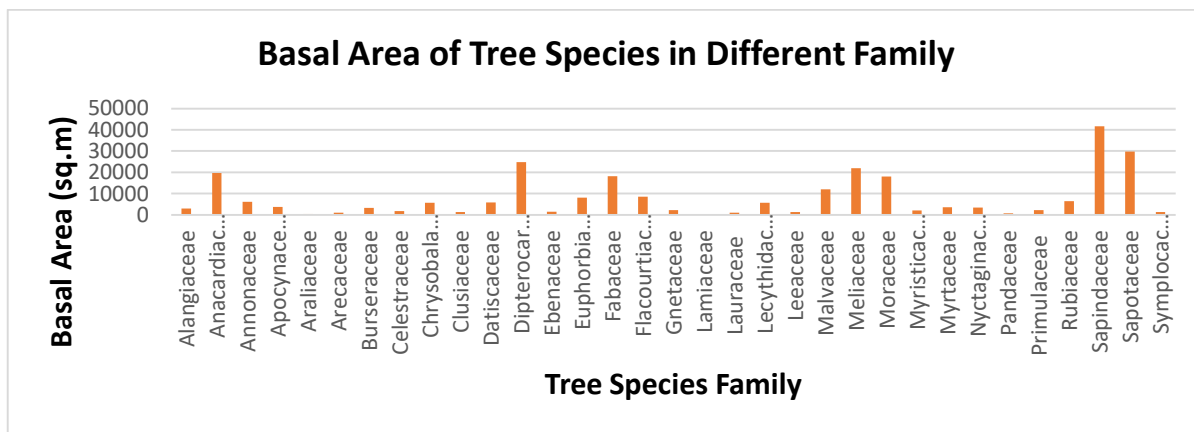


Fig. 9: Basal area.

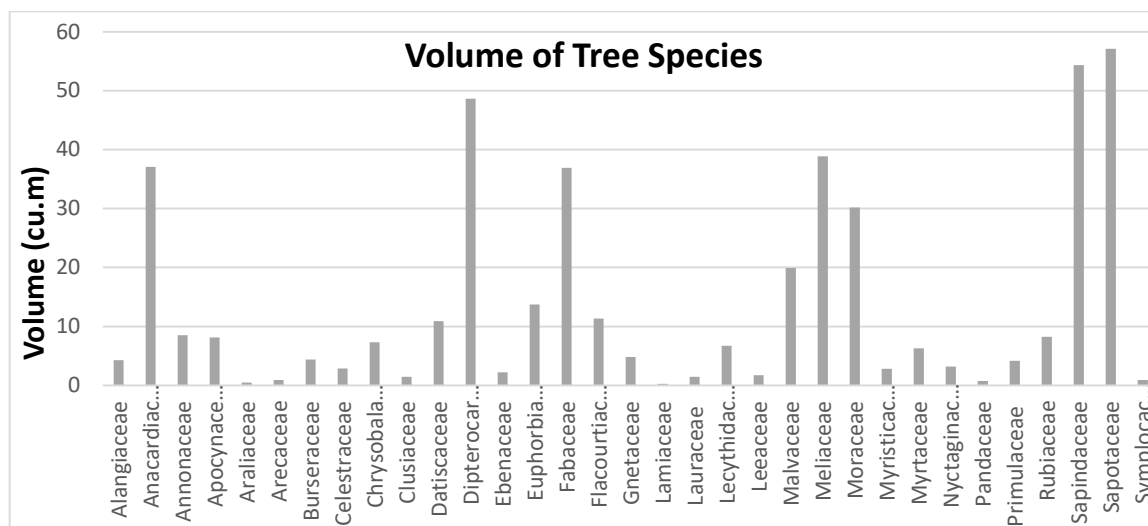


Fig. 10: Volume of tree species.

of the Environment and Natural Resources (DENR). Among these species, *Banga* (*Orania paraguayensis* Becc.), known locally among Tagbanua as “tangkaurin,” is a native of Palawan (Dransfield et al. 2008) and is considered a critically endangered palm species. The Tagbanua commonly use the leaves of this plant to build their houses (Fig. 11).

Meanwhile, *Manggis* (*Koompassia excelsa* (Becc.) Taub.) is a threatened plant under the IUCN endangered category due to habitat degradation such as kaingin. This species is recorded as native to Palawan and is usually found in forests in its low altitudes. Ecologically, *Manggis* is a resting or nesting place for important native birds in Palawan, such as Blue-naped parrots, Mynah, and Philippine cockatoo (MODECERA 2018). Flowers of this plant also serve as food for wild bees that exist in the area. The Tagbanua called this tree “Ginuu” (i.e., a respectable one or

person in the community); hence, it is a sacred tree amongst IPs.

Most of the threatened plants are in the vulnerable category. About 6 plant species are under this category. These vulnerable species are not endangered or critically endangered but are under threat due to deforestation, habitat destruction, overcollection, poaching, and land conversion, and are most likely to move to the endangered category in the future. In terms of abundance, quite a number of individuals have been observed i.e., *apalang* with 39 individuals, rambutan (28), apitong (25), nato (14) himaraan (6), kamagong (5) ipil (5).

There are 4 species listed under the “other threatened species” (OTS) i.e., *Amugis* (*Koordersiodendron pinnatum*), *Lanutan* (*Mitrephora lanotan*), *Kalingag/himaraan* (*Cinnamomum mercadoi*), *Nato* (*Palaquium bataanense*).

Table 9: List of threatened plant species found in the ancestral domain.

Common Name/Local Name	Scientific Name	Family	Conservation Status
Banga	<i>Orania paraguensis</i>	Arecaceae	Critically endangered
Manggis	<i>Koompassia excelsa</i>	Fabaceae	Endangered
Dao	<i>Dracontomelon dao</i>	Anacardiaceae	Vulnerable
Apitong	<i>Dipterocarpus grandifloras</i>	Dipterocarpaceae	Vulnerable
Kamagong	<i>Diospyros discolor</i>	Ebenaceae	Vulnerable
Ipil	<i>Intsia bijuga</i>	Fabaceae	Vulnerable
Apalang	<i>Barringtonia palawanensis</i>	Lecythidaceae	Vulnerable
Rambutan	<i>Nephelium lappaceum</i>	Sapindaceae	Vulnerable
Amugis	<i>Koordersiodendron pinnatum</i>	Anacardiaceae	Other threatened species
Lanutan	<i>Mitrephora lanotan</i>	Annonaceae	Other threatened species
Kalingag/Himaraan	<i>Cinnamomum mercadoi</i>	Lauraceae	Other threatened species
Nato	<i>Palaquium bataanense</i>	Sapotaceae	Other threatened species

Fig. 11: Banga (*Orania paraguensis* Becc.) is a raw material used by Tagbanuas for making house.

A taxon is *another* threatened species when it has been evaluated against the criteria and does not qualify to be critically endangered, endangered, or vulnerable but is under threat from adverse factors, such as over-collection throughout its range, and is likely to move to the vulnerable category in the near future (DAO 2017-11).

#### Avifaunal Description of the Ancestral Domain of the Tagbanua Tribe

A total of 372 birds representing 61 species from 29 families were recorded during the survey (Table 10). The family Pycnonotidae had the highest number of individuals (14.5%), followed by the families Dicaeidae (12.6%) and Nectariniidae (9.1%). Meanwhile, the Columbidae family had the most number of species representations (7 species), followed by Cuculidae (6 species), Pycnonotidae (4 species), and Nectariniidae (4 species). Either one or two species mostly represented the other families.

Table 10: Families, common names, scientific names, frequency, relative abundance, conservation status, and level of endemism of birds found in the ancestral domain.

Family	Common Name	Scientific Name	Conservation Status	Level of Endemism	Frequency [n]	Relative Abundance [%]
Pycnonotidae	Palawan Bulbul	<i>Alophotix frater</i>	P3	PHES*	17	4.57
Pycnonotidae	Ashy-Fronted Bulbul	<i>Pycnonotus cinereifrons</i>	LC	PHES*	14	3.76
Pycnonotidae	Sulphur-Bellied Bulbul	<i>Hypsipetes palawanensis</i>	P3	PHES*	15	4.03
Pycnonotidae	Black-Headed Bulbul	<i>Pycnonotus atriceps</i>	LC	R	8	2.15
Timaliidae	Pin-Striped Tit-Babbler	<i>Macronous gularis woodi</i>	LC	R**	20	5.38
Pellorneidae	Ashy-Headed Babbler	<i>Malacocincla cinereiceps</i>	P3	PHES*	9	2.42
Pellorneidae	Melodious Babbler	<i>Malacopteron palawanense</i>	NT / P3	PHES*	1	0.27
Muscicapidae	White-Vented Shama	<i>Copsychus niger</i>	P3	PHES*	11	2.96
Muscicapidae	Palawan Blue Flycatcher	<i>Cyornis lemprieri</i>	NT / P3	PHES*	5	1.34
Irenidae	Asian Fairy-Bluebird	<i>Irena puella tweeddalii</i>	LC	R**	16	4.30
Cisticolidae	Rufous-Tailed Tailorbird	<i>Orthotomus sericeus</i>	LC	R	19	5.11
Picidae	Red-Headed Flameback	<i>Chrysocolaptes erythrocephalus</i>	E/P2	PHES*	1	0.27
Picidae	Spot-Throated Flameback	<i>Dinopium everetti</i>	NT/P3	PHES*	2	0.54
Picidae	Great Slaty Woodpecker	<i>Mulleripicus pulverulentus</i>	V / P3	R	1	0.27
Pittidae	Hooded Pitta	<i>Pitta sordida</i>	LC	R	5	1.34
Pittidae	Red-Bellied Pitta	<i>Erythropitta erythrogaster</i>	LC	PHES	1	0.27
Monarchidae	Blue-Paradise Flycatcher	<i>Terpsiphone cyanescens</i>	NT / P3	PHES*	4	1.08
Monarchidae	Black-Naped Monarch	<i>Hypothymis azurea azurea</i>	LC	R	3	0.81
Dicaeidae	Pygmy Flowerpecker	<i>Dicaeum pygmaeum palawanorum</i>	LC	R**	26	6.99
Dicaeidae	Palawan Flowerpecker	<i>Prionochilus plateni</i>	P3	PHES*	21	5.65
Cuculidae	Chestnut-Breasted Malkoha	<i>Phaenicophaeus curvirostris</i>	LC	R	5	1.34
Cuculidae	Asian Koel	<i>Eudynamis scolopaceus</i>	LC	R	2	0.54
Cuculidae	Greater Coucal	<i>Centropus sinensis</i>	LC	R	2	0.54
Cuculidae	Lesser Coucal	<i>Centropus bengalensis javanensis</i>	LC	R	1	0.27
Cuculidae	Square-Tailed Drongo-Cuckoo	<i>Surniculus lugubris brachyurus</i>	LC	R	2	0.54
Cuculidae	Plaintive Cuckoo	<i>Cacomantis merulinus</i>	LC	R	2	0.54
Corvidae	Slender-Billed Crow	<i>Corvus enca</i>	LC	R	8	2.15
Nectariniidae	Pale Spiderhunter	<i>Arachnothera diluitor</i>	P3	PHES*	18	4.84
Nectariniidae	Olive-Backed Sunbird	<i>Cinnyris jugularis</i>	LC	R	6	1.61
Nectariniidae	Brown-Throated Sunbird	<i>Anthreptes malacensis paraguae</i>	LC	R**	4	1.08
Nectariniidae	Lovely Sunbird	<i>Aethopyga shelleyi shelleyi</i>	P3	PHES	6	1.61
Dicruridae	Hair-Crested Drongo	<i>Dicrurus hottentottus palawanensis</i>	LC	R**	14	3.76
Dicruridae	Ashy Drongo	<i>Dicrurus leucophaeus leucophaeus</i>	LC	R	4	1.08
Paridae	Palawan Tit	<i>Periparus amabilis</i>	NT / P3	PHES*	17	4.57
Estrildidae	White-Bellied Munia	<i>Lonchura leucogastra palawana</i>	LC	R	2	0.54

Table Cont....

Family	Common Name	Scientific Name	Conservation Status	Level of Endemism	Frequency [n]	Relative Abundance [%]	
Estrildidae	Scaly-Breasted Munia	<i>Lonchura punctulata cabanisi</i>	LC	R	2	0.54	
Alcedinidae	Oriental Dwarf Kingfisher	<i>Ceryx erithaca</i>	LC	R	6	1.61	
Alcedinidae	Collared Kingfisher	<i>Todiramphus chloris collaris</i>	LC	R	2	0.54	
Accipitridae	Crested Serpent-Eagle	<i>Spilornis cheela palawanensis</i>	AII / P2	R**	2	0.54	
Accipitridae	Crested Goshawk	<i>Accipiter trivirgatus palawanus</i>	AII / P2	R**	1	0.27	
Bucerotidae	Palawan Hornbill	<i>Anthracoceros marchei</i>	V / AII / P2	PHES*	3	0.81	
Columbidae	Green Imperial Pigeon	<i>Ducula aenea</i>	LC	R	2	0.54	
Columbidae	Common Emerald-Dove	<i>Chalcophaps indica</i>	LC	R	5	1.34	
Columbidae	Pink-Necked Green Pigeon	<i>Treron vernans</i>	LC	R	4	1.08	
Columbidae	Spotted Dove	<i>Spilopelia chinensis tigrine</i>	LC	R	2	0.54	
Columbidae	Zebra Dove	<i>Geopelia striata</i>	LC	R	2	0.54	
Columbidae	Black-Chinned Fruit Dove	<i>Ptilinopus leclancheri gironieri</i>	P3	R**	5	1.34	
Columbidae	Reddish Cuckoo-Dove	<i>Macropygia tenuirostris</i>	LC	R	2	0.54	
Campephagidae	Bar-Bellied Cuckoo-Shrike	<i>Coracina striata difficilis</i>	LC	R**	3	0.81	
Campephagidae	Fiery Minivet	<i>Pericrocotus igneus igneus</i>	NT	R	2	0.54	
Sturnidae	Common Hill Myna	<i>Gracula religiosa palawanensis</i>	AII / P1	R**	4	1.08	
Sturnidae	Asian Glossy Starling	<i>Aplonis panayensis</i>	LC	R	8	2.15	
Chloropseidae	Yellow-Throated Leafbird	<i>Chloropsis palawanensis</i>	P3	PHES*	8	2.15	
Coraciidae	Oriental Dollar Bird	<i>Eurystomus orientalis orientalis</i>	LC	R	2	0.54	
Aegithinidae	Common Iora	<i>Aegithina tiphia</i>	LC	R	3	0.81	
Psittaculidae	Blue-Naped Parrot	<i>Tanygnathus lucionensis salvadorii</i>	NT / AII / P1	R	3	0.81	
Psittaculidae	Blue-Headed Racket-Tail	<i>Prioniturus platenae</i>	V / P2	PHES*	2	0.54	
Phasianidae	Red Junglefowl	<i>Gallus gallus</i>	LC	R	2	0.54	
Phasianidae	Palawan Peacock-Pheasant	<i>Polyplectron napoleonis</i>	V / AI / P1	PHES*	1	0.27	
Oriolidae	Black-Naped Oriole	<i>Oriolus chinensis chinensis</i>	LC	R	2	0.54	
Artamidae	White-Breasted Woodswallow	<i>Artamus leucorynchus leucorynchus</i>	LC	R	2	0.54	
					Total	372	100

## Legend:

**Conservation Status:**

LC – IUCN Status “Least concern”

NT – IUCN Status “Near-threatened”

V – IUCN Status “Vulnerable”

AI – CITES Status “Appendix I”

AII – CITES Status “Appendix II”

P1 – PCSD Status “Critically Endangered”

P2 – PCSD Status “Endangered”

P3 – PCSD Status “Vulnerable”

**Level of Endemism:**

\* - Palawan endemic species

\*\* - with Palawan endemic subspecies

PHES – Philippine endemic species

R – Resident species

The first two commonly recorded species were the Pygmy Flowerpecker (*Dicaeum pygmaeum palawanorum*) (Fig. 12) and the Palawan Flowerpecker (*Prionochilus plateni*) (Fig. 13). These members of the Dicaeidae family have relative

abundances of 6.99% and 5.65%, respectively. The Pygmy Flowerpecker is a Palawan endemic subspecies, while the Palawan Flowerpecker is a Palawan endemic species. The Palawan Flowerpecker was considered “Vulnerable” by the Palawan Council for Sustainable Development (PCSD 2015). These birds are usually found in small groups of 2-4 individuals or mixed with other feeding birds in the canopy. As their diet is mainly fruits, these birds contribute a lot to seed dispersal (Corlett 1998, Sritongchuay et al. 2014).

The next well-represented species were both insectivores, the Pin-Striped Tit-Babbler (*Macronous gularis woodi*)

(Fig. 14) of the family Timaliidae and the Rufous-Tailed Tailorbird (*Orthotomus sericeus*) (Fig. 15) of the family Cisticolidae. These birds have relative abundances of 5.38% and 5.11%, respectively. Both birds are resident species but the Pin-Striped Tit-Babbler is a subspecies that is endemic to Palawan. Currently, these birds are not classified as threatened or near-threatened within their range.

The high Shannon-Weiner Diversity Index ( $H' = 3.69$ ) and Shannon's Evenness ( $H_E = 0.90$ ) values indicate high avifaunal diversity and equitable distribution among the detected bird species. These values together with species



**The Pygmy Flowerpecker** is the most common bird species recorded in the area. This bird is usually found feeding on fruits, nectars and small invertebrates in the canopy of trees in the forests and open areas. This bird is also common in farms and developed areas.

**Phylum:** Chordata

**Class:** Aves

**Order:** Passeriformes

**Family:** Dicaeidae

**Genus:** *Dicaeum*

**Species:** *D. pygmaeum*

**Subspecies:** *palawanorum*

**Endemism:** Palawan Endemic Subspecies

**Conservation Status:** Least Concern

**Location:** 9.453765N 118.438372E

Fig. 12: The Pygmy Flowerpecker.



**The Palawan Flowerpecker** is one of the most common species in the area. Like the other flowerpeckers it feeds on berries, nectars, pollen, and small invertebrates.

**Phylum:** Chordata

**Class:** Aves

**Order:** Passeriformes

**Family:** Dicaeidae

**Genus:** *Prionochilus*

**Species:** *P. plateni*

**Endemism:** Palawan Endemic Species

**Conservation Status:** Vulnerable (PCSD)

**Location:** 9.447200N 118.444033E

Fig. 13: Palawan Flower Pecker.



**The Pin-Striped Tit-Babbler** is also one of the commonly recorded species in the area. This bird usually hunts in noisy groups in the dense thickets and low-lying shrubs in the understory. It feeds on insects and small invertebrates.

**Phylum:** Chordata

**Class:** Aves

**Order:** Passeriformes

**Family:** Timaliidae

**Genus:** *Macronous*

**Species:** *M. gularis*

**Subspecies:** *woodi*

**Endemism:** Palawan Endemic Subspecies

**Conservation Status:** Least Concern

**Location:** 9.457532N 118.432311E

Fig. 14: The Pin-Striped Tit-Babbler.



**The Rufous-Tailed Tailorbird** is also one of the common species in the area. This bird usually hunts in pairs or small groups. It feeds on insects and small invertebrates in the dense understory vegetation.

**Phylum:** Chordata

**Class:** Aves

**Order:** Passeriformes

**Family:** Cisticolidae

**Genus:** *Orthotomus*

**Species:** *O. sericeus*

**Endemism:** Resident

**Conservation Status:** Least Concern

**Location:** 9.454969N 118.437976E

Fig. 15: The Rufous-Tailed Tailorbird.

richness and abundance, are important baseline information for possible monitoring and assessment in the future.

Out of the 61 identified bird species in the study area, 19 (31%) are Philippine endemic species, and 17 (89%) of them are confined only to the Palawan faunal region. The common Palawan endemic species recorded in the study area

are Palawan Flowerpecker (*Prionochilus plateni*) (Fig. 13), Pale Spiderhunter (*Arachnothera dilutior*) (Fig. 16), Palawan Bulbul (*Alophoixus frater*) (Fig. 17), Palawan Tit (*Periparus amabilis*) (Fig. 18), Sulphur-Bellied Bulbul (*Hypsipetes palawanensis*) (Fig. 19), Ashy-Fronted Bulbul (*Pycnonotus cinereifrons*) (Fig. 20), White-Vented Shama (*Copsychus*



**The Pale Spiderhunter** is one of the commonly recorded Palawan endemic species in the area. It feeds on nectars, fruit juices, small insects, and other invertebrates.

**Phylum:** Chordata

**Endemism:** Palawan Endemic Species

**Class:** Aves

**Conservation Status:** Vulnerable (PCSD)

**Order:** Passeriformes

**Location:** 9.447806N 118.445823E

**Family:** Nectariniidae

**Genus:** *Arachnothera*

**Species:** *A. dilutior*

Fig. 16.: The Pale Spiderhunter.



**The Palawan Bulbul** prefers forested areas and seldom ventures out in the open. This bird feeds on fruits and small invertebrates in the canopy and understory.

**Phylum:** Chordata

**Endemism:** Palawan Endemic Species

**Class:** Aves

**Conservation Status:** Vulnerable (PCSD)

**Order:** Passeriformes

**Location:** 9.448508N 118.438331E

**Family:** Pycnonotidae

**Genus:** *Alophoixus*

Fig. 17: The Palawan Bulbul.

*niger*) (Fig. 21), Ashy-Headed Babbler (*Malacocincla cinereiceps*) (Fig. 22), and Yellow-Throated Leafbird (*Chloropsis palawanensis*) (Fig. 23).

Meanwhile, the less common Palawan endemic species found during the survey are Palawan Blue Flycatcher (*Cyornis lemprieri*) (Fig. 24), Blue-Paradise

Flycatcher (*Terpsiphone cyanescens*) (Fig. 25), Palawan Hornbill (*Anthracoceros marchei*) (Fig. 26), Spot-Throated Flameback (*Dinopium everetti*) (Fig. 27), Blue-Headed Racket-Tail (*Prioniturus platenae*), Palawan Peacock-Pheasant (*Polyplectron napoleonis*) (Fig. 28), Red-Headed Flameback (*Chrysocolaptes erythrocephalus*) (Fig. 29),



**The Palawan Tit** is an insectivore bird that feeds in the canopy of the forest. It occurs from lowland forests to submontane forest habitats.

**Phylum:** Chordata

**Endemism:** Palawan Endemic Species

**Class:** Aves

**Conservation Status:**

**Order:** Passeriformes

Vulnerable (PCSD)

**Family:** Paridae

Near-Threatened (IUCN)

**Genus:** *Periparus*

**Location:** 9.454844N 118.4416613E

**Species:** *P. amabilis*

Fig. 18: The Palawan Tit.



**The Sulphur-Bellied Bulbul** is an omnivore bird that prefers to live in the mature stands of forest. It usually avoids young stages of secondary forests and fragmented forest.

**Phylum:** Chordata

**Endemism:** Palawan Endemic Species

**Class:** Aves

**Conservation Status:** Vulnerable (PCSD)

**Order:** Passeriformes

**Location:** 9.457496N 118.438446E

**Family:** Pycnonotidae

**Genus:** *Hypsipetes*

**Species:** *H. palawanensis*

Fig. 19: The Sulphur-Bellied Bulbul.





**The Ashy-Fronted Bulbul** has a wide range of foods which includes insects and other invertebrates. It also thrives in both forested and open areas with marginal vegetation. It also frequently visits home gardens and developed areas.

**Phylum:** Chordata

**Endemism:** Palawan Endemic Species

**Class:** Aves

**Conservation Status:** Least Concern

**Order:** Passeriformes

**Location:** 9.450243N 18.440648E

**Family:** Pycnonotidae **Genus:** *Pycnonotus* **Species:** *P. cinereifrons*

Fig. 20: The Ashy-Fronted Bulbul.



**The White-Vented Shama** is a noisy bird that lives in the lowland primary and secondary forests. It also thrives in severely fragmented areas and brush lands. It feeds on insects and small invertebrates.

**Phylum:** Chordata

**Endemism:** Palawan Endemic Species

**Class:** Aves

**Conservation Status:** Vulnerable (PCSD)

**Order:** Passeriformes

**Location:** 9.450134N 118.437649E

**Family:** Muscicapidae **Genus:** *Copsychus* **Species:** *C. niger*

Fig. 21: The White-Vented Shama.



**The Ashy-Headed Babbler** prefers to live in primary, secondary, and fragmented forests with dense shrub layer. It is commonly seen hunting for insects and small invertebrates close to the ground.

**Phylum:** Chordata

**Endemism:** Palawan Endemic Species

**Class:** Aves

**Conservation Status:** Vulnerable (PCSD)

**Order:** Passeriformes

**Location:** 9.450981N 118.443334E

**Family:** Pellorneidae **Genus:** *Malacocincla* **Species:** *M. cinereiceps*

Fig. 22: The Ashy-Headed Babbler.



**The Yellow-Throated Leafbird** is a Palawan endemic species. It is commonly found feeding on insects and berries in the canopy of the primary and secondary forests.

**Phylum:** Chordata

**Endemism:** Palawan Endemic Species

**Class:** Aves

**Conservation Status:** Vulnerable (PCSD)

**Order:** Passeriformes

**Location:** 9.446817N 118.444689E

**Family:** Chloropseidae **Genus:** *Chloropsis* **Species:** *C. palawanensis*

Fig. 23: The Yellow-Throated Leafbird.

and Melodious Babbler (*Malacopteron palawanense*). In addition, two Philippine endemic species that are not restricted to the Palawan faunal region were also recorded

in the area. These are the Lovely Sunbird (*Aethopyga shelleyi shelleyi*) and the Red-Bellied Pitta (*Erythropitta erythrogaster*).



**The Palawan Blue Flycatcher** is found only in forested areas in the Palawan region. This bird prefers to live in the interior part of the forest and avoids the open areas.

<b>Phylum:</b> Chordata	<b>Endemism:</b> Palawan Endemic Species
<b>Class:</b> Aves	<b>Conservation Status:</b> Vulnerable (PCSD)
<b>Order:</b> Passeriformes	Near-Threatened (IUCN)
<b>Family:</b> Muscicapidae	<b>Location:</b> 9.451836N 118.438265E
<b>Genus:</b> <i>Cyornis</i>	
<b>Species:</b> <i>C. lemprieri</i>	

Fig. 24: The Palawan Blue Flycatcher.



**The Blue-Paradise Flycatcher** is commonly found in the dense understory of primary and secondary forests catching insects while on the flight. This bird is also found in community green spaces in developed areas.

<b>Phylum:</b> Chordata	<b>Endemism:</b> Palawan Endemic Species
<b>Class:</b> Aves	<b>Conservation Status:</b> Vulnerable (PCSD)
<b>Order:</b> Passeriformes	<b>Location:</b> 9.451482N 118.439286E
<b>Family:</b> Monarchidae	<b>Genus:</b> <i>Terpsiphone</i>
	<b>Species:</b> <i>T. cyanescens</i>

Fig. 25. The Blue-Paradise Flycatcher



**The Palawan Hornbill** is one of the large frugivore birds in the forest of Palawan. This bird feeds on fruits and supports the forest health and plant diversity by helping in the dispersal of seeds.

**Phylum:** Chordata

**Endemism:** Palawan Endemic Species

**Class:** Aves

**Conservation Status:** Endangered (PCSD)

**Order:** Passeriformes

Vulnerable (IUCN), Appendix-II (CITES)

**Family:** Bucerotidae

**Location:** 9.453013N 118.438270E

**Genus:** *Anthracoceros* **Species:** *A. marchei*

Fig. 26: The Palawan Hornbill.



**The Spot-Throated Flameback** is one of the two flamebacks that are endemic in the Palawan region. Like the other members of the Picidae family, it feeds on insects and other invertebrates by foraging on trunks and branches of trees.

**Phylum:** Chordata

**Endemism:** Palawan Endemic Species

**Class:** Aves

**Conservation Status:** Vulnerable (PCSD)

**Order:** Passeriformes

Near-Threatened (IUCN)

**Family:** Picidae

**Location:** 9.458350N 118.430965E

**Genus:** *Dinopium* **Species:** *D. everetti*

Fig. 27: The Spot-Throated Flameback.



**The Palawan Peacock-Pheasant** is a ground-dwelling forest dependent species. It has strong legs used to scratch the forest floor while looking for berries, seeds, insects, and other invertebrates.

**Phylum:** Chordata

**Class:** Aves

**Order:** Passeriformes

**Family:** Phasianidae

**Genus:** *Polyplectron*

**Species:** *P. napoleonis*

**Endemism:** Palawan Endemic Species

**Conservation Status:**

Critically Endangered (PCSD)

Appendix II (CITES), Vulnerable (IUCN)

**Location:** 9.456357N 118.433898E

Fig. 28: The Palawan Peacock-Pheasant.



**The Red-Headed Flameback** is one of the two flamebacks found in Palawan. It feeds on insects by foraging on trunks of large trees.

**Phylum:** Chordata

**Class:** Aves

**Order:** Passeriformes

**Family:** Picidae

**Genus:** *Chrysocolaptes*

**Species:** *C. erythrocephalus*

**Endemism:** Palawan Endemic Species

**Conservation Status:** Endangered (PCSD)

Endangered (IUCN)

**Location:** 9.457159N 118.434153E

Fig. 29: The Red-Headed Flameback.

The high level of endemism is expected because Palawan is one of the endemic bird areas (EBA) in the Philippines, and the study area is within the eastern slopes of the Victoria-

Anipahan mountain range, one of the important bird areas (IBA) in the province (BirdLife International, 2020). Endemic birds are mostly forest-dependent and are sensitive

to habitat degradation. Thus, a good stand of old-growth forests is important to these species (Mallari et al. 2011). Seventy percent of all the Philippine endemic species found in Palawan were recorded in the study area. The presence of many endemic birds indicates that the forest habitat is still in good condition.

The ancestral domain is also home to many threatened and near-threatened bird species. Using the criteria of the International Union for the Conservation of Nature (IUCN) Red List of Threatened Species, Convention on International Trade in Endangered Species of Wild Fauna and Flora (CITES), and the Palawan Council for Sustainable Development (PCSD), a total of 24 (39%) species of birds found in the study area are on the conservation priority list of at least one of the aforementioned criteria.

Twelve species of birds were included on the conservation priority list of the IUCN Red List of Threatened Species (IUCN, 2020). Of these, seven were classified as “Near-Threatened,” four were classified as “Vulnerable,” and one was classified as “Endangered.” Meanwhile, based on the conservation priority criteria of PCSD (PCSD, 2015), twenty-three bird species found in the study area were already threatened by extinction. Among them, fifteen were identified

as “Vulnerable,” five were assessed as “Endangered,” and three were classified as “Critically Endangered.” Moreover, some of the commonly traded bird species found in the study area were also listed in the CITES Appendices. Five species were listed in Appendix II, which recommends regulating their trade in the international market, while one species was listed in Appendix I, which recommends prohibiting the international trade of that species.

Based on the highest conservation priority status given to each bird species, twenty-three species were considered threatened with extinction. Three species were classified as “Critically Endangered”, the Common Hill Myna (*Gracula religiosa palawanensis*) (Fig. 30), Blue-Naped Parrot (*Tanygnathus lucionensis salvadorii*) (Fig. 31), and Palawan Peacock-Pheasant (*Polyplectron napoleonis*) (Fig. 28). Another five species were classified as “Endangered”, the Red-Headed Flameback (*Chrysocolaptes erythrocephalus*) (Fig. 29), Crested Serpent-Eagle (*Spilornis cheela palawanensis*) (Fig. 32), Crested Goshawk (*Accipiter trivirgatus palawanus*) (Fig. 33), Palawan Hornbill (*Anthracoceros marchei*) (Fig. 26), and Blue-Headed Racket-Tail (*Prioniturus platenae*). Meanwhile, fifteen species were classified as “Vulnerable”, the Palawan



**The Common Hill Myna** is one of the most commonly sold bird species in the local and international pet trade. This species is an important seed dispersal agent in the forest.

**Phylum:** Chordata

**Class:** Aves

**Order:** Passeriformes

**Family:** Sturnidae

**Genus:** *Gracula*

**Species:** *G. religiosa* **Subspecies:** *palawanensis*

**Endemism:** Palawan Endemic subspecies

**Conservation Status:**

Critically Endangered (PCSD)

Appendix II (CITES)

**Location:** 9.454745N 118.440773E

Fig. 30: The Common Hill Mynah.



**The Blue-Naped Parrot** is also one of the common bird species sold in the local and international pet trade.

**Phylum:** Chordata

**Class:** Aves

**Order:** Passeriformes

**Family:** Psittaculidae

**Genus:** *Tanygnathus*

**Species:** *T. lucionensis*

**Subspecies:** *salvadorii*

**Endemism:** Resident (Near Philippine Endemic)

**Conservation Status:**

Critically Endangered (PCSD)

Appendix II (CITES),

Near-Threatened (IUCN)

**Location:** 9.458208N 118.430867E

Fig. 31: The Blue-Naped Parrot.



**The Crested Serpent-Eagle** is a Palawan endemic subspecies. This bird usually hunts prey while soaring in thermals above the forest, forest-edges and open areas.

**Phylum:** Chordata

**Class:** Aves

**Order:** Passeriformes

**Family:** Accipitridae

**Genus:** *Spilornis*

**Species:** *S. cheela*

**Subspecies:** *palawanensis*

**Endemism:** Palawan endemic subspecies

**Conservation Status:** Endangered (PCSD)

Appendix II (CITES)

**Location:** 9.454655N 118.438254E

Fig. 32: The Crested Serpent-Eagle.



**The Crested Goshawk** is a bird of prey that hunts small vertebrates in the forest such as rats, squirrels, lizards, and birds.

**Phylum:** Chordata

**Endemism:** Palawan endemic subspecies

**Class:** Aves

**Conservation status:** Endangered (PCSD)

**Order:** Passeriformes

Appendix II (CITES)

**Family:** Accipitridae

**Location:** 9.452050N 118.438951E

**Genus:** *Accipiter* **Species:** *A. trivirgatus* **Subspecies:** *palawanus*

Fig. 33: The Crested Goshawk.



**The Great Slaty Woodpecker** is one of the largest woodpeckers in the world. It feeds on invertebrates gleaned from barks and rotten tree trunks.

**Phylum:** Chordata

**Endemism:** Resident

**Class:** Aves

**Conservation Status:** Vulnerable (PCSD)

**Order:** Passeriformes

Vulnerable (IUCN)

**Family:** Picidae

**Location:** 9.457436N 118.432778E

**Genus:** *Mulleripicus* **Species:** *M. pulverulentus* **Subspecies:** *pulverulentus*

Fig. 34: The Great Slaty Woodpecker.





**The Black-Chinned Fruit Dove** is a medium sized dove that feed on fruits of trees in the forest. Occasionally, it also visits the fruit bearing trees in fragmented landscapes.

**Phylum:** Chordata

**Endemism:** Palawan endemic subspecies

**Class:** Aves

**Conservation Status:** Vulnerable (PCSD)

**Order:** Passeriformes

**Location:** 9.457037N 118.434562E

**Family:** Columbidae **Genus:** *Ptilinopus* **Species:** *P. leclancheri*

**Subspecies:** *gironieri*

Fig. 35: The Black-Chinned Fruit Dove.

Bulbul (*Alophoixus frater*) (Fig. 17), Sulphur-Bellied Bulbul (*Hypsipetes palawanensis*) (Fig. 19), Ashy-Headed Babbler (*Malacocincla cinereiceps*) (Fig. 22), Melodious Babbler (*Malacopteron palawanense*), White-Vented Shama (*Copsychus niger*) (Fig. 21), Palawan Blue Flycatcher (*Cyornis lemprieri*) (Fig. 24), Spot-Throated Flameback (*Dinopium everetti*) (Fig. 27), Great Slaty Woodpecker (*Mulleripicus pulverulentus pulverulentus*) (Fig. 34), Blue-Paradise Flycatcher (*Terpsiphone cyanescens*) (Fig. 25), Palawan Flowerpecker (*Prionochilus plateni*) (Fig. 13), Pale Spiderhunter (*Arachnothera dilutior*) (Fig. 16), Lovely Sunbird (*Aethopyga shelleyi shelleyi*), Palawan Tit (*Periparus amabilis*) (Fig. 18), Black-Chinned Fruit Dove (*Ptilinopus leclancheri gironieri*) (Fig. 35), Yellow-Throated Leafbird (*Chloropsis palawanensis*) (Fig. 23) (IUCN, 2020; PCSD, 2015).

Most of the conservation priority species recorded in the study area are also Palawan endemic species. Being restricted in Palawan, which is a small geographic region, the deforestation and habitat degradation in the province may drive these species to extinction. This observation further emphasized the importance of the forest in the ancestral

domain as a refuge for these endemic and conservation-priority species.

The supplementary bird watching in the area at night and during rest periods found seven more species. Four species were recorded at night. These are the Spotted Wood Owl (*Strix seloputo wiepkeni*), Palawan Scops Owl (*Otus fuliginosus*), Palawan Frogmouth (*Batrachostomus chaseni*), and Large-Tailed Nightjar (*Caprimulgus macrurus johnsoni*). Meanwhile, three species were found during the daytime, these are the Pied Triller (*Lalage nigra nigra*), Palawan Flycatcher (*Ficedula platenae*), and White-Bellied Woodpecker (*Dryocopus javensis hargitti*). The Palawan Scops Owl, Palawan Frogmouth, and Palawan Flycatcher are Palawan endemic species, while both the Palawan Scops Owl and Spotted Wood Owl were classified as “Endangered,” and Palawan Frogmouth and Palawan Flycatcher were classified as “Vulnerable.”

The avifaunal assemblage in the ancestral domain, particularly in the forested area, may reflect a healthy forest ecosystem, but the threat of habitat degradation and deforestation is always possible if the current anthropogenic activities intensify and become less sustainable. The current

habitat of birds and other wildlife will be affected if a large portion of the watershed is converted into swidden farms. Moreover, if the harvesting of timber and non-timber forest products exceeds the carrying capacity of the forest, it may end up in habitat degradation.

## CONCLUSIONS

The findings of the study show that the Tagbanuas are living in a fragile ecosystem characterized by a high diversity of both plants and animals. Using the diversity values for Shannon-Weiner classification, the forest area of the ancestral domain is considered *High* with a value of 3.42. The area also supports a high avifaunal diversity, as shown by the high species richness, abundance, diversity index, and evenness values. It supports many forest-dependent endemic birds and conservation priority species that are threatened by extinction. These avifaunal community attributes indicate that the forest ecosystem in the ancestral domain is still intact, healthy, in good condition, and stable amid existing anthropogenic activities taking place in the area. The high avifaunal diversity and the presence of many endemic and conservation priority bird species highlight the need to protect and conserve the forest of the ancestral domain.

## RECOMMENDATIONS

Government and other entities, including policymakers, need to consider the conduct of immediate rehabilitation activities and restore areas, especially near the watershed. Silvicultural practices must be introduced to enhance residual forest growth. Utilization of forest resources, particularly the non-timber forest products like rattan and almaciga resins, must be governed by permits. Forest Management Plans in the ancestral domain must be thorough in giving future direction to the IP. As the areas in Talakaigan River have great potential as eco-tourism destinations, management plans should be crafted by the academe or related institutions. Likewise, local communities should be involved in the development and implementation of any project to ensure its success. Government incentives such as payment for environmental services (PES) should be enforced to encourage and sustain better participation of the communities affected.

## ACKNOWLEDGMENT

Esteemed gratitude is extended to Associate Professor Alejandro A. Bernardo Jr.- an expert on bird identification who is based at the Western Philippines University, main campus, Aborlan, Palawan, Philippines.

## REFERENCES

- Aquino, A., Rookie, C. and Dacquo, O., 2010. Executive Order No. 26: Towards a Greener Philippines. Retrieved on February 18, 2016 from <http://ap.fttc.agnet.org/ap/db.php>.
- BMB-DENR and GIZ 2017. Biodiversity Management Bureau (BMB)- Department of Environment and Natural Resources (DENR) & Deutsche Gesellschaft für Internationale Zusammenarbeit (GIZ) GmbH. *Manual on Biodiversity Assessment and Monitoring System for Terrestrial Ecosystems*. Manila, 194p.
- DENR 2015. *Philippine Forest at a Glance*. On National Greening Program. Retrieved on March 25, 2016 from <https://legacy.senate.gov.ph/publications>.
- DENR 2019. *Terrestrial ecosystem biodiversity assessment and monitoring manual*.
- DENR-CENRO 2020. *The soil, elevation, slope, land cover, river systems maps of the ancestral domain of the Tagbanuas in Palawan*. Philippines
- Dransfield, J., N.W. Uhl, C.B. Asmussen, W.J. Baker, M.M. Harley and C.E. Lewis 2008. *Genera Palmarum: The Evolution and Classification of Palms*. *Royal Botanic Gardens*, Kew, 732 pp
- ESSC 1999. *The Decline of the Philippine Forest*. ESSC, Ateneo de Manila University, Quezon City.
- Food and Agriculture Organization of the United Nations (FAO)., 1973. *The state of food and agriculture*. Italy. Retrieved November 12, 2020 from <https://openknowledge.fao.org/server/api/core/bitstreams/c4281a74-d889-4f4b-8dde-280e2d5c9204/content>
- Food and Agriculture Organization of the United Nations (FAO)., 1976. *The state of food and agriculture*. Italy. Retrieved November 9, 2020, from <https://openknowledge.fao.org/server/api/core/bitstreams/>
- Forest Management Bureau (FMB) of the Department of Environment and Natural Resources (DENR)., 2019. *Philippine Forestry Statistics. Department of Environment and Natural Resources (DENR)*. 104p. Retrieved October 30, 2020, from <https://drive.google.com/file/d/1Cuy-Sup929NPOxqBdVcDml-3iYfG2Nhn/view>
- Guiang, E.S., Borlagdan, S.B. and Pulhin, J.M., 2001. *Community-Based Forest Management in the Philippines: A Preliminary Assessment*. Institute of Philippine Culture, Ateneo De Manila University, Quezon City.
- Hooker, J.D., 1890. *The Flora of British India*. Vol. 5. L. Reeve
- Hooker, J.D., (1872–1897) *Flora of British India*, Vol. I–VII. Reeve & Co., London.
- Kholia, B.S., 2010. *Ferns and fern-allies of Sikkim: Part I*. Beracah Printing & Stationeries, Gangtok.
- Revilla, A. Jr. V., 2016. *Sustainable Forest Management in the Philippines*. College of Forestry and Natural Resources, UPLB.
- Pradhan, U. C. and Lachungpa, S.T., 1990. *Sikkim Himalayan Rhododendrons*. Primulaceae Books, Kalimpong.
- Van Beijnen, J. and Jose, E., 2019. Botanical observations from a threatened riverine lowland forest in Aborlan, Palawan, Philippines. *The Palawan Scientist*, 12, pp. 64–73.
- Whitmore, T. C., 1984. *Tropical rain forests of the Far East*. (2nd edition). Oxford University Press, Oxford.
- Whitmore, T.C., 1990. *An Introduction to Tropical Rainforests*. Oxford University Press, Oxford
- Whitmore, T.C., 2017. *Terrestrial Ecosystems Biodiversity Assessment and Monitoring Manual*. Biodiversity Management Bureau and the Deutsche Gesellschaft für Internationale Zusammenarbeit (GIZ) GmbH.

## ORCID DETAILS OF THE AUTHORS

Reynald M. Quilang: <https://orcid.org/0009-0000-9118-4260>



# Dynamic Impact-Based Heavy Rainfall Warning with Multi-classification Machine Learning Approaches

Anand Shankar<sup>1, 2†</sup>

<sup>1</sup>Department of Electronics & Communication Engineering, National Institute of Technology, Patna, India

<sup>2</sup>Indian Meteorological Department, Ministry of Earth Sciences, Govt. of India, Patna, India

†Corresponding author: Anand Shankar; anand.shankar@imd.gov.in

Nat. Env. & Poll. Tech.  
Website: [www.neptjournal.com](http://www.neptjournal.com)

Received: 02-02-2024

Revised: 14-03-2024

Accepted: 29-03-2024

## Key Words:

Impact-based heavy rainfall warning

Multi-classification machine learning

Impacts of floods

Flood assessment

Cascading impact

## ABSTRACT

The majority of flood assessment and warning systems primarily focus on the occurrence of floods caused by river overflow, taking into account factors such as intense precipitation. Improving flood resilience, on the other hand, requires a deeper understanding of how these factors affect each other and how specific local conditions can have an impact. This study offers impartial tools for estimating the severity of the effects brought on by heavy rainfall to facilitate the prompt communication of effective measures, such as the evacuation of livestock and human settlements and the provision of medical assistance. These tools take into account the cascading effects of various causative factors contributing to heavy rainfall. This article aims to assess the various factors that contribute to the impacts of heavy rainfall, including the timestamp (indicating soil saturation and moisture levels), river gauges (determining water congestion in canal systems), average aerial precipitation (indicating runoff), and the rainfall itself, taking into account both in situ and ex-situ impacts. Support Vector Machine (SVM), Decision Tree (DT), K-Nearest Neighbour (KNN), and Naive Bayes are some of the machine learning methods used in the study to find out how dynamically vulnerable affected districts are to flooding in different compound scenarios. This analysis is conducted by leveraging historical observed datasets. The results demonstrate the feasibility of mitigating the issue of excessive and insufficient flood warnings resulting from the cumulative effects of intense precipitation. By implementing a categorization system that divides the affected areas into various portions, or districts, according to the main factors contributing to flooding, namely rainfall, river discharge, and runoff, The suggested model presents novel insights into the sequential consequences of intense precipitation in the regularly inundated regions of North Bihar, India. Innovative tools can serve as valuable resources for flood forecasters and catastrophe managers to comprehend the extent of flooding and the consequential effects of intense precipitation.

## INTRODUCTION

Several studies conducted by (Goswami et al. 2006), (Zou & Ren 2015), and (Abbas et al. 2023) have shown an increase in the frequency of heavy or extreme rainfall events in various regions, indicating a pan-Asian phenomenon. Similarly, global research conducted by (Brunetti et al. 2004), (Groisman et al. 2005), and (De Luis et al. 2011) has also observed a similar trend of extreme rainfall occurrences across different parts of the world. A higher concentration of greenhouse gases in the atmosphere may make it more likely for heavy rain to occur (Easterling et al. 2000, Groisman et al. 2005). This is supported by many studies and real-world evidence from observations or model predictions. Increasing concentrations of greenhouse gases are blamed for the shift in the frequency of severe rainfall (Meehl & Tebaldi 2004).

Regional land-use and land-cover changes (LULC) have been observed to have an impact on mesoscale convection, as noted by (Pielke et al. 2011) and (Niyogi et al. 2017). The frequency of floods has exhibited a notable upward trend during the past three decades, as documented by (Najibi & Devineni 2018). The susceptibility of different regions within the country to flooding is attributed to the unanticipated precipitation patterns resulting from the geographical and hydrological characteristics of the subcontinent. The primary factors contributing to floods, which frequently lead to the loss of human lives and property, include heavy precipitation, obstruction in river outflow and associated canal systems, uncontrolled urban development, and alterations in land use and land cover. The adverse impacts of floods, resulting from the overflow of water from various sources such as riverine flooding, runoff, in-situ rainfall, and groundwater status, can

be attributed to factors such as exposure, lack of resilience, and inadequate early warning systems. These negative effects encompass a wide range of areas, including infrastructure, human health, economic activity, and the environment (Beevers et al. 2012). According to (Mohapatra et al. 2021), there has been an improvement in the precision of predicting extreme precipitation within a short- to medium-term timeframe of up to five days. Nevertheless, the current level of proficiency in predicting and alerting to heavy precipitation is inadequate for mitigating the risks associated with potential casualties and property damage. To safeguard both human lives and economic stability, it is imperative to expand the scope of weather forecasting and warning systems beyond solitary predictions of severe weather events. This entails including impact-based forecasting systems, which utilize impact modeling techniques, and subsequently integrating impact estimation systems that employ impact-based modeling. This comprehensive approach is crucial for facilitating appropriate response actions.

According to reports, the flooding in North Bihar affected a significant proportion of the population, specifically 76%. Each year, a significant number of individuals, along with their domesticated animals, become displaced as a result of the catastrophic floods occurring in the Indian state of Bihar. The catchment areas of the rivers that comprise the primary river systems in northern Bihar, namely the Gandak, the Bagmati/Adhwara, and the Kosi/Mahananda, are located within the mountainous region of Nepal. Originating in Nepal, these rivers traverse densely populated regions of

North Bihar, including Supaul, Araria, west Champaran, east Champaran, Sitamarhi, and other locations. The slope of these rivers exhibits a gradual decline, transitioning from a rate of 6 meters per kilometer to 6 centimeters per kilometer near the Gangetic floodplain. During the monsoon season's intense precipitation, the lower catchment areas of the river basin experience a significant influx of run-off. The occurrence of intense precipitation in the vicinity of the Himalayan foothills, particularly near Nepal and other geographical regions, resulted in a sudden and significant rise in water levels, commonly catalyzing the onset of flooding events. Hence, the considerable inundation observed in these river systems can be attributed to the interplay between precipitation in the catchment areas and precipitation in the higher tributary regions. Hence, the comprehensive inundation of settlements situated on either side of the embankment of these rivers is a multifaceted interaction between the water level at a specific moment in a specific river section, the actual precipitation in the associated catchments, and the precipitation in the downstream catchment area. The understanding of both the individual and combined effects of these flooding mechanisms is often limited, resulting in either an underestimation or overestimation of the consequences of such an event, depending on the information source.

Meteorological systems that range in scale from the synoptic to the local scale have an impact on the occurrence of flooding (Reddy et al. 2008, Pandit 2009, Ranalkar et al. 2016, Kumar et al. 2021, Prasad et al. 2021). These systems contribute to the process of flooding by facilitating the transfer

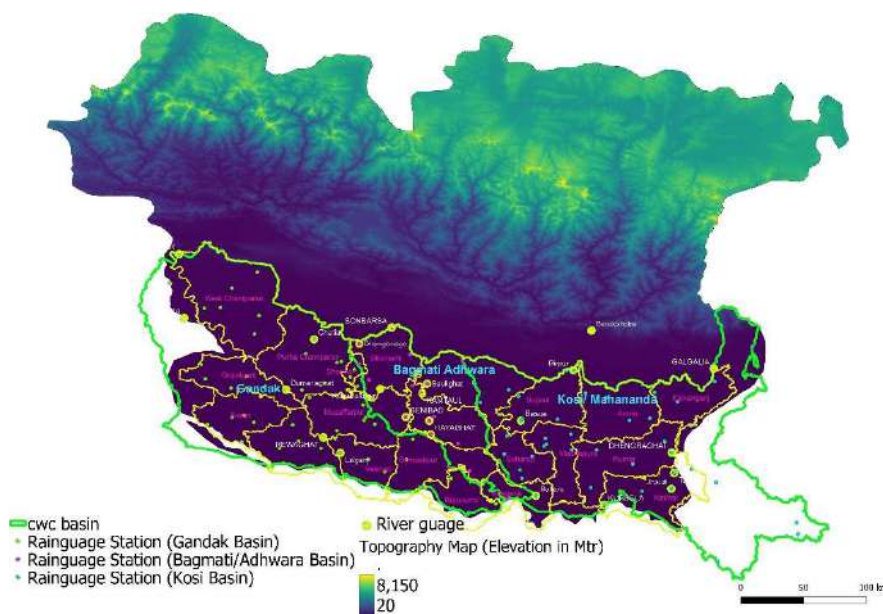


Fig. 1: The topographic map of the district of North Bihar, where the orography makes the location vulnerable to flooding.

of rainfall to river systems through numerous tributaries. This process occurs across a wide geographical area characterized by intricate orography, as illustrated in Fig. 1 The inundation of the Ganga River's catchment area, predominantly located in the northern region of Bihar, resulted in widespread flooding across the state. This occurrence was primarily attributed to the excessive precipitation experienced during the summer monsoon season, leading to the river's water exceeding its normal capacity and inundating floodplains and canals. The objective assessment conducted by (Shankar et al. 2022) examines the cascading impacts of substantial river releases and the accompanying high rainfall in North Bihar, India, which has led to recurrent flooding incidents. There isn't a lot of written material that fully talks about the dynamic vulnerability assessment of the cascading effects of in situ rainfall and how it affects river levels, as well as the right order of events over time. The objective of this study is to address the existing knowledge gap by implementing the techniques utilized by operational forecasters and disaster managers to do precise risk and vulnerability evaluations. This would consequently diminish the probability of both excessive and insufficient warnings.

In the realm of natural hazards, the most often employed vulnerability assessment approaches encompass historically derived impact data, evaluation indicator systems, hazard loss curves, and machine learning techniques. The presence of localized historical hazard data for every research site is crucial for the efficacy of the historical hazard-oriented approach. Although this methodology proves highly effective in facilitating cross-regional comparisons, its predominant use lies across expansive study domains, rendering the evaluation of specific phenomena challenging. Nevertheless, (Goyal et al. 2021) highlighted the fact that the assessment indicator system's methodology is highly subjective, primarily as a result of the arbitrary nature of weight computation. The use of expert scoring is a common method for assigning weight, as (Moghadas et al. 2019) and (Xu et al. 2023) demonstrate. However, it is important to note that this method is inherently subjective and has the potential for substantial errors in the ultimate evaluation outcomes. The use of a hazard damage curve, alternatively referred to as a vulnerability curve, facilitates the evaluation of the correlation between the magnitude of a cause and the resultant impact incurred by the entities that are most susceptible to its impact. The present methodology can assess vulnerability outcomes for a given geographical area through the measurement of the extent of harm incurred by distinct characteristics. The susceptibility of social and economic structures is an often-discussed subject when examining the impacts of catastrophic occurrences. To evaluate the susceptibility to disasters, scholars have conventionally placed significant

reliance on the direct use of machine learning methodologies. While the use of extensive data sets for training purposes can lead to precise vulnerability forecasts, the application of vulnerability mapping specifically for flood assessments remains unexplored and is considered a nascent topic.

This research provided a comparative analysis of several multiclassification methods, including Decision Tree (DT), Naive Bayes, Support Vector Machine (SVM), and K-Nearest Neighbour (KNN), in the context of dynamic impact-based forecasting utilizing machine learning techniques. This paper presents an analysis of the impacts resulting from rainfall and associated systems, utilizing the most up-to-date historical data sets of impacts specifically about the districts of north Bihar. This research article discusses the investigation of the impacts in three districts, specifically West Champaran, Darbhanga, and Vaishali. This work aims to address a research gap in the quantitative analysis of dynamic impact-based forecasting and its corresponding vulnerability assessment. The article's organizational structure is outlined as follows: the discussion of the datasets and their corresponding research areas is presented in Section 2. Following this, Section 3 explains the suggested strategy, and Section 4 presents the findings. Sections 5 and 6 then provide a thorough analysis and conclusion, respectively.

## STUDY AREAS AND DATASET

### Study Areas

The scope of this study is the prediction of dynamic impacts and the assessment of dynamic vulnerability related to rainfall and accompanying floods in three selected districts of North Bihar, namely West Champaran, Darbhanga, and Vaishali, as depicted in Fig. 2 The districts chosen for this study were based on a combination of different geographical settings and various causative factors for the impacts of floods. West Champaran, the largest district, was included due to its significant size and influence in the region and its proximity to the central region of Nepal. Additionally, the topography of the Himalayan mountain range has a significant impact on the rainfall patterns in this region. The second district, Vaishali, exemplifies the characteristics of flat lands located at a distance from the Himalayan foothills. The selection of the third district, Darbhanga, is based on its geographical location within the catchment areas of the Bagmati and Adhawara rivers (see Fig. 2). The geographical extent of the region under consideration encompasses the longitudes ranging from 84° E to 88.5° E, together with the latitudes spanning from 25° N to 27.6° N. The Upper Ganga basin has a multitude of rivers that traverse the northern region of Bihar. The Gandak River basin spans an area of

58,800 square kilometers, while the Bagmati/Adhawara River covers 18,845 square kilometers. Additionally, the Kosi/Mahananda river basin extends over an area of 95,552 square kilometers (see Fig. 2). The governments of Bihar (India) and Nepal have implemented several remedial steps to establish regular monitoring systems for floods and safeguard the low-lying regions of North Bihar (Sinha et al. 2008). Subtropical monsoons have a significant impact on the state of Bihar in India. The hydrological regime of this particular state is significantly impacted by its climate, thereby influencing a diverse range of geographical features. Approximately 84.8% of the state's yearly precipitation is derived from the monsoons, a meteorological phenomenon resulting from the interaction between easterly and westerly monsoonal winds, owing to the state's particular geographical positioning. The economic development of the local area is contingent upon the sectors of agriculture, aquaculture, horticulture, and tourism, all of which are susceptible to fluctuations in climatic conditions. Consequently, the effective control of floods in the rivers is of paramount importance.

## Dataset

The details of the datasets utilized for the creation of the dynamic impact-based rainfall forecasting system are presented in Table 1.

Therefore, the input characteristics are obtained from datasets containing information on river levels, average aerial precipitation, and district rainfall. The corresponding impact datasets are also collected, and the level of impacts is measured using the methods outlined in Fig. 3 and 4. The dataset comprised 70% of the total data, which was used for training the models. The remaining 30% of the dataset was utilized for evaluating the performance of the trained models. The time steps taken throughout the training process were also recorded. The impact datasets before quantification are displayed in Table 2.

## MATERIALS AND METHODS

### AI/ML-Based Impact Modeling

This approach involves the development of a model that

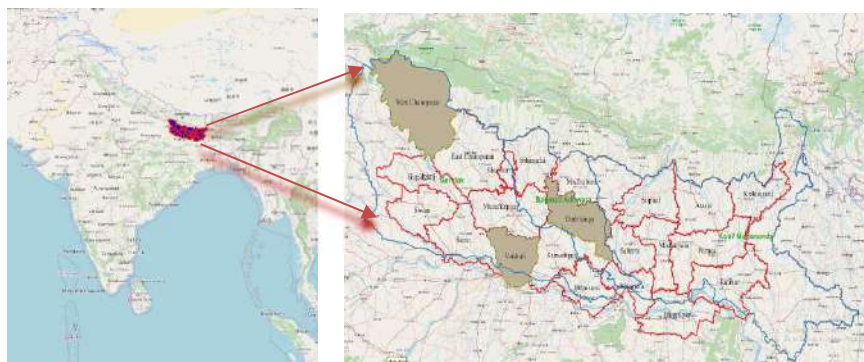


Fig. 2: Map of North Bihar (Districts, Catchments, Water Body) and the Sample Districts (West Cahmparan, Darbhanga, and Vaishali).

Table 1: The details of the datasets used in the dynamic impact-based rainfall prediction system.

Type of the Datasets	Name	Period	Unit	Source
River levels	River gauge of associated districts	June to October(2020-2022)	In metre	Central Water Commission, Govt. of India.
Rainfall	Point Rainfall		In mm	India Meteorological Department, Govt. of India
Overall Aerial Precipitation of the Catchment	Interpolated Rainfall( Storm Analysis)		In mm	Flood Meteorological Office, IMD, Govt. of India
Associated impacts datasets	Loss of Life( population)		quantification	Disaster Management Department, Govt. of Bihar, India
	Evacuation of population		quantification	
	Crop damages		quantification	
	Dwelling Unit damages		quantification	

Table 2: Sample of impact Dataset prepared by the executive agency and Compiled by the Disaster Management Department, Govt. of Bihar.

Date	Name of District	No. of Blocks	Panchayats		Village	Persons		Animals	Affected area (lac ha)	Estd crop damage (Rs lac)	Houses damaged					Total	No. of Damage Cattle Shade	Public property damaged (Rs lac)	Lives lost		Population evacuated	Population	No. of villages surrounded by water	Population on roads/rail tracks/roofops etc.		
			Fully	Partly		lac	lac				Fully	Partly	Huts	Human	Animal											
15-Aug-21	Vaishali	7	20	19	65	1.9	0.0	0.2	0	0	0	0	0	0	0	0	0	0	0	0	0	0	0	608	608	65
31-Aug-21		9	21	49	152	3.0	0.0	0.2	0	3	7	3	7	11	31	13	10.5	4	0	830	0	152				
01-Sep-21		10	21	61	176	3.4	0.0	0.2	0	3	7	3	7	11	31	13	10.5	4	0	830	0	176				
15-Sep-21		16	200	90	366	4.3	0.1	0.6	8286	0	0	0	0	0	0	0	0	6	5	830	0	366				
30-Sep-21		16	203	91	372	4.6	0.1	0.6	8286	0	0	0	0	0	0	0	0	6	5	830	0	372				
01-Oct-21		16	203	91	372	4.6	0.1	0.6	8286	0	0	0	0	0	0	0	0	6	5	830	0	372				
15-Oct-21		16	204	90	398	5.0	0.1	0.6	8286	0	0	0	0	0	0	0	0	16	10	830	0	392				

integrates impact magnitude( quantified) or vulnerability, exposure data sets, i.e., the causative factors of the floods (both in-situ and ex-situ), and the current states of the districts in terms of timeframe. Fig. 3 shows the four levels of impact quantification based on the combined impacts of the factors that caused the floods. These levels are green, yellow, orange, and red. The historical impact data is confirmed based on the flow chart outlined in Fig. 5. In cases of severe weather, the causative factor, which is based on its ability to have

an impact, is largely constant (the five factors outlined in Fig. 4). Conversely, the vulnerability of the affected population is contingent upon the extent of their exposure. Graded impact warning systems play a crucial role in the management of population vulnerability and exposure by providing a means to estimate the amount of impact. The causative factor, which is based on the potential for impact, is relatively constant in cases of severe weather events. Conversely, the vulnerability of the affected population is

contingent upon the degree of exposure. The implementation of impact-graded warning systems plays a crucial role in effectively managing and mitigating people’s exposure to various causative factors. Therefore, comprehending the detrimental effects of various meteorological phenomena is crucial for effectively mitigating natural disasters like floods. Based on the matrix presented in Fig. 3, the quantification of the graded impacts (0-green, 1-yellow, 2-orange, and 3-red)

at four levels was carried out. by following the standard operating procedure of the India Meteorological Department, India (IMD, Ministry of Earth Sciences 2021).

The current work uses machine learning techniques to create a decision tree model whose goal is to figure out the best level of graded warning issue when there is heavy rain and the impact systems that go with it. The local administrative body has used the precise graded warning to

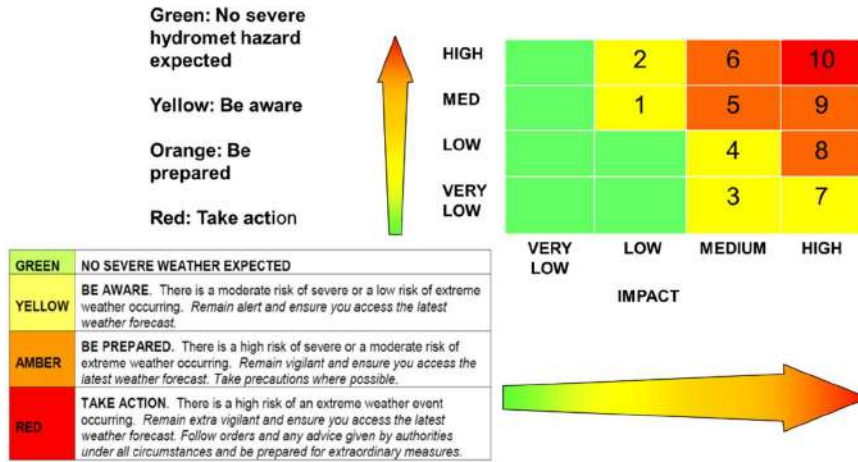


Fig. 3: Level of impacts and associated matrix (quantification of the graded impacts: 0-green, 1-yellow, 2-orange, and 3-red).

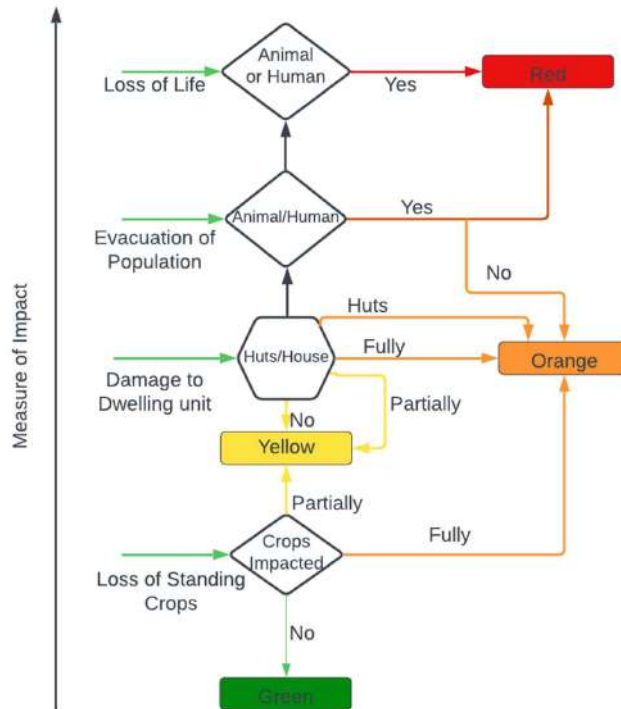


Fig. 4: Objective criteria (methodology) used for the quantification of the graded warning system (0-green, 1-yellow, 2-orange, and 3-red) for the studied areas.



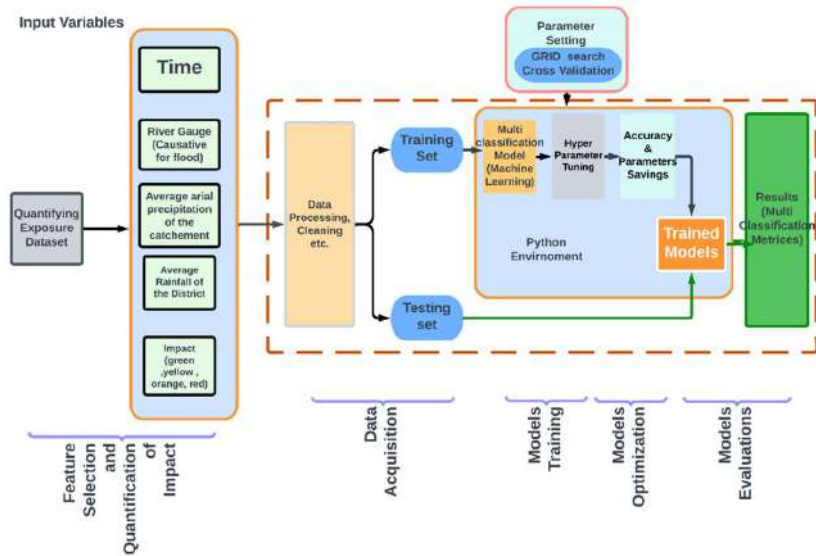


Fig. 5: Process block diagram of dynamic impact-based prediction system.

evaluate the extent of damage and potential threats resulting from the occurrence of heavy rainfall. The levels of impacts of flood assessment include the examination of existing crops, the assessment of damage to residential structures, the appraisal of population evacuation measures, and the analysis of casualties (presented in Fig. 4).

The proposed model exhibits considerable potential for utilization and possesses substantial value in terms of its practicality. Fig. 5: is a graph that shows the steps that were used to make the machine learning-based multiclassification algorithm that was used in the dynamic impact-based heavy rainfall prediction system. The steps included finding historical impact data, quantifying the exposure data, training the multiclassification algorithms, etc.

### Multi-Classification Algorithm(ML)

Machine learning, a branch within the broader domain of artificial intelligence, has become a focal point for addressing the challenges of digitalization, attracting significant attention within the digital realm. In this study, the multiclassification of the assessment and prediction of the impacts of heavy rainfall was conducted using four machine learning models: Support Vector Machines (SVM), Decision Trees (DT), k-Nearest Neighbors (KNN), and Naive Bayes (NB).

### Support Vector Machine

Support Vector Machines (SVM) are capable of handling difficulties including classification as well as regression. The decision boundary in this approach is a hyperplane, which must be determined. A decision plane is necessary to divide a set of objects into their respective classes when

there are several classes represented. Separating items into their respective classes may or may not need complex mathematical functions known as kernels if the objects are not linearly separable. SVM attempts to correctly classify objects based on examples in the training data set. The benefits of support vector machines (SVM) include: They work well with semi-structured and structured data, and they can even deal with complex functions if the right kernel function is generated. Overfitting is reduced by SVM's reliance on generalization.

This method works well with high-dimensional data and scales well. Local minima are not a problem for it. The longer it takes to train an SVM, the less well it performs with more data. An adequate kernel function will be hard to locate. When the dataset is noisy, SVM performs poorly. If there are a lot of features and observations, then SVM is worth a go (Ray 2019).

### Decision Tree

Decision trees are supervised machine learning that can be used to resolve classification and regression issues by continually separating data based on certain parameters. The leaves are where the decisions are made, whereas the nodes are where the data is divided up. In multiclassification decision variable is graded. The decision in the leaves and the data split in the nodes. The benefits of using a Decision Tree include its adaptability to both regression and classification problems, its straightforward interpretation, its ability to handle both quantitative and qualitative values, its capacity to fill missing values in attributes with the most likely value, and its high-performance thanks to the efficiency of its tree-

traversal algorithm. Over-fitting is an issue that can arise with Decision trees, but it can be remedied with the help of the ensemble modeling approach that Random Forest employs. It can be unstable, it's not always easy to regulate the tree's size, it's vulnerable to sampling error, and it only provides a locally optimal solution, not the best possible one.

### Naïve Bayes

This algorithm relies on conditional probability and is therefore easy to implement. In this approach, training data is used to define a probability table that serves as the model. The "probability table" uses feature values to anticipate fresh observations by looking up class probabilities. Predicting a new observation requires consulting a "probability table" whose columns include the feature values and whose rows contain the class probabilities. The term "naive" refers to the underlying premise of conditional independence. Taking into account all input features as though they were unrelated to one another is unrealistic in practice.

The benefits of Naive Bayes (NB) include straightforward implementation; high performance; use of a smaller sample of training data; linear scalability in terms of predictors and data points; the ability to deal with both continuous and discrete data; the capability to deal with multi-class classification problems; and the ability to make probabilistic predictions. Both continuous and discrete data types are supported. It has a low sensitivity to non-essential details. Properly trained and optimized models typically outperform NB models because NB models are overly simplistic. It is challenging to directly apply Naive Bayes if one of the features must be a "continuous variable," such as time. While "buckets" can be created for "continuous variables," they are not always accurate.

Because there is no genuine online form of Naive Bayes, all data must be retained for retraining the model. For a large enough number of classes, say above 100,000, it will not scale. It requires more memory at runtime for prediction than support vector machines or standard logistic regression. High-end central processing unit (CPU), especially for complex models with lots of variables.

### K Nearest Neighbour Algorithm (KNN)

It is an example of a classification method. The algorithm (KNN) uses a database partitioned into classes into which it must place a single sample data point and solve the ensuing classification problem. It is said that KNN is non-parametric since it does not make any assumptions about the underlying data distribution. It's a straightforward method with easy implementation. It's an adaptable system that works well with multi-modal classification. Several

category tags appear in the record set. The rate of error is no more than twice the Bayes error rate. In some cases, this is the most effective technique.

### Multi Classification Performances Metrics

Classification is a commonly used technique in data analysis that involves the categorization of data into more than two categories. While the traditional approach involves the separation of data into two groups, known as binary classification, it is also possible to extend this method to encompass more than two groups, which is known as multi-class classification. From an algorithmic perspective, (Mohandes et al. 2018) discuss how the prediction process is dependent on advanced mathematical techniques. These methodologies employ the provided input data (represented by the  $x$  variables) to provide precise predictions for the outcome variable  $y$ . Given that  $y$  is a variable that can take on values from 1 to  $K$ , where each value represents a unique class, it is possible to see both the response variable  $y$  and the prediction ( $\hat{y}$ ) as discrete random variables in the context of multi-class classification. The algorithm calculates the probability that a given unit is a member of a particular class and subsequently utilizes a classification rule to allocate each unit to one of these classes. In general, the rule is characterized by its simplicity: an object is allocated to the category that exhibits the greatest probability. In the context of employing a classification model, it is possible to make estimations regarding the probability of membership for each potential unit inside a given class. In the context of a binary classification task, it is customary to use a threshold value to determine the appropriate class prediction for each instance while taking the model's probability output into account (Grandini et al. 2020).

**Confusion Matrix:** The confusion matrix is a cross table that keeps track of the frequency with which the true/actual classification differs from the expected classification (Fig. 6).

The details of the performance metrics used in this research article are presented in Table 3.

## RESULTS AND DISCUSSION

This section focuses on assessing the efficacy of the quantification of causative factors contributing to floods in North Bihar. Additionally, it examines the effectiveness of a proposed multi-classification algorithm in categorizing the impact of floods in the districts of West Champaran, Darbhanga, and Vaishali in the studied areas. The selection of these districts was made by considering the geographical settings and the diverse factors associated with floods in these areas. The implementation code was developed using Python 3.10. A machine learning model for simple

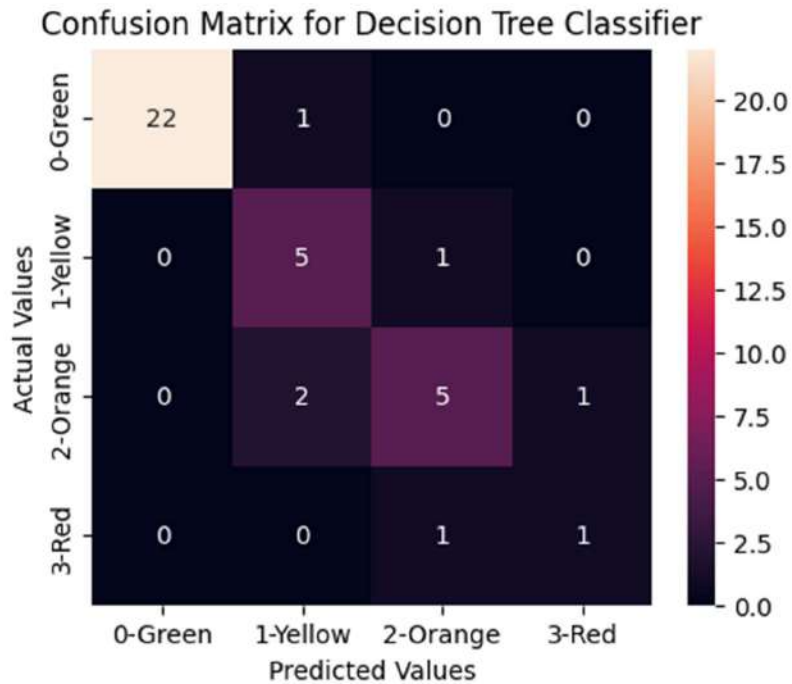


Fig. 6: Schematic of Confusion Matrix on the test datasets.

Table 3: Details of the performance matrices used in the assessment of multiclassification ML approaches.

Performance Metrics	Remarks
$Balanced Accuracy = \frac{\frac{TP}{Total_{row1}} + \frac{TN}{Total_{row2}}}{2} \quad (1)$	It is the average value of recall of each class. How likely is it that an individual of that class will be classified correctly? The recall value for each class response. Therefore, balanced accuracy provides a class-general mean measure of this idea.
$Macro F1 - Score = 2 * \left( \frac{Macro Average Precision * macro Average Recall}{macro Average Precision^{-1} + Macro Average Recall^{-1}} \right) \quad (2)$	Since the numerators of Macro Average Precision and Macro Average Recall are composed of values in the range [0, 1], macro-average methods often compute an overall mean of several metrics. There is no correlation between class size and the denominator because classes of varying sizes are counted the same. This means that the influence of the largest classes is just as significant as that of the smallest. High Macro-F1 values suggest that the method performs well across all classes, while low Macro-F1 values show classes that are poorly predicted by the system.
$Micro-Average F1 Score = \frac{\sum_{k=1}^K TP_k}{Grand Total} \quad (3)$	Macro F1-Score is an average measurement of the classes' average precision and average recall. This metric is calculated at the class level so that each class receives equal weight. Small classes are equivalent to large ones, and algorithm performance regardless of class size is of equal importance.
$Cross Entropy H(p(y_i), p(\hat{y}_i)) = -\sum_{k=1}^K \sum_{i=1}^n p(Y = k   X_i) \log p(\hat{Y}_i = k   X_i) \quad (4)$	Cross-entropy values of the individual units to derive a measure of agreement for the entire dataset. Cross-entropy exploits only the value of $p(\hat{Y}_i = k   X_i)$ for the k value representing the true class.

multiclassification was implemented on a laptop running the Windows 11 operating system. The laptop is equipped with an Intel (R) Core (TM) i5-1035G1 processor working at a frequency of 1.00 GHz and has 8 GB of memory. The

specifics regarding the datasets are outlined in Section 2. The process of the proposed methodologies is outlined in subsection 3.1, and the subsequent optimal hyperparameters are presented in Table 4.

## Quantification of Causative Factors of The Impact of Floods

The studied areas, i.e., districts of North Bihar, lie in the basins of the Gandak, Bagmati/Adhawara, and Kosi/Mahananda groups of rivers, which are prone to flooding. The catchments of the Gandak, Bagmati/Adhawara, and Koshi/Mahananda rivers are located in the mountainous central and eastern regions of Nepal (presented in Fig. 1). Consequently, any amount of rainfall in adjoining Nepal, even if it is of moderate quantity, leads to an increase in the water level of these river systems. Depending on the varying capacity of the rivers, floods occur in the downstream areas. The river system mentioned in this study causes flooding in the lowlands of northern Bihar, India, when it traverses the border from Nepal, where the terrain is steeper (Shankar et al. 2022). The steep topography of the region leads to sudden or flash floods in the downstream districts of North Bihar during periods of excessive rainfall in neighboring Nepal. Therefore, it is seen that floods can occur in the lowlands of Bihar even in the absence of significant in-situ rainfall. To establish a comprehensive warning system for heavy rainfall-induced floods, our objective is to uncover the underlying elements that contribute to these impacts. The assessment of impacts has been derived from historical data about several factors, including the loss of human lives, displacement of communities, destruction of

residential structures, and losses to crops. This technique is derived from the discussion in Fig. 4, which focuses on the quantification of the graded warning system. The objective of this approach is to verify that the graded warning aligns with the probability of potential impacts. The inputs for this study include various causative factors, such as the river gauges at different locations, which may be influenced by rainfall in neighboring regions of Nepal. Additionally, the average aerial precipitation response for water runoff and district rainfall are also considered. As shown in Fig. 5, these inputs come with the corresponding time data. The details of these elements have been assessed for each district. This study presents an assessment of three districts from the perspective of rational representation. A comprehensive examination of three districts, namely West Champaran, Vaishali, and Darbhanga, is presented in the following subsection. West Champaran is situated in the higher catchment area of the river, while Vaishali encompasses both the lower catchment area of the river and the region affected by the Ganga River. Lastly, Darbhanga is a district prone to flooding. This section focuses on the evaluation of the quantification of causative factors contributing to floods in North Bihar. It also checks how well a suggested multi-classification algorithm sorts the graded impact-based flood warning system or the dynamic impact-based vulnerability assessment works in the districts of Darbhanga, Vaishali, and West Champaran. The selection of these districts took into account their geographical settings

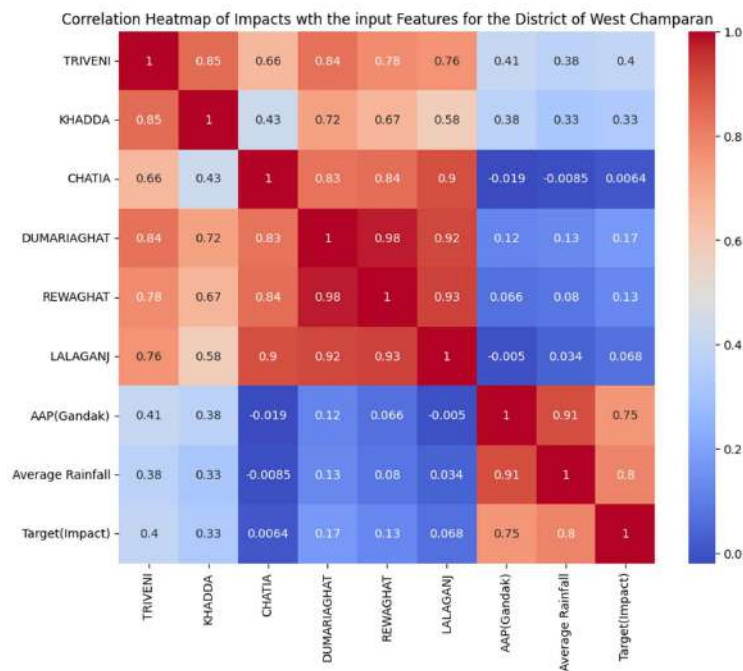


Fig. 7: The correlation matrix of the impacts of heavy rainfall with its causative feature in the districts of West Champaran, Bihar, India.

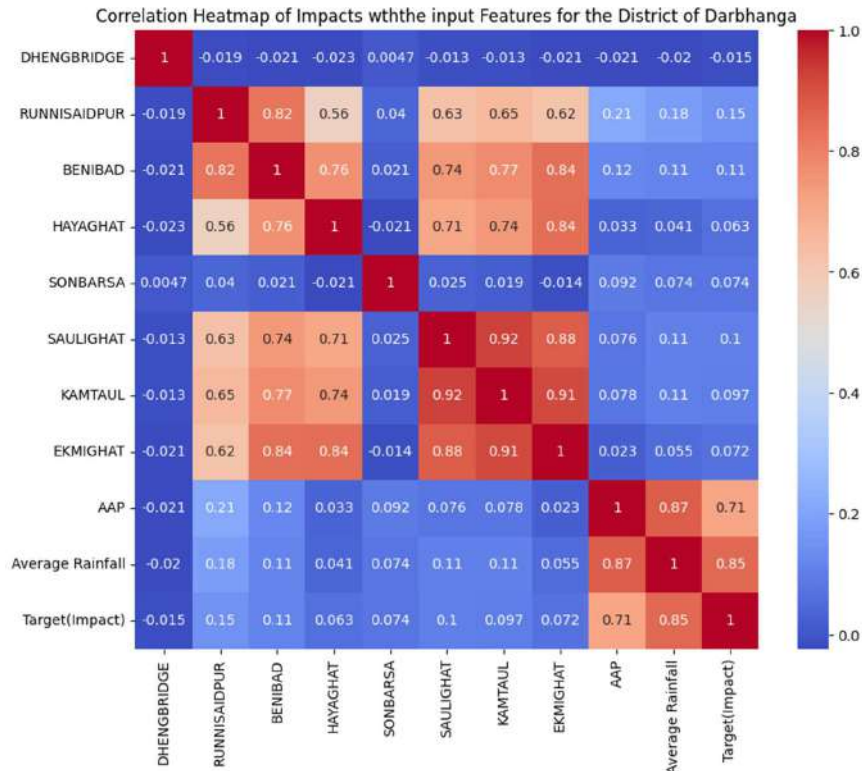


Fig. 8: The correlation matrix of the impacts of heavy rainfall with its causative feature in the districts of Darbhanga, Bihar, India.

and the diverse factors associated with floods in these areas.

**West Champaran**

The districts of West Champaran hold the distinction of being the largest in Bihar in terms of their geographical expanse. It is noteworthy that flash floods frequently affect this area. The primary cause of these floods may be attributed to the substantial precipitation in the Soemshwar Doon region. According to (Jha & Gundimeda 2019), the district experiences floods very frequently, with a frequency of 0.8 to 1. The districts exhibit a north-to-south slope, whereas the canal runs in an east-to-west direction. This configuration leads to congestion in the canal’s capacity at peak events. Nevertheless, due to the topography, the floodwaters dissipated swiftly. Fig. 7 displays the correlation matrix between the input attributes and the effects. The correlation coefficients of 0.8 for rainfall and 0.75 for AAP clearly show a strong correlation between heavy rainfall and its effects. This relationship is further supported by the data collected from the river gauges located at Triveni and Khadda, which are situated close to the border with Nepal.

**Darbhanga**

According to (Jha & Gundimeda 2019), the Darbhanga districts are classified as having a high frequency of floods, with a range of 0.6 to 0.8. The river group Bagmati/Adhawra is responsible for the floods in these two districts. Blocks such as Kusheshwar Asthan, Hayafghat, Jale, and others are susceptible to flooding. The duration of the flood is characterized as mild since the water recedes within a timeframe of around one to two weeks. The study conducted by (Kumar et al. 2016) examines the progress made in the regions affected by the significant flooding incidents. Fig. 8: displays the correlation matrix, illustrating the relationships between the impacts of the districts and the input attributes. The data indicates a strong correlation between severe rainfall impacts and the average rainfall (0.85) in the districts, as well as the average annual precipitation (AAP) (0.75) in the adjacent catchments, in conjunction with the river gauges at Benibad.

**Vaishali**

Flood-prone areas are often located in the downstream regions of the Ganga River, and the Vaishali district is categorized

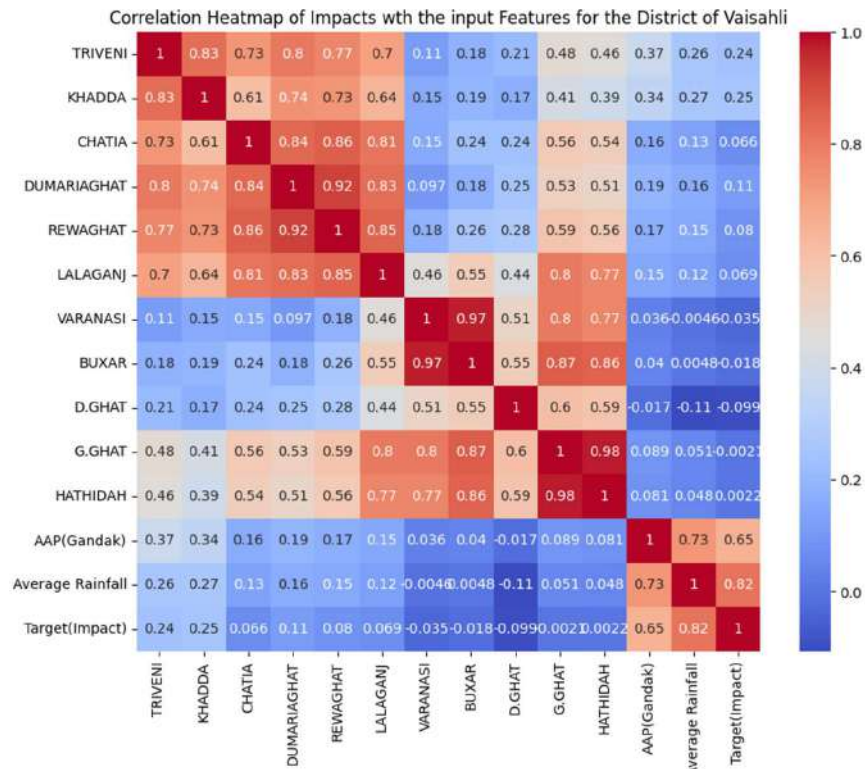


Fig. 9: The correlation matrix of the impacts of heavy rainfall with its causative feature in the districts of Vaishali, Bihar, India.

as one such area where flooding is mostly attributed to the combined influence of two river systems, namely the Ganga and the Gandak. Typically, amid the monsoon season, the lower regions known as Diyara have regular occurrences of flooding. According to (Jha & Gundimeda 2019), the district is within the range of medium flood frequency, namely between 0.4 and 0.6. The drainage process of floods in this district is often characterized by a prolonged duration. Fig. 9: displays the correlation matrix, illustrating the relationships between the districts' impacts and the input attributes. The data indicates a strong correlation between severe rainfall impacts and the average rainfall (0.82) in the districts, as well as the average annual precipitation (AAP) (0.65) in the connected catchments, in addition to the river gauges at Khadda (0.25) and Triveni (0.24).

### Assessment of the Proposed M/L Multi-classification Models

The performance indicators outlined in paragraph 3.3 were employed to assess the effectiveness of the proposed machine learning multi-classification models. The models were evaluated for four consecutive days: day 0, day 1, day 2, and day 3. The inputs used for each evaluation were

based on the characteristics of the corresponding day or the preceding days. The grid search methodology is employed to refine and optimize the selection of hyperparameters. Table 4 displays the ideal hyperparameters for the Decision Tree (DT), K-Nearest Neighbors (KNN), and Support Vector Machine (SVM) models that were trained in the districts of West Champaran, Darbhanga, and Vaishali. These districts are representative of the northern region of Bihar. The change of hyperparameters is deemed unnecessary for the Naïve Bayes multi-classification approach. The observed variation in the quantity of hyperparameterized parameters throughout the districts of northern Bihar can be ascribed to disparities in the number of input features and the heterogeneous attributes of floods.

The performance metrics from subsection 3.3 were used to rate the trained models. The results can be seen in Table 5 (Decision Tree and Support Vector Machine models) and Table 6 (KNN and Naïve Bays models).

To build an efficient early warning system and a thorough vulnerability assessment that considers the diverse causes of floods (Zhang et al. 2022), This methodology employs an innovative machine learning technique for multi-classification, which effectively combines diverse sources

Table 4: Best Hyperparameter of the Decision Tree, SVM, and KNN Multi classification algorithms for the proposed dynamic impact-based multi-classification algorithms for the districts of West Chamapran, Darbhanga, and Vaishali.

Algorithm/ Best Parameter	Decision Tree			SVM				KNN			
	max_ depth	min_ samples_ leaf	min_samples_ split	C	coef0	degree	gamma	kernel	n_ neighbors	p	weights
West Chamapran	3	2	2	0.1	-1	1	0.01	poly	3	1	distance
Darbhanga	3	1	5	10	-1	5	0.0001	poly	9	2	uniform
Vaishali	10	1	2	10	1	5	scale	poly	7	2	distance

Table 5: Presentation of performance metrics for the day (0–3) for DT and SVM.

Decision Tree Multi Classifier												
District(Days)/ Performance Parameter	West Champaran				Darbhanga				Vaishali			
	Day0	Day1	Day2	Day3	Day0	Day1	Day2	Day3	Day0	Day1	Day2	Day3
Balanced Accuracy	0.7287	0.7287	0.7287	0.7287	0.8068	0.8068	0.8068	0.7840	0.7174	0.6787	0.6816	0.6758
Binary Cross Entropy	2.1128	2.1128	2.1128	2.1128	0.0688	0.0688	0.0688	0.0741	3.656	3.9177	3.6566	4.1789
Macro F1 Score	0.71	0.71	0.71	0.71	0.80	0.80	0.80	0.77	0.58	0.56	0.57	0.54
Micro Weighted F1 Score	0.85	0.85	0.85	0.85	0.96	0.96	0.96	0.96	0.90	0.89	0.89	0.88
Support Vector Machine												
Balanced Accuracy	0.5729	0.5729	0.5729	0.5729	0.6717	0.6717	0.6717	0.6717	0.7412	0.7412	0.7412	0.5729
Binary Cross Entropy	0.3973	0.3782	0.3880	0.3847	0.5910	0.6063	0.6049	0.6067	0.2364	0.2522	0.2516	0.3847
Macro F1 Score	0.61	0.61	0.61	0.61	0.64	0.64	0.64	0.64	0.60	0.60	0.60	0.61
Micro Weighted F1 Score	0.74	0.74	0.74	0.74	0.94	0.94	0.94	0.94	0.91	0.91	0.91	0.74

Table 6: Presentation of performance metrics for the day (0–3) for KNN and Naïve Bays.

KNN												
District(Days)/ Performance Parameter	West Champaran				Darbhanga				Vaishali			
	Day0	Day1	Day2	Day3	Day0	Day1	Day2	Day3	Day0	Day1	Day2	Day3
Balanced Accuracy	0.6875	0.6875	0.6875	0.6875	0.6489	0.6489	0.6489	0.6489	0.8662	0.8662	0.8662	0.8662
Binary Cross Entropy	2.9199	2.9199	2.9199	2.9199	0.1380	0.1380	0.1380	0.1380	0.1662	0.1662	0.1662	0.1662
Macro F1 Score	0.65	0.65	0.65	0.65	0.63	0.63	0.63	0.63	0.87	0.87	0.87	0.87
Micro Weighted F1 Score	0.85	0.88	0.88	0.88	0.93	0.93	0.93	0.93	0.94	0.94	0.94	0.94
Naïve Bays Classifier												
Balanced Accuracy	0.8849	0.8849	0.8849	0.8849	0.7030	0.7030	0.7030	0.7030	0.5478	0.5478	0.5478	0.5478
Binary Cross Entropy	0.4672	0.4672	0.4672	0.4672	0.7065	0.7065	0.7065	0.7065	0.334	0.334	0.334	0.334
Macro F1 Score	0.84	0.84	0.84	0.84	0.60	0.60	0.60	0.60	0.55	0.55	0.55	0.55
Micro Weighted F1 Score	0.90	0.90	0.90	0.90	0.84	0.84	0.84	0.84	0.84	0.84	0.84	0.84

of both heterogeneous and homogeneous information. The implementation of this improvement resulted in the enhancement of the current early warning system while also enabling the retention of a greater quantity of information during the fusion process. The individual who bears the responsibility for decision-making holds the capacity to

evaluate the sources and extent of consequences, which might serve as important considerations for those tasked with disaster management. The Naïve Bayes algorithms exhibit noteworthy performance in the districts of West Chamapran, achieving a balanced accuracy of 0.88, which closely approaches the ideal value of 1. Furthermore, it can be

observed that the decision tree multi-classification algorithms exhibit a high level of effectiveness, ranking as the second most efficient models. One significant advantage of utilizing balanced accuracy is its fair assessment of all classes, which is especially important when dealing with imbalanced datasets that have significant differences in sample numbers between classes. Furthermore, the macro F1 score demonstrates a significant degree of efficacy when employed in conjunction with the naive Bayes multi-classifier. The ability to punish the model severely when it shows excessive confidence in an incorrect class is one of the benefits of using binary cross entropy. As a result, this contributes to improving the accuracy of the model. In the context of the Naive Bayes classifier, when the value tends towards 1, it signifies a desirable level of performance. In the districts of West Champaran, it is evident that the algorithms operate in the following sequence: The performance of Naive Bayes is seen to be the greatest, followed by Decision Tree, K-Nearest Neighbors (KNN), and Support Vector Machine (SVM). In the context of the Darbhanga districts, the performance of multiclassification algorithms may be rated as follows: The performance of the Decision Tree surpasses that of the Support Vector Machine (SVM), which in turn surpasses that of K-Nearest Neighbors (KNN), while Naive Bayes exhibits the least effective performance. In the Vaishali areas, where the possible ramifications of floods may be ascribed to the combined impacts of the Gandak and Ganga river systems, the algorithms can be hierarchically ordered based on their efficacy as follows: The K-Nearest Neighbors (KNN) algorithm has the highest level of effectiveness, followed by Support Vector Machines (SVM), Decision Trees (DT), and Naive Bayes (NB). Consequently, a thorough assessment was undertaken to evaluate the performance of several machine learning algorithms for multi-classification, to examine their effectiveness concerning the proposed methodologies. The comprehensive assessment of available sources is crucial to effectively enable the actual application of models in the field. The present study investigates the possible use of big data technologies in the evaluation of flood risk, as stated in the work of (Monrat et al. 2019). Furthermore, this study examines the practical use of graded impact-based warning systems in the context of severe rainfall events. The study also examines the issues that require attention and the tactics that must be implemented to effectively harness the capabilities of these technologies. The performance metrics outlined in paragraph 3.3 were employed to assess the effectiveness of the proposed machine learning multiclassification models. The models underwent evaluation for four consecutive days: day 0, day 1, day 2, and day 3. The evaluation process involved using input characteristics from the same day for day 0, while for subsequent days (day 1, day 2, and day 3),

inputs from prior days were used. The grid search method is employed to refine the optimal hyperparameterization. Table 4 displays the best hyperparameters for the Decision Tree (DT), K-Nearest Neighbor (KNN), and Support Vector Machine (SVM) models that were trained using data from the districts of West Champaran, Darbhanga, and Vaishali. There is no need for hyperparameter changes in the Naive Bayes multiclassification approach. The observed heterogeneity in the quantity of hyperparametrized parameters throughout the districts of northern Bihar may be ascribed to the disparities in the number of input features and the distinct attributes of floods in these regions.

Different multiclassification methods behave in different ways, especially when they are given datasets that aren't balanced and have a big difference in the number of cases in each class. The aforementioned disparity has the potential to result in models that exhibit bias and demonstrate inferior performance when it comes to underrepresented classes. To solve these challenges, a range of strategies are utilized. In this article, the Synthetic Minority Oversampling Technique (SMOTE) is employed to handle unbalanced datasets by producing synthetic samples for the minority class. The generation of synthetic examples is achieved by the process of interpolating between pre-existing cases, effectively equalizing the distribution of classes. Also, stratified cross-validation is employed to guarantee that every fold inside the cross-validation procedure maintains an equitable distribution of all classes. This methodology facilitates the assessment of the model's efficacy by ensuring that each class is equally represented. In our forthcoming stages, we intend to augment the efficacy of our models by capitalizing on the benefits of sophisticated methodologies, such as Easy-Ensemble or Balanced Random Forest. The efficacy of the presented models is contingent upon the caliber of previous flood impact data and the fundamental causal elements. The success of multiclassification models relies heavily on the presence of high-quality data. The incorporation of continuous input from real-time datasets is crucial to maintaining the real-time correctness of these models. Moreover, the precision and dependability of historical data play a crucial role in efficiently training the models. The outcomes derived from these models offer significant insights into the quantification of the economic implications associated with varying degrees of warning accuracy. This evaluation encompasses the estimation of possible cost savings that may arise as a consequence of less damage and improved procedures for disaster preparedness.

## CONCLUSION

The primary aim of this research is to improve our understanding of flood risk categorization and the impact



of individual or combined causative elements through the development of innovative ML approaches. The study sites were chosen from places located in northern Bihar, India, which are susceptible to frequent occurrences of flooding. The geography of the North Bihar region and its adjacent Tarai territories is characterized by a significant incline. Consequently, the development of an impact-based flood warning system in these regions necessitates consideration of the combined impacts of in-situ and runoff rainfall, as well as the overflow of rivers and associated canal systems. A novel machine learning approach has been devised to improve comprehension and communication regarding the diverse degrees of impacts of flood consequences arising from rainfall, average aerial precipitation in nearby catchment areas, and rises in river gauges due to rainfall in neighboring regions of Nepal. To accomplish this goal, we utilized a modeling methodology to evaluate the quantification of floods resulting from several causative factors. The utilization of multi-classification ML classifiers in tandem enhances the decision-making process by capitalizing on the collective proficiency of the machine learning algorithms. The tools that have been suggested aim to improve decision-making in the context of operational impact-based forecasting. Furthermore, this approach maximizes the likelihood of both over- and under-warnings. The ML models under consideration are evaluated in terms of their performance relative to the base models, to identify the optimal model that exhibits robustness in the presence of variations. The main objective of these proposed tools is to assist operational forecasters by generating a classification of flood impacts as a result. Hence, the executive line agency operates to the specific requirements of the situation, allocating resources as necessary to minimize the effects of flooding. This paper presents a conceptual framework for evaluating the dynamic consequences of intense precipitation, incorporating several additional contributing components. The suggested framework has the potential to be implemented in many geographical areas to improve flood management tactics. The presented model will be employed in further investigations to examine several facets of compound runoff and rainfall-induced flooding. While this study acknowledges the important influence of other contributing factors, such as land use and land cover, on impact-based flooding occurrences within the relevant period, it does not quantify their effects. Future research endeavors should prioritize the exploration of the integration of these components. However, the potential for intensified rainfall as a result of climate change might significantly amplify the likelihood of flooding in the area under study. Future evaluations employing this model aim to quantitatively evaluate the influence of altering climatic conditions on the susceptibility to flooding.

## ACKNOWLEDGMENTS

The authors are grateful to the Ministry of Earth Sciences, Govt. of India for implementing the Impact heavy rainfall warning system in the country.

## ABBREVIATIONS

This manuscript employs the following abbreviations:

AI/ML	Artificial Intelligence/Machine Learning
SVM	Support Vector Machine
DT	Decision Tree
KNN	k-Nearest Neighbour
NB	Naïve Bays
LU/LC	Land Use/Land Cover

## REFERENCES

- Abbas, S., Waseem, M., Yaseen, M., Latif, Y., Leta, M.K., Khan, T.H. and Muhammad, S., 2023. Spatial-temporal seasonal variability of extreme precipitation under warming climate in Pakistan. *Atmosphere (Basel)*, 14, 210. <https://doi.org/10.3390/atmos14020210>.
- Beevers, L., Douven, W., Lazuardi, H. and Verheij, H., 2012. Cumulative impacts of road developments in floodplains. *Transportation Research Part D: Transport and Environment*, 17, pp.398–404. <https://doi.org/10.1016/j.trd.2012.02.005>.
- Brunetti, M., Buffoni, L., Mangianti, F., Maugeri, M. and Nanni, T., 2004. Temperature, precipitation and extreme events during the last century in Italy. *Global and Planetary Change*, 40, pp.141–149. [https://doi.org/10.1016/S0921-8181\(03\)00104-8](https://doi.org/10.1016/S0921-8181(03)00104-8).
- De Luis, M., González-Hidalgo, J.C., Brunetti, M. and Longares, L.A., 2011. Precipitation concentration changes in Spain 1946-2005. *Natural Hazards and Earth System Sciences*, 11, pp.1259–1265. <https://doi.org/10.5194/nhess-11-1259-2011>.
- Easterling, D.R., Evans, J.L., Groisman, P.Y., Karl, T.R., Kunkel, K.E. and Ambenje, P., 2000. Observed variability and trends in extreme climate events: a brief review. *Bulletin of the American Meteorological Society*, 81(3), pp.417-426.
- Goswami, B.N., Venugopal, V., Sangupta, D., Madhusoodanan, M.S. and Xavier, P.K., 2006. Increasing trend of extreme rain events over India in a warming environment. *Science*, 314, pp.1442–1445. <https://doi.org/10.1126/science.1132027>.
- Goyal, D., Haritash, A.K. and Singh, S.K., 2021. A comprehensive review of groundwater vulnerability assessment using index-based, modelling and coupling methods. *Journal of Environmental Management*, 296, 113161. <https://doi.org/10.1016/j.jenvman.2021.113161>.
- Grandini, M., Bagli, E. and Visani, G., 2020. Metrics for multi-class classification: an overview. *arXiv preprint arXiv:2008.05756*.
- Groisman, P.Y., Knight, R.W., Easterling, D.R., Karl, T.R., Hegerl, G.C. and Razuvaev, V.N., 2005. Trends in intense precipitation in the climate record. *Journal of Climate*, 18, pp.1326–1350. <https://doi.org/10.1175/JCLI3339.1>.
- IMD, Ministry of Earth Sciences, 2021. Standard Operation Procedure - Weather Forecasting and Warning Services.
- Jha, R.K. and Gundimeda, H., 2019. An integrated assessment of vulnerability to floods using composite index – A district level analysis for Bihar, India. *International Journal of Disaster Risk Reduction*, 35, 101074. <https://doi.org/10.1016/j.ijdr.2019.101074>.

- Kumar, A., Sarthi, P.P., Kumari, A. and Sinha, A.K., 2021. Observed characteristics of rainfall indices and outgoing longwave radiation over the Gangetic Plain of India. *Pure and Applied Geophysics*, 178, pp.619–631. <https://doi.org/10.1007/s00024-021-02666-6>.
- Kumar, V., Yin, C.C.S., Kumar Singh, A., Yin, C.S. and Kumar, A., 2016. Impact of flood on rural population and strategies for mitigation: A case study of Darbhanga district, Bihar state, India. *Contemporary Rural Social Work Journal*, 8.
- Meehl, G.A. and Tebaldi, C., 2004. More intense, more frequent, and longer lasting heat waves in the 21st century. *Science*, 305, pp.994–998.
- Moghadas, M., Asadzadeh, A., Vafeidis, A., Fekete, A. and Kötter, T., 2019. A multi-criteria approach for assessing urban flood resilience in Tehran, Iran. *International Journal of Disaster Risk Reduction*, 35. <https://doi.org/10.1016/j.ijdr.2019.101069>.
- Mohandes, M., Deriche, M. and Aliyu, S.O., 2018. Classifiers Combination Techniques: A Comprehensive Review. *IEEE Access*, 6, pp.19626–19639. <https://doi.org/10.1109/ACCESS.2018.2813079>.
- Mohapatra, M., Kumar, N., Mishra, K. and Devi, S., 2021. Evaluation of heavy rainfall warnings of India National Weather Forecasting Service for monsoon season (2002–2018). *Journal of Earth System Science*, 130. <https://doi.org/10.1007/s12040-020-01549-z>.
- Monrat, A.A., Ul Islam, R., Hossain, M.S. and Andersson, K., 2019. A belief rule based flood risk assessment expert system using real time sensor data streaming. *Proceedings of the 43rd Annual IEEE Conference on Local Computer Networks, LCN Workshops 2018*, pp.38–45. <https://doi.org/10.1109/LCNW.2018.8628607>.
- Najibi, N. and Devineni, N., 2018. Recent trends in the frequency and duration of global floods. *Earth System Dynamics*, 9, pp.757–783. <https://doi.org/10.5194/esd-9-757-2018>.
- Niyogi, D., Lei, M., Kishtawal, C., Schmid, P. and Shepherd, M., 2017. Urbanization impacts on the summer heavy rainfall climatology over the eastern United States. *Earth Interactions*, 21, pp.1–17. <https://doi.org/10.1175/EI-D-15-0045.1>.
- Pandit, C., 2009. Some common fallacies about floods and flood management. *Current Science*, 97, pp.991–993.
- Pielke, R.A., Pitman, A., Niyogi, D., Mahmood, R., McAlpine, C., Hossain, F., Goldewijk, K.K., Nair, U., Betts, R., Fall, S., Reichstein, M., Kabat, P. and de Noblet, N., 2011. Land use/land cover changes and climate: Modeling analysis and observational evidence. *Wiley Interdisciplinary Reviews: Climate Change*, 2, pp.828–850. <https://doi.org/10.1002/wcc.144>.
- Prasad, K., Afroz, R., Sarker, M.A. and Rahman, M., 2021. A diagnostic study of some flood producing rainfall events in Bangladesh with a limited area analysis-forecast system. *Mausam*, 57, pp.475–488. <https://doi.org/10.54302/mausam.v57i3.492>.
- Ranalkar, M.R., Chaudhari, H.S., Hazra, A., Sawaisarje, G.K. and Pokhrel, S., 2016. Dynamical features of incessant heavy rainfall event of June 2013 over Uttarakhand, India. *Natural Hazards*, 80, pp.1579–1601. <https://doi.org/10.1007/s11069-015-2040-z>.
- Ray, S., 2019. Introduction to machine learning and different types of machine learning algorithms. *Proceedings of the International Conference on Machine Learning, Big Data, Cloud and Parallel Computing: Trends, Perspectives and Prospects*, pp.35–39.
- Reddy, D.V., Kumar, D., Saha, D. and Mandal, M.K., 2008. The 18 August 2008 Kosi river breach: an evaluation. *Current Science*, 95, pp.1668–1669.
- Shankar, A., Kumar, A., Sahana, B.C. and Sinha, V., 2022. A Case study of heavy rainfall events and resultant flooding during the summer monsoon season 2020 over the river catchments of north Bihar, India. *VayuMandal*, 48(2), pp.17–28.
- Sinha, R., Bapalu, G.V., Singh, L.K. and Rath, B., 2008. Flood risk analysis in the Kosi river basin, north Bihar using multi-parametric approach of analytical hierarchy process (AHP). *Journal of the Indian Society of Remote Sensing*, 36, pp.335–349. <https://doi.org/10.1007/s12524-008-0034-y>.
- Xu, C., Gong, A., Liang, L., Song, X. and Wang, Y., 2023. Vulnerability assessment method for immovable cultural relics based on artificial neural networks—an example of a heavy rainfall event in Henan Province. *International Journal of Disaster Risk Science*, 14, pp.41–51. <https://doi.org/10.1007/s13753-022-00461-y>.
- Zhang, Z.X., Wang, L., Duan, J.L. and Wang, Y.M., 2022. An early warning method based on fuzzy evidential reasoning considering heterogeneous information. *International Journal of Disaster Risk Reduction*, 82, 103356. <https://doi.org/10.1016/j.ijdr.2022.103356>.
- Zou, X. and Ren, F., 2015. Changes in regional heavy rainfall events in China during 1961–2012. *Advances in Atmospheric Sciences*, 32, pp.704–714. <https://doi.org/10.1007/s00376-014-4127-y>.

---

#### ORCID DETAILS OF THE AUTHORS

Anand Shankar: <https://orcid.org/0000-0001-8141-6400>



# Heavy Metals in Water and Sediments and Their Impact on Water Quality in Andean Micro-watersheds: A Study of the Colorado and Alajua Rivers in the Ambato River Watershed, Tungurahua, Ecuador

Rodny Peñafiel<sup>1†</sup>, Fabián Rodrigo Morales-Fiallos<sup>2</sup>, Bolívar Paredes-Beltrán<sup>2</sup>, Dilon Moya<sup>2</sup>,  
Adriana Jacqueline Frias Carrion<sup>1</sup> and Belén Moreano<sup>1</sup>

<sup>1</sup>Environmental Laboratory, Faculty of Food Science and Biotechnology Engineering, Technical University of Ambato, Ecuador

<sup>2</sup>Faculty of Civil and Mechanical Engineering, Technical University of Ambato, Ecuador

†Corresponding author: Rodny Peñafiel; rd.penafiel@uta.edu.ec

Nat. Env. & Poll. Tech.  
Website: [www.neptjournal.com](http://www.neptjournal.com)

Received: 05-03-2024

Revised: 16-04-2024

Accepted: 27-04-2024

## Key Words:

Heavy metals  
Water quality  
Ambato River watershed  
Colorado River  
Anthropogenic activities  
Coliforms

## ABSTRACT

The present study aims to characterize the water and sediment quality of the Colorado and Alajua rivers within Ecuador's Ambato River watershed, with a specific focus on the presence of heavy metals. Measurements were conducted at five sampling points along the upper and lower zones of each river, where both physicochemical and microbiological parameters, as well as concentrations of heavy metals in water and sediments, were analyzed. Most parameters exhibited statistically significant differences, as determined by the analysis of variance (ANOVA), between the values observed in the upper and lower zones of the micro-watersheds. Water quality in the mentioned rivers was assessed using specific water quality indices, WQI, namely the NSF-WQI and Dinius WQI. Additionally, the impact of heavy metal presence in the water and sediments was evaluated using the Heavy Metal Evaluation Index (HEI). While most parameters met the Ecuadorian quality standards for water sources intended for human consumption, concerns emerged regarding elevated levels of total and fecal coliforms along both rivers, which could limit the suitability of these rivers as a water source for human use and consumption. At various sampling points, water quality criteria for the preservation of aquatic life were not met for several heavy metals. For example, the Colorado River exhibited elevated levels of zinc ( $59\text{-}76\ \mu\text{g.L}^{-1}$ ), copper ( $12\text{-}47\ \mu\text{g.L}^{-1}$ ), lead ( $1.2\text{-}3.9\ \mu\text{g.L}^{-1}$ ), iron ( $0.33\text{-}0.37\ \text{mg.L}^{-1}$ ), and manganese ( $0.37\text{-}0.47\ \text{mg.L}^{-1}$ ), while the Alajua River showed excess copper ( $11\ \mu\text{g.L}^{-1}$ ), iron ( $0.61\text{-}0.72\ \text{mg.L}^{-1}$ ), and manganese ( $0.62\text{-}0.98\ \text{mg.L}^{-1}$ ). Geological factors likely contribute to the concentration of heavy metals in the upper segments of the rivers, while agricultural runoff may contribute to concentrations in the lower segments. Sediments exhibited higher average values of the Heavy Metal Evaluation Index (HEI) ( $20.6\text{-}26.7$ ) compared to water samples ( $13.9\text{-}15.4$ ), indicating a potential accumulation of heavy metals in the river sediments. Overall, both rivers exhibited contamination levels ranging from regular to moderate, as indicated by the calculated average Water Quality Indices (WQI), with certain areas showing slight contamination or meeting acceptable standards. These results highlight the influence of anthropogenic activities on water quality, emphasizing the necessity of continuous monitoring to assess and control their impact.

## INTRODUCTION

Water plays a crucial role in both human well-being and environmental integrity. The use of water is influenced by its condition, whether it is in its natural state or altered in its physical, chemical, or biological characteristics (WHO 2011). In this context, Ecuador has instituted a framework of standards and regulatory mechanisms intended to safeguard aquatic ecosystems, protect drinking water sources, and sustain agricultural irrigation (Ministerio del Ambiente del Ecuador, 2015). Nevertheless, the persistence of water pollutants and the economic and technological constraints

in rural Andean communities turn water quality preservation into a lasting challenge for emerging economies.

Rivers located in the high-altitude Andean regions of Ecuador, such as the Colorado River (4048-3876 meters above sea level, a.s.l.) and the Alajua River (3236-2784 meters a.s.l.), which belong to the Ambato River watershed, predominantly constitute lotic ecosystems. These ecosystems are characterized by their rapid transport of the contained substances, including contaminants, such as heavy metals, persistent organic pollutants (POPs), nutrients, and pathogenic microorganisms. The conveyance of these

pollutants poses potential detrimental impacts on human health and negative effects on the aquatic ecosystems (Timmerman 2011).

The quality of water in these rivers depends on both their intrinsic natural characteristics and the land use practices within their respective hydrographic watersheds. The concentration of various substances in these water bodies is influenced not only by the local geological and hydrogeological conditions but also by the introduction of compounds of anthropogenic origin (Fournier et al. 2019). Human-induced activities have negatively impacted the aquatic integrity of the main river systems within the Ambato River watershed. It is estimated that approximately 95% of the wastewater discharged into the water bodies of this watershed lacks proper treatment (Herrmann 2002). The presence of heavy metals in riverine systems can markedly influence their water quality. Metals such as lead, nickel, cadmium, chromium, and arsenic may enter water bodies via various routes. These include industrial operations, effluents and disposals, mining activities, and the mobilization of natural sedimentary deposits (Matta & Gjyli 2016).

The presence of metals in the rivers of Ecuador poses a significant environmental threat, particularly in the Cotopaxi and Tungurahua provinces, where the presence of heavy metals has been detected. Elevated concentrations of chromium have been documented at tannery wastewater discharge locations along the Ambato River, with recorded values between 8.2 and 30.2 mg.L<sup>-1</sup> (Sánchez et al. 2020). With respect to cadmium, the highest concentration was observed in the Ambato-Huachi-Pelileo irrigation canal, reaching a level of 0.23 mg.L<sup>-1</sup>. In the case of the Cutuchi and Pumacunchi rivers, arsenic emerges as the predominant contaminant, exhibiting maximum concentrations of 0.062 mg.L<sup>-1</sup> and 0.067 mg.L<sup>-1</sup>, respectively (Sánchez et al. 2020). On the other hand, lead (Pb), concentrations of 0.2 mg.L<sup>-1</sup> were detected in the Ambato-Huachi-Pelileo irrigation canal and 0.18 mg.L<sup>-1</sup> in the Ambato River.

Furthermore, in the study by Chiliquina & Donoso in 2012, the presence of chromium was found with an average concentration of 0.0628 mg.L<sup>-1</sup> in the Pachanlica River, located in the province of Tungurahua (Chiliquina & Donoso 2012, Sánchez et al. 2020). The detrimental impacts of heavy metals are not confined to aquatic life forms. These metals can modify biogeochemical cycles and alter the composition of aquatic communities, consequently disrupting the natural balance of these ecosystems (Sonone et al. 2020, Vajargah 2021).

The Alajua River originates from the Casahuala volcano in Tungurahua Province, covering an area of influence spanning 123 km<sup>2</sup>, accounting for 13% of the total watershed

area. It plays an important role in providing water resources for agricultural purposes and human consumption within the Ambato canton. On the other hand, the Colorado River originates in the highlands of the Chimborazo volcano located in the Ecuadorian Andean region and serves as a significant tributary of the Pastaza River basin. It has an approximate length of 100 km, and its influence area within the basin encompasses approximately 164 km<sup>2</sup>, constituting 18 % of the overall watershed area (Pérez 2015).

However, information regarding the presence of heavy metals in water and sediments in these Andean rivers is limited. Hence, the present study aims to characterize the water and sediment quality of these two rivers, which are the main ones in the Ambato River watershed in Ecuador. The study focuses on identifying the presence of heavy metals in both water and sediments and comparing the results with current environmental regulations in Ecuador. Additionally, water and sediment quality indices will be applied using the collected data, enabling the calculation of numerical values that reflect the environmental conditions of the Colorado and Alajua rivers, as well as the evaluation of the impact of heavy metals on the water quality of these rivers.

## MATERIALS AND METHODS

### Research Area

The study area, which encompasses the Ambato River watershed within Ecuador's Tungurahua province (Figs. 1 and 2), is located in the western Andes region of the country. It is geographically defined by neighboring catchment areas, with the Cutuchi River to the north, the Chambo River to the south, the Cutuchi and Patate Rivers to the east, and the Babahoyo and Yaguachi Rivers to the west. Covering an approximate land area of 130 173 hectares, this sub-basin constitutes 38% of the province's total territory (Pérez 2015). Serving as the primary water source for the Tungurahua province, it supports a wide range of uses in both urban and rural areas, including domestic consumption, agricultural activities, and industrial applications (Herrmann 2002).

The Ambato River watershed consists of 11 hydrological micro-catchments, with the Ambato, Pachanlica, Colorado, and Alajua rivers being the predominant ones (Fig. 3). The Colorado River is a significant tributary of the larger catchment area of the Pastaza River.

Field visits were conducted to identify pollution hotspots in the study areas, resulting in the determination of five sampling points in the upper and lower basins of each river. In the case of the Colorado River (Fig. 4), at point 1 (P1-AF) with an altitude of 4048 m, located near a meteorological station at coordinates 113.0'25''S 78°52'37.1''W, vicuñas



Fig. 1: Location map of the Tungurahua Province, Ecuador.



Fig. 2: Map of Tungurahua Province with Ambato Canton shaded.

were observed. At point 2, situated at an altitude of 3995 m at coordinates 1°24'55.5"S, 78°52'05.1"W, cows were seen along the river. On the other hand, at point 3, near the confluence of the middle tributary at 3994 m at coordinates

1°24'53.1"S, 78°51'49.5"W, no sources of contamination were identified. Additionally, residents testified that this site is used for human consumption without prior treatment. At point 4, located at 3881 m at coordinates 1°23'14.0''S

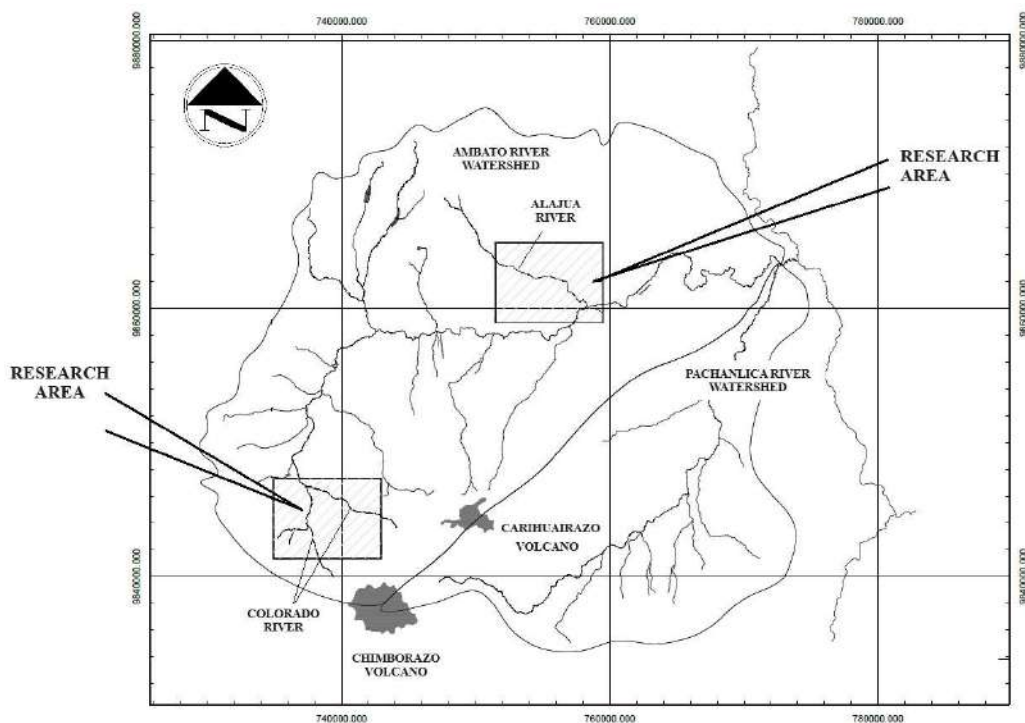


Fig. 3: Map of the Ambato River Watershed. Research Areas Colorado and Alajua Rivers.

78°51'59.1''W, washing of containers used in dairies and laundry discharge was observed. Llamas and domestic wastewater discharges were witnessed at point 5, located near an underpass at 3876 m with coordinates 1°23'09.2''S and 78°51'57.7''W.

At point 1 of the Alajua River (Fig. 5), situated at 3236 m at coordinates 1°14'29.8'' S 78°43'09.1''W, the waterway streamed amid forest vegetation. At point 2, on the Pumgoloma - Quisapincha road, located at 3191 m at coordinates 1°14'28.3'' S 78°43'23.2''W, cultivated areas were observed. Point 3, positioned 200 m downstream from the road at an elevation of 3207 m and coordinates 1°14'29.6''S 78°43'15.7''W, had pastures for livestock, cultivated areas, and recreational spots for sport fishing. Point 4, located 200 m upstream of the EMAPA-Tilulum drinking water treatment plant, operated by the Municipal Water Company of Ambato (EMAPA) at 2788 m and coordinates 1°15'40.5''S 78°40'45.6''W, exhibited signs of deforestation in the surrounding area. Lastly, point 5 at the EMAPA Tilulum drinking water treatment plant, at an elevation of 2784 m and coordinates 1°15'48.3''S, 78°40'41.1''W, showed water discharges and areas used for fruit cultivation.

### Water and Sediment Samples Collection

Simple sampling of water and sediments was conducted according to Ecuadorian standards (NTE-INEN 2176 2013),

which took place during the dry season of the year (August) to minimize the impact of rainfall on the collected samples. All samples were collected in triplicate. The collection of surface water at each point was done using a Van Dorn bottle, which was submerged to a depth of 0.3 meters below the water surface. The collected water volume was poured into one-liter amber bottles and sterile 100 mL containers for microbiological analysis, avoiding the formation of air bubbles. On the other hand, along the riverbanks, 300 grams of sediment were collected using spatulas and placed in polyethylene plastic jars, which were then sealed in airtight plastic bags (Vega 2021). Samples for the analysis of heavy metals, sulfates, and chlorides were acidified with 0.1% concentrated 65% nitric acid. Subsequently, the samples were transported in containers with ice to prevent alteration until they reached the facilities of the Environmental Analysis Laboratory of the Faculty of Food Science and Biotechnology at the Technical University of Ambato, where they were characterized.

The detection of in-situ parameters is carried out using the HANNA HI 9829 multiparameter meter, as well as the LaMotte turbidimeter. At each station, in-situ measurements of temperature, pH, turbidity, conductivity, dissolved oxygen (DO), and total dissolved solids (TDS) were conducted by directly immersing the meter probe 25 cm below the water surface (Quiroz et al. 2017).

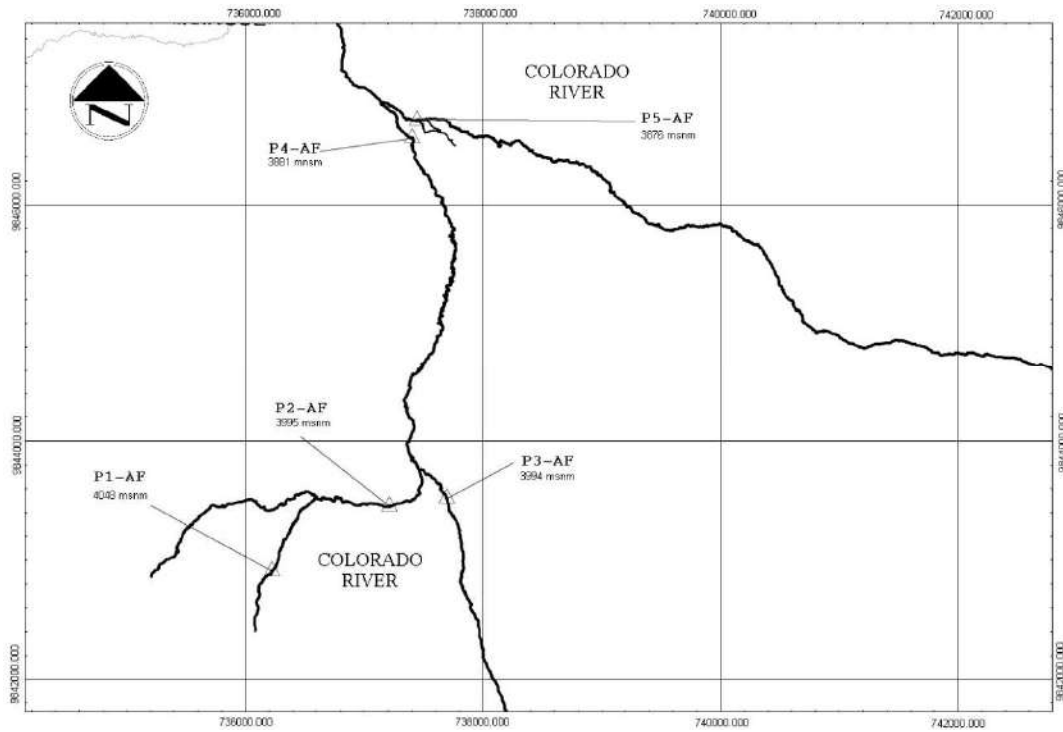


Fig. 4: Location of sampling points for the Colorado River.

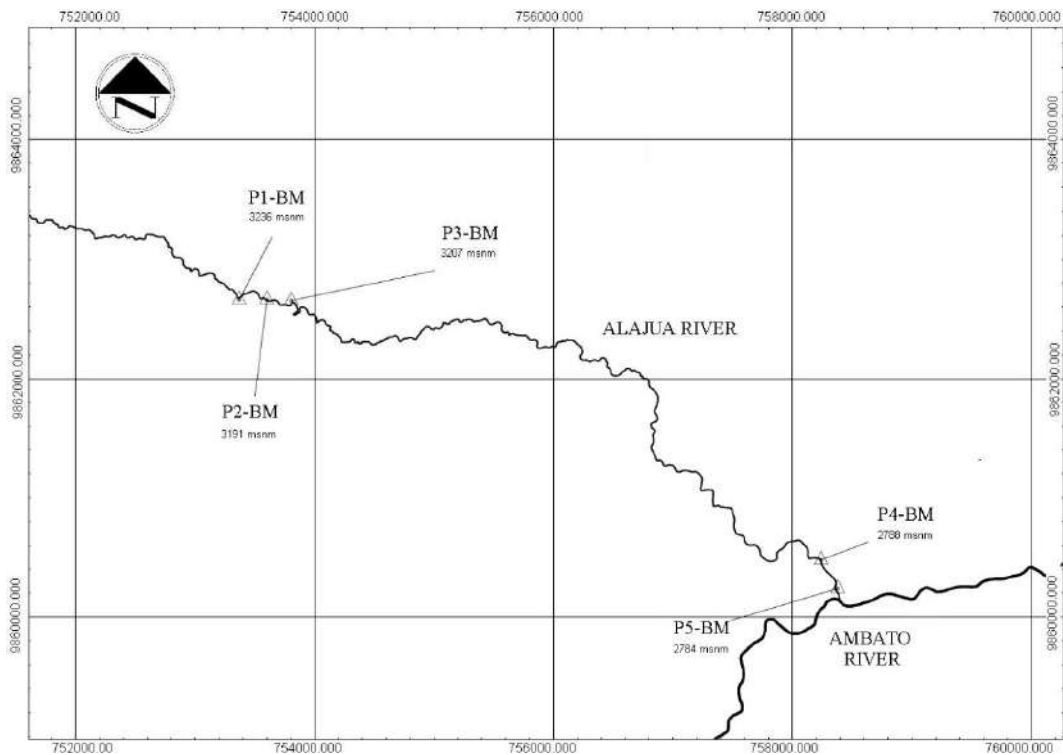


Fig. 5: Location of sampling points for the Alajua River.

## Analysis of Water and Sediment Samples

Total and fecal coliforms were determined using the membrane filtration (MF) technique. Samples were first agitated for 30 seconds, and then serial dilutions ranging from  $10^{-1}$  to  $10^{-3}$  were prepared using sterile buffered water (Plúas 2019). Next, sterile millipore membranes were placed in the funnels' receptacles, then the dilutions were transferred to the funnels of the vacuum equipment, filtration was initiated, and once completed, the membranes were removed and placed in Petri dishes with selective media, m-Endo for total coliform detection and rosolic acid for fecal coliforms. Finally, they were incubated at 37°C for 24 hours, and the colony-forming units (CFU.100.mL<sup>-1</sup>) were calculated (Larrea-Murrell et al. 2013).

The following ions were determined using the HI83399 Hanna photometer: nitrates, ammonia, phosphates, chlorides, sulfates, potassium, magnesium, calcium, hexavalent chromium, copper, zinc, and iron. The analyses were conducted following the Standard Methods for the Examination of Water and Wastewater (American Public Health Association, APHA, 2017). The total permanent hardness of the water, expressed as the mgL<sup>-1</sup> CaCO<sub>3</sub> equivalent, was calculated in the water samples using the following formula (Pal et al. 2018): Hardness (mgL<sup>-1</sup> CaCO<sub>3</sub>) = 2.5(mgL<sup>-1</sup> Ca) + 4.1(mgL<sup>-1</sup> Mg).

The analysis of heavy metals, specifically arsenic, lead, nickel, and cadmium, was conducted using Graphite Furnace Atomic Absorption Spectrometry (GFAAS) with the PG Instruments AA500 spectrometer. Acidified surface water samples were filtered using 0.45 µm syringe filters (Econofilter). The measurements were carried out following the specifications recommended in the PGI AA500 Analytical Cookbook. For each specific metal analysis, predetermined calibration curves developed by the Environmental Analysis Laboratory at the Technical University of Ambato were utilized. These calibration curves exhibited Pearson Correlation Coefficients (R<sup>2</sup>) above 0.98.

To determine the conductivity and pH in sediments, the procedure described by Romero et al. (2009) was employed. 200 grams of sediment were placed in a 1000 mL precipitation beaker along with 500 mL of distilled water. The mixture was stirred for 30 minutes to keep the particles suspended. Subsequently, conductivity and pH were measured using the portable photometer Hanna HI9829.

For the determination of heavy metals in sediments, prior digestion was conducted using the EPA 3051 method in a microwave oven (ETHOS UP). This involved weighing 5 grams of the sample into pre-labeled and pre-weighed crucibles, which were then dried at 105°C for 24 h. The

dried samples were subsequently pulverized, and 0.5 grams were placed into digestion tubes. Next, 5 mL of concentrated HNO<sub>3</sub> and 1 mL of 30% (V/V) hydrogen peroxide were added. The tubes were then subjected to microwave digestion for 50 min (American Public Health Association 2017). Once the samples were digested and cooled, they were transferred to 100 mL volumetric flasks and topped up with distilled water. The samples were stored at 5°C until analysis (United States Environmental Protection Agency (EPA) 2013, Vega 2021). The digested samples were then analyzed using the atomic absorption equipment, with prior filtration using the WELCH vacuum filtration apparatus with 0.45 µm cellulose acetate filters. Finally, the results obtained from the GFAAS equipment are expressed in units of mg.kg<sup>-1</sup> dry sediment.

## Water Quality Index (WQI) and Heavy Metal Evaluation Index (HEI)

Two different Water Quality Indices (WQI) were employed: the NSF-WQI (Water Quality Index according to the National Science Foundation), which primarily assesses water quality for human consumption, and the Dinius' WQI, which considers five water uses, including human consumption, industry and recreation, agriculture, fishing, and aquatic life (Torres et al. 2018). For the Water Quality Index (WQI), as outlined by Sierra (2011), the following parameters were considered: dissolved oxygen, pH, temperature, turbidity, total solids, total phosphate, nitrates, fecal coliforms, and Biochemical Oxygen Demand (BOD). This approach involves the utilization of a rating curve technique, linking the measured parameter concentrations (mg.L) to a quality sub-index value, S<sub>i</sub>, ranging from 0 (lowest quality) to 100 (highest quality). Relative fractional weights are denoted as were assigned to each parameter, reflecting their respective importance and the specific aspects of water quality they assess. Utilizing the formula (1), the WQI value was then computed for each sampling zone, as elaborated by (Uddin et al. 2021).

$$\text{NSF-WQI} = \sum_i^n S_i \cdot W_i \quad \dots(1)$$

The corresponds to the following water quality ranges: 91-100 (excellent), 71-90 (good), 51-70 (fair), 26-50 (poor), and 0-25 (very poor) (Méndez et al. 2020, Quiroz et al. 2017).

In addition, Dinius' Water Quality Index (WQI) was also employed, which encompasses 12 parameters, including dissolved oxygen (DO), Biochemical Oxygen Demand (BOD), total coliforms (CT), fecal coliforms (CF), nitrates, hardness, chlorides, alkalinity, pH, conductivity, temperature, and color (Flores 2022). Nine of these parameters were considered for the study, while three parameters—chlorides, which were undetectable (measuring below 0.5 mg.L<sup>-1</sup>), as



well as alkalinity and color, which were not measured—were excluded from the analysis. Consequently, weighting coefficients ( $W_i$ ) were adjusted, and subindex values ( $Q_i$ ) were determined using weighted geometric mean equations, with the results raised to the corresponding powers,  $n$ , (Dinius 1987). Finally, the DINIUS-WQI was calculated using the geometric mean with a multiplicative function:

$$\text{DINIUS-WQI} = \prod_{i=1}^n Q_i^{S_i} \quad \dots(2)$$

The DINIUS-WQI is associated with the following water quality ranges: 90-100 (excellent), 80-89 (acceptable), 51-79 (slightly contaminated), 30-50 (contaminated), 20-29 (highly contaminated), and 0-19 (excessively contaminated) (Dinius 1987, Flores 2022, Guananga-Diaz et al. 2022).

There are several water quality indices developed to assess and analyze metal pollution, including the Heavy Metal Pollution Index (HPI), the Metal Pollution Index (MPI), the Heavy Metal Evaluation Index (HEI), and the Contamination Degree (Cd) (Boateng et al. 2015). However, it has been suggested that the use of HEI, due to its simplicity, is preferable for conducting heavy metal pollution monitoring (Edet & Offiong 2002). The Heavy Metals Assessment Index (HEI) was employed to gain a comprehensive understanding of water quality in the Colorado and Alajua rivers concerning heavy metal pollution (Moyel et al. 2015). This index is defined as follows:

$$\text{HEI} = \sum_{i=1}^n \frac{H_c}{H_{mac}} \quad \dots(3)$$

Where  $H_c$  represents the measured value, while  $H_{mac}$  corresponds to the maximum allowable concentration of each trace metal (Rezaei et al. 2019).  $H_{mac}$  was determined based on the maximum permissible value specified according to the Ecuadorian environmental regulations, Annex 2 of Book VI of TULSMA (Ministerio del Ambiente del Ecuador 2015)

in “Water Quality criteria for the preservation of aquatic and wildlife in freshwater, marine, and estuarine waters.” However, for sediment samples,  $H_{mac}$  was chosen based on the maximum permissible value established in the “Criteria for soil quality,” of the mentioned regulation. According to the HEI index value, three levels of pollution categories are proposed, described as follows: (i) HEI < 10 indicates a low level of contamination; (ii) HEI = 10-20 signifies a moderate level of contamination; and (iii) HEI > 20 represents a high degree of contamination (Boateng et al. 2015).

## RESULTS AND DISCUSSION

### Physicochemical and Microbiological Characterization of Water Samples

Water samples were collected during the dry season, and Table 1 presents their in-situ measurements. Both the Colorado River and the Alajua River exhibit dissolved oxygen (DO) concentrations approaching saturation due to the increased turbulence levels in these water bodies (Carvajal 2017).

The pH fell within the allowable range of 6.5 to 9, as stipulated in Tables 1, 2, and 3 of TULSMA. These tables outline the Ecuadorian environmental regulations of criteria for quality water, encompassing various uses, including human consumption and domestic use (Table 1), the preservation of freshwater aquatic and wildlife (Table 2), and agricultural irrigation (Table 3) (MAE 2015).

Electrical conductivity is directly linked to the presence of total dissolved solids (TDS) due to their ionic activity, which can originate from both organic and inorganic substances in solution (Cantera et al. 2009). In the Colorado and Alajua rivers, an increase in conductivity downstream was observed, rising from 196 to 484  $\mu\text{S cm}^{-1}$  and from 127

Table 1: Physicochemical parameters and on-site meteorological conditions at surface water sampling points.

	Sampling Points	pH	Temperature (°C)	ORP (mV)	OD (ppm)	TDS (ppm)	Turbidity (NTU)	Conductivity ( $\mu\text{S cm}^{-1}$ )	Height (m)	Pressure mmHg)
Colorado River	P1 – AF	8.2±0.1	8.7±0.2	20.7±0.5	7.4±1.5	98±1	1.2± 0.1	196± 1	4048	472
	P2 – AF	8.2±0.1	9.6±0.2	61.5±0.5	6.8±1.5	64±1	0.7±0.1	129±1	3995	469
	P3 – AF	7.0±0.1	8,6±0.2	79.0±0.5	6.8±1.5	114±1	0.3±0.1	228±1	3994	470
	P4 – AF	8.8±0.1	13,1±0.2	57.5±0.5	6.7±1.5	98±1	0.3±0.1	196±1	3881	483
	P5 – AF	7.4±0.1	13,5±0.2	-38.8±0.5	6.9±1.5	242±1	0.5±0.1	484±1	3876	482
Alajua River	P1 – BM	8.3±0.1	13.0±0.2	9.4±0.5	8.4±1.5	64±1	2.6±0.1	127±1	3236	526
	P2 – BM	8.3±0.1	12.6±0.2	67.0±0.5	8.4±1.5	64±1	2,3±0.1	128±1	3191	527
	P3 – BM	7.7±0.1	12.7±0.2	71.3±0.5	8.5±1.5	64±1	2.7±0.1	128±1	3207	526
	P4 – BM	8.6±0.1	9.3±0.2	88.8±0.5	9.7±1.5	76±1	2.1±0.1	152±1	2788	550
	P5 – BM	8.9±0.1	9.5±0.2	63.3±0.5	9.9±1.5	80±1	1.9±0.1	161±1	2784	552

to 161  $\mu\text{S cm}^{-1}$ , respectively. This upward trend may be associated with increased agricultural and domestic activities since 2015. According to Vinueza et al. (2021), the average conductivity in surface waters of Andean rivers in Ecuador is approximately 137  $\mu\text{S cm}^{-1}$ , which aligns with the figures obtained in this study. When comparing both rivers, the Colorado River exhibits higher conductivity than the Alajua River, with averages of 247 and 139  $\mu\text{S cm}^{-1}$ , respectively. This difference could be attributed to a greater presence of salts discharged into the Colorado River, stemming from anthropogenic activities.

Regarding the Oxidation-Reduction Potential (ORP), Ecuador lacks specific regulatory standards for reference values concerning this parameter. Nevertheless, it is observed that samples from the Alajua River and the first four sampling points of the Colorado River exhibit oxidizing characteristics, indicated by their positive ORP values. Conversely, sampling point P5 displayed a negative ORP value. This anomaly could be linked to the elevated content of Total Dissolved Solids (TDS) at 242  $\text{mg.L}^{-1}$ , high conductivity at 484  $\mu\text{S cm}^{-1}$ , and a significant concentration of sulfates (35  $\text{mg.L}^{-1}$ ). These characteristics may result from agricultural runoff, the presence of farm animals, and native camelids in the area (Reichart et al. 2007)

### Total Coliforms (TC) and Fecal Coliforms (FC) in Water Samples

The water quality criterion, as specified in Tables 2 and 3 of the TULSMA regulations, is 1000 CFU/100 mL of FC. Regarding this criterion, in both rivers, all values exceeded the limit, except at sampling points P1-AF and P3-AF of the Colorado River, where coliforms were not detected. The highest recorded figure was observed in the Colorado River, specifically at sampling point P4-AF, where the value reached

$3.4 \times 10^4$  CFU  $\text{mL}^{-1}$  (see Table 3). This microbiological pollution can be attributed to anthropogenic contamination resulting from the improper disposal of organic animal waste and wastewater from human consumption.

The study conducted by Hong et al. (2010) demonstrated that TC is closely associated with physicochemical parameters of water, such as suspended solids, organic and inorganic content, pH, and temperature, as these factors influence the survival and growth of coliforms. In contrast, FC is linked to runoff, as it involves a greater transport of fecal matter into watercourses (Reitter et al. 2021).

### Determination of Metals and Ions in Water Samples

Table 4 displays the concentrations of metals and ions in water samples collected from various points in both rivers. No chlorides were detected in the samples taken from the Colorado River. Furthermore, sampled areas showed low levels of nitrates, ammonia, phosphates, and sulfates, indicating a reduced degree of anthropogenic contamination (Strokal et al. 2020). Downstream points in the Colorado River (points 4 and 5) tend to exhibit higher concentrations of metals and ions, notably nitrates (377% higher), sulfates (129% higher), and magnesium (103% higher) compared to points in the upper zone (points 1, 2, and 3). This difference may be attributed to increased agricultural activity in the lower Colorado River watershed (Badrzadeh et al. 2022).

Regarding the Alajua River, the concentrations of all metals and ions analyzed comply with the permissible limits established by legislation for the preservation of aquatic and wildlife (MAE 2015). The concentration of ammonia at sampling point 3 is slightly elevated (0.90  $\text{mg.L}^{-1}$ ) compared to the other sampling points. According to the United States Environmental Protection Agency (EPA 2013), an ammonia concentration at pH 7.0 and 20°C of 17  $\text{mg.L}^{-1}$  can lead to

Table 2: Determination of fecal and total coliforms.

	Sampling Points	Units	Fecal Coliforms	Total Coliforms	TULSMA Tables Annex 1 - Book VI		
					Table 1	Table 2	Table 3
Colorado River	P1 – AF	CFU.mL <sup>-1</sup>	ND	ND	1000	-	1000
	P2 – AF		$3.7 \cdot 10^3 \pm 2.5 \cdot 10^2$	$4.0 \cdot 10^3 \pm 5.6 \cdot 10^2$			
	P3 – AF		ND	ND			
	P4 – AF		$3.4 \cdot 10^4 \pm 5.5 \cdot 10^2$	$3.2 \cdot 10^4 \pm 8.0 \cdot 10^2$			
	P5 – AF		$1.6 \cdot 10^3 \pm 8.0 \cdot 10^2$	$9.0 \cdot 10^3 \pm 6.7 \cdot 10^2$			
Alajua River	P1 – BM		$3.7 \cdot 10^3 \pm 3.0 \cdot 10^2$	$7.7 \cdot 10^3 \pm 1.5 \cdot 10^2$			
	P2 – BM		$3.3 \cdot 10^3 \pm 2.5 \cdot 10^2$	$5.8 \cdot 10^3 \pm 5.2 \cdot 10^2$			
	P3 – BM		$1.3 \cdot 10^4 \pm 49.0 \cdot 10^2$	$1.9 \cdot 10^4 \pm 5.1 \cdot 10^2$			
	P4 – BM		$7.5 \cdot 10^3 \pm 4.0 \cdot 10^2$	$1.4 \cdot 10^4 \pm 7.0 \cdot 10^2$			
	P5 – BM		$3.4 \cdot 10^3 \pm 2.0 \cdot 10^2$	$6.1 \cdot 10^3 \pm 6.1 \cdot 10^2$			

Note: Values that were not detected are reported as (ND).

Table 3: Results of metal and anion concentrations in water samples.

Parameter	Units	Alajua River										Maximum permissible limit		
		Colorado River					Alajua River					Table		
		P1-AF	P2-AF	P3-AF	P4-AF	P5-AF	P1-BM	P2-BM	P3-BM	P4-BM	P5-BM	1	2	3
Calcium	mg.L <sup>-1</sup>	19.5 ± 0.1	7.1 ± 0.1	20.6 ± 0.1	21.3 ± 0.1	33.2 ± 0.1	7.6 ± 2.8	18.1 ± 2.1	17.0 ± 2.8	15.2 ± 0.3	11.7 ± 1.1	-	-	-
Potassium	mg.L <sup>-1</sup>	2.9 ± 0.1	2.7 ± 0.1	2.3 ± 0.2	2.6 ± 0.2	5.0 ± 0.1	2.1 ± 0.06	2.0 ± 0.1	1.9 ± 0.1	1.8 ± 0.1	1.8 ± 0.1	-	-	-
Magnesium	mg.L <sup>-1</sup>	1.3 ± 0.6	0.7 ± 0.2	1.7 ± 0.6	3.7 ± 0.6	1.3 ± 0.6	8.8 ± 0.7	10.1 ± 0.1	9.7 ± 2.2	10.7 ± 1.5	13.1 ± 1.4	-	-	-
Aluminum	mg.L <sup>-1</sup>	1.0 ± 0.1	ND	ND	ND	ND	ND	ND	ND	ND	ND	-	0.1	5
Fluoride	mg.L <sup>-1</sup>	ND	ND	ND	ND	ND	ND	ND	ND	ND	ND	1.5	-	1 <sup>fluorine</sup>
Ammonium	mg.L <sup>-1</sup>	0.26 ± 0.20	0.09 ± 0.04	0.02 ± 0.01	0.08 ± 0.01	0.07 ± 0.04	0.08 ± 0.01	0.08 ± 0.02	0.90 ± 0.04	0.12 ± 0.02	0.07 ± 0.03	-	-	-
Nitrate	mg.L <sup>-1</sup>	0.2 ± 0.1	0.2 ± 0.1	0.2 ± 0.1	1.8 ± 0.3	0.3 ± 0.2	0.9 ± 0.2	1.1 ± 0.2	1.2 ± 0.8	3.3 ± 0.2	3.2 ± 0.1	50	-	-
Phosphate	mg.L <sup>-1</sup>	2.0 ± 0.2	1.4 ± 0.2	2.5 ± 0.1	2.4 ± 0.1	2.6 ± 0.1	0.3 ± 0.1	1.7 ± 0.2	2.0 ± 0.3	2.3 ± 0.1	3.0 ± 0.3	-	-	-
Chlorides	mg.L <sup>-1</sup>	ND	ND	ND	ND	ND	1.6 ± 0.1	1.4 ± 0.2	0.9 ± 0.1	2.6 ± 0.3	2.2 ± 0.1	-	-	-
Sulfates	mg.L <sup>-1</sup>	2.2 ± 0.8	15.1 ± 1.1	11.4 ± 0.9	8.7 ± 0.5	35.1 ± 0.6	0.8 ± 0.4	2.0 ± 0.7	2.1 ± 1.1	1.1 ± 0.8	5.6 ± 1.2	500	-	250

Note: Values that were not detected are reported as (ND). Table 1 indicates “Water Quality Criteria for human consumption and domestic use,” Table 2 indicates “Water Quality criteria for the preservation of aquatic and wildlife in freshwater, marine, and estuarine waters,” and Table 3 indicates “Water quality criteria for water intended for agricultural use” (MAE, 2015).

acute adverse effects on freshwater aquatic life, while chronic effects may occur at levels as low as  $1.9 \text{ mg.L}^{-1}$ . Furthermore, Ding et al. (2021) suggest that in Australia and New Zealand, the recommended limit for ammonium ions is  $2.18 \text{ mg.L}^{-1}$  at pH 7.0 to safeguard aquatic life. It can be concluded from the above that the levels of ammonia found in this study (ranging from  $0.02$  to  $0.90 \text{ mg.L}^{-1}$ ) do not pose a threat to aquatic life as they are below the permissible limits of local regulations and are lower than the critical values established in different countries, indicating a limited impact from anthropogenic contamination.

Similar to the Colorado River, the lower zones of the Alajua River (points 4 and 5) exhibit higher concentrations of these pollutants: nitrates 207% higher, sulfates 105% higher, and phosphate 99% higher than at higher elevations (points 1, 2, and 3). Agriculture and communal wastewater discharges into the river are presumed sources of pollution (Mekuria et al. 2021). However, the presence of aluminum and fluoride was not detected in any of the samples taken in both rivers (except at point 1 in the Colorado River, with an aluminum concentration of  $1 \text{ mg.L}^{-1}$ ).

#### Determination of Heavy Metals in Water Samples

Table 4 presents the results of heavy metal determination, including arsenic, lead, nickel, zinc, copper, cadmium, hexavalent chromium, iron, and manganese, in the water samples collected from various points in the Colorado and Alajua rivers. In the Colorado River, concentrations of zinc exceeding the established water quality criterion for aquatic life, which is  $30 \text{ } \mu\text{g.L}^{-1}$ , have been observed at points 2, 3, and 4. These elevated zinc concentrations are attributed to factors such as runoff from roads, agricultural areas, and the release of zinc-containing minerals due to weathering (Prasad Ahirvar et al. 2023). The presence of zinc and other metals in water can also be influenced by the geological and mineral characteristics of the soil (Tu et al. 2020). Zinc was not detected in the water samples from the Alajua River. Regarding lead, the Colorado River exhibits levels exceeding the permissible limit ( $1 \text{ } \mu\text{g.L}^{-1}$ ) for the preservation of aquatic life at all sampling points (Table 4). This could be attributed to the atmospheric deposition of anthropogenic lead from sources like gasoline use, coal combustion, and vehicle emissions (González et al. 2020). The sampling areas of this river are influenced by the presence of roads and major routes connecting various cantons in the province, including the road to Guaranda. On the other hand, the Alajua River presented elevated lead concentrations ( $11.46$ - $2.64$ - $1.78 \text{ } \mu\text{g.L}^{-1}$ ) at sampling points 3, 4, and 5 (Table 4). The presence of this metal in the water of the Alajua River may be attributed to the fact that these areas are downstream of the Quisapincha-Pumgoloma route.

In sampling points 1, 3, and 5 of the Colorado River, iron (Fe) concentrations exceeding the established water quality standards for aquatic life ( $0.3 \text{ mg.L}^{-1}$ ) were detected. In contrast, at all 5 study points along the Alajua River, iron concentrations ranged from  $0.612$  to  $0.722 \text{ mg.L}^{-1}$ , surpassing the limits set by TULSMA for the preservation of aquatic life (Table 4). This is likely due to the presence of natural sources attributed to soil composition (Borja et al. 2020). The World Health Organization (WHO 2011) mentions that iron concentrations up to  $0.7 \text{ mg.L}^{-1}$  do not pose an immediate threat to public health. However, the accumulation of iron can lead to hemorrhagic necrosis and gastric mucosa disorders (WHO 2011). Furthermore, manganese levels in the Colorado River ( $0.433$ - $0.467 \text{ mg.L}^{-1}$ ) and the Alajua River ( $0.621$ - $0.983 \text{ mg.L}^{-1}$ ) exceeded the criteria for the preservation of aquatic and wildlife in freshwater ( $0.1 \text{ mg/L}$ ) and for agricultural use ( $0.2 \text{ mg.L}^{-1}$ ). Clearly, both rivers show an increase in manganese concentration downstream. The high levels of manganese in the river waters can be attributed to the natural presence of this element in the environment due to the erosion of manganese-containing rocks, volcanic activity, and plant decomposition (Bhuyan et al. 2019).

#### Determination of Metals in Sediment Samples

The concentrations of heavy metals in sediments serve as a key indicator of pollution within the aquatic ecosystem. In the sediment samples collected from the Colorado River, the following metals were detected: Cu, Cd, Ni, Cr, Pb, and  $\text{Cr}^{6+}$ . Similarly, sediment samples from the Alajua River revealed the presence of metals, including Fe, Cu, As, Pb, Ni,  $\text{Cr}^{6+}$ , and Cd.

Hexavalent chromium ( $\text{Cr}^{6+}$ ) exceeded the soil quality criterion of  $0.4 \text{ mg.kg}^{-1}$  in all five sampling stations of both rivers (MAE 2015). Chromium concentrations ranged from  $4.5$  to  $9.7 \text{ mg.kg}^{-1}$  in the Colorado River and from  $2.9$  to  $6.3 \text{ mg.kg}^{-1}$  in the Alajua River (Table 5). This may be due to the geological accumulation of volcanic origin in the soil and processes of erosion and sedimentation in the sampled areas (González et al. 2020).

In terms of copper (Cu), the established limit of  $25 \text{ mg.kg}^{-1}$  has been exceeded at all sampling points in both rivers. Specifically, the highest levels of this metal were recorded at points 1 and 3 of the Colorado River, reaching  $184 \text{ mg.kg}^{-1}$  and  $180 \text{ mg.kg}^{-1}$ , respectively (Table 5). Furthermore, significant copper content was also detected at sampling stations 2, 3, 4, and 5 of the Alajua River, ranging from  $194 \text{ mg.kg}^{-1}$  to  $228 \text{ mg.kg}^{-1}$ . These findings indicate that the Alajua River exhibited a higher copper concentration compared to the Colorado River. The elevated

Table 4: Results of heavy metals in water samples.

Parameter	Units	Colorado River									Alajua River									Maximum permissible limit														
		P1-AF			P2-AF			P3-AF			P4-AF			P5-AF			P1-BM			P2-BM			P3-BM			P4-BM			P5-BM			Table		
		1	2	3	1	2	3	1	2	3	1	2	3	1	2	3	1	2	3	1	2	3	1	2	3	1	2	3	1	2	3			
Arsenic	µg.L <sup>-1</sup>	5.1 ± 0.5	4.9 ± 0.8	5.1 ± 0.3	5.1 ± 0.3	5.1 ± 0.3	5.1 ± 0.3	5.1 ± 0.5	5.0 ± 0.3	5.0 ± 0.1	4.9 ± 0.6	5.9 ± 0.7	5.8 ± 0.9	100	50	100	50	100	100	50	100	50	100	50	100	50	100	50	100	50	100			
Lead	µg.L <sup>-1</sup>	2.8 ± 0.1*	3.9 ± 0.1*	2.2 ± 0.3*	1.2 ± 0.1*	1.2 ± 0.1*	3.3 ± 0.2*	3.3 ± 0.2*	ND	1.8 ± 0.1*	2.6 ± 0.5*	1.8 ± 0.1*	11.5 ± 1.2*	10	1	5000	10	1	5000	10	1	5000	10	1	5000	10	1	5000	10	1	5000			
Nickel	µg.L <sup>-1</sup>	ND	ND	ND	ND	ND	2.1 ± 0.1	2.1 ± 0.1	ND	3.2 ± 0.1	ND	ND	2.4 ± 0.1	-	25	200	-	25	200	-	25	200	-	25	200	-	25	200	-	25	200			
Zinc	µg.L <sup>-1</sup>	3.0 ± 0.1	76 ± 0.1*	67 ± 0.1*	59 ± 0.2*	19 ± 0.2	19 ± 0.2	19 ± 0.2	ND	ND	ND	ND	ND	-	30	2000	-	30	2000	-	30	2000	-	30	2000	-	30	2000	-	30	2000			
Copper	µg.L <sup>-1</sup>	47 ± 1	12 ± 1	4 ± 1	4 ± 1	23 ± 1	23 ± 1	23 ± 1	ND	4 ± 1	11 ± 1	2 ± 1	3 ± 1	2000	5	200	2000	5	200	2000	5	200	2000	5	200	2000	5	200	2000	5	200			
Cadmium	µg.L <sup>-1</sup>	0.2 ± 0.1	0.1 ± 0.1	0.2 ± 0.1	0.2 ± 0.1	0.2 ± 0.1	0.2 ± 0.1	0.2 ± 0.1	0.2 ± 0.1	0.2 ± 0.1	0.3 ± 0.1	0.2 ± 0.1	0.1 ± 0.1	20	1	50	20	1	50	20	1	50	20	1	50	20	1	50	20	1	50			
Hexavalent Chromium	µg.L <sup>-1</sup>	19 ± 3	22 ± 3	20 ± 3	17 ± 2	17 ± 2	17 ± 4	17 ± 4	5 ± 1	26 ± 1	26 ± 1	26 ± 1	26 ± 1	50	32 <sup>Cr</sup>	100	50	32 <sup>Cr</sup>	100	50	32 <sup>Cr</sup>	100	50	32 <sup>Cr</sup>	100	50	32 <sup>Cr</sup>	100	50	32 <sup>Cr</sup>	100			
Iron	mg.L <sup>-1</sup>	0.37 ± 0.01*	0.17 ± 0.04	0.33 ± 0.01*	0.17 ± 0.02	0.36 ± 0.06*	0.36 ± 0.06*	0.36 ± 0.06*	0.61 ± 0.02*	0.65 ± 0.03*	0.65 ± 0.03*	0.72 ± 0.02*	0.72 ± 0.02*	1	0.3	5	1	0.3	5	1	0.3	5	1	0.3	5	1	0.3	5	1	0.3	5			
Manganese	mg.L <sup>-1</sup>	0.43 ± 0.01**	0.43 ± 0.01**	0.47 ± 0.06**	0.37 ± 0.01**	0.47 ± 0.05**	0.47 ± 0.05**	0.47 ± 0.05**	0.62 ± 0.22**	0.79 ± 0.3**	0.81 ± 0.11**	0.98 ± 0.2**	0.90 ± 0.2**	-	0.1	0.2	-	0.1	0.2	-	0.1	0.2	-	0.1	0.2	-	0.1	0.2	-	0.1	0.2			

Note: Values that were not detected by the GFAAS were reported as (ND). Table 1 indicates "Water Quality Criteria for Water Sources for human consumption and domestic use," Table 2 indicates "Water Quality criteria for the preservation of aquatic and wildlife in freshwater, marine, and estuarine waters," and Table 3 indicates "Water quality criteria for water intended for agricultural use" (MAE, 2015). Values that exceed Table 2 are marked with (\*), and those that exceed the limits for agricultural use (Table 3) are marked with (\*\*).



Table 5: Results of heavy metals analyzed in sediment samples.

Parameter	Colorado River					Alajua River					Soil Quality Criterion (TULSMA)
	P1-AF	P2-AF	P3-AF	P4-AF	P5-AF	P1-BM	P2-BM	P3-BM	P4-BM	P5-BM	
pH	7.4±0.1	7.5±0.1	6.7±0.1	7.2±0.1	7.5±0.1	8.0±0.1	7.2±0.1	7.7±0.1	7.0±0.1	6.8±0.1	6-8
Cu	*5.3±0.2	*4.5±0.2	*9.7±0.3	*5.3±0.5	*6.7±0.1	*4.4±0.6	*2.9±0.5	*6.3±0.3	*2.9±0.3	*5.0±0.4	0.4
Cd	*1.1±0.1	*3.4±0.1	*0.8±0.1	*1.4±0.1	*0.7±0.1	*0.2±0.1	0.2±0.1	*1.8±0.3	2.0±0.1	0.6±0.1	25
Ni	11±2	12±1	12±1	16±2	4±2	0.9±0.1	13.8±1	3.7±0.7	4.1±0.7	8.5±4.6	19
Pb	16±5	16±7	3±1	6±4	2±1	2.2±0.5	2.7±1.0	9.0±2	10.5±1.5	2.1±0.4	19

Note: Results that exceeded the soil quality criteria established in Table 1, Annex 2 of Book VI of TULSMA (MAE, 2015) are indicated with (\*).

copper levels in both rivers may result from runoff carrying copper-containing fertilizers and pesticides. Notably, the lower basin of the Alajua River, where more fruit crops are present, shows higher copper accumulation. This suggests that these chemicals are possibly used more frequently in this region, explaining the increased copper content in the river sediments (Shaw et al. 2020).

Cadmium (Cd) exceeded the permissible limit of 0.5 mg.kg<sup>-1</sup> for soil quality in all samples from the 5 sampling zones of the Colorado River, with concentrations ranging from 0.7 to 3.4 mg.kg<sup>-1</sup>. In the case of the Alajua River, it exceeded the regulations in sampling zones 3 and 5, with concentrations of 1.8 and 0.6 mg.kg<sup>-1</sup>, respectively. The contamination of these rivers with cadmium is likely due to processes involving the deposition and release of sulfide minerals in sediments, as well as interactions with phosphate fertilizers used in agriculture or the presence of sedimentary rocks with high Cd levels (Hossain et al. 2019, Sarkar et al. 2021).

### Statistical Analysis of Results

The water and sediment characterization results were analyzed using the ANOVA method. The majority of parameters between the upper and lower zones of the micro-watersheds of both rivers exhibited significant differences with p-values less than 0.05, except for arsenic and cadmium concentrations in water samples collected from the Colorado River.

### The Determination of the Water Quality Index (WQI)

Table 6 displays the calculated values for the Water Quality Index (WQI) using the NSF and Dinius methods for the different sampling points in the Colorado and Alajua rivers.

The calculated NSF - WQI suggests that water quality in the Colorado River can be classified as moderate, as per Quiroz et al. (2017). Conversely, there was a decline in water quality in the sampling areas of the Alajua River, primarily due to elevated concentrations of fecal coliforms, as reported by Castro et al. (2022). This observation aligns with the findings of Pauta et al. (2019), who emphasize that fecal coliforms are the parameter with the most significant impact on water quality in Andean rivers. In some sampling areas of both rivers, signs of agricultural cultivation, livestock grazing, and domestic wastewater discharges were evident, and these activities intensified downstream in each river. Consequently, agricultural runoff can transport various contaminants into the rivers, including animal feces and organic fertilizers, leading to an overall increase in pollution levels, particularly in coliform counts (Pauta et al. 2019).

According to the Dinius Water Quality Index (Dinius 1987), water quality in the Colorado River was mostly classified as contaminated, except point 3, which was deemed acceptable. Consequently, agricultural use may not require treatment, but water treatment would be necessary for human consumption. Similarly, water quality at points 1, 2, and 3 in the Alajua River was deemed acceptable, suggesting that minimal purification may be necessary for agricultural uses. However, points 4 and 5 exhibited slight contamination, primarily due to anthropogenic activities in the area, such as fruit cultivation, domestic wastewater discharge, and mining. This contamination resulted in a decrease in the Water Quality Index (WQI) in the lower basin areas, as observed in Table 7 (Sierra 2011).

Additionally, it can be noted that the Colorado and Alajua Rivers have average NSF - WQI values of 59 and 67, respectively, indicating that the overall water quality is considered moderate for general use. However, the average DINIUS-WQI value for the Colorado River is 72, suggesting slight contamination, and thus, purification is necessary for crops requiring high-quality water. For human consumption, treatment is also required. In the case of the Alajua River, the average DINIUS-WQI value is 79, indicating acceptable water quality. Furthermore, for agricultural use, treatment is not necessary, but for human consumption, minimal purification will be required (Dinius 1987).

### Heavy Metal Evaluation Index (HEI)

Table 7 presents the calculated values of the Heavy Metal Evaluation Index (HEI) for water and sediment samples collected in the Colorado and Alajua Rivers.

In terms of heavy metal presence in the water samples collected from different points along the Colorado River, points 1, 2, 3, and 5 exhibit Heavy Metal Evaluation Index (HEI) values ranging from 12.0 to 18.7, indicating a moderate level of contamination. Point 4 is the only sampling location with an HEI value below 10, registering 9.1, signifying a low

level of contamination. The average HEI for the Colorado River stands at 13.9, placing it in the category of moderately contaminated with heavy metals (Boateng et al. 2015). The major contributors to the HEI in this river are manganese, copper, and lead. Furthermore, the HEI values in sediments exhibited a range between 24.1 and 33.8, signifying a higher degree of pollution in the sediments as compared to the water. This can be attributed to both the volcanic composition of the soil and the diminished transport of heavy metals in the sediments, resulting in their accumulation.

Conversely, the Alajua River displays a trend of increasing heavy metal contamination from its upper zones (points 1, 2, and 3, with low and moderate contamination levels) to the lower zones (points 4 and 5, with moderate and high contamination levels). The HEI value for the Alajua River reaches 15.4, surpassing the value recorded for the Colorado River. In the case of the Alajua River, the key metals contributing to HEI are manganese, lead, and iron. Ultimately, the HEI values within the sediment samples ranged from 16.4 to 28.0, with an average HEI of 20.6, signifying an increased level of pollution within the sediments when compared to the water. Similar to the situation observed in the Colorado River, this phenomenon could be attributed to the accumulation of heavy metals resulting from reduced mobility in the solid phase and the influence of the volcanic origin of the soil.

### CONCLUSIONS

The water quality of the Colorado and Alajua rivers was assessed through the analysis of physicochemical parameters, microbiological tests, and the measurement of heavy metal concentrations in surface water and sediment samples using various methods. This comprehensive approach provided precise data on substances exceeding acceptable water quality standards for human consumption, aquatic ecosystem preservation, and agricultural irrigation. Additionally, investigations into potential factors contributing to the

Table 6: Values obtained according to NSF-WQI and Dinius-WQI.

Sampling points	NSF - WQI		DINIUS - WQI	
	General criteria		Agricultural & Human consumption criteria	
	Colorado	Alajua	Colorado	Alajua
1	67 (fair)	75 (good)	69 (slightly contaminated)	84 (acceptable)
2	53 (fair)	69 (fair)	75 (slightly contaminated)	83 (acceptable)
3	69 (fair)	69 (fair)	79 (slightly contaminated)	83 (acceptable)
4	53 (fair)	62 (fair)	67 (slightly contaminated)	73 (slightly contaminated)
5	51 (fair)	60 (fair)	70 (slightly contaminated)	72 (slightly contaminated)
Average	59 (fair)	67 (fair)	72 (slightly contaminated)	79 (slightly contaminated)

Table 7: Values obtained from the Heavy Metal Evaluation Index (HEI) for water and sediment samples from the Colorado and Alajua rivers.

Sampling Points	Heavy Metal Evaluation Index in Water (HEI)		Heavy Metal Evaluation Index in Sediments (HEI)	
	Colorado River	Alajua River	Colorado River	Alajua River
1	18.7 (moderate)	8.7 (low)	24.2 (high)	18.7 (moderate)
2	14.6 (moderate)	12.1 (moderate)	26.3 (high)	16.4 (moderate)
3	12.0 (moderate)	16.3 (moderate)	33.8 (high)	28.0 (high)
4	9.1 (low)	15.5 (moderate)	24.1 (high)	16.4 (moderate)
5	15.4 (moderate)	24.7 (moderate)	25.6 (high)	23.6 (high)
Average	13.9 (moderate)	15.4 (moderate)	26.7 (high)	20.6 (moderate)

decline in water quality in the sampling areas were carried out, considering environmental, geological, and human-related factors.

Most parameters across the upper and lower zones of both rivers' micro-watersheds show significant differences with p-values below 0.05. However, exceptions were observed in the arsenic and cadmium concentrations within water samples collected from the Colorado River. When comparing the results of water characterization with the Ecuadorian environmental legal requirements, most parameters met acceptable limits for human and domestic consumption. However, certain parameters in the Colorado River exceeded the criteria for the preservation of aquatic life. For instance, fecal coliform levels exceeded the limit. However, the more challenging issue lies in the presence of heavy metals. Zinc (Zn) levels in Colorado River water samples were elevated at points 2 ( $76 \mu\text{g.L}^{-1}$ ), 3 ( $67 \mu\text{g.L}^{-1}$ ), and 4 ( $59 \mu\text{g.L}^{-1}$ ), surpassing the maximum permissible limit (MPL) of  $30 \mu\text{g.L}^{-1}$ . Additionally, lead levels ranged from  $1.2 \mu\text{g.L}^{-1}$  to  $3.9 \mu\text{g.L}^{-1}$ , exceeding the MPL of  $1 \mu\text{g.L}^{-1}$ . In terms of iron (Fe) concentration, points 1, 3, and 5 slightly exceeded the  $0.3 \text{ mg.L}^{-1}$  criteria, with values of  $0.37 \text{ mg.L}^{-1}$ ,  $0.33 \text{ mg.L}^{-1}$ , and  $0.36 \text{ mg.L}^{-1}$ , respectively. Furthermore, manganese (Mn) concentrations ranged between  $0.37 \text{ mg.L}^{-1}$  and  $0.47 \text{ mg.L}^{-1}$ , surpassing the irrigation water quality criterion for Mn, which has a maximum limit of  $0.2 \text{ mg.L}^{-1}$ .

Regarding the Alajua River, parameters that exceeded the permissible limit for the preservation of aquatic life included copper at point 3, measuring  $11 \mu\text{g.L}^{-1}$  (MPL of  $5 \mu\text{g.L}^{-1}$ ), iron, with concentrations ranging from  $0.61 \text{ mg.L}^{-1}$  to  $0.79 \text{ mg.L}^{-1}$  (MPL of  $0.30 \text{ mg.L}^{-1}$ ), and manganese, with values ranging from  $0.62 \text{ mg.L}^{-1}$  to  $0.98 \text{ mg.L}^{-1}$  (MPL of  $0.10 \text{ mg.L}^{-1}$ ).

The altered concentrations of heavy metals may originate from the volcanic geological conditions in both rivers. In most cases, sample points on the upper side of the micro-watershed (sampling points 1, 2, and 3) exhibited higher concentrations of heavy metals (lead, iron, zinc, copper, and

manganese) than the maximum permissible limits (MPL). Additionally, river sediments displayed an accumulation of heavy metals, including hexavalent chromium, copper, and cadmium, exceeding the MPL for these metals in soil.

Furthermore, the Heavy Metal Evaluation Index (HEI) in sediment samples showed higher values, ranging from 16.4 to 33.8, in comparison to HEI values in water samples, which ranged from 8.7 to 24.7. These results emphasize the necessity for further investigation into the sources of heavy metals, their transport in water and sediments, and the potential direct exposure to metals through human consumption of water, as well as indirect exposure through agricultural feedstock and livestock farming.

Overall, the assessment of water quality using the NSF-WQI indicated that the Colorado and Alajua rivers in all five sampling zones exhibited regular to moderate levels of contamination. According to the Dinius index, a "slightly contaminated" level was observed in all sampling points, except at points 1, 2, and 3 (84, 83, and 83) of the Alajua River, which showed an "acceptable" level. In relation to heavy metal pollution, it is recommended to purify the water for human consumption due to the excessive presence of coliforms, Zn, Pb, Fe, and Mn.

Finally, it is advisable to implement specific actions, such as limiting intensive agriculture and livestock in certain areas of the watershed and defining water source protection zones. This will help preserve water resource quality and protect consumer health.

## ACKNOWLEDGMENTS

The authors acknowledge the support and suggestions of the "Gestión de Recursos Naturales e Infraestructura Sustentable" (GeReNIS) research group of the Technical University of Ambato.

Authors acknowledge the support of the Project "Canje de Deuda Ecuador-España: Fortalecimiento de la unidad



operativa de investigación (FITA-UOITA)” Faculty of Food Science and Biotechnology Engineering, Technical University of Ambato, Ecuador.

## REFERENCES

- American Public Health Association, 2017. *Standard methods for the examination of water and wastewater*. 23rd ed. American Public Health Association.
- Badrzadeh, N., Samani, J., Mazaheri, M. and Kuriqi, A., 2022. Evaluation of management practices on agricultural nonpoint source pollution discharges into the rivers under climate change effects. *Science of the Total Environment*, 838, p.156643.
- Bhuyan, M.S., Bakar, M.A., Rashed-Un-Nabi, M., Senapathi, V., Chung, S.Y. and Islam, M.S., 2019. Monitoring and assessment of heavy metal contamination in surface water and sediment of the Old Brahmaputra River, Bangladesh. *Applied Water Science*, 9(5), pp.1-13.
- Boateng, T.K., Opoku, F., Acquah, S.O. and Akoto, O., 2015. Pollution evaluation, sources and risk assessment of heavy metals in hand-dug wells from Ejisu-Juaben Municipality, Ghana. *Environmental Systems Research*, 4(1), p.16.
- Borja, P., Ochoa, V., Maurice, L., Morales, G., Quilumbaqui, C., Tejera, E. and Machado, A., 2020. Determination of the microbial and chemical loads in rivers from the Quito Capital Province of Ecuador (Pichincha): A preliminary analysis of microbial and chemical quality of the main rivers. *International Journal of Environmental Research and Public Health*, 17(1), p.5048.
- Cantera, K., Carvajal, Y. and Castro, L., 2009. Environmental flow: Concepts, experiences, and challenges [Caudal ambiental: Conceptos, experiencias y desafíos]. *Universidad del Valle*.
- Carvajal, E., 2017. Análisis integral de la calidad de agua del río Ambato, mediante la utilización de indicadores biológicos, complementadas con variables fisicoquímicas, para la generación de propuestas de gestión [Comprehensive analysis of water quality in the Ambato River, using biological indicators, complemented with physicochemical variables, for the generation of management proposals]. (Thesis. *Escuela Politécnica Nacional*).
- Castro, R., Oliveira, S., Borges, D., da Silva, D. and dos Santos, W., 2022. Soil losses related to land use and rainfall seasonality in a watershed in the Brazilian Cerrado. *Journal of South American Earth Sciences*, 119 (November 2022), p.104020.
- Chiliquinga, C. and Donoso, H., 2012. Caracterización de la calidad de agua de la microcuenca del río Pachanlica de la provincia de Tungurahua tomando como base la metodología ICA de Montoya [Characterization of water quality of the Pachanlica River micro-basin in the province of Tungurahua using Montoya's ICA methodology]. (Thesis. *Facultad de Ciencias, Escuela Politécnica de Chimborazo*).
- Dinius, S.H., 1987. Design of an index of water quality. *JAWRA Journal of the American Water Resources Association*, 23(5), pp.833-843.
- Ding, T.T., Du, S.L., Huang, Z.Y., Wang, Z.J., Zhang, J., Zhang, Y.H., Liu, S.S. and He, L.S., 2021. Water quality criteria and ecological risk assessment for ammonia in the Shaying River Basin, China. *Ecotoxicology and Environmental Safety*, 215 (December 2020), p.112141.
- Edet, A.E. and Offiong, O.E., 2002. Evaluation of water quality pollution indices for heavy metal contamination monitoring. A study case from the Akpabuyo-Odukpani area, Lower Cross River Basin (southeastern Nigeria). *GeoJournal*, 57(4), pp.295-304.
- Flores, L., 2022. Evaluación de la calidad del agua del río Tomebamba basado en un análisis jerárquico para identificar los pesos de los parámetros de un índice propio de calidad del agua [Evaluation of the water quality of the Tomebamba River based on a hierarchical analysis to identify the weights of the parameters of a custom water quality index]. (Thesis. *Universidad de Cuenca*).
- Fournier, M., Castillo, L., Ramírez, F., Moraga, G. and Ruepert, C., 2019. Evaluación preliminar del área agrícola y su influencia sobre la calidad del agua en el Golfo Dulce, Costa Rica [Preliminary evaluation of the agricultural area and its influence on water quality in Golfo Dulce, Costa Rica]. *Revista de Ciencias Ambientales*, 53, pp.92-112.
- González, J., Martínez Robaina, A., Amaral Sobrinho, N.M. and Zonta, E., 2020. Los ambientes geológicos en la acumulación de metales pesados en suelos de Pinar del Río. *Cultivos Tropicales*, 41(2), pp.1-21.
- Guananga-Díaz, F., Carbonel, H.C., Escobar-Arrieta, S., Guerrero-Rivera, A., Mendoza, B. and Guananga-Díaz, N.I., 2022. Influence of geomorphology and flow on the water quality of Guano River, Ecuador. *Novasinergia*, 5(2), pp.174-192.
- Herrmann, P., 2002. Management conflicts in the Ambato River watershed, Tungurahua province, Ecuador. *Mountain Research and Development*, 22(4), pp.338-340.
- Hong, H., Qiu, J. and Liang, Y., 2010. Environmental factors influencing the distribution of total and fecal coliform bacteria in six water storage reservoirs in the Pearl River Delta Region, China. *Journal of Environmental Sciences*, 22(5), pp.663-668.
- Hossain, M.S., Latifa, G.A., Prianqa and Nayeem, A.A., 2019. Review of cadmium pollution in Bangladesh. *Journal of Health and Pollution*, 9(23).
- Ministerio del Ambiente del Ecuador, 2015. *Libro IV del texto unificado de legalización secundaria del Ministerio del Ambiente: Normativa de calidad ambiental y de descargas de efluentes al recurso agua* [Book IV of the unified text of secondary legislation from the Ministry of Environment: Environmental quality standards and effluent discharge regulations for water resources]. Registro Oficial No. 387.
- Matta, G. and Gjyli, L., 2016. Mercury, lead and arsenic: Impact on environment and human health. *Journal of Chemical and Pharmaceutical Sciences*, 9(2), pp.718-725.
- Mekuria, D.M., Kassegne, A.B. and Asfaw, S.L., 2021. Assessing pollution profiles along Little Akaki River receiving municipal and industrial wastewaters, Central Ethiopia: Implications for environmental and public health safety. *Heliyon*, 7(7), p.e07526.
- Méndez, P., Arcos, J. and Cazorla, X., 2020. Determination of the water quality index (NSF) of the Copueno River located in Morona Canton. *Dominio de Las Ciencias*, 6(2), pp.734-746.
- Moyel, M., Hassan, W.F. and Amteghy, A.H., 2015. Application and evaluation of water quality pollution indices for heavy metal contamination as a monitoring tool in Shatt Al Arab River. *Journal of International Academic Research for Multidisciplinary*, 3(4), pp.67-75.
- Larrea-Murrell, J.A., Rojas Badia, M.M., Romeu Alvarez, B., Rojas Hernandez, M.R. and Heydrich Pérez, M., 2013. Bacteria indicative of fecal contamination in the evaluation of water quality: literature review. *Revista CENIC. Ciencias Biológicas*, 44, pp.24-34.
- Pal, A., Pal, M., Mukherjee, P., Bagchi, A. and Raha, A., 2018. Determination of the hardness of drinking packaged water in the Kalyani area, West Bengal. *Asian Journal of Pharmacy and Pharmacology*, 4(2), pp.203-206.
- Pauta, G., Velasco, M., Gutiérrez, D., Vázquez, G., Rivera, S., Morales, Ó. and Abril, A., 2019. Evaluación de la calidad del agua de los ríos de la ciudad de Cuenca, Ecuador. *Maskana*, 10(2), pp.76-88.
- Pérez, S., 2015. Gestión actual de los recursos hídricos en la subcuenca del río Ambato desde los actores [Current management of water resources in the Ambato River sub-basin from the actors]. Provincial Government of Tungurahua.
- Plúas, A., 2019. Determination of Total Coliforms and Escherichia Coli in the Chullupe Estuary of the Santa Elena Canton, Province of Santa Elena. (Thesis. *University of Guayaquil*).
- Prasad Ahrivar, B., Das, P., Srivastava, V. and Kumar, M., 2023. Perspectives of heavy metal pollution indices for soil, sediment, and water pollution evaluation: An insight. *Total Environment Research Themes*, 6, p.100039.

- Quiroz, L., Izquierdo, E. and Menéndez, C., 2017. Aplicación del índice de calidad de agua en el río Portoviejo, Ecuador. *Revista de Ingeniería Hidráulica y Ambiental*, 38(3), pp.41-51.
- Reichart, O., Szakmár, K., Jozwiak, Á., Felföldi, J. and Baranyai, L., 2007. Redox potential measurement as a rapid method for microbiological testing and its validation for coliform bacteria determination. *International Journal of Food Microbiology*, 114(2), pp. 143-148.
- Reitter, C., Petzoldt, H., Korth, A., Schwab, F., Stange, C., Hamsch, B., Tiehm, A., Lagkouvardos, I., Gescher, J. and Hügler, M., 2021. Seasonal dynamics in the number and composition of coliform bacteria in drinking water reservoirs. *Science of The Total Environment*, 787, pp.2-15.
- Rezaei, A., Hassani, H., Hassani, S., Jabbari, N., Fard Mousavi, S.B. and Rezaei, S., 2019. Evaluation of groundwater quality and heavy metal pollution indices in Bazman basin, southeastern Iran. *Groundwater for Sustainable Development*, 9, p.100245.
- Romero, M., Santamiaría, D. and Zafra, C., 2009. Bioingeniería y suelo: Abundancia microbiológica, pH y conductividad eléctrica bajo tres estratos de erosión. *Umbra Científico*, 15(1), pp.67-74.
- Sánchez, M., Pérez, L., Córdova, M. and Cabrera, D., 2020. Heavy metal contamination in the Cotopaxi and Tungurahua rivers: a health risk. *Environmental Earth Sciences*, 79(6), p.144.
- Sarkar, B., Mukhopadhyay, R., Ramanayaka, S., Bolan, N. and Ok, Y.S., 2021. The role of soils in the disposition, sequestration, and decontamination of environmental contaminants. *Philosophical Transactions of the Royal Society B: Biological Sciences*, 376(1834), p.101145.
- Shaw, J.L.A., Ernakovich, J.G., Judy, J.D., Farrell, M., Whatmuff, M. and Kirby, J., 2020. Long-term effects of copper exposure to agricultural soil function and microbial community structure at a controlled and experimental field site. *Environmental Pollution*, 263, p.114411.
- Sierra, C., 2011. Calidad del agua: Evaluación y diagnóstico [Water quality: Evaluation and diagnosis]. (Undergraduate thesis, *Universidad de Medellín*). Institutional Repository UDEM.
- Sonone, S.S., Jadhav, S.V., Sankhla, M.S. and Kumar, R., 2020. Water contamination by heavy metals and their toxic effect on aquaculture and human health through food chain. *Letters in Applied NanoBioScience*, 10(2), pp.2148-2166.
- Strokal, M., Kahil, T., Wada, Y., Albiac, J., Bai, Z., Ermolieva, T. and Kroeze, C., 2020. Cost-effective management of coastal eutrophication: A case study for the Yangtze river basin. *Resources, Conservation & Recycling*, 154, p.104635.
- Timmerman, J., 2011. Bridging the water information gap: Structuring the process of specification of information needs in water management. (Doctoral thesis, *Wageningen University*).
- Torres, C., Valencia, N. and Bonilla, A., 2018. Planteamiento de una metodología para el cálculo de un índice de calidad del agua para el río Machángara, cuenca alta del río Guayllabamba [Proposal of a methodology for calculating a water quality index for the Machángara River, upper Guayllabamba River basin]. (Thesis, *Escuela Politécnica Nacional*).
- Tu, Y.J., You, C.F. and Kuo, T.Y., 2020. Source identification of Zn in Erren River, Taiwan: An application of Zn isotopes. *Chemosphere*, 248(100), p.126044.
- Uddin, M.G., Nash, S. and Olbert, A.I., 2021. A review of water quality index models and their use for assessing surface water quality. *Ecological Indicators*, 122, p.107218.
- United States Environmental Protection Agency, 2013. *Aquatic life ambient water quality criteria for ammonia - freshwater 2013* (Report No. EPA-822-R001-13-). United States Environmental Protection Agency.
- Vajargah, M.F., 2021. A review of the effects of heavy metals on aquatic animals. *Journal of Biomedical Research & Environmental Sciences*, 2(9), pp.865-869.
- Vega, C., 2021. Evaluación de la calidad del agua y sedimento de la subcuenca del río Birrís, en cuanto a su contenido de metales pesados [Evaluation of water and sediment quality in the Birrís River sub-basin, regarding its heavy metal content]. (Thesis, *Instituto Tecnológico de Costa Rica, Escuela de Química, Carrera de Ingeniería Ambiental*).
- Vinueza, D., Ochoa-Herrera, V., Maurice, L., Tamayo, E., Mejía, L., Tejera, E. and Machado, A., 2021. Determining the microbial and chemical contamination in Ecuador's main rivers. *Scientific Reports*, 11(1), pp.1-15.
- World Health Organization, 2011. *Guidelines for drinking-water quality*. 4th ed. World Health Organization.

---

#### ORCID DETAILS OF THE AUTHORS

- Rodny Peñafiel: <https://orcid.org/0000-0003-1923-2525>  
 Fabián Rodrigo Morales-Fiallos: <https://orcid.org/0000-0002-0655-8684>  
 Bolívar Paredes-Beltrán: <https://orcid.org/0000-0002-8071-8500>  
 Dilon Moya: <https://orcid.org/0000-0002-7692-3069>  
 Adriana Jacqueline Frias Carrion: <https://orcid.org/0009-0009-5634-886X>  
 Belén Moreano: <https://orcid.org/0009-0002-7746-3612>



# Hepatotoxic Effects of Gaseous Sulfur Dioxide (SO<sub>2</sub>), Nitrogen Dioxide (NO<sub>2</sub>), and Their Mixture on Sea Bass (*Centropristis striata*): Hematological, Biochemical and Genotoxic Studies

N. Gandhi<sup>1</sup>, Y. Rama Govinda Reddy<sup>2</sup> and Ch. Vijaya<sup>1†</sup>

<sup>1</sup>Department of Marine Biology, Vikrama Simhapuri University, Nellore, Andhra Pradesh, India

<sup>2</sup>Department of Physiology, Green Fields Institute of Agriculture Research and Training, Hyderabad, Telangana, India

†Corresponding author: Ch.Vijaya; vijayalch@gmail.com

Nat. Env. & Poll. Tech.  
Website: [www.neptjournal.com](http://www.neptjournal.com)

Received: 22-01-2024

Revised: 26-02-2024

Accepted: 22-03-2024

## Key Words:

Hepatotoxicity

Genotoxicity

Sea bass (*Centropristis striata*)

Gaseous pollutants

Aquatic environment

Physiological disturbances

Water quality

## ABSTRACT

This study meticulously explores the intricate hepatotoxic effects stemming from acute exposure to gaseous sulfur dioxide (SO<sub>2</sub>), nitrogen dioxide (NO<sub>2</sub>), and their amalgamation on sea bass (*Centropristis striata*). Employing a comprehensive approach involving hematological, cytotoxic, and histochemical analyses, the research provides crucial insights into the potential adverse impacts of these pollutants on fish health. The examination specifically focuses on the effects of SO<sub>2</sub>+NO<sub>2</sub> on hematological, histochemical, and serum biochemical parameters in *Centropristis striata*. Treatment groups, subjected to LC<sub>30</sub>, LC<sub>50</sub>, and LC<sub>90</sub> acute exposure of gaseous SO<sub>2</sub>, NO<sub>2</sub>, and SO<sub>2</sub>+NO<sub>2</sub>, alongside a control group, underwent evaluation of parameters such as red and white blood cells, hemoglobin, hematocrit, mean corpuscular hemoglobin, mean corpuscular volume, mean corpuscular hemoglobin concentration, alanine aminotransferase, aspartate aminotransferase, alkaline phosphatase, acid phosphatase, lactate dehydrogenase, total protein, albumin, serum creatinine, and blood urea. At the 96<sup>th</sup> hour, RBC values decreased, and WBC values increased in all experimental conditions compared to the control group (p>0.05). MCV and MCH increased with the concentration of gaseous pollutants and exposure time (p>0.05). Hematological parameter variations underscore disruptions in blood composition and immune responses. Simultaneously, alterations in serum biochemical parameters suggest potential impairments in liver and kidney functions, along with disturbances in lipid metabolism. Significant declines in albumin levels, indicating potential liver dysfunction or inflammation due to SO<sub>2</sub> and NO<sub>2</sub> exposures, were observed at all experimental conditions, while decreased globulin levels suggest immunosuppressive effects from combined pollutants. A substantial increase in the albumin/globulin ratio further signals an imbalance indicative of potential liver dysfunction or inflammation. Varied responses in liver enzyme levels (SGPT/ALT, SGOT/AST, ALP) underscore potential liver damage or injury (p<0.05). These findings deepen our understanding of environmental impacts on aquatic ecosystems, emphasizing the need for ongoing efforts to ensure the health and sustainability of fish populations in polluted environments.

## INTRODUCTION

The impact of sulfur dioxide (SO<sub>2</sub>), nitrogen dioxide (NO<sub>2</sub>), and other gaseous pollutants on marine fish has been the subject of numerous studies in recent years. These pollutants are produced by various human activities such as industrial processes, transportation, and energy production and have been found to have detrimental effects on the environment and its inhabitants. The following literature review provides an overview of the impact of SO<sub>2</sub>, NO<sub>2</sub>, and other gaseous pollutants on marine fish, with a focus on their growth and physiological, morphological, biochemical, and molecular response. Several studies have shown that exposure to SO<sub>2</sub>

and NO<sub>2</sub> can lead to decreased growth and development in marine fish. For example, a study by Liu et al. (2019) found that exposure to SO<sub>2</sub> resulted in decreased body weight and length in juvenile turbot. Similarly, exposure to NO<sub>2</sub> has been shown to reduce growth rates in juvenile Atlantic salmon (Collier et al. 2004). These studies suggest that gaseous pollutants may have a negative impact on the growth and development of marine fish. In addition to growth, exposure to gaseous pollutants can also have physiological effects on marine fish. For example, studies have shown that exposure to SO<sub>2</sub> and NO<sub>2</sub> can lead to changes in gill structure and function, which can affect respiration and ion regulation in fish (Aruoma et al. 1990, Bransden et al. 2002). Exposure

to SO<sub>2</sub> has also been shown to decrease heart rate and blood pressure in juvenile turbot (Liu et al. 2019). These findings suggest that gaseous pollutants can have a significant impact on the physiology of marine fish. Exposure to gaseous pollutants can also lead to morphological changes in marine fish. For example, a study by Choudhary et al. (2015) found that exposure to SO<sub>2</sub> resulted in abnormal development of the swim bladder in zebrafish. Similarly, exposure to NO<sub>2</sub> has been shown to cause damage to the liver and spleen in juvenile Atlantic salmon (Collier et al. 2004). These studies suggest that exposure to gaseous pollutants can have detrimental effects on the morphology of marine fish. Biochemical and molecular studies have also shown that exposure to gaseous pollutants can affect the metabolism and gene expression of marine fish. For example, a study by Wong et al. (2016) found that exposure to SO<sub>2</sub> and NO<sub>2</sub> led to changes in the expression of genes involved in oxidative stress and immune response in juvenile coibia. Similarly, exposure to SO<sub>2</sub> has been shown to increase the activity of antioxidant enzymes in the liver of juvenile turbot (Liu et al. 2019). These findings suggest that exposure to gaseous pollutants can have a significant impact on the biochemical and molecular response of marine fish. The literature suggests that exposure to SO<sub>2</sub>, NO<sub>2</sub>, and other gaseous pollutants can have significant impacts on the growth, physiology, morphology, and biochemical and molecular response of marine fish. These effects can lead to decreased growth rates, changes in gill structure and function, morphological abnormalities, and alterations in metabolism and gene expression. It is important to continue researching the impact of gaseous pollutants on marine fish in order to better understand the potential long-term effects on these important organisms and the ecosystems in which they reside.

Biochemical analysis is a valuable tool for identifying target organs affected by toxicity, assessing the overall health status of organisms, and providing early warning signs of stress (Dube et al. 2014, Sayed et al. 2011, 2017). In aquatic animals, histochemical examination of the liver serves as an indicator of the effects of toxin exposure in the aquatic environment (Fernandes et al. 2008, Ramesh & Nagarajan 2013, Singh et al. 2018). The liver structure of teleost fish is particularly sensitive to environmental changes, and exposure to nanoparticles has been shown to cause a notable decline in cell membrane integrity, reduced metabolic activity, and, in some cases, hepatocyte apoptosis or necrosis (Ahamed et al. 2009, Farkas et al. 2010, Hao et al. 2009). Fish are commonly employed as indicators to assess environmental pollution and the overall health of aquatic ecosystems, primarily due to their sensitivity to environmental changes and their physiological responses (Rajkumar et al. 2016). Among the fish species used for such studies, sea bass

(*Centropristis striata*) is particularly favored. This species exhibits remarkable adaptability, being capable of tolerating both well-oxygenated and poorly oxygenated waters, and can even survive for extended periods outside of water (Hecht et al. 1988, Safriel & Bruton 1984). As a result, sea bass (*Centropristis striata*) is extensively utilized as a biological indicator in ecotoxicological investigations. Its ability to withstand varying environmental conditions makes it a valuable model organism for assessing the impact of pollutants and studying the physiological changes that occur in response to environmental stressors. According to the aforementioned findings, the present work was suggested and was aimed at studying the hepatotoxicity of sea bass (*Centropristis striata*) exposed with acute dosages (LC<sub>30</sub>, LC<sub>50</sub>, and LC<sub>90</sub>) of gaseous SO<sub>2</sub>, NO<sub>2</sub>, and their mixture in an attempt to determine toxicity level and impact on biochemical, hematological and genotoxicity parameters.

## MATERIALS AND METHODS

### Determination of Hematological Parameters

To investigate the effects of gaseous pollutants on fish health, blood samples were collected from experimental fish exposed to different concentrations of gaseous SO<sub>2</sub>, NO<sub>2</sub>, and a mixture of SO<sub>2</sub>+NO<sub>2</sub> (LC<sub>30</sub>, LC<sub>50</sub>, and LC<sub>90</sub>). Control treatment fish were also included in the study. The blood samples were collected using a 24-gauge needle and stored in heparinized glass tubes to prevent clotting. To assess the hematological parameters, the method described by Dacie and Lewis (1984) was employed. This method allows for the evaluation of various blood parameters, including total Red Blood Cells (RBC), White Blood Cells (WBC), Hemoglobin (Hb), Hematocrit (Ht), Mean Cell Hemoglobin (MCH), and Mean Cell Hemoglobin Concentration (MCHC). The experiments were conducted in triplicates, and the mean values were calculated for further analysis and interpretation of the results.

### Enumeration of Red Blood Corpuscles (RBC)

A hemocytometer pipette collected blood samples up to the 0.5 mark, diluted at 1:200, mixed, and a drop transferred to a counting slide. Five sets of sixteen squares were examined with a microscope. Only squares on the upper and left-hand lines were counted. The total RBC count was calculated using a standard formula (Dacie & Lewis 1984). This method, employing a Neubauer chamber, ensures accurate RBC counts in hematological studies (Kanu et al. 2023, Rohani 2013), providing valuable insights into the health and physiological responses of organisms under different experimental conditions.

$$\text{Number of RBC/Cu mm} =$$

$$\frac{\text{Total no. of corpuscles counted}}{\text{Total no. of small squares counted}} \times \text{dilution} \times 10$$

#### Enumeration of White Blood Corpuscles (WBC)

The Neubauer Counting Chamber was used to determine WBC counts in control and treated fish. Blood samples were drawn using a WBC pipette, diluted 1:20 with Turk's fluid, and transferred to a counting slide (Dacie & Lewis 1984). Four sets of sixteen squares were counted. This method, introduced by Hans Neubauer, is widely employed in hematology studies for accurate WBC counts, providing insights into immune responses and overall health status in various organisms (Adhikari et al. 2004, Barcellos et al. 2004). Standardized protocols and Turk's fluid ensure reliable results for comparisons across studies, allowing assessment of factors like pollutants on immune systems in marine organisms.

$$\text{Number of WBC/Cu mm} =$$

$$\frac{\text{Total no. of leucocytes counted}}{\text{Total no. of large squares counted}} \times \text{dilution} \times 10$$

#### Estimation of Hemoglobin (Hb) Content

Sahli's Haemometer, produced by Superior, Germany, measures blood hemoglobin (Hb) content in grams per 100 mL. It employs permanent glass standards for accurate colorimetric Hb assessment, widely used in clinical and research settings. Introduced by Hermann Sahli in the late 19<sup>th</sup> century (Campbell 1999, Tavares & Moraes 2007), the instrument provides reliable and consistent Hb measurements, crucial for evaluating oxygen-carrying capacity and overall health in individuals or organisms (Agrawal & Srivastava 1980). Trusted in clinical diagnostics, hematology, and physiology, Sahli's Haemometer offers a practical and cost-effective solution for Hb estimation.

#### Determination of Haematocrit Value (Ht or Packed Cell Volume)

Hematocrit values were evaluated by centrifuging heparinized hematocrit tubes (Germany) at 7000 rpm for 30 min. The process separated blood components, allowing the calculation of hematocrit as a percentage based on packed cell volume (PCV). This widely recognized method in clinical and research settings involves centrifugation to quantify red blood cell concentration (Aguigwo 1998). The use of heparinized tubes ensures proper anticoagulation

during centrifugation. Hematocrit values are crucial for assessing blood composition, diagnosing conditions like anemia or dehydration, and monitoring hematological disorders (Annune et al. 1994).

#### Mean Corpuscular Volume (MCV)

The Mean Corpuscular Volume (MCV) content was determined based on the values of packed cell volume (PCV) and erythrocyte count using a specific formula. MCV is expressed in femtoliters (fL), which represents the average volume of individual red blood cells.

$$\text{MCV} =$$

$$\frac{\text{PCV} \times 10}{\text{Erythrocyte count (million cells/Cu mm blood)}}$$

#### Mean Corpuscular Hemoglobin (MCH)

The Mean Corpuscular Hemoglobin (MCH) content was estimated based on the values of hemoglobin content and erythrocyte count using a specific formula. MCH is expressed in picograms (pg), which represent the average amount of hemoglobin within individual red blood cells.

$$\text{MCH} =$$

$$\frac{\text{Hb (g/100 mL)} \times 10}{\text{Erythrocyte count (million cells/Cu mm blood)}}$$

#### Estimation of Mean Cell Hemoglobin Concentration (MCHC)

The Mean Cell Hemoglobin Concentration (MCHC) was determined based on the values of hemoglobin and the hematocrit percentage using a specific formula. MCHC represents the average concentration of hemoglobin within individual red blood cells and is expressed as a percentage.

$$\text{MCHC} = \frac{\text{Hb (g/100 mL)}}{\text{Hematocrit percentage}}$$

The estimation of MCHC using the hemoglobin content and hematocrit is a standard method employed in clinical hematology to assess the concentration of hemoglobin within red blood cells. MCHC serves as an important parameter in the diagnosis and classification of various types of anemia and other blood disorders. It provides insights into the hemoglobin status and the cellular characteristics of red blood cells, contributing to the overall evaluation of an individual's hematological profile (Dacie & Lewis 1984).

### Differential Leucocytes Count

Differential leucocyte counts were conducted using Leishman/Giemsa stained blood smears, a widely accepted method for identifying and quantifying various white blood cell types (Annune & Ahume 1998, Bouck & Ball 1996). Observation under a microscope at 10X and 100X magnifications involved a systematic scanning approach, examining at least 100 white blood cells. Types of white blood cells were identified based on morphology and staining patterns (Britton 1963, Brown et al. 2006). Counts of each cell type were recorded, and percentages were calculated by dividing the count of a specific cell type by the total observed and multiplying by 100. This method, crucial in research and clinical settings, provides insights into immune response, infections, and pathological conditions (Annino 1976, Larsson & Johansson 1976). Adherence to standard procedures and references is recommended for accurate differential leucocyte counts.

### Determination of Erythrocyte Sedimentation Rate (ESR)

The blood sample was thoroughly mixed, and 200 mm of the mixed sample was drawn into a Westergren tube. The Westergren tube was then positioned vertically and left undisturbed for 60 min. After the designated time, the level of sedimentation in the tube, known as the erythrocyte sedimentation rate (ESR), was measured and recorded. The measurement of ESR using the Westergren method is a widely recognized and standardized procedure for assessing inflammation and various medical conditions Westergren 1921 (Grzybowski et al. 2011, ICSH 1993). The rate of erythrocyte sedimentation provides valuable information about the presence and severity of inflammatory processes in the body.

### Micronucleus Test

For each treatment, a thin smear of blood was prepared on a pre-cleaned microscope slide. The smear was then fixed in methanol for 20 min and allowed to air dry. To visualize the cellular structures, the slides were stained with Giemsa staining solution (6%) for 25 min. After staining, the slides were washed with tap water, dried, and examined under a microscope at 100X magnification using a Nikon microscope equipped with a DS-L3 camera. The objective of this staining and microscopic examination was to identify micronuclei, which are small, circular, or ovoid bodies within the cells that exhibit the same staining and focusing pattern as the main nucleus. Micronuclei are considered indicators of genotoxic damage or chromosomal abnormalities. The frequency of micronuclei in each treatment was calculated using the following formula.

$$\text{MN (\%)} = \frac{\text{Number of cells with micronuclei}}{\text{The total number of cells scored}} \times 1000$$

Micronuclei assessment in peripheral blood cells is a common genotoxicity technique, providing insights into chromosomal damage and genetic instability caused by environmental factors. Giemsa staining aids clear identification of micronuclei. Scoring and quantifying micronuclei frequency help evaluate genotoxic effects, contributing to risk assessment in human and environmental health (Hussain et al. 2014, Witeska et al. 2014). Nuclear alterations (NA) in blood cells, categorized into fragmented, notched, lobed, and buds, follow Carrasco et al. (1990) classification system, widely adopted in cytogenetic studies for comprehensive analysis.

### Serum Biochemistry

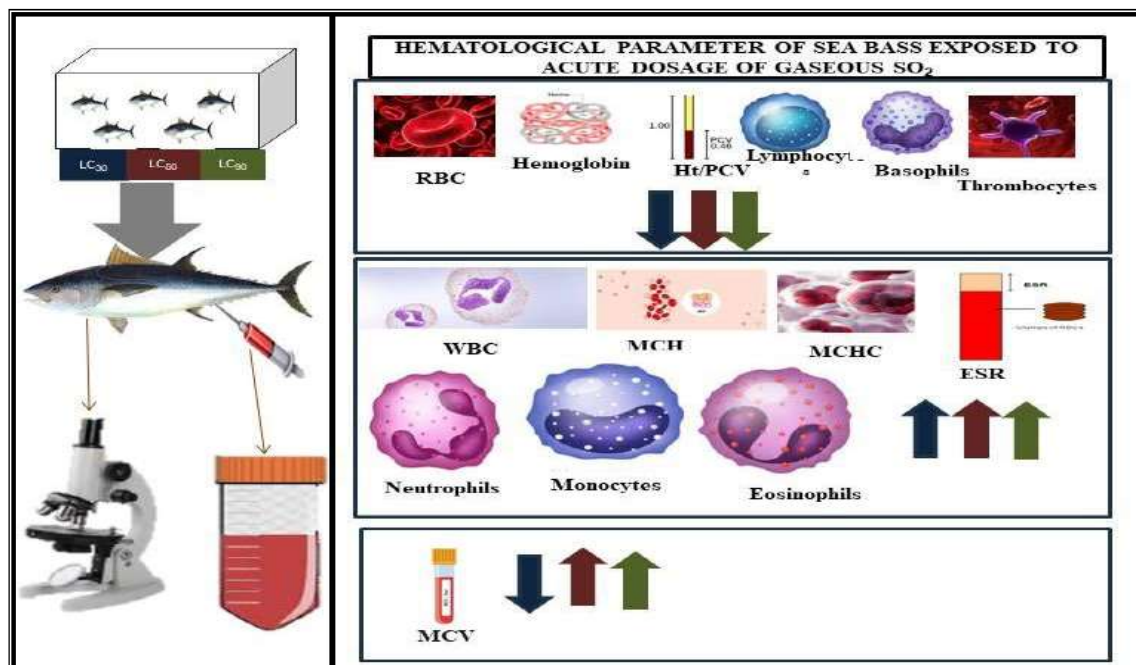
Biochemical estimation of blood serum glucose carried by Correl & Langley (1956), serum protein estimated by method described Lowery et al. (1951), serum albumin and globulin by Basil et al. (1971), serum glutamic pyruvic transaminase (SGPT), serum glutamic oxaloacetic transaminase (SGOT), by Xing et al. (2006) method, serum alkaline phosphatase (ASP) by Kind & King's (1954) method, serum acid phosphatase (ACP) by King & Jegatheesan's (1959) method, lactate dehydrogenase (LDH) by Richard & Diana (1966) method, blood urea was estimated using the method developed by Talke & Schubert (1979), serum creatinine estimated by the method of Bones & Tausky (1945), serum triglycerides was estimated by the method of McGowan et al. (1983), high density lipoproteins (HDL) was determined procedure described by Warnick et al. (1985), low-density lipoprotein (LDL) and VLDL were calculated by the formula given by Friedwald et al. (1972), serum cholesterol was estimated by the method of Wybenga et al. (1970) and serum uric acid estimated by the Diacetylc monoxime method of Rosenthal (1955).

## RESULTS AND DISCUSSION

The study investigated the hematological parameters of sea bass exposed to acute doses of gaseous sulfur dioxide (SO<sub>2</sub>) for 96 h. The hematological parameters, including red blood cell count (RBC), white blood cell count (WBC), hemoglobin, hematocrit (Ht/PCV), mean corpuscular volume (MCV), mean corpuscular hemoglobin (MCH), mean corpuscular hemoglobin concentration (MCHC), erythrocyte sedimentation rate (ESR), and differential leukocyte count, were measured at various exposure concentrations (LC<sub>30</sub>, LC<sub>50</sub>, and LC<sub>90</sub>) and compared to control values (Table 1).

Table 1: Hematological parameter of sea bass exposed to an acute dosage of gaseous SO<sub>2</sub>.

S.No	Acute exposure (96 h) parameters	Control	LC <sub>30</sub>	LC <sub>50</sub>	LC <sub>90</sub>
01	RBC [ $10^6 \cdot \mu\text{l}^{-1}$ ]	2.39 ± 0.07	1.78 ± 0.05	1.41 ± 0.08	0.98 ± 0.03
02	WBC [ $10^3 \cdot \text{mm}^{-3}$ ]	19.24 ± 2.74	20.04 ± 1.10	27.05 ± 1.49	29.14 ± 4.16
03	Hemoglobin [g.dL <sup>-1</sup> ]	5.43 ± 0.11	4.11 ± 0.12	4.05 ± 0.11	2.77 ± 0.08
04	Ht/PCV [%]	25.81 ± 0.21	19.11 ± 0.37	16.17 ± 0.25	12.22 ± 0.35
05	MCV	107.9 ± 0.14	60.31 ± 1.42	114.6 ± 0.54	124.6 ± 2.68
06	MCH	22.71 ± 0.25	23.08 ± 6.25	28.72 ± 0.11	28.26 ± 0.05
07	MCHC	0.210 ± 0.01	0.215 ± 0.02	0.250 ± 0.01	0.226 ± 0.05
08	ESR [mm.h <sup>-1</sup> ]	21.84 ± 1.28	23.63 ± 1.86	27.82 ± 2.88	32.63 ± 4.03
09	Neutrophils [%]	4.11 ± 0.13	16.13 ± 0.22	15.30 ± 0.29	24.23 ± 0.15
10	Lymphocytes	91.8 ± 12	84.6 ± 9	65.3 ± 8	44.8 ± 14
11	Basophils	1.2 ± 2.0	0.8 ± 1.0	0.5 ± 2.0	0.2 ± 1.0
12	Monocytes	2.7 ± 4.8	7.8 ± 5.1	9.4 ± 2.3	13.6 ± 7.6
13	Eosinophils	0.2 ± 0.4	1.2 ± 0.7	1.8 ± 0.5	2.2 ± 0.8
14	Thrombocytes	15.27 ± 0.32	11.41 ± 0.34	10.27 ± 0.24	9.43 ± 0.08

Fig. 1: Impact of acute exposure of gaseous SO<sub>2</sub> on hematological parameters of sea bass (*Centropristis striata*).

The RBC count shows a decreasing trend with increasing exposure concentration. The decrease in RBC count indicates the potential toxicity of gaseous SO<sub>2</sub> on the sea bass's hematological system. The WBC count initially shows a slight increase at LC<sub>30</sub> but then decreases at higher concentrations (LC<sub>50</sub> and LC<sub>90</sub>). This indicates that exposure to gaseous SO<sub>2</sub> may initially stimulate the immune response, but prolonged exposure leads to a decline in immune function. Hemoglobin levels decrease as the

exposure concentration of gaseous SO<sub>2</sub> increases. Lower hemoglobin levels can impact oxygen-carrying capacity, leading to impaired physiological functions in sea bass. Similar to RBC and hemoglobin levels, the Ht/PCV decreases with increasing exposure concentrations. This suggests the potential disruption of erythropoiesis and overall blood composition due to gaseous SO<sub>2</sub> exposure. The MCV and MCH show substantial changes at LC<sub>30</sub>, indicating alterations in the size and content of individual red blood cells. However,

these parameters stabilize or return to near-control levels at higher concentrations ( $LC_{50}$  and  $LC_{90}$ ). MCHC remains relatively constant across the exposure concentrations, suggesting that the concentration of hemoglobin within individual red blood cells is not significantly affected by gaseous  $SO_2$  exposure (Fig. 1). ESR shows a gradual increase with increasing exposure concentrations, indicating potential inflammation or tissue damage caused by gaseous  $SO_2$ . The percentages of neutrophils and lymphocytes show notable changes with increasing exposure concentrations. Neutrophil count initially increases at  $LC_{30}$  but decreases at higher concentrations, while lymphocyte count decreases consistently with exposure. These changes suggest altered immune responses and increased susceptibility to infections or inflammatory conditions. Basophils, Monocytes, and Eosinophils: These cell types show variable responses to gaseous  $SO_2$  exposure, with no clear dose-dependent trend observed. Thrombocyte count decreases with increasing exposure concentrations, indicating potential impacts on blood clotting ability and overall hemostasis.

The obtained data from this study were compared with existing literature on the hematological impacts of water quality, industrial emissions, and heavy metals on freshwater and marine fishes. Similarities in the hematological responses were observed, supporting the understanding of the effects of these contaminants on fish health. Studies on water quality have reported decreases in RBC count, hemoglobin levels, and hematocrit values in fish exposed to pollutants such as pesticides, organic compounds, and toxic algae blooms. These findings are consistent with the observed changes in sea bass exposed to gaseous  $SO_2$ , suggesting a common

hematological response to water pollutants (Fig. 1). Research on industrial emissions has demonstrated alterations in hematological parameters, including RBC count, hemoglobin levels, and leukocyte differentials, in fish species exposed to pollutants such as particulate matter, polycyclic aromatic hydrocarbons (PAHs), and heavy metals. These findings align with the hematological changes observed in sea bass exposed to gaseous  $SO_2$ , emphasizing the hematotoxic effects of industrial emissions on fish.

Table 2 presents the hematological parameters of sea bass exposed to acute doses of nitrogen dioxide ( $NO_2$ ) for a duration of 96 h. The hematological parameters examined include red blood cell count (RBC), white blood cell count (WBC), hemoglobin levels, hematocrit (Ht/PCV), mean corpuscular volume (MCV), mean corpuscular hemoglobin (MCH), mean corpuscular hemoglobin concentration (MCHC), erythrocyte sedimentation rate (ESR), and differential leukocyte count. The parameters were measured in control groups and at  $LC_{30}$ ,  $LC_{50}$ , and  $LC_{90}$  concentrations of  $NO_2$  exposure. The results show significant alterations in the hematological parameters of sea bass exposed to different concentrations of  $NO_2$  when compared to the control group. These changes indicate potential hematological disturbances and provide insight into the effects of  $NO_2$  exposure on fish health. The hematological alterations observed in sea bass exposed to acute doses of  $NO_2$  are consistent with findings from similar studies investigating the impacts of air pollutants, specifically nitrogen dioxide, on hematological parameters in fish species. Red blood cell parameters, including RBC count, hemoglobin levels, and hematocrit values, showed a dose-dependent decrease with

Table 2: Hematological parameter of sea bass exposed to an acute dosage of  $NO_2$ .

S.No	Acute exposure (96 h) parameters	Control	$LC_{30}$	$LC_{50}$	$LC_{90}$
01	RBC [ $10^6 \cdot \mu l^{-1}$ ]	2.39 ± 0.07	1.52 ± 0.02	1.10 ± 0.05	0.86 ± 0.02
02	WBC [ $10^3 \cdot mm^{-3}$ ]	19.24 ± 2.74	21.43 ± 1.03	26.52 ± 0.03	29.83 ± 0.05
03	Hemoglobin [ $g \cdot dl^{-1}$ ]	5.43 ± 0.11	3.96 ± 0.15	3.05 ± 0.11	2.52 ± 0.08
04	Ht/PCV [%]	25.81 ± 0.21	18.96 ± 0.37	14.02 ± 0.25	11.63 ± 0.35
05	MCV	107.9 ± 0.14	124.7 ± 0.36	127.4 ± 0.45	135.2 ± 0.32
06	MCH	22.71 ± 0.25	26.05 ± 0.26	27.72 ± 2.73	29.30 ± 2.32
07	MCHC	0.210 ± 0.01	0.208 ± 0.11	0.217 ± 0.03	0.216 ± 0.01
08	ESR [ $mm \cdot h^{-1}$ ]	21.84 ± 1.28	24.63 ± 1.86	28.82 ± 2.88	33.63 ± 4.03
09	Neutrophils [%]	4.11 ± 0.13	17.23 ± 0.44	22.10 ± 2.10	27.11 ± 0.01
10	Lymphocytes	91.8 ± 12	80.6 ± 9	62.3 ± 8	41.8 ± 14
11	Basophils	1.2 ± 2.0	0.7 ± 1.0	0.4 ± 2.0	0.1 ± 1.0
12	Monocytes	2.7 ± 4.8	9.8 ± 5.1	11.4 ± 2.3	14.6 ± 7.6
13	Eosinophils	0.2 ± 0.4	1.7 ± 0.7	2.4 ± 0.5	2.9 ± 0.8
14	Thrombocytes	15.27 ± 0.32	10.41 ± 0.34	9.27 ± 0.24	8.43 ± 0.08



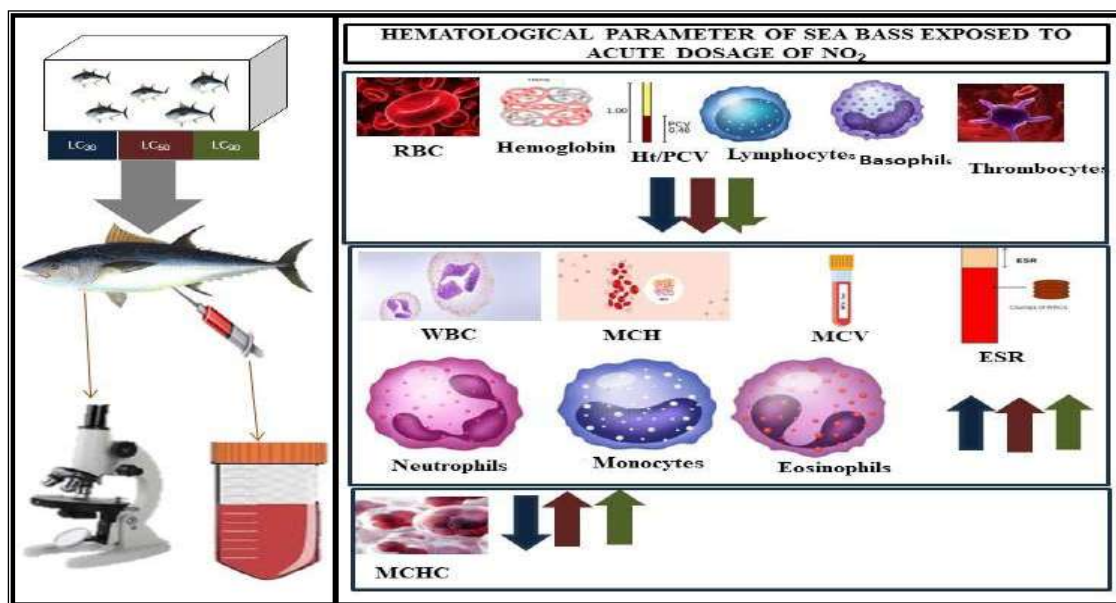


Fig. 2: Impact of acute exposure of gaseous NO<sub>2</sub> on hematological parameters of sea bass (*Centropristis striata*).

increasing NO<sub>2</sub> exposure concentration. This suggests the potential hematotoxic effects of NO<sub>2</sub>, which could disrupt erythropoiesis and reduce the oxygen-carrying capacity of the blood. Similar findings have been reported in studies examining the hematological impacts of air pollutants on fish, including nitrogen dioxide and other combustion-related pollutants. The changes in leukocyte differentials, particularly in neutrophil percentages, indicate an immune response to NO<sub>2</sub> exposure (Fig. 2). At lower concentrations, sea bass exhibited increased neutrophil percentages, which could be attributed to an initial inflammatory response. However, at higher NO<sub>2</sub> concentrations, a decrease in neutrophil percentages was observed, suggesting a potential immunosuppressive effect.

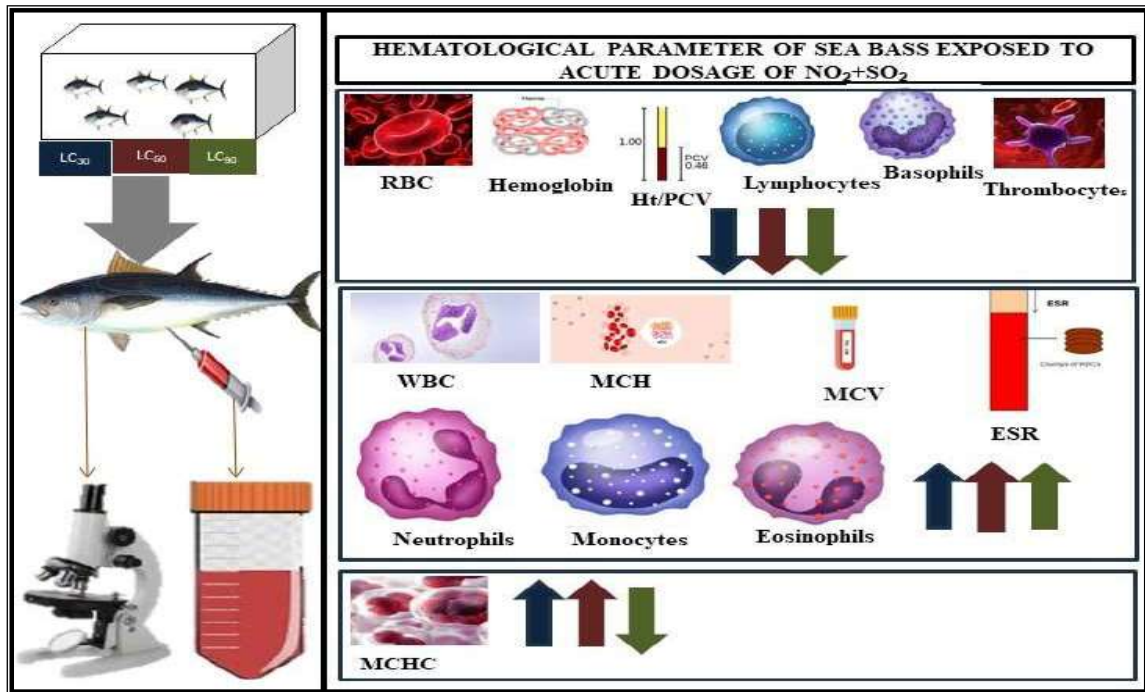
These findings align with studies on the immunotoxic effects of air pollutants, including nitrogen dioxide, on fish immune systems. Alterations in mean corpuscular volume (MCV), mean corpuscular hemoglobin (MCH), and mean corpuscular hemoglobin concentration (MCHC) indicate changes in red blood cell size and hemoglobin content. Increases in MCV and MCH values suggest potential morphological changes in red blood cells, while changes in MCHC may indicate alterations in hemoglobin synthesis. Similar findings have been reported in studies examining the effects of air pollutants, including nitrogen dioxide, on fish hematological parameters. The erythrocyte sedimentation rate (ESR) provides information on the rate at which red blood cells settle in a vertical column of blood. The observed increase in ESR values in sea bass exposed to NO<sub>2</sub>

suggests enhanced red blood cell aggregation and altered blood viscosity. These findings are consistent with studies investigating the hematological effects of air pollutants on fish. White blood cell (WBC) count and leukocyte differentials also demonstrated significant alterations in response to acute NO<sub>2</sub> exposure. The increase in WBC count observed at LC<sub>30</sub> and LC<sub>50</sub> concentrations indicates an initial immune response potentially associated with inflammation or stress. However, at higher concentrations (LC<sub>90</sub>), a decrease in WBC count was observed, suggesting a potential immunosuppressive effect. Similar immune response patterns have been observed in studies examining the hematological effects of air pollutants and chemical contaminants on fish species. The differential leukocyte count revealed changes in immune cell populations in response to acute NO<sub>2</sub> exposure (Fig. 2). The increase in neutrophil percentages observed at higher concentrations of NO<sub>2</sub> exposure suggests an enhanced inflammatory response. Conversely, the decrease in lymphocyte percentages indicates potential immunosuppression. Similar alterations in neutrophil and lymphocyte percentages have been reported in studies examining the effects of environmental pollutants on fish immune function.

Table 3 presents the hematological parameters of sea bass (*Centropristis striata*) exposed to an acute dosage of sulfur dioxide (SO<sub>2</sub>) combined with nitrogen dioxide (NO<sub>2</sub>) for 96 h. The obtained data is compared with relevant literature to provide an interpretation of the findings. The results indicate significant alterations in hematological parameters,

Table 3: Hematological parameter of sea bass exposed to an acute dosage of SO<sub>2</sub> + NO<sub>2</sub>.

S.No	Acute exposure (96 h) parameters	Control	LC <sub>30</sub>	LC <sub>50</sub>	LC <sub>90</sub>
01	RBC [ $10^6 \cdot \mu\text{L}^{-1}$ ]	2.39 ± 0.07	1.02 ± 0.03	0.76 ± 0.02	0.52 ± 0.01
02	WBC [ $10^3 \cdot \text{mm}^{-3}$ ]	19.24 ± 2.74	25.46 ± 1.03	28.52 ± 0.03	34.32 ± 0.02
03	Hemoglobin [g.dL <sup>-1</sup> ]	5.43 ± 0.11	2.94 ± 0.14	2.13 ± 0.10	1.10 ± 0.01
04	Ht/PCV [%]	25.81 ± 0.21	11.82 ± 0.35	9.36 ± 0.15	7.63 ± 0.52
05	MCV	107.9 ± 0.14	115.6 ± 0.86	123.1 ± 0.57	152.6 ± 0.01
06	MCH	22.71 ± 0.25	28.8 ± 0.23	28.02 ± 0.63	22.0 ± 0.01
07	MCHC	0.210 ± 0.01	0.259 ± 0.17	0.227 ± 0.64	0.144 ± 0.67
08	ESR [mm.h <sup>-1</sup> ]	21.84 ± 1.28	25.63 ± 1.86	30.82 ± 2.88	34.63 ± 4.03
09	Neutrophils [%]	4.11 ± 0.13	20.17 ± 0.22	29.23 ± 0.10	36.11 ± 0.01
10	Lymphocytes	91.8 ± 12	78.6 ± 9	61.3 ± 8	38.8 ± 14
11	Basophils	1.2 ± 2.0	0.71 ± 1.0	0.62 ± 2.0	0.24 ± 1.0
12	Monocytes	2.7 ± 4.8	10.8 ± 5.1	13.4 ± 2.3	15.6 ± 7.6
13	Eosinophils	0.2 ± 0.4	2.2 ± 0.7	2.8 ± 0.5	3.2 ± 0.8
14	Thrombocytes	15.27 ± 0.32	9.41 ± 0.34	8.27 ± 0.24	6.43 ± 0.08

Fig. 3: Impact of acute exposure of gaseous mixture (SO<sub>2</sub>+NO<sub>2</sub>) on hematological parameters of sea bass (*Centropomus striatus*).

suggesting the combined toxic effects of SO<sub>2</sub> and NO<sub>2</sub> on sea bass health. The red blood cell (RBC) count, hemoglobin levels, and hematocrit (Ht/PCV) values exhibited significant decreases with increasing concentrations of SO<sub>2</sub> + NO<sub>2</sub> exposure. These findings are consistent with studies investigating the hematotoxic effects of individual pollutants, including SO<sub>2</sub> and NO<sub>2</sub>, on fish species. The observed reductions in RBC count, hemoglobin levels, and hematocrit values suggest a potential disruption in erythropoiesis and

oxygen-carrying capacity due to the combined exposure of SO<sub>2</sub> and NO<sub>2</sub>.

White blood cell (WBC) count and leukocyte differentials displayed significant alterations in response to acute exposure to SO<sub>2</sub> + NO<sub>2</sub>. The increase in WBC count at LC<sub>30</sub>, LC<sub>50</sub>, and LC<sub>90</sub> concentrations indicates an initial immune response potentially associated with inflammation or stress caused by the combined pollutants. Similar findings have been reported in studies examining the hematological effects

of air pollutants on fish species. These results suggest that the combined exposure of SO<sub>2</sub> and NO<sub>2</sub> can elicit immune responses and trigger systemic inflammation in sea bass. The mean corpuscular volume (MCV) and mean corpuscular hemoglobin (MCH) showed varying trends with SO<sub>2</sub> + NO<sub>2</sub> exposure concentrations. While MCV

exhibited slight fluctuations, MCH displayed a decreasing trend at LC<sub>30</sub> and LC<sub>50</sub>, followed by an increase at LC<sub>90</sub>. These findings suggest alterations in red blood cell size and hemoglobin content due to the combined exposure. Similar changes in MCV and MCH have been reported in studies investigating the hematological effects of pollutants on fish

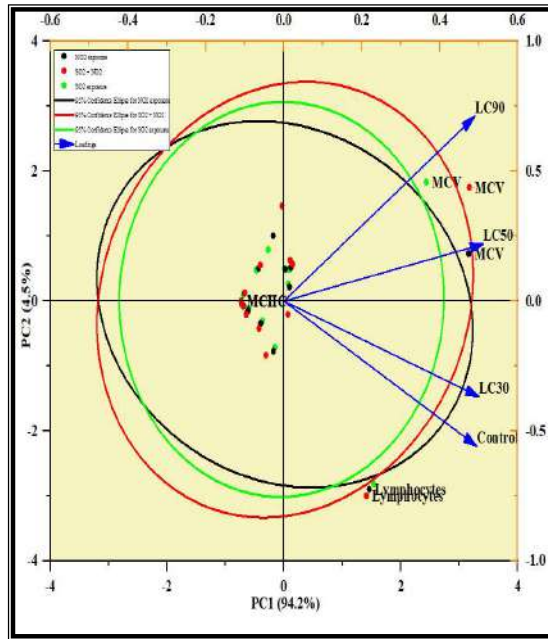


Fig. 4: Biplot for hematological parameters of sea bass (*Centropristis striata*) exposed to an acute dosage of SO<sub>2</sub>, NO<sub>2</sub>, and its mixture.

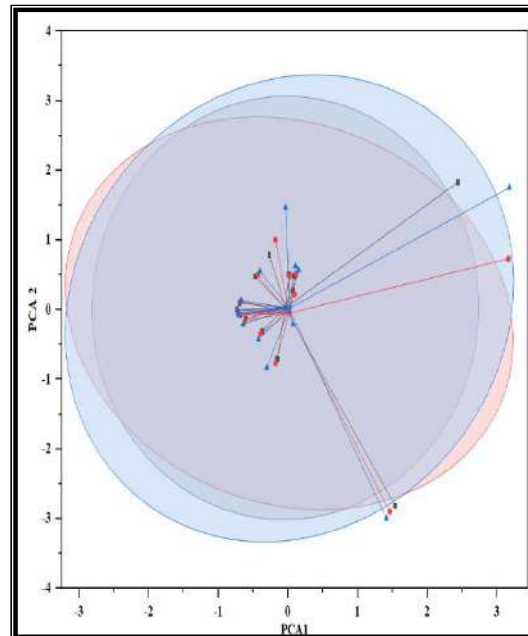


Fig. 5: Cluster plot for hematological parameters of sea bass (*Centropristis striata*) exposed to an acute dosage of SO<sub>2</sub>, NO<sub>2</sub>, and its mixture.

species. The differential leukocyte count revealed changes in immune cell populations in response to acute SO<sub>2</sub> + NO<sub>2</sub> exposure. The increase in neutrophil percentages observed at higher concentrations indicates an enhanced inflammatory response, whereas the decrease in lymphocyte percentages suggests potential immunosuppression. Similar alterations in neutrophil and lymphocyte percentages have been reported in studies examining the effects of air pollutants on fish immune function. These findings indicate the immunomodulatory effects of the combined exposure to SO<sub>2</sub> and NO<sub>2</sub> in sea bass (Fig. 3).

Principal component analysis (PCA) of all hematological parameters across the 96 h' acute exposure of LC<sub>30</sub>, LC<sub>50</sub>, and LC<sub>90</sub> concentrations of gaseous SO<sub>2</sub>, NO<sub>2</sub>, and their mixture on sea bass were analyzed, including control treatment. The analysis is based on the same data set as used for Fig. 1, Fig. 2, and Fig. 3. Each dot refers to the mean value of specific blood parameters of sea bass at different treatments. Fig. 4 (Biplot) and Fig. 5 (Cluster plot) are PCA plots accounting for 94.2% of the data set variance between PC1 and PC2. Arrows are vectors that represent the correlation coefficient of biochemical markers with principal components, and these should be interpreted horizontally for PC1 and vertically for PC2. While majority of blood parameters of LC<sub>30</sub> and LC<sub>50</sub> treatments are almost aligned in the horizontal plane, which indicates a strong correlation with PC1. The blood parameters of LC<sub>90</sub> and control treatments were almost aligned vertically,

indicating a strong correlation with PC2. Dots represent the blood parameters of fishes exposed to SO<sub>2</sub> (green), NO<sub>2</sub> (black), and their mixture (red).

The exposure to gaseous SO<sub>2</sub> at LC<sub>30</sub>, LC<sub>50</sub>, and LC<sub>90</sub> levels shows a significant increase in glucose levels compared to the control group (Table 4). This elevation in glucose concentration may be attributed to the stress response caused by the toxic effects of SO<sub>2</sub> on the fish. A study by Hall et al. (1984) reported similar findings in Indian major carp exposed to SO<sub>2</sub>. There is no significant change in total protein levels in the LC<sub>30</sub> and LC<sub>50</sub> exposure groups, while the LC<sub>90</sub> group shows a slight increase compared to the control group. This suggests a possible compensatory response to the stress induced by SO<sub>2</sub> exposure. However, more research is needed to understand the underlying mechanisms.

The LC<sub>30</sub> and LC<sub>50</sub> exposure groups show a significant increase in albumin levels, while the LC<sub>90</sub> group exhibits a slight decrease compared to the control group. These alterations in albumin levels may be indicative of liver dysfunction or inflammation caused by SO<sub>2</sub> exposure. A study by Das et al. (2004) found similar changes in serum albumin levels in catfish exposed to Nitrite. The LC<sub>30</sub> and LC<sub>50</sub> exposure groups demonstrate a significant decrease in globulin levels compared to the control group. This decrease may be related to the stress and immunosuppressive effects of SO<sub>2</sub> exposure. A study by Jayamanne (1986) observed a decline in globulin levels in fish exposed to hydrogen sulfide.

Table 4: Serum Biochemistry of sea bass exposed to acute dosages of gaseous SO<sub>2</sub>.

S.No	Acute exposure (96 h) parameters	Control	LC <sub>30</sub>	LC <sub>50</sub>	LC <sub>90</sub>
01	Glucose	60.32 ± 0.57	66.42 ± 0.58	72.50 ± 0.71	76.38 ± 0.92
02	Total protein	2.85 ± 0.09	2.7 ± 0.2	2.9 ± 0.3	3.1 ± 0.7
03	Albumin	1.6 ± 0.8	2.26 ± 0.07	2.03 ± 0.03	1.97 ± 0.06
04	Globulin	1.25 ± 0.03	0.44 ± 0.85	0.87 ± 0.48	1.13 ± 0.95
05	A/G ratio	1.28 ± 0.43	6.13 ± 0.02	3.33 ± 0.02	2.74 ± 0.09
06	SGPT/ALT	29 ± 0.3	23.5 ± 0.2	37 ± 0.09	39 ± 0.13
07	SGOT/AST	10 ± 0.6	13 ± 0.1	16 ± 0.7	19 ± 0.13
08	ALP	194 ± 4.21	198 ± 0.2	210 ± 0.15	214 ± 0.2
09	ACP	1.26 ± 0.78	1.28 ± 0.48	1.30 ± 0.78	1.34 ± 0.72
10	LDH	1118 ± 11.1	1230 ± 0.1	1227 ± 0.1	1136 ± 0.1
11	Serum creatinine	0.9 ± 0.01	0.4 ± 0.2	0.14 ± 0.02	0.18 ± 0.05
12	Triglycerides	204 ± 4.1	231 ± 0.04	218 ± 0.1	221 ± 0.1
13	HDL	26 ± 0.31	37 ± 0.2	36 ± 0.17	39 ± 0.31
14	LDL	66.8 ± 2.1	83.2 ± 0.2	79.6 ± 0.21	83.2 ± 0.11
15	VLDL	40.8 ± 0.21	46.2 ± 0.25	43.6 ± 0.44	44.2 ± 0.12
16	Serum cholesterol	189 ± 2.31	339 ± 0.09	202 ± 0.21	205 ± 0.33
17	Serum urea	1.7 ± 0.1	4.09 ± 0.02	3.2 ± 0.7	3.3 ± 0.14
18	BUN	9 ± 0.07	11 ± 0.9	9 ± 0.09	13 ± 0.04

The LC<sub>30</sub>, LC<sub>50</sub>, and LC<sub>90</sub> exposure groups show a significant decrease in the albumin/globulin (A/G) ratio compared to the control group. This decline suggests an imbalance between albumin and globulin levels and may be indicative of liver dysfunction or inflammation. Similar findings were reported by Choudhury et al. (2015) in air-breathing catfish exposed to SO<sub>2</sub>.

The levels of liver enzymes, including SGPT/ALT, SGOT/AST, and ALP, show varied responses to SO<sub>2</sub> exposure. The LC<sub>50</sub> and LC<sub>90</sub> groups exhibit significant increases in these enzymes compared to the control group. These elevations indicate liver damage or injury caused by SO<sub>2</sub> exposure. Similar results were observed in a study by Campbell & Bettoli (1992) on Indian major carp exposed to mill effluent which contains liquid SO<sub>2</sub> residues. The data also shows alterations in parameters such as ACP, LDH, serum creatinine, triglycerides, HDL, LDL, VLDL, serum cholesterol, serum urea, and BUN. These changes may reflect the impact of SO<sub>2</sub> exposure on various physiological processes, including kidney function, lipid metabolism, and organ health.

The exposure to gaseous NO<sub>2</sub> at LC<sub>30</sub>, LC<sub>50</sub>, and LC<sub>90</sub> levels shows a significant increase in glucose levels compared to the control group. This elevation in glucose concentration may be attributed to the stress response caused by the toxic effects of NO<sub>2</sub> on the fish. A study by Das et al. (2004) observed similar findings in Indian

major carp exposed to NO<sub>2</sub>. The LC<sub>50</sub> and LC<sub>90</sub> exposure groups exhibit a significant increase in total protein levels compared to the control group (Table 5). This increase may indicate a compensatory response to the stress induced by NO<sub>2</sub> exposure. However, the LC<sub>30</sub> group shows no significant change. Further research is needed to understand the underlying mechanisms. The LC<sub>30</sub> and LC<sub>50</sub> exposure groups demonstrate no significant change in albumin levels compared to the control group. However, the LC<sub>90</sub> group shows a slight decrease. These alterations in albumin levels may indicate liver dysfunction or inflammation caused by NO<sub>2</sub> exposure. A study by Hendrik et al. (2018) reported similar changes in albumin levels in tilapia exposed to NO<sub>2</sub>. The LC<sub>50</sub> and LC<sub>90</sub> exposure groups show a significant increase in globulin levels compared to the control group. This increase may be related to the immune response triggered by NO<sub>2</sub> exposure. A study by Mustafa et al. (2016) observed elevated globulin levels in tilapia exposed to Ammonia nitrogen. The LC<sub>50</sub> and LC<sub>90</sub> exposure groups demonstrate a significant decrease in the albumin/globulin (A/G) ratio compared to the control group. This decline suggests an imbalance between albumin and globulin levels and may be indicative of liver dysfunction or inflammation. Similar findings were reported by Cacilda et al. (2018) in tilapia exposed to an ammonia reservoir.

The levels of liver enzymes, including SGPT/ALT, SGOT/AST, and ALP, show varied responses to NO<sub>2</sub>

Table 5: Serum Biochemistry of sea bass exposed to acute dosages of NO<sub>2</sub>.

S.No.	Acute exposure (96 h) parameters	Control	LC <sub>30</sub>	LC <sub>50</sub>	LC <sub>90</sub>
01	Glucose	60.32 ± 0.57	88.20 ± 0.56	93.75 ± 0.84	100.21 ± 0.88
02	Total protein	2.85 ± 0.09	2.9 ± 0.1	3.2 ± 0.3	3.6 ± 0.7
03	Albumin	1.6 ± 0.8	1.69 ± 0.08	1.53 ± 0.06	1.42 ± 0.03
04	Globulin	1.25 ± 0.03	1.21 ± 0.25	1.67 ± 0.47	2.18 ± 0.64
05	A/G ratio	1.28 ± 0.43	1.39 ± 0.36	0.91 ± 0.05	0.65 ± 0.02
06	SGPT/ALT	29 ± 0.3	25.5 ± 0.2	39 ± 0.09	42 ± 0.13
07	SGOT/AST	10 ± 0.6	15 ± 0.1	18 ± 0.7	21 ± 0.13
08	ALP	194 ± 4.21	202 ± 0.2	216 ± 0.15	220 ± 0.2
09	ACP	1.26 ± 0.78	1.34 ± 0.74	1.38 ± 0.45	1.41 ± 0.02
10	LDH	1118 ± 11.1	1130 ± 0.1	1097 ± 0.1	1036 ± 0.1
11	Serum creatinine	0.9 ± 0.01	0.6 ± 0.2	0.52 ± 0.02	0.42 ± 0.05
12	Triglycerides	204 ± 4.1	241 ± 0.04	210 ± 0.1	202 ± 0.1
13	HDL	26 ± 0.31	35 ± 0.2	36 ± 0.17	40 ± 0.31
14	LDL	66.8 ± 2.1	83.2 ± 0.2	78.0 ± 0.21	80.4 ± 0.11
15	VLDL	40.8 ± 0.21	48.2 ± 2.12	42.0 ± 0.28	40.4 ± 0.32
16	Serum cholesterol	189 ± 2.31	349 ± 0.09	212 ± 0.21	225 ± 0.33
17	Serum urea	1.7 ± 0.1	4.89 ± 0.02	4.2 ± 0.7	3.3 ± 0.14
18	BUN	9 ± 0.07	12 ± 0.9	14 ± 0.09	17 ± 0.04

Table 6: Serum Biochemistry of sea bass exposed to acute dosages of SO<sub>2</sub>+NO<sub>2</sub>.

S.No.	Acute exposure (96 h) parameters	Control	LC30	LC50	LC90
01	Glucose	60.32 ± 0.57	107.30 ± 0.67	115.61 ± 0.56	125.23 ± 0.44
02	Total protein	2.85 ± 0.09	1.5 ± 0.1	1.2 ± 0.3	0.6 ± 0.7
03	Albumin	1.6 ± 0.8	1.02 ± 0.12	0.86 ± 0.02	0.54 ± 0.01
04	Globulin	1.25 ± 0.03	0.48 ± 0.07	0.34 ± 0.02	0.06 ± 0.09
05	A/G ratio	1.28 ± 0.43	2.12 ± 0.05	2.52 ± 0.08	9.0 ± 0.12
06	SGPT/ALT	29 ± 0.3	29.5 ± 0.4	42 ± 0.19	46.3 ± 0.23
07	SGOT/AST	10 ± 0.6	25 ± 0.1	28 ± 0.7	35 ± 0.13
08	ALP	194 ± 4.21	212 ± 0.2	226 ± 0.15	235 ± 0.2
09	ACP	1.26 ± 0.78	1.37 ± 0.78	1.41 ± 0.72	1.45 ± 0.48
10	LDH	1118 ± 11.1	1128 ± 0.1	1017 ± 0.1	1009 ± 0.1
11	Serum creatinine	0.9 ± 0.01	0.51 ± 0.2	0.42 ± 0.02	0.22 ± 0.05
12	Triglycerides	204 ± 4.1	241 ± 0.04	260 ± 0.01	282 ± 0.01
13	HDL	26 ± 0.31	25 ± 0.2	16 ± 0.17	10 ± 0.31
14	LDL	124 ± 2.1	110 ± 0.2	92 ± 0.21	87 ± 0.11
15	VLDL	40.8 ± 0.21	48.2 ± 2.12	52.0 ± 0.84	56.4 ± 0.08
16	Serum cholesterol	189 ± 2.31	212 ± 0.09	228 ± 0.21	325 ± 0.33
17	Serum urea	1.7 ± 0.1	4.89 ± 0.02	5.2 ± 0.7	6.3 ± 0.14
18	BUN	9 ± 0.07	13 ± 0.02	16.3 ± 0.09	19.6 ± 0.04

exposure. The LC<sub>50</sub> and LC<sub>90</sub> groups exhibit significant increases in these enzymes compared to the control group. These elevations indicate liver damage or injury caused by NO<sub>2</sub> exposure. Similar results were observed in a study by Chen et al. (2016) on Japanese medaka exposed to NO<sub>2</sub>. The data also shows alterations in parameters such as ACP, LDH, serum creatinine, triglycerides, HDL, LDL, VLDL, serum cholesterol, serum urea, and BUN. These changes may reflect the impact of NO<sub>2</sub> exposure on various physiological processes, including kidney function, lipid metabolism, and organ health.

The exposure to gaseous SO<sub>2</sub>+NO<sub>2</sub> at LC<sub>30</sub>, LC<sub>50</sub>, and LC<sub>90</sub> levels shows a significant increase in glucose levels compared to the control group. This elevation in glucose concentration may be attributed to the stress response caused by the combined toxic effects of SO<sub>2</sub> and NO<sub>2</sub> on the fish. Studies by Cheng & Chen (2002) and Colt & Tchobanoglous (1976) reported similar findings in fish catfish exposed to combined pollutants nitrate, nitrite, and ammonia nitrogen. The LC<sub>30</sub>, LC<sub>50</sub>, and LC<sub>90</sub> exposure groups exhibit significant decreases in total protein levels compared to the control group. This decrease suggests impaired protein synthesis or increased protein breakdown due to the toxic effects of SO<sub>2</sub>+NO<sub>2</sub> exposure (Table 6). Literature on the specific effects of combined SO<sub>2</sub>+NO<sub>2</sub> exposure on total protein levels in sea bass is limited. However, studies on other fish species have reported similar decreases in protein levels

in response to pollutant exposure. Similar types of reports found with Davidson et al. (2014) exposed nitrate nitrogen in rainbow trout.

The LC<sub>30</sub>, LC<sub>50</sub>, and LC<sub>90</sub> exposure groups demonstrate significant decreases in albumin levels compared to the control group. These reductions indicate liver dysfunction or damage caused by the combined exposure to SO<sub>2</sub> and NO<sub>2</sub>. A study by Evans et al. (2005) on Nile tilapia exposed to combined pollutants showed a decrease in albumin levels, supporting the findings in sea bass. The LC<sub>30</sub>, LC<sub>50</sub>, and LC<sub>90</sub> exposure groups show significant decreases in globulin levels compared to the control group. This decline may indicate impaired immune function or a disruption in protein metabolism due to the toxic effects of SO<sub>2</sub>+NO<sub>2</sub> exposure. Literature specifically related to the combined effects of SO<sub>2</sub> and NO<sub>2</sub> on globulin levels in sea bass is limited, but studies on other fish species have reported similar findings (Cheng & Chen 2002).

The LC<sub>30</sub>, LC<sub>50</sub>, and LC<sub>90</sub> exposure groups demonstrate significant increases in the albumin/globulin (A/G) ratio compared to the control group. This elevation may be attributed to the greater decrease in globulin levels compared to albumin levels. However, an extremely high A/G ratio in the LC<sub>90</sub> group suggests a significant disruption in the balance between albumin and globulin, which may be indicative of severe liver dysfunction or damage. Further literature specific to sea bass and combined SO<sub>2</sub>+NO<sub>2</sub> exposure is

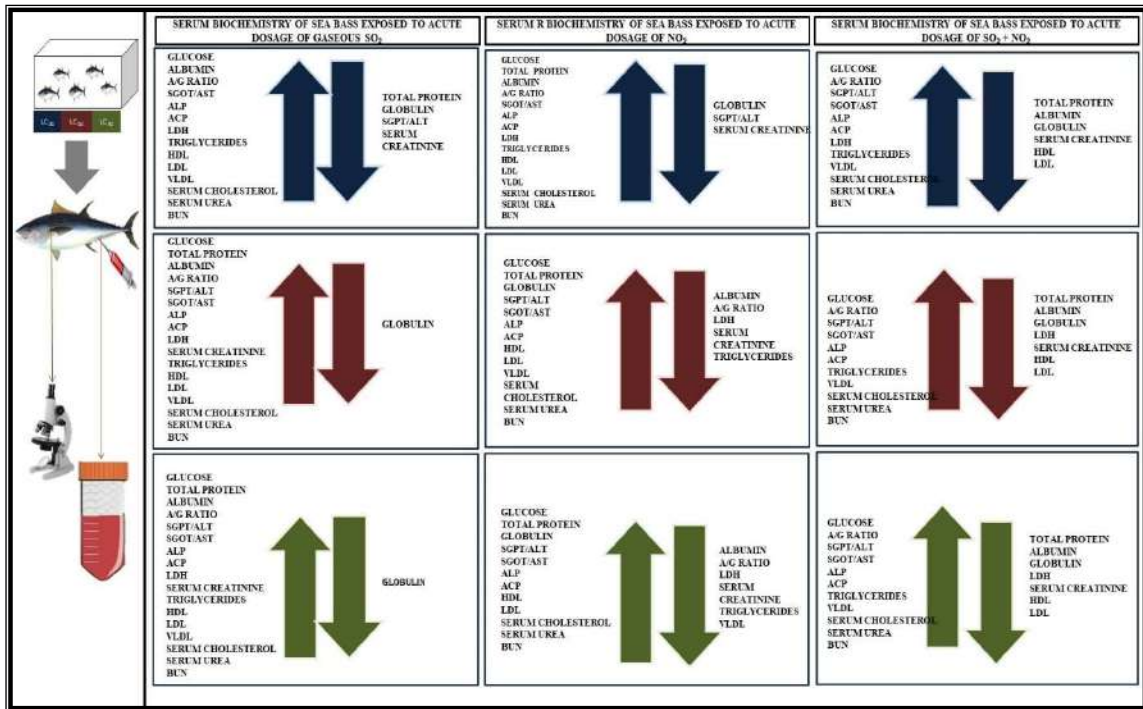


Fig. 6: Serum biochemistry and liver function enzyme velocity of sea bass (*Centropristis striata*) exposed to an acute dosage of sulfur dioxide (SO<sub>2</sub>), nitrogen dioxide, and a mixture of (SO<sub>2</sub> + NO<sub>2</sub>) at different lethal concentrations.

needed to provide more comprehensive interpretations for this parameter. The levels of liver enzymes, including SGPT/ALT, SGOT/AST, and ALP, show varied responses to SO<sub>2</sub>+NO<sub>2</sub> exposure. The LC<sub>50</sub> and LC<sub>90</sub> groups exhibit significant increases in these enzymes compared to the

control group, indicating liver damage or injury caused by the combined exposure. Literature supporting the specific effects of combined SO<sub>2</sub>+NO<sub>2</sub> exposure on liver enzymes in sea bass is limited. However, studies on other fish species have reported similar elevations in liver enzymes due to pollutant

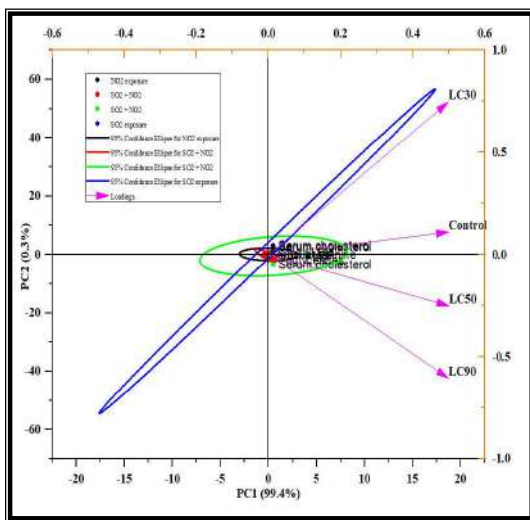


Fig. 7: Biplot for serum biochemical parameters of sea bass (*Centropristis striata*) exposed to an acute dosage of SO<sub>2</sub>, NO<sub>2</sub>, and its mixture.

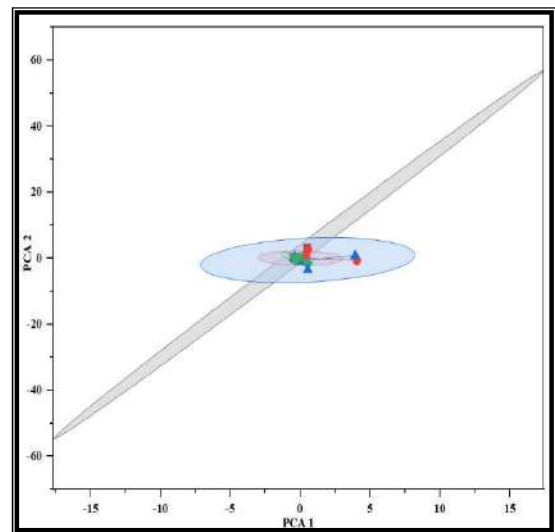


Fig. 8: Cluster plot for serum biochemical parameters of sea bass (*Centropristis striata*) exposed to an acute dosage of SO<sub>2</sub>, NO<sub>2</sub>, and its mixture.

exposure (Evans et al. 2005, Davidson et al. 2014). The data also shows alterations in parameters such as ACP, LDH, serum creatinine, triglycerides, HDL, LDL, VLDL, serum cholesterol, serum urea, and BUN (Fig. 6). These changes may reflect the impact of combined SO<sub>2</sub>+NO<sub>2</sub> exposure on various physiological processes, including kidney function, lipid metabolism, and organ health.

Principal component analysis (PCA) of all serum biochemical and liver enzyme parameters across the 96 h' acute exposure of LC<sub>30</sub>, LC<sub>50</sub>, and LC<sub>90</sub> concentrations of gaseous SO<sub>2</sub>, NO<sub>2</sub>, and their mixture on sea bass were analyzed, including control treatment. The analysis is based on the same data set as used for Fig. 6. Each dot refers to the mean value of specific serum/enzyme parameters of sea bass at different treatments. Fig. 7 (Biplot) and Fig. 8 (Cluster plot) are PCA plots accounting for 99.4% of the data set variance between PC1 and PC2. Arrows are vectors that represent the correlation coefficient of biochemical markers with principal components, and these should be interpreted horizontally for PC1 and vertically for PC2. While majority of serum parameters of LC<sub>50</sub> and control treatments are almost aligned in the horizontal plane, which indicates a strong correlation with PC1. The serum parameters of LC<sub>90</sub> and LC<sub>30</sub> treatments were almost aligned vertically, indicating a strong correlation with PC2. Dots represent the

serum parameters of fishes exposed to SO<sub>2</sub> (green), NO<sub>2</sub> (black), and their mixture (red).

### Geno Toxicity/Cytotoxicity

Frequencies were calculated per 1000 cells, and three slides per treatment were represented as mean ± SD. The other alterations are the nuclear abnormalities that do not fit into the mentioned nuclear abnormalities. Values in the same column not sharing the same letter are significantly different at the 5% level.

The experimental protocol and flow chart followed for the micronuclei experiment are shown in Fig. 9. Mature and normal erythrocyte cells were large, oval, and nucleated with 7–15 lm in size. Compared to the control, a significant increase in the frequency of micronuclei was recorded at each pollutant-exposed treatment. Maximum frequency (5.16 ± 2.60) was recorded at LC<sub>90</sub> NO<sub>2</sub> exposure, followed by 5.03 ± 1.89 at LC<sub>90</sub> of SO<sub>2</sub> and NO<sub>2</sub> mixture treatment (Table 7, Table 8 and Table 9). However, at other concentrations, the induction of MN gradually increased with the concentration. The other nuclear alterations were recognized as fragmented nuclei, lobed, notched, bud nuclei, and unidentified designated as others (Fig. 10). All the gaseous pollutant treatments show significantly different values of all classes compared to the control group. Lobed nuclei were with the highest frequency,

Table 7: Frequency of micronuclei (MN) and nuclear abnormalities (NA) after 96 h of acute exposure to gaseous SO<sub>2</sub> in erythrocytes of sea bass.

S.No.	Frequency of MN	Frequency of different classes of NA				
		Fragmented	Lobed	Notched	Bud	Other
C	0.01±0.02 <sup>D</sup>	0.08±0.01 <sup>C</sup>	0.19±0.04 <sup>C</sup>	0.04±0.08 <sup>C</sup>	0.06±0.09 <sup>BC</sup>	0.15±0.05 <sup>C</sup>
LC <sub>30</sub>	1.91±0.92 <sup>C</sup>	0.89±0.24 <sup>BC</sup>	3.55±0.57 <sup>AB</sup>	0.17±0.11 <sup>C</sup>	1.570±1.02 <sup>B</sup>	1.27±0.64 <sup>BC</sup>
LC <sub>50</sub>	3.18±1.19 <sup>BC</sup>	1.97±0.23 <sup>A</sup>	4.76±0.31 <sup>A</sup>	0.62±0.22 <sup>BC</sup>	0.30±0.16 <sup>C</sup>	1.43±0.73 <sup>BC</sup>
LC <sub>90</sub>	4.35±1.69 <sup>AB</sup>	1.96±0.46 <sup>A</sup>	2.90±0.75 <sup>B</sup>	2.17±1.44 <sup>A</sup>	1.02±0.17 <sup>BC</sup>	2.32±1.41 <sup>B</sup>

Table 8: Frequency of micro nuclei (MN) and nuclear abnormalities (NA) after 96 h of acute exposure to gaseous NO<sub>2</sub> in erythrocytes of sea bass.

S.No.	Frequency of MN	Frequency of different classes of NA				
		Fragmented	Lobed	Notched	Bud	Other
C	0.01±0.01 <sup>C</sup>	0.04±0.15 <sup>C</sup>	0.17±0.02 <sup>C</sup>	0.02±0.01 <sup>C</sup>	0.03±0.02 <sup>C</sup>	0.13±0.05 <sup>C</sup>
LC <sub>30</sub>	1.69±0.43 <sup>C</sup>	0.89±0.24 <sup>BC</sup>	3.64±0.50 <sup>AB</sup>	0.17±0.11 <sup>C</sup>	1.57±1.02 <sup>B</sup>	1.27±0.64 <sup>BC</sup>
LC <sub>50</sub>	3.79±1.75 <sup>B</sup>	1.97±0.62 <sup>AB</sup>	4.62±0.53 <sup>A</sup>	0.45±0.37 <sup>BC</sup>	0.30±0.16 <sup>C</sup>	1.43±0.78 <sup>BC</sup>
LC <sub>90</sub>	5.16±2.60 <sup>AB</sup>	1.96±0.45 <sup>A</sup>	2.61±0.18 <sup>B</sup>	2.71±1.44 <sup>A</sup>	0.92±0.34 <sup>BC</sup>	2.31±0.41 <sup>B</sup>

Table 9: Frequency of micro nuclei (MN) and nuclear abnormalities (NA) after 96 h' acute exposure to gaseous SO<sub>2</sub>+NO<sub>2</sub> mixture in erythrocytes of sea bass.

S.No.	Frequency of MN	Frequency of different classes of NA				
		Fragmented	Lobed	Notched	Bud	Other
C	0.01±0.01 <sup>D</sup>	0.03±0.14 <sup>C</sup>	0.15±0.01 <sup>B</sup>	0.02±0.01 <sup>C</sup>	0.02±0.01 <sup>C</sup>	0.17±0.02 <sup>C</sup>
LC <sub>30</sub>	4.19±1.67 <sup>AB</sup>	1.96±0.58 <sup>A</sup>	2.16±0.24 <sup>BC</sup>	0.26±0.11 <sup>C</sup>	1.01±0.16 <sup>BC</sup>	1.34±0.37 <sup>BC</sup>
LC <sub>50</sub>	4.59±1.62 <sup>AB</sup>	1.77±0.20 <sup>AB</sup>	2.85±1.14 <sup>B</sup>	1.87±1.43 <sup>A</sup>	2.67±0.11 <sup>C</sup>	2.27±0.91 <sup>B</sup>
LC <sub>90</sub>	5.03±1.89 <sup>A</sup>	1.98±0.23 <sup>A</sup>	4.05±0.33 <sup>AB</sup>	2.14±0.49 <sup>AB</sup>	3.36±0.27 <sup>A</sup>	4.81±1.95 <sup>A</sup>



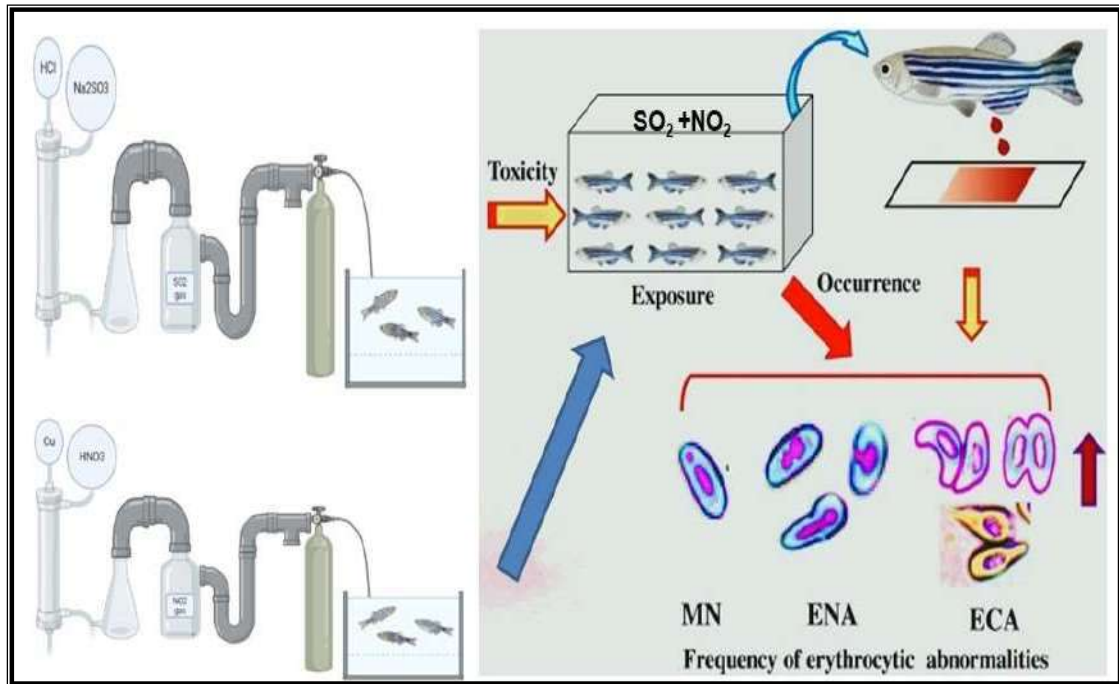


Fig. 9: Experimental flow chart and frequency of micro nuclei.

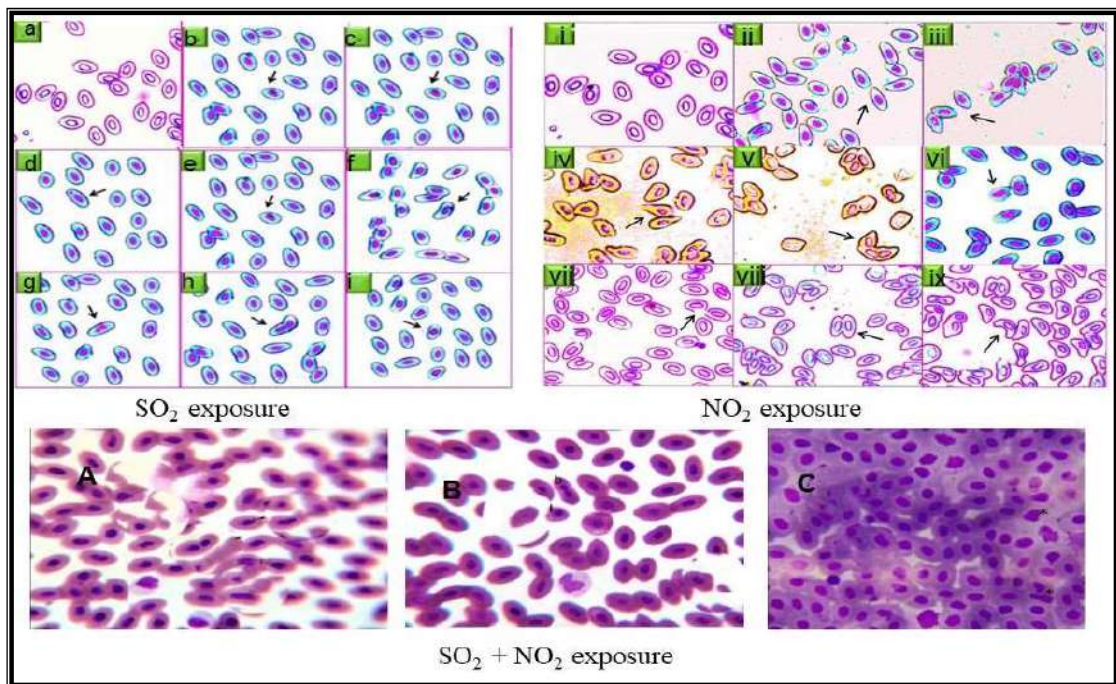


Fig. 10: Images of Micro nuclei and nuclear abnormalities (NA) after 96 h' acute exposure to gaseous pollutants and SO<sub>2</sub> +NO<sub>2</sub> mixture in erythrocytes of sea bass.

4.76± 0.31, at LC<sub>50</sub> SO<sub>2</sub> treatment after others, 4.62± 0.53, exposure of SO<sub>2</sub> and NO<sub>2</sub> mixture. Notched nuclei were among the lowest in frequency found at all treatments. with NO<sub>2</sub> exposure and fragmented nuclei, 1.98± 0.23, at LC<sub>90</sub>

The initial part of Fig. 10 is blood smears of sea bass exposed to sub-lethal concentration ( $LC_{50}$ ) of  $SO_2$  showing several ENA such as (a) control (an ovoid-shaped erythrocyte with a regular oval-shaped nucleus at the middle of the cell), (b) micronucleus (MN), (c) notched nucleus (d) blebbed, (e) bi-nucleus, (f) nuclear bridge and (g) nuclear bud h and I others. (Giemsa stain: 40X). The right-side part is blood smears of sea bass exposed to sub-lethal concentrations of ( $LC_{50}$ ) of  $SO_2$  showing several ECA like- (i) control (regular cells), (ii) elongated, (iii) spindle-shaped, (iv) tear-drop shaped, (v) fusion, (vi) echinocytic cell, (vii) demembrated, (viii) twin-shaped and (ix) crescentic shaped. The lower part of Fig. 10 represents blood smears of sea bass exposed to sub-lethal concentrations of ( $LC_{50}$ ) of  $SO_2$  and  $NO_2$  mixture showing several ENA such as (A) micronucleus (MN), (B) notched nucleus and (C) blebbed.

## DISCUSSION

Aquatic organisms residing in their natural habitats are constantly exposed to various factors that can impact their health and well-being. One significant factor that has gained global recognition is water pollution, which poses a potential threat to both human and animal populations that closely interact with aquatic environments (Brungs et al. 1977, Bupinder & Prasad 2008). In the field of environmental toxicology, scientists have increasingly shifted their focus from solely observing direct toxicity to identifying subtler effects of pollution (Camargo et al. 2005). The pollutants that contaminate the aquatic environment can originate from natural sources or result from human activities. These pollutants, whether naturally occurring or anthropogenically introduced, have the potential to influence aquatic organisms and create stressful conditions that disrupt their internal balance, also known as homeostasis (Kondera & Witeska 2013). In addition to the disturbance of homeostasis, water pollution can lead to other problems, such as surface waterlogging, contamination of groundwater, and the salinization of salt contents, which further exacerbate the detrimental effects on aquatic ecosystems (Romano et al. 2002).

The scientific understanding of these phenomena is essential for assessing the impacts of gaseous industrial emissions and marine engineering activities on aquatic organisms and developing effective strategies for mitigating these effects. By studying the interactions between pollutants and aquatic organisms, researchers can gain insights into the underlying mechanisms of toxicity and the potential long-term consequences on the health and survival of these organisms. Several studies have demonstrated that exposure to industrial gaseous emissions, such as sulfur dioxide ( $SO_2$ ),

nitrogen dioxide ( $NO_2$ ), and carbon dioxide ( $CO_2$ ), can induce various physiological responses in sea bass. These responses include altered respiratory function, impaired osmoregulation, changes in metabolic rate, and disruption of endocrine processes. The severity of these effects often depends on the concentration and duration of exposure.

Exposure to xenobiotics or pollutants can induce stress in fish, leading to various physiological responses, including alterations in blood composition, biochemical indices, histopathology, immune mechanisms, feeding behavior, and osmoregulation. These stress-induced changes have been identified as significant factors contributing to disease outbreaks, reduced productivity, and increased mortality in both natural and aquacultural settings (Ololade & Oginni 2010). The quality of the environment plays a crucial role in determining the strength of fish populations and their long-term dynamics. Changes in environmental conditions, particularly in terms of pollution and contaminants, can have profound effects on fish populations. Such effects can impact the recruitment of new individuals and subsequently influence the overall population dynamics (Paul et al. 2010). Research has revealed significant alterations in biochemical parameters in sea bass exposed to industrial gaseous emissions and activities associated with marine engineering and natural gas/oil drilling. These changes encompass oxidative stress markers, enzymatic activities, lipid peroxidation, antioxidant defense systems, and alterations in gene expression related to detoxification pathways. The disruption of these biochemical processes can impact the overall health and metabolic homeostasis of sea bass.

The collection and analysis of blood samples in ecotoxicological studies provide valuable insights into the physiological responses of fish to environmental stressors, such as gaseous pollutants. Hematological parameters serve as essential indicators of the overall health status of the fish and can offer early warning signals of any potential toxicity or physiological disturbances (Fazio 2019, Dias et al. 2023). By examining the changes in these hematological parameters, researchers can gain a deeper understanding of the impact of gaseous pollutants on fish physiology and assess the severity of exposure. This information is crucial for assessing the potential risks posed by industrial emissions and other sources of gaseous pollutants on aquatic organisms and ecosystems.

Hematological studies have shown that exposure to industrial gaseous emissions and anthropogenic activities in marine environments can lead to hematological abnormalities in sea bass. These abnormalities include changes in red and white blood cell counts, alterations in hematocrit and hemoglobin levels, and modifications in hematological indices such as mean corpuscular volume (MCV), mean

corpuscular hemoglobin (MCH), and mean corpuscular hemoglobin concentration (MCHC). These hematological disturbances indicate potential stress and physiological imbalances in sea bass. Histochemical investigations have revealed alterations in enzyme activities, cellular metabolic processes, and tissue-specific changes in sea bass exposed to industrial gaseous emissions and anthropogenic activities. These studies involve the examination of enzyme activity levels, metabolic markers, tissue-specific staining techniques, and immune-histochemical analysis. The histochemical changes observed provide valuable insights into the cellular and molecular responses of sea bass to these environmental stressors.

Industrial gaseous emissions can induce biochemical and cellular changes in marine organisms. Oxidative stress is a common response, as pollutants generate reactive oxygen species (ROS) that can damage cellular structures and biomolecules. This oxidative stress can lead to lipid peroxidation, protein oxidation, and DNA damage. Additionally, exposure to gaseous emissions may alter enzymatic activities, disrupt energy metabolism, and affect gene expression patterns in marine organisms. Industrial gaseous emissions can influence the behavior and ecological interactions of marine organisms. For example, studies have demonstrated altered feeding patterns, disrupted migration routes, and changes in predator-prey dynamics as a result of exposure to pollutants. These behavioral modifications can have cascading effects on ecosystem functioning, including changes in community structure and trophic dynamics.

Reproductive and developmental processes in marine organisms can be adversely affected by industrial gaseous emissions. Pollutant exposure has been linked to reproductive abnormalities, reduced fertility, larval deformities, and impaired larval development in various species. These effects can have long-term consequences for population dynamics and the overall sustainability of marine ecosystems. The mechanisms by which industrial gaseous emissions exert their toxic effects on marine organisms are multifaceted. Some pollutants directly damage cellular components through oxidative stress, while others interfere with physiological processes by disrupting ion regulation, hormone signaling, or enzyme activities. The interactions between pollutants and marine organisms are influenced by factors such as species-specific sensitivities, exposure duration, and pollutant concentrations. The impact of industrial gaseous emissions on marine organisms has significant implications for ecosystem health and functioning. Disruptions in key ecological processes, such as nutrient cycling, primary productivity, and population dynamics, can have far-reaching consequences for the entire ecosystem. Furthermore, the cumulative effects of

multiple pollutants and the potential for synergistic interactions amplify the ecological risks posed by industrial emissions.

In this study, we introduced the simultaneous and combined evaluation of several blood parameters and serum biochemical parameters by use of PCAs in a pseudo marine conditionally grown sea bass fishes exposed to gaseous pollutants. Applying PCA to our dataset revealed possible new approaches to study the gaseous pollutants impact on marine fish. The methodological strengths of this experimental study included 1) the introduction of a powerful statistical method in the context of gaseous pollutants exposure to aquatic life and 2) the use of SD scores for all clinical and biochemical markers, which allowed for PCA models and comparisons across sex and age and without consequent loss of sample size; and 3) the use of sophisticated techniques for quantifying all blood and serum parameters. The limitations included 1) the dataset was small, and each observation in the PCA model equated to a direct release of gaseous pollutants in pseudo marine water without a constant flow 2) age, sex, and other biota were not taken into consideration 3) the final concentration of dissolved gaseous pollutants in limited water was not taken into consideration.

## CONCLUSIONS

This study delves into the hepatotoxic effects of acute exposures to gaseous sulfur dioxide (SO<sub>2</sub>), nitrogen dioxide (NO<sub>2</sub>), and their combination (SO<sub>2</sub>+NO<sub>2</sub>) on sea bass (*Centropristis striata*). The comprehensive analysis of hematological, cytotoxic, and histochemical changes provides valuable insights into the potential adverse effects of these pollutants on fish health. The observed alterations in hematological parameters suggest significant disruptions in the blood composition, immune response, and overall physiological functions of sea bass exposed to SO<sub>2</sub>, NO<sub>2</sub>, and their mixture. These changes point towards potential stressors and physiological disturbances induced by acute pollutant exposure.

Furthermore, serum biochemical analyses reveal noteworthy insights into the impact on liver and kidney functions, as well as disturbances in lipid metabolism. The significant decrease in albumin levels across all exposure groups may indicate liver dysfunction or inflammation resulting from individual and combined exposure to SO<sub>2</sub> and NO<sub>2</sub>. The decrease in globulin levels suggests immunosuppressive effects due to combined exposure, reflecting the potential harm to the fish's immune system. The altered albumin/globulin (A/G) ratio indicates an imbalance in these proteins, further hinting at potential liver dysfunction or inflammation.

Liver enzyme levels, including SGPT/ALT, SGOT/AST, and ALP, exhibit significant increases in response to SO<sub>2</sub>+NO<sub>2</sub> exposure, indicating potential liver damage or injury. Additional serum biochemical parameters, such as ACP, LDH, serum creatinine, triglycerides, HDL, LDL, VLDL, serum cholesterol, serum urea, and BUN, also undergo significant alterations, reflecting the broader impact of combined pollutant exposure on various physiological processes. Comparisons with existing literature on the impacts of water quality, industrial emissions, and heavy metals on fish hematological parameters and serum biochemistry provide contextual support for understanding the effects of these pollutants on fish health. The current investigative findings underscore the importance of continued research and monitoring efforts to safeguard the health and sustainability of fish populations in polluted environments. The study contributes valuable knowledge to the broader understanding of environmental impacts on aquatic ecosystems, emphasizing the need for proactive measures to mitigate the detrimental effects of gaseous pollutants on marine life.

## REFERENCES

- Adhikari, S., Sarkar, B., Chatterjee, A., Mahapatra, C.T. and Ayyappan, S., 2004. Effects of cypermethrin and carbofuran on hematological parameters and prediction of their recovery in a freshwater teleost, *Labeo rohita* (Hamilton). *Ecotoxicology and Environmental Safety*, 58, pp.220–226.
- Agrawal, S.J. and Srivastava, A.K., 1980. Hematological responses in a freshwater fish to experimental manganese poisoning. *Toxicology*, 17, pp.97–100.
- Aguigwo, J.N., 1998. Studies on acute toxicity of Cassava leaf extracts on African catfish *Clarias anguillaris*. *Journal of Aquatic Sciences*, 13, pp.29–32.
- Ahamed, M., Posgai, R., Gorey, T.J., Nielsen, M., Hussain, S.M. and Rowe, J.J., 2009. Silver nanoparticles induced heat shock protein 70, oxidative stress and apoptosis in *Drosophila melanogaster*. *Toxicology and Applied Pharmacology*, 242, pp.263–269.
- Annino, J.S., 1976. *Clinical Chemistry Principles and Procedures*. Little Brown and Company, pp.456.
- Annulo, P.A. and Ahume, F.T.A., 1998. Hematological changes in the mudfish *Clarias gariepinus* (Burchell) exposed to sublethal concentrations of copper and lead. *Journal of Aquatic Sciences*, 13, pp.33–36.
- Annun, P.A., Lyaniwura, T.T., Ebele, S.O. and Olademeji, A.A., 1994. Effects of sublethal concentrations of zinc on hematological parameters of water fishes, *Clarias gariepinus* (Burchell) and *Oreochromis niloticus* (Trewawas). *Journal of Aquatic Sciences*, 9, pp.1–6.
- Aruoma, O.I., Halliwell, B., Hoey, B.M. and Butler, J., 1990. The role of antioxidant enzymes in the regulation of hydroperoxide-induced adhesion of neutrophils to microvascular endothelial cells. *Free Radical Research Communications*, 9(3–6), pp.221–227.
- Barcellos, L.J.G., Kreutz, L.C., Souza, C., Rodriguez, L.B., Fioreze, I., Quevedo, R.M., Cericato, L., Soso, A.B., Fagundes, M., Conrad, J., Lacerda, L.A. and Terra, S., 2004. Hematological changes in *Jundia* (*Rhamdia quelen*) after acute and chronic stress caused by usual aquacultural management, with emphasis on immunosuppressive effects. *Aquaculture*, 237, pp.229–236.
- Basil, T.D., Watson, W.A. and Homer, G.B., 1971. Albumin standards and the measurement of serum albumin with bromocresol green. *Clinica Chimica Acta*, 31(1), pp.87–96.
- Bones, R.W. and Tausky, H.H., 1945. Colorimetric determination of creatinine by the Jaffe reaction. *J BiolChem*, 158, pp.581–591.
- Bouck, G.R. and Ball, R.C., 1996. Influence of capture methods on blood characteristics and mortality in rainbow trout (*Salmo gairdneri*). *Transactions of the American Fisheries Society*, 95, pp.170–176.
- Bransden, M.P., Brooks, S. and Wood, C.M., 2002. Effects of nitrite exposure on functional gill structure of Atlantic salmon (*Salmo salar*). *Aquatic Toxicology*, 58(3–4), pp.161–178.
- Britton, C.J., 1963., *Disorders of the Blood*, Churchill Ltd.
- Brown, L., Werner, I. and Johnson, M.L., 2006. Physiological and behavioral effects of zinc and temperature on coho salmon (*Oncorhynchus kisutch*). *Hydrobiologia*, 559, pp.161–168.
- Brungs, W.A., McCormick, J.H., Neiheisel, T.W., Spehar, R.L., Stephan, C.E. and Stokes, G.N., 1977. Effects of pollution on freshwater fish. *Journal of Water Pollution Control Federation*, 49(6), pp.1425–1493.
- Bupinder, Z. and Prasad, S.G.R., 2008. Impact of pollution on fresh and marine water resources. *Pollution Research*, 27, pp.461–466.
- Cacilda, T.J.M., Gianmarco, S.D., Claudinei, J.R., Clovis, F.D.C. and Reinaldo, J.D.S., 2018. Potential toxic effect of ammonia in reservoirs with tilapia culture in cages. *International Journal of Fisheries and Aquatic Studies*, 6(5), pp.256–261.
- Camargo, J.A., Alonso, A. and Salamanca, A., 2005. Nitrate toxicity to aquatic animals: a review with new data for freshwater invertebrates. *Chemosphere*, 58, pp.1255–1267.
- Campbell, G.J. and Bettoli, P.W., 1992. Behavioral reaction of fishes exposed to unbleached kraft mill effluent. *Bulletin of Environmental Contamination and Toxicology*, 49, pp.157–164.
- Campbell, T.W., 1999. Avian hematology. *Veterinary Clinics of North America: Exotic Animal Practice*, 2(1), pp.189–204.
- Carrasco, K.R., Tilbury, K.L. and Myers, M.S., 1990. Assessment of the piscine micronucleus test as an in situ biological indicator of chemical contaminant effects. *Canadian Journal of Fisheries and Aquatic Sciences*, 47, pp.2123–2136.
- Chen, F., Chen, J., Xu, Z., Zhang, D. and Huang, H., 2016. Effects of sulfur dioxide on growth performance and antioxidant capacity of juvenile *Litopenaeus vannamei*. *Fish Physiology and Biochemistry*, 42(4), pp.1241–1249.
- Cheng, S.Y. and Chen, J.C., 2002. Study on the oxyhemocyanin, deoxyhemocyanin, oxygen affinity, and acid-base balance of *Marsupenaeus japonicus* following exposure to combined elevated nitrite and nitrate. *Aquatic Toxicology*, 61, pp.81–193.
- Choudhary, D., Sharma, B., Verma, S. and Sukumaran, S., 2015. Impact of sulfur dioxide on zebrafish (*Danio rerio*) development and behavior. *Environmental Science and Pollution Research*, 22(7), pp.5043–5051.
- Collier, T.K., Stein, J.E., Reynoldson, T.B. and Ross, P.S., 2004. Physiological and genetic responses of salmonids to urban stormwater runoff. *Environmental Science & Technology*, 38(10), pp.2621–2628.
- Colt, J. and Tchobanoglous, G., 1976. Evaluation of the short-term toxicity of nitrogenous compounds to channel catfish, *Ictalurus punctatus*. *Aquaculture*, 8, pp.209–224.
- Correl, N.V. and Langley, R.W., 1956. Glycogen determination in liver and muscle by use of anthrone reagent. *Journal of Biological Chemistry*, 26, pp.583–593.
- Dacie, J.V. and Lewis, S.M., 1984., *Practical Haematology*. Churchill Livingstone.
- Das, P.C., Ayyappan, S., Das, B.K. and Jena, J.K., 2004. Nitrite toxicity in Indian major carps, sublethal effect on selected enzymes in fingerlings of Catla catla, *Labeo rohita* and *Cirrhinus mrigala*. *Comparative Biochemistry and Physiology Part C: Toxicology and Pharmacology*, 138(1), pp.3–10.
- Davidson, J., Good, C., Welsh, C. and Summerfelt, S.T., 2014. Comparing

- the effects of high vs. low nitrate on the health, performance and welfare of juvenile rainbow trout (*Oncorhynchus mykiss*) within water recirculating aquaculture systems. *Aquacultural Engineering*, 59, pp.30–40.
- Dias, G.M.C., Bezerra, V., Risso, W.E., Martinez, C.B. and Simonato, J.D., 2023. Hematological and biochemical changes in the Neotropical fish (*Astyanax altiparanae*) after acute exposure to a cadmium and nickel mixture. *Water Air & Soil Pollution*, 234, pp.307-314.
- Dube, P.N., Shwetha, A. and Hosetti, B.B., 2014. Impact of copper cyanide on the key metabolic enzymes of freshwater fish *Catla catla* (Hamilton). *Biotechnology & Animal Husbandry*, 30, pp.499–508.
- Evans, D.H., Piermarini, P.M. and Choe, K.P., 2005. The multifunctional fish gill: dominant site of gas exchange, osmoregulation, acid-base regulation, and excretion of nitrogenous waste. *Physiological Reviews*, 85, pp.97–177.
- Farkas, J., Christian, P., Urrea, J.A.G., Roos, N. and Hasselov, M., 2010. Effects of silver and gold nanoparticles on rainbow trout (*Oncorhynchus mykiss*) hepatocytes. *Aquatic Toxicology*, 96, pp.44–52.
- Fazio, F., 2019. Fish hematology analysis as an important tool of aquaculture: A review. *Aquaculture*, 500, pp.237–242.
- Fernandes, C., Fontainhas, A.F., Rocha, E. and Salgado, M.A., 2008. Monitoring pollution in Esmoriz-Paramos lagoon, Portugal: liver histological and biochemical effects in *Liza saliens*. *Environmental Monitoring and Assessment*, 145, pp.315–322.
- Friedewald, W.T., Levy, R.I. and Fredrickson, D.S., 1972. Estimation of the concentration of low-density lipoprotein cholesterol in plasma, without use of the preparative ultracentrifuge. *Clinical Chemistry*, 18, pp.499–502.
- Grzybowski, A., Sak, J. and Edmund, B., 2011. (1866-1911) Discoverer of the erythrocyte sedimentation rate. On the 100th anniversary of his death. *Clinical Dermatology*, 29(6), pp.697-703.
- Hall, L.W., Burton, D.T., Graves, W.C. and Margrey, S.L., 1984. Behavioral modification of estuarine fish exposed to sulfur dioxide. *Journal of Toxicology and Environmental Health*, 13, pp.969–978.
- Hao, L., Wang, Z. and Xing, B., 2009. Effect of sub-acute exposure to TiO<sub>2</sub> nanoparticles on oxidative stress and histopathological changes in juvenile carp (*Cyprinus carpio*). *Journal of Environmental Sciences*, 21, pp.1459–1466.
- Hecht, T., Uys, W. and Britz, P.J., 1988. Culture of Sharptooth Catfish, *Clarias gariepinus*, in southern Africa. *National Scientific Programmes Unit: CSIR, SANSP Report*, 153, pp.146-156.
- Hendrik, M., Laura, K., Werner, K. and Sven, W., 2006. Chronic exposure to nitrate significantly reduces growth and affects the health status of juvenile Nile tilapia (*Oreochromis niloticus* L.) in recirculating aquaculture systems. *Aquaculture Research*, 48(7), pp.01-16.
- Hussain, R., Mahmood, F., Khan, A., Javed, M.T., Rehan, S. and Mehdi, T., 2014. Cellular and biochemical effects induced by atrazine on blood of male Japanese quail (*Coturnix japonica*). *Pesticide Biochemistry and Physiology*, 103(1), pp.38–42.
- ICSH, 1993. Recommendations for measurement of erythrocyte sedimentation rate. *International Council for Standardization in Haematology (Expert Panel on Blood Rheology)*. *Journal of Clinical Pathology*, 46(3), pp.198-203.
- Jayamanne, S.C., 1986. A preliminary study of hydrogen sulphide toxicity on juveniles of *Macrobrachium rosenbergii*. *Network of Aquaculture Centres in Asia*, Bangkok, Thailand. November 1986.
- Kanu, K.C., Okoboshi, A.C. and Otitololu, A.A., 2023. Haematological and biochemical toxicity in freshwater fish *Clarias gariepinus* and *Oreochromis niloticus* following pulse exposure to atrazine, mancozeb, chlorpyrifos, lambda-cyhalothrin, and their combination. *Comparative Biochemistry and Physiology C: Toxicology & Pharmacology*, 270, p.109643.
- Kind, P.R.N. and King, E.J., 1954. Estimation of plasma phosphatase by determination of hydrolysed phenol with amino antipyrine. *Journal of Clinical Pathology*, 7(4), pp.322-326.
- King, E.J. and Jegatheesan, K.A., 1959. A method for the determination of tartrate-labile prostatic acid phosphatase in serum. *Journal of Clinical Pathology*, 12(1), pp.85–89.
- Kondera, E. and Witeska, M., 2013. Cadmium and copper reduce hematopoietic potential in common carp (*Cyprinus carpio* L.) head kidney. *Fish Physiology and Biochemistry*, 39(4), pp.755-764.
- Larsson, A. and Johansson, S.F.M.L., 1976. Comparative study of some haematological and biochemical blood parameters in fishes from Skagerrak. *Journal of Fish Biology*, 9, pp.425-440.
- Liu, Y., Ma, Q., Feng, M., Liu, L., Gao, M. and Yang, Z., 2019. Impact of SO<sub>2</sub> on juvenile turbot: growth, antioxidant responses, and tissue-specific bioaccumulation. *Aquatic Toxicology*, 21, pp.53-60.
- Lowery, O.H., Rosebrough, N.J., Farr, A.L. and Randall, R.J., 1951. Protein measurement with Folin phenol reagent. *The Journal of Biological Chemistry*, 193, pp.265-275.
- McGowan, M.W., Artiss, J.D., Donald, R.S. and Bennie, Z., 1983. A peroxidase-coupled method for the colorimetric determination of serum triglycerides. *Journal of Clinical Chemistry*, 29(3), pp.538-542.
- Mustafa, M.Z., Kheir, E.D.M., Azrak, E.L., Zaki, M.A., Bahig, R.N.A. and Mehana, E.S.E., 2016. Effect of ammonia toxicity on growth performance, cortisol, glucose, and hematological response of Nile tilapia (*Oreochromis niloticus* L.). *ACEB Journal of Animal Science*, 1(1), pp.21-28.
- Ololade, I.A. and Oginni, O., 2010. Toxic stress and hematological effects of nickel on African catfish (*Clarias gariepinus*) fingerlings. *Journal of Environmental Chemistry & Ecotoxicology*, 2, pp.14-19.
- Paul, A.V., Cheryl, A.M., Brian, J.S., Thomas, A.J., Peter, J.C., Peter, T.B., John, M.C., Robert, M., Murray, D.W. and William, C.L., 2010. Maternal influences on population dynamics: evidence from an exploited freshwater fish. *Ecology*, 91(7), pp.2003–2012.
- Rajkumar, K.S., Kanipandian, N. and Thirumurugan, R., 2016. Toxicity assessment on hematology, biochemical, and histopathological alterations of silver nanoparticles-exposed freshwater fish *Labeo rohita*. *Applied Nanoscience*, 6, pp.19–29.
- Ramesh, F. and Nagarajan, K., 2013. Histopathological changes in the muscle tissue of the fish *Clarias batrachus* exposed to untreated and treated sago effluent. *Advances in Bioscience and Bioengineering*, 1, pp.74–80.
- Richard, S. and Diana, P., 1966. A spectrophotometric method for the assay of lactic dehydrogenase subunits. *Analytical Biochemistry*, 15(3), pp.470-480.
- Rohani, M.F., 2023. Pesticides toxicity in fish: Histopathological and hemato-biochemical aspects-A review. *Emerging Contaminants*, 9, p.100234.
- Romano, N., Ceccariglia, S., Mastroli, L. and Mazzini, M., 2002. Cytology of lymphomyeloid head kidney of Antarctic fishes: *Trematomus bernacchii* (Nototheniidae) and *Chionodraco hamatus* (Channichthyidae). *Tissue and Cell*, 34, pp.63–72.
- Rosenthal, H.L., 1955. Determination of urea in blood and urine with diacetyl monoxime. *Analytical Chemistry*, 27(12), pp.1980-1982.
- Safriel, O. and Bruton, M.N., 1984. A cooperative aquaculture research programme for South Africa. *South African National Scientific Programmes Report*, 89, CSIR, Pretoria, p.79.
- Sayed, A.H. and Hamed, H.S., 2017. Induction of apoptosis and DNA damage by 4-nonylphenol in African catfish (*Clarias gariepinus*) and the antioxidant role of *Cydonia oblonga*. *Ecotoxicology and Environmental Safety*, 139, pp.97–101.
- Sayed, A.H., Mekkawy, I.A.A. and Mahmoud, U., 2011. Effects of 4-nonylphenol on metabolic enzymes, some ions, and biochemical blood parameters of the African catfish *Clarias gariepinus* (Burchell, 1822). *African Journal of Biochemistry Research*, 5, pp.287–297.
- Singh, A., Dar, M.Y., Joshi, B., Sharma, B., Shrivastava, S. and Shukla, S.,

2018. Phyto-fabrication of silver nanoparticles: novel drug to overcome hepatocellular ailments. *Toxicology Reports*, 5, pp.333-342.
- Talke, H. and Schubert, G.E., 1965. Enzymatic urea determination in the blood and serum in the Warburg optical test. *Klinische Wochenschrift (Journal of Molecular Medicine)*, 43, pp.174-175.
- Tavares, D.M. and Moraes, F.R., 2007. Hematology of teleost fish. *Veterinary Clinics of North America: Exotic Animal Practice*, 10(3), pp.859-876.
- Warnick, G.R., Benderson, J. and Albers, J.J., 1982. Dextran sulphate-Mg<sup>2+</sup> precipitation procedure for quantitation of high-density lipoprotein cholesterol. *Clinical Chemistry*, 28, pp.1379-1388.
- Witeska, M., Sarnowski, P., Ługowska, K. and Kowal, E., 2014. The effects of cadmium and copper on embryonic and larval development of *Ide Leuciscus idus* L. *Fish Physiology and Biochemistry*, 40(1), pp. 151-163.
- Wong, C.K., Wu, R.S., Kuah, M.K., Lee, S.M. and Richardson, B.J., 2016. Gene expression profiling revealed diverse molecular mechanisms underlying differential responses of cobia juveniles to elevated carbon dioxide. *PLOS ONE*, 11(1), p.e0145695.
- Wybenga, D.R., Pileggi, P.H., Dirstine, J. and Giorgio, J.D., 1970. Direct manual determination of serum total cholesterol with a single stable reagent. *Clinical Chemistry*, 16, pp.980-984.
- Xing, J.H., Yang, K.C., Hyung, S.I., Oktay, Y., Euisiky, Y. and Hak, S., 2006. Aspartate amino transferase (AST/GOT) and alanine aminotransferase (ALT/GPT) detection techniques. *Sensors (Basel)*, 6(7), pp.756-782.



# Analysis of the Lebanese Society's Behavior Regarding Electronic Waste Management

M. Trad<sup>†</sup> and A. Harb

Faculty of Business Administration and Economics, Notre Dame University, Lebanon

<sup>†</sup>Corresponding author: M. Trad; mtrad@ndu.edu.lb

Nat. Env. & Poll. Tech.  
Website: [www.neptjournal.com](http://www.neptjournal.com)

Received: 03-03-2024

Revised: 16-04-2024

Accepted: 26-04-2024

## Key Words:

E-waste

E-cycling

Waste management

Environmental awareness

Refurbished products

Recycled materials

## ABSTRACT

This paper examines electronic waste and cycling in Lebanon. It describes the current situation regarding e-waste among government agencies and non-governmental organizations. It addresses two research questions: The first one asks if the Lebanese society and government are aware of the dangers posed by electronic waste and whether any action has been taken to prevent an environmental catastrophe. The second question asks about Lebanese attitudes toward e-waste and whether they are willing to fight against it. Interviews provided the first question's responses. The authors have visited Organization A and NGO B. The first is worried about gathering waste in more prominent Beirut, while the second targets spreading attention to e-waste's risks on legislative and social levels the same. Question two was discussed through surveys filled out by arbitrary people from Lebanese society. The answers to both research questions came in a manner that demonstrates the two hypotheses expected toward the start of the study, specifically that e-waste represents an incredible danger to the Lebanese climate. Hypothesis two, if climate neighborliness and proclivity to right e-garbage removal rely upon the instructive level of some random resident, has been confirmed while analyzing the answers in the survey.

## INTRODUCTION

The reliance on technology is what most defines the twenty-first century and sets it apart from previous eras. These days, it is difficult to envision existence without PCs, cell phones, TVs, or some other electronic appliance; Furthermore, it is insufficient to use with about any computer, mobile device, or television: these should be ultramodern, or if nothing else present day for them to enough work. The consumer is being forced to follow technology's rapid development and occasionally purchase new electronic appliances, putting older devices that are no longer compatible with modern technology in the basement or junkyard. This unused electronic equipment will eventually be thrown out. The buyer electronics industry has been developing at an incredibly high rate. Interest in buying electronic products has forever been there, however, it has arrived at its peak in the past couple of years. This has brought about the extension of this area, which is presently one of the most productive in the worldwide economy (Nagajothi & Kala 2018, Chen 2010). Electronic waste, also known as e-waste or e-scrap, is discarded, broken, surplus, and obsolete electrical and electronic equipment; Additionally, the term "Waste Electrical and Electronic Equipment" (WEEE) is frequently utilized. E-squander signifies any item that holds

an electronic board, a battery, or just electronic parts like a screen, capacitors, diodes, and transformers that are broken or presently not utilized. Examples of electrical and electronic devices that could turn into WEEE are TV and PC monitors, computers and computer peripherals (e.g., webcams, keyboards, scanners, printers, USB flash memory, etc.), Audio and stereo equipment (e.g., MP3 players, DVD, VCR, CD players, etc.), Corded & Wireless communication devices, Cameras, Fax and copy machines, video game consoles, batteries, adaptors, chargers and UPS, Home appliances such as Microwaves, Fridges, Irons etc. (Bortoleto 2015, Mor et al. 2021, Hong et al. 2015, Xue & Xu 2017). Throughout this paper, the terms electronic waste, e-scrap, WEEE, and e-waste are used interchangeably. As hardware keeps on propelling, there is more in innovation to anticipate. The development of electronic technology may improve the world, but it poses a greater threat to the environment. Pollution and the construction of buildings brought about by modernization harm trees and animal habitats. Flooding happens considering timberland deforestation. Electronic gadgets should be eco-friendly, so developers should think about that. Innovation must not ignore environmental concerns. Worldwide, waste of electrical and electronic equipment ranges from 20 to 50 million tons annually;

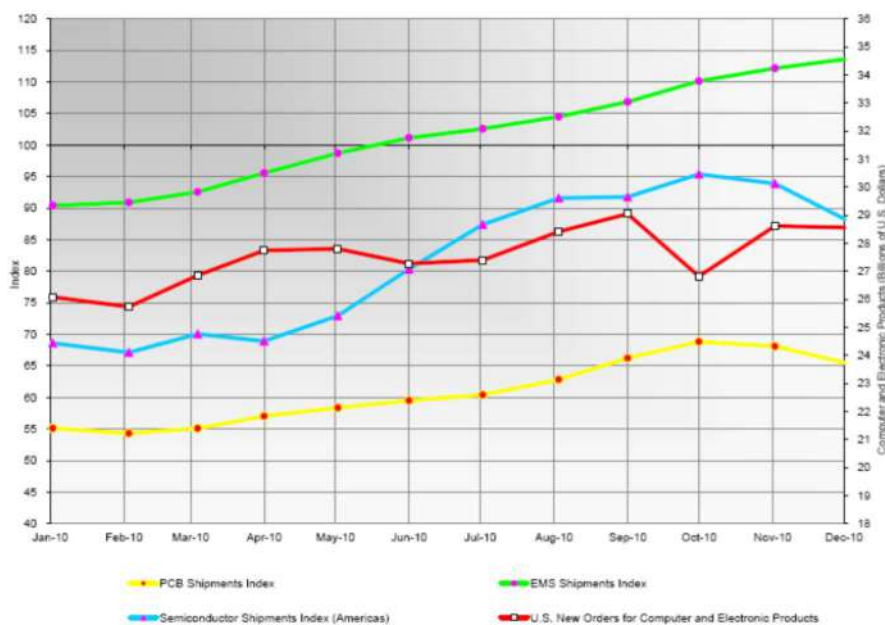
these electronic gadgets are, made of a wide assortment of material constituents. Constituents, like lead, nickel, cadmium, and mercury could present dangers to human wellbeing or the climate whenever fumbled at their finish of life. On the other hand, these components of e-waste are made of valuable resources like copper, precious metals, and engineered plastics, all of which take a lot of energy to process and make. By recovering these valuable materials through recycling (E-Cycling) or reusing less raw materials are taken from the earth, air and water pollution is reduced, gas emissions are reduced, and energy and resources are saved (Kaza et al. 2018, Murthy & Ramakrishna 2022, Islam et al. 2020, Kiddee et al. 2014). Hereby is an example of a study done by the EPA (Environment Protection Agency) of the United States of America. This study shows that recycling one million laptops saves energy equivalent to the electricity used by 3,657 US homes in a year. Given that study and other examples, a worldwide appeal for proper processing and management lately increased. The European Association has as of late fostered a progression of new strategy drives to additional location negative natural and human well-being effects of risky substances. In EU terms, three recent policy developments—two “directives” and one “regulation”—have a significant impact on the management of hazardous chemicals and e-waste in the future. The first directive covers waste electrical and electronic equipment (WEEE), and the second outlines restrictions on the use of certain hazardous substances in electrical and electronic equipment (RoHS). WEEE and RoHS entered into force in February 2003. In Lebanon, there are still no legislative guidelines or arrangements that treat the waste issue. As a result, citizens should be made more aware, and the government should deal with WEEE in accordance with international standards. The management of electronic waste in Lebanon will be illuminated in this paper. It will report on the existence of governmental and non-governmental organizations concerned with e-waste regulation or recycling as well as statistics regarding people’s awareness of this issue. Through our research and interviews with various Lebanese parties, we intend to determine whether improper disposal of e-waste poses a threat to human and environmental health. Additionally, we target upgrading mindfulness among Lebanese residents, beginning with understudies in schools and colleges to any party worried about saving the earth from these perilous materials and edifying them about the approaches to taking care of waste created and what might be the advantage if fittingly managed. To effectively manage e-waste through either e-cycling (electronic recycling), reuse, or donation, the government and the public must acknowledge the issue and implement policies.

## SIMILAR STUDIES IN THE PAST

The results of earlier research that was conducted by nations all over the world, such as the United States, Europe, and Japan, are presented in this section. Data is accumulated from articles, distributed booklets and studies led about the impact of E-Waste on the climate and the human well-being living around and its control cycle. People’s lives have been drastically altered by the Industrial Revolution, which was followed by advances in information technology over the past century. Even though humans have benefited from this development, poor management has resulted in recent contamination and pollution issues. The technological competence acquired over the past century has brought about a new obstacle in waste management. A study on computer trends found that the steady rise in demand was remarkable. Computers are now used in a wider variety of settings, including schools, offices, homes, and manufacturing facilities, than ever before (Rathi & Shyamalendu 2015, Stoeva & Alriksson 2017). Regarding the expansion and availability of electronics in the United States, an IPC study demonstrates the rising demand for electronic goods:

Fig. 1 shows that the U.S. economy grew at an annualized rate of 3.2 percent in the fourth quarter of 2018. The solid growth was attributed to consumer spending and foreign trade. Besides, a UN study found that the manufacturing of a computer and its screen takes at least 240 kg (530 pounds) of fossil fuels, 22 kg (48 pounds) of chemicals, and 1.5 tons of water – more than the weight of a rhinoceros or a car. As a result, household appliances, personal computers, and other electrical and electronic equipment (WEEE) waste is regarded as one of the hazardous waste categories with the fastest global growth. The preceding section cites research conducted by several organizations, which demonstrates that the volume of e-waste is without a doubt expanding at unprecedented rates. However, what is so distinctive about this kind of waste? What makes it unique in relation to various kinds of trash like biodegradable waste or paper and cardboard waste? Well, the toxicity and high value of its components are what make e-waste unique. A variety of substances, both non-hazardous and toxic, are contained in typical electrical waste. Take, for instance, a discarded small radio: This device has metal parts like the antenna and screws in a plastic casing. Inside the casing are one or more PCBs (Printed Circuit Boards) made of plastic or resin with thin copper layers and small electronic components and ICs (Integrated Circuits) that are attached to the PCB with lead solder. While copper, tin, tar, and plastic are nontoxic, nonetheless they can be reused and reused in the creation of new plastic and metal parts. Other non-risky materials can be found in small amounts in electrical and electronic





Note on the graph:

All indices are based on the same baseline of the average month in 2000=100, and reflect a 3-month rolling average.

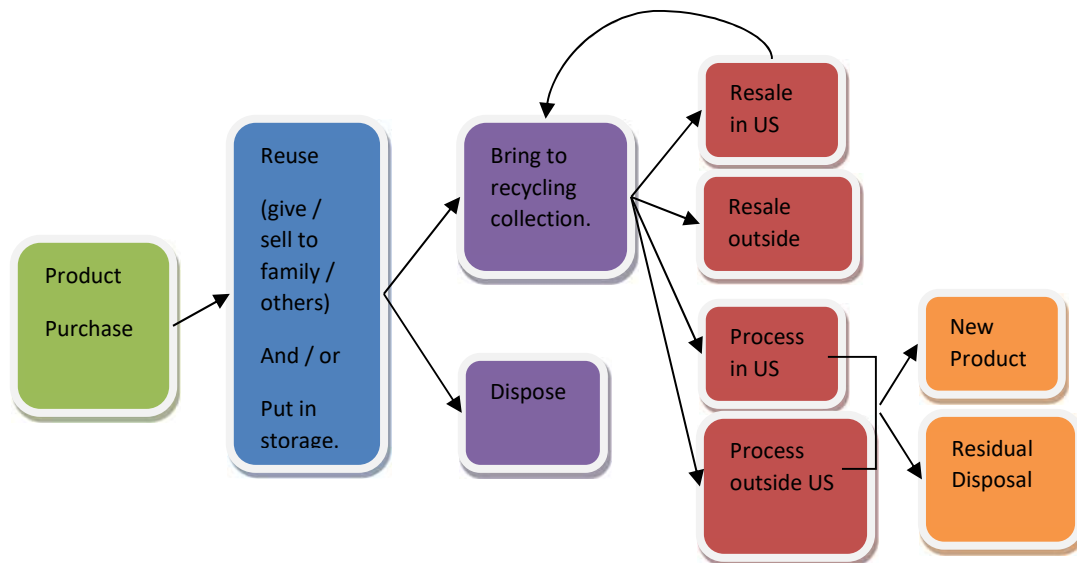
Sources: IPC statistical programs for the EMS and PCB industries; SIA for semiconductor data; U.S. Census Bureau for U.S. new orders for computer and electronic products.

(Source: www.ipc.org)

Fig. 1: Trends in U.S. Computer and Electronic Products New orders and North American Sales Indices of Selected Supplier Industries in 2018.

items like this radio are aluminum (utilized in electrolytic capacitors), silicon (utilized in ICs), gold utilized as plating for connectors, and different components like zinc, lithium, germanium (Bhat & Patil 2021, Abbas et al. 2019, Ilankoon 2018, Song & Li 2015). The toxic substances in the radio are the lead contained in the solder, BFRs (Brominated Flame Retardants) used as a flame retardant in most electronic parts subject to prominent levels of heat, and cadmium used in batteries. Other toxic elements known to be used in various electronic devices are Americium, a radioactive element used in smoke detectors. Mercury: found in flat screens, mechanical doorbells, and fluorescent tubes. Sensory impairments, dermatitis, memory loss, and muscle weakness are negative health effects. Death, diminished fertility, and diminished growth are animal effects of the environment. Sulfur: utilized in lead-acid batteries. Health effects incorporate liver harm, kidney harm, heart harm, eye, and throat bothering. Sulfuric acid can result from its release into the environment. Cadmium: found in nickel-cadmium batteries, corrosion-resistant alloys, and light-sensitive resistors. Nickel-cadmium rechargeable batteries contain the most usual form of cadmium. It can leach into the soil, harming microorganisms and disrupting the soil ecosystem if it is not properly recycled. Cadmium exposure through inhalation has been linked to kidney damage and severe lung damage. Oxide of beryllium: filler

in some materials used at the thermal interface, like the thermal grease on CPU and power transistor heatsinks. If taken orally, beryllium oxide is extremely harmful. One will find at least one of these harmful substances recorded above in each piece of electronics conveying genuinely a threat to the climate and the people. Since the nineties, developed nations have mitigated the risks associated with irresponsible e-waste disposal (Bell et al. 2010, Adeola & Othman 2011, Sthiannopkao & Wong 2013). As previously stated, developed nations have conducted research and raised public awareness of this pressing issue because e-waste poses a risk to citizens and the environment. In the US, electronic gear has turned into a pillar of their lifestyle. Somehow, it is a fundamental piece of all that they do and possess TVs in homes, automobile GPSs, MP3 players and cell phones in their pockets, and laptops on desks and laps. Every year, the electronics industry makes \$2 billion. Americans own three billion electronic items. For every new product that is introduced, one or more become out of date or obsolete. As a result, they are throwing away or storing older electronics more quickly than ever before. In 2015, the Environmental Protection Agency (EPA) estimated that between twenty-six and thirty-seven million computers became obsolete. In addition to that, the amount of used or unwanted electronics ranged between 1.9 and 2.2 million tons. Of these, about 1.5 to 1.8 million tons were primarily disposed of in landfills,



(Source: Electronics Waste Management in the U.S, Office of Solid Waste U.S Environmental Protection Agency)

Fig. 2: Framework for Modeling the Product Lifecycle.

and only 345,000 to 379,000 tons were recycled. So, the EPA has been collaborating with stakeholders to help improve awareness of the need for the recovery of electronics and access to safe reuse and recycling options. State and neighborhood legislatures, producers, and retailers, who are as of now mindful of the squeezing need to more likely deal with these materials, are providing more chances to recycle and reuse this equipment. Electronics cannot be disposed of in landfills in at least seven states, and four have established recovery programs. A form of legislation to regulate used electronics is being considered by a few additional states. To assist in the management of discarded household electronics, over eight hundred communities have established electronics collection events (Seeberger et al. 2016, Kahhat et al. 2008, Abalansa et al. 2021).

### Key Findings

**The electronic products lifecycle:** Almost half or 976 million units, of all the products sold between 2000 and 2014 are still in use or reuse (Fig. 2). About 42 percent, or 842 million units, of the products sold between 2000 and 2014 have been recycled or disposed of.

**The storage:** From 1980 until 2005, 180 million electronic products had accumulated in storage. In 2005 alone, approximately 460 million products were put into storage and/or reuse. TVs account for 34-52 percent (by weight) of the units in storage. Desktop PCs account for approximately 24 percent (by weight) of stored units.

**Recycling vs Disposal:** In the period from 2003 to 2005,

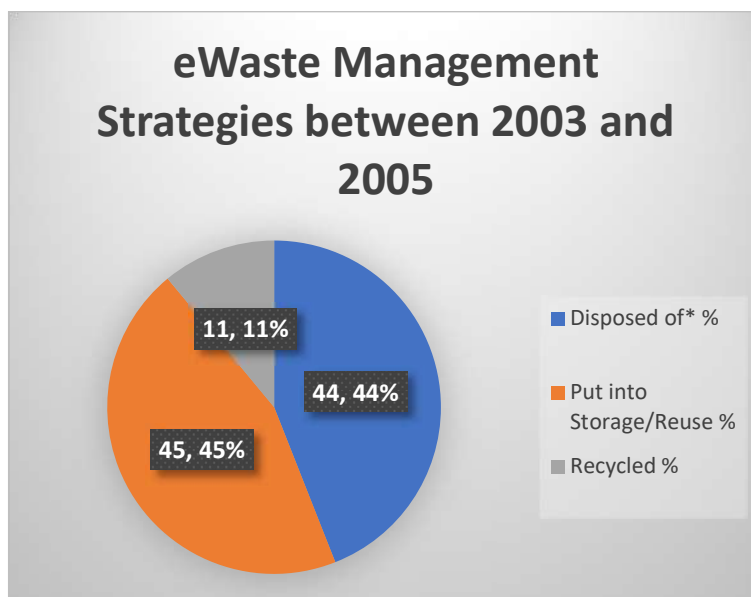
electronic products available for EOL management were recycled or disposed of in the following approximate percentages: About 15-20 percent was collected for recycling. The recycled/disposed split remained constant in the years from 1999 until 2005. Although recycling continues to increase, the percentage recycled is still constant because of the ever-increasing number of electronics available for EOL management. About 80-85 percent was disposed of (in landfills). In the two years period from 2003 until 2005, when products are included into storage or reuse. Approximately 44 percent of products were disposed of, and 11 percent recycled.

**End markets:** In 2005, approximately 61 percent, or 107,500 tons, of CRT monitors and TVs collected for recycling were exported for remanufacture or refurbishment. The next largest part (about 14 percent or 24,000 tons) was CRT glass sold to markets abroad for glass-to-glass processing, while lead recovery in North America accounts for about 6 percent (10,000 tons) of the materials. (Gibson & Tierney 2006, Ogunseitan et al. 2004, Kang & Schoenung 2005, Abalansa et al. 2021).

Fig. 3 stands for the average amount of electronics recycled, disposed of, or put into storage or reused from 2003 till 2005. In 2005 alone, approximately 460 million units were put into storage and/or reuse.

As for TVs and CRT monitors collected by electronic recyclers in the U.S., information is presented in Table 1.

According to the data, 61% of the CRT monitors and TVs that were collected for recycling are exported to produce



(Source: www.epa.gov)

Fig. 3: Electronic products, recycled, disposed, or Going into Storage/Reuse 2011-2017.

re-manufactured or refurbished CRT monitors and TVs. In terms of European nations, statistics from Euro stat indicate that the European Union alone generates three billion tons of waste each year, approximately ninety million of which are hazardous. This amounts to about six tons of solid waste for every man, woman, and child. Between 1990 and 1995, the amount of waste generated in Europe increased by 10%, according to the Organization for Economic Cooperation and Development (OECD). Additionally, waste is either

Table 1: End Markets for EOL TVs and CRT Monitors Collected for Recycling in the U.S. in 2012 .

End Market	Tons/Year	% of Total
Resale 'as is' or after some repair/ upgrade in the US	3000	2%
Resale 'as is' or after some repair/ upgrade abroad	3500	2%
Refurbishing or remanufacturing into specialty monitors in the US	2500	1%
Refurbishing or remanufacturing into specialty monitors abroad	107500	61%
CRT glass-to-glass factories in the US	4000	2%
CRT glass-to-glass factories abroad	24000	14%
CRT glass to smelters in North America for lead recovery	10000	6%
Plastic, metal and other material recovery from remanufacturing	20500	12%
Total	175000	100%

(Source: World Reuse, Repair and Recycling Association)

disposed of in landfills or burned in incinerators (67 percent). However, these two methods harm the environment. In addition to taking up increasingly valuable land, landfilling pollutes the air, water, and soil by releasing carbon dioxide (CO<sub>2</sub>) and methane (CH<sub>4</sub>) into the atmosphere and chemicals and pesticides into the ground and groundwater. In turn, this is bad for people's health as well as for plants and animals (Propescu 2015). By 2020, the OECD estimates, that they would generate 45% more waste than they did in 1995. One of the four top priorities in the EU's Sixth Environment Action Program is waste prevention and management. Its essential objective is to decouple waste generation from financial action, so EU development will never again prompt expanded junk, and there are signs that this is starting to occur. The generation of municipal waste, for instance, decreased in the Netherlands and Germany during the 1990s. Through new waste prevention initiatives, improved resource utilization, and encouraging a shift to more sustainable consumption patterns, the EU is aiming for a significant reduction in garbage production (Vadoudi et al. 2015, Skinner et al. 2010, Mohanty et al. 2015).

The three guiding principles of the European Union's waste management strategy are:

1. Preventing waste: Any strategy for managing waste must include this. By reducing the presence of hazardous substances in products, we can reduce the amount of waste that is generated and make it less hazardous. This will make it easier to get rid of waste.
2. Improving



Fig. 4: E-waste disposal container at a German electronics company



Fig. 5: All out-of-order electronic parts end up here.

manufacturing techniques and influencing consumers to demand greener products and less packaging are all intertwined with waste prevention. 3. Recycling and reuse: Recovering as much of the materials as possible, preferably through recycling, should be done if waste cannot be avoided. The European Commission has characterized explicit ‘waste streams’ for need consideration, the point being to lessen their ecological

effect. Waste from packaging, used cars, batteries, and electrical and electronic waste are all included in this. The collection, reuse, recycling, and disposal of these waste streams must now be regulated by Member States in accordance with EU directives. Over fifty percent of the waste packaging is already recycled in EU countries. Enhancing surveillance and final disposal: Waste that cannot be recycled or reused should be safely burned

Table 2: Estimated amount of WEEE currently collected and treated as a percentage of the total amounts of WEEE for the EU27, 2005.

Large household appliances (smaller items)	40%
Small household appliances, lighting equipment – luminaires and domestic medical devices	26.6%
IT and telecom excl. CRT's	27.8%
CRT monitors	35.3%
LCD monitors	40.5%
Consumer electronics excl. CRT's	40.1%
CRT TV's	29.9%
Flat-panel TVs	40.5%
Lighting equipment – Lamps	27.9%
Electrical and electronic tools	20.8%
Toys, leisure and sports equipment	24.3%
Medical devices	49.7
Monitoring and control instruments	65.2%
Automatic dispensers	59.4%

(Source: Best Practices for E-Waste Management in Developed countries)

instead of dumped in a landfill whenever possible. Both these techniques need close checking considering their true capacity for causing extreme natural harm. A directive with stringent management guidelines for landfills was recently approved by the EU. It boycotts specific sorts of waste, like utilized tires, and focuses on diminishing amounts of biodegradable garbage. Incinerator emission levels are tightly controlled by another recent directive. The Union also wants to reduce emissions of dioxins and acid gases such as nitrogen oxides ( $\text{NO}_x$ ), Sulphur dioxides ( $\text{SO}_2$ ), and hydrogen chlorides (HCL), which can be harmful to human health (Sthiannopkao et al. 2013, Mohanty et al. 2015, Vadoudi et al. 2015).

Regarding the infrastructure of e-waste management, Europe is considering three main types of e-waste management systems, namely, Take-back systems (collective-model), clearinghouse-model and European Recycling Platform (ERP).

**National collective system:** is the most widely used national system for managing WEEE collection within national boundaries (Table 2). Although their legal status varies from country to country, they are non-profit, non-governmental businesses owned by one or more trade associations. They are organized into product categories so that they can find markets for recycled material and product reuse and focus on making their recycling operations as efficient as possible. This framework has drawbacks: Cost prohibitive in comparison to the clearing house model in terms of enforcement and does not encourage cost reduction. On

the other hand, this is the case in an environment where competition is constant, and the economics of the supply chain are a major driving factor.

**Competitive clearing house system:** is again a public system in which different accomplices. However, it lacks the knowledge and data necessary to effectively analyze and compare it to other collective schemes.

**European recycling platform:** enables member businesses to meet the WEEE's product take-back obligations at a competitive cost, benefiting both customers and the environment (Sthiannopkao et al. 2013).

In conclusion, previous experiences with electronic waste policies in developed nations demonstrate that legislation ought to serve a variety of broader societal objectives. It ought to likewise obviously characterize the jobs, obligations, and meanings of waste included under the umbrella of the regulation to limit managerial burden and confusion. It is essential and beneficial for implementation to separate operational standards from the fundamental legal framework. E-waste management is a long-term process that requires collaboration among various stakeholders and technological advancements to better manage the issue and reduce e-waste through the design of future electronic products. Even in developed nations like Japan and the EU, where e-waste management has been practiced for a long time, there is a lot of room for improvement in the way e-waste is collected and managed in the future. Notwithstanding, existing great practices from created nations give significant illustrations and bits of knowledge to developing nations to manage e-waste and its management both as far as great practices can be taken on and thought about in figuring out or auditing existing e-waste regulation in the country. Once we see the success of the other countries around the world in dealing with e-waste management, we deduce the necessity of such policies and regulations' implementation as well as rising awareness among citizens. All these facts have driven us to focus on the current Lebanese situation and the e-waste status. Our paper will be looking at this issue in terms of current circumstances, management, and awareness.

## MATERIALS AND METHODS

This study will make use of both primary and secondary data. Interview-based primary data and reliable secondary data, such as articles in journals and magazines, previous studies and research, published books, and websites. We found that Lebanon is in great danger for the environment if society does not change its perception of undifferentiated waste disposal at the nearest dumping site or valley, and it was urgent to assess the local situation to determine which

organizations are working on this matter, which laws or drafts of laws are in place to curb the environmental disaster that is about to occur and to determine whether citizens are aware of the e-waste danger, how they deal with their old electronic appliances, and whether they would be willing to do more to save nature. Hence, in essence, this paper will answer two questions through research

1. Is there such hazardous waste in Lebanon, and if so, what campaigns have been launched to combat it? In addition, does the government of Lebanon enact any legislation to combat waste?
2. How does the typical Lebanese feel about e-waste, and how willing is he or she to fight it?

Following our research questions, two theories are molded. These hypotheses help in guiding the study, showing realities, and providing a system for diving into conclusions and suggestions. In our study, two hypotheses are developed.

The first hypothesis says the following:

Governmental and NGO actions, translated into easing e-cycling and raising awareness among the citizens, will have a positive impact on cutting environmental hazards, reducing pollution, and saving natural resources.

As for the second hypothesis, it claims that:

The purchase of recycled products is highly affected by the consumer's prejudgment and status.

In our stated hypotheses, the independent variables are as follows: In the first hypothesis, awareness campaigns and facilitation of e-cycling are the independent variables that have a direct effect on human health and nature. E-cycling refers to the recycling of waste associated with electrical or electronic products like computers, mobile phones, televisions, and microwaves, as opposed to throwing them away and creating e-waste. Encouraging people and raising their awareness to be socially and environmentally involved in saving the planet and their health through buying refurbished products will also save natural resources and reduce costs. In the second hypothesis, the purchase of electronics is the dependent variable while it is linked to the independent ones: consumer's prejudgment and status. The level of consumption of such recycled goods would rise because of raising awareness among Lebanese people, and it is important to note that status would play a significant role in influencing buyers' actions. In our paper, we can notice that the dependent and independent variables are more qualitative than quantitative due to the type of primary data collected. They assist us in providing useful recommendations and are utilized for the evaluation of e-waste in Lebanon. The authors of this paper, for reasons of confidentiality, refer to interviews with Company A and NGO B to support their

hypothesis regarding the Lebanese actions and their impact on e-waste to demonstrate that hypothesis one is true.

Data used to support hypothesis #1 is extracted from two diverse sources: To demonstrate that e-cycling is the most practical approach to addressing the e-waste issue, the authors rely on online literature on a global scale. Due to the lack of literature on the effect of laws and recycling initiatives in Lebanon, the authors resorted to interviewing officials in two local organizations concerned with e-waste treatment in Lebanon. As mentioned, if we go through the hazards engendered by e-waste, we remark that this e-waste has toxic substances that are harmful to humans and the environment. Electronic products and their components, such as semiconductor chips, circuit boards, and disk drives, are made of over one thousand different elements, including chlorinated solvents, PVC (polyvinyl chloride), heavy metals, plastics, and gases. E-waste risks are minimal when these components are securely encased in the purchased goods. Issues can happen when devices break. They can leak and contaminate their immediate surroundings—the house, the school, the street, the natural world, or the landfill—at this point. Over time, the toxic chemicals of landfill e-waste can seep into the ground, enter the water supply, or they can escape into the atmosphere, thus affecting the health of nearby communities. Hazardous waste reuse, recycling, and reclamation can avoid environmental hazards and pollution. In terms of environmental benefits, recycling hazardous waste fulfills two of RCRA's (Resource Conservation & Recovery Act) goals by reducing the consumption of raw materials and reducing the volume of waste materials that must be treated or disposed of. Primary data has been gathered through qualitative interviews conducted with an NGO named B, founded in 2008, whose primary goal is to promote good environmental practices among the MENA communities for sustainable development, and with Company A, which takes care of cleaning the cities from streets to urban areas to parks and public spaces. Starting in Beirut, they now cover the Greater Beirut area and Mount Lebanon, serving more than two million residents. Interview protocols were structured following the research questions developed and addressed in our paper, one for the president of NGO B and one for the representative of company A. Regarding the second hypothesis, which says that the environmentally aware behavior of the consumer in Lebanon varies depending on his education and social status, the authors support their hypothesis by conducting a survey on a sample of fifty individuals, chosen randomly but of diversified age span, gender, and education level. After analyzing our data via the Statistical Software "SPSS," the indicators that shall be noted are mentioned in Tables 3 and 4. The educational level of the polled sample is distributed as in Table 4.

Table 3: Population.

		Frequency	Percent	Valid Percent	Cumulative Percent
Valid	Male	26	52.0	52.0	52.0
	Female	24	48.0	48.0	100.0
	Total	50	100.0	100.0	

Table 4: Educational Level.

		Frequency	Percent	Valid Percent	Cumulative Percent
Valid	Brevet	2	4.0	4.0	4.0
	Official Baccalaureate (Lebanese or equivalent)	5	10.0	10.0	14.0
	University degree	43	86.0	86.0	100.0
	Total	50	100.0	100.0	

As a conclusion, research questions and hypotheses were developed and stated explicitly. The dependent and independent variables were identified, and the collection of secondary and primary data was performed through various research instruments that were introduced and explained above. The basis of the SPSS survey was defined, and the general framework for the two interviews with company A and NGO B was described.

## RESULTS AND DISCUSSION

This part presents the results of the interviews conducted with the two parties involved with e-waste management in Lebanon, namely company A and NGO B. It also lists the results of the conducted survey on a sample of 150 Lebanese citizens and concludes the given answers in the form of statistics. The president of NGO B started the interview by introducing the organization as a non-governmental (NGO) founded in 2008 and aims to promote good environmental practices among the MENA communities for sustainable development. The organization's mission is to induce a change in the behavior of the MENA region communities to protect and save the environment. To promote public-private partnerships to successfully implement community-based environmental development projects. To lobby for the practice of sustainable environmental behavior in the MENA region both at grassroots and national levels and to adopt and adapt environmentally sound technologies for solid and wastewater management.

NGO B representative afterward cited a couple of events recently held across Lebanon to promote awareness for e-waste in society and at the official level. The most notable events were:

### The NGO Launches the Arab Forum for E-Waste Management

The workshop was held in Beirut with the presence of well-respected officials from both the public and private

sectors who spoke about their partnership with NGO B, which focuses on encouraging the reuse of computers before recycling them by providing licensed software that is compatible with refurbished computers. This process is part of their environmental initiative in the Middle East and North Africa.

And to sum up the event, the below list of recommendations that will be addressed to the board of the Arab Ministries for further advocacy includes enacting and amending legislation to conform with the needs of e-waste management. Preparing national action plans that tackle the e-waste issue. Applying and issuing internationally approved guidelines for the sound management of e-waste and adjusting them to suit the participating countries. Building the abilities of relevant institutions (Government, private sector, civil society, and media) on e-waste hazards and proper management. Raising the level of awareness and knowledge among producers, importers, and wholesalers of electrical and electronic devices, setting up a mechanism to communicate with them through Chambers of Commerce. Strengthening the partnership between the public and the private sector and the civil society organizations for e-waste management. Creating coordination mechanisms between the institutions of civil society and introducing e-waste awareness in schools, technical institutes, and universities' curricula.

### The NGO Collaborates with the American University of Beirut to Spread Awareness of the Dangers of E-Waste

The event took place with the collaboration of the American University of Beirut's Center of Civic Engagement and Community Services and the University's environmental club. It was under the patronage and presence of a top-level representative of the Ministry of Environment that NGO B organized this E-Waste awareness and collection day at the American University of Beirut. Through this collaboration, NGO B and the latter university aim to spread awareness on the E-Waste issue where they pointed out that 65% of the

Lebanese population keep their E-waste at home, “ignoring the health risks of this silent killer” and help guide university students along with the surrounding to support this movement and encouraging the sustainability of the operation. The named university will be acting as an official E-Waste collection point.

### **The NGO Launches “E-waste Best Management in Public Administrations and Institutions”**

NGO B’s president pointed out the dangers of the improper disposal of e-waste, knowing that it has more than one thousand toxic substances. He then declared that the project aims to raise the level of awareness on this matter among workers of public administrations and institutions. As for the director of the NGO, she declared that currently, e-waste occupies approximately 22,000 cubic meters of storage in public institutions.

### **The NGO Lobbies for the Approval of a Decree for the Best Management of E-Waste in Public Administrations and Institutions**

This event was organized with the presence of other NGOs alongside ministries’ representatives and officials.

The key achievements of the NGO’s project were announced by its president as follows: Raising awareness in the ministries and public institutions about the dangers of E-waste and the environmental and health problems attributed to it. Drafting a decree that would set up guidelines to check and collect e-waste in the ministries. It has been sent to the Lebanese Ministry of Environment to be reviewed and then to be given to the Council of Ministers. Setting up an inter-ministerial committee that would sustain the E-waste collection in the ministries, in cooperation with NGO B, including more public and private schools that receive help from awareness material. Launching a TVC that used social media like Facebook and YouTube to reach a wider range of the public, and which will soon be on television.

A USAID representative discussed the importance of initiatives as such, targeting extremely dangerous issues like the e-waste problem. He affirmed that USAID is always willing to encourage civil society organizations in Lebanon to play a more active role in promoting good governance in both the public and the private sectors. One representative from the Ministry of Environment (MoE) talked about the sustainability of the cooperation between the Lebanese MoE and NGO B, stressing the importance of this environmental initiative, knowing that Lebanon has signed International Conventions that include e-waste management within their scope of work. She declared that environmental safety is one of the most fundamental rights for the generations to come,

and it is our duty to provide them with the best conditions possible. Besides, the results of the conducted assessment by NGO B on the status of e-waste in ministries were as per the following: When stored, the electronic waste is revealed to be a costly operation for the ministries, which can reach up to 12,000 USD a year. The average turnover rate is 4 years; however, a computer’s lifespan could reach up to 7 years or until it is broken before disposing of it. There are no common procedures for the disposal of E-waste nor is there a department responsible for their disposal.

### **Microsoft and NGO B Launch “The Responsible E-learning through E-Waste Best Management”**

Together, NGO B and Microsoft organized a connection day/workshop. This workshop was under the high patronage of the Lebanese Ministry of Environment. During this event, Lebanon Country Manager in Microsoft, spoke of the corporation’s green initiative and the support it provides to the civil society through technology. Also, she portrayed the environmental policies applied at Microsoft’s buildings worldwide. The purpose of this workshop was explained to the participants as follows: “Our goal is to set an action plan that helps provide the public with a realistic and sustainable solution for the E-waste problem by making use of technology; hence, we would be forming responsible E-generators through our educational activities.” Increased events and projects were and will be launched by this NGO aiming at raising awareness about E-Waste dangers and the best way of managing it. They are highly focused on the new generation through workshops organized at schools and summer camps, in addition to the competitions that improve commitment and excitement about this issue. Besides, during their organized events and workshops, they insisted on the hazards of E-Waste on human health and the environment and the way to prevent such impacts. NGO B has prepared a hierarchy of e-waste management standing for a continuum from the least favored choice to the most favored one: disposal, energy recovery, recycling, reuse, minimization, and prevention. They consider that prevention is the most desired action that should be admitted by users since once they are aware of their impact, people will think twice before acting. On the other hand, we should recognize that the Ministry of Environment and the EU are getting the proper approval for NGO B to ship the e-waste collected in Lebanon to recycling plants in Europe. However, this exporting procedure faces difficulties due to the Basel Convention, which is an international treaty that was issued to reduce and prevent the movement of hazardous waste between nations. As for the recycling process, named “E-cycle,” which is encouraged by NGO B through their e-cycle program, it is the act of reprocessing the waste to produce the latest items.



Instead of throwing unwanted materials away, recycling is the process of breaking down and reusing parts to make new things. By recycling, the amount of waste that goes into landfills is being reduced; thus reducing the amount of toxic chemicals absorbed into the earth. The e-cycling process includes four steps:

**Detoxication:** It is the removal of critical components from the E-waste to avoid contamination with toxic substances during the dismantling process. Such critical components include lead, glass from screens, CFC gases from refrigerators, light bulbs, and batteries. For example, tube lights have mercury in the fill gas, and the starter electronic may use capacitors holding Polychlorinated Biphenyls (PCB). Both mercury and PCBs are highly toxic substances and need to be carefully removed before dismantling. As for batteries, they hold mercury, cadmium, and lead. Batteries should be managed carefully to avoid leakage during usage and transport.

**Dismantling:** Equipment is then dismantled in various parts (metal frames, power supplies, circuit boards, plastics), often by hand. The advantages of using manual labor are the ability of human workers to recognize and save working and repairable parts, including chips, transistors, and RAM, and the disadvantage is that labor is often cheapest in countries with the lowest health conditions and safety standards.

**Shredding:** Mechanical processing is the next step in E-Waste treatment. This is usually a large-scale industrial operation to obtain concentrates of recyclable materials in a dedicated fraction and to further separate hazardous materials. Typical components of a mechanical processing plant are crushing units, shredders, and magnetic and air separators. The gas emissions are filtered, and effluents are treated to minimize environmental impact. Indoor exposure is checked and assessed and kept within Maximum Allowable Concentration (MAC) levels to assure workers' safety. For instance, the Glass and metal parts of a light bulb are separated. Luminescent substances from new-generation lamps are recovered separately to ease the direct re-use of phosphorus powder. The luminescent powder of older fluorescent lamp models must be disposed of in a special storage facility. Clean glass tubes are shredded and the remaining metal parts are stored with a metal stripper.

**Refining:** The last step of the "E-Cycling" is refining. Refinement of resources in e-waste is possible, and technical solutions exist to recover raw materials with minimal environmental impact. On the other hand, the fractions need to be refined or conditioned to be sold as secondary raw materials or to be disposed of in a final disposal site, respectively. Throughout the refining process, attention

must be paid to three flows of materials: metals, plastics, and glass.

Metals are recovered in a large refinery. Due to economies of scale, specialization, and division of labor, such large installations are not needed in every country. This "integrated smelting" process is a combination of metallurgical and chemical unit processes, which recovers seventeen different metals in total. As for plastics, not all of them can be reused since they are often chemically treated and contaminated with undesired flame retardants. Plastics need to be separated according to their contents and treated separately. Plastics that cannot be reused are recycled thermally as fuel oil in cement works for example. Whereas the glass from fluorescent lamps used in CRT computers and television monitors has lead and other harmful substances. CRT glass is now being recycled into glass wool, a material used for sound and heat insulation. Once these hazardous wastes are recycled, less energy is needed to extract, transport, and process raw materials used in goods manufacture. Consequently, when energy demand decreases, fewer fossil fuels are burned, and less CO<sub>2</sub> is emitted into the atmosphere. Not to forget that the emissions of other air pollutants can be reduced, too, as recycling can decrease releases of air toxins from waste incineration. For instance, recycling aluminum cans would save about 95 percent of the energy needed to make the same amount of aluminum from raw materials. Besides, each ton of aluminum would save approximately ten cubic yards of landfill space. The Glass Packaging Institute in the US provides another example. It says that recycling glass reduces related air pollution by 20% and water pollution by 50%. Also, in the same context, electronics hold plastic, glass, steel, copper, lead, and cadmium, among others. Those, if recycled, will save natural resources and reduce pollution and energy usage during production. As an example, one of the substances used in making capacitors for cell phones, iPods, and computers is coltan or columbo tantalite. Coltan, found in few places in the world, has sold for as much as \$400 per pound. Eighty percent of coltan deposits are found in the Congo, home to the highly endangered eastern lowland gorilla. Logging in the forests and reserves of the Congo seems to take a worse toll on habitat and wildlife than mining. Thus, recycling and processing of used materials into new products to prevent waste of potentially useful materials, reduce the consumption of virgin components, use of energy, air pollution through incineration, and water pollution from landfilling. In view of the above, here are a few examples of the Metal and Material composition of E-Waste: A laptop is composed of 40% metals, 23% plastics, 11% printed circuit boards, 1% cables, 4% glass, and 8% pollutants. As for a CRT monitor, it has about 53% metals, 9% glass, 36% plastics, and 2% metal/plastic mix. Besides, to highlight the importance of proper

Table 5: Population.

		Frequency	Percent	Valid Percent	Cumulative Percent
Valid	Male	26	52.0	52.0	52.0
	Female	24	48.0	48.0	100.0
	Total	50	100.0	100.0	

(Source: Author's Own Elaboration)

Table 6: Awareness Level.

		Frequency	Percent	Valid Percent	Cumulative Percent
Valid	Yes	50	100.0	100.0	100.0

(Source: Author's Own Elaboration).

e-waste disposal, a survey was conducted in collaboration with Microsoft, showing the usage of ICT (Information Communications Technology). It was found that people aged between 16 and 22 use 90% of this ICT, while usage of IT decreases inversely proportional to age to reach a 3% level for people aged above 55. Another study conducted by this NGO showed that 65% of the people store these electronics at home, ignoring their hazards, 19% donate them, 9% throw them in municipal waste, and 7% resell these items. To find out what happens with e-waste collected throughout Beirut and large parts of Mount Lebanon, the authors resorted to interviewing a company A official. Company A is the company entrusted by the Lebanese government to collect all kinds of waste and garbage in the greater Beirut area and the Mount Lebanon region, thus serving around two million inhabitants. The interview was conducted in July 2011 with Company A representative. When asked to describe actions and procedures that the company has in place to collect, separate, and recycle electrical appliances and electronics, the representative declined to give any details about that, commenting that it is a bit of a complicated issue since their collection process is random and the sorting is done in part

manually. The mechanical separators only distinguish between non-organic and organic waste for later treatment. When asked to reveal the quantities of e-waste collected monthly and whether there are any companies which company A cooperates with, she said that they do not have statistics or Fig. 4 and 5 about electronic quantities collected, but she assured the company is committed to preserving the environment through recycling. To explore the society's opinion of e-waste and e-cycling and find out whether the Lebanese attitude towards the environment depends anyhow on education or gender, the authors put together seven questions into a survey that was then distributed to fifty adult subjects. The poll included 52% males and 48% females, as given in Table 5.

The survey started by mentioning a goal to understand whether people are aware of the Lebanese environment and the importance of protecting it.

The result came 100% positive as shown in Table 6.

Since all subjects declared being concerned about protecting the environment, there was a need to recognize whether any actions were taken to preserve our environment.

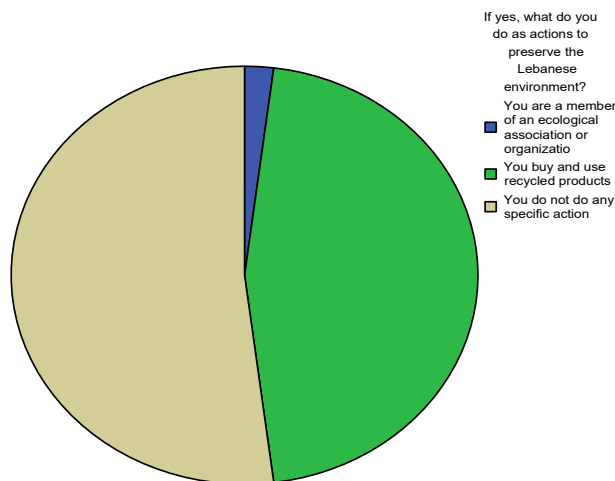


Fig. 6: Preservation actions/Authors' elaboration.

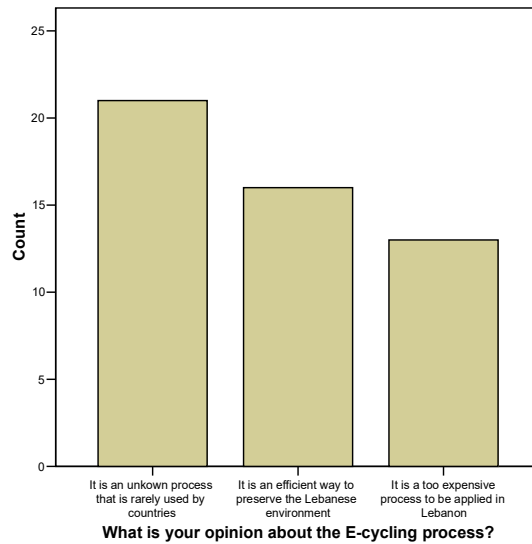


Fig. 7: E-cycling Opinion.

Fifty-five percent could not remember any specific action they took to preserve the environment, while 40% said they buy and use recycled or refurbished products. Five percent announced being members of a certain ecologic organization. The pie chart in Fig. 6 depicts the result.

The concern then is related to the recycling of e-waste in Lebanon. The aim is to find citizens who are familiar with

the notion of e-cycling and to know, out of those familiar with the process, the number of people who think that it is a workable possibility for Lebanon. Results as shown in Fig. 7.

Twenty-one people claimed that they were not familiar with e-cycling, while thirteen thought that this choice was too expensive to be realized in Lebanon. Only sixteen subjects

Table 7: Purchase of recycled/refurbished products

		Frequency	Percent	Valid Percent	Cumulative Percent
Valid	Yes	25	50.0	50.0	50.0
	No	25	50.0	50.0	100.0
	Total	50	100.0	100.0	

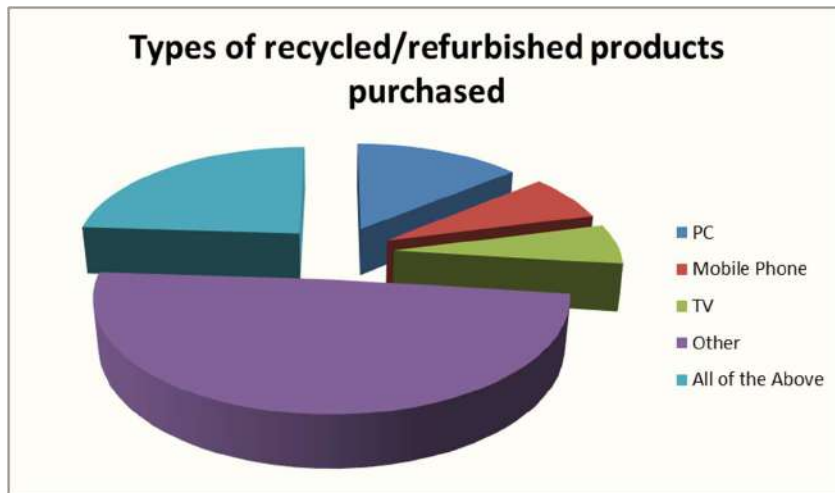


Fig. 8: Types of recycled/refurbished products purchased.

(32%) were optimistic about the benefits of e-cycling in Lebanon.

Furthermore, it is worth knowing whether the respondents own or plan to buy any electronic recycled/refurbished products. Answers were fifty-fifty, showing that half of the polled subjects already support e-waste recycling by buying products either made of recycled material or revamped and refurbished. The numbers are presented in Table 7.

For the 50% who answered yes to question 4 (25 persons), the authors asked them to specify what type of recycled or refurbished instrument they bought. The answers came as follows: 17% said they bought a used PC/Laptop. Seven percent specified a mobile phone, and

another 6% opted for secondhand TVs. Surprisingly, a considerable number, 24%, have stated having purchased all the above-mentioned appliances they used before, and 49% allegedly have at one point in the past bought a refurbished electrical or electronic machine other than the ones above. The pie chart in Fig.8 gives a better view of the proportions.

For the 50% who said they have not and would not buy any recycled or refurbished products, the authors tried to understand the reason mostly influencing their decision. The answers were: 30% chose to buy new products because of better quality or features, 20% justified their choice by a longer life, and the rest (50%) did not

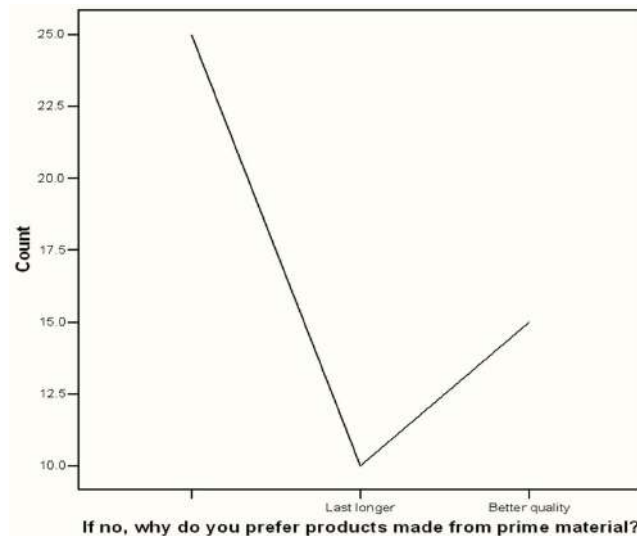


Fig. 9: Purchase of prime products.

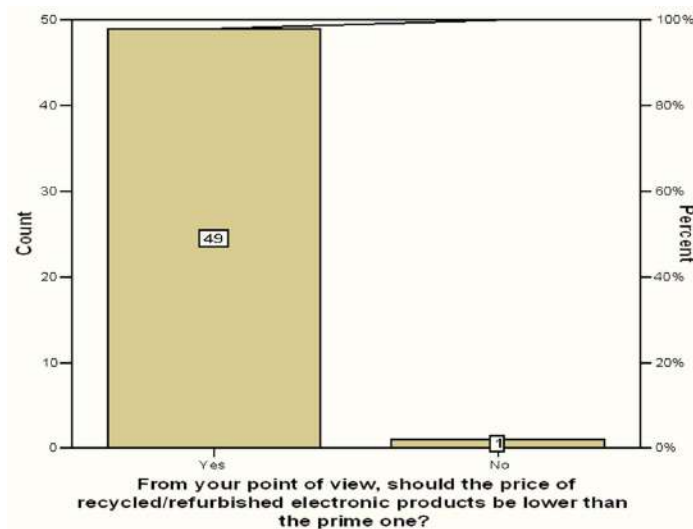


Fig. 10: Price of recycled/refurbished products.

specify a particular reason, as depicted in the following Fig. 9.

Moreover, the authors tried to understand the respondent's perspective on price and to what extent they believe that the price of recycled and refurbished products should be lower than that of prime, brand-new equivalents. The aim is to find out if subjects realize that recycling and refurbishment of products, including collection, marketing, and redistribution, might cost as much or even more than a new product. In addition, the authors wanted to have an idea about people who would accept

a not-so-competitive price just for the well-being of the environment.

Results in Fig. 10 show that 98% of polled individuals are unaware of the recycling costs issue, or they are willing to buy a used product only if it offers a cost advantage.

So, it is crucial to recognize from the authors' perspective the factors that primarily influence the purchase decision when it comes to buying electrical and electronic appliances. Among the answers to choose from are price, quality, discounts, advertisement campaigns, advertisement on the internet, government subsidy, or TV commercials.

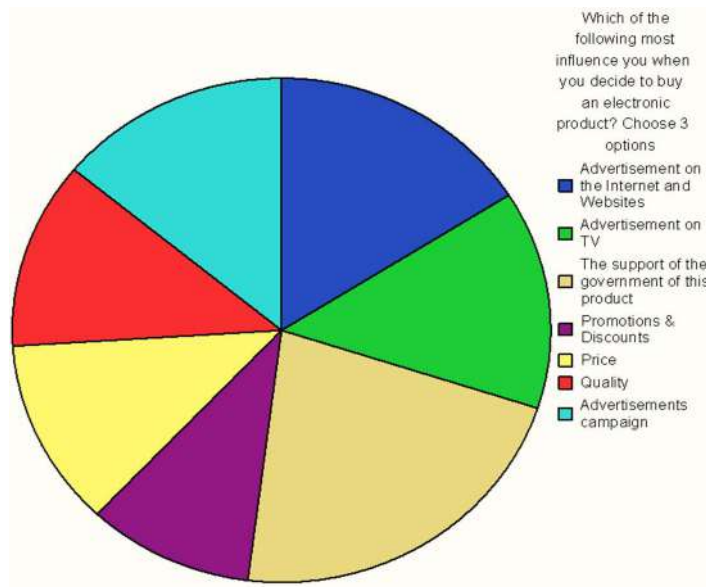


Fig. 11: Influence methods.

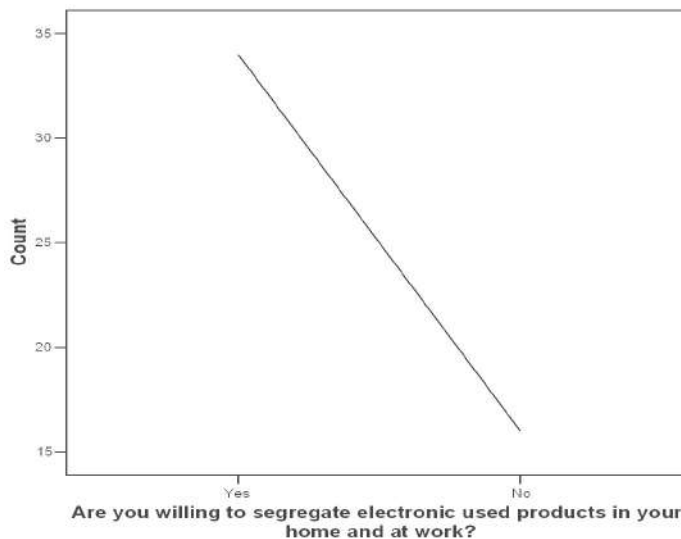


Fig. 12: Segregation Willingness.

Government subsidy was the most chosen answer with 19%, followed by advertisement on the internet with 17%. Advertising campaigns and TV commercials got each 15%. Price and quality were selected by 13% each. Eight percent went to promotion and discount, as shown in Fig. 11 .

At the end of the survey, the authors attempted to assess the future trend in e-waste acceptance in Lebanon. Survey participants were asked if they would be willing to use special

containers or disposal procedures for e-waste as opposed to other kinds of domestic garbage. 35 of 50 participants answered positively while the remaining fifteen said they were not willing to bother themselves going the extra mile to separate e-waste from the rest. Refer to Fig. 12 for a graphical representation of the results.

Furthermore, to see if these numbers relate anyhow to the educational level of the participant, we present the results in Table 8 and Fig. 13.

Table 8: Correlation of Education Level to Acceptance of E-waste Segregation.

		Count	%	In Favor of e-cycling (% of count)	Indifferent to e-cycling (% of count)
Valid	Brevet or Less	2	4.0	50	50
	Official Baccalaureate (Lebanese or equivalent)	5	10.0	40	60
	University degree	43	86.0	74.5	25.5
	Total	50	100.0		

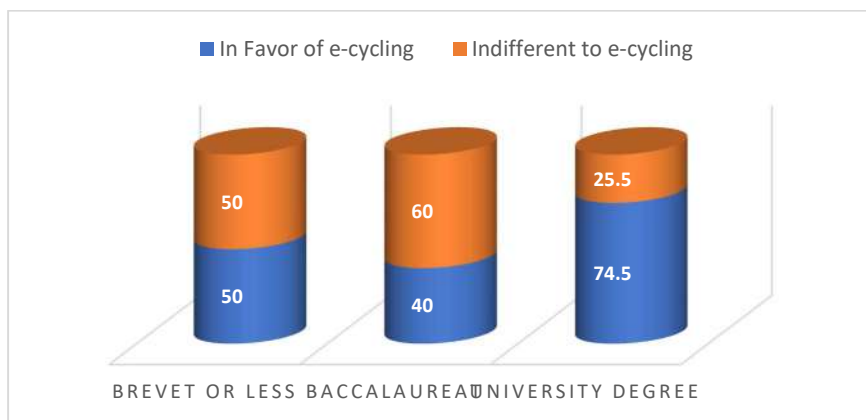


Fig. 13: Correlation of Education Level to Acceptance of E-waste Segregation.

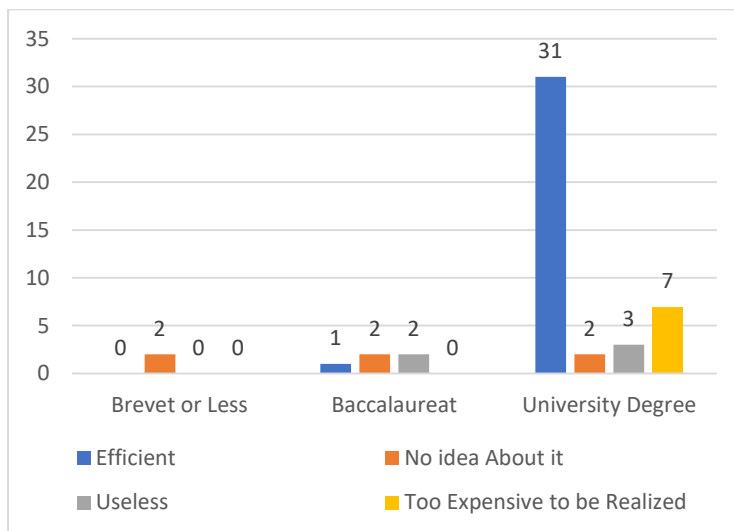


Fig. 14: Correlation of Education Level with Opinion about e-cycling.

This statistic proves the validity of hypothesis two; except for the “Brevet or Less” category, the other two categories show that people of higher education are more aware of the e-waste dangers and are more willing to do something about it. The sample of people with a Brevet degree or less consists only of two people, which is too little a sample to be considered of statistical significance. The next analytical statistics correlate the educational class of the survey participants with their answers in relation to opinions about e-cycling.

As shown in Fig. 14, only participants with an academic degree thought that e-cycling is an efficient way to curb pollution resulting from WEEE. Below that level of education, participants do not seem to be informed enough about that process; neither do they recognize its virtues and disadvantages.

## CONCLUSIONS

The paper comes with suggestions for making Lebanon a better place free of electronic waste and an outlook on how electronic waste management might change in the future. The authors used two tools to conduct their research on the e-waste and e-cycling situation in Lebanon, as was extensively discussed in the preceding section: interviews with concerned associations and a survey. While the interviews provided information about the state of organized work on e-waste and the government's stance on the issue, the survey was an effective way to find out what people think and how they feel about e-waste, and how to solve it. Company A, a private company contracted by the Lebanese government to collect all waste in Greater Beirut, and NGO B, whose mission is to raise awareness of the dangers of electronic waste throughout the Arab world and collaborate with societies and governments to define frameworks for electronic waste management, were questioned by the authors. These interviews were conducted to learn more about the current situation and potential future of e-waste in Lebanon. Since there is practically no literature on the position of the Lebanese government in regard to e-waste, and on the grounds that the service of Climate declined to accord the authors an interview or supply them with dependable sources, the last option turned to reaching the main NGO that they accept may be useful and has an involvement with e-waste circumstance in Lebanon - NGO B, and the main organization gathering trash in the capital - Organization A. A representative of NGO B claims that their organization has been successful in educating officials and citizens alike about the danger posed by e-waste up until this point. She provided examples of workshops and events that they had been organizing with the help of other universities, USAID,

and the ministry of the Environment. She said that e-waste recycling, collection, and disposal are being regulated by laws but that they are working toward it. She also said that she hoped the government would pass a law through the Ministry of the environment that would prohibit the random and uncontrolled disposal of WEEE in backyards, landfills, and nature in general. She also expressed the hope that the government would, in the future, encourage the recycling and repurposing of e-waste as much as possible by providing subsidies. The other interview was more informative than the one with Company A. Even though the representative of company A assured them that they are aware of the dangers associated with e-waste and are treating this issue with the utmost seriousness, the authors observed a significant hesitation from the representative to provide tangible, hard facts. A request to visit the locales where e-waste arranging is done was turned down on the premise that it is against the organization's strategy.

While conducting this research, the authors faced a few limitations: The literature review was based on secondary data collection, where this data, for instance, cannot be checked by the researcher personally in terms of reliability, accuracy, and credibility. Internal policy issues have driven a few interviewed people at the waste management company in Lebanon, “Company A,” to refuse to provide us with statistics and documents other than the leaflet to be able to use in this paper. After going through this study about e-waste management in terms of effective and efficient processes and regulations, we can formulate some useful recommendations targeting the government, manufacturers, and consumers: The government, when developing an e-waste management strategy or regulation, should aim to encourage resource efficiency and minimize the risks and impacts to the environment associated with the treatment and disposal of e-waste. The Lebanese Ministry ought to approve the decree as soon as possible, considering the lessons learned from the case studies to guarantee a secure disposal and an adequate collection system. To follow the law, citizens should attend awareness seminars. In terms of their products in the future, manufacturers must bear the responsibility. These producers ought to utilize creative systems for renting and growing secondhand business sectors. Producers can make their products last longer by doing this. Along these lines, the interest in fresh out of the, out-of-the-box new products will diminish as well with respect to assets. Not to mention that encouraging reconditioned and secondhand goods will save energy and reduce pollution. The customers receive the primary recommendation. They must make use of their market power to change the stages before and after consumption. Consumers, for instance, have the option of donating their old computers to charitable organizations

that support literacy programs or low-income families. In addition, these consumers must consider any electronic device to be an investment. By purchasing quality things that are viable for overhauls and add-ons, assets and energy will be saved in a roundabout way and, subsequently, changes in the climate. Finally, educating the Lebanese about the dangers of electronic waste is essential eventually. In schools, children should be taught to respect nature and protect the environment. Television shows, particularly those geared toward children, can play a significant role in raising public awareness. The purpose of this paper is to explore multiple sides of e-waste management to develop a sound understanding of the problem and the measures that should be taken to overcome such issues. This research supplies insights on e-waste management, particularly about Lebanese consumers' willingness to support e-cycling and pay for environmentally friendly electronics. The acknowledgment of the e-waste issue and its risks by the Lebanese parties will straightforwardly affect the climate and the well-being of people living around it. It was found that these electronic devices contained a wide range of toxic materials, including mercury, lead, and cadmium, which, if disposed of improperly, could harm human and environmental health. The typical life expectancy of these things has dropped altogether in the previous years, with shoppers progressively purchasing the most up-to-date stuff and discarding the more seasoned and less high-level ones.

Consequently, e-waste management has drawn impressive consideration from NGOs, administrative associations as well as companies. In Lebanon, NGO B, in conjunction with the Ministry of Environment and well-known parties like Microsoft and AUB, frequently organizes seminars, presentations, and competitions in schools to raise awareness of this risky issue and develop a strategy for dealing with it. They believe that the new generation will easily adapt to change and will readily embrace the green idea, which is why they are targeting them with summer camps and school competitions. On the legislative and official front, NGO B has sent the Ministry of Environment a draft decree on e-waste management, which will be reviewed and sent to the Council of Ministries. The project will be launched first in the private sector and then in the public sector, which is their goal. Concerning waste administration organizations, for example, organization A they are worried about keeping the urban communities clean yet at the same time does not systematically sort e-waste and treat it by isolating the plastic from the metal and electronic parts (resistors, capacitors, ICs) in view of raised costs.

## REFERENCES

- Abalansa, S., El Mahrad, B., Icely, J. and Newton, A., 2021. Electronic waste, an environmental problem exported to developing countries: The good, the bad and the ugly. *Sustainability*, 13(9), pp.5302.
- Abbas, I., Chaaban, J., Al-Rabaa, A. and Shaar, A., 2019. Solid waste management in Lebanon: Challenges and recommendations. *Journal of Environment and Waste Management*, 4(2), pp.53-63.
- Adeola, A.M. and Othman, M., 2011. An overview of ICT waste management: suggestions of best practices from developed countries to developing nations (Nigeria). *7th International Conference on Networked Computing*, 161, pp.109-115.
- Bell, J., Huber, J. and Viscusi, W., 2010. Alternative policies to increase recycling of plastic water bottles in the United States. *Review of Environmental Economics and Policy*, 6(2), pp.190-211.
- Bhat, V. and Patil, Y., 2021. An integrated and sustainable model for e-waste management for Pune City households. *Journal of Physics: Conference Series*, 14, pp.1-10.
- Bortoleto, A., 2015. *Waste Prevention Policy and Behavior: New Approaches to Reducing Waste Generation and its Environmental Impacts*. Oxon.
- Chen, C.C., 2010. Spatial inequality in municipal solid waste disposal across regions in developing countries. *International Journal of Environmental Science and Technology*, 7, pp.447-456.
- Gibson, K. and Tierney, J., 2006. Electronics waste management and disposal issues and alternatives. *Environmental Claims Journal*, 18(4), pp.321-332.
- Hong, J., Shi, W., Wang, Y., Chen, W. and Li, X., 2015. Life cycle assessment of electronic waste treatment. *Waste Management*, 38, pp.357-365.
- Ilanakoon, I., 2018. E-waste in the international context: a review of trade flows, regulations, hazards, waste management strategies and technologies for value recovery. *Waste Management*, 82, pp.258-275.
- Islam, A., Ahmed, T., Awual, M.R., Rahman, A., Sultana, M., Aziz, A.A., Monir, M.U., Teo, S.H. and Hasan, M., 2020. Advances in sustainable approaches to recover metals from e-waste: A review. *Journal of Cleaner Production*, 244, 118815.
- Kahhat, R., Kim, J., Xu, M., Allenby, B., Williams, E. and Zhang, P., 2008. Exploring e-waste management in the United States. *Resources, Conservation and Recycling*, 52(7), pp.955-964.
- Kang, H.Y. and Schoenung, J.M., 2005. Electronic waste recycling: A review of U.S. infrastructure and technology options. *Resources, Conservation and Recycling*, 45(4), pp.368-400.
- Kaza, S., Lisa, C., Bhada-Tata, P. and Van Woerden, F., 2018. *What a Waste 2.0: A Global Snapshot of Solid Waste Management to 2050*. World Bank.
- Kiddee, P., Naidu, R. and Wong, M.H., 2013. Electronic waste management approaches: An overview. *Waste Management*, 33, pp.1237-1250.
- Mohanty, S., Vermeersch, E., Di Cortemiglia, H.J., Vittoria, L. and Liddane, M., 2015. Weaknesses in European e-waste management. *Proceedings of the Hamburg International Conference of Logistics (HICL)*, 22, pp.535-561.
- Mor, R.S., Sangwan, K.S., Singh, S., Singh, A. and Kharub, M., 2021. E-waste management for environmental sustainability: An exploratory study. *28th CIRP Conference on Life Cycle Engineering*, 98, pp.193-198.
- Murthy, V. and Ramakrishna, S., 2022. A review on global e-waste management: Urban mining towards a sustainable future and circular economy. *Sustainability*, 14, pp.647.
- Nagajothi, P.G. and Kala, F., 2018. Electronic waste management: A review. *International Journal of Applied Engineering Research*, 10(68), p.4123.
- Ogunseitun, O.A., Saphores, J. and Shapiro, A.A., 2004. Environmental and economic trade-offs in consumer electronic products recycling: A case study of cell phones and computers. In: *Proceedings of the 2004 IEEE International Symposium on Electronics and the Environment*, IEEE, pp.74-79.
- Propescu, M., 2015. Waste electrical and electronic equipment management in Romania: harmonizing National Environmental Law with the EU Legislation. *Social and Behavioral Sciences*, 188, pp.264-269.
- Rathi, S. and Shyamalendu, N., 2015. E-waste management: Save earth. *International Journal of Computer Applications*, 127(4).



- Seeberger, J., Gandhi, R., Kim, S. S., Mase, W.A., Reponen, T., Ho, S. and Chen, A., 2016. SPECIAL REPORT: E-Waste Management in the United States and Public Health Implications. *Journal of Environmental Health*, 79(3), pp.8–17.
- Skinner, A., Dinter, Y., Lloyd, A. and Strothmann, P., 2010. The challenges of e-waste management in India: Can India draw lessons from the EU and the USA? *ASIEN*, 117, pp.7-26.
- Song, Q. and Li, J., 2015. A review on human health consequences of metals exposure to e-waste in China. *Environmental Pollution*, 196, pp.450–461.
- Spišáková, M., Mandičák, T., Mésároš, P. and Špak, M., 2022. Waste management in a sustainable circular economy as a part of design of construction. *Applied Sciences*, 12, pp.4553.
- Sithiannopkao, S. and Wong, M.H., 2013. Handling e-waste in developed and developing countries: initiatives, practices, and consequences. *Science of the Total Environment*, 463, pp.1147–1153.
- Stoeva, K. and Alriksson, S., 2017. Influence of recycling programs on waste separation behavior. *Waste Management*, 68, pp. 732-741.
- Vadoudi, K., Kim, J., Laratte, B., Lee, S.J. and Troussier, N. E., 2015. Waste management and resources recovery in France. *Waste Management & Research*, 33(10), pp.919-929.
- Xue, M. and Xu, Z., 2017. Application of life cycle assessment on electronic waste management: A review. *Environmental Management*, 59, pp.693–707.





# Transforming Soil Stability: A Review on Harnessing Plant Cell Compounds and Microbial Products for Modifying Cation Exchange Capacity

M. V. Shah<sup>1†</sup>, N. M. Rathod<sup>1</sup>, D. N. Prajapati<sup>2</sup>, P. J. Mehta<sup>1</sup>, R. R. Panchal<sup>2</sup> and Vijay Upadhye<sup>3</sup>

<sup>1</sup>Department of Applied Mechanics, L.D. College of Engineering, Navrangpura, Ahmedabad-380015, Gujarat, India

<sup>2</sup>Department of Microbiology and Biotechnology, Gujarat University, Navrangpura, Ahmedabad-380009, Gujarat, India

<sup>3</sup>Parul Institute of Applied Sciences, Parul University, PO Limda, Tal Waghodia, Vadodara-391760, Gujarat, India

†Corresponding author: M. V. Shah; drmvshah@ldce.ac.in

Nat. Env. & Poll. Tech.  
Website: [www.neptjournal.com](http://www.neptjournal.com)

Received: 01-02-2024

Revised: 16-04-2024

Accepted: 01-05-2024

## Key Words:

Cation exchange capacity  
Plant extraction  
Methylene blue spot test  
Soil stabilization  
Cellulose degradation  
Lignin degradation

## ABSTRACT

Soil stabilization is a very important method of science and engineering for improving the properties of soil. This paper aims to stabilize expansive black cotton soil through a biological approach involving plant extracts, plant waste materials, and microorganisms. While chemical methods exist, i.e., lime stabilization, geotextiles, etc., they are not economically feasible for large-scale applications. The primary issue with black cotton soil is due to the presence of montmorillonite clay mineral, which makes it unsuitable for the construction of roads and airfields. The cation exchange capacity (CEC) can be defined as the ability of soil to absorb and exchange positively charged ions; thus, if free positively charged ions are not available, the soil will not exchange them with others. The CEC of the soil is diminished, and ultimately, the soil is stabilized to some extent. This paper explores the preparation of plant extract, which contains a high number of anions, and directly inoculates it with soil, which nullifies the positive charge of the soil and diminishes the CEC. The use of cellulose and lignin-degrading microorganisms as an energy source and other minerals that are needed for their growth will be utilized from the soil to reduce CEC, i.e., Mg required for DNA replication and Ca required for their growth and maintenance. Another approach to diminishing the CEC is to use the microorganisms that produce EPS, which require Ca and Mg as adhesions for the formation of biofilm, i.e., *Pseudomonas aeruginosa*, *Bacillus subtilis*, and *Escherichia coli*. The use of microorganisms that have specific enzymes is also used in the diminishing soil CEC, i.e., by using ureolytic enzyme-producing bacteria like *Sporosarcina pasteurii*, *Bacillus paramycooides*, *Citrobacter sedlakii*, and *Enterobacter bugadensis*.

## INTRODUCTION

Some of the partially saturated clayey soils are very sensitive to variations in water content and show excessive volume changes; such soils are classified as expansive soils. It can also be known as swell soil or black cotton soil. Many stabilization techniques are in practice for improving expansive soils in which the characteristics of the soils are altered or the problematic soils are removed and replaced, which can be used alone or in conjunction with specific design alternatives. These types of soil are spread mostly across interior Gujarat, Maharashtra, Karnataka, and Madhya Pradesh.

Black clays, tropical black earth, or black cotton are known to be potentially expansive soils that are “black” or “greyish black” or, in their eroded phase, “greyish white” heavy loam or clay (usually 50%), with a predominant clay mineral of the smectite group, rich in alkali earth elements,

and the horizons sometimes contain calcium carbonate or magnesium oxide concretions as shown in Fig.1. Many other terms have been applied locally, such as “regur” soils in India, “margalitic” soils in Indonesia, “black turf” in Africa, and “tirs” in Morocco. Although there are several names, the term “black cotton soil” is adopted in this paper because of its extensive use in India. The term “black cotton” is believed to have originated in India, where the locations of these soils favor cotton growth (Gidigas & Gawu 2013).

The main characteristics of black cotton soils, among others, are:

1. Black or darkish gray to brown color.
2. High content of expansive clay mineral montmorillonite.
3. Possess the tendency to shrink and swell with changes in moisture conditions.
4. Exhibits heave and crack as geo-environmental phenomena.

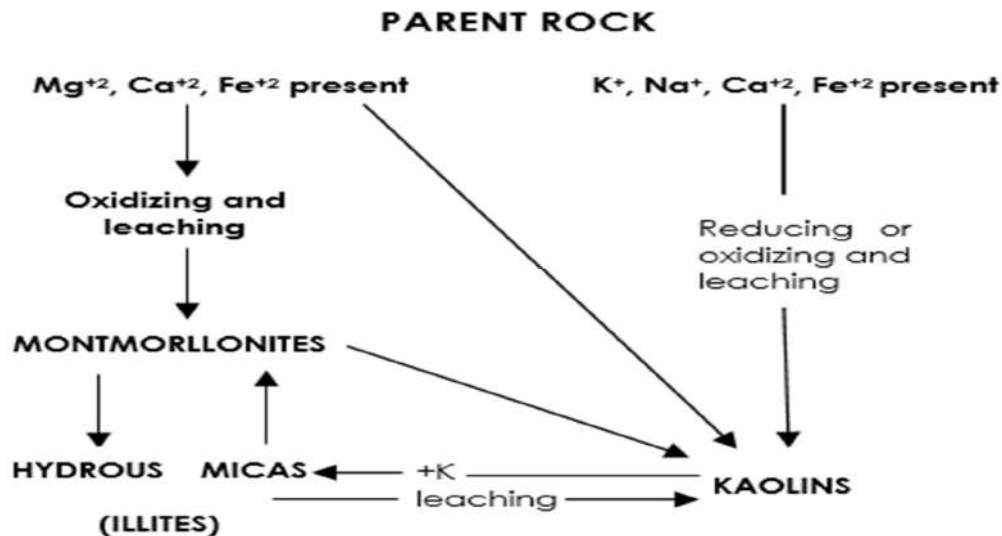


Fig. 1: The environment of formation of illite, kaolinite and montmorillonite (Frederickson 1952).

### Problems Associated with Black Cotton Soil

Major issues with several tropical countries, particularly in Africa and India, are their black cotton soils. Because they are frequently expansive due to the presence of substantial percentages of expansive clay minerals, such as montmorillonite, they are poor materials by temperate zone standards and challenging to employ for road and airfield construction. When these soils come into touch with water, they swell and shrink. Because the soil deposits are typically thick, it is impossible to avoid or bypass them when building engineering projects. The seasonal volume variation (i.e., swell and shrinkage) of these soils has been documented to have caused discomfort to many roads and light-building foundations (Chen 1988). According to reports, these soils cause annual damages and repairs to earth buildings and infrastructure, totaling billions of dollars (Gidigas & Gawu 2013).

Soils made of black cotton absorb a lot of water, expand, get mushy, and lose their strength. These soils have a propensity to heave in damp conditions and are readily compressible when damp. During the heat, black cotton soils lose volume and start to break. When dry, they exhibit severe hardness and fractures. They are not good earth construction materials or foundation soils because of these characteristics. Since the subgrade and embankment act as pavement foundations, they have a significant impact on the stability and performance of the pavements. In places with black cotton soil, a thorough understanding of the characteristics of the soil is necessary for the development of a good and long-lasting road network. Adopting appropriate construction techniques and sophisticated design approaches is necessary for such soils (Nadgouda & Hegde 2010).

### CATION EXCHANGE CAPACITY

The cation exchange capacity of CEC is the total amount of exchangeable cations that a soil can absorb. Positively charged ions ( $\text{Na}^+$ ,  $\text{Ca}^{2+}$ , and  $\text{K}^+$ ) that are present on or close to negatively charged soil particles make up the majority of these exchangeable cations. These are easily interchangeable cations that can be swapped out for other positively charged ions, as seen in Fig. 2. The plants can also easily access them. Terrestrial ecosystems cannot sustain plant development without cation exchange, which is a vital life-supporting activity that works in tandem with photosynthesis.

Cation exchange capacity is measured by one of several standard methods where all adsorbed cations in soil are replaced by a common ion (such as  $\text{NH}_4^+$ ), and then the amount of adsorbed common ion is determined. The standard way to describe soil CEC is as one of two numerically identical sets of units:  $\text{cmolc.kg}^{-1}$  (centimoles of charge per kilogram of dry soil) or  $\text{meq.100g}^{-1}$  (milliequivalents of charge per 100 g of dry soil).

The exchangeable cations and cation exchange capacity (CEC) of soils can be measured using a variety of techniques. Some employ buffered solutions, including barium chloride, sodium acetate, or ammonium acetate. For the others, unbuffered salts like ammonium chloride or barium chloride are used to carry out the exchange process. CEC values can be calculated for a given reagent by counting the amount of a fixed cation (index cation) or by adding up the exchanged cations. Numerous methods are proposed to measure the cation exchange capacity (CEC) and exchangeable cations in soils. Some of them are the ammonium acetate method at pH 7, the barium chloride compulsive exchange method,

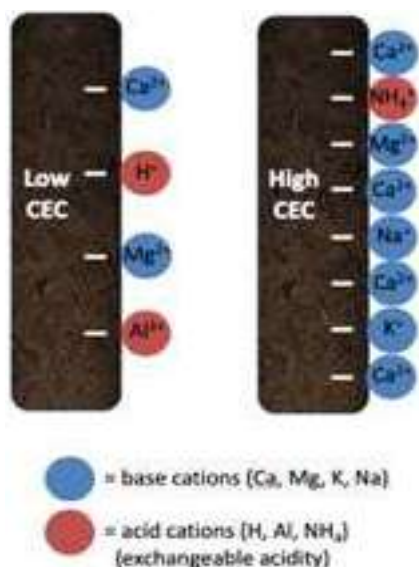


Fig. 2: Cation exchange capacity of soil.

the methylene blue test (spot test and turbidimetric test), the cobalt-III hexamine chloride method, and the silver thiourea (AGTU) method. The methylene blue test is a quicker, easier, and more affordable procedure than other methods.

### Methylene Blue Test for Measurement of CEC

The Methylene blue test was created in France to identify the clay content of granular material and assess its viability for use in the production of concrete. The chemical formula for methylene blue powder is  $C_{16}H_{18}N_3SCl$ , and it reacts with water like a cationic dye. Chloride ions in methylene solution exchange places with cations in clay minerals when combined with soil solution, where they are adsorbed on the surface of clay minerals. The amount of adsorbed methylene solution changes according to the number of clay minerals and clay type, cation exchange capacity, and specific surface area (Turkoz & Tosun 2011). The methylene blue test is a widely used test procedure (as shown in Fig. 3) since it is relatively simple to perform and doesn't require any specialized equipment. The methylene blue adsorption test is a dependable and uncomplicated technique for determining whether clay minerals are present in soils and what their characteristics are. In actual practice, two test methods—the “turbidimetric” approach and the “spot method”—have been employed. A titration procedure that is simplified is the spot method.

By confirming how much methylene blue is needed to cover the whole surface area of the clay particles in the soil, the test allows one to determine the ion adsorption capacity of the soil. This test method is based on titration created by a chemical reaction between free methylene blue cations acquired by dissolving methylene blue in water and

replaceable clay cations. The greatest potential for cation exchange is possessed by clay particles with the largest specific surface area and the highest negative electrical charge. The particular surface area and electrical charge of the clay particle both influence the adsorption (Turkoz & Tosun 2011). It is advised to collect soil test samples for ANFOR standard analysis, taking into account the soil's clay content; 30 to 60 g should be taken from clayey or overly clayey soils, and 60 to 120 g from less clayey soils. 500 milliliters of distilled water are used to dissolve soil samples collected at this ratio.

The soil sample solution is then supplemented with 5 milliliters of methylene blue solution, which is made at a concentration of 10 g/L. One drop of the mixed solution is applied to the filter paper one minute later. When the dye around the aggregate dye area creates a second, lighter-colored blue halo and remains stable for five minutes, the test is considered to have ended (Turkoz & Tosun 2011).

In the end, it is said that (Chiappone et al. 2004), the ANFOR standard defined test method yields results that represent the entire material and should be used in heterogeneous samples, while the ASTM standard test method is appropriate to use for homogenous, fine-grained material; in other words, only verifying the clay content. The most popular technique used by all researchers to determine the CEC of soil is the methylene blue spot test.

### PLANT EXTRACTION METHODS

Extraction is the process of separating a variety of plant metabolites that are used medicinally, including alkaloids,

glycosides, phenolics, terpenoids, and flavonoids, utilizing established techniques and selected solvents. Separating the soluble plant metabolites from the insoluble cellular marc is the goal of all solvent extraction techniques. The following are popular methods for extracting plant material: Certain plants offer significant benefits when utilized as a simple and affordable method for extracting plant material. Phytonic procedures are one of them, and they have a lot of benefits and a broad variety of applications over other techniques. The selection of the desired solvent and extraction method is quite a difficult task.

### **Maceration, Infusion, Percolation and Decoction**

According to Azwanida (2015), the maceration extraction method is utilized to extract bioactive compounds from plants as well as in the wine-making process. Plant materials (coarse or powdered) were macerated by soaking them in a solvent in a stoppered container and letting them stand at room temperature for at least three days while stirring often. Pressing, straining, and filtering were the next steps in the process. Conventional methods involve the transfer of heat by convection and conduction, with the solvent chosen following the target compound for extraction. Similar to maceration, infusion, and decoction involve immersing the ingredients in either boiling or cold water (Azwanida 2015). Decoction often produces more oil-soluble chemicals than maceration and infusion, and it is only appropriate for extracting heat-stable compounds from hard plant materials like roots and barks (Azwanida 2015).

### **Hot Continuous Extraction (Soxhlet)**

Using this technique, coarsely powdered crude plant material is put into the soxhlet apparatus's chamber in a porous bag

or “thimble” composed of sturdy filter paper. Vapors from the heated solvent in the flask condense in the condenser. By dripping into the thimble holding the raw plant material, the condensed extractant facilitates extraction by contact. Until a drop of solvent from the siphon tube evaporates without leaving any trace, the procedure is ongoing. Notably, this process saves a significant amount of time, energy, and money by enabling the extraction of vast amounts of plant material with a far smaller amount of solvent.

### **Accelerated Solvent Extraction (ASE)**

When compared to maceration and Soxhlet extraction techniques, accelerated solvent extraction is a more effective solvent extraction procedure. Compared to maceration and Soxhlet extraction techniques, this method uses the least amount of solvent (Gomes et al. 2017). To keep the sample from aggregating and clogging the system tubes, the ASE uses inert packing material, like sand, packed inside stainless-steel containers (Barros et al. 2013). According to Gomes et al. (2017), the extraction process takes less than an hour to finish, and the technique regulates temperature and pressure for every single sample.

### **Microwave-Assisted Extraction (MAE)**

This extraction method uses microwave energy to enhance the partition of analytes from the sample matrix into the solvent (Zhao et al. 2012). As a result of interactions between microwave radiation and the dipoles of polar and polarizable materials, such as solvent, a plant sample heats up close to the material's surface, and conduction transfers heat. Dipole rotation of the molecules caused by microwave electromagnetics breaks hydrogen bonding, boosts the movement of dissolved ions, and improves

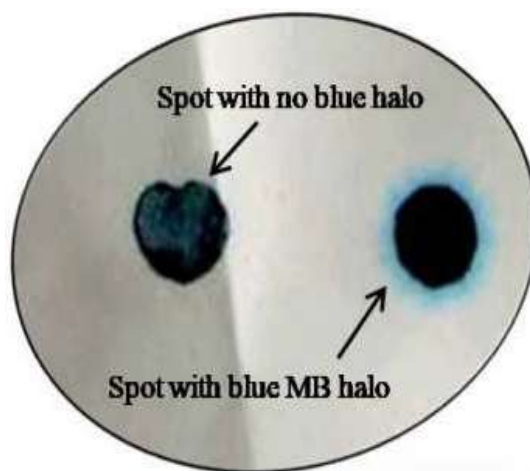


Fig. 3: Methylene blue spot test result capacity.

solvent penetration into the matrix (Kaufmann & Christen 2002).

### Ultrasound Extraction (Sonication)

The extraction method known as ultrasound-assisted extraction (UAE) is noted for using low temperatures, shortening extraction periods, and increasing extraction yield. With the use of ultrasonic frequencies between 20 and 2000 kHz, this extraction technique increases cavitation and permeability of the cell wall. Although it works well for some uses, including the extraction of *rauwolfia* roots, high prices prevent it from being widely used. One significant disadvantage is that ultrasonic radiation (over 20 kHz) can occasionally have a detrimental effect on the active ingredients in medicinal plants, resulting in the production of free radicals and unfavorable molecular changes.

### Supercritical Fluid Extraction (SFE)

The method of separating one component (the extractant) from another (the matrix) by employing supercritical fluids as the extracting solvent is known as supercritical fluid extraction or SFE. SFE is an alternate technique for preparing samples that aims to increase sample throughput while using less organic solvent. Temperature, pressure, sample volume, analyte collection, modifier addition, flow and pressure control, and restrictors are examples of critical parameters. Because of its abundance, affordability, safety, and favorable physical characteristics, CO<sub>2</sub> is the recommended extraction solvent. However, the use of organic solvents is required due to their polarity limits. Because argon is inexpensive and inert, it has been investigated as a possible substitute recently. Significant capital investment requirements impede the practical deployment of SFE, notwithstanding its benefits in extracting different chemicals.

### Enzyme-Assisted Extraction (EAE)

Enzymes, known as biocatalysts, are obtained from fruits, vegetables, animal organs, and microbes (bacteria and fungi). The fundamentals of enzyme-assisted extraction (EAE) entail a catalytic hydrolysis reaction that releases intracellular components into the extraction medium by disrupting the plant cell wall under ideal experimental conditions. Disentangling phytochemicals from the polysaccharide-lignin network supported by hydrogen bonding and hydrophobic interactions like van der Waal forces can be difficult in some plants. The solvent extraction technique does not make the phytochemicals in their matrices accessible; instead, they stay scattered in the cell cytoplasm. By dissolving cellular walls, these enzymes are added during extraction to increase phytochemical output.

Moreover, these enzymes hydrolyze lipid bodies and other carbohydrates, like cellulose. Particular enzymes, including amylase, pectinase, and cellulase, are employed. Two prominent techniques that involve enzymes during extraction are enzyme-assisted aqueous extraction (EAAE) and enzyme-assisted cold pressing (EACP). While the first technique has been used largely to extract oils from various seeds, the latter has been utilized to hydrolyze the plant's seed cellular wall (Yi et al. 2009). By pre-treating the plant material with particular enzymes, the bound phytochemicals in such samples are efficiently released at high yields (Yi et al. 2009).

### Phytonic Process

Advanced Phytonics Limited has developed a patented "phytonics process" using hydrofluorocarbon-134a as a non-flammable, non-toxic, and ozone-friendly solvent. This process allows for the selective extraction of specific phytoconstituents, resulting in low residual solvent levels. The closed-loop processing plant ensures solvent recycling, minimal energy consumption, and no environmental emissions, making it a sustainable and efficient extraction technique.

### Advantages of the Process

The phytonics process is a gentle, cool, and environmentally friendly method that does not damage products by high temperatures. It does not require vacuum stripping, and the process is conducted at a neutral pH, preventing acid hydrolysis damage or oxidation. The technique offers a variety of operating conditions and end products, is less threatening to the environment, requires minimal electrical energy, releases no harmful emissions, and produces innocuous waste products.

The solvents used are non-flammable, toxic, and ozone-depleting.

### Applications

Phytonic procedures are used in a wide range of businesses, including the food, essential oil, and taste sectors, as well as biotechnology for the synthesis of antibiotics and herbal drugs. Notably, it is used in the manufacturing of phytopharmaceuticals, pharmacologically active intermediates, antimicrobial extracts, and premium pharmaceutical-grade extracts. Its versatility goes beyond these fields and includes the extraction from a variety of plant materials of essential oils, oleoresins, natural food colors, tastes, and aromatic oils. The method is also used to refine crude products that come from other extraction methods; it guarantees that only pure chemicals free of waxes and

impurities are extracted, and it makes it easier to remove biocides from contaminated biomass.

#### Parameters Governing the Selection of an Appropriate Extraction Method (Fig. 4)

1. Verification of plant material authenticity, including careful removal of extraneous material.
2. Using the appropriate plant portion and documenting information for quality control, such as plant age, collection time, season, and location.
3. Customizing the drying environment to the chemical makeup of the plant components, preferring techniques such as hot or cold airflow.
4. Specification of grinding procedures, avoiding techniques creating heat.
5. Plant material powder is sieved to ensure consistent particle size.
6. Consideration of the nature of constituents, such as selecting a non-polar solvent for non-polar medicinal constituents and utilizing acceptable extraction procedures based on thermo ability.
7. Implementation of measures for constituents sensitive to organic solvents.
8. Standardization of extraction duration to provide comprehensiveness while avoiding extraction of undesired components
9. Determining and managing the water or extraction solvent quality.
10. Adoption of concentration and drying techniques, such as lyophilization and reduced pressure drying,

that guarantee the stability and safety of active ingredients.

11. Consideration of extractor design and construction material.
12. Recording analytical metrics, like TLC and HPLC fingerprints, to keep an eye on the quality of various extract batches.

#### MICROBIAL PROCESSING OF PLANT MATERIALS

Microorganisms are essential to the effective recycling of agricultural wastes because they help to bioconvert agricultural residues into compost, which has many advantages. In addition to improving soil fertility, this procedure also improves soil health, which lowers ecological hazards, increases agricultural output, increases soil biodiversity, and creates a better environment. One particularly good solution for handling the large amounts of agro-waste produced worldwide is composting. Crop leftovers are a major but underutilized source of renewable biomass produced in large numbers in the context of agriculture. The amount of crop waste in India alone is estimated to be around 620 million tons. Remarkably, 50% of all residues generated are attributed to three key crops: oilseed, wheat, and rice. On average, these residues contain 1.5% potassium oxide ( $K_2O$ ), 0.2% phosphorus pentoxide ( $P_2O_5$ ), and 0.5% nitrogen (N).

With half of the agricultural residues being used for fuel and cow feed, the remaining residue has a significant amount of nutrients left in it; 6.5 million tons of NPK (nitrogen, phosphorous, and potassium) can be produced annually. This makes up 30 percent of India's overall

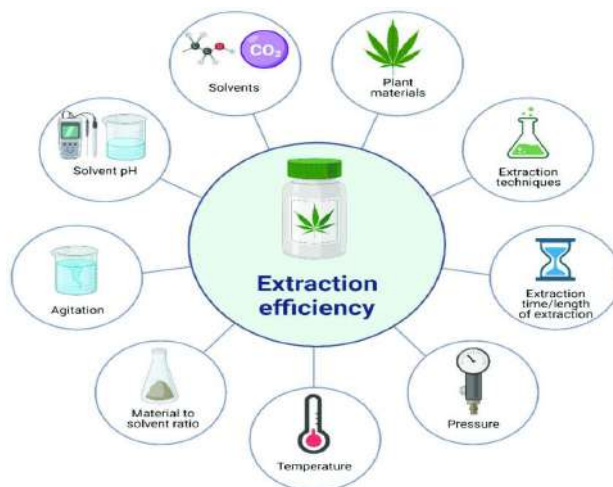


Fig. 4: Factors affecting on extraction of plant material.



NPK consumption. Composting agricultural leftovers is a feasible and cost-effective technique that is made possible by lignolytic, lignocellulolytic, and cellulolytic bacteria. It efficiently recycles cellulosic, lignocellulosic, and lignin waste, supporting nutrient management and sustainable farming methods.

### Lignin Degradation

The most common naturally occurring aromatic heteropolymer and one of the fundamental components of lignocellulosic biomass is lignin. As part of the secondary cell wall of plants, lignin (15–30%), cellulose (30–50%), and hemicellulose (15–30%) work together to maintain the integrity of the cellulose/hemicellulose/pectin matrix (Boerjan et al. 2003). Nearly all forms of lignin are composed of three basic monolignols, or phenol derivatives: p-coumaryl alcohol (M1H), coniferyl alcohol (M1G), and sinapyl alcohol (M1S). Lignin is a complex, highly branching, three-dimensional phenolic structure. In the polymer, every monolignol yields p-hydroxyphenyl, guaiacyl, and syringyl subunits (Calvo & Dobado 2010). Lignin has a variable molecular mass due to random cross-linking by polymerization of phenolic groups, which results from radical coupling processes between phenolic radicals (Boerjan et al. 2003).

Lignin comprises functional groups such as phenol hydroxyl, methoxyl, carboxyl groups, and alcohol hydroxyl, which impact the reactivity of lignin (Christopher et al. 2014). Lignin is synthesized by combining monolignol units through peroxidase-mediated dehydrogenation, in which the structures of linked basic units are created and linked to one another by aryl ether linkages with  $\beta$ -aryl ether and aryl-glycerol as well as C–C bonds. The biggest proportion is  $\beta$ -O-4 aryl ether bonds, about 50–70%, followed by  $\beta$ - $\beta$ ,  $\beta$ -5, 5-5, and 5-O-4 bonds (Calvo & Dobado 2010). Among the bonds that are hardest to break are carbon-carbon ones (Christopher et al. 2014). Through interactions with other polymers found in the cell wall, such as cross-linking proteins and polysaccharides, monolignols form a complex three-dimensional matrix (Calvo & Dobado 2010), giving the tissues and cell walls of all vascular plants strength, rigidity, and resistance to microbial degradation (Fisher & Fong 2014).

Lignin can be categorized into four main categories as shown in Fig. 5 according to the number of basic phenol units such as guaiacyl (G), syringyl (S), and p-hydroxyphenyl(H) in the polymer into type G, type G-S, type H-G-S, and type H-G (Calvo & Dobado 2010). Because lignocellulosic material can replace high-value chemicals made from petroleum derivatives, there is growing interest in it (Asina

Table1: Details of lignin and its application.

Sr. No.	Main Lignin Preparation	Degradation of Lignin	Application	Derived from Monolignol units
1.	Organosolv lignin	Physical	Biofuels	Guaiacyl (G)
2.	Steam-exploded lignin	Microbial 1. Bacterial 2. Fungal	Component for composites & co-polymers	4-hydroxy-phenyl (H)
3.	Lignin sulfonates	Chemical	Dispersant agent for pesticide	Syringyl (S)
4.	Kraft lignin	-	Biner	-
5.	-	-	Heavy metal sequestration	-
6.	-	-	Emulsifier	-
7.	-	-	High-value products	-

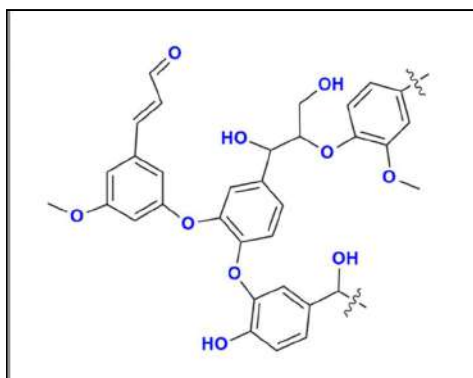


Fig. 5: Chemical structure of lignin.

et al. 2016). It can also be used to produce biofuels (Fisher & Fong 2014), paper (Calvo & Dobado 2010), sorbents, activated carbon, carbon fibers with a very large surface area and pore volume, and bioplastics.

Referring to Table 1, lignin degradation can be carried out chemically and thermally by sophisticated oxidation processes: photocatalytic, pyrolysis, electrochemical, or enzymatically/biologically. Because of its complicated and irregular structure and the absence of conventional repeating covalent connections, lignin is a refractory material that cannot be broken down by most degradation techniques (Yadav et al. 2022). The use of selective ligninolytic enzymes and microorganisms to control lignin biodegradation and prevent the formation of undesirable byproducts makes biological methods of lignin degradation preferable to chemical ones. Biological processes also do not result in yield loss, unlike thermal lignin decomposition.

The lignin-degrading bacteria can be isolated on the MSML (minimal salt medium containing alkaline lignin) medium or LB medium supplemented with guaiacol or tannic acid from a soil sample, and the confirmation of the lignin-degrading bacteria can be done by using methylene blue as an indicator for the MSML medium, while for the LB medium, the lignin-degrading bacteria will give rise to a brown-colored zone surrounding the colony.

### Biological Lignin Degradation

Fungi and bacteria do not produce any toxic chemicals; therefore, the biological breakdown or decomposition of lignin is considered a green and environmentally beneficial process (Niu et al. 2021). Hydrolytic enzymes cannot cleave lignin due to the branching three-dimensional structure and C-C and C-O ether bonds (Abdel-Hamid et al. 2013). Moreover, low-potential oxidoreductases, like plant oxidases, which start lignin polymerization, are unable to oxidize the non-phenolic aromatic subunits of lignin. Because of this composition of lignin, bacteria, and fungi have evolved to produce a variety of groups of enzymes with ligninolytic activity (Bugg et al. 2011). The oxidative process of lignin biodegradation necessitates the synthesis of extracellular ligninolytic enzymes, which include dye-decolorizing peroxidase (DyP), lignin peroxidase (LiP), manganese-dependent peroxidase (MnP), versatile peroxidase (VP), and laccases (LaC) (Yadav et al. 2022). The type and structure of lignin are related to the binding affinity of enzymes that break down lignin. The interactions between lignin and amino acids in the enzymes involve the three primary types of non-covalent bonds: hydrogen, hydrophobic, and electrostatic.

According to Fisher & Fong (2014), there is considerable variation in both the lignin's chemical structure and the

degradation products produced by the enzymes that break it down. C-C and C-O monomer bonds break during many metabolic transformations, while side chain modifications, hydroxylation, and demethylation also take place. Most modifications take place at the same time (Sanchez 2009). There are two stages to the breakdown of lignin (Bugg et al. 2011).

The breaking of the  $\beta$ -O-4 aryl ether bond in the phenyl-*en* unit is the primary process of the first phase of lignin degradation (Niu et al. 2021). The cleavage of the core ring results in the formation of a number of intermediates during the second phase. During the biochemical conversion of lignin, the main intermediates are the aromatic chemicals that are generated, specifically catechol and protocatechuic acid (Abdelaziz et al. 2016). According to Bugg et al. (2011), several catabolic pathways lead to the breakdown of lignin components. These pathways include the breakdown of  $\beta$ -aryl ether by bacteria and fungi, biphenyl by bacteria, diarylpropane by bacteria, phenyl coumarane, and pinoresinol by bacteria, bacterial degradation of ferulic acid, and oxidative cleavage of protocatechuic acid by bacteria.

One of the methods by which biodegradation of lignin happens is composting. The diverse microbial community in the compost pile is active during the composting process, and microorganisms break down organic material to produce compost (humus), carbon dioxide, water, and heat. It is thought that lignin, polysaccharides, and nitrogenous chemicals make up the majority of humus, preventing lignin from fully mineralizing throughout the composting process. Actinomycetes and thermophilic microfungi break down lignin during composting (Grgas et al. 2023). The majority of research on lignin modification and degradation has been done on basidiomycetes (Fisher & Fong 2014). Because they secrete extracellular ligninolytic enzymes, white and brown rotting fungi are crucial in the decomposition of lignocellulosic biomass (Sanchez 2009). Various combinations of enzymes, such as LiP and MnP, MnP and LaC, and LiP and LaC, are produced by distinct white-rot fungi. Fungi that cause brown rot may effectively break down cellulose and hemicellulose but not lignin, at least not completely. Basidiomycetes, an aerobic white-rot fungus, are capable of completely breaking down lignin. Since high yields and productivity are necessary, the industrial application of fungi is restricted due to their demanding growth requirements (Niu et al. 2021). Laccase genes, mostly identified in Firmicutes, Proteobacteria, and Actinobacteria, vary in occurrence across bacterial strains.

Actinomycetes such as *Streptomyces viridosporus* T7A, *Sphingomonas paucimobilis* SYK-6, *Comamonas*, *Nocardia*, and *Rhodococcus* are examples of bacteria that break down

lignin. These bacteria can release extracellular peroxidases and break down both lignin and lignocellulose carbohydrates. Noteworthy eubacteria and actinomycetes include *Bacillus*, *Acinetobacter*, *Xanthomonas*, *Micromonospora*, and *Streptomyces*, underlining the vast spectrum of bacteria adept in lignin breakdown. A well-researched lignin-degrading bacteria called *Streptomyces viridosporus T7A* generates extracellular peroxidases that break the  $\beta$ -aryl ether bond in lignin to depolymerize it and release low-molecular-weight phenols (Yadav et al.2022). There are also identified bacteria that can break down lignin, like *Rhodococcusjostii RHA1* and *Pseudomonas putida mt-2*. Fungi are superior to bacteria in the breakdown of lignin, while bacteria alter lignin by producing smaller aromatic molecules that are then imported into cells and metabolized.

### Cellulose Degradation

The main type of carbohydrate that plants synthesize is cellulose. Therefore, a significant portion of the carbon cycle in the biosphere, is represented by the breakdown of cellulosic biomass. For the same reason, biotechnologists' interest in using cellulolytic enzymes to treat cellulose for practical uses has not abated. However, a lack of fundamental understanding of the process prevents cellulose hydrolysis from being improved. Made up of glucose subunits connected by 1,4  $\beta$  linked bonds, cellulose is a linear polymer. Since each glucose residue is 180 degrees rotated in relation to its neighbors, cellobiose is the fundamental repeating unit. The range of chain lengths is 100–14000 residues. Rigid, insoluble microfibrils are formed when an abundance of intra- and intermolecular hydrogen bonds is formed by cellulose chains. The lateral diameter of microfibrils varies from 3–4 nm in higher plants and up to 20 nm in the case of

the alga *Valoniarnacrophysa*, whose microfibrils can contain several hundred cellulose chains.

The chains are parallelly aligned and create highly structured crystalline domains with more amorphous, disordered areas strewn in between as shown in Fig. 6. Depending on origin and pre-treatment, the degree of crystallinity of cellulose can vary from 0% for amorphous, acid-swollen cellulose to over 100% for the cellulose isolated from Valoniamacrophysa (Beguin & Aubert 1994). There are various commercially accessible types of pure cellulose, including cotton, filter paper, and Avicel. Usually, these forms are employed to evaluate the effectiveness of whole cellulase systems. However, their physical variability (degree of crystallinity, accessible surface area, pore size) hinders detailed enzymological research. Because of their quick rate of hydrolysis, amorphous forms such as soluble carboxymethyl cellulose (CMC) and acid-swollen cellulose are commonly utilized in tests. The most popular media for testing bacteria that break down cellulose is carboxymethyl cellulose, which is then washed with NaCl after being flooded with Congo red (Beguin & Aubert 1994).

### Cellulolytic Microorganisms

One method that cellulases catalyze is cellulose hydrolysis. Cellulose, a nearly limitless carbon, and renewable energy source, is a linear polymer composed of D-glucopyranose units joined by  $\beta$ -(1-4) glycosidic bonding. Since each glucose residue is 180 degrees rotated in relation to its neighbors, cellobiose is the fundamental repeating unit. The range of chain lengths is 100–14000 residues. Rigid, insoluble microfibrils are formed when an abundance of intra- and intermolecular hydrogen bonds are formed by

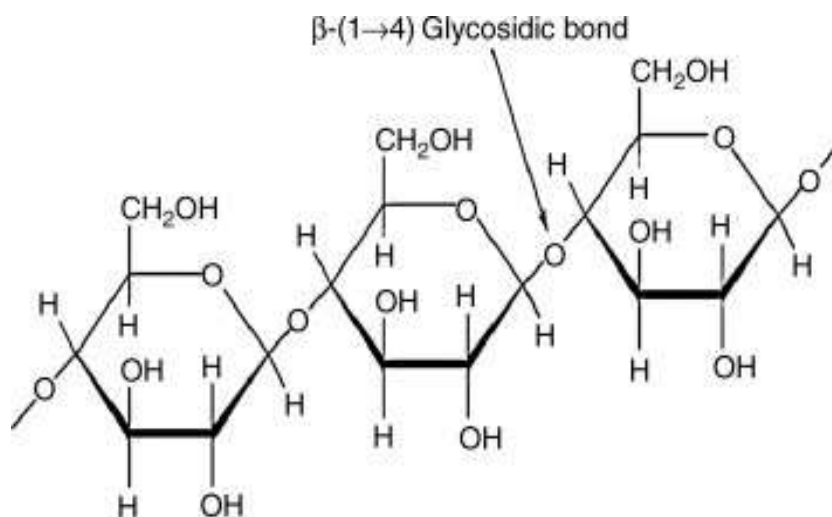


Fig. 6: Chemical structure of cellulose.

cellulose chains. The chains are parallelly aligned and create highly structured crystalline domains with more amorphous, disordered areas strewn in between. Hemicellulose is formed of complex carbohydrate polymers, with xylans and glucomannans as the primary components. Despite the complexity of the transformation processes, cellulose offers the best opportunities for lowering the production costs of many products because it is abundant and may be less expensive than other substrates (Silalertruksa & Gheewala 2020). Hemicellulose and lignin combine to generate cellulose (both crystalline and amorphous), which is limited in its destruction by a compact network structure that is insoluble in water (Faria et al. 2020).

Because of the quick rate of hydrolysis, amorphous forms of cellulose, such as soluble carboxymethyl cellulose (CMC) and acid-swollen cellulose, are commonly utilized in tests. Grown on CMC agar, Reasoner's 2A agar, or LB broth medium, the cellulose-degrading organisms are subsequently screened and verified by flooding congo red onto a plate and then being washed with NaCl as shown in Fig. 7. These organisms are employed to degrade and decompose the plant waste material into simpler forms.

**Biological cellulose degradation:** Fermentable sugar release requires the physical, chemical, and biological pre-treatment. Because it is environmentally friendly, biological pre-treatment using enzymes and cellulolytic microorganisms is still the best way to deal with this problem. Cellulase is a complete enzyme system comprising endoglucanase and exoglucanases, including cellobiohydrolases and  $\beta$ -glucosidase (Paudel & Qin 2015), which breaks down  $\beta$ -1,4-linkages in cellulose polymer to liberate glucose units. Numerous researchers have documented those fungi, actinomycetes, and both aerobic and anaerobic bacteria may manufacture cellulase enzymes (Shida et al. 2016). These

microorganisms have an effective enzyme breakdown system and secrete free or cell surface-bound cellulases.

Among several types of microorganisms, bacteria are the most efficient cellulose degraders because they develop fast and have high cellulase synergistic activity (Bilal & Iqbal 2020). Cellulases have proven to be highly effective in the industrial utilization of lignocellulosic biomass degradation. Numerous industries, including chemicals, food and feed, pulp and paper, textiles, drinks, cars, electronics, and, most significantly, energy, use cellulases in a variety of ways (De Souza & Kawaguti 2021). From a phylogenetic perspective, the aerobic cellulolytic bacterial community found in soil is highly diverse, with members of several phyla such as Actinobacteria, Firmicutes, Bacteroidetes, and Proteobacteria. Prominent taxa include *Streptomyces*, *Bacillus*, *Cellulomonas*, *Cytophaga*, *Cellvibrio*, and *Pseudomonas*. The taxonomic categories in which cellulolytic microbes are found are incredibly diverse. The majority are eubacteria and fungi, but the rumen has also been found to include anaerobic protozoa that break down cellulose.

Although cellulolytic enzymes are also produced by the avocado fruit and the slime mold *Dictyostelium discoideum* (Blume & Ennis 1991), it is believed that the primary purpose of these enzymes is connected to the development of the corresponding fruits and spores. The most significant aerobic biota where cellulosic wastes build up is the topsoil. Because wood has a high lignin content, it is the component that cellulolytic microbes destroy the slowest. *Phanerochaete chrysosporium*, the fungus that causes white rot, is one of the rare microorganisms that can fully degrade lignin by oxidation. On the other hand, a wider range of organisms, especially Actinomycetes, can cause partial delignification to get access to the cellulose substrate.

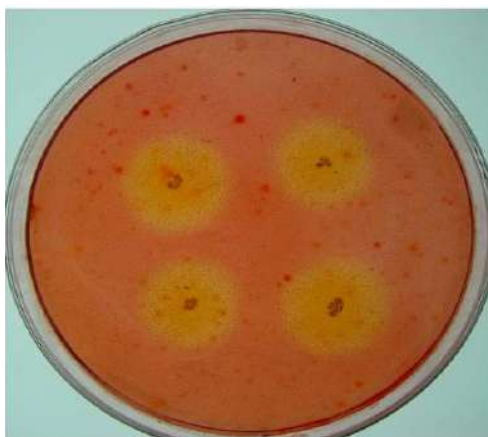


Fig. 7: Screening of cellulolytic organism.

The aerobic, highly cellulolytic Deuteromycete fungus *Trichoderma reesei* is most likely the microbe whose cellulase system has been studied the most. Numerous species of aerobic, cellulolytic soil bacteria have been thoroughly investigated. These include members of the genera *Cellulomonas*, *Pseudomonas* (*Cellovibrio*), *Thermomonospora*, and *Microbiopora*.

The hydrolysis reaction that is catalyzed by glycosidases, such as xylanases and cellulases, is typically thought to operate by an acid-base mechanism that involves two residues. The oxygen of the acidic bond is protonated by the first residue, which also functions as a general acid catalyst. The second residue works as a nucleophile, which either interacts with the oxocarbenium intermediate (for retaining enzymes) or stimulates the production of an OH<sup>-</sup> ion from a water molecule (for inverting enzymes). A two-step mechanism involving a double inversion of configuration at the anomeric carbon and the production of an oxocarbenium intermediate is responsible for reactions that result in configuration retention (Sinnott 1990). The lysozyme mechanism serves as the model for this kind of response. Reactions leading to inversion of configuration proceed via a single nucleophilic substitution (Sinnott 1990).

The non-catalytic cellulose-binding domains (CBDs) of numerous cellulolytic enzymes are present. These are typically found at the NH<sub>2</sub> or COOH terminus of the enzymes, and glycosylated, Pro/Thr/Ser rich linker sequences frequently divide them from the catalytic domains. Only a small percentage of the putative domains that can be identified by sequence similarity have been shown to exhibit cellulose-binding characteristics. Currently, there is no evidence to refute the latter's functionality; however, expected variations in binding affinity are quantifiable. These cellulolytic bacteria break down plant waste and use the cellulose as a carbon source. They also use the soil to get other cations that are necessary for their growth.

### The Role of EPS of Bacteria in CEC Changes

When it comes to how variable charge soils interact with cations and anions, their charge characteristics are crucial. An increase in the surface negative charge or a decrease in the surface positive charge of the soils might be caused by the selective adsorption of anions. Because of their low pH and cation exchange capacity (CEC), variable charge soils are unique in that heavy metal pollution can occur in them. By adding biochar from various sources, several researchers have tried to raise the pH buffering capacity and CEC of variable charge soils (Shi et al. 2017). Low molecular weight organic anions have also been shown to modify the electrokinetic characteristics of variable charge soils; this has

a significant impact on the sorption of cations and anions.

Extracellular polymeric substances (EPS) are produced by bacterial cells and coat their cell surfaces. EPS is a diverse biomolecule mostly made up of proteins, lipids, nucleic acids, and polysaccharides. This heterogeneous biomolecule has acidic functional groups that are pH-dependent and progressively become negatively charged as pH increases. According to reports, interactions including electrostatic, covalent, polymer-polymer, and hydrophobic control bacterial adhesion to surfaces, with hydrogen bonding being a significant factor (Hong et al. 2012). *Escherichia coli* cells in the stationary phase exhibited a greater capacity for adhesion compared to those in the mid-exponential phase.

According to Tsuneda et al. (2003), bacterial deposition on surfaces was thought to be promoted by the presence of a comparatively greater amount of EPS on the cell surface. According to other research (Liu et al. 2007), the EPS-deficient strains of *Pseudomonas aeruginosa* had a lower deposition potential on surfaces under comparable conditions, even though there was no discernible difference in their zeta potentials. Additionally, it was observed by Long et al. (2009) that bacterial deposition on silica surfaces was decreased when EPS was removed from bacterial surfaces. It has also been demonstrated that bacterial adherence depends on the surface on which it occurs, both in the presence and absence of extracellular polymer shielding (EPS). In contrast, *Pseudomonas aeruginosa* SG81, which produces EPS, and *Pseudomonas aeruginosa* SG81R1, a strain that does not produce EPS, showed comparable deposition capabilities on surfaces with varying levels of hydrophobicity. These opposing opinions were noted elsewhere as well, and it was believed that some bacterial species secreted uronic acids (mannuronic and glucuronic acids), which prevented the germs from depositing (Liu et al. 2015).

Bacteria have employed EPS secretion as a useful defense against heavy metal toxicity or to control the bioavailability of heavy metals in the environment (Wei et al. 2011). Plant growth-boosting properties have been demonstrated by bacteria such as *P. fluorescens*. According to Cardoso et al. (2018), rhizobacteria can promote plant growth in two ways: either by promoting the adsorption of nutrients like nitrates, phosphates, and important minerals or by controlling the negative impacts of pathogens on plant growth. In the last several years, there has been increased interest in the interactions of bacteria with soil colloids or minerals. Nevertheless, little research and understanding have been done on the part of EPS in bulk soil bacterial motility.

Nkoh et al. (2020) employed four bulk variable charge soils that included three species of *Escherichia coli*, *Bacillus subtilis*, and *Pseudomonas fluorescens*, as well

as three Ultisols and three Oxisols. Alfisol, a soil with a constant charge, was added for comparison. The alterations on the surfaces of the bacteria both before and after treatment with cation exchange resin (CER) and the soils following interactions with the bacteria were examined using zeta potential and spectroscopic techniques. The term “adsorption isotherm” refers to the relationship that exists between the amounts of a material adsorbed at a specific temperature and its equilibrium concentration. The Langmuir (Equation 1) isotherm was utilized to examine the bacterial adhesion behaviors on soil surfaces (Nkoh et al. 2020).

$$\frac{C}{Q} = \frac{1}{KQm} + \frac{C}{Qm} \quad \dots(1)$$

Where C represents the equilibrium concentration of the bacteria, Q is the number of bacterial cells adsorbed per unit mass of soils, Qm is the maximum adsorption capacity, and the constant K is related to the binding capacities of the soils.

With the majority of the  $r^2 > 0.8$ , the adsorption behavior of the bacteria to varying charge soils fit the Langmuir isotherm well. The Langmuir isotherm was not well-fitted by the adherence of *E. coli* to the Oxisol and Alfisol ( $r^2 < 0.2$ ). Ultisol>Oxisol>Alfisol was the order of adhesion for the soils. In contrast, *B. subtilis* > *P. fluorescens* > *E. coli* was the natural bacteria’s order of attachment for Ultisol and Oxisol. The native bacterial attachment order for the Alfisol was *P. fluorescens* > *B. subtilis* > *E. coli*. This is because *E. Coli* cells and soil particles resisted each other more electrostatically than the other bacteria did. The electrostatic repulsion at pH values above their IEP inhibited *E. coli*’s migration to binding sites on soil surfaces, which in turn reduced the bacteria’s ability to adhere to soil particles because of the increased quantity of negative charges on the surface of the bacteria (Nkoh et al. 2020).

According to Hong et al. (2012), the oxides of Fe and Al are the primary adsorbents for anions in soils with varying charges. The oxides are said to have a greater affinity for bacterial cells than silicate minerals. These oxides are thought to play a major role in the overall positive charge of variable-charge soils in acidic environments. Compared to the other soils, the Ultisol’s higher Fe<sub>2</sub>O<sub>3</sub> content significantly improved its ability to adsorb negatively charged bacterial cells. Although Oxisol’s amount of free Fe<sub>2</sub>O<sub>3</sub> is higher than Ultisol’s, it has a reduced ability to cling to these germs. The bacterial cells’ ability to adhere to one another was dramatically changed after they were treated with CER to eliminate EPS. The quantity of adherent native cells was substantially ( $p < 0.05$ ) higher for all species of bacteria than the quantity of EPS-free cells adhered to Ultisol, Oxisol, Ultisols, and Jinxian. *P. fluorescens* and *B. subtilis* adhesion, however, displayed an unusual pattern when the constant

charge Alfisol was used (Nkoh et al. 2020). *B. subtilis*’s surface functional group concentration increased as a result of CER treatment, which increased the cells’ deposition on goethite but decreased it on clay minerals (kaolinite and montmorillonite). Furthermore, Hong et al. (2012) employed the DLVO theory to describe how hydrophobicity, Van der Waals forces, and electrostatic interactions between bacteria and soil particles interact. Furthermore, Tsuneda et al. (2003) showed that electrostatic interaction prevented bacterial cell attachment when the EPS covering bacterial surfaces was tiny. The scientists also noticed that polymeric interaction improved bacterial cell adherence when a comparatively higher quantity of EPS coated the cells.

**Bacterial adhesion enhanced cation sorption:** The sorption of Mg<sup>2+</sup> by Ultisol in the presence and absence of *E. coli* was investigated to determine whether bacterial adherence increased the surface negative charge of variable charge soils. With an initial Mg<sup>2+</sup> concentration, the Ultisol and Ultisol-bacteria composite absorbed more Mg<sup>2+</sup>. As the initial concentration of *E. coli* introduced rose, so did the sorption of Mg<sup>2+</sup> by the soil bacterium composite. In contrast, the amount of Mg<sup>2+</sup> adsorbed by the Ultisol-bacteria composite was substantially larger ( $p < 0.05$ ) than the amount adsorbed by the free Ultisol and *E. coli* individually. The zeta potential tests showed that *E. coli* adherence to the soil surface increased the soil’s surface negative charge, making the soil composites more negative than the individual soil systems devoid of *E. coli*. A rise in the soil’s ability to retain cations is implied by an increase in the effective negative charge on the soil surface. The concentration of *E. coli* that was deposited on the soil surface was directly correlated with the degree to which *E. coli* adhesion improved the adsorption of Mg<sup>2+</sup>.

### The Use of Bioenzymes for Soil Stabilization

Bioenzymes are naturally occurring liquid enzyme compositions that are non-toxic, non-flammable, and non-corrosive. They are produced from fermented carbohydrates. They are known to boost stability, enable higher soil compaction densities, and enhance the engineering properties of soil. It is expected that bioenzymes will speed up the cationic exchange process to lower the thickness of the adsorbed layer and catalyze the reactions between the clay and large organic cations (Rajoria & Kaur 2014).

Enzymes are used by some soil microbes to maintain environmental equilibrium. They generate particular enzymes that catalyze the interactions between organic cations and clay particles, resulting in the formation of stable soil clods around the roots of the plants (Rajoria & Kaur 2014). Among these microbes are ureolytic bacteria. Numerous taxa of urease-producing bacteria have possibly been researched, including

*Lactobacillus*, *Streptococcus*, *Arthrobacter*, *Weissella*, *Enterococcus*, *Enterobacter*, *Citrobacter*, *Pseudomonas*, and *Yersinia* (Alizadeh et al. 2014). *Bacillus*, *Sporosarcina*, *Sporolactobacillus*, *Clostridium*, *Desulfotomaculum*, *Lactobacillus*, *Streptococcus*, *Arthrobacter*, *Weissella*, *Enterococcus*, *Enterobacter*, and *Providenciarettgeri* (Phang et al. 2018). These microbes not only produce urease but also a variety of other enzyme groups such as transferase, lyase, aspartase, amidohydrolase, oxido reductase, hydrolase, L. glutaminase, dehydrogenase, acid phosphatase, alkaline phosphatase, arylsulfatase, betaglucoosidase, amylase, catalase, alkaline phosphomonoesterase, phosphodiesterase, deaminase, invertase, cellulase, protease, asparaginase, amidase, chitinase, lipase, carbohydase, phenoloxidase, peroxidase, laccase, lipase, aminopeptidase, and glucoseoxidase.

## CONCLUSION

Address the challenges posed by expansive soil's swelling and shrinkage involves three main strategies: chemical, mechanical, and biological stabilization, having the following outcomes:

- Chemical stabilization utilizes lime, cement, and polymers to reduce cation exchange capacity (CEC).
- Mechanical methods include re-molding and compaction, fill replacement, pre-wetting, and sub-drainage. These approaches collectively offer effective solutions to mitigate the detrimental effects of expansive soil.
- Among these methods, we recommended the biological methods, which are economical, feasible, and environment friendly compared to other methods.
- It involves the use of plant extract with different concentrations, which are commonly available at every location, and also the use of microorganisms that produce enzymes and EPS.
- Lignin degradation can be carried out chemically and thermally by advanced oxidation processes: photocatalytic, pyrolysis, electrochemical, or enzymatically/biologically. Since the chemical structure of lignin is highly variable, as well as the enzymes used to degrade lignin, the degradation products also vary.
- During multiple biochemical transformations, C–C and C–O monomer bonds are split, and hydroxylation, demethylation, modification of side chains, and other transformations occur.
- It is generally assumed that the hydrolysis reaction catalyzed by glycosidases, including cellulases and xylanases, proceeds via an acid-base mechanism involving two residues. The first residue acts as a general

acid catalyst and protonates the oxygen of the acidic bond.

- The second residue acts as a nucleophile, which either interacts with the oxocarbonium intermediate (for retaining enzymes) or promotes the formation of an OH- ion from a water molecule.
- EPS-producing microbes like *E.coli*, *Pseudomonas fluorescens*, and *Bacillus subtilis* also require Mg and Ca-like cations as adhesion factors for the production of biofilms.
- The use of ureolytic enzymes will diminish CEC by catalyzing the reaction between organic cation and clay minerals and producing clods of stabilized soil.

Based on the above review done for various aspects of biological stabilization, the application of natural microbes available in nature itself can resolve such engineering issues with the added advantage of ecology, environment, economics, and ease with an application for large project areas.

## ACKNOWLEDGEMENT

The authors are very thankful to Prof. Dr. N. N. Bhuptani, Principal, L D College of Engineering, Ahmedabad, and Prof. Dr. C S Sanghvi, Head of Applied Mechanics Department, L D College of Engineering, Ahmedabad, for their valuable support for this project. Special thanks to Dr. Prof. Meenu Saraf, Director of the School of Science, Gujarat University, and Head of the Department for the use of laboratory and library facilities for this project.

## REFERENCES

- Abdelaziz, O.Y., Brink, D.P., Microbiology and Biotechnology, Gujarat University, Ahmedabad, for extending the Prothmann, J., Ravi, K., Sun, M., Garcia-Hidalgo, J., Sandahl, M., Hulteberg, C.P., Turner, C., Liden, G. and Gorwa-Grauslund, M.F., 2016. Biological valorization of low molecular weight lignin. *Biotechnology Advances*, 34(8), pp.1318-1346. <https://doi.org/10.1016/j.biotechadv.2016.10.001>.
- Abdel-Hamid, A.M., Solbiati, J.O. and Cann, I.K.O., 2013. Insights into lignin degradation and its potential industrial applications. *Advances in Applied Microbiology*, 82, pp.1-28. <https://doi.org/10.1016/B978-0-12-407679-2.00001-6>.
- Alizadeh, H., Kandula, D., Hampton, J., Stewart, A., Leung, D. and Edwards, Y., 2014. Screening and identification of urease-producing microorganisms from New Zealand pasture soils. *Australia Society of Soil Science Incorporated*. <https://hdl.handle.net/10182/8961>.
- Asina, F., Brzonova, I., Voeller, K., Kozliak, E., Kubatova, A., Yao, B. and Ji, Y., 2016. Biodegradation of lignin by fungi, bacteria, and laccases. *Bioresource Technology*, 220, pp.414-424. <https://doi.org/10.1016/j.biortech.2016.08.016>.
- Azwanida, N., 2015. A review of the extraction methods used in medicinal plants, principle, strength, and limitation. *Medicinal & Aromatic Plants*, 4(3), p.196. <https://doi.org/10.4172/2167-0412.1000196>.
- Barros, F., Dykes, L., Awika, J.M. and Rooney, L.W., 2013. Accelerated solvent extraction of phenolic compounds from sorghum brans. *Journal of Cereal Science*, 58(2), pp.305-312. <https://doi.org/10.1016/j.jcs.2013.05.011>.

- Beguin, P. and Aubert, J.P., 1994. The biological degradation of cellulose. *FEMS Microbiology Reviews*, 13, p.33. <https://doi.org/10.1111/j.1574-6976.1994.tb00033.x>.
- Bilal, M. and Iqbal, H.M.N., 2020. State of the art strategies and applied perspectives of enzyme biocatalysis in food sector: Current status and future trends. *Critical Reviews in Food Science and Nutrition*, 60(12), pp.2052-2066. <https://doi.org/10.1080/10408398.2019.1627284>.
- Blume, J.E. and Ennis, H.L., 1991. A dictyostelium discoideum cellulase is a member of a spore germination-specific gene family. *Journal of Biological Chemistry*, 266(23), pp.15432-15437. [https://doi.org/10.1016/s0021-9258\(18\)98634-5](https://doi.org/10.1016/s0021-9258(18)98634-5).
- Boerjan, W., Ralph, J. and Baucher, M., 2003. Lignin biosynthesis. *Annual Review of Plant Biology*, 54, pp.519-546. <https://doi.org/10.1146/annurev.arplant.54.031902.134938>.
- Bugg, T.D.H., Ahmad, M., Hardiman, E.M. and Rahmanpour, R., 2011. Pathways for degradation of lignin in bacteria and fungi. *Natural Product Reports*, 28(12), pp.1883-1896. <https://doi.org/10.1039/c1np00042j>.
- Calvo, F.G. and Dobado, J.A., 2010. Lignin is a renewable raw material. *Chemsuschem*, 3(11), pp.1227-1235. <https://doi.org/10.1002/cssc.201000157>.
- Cardoso, P., Alves, A., Silveira, P., Sa, C., Fidalgo, C., Freitas, R. and Figueira, E., 2018. Bacteria from nodules of wild legume species: Phylogenetic diversity, plant growth promotion abilities, and osmotolerance. *Science of The Total Environment*, 645, pp.1094-1102. <https://doi.org/10.1016/j.scitotenv.2018.06.399>.
- Chen, F.H., 1988. *Foundations on Expansive Soils. Development in Geotechnical Engineering*. Elsevier Scientific Publishing Company, Amsterdam, 12, pp.9-29.
- Chiappone, A., Marelllo, S., Scavia, C. and Setti, M., 2004. Clay mineral characterization through the methylene blue test: Comparison with other experimental techniques and applications of the method. *Canadian Geotechnical Journal*, 41(6), pp.1168-1178. <https://doi.org/10.1139/t04-060>.
- Christopher, L.P., Yao, B. and Ji, Y., 2014. Lignin biodegradation with laccase-mediator systems. *Frontiers in Energy Research*, 2. <https://doi.org/10.3389/fenrg.2014.00012>.
- De Souza, T.S.P. and Kawaguti, H.Y., 2021. Cellulases, hemicellulases, and pectinases: Applications in the food and beverage industry. *Food Bioprocess Technology*, 14, pp.1446-1477. <https://doi.org/10.1007/s11947-021-02678-z>.
- Faria, S.P., de Melo, G.R., Cintra, L.C., Ramos, L.P., AmorimJesuino, R.S., Ulhoa, C.J. and de Faria, F.P., 2020. Production of cellulases and xylanases by *Humicola grisea* var. *thermoidea* and application in sugarcane bagasse arabinoxylan hydrolysis. *Industrial Crops and Products*, 158, 112968. <https://doi.org/10.1016/j.indcrop.2020.112968>.
- Fisher, A.B. and Fong, S.S., 2014. Lignin biodegradation and industrial implications. *AIMS Bioengineering*, 1(2), pp.92-112. <https://doi.org/10.3934/bioeng.2014.2.92>.
- Gidigas, S. and Gawu, S., 2013. The mode of formation, nature, and geotechnical characteristics of black cotton soils: A review. *Standard Scientific Research and Essays*, 1(14). <http://www.standresjournals.org/journals/ssre>.
- Gomes, S.V.F., Portugal, L.A., dos Anjos, J.P., de Jesus, O.N., de Oliveira, E.J., David, J.P. and David, J.M., 2017. Accelerated solvent extraction of phenolic compounds exploiting a Box-Behnken design and quantification of five flavonoids by HPLC-DAD in *Passiflora* species. *Microchemical Journal*, 132, pp.28-35. <https://doi.org/10.1016/j.microc.2016.12.021>.
- Grgas, D., Stefanac, T., Baresic, M., Toromanovic, M., Ibrahimasic, J., VukusicPavicic, T., Habuda-Stanic, M., Herceg, Z. and LandekaDragicevic, T., 2023. Co-composting of sewage sludge, green waste, and food waste. *Journal of Sustainable Development of Energy, Water and Environment Systems*, 11(1), pp.1-14. <https://doi.org/10.13044/j.sdewes.d10.0415>.
- Hong, Z., Rong, X., Cai, P., Dai, K., Liang, W., Chen, W. and Huang, Q., 2012. Initial adhesion of *Bacillus subtilis* on soil minerals as related to their surface properties. *European Journal of Soil Science*, 63(4), pp.457-466. <https://doi.org/10.1111/j.1365-2389.2012.01460.x>.
- Kaufmann, B. and Christen, P., 2002. Recent extraction techniques for natural products: Microwave-assisted extraction and pressurized solvent extraction. *Phytochemical Analysis*, 13(2), pp. 105-113. <https://doi.org/10.1002/pca.631>.
- Liu, Y., Yang, C.H. and Li, J., 2007. Influence of extracellular polymeric substances on *Pseudomonas aeruginosa* transport and deposition profiles in porous media. *Environmental Science and Technology*, 41(1), pp.198-205. <https://doi.org/10.1021/es061731>.
- Liu, Z.D., Hong, Z.N., Li, J.Y., Jiang, J. and Xu, R.K., 2015. Interactions between *Escherichia coli* and the colloids of three variable charge soils and their effects on soil surface charge properties. *Geomicrobiology Journal*, 32(6), pp.511-520. <https://doi.org/10.1080/01490451.2014.967419>.
- Long, G., Zhu, P., Shen, Y. and Tong, M., 2009. Influence of extracellular polymeric substances (EPS) on deposition kinetics of bacteria. *Environmental Science and Technology*, 43(7), pp. 2308-2314. <https://doi.org/10.1021/es802464v>.
- Niu, J., Li, X., Qi, X. and Ren, Y., 2021. Pathway analysis of the biodegradation of lignin by *Brevibacillus thermoruber*. *Bioresource Technology*, 341, 125875. <https://doi.org/10.1016/j.biortech.2021.125875>.
- Nadgouda, K.A. and Hegde, R.A., 2010, December. The effect of lime stabilization on properties of black cotton soil. In *Indian Geotechnical Conference* (pp. 514-511).
- Nkoh, N.J., Liu, Z.D., Yan, J., Cai, S.J., Hong, Z.N. and Xu, R.K., 2020. The role of extracellular polymeric substances in bacterial adhesion onto variable charge soils. *Archives of Agronomy and Soil Science*, 66(13), pp.1780-1793. <https://doi.org/10.1080/03650340.2019.1696016>.
- Paudel, Y.P. and Qin, W., 2015. Characterization of novel cellulase-producing bacteria isolated from rotting wood samples. *Applied Biochemistry and Biotechnology*, 177, pp.1186-1198. <https://doi.org/10.1007/s12010-015-1806-9>.
- Phang, I.R.K., Chan, Y.S., Wong, K.S. and Lau, S.Y., 2018. Isolation and characterization of urease-producing bacteria from tropical peat. *Biocatalysis and Agricultural Biotechnology*, 13, pp. 168-175. <https://doi.org/10.1016/j.bcab.2017.12.006>.
- Rajoria, V. and Kaur, S., 2014. A review on stabilization of soil using bio-enzyme. *International Journal of Research in Engineering and Technology*, 14, pp.61-73.
- Sanchez, C., 2009. Lignocellulosic residues: Biodegradation and bioconversion by fungi. *Biotechnology Advances*, 27(2), pp.185-194. <https://doi.org/10.1016/j.biotechadv.2008.11.001>.
- Shida, Y., Furukawa, T. and Ogasawara, W., 2016. Deciphering the molecular mechanisms behind cellulase production in *Trichoderma reesei*, the hyper-cellulolytic filamentous fungus. *Bioscience, Biotechnology, and Biochemistry*, 80(9), pp.1712-1729. <https://doi.org/10.1080/09168451.2016.1171701>.
- Shi, R.Y., Hong, Z.N., Li, J.Y., Jiang, J., Baquy, M.A.A., Xu, R.K. and Qian, W., 2017. Mechanisms for increasing the pH buffering capacity of an acidic Ultisol by crop residue-derived biochars. *Journal of Agricultural and Food Chemistry*, 65(37), pp.8111-8119.
- Silalertruksa, T. and Gheewala, S.H., 2020. Competitive use of sugarcane for food, fuel, and biochemical through environmental and economic factors. *International Journal of Life Cycle Assessment*, 25, pp.1343-1355. <https://doi.org/10.1007/s11367-019-01664-0>.
- Sinnott, M.L., 1990. Catalytic mechanisms of enzymic glycosyl transfer. *Chemical Reviews*, 90(7), pp.1171-1202. <https://doi.org/10.1021/cr00105a006>.
- Tsuneda, S., Aikawa, H., Hayashi, H., Yuasa, A. and Hirata, A., 2003.



- Extracellular polymeric substances are responsible for bacterial adhesion onto solid surfaces. *FEMS Microbiology Letters*, 223(2), pp.287-292. [https://doi.org/10.1016/s0378-1097\(03\)00399-9](https://doi.org/10.1016/s0378-1097(03)00399-9).
- Turkoz, M. and Tosun, H., 2011. The use of methylene blue test for predicting swell parameters of natural clay soils. *Scientific Research and Essays*, 6(8), pp.1780-1792. <https://doi.org/10.5897/sre10.629>.
- Wei, X., Fang, L., Cai, P., Huang, Q., Chen, H., Liang, W. and Rong, X., 2011. Influence of extracellular polymeric substances (EPS) on Cd adsorption by bacteria. *Environmental Pollution*, 159(5), pp.1369-1374. <https://doi.org/10.1016/j.envpol.2011.01.006>.
- Yadav, V.K., Gupta, N., Kumar, P., Dashti, M.G., Tirth, V., Khan, S.H., Yadav, K.K., Islam, S., Choudhary, N., Algahtani, A., Bera, S.P., Kim, D.H. and Jeon, B.H., 2022. Recent advances in synthesis and degradation of lignin and lignin nanoparticles and their emerging applications in nanotechnology. *Materials*, 15(3), p.953. <https://doi.org/10.3390/ma15030953>.
- Yi, C., Shi, J., Xue, S.J., Jiang, Y. and Li, D., 2009. Effects of supercritical fluid extraction parameters on lycopene yield and antioxidant activity. *Food Chemistry*, 113(4), pp.1088-1094. <https://doi.org/10.1016/j.foodchem.2008.08.083>.
- Zhao, L.C., He, Y., Deng, X., Yang, G.L., Li, W., Liang, J. and Tang, Q.L., 2012. Response surface modeling and optimization of accelerated solvent extraction of four lignans from *FructusSchisandrae*. *Molecules*, 17(4), pp.3618-3629. <https://doi.org/10.3390/molecules17043618>.

---

#### ORCID DETAILS OF THE AUTHORS

- M. V. Shah: <https://orcid.org/0000-0003-0348-4816>  
R. R. Panchal: <https://orcid.org/0000-0001-8715-8553>





# Landslide Susceptibility Zonation Mapping Using Machine Learning Algorithms and Statistical Prediction at Hunza Watershed Basin, Pakistan

A. Khan<sup>1†</sup>, G. Khan<sup>1</sup>, M. Minhas<sup>2,3</sup>, S. A. Hussain Gardezi<sup>5,6,7</sup>, J. Ahmed<sup>2,4</sup> and N. Abbas<sup>1,2</sup>

<sup>1</sup>Department of Earth Sciences, Karakoram International University (KIU), Gilgit, 15100, Pakistan

<sup>2</sup>Faculty of Land Resources Engineering, Kunming University of Science and Technology, Yunnan, 650093, China

<sup>3</sup>Centre of Excellence in Mineralogy, University of Balochistan, Quetta, Pakistan

<sup>4</sup>Department of Geology, University of Balochistan, Quetta, Pakistan

<sup>5</sup>Key Laboratory of Ocean and Marginal Sea Geology, South China Sea Institute of Oceanology, Chinese Academy of Science, Guangzhou, 510301, China

<sup>6</sup>University of Chinese Academy of Science, Beijing, 100049, China

<sup>7</sup>Azad Jammu and Kashmir Directorate, Geological Survey of Pakistan, Muzaffarabad 13100, Pakistan

†Corresponding author: Asghar Khan: [Asghar.khan@kiu.edu.pk](mailto:Asghar.khan@kiu.edu.pk)

Nat. Env. & Poll. Tech.  
Website: [www.neptjournal.com](http://www.neptjournal.com)

Received: 14-01-2024

Revised: 04-03-2024

Accepted: 02-04-2024

## Key Words:

Seed cell area index  
Intuitionistic fuzzy divergence  
Karakoram highway  
Susceptibility mapping  
Prediction rate curve

## ABSTRACT

The mountainous region of the Hunza River watershed basin, especially along the Karakoram highway, and also known as a third pole for the high accumulation of glaciers, which leads to huge devastating landslides occurring every year. Landslide susceptibility mapping was carried out using two deep machine learning techniques (DeeplabV3<sup>+</sup> & universal network U-Net) and two statistical models (Intuitionistic Fuzzy divergence IF-D & Frequency ratio FR). The landslide susceptibility mapping is conducted using landslide inventory data and twelve conditional factors. The landslide susceptibility maps obtained from the two statistical models were compared with those generated by two deep machine learning models based on prediction accuracy measures, such as the Area Under the Curve (AUC) and Seed Cell Area Index (SCAI). The Success Rate Curve (SRC) was obtained using the training dataset, and the AUC values for the four models were as follows: 76.9% for IF-D, 76.9% for FR, 80.4% for DeeplabV3<sup>+</sup>, and 76.3% for U-Net. In terms of the Prediction Rate Curve (PRC) obtained from the validation dataset, the AUC values were found to be 80.8% for IF-D, 80.8% for FR, 81% for DeeplabV3<sup>+</sup>, and 77.8% for U-Net. To assess the classification ability of the models, the Seed Cell Area Index (SCAI) test was conducted. The results indicated that the SCAI (D-value) was 7.3 for U-Net, 10 for DeeplabV3<sup>+</sup>, 7.6 for IF-D, and 9.1 for FR. Overall, the findings revealed that DeeplabV3<sup>+</sup> exhibited the highest prediction accuracy and classification ability, making it the most suitable choice for landslide susceptibility mapping in the relevant study area.

## INTRODUCTION

Landslides are widely recognized as the most common and devastating geohazards in mountainous regions (Panchal & Shrivastava, 2022), significantly impacting both socioeconomic factors and human lives (Panahi et al. 2022). The occurrence and severity of landslides have been on the rise globally, attributed to the influences of climate change and human activities (Sajadi et al. 2022). Various factors contribute to these events, including frequent earthquakes, human activities such as road expansion on steep slopes, volcanic activities, and prolonged rainfall (Youssef & Pourghasemi 2021). The Karakoram and Himalayan mountainous terrain in the extreme northern part of Pakistan

is prone to numerous landslides. The frequent occurrence of landslides in these rugged terrains can be attributed to factors such as repeated seismic activity, highly weathered lithologies, unstable slopes, and human activities (Shafique et al. 2016). The presence of active thrust faults, fractured lithologies, exposed geomorphology, and unconsolidated glacial-fluvial moraine on steep slopes further contributes to the susceptibility of the area to landslides (Hewitt 1998). In recent years, the Hunza River watershed basin located within the Karakoram Mountain range has experienced frequent devastating landslides (Derbyshire 2001). In January 2010, an especially destructive landslide occurred in Attabad village in Upper Gojal, resulting in the loss of twenty lives, the destruction of over three hundred houses,

and the formation of a new natural lake that persists to this day (Kargel et al. 2010). To address these natural hazards, landslide susceptibility maps can prove to be valuable tools for identifying areas vulnerable to landslides (Youssef & Pourghasemi 2021). These maps can be developed by considering various geo-environmental factors, including lithology, geomorphology, soil types, human activities, and drainage patterns.

Several approaches have been proposed for studying landslide susceptibility mapping, driven by advancements in computer science technologies and the availability of geospatial data. Many of these approaches utilize remote sensing data and Geographic Information Systems (GIS) (Chang et al. 2020). However, these methods often require extensive preparation related to landslides, including environmental, pedagogical, physical, geomorphological, and topographic considerations, as well as considerable knowledge and determination. Traditional approaches to landslide modeling rely on field excursions, which can be costly, site-specific, and time-consuming. Consequently, in the past few decades, statistical approaches for landslide susceptibility modeling have gained popularity (Al-Najjar & Pradhan 2021).

In general, landslide susceptibility mapping approaches encompass objective quantitative methodologies based on mathematical analysis, as well as qualitative methodologies involving subjective expert judgment (Bopche & Rege 2022). The heuristic technique involves the creation of susceptibility classes by assessing the relative contribution of landslide conditional factors to landslide formation (Dahal et al. 2008). The main limitation of heuristic methods, which fall under the qualitative approach, is the subjective nature of susceptibility assessments. On the other hand, the quantitative approach allows for the evaluation of the statistical relationship between the spatial distribution of known landslides and conditional factors (Chen et al. 2019). However, among the various landslide susceptibility techniques available, statistical approaches have gained popularity due to their accuracy and reliability in addressing the challenges of large-scale landslide mapping.

These methods can be categorized into qualitative, semi-quantitative, and quantitative approaches. The availability of remote sensing data, including topography and land cover information, has greatly facilitated the application of these techniques at large scales (Al-Najjar & Pradhan 2021). In recent years, researchers have extensively evaluated and applied various statistical models for landslide susceptibility analysis. These models include the Weight of Evidence (WOE) (Bopche & Rege 2022), Entropy Index (IOE) (Mondal & Mandal 2019), Support Vector Machine (Pandey

et al. 2020), Neural Network (Abbaszadeh Shahri et al. 2019), Decision Tree methods (Wu et al. 2020), and Logistic Regression (Shan et al. 2020). However, each landslide susceptibility mapping (LSM) model has its advantages and disadvantages. It is common for different models to yield diverse evaluation outcomes when applied in the same region. To address these differences in prediction accuracies, many researchers have opted for multi-LSM models and conducted comparative analyses (Chen et al. 2019).

In recent years, various machine learning techniques (MLTs) have been utilized for tasks such as landslide susceptibility mapping, debris classification, and glacier lake mapping. Specifically, for landslide susceptibility mapping, several MLT techniques have been applied, including Artificial Neural Network (Youssef & Pourghasemi 2021), Support Vector Machine (X. Zhang et al. 2019), Decision Tree (Dou et al. 2019), and Random Forest (RF) (Sun et al. 2021).

Landslide occurrences depend on multiple factors (Zhang et al. 2019), including man-made activities, geomorphological conditions, weathering conditions, and others. While some factors can only be analyzed using qualitative or semi-qualitative methods (Zhang et al. 2021), there is inherent uncertainty in the landslide system (Zou & Xiao 2008). Fuzzy mathematical methods have been widely applied for landslide assessment to capture the complexity of these factors (Zhang et al. 2012). However, in classical fuzzy methods, the fuzzy nature is only represented by the membership function, whereas in intuitionistic fuzzy sets, the non-membership function is introduced to further explain the fuzzy concept (Zhang et al. 2021).

With the advancement of fuzzy set theory, various fuzzy models have been widely applied in various decision-making scenarios (Gu & He 2021). In the context of landslide susceptibility mapping, several entropy models and fuzzy models have been employed in landslide-prone areas. These include Shannon entropy (SE) (Nohani et al. 2019), index of entropy (IE) (Pourghasemi et al. 2012), Renyi divergence (RI) (Qin et al. 2001), intuitionistic fuzzy Jensen-Renyi divergence (IFJ-D) (Verma & Sharma, 2013), fuzzy gamma ray operator and AHP (Bera et al. 2019), and intuitionistic fuzzy set (Gu et al. 2022).

The concept of intuitionistic fuzzy sets, developed by Atanassov (1986), incorporates the degree of membership and non-membership functions with hesitancy such that their sum equals 1. Various modifications have been made to the classical fuzzy divergence model, with the latest version of modification being the Jensen-Renyi divergence. In the context of intuitionistic fuzzy sets, the Jensen-Renyi divergence is referred to as the Intuitionistic Fuzzy Jensen-

Renyi Divergence (IFJR). This divergence provides more precise results than previous models, particularly in decision-making problems. However, it involves lengthy calculations and may fail for certain pattern sets (Verma & Sharma 2013).

In this study, the author introduces a refined fuzzy model, IF-D, derived from the intuitionistic fuzzy Jensen-Renyi divergence. This model streamlines computations and enhances performance on pattern sets. IF-D leverages original data effectively, employing straightforward mathematical calculations for probability analysis, resulting in superior accuracy compared to conventional models. Additionally, this research also aims to evaluate the efficacy of IF-D and classical models in landslide susceptibility mapping, focusing on classification capabilities and prediction accuracies. Furthermore, the study seeks to assess the accuracy, reliability, and suitability of deep machine learning techniques and statistical methods through a comparative analysis in the study area.

### Study Area

Hunza watershed basin in the Karakoram mountainous range is in the Northern part of Pakistan. This watershed basin is fenced by the world's highest mountain ranges, i.e., Karakoram, Hindu-Kush, and the Himalayas. These mountain ranges comprise the world's highest and steep slopes with more than 45° slopes. The geographical location of the study area falls between the latitudes of 36°51'38.359" N, 35°55'22.231" N and longitudes of 76°0'45.354" E, 73°59'26.466" E. The elevation ranges from 1746 m to 7315 m above sea level. This watershed basin covers an area of 14305.07 km<sup>2</sup>.

In Pakistan, particularly in the Karakoram mountainous range, landslides pose a common and significant threat to settlement areas (Ahmed et al. 2019). The study area, Hunza watershed basin, is situated in the Northern Karakoram Range of Pakistan (Fig. 1). The area is traversed by the Karakoram Highway (KKH), which serves as the primary trade and transportation route between China and Pakistan and has experienced numerous large-scale landslides in the past. The geomorphology of the study area is diverse, encompassing glacial-fluvial terraces, ancient moraines, loose material on steep scree slopes, debris fans, colluvium deposits, and talus deposits at the base of high cliffs (Hewitt 1998). The study area is characterized by a unique geology known as the Karakoram block. This block originated from the pre-Gondwanan supercontinent and drifted away during the late Paleozoic era before colliding with the Indian plate. The Hunza watershed basin is situated between two regional thrust faults: the Shyok Suture Zone to the south (Searle

& Tirrul 1991) and the Rushan-Pshart Suture to the north (Pashkov & Shvol'man 1979).

Consequently, the rocks in the area are highly fragile due to the intense tectonic compressional regime, making the slopes highly susceptible to landslides exacerbated by frequent earthquakes. The Hunza River watershed covers an area of 13,571 km<sup>2</sup> and is nourished by some of the highest glaciers in the region. The Hunza River originates from this basin, serving as the starting point of the Indus River. The Indus River begins at the Khunjerab Pass and passes through the Hunza watershed basin, which is characterized by a network of long valley glaciers. See Fig. 1.

### MATERIALS AND METHODS

The research methodology employed in this study involves seven main steps. (1) a detailed landslide inventory map of the study area is constructed by utilizing previous records, satellite imagery, and thorough field investigations. This map serves as the foundational map for data analysis, capturing the spatial distribution and occurrences of landslides in the study area. (2) twelve landslide conditional factors, including Slope, Aspect, Curvature, Geology, Distance to Fault, Distance to River, Distance to Road, Land cover, Topographic Wetness Index, Stream Power Index, and rainfall data, are selected through comprehensive field surveys of the study area. (3) Weight estimations of statistical models are analyzed to identify the spatial relationship between landslide conditional factors and landslide occurrence. (4) The landslide susceptibility maps are prepared using three state-of-the-art deep machine-learning techniques and statistical models. (5) The susceptibility maps generated from the machine learning techniques undergo validation using metrics such as F1 Score, Confusion Matrix, Precision, and IOU curve. (6) The landslide susceptibility maps produced from all four models are analyzed using the AUC (Area Under the Curve) and Seed Cell Area Index (SCAI). (7) A comparative analysis is conducted based on the results obtained from the models to determine their suitability and applicability for the specific study area, see Fig. 2.

### Landslide Inventory Map

A global-scale landslide inventory was introduced by the International Geotechnical Societies' UNESCO Working Party on the World Landslide Inventory (deLugt & Cruden 1990). This inventory was later integrated into a database management system (Brown 1992). Mapping the spatial distribution of landslides is considered crucial before studying the relationship between landslide occurrence and its conditional factors, as highlighted by (van Westen et al. 1997). Various approaches, such as satellite images, aerial

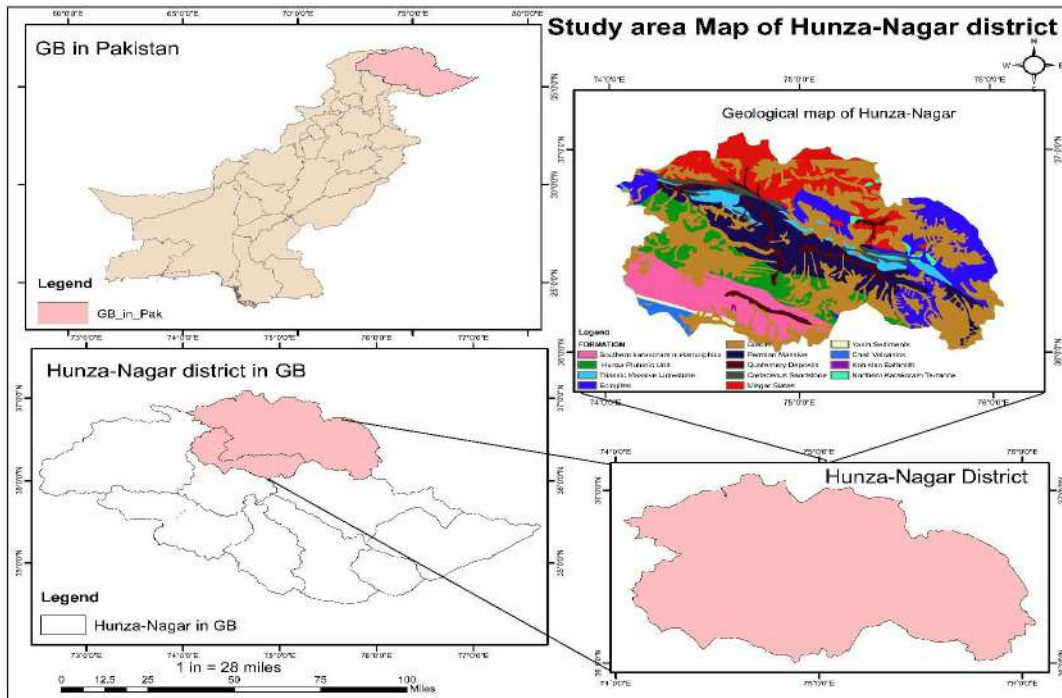


Fig. 1: Study area map, showing demographic boundaries and geological of area.

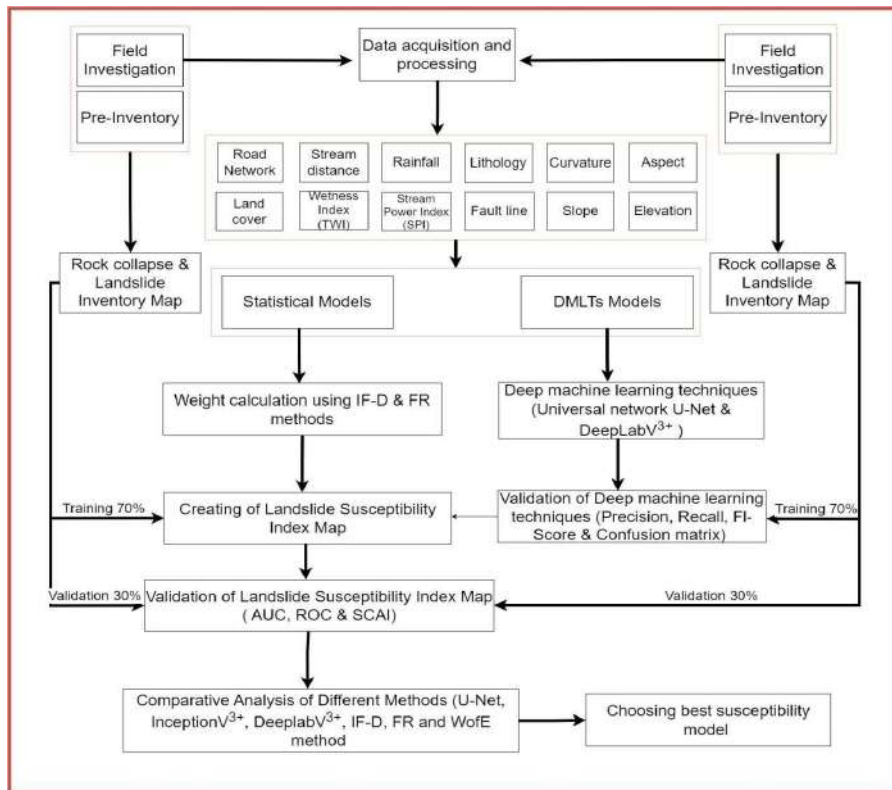


Fig. 2: Schematic flow chart for the adopted methodology.

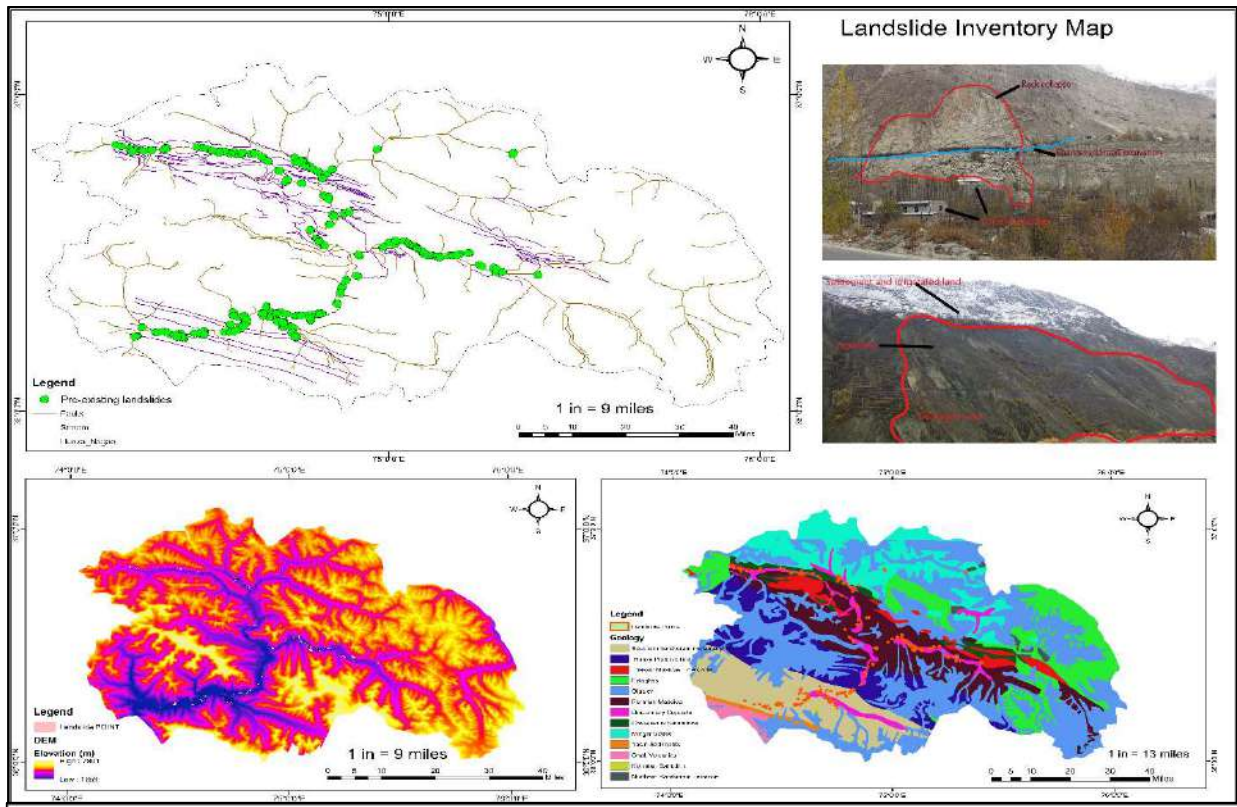


Fig. 3: Landslide inventory map of the study area, showing landslide locations, geological map, fault lines and some of the pictures of existing landslides.

photographs, and digital representations of topographic surfaces, can be used to map and identify landslides (Guzzetti, 2000). Therefore, landslide inventory maps play a vital role in regional landslide susceptibility mapping (Yan et al. 2019).

In this study, a comprehensive approach was employed, which involved the interpretation of aerial photographs, satellite images, earlier reports, and meticulous field investigations. Geologists and subject specialists were involved in the precise identification and marking of landslide sites. A total of 148 landslides were identified and marked in the study area using Garmin GPS with an accuracy of 3m. See Fig. 3 inventory map of the study area.

### Landslide Conditional Factors

Landslide conditional factors are temporally and spatially dependent on the geomorphology of the study area. According to Yan et al. (2019), understanding the factors influencing landslide occurrences is crucial for landslide susceptibility mapping. Many researchers have conducted extensive investigations to identify the factors contributing to landslides and construct landslide susceptibility maps. These events are influenced by a combination of topographic,

hydrological, and geological factors (Dou et al. 2019). The quality of landslide susceptibility maps relies not only on the selected models but also on the quality of the input data (Pourghasemi et al. 2013). Hong et al. (2016) emphasize that the selection of landslide conditioning factors is a key step in evaluating and mapping landslide susceptibility, as it directly impacts the quality of the resulting models. Based on the available literature, prior knowledge of landslide occurrence characteristics in the Hunza watershed basin, and the data availability for the study area, twelve landslide conditional factors were selected: slope, slope curvature, elevation, aspect, lithology, distance to faults, distance to rivers, distance to roads, topographic wetness index TWI, stream power index (SPI), land cover, and rainfall. All the thematic layer maps are shown in Fig. 4.

### LSM Applying (DeeplabV3<sup>+</sup>)

DeeplabV3<sup>+</sup> is the latest state of art machine learning model that has an encoder-decoder-based network for semantic segmentation. The DeeplabV3<sup>+</sup> has a setup of deeplabV3 architecture as an encoder at the backup of ResNet. The architecture is divided into three parts: the encoder used for

feature extraction, ASPP to convert them into a wide scale information, and the encoder part arrayed to recuperate the spatial information. The extracted features in the encoder level are bilinearly up-sampled and then finally concatenated with the respective low-level features in the subsequent stage.

This model is built on the conception of Atrous Convolution and Atrous Spatial Pyramid Pooling (ASPP). In the Atrous convolution, the active field of view of the convolution is governed by a rate parameter. This Atrous convolution can be generalized as follows.

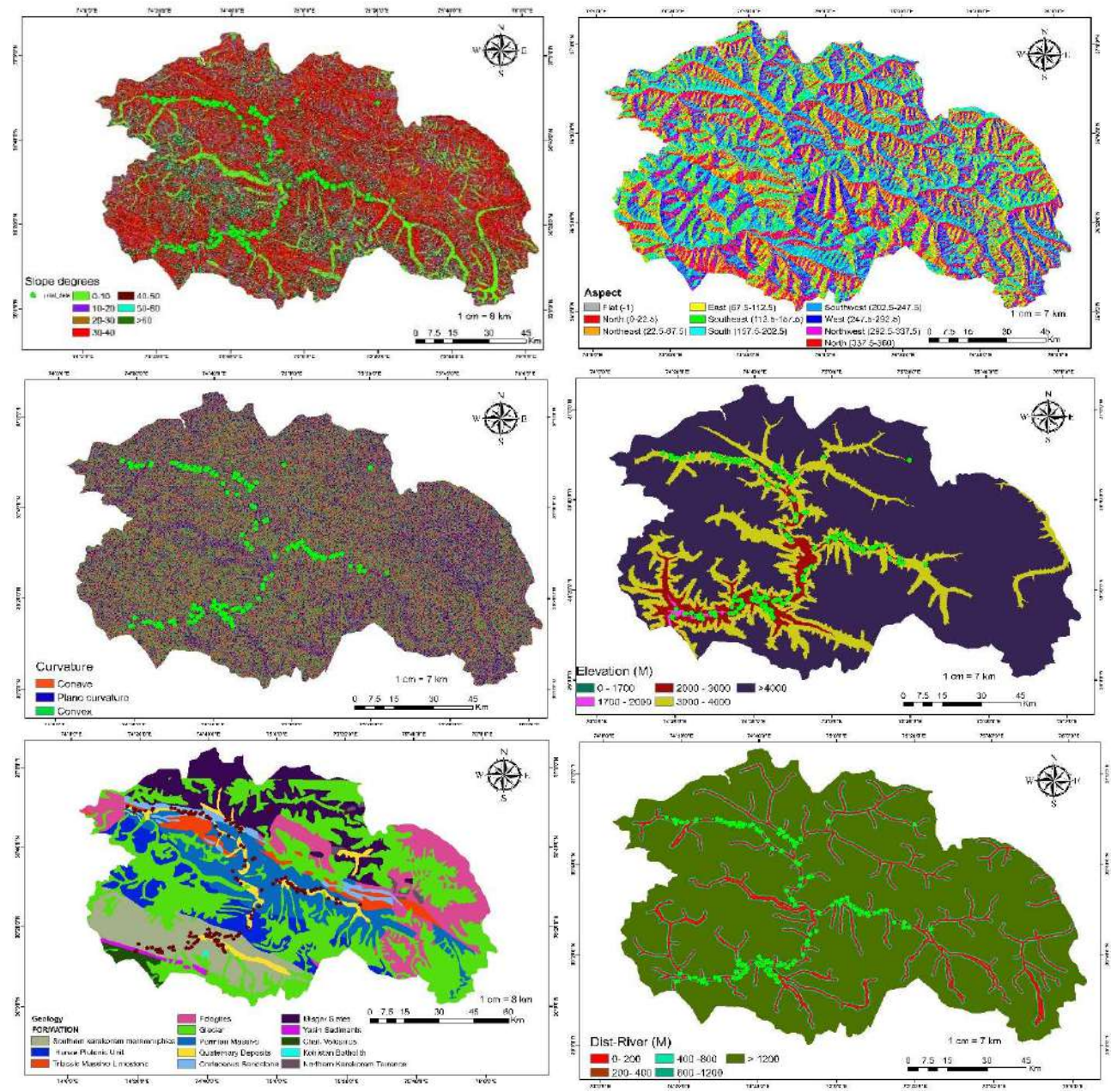


Figure Cont....



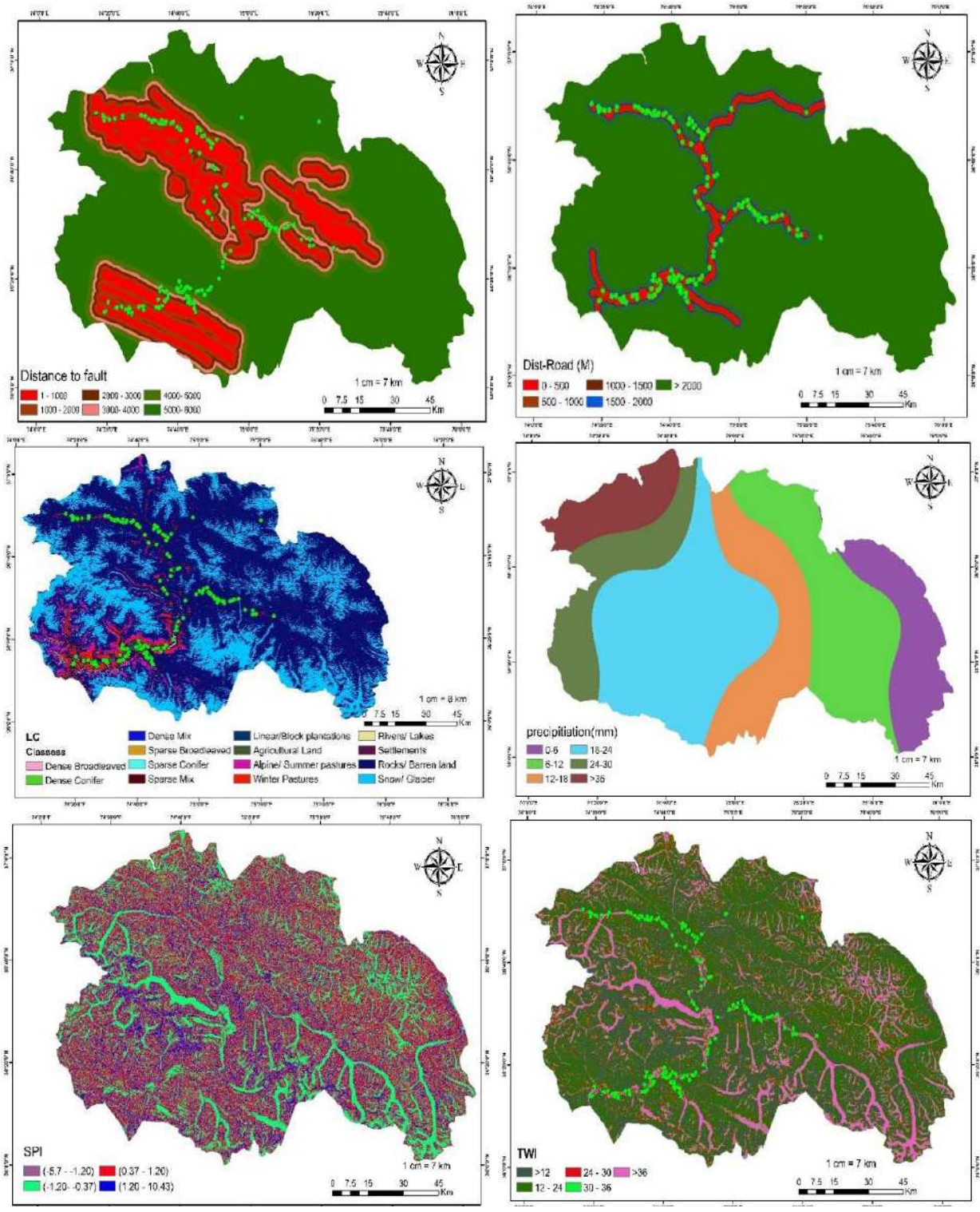


Fig. 4: Thematic layers of all 12 landslides conditional factors, the thematic layers have been classified into various classes for the probability analysis, the 12 landslide conditional factors are slope, aspect, curvature, elevation, distance to fault, distance to river, distance to road, land cover, topographic wetness index, stream power index, lithology and precipitation.

$$y[i] = \sum_k x [i + r \cdot k]w[k]$$

Where  $w$  represents the filter,  $i$  denotes each location of output  $y$ ,  $x$  is the input feature map, and  $r$  denotes the Atrous rate.

To regain information on different scales, several Atrous convolution layers can be applied. The ASPP can detain multi-scale data more capably with enormous Atrous rates. Thus DeeplabV3<sup>+</sup> works as an encoder and depicts useful features at capricious resolution. Moreover, the ASPP can discover the convolutional features at several scales with multi-dilation rates. Therefore, better semantic information can be obtained from the output feature map of the encoder networks, which often contain 256 channels and are 32 times smaller than the resolution of the input image.

### LSM Applying (U-Net)

U-Net is a deep machine-learning model that is useful for semantic segmentation purposes (Ronneberger et al. 2015). The architecture of the model has been modified to enable precise segmentation of targets even with limited training samples. U-Net has demonstrated excellent performance in remote sensing and segmentation tasks. The model follows an encoder-decoder structure, where the encoder path primarily consists of two 3×3 convolutional layers followed by 2×2 max-pooling layers. The convolutional layers act as moving windows that traverse the image (Zhang et al. 2019). Typically, U-Net takes input images with three channels, but for landslide susceptibility mapping, we have 12 channels or bands representing the thematic layers of landslide conditional factors. Therefore, it is essential to add additional layers to accommodate the increased input channels. In our model, we use the ResNet34 architecture as the encoder, allowing the extraction of multi-scale features from the input remote sensing data. The max-pooling operation in the encoder down samples the data with a stride of 2.

In contrast, the up-sampling in the decoder part is achieved by increasing the spatial size by a factor of 2 using bilinear interpolation. For this study, we utilized pre-trained weights from the ImageNet dataset for our encoder. To enhance the model's performance and prevent overfitting, we incorporated additional convolutional layers, such as Batch Normalization layers and dropout layers, with a rate of 0.2. The last convolutional layer consists of 5 neurons, and all the convolutional layers employ the Rectified Linear Unit (ReLU) activation function. The final output layer uses the Softmax activation function, which assigns a probability to each pixel indicating its belonging to a particular class in the LSM.

### LSM Applying (Frequency Ratio FR)

The FR (Frequency Ratio) model is a statistical analysis approach that considers the spatial distribution of landslides and their conditional factors (Yan et al. 2019). It examines the number of pixels affected by landslides in a specific study area. The FR method applies conditional probability, whereby a stronger relationship between landslides and their influencing factors exists when the landslide-to-factor ratio is higher. This approach is in line with the works of Lee and Talib (2005), Pourghasemi (2008), Karim et al. (2011a), and (Khan et al. 2022), who also considered each class of landslide conditional factors and their associated pixels in landslide susceptibility mapping.

To implement the FR model for each class of landslide conditional factors, a combination is established between the landslide inventory map and criterion map Karim et al. (2011a). Therefore, in the process of landslide susceptibility mapping, it is essential to consider each class of landslides, their causative and conditional factors, as well as associated pixels both with and without landslides (Mandal & Mondal 2019).

To calculate the frequency ratio for each class of all the data layers, a combined expression will be used by using the following statistical expression (Karim et al. 2011b). Eq. 1.

$$Fr_i = \frac{N_{Pix(S_i)}/N_{Pix(N_I)}}{\sum N_{Pix(S_j)}/\sum N_{Pix(N_I)}} \quad \dots(1)$$

$N_{Pix(S_i)}$  The number of pixels contains slides in each class ( $i$ )

$N_{Pix(N_I)}$  The total number of pixels having class in the whole watershed area

$\sum N_{Pix(S_j)}$  The total number of pixels containing landslide

$\sum N_{Pix(N_I)}$  The total number of pixels in the whole watershed area

### LSM Applying (Intuitionistic Fuzzy Divergence IF-D)

The concept of fuzzy logic, proposed by Zadeh (1965), is based on the idea that each element should belong to a set with a membership value ranging between 0 and 1. Fuzzy logic allows for dealing with uncertainties in data using the Interval-Valued Fuzzy Sets (IFS) theory, which has proven beneficial in various research fields due to its ability to handle imprecise analysis. In probability theory, statistical divergence measures are commonly employed to quantify the differences between two probability distributions, as seen in the works of Kullback and Leibler (1951) and Rao (1985).

One specific divergence measure used in IFSs is known as the Intuitionistic Fuzzy Jensen-Rényi divergence (IFJRD).

While this divergence provides precise results in decision-making problems compared to classical fuzzy models, it involves lengthy calculations and has limitations when applied to certain pattern sets (Verma & Sharma 2013). To address these limitations, a new model called Intuitionistic Fuzzy Divergence (IF-Divergence) has been proposed, which overcomes the limitations of the Fuzzy Jensen-Rényi divergence model and is based on simpler calculations. In this study, the proposed IF-Divergence model is applied for landslide susceptibility mapping and probability analysis.

The fuzzy membership values can be derived from various methods of normalization of the frequency ratio (Abedi Gheshlaghi & Feizizadeh 2017). In the present study, fuzzy membership values were normalized from information values.

**Step 01:**

Normalized the Intuitionistic Fuzzy Matrix  $R = (r_{ij})_{(n \times m)}$

$$\gamma_{ij} [\pi_{ij}, v_{ij}, \pi_{ij}] = \begin{cases} d_{ij} & \text{for stable pixels} \\ d_{ij} & \text{for non - stable pixel} \end{cases} \dots(2)$$

**Step 02:**

Find the Ideal Solution

$$A^* = \{(\mu_{1*}, v_{1*}, \pi_{1*}), (\mu_{2*}, v_{2*}, \pi_{2*}), \dots, (\mu_{m*}, v_{m*}, \pi_{m*})\} \dots(3)$$

Where  $i = 1, 2, \dots, n$

$$(\mu_{*i}, v_{*i}, \pi_{*i}) = \{ \max_j \mu_{ij}, \min_j v_{ij}, 1 - \max_j \mu_{ij}, 1 - \min_j v_{ij} \} \dots(4)$$

**Step 03:**

$$D_n(A_j, A^*) = \frac{1}{2|X|} \sum_{i=1}^n \left\{ \left| \mu_{A_j}(x_i) - \mu_{A^*}(x_i) \right| + \left| v_{A_j}(x_i) - v_{A^*}(x_i) \right| + \left| \pi_{A_j}(x_i) - \pi_{A^*}(x_i) \right| \right\}^n \dots(5)$$

Where  $n = 1, 2, \dots$

**Step 05:**

$$S(A, B) = 1 - D_n \dots(6)$$

**RESULTS AND DISCUSSION**

**Weight Estimation Using (FR & IF-D)**

In the investigation, all the conditional factors contributing to landslides were transformed into a binary pattern, indicating the presence or absence of landslides, using the FR and divergence values. For continuous data such

as slope, elevation, distance to fault, distance to the river, and road distance, they were first classified into different classes, and weights were separately estimated using the FR and IF-D models. In the case of continuous data, cutoff values were determined using the IF-D model, where the influence of a factor class on landslide occurrence is no longer statistically significant. The IF-D model identifies these cutoff values by examining the intersection points of similarity and divergence, enabling multi-generalization for continuous data.

For categorical data such as lithology, land cover, precipitation, curvature, SPI, TWI, and aspect, they were converted into a binary pattern based on the calculated weights from the FR and IF-D models for each factor class. The weights derived from the FR and IF-D models were then used to interpret the importance of each class of landslide conditional factor on landslide occurrences.

**Cumulative Weights Using FR and IF-D**

The influence of slope gradient below 20° and intersection point below 50° indicates that there is no influence of landslides. Therefore, this indicates that the cutoff valve for the slope gradient is 50°. Additionally, the minimum value of divergence D=0 and maximum valve of S=1 for the slope gradient 30°-40° indicates the maximum probability of landslide occurrence. In the case of frequency ratio, the weighted value of FR=1.62 represents the maximum value indicating the maximum probability of landslide occurrence for the slope gradient between slope class 30°-40° slope degrees.

**Cumulative weights of elevation:** The influence of elevation range intersection point is between 0-1700 m. This indicates that there is no influence of elevation on landslides. moreover, below 4000 m, the range of membership values tends to a maximum. Therefore, the results indicate the cutoff valve is below 4000 m. However, the maximum values indicated by S=1 and minimum values D=0 for the range of 2000 to 3000 m indicate the maximum probability and maximum influence of elevation on landslide occurrence. Furthermore, the results reveal that the similar highest value for frequency ratio FR=10.16 is the maximum for the same range of 2000 to 3000 m. This reflects that the highest association of landslide occurrence and maximum influence of elevation on landslide occurrence is in the range of 2000 to 3000 m.

**Cumulative weights of distance to fault:** For IF-D weight estimation, the boundary and intersection point lie below 5000 m. This indicates the cutoff value is below 5000 m, and the influence of distance to fault on landslide occurrence is below 5000 m. The number of landslides is about 11% for the range of 4000-5000 m; therefore, the cutoff point lies below

5000 m. Additionally, the similarity remains maximum, and divergence remains minimum from the range of 0-5000 m for the distance of fault. The result showed that the maximum influence of distance to fault on landslide occurrence is between 0-5000 m. Similarly, for frequency ratio weight estimation, the ascending trend in FR values from FR=2.02-2.95 for the class starts from 0-4000 m; additionally, the maximum value of FR = 2.95 for the same range between 3000 to 4000 m indicates that the influence of distance to fault on landslide occurrence can be found from 0 to 4000 m but maximum influence reached at 4000 m.

**Cumulative weights for distance to river.** Moreover, the weight values evaluated from IF-D showed a precise estimation regarding the weight cutoff value, which is indicated by the support and boundary of membership values. The cutoff value indicated by the cross-section point at 800 m indicates that there is no influence of distance to the river on landslide occurrence. Additionally, the values of divergence are minimum, and the values of similarity maximum for the class ranges from 0-800, indicating the maximum probability of landslide and maximum influence of distance to river on landslide occurrence.

**Cumulative weights for distance to road.** Therefore, the results indicate the cutoff value for the distance is below 2000 m. Additionally, the maximum value of similarity and minimum value of divergence is between the ranges of 0-500, this reflects that the maximum probability of spatial association of landslide and the influence of distance to the road lies between 0-500 m. On the other hand, the frequency ratio value FR= 4.00 indicates the maximum influence of distance to the river on landslides is 0 to 500 m. But at the same time, there is a decreasing trend in FR values for the classes from 0-2000 m. The result indicates that the influence of road distance has a substantial role in the distance ranges from 0-2000 m.

**Slope aspect:** Moreover, the weights estimated from IF-D represent the maximum value of S=1, and the minimum value D=1 indicates the maximum probability of landslide occurrence for the class flat aspect. Similarly, for the frequency ratio FR, the highest value of FR=1.50, with the highest frequency ratio value representing the highest probability of landslide occurrence for the class flat (-1).

**Lithology:** In the case of IF-D weight values, the maximum value of indicated by southern Karakorum metamorphic, cretaceous sandstone, Permian massive, and quaternary deposits. The support and boundary of the membership and non-membership functions represent the maximum probability of landslide occurrence on these lithological units. In the case of the frequency ratio model, the weight value of (FR= 5.0) corresponds to quaternary deposits

followed by (FR= 3.74) cretaceous sandstone and (FR=2.16) Permian massive rocks. This indicates the highest landslide susceptibility class in these geological rock formations. This is because of the tectonic disturbance and active fault movement of the Klik fault in the upper Hunza Gojal area.

**Stream Power Index (SPI):** The weight derived from intuitionistic fuzzy divergence, indicates that the maximum value of S=1 and minimum value of D=0 is at the class (-5.7 - -1.23). The result showed the maximum probability of landslide and the highest probability of the influence of SPI for this class on landslide occurrence. Similarly, for the frequency ratio weight calculations from statistical analysis, the highest value of frequency ratio (FR=1.57) represents the highest value for the same class (1.2-10.43), indicating the highest probability of landslide occurrences among other classes for SPI classes. **Land cover (LC)** For intuitionistic fuzzy divergence the minimum divergence value and similarity value indicated that the highest probability of landslide is on barren land. The study area is at a high altitude, the area lacks natural forest, and most of the slopes are barren, settlements and irrigated lands lie below the water channels. Therefore, most of the landslides in the study area are due to channel excavation. It is, therefore, the derived values indicate most of the probability of landslides occurring on barren land. Besides the highest weight positive, the weight calculations for the frequency ratio of the highest value (FR=2.96) indicate the maximum landslide susceptibility refers to orchards. The agricultural activities in orchards in hilly areas made the slopes vulnerable and accelerated landslides. On the other hand, the second highest value of FR=1.36 also indicates the maximum probability of landslide susceptibility.

**Topographic Wetness Index (TWI):** Additionally, from the statistical analysis of Frequency ratio weight estimation, the results revealed that the highest frequency ratio value (FR=1.12) with the highest value for the range below >12 indicates the most landslide occurrence for TWI. However, the weight estimation from IF-D showed that the probability of landslide occurrence is below >12 for the TWI factor. The descending trend of similarity and ascending trend in divergence reflect that the influence of TWI decreases with an increase in classes (Table 1).

**Precipitation:** In the case of the intuitionistic fuzzy divergence model, the similarity S=1 and divergence D=0 for the class 18-24 mm of precipitation indicates the maximum probability of landslides occurrence. However, 93% of landslides exist in this class for precipitation. Therefore, based on acquired data and weight values derived from IF-D, the highest probability of landslide and influence of

precipitation is between 18-24mm in the case of precipitation. From frequency weight estimation, the highest value of FR= 2.9 for the class ranges (18-24). The results indicated that the high susceptibility of landslide occurs is in the range of 18-24 (Table 1).

**Validation and Construction of Landslide Index Maps**

The machine learning models are sensitive to data within their desired range. In this research assessment, the dependent factors were expressed as a binary variable, representing landslides and non-landslides. Therefore, the landslide causal factors were normalized to a range of 0 to 1, where 0 indicates non-landslides and 1 indicates landslides. The normalized data of the conditional factors were used as input for the machine learning models. To address the issue of overfitting, the dataset was divided into 70:30 ratios. 70% of the dataset was randomly selected for training the models, while the remaining 30% was used for validating the performance of the models. It's important to note that both negative and positive data were equally considered to generate the landslide susceptibility map.

The machine learning models were implemented and trained using the KERAS Python programming framework.

Once the models were trained and validated, the final outputs were extracted to a GIS environment to validate the landslide susceptibility map. The validation of the susceptibility maps was performed using metrics such as the AUC curve and SCAI values. Finally, the landslide susceptibility indices (LSIs) were reclassified into different susceptibility zones using the ArcGIS 10.2 environment.

**Validation of DMLT Models Using IOU and Loss Curve**

The validation and training data for the deeplabV3+ DMLT model provided insightful results. The IOU (Intersection over Union) and Loss curves were utilized to assess the model's performance. For the training dataset, the IOU curve started at 0.35 and steadily increased, reaching a value of 0.74. Similarly, for the validation data, the IOU curve began at 0.1 and progressively rose to 0.7. These results indicate that the model demonstrates good detection and prediction accuracy. Furthermore, the Loss curve results showed a validation value of approximately 0.25, which is considered ideal and suggests that the model possesses excellent prediction accuracy. See the graphical representation of IOU in Fig. 5.

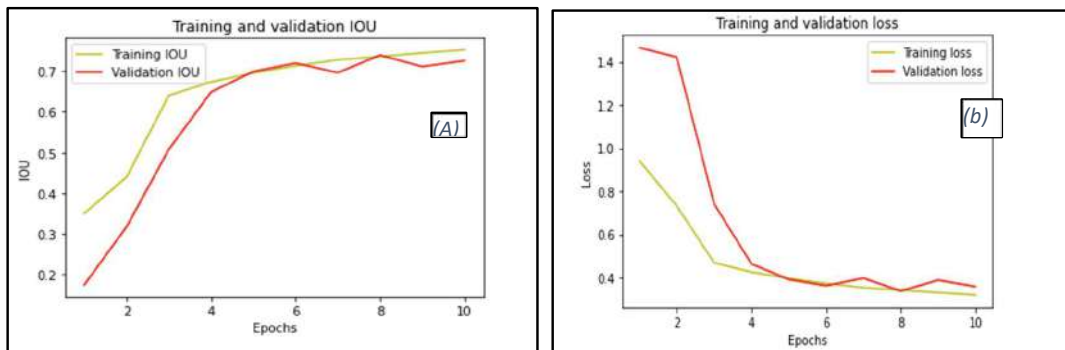


Fig. 5: IOU and loss curve for deeplabV3+, DMLTs. IOU (a), Loss curve (b).

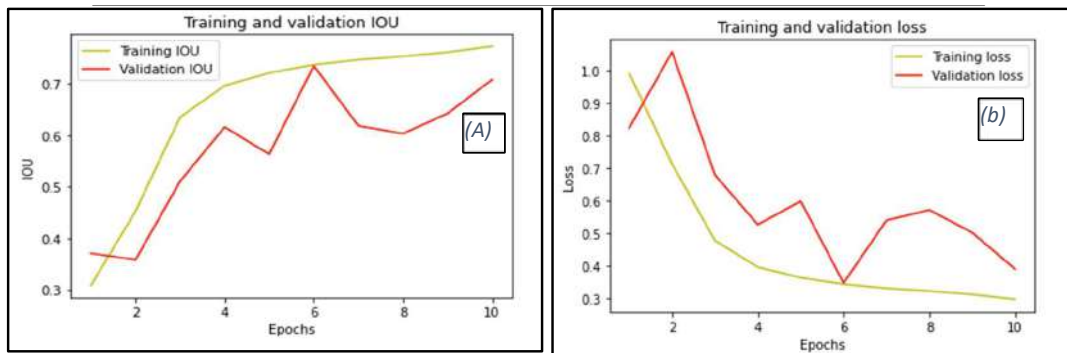


Fig. 6: IOU and Loss curve for U-Net, DMLTs. (a) IOU, (b), Loss curve.

Table 1: Weight estimation of all landslide conditional factors using bi-variate statistical models.

Factor	Classes	(STP) Stable Pixel	(LDP) Landslide Pixel	Intuitionistic Fuzzy Divergence (IF-D)			FR
				Hesitancy	Divergence ( $\wedge$ 1)	Similarity	FR
Slope	0-10	10673912	7963	0.9	0.6	0.4	0.0
	10-20	12222692	13645	0.8	0.5	0.5	0.4
	20-30	16617234	53055	0.6	0.3	0.7	1.1
	30-40	24525672	120091	0.3	0.0	1.0	1.6
	40-50	17540848	61826	0.6	0.3	0.7	1.2
	50-60	7842431	16212	0.9	0.6	0.4	0.7
	>60	2325655	3899	1.0	0.7	0.3	0.6
Aspect	Flat (-1)	810004	4559	1.0	0.0	1.0	1.9
	North (0-22.5)	6402821	28974	0.8	0.1	0.9	1.5
	Northeast (22.5-67.5)	12467219	47337	0.7	0.3	0.7	1.3
	East (67.5-112.5)	11039494	9454	0.8	0.1	0.9	0.3
	southeast (112.5-157.5)	11073594	19762	0.8	0.2	0.8	0.6
	South (157.5-202.5)	11541955	60733	0.7	0.3	0.7	1.7
	Southwest (202.5-247.5)	12256765	52173	0.7	0.3	0.7	1.4
	West (247.5-292.5)	10294776	19912	0.8	0.2	0.8	0.6
	Northwest (292.5-337.5)	10521353	17456	0.8	0.2	0.8	0.6
North (337.5-360)	5340463	16331	0.9	0.0	1.0	1.0	
Elevation	0-1700	6	0	1.0	0.5	0.5	0.0
	1700-2000	290915	6980	1.0	0.5	0.5	8.0
	2000-3000	4426712	135690	0.5	0.0	1.0	10.2
	3000-4000	16380340	131055	0.3	0.1	0.9	2.7
	>4000	70650471	2965	0.2	0.2	0.8	0.0
Curvature	Concave (-1.28- -0.001)	25940251	80636	0.0	0.1	0.9	1.0
	Flat (-0.001- 1.29)	55773965	171292	0.0	0.0	1.0	1.0
	Convex (1.29-88.32)	10034228	24762	0.1	0.3	0.7	0.8
Lithology	southern Karakoram metamorphic	9357596	70470	0.6	0.0	1.0	2.5
	Hunza plutonic unit	6146242	5614	0.9	0.3	0.7	0.3
	Triassic massive limestone	2582095	5946	1.0	0.3	0.7	0.8
	eclogites	10353152	0	0.9	0.3	0.7	0.0
	glacier	35163540	566	0.6	0.0	1.0	0.0
	Permian massive	10934340	71399	0.6	0.1	0.9	2.2
	quaternary deposits	2938134	94377	0.6	0.0	1.0	10.6
	cretaceous sandstone	1881467	21219	0.9	0.3	0.7	3.7
	Misgar slates	10143545	5383	0.9	0.2	0.8	0.2
	Yasin sediments	493283	633	1.0	0.4	0.6	0.4
	Chalt volcanic	884343	0	1.0	0.4	0.6	0.0
	Kohistan batholith	41605	0	1.0	0.4	0.6	0.0
	Northern Karakoram Terrance	435112	0	1.0	0.4	0.6	0.0

Table Cont....

...Cont. Table 1

Factor	Classes	(STP) Stable Pixel	(LDP) Landslide Pixel	Intuitionistic Fuzzy Divergence (IF-D)			FR
				Hesitancy	Divergence ( $\wedge$ 1)	Similarity	FR
Dist_Fault	0-1000	12345198	75160	0.6	0.0	1.0	2.0
	1000-2000	7116810	46309	0.8	0.1	0.9	2.2
	2000-3000	4813319	52215	0.8	0.1	0.9	3.6
	3000-4000	4390897	39129	0.8	0.0	1.0	3.0
	4000-5000	7474161	32764	0.8	0.0	1.0	1.5
	>5000	55608059	31113	0.3	0.5	0.5	0.2
Dist_River	0-200	4911209	38647	0.8	0.0	1.0	2.6
	200-400	4427540	62049	0.7	0.1	0.9	4.6
	400-600	4105746	57210	0.7	0.1	0.9	4.6
	600-800	3963514	45730	0.8	0.0	1.0	3.8
	>800	74340288	73054	-0.1	0.9	0.1	0.3
Dist_Road	0-500	2889524	129326	0.5	0.0	1.0	14.8
	500-1000	2402126	88376	0.7	0.2	0.8	12.2
	1000-1500	2287711	36399	0.8	0.3	0.7	5.3
	1500-2000	2214121	10905	0.9	0.4	0.6	1.6
	>2000	81954962	11684	0.1	0.4	0.6	0.0
SPI	(-5.7 - -1.20)	7395668	22606	0.8	0.0	1.0	1.0
	(-1.20 - 0.37)	31839391	55789	0.5	0.4	0.6	0.6
	(0.37 - 1.20)	38492081	131706	0.1	0.7	0.3	1.1
	(1.20 - 10.43)	14021304	66589	0.6	0.2	0.8	1.6
LC	Natural forest	342085	48	1.0	1.0	0.0	0.0
	Orchards	410062	3678	1.0	1.0	0.0	3.0
	Agriculture land	199084	623	1.0	1.0	0.0	1.0
	Summer Pasture	2399038	2649	1.0	1.0	0.0	0.4
	Winter Pasture	2244705	16382	0.9	0.9	0.1	2.4
	River/Lakes	113378	33	1.0	1.0	0.0	0.1
	Settlements	27535	124	1.0	1.0	0.0	1.5
	Barren land	61298772	253131	-0.6	0.0	1.0	1.4
	Snow/Glacier	24189260	22	0.7	0.7	0.3	0.0
Precipitation	>6	10679048	0	0.9	1.1	-0.1	0.0
	6 - 12	19270617	9081	0.8	1.0	0.0	0.1
	12-18	14131172	29114	0.8	1.0	0.0	0.3
	18 - 24	29012457	565691	-0.3	0.0	1.0	2.9
	24 - 30	10731572	2271	0.9	1.1	-0.1	0.0
	30-36	7153291	0	0.9	1.2	-0.2	0.0
TWI	>12	78961564	267502	-0.8	0.0	1.0	1.1
	12- 24	7237810	3186	0.9	0.9	0.1	0.1
	24- 36	2559283	713	1.0	1.0	0.0	0.1
	36-48	614958	165	1.0	1.0	0.0	0.1
	>48	2374829	5124	1.0	1.0	0.0	0.7

Fig. 5 showcases the validation of the U-Net model using 70% of the training dataset for 10 epochs. The IOU curve displayed an initial value of 0.3, eventually reaching 0.79. Likewise, the IOU value of 0.69 for the 30% validation dataset indicates good prediction accuracy and alignment with the ground truth. Additionally, the Loss curve validation for the U-Net model yielded a value of 0.4, further affirming the model's reliable prediction accuracy. See Fig. 6. Overall, the IOU and Loss curves demonstrate that both the deeplabV3+ and U-Net models exhibit excellent detection and prediction accuracy.

### Validation of DMLT Models Using Confusion Matrix

The confusion matrix is an N\*N matrix that evaluates the classification performance of the ML model. In the confusion matrix, the matrix compares the actual target values with predicted values by machine learning technique for a given set of data. In ML, a good model is with those high true positive and true negative rates. Additionally, in this study, three DML models were also validated based on the scores of the confusion matrix. The results showed that the three ML models have good classification performance in landslide detection for the given data set. See Fig. 7.

### Validation of DMLT Models Using Recall, Precision and F1 Score

Based on the comparative assessment of the three executed models, namely DeeplabV3+ and U-Net, the results indicate favorable performance for classification in the relevant study area. For both the DeeplabV3+ and U-Net models, the precision and recall values were found to be 0.85 and 0.89, respectively. These results suggest that all the models performed well and exhibited good classification abilities.

The F1 score is a crucial evaluation metric used to validate the models' performance. It combines multiple competing metrics to provide an overall assessment of the model's analytical performance. In machine learning, an F1 score of 1 represents a perfect score, while a score of 0 signifies model failure. In the case of the three executed DMLTs models, the results revealed that DeeplabV3+ achieved an F1 score of 0.89 and an accuracy of 0.8, while U-Net attained an F1 score of 0.89. These findings indicate that both DMLT models exhibited satisfactory performance based on their F1 scores and accuracy. Overall, the comparative assessment demonstrates that the DeeplabV3+ and U-Net models performed well as classifiers, showcasing their effectiveness in the classification task for the specific study area. See Fig. 8.

### Validation Landslide Susceptibility Index Maps Based on AUROC

According to Fabbri and Chung (2019), validating the performance of a model requires splitting the dataset into separate subsets. In this study, particularly the dataset was divided into two sets for validation and prediction of susceptibility maps. However, no specific criteria were applied for the selection of the splitting datasets (Pradhan 2013). The dataset was divided into a 30:70 ratio, where 30% of the dataset was used for validation and 70% for model building, also known as the training dataset. This validation method has been commonly employed in previous studies (Suzen & Doyuran 2004, Zhang et al. 2019).

The area under the ROC curve (AUC) values are utilized to assess the accuracy, often referred to as the "prediction rate," of the models. The AUC value ranges from 0.5, indicating random prediction represented by the diagonal reference line, to 1, representing perfect prediction (Huang

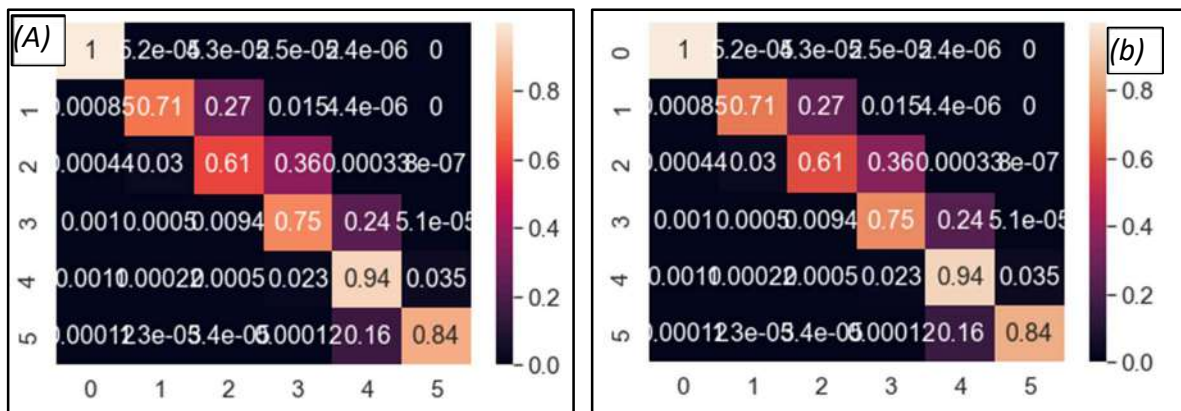


Fig. 7: Confusion matrix, deeplabV3+ (A) and U-Net (B).



(a)	precision	recall	f1-score	support
0	1.00	1.00	1.00	27461588
1	0.96	0.71	0.82	3837326
2	0.67	0.61	0.64	3760218
3	0.82	0.75	0.78	9709555
4	0.77	0.94	0.84	9895272
5	0.89	0.84	0.86	3218665
accuracy			0.89	57882624
macro avg	0.85	0.81	0.82	57882624
weighted avg	0.90	0.89	0.89	57882624

(b)	precision	recall	f1-score	support
0	1.00	1.00	1.00	27461588
1	0.96	0.71	0.82	3837326
2	0.67	0.61	0.64	3760218
3	0.82	0.75	0.78	9709555
4	0.77	0.94	0.84	9895272
5	0.89	0.84	0.86	3218665
accuracy			0.89	57882624
macro avg	0.85	0.81	0.82	57882624
weighted avg	0.90	0.89	0.89	57882624

Fig. 8: Precision, recall and F1 scores for DeeplabV3+ (a), U-Net (b).

2012). An AUC value of 1 signifies a perfect model, while a value of 0.5 indicates incorrect models (Tien Bui et al. 2016). Overall, splitting the dataset for validation and utilizing the AUC values provide a means to evaluate the accuracy and performance of the models, as mentioned by Fabbri and Chung (2019) and supported by previous studies (Suzen & Doyuran, 2004, Zhang et al. 2019).

The ROC curve indicates the correlation between “Sensitivity and “Specificity, which are as follows:

$$\text{Sensitivity} = \frac{TP}{TP+F} \quad \dots(7)$$

$$\text{Specificity} = \frac{TN}{FP+TN} \quad \dots(8)$$

TP is a true positive rate, FN is a false-negative rate, TN is a true negative rate, and FP is a false positive rate.

For the training and validation of LSI for statistical models. The results indicated the success rate cure for FR was 81% and IF-D 81%. The result revealed from the prediction

rate curve for FR 77% and IF-D 77%. The prediction accuracy for the three statistical models is satisfactory to estimate the newly proposed model IF-D performed well whose prediction accuracy is equal to FR. This concludes that the newly proposed model fits the landslide susceptibility mapping for the pertinent study area. See the graphical representation of the prediction and success rate cure in Fig. 9.

### Validation of Landslide Index Maps Based on Seed Cell Area Index (SCAI)

The Seed cell area index (SCAI) (Suzen & Doyuran 2004) was used to estimate the differences between the divided zones for LSM models. In this study, SCAI was applied to evaluate the classification capabilities of four LSM models more precisely and also to identify the differences between the divided zones of LSM models. The best classifier could make large differences between the divided zones. Likewise, the lower difference between the divided zones indicates the

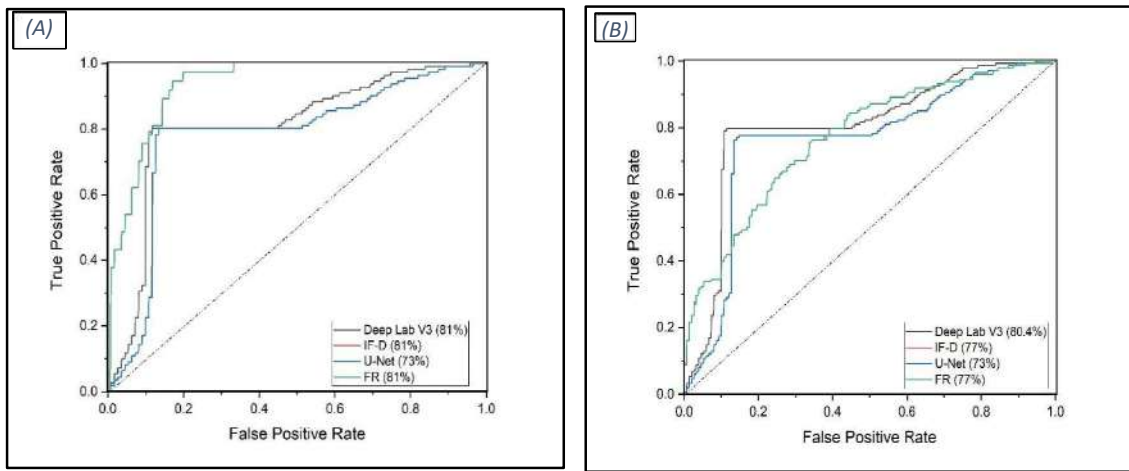


Fig. 9: Training and Validation of landslide susceptibility index maps based on AUROC. (a) Success Rate Curve (SRC) and (b) Prediction Rate Cure (PRC).

low classification capability of LSM. The landslide grid cell is called the “Seed cell,” and the SCAI can be calculated using the following equation (Tang et al. 2021).

$$SCAI = \frac{\% Area}{\% seed} \quad \dots(9)$$

Where  $\%_{area}$  indicates the percentage of grid cells in each susceptibility class to total grid cells in the whole area, while  $\%_{seed}$  indicates the percentage of landslide grid cells in each susceptibility class to grid cells of all landslides. The values of SCAI represent the proneness of landslide. The higher value of SCAI shows the low-proneness of the landslide, while the low value of SCAI indicates the high proneness of the landslide. Similarly, the Differential value (D-value) represents the difference in SCAI for each susceptibility zone. The higher difference in D-value is the low proneness of the landslide, and the lower difference in D-value, the higher proneness of landslide probability. The higher value of SCAI shows the low-proneness of the landslide, while the low value of SCAI indicates a high proneness of the landslide.

Additionally, the difference in SCAI indicated by D-Value between low and very high for DeeplabV3<sup>+</sup> is 672, U-Net 7.34, IF-D 7.6, and FR 9.1. The result indicates deeplabV3<sup>+</sup> D=6.7 showed that the model has the highest accuracy of classification capability among the other three models. See Table 2.

## DISCUSSION

In general, the evaluation of landslide occurrences involves

analyzing past landslide events caused by predisposing factors, which serves as a guideline for predicting future landslides. This connection between landslide occurrence and the underlying conditional factors can be identified. In this regard, intuitionistic fuzzy divergence provides a means to assess the relationship and membership among factor classes. The models also offer insights into the influence of conditional factors on landslide occurrences through similarity and divergence values. The present study aimed to assess landslide susceptibility models (LSMs) and weight estimation using Intuitionistic Fuzzy Divergence (IF-D) in comparison with Frequency Ratio (FR). The susceptibility maps generated were based on a pixel-based analysis of twelve landslide conditional factors that contribute to the level of landslide susceptibility. Moreover, the weights assigned to each geo-environmental factor for each class were objectively determined through a precise mathematical solution using intuitionistic fuzzy divergence, and these weights were compared to those derived from the frequency ratio model.

Moreover, this study evaluates the performance of two statistical models (FR and IF-D) and two deep machine learning models (U-Net and DeeplabV3<sup>+</sup>) for landslide susceptibility mapping (LSM) in the Hunza watershed basin of Northern Pakistan. The utilization of remote sensing, GIS, and Karas Python programming proved beneficial in developing a spatial database for susceptibility analysis. This research contributes to understanding the spatial contribution of landslide factors and predicting landslide susceptibility values for specific geographic locations. Previous studies

Table 2: Results of Seed Cell Area Index (SCAI) for all four statistical LSM models.

LSM Models	Class	Total no of Pixel	% Area	No Landslide Pixels	Seed %	SCAI	D-Value
U-Net	Very high	45961427	50.1	199003	71.9	0.7	
	High	26921671	29.4	63016	22.8	1.3	0.6
	Moderate	10268183	11.2	11467	4.1	2.7	1.4
	Low	8527751	9.3	3202	1.2	8.0	5.3
DeepLabV3 <sup>+</sup>	Very high	40185752	43.8	201751	72.9	0.6	
	High	29521577	32.2	61660	22.3	1.4	0.8
	Moderate	10902779	11.9	10095	3.6	3.3	1.8
	Low	11137190	12.1	3156	1.1	8.0	5.0
IF-D	Very high	16447576	18.4	124273	44.9	0.4	
	High	62105787	69.4	147914	53.5	1.3	0.9
	Moderate	10890117	12.2	4502	1.6	7.5	6.2
	Low	34356	0.0	1	0.0	8.0	0.5
FR	Very high	16447576	18.4	124273	44.9	0.4	
	High	62105787	69.4	147914	53.5	1.3	0.9
	Moderate	10890117	12.2	4502	1.6	7.5	6.2
	Low	34356	0.0	1	0.0	9.5	2.0

have indicated that slopes with degrees between 30 and 50 are more prone to landslides in the region, while slopes greater than 50 degrees have a lower influence on landslide susceptibility (Bacha et al. 2018). The findings of this research align with these previous studies, particularly with the slope of the study area.

Furthermore, regarding the slope gradient, the weights derived from IF-D (with minimum  $D=0$ ,  $S=1$ ) and the maximum value of FR (1.62) indicate a higher probability of a spatial relationship between landslide occurrence and slopes ranging from 30–40 degrees. Similarly, for continuous data such as elevations, the results show that the maximum value of FR (10.16),  $S=1$ , and  $D=0$  correspond to the class of elevations between 2000–3000 m, suggesting a spatial relationship with landslide occurrences. However, in the case of the influence of the river, the study reveals that the distance to the river does not perform well when using FR as a measure. It is evident that as the distance to the river decreases, the influence of the river on landslide occurrences increases. In the case of FR, the weight values follow an ascending order, indicating imprecise estimation. On the other hand, the weight values derived from IF-D provide a more accurate estimation of the influence of distance from the river on landslide occurrences. Specifically, for distances between 0–200 m, the divergence values exhibit an ascending order with  $D=0$ . See Table 2.

Faults play a significant role as conditional factors for landslides. In the study area, regional faults to the south and the local fault system to the north are the dominant factors contributing to landslide occurrences. The landslide inventory map of the study area confirms that most landslide clusters are concentrated in the northern and southern parts. The weight derived from the statistical analysis of IF-D indicates that most landslides occur within a circumference of 0–1000 m from the faults. The analysis also reveals that proximity to roads is a significant factor in destabilizing slope stability. Areas within a radius of 0–500 m from roads are more susceptible to landslides. Blasting for construction purposes has weakened slopes and made them vulnerable to landslides. In the construction of the Karakoram Highway, extensive blasting activities have contributed to slope instability in the region.

Furthermore, the weight values derived from FR do not precisely indicate the effect of faults on landslide occurrences. The valley in the study area predominantly follows an east-west direction, with slopes dipping towards the south and north. This topographical characteristic results in less natural vegetation, rendering the slopes more vulnerable to landslides. The slope aspect categories—Flat ( $FR=1.9$ ,  $D=0.0$ ), North ( $FR=1.5$ ,  $D=0.1$ ), and South

( $FR=1.7$ ,  $D=0.3$ )—exhibit the highest probability of landslide occurrences in this terrain. Regarding categorical data such as geology, the weight values suggest that certain lithological units have a higher probability of landslide occurrence. The southern Karakoram metamorphic unit ( $FR=2.5$ ,  $D=0.02$ ), quaternary deposits ( $FR=10.6$ ,  $D=0.00$ ), Permian massive ( $FR=2.2$ ,  $D=0.07$ ), and cretaceous sandstone ( $FR=3.5$ ,  $D=0.2$ ) show the highest likelihood of landslides. These lithological units in the northern and southern parts of the study area are highly influenced by two major regional faults present in the north and south. Man-made activities play a crucial role in destabilizing slopes in the study area, as indicated by the maximum FR value of 3.0 for orchards,  $FR=2.4$ ,  $D=0$  for winter pastures, and  $FR=1.4$ ,  $D=0$  for barren land. These activities have altered the natural landscape, contributing to increased landslide susceptibility.

Deep machine learning techniques (DMLTs) have gained significant popularity in the scientific community for modeling various environmental phenomena, as they enable the exploration of complex relationships. In the context of landslide susceptibility analysis, several machine-learning techniques have been employed. In this study, the DeeplabV3<sup>+</sup> and U-Net models were utilized to assess landslide susceptibility in the Hunza watershed basin. The LSMs for the study area were developed using Python programming in the KARAS software environment and subsequently exported to GIS for final mapping. To address the issue of overfitting, a sampling ratio of 70% for training the model and 30% for validation was employed. The data was partitioned into 126/256 patches, and the model was trained for 10 epochs.

To comprehensively evaluate the training and validation of DMLT models, a wide range of state-of-the-art deep machine learning techniques were employed, utilizing accuracy statistics. Validation of the prediction map is crucial for assessing the implications of the results in landslide prediction modeling. Various validation tests, including the F1 score, IOU curve, and ACC score, were performed to validate the deep machine learning models (DMLTs). The validation results for IOU (0.74, 0.69) and the loss curve for DeeplabV3<sup>+</sup> and U-Net (0.25, 0.1) indicate excellent prediction accuracy for this study. Similarly, the precision and recall values (0.85, 0.89) for DeeplabV3<sup>+</sup> and U-Net suggest that both models are effective classifiers and demonstrate strong classification ability for the study area. After training and validating the models, landslide susceptibility maps were generated using DeepLabV3<sup>+</sup> and U-Net. These maps were categorized into distinct susceptibility classes, namely very high, high, medium, and low, within the GIS 10.2 environment. Furthermore, to produce LSMs

using IF-D and FR, parameter scores and FR values were combined from the respective parameter maps. These values were then aggregated from twelve scaled parameters within the ArcGIS 10.2 environment to obtain a landslide susceptibility map. The resulting LSI map from IF-D and FR was subsequently classified into four susceptibility zones Fig. 10.

To assess the goodness of fit and prediction accuracy of LSMs, this research utilized the AUC curve and Seed Cell Area Index (SCAI). The AUC curve was employed to generate the Success Rate Curve (SCR) and Prediction Rate Curve (PCR) using the training and validation datasets. Verification and testing of the LSMs' accuracy are crucial aspects that need to be addressed. In this study, we applied the Receiver Operating Characteristic (ROC) curve and calculated the Area Under the Curve (AUC). This validation method has been widely used in previous studies (Suzen & Doyuran, 2004, X. Zhang et al. 2019).

For the Prediction Rate Curve (PRC) obtained from the validation dataset, the AUC values were determined as 80.8% for IF-D, 80.8% for FR, 81% for DeeplabV3+, and 77.8% for U-Net (refer to Fig. 9). To assess the classification ability of the models, the Seed Cell Area Index (SCAI) test was employed. See Table 2. The results indicated that the SCAI D-value was 7.3 for U-Net, 10 for DeeplabV3+, 7.0 for IF-D, and 9.1 for FR.

Furthermore, the accuracy statistics revealed that the IF-D model exhibited 44.9% of landslides in the very high susceptibility zone and 53.5% in the high susceptibility class. Similarly, the percentage area of landslides was 44.8% for the very high susceptibility class and 53% for the high susceptibility class. Table 2.

## CONCLUSIONS

Landslide susceptibility mapping plays a crucial role in reducing the risk of disasters in landslide-prone areas.

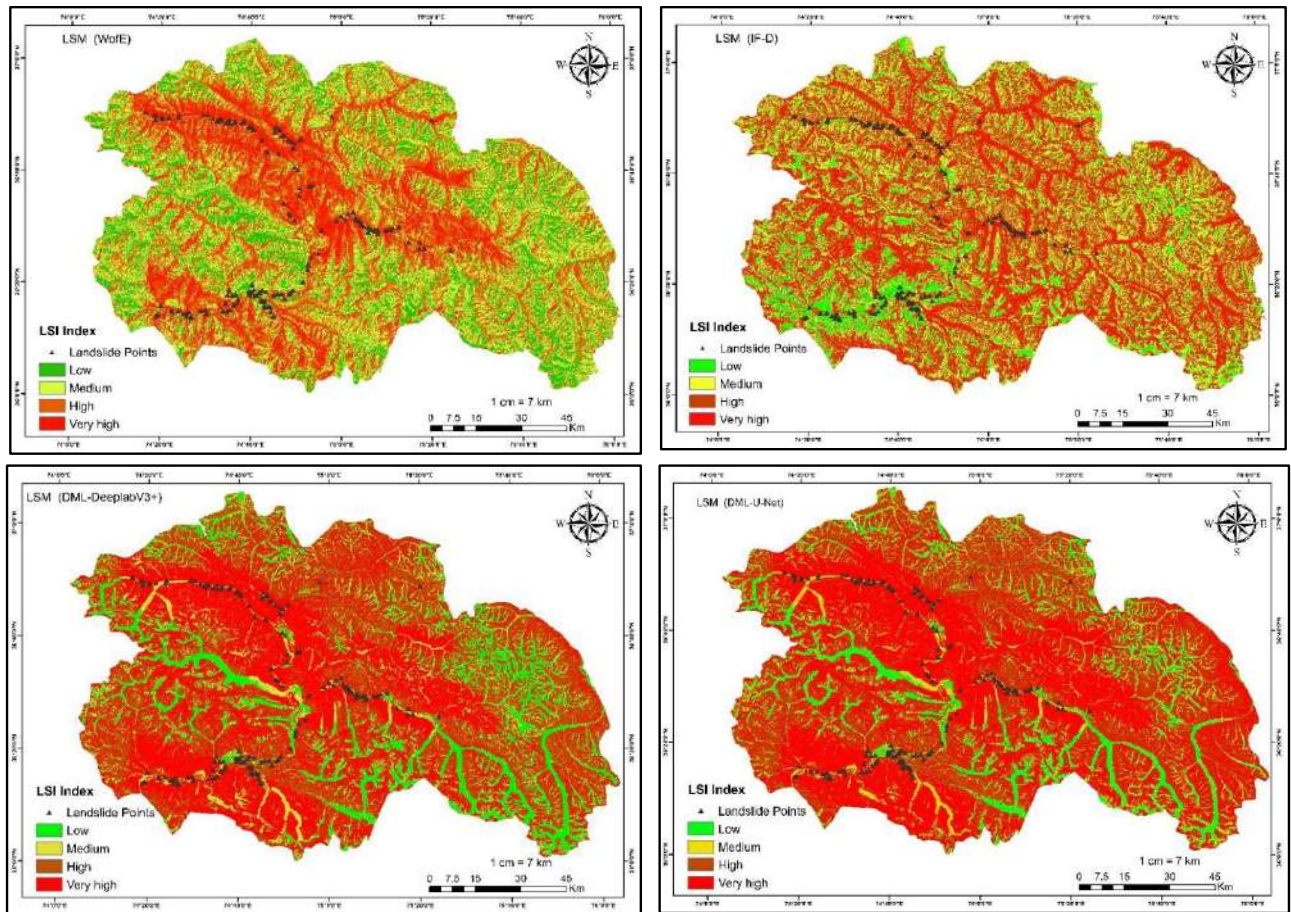


Fig. 10: Landslide susceptibility maps (LSMs) using static techniques (IF-D & FR) and Deep Machine Learning models (DeeplabV3+ & U-Net). Final susceptibility maps classified into four susceptibility zones.

This study focused on the Hunza watershed basin in northern Pakistan, which experiences frequent rockslides and landslides as geological phenomena. The occurrence of landslides is directly influenced by various conditional factors, and each factor class contributes differently to the modeling and mapping of the area. To assess the significance of each factor class in landslide occurrences, a proposed model and FR model were utilized. In terms of weight estimation for each conditional factor, the proposed model demonstrated greater reliability in identifying the spatial relationship of the conditional factors.

Two advanced deep machine learning techniques, DeeplabV3<sup>+</sup> and U-Net, along with two bi-variate statistical models, IF-D and FR, were executed to assess and map landslide susceptibility in the study area. The performance of these models was compared based on prediction accuracy, accuracy statistics, and SCAI. DeeplabV3<sup>+</sup> demonstrated a prediction accuracy of 80% and an SCAI of 7.6 D-value, making it the recommended choice for landslide susceptibility mapping in the study area.

## REFERENCES

- Abbaszadeh Shahri, A., Spross, J., Johansson, F. and Larsson, S., 2019. Landslide susceptibility hazard map in southwest Sweden using artificial neural network. *CATENA*, 183, p.4225. <https://doi.org/10.1016/j.catena.2019.104225>.
- Abedi Gheshlaghi, H. and Feizizadeh, B., 2017. An integrated approach of analytical network process and fuzzy-based spatial decision-making systems applied to landslide risk mapping. *Journal of African Earth Sciences*, 133, pp.15–24. <https://doi.org/10.1016/j.jafrearsci.2017.05.007>.
- Ahmed, M.F., Ali, M.Z., Rogers, J.D. and Khan, M.S., 2019. A study of knick point surveys and their likely association with landslides along the Hunza River longitudinal profile. *Environmental Earth Sciences*, 78(5), p. 176. <https://doi.org/10.1007/s12665-019-8178-3>.
- Al-Najjar, H.A.H. and Pradhan, B., 2021. Spatial landslide susceptibility assessment using machine learning techniques assisted by additional data created with generative adversarial networks. *Geoscience Frontiers*, 12(2), pp. 625–637. <https://doi.org/10.1016/j.gsf.2020.09.002>.
- Atanassov, K., 1986. Intuitionistic fuzzy sets. *Fuzzy Sets and Systems*, 20, pp. 87–96.
- Bera, S., Guru, B. and V. R., 2019. Evaluation of landslide susceptibility models: A comparative study on the part of Western Ghat Region, India. *Remote Sensing Applications: Society and Environment*, 13, pp.39–52. <https://doi.org/10.1016/j.rsae.2018.10.010>.
- Bopche, L. and Rege, P.P., 2022. Landslide susceptibility mapping: An integrated approach using geographic information value, remote sensing, and weight of evidence method. *Geotechnical and Geological Engineering*, 40(6), pp. 2935–2947. <https://doi.org/10.1007/s10706-022-02070-4>.
- Brown, D., 1992. Ohmeda archive1 patient information management system—an operating room-based database analysis network. In: Ikeda, K., Doi, M., Kazama, T., Sato, K. and Oyama, T. (eds.), *Computing and Monitoring in Anesthesia and Intensive Care*, Springer, pp. 201–202. [https://doi.org/10.1007/978-4-431-68201-1\\_56](https://doi.org/10.1007/978-4-431-68201-1_56).
- Chang, Z., Du, Z., Zhang, F., Huang, F., Chen, J., Li, W. and Guo, Z., 2020. Landslide susceptibility prediction based on remote sensing images and GIS: Comparisons of supervised and unsupervised machine learning models. *Remote Sensing*, 12(3), p. 3. <https://doi.org/10.3390/rs12030502>.
- Chen, W., Zhao, X., Shahabi, H., Shirzadi, A., Khosravi, K., Chai, H., Zhang, S., Zhang, L., Ma, J., Chen, Y., Wang, X., Bin Ahmad, B. and Li, R., 2019. Spatial prediction of landslide susceptibility by combining evidential belief function, logistic regression, and logistic model tree. *Geocarto International*, 34(11), pp. 1177–1201. <https://doi.org/10.1080/10106049.2019.1588393>.
- Dahal, R.K., Hasegawa, S., Nonomura, A., Yamanaka, M., Dhakal, S. and Paudyal, P., 2008. Predictive modeling of rainfall-induced landslide hazard in the Lesser Himalayas of Nepal based on weights-of-evidence. *Geomorphology*, 102(3), pp. 496–510. <https://doi.org/10.1016/j.geomorph.2008.05.041>.
- deLugt, J.S. and Cruden, D.M., 1990. The world landslide inventory. *Infrastructure Management, Transportation Public Safety, Land Records Modernization, Natural Resource Management*, 64, pp. 112–124.
- Derbyshire, E., 2001. Geological hazards in loess terrain, with particular reference to the loess regions of China. *Earth-Science Reviews*, 54(1), pp. 231–260. [https://doi.org/10.1016/S0012-8252\(01\)00050-2](https://doi.org/10.1016/S0012-8252(01)00050-2).
- Dou, J., Yunus, A.P., Tien Bui, D., Merghadi, A., Sahana, M., Zhu, Z., Chen, C.-W., Khosravi, K., Yang, Y. and Pham, B.T., 2019. Assessment of advanced random forest and decision tree algorithms for modeling rainfall-induced landslide susceptibility in the Izu-Oshima Volcanic Island, Japan. *Science of The Total Environment*, 662, pp. 332–346. <https://doi.org/10.1016/j.scitotenv.2019.01.221>.
- Fabbri, A.G. and Chung, C.J., 2019. Landslide susceptibility prediction maps: From blind-testing to uncertainty of class membership: A review of past and present developments. In: Pourghasemi, H.R. and Rossi, M. (Eds.), *Natural Hazards GIS-Based Spatial Modeling Using Data Mining Techniques*. Springer International Publishing, pp. 127–144. [https://doi.org/10.1007/978-3-319-73383-8\\_6](https://doi.org/10.1007/978-3-319-73383-8_6).
- Gu, X.B., Ma, Y., Wu, Q.H., Ji, X.J. and Bai, H., 2022. The risk assessment of landslide hazards in Shiwangmiao based on intuitionistic fuzzy sets-TOPSIS model. *Natural Hazards*, 111(1), pp. 283–303. <https://doi.org/10.1007/s11069-021-05053-5>.
- Gu, Z. and He, C., 2021. Application of fuzzy decision tree algorithm based on mobile computing in sports fitness member management. *Wireless Communications and Mobile Computing*, 21, pp. 1–10. <https://doi.org/10.1155/2021/4632722>.
- Guzzetti, F., 2000. Landslide fatalities and the evaluation of landslide risk in Italy. *Engineering Geology*, 58(2), pp.89–107. [https://doi.org/10.1016/S0013-7952\(00\)00047-8](https://doi.org/10.1016/S0013-7952(00)00047-8).
- Hewitt, K., 1998. Catastrophic landslides and their effects on the Upper Indus streams, Karakoram Himalaya, northern Pakistan. *Geomorphology*, 26(1–3), pp. 47–80. [https://doi.org/10.1016/S0169-555X\(98\)00051-8](https://doi.org/10.1016/S0169-555X(98)00051-8).
- Hong, H., Pourghasemi, H.R. and Pourtaghi, Z.S., 2016. Landslide susceptibility assessment in Lianhua County (China): A comparison between a random forest data mining technique and bivariate and multivariate statistical models. *Geomorphology*, 259, pp. 105–118. <https://doi.org/10.1016/j.geomorph.2016.02.012>.
- Huang, R., 2012. Mechanisms of large-scale landslides in China. *Bulletin of Engineering Geology and the Environment*, 71(1), pp. 161–170. <https://doi.org/10.1007/s10064-011-0403-6>.
- Kargel, J.S., Leonard, G., Crippen, R.E., Delaney, K.B., Evans, S.G. and Schneider, J., 2010. Satellite monitoring of Pakistan's rockslide-dammed Lake Gojal. *Eos, Transactions American Geophysical Union*, 91(43), pp. 394–395. <https://doi.org/10.1029/2010EO430002>.
- Karim, S., Jalileddin, S. and Ali, M.T., 2011a. Zoning landslide by use of frequency ratio method (case study: Deylaman Region). *Middle-East Journal of Scientific Research*, 9(5), pp. 578–583.
- Karim, S., Jalileddin, S. and Ali, M.T., 2011b. Zoning landslide by use of frequency ratio method (case study: Deylaman Region). *Middle-East Journal of Scientific Research*, 9(5), pp. 578–583.

- Khan, A., Shitao, Z. and Khan, G., 2022. Comparative analysis and landslide susceptibility mapping of Hunza and Nagar Districts, Pakistan. *Arabian Journal of Geosciences*, 15(21), 1644. <https://doi.org/10.1007/s12517-022-10865-1>.
- Kullback, S. and Leibler, R.A., 1951. On information and sufficiency. *The Annals of Mathematical Statistics*, 22(1), pp. 79–86.
- Lee, S. and Talib, J.A., 2005. Probabilistic landslide susceptibility and factor effect analysis. *Environmental Geology*, 47(7), pp. 982–990. <https://doi.org/10.1007/s00254-005-1228-z>.
- Mandal, S. and Mondal, S., 2019. Frequency ratio (FR) model and modified information value (MIV) model in landslide susceptibility assessment and prediction. In: Mandal, S. and Mondal, S. (Eds.), *Statistical Approaches for Landslide Susceptibility Assessment and Prediction*. Springer International Publishing, pp. 77–105. [https://doi.org/10.1007/978-3-319-93897-4\\_3](https://doi.org/10.1007/978-3-319-93897-4_3).
- Mondal, S. and Mandal, S., 2019. Landslide susceptibility mapping of Darjeeling Himalaya, India using index of entropy (IOE) model. *Applied Geomatics*, 11(2), pp. 129–146. <https://doi.org/10.1007/s12518-018-0248-9>.
- Nohani, M., Moharrami, M., Sharafi, M., Khosravi, K., Pradhan, B., Pham, B.T., Lee, J. and Melesse, A.M., 2019. Landslide susceptibility mapping using different GIS-based bivariate models. *Water*, 11(7), 1402. <https://doi.org/10.3390/w11071402>.
- Panahi, M., Rahmati, O., Rezaie, F., Lee, S., Mohammadi, F. and Conoscenti, C., 2022. Application of the group method of data handling (GMDH) approach for landslide susceptibility zonation using readily available spatial covariates. *CATENA*, 208, 105779. <https://doi.org/10.1016/j.catena.2021.105779>.
- Panchal, S. and Shrivastava, A.K., 2022. Landslide hazard assessment using analytic hierarchy process (AHP): A case study of National Highway 5 in India. *Ain Shams Engineering Journal*, 13(3), p. 101626. <https://doi.org/10.1016/j.asej.2021.10.021>.
- Pandey, V.K., Pourghasemi, H.R. and Sharma, M.C., 2020. Landslide susceptibility mapping using maximum entropy and support vector machine models along the highway corridor, Garhwal Himalaya. *Geocarto International*, 35(2), pp.168–187. <https://doi.org/10.1080/10106049.2018.1510038>.
- Pashkov, B.R. and Shvol'man, V.A., 1979. Rift margins of Tethys in the Pamirs. *Geotectonics*, 13.
- Pourghasemi, H.R., 2008. Landslide hazard assessment using fuzzy logic (Case Study: A part of Haraz Watershed) [Ph.D. Thesis]. Tarbiat Modarres University International Campus, Iran.
- Pourghasemi, H.R., Jirandeh, A.G., Pradhan, B., Xu, C. and Gokceoglu, C., 2013. Landslide susceptibility mapping using support vector machine and GIS at Golestan Province, Iran. *Journal of Earth System Science*, 122(2), pp. 349–369. <https://doi.org/10.1007/s12040-013-0282-2>.
- Pourghasemi, H.R., Mohammady, M. and Pradhan, B., 2012. Landslide susceptibility mapping using an index of entropy and conditional probability models in GIS: Safarood Basin, Iran. *CATENA*, 97, pp. 71–84. <https://doi.org/10.1016/j.catena.2012.05.005>.
- Pradhan, B., 2013. A comparative study on the predictive ability of the decision tree, support vector machine, and neuro-fuzzy models in landslide susceptibility mapping using GIS. *Computers & Geosciences*, 51, pp. 350–365. <https://doi.org/10.1016/j.cageo.2012.08.023>.
- Qin, S.Q., Jiao, J.J. and Wang, S.J., 2001. The predictable time scale of landslides. *Bulletin of Engineering Geology and the Environment*, 59(4), pp. 307–312. <https://doi.org/10.1007/s100640000062>.
- Rao, C.R., 1985. Weighted distributions arising out of methods of ascertainment: What population does a sample represent? In: Atkinson, A.C. and Fienberg, S.E. (Eds.), *A Celebration of Statistics* (pp. 543–569). Springer. [https://doi.org/10.1007/978-1-4613-8560-8\\_24](https://doi.org/10.1007/978-1-4613-8560-8_24).
- Ronneberger, O., Fischer, P. and Brox, T., 2015. U-Net: Convolutional networks for biomedical image segmentation. In: Navab, N., Hornegger, J., Wells, W.M. and Frangi, A.F. (Eds.), *Medical Image Computing and Computer-Assisted Intervention – MICCAI 2015* (pp. 234–241). Springer International Publishing. [https://doi.org/10.1007/978-3-319-24574-4\\_28](https://doi.org/10.1007/978-3-319-24574-4_28).
- Sajadi, P., Sang, Y.-F., Gholamnia, M., Bonafoni, S. and Mukherjee, S., 2022. Evaluation of the landslide susceptibility and its spatial difference in the whole Qinghai-Tibetan Plateau region by five learning algorithms. *Geoscience Letters*, 9(1), 9. <https://doi.org/10.1186/s40562-022-00218-x>.
- Searle, M.P. and Tirrul, R., 1991. Structural and thermal evolution of the Karakoram crust. *Journal of the Geological Society*, 148(1), pp. 65–82. <https://doi.org/10.1144/gsjgs.148.1.0065>.
- Shafique, M., van der Meijde, M. and Khan, M.A., 2016. A review of the 2005 Kashmir earthquake-induced landslides, from a remote sensing perspective. *Journal of Asian Earth Sciences*, 118, pp. 68–80. <https://doi.org/10.1016/j.jseas.2016.01.002>.
- Shan, Y., Chen, S. and Zhong, Q., 2020. Rapid prediction of landslide dam stability using the logistic regression method. *Landslides*, 17(12), pp. 2931–2956. <https://doi.org/10.1007/s10346-020-01414-6>.
- Sun, D., Shi, S., Wen, H., Xu, J., Zhou, X. and Wu, J., 2021. A hybrid optimization method of factor screening predicated on GeoDetector and Random Forest for landslide susceptibility mapping. *Geomorphology*, 379, 107623. <https://doi.org/10.1016/j.geomorph.2021.107623>.
- Suzen, M.L. and Doyuran, V., 2004. Data-driven bivariate landslide susceptibility assessment using geographical information systems: A method and application to Asarsuyu catchment, Turkey. *Engineering Geology*, 71(3), pp. 303–321. [https://doi.org/10.1016/S0013-7952\(03\)00143-1](https://doi.org/10.1016/S0013-7952(03)00143-1).
- Tang, R.X., Yan, E.C., Wen, T., Yin, X.M. and Tang, W., 2021. Comparison of logistic regression, information value, and comprehensive evaluating model for landslide susceptibility mapping. *Sustainability*, 13(7), Article 7. <https://doi.org/10.3390/su13073803>.
- Tien Bui, D., Tuan, T.A., Klempe, H., Pradhan, B. and Revhaug, I., 2016. Spatial prediction models for shallow landslide hazards: A comparative assessment of the efficacy of support vector machines, artificial neural networks, kernel logistic regression, and logistic model tree. *Landslides*, 13(2), pp.361–378. <https://doi.org/10.1007/s10346-015-0557-6>.
- van Westen, C.J., Rengers, N., Terlien, M.T.J. and Soeters, R., 1997. Prediction of the occurrence of slope instability phenomena through GIS-based hazard zonation. *Geologische Rundschau*, 86(2), pp. 404–414. <https://doi.org/10.1007/s005310050149>.
- Verma, R. and Sharma, B.D., 2013. Intuitionistic fuzzy Jensen-Rényi divergence: Applications to multiple-attribute decision making. *Informatica*, 37(4), pp. 276–291.
- Wu, Y., Ke, Y., Chen, Z., Liang, S., Zhao, H. and Hong, H., 2020. Application of alternating decision tree with AdaBoost and bagging ensembles for landslide susceptibility mapping. *CATENA*, 187, 104396. <https://doi.org/10.1016/j.catena.2019.104396>.
- Yan, F., Zhang, Q., Ye, S. and Ren, B., 2019. A novel hybrid approach for landslide susceptibility mapping integrating analytical hierarchy process and normalized frequency ratio methods with the cloud model. *Geomorphology*, 327, pp. 170–187. <https://doi.org/10.1016/j.geomorph.2018.10.024>.
- Youssef, A.M. and Pourghasemi, H.R., 2021. Landslide susceptibility mapping using machine learning algorithms and comparison of their performance at Abha Basin, Asir Region, Saudi Arabia. *Geoscience Frontiers*, 12(2), 639–655. <https://doi.org/10.1016/j.gsf.2020.05.010>.
- Zadeh, L.A., 1965. Fuzzy sets. *Information and Control*, 8(3), 338–353. [https://doi.org/10.1016/S0019-9958\(65\)90241-X](https://doi.org/10.1016/S0019-9958(65)90241-X).
- Zhang, S., Zhang, L.M., Peng, M., Zhang, L.L., Zhao, H.F. and Chen, H.X., 2012. Assessment of risks of loose landslide deposits formed by the 2008 Wenchuan earthquake. *Natural Hazards and Earth System Sciences*, 12(5), 1381–1392. <https://doi.org/10.5194/nhess-12-1381-2012>.

- Zhang, X., Song, J., Peng, J. and Wu, J., 2019. Landslides-oriented urban disaster resilience assessment—A case study in Shenzhen, China. *Science of The Total Environment*, 661, 95–106. <https://doi.org/10.1016/j.scitotenv.2018.12.074>
- Zhang, Z., Zhou, A., Huang, P., Yang, R. and Ma, C., 2021. Using AHP-VW model to evaluate the landslide susceptibility-A case study of Zigui County, Hubei Province, China. *Arabian Journal of Geosciences*, 14(20), 2095. <https://doi.org/10.1007/s12517-021-08476-3>
- Zou, Y. and Xiao, Z., 2008. Data analysis approaches of soft sets under incomplete information. *Knowledge-Based Systems*, 21(8), 941–945. <https://doi.org/10.1016/j.knosys.2008.04.004>

---

**ORCID DETAILS OF THE AUTHORS**

A. Khan: <https://orcid.org/0000-0003-0401-3020>







# Optimization, Characterisation and Evaluation of Biochar Obtained from Biomass of Invasive Weed *Crotalaria burhia*

Loveena Gaur<sup>id</sup> and Poonam Poonia<sup>†id</sup>

Department of Zoology, Jai Narain Vyas University, Jodhpur, Rajasthan, India

<sup>†</sup>Corresponding author: Poonam Poonia; [poonam.poonia@yahoo.com](mailto:poonam.poonia@yahoo.com)

Nat. Env. & Poll. Tech.  
Website: [www.neptjournal.com](http://www.neptjournal.com)

Received: 16-01-2024

Revised: 13-03-2024

Accepted: 22-03-2024

## Key Words:

Biochar  
Invasive weed  
*Crotalaria burhia*  
Response surface methodology  
Biomass

## ABSTRACT

Invasive weed plants are unwanted and hazardous waste biomass; and have extraordinary potential to serve as raw materials for biochar production. To evaluate the potentiality of invasive weed for bioenergy production in the form of biochar, *Crotalaria burhia* was investigated. The response surface modeling and optimization of the biochar parameters were conducted using the experimental design expert 13.0. The optimum value of the desirability function was obtained at a pyrolysis temperature of 450°C and a particle size of 50-100 mm. The model represents a p-value less than 0.0500 and a high F value, which denotes its reliable and accurate prediction of experimental data. A strong correlation was observed between actual and predicted values for biochar composites fixed carbon, carbon, surface area, pore size, and pore volume. In the present study, *C. burhia* biochar production was carried out by slow pyrolysis at 450°C under vacuum conditions. Biochar was found to be alkaline, with a 33.23% yield. Proximate analysis of *C. burhia* revealed 3.35% moisture content, 8.48% volatile matter, 81.24% fixed carbon and 6.94% ash content. The elemental analysis shows major concentrations of carbon, hydrogen, and oxygen as 57.77%, 6.123%, and 27.60%, respectively. Low H/C and O/C molar ratios were quantified as 0.10% and 0.47%, respectively. It possesses a honeycomb structure having mesoporous surface porosity with a surface area of 155.19m<sup>2</sup>/g and the presence of a remarkable concentration of mineral elements calcium and potassium. Biochar rich in hydroxyl, carboxylic, and alkene functional groups enhances its applicability areas. These findings make *C. burhia* a potential feedstock for the production of good-quality biochar.

## INTRODUCTION

Weed plant biomass can be used as a potential source for biochar production. High dry matter, low water, and nutrient requirement, presence of high cellulose content, and ubiquitous nature make weeds very attractive feedstock for biochar production (Priya et al. 2014, Premjet 2018). Thus, the conversion of invasive weed biomass into biochar can be very helpful in the efficient management of weed species and the production of energy-valuable by-products such as biochar (Feng et al. 2021).

Biochar is defined as a porous carbon-rich product obtained from the thermal degradation of biomass, such as wood, agricultural residues, manures, activated sludge, energy crops, etc. Pyrolysis is one of the most common thermochemical processes to convert dry biomass into by-products like biochar, bio-oil, and non-condensable gases (Kambo & Dutta 2015, Sik et al. 2016). In this process, thermal decomposition of organic material is carried out under a limited supply of oxygen and at relatively low temperatures (<700°C) (Lehmann & Joseph 2009). Biochar yield depends on the type and properties

of feedstock and pyrolysis conditions such as temperature, heating rate, pressure, etc. (Song & Guo 2012, Roy & Dias 2017). On the basis of temperature, heating rate, and residence time, pyrolysis is mainly of two types, i.e., fast pyrolysis and slow pyrolysis. The type of pyrolysis is employed according to the requirement of by-product (Tripathi et al. 2016). Fast pyrolysis is carried out for high liquid yield, i.e., bio-oil, whereas slow pyrolysis produces solid char as the main product (Bridgwater 2003). High temperatures yield less biochar due to more volatile production, which in turn generates more gases and liquid (Cheah et al. 2016, Daful & Chandraratne 2020). Slow pyrolysis efficiently yields biochar of about 35.0% from dry biomass weight and is typically operated at the temperature range of 300-550°C, a slow heating rate of 0.1 C/s to 0.8 C/s and a longer residence time of 5-30 min or 25-35 hat atmospheric pressure (Roy & Dias 2017, Tomczyk et al. 2020).

Around 700 species of *C. burhia* are found throughout the tropical and subtropical regions of the world, and about 300 species have been reported in India (Wanjala & Majinda 1999, Lewis 2005). *C. burhia* is an undershrub fibrous plant

of the family Fabaceae. It is most commonly found weed in arid parts of India (Punjab, Rajasthan, and Gujarat), West Pakistan, and Afghanistan. It grows extensively on dunes all over the desert region. Its common name is 'Khimp,' and in Rajasthan, it is locally known as 'Shiniyo' (Kumar et al. 2008). In the present study, a weedy biomass *C. burhia* was used as feedstock to produce biochar through slow and vacuum pyrolysis at 450°C and further characterized and evaluated for determining its application. Under the optimal condition, derived biochar was characterized using proximate analysis, elemental analysis, Brunauer-Emmet-Teller method (BET), Scanning Electron Microscopy (SEM), X-ray Energy Dispersive Spectrometry (EDX), and Fourier Transform Infrared Spectroscopy (FTIR).

## MATERIALS AND METHODS

### Biomass Collection, Preparation and Biochar Production

*C. burhia* was collected from Kasti village of Baori tehsil located in Jodhpur, Rajasthan, India (Fig. 1). The biomass samples were washed with water to remove any contamination and sun-dried for 10 days in an open, clean area. Dry Biomass was chopped to attain a uniform size of 50-100mm. After this, the dried samples were packed, weighed, and further processed for vacuum pyrolysis at the Department of Renewable Energy Engineering, MPUAT, Udaipur, Rajasthan, India (Fig. 2).

A vacuum pyrolyzer is composed of various components such as a biomass cartridge, pyrolysis chamber, vacuum

pump, electric heaters, insulation, condensers (shell and tube type), and vacuum pump. Initially, the chopped dry feedstock was filled into a biomass cartridge. This cartridge was then inserted into a pyrolysis chamber, which is connected to shell and tube-type condensers and a vacuum pump. To achieve the desired temperature for pyrolysis, electric coils are rolled over the pyrolysis chamber (Pawar & Panwar 2022). In vacuum pyrolyzer, biochar was produced at the temperature of 450°C with a residence time of 1 hour and a reduced pressure of 10-12kPa. A carbon-rich solid material, 'biochar,' was collected and weighed after a cooling session of about three hours. Gases and vapors produced during pyrolysis were removed from the pyrolysis chamber by the vacuum pump. Shell and tube-type condensers trapped the gases produced and converted them into liquid oil, i.e., bio-oil. The yield of the biochar has been calculated by using the following formula given by Sadaka et al. (2014)

$$\text{Biochar yield (\%)} = \frac{\text{weight of biochar (gms)}}{\text{weight of biomass (gms)}} \times 100$$

### Characterisation of Biomass and Biochar

For pH analysis, the biochar sample was crushed into powdered form, and the solution was prepared in deionized water in a ratio of 1:10 (biochar: deionized water). The prepared solution was shaken for about one hour and then allowed to stand for 30 min. The pH was measured in Systronics 1010 pH meter after calibrating using buffers of pH 7 and 10. The proximate analysis of raw material and biochar was carried out for moisture content, volatile content, fixed carbon content, and ash content utilizing ASTM 3173-87 method. Carbon,



Fig. 1: *C. burhia* plant in field.



Fig. 2: Dried biomass and biochar of *C. burhia*.

hydrogen, nitrogen, sulfur of feedstock, and biochar were determined by elemental analyzer vario MICRO Cube. The total surface area, pore volume, and pore size of the biochar sample were determined by the BET analyzer Micromeritics, ASAP, 2010. The biochar samples were subjected to high-resolution Field Emission scanning electron microscope (FE-SEM), JEOL JSM 7100F, to study the microstructures of biochar, and some localized elemental compositions such as C, O, Na, Mg, and K were analyzed by EDX. The thermogravimetric analysis of the feedstock was performed on a TG-DTG analyzer (Model: STA 7300, Hitachi, Germany) to find out the mass loss with an increase in carbonized temperature. The infrared spectrum of powdered biochar was recorded on  $8\text{ cm}^{-1}$  resolution by Cary 630 FTIR spectrometer to identify the presence of the functional group.

### Optimization of Biochar Preparation Conditions by Response Surface Methodology (RSM)

To obtain the best quality of *C. burhia* biochar, RSM, a multivariate statistical technique, was used to optimize the preparation parameters and their responses. One of the frequently used RSM techniques is the central composite design (CCD). CCD was used to optimize the preparation conditions using feedstock particle size and pyrolytic temperature as independent variables and fixed carbon, carbon, surface area, pore size, and pore volume as responses. In the present application of RSM, -1 denotes less than 50 mm particle size, 0 denotes 50 to 100 mm particle size, and +1 denotes more than 100 mm particle size. In this design total of 13 runs were found, compared, and tested on the surface response. The Design Expert 13.0 was employed for experimental design, tabulation, and data analysis. For the

evaluation of RSM results, analysis of variance (ANOVA), coefficient of determination ( $R^2$ ), three-dimensional plots, and contour plots were analyzed. The ANOVA finding gives p-value and model F values. To optimize the process variables, the  $R^2$  value, coefficient of variation (CV %), adjusted  $R^2$  value, and predicted  $R^2$  values were analyzed.

## RESULTS AND DISCUSSION

### Yield and pH of Biochar

A high yield of *C. burhia* was found at 33.23%. This is attributed to the slow pyrolysis with vacuum conditions and lignocellulosic herbaceous weedy feedstock with the presence of high inorganic elements (Tomczyk et al. 2020, Carrier et al. 2012). Biochars are mostly alkaline. The pH of *C. burhia* biochar was observed as 10.0. Similar observations of pH have been confirmed by various researchers (Zama et al. 2017) (Table 1). pH of biochar increases with an increase in pyrolysis temperature due to the removal of acidic functional groups and accumulation of alkaline inorganic substances (Yuan et al. 2011, Zhang & Liy 2015). The application of biochar as a fuel or soil fertility or as an adsorbent of organic and inorganic contaminants depends upon the pH of biochar. An increase in pH from 2.0 to 5.0 has been reported for the increase in the adsorption capacity of the metallic cations (Chen et al. 2011). Alkaline pH has been reported for enhanced adsorption of organic contaminants of industrial wastewater (Parshetti et al. 2013) and to correct the acidity of agricultural soil by increasing pH (Daful et al. 2021).

### Proximate and Elemental Analysis

The proximate analysis of biomass and biochar of *C. burhia*

Table 1: pH of various biochars.

Biomass	Pyrolysis temperature [°C]	Residence time [min]	pH	Reference
<i>C. burhia</i>	450	60	10	Present study
Green waste	450	60	10	Ronsse et al. 2013
Buckwheat husk	450	-	9.7	Zama et al. 2017

is shown in Table 2. An increase in pyrolytic temperature increases carbon and ash content, whereas it decreases the volatile content and moisture content of biochar (Zhao et al. 2017, Domingues et al. 2017). In the present study also, thermo-degradation of raw biomass into biochar results in an increase in fixed carbon and ash content by 325.56 % and 92.77%, respectively, and a decrease in moisture content and volatile content by 52.54% and 87.93%, respectively. At higher temperatures, further cracking of volatiles into low molecular weight products like liquids and gases occurs, resulting in low volatile content in biochar (Park et al. 2014, Usman et al. 2015).

The composition of carbon and hydrogen determines the quality and calorific value of biochar. The molar ratios of O/C, H/C, N/C, and S/C decrease with an increase in temperature (Usman et al. 2015, Domingues et al. 2017). Devolatilization of biomass during pyrolysis causes the removal of hydrogen and oxygen over carbon, resulting in carbon-rich biochar (Lehmann & Joseph 2009). In the present study, the carbon content observed is 57.77%, whereas hydrogen, nitrogen, and oxygen contents are 6.123%, 1.52%, and 27.60%, respectively (Table 2). The H/C ratio indicates the degree of aromaticity in biochar (Uchimiya et al. 2010). The O/C molar ratio represents the extent of carbonization and its stability in the environment (Rodriguez et al. 2020). The H/C and O/C ratio were found as 0.10 and 0.47, respectively. Biochar with O/C less than 0.2-0.6 shows moderate stability with a half-life between 100-1000 years (Spokas 2010). Biochar with an H/C ratio less than 0.7 indicates a high degree of aromaticity (i.e., greater fused aromatic ring) in comparison to an H/C ratio greater than 0.7 (IBI 2015). Decreased H/C and O/C ratios in pine needles biochars were reported to be correlated with higher aromaticity and lower polarity (Chen et al. 2008). Thus, obtained biochar possesses good quality properties with an enduring ability in soil for 100-1000 years and could be used for soil fertility enhancement and carbon sequestration.

### BET Analysis

The surface area, pore volume, and pore size of *C. burhia* were observed as 155.19 m<sup>2</sup>.g<sup>-1</sup>, 0.0545 cm<sup>3</sup>.g<sup>-1</sup>, and 2.37 nm, respectively. Surface area increases with temperature due to thermal cracking and the elimination of pore-blocking materials, whereas pore volume increases due

to the gradual degradation of lignin, cellulose, and organic matter, resulting in the creation of channels or tubular structures (Li et al. 2013, Rafiq et al. 2016, Zhao et al. 2017). The release of more volatiles at high temperatures causes an increase in the number of pores (Shaaban et al. 2014). Biochar's surface has been reported to vary from 3 m<sup>2</sup>.g<sup>-1</sup> for rice husk to 500 m<sup>2</sup>.g<sup>-1</sup> for wood (Kan et al. 2016). Surface area and pore volume play a crucial role in adsorption, water holding, and cation exchange capacity in the removal of pollutants from soil and water and soil restoration in agriculture (Weber & Quicker 2018).

### SEM/EDX Analysis

SEM micrographs give a detailed description of the distribution and arrangement of pores present in the biochar (Fig. 3). The observed range of pore diameter of *C. burhia* (2.37nm) lies between 2 to 50 nm. Thus they possess mesoporous structures (Wang et al. 2022). Based on outward appearance, pores resemble honey-comb like structures and are observed as polygonal, uneven, and fibrous due to aggregation of mineral components over the surface. The formation of pores occurs due to de-volatilization during the pyrolysis process (Masto et al. 2013).

Table 2: The proximate and elemental analysis of biomass and biochar of *C. burhia*.

<i>C. burhia</i>	Biomass	Biochar
<b>Proximate analysis</b>		
Moisture content [%]	7.06	3.35
Volatile content [%]	70.26	8.48
Fixed carbon [%]	19.09	81.24
Ash content [%]	3.60	6.94
<b>Elemental analysis</b>		
Carbon	39.59	57.77
Nitrogen	2.25	1.52
Hydrogen	9.942	6.123
Sulfur	0.000	0.067
Oxygen	44.618	27.60
H/C	0.25	0.10
O/C	1.12	0.47
N/C	0.05	0.02
S/C	0.000	0.001

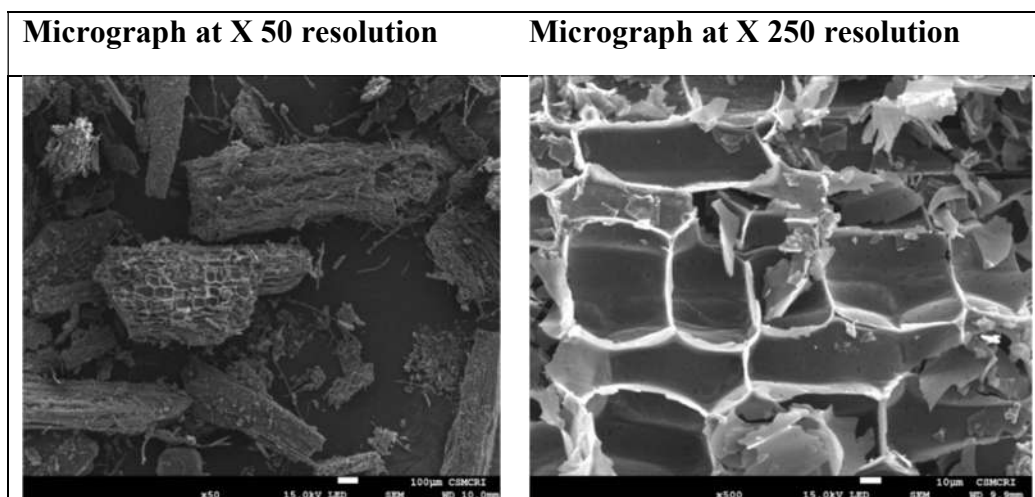


Fig. 3: SEM micrographs of *C. burhia* at different resolutions.

Biochars have profused mineral elements (Jha et al. 2010). Their concentration increases with an increase in temperature and varies with the type of biomass (de la Rosa et al. 2014). EDX indicated carbon (83.87%) and oxygen (13.78%) are major elements of the biochar. Some mineral elements in trace amount, such as Mg (0.35), Si (0.40), Cl (0.14), K (0.52), Ca (0.89), Br (0.05), were also detected (Table 3 and Fig. 4). Magnesium, potassium, and calcium are nutrient elements for plant growth (Qian et al. 2013, Rivka et al. 2017). A decrease in oxygen content indicates an increase in biochar surface hydrophobicity, which is an important factor in the removal of contaminants from an aqueous medium (Shaaban et al. 2014, Sik et al. 2016).

### TG/DTG Analysis

Thermal gravimetry analysis (TGA) and differential thermal gravimetry (DTG) analysis provide a correlation between weight loss and temperature (Fig. 5). The TGA curve represents the thermal stability of biomass (Salavati-niasari

Table 3: Percentage of localized carbon, oxygen, and some minerals contents.

S.No.	Element	Weight [%]	Atomic [%]
1	Carbon (C)	76.74	83.87
2	Oxygen (O)	16.80	13.78
3	Magnesium (Mg)	0.65	0.35
4	Silicon (Si)	0.86	0.40
5	Chloride (Cl)	0.37	0.14
6	Potassium (K)	1.54	0.52
7	Calcium (Ca)	2.71	0.89
8	Bromide (Br)	0.33	0.05

et al. 2010). The thermal decomposition occurs in three zones. The first zone is the drying stage, in which thermal degradation occurs between 30°C - 150°C, with a mass loss of 8.33%. In this stage moisture content of biomass is removed by heating up to a temperature of 150°C (Yang et al. 2007). At a temperature of about <220°C devolatilisation of extractives of biomass takes place. The devolatilization stage is the second zone and is the most active stage of pyrolysis. The mass loss of about 83% occurred between temperatures of 150°C -400°C. In the de-volatilization stage, degradation of hemicellulose, cellulose, and lignin occurs. Hemicellulose degradation is observed at 150°C-270°C followed by degradation of cellulose at temperature range 270°C -400°C. Thermal degradation of lignin starts at 400°C and ends at 580°C, followed by carbonization. According to Yang et al. (2007), thermal degradation of hemicellulose and cellulose takes place in the temperature range of around 220°C-315°C and 315°C-400°C respectively, with maximum mass loss at 270°C and 355°C. Thermal decomposition of lignin occurs in the range from 180°C-900°C with undefined maximum mass loss. The minimum mass loss of 2% was observed in the temperature range from 400°C-900°C. This is referred to as the char formation zone of thermal decomposition, indicating the presence of fixed carbon and non-combustion products (Rout et al. 2016). From the TGA and DTG results, it was found that 200°C-600°C is the suitable temperature for the pyrolysis zone.

### FTIR Analysis

FTIR is informative in the determination of various functional groups on the surface of material produced at different conditions. The FTIR spectrum of *C. burhia* biochar represented in Fig. 6 shows a very weak banding at

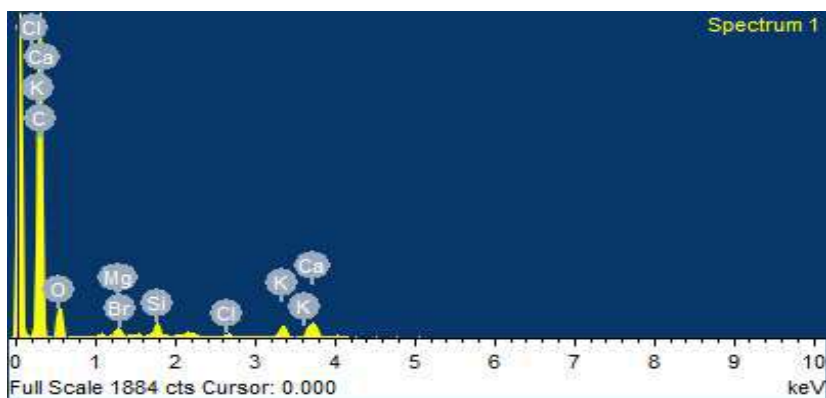
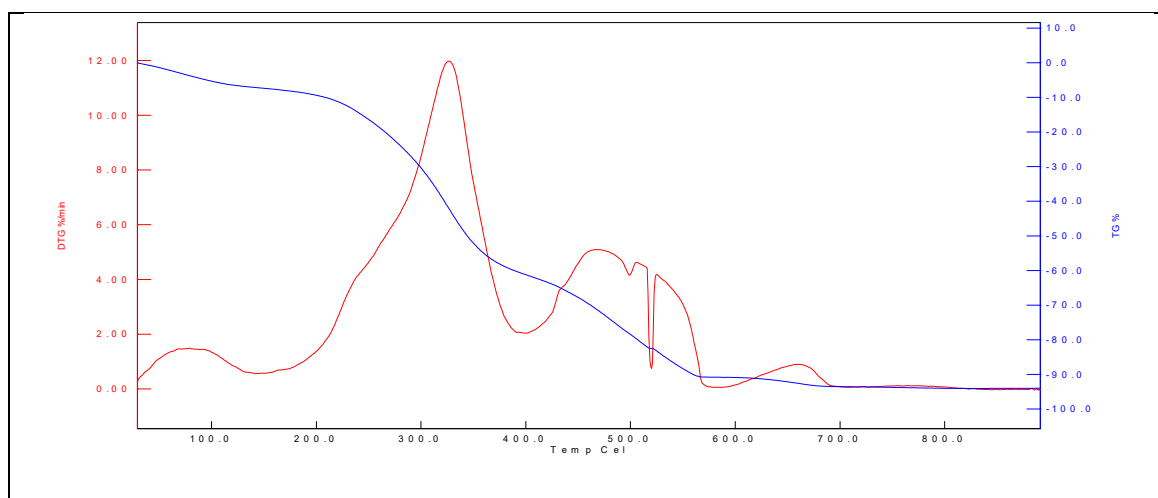


Fig. 4: EDX curves of biochars.

Fig. 5: TG (Thermogravemetric) and DTG (derived thermogravemetric) curve of *C. burhia*.

2877  $\text{cm}^{-1}$ , which represents symmetrical  $-\text{CH}$  stretching of the aliphatic alkane group. This is similar to a study by Ferreira et al. (2013), who found that major peaks at 2920  $\text{cm}^{-1}$  and 2851  $\text{cm}^{-1}$  are mainly attributed to the aliphatic chains of suberin, accounting for asymmetric and symmetric  $-\text{CH}$  stretching vibrations, respectively. Clear peaks representing hemicellulose and cellulose (3200  $\text{cm}^{-1}$  -3000  $\text{cm}^{-1}$  for OH or 3100  $\text{cm}^{-1}$  -3000  $\text{cm}^{-1}$  for CH) show degradation of hemicellulose and cellulose at given pyrolytic temperature (Jouiad et al. 2015). Bending at 2340  $\text{cm}^{-1}$  indicates the presence of  $\text{CO}_2$  (Schott et al. 2021). Between 2000  $\text{cm}^{-1}$ -1500  $\text{cm}^{-1}$ , two peaks are observed at 1798  $\text{cm}^{-1}$  and 1561  $\text{cm}^{-1}$ . The absorption band at 1798  $\text{cm}^{-1}$  represents the  $\text{C}=\text{O}$  stretching of aldehydes and ketones formed due to the degradation of hemicellulose and cellulose, and the peak at 1561  $\text{cm}^{-1}$  denotes plane  $\text{C}=\text{C}$  aromatic vibrations of skeletal compounds in lignin and its extractives (Azargohar et al. 2014, Jouiad et al. 2015). Peaks between a

range of 1400  $\text{cm}^{-1}$  -900  $\text{cm}^{-1}$  represent  $\text{C}=\text{C}$  rings of lignin. Emergences of peaks at 1375  $\text{cm}^{-1}$  and 1021  $\text{cm}^{-1}$  could be attributed to symmetrical and asymmetrical aryl alkyl ethers showing changes in vibration due to the transformation products of cellulose and lignin components of the biomass. These peaks are more pronounced than those for cellulose and hemicellulose, which can be attributed to lignin degradation temperature between 200°C -and 700°C (Cantrell et al. 2012, Azargohar et al. 2014, Jouiad et al. 2015). Between 900  $\text{cm}^{-1}$  -700  $\text{cm}^{-1}$ , peaks are observed at 872  $\text{cm}^{-1}$ , 808  $\text{cm}^{-1}$ , and 745  $\text{cm}^{-1}$ , representing aromatic  $\text{C}-\text{H}$  bending vibration of benzene rings (Xu et al. 2013). The presence of various functional groups, such as hydroxyl, aldehyde, and ketone, provides surface binding of polar contaminants (Inyang et al. 2016). Biochar rich in oxygen contains functional groups such as ether that can be considered for the adsorption of heavy metals like cadmium by ion exchange and surface complexation (Fan et al. 2018). FTIR results



Table 4: ANOVA for quadratic model based on RSM design for various responses of *C. burhia*.

Response	Source	Sum of Squares	Df	Mean Square	F-value	p-value	
Fixed carbon	Model	0.1187	5	0.0237	69.90	< 0.0001	Significant
	A-Temperature	0.0622	1	0.0622	183.15	< 0.0001	
	B-Particle size	0.0065	1	0.0065	19.07	0.0033	
	AB	0.0028	1	0.0028	8.26	0.0239	
	A <sup>2</sup>	0.0432	1	0.0432	127.27	< 0.0001	
	B <sup>2</sup>	0.0004	1	0.0004	1.27	0.2967	
Carbon	Model	0.1445	5	0.0289	113.40	< 0.0001	Significant
	A-Temperature	0.0921	1	0.0921	361.34	< 0.0001	
	B-Particle size	0.0151	1	0.0151	59.19	0.0001	
	AB	0.0053	1	0.0053	20.79	0.0026	
	A <sup>2</sup>	0.0318	1	0.0318	124.92	< 0.0001	
	B <sup>2</sup>	0.0030	1	0.0030	11.86	0.0108	
Surface area	Model	0.0058	5	0.0012	1238.31	< 0.0001	Significant
	A-Temperature	0.0015	1	0.0015	1596.29	< 0.0001	
	B-Particle size	0.0009	1	0.0009	937.94	< 0.0001	
	AB	1.435E-06	1	1.435E-06	1.52	0.2568	
	A <sup>2</sup>	0.0028	1	0.0028	2986.13	< 0.0001	
	B <sup>2</sup>	9.100E-06	1	9.100E-06	9.67	0.0171	
Pore volume	Model	0.0000	5	2.165E-06	21.21	0.0004	Significant
	A-Temperature	1.299E-06	1	1.299E-06	12.72	0.0091	
	B-Particle size	5.168E-06	1	5.168E-06	50.61	0.0002	
	AB	1.489E-07	1	1.489E-07	1.46	0.2664	
	A <sup>2</sup>	3.109E-06	1	3.109E-06	30.45	0.0009	
	B <sup>2</sup>	8.928E-08	1	8.928E-08	0.8744	0.3809	
Pore Size	Model	0.0003	5	0.0001	19.16	0.0006	Significant
	A-Temperature	0.0000	1	0.0000	7.59	0.0283	
	B-Particle size	0.0001	1	0.0001	18.71	0.0035	
	AB	7.635E-07	1	7.635E-07	0.2353	0.6424	
	A <sup>2</sup>	0.0002	1	0.0002	60.47	0.0001	
	B <sup>2</sup>	1.547E-07	1	1.547E-07	0.0477	0.8334	

Table 5: Fit statistics of fixed carbon, carbon, surface area, pore volume and pore size

Responses	Std. Dev.	Mean	C.V.%	R <sup>2</sup>	Adjusted R <sup>2</sup>	Predicted R <sup>2</sup>	Adeq Precision
Fixed carbon	0.0184	8.95	0.2060	0.9804	0.9663	0.8126	25.4881
Carbon	0.0160	9.21	0.1734	0.9878	0.9791	0.8764	33.9242
Surface area	0.0010	9.97	0.0097	0.9989	0.9981	0.9934	110.1255
Pore Volume	0.0003	0.1980	0.1614	0.9381	0.8938	0.6175	16.4706
Pore size	0.0018	2.89	0.0624	0.9319	0.8833	0.7102	14.0979

and pore volume. At ideal temperatures, the bigger surface area and pore volume are desirable for effective adsorption. At 450°C, three distinct *C. burhia* particle sizes were examined. From the overlay optimization plot of the RSM

model, it is deduced that maximum fixed carbon, carbon, surface area, pore volume, and pore size may be found at 462.930°C, which is in good agreement with the outcomes at 450°C.



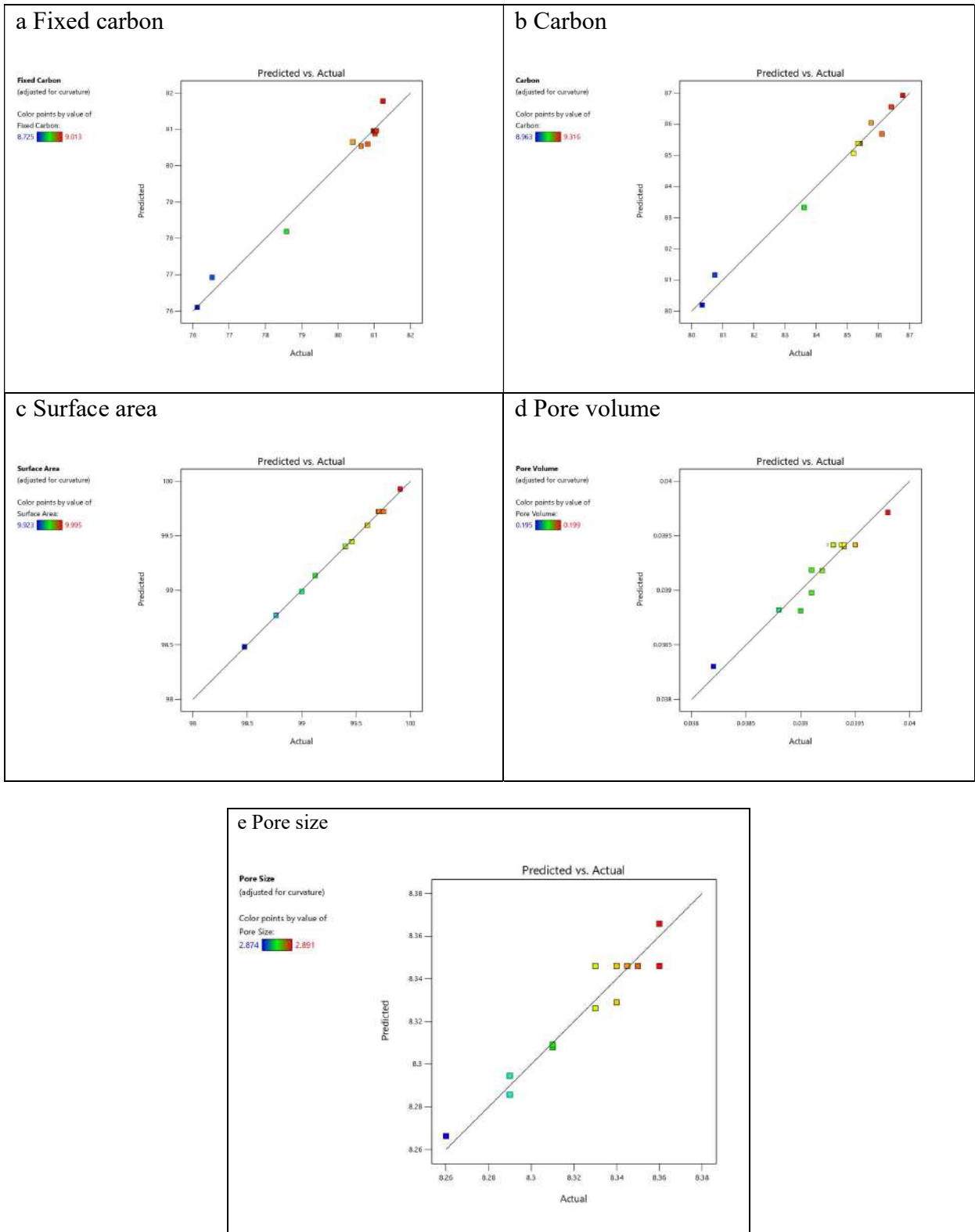


Fig. 7: Predicted vs. actual plots of responses for *C. burhia*.

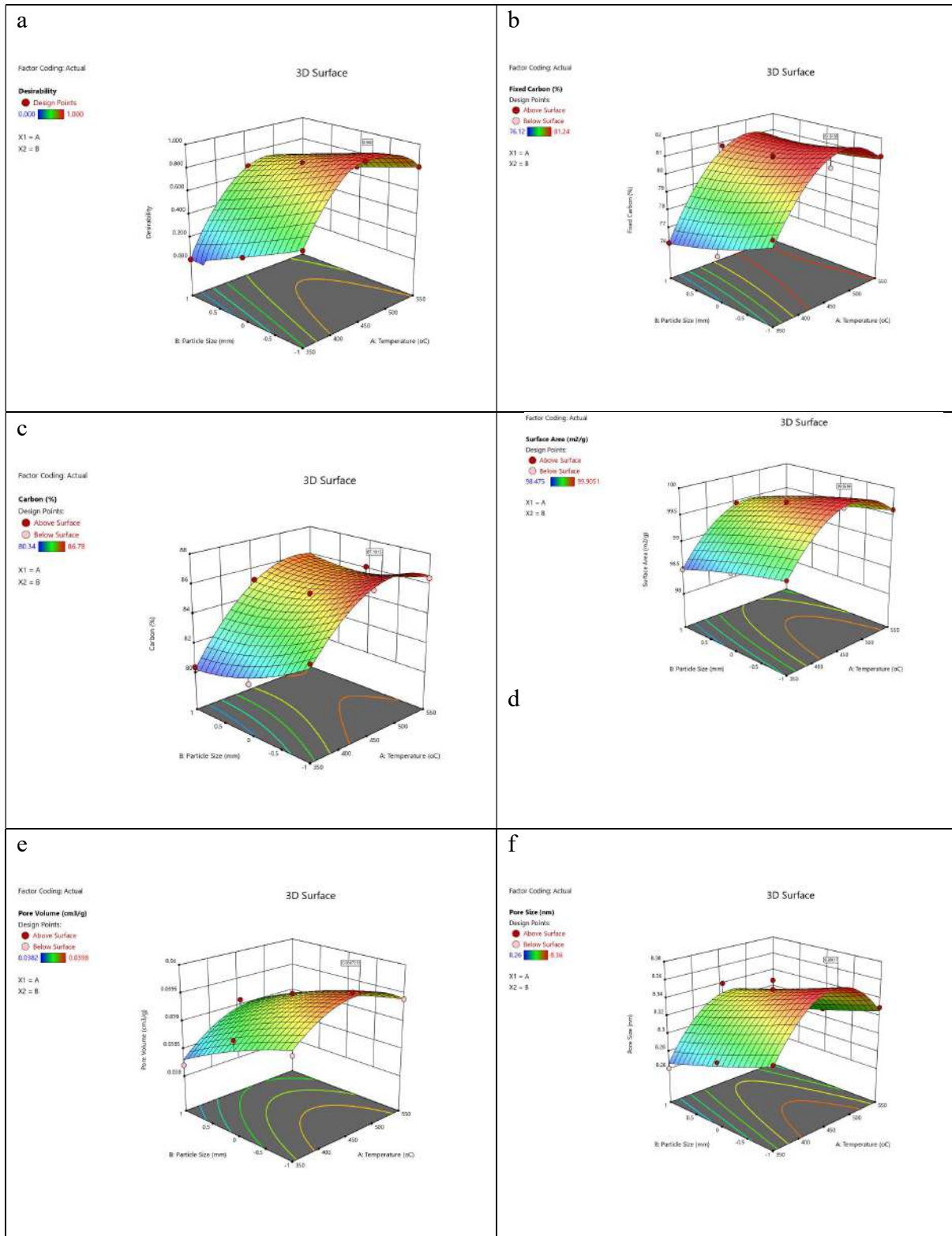


Fig. 8: Three-dimensional response surface plots for desirability, fixed carbon, carbon, surface area, pore volume, and pore size of *C. burhia*.

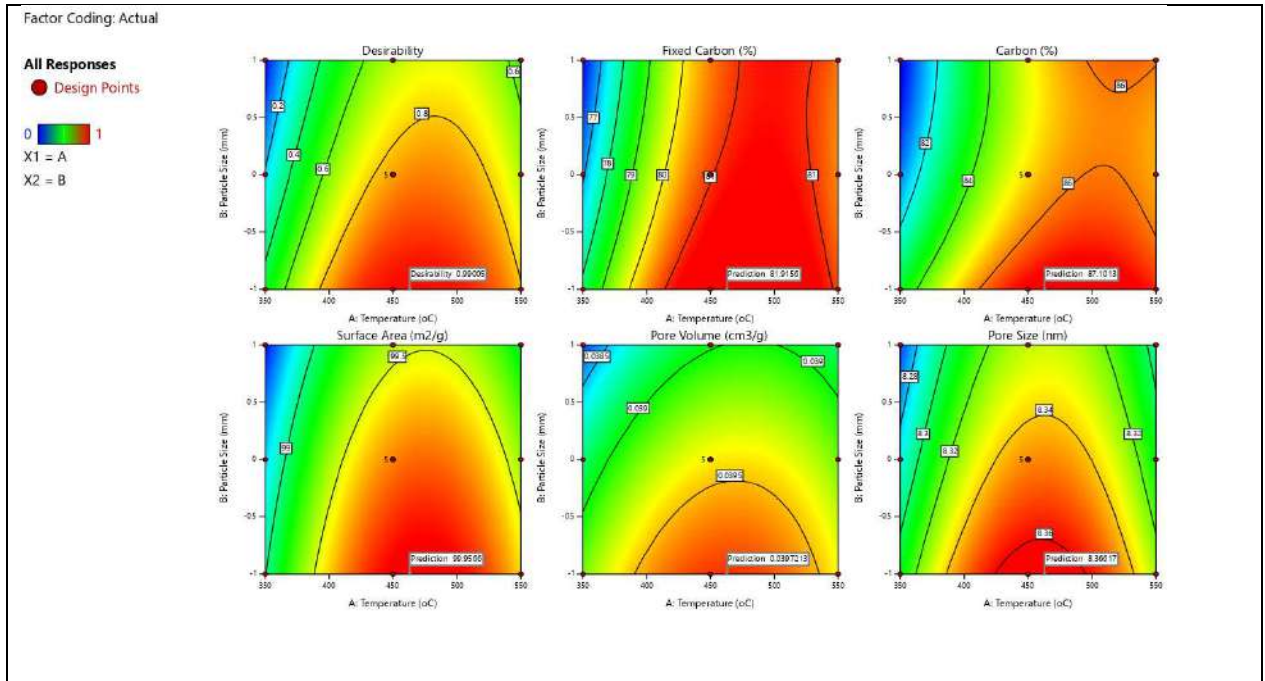


Fig. 9: Contour plots of different responses with particle size and temperature of *C. burhia*.

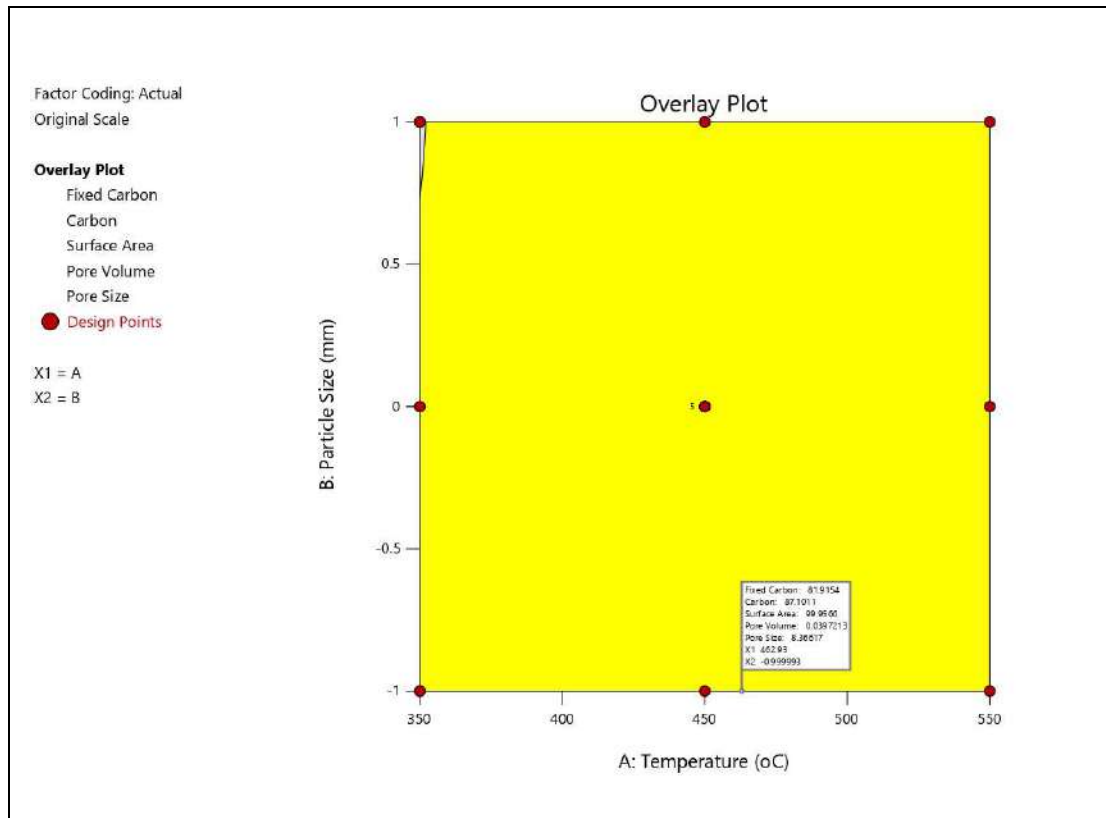


Fig. 10: Overlay plot of *C. burhia*.

## CONCLUSIONS

The invasive weed plant feedstock as a resource for biochar production not only reduces the negative environmental impact but also contributes as a bioenergy source for ecological and economic profits. The findings of this study demonstrate that the invasive weed *C. burhia* is a potential source of raw material for biochar production due to its huge biomass, rapid growth, and easy availability. The present study utilized response surface methodology using CCD for the optimization of preparation conditions to obtain good quality biochar. RSM displayed that pyrolytic temperature and feedstock particle size greatly influence the biochar quality parameters such as fixed carbon, carbon, surface area, pore volume, and pore size. The pyrolytic temperature of 450°C (predicted value-462.90°C) and particle size of 50-100mm have been observed for maximum fixed carbon, carbon, surface area, pore volume, and pore size. The slow pyrolysis, along with vacuum conditions, has proven its potential for the production of good quality biochar with high yield, increased surface area, and enhanced fixed carbon content. A low molar ratio of H/C and O/C indicates that biochar is highly carbonized and hydrophobic in nature. SEM/EDX analysis confirms its porous structure with the presence of meso-pores along with some inorganic elements such as calcium, silicon, magnesium, etc. FTIR analysis reports its richness in hydroxyl and carboxyl functional groups. It is expected that obtained biochar is multifunctional and can contribute to climate mitigation, increase carbon sequestrations, enhance soil fertility, and remediation of organic and inorganic pollutants from soil and water.

## ACKNOWLEDGEMENTS

The authors are very grateful to Dr. N.L. Panwar Head of Department, Renewable Energy Engineering, Maharana Pratap University of Agriculture and Technology (MPUAT), Udaipur, Rajasthan, India for their support and guidance to drive towards quality research and providing necessary laboratory facilities.

## REFERENCES

Azargohar, R., Nanda, S., Kozinski, J., Dalai, A. and Sutarto, R., 2014. Effects of temperature on the physicochemical characteristics of fast pyrolysis bio-chars derived from Canadian waste biomass. *Fuel*, 125, pp.90-100. <http://doi.org/10.1016/j.fuel.2014.01.083>

Bridgwater, A.V., 2003. Renewable fuels and chemicals by thermal processing of biomass. *Journal of Chemical Technology & Biotechnology*, 91(2-3), pp.87-102

Cantrell, B., Hunt, P.G., Uchimiya, M., Novak, J.M. and Ro, K.S., 2012. Impact of pyrolysis temperature and manure source on physic-chemical characteristics of biochar. *Bioresource Technology*, 107, pp.419-428.

Carrier, M., Hardie, A.G., Uras, Ü., Görgens, J. and Knoetze, J., 2012. Production of char from vacuum pyrolysis of South African sugar cane bagasse and its characterization as activated carbon and biochar. *Journal of Analytical and Applied Pyrolysis*, 96, pp.24-32. <https://doi.org/10.1016/j.jaap.2012.02.016>

Cheah, S., Jablonski, W.S., Olstad, J.L., Carpenter, D.L., Barthelemy, K.D., Robichaud, D.J., Andrews, J.C., Black, S.K., Oddo, M.D. and Westover, T.L., 2016. Effects of thermal pretreatment and catalyst on biomass gasification efficiency and syngas composition. *Green Chemistry*, 18, pp.6291-6304

Chen, B., Zhou, D. and Zhu, L., 2008. Transitional adsorption and partition of nonpolar and polar aromatic contaminants by biochars of pine needles with different pyrolytic temperatures. *Environmental Science & Technology*, 42, pp.5137-5143

Chen, X., Chen, G., Chen, L., Chen, Y., Lehmann, J., McBride, M.B. and Hay, A.G., 2011. Adsorption of copper and zinc by biochars produced from pyrolysis of hardwood and corn straw in aqueous solution. *Bioresource Technology*, 102(19), pp.8877-8884

Daful, A.G., Chandraratne, M.R. and Loridon, M., 2021. Recent perspectives in biochar production, characterization and applications. In: Bartoli, M. and Giorelli, M. (eds.) *Recent Perspectives in Pyrolysis Research*. IntechOpen, pp. 327-344.

Daful, A.G. and Chandraratne, M.R., 2020. Biochar production from biomass waste-derived material. In: Hashmi, S., Choudhury, I.A. (eds.). *Encyclopedia of Renewable and Sustainable Materials*. Oxford: Elsevier; pp. 370-378.

De la Rosa, J.M., Paneque, M., Miller, A.Z. and Knicker, H., 2014. Relating physical and chemical properties of four different biochars and their application rates to biomass production of *Lolium perenne* on a Calcic Cambisol during a pot experiment of 79 days. *Science of The Total Environment*, 499, pp.175-184.

Domingues, R.R., Trugilho, P.F., Silva, C.A., de Melo, I.C.N.A., Melo, L.C.A., Magriotis, Z.M. and Sánchez-Monedero, M.A., 2017. Properties of biochar derived from wood and high-nutrient biomasses with the aim of agronomic and environmental benefits. *PLoS ONE*, 12, e0176884.

Fan, S.S., Wang, Y., Li, Y., Wang, Z., Xie, Z.X. and Tang, J., 2018. Removal of tetracycline from aqueous solution by biochar derived from rice straw. *Environmental Science and Pollution Research*, 25(29), pp.29529-29540.

Feng, Q., Wang, B., Chen, M., Wu, P., Lee, X. and Xing, Y., 2021. Invasive plants as potential sustainable feedstocks for biochar production and multiple applications: A review. *Resources, Conservation and Recycling*, 164, 105204.

Ferreira, R., Garcia, H., Sousa, A.F., Freire, C.S.R., Silvestre, A.J.D., Rebelo, L.P.N. and Pereira, C.S., 2013. Isolation of suberin from birch outer bark and cork using ionic liquids: a new source of macromonomers. *Industrial Crops and Products*, 44, pp.520-527. <https://doi.org/10.1016/j.indcrop.2012.10.002>

IBI, 2015. Standardized product definition and product testing guidelines for biochar that is used in soil. *International Biochar Initiative*, Version 2.1.

Inyang, M.I., Gao, B., Yao, Y., Xue, Y., Zimmerman, A., Mosa, A., Pullammanappallil, P., Ok, Y.S. and Cao, X., 2016. A review of biochar as a low-cost adsorbent for aqueous heavy metal removal. *Critical Reviews in Environmental Science and Technology*, 46, pp.406-433.

Jha, P., Neenu, S., Rashmi, I., Meena, B.P., Jatav, R.C., Lakaria, B.L., Biswas, A.K., Singh, M. and Patra, A.K., 2010. Ameliorating effects of Leucaena biochar on soil acidity and exchangeable ions. *Communications in Soil Science and Plant Analysis*, 47(10), pp.1252-1262.

- Jouiad, M., Al-Nofeli, N., Khalifa, N., Benyettou, F. and Yousef, L.F., 2015. Characteristics of slow pyrolysis biochars produced from Rhodes grass and fronds of edible date palm. *Journal of Analytical and Applied Pyrolysis*, 111, pp.183.
- Kambo, H. and Dutta, A., 2015. A comparative review of biochar and hydrochar in terms of production, physico-chemical properties, and applications. *Renewable and Sustainable Energy Reviews*, 45, pp.359–378. <http://doi.org/10.1016/j.rser.2015.01.050>
- Kan, T., Strezov, V. and Evans, T.J., 2016. Lignocellulosic biomass pyrolysis: A review of product properties and effects of pyrolysis parameters. *Renewable and Sustainable Energy Reviews*, 57(C), pp.1126–1140.
- Kumar, S., Praveen, F., Goyal, S. and Chauhan, A., 2008. Indigenous herbal coolants for combating heat stress in the hot Indian Arid Zone. *Indian Journal of Traditional Knowledge*, 7(4), pp.679–682.
- Lehmann, J. and Joseph, S., 2009. *Biochar for Environmental Management: Science and Technology*. Earthscan.
- Lewis, G.P., 2005. *Legumes of the World*. Royal Botanic Gardens Kew.
- Li, X., Shen, Q., Zhang, D., Mei, X., Ran, W., Xu, Y., Yu, G. and Motta, A., 2013. Functional groups determine biochar properties (pH and EC) as studied by two-dimensional <sup>13</sup>C NMR correlation spectroscopy. *PLoS ONE*, 8(6), e65949.
- Masto, L.E., Kumar, S., Rout, T.K., Sarkar, P., George, J. and Ram, L.C., 2013. Biochar from water hyacinth (*Eicchornia crassipes*) and its impact on biological activity. *CATENA*, 111, pp.64–71.
- Park, J., Lee, Y., Ryu, C. and Park, Y.K., 2014. Slow pyrolysis of rice straw: Analysis of product properties, carbon and energy yields. *Bioresource Technology*, 155, pp.63–70. <https://doi.org/10.1016/j.biortech.2013.12.084>
- Parshetti, G.K., Hoekman, S.K. and Balasubramanian, R., 2013. Chemical, structural, and combustion characteristics of carbonaceous products obtained by hydrothermal carbonization of palm empty fruit bunches. *Bioresource Technology*, 135, pp.683–689.
- Pawar, A. and Panwar, N.L., 2022. A comparative study on morphology, composition, kinetics, thermal behavior, and thermodynamic parameters of *Prosopis juliflora* and its biochar derived from vacuum pyrolysis. *Bioresource Technology Reports*, 18, 101053.
- Premjet, S., 2018. *Potential of Weed Biomass for Bioethanol Production in Fuel Ethanol Production from Sugarcane*. Intech Open, pp.83–98.
- Priya, H.R., Veena, A.H., Pavithra, D. and Joythi, A., 2014. Prospects and problems of utilization of weed biomass: A review. *Research & Reviews: Journal of Agricultural and Allied Sciences*, 3, pp.1–11.
- Qian, K., Kumar, A., Patil, K., Bellmer, D., Wang, D., Yuan, W. and Huhnke, R., 2013. Effects of biomass feedstocks and gasification conditions on the physicochemical properties of char. *Energies*, 6(8), pp.3972–3986. <http://doi.org/10.3390/en6083972>
- Rafiq, M.K., Bachmann, R.T., Rafiq, M.T., Shang, Z., Joseph, S. and Long, R., 2016. Influence of pyrolysis temperature on physico-chemical properties of corn stover (*Zea mays* L) biochar and feasibility for carbon capture and energy balance. *PLoS ONE*, 11, e0156894.
- Rivka, B., Laird, D., Thompson, M. and Lawrinenko, M., 2017. Characterization and quantification of biochar alkalinity. *Chemosphere*, 167, pp.367–373. <http://doi.org/10.1016/j.chemosphere.2016.09.151>
- Rodriguez, J.A., Lustosa, J.F., Melo, L.C.A., de Assis, I.R. and de Oliveira, T.S., 2020. Influence of pyrolysis temperature and feedstock on the properties of biochars produced from agricultural and industrial wastes. *Journal of Analytical and Applied Pyrolysis*, 149, 104839.
- Ronsse, F., Dickinson, D., Nachenius, R. and Prins, W., 2013. Biomass pyrolysis and biochar characterization. In *Proceedings of the 1st FOREBIOM Workshop*, 4(4).
- Rout, T., Pradhan, D., Singh, R.K. and Kumari, N., 2016. An exhaustive study of products obtained from coconut shell pyrolysis. *Journal of Environmental Chemical Engineering*, 4(3), pp.3696–3705.
- Roy, P. and Dias, G., 2017. Prospects for pyrolysis technologies in the bioenergy sector: A review. *Renewable and Sustainable Energy Reviews*, 77, pp.59.
- Sadaka, S., Sharara, M.A., Ashworth, A., Keyser, P., Allen, F. and Wright, A., 2014. Characterization of biochar from switchgrass carbonization. *Energies*, 7, pp.548–567.
- Salavati-Niasari, M., Davar, F. and Loghman-Estarki, M.R., 2010. Controllable synthesis of thioglycolic acid capped ZnS (Pn)0.5 nanotubes via simple aqueous solution route at low temperatures and conversion to wurtzite ZnS nanorods via thermal decomposition of precursor. *Journal of Alloys and Compounds*, 494(1–2), pp.199–204.
- Schott, J.A., Do-Thanh, C.L., Shan, W., Puskar, N.G., Dai, S. and Mahurin, S.M., 2021. FTIR investigation of the interfacial properties and mechanisms of CO<sub>2</sub> sorption in porous ionic liquids. *Green Chemistry*, 2(4), pp.392–401.
- Shaaban, A., Se, S.M., Dimin, M.F., Juoi, J.M., Husin, M.H. and Mitan, N.M., 2014. Influence of heating temperature and holding time on biochars derived from rubber wood sawdust via slow pyrolysis. *Journal of Analytical and Applied Pyrolysis*, 107, pp.31–39.
- Sik, Y., Uchimiya, S., Chang, S. and Bolan, N., 2016. *Biochar: Production, Characterization and Applications*. CRC Press.
- Song, W. and Guo, M., 2012. Effect of pyrolysis temperature and feedstock type on agricultural properties and stability of biochars. *Journal of Analytical and Applied Pyrolysis*, 94, p.138.
- Spokas, K., 2010. Review of the stability of biochar in soils: Predictability of Omolar ratios. *Carbon Management*, 1(2). <https://doi.org/10.4155/cmt.10.32>
- Tomczyk, A., Sokołowska, Z. and Boguta, P., 2020. Biochar physicochemical properties: Pyrolysis temperature and feedstock kind effects. *Reviews in Environmental Science and Bio/Technology*, 19, pp.191–215.
- Tripathi, M., Sahu, J.N. and Ganesan, P., 2016. Effect of process parameters on production of biochar from biomass waste through pyrolysis: A review. *Renewable and Sustainable Energy Reviews*, 55, pp.467.
- Uchimiya, M., Ohno, T. and He, Z., 2013. Pyrolysis temperature-dependent release of dissolved organic carbon from plant, manure, and biorefinery wastes. *Journal of Analytical and Applied Pyrolysis*, 104, pp.84–94.
- Usman, R., Abduljabbar, A., Vithanage, M., Ok, Y.S., Ahmad, M., Elfaki, J., Abdulazeem, S.S., Al-Wabel, M.I., 2015. Biochar production from date palm waste: Charring temperature-induced changes in composition and surface chemistry. *Journal of Analytical and Applied Pyrolysis*, 115, pp.392.
- Wang, L., Olsen, M.N.P., Moni, C., Dieguez-Alonso, A., de la Rosa, M., Stenrød, M., Liu, X. and Mao, I., 2022. Comparison of properties of biochar produced from different types of lignocellulosic biomass by slow pyrolysis at 600 °C. *Applied Energy Combustion Science*, 12, 100090.
- Wanjala, C.W. and Majinda, R.T., 1999. Flavonoid glycosides from *Crotalaria podocarpa*. *Phytochemistry*, 51, pp.705–707.
- Weber, K. and Quicker, P., 2018. Properties of biochar. *Fuel*, 217, pp.240–261.
- Xu, X., Cao, X. and Zhao, L., 2013. Comparison of rice husk-and dairy manure-derived biochars for simultaneously removing heavy metals from aqueous solutions: Role of mineral components in biochars. *Chemosphere*, 92(8), pp.955–961.
- Yang, H., Yan, R., Chen, H., Lee, D.H. and Zheng, C., 2007. Characteristics of hemicellulose, cellulose, and lignin pyrolysis. *Fuel*, 86, pp.1781–1788.
- Yuan, J.H., Xu, R.K. and Zhang, H., 2011. The forms of alkali in biochar produced from crop residues at different temperatures. *Bioresource Technology*, 102, pp.3488–3497.
- Zama, E.F., Zhu, Y.G., Reid, B.J. and Sun, G.X., 2017. The role of biochar properties in influencing the sorption and desorption of Pb (II), Cd

- (II), and As (III) in aqueous solution. *Journal of Cleaner Production*, 148, pp.127-136.
- Zhang, J. and Liy, R., 2015. Effects of pyrolysis temperature and heating time on biochar obtained from pyrolysis of straw and lignosulphonate. *Bioresource Technology*, 176, pp.288-291.
- Zhao, S.X., Na, T. and Wang, X.D., 2017. Effect of temperature on the structural and physicochemical properties of biochar with apple tree branches as feedstock material. *Energies*, 10, 1293.

---

**ORCID DETAILS OF THE AUTHORS**Loveena Gaur: <https://orcid.org/0009-0008-4613-3905>Poonam Poonia: <https://orcid.org/0000-0002-7766-1830>



# The Waste Management System in the Parking and Traders Arrangement in the Borobudur Temple Area, Central Java, Indonesia

S. Isworo<sup>1†</sup> , E. Jasmieni<sup>2</sup> and P. S. Oetari<sup>1</sup>

<sup>1</sup>Department of Environmental Health, Dian Nuswantoro University, Semarang, Indonesia

<sup>2</sup>Urban and Regional Planning Doctoral Study Program, Diponegoro University, Semarang, Indonesia

†Corresponding author: Slamet Isworo; slamet.isworo@dsn.dinus.ac.id

Nat. Env. & Poll. Tech.  
Website: [www.neptjournal.com](http://www.neptjournal.com)

Received: 03-01-2024  
Revised: 19-03-2024  
Accepted: 05-04-2024

## Key Words:

Waste management system  
Reduce-reuse-recycle  
Borobudur temple  
Water quality  
Plankton  
Benthos  
Diversity index

## ABSTRACT

The Indonesian government continues to accelerate the resolution of all problems related to the planning, infrastructure development, and arrangement of tourist visits, including the arrangement of parking spaces and commercial areas in the Borobudur temple area. The purpose of this study is to develop a waste management system in the parking and commercial areas of Kujon as an alternative to structuring the Borobudur temple area. The research method is a descriptive-qualitative observational approach. Surface water and groundwater examinations are carried out in laboratories and compared with quality criteria determined by the Indonesian government. Toxic and hazardous waste is stored in temporary facilities until it is collected by a company licensed by the Indonesian environmental ministry. The Shannon-Wiener Plankton and Benthos Diversity Index measures the diversity of organisms in a community. The study's findings highlight the need to establish a waste processing facility based on the reduction, reuse, and recycling principles. Waste will be collected at a certain site and stored temporarily in line with the technical instructions for the Minister of Environment and Forestry's Regulation. The findings of surface water and groundwater studies demonstrate that all measured parameters continue to meet the Indonesian government's quality thresholds. Plankton Bioindicator Measurements: Plankton diversity index values range from 1.040 to 1.943, indicating moderate pollution, while benthos values range from 0.811 to 0.918, indicating weakly to moderately contaminated conditions. Sustainable environmental management is critical and should serve as a baseline for environmental quality in the activity area.

## INTRODUCTION

Tourism is one of Indonesia's fastest-expanding economic sectors, both in terms of variety and growth. The positive consequence of tourism activities will be the construction of new hotels, restaurants, and retail complexes, which will result in the creation of more jobs and an increase in regional income. According to the United Nations World Tourism Organization (UNWTO), tourism has contributed to the gross domestic product (GDP) of numerous countries across the world (Khan et al. 2020). Tourism may also be detrimental to the environment, particularly in terms of garbage (waste) generation brought on by the large number of tourists and activities at tourist destinations. The conservation and preservation of historical sites, natural regions, and archeological artifacts are also hampered by this (Barakazi 2023). Borobudur Temple Tourist Park is a major tourist destination for both domestic and international visitors, as well as a cultural heritage site. Borobudur Temple Tourist Park has already been declared one of the world's seven

wonders (Scolaro 2016). The Magelang Regency Central Statistics Agency projects that 1.44 million tourists will visit Borobudur Temple in 2022.

The Borobudur Temple Tourist Park presents a bright prospect for state revenue. Annual increases in tourism have both beneficial and detrimental effects on the environment. The amount of rubbish generated by the growing number of visitors to Borobudur Temple is one of the negative effects. (Ahmed et al. 2019). The waste processing process in the Borobudur Temple area includes physical, chemical, and biological processes, all of which must meet the criteria set by the government. (Bravi et al. 2020). The establishment of a waste management system requires a paradigm shift that prioritizes an environmentally friendly waste management process by reducing and utilizing waste before it is disposed of in the landfill or into the environment. Referring to Presidential Regulation Number 1 of 1992 concerning Waste Management and Control implemented by the State-Owned Enterprise (BUMN) PT Taman Wisata Candi Borobudur, Prambanan,

and Ratu Boko (Persero) (Purwaningsih et al. 2021). The protection of the Borobudur World Cultural Heritage Area is carried out in accordance with Law Number 11 of 2010 concerning Cultural Heritage, while the surrounding cultural landscape is carried out in accordance with Law Number 26 of 2007 concerning Spatial Planning, with the Borobudur Temple Complex designated as a National Strategic Area. (Susilo & Suroso 2015). The waste management system plan consists of sorting and containerization, collection, and processing at the waste processing site using the Waste Management Site reduce-reuse-recycle method (TPS 3R), transfer, and transportation to the final processing site. The management results are validated based on physical and chemical parameters. and biology and parameters do not exceed quality standards that have been determined based on government regulations (Perdana 2023)

The waste management system is a systematic, comprehensive, and sustainable activity that includes reducing and handling waste (Heidari et al. 2019). The waste management system in Indonesia is governed by Law No. 18 of 2008. It aims to promote public and environmental health by converting waste into resources that can be sustainably handled. The waste management system includes both technical and non-technical components. Waste management technically refers to decreasing and handling waste, which involves storing and segregating waste, collecting, transferring, and transporting it. Non-technical handling comprises institutions, regulatory and legal subsystems, financing, and community participation. These two factors are mutually sustainable and must be carried out in tandem to build a good waste management system (Karjoko et al. 2022). Waste generated from the operations of the Borobudur Temple tourist area must be managed first so that it does not cause ecological disturbance. This waste must meet environmental quality standards with physical, chemical, and biological parameters. River water quality standards must meet the requirements set by the Indonesian government, especially regarding National Water Quality Standards based on Government Regulation Number 22 of 2021 (Susanto 2023), Minister of Health Regulation Number 32 of 2017 for Environmental Health Quality Standards, and Clean Water Health Requirements. The water quality standard for biological parameters is to know the plankton and benthos diversity index. Management of toxic and hazardous waste must be in accordance with Regulation Number 6 of 2021 concerning procedures and techniques for managing hazardous and toxic waste. (Astuti et al. 2020)

The concept of the Borobudur Destination Development Acceleration program guides the spatial planning of the temple area, including the arrangement of parking lots and merchant spaces, to preserve the temple as a top priority for

the Indonesian government. To maintain and preserve the extraordinary special value that Borobudur Temple has, a sustainable waste management system must go hand in hand with the creation of this policy.

The research question is whether the waste management system for parking and trading locations in the Kujon area can provide an alternative solution for the Borobudur temple area, as well as whether groundwater and surface water quality standards can be managed following established quality standards. Likewise, with the management of solid waste, toxic, and hazardous materials related to research questions, this research aims to design an environmental management system that is suitable for structuring parking allocations and trade activity zones in the tourist area around Borobudur Temple, including standard management. Quality of surface water and groundwater, and management of toxic and hazardous waste as per the regulations set by the Indonesian government.

## MATERIALS AND METHODS

On March 18-21, 2021, this study was conducted in the Borobudur temple tourism region of Magelang Regency. The sample conditions were sunny, wind speed 0.50-2.1 m.s<sup>-1</sup>, the total wind direction was dominated by the east by 23%, the air temperature was 28.6°C, air pressure mmHg was 739.7 mmHg, and air humidity was 76.7%.

### Management of Solid Waste

Waste management is the practice of managing waste from conception to disposal, which includes collection, transportation, processing, and disposal, as well as waste management rules. Clear environmental boundaries are needed to manage and comply with waste impact analysis and solid waste management so that assessments in environmental monitoring can be more thoroughly confirmed. The ecological boundary of waste management is the location where waste is collected, sorted, reused, recycled, processed, and finally processed (Quilley & Kish 2019).

The waste produced can be evaluated by calculating the amount of waste at temporary and final disposal sites using the SNI 19-3964-1995 standard, with the standard unit for large cities being 2-2.5 L.person.day<sup>-1</sup> or 0.4-0.5 kg.person<sup>-1</sup>. day<sup>-1</sup> and the standard unit for medium or small cities is 1.5-2 L.person<sup>-1</sup>.day<sup>-1</sup> or 0.3-0.4 kg.person.hour<sup>-1</sup> with waste management criteria based on Minister of Health Regulation Number 17 of 2020 (Kastolani 2019). The quantity of waste generated in a tourist location is directly correlated with the number of tourists, including vendors, and the local population. SNI 19-3964-1995 states that estimates from



landfills for traditionally generated garbage (waste) can be utilized to estimate the volume of waste in a tourism region (Butar-Butar et al. 2020).

The data collection method used is observation, namely observing the availability of waste collection places and locations, the availability of cleaning staff, daily waste handling, the amount of organic and inorganic waste produced, the type of waste management facilities, and secondary data from the Magelang Regency Cleaning Service using the method of descriptive-qualitative analysis.

### Surface Water Quality

The ecological boundaries for surface water parameters (river water) are based on water bodies in the vicinity of the research site. The Elo River is a river to the south of the research site, with an ecological border of surface water about 100 meters downstream.

The discharge of wastewater from anthropogenic activities in the Borobudur Temple tourist area into water bodies can impair the quality of surface water. Because wastewater typically flows into rivers, river water quality can be used to assess the success of wastewater treatment as well as the overall quality of a water body (Arum et al. 2019). Surface water quality measurements in the Elo River were carried out using a surface water sampling methodology based on SNI 6989.57:2008. The analysis was carried out experimentally in the laboratory using a spectrophotometer and then compared to the National Water Quality Standards, which are based on Government Regulation No. 22 of 2021 (Cahyadi et al. 2023). The coordinates of the surface water sampling location are at Location AP-1: LS: 07°36'11.76" - BT: 110°11'47.11" and LS: 07°36'18.63" - BT: 110°11'46.34".

Water samples are collected in phases using a 1-liter water sampler before being composited, divided, and conserved for laboratory analysis. Water samples are collected based on the analytical designation, including metals, BOD, COD, and other parameters. Temperature, TDS, electrical conductivity, pH, and dissolved oxygen parameters, which can change quickly and cannot be preserved, are tested at the site where the water samples were collected, and the results are recorded on a field sheet or special notebook. Research on ecological boundaries is required in this study to direct the selection of sites for the first environmental baseline data collection and impact dispersion analysis. Every aspect of the impacted biophysical and chemical environment must be taken into account when determining ecological limitations (Strayer 2003).

### Residential Well Water Quality

The ecological boundaries for well water are based on

the impact of lowering the quality of well water within a 100-meter radius of the research site (Van Geen et al. 2016)

This study's sample was excavated using well water gathered utilizing purposive sampling procedures. SNI 6989 58 2008 Concerning Methods for Sampling Groundwater is the foundation for groundwater sampling (Lusiana et al. 2020). The analytical method relies on laboratory analysis with a spectrophotometer and comparison to quality standards of Minister of Health Regulation No. 32 of 2017 concerning Environmental Health Quality Standards and Water Health Requirements for Cleanliness, Sanitation, Swimming Pools, and Public Baths (Erlinawati et al. 2021). Sampling location determined by coordinates: AB-1: Residents of Kujon Hamlet to the west of the location (LS: 07°36'09.6" - BT: 110°11'46.6") and location AB-2: a residents' well close to the location's south (LS: 07°36'21.85"; BT: 110°11'51.22").

Residential well water sampling: Before utilizing a water sampler, agitate the bottom of a dug well for 2-3 minutes. The sample was then placed in a plastic container with a capacity of 2000 mL without preservative, a 1000 mL bottle with HNO<sub>3</sub>, a 500 mL bottle with H<sub>2</sub>SO<sub>4</sub>, and a 100 mL glass bottle for microbiological parameters, all of which were wrapped in aluminum foil.

### Waste Management of Toxic Hazardous Materials

Ecological boundaries for managing toxic and hazardous waste include storage, collection, utilization, transportation, and processing in temporary storage areas before being taken by a third party and having permission from the Ministry of Environment based on the requirements of the Minister of Environment and Forestry Regulation Number 6 of 2021 (Widyaningsih & Sembiring 2021).

The management plan takes the form of temporary storage, and it refers to the Minister of Environment and Forestry Regulation Number 6 of 2021, which governs the procedures and techniques for managing hazardous and toxic waste (Budihardjo et al. 2023)

### Plankton and Benthos Species Diversity Index Value

The ecological limits for plankton and benthos characteristics are the same as for surface water. The plankton sampling approach is carried out at two sites along the Elo River by filtering river water samples using a plankton net, while the benthos (macro-invertebrate) sampling method is carried out by taking mud and substrate samples from the river surface with a Grab and stream-net sampler. The Shannon-Wiener equation is used to get the species diversity index value. (Putri et al. 2019) Coordinates of Plankton/ benthos sampling locations at Location AP-1: LS: 07°36'11.76" - BT: 110°11'47.11" and Location AP-2: B LS: 07°36'18.63" - E:

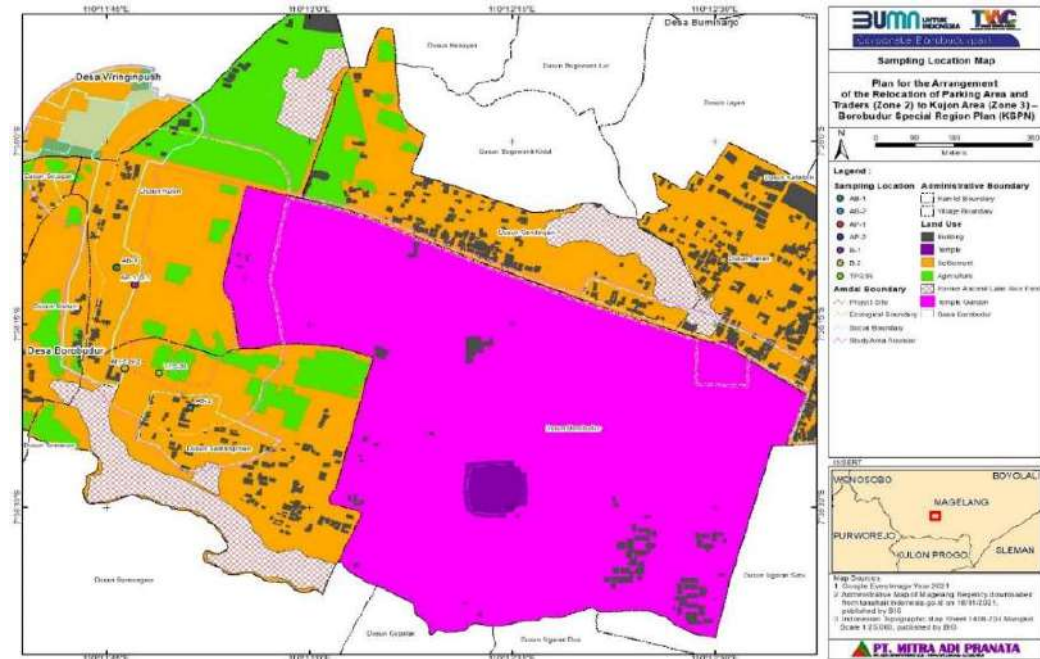


Fig 1: Research area boundaries.

110°11'46.34". Fig. 1 shows the sampling locations and ecological boundaries of the research.

## RESULTS AND DISCUSSION

### Management of Solid Waste, Waste Water, and Toxic Hazardous Materials

According to Waste Management Law Number 18 of 2008, waste is defined as the remains of anthropogenic activities or natural processes in solid or semi-solid form, in the form of biodegradable or non-biodegradable organic or inorganic substances that are no longer useful and are thrown into the environment. Tourist locations produce large amounts of waste due to tourist activities and supporting facilities; therefore, these places require a sustainable waste management system. The growth of tourist attractions in the Borobudur Temple area is a priority, especially plans for the development and arrangement of parking lots and merchant areas, so waste management is needed that meets technical requirements (Ernawaty 2018). Activities in parking areas, souvenir/culinary kiosks, open-air amphitheatres, bicycle & tourist car terminals, shuttle services, lobbies, courtyards, multi-purpose buildings, educational galleries, and parks are estimated to produce organic and inorganic waste. The amount of waste produced in tourist areas is determined by the number of visitors, traders, managers, and local communities based on SNI 19-3964-1995. If field observation standards for waste at the research location are not yet available, then to calculate

waste heaps, the standard for the amount of waste heaps can be used. Residential areas, or using the standard waste collection unit for large cities, namely  $2-2.5 \text{ L.person.day}^{-1}$  or  $0.4-0.5 \text{ kg.person.day}^{-1}$ , while the standard waste collection unit for medium/small cities is  $1.5-2 \text{ L.person.day}^{-1}$  or  $0.3-0.4 \text{ kg.person}^{-1}.\text{day}^{-1}$  (Widyarsana & Salmaa 2019).

The analysis of waste heaps in the Borobudur Temple tourist area is as follows: The producer or source of waste is mostly due to visitor activities, traders' areas, and parking areas in the Borobudur Temple tourist area, which is under the administration of Magelang Regency with the criteria of a metropolitan city with a population of 1,279,625 people. The assumption is that the amount of waste produced is  $2-2.5 \text{ L.person}^{-1}.\text{day}^{-1}$  or  $0.4-0.5 \text{ kg.person}^{-1}.\text{day}^{-1}$ . The merchant and parking area in the Borobudur temple area is a non-residential market and public space. According to Aziz (2019), the usual unit for storing non-residential market-type garbage (waste) is  $0.20-0.60 \text{ L.m}^{-2}.\text{day}^{-1}$  or  $0.100-0.30 \text{ kg.m}^{-2}.\text{day}^{-1}$ . The following is an explanation of waste heap analysis: Estimated waste heaps =  $0.6 \text{ L.m}^{-2}.\text{day}^{-1}$ , land area = 10.74 Ha, hence total waste generation =  $0.6 \text{ L.m}^{-2}.\text{day}^{-1} \times 10.74 \text{ Ha} \times 10,000 \text{ m}^2.\text{ha}^{-1} = 64,440 \text{ L.day}^{-1}$  (Aziz 2019). Based on the trash pile analysis, it is projected that waste heaps in Borobudur's merchant and parking areas, as well as visitor activities, will expand, necessitating the calculation of waste forecasts that refer to the increase in visitors. Table 1 shows the projected number of visitors in the Borobudur Temple area.

Table 1: Projection of the number of visitors.

Year of Visit	2021	2022	2023	2024	2025
Number of Visitors (people)	736222	846752	967838	1084891	1216285
Increase in Visitors (people)		110531	121086	117053	131393
Increase in Visitors [%]		15.00%	14.30%	12.10%	12.10%
Average Increase in Visitors [%]	13.40 % with linear prediction is $y = 122565+722829$				

Table 2: Projection of waste piles in the area in Borobudur temple area (L.day<sup>-1</sup>).

Year of Foundation (2020)	73,074	82,867	93,971	106,563	120,842
64.44	65.3 % with linear prediction is $y = 122565+722829$				

The estimated garbage (waste) pile in the Kujon merchant and parking area of the Borobudur temple area is computed using a 13.4% increase in tourist numbers. Table 2 summarizes the trash generation projections for the Borobudur temple region.

A waste processing site with the Waste Management Site Reduce-Reuse-Recycle (TPS3R) concept will be built in the study area. The Waste Management Site Reduce-Reuse-Recycle (TPS3R) is a waste management pattern at the local or regional level that involves active government participation and community empowerment. This effort is expected to reduce the burden of waste processing at temporary waste storage areas (TPS) and integrated waste processing sites (TPST) in the study area (Fig 2).

- a. The waste storage system is planned to use trash cans, while the waste transportation system to the A waste processing site with The Waste Management Site Reduce-Reuse-Recycle (TPS3R) is planned to use trash motorbikes, and waste transportation from The Waste Management Site Reduce-Reuse-Recycle (TPS3R) to the final processing site (TPA) or waste processing site integrated (TPST) is planned to use an arm roll truck. The waste management system is designed based on the following criteria:
  - b. Storage facilities: trash cans with a capacity of 40-50 liters (0.05 m<sup>3</sup>)
    - a) Means of Transportation: a) Garbage (waste) transport motorbike with capacity: 1.5 m<sup>3</sup>.day<sup>-1</sup>, recycling: 2 times per day. b) Arm roll Truck Ca-

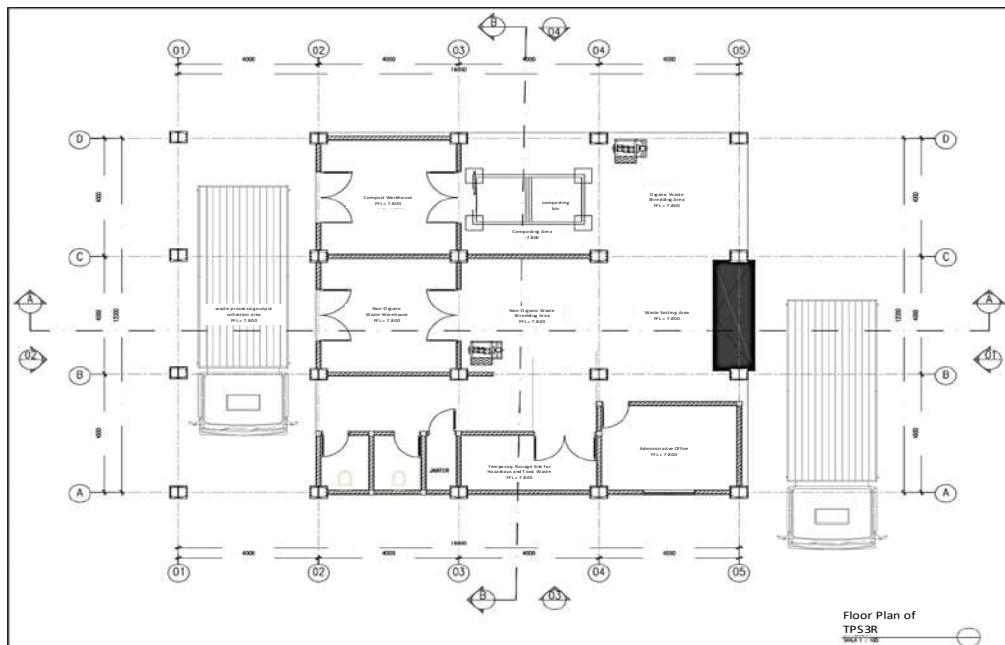


Fig. 2: Building plan the waste management site reduce-reuse-recycle (TPS3R).

capacity: 6 m<sup>3</sup>; Rotation: 2 times per day. c) The Waste Management Site - Reduce-Reuse-Recycle (TPS3R) facilities capacity is 30 m<sup>3</sup>

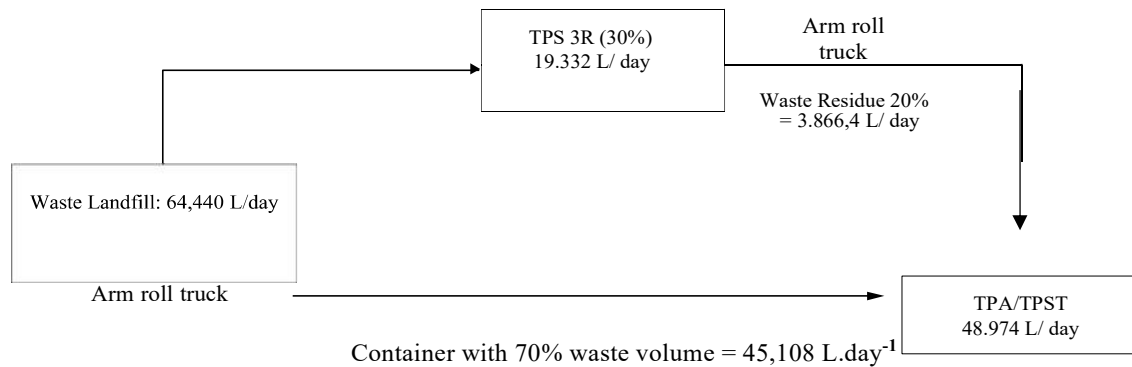
Waste management operational technicalities include sorting and containing, collection, transportation, processing, and final processing activities.

Waste Container System: The container design must meet the following requirements: a) Comply with the specifications for use as a temporary waste storage device, including the design. b) Tool uniformization can aid in the smooth execution of operations. c) The equipment includes a separate container for wet and dry garbage (waste) to aid in the process of minimizing waste at the source. Specifications for a container with a capacity of 40-50 liters manufactured of polyethylene plastic bin material and a service life of 3 years. The garbage (waste) container pattern is as follows: 1) Domestic garbage (waste), institutional waste (offices, hotels, stores, restaurants, and health facilities), and street waste are anticipated to be divided into organic and inorganic waste

to aid in the reduction process. 2) Every morning at 05.00, traders collected the rubbish created so that the cleaning crew could collect and transport the waste around 06.00-07.00. 3) Make certain that the waste is not scattered; if there is surplus waste, place it in a plastic bag so that the cleaning crew can quickly collect it. 4) Waste containers will be provided at each trader's kiosk and in public locations. Meanwhile, the waste container from street sweeping is a zinc garbage (waste) can with a capacity of 40-50 liters, with a placement pattern on the road lane on the right and left of the road at a distance of 50 meters alternately. The waste management system plan diagram is shown in Fig. 3

The number of waste containers needed is described in Table 3.

Cleaning personnel then collect the gathered trash every morning between 6:00 and 7:00 a.m. and collect it using a waste motorbike for waste that will be processed at Waste Disposal - The Waste Management Site Reduce-Reuse-Recycle (TPS3R). Meanwhile, garbage (waste) is carried to



Note: Waste Management Site for The Waste Management Site Reduce-Reuse-Recycle (TPS3R) Integrated Waste Processing Site (TPST) Final Processing Place (TPA)

Fig. 3: Waste Management System Plan.

Table 3: Number of trash cans required.

Description	Number of trash cans	Information
Trader	1284	Waste containers are segregated and closed and provided by each trader
Courtyard with (Entrance hall)	4	Provided by the kujon merchant and parking area manager
Outdoor space-rock garden	8	Provided by the kujon merchant and parking area manager
Green-Landscape / Rare Forest Plants	15	Provided by the kujon merchant and parking area manager
Open Stage-creative space	10	Provided by the kujon merchant and parking area manager
Deck-Feeder Shuttle	20	Provided by the kujon merchant and parking area manager
Parking area	15	Provided by the kujon merchant and parking area manager
Bike & VW Safari Station	15	Provided by the kujon merchant and parking area manager
Number of containers/trash cans	1371	

Table 4: Power requirements for sweepers.

Areas	Number of Sweepers (People)	Information
Courtyard with (Entrance hall)	5	Every morning between 05.00 and 07.00, street sweeping takes place.
Outdoor space-rock garden	15	
Green-Landscape/Rare Forest Plants	20	
Open Stage-creative space	10	
Deck-Feeder Shuttle	25	
Parking area	20	
Bike & VW Safari Station	15	
Number of sweepers	110	

the Final Waste Processing Site (TPA) or Integrated Waste Processing Site (TPST) using an arm-roll truck. Sweeping is used to gather garbage (waste) in public areas and on roads. Sweeping power will be split into the locations as given in Table 4.

Each sweeping worker should be outfitted with the following items: 1 set of work clothes (striking color), 1 work safety hat, 1 broomstick, 1 bamboo cradle, 1 dust protection mask, 1 pair of work shoes, and 1 broomstick and bamboo cradle. Sweeping command. It is vital to inspect the sweepers regularly. It is vital to vary the work location regularly to create a new and pleasant working environment.

### Transport System

The waste transportation system is carried out in the morning after sweeping, and traders have collected all the waste produced. Garbage (waste) transportation is carried out at 7:00 a.m. Transporting waste from waste containers to Waste Management Site - Reduce-Reuse-Recycle (TPS3R) uses a trash motorbike while transporting waste from waste containers and residue from Waste Management Site - Reduce-Reuse-Recycle (TPS3R) is carried out using an arm roll truck. garbage (waste) Motor Capacity:  $1.5 \text{ m}^3 \cdot \text{day}^{-1}$ ; Processing: 2 times per day Arm roll truck capacity:  $6 \text{ m}^3$ ; recitation: 2 times per day.

The waste transportation system requires that the waste transportation equipment be equipped with a waste cover, at least using a net so that the waste is scattered, that the maximum height of the transportation tank is 1.6 m, that it has a lever, that the capacity of the waste is determined by the class of road that will be traversed, and that the truck body is equipped with wastewater protection. The trash transportation system is planned in collaboration with Magelang Regency sanitation officials to transfer waste to the Final Processing Site / Integrated Waste Processing Sites (TPST), while the management provides waste transportation equipment to Waste Management Site - Reduce-Reuse-Recycle (TPS3R) in the form of a waste motorbike.

Analysis of the need for waste transport motorbikes is described as follows: Volume of waste transported to Waste Management Site - Reduce-Reuse-Recycle (TPS3R) =  $19,332 \text{ L} \cdot \text{day}^{-1}$ , the capacity of motorbike transport =  $1.5 \text{ m}^3 \cdot \text{day}^{-1}$  with rotation: 2 times a day = 7 motorbikes carrying waste, the number of waste motorbikes required is 7 units; therefore, 7 riders are needed.

### Wastewater Management

Wastewater management planning refers to the Regulation of the Minister of Public Works and Public Housing Number 04/PRT/M/2017 concerning the Implementation of Domestic Wastewater Management Systems. The planned dirty water treatment system or sewage treatment plant uses a biofilter septic tank. The Sewage Treatment Plant (STP) is utilized to handle all wastewater generated by building activities. (Vindriani et al. 2023). Biotank is a bioseptic tank that treats home wastewater and is an advancement of simple septic tank technology. Domestic wastewater treatment systems will be differentiated based on building clusters, namely buildings with culinary clusters and buildings without culinary clusters (Fig. 4 & 5). The domestic wastewater treatment system in buildings with culinary clusters will have a grease trap added before it enters the bio-filter septic tank. The grease trap that will be used is made of fiberglass with a volume of 35 L. In general, the grease trap functions to Filter and wash cooking and dining utensils after removing waste fat and oil from kitchen garbage (waste) and Separating fat or oil with water so that the oil does not clump and freeze in the drain pipe, clogging the line.

Domestic wastewater treatment systems in non-culinary buildings do not have grease traps before entering the bio-filter septic tank.

34 biofilter septic tanks will be used, each with a capacity of  $8 \text{ m}^3$ . The biofilter septic tank has 4 (four) segments/bulks, namely:

**The initial settling tank:** It serves as an initial filter media to separate solid and liquid waste; solid waste

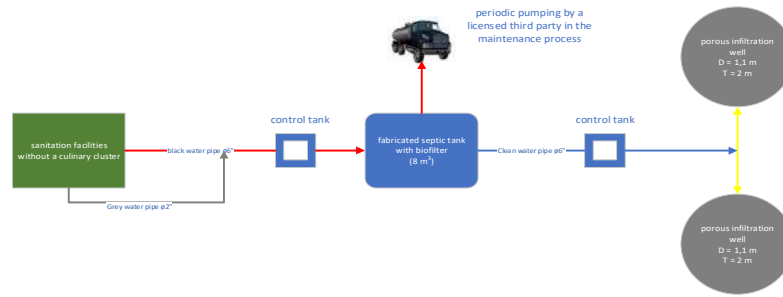


Fig. 4: Domestic wastewater treatment system scheme for facilities without culinary clusters.

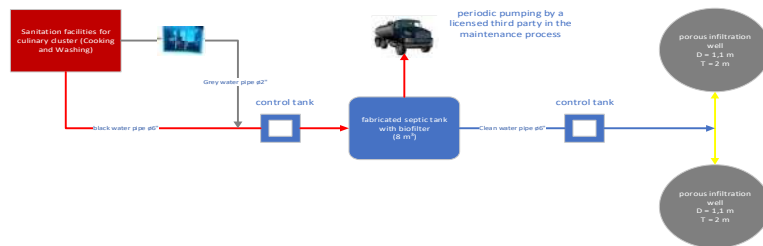


Fig. 5: Domestic wastewater treatment system scheme for facilities with culinary clusters.

is removed from unclean water and allowed to settle fully.

**Anaerobic Zone 1:** Sewage waste will be divided into solid waste and liquid waste using a filtration system, allowing for perfect separation of unclean water and solid waste.

**Anaerobic Zone 2:** It is the third filter, which produces better and clearer water that no longer harms the environment. In this filter, there are balls, also called bioballs, which influence the final results of wastewater treatment.

**Anaerobic zone:** It is a wastewater treatment filter equipped with decomposing bacteria whose job is to break down residual waste so that it is not harmful to the soil and water areas. Concentrated bacterial tablets will be inserted into this filter periodically so that the decomposition process can take place efficiently and effectively.

**A chlorination tank (disinfectant medium):** It is a wastewater treatment component that is beneficial for destroying germs in wastewater. Chlorine will be injected into this chlorination tank before it flows through the biofilter section tank's outlet or effluent (Fig. 6). The water treated by the biofilter septic tank will subsequently be directed to the water catchment (Da Silva et al. 2013).

**Management of Hazardous and Toxic Waste**

The trade and parking areas in the Borobudur temple area will produce hazardous and toxic waste (B3) during operational activities, namely Toxic and Hazardous Waste originating from non-specific sources (not otherwise

specified) in the form of used batteries, used electronic equipment refrigerants, and electronic waste (PCB/Print Circuit)., TL lamp, and battery. The management plan in the form of temporary storage before being taken by a second party will be related to the Minister of Environment and Forestry Regulation Number 6 of 2021 concerning Procedures and Requirements for Management of Hazardous and Toxic Waste (Zulfikri 2023). An estimate of the amount of hazardous and toxic waste produced during operational activities (peak conditions) is shown in Table 5.

Toxic and hazardous waste will be collected at a certain location in a temporary storage area with an area of 8 m<sup>2</sup>. The Waste Management Site - Reduce-Reuse-Recycle (TPS3R) building must be flood-free, closed, and protected from rain, have an air circulation ventilation system, and have a watertight and non-way floor.

The amount of toxic and hazardous waste produced is less than 50 kg.day<sup>-1</sup> (Category 1). The longest storage period

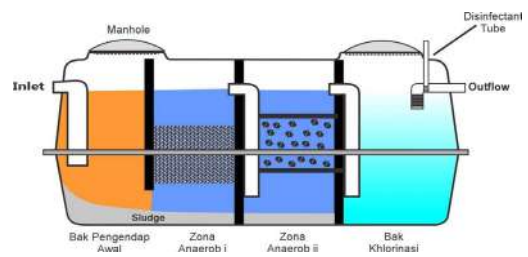


Fig. 6: Bio Filter Septic Tank Scheme.

Table 5: Name, characteristics, and amount of toxic and hazardous waste.

No	Name and Code	Source	Type	Characteristics	Amount
1.	Used battery Code: A102d	Electronic equipment includes: wall clock, remote, microphone	Congested	Toxic and corrosive	20 kg.month <sup>-1</sup>
2.	Refrigerant used for electronic equipment, Code: A111d	Electronic equipment includes AC, refrigerator, dispenser, and freezer.	Liquid	Poisonous	250 L.month <sup>-1</sup>
3.	Electronic waste (Printed Circuit Boards, TL lamps), Code: B107d	Electronic equipment includes lights	Congested	Poisonous	60 pcs.month <sup>-1</sup>

is 180 days from the time the toxic and hazardous waste is produced. Supervision of Toxic Waste Storage activities in the form of supervision during the placement and/or removal of Toxic Waste from the toxic and hazardous Waste Storage room; inspection of toxic and hazardous waste packaging; documentation of storage activities. Toxic and hazardous waste will be collected at a certain location in a temporary storage area with a room area of 8 m<sup>2</sup>. The Waste Management Site - Reduce-Reuse-Recycle (TPS3R) building must be flood-free, closed, and protected from rain, have an air circulation ventilation system, and have a watertight and non-wavy floor.

The amount of toxic and hazardous waste produced is less than 50 kg.day<sup>-1</sup> (Category 1). The longest storage period is 180 days from the time the toxic and hazardous waste is produced. Supervision of Toxic and Hazardous Waste Storage activities in the form of supervision during the placement and/or removal of Toxic and Hazardous Waste from the Toxic Waste Storage room; inspection of Toxic and hazardous waste packaging; documentation of toxic and hazardous waste storage activities; and supervision of housekeeping procedures.

Every toxic and hazardous material waste that is included in the toxic and hazardous material waste is recorded and reported. Transport and handling of toxic and hazardous waste is delegated to other parties who have permits. The storage flow for toxic and hazardous waste; and supervision of housekeeping procedures are shown in Fig. 7.

Every toxic and hazardous material waste that is included in the toxic and hazardous material waste is recorded and reported. Transport and handling of toxic and hazardous waste is delegated to other parties who have permits. The storage flow for toxic and hazardous waste is shown in Fig. 7.

The general procedure for storing hazardous waste is as follows: a) hazardous waste is produced from the Kujon merchant and parking area in the form of used batteries, used refrigerants, and electronic waste. b) Toxic and hazardous waste will be packaged according to its characteristics. Temporary storage of Toxic and hazardous waste will use packaging in accordance with the waste code, type, and characteristics of Toxic and hazardous waste. Used refrigerant (A111d) uses the original packaging or other watertight packaging if the original packaging is not available (in the form of a drum), while used batteries (A102d) and electronic waste (B107d) will use packaging/containers in the form of sacks or plastic. c) Packages containing Toxic and hazardous waste will be given labels and symbols in accordance with the Minister of Hazardous Environment Regulation Number 14 of 2013 concerning Symbols and Labels for Hazardous and Toxic Waste. d) Toxic and hazardous waste that has been packaged and given a symbol will be stored Special Temporary Storage Area e) Stored according to its characteristics and not exceeding the storage time limit. f) Managed further by a third party who has a Toxic and hazardous waste processing permit, namely in the form of transporting Toxic and hazardous waste.

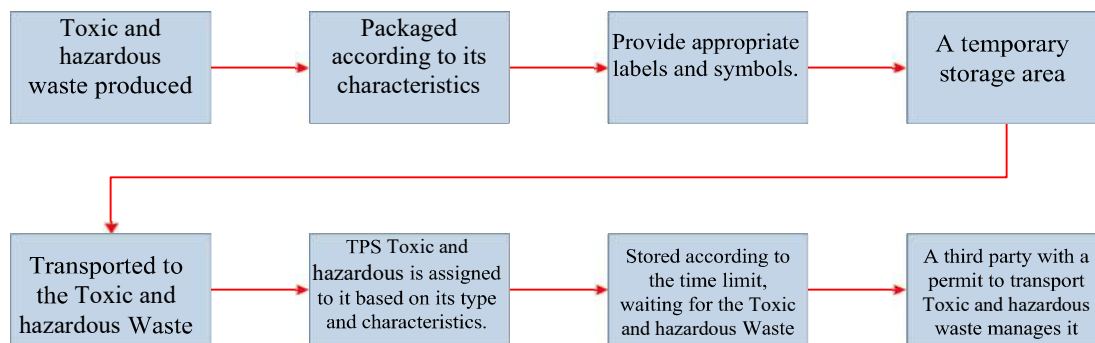


Fig. 7: Toxic and hazardous waste storage flow.

## Environmental Quality Indicators

### Surface Water Quality and Ground Water Quality

The quality of surface water at a location can be used as an indicator of environmental quality. This is because, generally,

the impact of an activity, especially liquid waste, will end up in water bodies (Akhtar et al. 2021). Measurements of surface water quality in water bodies (class III category designated as urban drainage channels) are known to provide results, except for the BOD parameters at the measurement location to the south of the

Table 6: Measurement results for surface water quality.

No.	Parameter	Unit	Result		Environmental Quality standards			
			AP-1	AP-2	Class1	Class 2	Class 3	Class 4
<b>PHYSICS</b>								
1.	Temperature	°C	27.4	27.6	Deviasi 3	Deviasi 3	Deviasi 3	Deviasi 5
2.	Total dissolved solids (TDS)	mg.L <sup>-1</sup>	148	173	1000	1000	1000	2000
3.	Total suspended solids (TSS)	mg.L <sup>-1</sup>	< 3	< 3	40	50	100	400
4.	Color	Pt-Counit	32.7	< 3	15	50	100	-
5.	Rubbish		Nil	Nil	Nil	Nil	Nil	Nil
<b>CHEMISTRY</b>								
6.	Degree of acidity (pH)		6.50	6.83	6-9	6-9	6-9	5-9
7.	Biochemical oxygen demand (BOD)	mg.L <sup>-1</sup>	< 2	3	2	3	6	12
8.	Chemical oxygen demand (COD)	mg.L <sup>-1</sup>	4	12	10	25	40	80
9.	Dissolved oxygen (DO)	mg.L <sup>-1</sup>	5.9	5.2	6	4	3	1
10.	Sulfate (SO <sub>4</sub> )	mg.L <sup>-1</sup>	11	8	300	300	300	400
11.	Chloride (Cl)	mg.L <sup>-1</sup>	9	13	300	300	300	600
12.	Nitrate (as N)	mg.L <sup>-1</sup>	3	4	10	10	20	20
13.	Nitrite (as N)	mg.L <sup>-1</sup>	0.02	0.01	0.06	0.06	0.06	-
14.	Ammonia (as N)	mg.L <sup>-1</sup>	0.07	0.05	0.1	0.2	0.5	-
15.	Total Nitrogen	mg.L <sup>-1</sup>	3	4	15	15	25	-
16.	Total Phosphate as P	mg.L <sup>-1</sup>	0.004	< 0.003	0.2	0.2	1	-
17.	Fluoride	mg.L <sup>-1</sup>	0.4	0.3	1	1.5	1.5	-
18.	Sulfur as H <sub>2</sub> S	mg.L <sup>-1</sup>	0.001	0.002	0.002	0.002	0.002	-
19.	Cyanide (CN)	mg.L <sup>-1</sup>	< 0.002	< 0.002	0.02	0.02	0.02	-
20.	Free chlorine	mg.L <sup>-1</sup>	0.08	0.01	0.03	0.03	0.03	-
21.	Oil and fat	mg.L <sup>-1</sup>	< 0.3	< 0.3	1	1	1	10
22.	Total detergent	mg.L <sup>-1</sup>	< 0.008	< 0.008	0.2	0.2	0.2	-
23.	Phenol	mg.L <sup>-1</sup>	< 0.0005	< 0.0005	0.002	0.005	0.01	0.02
24.	Barium (Ba) is dissolved	mg.L <sup>-1</sup>	0.02	0.03	1	-	-	-
25.	Boron (B) is dissolved	mg.L <sup>-1</sup>	0.5	0.3	1	1	1	1
26.	Dissolved mercury (Hg)	mg.L <sup>-1</sup>	< 0.002	< 0.0002	0.001	0.002	0.002	0.005
27.	Dissolved Arsenic (As)	mg.L <sup>-1</sup>	0.0005	0.0003	0.05	0.05	0.05	1
28.	Selenium (Se) is dissolved	mg.L <sup>-1</sup>	0.0003	0.0009	0.01	0.05	0.05	0.05
29.	Dissolved cadmium (Cd)	mg.L <sup>-1</sup>	< 0.002	< 0.0002	0.01	0.01	0.01	0.01
30.	Dissolved cobalt (Co)	mg.L <sup>-1</sup>	0.0008	0.0004	0.2	0.2	0.2	0.2
31.	Manganese (Mn) is dissolved	mg.L <sup>-1</sup>	0.2	0.11	0.1	-	-	-
32.	Dissolved nickel (Ni)	mg.L <sup>-1</sup>	0.0006	0.0005	0.05	0.05	0.05	0.1
33.	Zinc (Zn) is dissolved	mg.L <sup>-1</sup>	0.01	0.06	0.05	0.05	0.05	2
34.	Dissolved copper (Cu)	mg.L <sup>-1</sup>	0.004	0.006	0.02	0.02	0.02	0.2
35.	Lead (Pb) is dissolved	mg.L <sup>-1</sup>	0.0005	0.0007	0.03	0.03	0.03	0.5
36.	Hexavalent chromium (Cr <sup>6+</sup> )	mg.L <sup>-1</sup>	< 0.002	< 0.002	0.05	0.05	0.05	1
37.	DDT	mg.L <sup>-1</sup>	< 0.008	< 0.008	2	2	2	2
<b>MICROBIOLOGY</b>								
38.	Fecal Coliforms	MPN.100 mL <sup>-1</sup>	622	790	100	1.000	2.000	2.000
39.	Total Coliforms	MPN.100 mL <sup>-1</sup>	1.013	1.300	1.000	5.000	10.000	10.000

Information: Environmental Quality Standards for River Water Quality Standards and the like are in accordance with Republic of Indonesia Government Regulation Number 22 of 2021 concerning the Implementation of Environmental Protection and Management (Soeprbowati 2023). The sign (-) indicates that the parameter is not required for quality standards, and the sign (<) indicates results below the detection limit. Sampling location: Location AP-1: Water body west of the planned activity location; LS: 07° 36' 11.76" - BT: 110° 11' 47.11" and Location AP-2: Water body south of the planned activity location; S: 07°36'18.63" - E: 110°11'46.34"



planned activity location, all of which are still below standard quality in accordance with Republic of Indonesia Government Regulation Number 22 of 2021 concerning the Implementation of Environmental Protection and Management (Widodo & Hossain 2022). The analysis and measurement findings related to surface water quality are shown in Table 6.

Based on analysis of surface water, it is known that the BOD results have almost reached the quality standard limit, especially at the AP-2 sampling point, where the BOD results for class 2 (which includes water used for planting irrigation, fresh water for fish cultivation, livestock, and recreational purposes) are with value is 3. Biochemical Oxygen Demand, or BOD, is a property that indicates how much-

dissolved oxygen a microorganism needs to break down organic matter under aerobic conditions. BOD conditions are a measurement of the amount of oxygen consumed by microbial populations living in water as a reaction to the entry of decomposed organic matter (Sonawane et al. 2020). Based on the analysis findings, organic materials are a source of pollution, so oxygen intervention is needed to support the healthy growth of aerobic microorganisms. An aerator needs to be introduced to organic waste processing facilities in order to lower the BOD.

### *The Quality of Clean Water (Well Water)*

The average depth of groundwater in the research location

Table 7: Results of Well Water Quality Measurements.

No.	Parameter	Unit	Location AB-1	Location AB-2	SBM *
MANDATORY PARAMETERS					
I PHYSICS					
1	Turbidity	NTU	0.3	0.2	25
2	Color	Pt. Co	<3	<3	50
3	Total Dissolved Solids, TDS	mg.L <sup>-1</sup>	217	195	1000
4	Temperature	°C	28.6	28.9	Suhu Udara ± 3
5	Smell	-	Tidak Berbau	Tidak Berbau	Tidak Berbau
6	Flavor	-	Tidak Berasa	Tidak Berasa	Tidak Berasa
II BIOLOGY					
1	Total Coliforms	CFU.100 mL <sup>-1</sup>	8	49	50
2	E. Coli	CFU.100 mL <sup>-1</sup>	0	0	0
III CHEMISTRY					
1	pH	-	6.89	6.85	6.5-8.5
2	Fluoride, F	mg.L <sup>-1</sup>	0.26	0.14	1.5
3	Iron, Fe	mg.L <sup>-1</sup>	0.06	0.02	1
4	Total Hardness, CaCO <sub>3</sub>	mg.L <sup>-1</sup>	85	162	500
5	Mangan, Mn	mg.L <sup>-1</sup>	<0.00003	<0.00003	0.5
6	Nitrate, NO <sub>3</sub> -N	mg.L <sup>-1</sup>	3	1	10
7	Nitrite, NO <sub>2</sub> -N	mg.L <sup>-1</sup>	<0.003	0.007	1
8	Cyanide, CN <sup>-</sup>	mg.L <sup>-1</sup>	<0.002	<0.002	0.1
9	Surfactant (Detergent), MBAS	mg.L <sup>-1</sup>	<0.008	<0.008	0.05
0	Total Pesticide	mg.L <sup>-1</sup>	<0.000006	<0.000006	
ADDITIONAL PARAMETERS					
IV CHEMISTRY					
1	Mercury, Hg	mg.L <sup>-1</sup>	<0.0002	<0.0002	0.001
2	Arsen, As	mg.L <sup>-1</sup>	0.0001	0.0007	0.05
3	Cadmium, Cd	mg.L <sup>-1</sup>	<0.0002	<0.0002	0.005
4	Hexavalent Chromium, Cr <sup>6+</sup>	mg.L <sup>-1</sup>	<0.002	<0.002	0.05
5	Selenium, Se	mg.L <sup>-1</sup>	0.0003	0.0006	0.01
6	Zinc, Zn	mg.L <sup>-1</sup>	0.03	0.2	15
7	Timbal, Pb	mg.L <sup>-1</sup>	0.001	0.0005	0.05

Information: \* SBM is a Quality Standard for Sanitation Hygiene Needs, in accordance with Minister of Health Regulation No. 32 of 2017 concerning Environmental Health Quality Standards and Water Health Requirements for Sanitation Hygiene, Swimming Pools, Solus Per Aqua, and Public Baths (Table 1, 2 & 3) (Astuti et al. 2020). The sign (<) indicates results below the detection limit. Sampling location: Location AB-1: Kujon Hamlet Resident's Well to the west of the location (LS: 07°36'09.6" - BT: 110°11'46.6") and Location AB-2: Resident's Well to the south of the location (LS: 07°36'21.85" - E: 110°11'51.22")

area and its surroundings ranges from 8 to 15 meters (Widodo 2019). The geological conditions below the groundwater surface affect its depth. Field observations and interviews with residents around the proposed location of the Kujon Hamlet trading and parking area show that a number of residents' wells in Kujon Hamlet, Borobudur Village, have an average water surface depth of around 13 meters.

Measurement of the quality of clean groundwater was carried out at residents' wells near the research location area (trader arrangement area and Kujon Hamlet parking) at 2 (two) points, as shown in Table 7.

Based on the results of measurements of groundwater quality in 2 (two) resident's wells around the area where

traders and parking are arranged in Kujon Hamlet, it is known that all measured parameters still meet the threshold values according to Minister of Health Regulation No. 32 of 2017 concerning Environmental Health Quality Standards and Health Requirements for Water for Sanitation Hygiene, Swimming Pools, Solus Per Aqua, and Public Baths, for sanitary hygiene purposes (Erlinawati et al. 2021). The parameter that almost reaches the threshold value is the total coliform measured at location AB-2 (south of the location), which is 49 CFU.100 mL<sup>-1</sup>, where the threshold value is 50 CFU.100 mL<sup>-1</sup>. This is possibly due to poor sanitation in the surrounding area, so the well is contaminated with coli bacteria, and it is also possible that the well is close to a source of household waste disposal.

Table 8: Phytoplankton types and amounts discovered.

No.	Types of Organisms (Genera)	Phytoplankton			
		Location B-1		Location B-2	
		sel.L <sup>-1</sup>	%	sel.L <sup>-1</sup>	%
	Bacillariophyceae				
1	<i>Asterionella</i> sp.	170	10.33	70	22.58
2	<i>Bacillaria</i> sp.	10	0.61	25	8.06
3	<i>Fragilaria</i> sp.	20	1.22	25	8.06
4	<i>Navicula</i> sp.	5	0.30	5	1.61
5	<i>Synedra</i> sp.	-		10	3.23
	Chlorophyceae				
6	<i>Pediastrum</i> sp.	215	13.07	-	
7	<i>Tetraedron</i> sp.	10	0.61	-	
	Coccinodiscophyceae				
8	<i>Coccinodiscus</i> sp.	-		5	1.61
9	<i>Melosira</i> sp.	195	11.85	35	11.29
	Cyanophyceae				
10	<i>Aphanizomenon</i> sp.	875	53.19	50	16.13
11	<i>Aphanocapsa</i> sp.	120	7.29	80	25.81
	Euglenophyceae				
12	<i>Trachelomonas</i> sp.	5	0.30	-	
	Trebouxiophyceae				
13	<i>Chlorella</i> sp.	5	0.30	5	1.61
	Zygnematophyceae				
14	<i>Staurastrum</i> sp.	15	0.91	-	
	Abundance (cells/L)	1645	100	310	100
	Taxa (S)	12	1.943	10	
	Diversity (H')	1.491	0.844		
	Equalization (E)	0.600	0.171		
	Domination (D)	0.330			

Description: Sampling location: AP-1 Location: LS: 07°36'11.76" - BT: 110°11'47.11" and LS: 07°36'18.63" - BT: 110°11'46.34"

Table 9: Zooplankton types and amounts discovered.

No	Types of Organisms (Genera)	Zooplankton			
		Location B-1		Location B-2	
		sel.L <sup>-1</sup>	%	sel.L <sup>-1</sup>	%
1	IMBRICATEA				
	Trinema sp.	10	40	-	
2	TUBULINEA				
	Arcella sp.	10	40	10	50
3	Centropyxis sp.	-		5	25
4	Diffugia sp.	5	20	5	25
	Abundance (cells/L)	25	100	20	100
	Taksa (S)	3		3	
	Diversity (H')	1.055		1.040	
	Equalization (E)	0.960		0.946	
	Domination (D)	0.360		0.375	

Sampling location: Location AP-1: Water body west of the planned activity location; LS: 07°36'11.76" - BT: 110°11'47.11" and Location AP-2: Water body south of the planned activity location; S: 07°36'18.63" - E: 110°11'46.34"

## Plankton

Plankton is a heterogeneous group of microorganisms consisting of plants and animals, very small in size and microscopic in nature, living floating in water, moving passively, and whose movements are strongly influenced by water movements or waves. Water quality can be determined by looking at the presence of plankton. The more plankton species that live in a body of water shows that the quality of the water is still good. To determine the condition of the composition, abundance, and diversity of plankton types found in the water bodies around the research location (planned activities for structuring the trading and parking areas of Kujon Hamlet, Borobudur Village). Plankton samples were taken at 2 (two) points at the same location as surface water quality measurements, namely water bodies to the west and south of the planned activity location. Sample collection and analysis were carried out by the Environmental Quality Testing Laboratory. The types and amounts of plankton and zooplankton found are presented in Tables 8 and 9 respectively.

Otene et al. (2023), plankton species diversity index value, criteria for the quality of the aquatic environment can be categorized as shown in Table 10 (Otene et al. 2023).

Based on the data above, it can be seen that the plankton diversity index value ranges between 1.040 to 1.943, so it is included in the medium category. The condition of the water body at the research location according to environmental quality criteria based on the plankton diversity index is included in the moderately polluted category.

## Benthos

Benthos are organisms, whether sessile, crawling, or burrowing, that reside at the bottom of the sea (substrate). Benthos can be found in dead or broken coral, dirt, rocks, or sand. Many organic compounds have a major impact on their occurrence in water. Similar to the presence of plankton, benthos can likewise be utilized as an aquatic bioindicator. When estimating imbalances in the biological, chemical, and physical environments of waterways, benthos is frequently utilized. Polluted waters will affect the survival of aquatic organisms, including macrozoobenthos, because macrozoobenthos are aquatic organisms that have been affected by pollutants, both chemical and physical (Rahayu & Fanni 2022), to determine the condition of the composition, abundance, and diversity of benthos types found in the bottom substrate of water bodies around the location of planned activities for structuring the trading and parking areas of Kujon Hamlet, Borobudur Village. Benthos samples were taken at two points at the same location as surface water quality measurements, namely water bodies to the west and south of the planned activity location. Sample collection and analysis were carried out by the Environmental Quality

Table 10: The plankton diversity index is the basis for the environmental quality criteria (Hossain et al. 2017).

Diversity Index Value Plankton	Category	Water Conditions
$H \geq 3$	High	Not polluted
$1 < H < 3$	Medium	Moderately polluted
$H \leq 1$	Low	Heavily polluted

Table 11: Types and numbers benthos.

No	Types of Organisms (Genera)	Macrozoobenthos			
		Location B-1		Location B-1	
		Ind.m <sup>-2</sup>	%	Ind.m <sup>-2</sup>	%
	INSECTA				
	Chironomus sp.	57	25	114	66.67
	Tanytarsus sp.	171	75	57	33.33
	Kelimpahan [ind.m <sup>-2</sup> ]	228	100	171	100
	Taksa (S)	2		2	
	Diversity (H')	0.811		0.918	
	Evenness (E)	0.811		0.918	
	Dominance (D)	0.625		0.556	

Information:

Sampling location: Location AP-1: Water body west of the planned activity location; LS: 07°36'11.76" - BT: 110°11'47.11" and Location AP-2: Water body south of the planned activity location; S: 07°36'18.63" - E: 110°11'46.34"

Table 12: Environmental quality criteria based on the Benthos Diversity Index (Ni et al. 2019).

Benthos Diversity Index Value	Category	Water Conditions
$H \geq 2,0$	Very high	Not polluted
$1,6 < H < 2,0$	High	Lightly polluted
$1 < H < 1,6$	Medium	Moderately polluted
$H \leq 1$	Low	Heavily Polluted

Testing Laboratory. The types and amounts of benthos found in the study area are presented in Table 11.

Aquatic environmental quality criteria can be grouped based on plankton and benthos species diversity index values according to Ni et al. (2019), as presented in Table 12.

The benthos diversity index values of 0.811 and 0.918 indicate that only two benthos species were discovered, placing them in the low group according to the previously mentioned statistics. Based on benthos diversity index-based environmental quality criteria, the research location's water body is classified as extremely polluted.

## CONCLUSION

The waste processing site that will be implemented at the research location follows the waste management site - reduce-reuse-recycle (TPS3R) concept. This effort is expected to reduce the burden of waste processing at temporary waste storage areas (TPS) and integrated waste processing sites (TPST) in the study area. The waste processing installation system is planned to use a biofilter septic tank. Management of wastes in compliance with the technical guidelines for toxic and hazardous waste management specified in Minister of Environment and Forestry Regulation No. 3/2021, toxic

and hazardous trash will be gathered at certain sites in the temporary storage facility with a room space of 8 m<sup>2</sup>.

**Surface Water Quality:** The BOD findings at the AP-2 sample point, with BOD results = 3 in the class 2 category, were determined to be in close proximity to the quality standard limit, according to the study of surface water.

**Ground Water Quality:** All measured parameters continue to fall below the threshold levels specified by Minister of Health Regulation No. 32 of 2017, based on data from the assessment of the groundwater quality in two (two) residents' wells. The whole coliform measured at the AB-2 sampling point, 49 CFU.100 mL<sup>-1</sup> (Quality Standard = 50 CFU. 100 mL<sup>-1</sup>), is the metric that nearly reaches the threshold value.

**Plankton:** The data above shows that the plankton diversity index value is in the medium range, namely between 1.040 and 1.943. The waters at the research location are included in the moderately polluted category based on environmental quality standards. **Benthos:** The condition of benthos at the research location for Benthos diversity was 0.811 and 0.918 (< 1 lightly polluted)

## ACKNOWLEDGMENTS

The author is very grateful to the management of PT Taman Wisata Candi Borobudur Prambanan Ratu Boko (Persero) and Environmental Consultant PT. Mitra Adi Pranata so that this research can run well.

## REFERENCES

- Ahmed, A.S.S., Rahman, M.M., Hasan, M.T., Habibullah-Al-Mamun, M., Islam, M.S. and Hossain, M.B., 2019. Bioaccumulation and heavy metal concentration in tissues of some commercial fishes from the Meghna River Estuary in Bangladesh and human health implications. *Marine Pollution Bulletin*, 145, pp.436-447.
- Akhtar, N., Ishak, M.I.S., Bhawani, S.A. and Umar, K., 2021. Various natural and anthropogenic factors responsible for water quality degradation: A review. *Water*, 13(19), p.2660.
- Arum, S.P.I., Harisuseno, D. and Soemarno, S., 2019. Domestic wastewater contribution to the water quality of Brantas River at Dinoyo Urban Village, Malang City. *Indonesian Journal of Environment and Sustainable Development*, 10(2), p. 641-666.
- Astuti, D., Mayra, A., Larasati, E. and Arifin, H.A., 2020. Analysis of the impact of leachate on the quality of groundwater and river water in Putri Cempo Landfill in Mojosoong Surakarta, Indonesia. *International Journal of Multi-Science*, 1(04), pp.69-86.
- Aziz, R., 2019. Study of recycling potential of solid waste of tourist area in Pariaman City. *IOP Conference Series: Materials Science and Engineering*, 452, p.12059.
- Barakazi, M., 2023. Unsustainable tourism approaches in touristic destinations: A case study in Turkey. *Sustainability*, 15(6), p.4744.
- Bravi, L., Santos, G., Pagano, A. and Murmura, F., 2020. Environmental management system according to ISO 14001: 2015 as a driver to sustainable development. *Corporate Social Responsibility and Environmental Management*, 27(6), pp.2599-2614.
- Budihardjo, M.A., Sutrisno, B.Z.E., Ramadan, B.S. and Arumdani, I.S.,

2023. Hazardous and toxic waste management scenario from the domestic and office sectors in Semarang City. *Journal of Sustainable Science and Management*, 18(2), pp.1-14.
- Butar-Butar, E.S., Priantoro, E.A. and Sembiring, T., 2020. Potential of organic waste from Caringin central market as raw material for biogas and compost. *IOP Conference Series: Earth and Environmental Science*, 12019.
- Cahyadi, T.A., Apriyanti, D. and Susanti, H., 2023. Water quality assessment based on government regulation standards in Sangkalami River, North Kalimantan, Indonesia. *IOP Conference Series: Earth and Environmental Science*, 12020.
- Da Silva, F.J.A., Lima, M.G.S., Mendonça, L.A.R. and Gomes, M.J.T.L., 2013. Septic tank combined with anaerobic filter and conventional UASB: Results from full scale plants. *Brazilian Journal of Chemical Engineering*, 30, pp.133-140.
- Erlinawati, D., Wibisana, M.R., Putra, D.P.E. and Titisari, A.D., 2021. Analysis of water quality of springs on the east slope of Mount Sumbing, Central Java, Indonesia, for sanitation hygiene purposes based on the physical and chemical properties. *IOP Conference Series: Earth and Environmental Science*, 12013.
- Ernawaty, E., 2018. *Implementation of Law Number 18 Year 2008 Regarding Waste Management*. Universitas Riau.
- Heidari, R., Yazdanparast, R. and Jabbarzadeh, A., 2019. Sustainable design of a municipal solid waste management system considering waste separators: A real-world application. *Sustainable Cities and Society*, 47, p.101457.
- Hossain, M.R.A., Pramanik, M.M.H. and Hasan, M.M., 2017. Diversity indices of plankton communities in the River Meghna of Bangladesh. *International Journal of Fisheries and Aquatic Studies*, 5(3), pp.330-334.
- Karjoko, L., Handayani, I.G.A.K.R., Jaelani, A.K. and Hayat, M.J., 2022. Indonesia's sustainable development goals resolving the waste problem: Informal to a formal policy. *International Journal of Sustainable Development & Planning*, 17(2), pp.83-91.
- Kastolani, W., 2019. Utilization of BSF to reduce organic waste in order to restoration of the Citarum River ecosystem. *IOP Conference Series: Earth and Environmental Science*, 619, p. 12017.
- Khan, N., Hassan, A.U., Fahad, S. and Naushad, M., 2020. Factors affecting the tourism industry and its impacts on the global economy of the world. *SSRN*, 35, 593-603.
- Lusiana, N., Rahadi, B. and Anggita, Y., 2020. Determination of pollution load capacity of Ngrowo River as wastewater receiver from hospital activities. *IOP Conference Series: Earth and Environmental Science*, 12067.
- Ni, D., Zhang, Z. and Liu, X., 2019. Benthic ecological quality assessment of the Bohai Sea, China, using marine biotic indices. *Marine Pollution Bulletin*, 142, pp.457-464.
- Otene, B.B., Thornhill, I. and Amadi, J., 2023. A comparison of the water quality and plankton diversity of the Okamini Stream to the freshwater systems within the New Calabar River catchment, Port Harcourt, Nigeria. *African Journal of Aquatic Science*, 48(1), pp.97-104.
- Perdana, A.S., 2023. Plastic waste management education through the waste management unit (UPS) in Borobudur Village. *Research Journal on Teacher Professional Development*, 1(2), p. 72.
- Purwaningsih, R., Rahmawati, I., Saputra, M., Kurniawan, H. and Muhaimin, T., 2021. Sustainability status assessment of the Borobudur Temple using the Rap-Tourism with multi-dimensional scaling (MDS) approach. *E3S Web of Conferences*, 5004.
- Putri, M., Azza, T., Wimbaningrum, R. and Setiawan, R., 2019. Diversity of dragonfly species belonging to the order Odonata in the rice fields of Summersari District, Jemb Regency. *Bioma: Jurnal Ilmiah Biologi*, 8(1), pp.324-336.
- Quilley, S. and Kish, K., 2019. *The Ecological Limits of the Sustainable Development Goals*. Routledge, pp.170-189.
- Rahayu, A.P. and Fanni, N.A., 2022. Study of Macrozoobentos diversity in the secondary flow of the Bengawan solo river, Tunjungmekar village, Kalitengah District, Lamongan Regency. *Environmental Sciences*, 6(1), pp.22-28.
- Scolaro, E., 2016. *Nationalism and Cultural Heritage in Indonesia: A Local Study of Borobudur Temple*. The Ohio State University, Ohio.
- Soeprubowati, R.T., Jumari, J., Wasiq Hidayat, J., Muhammad, F., Hanif Al Falah, M., Kadek Dita Cahyani, N. and Gell, P., 2023. Water quality status of mangrove ecosystem in Bedono, Sayung, Demak, Central Java. *Pollution*, 9(4), pp.1374-1385.
- Sonawane, J.M., Ezugwu, C.I. and Ghosh, P.C., 2020. Microbial fuel cell-based biological oxygen demand sensors for monitoring wastewater: State-of-the-art and practical applications. *ACS sensors*, 5(8), pp.2297-2316.
- Strayer, D.L., 2003. Classification of ecological boundaries. *BioScience*, 53(8), pp.723-729.
- Susanto, A., 2023. Identification and management of toxic & hazardous wastes (waste) based on the Indonesian Government Regulation Number 22 of 2021. *IOP Conference Series: Earth and Environmental Science*, 1241, p.12023.
- Susilo, Y.S. and Suroso, A., 2015. Integrated management of Borobudur World Heritage Site: A conflict resolution effort. *Asia Pacific Management and Business Application*, 3(2), pp.116-134.
- Vindriani, E., Sofiyah, E. and Zahra, N., 2023. Domestic wastewater treatment units design in the coastal area with high groundwater level: A case study in Cilincing District. *Proceedings of the International Conference on Sustainable Engineering, Infrastructure and Development, ICO-SEID 2022, 23-24 November 2022, Jakarta, Indonesia*.
- Widodo, A. and Hossain, M.B., 2022. The reconstruction of legal policies for the management and control of environmental impacts for industrial areas in urban Central Java. *International Journal of Law Reconstruction*, 6(2), pp.241-256.
- Widyarsana, I.M.W. and Salmaa, K., 2019. Evaluation of Waste Management Achievement in Padangtegal Pekraman Village, Ubud Sub District, Gianyar Regency, Bali. *IOP Conference Series: Earth and Environmental Science*, 12029.
- Yunita, R., 2023. River Waste Management Education Program in the Regency of Semarang. *Waste Management*, 15, pp. 508-519.

---

#### ORCID DETAILS OF THE AUTHORS

Slamet Isworo: <https://orcid.org/0000-0001-6332-4713>





# Integrating Satellite Data and *In-situ* Observations for Trophic State Assessment of Renuka Lake, Himachal Pradesh, India

Sujit Kumar Jally<sup>1†</sup> , Rakesh Kumar<sup>2</sup> and Sibabrata Das<sup>3</sup>

<sup>1</sup>School of Geography, Gangadhar Meher University, Sambalpur, Odisha, India

<sup>2</sup>Indian Council of Forestry Research and Education, Dehradun, India

<sup>3</sup>Department of Geography, Ravenshaw University, Cuttack, Odisha, India

†Corresponding author: Sujit Kumar Jally; [sujit.graphy@gmail.com](mailto:sujit.graphy@gmail.com)

Nat. Env. & Poll. Tech.  
Website: [www.neptjournal.com](http://www.neptjournal.com)

Received: 23-02-2024

Revised: 28-03-2024

Accepted: 02-04-2024

## Key Words:

LISS-III

Landsat-8 OLI

Renuka Lake

Trophic State Index

## ABSTRACT

The present study focuses on estimating the Trophic State Index (TSI) of Renuka Lake, the smallest Ramsar site in India, utilizing in-situ observed Secchi disk transparency (SDT) and satellite data. Site-specific algorithms were developed by establishing the relationship between the spectral band ratio of Landsat 8 OLI and LISS-III with that of in-situ measured SDT data. Notably, the exponential regression model outperformed other regression models (linear, logarithmic, polynomial, and power), achieving a better model output ( $R^2=0.94$ ). Additionally, water quality parameters, namely pH and dissolved oxygen (DO), were measured using the TROLL 9500 multi-parameter instrument. Various interpolation methods were applied to the in-situ data, with the exponential regression model yielding the most accurate results. This method was subsequently selected to generate two-dimensional water-quality images of Renuka Lake. The combined analysis of in-situ and satellite-derived trophic status indicates the eutrophic to hypereutrophic condition of the lake's eastern and western parts. Satellite imagery spanning 2010-2019 consistently reveals a eutrophic state in the lake, with fluctuations in intensity over the period. The sustained eutrophic condition is attributed to escalating human-induced activities surrounding the lake, particularly in the western region.

## INTRODUCTION

The Himalayan lakes hold unique significance as self-sustaining entities supporting harmonious freshwater ecosystems, vital for promoting aquatic biodiversity. Lake water, an indispensable natural resource for both human populations and their environments, faces global degradation due to natural processes and escalating human-induced activities (Brönmark & Hansson 2002, Mishra & Garg 2011). This degradation of lake water quality stands as a pressing global water issue, especially given the lakes' pivotal role as lifelines for both humans and ecosystems (Rast 2009, Mohamed M.F 2015, Gholizadeh et al. 2016, Sent et al. 2021). The increasing trophic status of lakes serves as an indicator of this degradation, as highlighted in existing literature, attributing it to factors such as organic and inorganic pollution, siltation, eutrophication, morphological changes, and the impact of climate change, notably manifested through rising water temperatures (Brönmark & Hansson 2002, Dudgeon et al. 2006, Mabwoga et al. 2010, Mishra & Garg 2011, Torbick et al. 2013).

The quality of water not only influences the development of organisms but also determines their survival. Therefore, it is crucial to assess the lake's health through water quality measurements. Various monitoring methods are employed for a comprehensive study to fully understand the lake's water quality and ecosystem (Hestir et al. 2015, van Puijenbroek et al. 2015, Bresciani et al. 2019, Bonansea et al. 2019, Cahalane et al. 2019, Torres-Bejarano et al. 2020). The assessment of trophic states of lakes through in-situ measurements has long been a cornerstone of limnological research. Studies by Carlson (1977) and Vollenweider (1968) laid the foundation for this approach, emphasizing the relevance of key parameters such as chlorophyll-a, total phosphorus, and Secchi disk transparency. The Secchi disk transparency test, introduced by Carlson (1977), emerged as a fundamental tool in categorizing lakes into trophic states. This method involves lowering a white disk into the water until it disappears, providing a measure of water clarity.

While in-situ methods are crucial for understanding the ecological dynamics of lakes, they come with inherent limitations. One major constraint lies in the spatial coverage,

as in-situ measurements are often point-specific and labor-intensive. The challenge of extrapolating localized data to represent entire lake ecosystems is acknowledged by Hestir et al. (2015). Additionally, the temporal resolution of in-situ observations may not capture short-term fluctuations in trophic conditions, as noted by Bresciani et al. (2019) and Bonansea et al. (2019). Despite these limitations, the wealth of information obtained through in-situ measurements remains invaluable for validating satellite-derived algorithms and enhancing the overall accuracy of trophic state assessments. In recent years, the use of satellite-based observations alongside traditional in-situ methods has emerged as a powerful approach for studying the trophic states of lakes. This integrated methodology offers a comprehensive understanding of water quality dynamics.

Numerous studies have recognized the limitations of relying solely on in-situ data and have explored the potential of satellite observations to bridge gaps in lake monitoring. Remote sensing applications have proven effective in both terrestrial and aquatic ecosystem monitoring (Andrew et al. 2014, Walshe et al. 2014, de Araujo Barbosa et al. 2015). Optical satellite data is used to monitor water quality indicators, including trophic status, suspended sediment concentration, turbidity, and chlorophyll content. Various studies have utilized different band ratios of satellite data (Landsat TM, Landsat ETM, Landsat-8 OLI, LISS-III, SeaWiFS, MERIS, MODIS, Sentinel-2A, NOAA AVHRR) to assess water quality, with the Landsat series data being particularly successful globally due to its spatial, temporal, spectral resolution, and cost-effectiveness in water quality assessment (Khorram & Cheshire 1985, Harrington et al. 1989, Koponen et al. 2002, Wang et al. 2004, Usali & Ismail 2010, Bilgehan et al. 2010, Mishra & Garg 2011, Palmer et al. 2015). Satellite data offers a synoptic perspective and spatiotemporal coverage over wider areas, providing features unattainable during ground truth observations.

The significance of this study lies in its approach to assessing the trophic state of Renuka Lake, the smallest Ramsar site in India, by integrating satellite-based observations with traditional in-situ methods. Several studies have contributed to understanding Renuka Lake's limnology. Previous works by Das & Kaur (2001) and Das et al. (2008) explored major ion chemistry and geochemistry, providing insights into weathering processes affecting the lake's trophic state. Subsequent studies by Singh & Sharma (2012) and Kumar et al. (2019) focused on trophic status assessment, contributing valuable information on local ecological dynamics. However, these studies relied solely on traditional in-situ methods to explore the trophic condition of Renuka Lake. Unlike these predecessors, our study is novel and unique as it employs advanced satellite-

based observations, a methodology successfully used in various lake studies but not yet applied to Renuka Lake, the smallest Ramsar lake site. By combining satellite technology with in-situ observations, our research aims to provide a more comprehensive understanding of Renuka Lake's trophic state. This innovative approach not only adds a new dimension to the current understanding of the lake's dynamics but also addresses a significant research gap in the monitoring and assessment methodologies applied to the unique ecological setting of Renuka Lake. The integration of satellite-based observations is expected to enhance the precision and scope of trophic state assessments, ultimately contributing to more effective conservation and management strategies for this ecologically vital Ramsar site.

## MATERIALS AND METHODS

### Study Area

Renuka Lake is an oval-shaped lake situated in the foothills of the Lesser Himalaya, with geographical coordinates between 30°36'30" N latitude and 77°27'6" E longitude in the Sirmaur district of Himachal Pradesh (Fig. 1). The lake is 204 m wide, 1.05 m long, and 13 m deep, with a catchment area of 254.3 hectares. The subtropical climate of the lake area receives an annual rainfall of 150 to 199.9 cm (Das & Kaur 2001). The lake is surrounded by Lesser Himalayan rocks (Das et al. 2008) and flows along a riparian path between two forested, steep hill slopes. Renuka Lake is connected to Parashram Tal through a narrow channel, both located along the course of the Giri River. The majority of the lake's water is sourced from small watersheds, collected as surface runoff or groundwater seepage. The lake continuously discharges water to low-lying areas through Parshuram Taal. Declared a Ramsar site and protected as a National Wetland on 8th November 2005, the lake hosts rare, endangered plant and animal species, attracting large populations of avifauna during winter from Siberia and Eastern Europe. A popular tourist attraction in Himachal Pradesh, the lake's natural beauty, boating facility, and abundant wildlife draw thousands of visitors annually. The lake is a socio-economic lifeline for the mountain people directly or indirectly dependent on its resources. The Wildlife Wing of the Himachal Pradesh Forest Department implements various development programs to safeguard the lake ecosystem and monitor its condition through water quality evaluation.

### Satellite Data Collection and Processing

One critical aspect of the satellite and field data-based integrated approach lies in the selection of suitable satellite platforms and sensors. This study utilized remotely sensed satellite imagery from Landsat-8 OLI for 2013-2020 and



LISS-III for the 2010-2012 period. Cloud-free continuous data was available for the post-monsoon season only, so only data of this season (October to December) has been used and analyzed. The Landsat-8 OLI data is chosen in this study due to its improved sensor features over the previous Landsat series. The Resourcesat-2 LISS-III and Landsat-8 OLI (Operational Land Imager) satellite data are obtained from the National Remote Sensing Centre (NRSC), Hyderabad, India, and the USGS Earth Explorer site (USGS Earth Explorer 2023), respectively. The integration of satellite data with in-situ observations requires careful consideration of atmospheric correction and image pre-processing to ensure reliable results. The spectral image processing and analysis were conducted using ERDAS Imagine software. The Landsat-8 OLI radiance image was obtained using equation 1 (USGS 2023), and similarly, the Resourcesat-2 LISS-III radiance image was obtained using equation 2 (Robinove 1982).

$$L = M \times Q_{CAL} + A \quad \dots(1)$$

Where,

$L$  = cell value as radiance

$M$  = multiplicative factor in  $(W/m^2sr*\mu m)/DN$

$A$  = the additive factor in  $(W/m^2sr*\mu m)$

$Q_{cal}$  = quantized and calibrated standard pixel values (DN)

$$L_{\lambda} = (D_n/D_{max}) * (L_{max}-L_{min}) + L_{min} \quad \dots(2)$$

$L_{\lambda}$  = radiance in a single band

$D_n$  = digital value of a pixel

$D_{max}$  = maximum digital number

$L_{max}$  = maximum radiance measured at detector saturation in  $(mW\ cm^{-2}\ sr^{-1})$

$L_{min}$  = minimum radiance measured at detector saturation in  $(mW\ cm^{-2}\ sr^{-1})$

**In-Situ Data Collection**

For in-situ data collection, field observation data, including

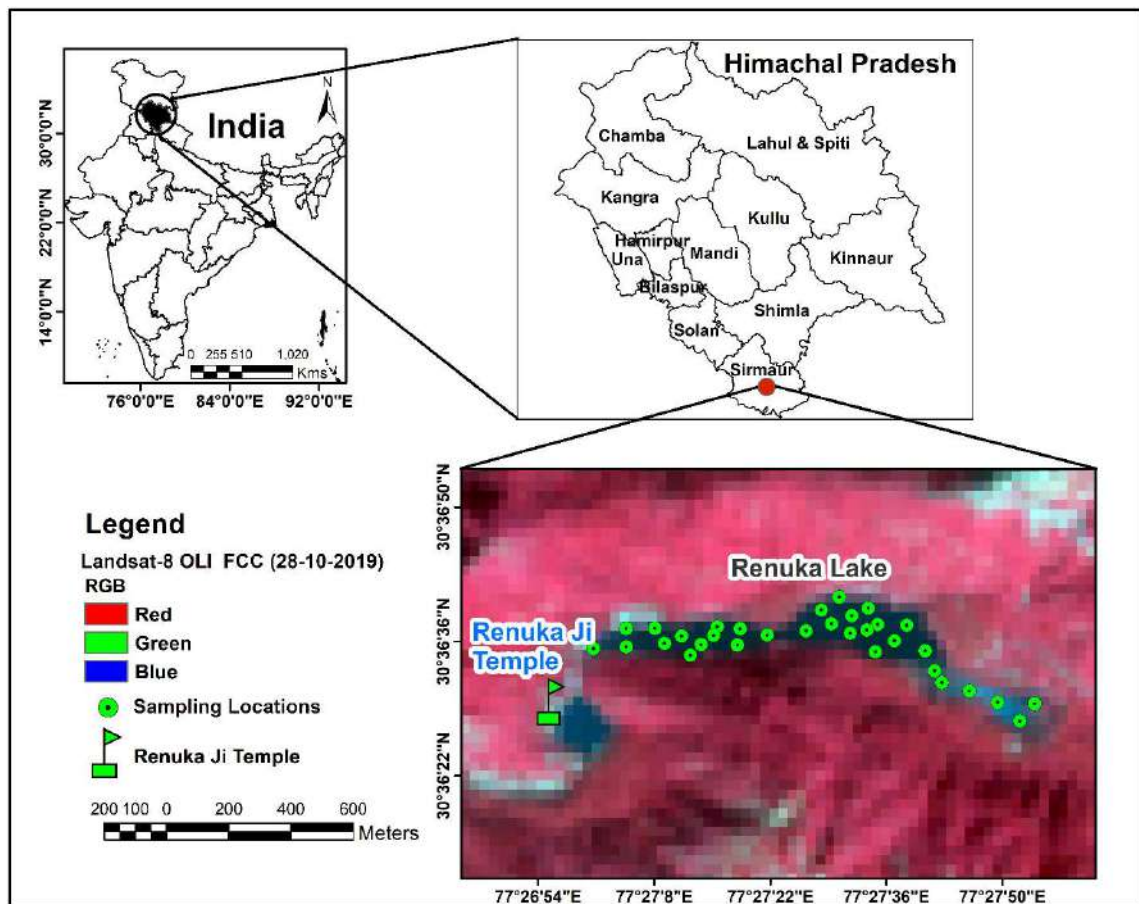


Fig. 1: Landsat-8 OLI satellite map showing water sampling locations in the Renuka Lake.

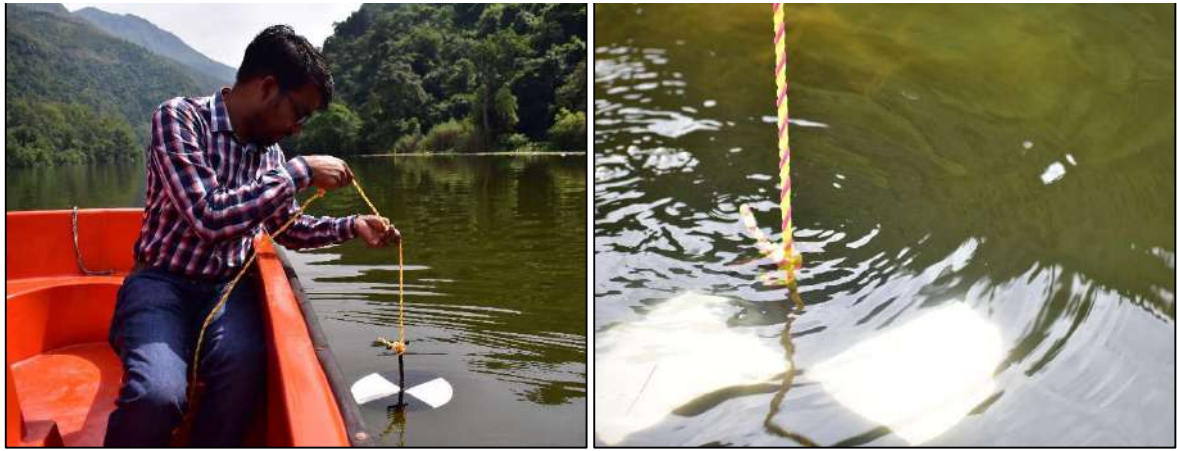


Fig. 2: Use of Secchi disk in the Renuka Lake.

Table 1: *In-situ* data collected over Renuka Lake on 28 October 2019.

Station	Latitude	Longitude	SDT[m]	pH	DO (Dissolved Oxygen)	Time
1	30.60972	77.45027	0.98	7.12	7.42	7.30 a.m
2	30.60975	77.45138	1.24	7.38	7.49	7.37 a.m
3	30.61028	77.45139	1.50	7.31	7.58	7.43 a.m
4	30.61028	77.45444	1.30	7.21	7.62	7.52 a.m
5	30.61000	77.45611	1.42	8.11	9.87	7.58 a.m
6	30.61000	77.45889	1.32	7.63	8.26	8.05 a.m
7	30.60944	77.45972	1.30	8.82	9.47	8.13 a.m
8	30.60944	77.46139	1.10	8.11	8.01	8.21 a.m
9	30.60982	77.45266	1.40	8.01	9.47	8.32 a.m
10	30.60976	77.45389	1.33	7.32	10.57	8.41 a.m
11	30.60973	77.45511	1.21	7.63	9.89	8.49 a.m
12	30.61010	77.45741	1.40	8.53	8.32	8.57 a.m
13	30.61069	77.45795	1.21	7.48	8.12	9.08 a.m
14	30.61029	77.45827	1.05	7.43	8.35	9.17 a.m
15	30.61050	77.45896	1.23	7.13	6.68	9.26 a.m
16	30.61024	77.45982	1.50	6.98	8.92	9.35 a.m
17	30.61019	77.46079	1.32	7.84	9.89	9.44 a.m
18	30.60975	77.46036	1.43	7.49	10.34	9.55 a.m
19	30.60851	77.46192	1.34	7.30	6.99	10.05 a.m
20	30.60790	77.46379	1.50	7.27	7.56	10.14 a.m
21	30.60784	77.46503	1.31	7.23	7.49	10.23 a.m
22	30.60735	77.46451	1.30	7.09	6.53	10.32 a.m
23	30.61027	77.45235	1.32	7.65	8.32	10.41 a.m
24	30.61002	77.45324	1.30	7.96	7.69	10.50 a.m
25	30.61002	77.45431	1.40	7.34	9.74	11.00 a.m
26	30.61021	77.45521	1.20	7.39	8.14	11.09 a.m
27	30.61071	77.45952	1.31	7.05	6.87	11.20 a.m
28	30.61008	77.45945	1.40	7.41	6.67	11.29 a.m
29	30.60886	77.46169	0.96	7.16	7.56	11.38 a.m
30	30.60947	77.45352	1.30	7.89	10.32	11.47 a.m
31	30.60825	77.46285	1.02	7.21	7.40	11.54 a.m
32	30.61105	77.45855	0.93	7.11	7.31	11.59 a.m

Secchi disk transparency (SDT), pH, and dissolved oxygen (DO), were collected during the post-monsoon season of 2019 at 32 sampling locations across Renuka Lake (Table 1). Secchi disk transparency (SDT) analysis is a simple and cost-effective method for identifying the best indicator for water quality. The Secchi disk, a black and white round metal disk with an approximate diameter of 20 cm, was employed for this purpose. While it was lowered into the lake's water through a calibrated rope, the disk was gradually submerged until it became invisible, marking the Secchi disk transparency (SDT) at that specific depth (Fig. 2). The *in-situ* collected SDT data of Renuka Lake was used to calculate its Trophic State Index (TSI), which classifies lake water into four categories: (1) oligotrophic (clean and nutrient-poor), (2) mesotrophic (good clarity, moderate nutrient content), (3) eutrophic (turbid water, increased nutrient content), and (4) hypereutrophic (extremely nutrient-enriched water) (Carlson 1977). The TSI of sampling locations derived from Secchi disk transparency (SDT) data was further used for estimating the trophic state of the entire lake by developing a regression model with satellite data spectral bands. The pH and DO data collected through TROLL 9500 (a multi-parameter water quality measuring instrument) were used as two additional data to supplement and validate the satellite-derived TSI of the lake.

## Methodology

The objective of the study was to assess the trophic status of Renuka Lake using both field observations and satellite data. Therefore, both satellite and ground truth observation data were integrated to assess the trophic state of the lake. The Secchi disk is widely used by lake management experts for monitoring lake water quality. Numerous organizations and institutions are actively researching these issues to improve water quality, identify challenges, and implement sustainable development plans through systematic monitoring efforts (Vörösmarty et al. 2010, Gray & Shimshack 2011, Torbick et al. 2013, Birk et al. 2012, Birk & Ecke 2014, Lim et al. 2015). Monitoring lake transparency is vital for lake ecology, and the trophic state index (TSI) serves as an essential factor in this assessment. The relationship between SDT and TSI has been extensively used by researchers for lake water quality assessment (Carlson 1977, Paukert & Willis 2003, Bio et al. 2008, Mabwoga et al. 2010, Mishra & Garg 2011, Sheela et al. 2011, Torbick et al. 2013, Gholizadeh et al. 2016, Bonansea et al. 2019, Bresciani et al. 2019, Sent et al. 2021). Equation 3 demonstrates this relationship:

$$TSI(SDT) = 10(6 - \ln SDT / \ln 2) \quad \dots(3)$$

Both *in-situ* observations and satellite data were utilized for TSI estimation, with *in-situ* data collected during the

Table 2: Lake Trophic State and Carlson TSI.

Lake Trophic State	Carlson TSI
Oligotrophic	<38
Mesotrophic	38-48
Eutrophic	49-61
Hyper eutrophic	>61

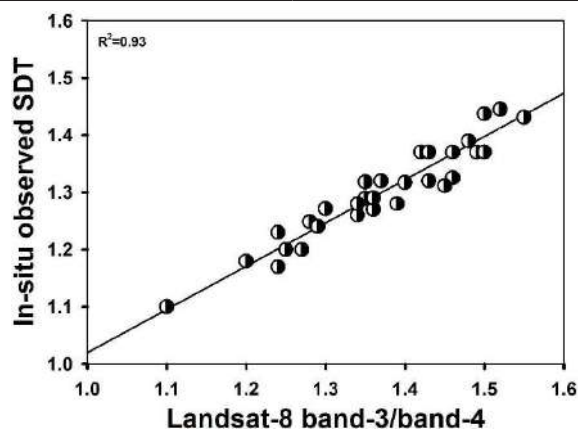


Fig. 3: Scatter plot showing relationship between the *in-situ* observed SDT and band ratio of Landsat-8 OLI band-3/band-4.

post-monsoon season. The lake water is categorized into four classes based on the TSI range, as shown in Table 2 (Fuller & Minnerick 2007). In this study, an algorithm using Landsat-8 OLI radiance data was developed to predict the SDT of Renuka Lake. Field data collection was synchronized with Landsat-8 OLI passes. Fig. 3 illustrates the correlation between SDT and the ratio of Landsat-8 OLI bands (OLI-3:OLI-4). Various regression models (linear, exponential, logarithmic, polynomial, and power) were applied in the statistical analysis. Among these models, the exponential regression model yielded the best result ( $R^2=0.94$ ), as shown in Equation 4:

$$SDT = 0.5869 \exp^{0.5783(OLI3/OLI4)} \quad \dots(4)$$

The Landsat-8 OLI bands 3 and 4 spectral wavelength ranges are similar to LISS-III (Linear Imaging Self Scanning) bands 2 and 3. Therefore, using LISS-III satellite data, Equation (4) can be applied to monitor Secchi disk transparency. For the period before 2013, LISS-III data were employed for SDT quantification in the absence of Landsat-8 OLI data.

In this study, ground-observed data were interpolated to create two-dimensional images. Various interpolation approaches (Table 3) were tested, and the most effective one was selected. Eleven randomly selected points were used to assess both the absolute difference (AD) and the absolute percentage difference (APD) to determine the agreement between the observed and interpolated values. The AD and

APD values were calculated using Equations 5 and 6 (Melin et al. 2007):

$$AD = (1/N) \sum_{i=1}^{i=N} (ly_i - x_i) \quad \dots(5)$$

$$AD = 100 * (1/N) \sum_{i=1}^{i=N} \frac{(ly_i - x_i)}{x_i} \quad \dots(6)$$

Where  $x$  represents the observed value,  $y$  is the interpolated value, and  $N$  is the number of points. Satellite data were employed to monitor the trophic status of the lake during the post-monsoon season from 2010 to 2019.

## RESULTS AND DISCUSSION

The primary objective of this study was to monitor the trophic status of the lake using satellite data. Measurements of Secchi disk transparency (SDT), dissolved oxygen (DO), and pH were conducted during the post-monsoon season of 2019. DO, and pH are crucial water quality metrics routinely monitored to assess the health condition of water bodies (Boavida & Marques 1996, Mullins & Whisenant 2004, Parinet et al. 2004, Nayak et al. 2004, Riduan et al. 2009, Azary et al. 2010, Sharma et al. 2010). The field data were meticulously analyzed and processed using SURFER software. A concerted effort was made to identify the optimal interpolation method, and the statistical outcomes comparing various techniques are presented in Table 3. The optimal interpolation method was determined by assessing how well the interpolated values align with in-situ observations. The

evaluation, based on in-situ observed SDT, is graphically represented in Fig. 4(a-k). Statistical comparisons of the absolute differences (AD) and absolute percentage differences (APD) between measured and extrapolated values at selected sites are detailed in Table 3. Upon an overall examination of shape and interpolated value range, the Kriging interpolation method emerged as the most effective. The AD and APD values of Kriging closely align with inverse distance to power, natural neighbor, and modified Shephard's method. However, values for inverse distance to power and modified Shephard's method fall outside the acceptable range, and the natural neighbor method produces an out-of-shape image, along with other approaches. Consequently, the Kriging interpolation method is employed for extrapolating field data in the present research.

The dissolved oxygen (DO) and pH of water bodies exert a significant influence on the spatial and seasonal distribution of aquatic species, particularly fish. These parameters have direct or indirect effects on various crucial limnological characteristics, encompassing clarity, viscosity, total dissolved solids, and conductivity (Whitney 1942, Araoye 2009). pH, a critical parameter of water bodies, supports aquatic life within a specific range conducive to optimal growth and survival. Although every aquatic species exhibits a preferred pH range, the majority favor a pH range of 6.5 to 9.0 (US EPA 1986). Deviations from this range induce physiological stress, and extreme pH levels can lead to severe consequences, including mortality. The concentration of dissolved oxygen (DO) in a water body serves as a key indicator for biological livelihood and is essential for water quality assessment. Oxygen depletion negatively affects aquatic life, influencing their growth. Analyzing oxygen levels is crucial for understanding the health of aquatic ecosystems, revealing the extent to which water has been contaminated, lost organic substances, and undergone self-purification (Chapman & Kimstach 1996). As a result, measuring the DO of a water body is crucial for determining water quality because oxygen is involved in or influences virtually all chemical and biological processes. The significance of DO in the aquatic ecosystem has been examined by numerous researchers (Walker 1979, Carr & Neary 2006, Ashraf et al. 2010, Saluja & Garg 2017). It is noteworthy that this study does not intend to estimate additional water quality parameters, such as Total Suspended Matter (TSM), Chlorophyll, and Nutrients. Consequently, the analysis is confined to selected water quality parameters, and the kriging method is employed to create in-situ observed interpolated images of DO, pH, SDT, and Trophic State Index (TSI), as illustrated in Fig.5 (a-d). A detailed analysis of these water quality parameters is described below.

Table 3: The different interpolation methods and values of AD and APD derived from the observed and interpolated values of SDT.

Sl. No.	Methods	AD	APD
(a)	Kriging	0.018873545	1.443803073
(b)	Inverse distance to power	0.027220545	2.329114213
(c)	Minimum curvature	0.033879364	2.743505355
(d)	Modified Shephards Method	0.019928455	1.569698211
(e)	Natural neighbour	0.024400000	1.913597509
(f)	Nearest neighbor	0.036363636	2.955635274
(g)	Polynomial regression	0.119352727	9.543133332
(h)	Radial basis function	0.035463818	2.725649744
(i)	Triangulation with linear interpolation	0.030948273	2.431568419
(j)	Moving average	0.126437182	10.11023505
(k)	Local polynomial	0.085441273	6.639062398

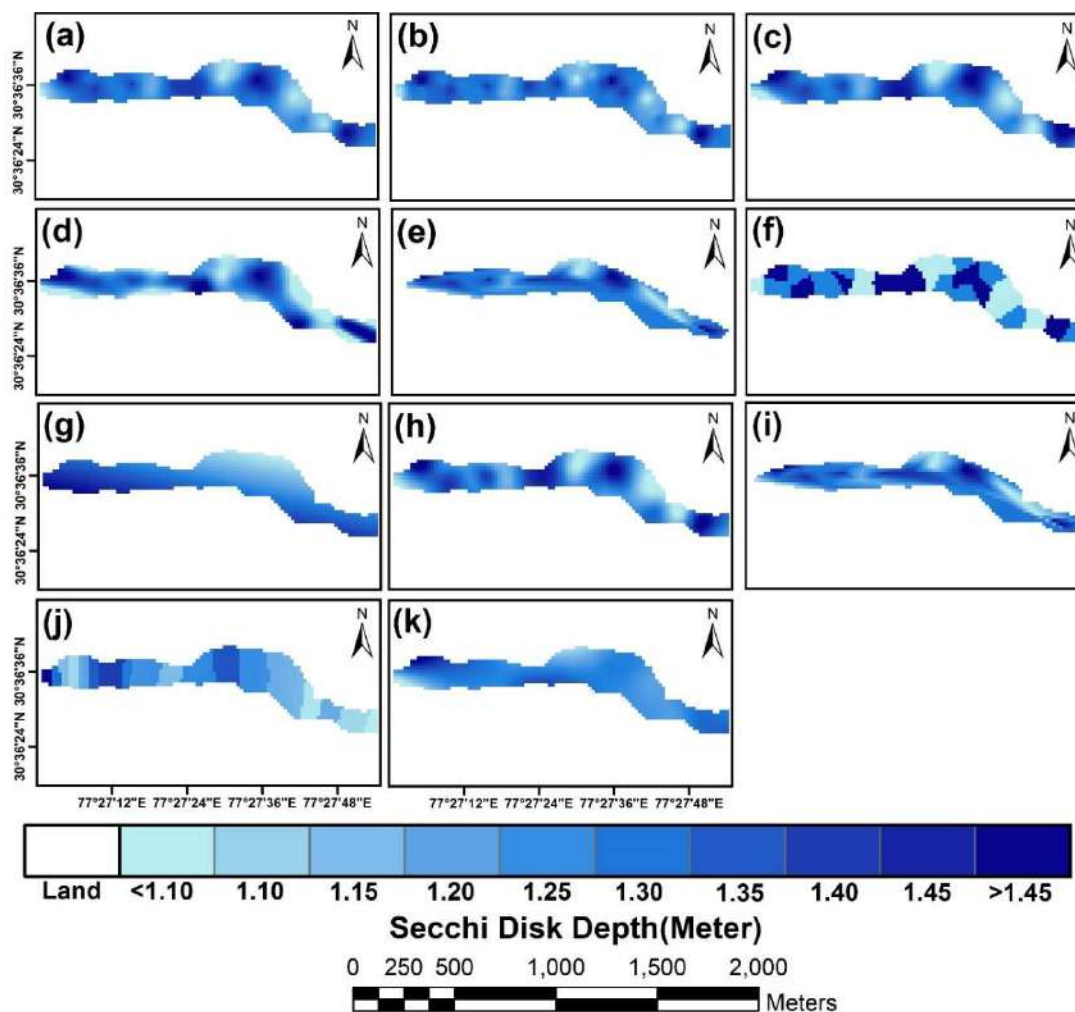


Fig. 4: The interpolated images of in-situ Secchi disk transparency data: (a) Kriging, (b) Inverse distance to power, (c) Minimum curvature Method, (d) Modified shepherds Method, (e) Natural Neighbor, (f) Nearest Neighbor, (g) Polynomial regression, (h) Radial Basis Function, (i) Triangulation with linear interpolation, (j) Moving Average and (k) Local Polynomial.

Fig. 5(a) depicts varying DO concentrations across different areas of the lake during the post-monsoon season of 2019. Higher DO levels are observed in some pockets of the western part ( $9.47 \text{ mg.L}^{-1}$ ), south-western part ( $10.57 \text{ mg.L}^{-1}$ ), and central part ( $10.34 \text{ mg.L}^{-1}$ ) of the lake, while the lowest DO concentrations are found in the western part ( $7.42 \text{ mg.L}^{-1}$ ), eastern part ( $7.49 \text{ mg.L}^{-1}$ ), and central parts ( $6.87 \text{ mg.L}^{-1}$ ) of the lake. The range of DO values in the present study is from  $6.67$  to  $10.57 \text{ mg.L}^{-1}$ , with an average DO value of approximately  $8.28 \text{ mg/L}$ . The maximum concentration of DO is found in the southwestern part of the lake, attributed to clear water and minimal anthropogenic activity (Singh & Sharma 2012, Gupta et al. 2018, Kumar et al. 2019). Conversely, the minimum DO levels observed in the western, central, and eastern pockets of the lake may

be attributed to weed growth and anthropogenic activities, leading to eutrophic conditions and resulting fish mortality in the lake (Das et al. 2001, 2008).

The pH of water serves as an indicator of its acidity or alkalinity, gauged through the concentration of hydrogen ions ( $\text{H}^+$ ) and hydroxyl ions ( $\text{OH}^-$ ) in water (Dhillon & Mishra, 2013). Our observations reveal that the entire lake water exhibits a slight acidity to alkalinity. Fig. 5(b) illustrates the spatiotemporal pattern of pH concentration across different locations during the post-monsoon season. In this study, the pH of lake water ranged from a maximum of  $8.82$  to a minimum of  $6.98$  in October, aligning closely with previous observations (Singh & Sharma 2012, Kumar et al. 2019). The average pH value during the post-monsoon season was  $7.52$ . Some pockets in the western part ( $7.12$ ), central part ( $6.98$ ),

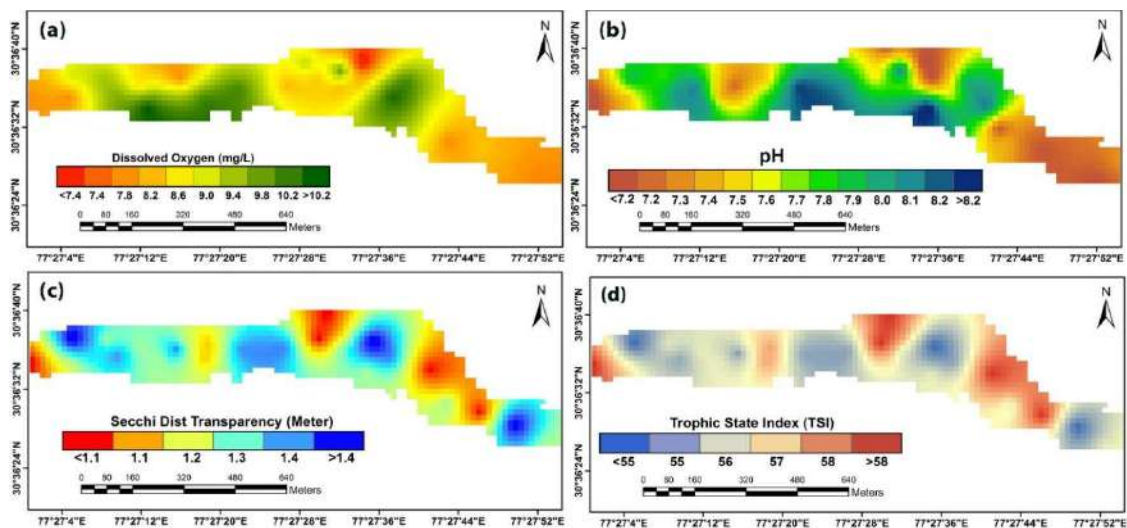


Fig. 5(a-d): Interpolated images of in-situ data (a) Secchi Disk Transparency (SDT), (b) DO, (c) pH and (d) Trophic State Index during October 2019.

and the entire eastern part (7.09) of the lake exhibited a lower pH concentration. The remaining areas of the lake displayed a large variation in pH (7.16 - 8.82), indicating an alkaline nature associated with the presence of submerged weeds. The uptake of carbon dioxide ( $\text{CO}_2$ ) during photosynthesis by these weeds may contribute to increased alkalinity in the lake water (Suba Rao et al. 1981, Panda et al. 1989, 2008, Nayak et al. 2004). Conversely, low pH values suggest a slightly acidic character in different locations, potentially attributed to pollution, weed decay, and the decomposition of carbonaceous material from the deciduous forest around the lake/catchment (Singh & Sharma 2012).

The spatiotemporal variability in Secchi disk transparency (SDT) during the post-monsoon season was analyzed. In-situ observed transparency ranged from 0.93 to 1.5 m, with an average transparency of 1.28 m. Fig. 5(c) illustrates that certain pockets of the eastern, western, and central parts of the lake displayed high transparency, with SDT measurements between 1.4 and 1.5 m, potentially due to minimal anthropogenic activity. However, pockets in the western and central parts exhibited low transparency (<1 m), indicating highly polluted water in terms of SDT. This could be associated with lower layers mixing with upper layers due to upwelling activities, human interference (boating, bathing), pollution, soil erosion, weed growth, and the influx of stream water from the surrounding drainage basin (Sehgal 1980, Das et al. 2001, 2008, Singh & Sharma 2012, Gupta et al. 2018). Some pockets in the eastern parts of the lake exhibited shallow depth, turbid water, and widespread weed growth, contributing to the overall low transparency. Notably, the eastern part of the lake near the Zoo area displayed maximum hydrophytes, indicating high productivity.

Renuka Lake exhibits signs of accelerated eutrophication due to human activities in the catchment area, resulting in high nutrient content and supporting rich biological diversity (Melkania 1988). The lake boasts a macro-phytic vegetation cover spanning approximately 39,969 square meters. A study by Singh & Mahajan (1987) identifies 42 different types of macrophytes, with Phragmites, Acorus, Typha, Carex, Pontederia, and Veronica being the most common. This abundance of macrophytic genera shows the high biological diversity of the lake. The nutrient concentration in the lake water shows an increasing trend, indicative of rising pollution, nutrient-rich water, and planktonic population. Given its status as a key indicator of lake health, regular monitoring of the Trophic State Index (TSI) is imperative.

TSI is measured using both in-situ observed SDT and Landsat-8 OLI satellite data, as depicted in Fig. 5(d). The majority of TSI values are highest in some pockets of the eastern part (58.46), central part (58.62), and western part (58.25) of the lake. However, except for these areas, minimum TSI values range from 54.15 to 54.45. The average in-situ observed TSI value for the lake is 56.38. Overall, the TSI values suggest that the lake water exhibits a eutrophic to hypereutrophic condition. A standard set by Caspers (1982) deems a lake hypereutrophic if its SDT values fall within the range of 0.7-1.5. Following this standard, the SDT values for Renuka Lake (0.93-1.5 m) from this study confirm its hypereutrophic condition. This finding is supported by a previous study by Kumar et al. (2019), which reported SDT values within the range of 0.9-1.14 m.

Various optical remote sensing satellite data, including Landsat-TM (Brezonik et al. 2005, Olmanson et al. 2008, Kulkarni 2011, Torbick et al. 2013), Landsat ETM (Allan et

al. 2007, Mishra & Garg 2011), Landsat-8 OLI (Lim et al. 2015, Lee et al. 2016, Urbanski et al. 2016, Olmanson et al. 2016, Liu et al. 2019, Jally et al. 2020), LISS-III (Coskun et al. 2006, Sheela et al. 2011, Gholizadeh 2016), LISS-IV (Mobwoga et al. 2010), Sentinel-2 (Toming et al. 2016, Bonansea et al. 20219, Bhangale et al. 2020, Bresciani et al. 2019, Torres Bejarano et al. 2020, Sent et al. 2021), MODIS (Wu et al. 2009, Knight et al. 2012), MERIS (Giardino et al. 2014, Mohamed 2015), and Rapid Eye (Fritz et al. 2017, Mishra et al. 2018, Avdan et al. 2019, Cahalane et al. 2019), have been utilized for the study of water quality assessment and eutrophication of the lake.

Landsat-8 and LISS-III satellite data were employed to monitor changes in the lake's trophic status during the post-monsoon period of 2010-19. The trophic status was

analyzed annually, revealing distinct patterns (Fig. 6(a-j)). In 2010, certain areas in the western, central, and eastern parts of the lake exhibited high Trophic State Index (TSI) values, indicating eutrophic to hypereutrophic conditions. The southwestern and central parts transitioned from oligotrophic to mesotrophic. Similar patterns persisted in 2011-12 (Fig. 6(b, c)), and 2013 saw high TSI values in specific pockets of the lake, with the remaining areas demonstrating oligotrophic to mesotrophic conditions. The years 2014-15 (Fig. 6(e, f)) showed high TSI values in the entire eastern part and some western pockets, while the central and southwest parts indicated mesotrophic to eutrophic conditions. In 2016-17 (Fig. 6(g, h)), the central and southwest parts exhibited mesotrophic conditions, whereas the western and eastern parts displayed high TSI values. In 2018 (Fig.

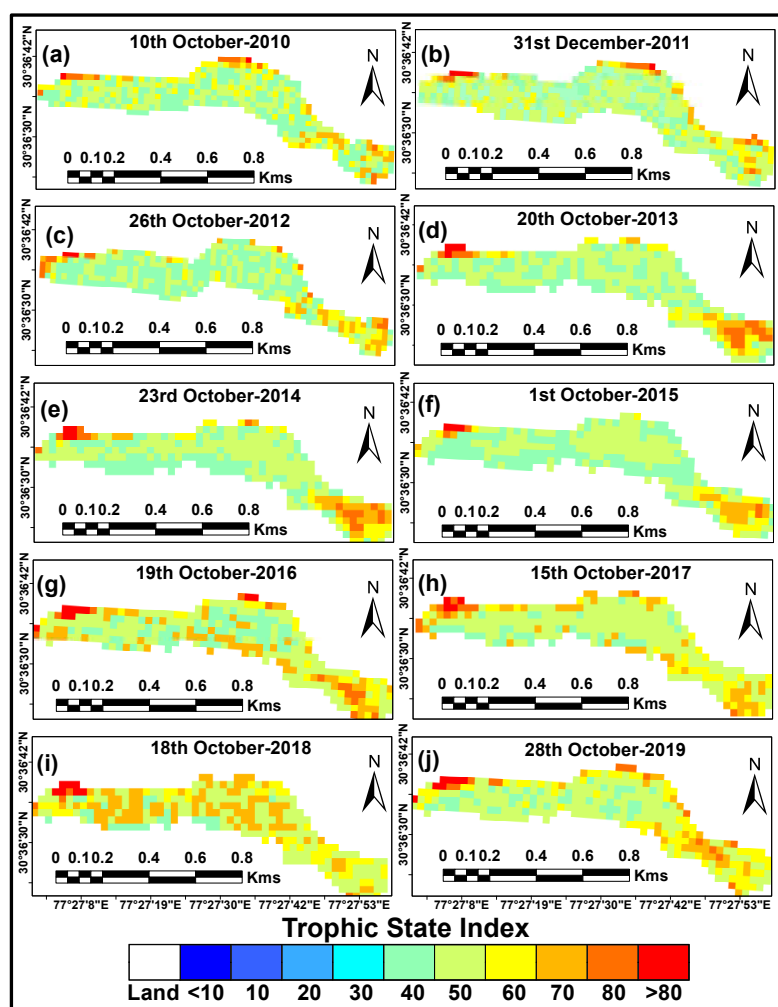


Fig. 6(a-j): TSI images derived from Landsat-8 OLI and LISS-III for 2010 to 2019.

6(i)), a substantial area of the lake showed high TSI values (hypereutrophic condition), except for some central pockets. 2019 (Fig. 6(j)) exhibited TSI patterns similar to 2017 (Fig. 6(h)).

Tourist-generated garbage and sewage seepage, contributing to macrophyte growth, especially in the lake's extreme west where tourist facilities are located, may explain the high trophic status observed during different years (Sehgal 1980, Das et al. 2001, 2008, Singh & Sharma 2012, Gupta et al. 2018, Kumar et al. 2019). The decrease in lake water transparency during winter months may result from the mixing of lower and upper layers due to upwelling activity (Sehgal 1980, Gupta et al. 2018). Human activities like grazing and road construction accelerate silt flow into the

lake, as determined at 3.3 mm/year using the Pb210 isotope method (Das & Kaur 2001). Despite this, some pockets in the central and southwest areas showed fairly clear water (mesotrophic) in 2019, possibly due to conservation efforts by the lake development authority, including regular cleaning of weeds and hydrophytes.

To understand the increasing impact of TSI values in the lake, TSI derived from satellite data and Secchi disk transparency (SDT) are presented in Fig. 7 and Fig. 8. Fig.7 illustrates the average TSI values exhibiting an initial increase followed by a decrease with slight fluctuations in SDT values. The lowest average TSI values were observed in 2015 and 2017. Conversely, Fig.8 depicts a decreasing to increasing trend in SDT values from 2010 to 2019. The

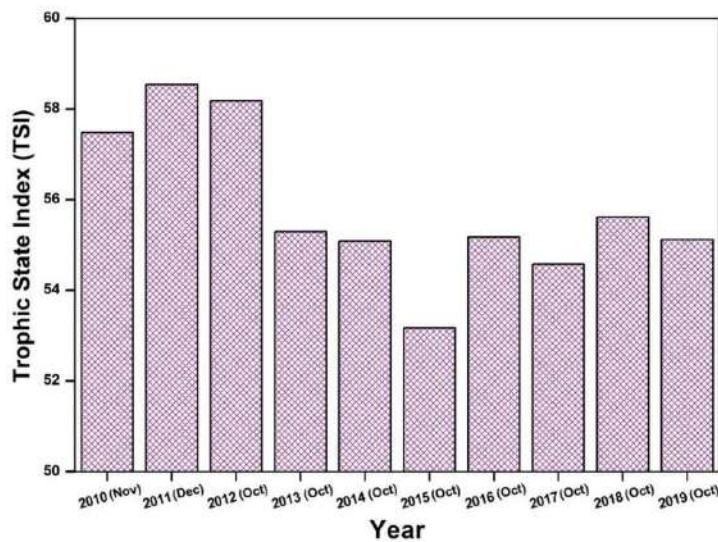


Fig. 7: Comparison of average TSI from Landsat-8 OLI and LISS-III during 2010-19.

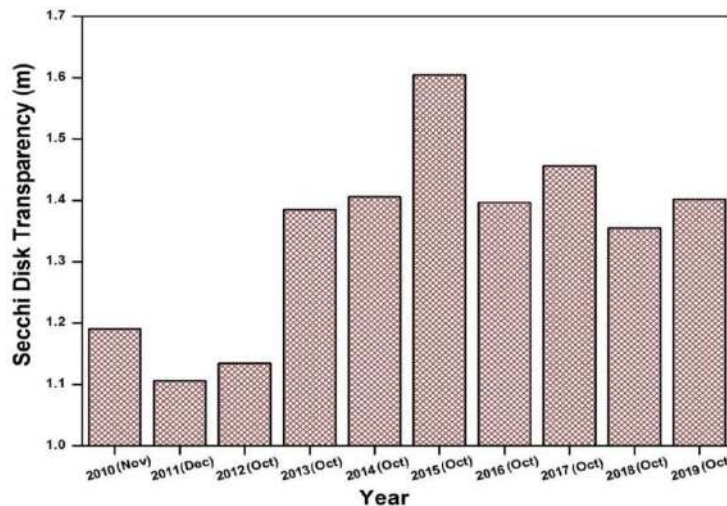


Fig. 8: Comparison of average SDT (m) from Landsat-8 OLI and LISS-III during 2010-19.



minimum transparency was observed in 2010-12. High TSI values leading to substantial development of algae, weeds, and hydrophytes, coupled with a decline in lake transparency, underscore the lake's extreme nutrient richness, impacting its clarity. Table 1 presents in-situ observations, indicating the disappearance of the Secchi disc at a depth of less than 1 meter in certain locations. A comparison of the mean TSI value derived from in-situ measurements with that from satellite observations for 2019 shows a close correspondence, with a difference of only 1.25%. The analysis of Fig. 7 and 8 reveals that the average in-situ measured TSI pattern aligns consistently with TSI values estimated from Landsat-8 OLI and LISS-III.

This study, while providing valuable insights into the trophic state of Renuka Lake, exhibits certain limitations that call for further exploration. Firstly, the focus on key water quality parameters, such as SDT, pH, and DO, leaves room for additional investigation into other critical contributors to the lake's overall health, including nutrient concentrations, chlorophyll, and pollutants. Expanding the scope to encompass a broader array of water quality parameters would enrich the study's comprehensiveness. Secondly, the paper briefly addresses post-monsoon season data, hinting at potential seasonal variability in water quality. A more thorough exploration of seasonal dynamics throughout the year could enhance our understanding of the lake's trophic state fluctuations and provide a more nuanced portrayal of its trophic status. Additionally, investigating the specific sources and relative impacts of anthropogenic activities, such as tourism and sewage, would contribute depth to the study. Furthermore, the research could further advance by exploring the integration of diverse data sources beyond Landsat-8 OLI, such as UAVs or high-resolution satellite imagery, to augment the accuracy and resolution of findings and a focus on long-term trends and predictive modeling could elevate the precision and forecasting capability of future assessments.

## CONCLUSION

In this study, we have demonstrated the utility of remote sensing satellite data in enhancing lake research and monitoring, specifically focusing on crucial water quality metrics, trophic status, and water transparency. The *in-situ* measured Secchi Disk Transparency (SDT) indicates that the water quality of the entire Renuka Lake is within the eutrophic to hypereutrophic range. Trophic status is particularly pronounced in certain areas of the extreme western, central, and eastern parts of the lake, primarily attributed to their proximity to hotels, temples, and bathing Ghats, where human activities and pollution reach maximum

levels. Factors such as upwelling, agricultural runoff, weed growth, drainage influx, and siltation from surrounding drainage basins contribute significantly to the increasing Trophic State Index (TSI) in Renuka Lake. Conversely, the central portion of the lake, where TSI is the lowest, exhibits relative clarity and greater depth due to minimal siltation and reduced human activity. The analysis of satellite data over the past decade unequivocally indicates that Renuka Lake has been consistently in a eutrophic to hypereutrophic condition, confirming the deterioration in water quality, as corroborated by TSI from ground observations. The Secchi disc transparency test emerges as a quick, easy, and accurate method for determining the trophic state of the lake. Notably, rigging interpolation stands out as a superior technique for generating water quality maps from in-situ data compared to alternative approaches.

The current pH and dissolved oxygen (DO) levels in Renuka Lake suggest favorable water quality conditions for aquatic life. However, to establish a comprehensive database and unravel the intricate relationships between physical, chemical, and biological processes in the lake, ongoing extensive monitoring programs are imperative. These programs should be implemented as part of an integrated development strategy aimed at safeguarding the wetland ecosystem from siltation, eutrophication, floodwater influx, and preserving aquatic life. Furthermore, afforestation initiatives in the lake's vicinity can effectively mitigate siltation and curb rapid soil erosion. Protective measures for the smallest Ramsar Wetland Ecosystem in the Shiwalik Range of the Lower Himalaya must include a complete prohibition on discarding household waste into the lake, regular cleaning of emergent and submerged aquatic weeds to reduce nutrient levels, and routine monitoring of water quality parameters to assess pollution. Thus, the consistent monitoring of water quality, both through in-situ observations and satellite data, is crucial for assessing and preserving the trophic status of the lake and safeguarding its Ramsar site wetland designation.

For an effective lake hydrological environment monitoring, the extensive utilization of continuous time-series satellite data, coupled with field-observed water quality data, proves beneficial. Landsat-8 OLI data, with its spatial, spectral, and radiometric resolutions, can intricately retrieve water quality indicators such as SDT and TSI. Recognizing the constraints of Landsat-8 OLI's 16-day revisit time and frequent cloud obscuration, incorporating other high-temporal-resolution satellite data sources like MODIS, Sentinel-2A, Rapid-Eye, and NOAA AVHRR can offer valuable insights into long-term trends in water quality metrics. The integration of field observations and remote

sensing data becomes a valuable resource for limnologists and lake management authorities. Future research endeavors should delve into assessing the mechanisms essential for protecting Renuka Wetland from rapid eutrophication. Embracing readily accessible and upcoming satellite data, adhering to open access and public data policies, leveraging existing algorithms, and employing open-source data will undoubtedly enhance the efficacy of remote sensing applications in lake research.

## ACKNOWLEDGMENTS

The authors acknowledge the financial assistance support from Gangadhar Meher University, Sambalpur, in terms of the SEED Money Research Grant. Additionally, sincere thanks are extended to the Director of the Indian Institute of Remote Sensing (ISRO), Dehradun, for providing essential support and access to laboratory facilities crucial for the research endeavor. The authors acknowledge with gratitude Earth Explorer (USGS) and NRSC for generously providing the Landsat-8 OLI and LISS-III data. Special appreciation is extended to Dr. A.K. Mishra, Scientist-SG, Marine and Atmospheric Sciences Department at the Indian Institute of Remote Sensing (ISRO), Dehradun, Uttarakhand, for valuable and constructive inputs. The authors extended their sincere appreciation to Imtijongshi Imchen and Abhishek Choudhary for their crucial role in facilitating field data collection. The authors are also thankful to the administration of Renuka Lake for facilitating the boat facility during the collection of water samples. The authors are also thankful to editors and anonymous reviewers for their insightful comments and suggestions which have helped to improve the quality of the manuscript.

## REFERENCES

- Allan, M.G., Hicks, B.J. and Brabyn, L., 2007. Remote sensing of water quality in the Rotorua lakes. *CBER Contract Report*, 51, pp.1-27, Hamilton, New Zealand: The University of Waikato.
- Andrew, M.E., Wulder, M.A. and Nelson, T.A., 2014. Potential contributions of remote sensing to ecosystem service assessments. *Progress in Physical Geography: Earth and Environment*, 38(3), pp.328-353.
- Araoye, P.A., 2009. The seasonal variation of pH and Dissolved oxygen concentration in Asa lake Ilorin, Nigeria. *International Journal of Physical Sciences*, 4(5), pp.271-274.
- Ashraf, M.A., Maah, M.J. and Yusoff, I., 2010. Water quality characterization of varsity lake, University of Malaya, Kuala Lumpur, Malaysia. *E-Journal of Chemistry*, 7(S1), pp.S245-S254.
- Avdan, Z.Y., Kaplan, G., Goncu, S. and Avdan, U., 2019. Monitoring the water quality of small water bodies using high-resolution remote sensing data. *International Journal of Geo-Information*, 8, p. 553.
- Azary, A.M., Mohebbi, F., Eimanifar, A., Javanmard, A. and Aliyev, A.F.Q., 2010. Species composition, ecological parameters, and seasonal changes of planktonic ciliates population in Bukan Dam reservoir. *American Journal of Agricultural and Biological Sciences*, 5(1), pp.102-106.
- Barnes, B.B., Hu, C., Kovach, C. and Silverstein, R.N., 2015. Sediment plumes induced by the Port of Miami dredging: Analysis and interpretation using Landsat and MODIS data. *Remote Sensing of Environment*, 170, pp.328-339.
- Bhangale, U., More, S., Shaikh, T., Patil, S. and More, N., 2020. Analysis of surface water resources using sentinel-2 imagery. *Procedia Computer Science*, 171, pp. 2645-2654.
- Bilgehan, N., Semih, E., Hakan, K., Ali, B. and David, M., 2010. An application of Landsat-5 TM image data for water quality mapping in Lake Beysehir, Turkey. *Water, Air, & Soil Pollution*, 212, pp.183-197.
- Bio, A., Couto, A., Costa, R., Prestes, A., Vieira, N., Valente, A. and Azevedo, J., 2008. Effects of fish removal in the Furnas Lake, Azores. *Arquipelago. Life and Marine Sciences*, 25, pp.77-87.
- Birk, S. and Ecke, F., 2014. The potential of remote sensing in ecological status assessment of colored lakes using aquatic plants. *Ecological Indicators*, 46, pp.398-406.
- Birk, S., Bonne, W., Borja, A., Brucet, S., Courrat, A., Poikane, S., Solimini, A., van de Bund, W., Zampoukas, N. and Hering, D., 2012. Three hundred ways to assess Europe's surface waters: an almost complete overview of biological methods to implement the Water Framework Directive. *Ecological Indicators*, 18, pp.31-41.
- Boavida, M.J. and Marques, R.T., 1996. Total phosphorus as an indicator of the trophic state of Portuguese reservoirs. *Limnetica*, 12(2), pp.31-37.
- Bonansea, M., Bresciani, M., Bolpagni, R., Braga, F. and Laini, A., 2019. Application of radiative transfer models for interpreting hyperspectral remote sensing data of a small lake. *ISPRS Journal of Photogrammetry and Remote Sensing*, 147, pp. 85-99.
- Bresciani, M., Giardino, C., Cazzaniga, I., Laini, A., Bresciani, M. and Brtoli, M., 2019. Lake water quality assessment using Hyperspectral Imagery (HSI). *Water Research*, 154, pp.337-349.
- Brezonik, P., Menken, K.D. and Marvin, B., 2005. Landsat-based remote sensing of lake water quality characteristics, including chlorophyll and Colored Dissolved Organic Matter (CDOM). *Lake and Reservoir Management*, 21(4), pp.373-382.
- Brönmark, C. and Hansson, L.A., 2002. Environmental issues in lakes and ponds: current state and perspectives. *Environmental Conservation*, 29(3), pp.290-307.
- Cahalane, C., Magee, A., Monteys, X., Casal, G., Hanafin, J. and Harris, P., 2019. A comparison of Landsat 8, RapidEye and Pleiades products for improving empirical predictions of satellite-derived bathymetry. *Remote Sensing of Environment*, 233, p.111414.
- Carlson, R.E., 1977. A trophic state index for lakes. *Limnology and Oceanography*, 22(2), pp.361-369.
- Carr, G.M. and Neary, J.P., 2006. *Water Quality for Ecosystem and Human Health*, United Nations Environment Programme Global Environment Monitoring System (GEMS)/Water Programme, pp. 1-120.
- Caspers, H., 1982. OECD: Eutrophication of waters. Monitoring, assessment and control; Organisation for Economic Co-Operation and Development: Paris, France, p.154.
- Chapman, D. and Kimstach, V. 1996. *Water quality assessments - A Guide to use of Biota, Sediments and Water in Environmental Monitoring*. UNESCO/WHO/UNEP, pp. 1-651, Cambridge: Cambridge University Press.
- Coskun, H.G., Gulergun, O. and Yilmaz, L., 2006. Monitoring of protected bands of Terkos drinking water reservoir of metropolitan Istanbul near the Black Sea coast using satellite data. *International Journal of Applied Earth Observation and Geoinformation*, 8, pp. 49-60.
- Das, B.K. and Kaur, P., 2001. Major ion chemistry of Renuka Lake and weathering process, Sirmour District, Himachal Pradesh, India. *Environmental Geology*, 40, pp.908-917.
- Das, B.K., Gaye, B. and Kaur, P., 2008. Geochemistry of Renuka Lake and wetland sediments, lesser Himalaya (India): Implication for source-area weathering, provenance and tectonic setting. *Environmental Geology*, 54, pp.147-163.

- de Araujo Barbosa, C.C., Atkinson, P.M. and Dearing, J.A., 2015. Remote sensing of ecosystem services: A systematic review. *Ecological Indicators*, 52, pp.430-443.
- Dhillon, J.K. and Mishra, A.K., 2013. Estimation of Trophic State Index of Sukhna Lake Using Remote Sensing and GIS. *Journal of the Indian Society of Remote Sensing*, 42, pp.469-474.
- Dudgeon, D., Arthington, A.H., Gessner, M.O., Kawabata, Z.I., Knowler, D.J., Leveque, C., Naiman, R.J., Prieur-Richard, A.H., Soto, D., Stiassny, M.L.J. and Sullivan, C.A., 2006. Freshwater biodiversity: importance, threats, status and conservation challenges. *Biological Reviews*, 81, pp.163-182.
- Fritz, C., Dörnhöfer, K., Schneider, T., Geist, J. and Oppelt, N., 2017. Mapping submerged aquatic vegetation using Rapideye satellite data: the example of Lake Kummerow (Germany). *Water*, 9, p. 510.
- Fuller, L.M. and Minnerick, R.J., 2007. Predicting water quality by relating Secchi disk transparency and chlorophyll-a measurement to Landsat satellite imagery for Michigan Inland Lakes 2001-2006, Fact sheet 2007-2022. U.S. Geological Survey, Science for Changing World.
- Gholizadeh, M.H., Melesse, A.M. and Reddi, L., 2016. A comprehensive review on water quality parameters estimation using remote sensing techniques. *Sensors*, 16, p.1298.
- Giardino, C., Bresciani, M., Stroppiana, D., Oggioni, A. and Morabito, G., 2014. Optical remote sensing of lakes: an overview on Lake Maggiore Claudia. *Journal of Limnology*, 73, pp.201-214.
- Gray, W.B. and Shimshack, J.P., 2011. The effectiveness of environmental monitoring and enforcement: a review of the empirical evidence. *Review of Environmental Economics and Policy*, 5(1), pp.3-24.
- Gupta, S., Singh, D., Rawat, M.S. and Ahmed, R., 2018. Phytoplankton community in relation to physicochemical characteristics of Renuka Lake and Parshuram Tal (H.P.), India. *International Journal of Scientific Research and Reviews*, 7(3), pp.769-780.
- Harrington, J.A., Schicbe, F.R. and Morrison, F.E., 1989. Monitoring lake recovery using the Landsat MSS. In: *Regional Characterization of Water Quality* (Proceedings of the Baltimore Symposium, May 1989), pp.143-150.
- Hestir, E.L., Brando, V.E., Bresciani, M., Giardino, C., Matta, E., Villa, P. and Dekker, A.G., 2015. Measuring freshwater aquatic ecosystems: the need for a hyperspectral global mapping satellite mission. *Remote Sensing of Environment*, 167, pp.181-195.
- Jally, S.K., Mishra, A.K. and Balabantary, S., 2020. Estimation of Trophic State Index of Chilika Lake using Landsat-8 OLI and LISS-III satellite data. *Geocarto International*, 35(7), pp.759-780.
- Khorram, S. and Cheshire, M.H., 1985. Remote Sensing of Water Quality in the Neuse River Estuary, North Carolina. *Photogrammetric Engineering and Remote Sensing*, 51, pp.329-341.
- Knight, J.F. and Voth, M.L., 2012. Application of MODIS imagery for intra-annual water clarity assessment of Minnesota lakes. *Remote Sensing*, 4(7), pp.2181-2198.
- Koponen, S., Pulliainen, J., Kallio, K. and Halliainen, M., 2002. Lake water quality classification with airborne hyperspectral spectrometer and simulated MERIS data. *Remote Sensing of Environment*, 79, pp.51-59.
- Kulkarni, A., 2011. Water quality retrieval from landsat TM imagery. *Procedia Computer Science*, 6, pp. 475-480.
- Kumar, P., Mahajan, A.K. and Meena, N.K., 2019. Evaluation of trophic status and its limiting factors in the Renuka Lake of Lesser Himalaya, India. *Environment Monitoring & Assessment*, 191, p.105.
- Lee, Z., Shang, S., Qi, L., Yan, J. and Lin, G., 2016. A semi-analytical scheme to estimate Secchi-disk depth from Landsat-8 measurements. *Remote Sensing of Environment*, 177, pp.101-106.
- Lim, J., and Choi, M., 2015. Assessment of water quality based on Landsat 8 operational land imager associated with human activities in Korea. *Environment Monitoring Assessment*, 187, p. 384.
- Liu, L and Wang, Y., 2011. Modelling reservoir turbidity using Landsat 8 satellite imagery by gene expression programming. *Water*, 11, p. 1479.
- Mabwoga, S.O., Chawla, A. and Thukral, A.K., 2010. Assessment of water quality parameters of the Harike wetland in India, a Ramsar site, using IRS LISS IV satellite data. *Environmental Monitoring and Assessment*, 170, pp.117-128.
- Melin, F., Zibordi, G. and Djavidnia, S., 2007. Development and validation of a technique for merging satellite-derived aerosol optical depth from Sea-WiFS and MODIS. *Remote Sensing of Environment*, 108(4), pp.436-450.
- Melkania, N.P., 1988. The Himalayan Lakes and Wetland Overview. *Indian Journal of Environmental Protection*, 8.
- Mishra, A.K. and Garg, N., 2011. Analysis of Trophic State Index of Nainital Lake from Landsat-7 ETM data. *Journal of Indian Society of Remote Sensing*, 39(4), pp.463-471.
- Mohamed, M.F., 2015. Satellite data and real time stations to improve water quality of Lake Manzalah. *Water Science*, 29, pp. 68-76.
- Mullins, M.L. and Whisenant, A.S., 2004. Somerville Reservoir Water Quality Study. *Texas Parks and Wildlife Department*, Austin, Texas. Water Quality Technical Series, WQTS-2004-02, pp.1-20.
- Nayak, B.K., Acharya, B.C., Panda, U.C., Nayak, B.B. and Acharya, S.K., 2004. Variation of water quality in Chilika Lake, Orissa. *Indian Journal of Marine Science*, 33, pp.164-169.
- Olmanson, L.G., Bauer, M.E. and Brezonik, P.L., 2008. A 20-year Landsat water clarity census of Minnesota's 10,000 lakes. *Remote Sensing of Environment*, 112(11), pp.4086-4097.
- Olmanson, L.G., Brezonik, P.L., Finlay, J.C. and Bauer, M.E., 2016. Comparison of Landsat 8 and Landsat 7 for regional measurements of CDOM and water clarity in lakes. *Remote Sensing of Environment*, 185, pp.119-128.
- Palmer, S.C., Kutser, T. and Hunter, P.D., 2015. Remote sensing of inland waters: challenges, progress, and future directions. *Remote Sensing of Environment*, 157, pp.1-8.
- Panda, D., Tripathy, S.K., Pattanaik, D.K., Choudhury, S.B., Goud, R. and Panigrahy, R.C., 1989. Distribution of Nutrients in Chilika Lagoon, East Coast of India. *Indian Journal of Marine Sciences*, 18, pp.286-288.
- Parinet, B., Lhote, A. and Legube, B., 2004. Principal component analysis: an appropriate tool for water quality evaluation and management application to a tropical lake system. *Ecological Modelling*, 178, pp.295-311.
- Paukert, C.P. and Willis, D.W., 2003. Population characteristics and ecological role of Northern Pike in shallow natural lakes in Nebraska. *North American Journal of Fisheries Management*, 23(1), pp.313-322.
- Rast, W., 2009. Lakes: Freshwater Storehouses and Mirrors of Human Activities. *Briefing Note*, United Nations World Water Assessment Programme, Programme Office for Global Water Assessment, Division of Water Sciences, UNESCO, 06134 Colomabella, Perugia, Italy.
- Riduan, S.D., Hamzah, Z. and Satt, A., 2009. In-situ measurement of selected water quality parameters in Ringlet's Lake, Cameron Highlands. *Malaysian Journal of Chemistry*, 11(1), pp.122-128.
- Robinove, C.J., 1982. Computation with physical values from Landsat digital data. *Photogrammetric Engineering and Remote Sensing*, 48(5), pp.781-784.
- Saluja, R. and Garg, J.K., 2017. Trophic state assessment of Bhindawas Lake, Haryana, India. *Environmental Monitoring and Assessment*, 189, p.32.
- Sehgal, H.S., 1980. Limnology of Lake Surinsar, Jammu, with reference to zooplankton and fishery prospects. Ph.D. Thesis, University of Jammu, Jammu.
- Sent, G., Biguino, B., Favareto, L., Cruz, J., Sá, C., Dogliotti, A.I., Palma, C., Brotas, V. and Brito, A.C., 2021. Deriving water quality parameters using Sentinel-2 Imagery: a case study in the Sado Estuary, Portugal. *Remote Sensing*, 13, p. 1043.
- Sharma, A., Ranga, M.M. and Sharma, P.C., 2010. Water quality status of historical Gundolav Lake at Kishangarh as primary data for sustainable management. *South Asian Journal of Tourism and Heritage*, 3(2), pp.151-158.

- Sheela, A.M., Letha, J., Joseph, S., Ramachandran, K.K. and Sanalkumar, S.P., 2011. Trophic state index of a lake system using IRS (P6-LISS III) satellite imagery. *Environmental Monitoring and Assessment*, 177, pp.575-592.
- Singh, O. and Sharma, M.K., 2012. Water quality and eutrophication status of the Renuka Lake, district Sirmour (H.P.). *Journal of Indian Water Resources Society*, 32, pp.1-7.
- Singh, R. and Mahajan, I., 1987. Phytoplankton and water chemistry of Rewalsar and Renuka Lakes, Himachal Pradesh. *Indian Journal of Ecology*, 14(2), pp.273-277.
- Suba Rao, M.V., Rao, B.M.G., Rao, B.R. and Nanda, N.K., 1981. Hydrological studies of the brackish water Chilika Lagoon, Orissa. *Journal of Environmental Biology*, 2, pp.59-62.
- Toming, K., Kutser, T., Laas, A., Sepp, M., Paavel, B. and Noges, T., 2016. First experiences in mapping lake water quality parameters with Sentinel-2 MSI imagery. *Remote Sensing*, 8(8), p.640.
- Torbick, N., Hession, S., Hagen, S., Wiangwang, N., Becker, B and Qi, J., 2013. Mapping inland lake water quality across the Lower Peninsula of Michigan using Landsat TM imagery. *International Journal of Remote Sensing*, 34(21), pp.7607-7624.
- Torres-Bejarano, F., Arteaga-Hernandez, F., Rodriguez-Ibarra, D., Mejia-Avila, D. and Gonzalez-Marquez, L.C., 2020. Water quality assessment in a wetland complex using Sentinel 2 satellite images. *International Journal of Environmental Science and Technology*, 18, pp. 2345-2356.
- Urbanski, J.A., Wochnaa, A., Bubakb, I., Grzybowski, W., Lukawska-Matuszewskab, K., Lackad, M., Sliwinski, S., Wojtasiewicz, B. and Zajaczkowski M., 2016. Application of Landsat 8 imagery to regional-scale assessment of lakewater quality. *International Journal of Applied Earth Observation and Geoinformation*, 51, pp. 28-36.
- US EPA, 1986. Quality criteria for waters, regulations, and standards. Washington, DC 20460, EPA 440/5-86-001.
- Usali, N. and Ismail, M.H., 2010. Use of remote sensing and GIS in monitoring water quality. *Journal of Sustainable Development*, 3(3), E-ISSN:1913-9071.
- USGS EarthExplorer, 2023. Landsat-8. Retrieved October 23, 2024 from <https://earthexplorer.usgs.gov/>
- USGS, 2023. Landsat-8. Retrieved October 23, 2024 from <https://www.usgs.gov/land-resources/nli/landsat/using-usgs-landsat-level-1-data-product>
- van Puijenbroek, P., Evers, C. and van Gaalen, F.W., 2015. Evaluation of Water Framework Directive metrics to analyze trends in water quality in the Netherlands. *Sustainable Water Quality Ecology*, 6, pp.40-47.
- Vollenweider, R.A., 1968. Scientific fundamentals of the eutrophication of lakes and flowing waters, with particular reference to nitrogen and phosphorous as factors in eutrophication. OECD Rep. *Water Management Research*, p. 159.
- Vörösmarty, C., McIntyre, P.B., Gessner, M.O., Dudgeon, D., Prusevich, A., Green, P., Glidden, S., Bunn, S.E., Sullivan, C.A., Reidy Liermann, C. and Davies, P.M., 2010. Global threats to human water security and river biodiversity. *Nature*, 467, pp. 555-561.
- Walker, W.W.J.R., 1979. Use of hypolimnetic oxygen depletion rate as a trophic state index for lakes. *Water Resources Research*, 15(6), pp.1463-1470.
- Walshe, T., MacNeil, A., Archer, A., Sweatman, H., Lawrey, E., Bay, L., Addison, P. and Anthony, K., 2014. Integrated Monitoring, Modelling, and Management of the Great Barrier Reef World Heritage Area - Demonstration Case for the Mackay Region, Final Report to the Department of the Environment December 2014. Townsville, Australia: Australian Institute of Marine Science.
- Wang, Y., Xia, H., Fu, J. and Sheng, G., 2004. Water quality change in reservoirs of Shenzhen, China: detection using Landsat/TM data. *Science of the Total Environment*, 328, pp.195-206.
- Whitney, R.J., 1942. Diurnal fluctuations of oxygen and pH in two small ponds and a stream. *Journal of Experimental Biology*, 19(1), pp.92-99.
- Wu, M., Zhang, W., Wang, X. and Luo, D., 2009. Application of MODIS satellite data in monitoring water quality parameters of Chaohu Lake in China. *Environmental Monitoring and Assessment*, 148, pp.255-264.

---

#### ORCID DETAILS OF THE AUTHORS

Sujit Kumar Jally: <https://orcid.org/0000-0002-9133-967X>



# Economic Feasibility of On-Grid Photovoltaic Solar Power Plants at Private Universities in Indonesia

Rijal Asnawi<sup>1†</sup>, Antariksa<sup>2</sup>, Sukir Maryanto<sup>3</sup> and Aminudin Afandhi<sup>4</sup>

<sup>1</sup>Postgraduate Study of Environmental Science, Brawijaya University, Malang, Indonesia

<sup>2</sup>Department of Architecture Engineering, Brawijaya University, Malang, Indonesia

<sup>3</sup>Brawijaya Volcano and Geothermal Research Center, University of Brawijaya, Malang, Indonesia

<sup>4</sup>Plant Protection Department, Agriculture Faculty, Universitas Brawijaya, Malang, Indonesia

†Corresponding author: Rijal Asnawi; rijalasnawi06@gmail.com

Nat. Env. & Poll. Tech.  
Website: [www.neptjournal.com](http://www.neptjournal.com)

Received: 05-03-2024

Revised: 09-04-2024

Accepted: 29-04-2024

## Key Words:

Cultural livelihood  
Environment  
Solar power plants  
Kogi State

## ABSTRACT

Campus 2 of the National Institute of Technology (ITN) Malang shows its commitment to utilizing solar energy by adopting a 500 kWp photovoltaic solar power plant (PV), making it the largest in Indonesia for a private university. This research aims to evaluate the economic feasibility of photovoltaic solar power plants (PV) at Campus 2 of the National Institute of Technology Malang. The implementation of renewable energy, particularly photovoltaic solar power, is gaining attention due to its contribution to reducing greenhouse gas emissions and economic growth. However, the development of renewable energy sources faces several challenges, including the limitations of economic feasibility studies in Indonesia. A mixed-methods research approach is used, combining qualitative and quantitative data. Qualitative data are obtained from interviews with PV management staff, while quantitative data include net present value (NPV) calculations and payback periods (PBP). The research findings indicate that the on-grid photovoltaic solar power plant at Campus 2 of the National Institute of Technology (ITN) Malang has a capacity of 500 kWp, with a peak load reaching 380 kVA. The total project cost is Rp. 4,084,498,826, with annual operational and maintenance costs of Rp. 81,595,607. The price of electricity from the on-grid photovoltaic solar power plant is Rp. 930 per kWh. An NPV value of Rp. 7,789,395,602 indicates future profitability, while a PBP of 8.55 years demonstrates feasibility in terms of return on investment. In conclusion, the on-grid photovoltaic solar power plant at Campus 2 of the National Institute of Technology Malang has good economic feasibility due to factors such as controlled costs, competitive prices, a positive NPV, and a short PBP. Regular evaluations are necessary to ensure efficient operation and maximum benefits.

## INTRODUCTION

Electricity is currently a vital factor in society's life and the functioning of the economy. The energy sector is transitioning from fossil fuels to renewable energy sources. In many countries, the use of renewable energy continues to increase. Renewable energy sources (RES) are replacing conventional energy sources to achieve emission-free economies (Czepło & Borowski 2024). Photovoltaic solar power generation has become an increasingly important topic in the context of energy sustainability worldwide. Photovoltaic technology harnesses solar energy to generate electricity, which is a clean and renewable energy source (Etukudoh et al. 2024). Photovoltaic technology is a suitable option for distributed power generation, which has the potential to replace conventional centralized stations and reduce network reinforcement costs (Jamil et al. 2012).

According to Boruah & Chandel (2024), photovoltaic solar power generation systems (PV) are cost-effective and environmentally friendly solutions for energy conservation. In this context, it provides a significant contribution to solving some of the most urgent energy problems facing the world today.

The International Renewable Energy Agency (IRENA) reported in 2022 that global progress in renewable energy has added 257 GW of renewable energy sources, with 133 GW (>50%) of this energy coming from solar power (Huda et al. 2024). Meanwhile, the International Energy Agency (IEA) predicts a 60% increase in installed renewable energy capacity by 2026, totaling over 4800 GW. According to the report, 1,100 GW of capacity will come from photovoltaic solar power generation, doubling compared to five years prior (Minazhova et al. 2023). The significant percentage of solar

energy is due to the maturity of the photovoltaic solar power generation market in terms of technology and large-scale movements toward global climate awareness. Additionally, photovoltaic solar power generation technology has gradually reduced investment costs and energy costs, making it the most cost-effective electricity source worldwide (Huda et al. 2024).

However, a significant obstacle to the development and implementation of renewable energy resources is the low level of research on local renewable resources (Obeng et al. 2020). Yet, higher education institutions can contribute to energy consumption reduction by implementing green campus policies that include the installation of medium-scale solar power systems (Kristiawan et al. 2018). According to Bouraima et al. (2024), potential challenges to sustainable photovoltaic solar power development offer four alternatives to address these challenges, focusing on energy resilience, economic growth, and greenhouse gas emission reduction. Therefore, universities should be involved in accelerating the implementation of photovoltaic solar power generation systems, especially in Indonesia, considering their potential in terms of human resource availability. Government incentives should encourage campus involvement to attract customers or campuses to install such systems (Pramadya & Kim 2024).

In the context of the research “Economic Feasibility of Photovoltaic Solar Power Generation at Campus 2 of the National Institute of Technology Malang,” the importance of implementing renewable energy, such as photovoltaic solar power, in the campus environment becomes increasingly evident. Considering global trends and their potential positive contribution to greenhouse gas emission reduction and economic growth, the involvement of universities in adopting photovoltaic solar power generation systems has become increasingly necessary (Shahsavari & Akbari 2018, Al-Shetwi 2022). The existence of barriers to the development of renewable energy sources indicates the need for collective efforts to promote the adoption of photovoltaic solar power generation technology in higher education institutions as a step toward better energy sustainability (Suheri et al. 2019).

The urgency of raising research regarding the use of photovoltaic solar power plants as an attractive alternative to facing current energy and environmental challenges has become a major concern, and photovoltaic solar power plant energy continues to experience growth. According to Draou et al. (2024), this growth has the potential to result in a reduction in prices and an increase in the use of solar photovoltaic power generation systems in the country by 2030. However, from an economic perspective, solar photovoltaic power generation technology is considered

expensive and requires investment. Significant start. Limitations in economic feasibility studies in Indonesia are an obstacle to increasing investment interest and community participation in investment (Huda et al. 2024). According to Hamad et al. (2024), most research focuses on analyzing location suitability and ignores considerations of assessing techno-economic potential.

This study raises and questions the economic feasibility of photovoltaic solar power plants due to the urgency of exploring the potential utilization of this technology as an attractive alternative to address the increasingly pressing energy and environmental challenges (Dehler-Holland et al. 2022). With continuous growth, photovoltaic solar power generation technology has the potential to reduce prices and increase its usage domestically by 2030, as mentioned by Draou et al. (2024). However, economically, this technology is considered expensive and requires a significant initial investment. Limitations in economic feasibility studies in Indonesia pose a barrier to attracting investment interest and public participation in the development of this technology. Haber et al. (2021) emphasize that the success of implementing new and renewable energy (NRE) requires a comprehensive understanding of economic considerations. Therefore, it is important to analyze the economic feasibility of photovoltaic solar power plants holistically to identify potential economic benefits and overcome existing investment barriers.

Referring to the data, out of the total installed capacity of new and renewable energy power plants of 12,736.7 megawatts (MW), solar power plants account for 322.6 MW. Thus, the realization of solar power plants in 2023 only contributed approximately 2.53% of the total capacity of national renewable energy power plants (Humas EBTKE 2023). Certainly, the use of solar energy is still far behind compared to neighboring countries in the Association of Southeast Asian Nations (ASEAN), such as Vietnam, Thailand, the Philippines, and Malaysia. These countries contributed 16,600 MW, 3,049 MW, 1,370 MW, and 1,787 MW, respectively, in 2022. This situation arises because the current government is unable to bear the high investment costs. Additionally, large-scale photovoltaic solar power plants require vast amounts of land. This issue is considered one of the biggest obstacles for Indonesia in infrastructure development (Pramadya & Kim 2024).

This problem must be addressed because, according to Manoo et al. (2024), expanding alternative energy sources such as solar power is a potential solution to address the problems caused by non-renewable resources. Universities play a crucial role in environmental awareness, training, research, and innovative solutions, yet university involvement

in environmentally friendly energy development efforts is often overlooked (Tshivhase & Bisschoff 2024). According to Basabien et al. (2024), photovoltaic solar power plants have the potential to support the research, academic, and practical goals of a university.

Campus 2 of the National Institute of Technology Malang, a private university that adopts and uses sustainable energy, has a solar photovoltaic power generation system with the largest capacity in Indonesia, reaching 500 kWp and using an area of 0.5 hectares. Certainly, this requires significant economic resources both in terms of the development and maintenance of the photovoltaic solar power generation system. Therefore, this research is urgent to evaluate the economic feasibility of photovoltaic solar power generation systems at Campus 2 of the National Institute of Technology Malang.

The findings from Paudel et al. (2021) research indicate that installing a 1 MW photovoltaic solar power generation system connected to the electricity grid is feasible for implementation on campus. Similar results were found by Basabien et al. (2024), who found that, overall, photovoltaic solar power plants will enable the Faculty of Engineering to use renewable energy and benefit from cost savings in the long term. However, a study by Pramadya and Kim (2024) found that photovoltaic solar power plants based on Net-metering (NEM) scheme calculations are not sufficient to make the photovoltaic solar power generation system economically viable. This directly reinforces the urgency of research in considering the economic feasibility of photovoltaic solar power plants at Campus 2 of the National Institute of Technology Malang, as well as their benefits in achieving sustainable development goals and reducing the negative environmental impacts resulting from the use of fossil energy sources.

The research conducted by Mulyani et al. (2024) supports previous research findings and introduces three new topics identified in both media channels. These findings include aspects of knowledge, misconceptions, and skepticism; economically viable alternative solar panel technology; as well as government regulations and policies. Aspects such as social and visual impressions like aesthetics, hedonic motivation, and social influence were not discussed in the study. Public perceptions of solar panels vary, with mainstream media tending to present solar panel technology more positively than social media. In general, the public has a positive view of solar panels regarding their practicality, installation, safety, and information accessibility. However, there are also negative views regarding investment costs, regulations, government policies, and the perceived inadequate level of government support.

This study differs from previous studies in several aspects. First, this study focuses on Campus 2 of the National Institute of Technology Malang, which is a different location from previous research. Different locations can affect the potential of solar energy and relevant economic factors. Second, this research examines the economic feasibility of a 500 kWp solar power plant, while previous studies considered different capacities. The difference in capacity will impact the costs and profits generated. Third, this study uses an on-grid scheme with net metering, allowing the solar power plant to sell excess energy to the national electricity company and increase profit potential. Additionally, this research also considers social and visual factors such as aesthetics, hedonic motivation, and social influence, which have not been extensively discussed in previous studies. Lastly, the study by Mulyani et al. (2024) focuses on public perceptions of solar power plants in mainstream and social media, while this study does not address those aspects. Therefore, this study provides a more comprehensive analysis of the economic feasibility of solar power plants at Campus 2 of the National Institute of Technology Malang, with a greater focus on techno-economic aspects.

Based on the description above, the economic feasibility of photovoltaic solar power plants faces challenges, including limitations in economic feasibility studies in Indonesia, the low contribution of solar power plants to the total national electricity generation capacity, barriers to investment, and extensive land use. This study aims to analyze the economic feasibility of photovoltaic solar power plants (PV) at Campus 2 of the National Institute of Technology Malang in response to the urgency of exploring the potential use of this technology as an alternative to address the increasingly pressing energy and environmental challenges today.

## MATERIALS AND METHODS

### Research Approach

The method to be used in this research is mixed-methods research, where one issue will be analyzed using two approaches: qualitative data and quantitative data. Conceptually, mixed-methods research combines qualitative and quantitative data in analysis (Azhari et al. 2023). By employing a mixed-methods approach, this research can integrate qualitative and quantitative data to obtain more comprehensive and in-depth information regarding the economic feasibility of photovoltaic solar power generation. Qualitative data can provide contextual insights and profound understanding, while quantitative data can offer concrete numbers and supporting statistics. Additionally, combining both types of data can enhance validity and strengthen

research findings (Sarie et al. 2023). By corroborating findings from both data sources, we can ensure that the research results are stronger and more reliable.

### Data Source

Qualitative data will be obtained through interviews with the staff members responsible for managing the photovoltaic solar power generation plant at the National Institute of Technology Malang. The interviews will focus on information related to initial investment costs, operational costs, and maintenance costs, as well as the energy costs of the photovoltaic solar power generation plant produced. This information can provide a deeper understanding of these aspects. Meanwhile, quantitative data will be obtained from the calculation of the net present value (NPV) and payback period (PBP) to evaluate the economic feasibility of the photovoltaic solar power generation plant project. This research was conducted from December 26, 2023, to January 26, 2024.

### Data Collection Technique

This is done by conducting structured interviews with relevant informants to gather qualitative data. Interviews are conducted either in person or via telephone.

### Data Analysis

#### 1) Qualitative data analysis

Qualitative data from interviews will be analyzed using the qualitative analysis technique known as thematic analysis. The data will be categorized, coded, and interpreted to identify patterns, themes, and relevant findings related to the initial investment costs, operational and maintenance costs, as well as the energy costs of the photovoltaic solar power generation plant.

#### 2) Quantitative data analysis

The quantitative data obtained from the NPV and PBP calculations will be analyzed using economic statistical analysis. The results of these calculations will be used to evaluate the economic feasibility of the Photovoltaic Solar Power Generation Plant project at the National Institute of Technology Malang, such as whether the project yields positive value, adequate return rates, and the period required to recoup the initial investment.

Using this mixed-methods approach, the research will combine in-depth insights from interviews with objective quantitative analysis, thus providing a more comprehensive and accurate picture regarding the economic feasibility of the photovoltaic solar power generation plant project at the National Institute of Technology Malang.

## RESULTS AND DISCUSSION

This study analyzes two important aspects at Campus 2 of the National Institute of Technology Malang. Firstly, it analyzes the existing electrical load on the campus. Through this analysis, we can understand the magnitude of the electrical load that needs to be handled at Campus 2 of the National Institute of Technology Malang. Secondly, it conducts an economic feasibility analysis of photovoltaic solar power generation at Campus 2 of the National Institute of Technology Malang (Fig. 1). In this analysis, it evaluates whether photovoltaic solar power generation at the campus is economically feasible. Considering various factors such as initial investment, operational costs, and potential energy savings, it aims to determine whether photovoltaic solar power generation is an economical solution to meet the campus's electricity needs.

Based on this image, the installation location of the on-grid photovoltaic solar power generation plant with a capacity of 500 kWp is situated at Campus 2 of the National Institute of Technology Malang, Tasikmadu, Malang City. It can be observed that the installation is done in an empty field, allowing for the use of a ground-mount photovoltaic solar power generation plant installation. Approximately 5000 m<sup>2</sup> of land area is required for the construction of this photovoltaic solar power generation plant. Additionally, at the installation location, there are no tall trees or buildings that could cause shading on the solar modules, ensuring the efficiency of the system.

From the perspective of access to Campus 2 of the National Institute of Technology Malang, it is relatively easy as it is close to the Singosari Toll Exit, facilitating transportation and logistics during the installation and maintenance process of the photovoltaic solar power generation plant. In terms of temperature, the surrounding area of Campus 2 of the National Institute of Technology Malang has a tropical climate with temperatures ranging from 24.7°C to 32.8°C. The duration of sunlight exposure at the National Institute of Technology Malang ranges from 8 to 10 hours, creating ideal conditions to maximize the potential of the photovoltaic solar power generation plant's energy output.

### Electric Load at Campus 2 of the National Institute of Technology Malang

Based on the data obtained, the total power capacity at Campus 2 of the National Institute of Technology Malang is 465 kVA. Peak load occurs during the daytime when all activities in the building are operational in almost all sectors. At night, only a few rooms are still operational using electric energy. In peak load conditions, the total power consumed





(Source: Google Maps).

Fig. 1: Photovoltaic solar power plant at the National Institute of Technology Malang.

is 380 kVA. Since the building operates 24 hours a day, the daily energy consumed by the load throughout the building is approximately 380 kWh. Based on interview results, informants revealed that:

*“..., after the installation of solar photovoltaic power plants, it is able to fulfill all operational energy needs of the campus. Therefore, at present, the campus only pays the basic load bill from the State Electricity Company (Perusahaan Listrik Negara/PLN)”*.

The project installation of a 500.850 kWp grid-connected photovoltaic solar power plant at Campus 2 of the National Institute of Technology Malang utilizes 1113 monocrystalline JA solar photovoltaic modules with a capacity of 450 Wp each. It is capable of generating daily energy, reaching 680,980 kWh per year. Four inverters will convert direct current (DC) electricity into alternating current (AC), with each inverter having a capacity of 100 kW. The DC/AC ratio obtained is 1.25, considered ideal for enhancing the conversion rate of current before distribution to the loads. The output distribution of the inverters will supply power to the loads at Campus 2 of the National Institute of Technology Malang and the Rusunawa Building. The grid-connected photovoltaic solar power plant system is equipped with protection devices such as MCBs, arresters, and energy meters, as well as monitoring systems to monitor voltage, current, frequency, power, and energy consumption by the loads.

Data in the report document of the grid-connected photovoltaic solar power plant at the National Institute of

Technology Malang shows that Campus 2 of the National Institute of Technology Malang requires 380 kWh of energy per day for its operations. On the other hand, the grid-connected photovoltaic solar power plant at the National Institute of Technology Malang is capable of producing 1865.7 kWh of energy per day, indicating that the campus experiences an energy surplus. The energy generated by the photovoltaic solar power plant is converted into power through inverters, with the output voltage of each inverter being 95.1 kW. Each inverter experiences a power decrease of 1.9 kW due to losses in the AC cables. The total power generated by the four inverters is 372.8 kW. Out of this amount, 257.3 kW is directed to the Campus 2 Building of the National Institute of Technology Malang and 64.9 kW to the Student Dormitory Building. Meanwhile, the excess power of 50.6 kW is exported to the State Electricity Company (PLN). This means that 13.57% of the total power generated by the grid-connected photovoltaic solar power plant at the National Institute of Technology Malang is supplied to the State Electricity Company (PLN).

In an interview with an online media outlet, the rector of the National Institute of Technology Malang stated that some of the energy generated by the grid-connected photovoltaic solar power plant at the National Institute of Technology Malang can be supplied to the State Electricity Company. This brings efficiency benefits to the electricity financing of the Campus 2 Building of the National Institute of Technology Malang, which is 10–15% lower compared to the previous electricity payment to the State Electricity Company. The process of exporting energy has a significant

positive impact on managing the campus building's electricity costs. Thus, the grid-connected photovoltaic solar power plant at the National Institute of Technology Malang is capable of generating energy that is converted into power to meet the campus's needs and send excess power to the State Electricity Company.

The most important thing to understand is that in the energy transaction process with the State Electricity Company, cash transactions are not used. This was revealed by the informant:

*“The electricity from the on-grid photovoltaic solar power plant that is not used by the customers will automatically be sent to the State Electricity Company's grid and counted as exported electricity. The State Electricity Company will recognize this exported electricity as a deduction from the electricity bill in the following month, but only at 65% of the total kWh recorded on the export meter. This concept is known as net billing in the rooftop solar power plant scheme without using batteries, in accordance with Regulation of the Minister of Energy and Mineral Resources Number 49 of 2018. With net billing, there are no cash transactions involved in the calculation of electricity exports and imports for rooftop solar power plant customers.”*

The implementation of solar power plants at Campus 2 of the National Institute of Technology Malang has brought significant benefits in terms of economic feasibility. With the ability of the solar power plants to meet the campus energy needs and generate surplus energy that can be exported to the State Electricity Company, the electricity costs of Building Campus 2 of the National Institute of Technology Malang can be reduced by up to 10-15% compared to before. The energy export process without cash transactions through the net billing concept also has a positive impact on managing the campus building's electricity costs. Thus, the Solar Power Plant at the National Institute of Technology Malang not only provides a sustainable energy solution but also contributes to improving the economic feasibility of campus operations.

### **Feasibility Analysis of a Photovoltaic Solar Power Plant at Campus 2 of the National Institute of Technology Malang**

The economic feasibility of a photovoltaic solar power generation plant at Campus 2 of the National Institute of Technology Malang is inseparable from the chosen investment mechanism because the installation project requires significant investment. Therefore, a flexible and affordable investment scheme is required. This flexible investment scheme provides clients with the flexibility to adjust the rental costs of the photovoltaic solar power

generation plant according to their abilities. By using a flexible investment scheme, clients only need to pay the rental costs of the photovoltaic solar power generation plant. The rental costs of the photovoltaic solar power generation plant can be adjusted based on the client's abilities, allowing the installation project to be carried out more affordably.

The flexible and affordable investment scheme is the chosen option by Campus 2 of the National Institute of Technology Malang to facilitate the installation of a photovoltaic solar power generation plant more affordably and efficiently. With this flexible investment scheme, it is hoped that the installation project of the photovoltaic solar power generation plant at Campus 2 of the National Institute of Technology Malang can be successfully implemented and provide optimal long-term benefits in the installation project at Campus 2 of the National Institute of Technology Malang, PT. Sun Energy acts as the developer.

This analysis will involve several important aspects that need to be comprehensively evaluated. The objective of this analysis is to assess whether investing in a photovoltaic solar power generation plant at Campus 2 of the National Institute of Technology Malang is an economically sound decision and provides long-term benefits. Here are some aspects that will be examined in the economic feasibility analysis of the photovoltaic solar power generation plant at Campus 2 of the National Institute of Technology Malang. The economic feasibility analysis of the photovoltaic solar power generation plant at Campus 2 of the National Institute of Technology Malang includes several aspects, including:

**Initial investment costs:** Evaluation of the costs required to build the photovoltaic solar power generation plant system at Campus 2 of the National Institute of Technology Malang. Based on the interview results and document research provided, the initial investment cost of the centralized photovoltaic solar power generation plant reaches IDR. 4,084,498,826 (Table 1). The breakdown is as follows:

The total project cost of the solar power generation plant at Campus 2 of the National Institute of Technology Malang amounts to IDR 4,084,498,826, which is divided into six main components. The main component, including solar modules and inverters, has a cost of IDR 3,005,825,216. The monitoring system, including the remote monitoring system, Huawei Smart Logger, RS485 cable, SPD RS486, and monitoring box, has a cost of IDR 51,921,500. Cable and Conduit covering DC cables, AC cables, grounding cables, and cable trays costs IDR 256,567,504. Switchgear and Protection, including fuse, MCB DC, circuit breaker, AC and DC distribution panels, and external lightning protection, costs IDR 25,921,500. The mounting system, with mounting rails, end clamps, mid clamps, splices, and

Table 1: Initial Investment Costs for Solar Photovoltaic Power Plants.

Price	Component	Information
IDR 625.695.000	Services	-
IDR 91.568.106	Mounting System	Mounting rails, end clamps, mid clamps, splices, and brackets, along with installation costs
IDR 25.921.500	Switchgear and Protection	Fuse, MCB (miniature circuit breaker), DC circuit breaker, AC and DC distribution panels, and external lightning protection.
IDR 256.567.504	Cable and Conduit	DC cable, AC cable, grounding cable, and cable tray.
IDR 51.921.500	Monitoring System	Remote Monitoring System, Huawei Smart Logger, RS485 Cable, SPD RS486, and Monitoring Box.
IDR 3.005.825.216	Main Component	solar modules and inverters
<b>Total Price = IDR.4.084.498.826,-</b>		

brackets, along with installation costs, costs IDR 91,568,106. Finally, services have a cost of IDR 625,695,000. All these components contribute to the significant total project cost for implementing the solar power generation plant at Campus 2 of the National Institute of Technology Malang.

**Operational and maintenance (O&M) costs:** Knowing the costs associated with the operation and maintenance of the photovoltaic solar power generation plant after construction is crucial. According to the managers of the solar power generation plant at Campus 2 of the National Institute of Technology Malang, interview results reveal that maintenance of the solar power generation system is vital to maintaining the reliability and sustainability of the system. Therefore, in carrying out the operation and maintenance of the solar power generation plant, there are separate costs that need to be considered. The annual operational and maintenance (O&M) costs for the photovoltaic solar power generation plant amount to IDR 81,595,607, demonstrating a commitment to maintaining the performance of the photovoltaic solar power generation plant to remain optimal and efficient in generating electricity from solar energy.

**Cost of Energy from photovoltaic solar power plants:** Estimating the cost of energy generated by the photovoltaic solar power plant at Campus 2 of the National Institute of Technology Malang. Based on interview data, the total electricity price analysis from the Solar Power Plant system at Campus 2 of the National Institute of Technology Malang

Table 2: Analysis of Total Electric Energy Prices for Solar Photovoltaic Power Plants Campus 2 National Institute of Technology Malang.

Component	Cost [Rp. kWh <sup>-1</sup> ]	Information
A	780	Initial investment value
B	120	Operation and maintenance costs (2% of the total price)
C	30	Unexpected fees (0.5%)
Total	930	Total cost of electricity per kilowatt-hour

is obtained by summing up the price per kWh of each component (Table 2), as detailed below:

Therefore, the total price per kWh of electrical energy from the Photovoltaic Solar Power Plant system at the National Institute of Technology Malang is IDR 930, calculated by considering the contribution of each component A, B, and C as provided.

**Calculation of the net present value (NPV) of the photovoltaic solar power plant at the National Institute of Technology Malang:** Calculating the net present value (NPV) of the cash flow generated by the photovoltaic solar power plant to evaluate the project’s financial feasibility. In computing the net present value (NPV) of the solar power plant project at the National Institute of Technology Malang campus, the difference between discounted revenues and expenditures is calculated. Here is the interview data regarding the NPV calculation results:

*“The net cash flow is IDR 11,873,894,464 calculated over the lifetime of the solar power plant project at the National Institute of Technology Malang campus, which typically spans 25 years. The total investment cost is IDR 4,084,498,862”.*

Based on the data, determine the NPV value of the photovoltaic solar power plant at the National Institute of Technology Malang campus based on the following formula:

$$NPV = \text{Net cash flow} - \text{Total investment}$$

$$NPV = \text{IDR } 11.873.894.464 - \text{IDR } 4.084.498.862$$

$$NPV = \text{IDR } 7.789.395.602$$

Nilai NPV Pembangkit Listrik Tenaga Surya Kampus 2 Institut Teknologi Nasional Malang adalah IDR 7.789.395.602. Nilai NPV yang positif menunjukkan bahwa proyek tersebut menghasilkan keuntungan di masa depan. Karena nilai NPV > 0, maka Pembangkit Listrik Tenaga Surya Kampus 2 Institut Teknologi Nasional Malang layak dijalankan. Semakin besar nilai NPV, semakin besar keuntungan yang diharapkan.

**Calculation of the Payback Period (PBP) for the Photovoltaic Solar Power Plant at the National Institute of Technology Malang:** Calculating the time required to recover the initial investment in the photovoltaic solar power plant to evaluate the speed of the investment return. In the Payback Period (PBP) analysis for the on-grid photovoltaic solar power plant at Campus 2 of the National Institute of Technology Malang, based on the data of net cash flow amounting to IDR 477,561,959. The calculated PBP result is as follows:

$$\text{PBP} = \text{Initial investment} / \text{Net cash flow}$$

$$\text{PBP} = \text{IDR } 4.084.498.862 / \text{IDR } 477.561.959$$

$$\text{PBP} = 8.55 \text{ Years}$$

Based on the calculations conducted, it can be concluded that the on-grid photovoltaic solar power plant at Campus 2 of the National Institute of Technology Malang has a payback period of 8.55 years, equivalent to 8 years and 6 months. A shorter PBP compared to the device's lifespan indicates that the photovoltaic solar power plant project at Campus 2 of the National Institute of Technology Malang is deemed feasible in terms of the payback period for the initial investment. This suggests that the investment in the photovoltaic solar power plant can be recovered in a relatively short time, demonstrating the project's efficiency in generating savings on electricity costs. Therefore, the on-grid photovoltaic solar power plant project at Campus 2 of the National Institute of Technology Malang can be considered a profitable and sustainable long-term investment.

The on-grid Photovoltaic Solar Power Plant at Campus 2 of the National Institute of Technology Malang demonstrates good economic feasibility. The energy generated annually is 680,980 kWh/year, with the annual operational and maintenance (O&M) costs reaching IDR 81,595,607. This indicates the commitment of Campus 2 of the National Institute of Technology Malang to maintain the performance of the Photovoltaic Solar Power Plant to remain optimal and efficient in generating electricity from the sun. These costs are relatively low compared to the long-term benefits when compared to the annual operation and maintenance (O&M) costs of the Solar Power Plant at the Regional Hospital (RSUD) of Mimika Regency, which reached IDR 100,477,114, with an annual energy output of 90,474 kWh. year<sup>-1</sup> (Kariongan & Joni 2022).

The total price per kWh of electricity from the photovoltaic solar power plant system at Campus 2 of the National Institute of Technology Malang is Rp 930, which is considered competitive compared to the electricity price from the State Electricity Company (PLN). Economic analysis values indicate a positive net present value, and energy costs

can be averaged over 25 years (Ennemiri et al. 2024). This indicates that photovoltaic solar power plants can be a more economical alternative energy source. The difference in the total price per kWh, according to Wang et al. (2024), can be the right choice based on its energy consumption to reduce energy bills. According to Tarigan (2024), the photovoltaic solar power plant system will not only reduce its electricity bills but also balance energy for 10 years.

The net present value (NPV) of the photovoltaic solar power plant at Campus 2 of the National Institute of Technology Malang is IDR 7,789,395,602, indicating that the project yields future profits. Based on the net cash flow data, the payback period (PBP) of the photovoltaic solar power plant at Campus 2 of the National Institute of Technology Malang is 8.55 years from the lifespan or device age of the solar panels. This indicates that this positive NPV value serves as a strong indicator that the photovoltaic solar power plant project is viable. Additionally, the initial investment in photovoltaic solar power plants will be recouped in a relatively short time. This short PBP enhances the project's attractiveness to investors. These research findings align with Zebua and Huda's (2024) study, which found that on-grid photovoltaic solar power plants have a larger NPV and a smaller PBP value. In essence, investing in photovoltaic solar power plant technology is quite profitable for universities (Ali & Alomar 2023).

Thus, the benefits of the economic feasibility of the on-grid photovoltaic solar power plant at Campus 2 of the National Institute of Technology Malang include: 1) generating clean and environmentally friendly electricity; 2) saving electricity costs in the long term; and 3) enhancing the image of the National Institute of Technology Malang as an institution that cares about the environment. Therefore, the National Institute of Technology Malang needs to conduct periodic studies and evaluations of the performance of the photovoltaic solar power plant to ensure and optimize its maximum operation.

## CONCLUSIONS

Based on the analysis conducted, it can be concluded that the on-grid photovoltaic solar power generation plant at Campus 2 of the National Institute of Technology Malang is economically feasible. Factors such as controlled operational and maintenance costs, competitive electricity prices, a positive net present value (NPV), and a short payback period indicate that this project is viable to proceed with. The success of this photovoltaic solar power generation plant project can also provide significant economic benefits to the National Institute of Technology Malang while enhancing the institution's image as an environmentally conscious

educational institution. However, to ensure the sustainability and optimization of the performance of the photovoltaic solar power generation plant at the National Institute of Technology Malang, periodic studies and evaluations are needed. This is aimed at ensuring that the photovoltaic solar power generation plant operates efficiently and provides maximum economic benefits to the institution. Thus, these measures will support the National Institute of Technology Malang in achieving sustainable goals and making positive contributions to the surrounding environment.

The implications of this research for future practice and research are significant. First, the study demonstrates that the implementation of photovoltaic solar power plants (PV) is economically feasible, particularly in campus environments. This serves as an encouragement for other higher education institutions to adopt similar technologies as part of their efforts to promote energy and environmental sustainability. Second, the research underscores the need for further investigation into addressing economic barriers associated with the development of photovoltaic solar power plants, such as significant initial investments and limitations in economic feasibility studies. Future research could focus on developing innovative business models and financial strategies to promote investment in photovoltaic solar power plants (PV). Third, the study highlights the importance of regular evaluation and monitoring of the performance of photovoltaic solar power plants (PV). Further studies could explore more advanced and effective evaluation methods to ensure the efficient and optimal operation of photovoltaic solar power plants (PV). Lastly, this research provides a foundation for higher education institutions to serve as role models in the adoption of renewable technologies and contribute to global efforts to reduce greenhouse gas emissions. This expands the scope of future research to understand the social, economic, and environmental impacts of using photovoltaic solar power plants (PV) in various higher education contexts.

## ACKNOWLEDGMENT

We would like to express our sincere gratitude to the administration and staff of Institut Teknologi Nasional (ITN) Malang for their invaluable support and assistance throughout the course of this research. Their cooperation and provision of resources have been instrumental in facilitating the data collection process and ensuring the success of this study. We are particularly grateful for their commitment to promoting research initiatives and fostering an environment conducive to academic inquiry. Their dedication to academic excellence and scholarly endeavors has greatly contributed to the advancement of knowledge in our field.

## REFERENCES

- Ali, O.M. and Alomar, O.R., 2023. Technical and economic feasibility analysis of a PV grid-connected system installed on a university campus in Iraq. *Environmental Science and Pollution Research*, 30(6), pp.15145–15157. <https://doi.org/10.1016/j.applthermaleng.2019.114678>
- Al-Shetwi, A.Q., 2022. Sustainable development of renewable energy integrated power sector: Trends, environmental impacts, and recent challenges. *Science of The Total Environment*, 822(20), p.153645. <https://doi.org/10.1016/j.scitotenv.2022.153645>
- Azhari, D.S., Afif, Z., Kustati, M. and Sepriyanti, N., 2023. Mixed method research for dissertations. *Innovative: Journal of Social Science Research*, 3(2), pp.8010–8025. <https://doi.org/10.31004/innovative.v3i2.1339>
- Basabien, W., Alzuhair, A., Badahya, M., Mogaitoof, A. and Ismail, M.A., 2024. Utilizing solar energy for higher education: design and implementation of a 500 kw rooftop solar array for College of Engineering, King Faisal University. *Journal of Engg. Research*, 11, p.119
- Boruah, D. and Chandel, S.S., 2024. Techno-economic feasibility analysis of a commercial grid-connected photovoltaic plant with battery energy storage achieving a net zero energy system. *Journal of Energy Storage*, 77, p.109984. <https://doi.org/10.1016/j.est.2023.109984>
- Bouraima, M.B., Ayyıldız, E., Badi, I., Özçelik, G., Yeni, F.B. and Pamucar, D., 2024. An integrated intelligent decision support framework for the development of photovoltaic solar power. *Engineering Applications of Artificial Intelligence*, 127, p.107253. <https://doi.org/10.1016/j.engappai.2023.107253>
- Czepto, F. and Borowski, P.F., 2024. Innovation Solution in Photovoltaic Sector. *Energies*, 17(1), p.265. <https://doi.org/10.3390/en17010265>
- Dehler-Holland, J., Okoh, M. and Keles, D., 2022. Assessing technology legitimacy with topic models and sentiment analysis—The case of wind power in Germany. *Technological Forecasting and Social Change*, 175, p.121354. <https://doi.org/10.1016/j.techfore.2021.121354>
- Draou, M., Brakez, A. and Bennouna, A., 2024. Techno-economic feasibility assessment of a photovoltaic water heating storage system for self-consumption improvement purposes. *Journal of Energy Storage*, 76, p.109545. <https://doi.org/10.1016/j.est.2023.109545>
- Ennemiri, N., Berrada, A., Emrani, A., Abdelmajid, J. and El Mrabet, R., 2024. Optimization of an off-grid PV/biogas/battery hybrid energy system for electrification: A case study in a commercial platform in Morocco. *Energy Conversion and Management*, 10(21), p.100508. <https://doi.org/10.1016/j.ecmx.2023.100508>
- Etukudoh, E.A., Nwokediegwu, Z.Q.S., Umoh, A.A., Ibekwe, K.I., Ilojiyanya, V.I. and Adefemi, A., 2024. Solar power integration in Urban areas: A review of design innovations and efficiency enhancements. *World Journal of Advanced Research and Reviews*, 21(1), pp.1383–1394. <https://doi.org/10.30574/wjarr.2024.21.1.0168>
- Haber, I.E., Toth, M., Hajdu, R., Haber, K. and Pinter, G., 2021. Exploring public opinions on renewable energy by using conventional methods and social media analysis. *Energies*, 14(11), p.3089. <https://doi.org/10.3390/en14113089>
- Hamad, J., Ahmad, M. and Zeeshan, M., 2024. Solar energy resource mapping, site suitability and techno-economic feasibility analysis for utility scale photovoltaic power plants in Afghanistan. *Energy Conversion and Management*, 303, p.118188. <https://doi.org/10.1016/j.enconman.2024.118188>
- Huda, A., Kurniawan, I., Purba, K.F., Ichwani, R. and Fionasari, R., 2024. Techno-economic assessment of residential and farm-based photovoltaic systems. *Renewable Energy*, 222, p.119886. <https://doi.org/10.1016/j.renene.2023.119886>
- Humas EBTKE., 2023. *Installed EBT Capacity Reaches 12.7 GW. This is the Government's Quick Action to Absorb the Potential of EBT. Ministry General of New, Renewable Energy and Energy Conservation*



- (EBTKE). Retrieved February 02, 2024, from <https://ebtke.esdm.go.id/post/2023/07/24/3536/kapasitas.terpasang.ebt.capai.127.gw.ini.gerak.cepat.pemerintah.serap.potensi.ebt>
- Jamil, M., Kirmani, S. and Rizwan, M., 2012. Techno-economic feasibility analysis of solar photovoltaic power generation: A review. *Smart Grid and Renewable Energy*, 3(4), pp.266-274. <https://doi.org/10.4236/sgre.2012.34037>
- Kariongan, Y. and Joni, J., 2022. Planning and economic analysis of rooftop solar power plant with on grid system as additional power supply at Mimika Regency Regional Hospital. *Jurnal Pendidikan Tambusai*, 6(1), pp.3763-3773. <https://doi.org/10.31004/jptam.v6i1.3453>
- Kristiawan, R.B., Widiastuti, I. and Suharno, S., 2018. Technical and economical feasibility analysis of photovoltaic power installation on a university campus in Indonesia. *MATEC Web of Conferences*, 197, p.08012. <https://doi.org/10.1051/mateconf/201819708012>
- Manoo, M.U., Shaikh, F., Kumar, L. and Arıcı, M., 2024. Comparative techno-economic analysis of various stand-alone and grid connected (solar/wind/fuel cell) renewable energy systems. *International Journal of Hydrogen Energy*, 52(2), pp.397-414. <https://doi.org/10.1016/j.ijhydene.2023.05.258>
- Minazhova, S., Akhambayev, R., Shalabayev, T., Bekbayev, A., Kozhageldi, B. and Tvaronavičienė, M., 2023. A review on solar energy policy and current status: Top 5 countries and Kazakhstan. *Energies*, 16(11), p.4370. <https://doi.org/10.3390/en16114370>
- Mulyani, Y.P., Saifurrahman, A., Arini, H.M., Rizqiawan, A., Hartono, B., Utomo, D.S., Spanellis, A., Beltran, M., Nahor, K.M.B. and Paramita, D., 2024. Analyzing public discourse on photovoltaic (PV) adoption in Indonesia: A topic-based sentiment analysis of news articles and social media. *Journal of Cleaner Production*, 434, p.140233. <https://doi.org/10.1016/j.jclepro.2023.140233>
- Obeng, M., Gyamfi, S., Derkyi, N.S., Kobo-bah, A.T. and Peprah, F., 2020. Technical and economic feasibility of a 50 MW grid-connected solar PV at UENR Nsoatre Campus. *Journal of Cleaner Production*, 247, p.119159. <https://doi.org/10.1016/j.jclepro.2019.119159>
- Paudel, B., Regmi, N., Phuyal, P., Neupane, D., Hussain, M.I., Kim, D.H. and Kafle, S., 2021. Techno-economic and environmental assessment of utilizing campus building rooftops for solar PV power generation. *International Journal of Green Energy*, 18(14), pp.1469-1481. <https://doi.org/10.1080/15435075.2021.1904946>
- Pramadya, F.A. and Kim, K.N., 2024. Promoting residential rooftop solar photovoltaics in Indonesia: Net-metering or installation incentives? *Renewable Energy*, 222, p.119901. <https://doi.org/10.1016/j.renene.2023.119901>
- Sarie, F., Sutaguna, I.N.T., Par, S.S.T., Par, M., Suiraoka, I.P., ST, S., Darwin Damanik, S.E., SE, M., Efrina, G. and Sari, R., 2023. Research methodology. *Cendikia Mulia Mandiri*, 16, pp.105-113.
- Shahsavari, A. and Akbari, M., 2018. Potential of solar energy in developing countries for reducing energy-related emissions. *Renewable and Sustainable Energy Reviews*, 90, pp.275-291. <https://doi.org/10.1016/j.rser.2018.03.065>
- Suheri, S., Febri, S.P., Arif, Z. and Amir, F., 2019. Study of the use of rooftop photovoltaic power plants as an effort to implement a green campus. *JURUTERA-Jurnal Umum Teknik Terapan*, 6(02), pp.14-18. <https://doi.org/10.55377/jurutera.v6i02.1911>
- Tarigan, E., 2024. Techno-economic analysis of residential grid-connected rooftop solar PV systems in Indonesia under MEMR 26/2021 Regulation. *International Journal of Energy Economics and Policy*, 14(1), pp.412-417. <https://doi.org/10.32479/ijeep.15277>
- Tshivhase, M.L. and Bisschoff, C.A., 2024. Investigating green initiatives at South African public universities. *Nurture*, 18(2), pp.245-263. <https://orcid.org/0000-0002-8128-5479>
- Wang, Z., Luther, M., Horan, P., Matthews, J. and Liu, C., 2024. Technical and economic analyses of PV battery systems considering two different tariff policies. *Solar Energy*, 267, p.112189. <https://doi.org/10.1016/j.solener.2023.112189>
- Zebua, O. and Huda, Z., 2024. Analysis of the economic feasibility and self-consumption of on-grid and hybrid PLTS with a capacity of 1328 kWp. *Electrician: Jurnal Rekayasa Dan Teknologi Elektro*, 18(1), pp.41-49. <https://doi.org/10.23960/elc.v18n1.2617>

---

#### ORCID DETAILS OF THE AUTHORS

Rijal Asnawi: <https://orcid.org/0000-0002-4202-5498>



# Impact of Urban Xenobiotics on Mycorrhizal Associations in Urban Plants

Aashutosh Kumar Mandwa<sup>1</sup>, Atul Kumar Bhardwaj<sup>1</sup>, Rajesh Kumar<sup>2†</sup>, K.K. Chandra<sup>1</sup>, Chanchal Kumari<sup>1</sup> and S. K. Padey<sup>3</sup>

<sup>1</sup>Department of Forestry, Wildlife and Environmental Sciences, Guru Ghasidas Vishwavidyalaya (A Central University), Bilaspur (C.G.), India

<sup>2</sup>Mahatma Gandhi University of Horticulture and Forestry, Sankra, Patan, Durg, C.G., India

<sup>3</sup>IGNOU Regional Centre Gandhi Bhawan, B.H.U. Campus, Varanasi, 221005, India

†Corresponding author: Rajesh Kumar; Rajesh.dewangan0506@gmail.com

## Nat. Env. & Poll. Tech.

Website: [www.neptjournal.com](http://www.neptjournal.com)

Received: 25-02-2024

Revised: 09-04-2024

Accepted: 29-04-2024

## Key Words:

Urban plants  
Xenobiotics  
Mycorrhiza  
Heavy metals  
Pollution

## ABSTRACT

Urban xenobiotics are a vital contamination phenomenon of urban plants in the overall country. They are a result of human activity due to growing urbanization and population growth. There are extensive sources of both natural (soil or rock erosion, fires, biodegradation, and volcanic eruptions) and anthropogenic (soil pollution, air, and herbicides). Currently, the demand for pharmaceuticals, compared to the growing population, has placed a risk on the urban plant. Additionally, the production of illegal drugs has caused the release of dangerous carcinogens into fungal activities, which will have an impact on plant health, microbial structure, and fungal interaction. Because of the harsh environment, higher temperatures, heavy metals, and higher N deposition, most urban trees suffer from stress conditions, and mycorrhiza is negatively impacted by plant conditions. Some mycorrhiza fungi are unable to sporulate and hyphal at higher xenobiotic concentrations in urban areas. This chapter takes a look at the sources and compounds of xenobiotics and their harmful impact on mycorrhiza; and its association with the urban plants.

## INTRODUCTION

Urbanization has both positive and negative effects on the plant, but it is undoubtedly bringing about change. According to UN estimates, more than half of the world's population already lives in cities, and by the year 2050, that percentage will rise to 64% in developing countries and 86% in developed countries. The effects of climate change will be especially felt in urban areas because of how quickly urbanization grows globally (Bazaz et al. 2018). As a result, the temperature rise brought on by global warming is problematic for the ensuing decades because it will have a variety of effects on urban areas, which will have an impact on plant health, microbial structure, and fungal interaction. Urban pollution is a major challenge due to the steadily growing urban population. Human demand is rising as a result of the growing population, which has a negative impact on the urban area's plant environment (Liang et al. 2008). Although most urban xenobiotics come from natural sources, human-related emissions are the most dangerous. Cities frequently have worsened anthropogenic sources of xenobiotics, such as factories, industries, transportation, and so forth, because of the local concentration of people and

human activity (Stefanac et al. 2021). For instance, fungus activity and the connection between fungi and plant roots affect xenobiotics in urban areas. Xenobiotics are chemicals or other substances that cannot be utilized by plants for the production of energy and are typically absent from ecosystems. Similar to other organisms in the environment, plants are constantly exposed to xenobiotics such as pesticides (such as atrazine, chlorpyrifos, cypermethrin, endosulfan, etc.), allelochemicals (such as cinnamic acid, benzoic acid), organic pollutants (such as trinitrotoluene, phenanthrene), heavy metals/metalloids (such as lead, cadmium, arsenic) (Zhang et al. 2007, Riechers et al. 2010). These xenobiotics can come from both anthropogenic (air and soil pollution, herbicides) and natural (fires, volcanic eruptions, soil or rock erosion, biodegradation) sources. Urban plants typically consist of tiny, isolated forest fragments and are subjected to very harsh environmental conditions (Ruddiman 2013). Urban forests experience higher temperatures than their rural counterparts because of heat island effects (Oke 1973), an increase in N deposition (Hosseini et al. 2015, O'Brien et al. 2012), and heavy metal buildup (Sun et al. 2009). Mycorrhizal fungi can be

negatively impacted by specific environmental conditions present in most urban environments, despite the fact that plant-mycorrhizal associations appear to be very resilient to disturbances and can persist in the soil despite clear-cutting and weathering (Haug et al. 2013, Bhardwaj & Chandra 2016, Kumar et al. 2023). Mycorrhizal diversity was found to be lower in urban and highly disturbed soils, and Karpati et al. (2011) theorized that this change may be due to pollution and increased anthropogenic nitrogen deposition. According to Egerton-Warburton and Allen (2000), some AMF fungi fail to sporulate in high nitrogen environments, and hyphal growth is frequently inhibited by N deposition (Treseder & Allen 2000, Bhardwaj & Chandra 2017, Kumar et al. 2024). Additionally, mycorrhizal colonization can be hampered or reduced by heavy metals like zinc and lead (Yang et al. 2015). Another helpful mycorrhizal indicator is the fact that mycorrhizal communities are less diverse in soils with more recent physical disturbance and smaller soil aggregates (Duchicela 2013, Bhardwaj et al. 2023a, Kumar et al. 2022). Mycorrhiza is a symbiotic relationship between plant roots and soil fungi. About 80% of terrestrial plants can establish associations with mycorrhizal fungi (Smith & Read 2008, Chandra 2014, Bhardwaj et al. 2023b). Mycorrhizal fungi help plants acquire water, phosphorus (P), and other essential nutrients, and the colonizing fungi, in turn, obtain carbon from their host plant (Smith & Smith 2011, Chandra & Bhardwaj 2018). In this chapter, we focus on the xenobiotics that alter the soil's beneficial fungi for urban plants and identify the key urban xenobiotics that are primarily to blame for the decline in mycorrhizal associations.

## XENOBIOTICS: SOURCES AND TYPES

The words "xenobiotic" come from Greek words that originally meant "foreign or strange" and "exotic," which means life. Xenobiotics are chemicals with peculiar structural characteristics (Fetzner 2002). Numerous xenobiotics have the potential to be harmful to organisms that come into contact with them in the environment. However, these bioavailable substances depend on the characteristics of the organism, the chemicals, and the environment. According to Maenpaa (2007), the bioaccumulation of chemical byproducts within the organism is correlated with the toxicity of any xenobiotic. Xenobiotics can linger in the environment for months or even years. For instance, the polymer structure of lignin or the components of a small number of fungi's cell walls (melanin polymers) may not break down quickly in the environment (Fetzner 2002). The same is true for hydrophobic pollutants in aquatic environments, which are eventually stored in sediments and turn dangerous when they come into contact with benthic organisms. Any exposure to xenobiotic-contaminated sediments may have an impact on the lower trophic levels.

At higher trophic levels, it might also cause biomagnification or more harmful toxic effects (Landrum & Robbins 1990, Lee 1992, Streit 1992, Newman 1998).

Xenobiotics are a significant urban plant contamination phenomenon across the entire country. They are the result of human activity sparked by escalating urbanization and population growth. There are many anthropogenic and natural sources of pollution, including volcanic eruptions, biodegradation, soil erosion, and fires (soil pollution, air, and herbicides) (Musolff et al. 2010). Due to the imbalance between the demand for pharmaceuticals and the growing population, the urban plant is currently in danger. In addition, harmful carcinogens have been released into the metabolism of urban plants as a result of the production of illegal drugs. The release of these dangerous xenobiotics has an immediate and long-term effect on the urban plant (Brooks 2018). Plants growing in highly soil xenobiotics environments have disruptions in the physiology and biochemical processes like CO<sub>2</sub> fixation, gaseous exchange, nutrient absorption, and respiration (Fig. 1). These disturbances cause the urban plant to produce less biomass and grow more slowly.

As a result of technological development in the 20<sup>th</sup> century, a large number of substances that are used to improve daily life (such as antibiotics, pesticides, dyes, PCPs, and additives) either do not necessarily occur naturally in the environment or whose naturally occurring concentrations are very different from those caused by anthropogenic activity.

The main problem is their physicochemical structures, which make them difficult to identify, quantify, and eliminate (De Oliveira et al. 2020). These structures include small molecular size, ionizability, water solubility, lipophilicity, polarity, and volatility.

Xenobiotics are chemicals that exist in both the environment and living things but are not created there. When found in high concentrations in the environment, some naturally occurring chemicals (endobiotics) turn into xenobiotics (Soucek 2011). They are classified as pesticides, pharmaceutical compounds, personal care products, illicit drugs, industrial products, and nuclear waste (Kumar et al. 2020) and can be found in the air, soil, water, plants, animals, and humans, as shown in Fig. 2. According to WFD, priority substances are divided into 17 categories (organophosphorus polyaromatic, herbicides, hydrocarbons, chlorinated solvents, organochlorine insecticides, aromatic organochlorine compounds, PBBs, dioxins, BDEs, phthalate, metals, anti-fouling biocide, pyrethroid insecticides, alkylphenols, perfluorinated surfactant, quinoline fungicide, benzene, hexabromocyclododecane, and chloroalkanes). Substances on the watch list are divided into eight categories (hormones, antibiotics, pharmaceuticals, neonicotinoid



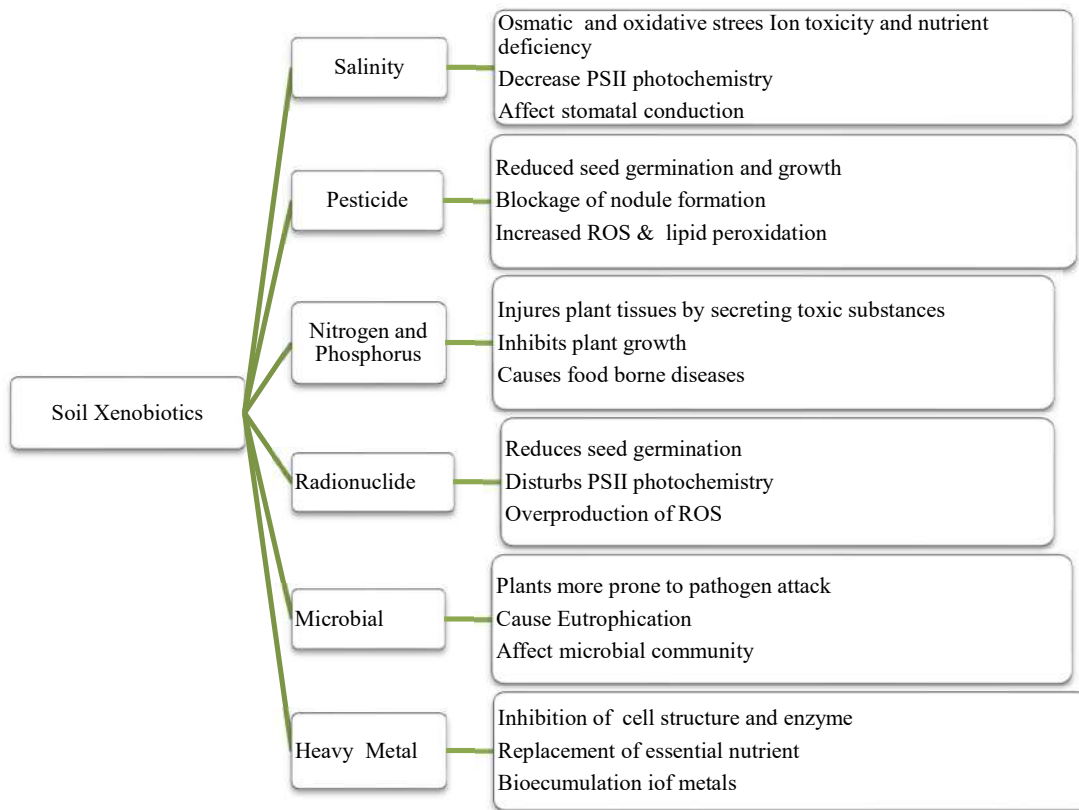


Fig. 1: Various soil xenobiotics influence the plant growth and physiology metabolism activity in plants.

insecticides, herbicides, antioxidant, carbamate insecticides, and sunscreen agent), and candidate substances, such as sulfonylurea herbicide, pyrethroid insecticides, organophosphorus insecticides, and metals and non-metals

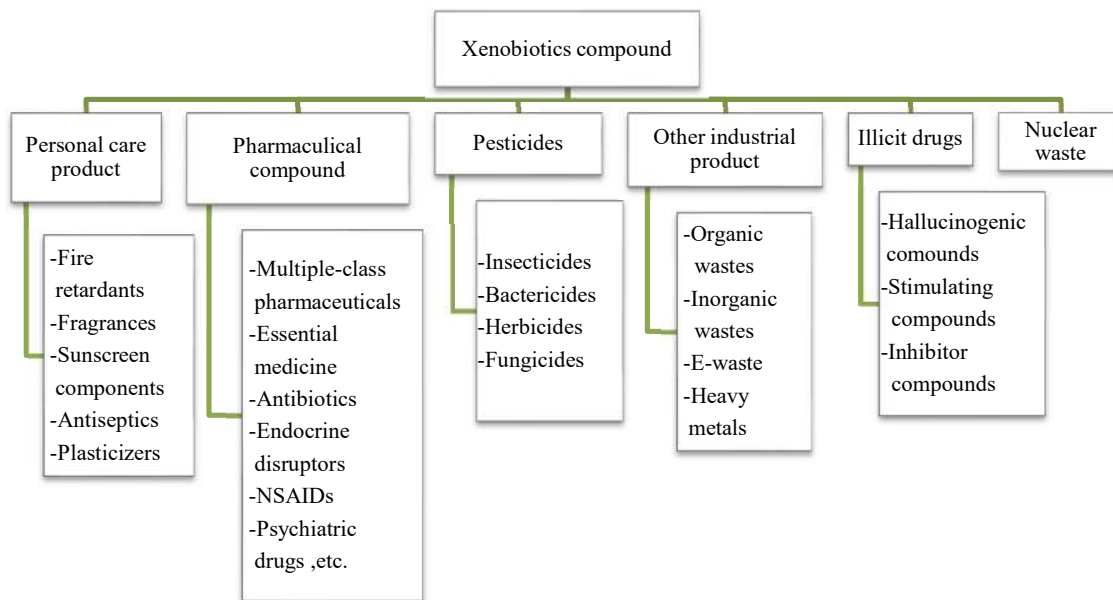


Fig. 2: Xenobiotics compounds (Kumar et al. 2020).

are present in traces. These are the different anthropogenic actions for entering xenobiotics into the environment, such as human consumption and excretion, livestock treatment and excretion, wastewater and sewage treatment plants, agriculture practices and industries, and production plants (Kumar & Chopra 2020). Pesticides are applied directly to the soil, where they are then washed into nearby rivers and groundwater, etc. When PPCPs are consumed by humans, they indirectly enter the environment because some of the metabolites cannot be completely metabolized and are, therefore, more toxic than the original compound. After excretion, they eventually find their way into sewage/wastewater treatment facilities, soil, groundwater, rivers, lakes, and oceans. Plants absorb PPCPs and pesticides, which then enter the food chain. Xenobiotic sources and substances can be categorized in Fig. 2 (Mathew et al. 2017).

### **XENOBIOTICS IN URBAN SOIL**

Urban soil pollution can be caused by both man-made (industry, land-based farming, extractives, wastewater, waste, energy production, and transportation) and unnatural (soil geochemistry, landslides geology, and salt) sources (UNEP 2017). All systems, whether they are made by humans or the natural world, have soil as their foundation. The soil in urban areas serves two crucial functions: promoting urban development and sustaining parks and gardens, which are crucial for the environmental well-being of urban areas (Cachada et al. 2018).

The main factors causing soils used for urban development or transportation infrastructures to lose the majority of their functions are disrupted water, nutrient, and biological cycles (European Commission 2012). Depending on its intended use, soil quality is evaluated. Through the use of chemical, physical, and biological indicators, this assessment is carried out (Cachada et al. 2018).

### **URBAN MYCORRHIZA**

Mycorrhizal symbiosis refers to the association of fungi with plant roots. This relationship is predominantly mutualistic, that is, with both partners benefiting from the association. There are seven types of mycorrhizal association, but common to all types is the net movement of carbon, generally (but not always) from the plant host to the fungus partner. In return, a fungus may confer increased nutrient supply, defense against pathogenic attack, and drought resistance to its partner plant. More than 90% of all plant families studied (80% of species) in both agricultural and natural environments form mycorrhizal associations, and they can be essential for plant nutrition. Mycorrhizas are found in a wide range of habitats, including deserts, lowland tropical rainforests,

high latitudes and altitudes, and aquatic ecosystems. There are a few exceptions to the rule that mycorrhizas are found in all plant species that are economically important to man.

### **URBAN RHIZOSPHERE**

The rhizosphere is the area of soil that surrounds plant roots. This region is characterized by root activity, including the related soil microbes and exudate production. The rhizosphere contains many microorganisms, which promotes their diversity, activity, and other interactions. This makes it a haven for a variety of organisms (Hinsinger et al. 2009). Rhizosphere processes include microbial colonization and biological, chemical, and physical changes caused by the plants' movement of water and minerals, which releases carbon dioxide, nutrients, and a variety of chemical compounds (Philippot et al. 2013). The secretion of chemical exudates into the rhizosphere region by the root cells is the process of rhizodeposition; these exudates are referred to as rhizodeposits (Hinsinger et al. 2005). Plants release a variety of substances into the soil around their roots, including organic acids, secondary metabolites, polysaccharides, amino acids, nitrogen (N), and organic carbon (Dennis et al. 2010, Baetz & Martinoia 2014). One of the key rhizosphere effect phenomena is the carbon released by germination-initiating seeds or plant roots, which permeates the soil and encourages microbial activity and proliferation (Farrar et al. 2003). Numerous studies have documented the effects of the rhizosphere on biotransformation for various compounds, such as improving plants' tolerance to phytotoxic elements in the soil because plants can encourage microorganisms that detoxify the xenobiotics (Dubey & Fulekar 2013, Agrawal & Dixit 2015).

Interactions between microbes and plants in the rhizosphere can be advantageous, neutral, or harmful depending on the particular host plant and the microbe involved in the current environmental conditions (Raaijmakers et al. 2009, Bais et al. 2006, Gianfreda 2015). While some pathogenic microbes, parasitic plants, and other harmful invertebrates associate with one another in the negative interactions, mycorrhizal fungi, rhizobacteria that encourage plant growth, and other beneficial microbes favor the positive interactions (Raaijmakers et al. 2009).

### **RHIZODEGRADATION IN URBAN AREA**

Rhizodegradation is the process of influencing plant roots to accelerate soil's natural degradation processes, which can lead to the best detoxification of these organic pollutants. This process involves a variety of organic compounds, such as chlorinated solvents, petroleum hydrocarbons, pesticides, PAHs, surfactants, and polychlorinated biphenyls (Rentz et

al. 2005). A few organic compounds that provide carbon and nitrogen are found in the root exudates of plants, which help the microorganisms that break down organic toxins grow and live longer. Additionally, studies revealed that plant roots stimulate the growth of microorganisms because they release certain organic compounds known as organic acids, enzymes, amino acids, sugars, and complex carbohydrates that are necessary for the development of microorganisms (Shim et al. 2000, Singer et al. 2003). Rhizospheric microbial populations contribute to the creation of substances that lessen plant stress, transport nutrients, protect against pathogens, and degrade pollutants (Gerhardt et al. 2009). As a result, certain plants and rhizospheric and endophytic microorganisms (bacteria) can work together to degrade poisonous organic compounds.

The density of microorganisms in the rhizosphere, which can be two to four times greater than the microbial population in the non-rhizospheric soil, promotes the degradation of polycyclic hydrocarbons (PAHs) in rhizospheric soils (Alkorta & Garbisu 2001, Anderson et al. 1994, Sheng-you et al. 2005). After annual plant growth, the PAH kills 100 times more microbial colonies in vegetated management than in unvegetated groups, according to research by Gerhardt et al. (2009). It was found that the degradation of phenanthrene is significantly accelerated by the addition of plant debris and root exudates (Miya & Firestone 2001).

The microbial community in the rhizosphere is influenced by a variety of factors, including the species of plant, root type, age of the plant, soil type, and previous exposure of the plant roots to xenobiotics. In general, gram-negative microbial communities predominate in the rhizosphere (Atlas & Bartha 1986). When compared to non-vegetated soil, the carbon dioxide concentration in the rhizosphere is typically higher, and the pH of rhizosphere soil is 1-2 units lower. The oxygen levels, moisture content, redox potentials, and osmotic potentials are some other variables that are affected by vegetation. Some characteristics of specific plant species are among the additional variables that affect these parameters. Physical and chemical changes that occur frequently at the root-soil interface lead to stable changes in the soil's structure and microbial community (Dzantor 2007).

Plant-microbe interactions lead to an increase in microbial biomass relative to soil bulk levels. The rhizosphere effect is typically defined as the ratio of organisms in rhizosphere-containing soil to those in rhizosphere-free soil. Although this ratio can be greater than 100, it typically falls between 5 and 20. The increased microbial activity and growth in the rhizosphere may be the cause of the increased metabolic degradation rate of different xenobiotic compounds. It is, therefore, intriguing to think about whether selecting

plants with super-modulating roots, increasing root hairs, or breeding plants with roots that are more firmly set genetically would speed up the rate at which specific toxicants in the rhizosphere are broken down by microbes (Kidd et al. 2008).

## CHANGES IN THE STRENGTH OF MYCORRHIZAL ASSOCIATIONS UNDER URBANIZATION

In urban areas, Shannon's diversity and Simpson's diversity of root AMF were significantly higher than in rural areas. Numerous studies have documented how important AM fungi are for increasing host plant resistance to heavy metal toxicity as well as host plant resistance to disease and insects (Hildebrandt et al. 2007, Khade & Adholeya 2008, Joy 2013, Schneider et al. 2016).

It is anticipated that plants in urban areas will rely more on mycorrhizal symbioses than plants in rural areas because of their increased exposure to biotic and abiotic stresses (Pourrut et al. 2011, Alzetta et al. 2012). As a result, when exposed to environmental stress, plants in urban areas with comparable biomass produce a wider variety of AM fungal communities.

In urban areas, trees increase the need for environmental stress tolerance while decreasing the need for nutrients. In urban areas, trees can be found with a range of fungal association compositions. Urbanization significantly increased the relative abundance of the *Glomus* Group II, which has a high degree of environmental adaptability and is frequently found in harmed ecosystems. Because of this, some environmental stress tolerance or resistance filters might encourage the growth of root mycorrhizal associations (Knapp et al. 2008). The patterns of significant plant-AM fungal links in the networks were very different in the urban area. The driving force behind niche differentiation is competition (Wright 2002). Urban xenobiotics in this study reduced the level of competition among AM fungi, as evidenced by a lower C-score value in the urban network. As a result, plants in urban areas may tend to work together with a variety of readily available, robust AM fungi to lessen the risk of species loss in ways other than through diffusion and host species selectivity.

## CHANGES THE FUNGAL GROWTH

As xenobiotics contain a variety of potentially toxic additives, they can directly harm soil biota (Kim et al. 2020). Furthermore, a growing body of research indicates that organic xenobiotics like polycyclic aromatic hydrocarbons and organochlorines like DDT, as well as polychlorinated biphenyls, herbicides, pesticides, antibiotics, and trace metals, can all be absorbed by trees (Wang et al. 2019). Particularly,

small xenobiotics particles or high concentrations can stimulate stress reactions, reproduction, and mortality of the plant and induce metabolic processes (Buks et al. 2020). Xenobiotics have the ability to significantly change the composition of the fungal communities (Kettner et al. 2017, Fei et al. 2020).

Xenobiotics, such as heavy metals or hydrocarbons, can have a negative impact on AMF, just like they can on other soil biota (Cabello 1997, Joner & Leyval 2003, Wang et al. 2020). Thus, we anticipate the direct effects of the additives or pollutants absorbed on the surface of the plant, which will ultimately be released upon degradation. Although heavy metals and hydrocarbons are tolerable to AMF and can even help reduce their toxicity to plants, they have adverse effects at high concentrations (Cabello 1997, Ferrol et al. 2016). AMF typically exhibits reduced root colonization and infectivity, decreased arbuscular and spore numbers, or cell damage in response to soil xenobiotics (Cabello 1997, Leyval et al. 1997, Desalme et al. 2012, Ferrol et al. 2016). Drugs like antibiotics can also be mycotoxic for AMF, reducing hyphal length and spore counts (Hillis et al. 2008). Additionally, changes in the AMF community structure can result from soil xenobiotics. For instance, in soils with high lead contamination, the relative abundance of Paraglomeraceae increased while the abundance of Acaulosporaceae and Glomeraceae decreased (Faggioli et al. 2019).

Xenobiotics can also affect AMF directly by producing breakdown byproducts. One recent study revealed that the diversity and composition of AMF communities were significantly altered by xenobiotics (Wang et al. 2020). The authors discovered that the type and concentration of xenobiotics affected the relative abundance of AMF taxa. For instance, Glomeraceae were less abundant in treatments with biodegradable polylactic acid (PLA) compared to the control and treatments with polyethylene (PE); OTU numbers of Ambispora and Archaeosporaceae were more abundant at higher application rates of microplastic (pollutant) (10% addition compared to 1% addition) under PLA and PE for Ambispora and only under PLA for Archaeosporaceae.

## XENOBIOTICS INFLUENCE SEEDLING SURVIVAL

In some urban areas, xenobiotics have reduced seedling survival rates (Broshot 2007, Lehvavirta et al. 2014). This might be a result of the effects of drought and pollution, which have been well-researched in urban environments (Guerrero et al. 2013, Gillner et al. 2013, McDonald & Urban 2004). Even though the below-ground dynamics of urban forests are less well understood, a growing body of research indicates that they may be just as important to ecosystems as many changes seen on the surface (O'Brien

et al. 2011, Horton et al. 1999, 2005). Possibly, Mycorrhizal fungi species and the degree to which they colonize plant roots may be influenced by the microclimate, soil nutrients or heavy metal accumulation, and restricted dispersal characteristics of urban environments (Treseder 2013, Fitter et al. 2004, Bainard et al. 2011). As mycorrhizal fungi are significant drivers of forest population dynamics, a better understanding of how plants and mycorrhizal fungi interact in urban environments will help assess and manage urban trees (Hetrick et al. 1989).

## CONCLUSION

Mycorrhiza plays a vital role in the growth and development of urban plants. Currently, increasing urbanization is a major challenge for urban areas. The increasing population sharply increases xenobiotic substances like pollution, heavy metals, pharmaceuticals, insecticides, pesticides, etc. They impact plant health, microbial structure, and fungal association and sporulation in urban areas. Xenobiotics mostly affect the rhizosphere in the area; they mostly cause a decrease in the growth of mycorrhizal fungal growth and the interaction of the urban plant.

## ACKNOWLEDGMENTS

The authors gratefully acknowledge the contributions of the Department of Forestry, Wildlife, and Environmental Science, Guru Ghasidas University, Bilaspur. They provide the working instruments and the research area for the work.

## REFERENCES

- Agrawal, N. and Dixit, A.K., 2015. An environmental cleanup strategy— Microbial transformation of xenobiotic compounds. *International Journal of Current Microbiology and Applied Sciences*, 4(4), pp.429-461.
- Alkorta, I. and Garbisu, C., 2001. Phytoremediation of organic contaminants in soils. *Bioresource Technology*, 79(3), pp.273-276. [https://doi.org/10.1016/S0960-8524\(01\)00016-5](https://doi.org/10.1016/S0960-8524(01)00016-5).
- Alzetta, C., Scattolin, L., Scopel, C. and Accordi, S.M., 2012. The ectomycorrhizal community in urban linden trees and its relationship with soil properties. *Trees - Structure and Function*, 26, pp.751-767. <https://doi.org/10.1007/s00468-011-0641-z>.
- Anderson, T., Kruger, E. and Coats, J., 1994. Enhanced degradation of a mixture of three herbicides in the rhizosphere of a herbicide-tolerant plant. *Chemosphere*, 28(8), pp.1551-1557. [https://doi.org/10.1016/0045-6535\(94\)90248-8](https://doi.org/10.1016/0045-6535(94)90248-8).
- Atlas, R.M. and Bartha, R., 1986. *Microbial Ecology: Fundamentals and Applications*. Benjamin/Cummings.
- Bainard, L.D., Klironomos, J.N. and Gordon, A.M., 2011. The mycorrhizal status and colonization of 26 tree species growing in urban and rural environments. *Mycorrhiza*, 21, pp.91-96. <https://doi.org/10.1007/s00572-010-0314-6>.
- Bais, H.P., Weir, T.L., Perry, L.G., Gilroy, S. and Vivanco, J.M., 2006. The role of root exudates in rhizosphere interactions with plants and other organisms. *Annual Review of Plant Biology*, 57, pp.233-266. <https://doi.org/10.1146/annurev.arplant.57.032905.105159>.

- Baetez, U. and Martinoia, E., 2014. Root exudates: The hidden part of plant defense. *Trends in Plant Science*, 19(2), pp.90-98. <https://doi.org/10.1016/j.tplants.2013.11.006>.
- Bazaz, A., Bertoldi, P., Buckeridge, M., Cartwright, A., De Coninck, H., Engelbrecht, F., Jacob, D., Hourcade, J.C., Klaus, I., Kleijne, K., Lwasa, S., Markgraf, C., Newman, P., Revi, A., Rogeli, J., Shultz, S., Shindell, D., Singh, C., Solecki, W., Steg, L. and Waisman, H., 2008. *Summary for Urban Policymakers: What the IPCC Special Report on L5C means for cities*. Global Covenant of Mayors for Climate & Energy/C40 Cities.
- Bhardwaj, A.K. and Chandra, K.K., 2016. Biomass and carbon stocks of different tree plantations in entisol soil of eastern Chhattisgarh, India. *Current World Environment*, 11, pp.1-15. <http://dx.doi.org/10.12944/CWE.11.3.17>.
- Bhardwaj, A.K. and Chandra, K.K., 2017. AMF symbiosis in forest species plantations and its relationship with major soil nutrients in entisol soil of Bilaspur, (C.G.). *Life Science Bulletin*, 14, pp.27-32.
- Bhardwaj, A.K., Chandra, K.K. and Kumar, R., 2023a. Water stress changes on AMF colonization, stomatal conductance, and photosynthesis of *Dalbergia sissoo* seedlings grown in entisol soil under nursery conditions. *Forest Science and Technology*, 21, pp.1-13. <https://doi.org/10.1080/21580103.2023.2167873>.
- Bhardwaj, A.K., Chandra, K.K. and Kumar, R., 2023b. Mycorrhizal inoculation under water stress conditions and its influence on the benefit of host microbe symbiosis of *Terminalia arjuna* species. *Bulletin of the National Research Centre*, 47, pp.1-13. <https://doi.org/10.1186/s42269-023-01048-3>.
- Brooks, B.W., 2018. Urbanization, environment and pharmaceuticals: advancing comparative physiology, pharmacology and toxicology. *Conservation Physiology*, 6(1), pp.1-8. <https://doi.org/10.1093/conphys/cox079>.
- Broshot, N.E., 2007. The influence of urbanization on forest stand dynamics in Northwestern Oregon. *Urban Ecosystems*, 10, pp.285-298. <https://doi.org/10.1007/s11252-007-0023-x>.
- Buys, F., Schaik, N.L.V. and Kaupenjohann, M., 2020. What do we know about how the terrestrial multicellular soil fauna reacts to microplastic? *Soil*, 6(2), pp.245-267. <https://doi.org/10.5194/soil-6-245-2020>.
- Cabello, M.N., 1997. Hydrocarbon pollution: its effect on native arbuscular mycorrhizal fungi (AMF). *FEMS Microbiology Ecology*, 22, pp.233-236. <https://doi.org/10.1111/j.1574-6941.1997.tb00375.x>.
- Cachada, A., Rocha-Santos, T. and Duarte, A.C., 2018. Chapter 1: Soil and pollution: an introduction to the main issues. In: *Soil Pollution*. American Press, Cambridge, Massachusetts.
- Chandra, K.K., 2014. Recovery pattern in diversity and species of ground vegetation and AMF in reclaimed coal mine dumps of Korba (India). *Expert Opinion Environmental Biology*, 3, pp.1-12. <https://doi.org/10.4172/2325-9655.1000110>.
- Chandra, K.K. and Bhardwaj, A.K., 2018. Growth, biomass, and carbon sequestration by trees in nutrient-deficient Bhatia land soil of Bilaspur, Chhattisgarh, India. In *Energy and Environment*, pp.39-45. [https://doi.org/10.1007/978-981-10-5798-4\\_4](https://doi.org/10.1007/978-981-10-5798-4_4).
- De Oliveira, M., Frihling, B.E.F., Velasques, J., Filho, F.J.C.M., Cavalheri, P.S. and Migliolo, L., 2020. Pharmaceuticals residues and xenobiotics contaminants: occurrence, analytical techniques and sustainable alternatives for wastewater treatment. *Science of the Total Environment*, 705, pp.1-7. <https://doi.org/10.1016/j.scitotenv.2019.135568>.
- Dennis, P.G., Miller, A.J. and Hirsch, P.R., 2010. Are root exudates more important than other sources of rhizodeposits in structuring rhizosphere bacterial communities? *FEMS Microbiology Ecology*, 72(3), pp.313-327. <https://doi.org/10.1111/j.1574-6941.2010.00860.x>.
- Desalme, D., Chiapusio, G., Bernard, N., Gilbert, D., Toussaint, M.L. and Binet, P., 2012. Arbuscular mycorrhizal fungal infectivity in two soils as affected by atmospheric phenanthrene pollution. *Water Air Soil Pollution*, 223, pp.3295-3305.
- Dubey, K.K. and Fulekar, M.H., 2013. Investigation of potential rhizospheric isolate for cypermethrin degradation. *Biotech*, 3(1), pp.33-43.
- Duchicela, J., Sullivan, T.S., Bontti, E. and Bever, J.D., 2013. Soil aggregate stability increase is strongly related to fungal community succession along an abandoned agricultural field chronosequence in the Bolivian Altiplano. *Journal of Applied Ecology*, 50, pp.1266-1273.
- Dzantor, E.K., 2007. Phytoremediation: The state of rhizosphere 'engineering' for accelerated rhizodegradation of xenobiotic contaminants. *Journal of Chemical Technology and Biotechnology*, 82, pp.228-232.
- Egerton-Warburton, L.M. and Allen, E.B., 2000. Shifts in Arbuscular Mycorrhizal Communities along an Anthropogenic Nitrogen Deposition Gradient. *Ecological Applications*, 10(2), pp.484-496.
- European Commission, 2012. Guidelines on best practices to limit, mitigate or compensate soil sealing. *Commission Staff Working Document*.
- Faggioli, V., Menovo, E., Geml, J., Kemppainen, M., Pardo, A. and Salazar, M.J., 2019. Soil lead pollution modifies the structure of arbuscular mycorrhizal fungal communities. *Mycorrhiza*, 29, pp.363-373.
- Farrar, J., Aawes, M., Tones, D. and Lindow, S., 2003. How roots control the flux of carbon to the rhizosphere. *Ecology*, 84, pp.827-837.
- Fei, Y., Huang, S., Zhang, H., Tong, Y., Wen, D. and Xia, X., 2020. Response of soil enzyme activities and bacterial communities to the accumulation of microplastics in an acid cropped soil. *Science of the Total Environment*, 707, pp.1-15.
- Ferrol, N., Tamayo, E. and Vargas, P., 2013. The heavy metal paradox in arbuscular mycorrhizas: from mechanisms to biotechnological applications. *Journal of Experimental Botany*, 67(22), pp.6253-6265.
- Fetzner, S., 2002. Biodegradation of xenobiotics. In: *Encyclopedia of Life Support Systems (EOLSS) Publishers, developed under the Auspices of UNESCO*. In *Biotechnology, Doelle and Da Silva, eds*. EOLSS Oxford, U.K., pp.32.
- Fitter, A.H., Heinemeyer, A., Husband, R., Olsen, E., Ridgway, K.P. and Staddon, P.L., 2004. Global environmental change and the biology of arbuscular mycorrhizas: gaps and challenges. *Canadian Journal of Botany*, 82(8), pp.1133-1139.
- Gerhardt, K.E., Huang, X.D., Glick, B.R. and Greenberg, B.M., 2019. Phytoremediation and rhizoremediation of organic soil contaminants: potential and challenges. *Plant Science*, 176(1), pp.20-30.
- Gianfreda, L., 2015. Enzymes of importance to rhizosphere processes. *Journal of Soil Science and Plant Nutrition*, 15(2), pp.283-306.
- Gillner, S., Vogt, J. and Roloff, A., 2013. Climatic response and impacts of drought on oaks at urban and forest sites. *Urban Forestry & Urban Greening*, 12(4), pp.597-605.
- Guerrero, C.C., Gunthardt-Goerg, M.S. and Vollenweider, P., 2013. Foliar symptoms triggered by ozone stress in irrigated holm oaks from the city of Madrid, Spain. *PLOS One*, 8(1), pp.1-12.
- Haug, I., Setaro, S. and Suarez, J.P., 2013. Reforestation sites show similar and nested AMF communities to an adjacent pristine forest in a tropical mountain area of South Ecuador. *PLOS One*, 8(5), pp.1-10.
- Hetrick, B.A.D., Wilson, G.W.T. and Hartnett, D.C., 1989. Relationship between mycorrhizal dependence and competitive ability of two tall grass prairie grasses. *Canadian Journal of Botany*, 67(9), pp.2608-2615.
- Hildebrandt, U., Regyar, M. and Bothe, H., 2007. Arbuscular mycorrhiza and heavy metal tolerance. *Phytochemistry*, 68(1), pp.139-146.
- Hillis, D.G., Antunes, P., Sibley, P.K., Klironomos, J.N. and Solomon, K.R., 2018. Structural responses of *Daucus carota* root-organ cultures and the arbuscular mycorrhizal fungus, *Glomus intraradices*, to 12 pharmaceuticals. *Chemosphere*, 73, pp.344-352.
- Hinsinger, P., Bengough, A.G., Vetterlein, D. and Young, I.M., 2009. Rhizosphere: biophysics, biogeochemistry and ecological relevance. *Plant and Soil*, 321, pp.117-152.

- Hinsinger, P., Gobran, G.R., Gregory, P.J. and Wenzel, W.W., 2005. Rhizosphere geometry and heterogeneity arising from root-mediated physical and chemical processes. *The New Phytologist*, 168, pp.293–303.
- Horton, T.R., Bruns, T.D. and Parker, V.T., 1999. Ectomycorrhizal fungi associated with *Arctostaphylos* contribute to *Pseudotsuga menziesii* establishment. *Canadian Journal of Botany*, 77, pp.93–102.
- Horton, T.R., Molina, R. and Hood, K., 2005. Douglas-fir ectomycorrhizae in 40- and 400-year-old stands: Mycobiont availability to late successional western hemlock. *Mycorrhiza*, 15, pp.393–403.
- Hosseini, B.S., Xu, Z., Blumfield, T.J. and Reverchon, F., 2015. Human footprints in urban forests: implication of nitrogen deposition for nitrogen and carbon storage. *Journal of Soils and Sediments*, 15, pp.1927–1936. <https://doi.org/10.1007/s11368-015-1205-4>.
- Joner, E.J. and Leyval, C., 2003. Rhizosphere gradients of polycyclic aromatic hydrocarbon (PAH) dissipation in two industrial soils and the impact of arbuscular mycorrhiza. *Environment Science Technology*, 37(11), pp.2371–2375. <https://doi.org/10.1021/es020196y>.
- Joy, J.B., 2013. Symbiosis catalyses niche expansion and diversification. *Proceedings of the Royal Society B: Biological Sciences*, 280, pp.1–10. <https://doi.org/10.1098/rspb.2012.2820>.
- Karpati, A.S., Handel, L.S.N., Dighton, J. and Horton, T.R., 2011. Quercus rubra-associated ectomycorrhizal fungal communities of disturbed urban sites and mature forests. *Mycorrhiza*, 21, pp.537–547. <https://doi.org/10.1007/s00572-011-0362-6>.
- Kettner, M.T., Rojas-Jimenez, K., Oberbeckmann, S., Labrenz, M. and Grossart, H.P., 2017. Microplastics alter composition of fungal communities in aquatic ecosystems. *Environmental Microbiology*, 19(11), pp.4447–4459. <https://doi.org/10.1111/1462-2920.13891>.
- Khade, S.W. and Adholeya, A., 2008. Effects of heavy metal (Pb) on arbuscular mycorrhizal fungi in vitro. *World Journal Microbiology Biotechnology*, 24, pp.1663–1668. <https://doi.org/10.1007/s11274-008-9681-y>.
- Kidd, P., Prieto-Fernandez, A., Monterroso, C. and Acea, M., 2008. Rhizosphere microbial community and hexachlorocyclohexane degradative potential in contrasting plant species. *Plant and Soil*, 302, pp.233–247. <https://doi.org/10.1007/s11104-007-9475-2>.
- Kim, S.W., Waldman, W.R., Kim, T.Y. and Rillig, M.C., 2020. Effects of different microplastics on nematodes in the soil environment: tracking the extractable additives using an ecotoxicological approach. *Environment Science Technology*, 54, pp.13868–13878. <https://doi.org/10.1021/acs.est.0c04641>.
- Knapp, S., Kuhn, I., Schweiger, O. and Klotz, S., 2008. Challenging urban species diversity: contrasting phylogenetic patterns across plant functional groups in Germany. *Ecology Letters*, 54(21), pp.1054–1064. <https://doi.org/10.1021/acs.est.0c04641>.
- Kumar, D. and Chopra, S., 2020. Xenobiotic compounds in the environment: Their fate, transport and removal. In: *Proceedings of the 3rd National Conference on Medical Instrumentation, Biomaterials and Signal Processing (NCMBS-20)*, Sonapat, India, 26–27 February, pp.96–102.
- Kumar, R., Bhardwaj, A.K., Chandra, K.K. and Singh, A.K., 2022. Mycorrhizae: An Historical Journey of Plant Association. *Chhattisgarh Journal of Science and Technology*, 19, pp.437–447.
- Kumar, R., Bhardwaj, A.K. and Chandra, K.K., 2023. Effects of arbuscular mycorrhizal fungi on the germination of terminalia arjuna plants grown in fly ash under nursery conditions. *Forestist*, 1, pp.1–5. DOI:10.5152/forestist.2023.23015.
- Kumar, R., Bhardwaj, A.K., Chandra, K.K., Dixit, B. and Singh, A.K., 2024. Diverse role of mycorrhiza in plant growth and development: Review. *Solovoyov Studies ISPU*, 72, pp.37–61.
- Landrum, P.F. and Robbins, J.A., 1990. Bioavailability of sediment-associated contaminants to benthic invertebrates. In: Baudo R, Giesy JP, Muntau H (eds) *Sediments: chemistry and toxicity of in-place pollutants*. Lewis Publishers Inc, Chelsea.
- Lee, I.I., 1992. Models, muddles, and mud predicting bioaccumulation of sediment-associated pollutants. In: Burton Jr. GA (ed) *Sediment toxicity assessment*. Lewis Publishers Inc, Chelsea.
- Lehvirvita, S., Vilisics, F., Hamberg, L., Malmivara-Lamsa, M. and Kotze, D.J., 2014. Fragmentation and recreational use affect tree regeneration in urban forests. *Urban Forestry and Urban Greening*, 13(4), pp.869–877. <https://doi.org/10.1016/j.ufug.2014.10.003>.
- Leyval, C., Turnau, K. and Haselwandter, K., 1997. Effect of heavy metal pollution on mycorrhizal colonization and function: physiological, ecological and applied aspects. *Mycorrhiza*, 7, pp.139–153. <https://doi.org/10.1007/s005720050174>.
- Liang, Y.Q., Li, J.W., Li, J. and Valimaki, S., 2008. Impact of urbanization on plant diversity: A case study in built-up areas of Beijing. *Forestry Studies in China*, 10, pp.179–188. <https://doi.org/10.1007/s11632-008-0036-4>.
- Lipson, D.A., Monson, R.K., Schmidt, S.K. and Weintraub, M.N., 2009. The trade-off between growth rate and yield in microbial communities and the consequences for under-snow soil respiration in a high elevation coniferous forest. *Biogeochemistry*, 95, pp.23–35. <https://doi.org/10.1007/s10533-008-9252-1>.
- Maenpaa, K.A., 2007. The toxicity of xenobiotics in an aquatic environment: connecting body residues with adverse effects. *PhD Dissertation, University of Joensuu, Finland*.
- Mathew, B.B., Singh, H., Biju, V.G. and Krishnamurthy, N.B., 2017. Classification, source, and effect of environmental pollutants and their biodegradation. *Journal of Environment Pathology Toxicology Oncology*, 36(1), pp.55–71. <https://doi.org/10.1615/JEnvironPatholToxicolOncol.2017015804>.
- Mcdonald, R.I. and Urban, D.L., 2004. Forest edges and tree growth rates in the North Carolina Piedmont. *Ecology*, 85, pp.2258–2266. <https://doi.org/10.1890/03-0313>.
- Miya, R.K. and Firestone, M.K., 2011. Enhanced phenanthrene biodegradation in soil by slender oat root exudates and root debris. *Journal of Environmental Quality*, 30(6), pp.1911–1918. <https://doi.org/10.2134/jeq2001.1911>.
- Musolf, A., Leschik, S., Schafmeister, M.T., Strauch, G., Krieg, R. and Schirmer, M., 2010. Evaluation of xenobiotic impact on urban receiving waters by means of statistical methods. *Water Science and Technology: A Journal of the International Association on Water Pollution Research*, 62(3), pp.684–92. <https://doi.org/10.2166/wst.2010.930>.
- Newman, M.C., 1998. Fundamentals of Ecotoxicology. Ann Arbor Press.
- O'Brien, A.M., Ettinger, A.K. and Hillerslammers, J., 2012. Conifer growth and reproduction in urban forest fragments: Predictors of future responses to global change? *Urban Ecosystems*, 15, pp.879–891. <https://doi.org/10.1007/s11252-012-0250-7>.
- O'Brien, M.J., Gomola, C.E. and Horton, T.R., 2011. The effect of forest soil and community composition on ectomycorrhizal colonization and seedling growth. *Plant and Soil*, 341, pp.321–331. <https://doi.org/10.1007/s11104-010-0646-1>.
- Oke, T.R., 1973. City size and the urban heat island. *Atmospheric Environment*, 7, pp.769–77. [https://doi.org/10.1016/0004-6981\(73\)90140-6](https://doi.org/10.1016/0004-6981(73)90140-6).
- Philippot, L., Raaijmakers, J.M., Lemanceau, P. and Van Der Putten, W.H., 2013. Going back to the roots: The microbial ecology of the rhizosphere. *Nature Reviews Microbiology*, 11, pp.789–799. <https://doi.org/10.1038/nrmicro3109>.
- Pourrut, B., Shahid, M., Dumat, C., Winterton, P. and Pinelli, E., 2011. Lead uptake, toxicity, and detoxification in plants. *Reviews of Environmental Contamination and Toxicology*, 213, pp.113–136.
- Raaijmakers, J.M., Paulitz, T.C., Steinberg, C., Alabouvette, C. and Mocenne-Loccoz, Y., 2011. The rhizosphere: A playground and battlefield for soil borne pathogens and beneficial microorganisms. *Plant and Soil*, 321, pp.341–361. <https://doi.org/10.1007/s11104-008-9568-6>.



- Rentz, J.A., Alvarez, P.J. and Schnoor, J.L., 2005. Benzo [a] pyrene co-metabolism in the presence of plant root extracts and exudates: implications for phytoremediation. *Environmental Pollution*, 136(3), pp.477-484. <https://doi.org/10.1016/j.envpol.2004.12.034>.
- Riechers, D.E., Kreuz, K. and Zhang, Q., 2010. Detoxification without intoxication: Herbicide safeners activate plant defense gene expression. *Plant Physiology*, 153(1), pp.3–13. <https://doi.org/10.1104/pp.110.153601>.
- Ruddiman, W.F., 2013. The Anthropocene. *Annual Review of Earth and Planetary Sciences*, 41, pp.45–68.
- Schneider, J., Bundschuh, J. and Do Nascimento, C.W.A., 2016. Arbuscular mycorrhizal fungi-assisted phytoremediation of a lead-contaminated site. *Science of the Total Environment*, 572, pp.86–97. <https://doi.org/10.1016/j.scitotenv.2016.07.185>.
- Sheng-You, X., Ying-Xu, C., Qi, L., Wei-Xiang, W., Sheng-Guo, X. and Chao-Feng, S., 2005. Uptake and accumulation of phenanthrene and pyrene in spiked soils by ryegrass (*Lolium perenne* L.). *Journal of Environmental Sciences*, 17(5), pp.817-822.
- Shim, H., Chauhan, S., Ryoo, D., Bowers, K., Thomas, S.M. and Burken, J.G., 2000. Rhizosphere competitiveness of trichloroethylene-degrading, poplar-colonizing recombinant bacteria. *Applied and Environmental Microbiology*, 66(11), pp.4673-4678. <https://doi.org/10.1128/AEM.66.11.4673-4678.2000>.
- Singer, A.C., Crowley, D.E. and Thompson, I.P., 2003. Secondary plant metabolites in phytoremediation and biotransformation. *Trends in Biotechnology*, 21(3), pp.123-130. [https://doi.org/10.1016/S0167-7799\(02\)00041-0](https://doi.org/10.1016/S0167-7799(02)00041-0).
- Smith, S.E. and Read, D., 2011. *Mycorrhizal Symbiosis*. Academic Press.
- Smith, S.E. and Smith, F.A., 2011. Roles of arbuscular mycorrhizas in plant nutrition and growth: New paradigms from cellular to ecosystem scales. *Annual Review of Plant Biology*, 62, pp.227–250. <https://doi.org/10.1146/annurev-arplant-042110-103846>.
- Soucek, P., 2017. *Xenobiotics*. Springer. [https://doi.org/10.1007/978-3-662-46875-3\\_6276](https://doi.org/10.1007/978-3-662-46875-3_6276).
- Stefanac, T., Grgas, D. and Dragicevic, T.L., 2021. Xenobiotics—Division and methods of detection: A review. *Journal of Xenobiotics*, 11(4), pp.130-141. <https://doi.org/10.3390/jox11040009>.
- Streit, B., 1992. Bioaccumulation processes in ecosystems. *Experientia*, 48(10), pp.955–970. <https://doi.org/10.1007/BF01919142>.
- Sun, F.F., Wen, D.Z., Kuang, Y.W., Li, J. and Zhang, J.G., 2009. Concentrations of sulphur and heavy metals in needles and rooting soils of Masson pine (*Pinus massoniana* L.) trees growing along an urban-rural gradient in Guangzhou, China. *Environmental Monitoring and Assessment*, 154, pp.263–274. <https://doi.org/10.1007/s10661-008-0394-3>.
- Treseder, K.K., 2013. The extent of mycorrhizal colonization of roots and its influence on plant growth and phosphorus content. *Plant and Soil*, 371, pp.1–13. <https://doi.org/10.1007/s11104-013-1681-5>.
- Treseder, K.K. and Allen, M.F., 2000. Mycorrhizal fungi have a potential role in soil carbon storage under elevated CO<sub>2</sub> and nitrogen deposition. *New Phytologist*, 147, pp.189–200.
- United Nations Environment Programme, 2017. Towards a pollution-free planet background report. United Nations Environment Programme, Nairobi.
- Wang, J., Liu, X., Li, Y., Powell, T., Wang, X., and Wang, G., 2019. Microplastics as contaminants in the soil environment: a mini-review. *Science of the Total Environment*, 691, pp.848–857. <https://doi.org/10.1016/j.scitotenv.2019.07.209>.
- Wright, J.S., 2002. Plant diversity in tropical forests: a review of mechanisms of species coexistence. *Oecologia*, 130(1), pp.1–14. DOI: 10.1007/s004420100809
- Yang, Y., Song, Y., Schellhorn, H.V., Ghosh, A., Ban, Y., Chen, H., and Tang, M., 2015. Community structure of arbuscular mycorrhizal fungi associated with *Robinia pseudoacacia* in uncontaminated and heavy metal contaminated soils. *Soil Biology and Biochemistry*, 86, pp.146–158. <https://doi.org/10.1016/j.soilbio.2015.03.018>
- Zhang, Q., Xu, F.X., and Lambert, K.N., 2007. Safeness co-ordinately induces the expression of multiple proteins and MRP transcripts involved in herbicide metabolism and detoxification in *Triticum tauschii* seedling tissues. *Proteomics*, 7(8), pp.1261–1278. <https://doi.org/10.1002/pmic.200600423>







# Cost Assessment of Emission Mitigation Technology for the Palm Oil Sector in Indonesia

A. S. Nur Chairat<sup>1,2</sup>, L. Abdullah<sup>2†</sup>, M. N. Maslan<sup>2</sup>, M. S. M. Aras<sup>2</sup>, M. H. F. Md Fauadi<sup>2</sup>, R. A. Hamid<sup>2</sup> and H. Batih<sup>1</sup>

<sup>1</sup>Faculty of Technology and Business Energy, Institut Teknologi PLN, Jakarta 11750, Indonesia

<sup>2</sup>Fakulti Teknologi dan Kejuruteraan Industri dan Pembuatan, Universiti Teknikal Malaysia, Melaka, Durian Tunggal 76100, Malaysia

†Corresponding author: Lokman Abdullah; lokman@utem.edu.my

Nat. Env. & Poll. Tech.  
Website: [www.neptjournal.com](http://www.neptjournal.com)

Received: 23-02-2024

Revised: 22-04-2024

Accepted: 25-04-2024

## Key Words:

Marginal abatement cost  
Mitigation technology  
Palm oil sector  
Greenhouse gas emissions

## ABSTRACT

Indonesia must establish a policy on the application of technology for mitigating greenhouse gas emissions because it is the nation that produces the most palm oil. When evaluating different technologies, policymakers should consider how much the technology will cost compared to the potential emissions abated, in terms of marginal abatement cost (MAC), which reflects priorities in the form of marginal abatement cost curves (MACC). The objective of this research is to evaluate and estimate the ranking of MAC from eight mitigation technologies used in Indonesia's palm oil sector between 2020 and 2030. The least MAC is given as technology ranked first, namely the high-capacity boiler, with a value of \$-19.61/tonne CO<sub>2</sub>eq followed by the high-efficiency steam turbine with \$-7.2/tonne CO<sub>2</sub>eq, and the POME-to-biogas technology with \$-0.1/tonne CO<sub>2</sub>eq. Additionally, the MAC of five additional technologies is positive, suggesting that implementation expenses were incurred. Subsequently, a sensitivity analysis is performed to see which technology ranks are impacted by interest rate fluctuations. Biogas upgrading technology is therefore liable to changes in the discount rate, which occur at different values. Other mitigation technologies, however, are also increasing their parameters, although less significantly than biogas upgrading, therefore this has no bearing on mitigation technology ranking.

## INTRODUCTION

The world is grappling with a pressing issue concerning fossil energy, as the detrimental environmental effects of its extraction and consumption become increasingly apparent. The combustion of fossil fuels, such as coal, oil, and natural gas, releases vast amounts of carbon dioxide and other greenhouse gases into the atmosphere, contributing significantly to climate change. This global predicament has spurred countries to adopt multifaceted approaches to mitigate the adverse impacts of fossil energy. Several nations have invested heavily in renewable energy sources like solar, wind, and hydropower, aiming to diversify their energy portfolios and reduce reliance on fossil fuels. Additionally, international collaborations and agreements, such as the Paris Agreement, have sought to unite countries in collective efforts to limit global temperature rise. Governments are implementing policies to incentivize clean energy initiatives, promote energy efficiency, and phase out subsidies for fossil fuels. The transition to sustainable energy is not without challenges, including economic considerations and

the need for technological advancements. However, the global commitment to addressing the fossil energy problem underscores the urgency of finding innovative solutions to secure a more sustainable and environmentally responsible energy future.

In January 2022, Indonesia has been making notable strides in contributing to sustainable development, recognizing the imperative of balancing economic growth with environmental and social considerations. One key aspect is the country's commitment to reducing carbon emissions and combating climate change. Indonesia has implemented policies and initiatives to address deforestation and promote sustainable forestry practices. Efforts such as the moratorium on new licenses for primary forests and peatlands, as well as the establishment of the REDD+ program (Reducing Emissions from Deforestation and Forest Degradation), aim to preserve the country's rich biodiversity and mitigate carbon emissions. Furthermore, Indonesia has been actively promoting renewable energy sources to diversify its energy mix and decrease reliance on fossil fuels. Initiatives include

the development of geothermal, solar, and wind energy projects, with a focus on increasing the share of renewables in the overall energy grid. The government has also launched programs to enhance energy efficiency and reduce the environmental impact of industries.

Currently, Indonesia is also the largest producer of palm oil globally, and the industry has played a pivotal role in the country's economic development, contributing to job creation and export revenue. Each year, the country generates around thirty million tons of palm oil, accounting for 4.5% of its GDP and employing 3 million people (Edwards 2019). International demand for palm oil products has contributed significantly to those positive impacts. The cultivation of oil palm, coupled with the subsequent processing of fresh fruit bunches (FFBs) into crude palm oil (CPO) and various derivative products, has created a robust supply chain that spans agricultural activities, processing facilities, and downstream industries.

However, the expansion of palm oil plantations has been associated with deforestation, habitat loss, and increased greenhouse gas (GHG) emissions. The conversion of large areas of tropical forests, particularly peatlands, into palm oil plantations is a major driver of GHG emissions. The production of palm oil leads to a variety of concerns regarding the environment. It has already been confirmed

throughout the manufacturing chain, most notably methane ( $\text{CH}_4$ ) emissions coming from wastewater in open-water ponds during the milling cycle (Stichnothe & Bessou 2017).

These circumstances prompted consumer awareness and international pressure throughout the palm oil industry to shift toward more sustainable practices. The government has implemented policies and regulations to curb deforestation, including moratoriums on new licenses for primary forests and peatlands. The use of mitigation technology (MT) to enhance mill efficiency and limit environmental impacts is essential for the industry to minimize its contribution to GHG emissions and support a more sustainable and responsible future for palm oil production in Indonesia. To assess the allocation of energy-related options and identify which resources are essential for climate measures, the Marginal Abatement Cost (MAC) is used to incorporate both economic and technical aspects of accomplishing GHG emission reduction targets.

To demonstrate the relationship involving abatement quantity and MAC, policymakers utilized the Marginal Abatement Cost Curve (MACC), a visual instrument that highlights the performance measures of economic effectiveness of a variety of GHG mitigation options like an established performance measures of maximum tracking error for machine tools application (Chiew et al. 2017). Fig. 1 shows an example of MACC with five MTs.

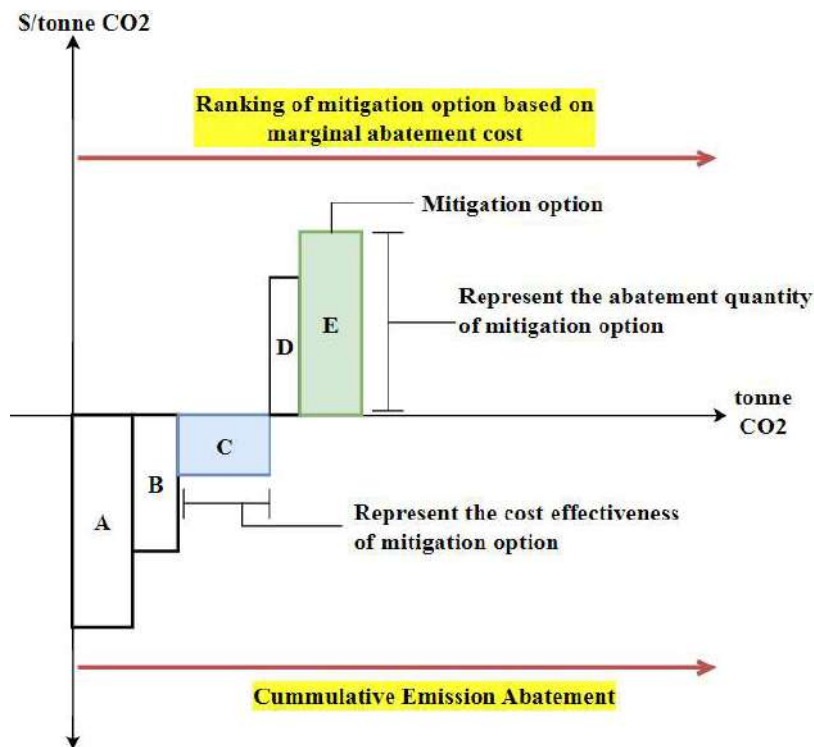


Fig. 1: Illustration of five mitigation technologies in MACC.

On the x-axis, the abatement quantity is presented, representing the volume of GHG emissions reductions achievable through diverse mitigation activities. This axis is organized from left to right, signifying an increasing scale of emission reduction efforts. Each point along the x-axis corresponds to a specific mitigation option, ranging from low-cost measures on the left to more expensive alternatives on the right. Conversely, the y-axis represents the Marginal Abatement Cost, measuring the cost incurred to achieve each additional unit of emission reduction. The MAC is expressed in monetary units and is arranged from bottom to top, indicating an ascending cost scale. As one moves upward along the y-axis, the cost of achieving additional emission reductions rises, reflecting diminishing returns on investment. The MACC, therefore, slopes upward, highlighting the economic efficiency of each mitigation option. The intersection of the MACC with the x-axis denotes measures that are both environmentally effective and economically viable without incurring additional costs. This crucial point indicates a balance between cost-effectiveness and emission reduction goals. By offering a visual representation of the costs associated with different mitigation measures, the MACC assists decision-makers in identifying the most economically efficient strategies to achieve specific emission reduction targets.

In Indonesia, only a few industries are relatively conscious of how much potential for mitigation exists and how much it would cost to realize this potential (Pambudi et al. 2018). Calculating the abatement costs of CO<sub>2</sub> is a key step to realizing CO<sub>2</sub> emission reduction (Duan et al. 2018) and can be summarized that MAC curves are a widely used method to support policy recommendations on carbon mitigation. To the best of the authors' knowledge, there is currently only one study available on the MAC curve and its application for the assessment of GHG emission reduction solutions for their costs in Indonesia. MAC applications have been used for energy, transport, residence, and agriculture, but are still not widely used in the palm oil sector, particularly in Indonesia. Extension to developing countries would bring greater challenges to MAC research. Thus, this study aims to fill this gap by using the concept of the "CO<sub>2</sub> abatement cost" to construct a bottom-up model to capture both the cost-effective and the technical potential for CO<sub>2</sub> emission reduction in the Indonesian palm oil sector. Research and development for CO<sub>2</sub> emission reduction in the palm oil production sector is also needed to ensure sustainable palm oil development. Reducing GHG emissions all along the production chain can help to reduce global impact while generating additional energy and farm income at the local

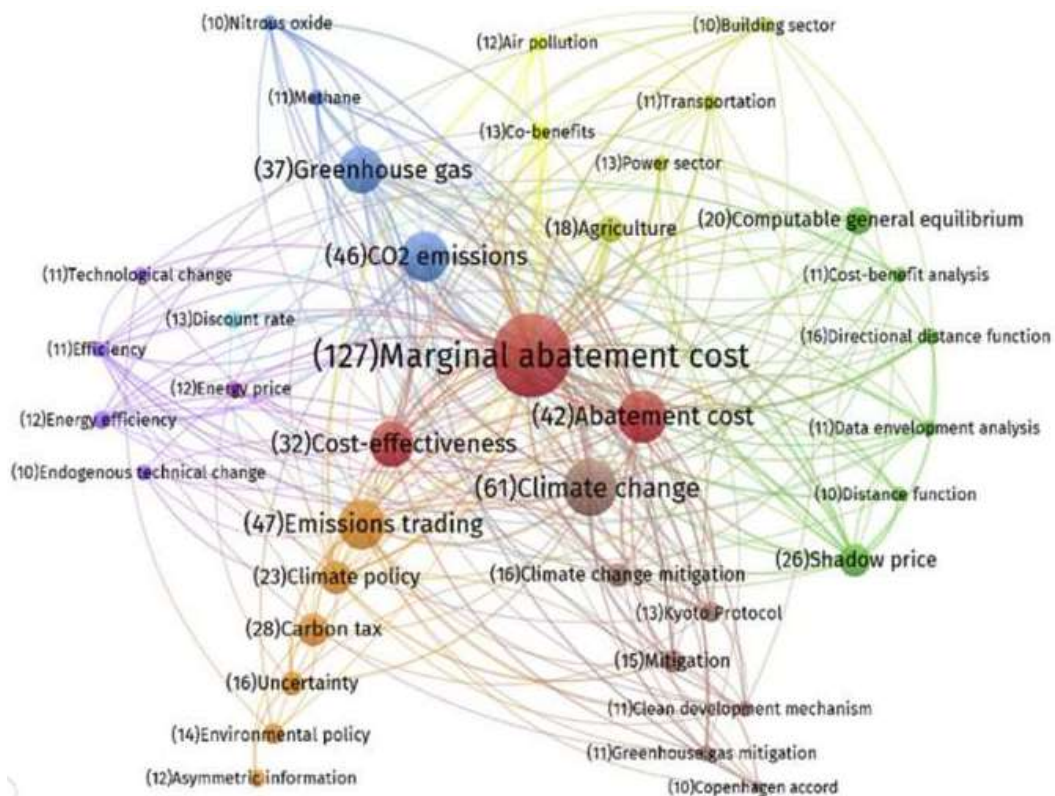


Fig. 2: The co-occurrence network of high-frequency keywords on MACC study.

level. The results are intended to help researchers and policymakers evaluate palm oil policies before 2060 and to develop new policies which in line with national and global climate mitigation targets.

## MAC STUDIES IN PAST

Recently, research on the Marginal Abatement Cost Curve (MACC) has been widely used by policymakers in climate change issues, which reveals that MACC is an important analysis tool for decision-making on climate change. The trend shows that the volume of research on MACC has generally been increasing from 1993 to 2022, indicating a popular trend in MACC research, mainly because of the wide application of MACC to evaluate the effects of the Kyoto Protocol and carbon trading as shown in Fig. 2. The co-occurrence network is drawn around high-frequency keywords (with a frequency exceeding 10) in the MACC field.

The MAC study field of interest is divided into three primary groups determined by the keyword frequency findings: decision-making aims, MAC applications, and stakeholder type. In essence, the three categories represent

the growing popularity of MAC-related research interest. Table 1 provides an overview of MAC's progress in research for the last ten years, based on credible journal sources, with an emphasis on applications across many industries to support the greenhouse emission reduction strategy.

MACC is applied in many different industries but is more common in high-emission industries, such as transportation, renewable energy, industry, power generation, and agriculture. MACC is also used for a series of sectors, such as the industrial, transportation, residential, commercial, and power generation sectors. Determined national MAC averages in four sectors: household, services, transportation, and EE solutions. The use of MACC for industrial aggregates is common in smaller contexts, such as cities or provinces. The efficacy and cost-effectiveness of various reduction strategies in waste management, energy, transport, and buildings were evaluated in London. Similarly, the cost-effectiveness and abatement potential of seventy measures belonging to the same four sectors were also examined in New York City. Seventy measures from the same four sectors were studied to determine their reduction potential and cost-effectiveness. MACCs have also been constructed for 58 cross-sector abatement technologies in Shanghai to

Table 1: MAC Research Trends.

Authors	Stakeholder		Sector (Country)	Methodologies	GHG Emission (Period)
	G	I			
(Kesicki 2013)	√		Transportation (UK)	Energy System Model (UK MARKAL) and Decomposition Analysis	CO <sub>2</sub> (2000-2050)
(Promjiraprawat et al. 2014)	√		Residential and building (Thailand)	Asia-Pacific Integrated Model	CO <sub>2</sub> (2005-2050)
(Tomaschek 2015a)	√		Transportation (South Africa)	TIMES-GEECO model	CO <sub>2</sub> (2007-2040)
(Contreras 2016)		√	Building (Spain)	Finance-accounting	CO <sub>2</sub> (N/A)
(Zhang et al. 2017)	√		Rural households (China)	Levelized Production Cost (LPC)	CO <sub>2</sub> (2015-2035)
(Luu et al. 2018)	√		Energy (Vietnam)	Finance-accounting	CO <sub>2</sub> (2015-2020)
(Johnsson et al. 2019)		√	Wood industry (Sweden)	Energy key performance indicators	CO <sub>2</sub> (2010-2018)
(Chen 2020)	√		Power (China)	Micro-technology and macro-industry model	CO <sub>2</sub> (2015-2030)
(Janzen et al. 2020)		√	Oil sands (Canada)	Market penetration model and Finance-accounting	CO <sub>2</sub> (2019-2050)
(Lameh et al. 2022)utilization, and sequestration (CCUS)	√		Power (N/A)	Mini-MAC	CO <sub>2</sub> (2020-2040)
This study (2024)		√	Palm oil Mill (Indonesia)	Finance-accounting	CO <sub>2</sub> (2020-2030)

G: Government, I: Industry

analyze GHG emission reductions and capital investments in 2015 and 2020 (Ibrahim & Kennedy 2016, Jiang et al. 2022, Tomaschek 2015b, Xiong et al. 2016).

In the energy sector, many studies conducted in large emitting countries and developed countries show that MAC varies widely between countries, and the average technology abatement cost of wind power technology in China is 75 Chinese Yuan/tCO<sub>2</sub>e or 11 USD/tCO<sub>2</sub>e. This figure is much lower than the average abatement cost of EE technology in thermal power plants in the same country, which is 316.51 Chinese Yuan/tCO<sub>2</sub>e, or 48 USD/tCO<sub>2</sub>e (Xiong et al. 2016). Using wind power as an example, the abatement costs for wind power technology in Austria are even negative, amounting to -31 EUR/tCO<sub>2</sub>e (or -37 USD/tCO<sub>2</sub>e) (Jiang et al. 2022). The different circumstances of these countries, such as resource potential, generation capacity, and generation costs, account for the varying ranges of abatement costs.

Based on the studies review, for the last several years, it is widely known that different stakeholders and the MAC approach have been explored and applied in various sectors by previous scholars. However, to the best of the author's knowledge, the approach of finance-accounting method for industrial stakeholders in the application of the palm oil sector is still limited and infrequent. Therefore, the current study attempts to assess the marginal costs of GHG emission mitigation technology abatement in Indonesian palm oil mill manufacturing operations. Particularly within the domain of the Indonesian palm oil industry, this study represents a pioneering effort aimed at bridging this evident gap in MACC implementation by undertaking a rigorous evaluation of energy-related mitigation options. The study's findings from empirical research have the potential to provide significant contributions to the development of evidence-based policy recommendations. This will assist in ensuring the adoption of well-informed decisions regarding the most effective use of national and regional resources for climate change mitigation initiatives.

## METHODS AND DATA

### Scope Setting

This scope includes the establishment of time intervals, geographic limits, and emission sectors. Compared to other Indonesian provinces, Riau province has produced the most CPO, supplying over one-fifth of the total national production. Samples from four palm oil mills that differed in capacities, ownership, and years of operation in relation to greenhouse gas emissions were assessed to gain the ranking of MAC. Geographic boundaries encompassing the years

2020 to 2030 are found in the Rokan Hulu Region and are defined by the administrative boundaries between the cities of Tandun, Kepenuhan, Ujung Batu, and Pasir Pengaraian.

### Identification and Evaluation of Mitigation Alternatives

The extraction and processing of palm oil involves several processes that result in GHG emissions, and every phase has the opportunity to increase GHG efficiency. Technology aimed at lowering greenhouse gas emissions in palm oil mills has primarily concentrated on increasing waste reuse. Examples involve composting mill waste, which is then used as fertilizers on plantations, and utilizing biogas as a source of energy generated by facilities that capture methane from POME.

Indirect and direct MTs that lower GHG emissions in mills are covered in the following subsection. A similar set of criteria, including the potential for reducing greenhouse gas emissions and cost aspects, were applied to evaluating the identified MTs. It is significant to take into consideration that the use of MT in a mill may encourage the reduction of GHG emissions elsewhere or make a difference in a larger context. For instance, methane-captured biogas can be used as captive power or to replace fossil fuel-based electricity generation on the grid.

### Research Design

The study flowchart presented in Fig. 3 illustrates a systematic research technique that is segmented into three primary stages to develop and analyze the MACC relevant to the palm oil industry.

In the initial phase of problem formulation, the commencement of this process entails the systematic acquisition of secondary data, primarily facilitated through an extensive literature review, focusing on elucidating the application of the MACC methodology within the industrial domain, with a specific emphasis on its implementation within the palm oil sector. Subsequently, this scholarly inquiry delineates the precise problem to be addressed, thereby laying the foundational framework for the formulation of research objectives. The process then proceeds to the critical task of delineating the most appropriate MACC approach, a decision-making endeavor that is rigorously aligned with the stipulated research objectives. Should the initially chosen MACC approach prove incongruent with the predefined research objectives, a systematic iterative process ensues, wherein alternative approaches are meticulously considered and evaluated until an optimal alignment between the selected approach and the research objectives is achieved? This methodological rigor

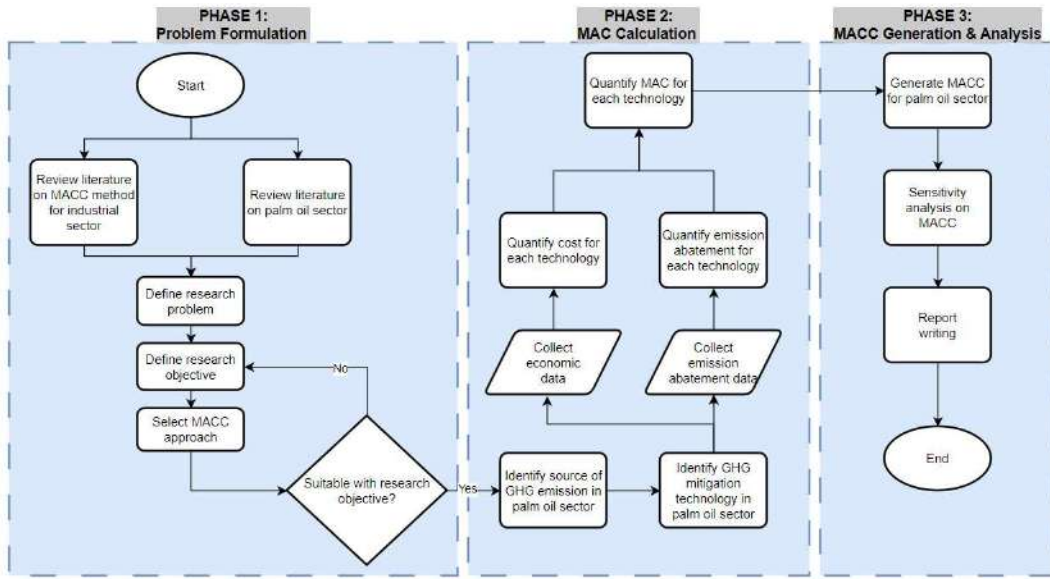


Fig. 3: The present research flowchart.

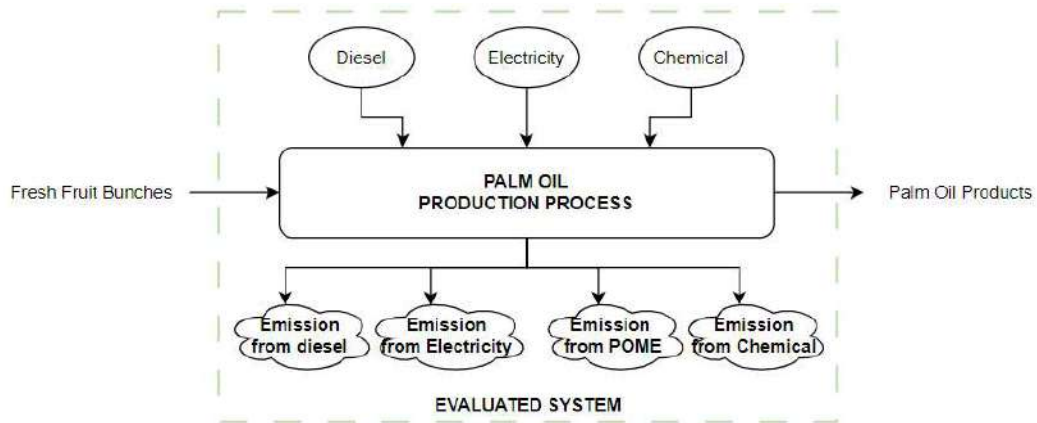


Fig. 4: Scope of the evaluated system in palm oil mill.

ensures that the ensuing research endeavors are conducted with a coherent and purposeful alignment toward the attainment of the established objectives, thereby enhancing the efficacy and robustness of the investigative process.

The subsequent phase of the study encompasses a comprehensive examination aimed at delineating the sources of greenhouse gas emissions prevalent within the palm oil sector. The burning of fossil fuels, Palm Oil Mill Effluent (POME), and the use of grid energy are the primary contributors to emissions that are identified throughout the milling stages (Fig. 3). These emissions arise from burning fossil fuels that are used for a variety of operational functions, such as machinery operation and steam production. They also come from the anaerobic digestion of POME to create biogas

and the grid-based electricity that is obtained to meet the energy demands of milling operations (Acobta et al. 2023).

Building upon this foundational understanding, the research endeavors progress to the quantification of MAC attributed to each discerned technological intervention. This intricate undertaking necessitates the meticulous collection and analysis of economic data pertinent to each technological avenue, facilitating the precise quantification of associated costs. Following the current study, the difference between the cost of producing palm oil in the MT condition and the baseline condition, divided by the difference between the GHG emissions in the baseline condition and the MT condition, is the marginal abatement cost of utilizing one MT. The MAC equation can be written as follows:

$$MAC_{MT(i)} = \frac{TC_{MT(i)} - TC_{BAU}}{TE_{BAU} - TE_{MT(i)}} \quad \dots(1)$$

Where  $MAC_{MT(i)}$  is the marginal abatement cost of utilizing selected MT (\$/ton CO<sub>2</sub>eq),  $TC_{MT(i)}$  is the total cost of applying selected MT in palm oil production (\$) and  $TC_{BAU}$  is the total cost in the baseline condition (\$).  $TE_{BAU}$  is the quantity of GHG emissions (ton CO<sub>2</sub>eq) in the baseline condition and  $TE_{MT(i)}$  is the quantity of GHG emissions (ton CO<sub>2</sub>eq) with selected MT in palm oil production. The total cost consists of capital expenditure (capex) and operational expenditure (opex) for baseline condition and utilizing a single MT in palm oil mill, which can be expressed as follows:

$$TC_{MT(i)} = \sum_{t=1}^n \frac{CAPEX_{MT(i)}^t + OPEX_{MT(i)}^t}{(1+r)^t} \quad \dots(2)$$

$$TC_{BAU} = \sum_{t=1}^n \frac{CAPEX_{BAU}^t + OPEX_{BAU}^t}{(1+r)^t} \quad \dots(3)$$

Where  $CAPEX_{MT(i)}^t$  is the total capital cost (\$) and  $OPEX_{MT(i)}^t$  is total operational cost (\$) when utilizing selected MT with the discount rate,  $r$ , and in the year of  $t$ .  $CAPEX_{BAU}^t$  and  $OPEX_{BAU}^t$  is total capital cost (\$) and operational cost (\$) in the baseline conditions with the discount rate,  $r$ , and in the year of  $t$ , respectively. The formula assesses the total of Capex and Opex for each type of MT determined by the cost of technology.

Within the present study, a bottom-up MAC approach involving financial accounting was utilized to determine the amount of abatements and corresponding costs on each MT. This methodology is appropriate in comparison to top-up methods, which are focused on analyzing the possible opportunity cost of accomplishing a specific emission reduction goal, due to its computational simplicity and high visibility in ranking cost-effectiveness measures (Huang et al. 2016).

Data is collected and compiled through desk studies and site visits. The data collected is techno-economic data from palm oil mills, with references such as performance reports and publications. For both the BAU and the alternative option, statistical data on investment cost, yearly cost of fuel, periodic operation and maintenance cost, lifespan of the technology, and replacement rates for the alternating solution must be collected.

By assessing the potential savings per ton of abatement against the construction and operating costs, the MAC calculates the net cost of measure implementation. The measures are then categorized and ranked according to their cost-effectiveness after each measure's technical mitigation

potential and marginal abatement cost have been measured. Along the x-axis, the mitigation strategies are sorted from smallest to greatest MAC, left to right.

The culminating phase of this research endeavor entails the generation of a tailored curve of marginal abatement cost, specifically tailored to the intricate dynamics of the palm oil sector. This pivotal stage encompasses a meticulous sensitivity analysis conducted upon the resultant MACC, aimed at scrutinizing the impact of parameter variations on the derived outcomes. The conclusion of this phase is marked by the comprehensive compilation of a detailed research report, meticulously encapsulating all pertinent facets of the investigative journey.

Through the dissemination of this comprehensive research report, the culmination of rigorous empirical inquiry, the scholarly community and stakeholders within the palm oil sector are furnished with invaluable insights and evidence-based recommendations pivotal for informed decision-making processes and strategic planning endeavors conducive to fostering sustainable practices and mitigating environmental impacts.

## RESULTS AND DISCUSSION

The MACC findings and analysis for mitigating technologies in the palm oil industry are covered in this section. The data sheet was collected using steps involved in the previous section to assess CO<sub>2</sub> emissions in the palm oil industry and develop efficient and cost-effective mitigation technologies. Data collection was focused on investment costs, fixed and variable Operation and Maintenance (O&M) costs, fuel costs, economic lifetime, capacity factor, efficiency or heat rate, specific fuel consumption, fuel prices, and the capacity of the reference palm oil mill.

There are currently eight methods that are capable of being used to lower GHG emissions depending on the conditions in the production process. Improvement aimed at lowering emissions in the mills has primarily concentrated on increasing waste reuse. A few of these include composting mill waste, which can be employed as fertilizer on plantations, and using biogas as a source of energy generated by facilities that capture methane from POME.

The MAC curve is shown in Fig. 5 and Table 2 shows the results of the research's marginal abatement costs for the palm oil industry in Indonesia.

The implementation of CO<sub>2</sub> mitigation technologies in the Rokan Hulu region of Riau, involving four palm oil producers, is projected to yield significant reductions in emissions. Specifically, it is estimated that these initiatives will lead to a reduction of approximately 87,255 tonnes

Table 2: MAC calculations for eight mitigation technologies in the palm oil sector.

Mitigation Technology	Capital cost	Operation and maintenance cost	Annual average CO <sub>2</sub> savings for the project	Project life	NPV	Cumulative savings for all projects	MAC
	(\$)	(\$)	(tonnes/year)	(years)	(\$)	(thousand tonnes/year)	(\$/tonne CO <sub>2</sub> eq)
A	100,000	78,000	8,950	15	-493,274	9.0	-7.2
B	15,000	5,000	15,000	8	-11,675	24.0	-0.1
C	500,000	62,500	4,875	10	115,965	28.8	3.9
D	200,000	20,000	2,390	10	77,109	31.2	5.3
E	120,000	8,000	9,400	15	59,151	40.6	0.8
F	550,000	25,000	27,530	15	359,848	68.1	1.7
G	823,000	91,000	11,630	20	48,266	79.8	0.49
H	343,000	202,500	7,480	10	-901,275	87.3	-19.61

A: High Efficiency Steam Turbine; B: POME-to-Biogas Electricity; C: Co-Composting  
 D: Solid-Liquid Separation; E: Biomass Waste Utilization; F: Biofuel Production  
 G: Biogas Upgrading; H: High-Capacity Boiler

of CO<sub>2</sub> emissions per year. This substantial decrease in emissions highlights the effectiveness of the applied mitigation strategies in mitigating the environmental impact of palm oil production activities in the region. When compared to the BAU scenario, wherein no mitigation technologies are implemented, the projected reduction in CO<sub>2</sub> emissions amounts to approximately 11.6%. This comparison underscores the importance and impact of adopting CO<sub>2</sub> mitigation technologies in the palm oil sector. By implementing these measures, palm oil producers can significantly contribute to reducing their carbon footprint and mitigating climate change effects.

Additionally, the calculations reveal that biofuel production technology emerges as the most significant contributor to emission reduction efforts, with an estimated reduction of 27,530 tons of CO<sub>2</sub> per year. This technology alone accounts for approximately 31.5% of the total emissions reduction achieved by the implemented solutions. Following closely behind, technologies such as POME-to-biogas electricity and biogas upgrading collectively contribute 30.5% to the emissions reduction efforts, resulting in a combined reduction of 26,630 tons of CO<sub>2</sub> per year. These three solutions, when considered together, demonstrate the potential to substantially mitigate CO<sub>2</sub> emissions by a combined total of 54,160 tons per year. Moreover, the analysis highlights the collective contribution of the remaining five technologies, which account for approximately 37.9% of the total emissions reduction. Among these, solid-liquid separation technology emerges as the least effective, with a relatively modest reduction of 2,390 tonnes of CO<sub>2</sub> per year, constituting only about 2.7% of the total emissions reduction achieved by all technologies combined.

Furthermore, In the realm of climate change mitigation, the evaluation of marginal abatement costs (MAC) represents

a crucial aspect of devising effective emission reduction strategies. Our comprehensive analysis delves deeply into this metric, offering nuanced insights into the cost-effectiveness and economic viability of a range of emission reduction technologies within the palm oil production sector.

Notably, high-efficiency steam turbine technology emerges as a standout performer, boasting a negative MAC of -7.2 (\$/tonne CO<sub>2</sub>eq). This remarkable finding not only underscores its efficacy in curbing emissions but also highlights its potential to generate substantial cost savings over time. By harnessing the power of advanced steam turbine systems, palm oil producers can not only reduce their carbon footprint but also enhance their bottom line, demonstrating the symbiotic relationship between environmental sustainability and economic prosperity.

Furthermore, the high-capacity boiler technology stands out as a transformative force in emission reduction efforts, with an exceptionally low MAC of -19.6 (\$/tonne CO<sub>2</sub>eq). This striking figure underscores its unparalleled capacity to drive significant emissions reductions while simultaneously yielding substantial cost benefits. As a cornerstone of sustainable palm oil production practices, high-capacity boilers offer a compelling pathway towards achieving ambitious emission reduction targets while bolstering the economic resilience of the industry.

In contrast, technologies such as POME-to-biogas electricity, solid-liquid separation, and biofuel production exhibit varying degrees of cost-effectiveness, with MACs ranging from marginally negative to moderately positive values. While these technologies offer promising avenues for emissions reduction, their economic viability may be contingent upon factors such as scale of implementation, technological maturity, and market dynamics.



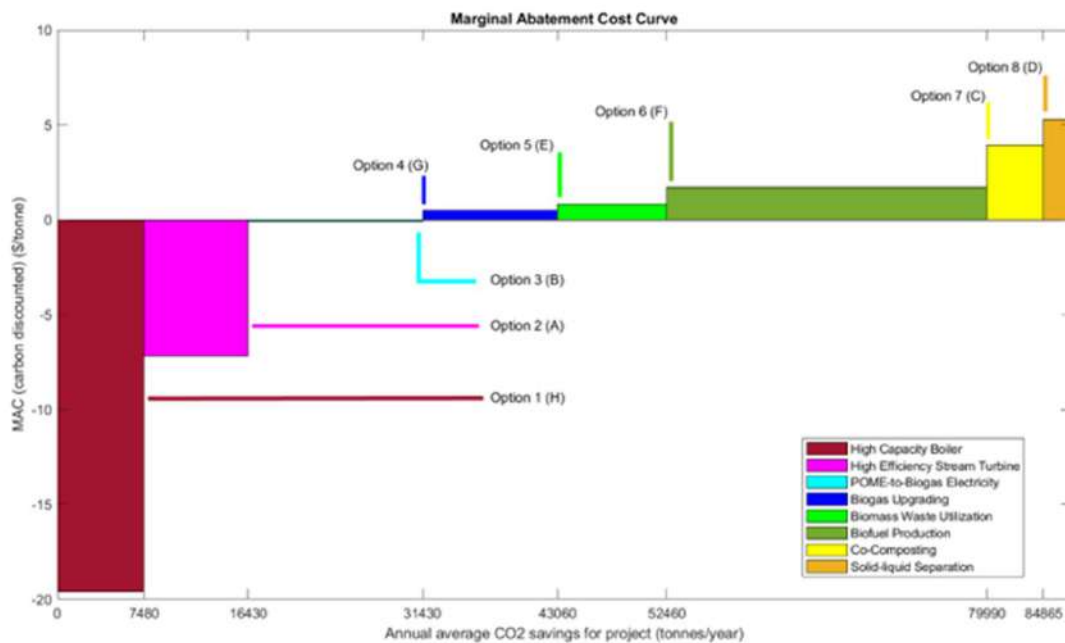


Fig. 5: MACC for the palm oil sector.

This in-depth analysis provides stakeholders with a comprehensive understanding of the intricate trade-offs and opportunities inherent in the pursuit of emission reduction within the palm oil production sector. By leveraging the insights gleaned from our analysis, policymakers, industry stakeholders, and environmental advocates can make informed decisions regarding the adoption and deployment of emission reduction technologies, paving the way for a more sustainable and prosperous future.

The MAC curve is typically displayed as a bar chart, with the horizontal axis representing abatement potential (tonne CO<sub>2</sub>eq) and the vertical axis representing marginal abatement costs (\$/tonne CO<sub>2</sub>eq). The curve can be plotted by using the provided data for “Annual Average CO<sub>2</sub> Savings for Project (tonnes/year)” and “MAC (Carbon Discounted) (\$/tonne)” columns. It arranges the projects in ascending order based on their “MAC (Carbon Discounted) (\$/tonne)” by presenting the marginal abatement cost while “Annual Average CO<sub>2</sub> Savings for Project (tonnes/year)” was presenting cumulative abatement potential that resulting to identify that offer the most cost-effective abatement options. These projects are located at the lower end of the MACC curve which will enable it to offer greater abatement potential at lower costs, making it more economically viable than other choices for reducing emissions.

The ranking basically can be observed by the MAC value of approximately ((\$/tonne). The graph shows that High-capacity boiler technology is better other than technologies.

This is followed by the High-Efficiency Stream Turbine technology and POME-to-biogas electricity technology that have a negative value of the cost of MAC. The other positive value of marginal abatement cost is defined using the higher cumulative abatement of emission. It shows the Biogas upgrading technology, followed by Biomass waste utilization technology, Biofuel production technology, Co-composting technology, and Solid-liquid separation technology.

### Sensitivity Analysis

Sensitivity analysis is a useful tool for determining which factors have the biggest impact on the results and for guiding decision-making by taking many scenarios and possible uncertainties into account. It shows how to assess the investment’s cost-effectiveness using a discount rate that can be seen by changes in the outcomes. This aids in decision-makers’ comprehension of the degree of risk or uncertainty related to the outcomes and enables them to evaluate the possible effects of changes in important parameters. Table 3 displays the results of a sensitivity study that identified the mitigating technologies as being sensitive to various rates.

The mitigation technology B is still the value in where it doesn’t change at any various rates starting at a 10% discount rate. It is demonstrated that mitigation technology G is sensitive to the discount rate, which is increasing at varying rates. However, in contrast to mitigation technology G, other mitigation technologies are also raising their

Table 3: Sensitivity analysis for MAC.

Mitigation Technology	MAC (\$/tonne CO <sub>2</sub> eq)									
	Discount rate									
	9%	10%	11%	12%	13%	14%	15%	16%	17%	18%
A	-7.3	-7.2	-7.2	-7.1	-7.0	-6.9	-6.8	-6.7	-6.6	-6.5
B	-0.2	-0.1	-0.1	-0.1	-0.1	-0.1	-0.1	-0.1	-0.1	-0.1
C	3.2	3.9	4.6	5.3	6.1	6.8	7.6	8.4	9.2	10.0
D	4.7	5.3	5.8	6.4	7.1	7.7	8.3	8.9	9.6	10.3
E	0.7	0.8	0.9	1.0	1.1	1.2	1.3	1.4	1.5	1.7
F	1.6	1.7	1.9	2.0	2.2	2.3	2.5	2.7	2.8	3.0
G	-0.07	0.49	1.06	1.65	2.25	2.86	3.48	4.11	4.75	5.40
H	-19.93	-19.61	-19.29	-18.96	-18.62	-18.28	-17.94	-17.58	-17.23	-16.87

A: High Efficiency Stream Turbine; B: POME-to-Biogas Electricity; C: Co-Composting  
 D: Solid-Liquid Separation; E: Biomass Waste Utilization; F: Biofuel Production  
 G: Biogas Upgrading; H: High-Capacity Boiler

parameter, just not as noticeably, and this does not affect their ranking.

## CONCLUSIONS

This study aims to evaluate the eight mitigation technologies that contribute to making the estimated marginal abatement costs (MAC) of Indonesia's palm oil sector from 2020 to 2030. In conclusion, the prospects of implementing CO<sub>2</sub> mitigation technologies in the Rokan Hulu region of Riau are promising, with anticipated substantial reductions in emissions amounting to approximately 87,255 tonnes of CO<sub>2</sub> annually. Among the various technologies, biofuel production emerges as the most impactful contributor, spearheading the emissions reduction efforts with a significant share of 31.5% of the total reduction. This underscores the pivotal role of innovative approaches in biofuel production within the palm oil industry's sustainability agenda.

Following closely behind are POME-to-biogas electricity and biogas upgrading technologies, collectively contributing 30.5% to the emissions reduction endeavor. Their integration into the operational framework of palm oil producers demonstrates a multifaceted approach to emissions reduction, leveraging waste-to-energy solutions for environmental gain.

Moreover, the evaluation of marginal abatement costs reveals compelling insights into the economic feasibility of emission reduction technologies. Notably, high-efficiency steam turbine and high-capacity boiler technologies emerge as cost-effective options, presenting opportunities for both emissions reduction and potential cost savings. This underscores the importance of adopting technologically advanced solutions that align with both environmental and economic sustainability goals. Future research must take into account different perspectives, such as those related to

renewable energy technology, carbon taxes, or subsidies, even though the costs of mitigation technologies have been examined in this study.

## ACKNOWLEDGEMENT

The authors gratefully acknowledge the facilities provided by the Faculty of Industrial and Manufacturing Technology and Engineering, Universiti Teknikal Malaysia Melaka, and Institut Teknologi PLN for this research work. This research work was funded by Universiti Teknikal Malaysia Melaka.

## REFERENCES

- Acobta, A. N., Ayompe, L. M., Wandum, L. M., Tambasi, E. E., Muyuka, D. S. and Egoh, B. N., 2023. Greenhouse gas emissions along the value chain in palm oil producing systems: A case study of Cameroon. *Cleaner and Circular Bioeconomy*, 6, p.100057. <https://doi.org/10.1016/j.clcb.2023.100057>
- Chen, L., 2020. Technology-side carbon abatement cost curves for China's power generation sector.
- Chiew, T. H., Jamaludin, Z., Bani Hashim, A. Y., Abdullah, L., Rafan, N. A. and Maharof, M., 2017. Second-order sliding mode control for direct drive positioning system. *Journal of Mechanical Engineering and Sciences*, 11(4), pp.3206–3216.
- Contreras, R. F., 2016. Analysis and Comparison of Energy Saving Measures Through Marginal Abatement Cost Curves. <https://doi.org/10.1007/978-3-319-26459-2>
- Duan, F., Wang, Y., Wang, Y. and Zhao, H., 2018. Estimation of marginal abatement costs of CO<sub>2</sub> in Chinese provinces under 2020 carbon emission rights allocation: 2005–2020. *Environmental Science and Pollution Research*, 25(24), pp.24445–24468. <https://doi.org/10.1007/s11356-018-2497-x>
- Edwards, R. B., 2019. Export agriculture and rural poverty: Evidence from Indonesian palm oil.
- Huang, S. K., Kuo, L. and Chou, K.-L., 2016. The applicability of marginal abatement cost approach: A comprehensive review. *Journal of Cleaner Production*, 127, pp.59–71. <https://doi.org/10.1016/j.jclepro.2016.04.013>

- Ibrahim, N. and Kennedy, C., 2016. A methodology for constructing marginal abatement cost curves for climate action in cities. *Energies*, 9(4), p.227.
- Janzen, R., Davis, M. and Kumar, A., 2020. An assessment of opportunities for cogenerating electricity to reduce greenhouse gas emissions in the oil sands. *Energy Conversion and Management*, 211(January), p.112755. <https://doi.org/10.1016/j.enconman.2020.112755>
- Jiang, H. D., Purohit, P., Liang, Q.-M., Dong, K. and Liu, L.-J., 2022. The cost-benefit comparisons of China's and India's NDCs based on carbon marginal abatement cost curves. *Energy Economics*, 109, p.105946.
- Johnsson, S., Andersson, E., Thollander, P. and Karlsson, M., 2019. Energy savings and greenhouse gas mitigation potential in the Swedish wood industry. *Energy*, 187, p.115919. <https://doi.org/10.1016/j.energy.2019.115919>
- Kesicki, F., 2013. Marginal Abatement Cost Curves: Combining Energy System Modelling and Decomposition Analysis. *Environmental Modeling and Assessment*, 18(1), pp.27–37. <https://doi.org/10.1007/s10666-012-9330-6>
- Lameh, M., Al-Mohannadi, D. M. and Linke, P., 2022. Minimum marginal abatement cost curves (Mini-MAC) for CO<sub>2</sub> emissions reduction planning. *Clean Technologies and Environmental Policy*, 24(1), pp.143–159. <https://doi.org/10.1007/s10098-021-02095-y>
- Luu, Q. Le, Nguyen, N. H., Halog, A. and Bui, H. Van., 2018. GHG emission reduction in energy sector and its abatement cost: Case study of five provinces in Mekong delta region, Vietnam. *International Journal of Green Energy*, 15(12), pp.715–723. <https://doi.org/10.1080/15435075.2018.1525556>
- Pambudi, R., Aufar, A. and Nathalia, D., 2018. Strategi Implementasi Instrumen Potensi Dan Biaya Mitigasi. pp.1–8.
- Promjiraprawat, K., Winyuchakrit, P., Limmeechokchai, B., Masui, T., Hanaoka, T. and Matsuoka, Y., 2014. CO<sub>2</sub> mitigation potential and marginal abatement costs in Thai residential and building sectors. *Energy & Buildings*. <https://doi.org/10.1016/j.enbuild.2014.02.050>
- Stichnothe, H. and Bessou, C., 2017. Challenges for life cycle assessment of palm oil production system. *Indonesian Journal of Life Cycle Assessment and Sustainability*, 1(2). <https://doi.org/10.52394/ijolcas.v1i2.28>
- Tomaschek, J., 2015a. Marginal abatement cost curves for policy recommendation – A method for energy system analysis. *Energy Policy*, 85, pp.376–385. <https://doi.org/10.1016/j.enpol.2015.05.021>
- Tomaschek, J., 2015b. Marginal abatement cost curves for policy recommendation—A method for energy system analysis. *Energy Policy*, 85, pp.376–385.
- Xiong, W., Yang, Y., Wang, Y. and Zhang, X., 2016. Marginal abatement cost curve for wind power in China: A provincial-level analysis. *Energy Science & Engineering*, 4(4), pp.245–255.
- Zhang, W., Stern, D., Liu, X., Cai, W. and Wang, C., 2017. An analysis of the costs of energy saving and CO<sub>2</sub> mitigation in rural households in China. *Journal of Cleaner Production*, 165, pp.734–745. <https://doi.org/10.1016/j.jclepro.2017.07.172>

---

#### ORCID DETAILS OF THE AUTHORS

L. Abdullah: <https://orcid.org/0000-0001-9181-826X>  
A. S. Nur Chairat: <https://orcid.org/0000-0002-1069-6860>





# Advancements in Machine Learning and Deep Learning Techniques for Crop Yield Prediction: A Comprehensive Review

V. Ramesh and P. Kumaresan<sup>†</sup>

School of Computer Science Engineering and Information Systems (SCORE), Vellore Institute of Technology, Vellore-632014, Tamil Nadu, India

<sup>†</sup>Corresponding author: P. Kumaresan; pkumaresan@vit.ac.in

Nat. Env. & Poll. Tech.  
Website: [www.neptjournal.com](http://www.neptjournal.com)

Received: 04-03-2024

Revised: 19-04-2024

Accepted: 01-05-2024

## Key Words:

Crop yield prediction

Machine learning

Deep learning

Artificial neural networks

Optimization algorithms

## ABSTRACT

Agriculture is the crucial pillar and basic building block of our nation. Agriculture plays a key role as the major source of revenue for our nation. Farming is the primary financial source of India. Abrupt environmental changes affect crop yield prediction. Unpredictable climate changes, lack of water resources, deficiency of nutrients, depletion of soil fertility, unbalanced irrigation systems, and conventional farming techniques are the major causes of crop yield prediction. Today, AI, the use of machine learning, and deep learning techniques provide an achievable solution to improve crop yields. The key intent of the survey is to accurately predict and improve crop yield by combining agricultural statistics with machine learning and deep learning models. To accomplish this, we have surveyed the optimization algorithms implemented in conjunction with the Random Forest and Cat Boost models. A survey made across multiple databases to determine the effectiveness of crop yield prediction and analysis was performed on the included articles. The survey results show that a hybrid CNN DNN and RNN model with optimization algorithms outperforms the other existing traditional models.

## INTRODUCTION

Indian economy is contingent on agriculture because it is crucial for the survival of both humans and animals in the country (Durai & Shamili 2022). From 2009 to 2030, the global population is projected to grow from 1 billion to 5 billion, leading to a significant increase in the need for agricultural commodities. As a result, there will be a greater demand for agricultural products among people, necessitating the efficient utilization of farmland and an increase in agricultural yields. Harmful climatic conditions caused by global warming frequently lead to spoiled harvests (Tseng et al. 2019). When a crop fails due to insufficient soil fertility, climate change, groundwater scarcity, flooding, or other similar circumstances, it directly affects farmers. Depending on geographical conditions and environmental factors, society in other countries recommends that farmers increase the production of certain crops (Reddy & Kumar 2021). Assessing and tracking crop productivity is crucial because of the population's faster growth (Alagurajan & Vijayakumaran 2020). Consequently, to select crops more effectively based on seasonal variation, it is critical to develop a suitable model that takes into account the relevant factors (Kumari et al. 2020).

Machine learning, a significant field of AI that focuses on the method of learning, can significantly enhance the

accuracy of yield prediction. It incorporates several features to achieve this. Machine learning can extract information from datasets and identify patterns and correlations. Datasets should be used to train models, and experience should be used to describe the findings. To create a predictive model, several features are combined, and its parameters are derived using historical data collected during the training stage. Performance evaluation is conducted using a subset of historical data that is separate from the data used for training (Klompenburg et al. 2020).

Machine learning, deep learning, and hybrid models with optimization techniques are being widely used worldwide due to their efficiency in different sectors, including predicting weed detection and disease. These algorithms also aid in improving crop yield prediction in unfavorable conditions. Regardless of the distracting environment, ML, DL, Hybrid, and Optimization algorithms are used in predicting crop yields and minimizing losses.

Fig. 1 shows the proposed RF-CatBooster crop yield prediction, indicating that yield increases under different circumstances when ML, DL, Hybrid, and Optimization Techniques are utilized. The machine learning approach has been adopted as the foundation for accurate predictions. Crop prediction leverages a classification model, while yield prediction utilizes regression models to learn insights

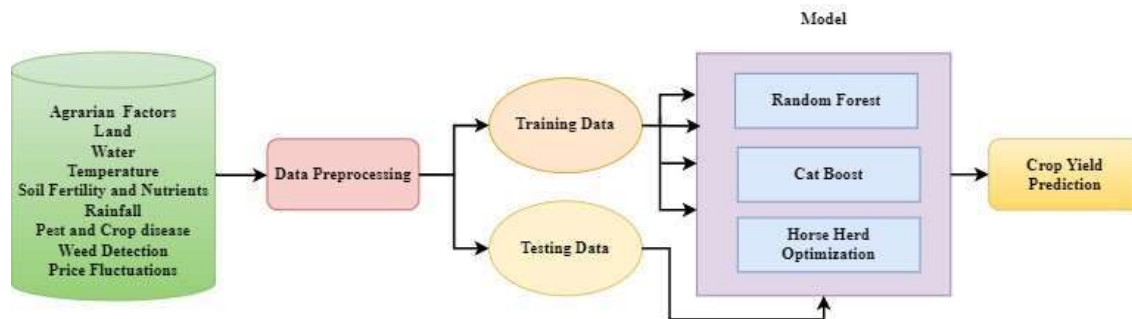


Fig. 1: Proposed RF-CatBoost architecture for crop yield prediction.

from the data. Multiple machine learning models have been surveyed based on performance metrics using a publicly accessible dataset spanning from 1999 to 2020. We propose a Random Forest and CatBoost model for predicting crop yield using preprocessed data. The dataset incorporates numerical attributes such as Crop\_Name, Area, Crop\_Year, Annual\_Rainfall, Fertilizer, and Yield\_Data. Preprocessing steps encompass encoding categorical variables like Area and Crop\_Name in preparing data for the proposed model. The standardization of attributes Crop\_Year, Annual\_Rainfall, Fertilizer, and Yield\_Data enhances consistency through the utilization of the Standard Scaler. A model is trained on 80% of the training dataset with the remaining 20% utilized to test the trained model. Prior pre-processing steps include handling missing data points, noisy entries, outlier removal, and duplication removal. MinMax Scaler resizes data proportionally within a stipulated range of 0 to 1, transforming features while retaining their original distribution shape by rescaling value to a specific range without modifying original distribution shapes. The proposed Hybrid model RF-CatBooster effectively handles non-linear data, manages categorical data, and reduces overfitting. The Horse Herd optimization algorithm is used to determine the most effective link weights in the classifier through error value computation and storage of the superior weight along with its position. Performance was measured using metrics like Mean Absolute Error (MAE) and Mean Squared Error (MSE). The results demonstrated that RF-CatBoost Regressor outperformed other models, with lower MAE and MSE scores (Moussaid et al. 2022).

The structure of this article is as follows. Section 2 presents a survey methodology for crop yield prediction. Section 3 discusses how environmental factors influence crop yield prediction. Section 4 analyzes the features and related datasets for crop yield prediction. Section 5 presents an overview of the existing machine learning, deep learning, and hybrid models for crop yield prediction. Section 6 presents the findings and discussion, and Section 7 concludes the article.

## MATERIALS AND METHODS

### Review Methodology

The Systematic Literature Review incorporates and provides research studies with the research questions presented in this literature, in addition to gathering them from conferences, journals, and other electronic sources.

### Research Questions

The following questions served as the foundation for the review paper's analysis and exploration of each study's various facets. The following is a list of the research questions:

- RQ1: How are the features used to classify in predicting crop yield?
- RQ2: How are the data sources utilized in the crop yield prediction process?
- RQ3: How can machine learning methods be used to identify various crops in yield prediction?
- RQ4: How have crop yield predictions been implemented using machine learning models?
- RQ5: Determine the methodologies utilized to evaluate the efficacy of machine learning algorithms.

The article search was meticulously designed around the central theme of the systematic literature review and its guiding research questions. To avoid the pitfalls of generic keywords, the search strategy went beyond simply encompassing "machine learning." Instead, it focused on the intersection of "crop yield prediction" and "machine learning." This targeted approach was initially executed across nine databases (Elsevier, Springer, IEEE Explorer, MDPI, Taylor & Francis, Tech Science Press, Frontiers in Plant Science, Earth System Science Data, and Journal of Ecological Engineering), ensuring relevant results. A total of 81 documents were found during this search for evaluation and analysis.

The article identifies the records retrieved after searching through 326 papers. The duplicated records were removed and the remaining records were screened in 317 papers. 180 records not related to our research were excluded. Out of the remaining 137 papers with full-text records, 56 papers were excluded for various agri-model predictions. Finally, 81 papers were assessed for crop yield and included in the review.

### **Impact of Environmental Factors on Crop Yield Prediction**

Developing an accurate and understandable prediction model for yield is a critical and arduous task. This is of fact that crop production is influenced by various crop-specific metrics, environmental factors, and management choices. Traditionally, crop yield predictions have been made using a combination of crop growth models, field surveys, and statistical models. A different facet of crop production prediction is addressed by each of these methods. Surveys in the field aim to obtain the truth on the ground. According to agronomic concepts of plant, environment, and management interactions, crop growth models simulate the growth and development of crops. To determine linear correlations between the predictors and crop yield, statistical models are used to predict meteorological variables and the results of the three preceding techniques as Field observations, Crop growth models, and Statistical models (Paudel et al. 2020).

**Abiotic and biotic factors influencing crop yield:** Abiotic factors and Biotic factors include soil, sunlight, temperature, wind, atmosphere, pH, and water, pests, and diseases, which affect the entire crop production. For example, droughts, wind, and heavy rainfall affect the crops sometimes, destroying the entire crops.

Crop yield is primarily influenced by four major agrarian factors: availability of water, soil productivity, illnesses, climate, and pests. These issues can put farmers in danger if they are not sufficiently assessed and handled. To maximize crop output while reducing risk, it is critical to examine the elements that influence crop productivity and the risks involved (Elavarasan et al. 2018).

**Land, rainfall and temperature variation:** Annual crop inventory maps that display both agricultural and non-agricultural land usage within Canada's agricultural area are published by Agricultural and Agri-Food Canada (AAFC). The maps are space-based operational and sensing tools that can boost agricultural productivity (Cravero et al. 2022). In a similar vein, (Amani et al. 2020) have produced high-resolution reference maps of South Asian cropland, discussing the necessity of raising output in light of regional food shortages. Too little rainfall causes crops to shrivel and

die, while too much rain leads to flooding, which wastes water, fertilizer, labor, and energy, while excessive rainfall harms crop growth (Ndehedehe et al. 2018, Kalaivanan & Vellingiri 2022). Crop growth properties, such as cell division, water transport, survival, photosynthesis, growth, and yield, are impacted by low temperatures (Su et al. 2017). Additionally, advanced technologies like remote sensing, weather satellites, and weather stations help monitor and analyze rainfall patterns more accurately. By understanding how rainfall impacts crops, agricultural experts can make decisions on irrigation, selection of crops, and planting season to optimize yield and mitigate potential risks caused by rainfall variability (Khosla et al. 2019).

**Soil fertility and nutrients:** Many factors influence agricultural productivity, but the most important ones are soil fertility, climate, availability of water, plant diseases, and pests. Farmers can be put at significant risk if these issues are not properly managed. A crop's ability to develop as healthily as possible depends on the soil's fertility. Healthy crops require 18 essential nutrients, which are divided into macronutrients and micronutrients. Macronutrients (N, P, K, Ca, S, Mg) are needed in larger amounts, while micronutrients (Fe, Zn, Cu, B, Mn, Mo, Cl, Si) are needed in smaller amounts (Raut et al. 2020).

**Pest, crop disease, and weed detection:** Pest and disease activity is another important factor that affects crop output (Ip et al. 2018). The most common plant diseases are spot, blight, canker, and rust (Amudha & Brindha. 2022). Pests and diseases come in various sizes and shapes, and they pose different risks to crops. Some insects, such as plant parasites, can harm crops both directly and indirectly (Serra & Tagliaferri. 2018, Roldán-Serrato et al. 2018). Weed control is a major problem for farmers during the growing season. For example, a single weed can grow approximately 10 million weed seeds, which, if not quickly eliminated, can drastically lower agricultural production or cause difficulties for years (Kumar Nagothu et al. 2023).

**Price fluctuations:** Advanced data analytics, satellite imagery, and machine learning models are commonly used to forecast crop yields. The forecasts can provide valuable information to farmers, merchants, and policymakers, helping them make effective decisions regarding harvesting, planting, and marketing strategies. Even though these methods can be accurate, they are not infallible, and unexpected events can still impact prices (Sun et al. 2023).

### **Features and Related Dataset for Crop Yield Prediction**

A study question (RQ1) was addressed by analyzing and presenting the features used with the machine learning

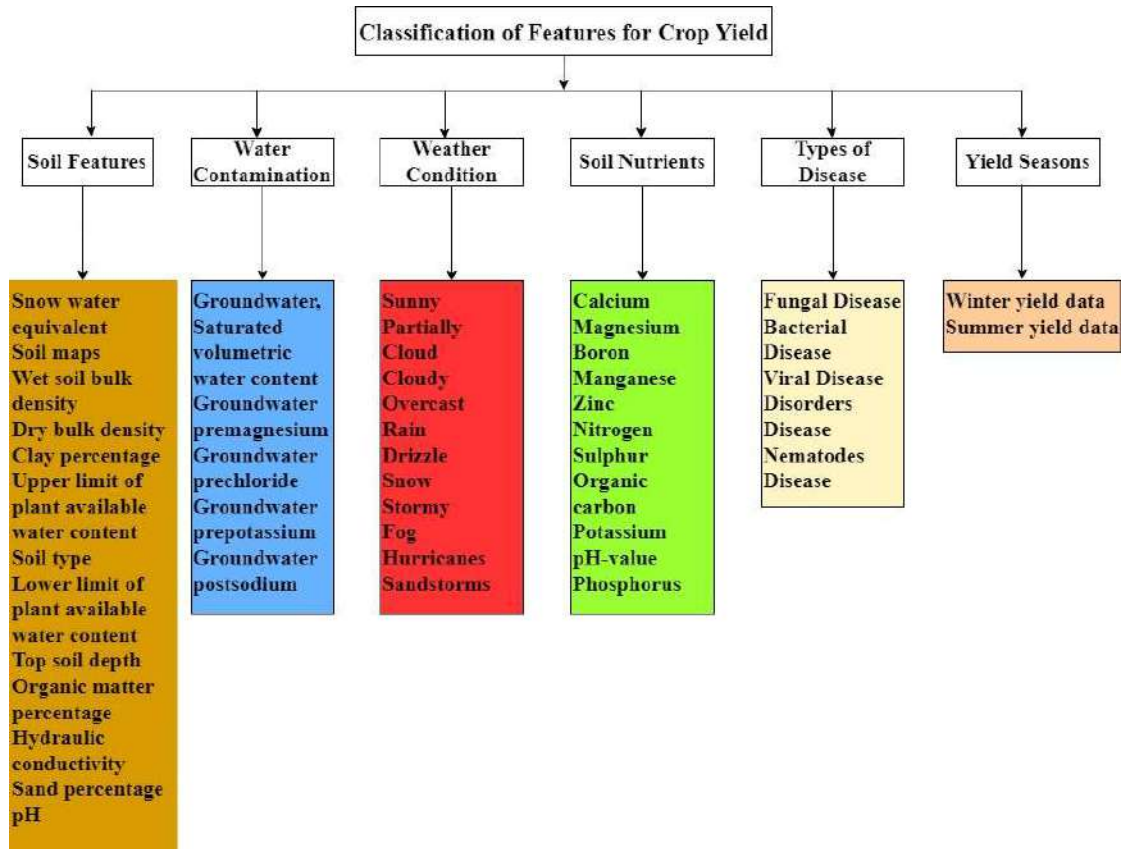


Fig. 2: Features classification for crop yield prediction.

techniques used for yield prediction. The vast quantity of data features used in yield estimation improves feature comprehension. Six categories were created from the features: soil features, water contamination, weather conditions, soil nutrients, types of disease, and yield seasons. The categorization of crop yield prediction features is seen in Fig. 2.

For instance, all satellite and aerial data features were combined, and data features of groundwater magnesium, groundwater sodium, groundwater chloride, and groundwater potassium were grouped with water content. Together with soil features, soil characteristics such as pH, type, wet soil density, dry bulk density, organic matter percentage, soil maps, snow water equivalent, clay percentage, and the upper and lower limits of plant-available water content were combined into one category. Weather data was combined with weather-related features, such as vapor pressure, daily minimum and maximum air temperatures, daily solar radiation, wind speed, temperature, rain, and precipitation. Data on diseases and yield seasons were grouped together with the names of other participants. Table 1 shows dataset features utilized in the survey article to forecast crop yields, specifically in relation to the Research Question (RQ2).

### Crop selection for yield prediction using machine learning methods:

A wide range of crop yields are estimated using machine learning techniques. Research Question (RQ3) was addressed through an analysis and presentation of the crops used in the machine learning techniques. Various crops such as Rice, Potato, Soybean, Cotton, Ragi, Barley, Apple, Coffee, Wheat, and Mango were examined in the articles that were reviewed. Fig. 3 shows the distribution of the various crop kinds employed in the examined articles. A machine learning algorithm has been used to predict crop yield including rice, soybeans, and wheat. The most prevalent crop whose output can be broadly predicted with machine learning approaches is rice.

In the reviewed articles, 19 papers were used to predict rice yield, 12 for maize yield, 10 for wheat yield, 3 for groundnut, cotton, and banana yield, and 2 for ragi, jowar, bajra, apple yield, and other crops.

### Overview of the Existing Machine Learning, Deep Learning, and Hybrid Models for Crop Yield Prediction

**Machine learning approaches:** In supervised machine learning, the machines are trained using labeled datasets,



Table 1: Overview of features of Machine Learning and Dataset Description.

Authors	Dataset	Soil Info.	Water Info.	Weather Data	Nutrients	Yield Data	Synthetic Image
Goldstein et al. (2018)	MANAGE, Meteorological data	√		√			
Aghighi et al. (2018)	Silage maize dataset, the United States Geological Survey data center.					√	√
Zhong et al. (2018)	Syngenta dataset	√		√			
Kouadio et al. (2018)	Food and Agriculture Organization data	√		√		√	
Taherei Ghazvinei et al. (2018)	Daily Basis dataset	√		√			
Deepa and Ganesan (2019)	Agriculture sites of Tamilandu(Tiruvannamalai)	√	√	√			
Bondre and Mahagaonkar (2019)	The past five years' data	√			√	√	
Khosla et al. (2019)	Rainfall Data and Crop Related Data collected from data.gov.in		√	√			
Leroux et al. (2019)	MODIS - MOD13Q1, MOD11A2, NDVI, LST	√		√		√	√
Maya Gopal and Bhargavi (2019 a)	Statistical Department of Tamilnadu,		√	√	√	√	
Filippi et al. (2019)	spatial and temporal data collected on-farm	√		√			√
Cai et al. (2019)	MODIS MOD13C1 EVI, Spatial Production Allocation Model (SPAM), Australian Bureau of Statistics (ABS) from 2000 to 2014 at the SD level (unit: t/ha).					√	√
Shiu and Chung (2019)	Spot-7 Multispectral Satellite Image						√
Elavarasan et al. (2020)	Meteorological Department of India, Agricultural Department of Tamilnadu	√	√	√		√	
Kamir et al. (2020)	MODIS dataset - MOD13Q1	√		√		√	√
Guo et al. (2021)	Chinese Meteorological Administration			√			
Nyeki et al. (2021)	spatiotemporal database	√		√			
Pant et al. (2021)	Food and Agriculture Organization data			√	√	√	
Joshua et al. (2021)	data.gov.in and indiastat.org data	√		√	√	√	
Batool et al. (2022)	Data collected from NTHRI.	√		√		√	√
Burdett and Wellen (2022)	Professional agronomists(Last year)	√				√	
Jeevaganesh et al. (2022)	Over the past two decades, agricultural data from across India has been analyzed.	√		√		√	
Cedric et al. (2022)	World Bank's knowledge portal CCKP,			√	√	√	
Croci et al. (2022)	Crop and Yield Data, Meteorological, Soil, Satellite	√		√		√	√
Gopi and Karthikeyan (2022)	Kaggle - Crop Recommendation and Crop Yield Prediction			√	√	√	
Rahman and Aktar (2022)	Food and Agriculture Organization data	√		√		√	
Joshua et al. (2022)	Agricultural Department of Tamilnadu, Regional Meteorological Centre - Chennai, Tata-Cornell Institute for Agriculture and Nutrition, Statistical Department of Tamilnadu.			√	√	√	
Iniyar et al. (2023)	Agriculture csv dataset for Crop Yield Prediction	√		√		√	
Ed-Daoudi et al. (2023)	The Regional Agricultural Development Office Ouarzazate Morocco.	√		√		√	
Sathya and Gnanasekaran (2023)	Joint Director of Agriculture Office, Kattuthottam, Thanjavur and Indian Meteorological Department, Chennai.	√	√	√	√		

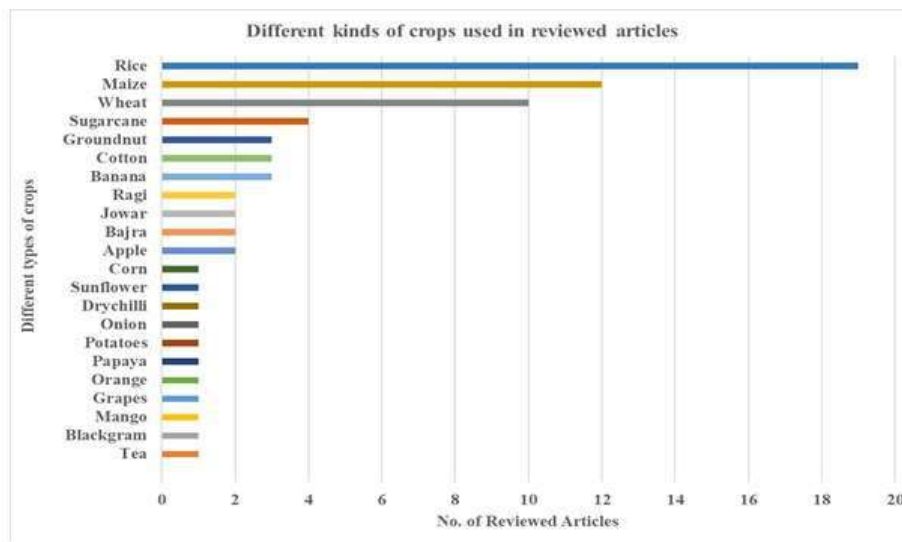


Fig. 3: Various crops distribution.

allowing them to predict outputs based on the training. The labeled data shows that certain inputs are already linked to the output. The process involves training the machine by providing it with input data and corresponding output data. After this training phase, the machine is then tested for predicting the output using separate test data. Unsupervised machine learning is trained using an unlabeled dataset to make predictions without any supervision. Semi-supervised lies between supervised learning and unsupervised learning algorithms. During the training process, it utilizes the merging of labeled and unlabeled datasets. Reinforcement learning operates through a feedback-based process. AI software agent explores their surroundings by taking action and learning from their training. Performance is improved, and the agent automatically adapts and becomes more proficient. Fig. 4 shows the general classification of Machine Learning Models.

Machine learning algorithms are crucial in predicting crop yields. The review paper examined various machine learning approaches, including Linear Regression, Logistic Regression, K-Nearest Neighbour, Gradient Boosting, Decision Tree, Random Forest, Cat Boost, XGBoost, CNN, DNN, RNN, Long Short-Term Memory, Artificial Neural Network and Hybrid Networks. The various algorithms were listed to address the Research Question (RQ4) to highlight their benefits.

**Linear, logistic, and gradient-boosting regression:** The most straightforward machine learning method is linear regression. Liang et al. (2023) predicted crop yield using the multiple linear regression method while considering socioeconomic and natural factors. The example phrase is:

$$y = b_1x_1 + b_nx_n + b_0 \quad \dots(1)$$

When  $y$  is the crop yield,  $x_1 \dots x_n$  are natural and socioeconomic factors,  $b_0$  is a constant term, and  $b_1 \dots b_n$  is the regression coefficient. Logistic regression, a statistical model with a logistic function, represents a binary dependent variable in its simplest form. Islam et al. (2022) proposed a model called the attention-based dilated CNN logistic regression for the detection of tomato leaf disease with the highest accuracy rate. Gradient boosting, an ensemble approach, is a powerful technique in practical machine learning. Nihar et al. (2022) predicted the regional wise sugarcane crop yields from the Uttar Pradesh agriculture dataset using satellite images. Verma (2022) predicted the crop yield from weather and soil conditions. The five ML models were used, such as KNN, SVC, RF, DT, and Gradient Boosting. Gradient Boosting has achieved the highest accuracy.

**Random forest and cat boost models:** Random Forest is widely recognized for its high accuracy, robustness, versatility, scalability, and importance in determining features in classification and regression tasks. Random Forest reduces overfitting by incorporating the average predictions of multiple decision trees. This averaging process enhances its robustness against noise and outliers present in the data. It offers a way to determine the importance of features, which can help select features and interpret data. Random Forest architecture is shown in Fig. 5. Choudhary et al. (2022) developed Sentinel-2 data that is suitable for predicting rice yield and conducting advanced classification with high yield prediction accuracy. Jain & Choudhary (2022) have developed a Soil-Based Machine Learning Comparative

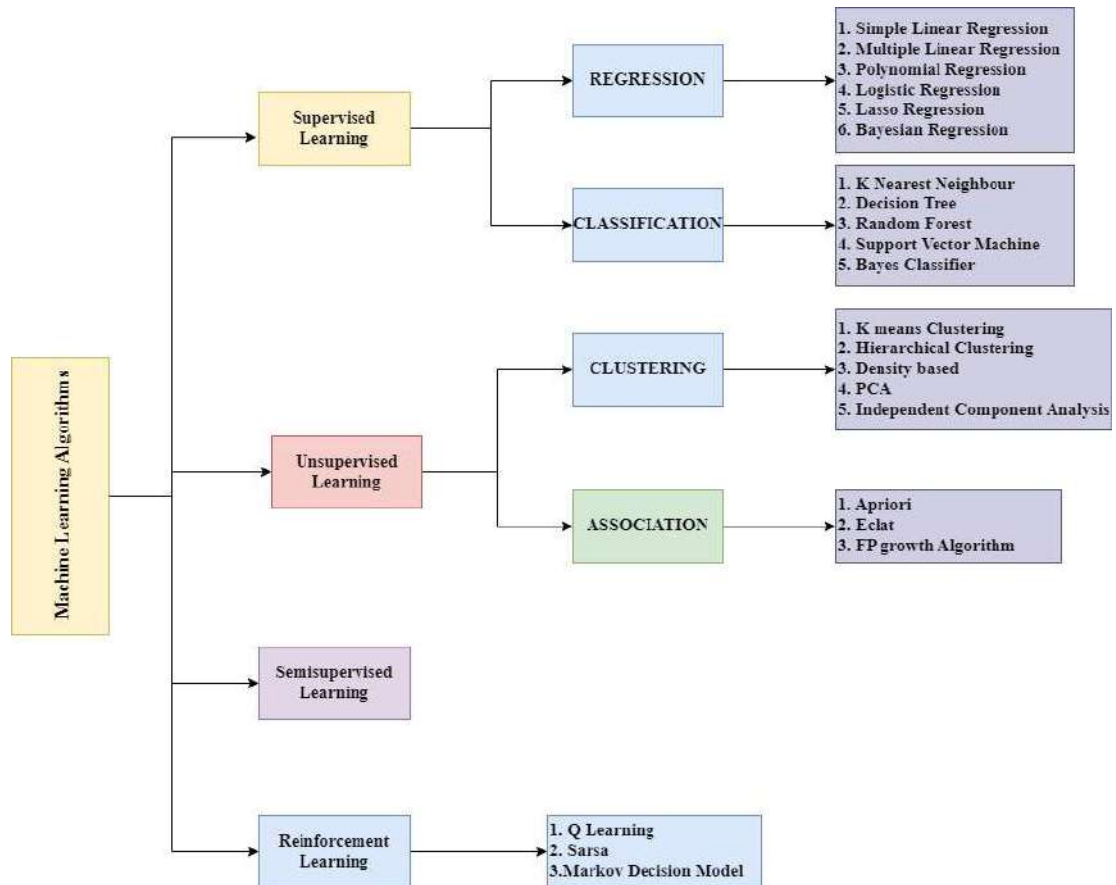


Fig. 4: Classification of Machine Learning Models.

Analytical Framework to forecast crop yield production. The SMLF utilizes soil features and climate factors to create a feature vector. The performance of SMLF is higher than other methods in the yield prediction. Croci et al. (2022) developed a machine-learning framework to predict maize yield. They incorporated different data sources, namely vegetation indices, soil, and meteorological data. The framework is used to identify the machine learning configuration that performs the best and the optimal lead time.

Cat Boost is an algorithm for gradient boosting that is specifically designed to handle datasets containing numerous categorical variables. It employs gradient descent to optimize the decision tree parameters, thereby enhancing the model's performance. The study evaluated various algorithms, including CatBoost Regressor, for predicting tree crop yield.

**XGBoost:** The XGBoost algorithm, short for eXtreme Gradient Boosting, is a combination of gradient-boosted regression trees. It is an improved gradient-boosting machine developed specifically for enhancing the output prediction speed and performance. Hazra et al. (2023) used seven machine-learning algorithms for predicting crop yields,

such as KNN, RF, XGBoost, LightGBM, ANN, SVM, and MLP. Among these, the XGBoost model gave the highest accuracy. Panigrahi et al. (2022) conducted a study in the Telangana region of India from 2016 to 2018, where they developed a crop yield prediction model using XGBOOST. The model was specifically designed for maize, groundnut, and Bengal gram. The researchers obtained the data from the Open Data Source of the State of Telangana, India, which was provided by the Department of Agriculture and Cooperation, Government of Telangana. Their findings showed that the accuracy of the XGBoost model surpassed that of other models. Kaur Dhaliwal et al. (2022) predicted historical cotton lint yield in the southeastern United States using six different ML techniques. Among these six techniques, the XGBoost showed the highest accuracy.

### Deep Learning Approaches

A deep learning algorithm is a component of a machine learning algorithm that is utilized to execute complex calculations on a large amount of data in sophisticated manners (Muruganatham et al. 2022). The input, hidden,

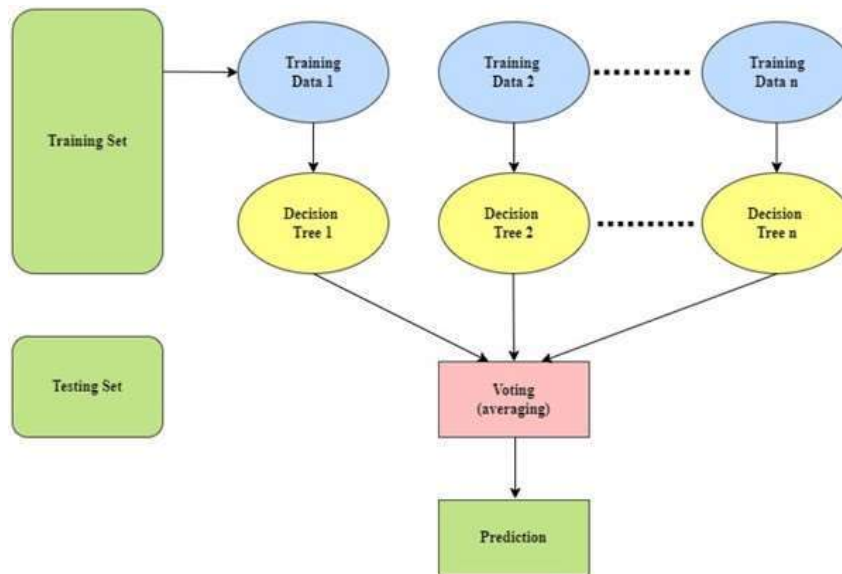


Fig. 5: Architecture of Random Forest.

and output layers of the neural network are all made up of nodes or artificial neurons. Each node receives data inputs and combines them with random weights. Finally, activation functions determine which neuron should be activated. By automatically detecting hidden patterns in the data, deep learning methods can develop more effectual decision rules. Deep learning algorithms generally outperform conventional machine learning algorithms in terms of prediction accuracy (Elavarasan & Vincent 2021).

Deep learning techniques can capture the spatio-temporal relationships in datasets (Tian et al. 2021a). Several deep learning approaches, including MLP, RNN, DNN, CNN, LSTM, and autoencoders, have been used in numerous studies to predict crop yields. Deep learning algorithms can automatically extract salient features from the data, eliminating the need for manual data preparation. An LSTM (Long Short-Term Memory) network can effectively mitigate the vanishing gradient problem that can occur with deep recurrent neural networks (RNNs) (Liu et al. 2022).

**Neural networks for crop yield prediction:** Several artificial neurons stacked on top of one another make up a CNN. The layers that make up a CNN consist of the pooling layer, the convolution layer, and the fully connected layer. The CNN Layers are used to process the dataset and extract its features (Wang et al. 2020). To identify crops and weeds, assess biomass, and forecast the production of wheat and barley crops with multispectral data, Nevavuori et al. (2019) developed a model using Deep CNN. The technique of convolutional neural networks produces outstanding results in problems related to object detection and image classification.

The results show that using RGB images improves the accuracy of yield estimates made by CNN algorithms. A deep neural network is a form of feed-forward neural network containing multiple fully connected hidden layers. Ang et al. (2022) predicted the yield for oil palm at the block level from multi-source data using Multiple Linear Regression, XGBoost, SVR, RF, and DNN approaches. Kalaiarasi & Anbarasi. (2022) introduced the concept of MDNN (Multi-parametric Deep Neural Network) for predicting crop yield by incorporating various factors like climate and soil conditions. The RNN can process the arbitrary length of an input sequence, extract the features from the input sequence, and store them in its hidden state (Fig. 6).

Long Short-Term Memory (LSTM) is a type of recurrent neural network (RNN) known for its ability to learn long-term dependencies and retain sequential data, including relevant information from previous inputs (Tian et al. 2021 b). The LSTM was developed to overcome the challenges faced by traditional RNNs, specifically the issues of exploding and vanishing gradients. It is particularly valuable in time series forecasting due to its ability to remember past inputs. The LSTM unit consists of a cell (Fig. 7), which includes an input gate, an output gate, and a forget gate. These gates regulate the flow of data within the cell and retain values for an unlimited duration. Elavarasan and Vincent (2020a) have developed a framework that uses a deep recurrent Q-learning network with 38 features to accurately estimate agricultural yield. This algorithm, known as Q-learning, offers improved accuracy and reliability in crop yield forecasts when compared to other models.

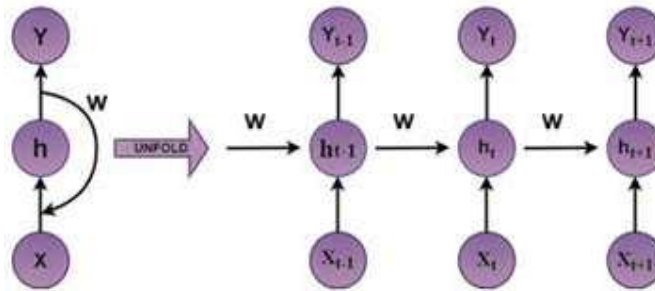


Fig. 6: Architecture of RNN.

Fig. 8 shows the standard architecture of an Artificial Neural Network (ANN) consisting of three layers: the input layer, the hidden layer, and the output layer. Each layer is comprised of multiple neurons or nodes. The input is initially received through the input layer and then forwarded to the hidden layer, commonly referred to as the core of the ANN. There may be one or more hidden layers, which are responsible for processing the information and uncovering hidden patterns or features. The output layer, which takes input from the last hidden layer, is the final layer responsible for providing the output. An ANN model was utilized by Anurag Satpathi et al. (2023) to predict rice yield.

**Hybrid and Optimization Algorithms for Crop Yield Prediction**

The purpose of optimization is to decrease the loss function, leading to improved prediction accuracy. The horse Herd optimization algorithm derives the optimal weights of the classifier links. Krishna et al. (2023) utilized A-BiLSTM-MFA to predict crop yields in India, focusing on specific features. The resulting predictions were both accurate and fast.

**RESULTS AND DISCUSSION**

The selected articles are analyzed and summarized in the review. Fig. 9. shows the number of articles published from 2016 and 2023.

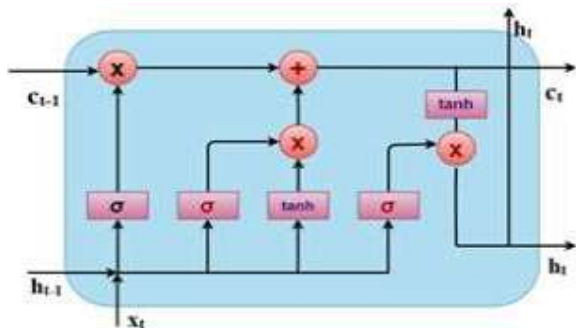


Fig. 7: Architecture of LSTM.

**Selection of Crops for Yield Prediction Based on ML Approaches**

In the articles reviewed, authors have utilized approximately 37 different crops for yield prediction. Among these, 7 crops are the most commonly used and are illustrated in Fig. 10. The remaining 30 crops, which are either used solely for comparison or to support yield prediction, have been grouped under others.

**Performance Evaluation Metrics**

Different evaluation metrics are used to measure the performance of machine learning in predicting crop yield. A total of 18 metrics are considered, including RMSE, Coefficient of determination (R<sup>2</sup>), MAE, MSE, Precision, Accuracy, F1-Score, Recall, MAPE, Correlation Coefficient(R), NMSE, RRMSE, Sensitivity, Specificity, ME, CV, RMAE, MCC, Index of Agreement were investigated in the reviewed papers. Fig. 11 shows performance evaluation metrics for crop yield prediction Algorithm.

**Mean Absolute Error (MAE)**

The mean absolute error refers to the absolute difference between the predicted value and the actual value (Aghi et al. 2018). Eq. 2. Gives the mathematical expression of MAE.

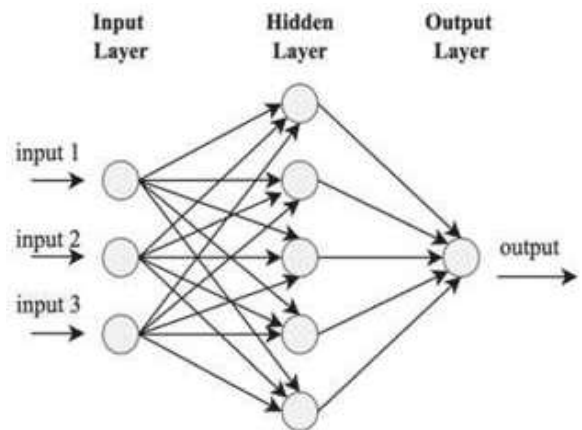


Fig. 8: Architecture of Artificial Neural Networks.

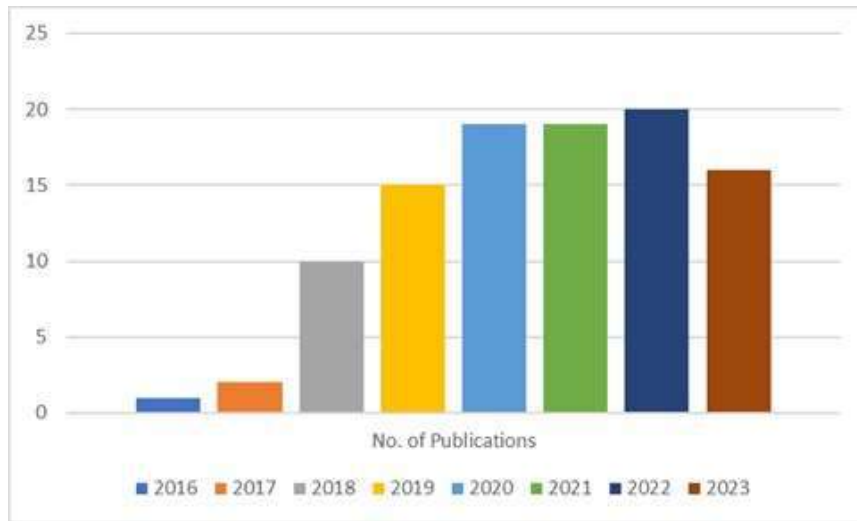


Fig. 9: The number of reviewed articles with respect to the publication year.

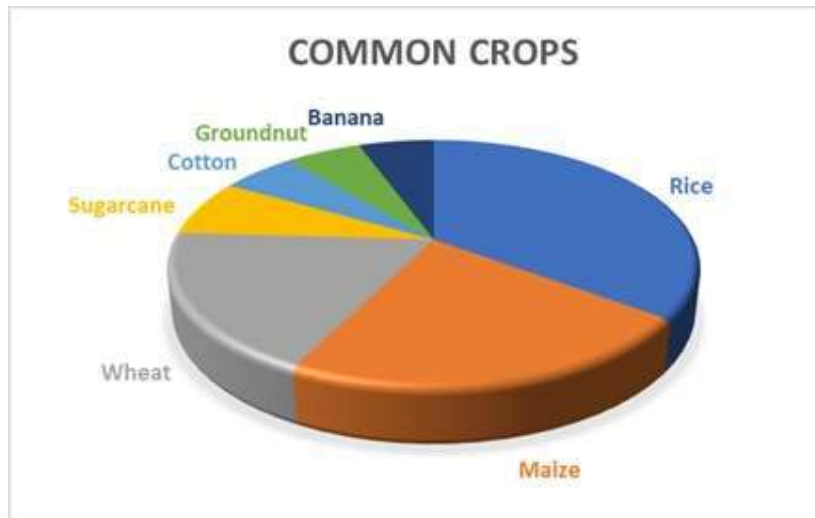


Fig. 10: Analysis of Common Crops.

$$MAE = \frac{1}{n} \sum_{i=1}^n |Y_i - \hat{Y}_i| \quad \dots(2)$$

**Mean Square Error (MSE)**

The mean square error is obtained by average squared errors. This value represents the average of the squared differences between the predicted and actual values (Elavarasan et al. 2020 b). Eq. 3. Gives the mathematical expression of MSE.

$$MSE = \frac{1}{n} \sum_{i=1}^n (\hat{y}_i - y_i)^2 \quad \dots(3)$$

**Precision**

Precision is determined by calculating the sum of accurately predicted crop yield ratings (True Predicted) divided by

the total number of crop yield predictions (True Predicted, False Predicted) (Deepa and Ganesan. 2019). Eq. 4. Gives the mathematical expression of Precision.

$$Precision = \frac{TP}{TP+FP} \quad \dots(4)$$

**Accuracy**

Accuracy refers to the proportion of accurate crop yield predictions out of the total number of crop yield predictions made (Nyeki et al. 2021). Eq. 5. Gives the mathematical expression of Accuracy.

$$Acc = \frac{TP+TN}{TP+TN+FP+FN} \quad \dots(5)$$

**F1 Score**

The F1 Score is a measurement of accuracy for a test. It considers both precision and recall when determining the score. The F1 score is calculated by taking the harmonic mean of precision and recall (Bondre & Mahagaonkar 2019). Eq. 6. Gives the mathematical expression of F1 Score.

$$F1 = \frac{(2TP)}{(2TP+FP+FN)} \quad \dots(6)$$

The F1 score is calculated as the weighted average of precision and recall. A value of 1 represents the best performance, while a value of 0 indicates the worst.

**Recall**

Recall is defined as the sum of the crop yield ratings that were accurately predicted, divided by the total number of attempts made to predict crop yield (both successful and unsuccessful predictions) (Singh Boori et al. 2023). Eq. 7. Gives the mathematical expression of Recall.

$$Recall = \frac{TP}{TP+FN} \quad \dots(7)$$

**Correlation Coefficient (R)**

The correlation coefficient (R) is included to quantify the

strength of the linear relationship between the predictions of the regression model and the actual values (Aghighi et al. 2018). Eq. 8. Gives the mathematical expression of correlation coefficient (R).

$$r = \frac{\sum(x_i - \bar{x})(y_i - \bar{y})}{\sqrt{\sum(x_i - \bar{x})^2 \sum(y_i - \bar{y})^2}} \quad \dots(8)$$

**Specificity**

Specificity is determined by dividing the number of individuals who test negative by the total number of individuals without the disorder (Gopi & Karthikeyan. 2023). Eq. 9. Gives the mathematical expression of Specificity.

$$Specificity = \frac{TN}{TN+FP} \quad \dots(9)$$

**Square Root of Mean Absolute Error (RMAE)**

RMAE stands for the square root of the Mean Absolute Error (MAE). Its naming convention is similar to that of Root Mean Square Error (RMSE), which is the square root of Mean Square Error (MSE) (Kouadio et al. 2018). Eq. 10. Gives the mathematical expression of RMAE.

$$RMAE = 100 * \frac{MAE}{\bar{Y}_m} \quad \dots(10)$$

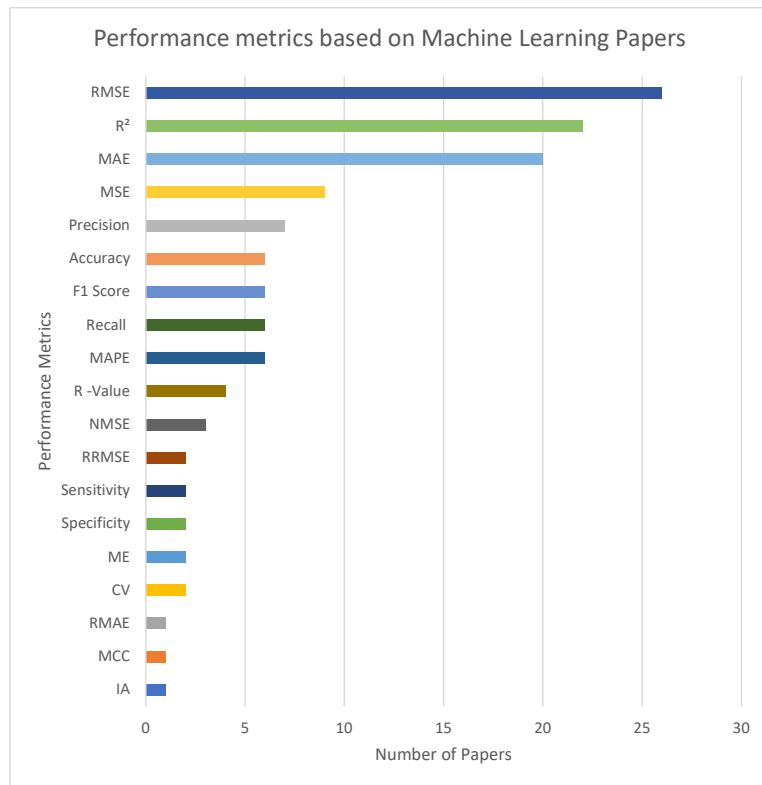


Fig. 11: Performance evaluation metrics for crop yield prediction Algorithm.

Table 2: Overview of different machine learning algorithms, crop utilized, and evaluation metrics used in crop yield prediction.

Authors	Machine Learning Algorithms	Crops	Performance Evaluation Metrics
Goldstein et al. (2018)	LR, GBRT, BTC	Alfalfa, Barley, Corn	RMSE, ME
Aghighi et al. (2018)	BRT, RFR, SVR, GPR	Maize	R, RMSE, MAE
Zhong et al. (2018)	RF, Stochastic decision model	Soyabean	RMSE, MAE
Kouadio et al. (2018)	ELM, RF, MLR	Coffee	RMSE, MAE, RRMSE, RMAE
Taherei Ghazvinei et al. (2018)	ELM, ANN, GP	Sugarcane	RMSE, r, R <sup>2</sup>
Deepa and Ganesan (2019)	SVM, NB, J48	Rice, Groundnut, Sugarcane, Cumbu, Ragi	Accuracy, Precision, Sensitivity, Specificity
Bondre and Mahagaonkar (2019)	SVM, RF	Rice, Jowar, Wheat, Soybean, Sunflower, Cotton, Sugarcane, Tobacco, Onion, Drychilli	Precision, Recall, F1-Score
Khosla et al. (2019)	MANN, SVR	Bajra, Maize, Rice, Ragi	Not Available
Leroux et al. (2019)	MLR, RF	Maize	R <sup>2</sup> , RMSE, RRMSE, MAE
Maya Gopal and Bhargavi (2019 a, b)	SVR, KNN, RF, MLR, ANN, Hybrid MLR-ANN	Rice	RMSE, MAE, R
Filippi et al. (2019)	RF	Wheat, Barley, Canola	MSE, RMSE
Khaki and Wang (2019)	LASSO, SNN, RT, DNN	Maize	RMSE
Cai et al. (2019)	SVM, RF, NN, LASSO	Wheat	R <sup>2</sup>
Shiu and Chung (2019)	OLS, SVR, GWR	Rice	R <sup>2</sup>
Elavarasan et al. (2020)	RF, DT, Gradient Boosting	Rice	MSE, MAE, RMSE, MAPE, R <sup>2</sup>
Kamir et al. (2020)	CUB, XB, RF, SVMl, MARS, GP, SVMr, KNN, MLP	Wheat	RMSE,R <sup>2</sup>
Guo et al. (2021)	MLR, BP, SVM, RF	Rice	R <sup>2</sup> , RMSE, MAE
Nyeki et al. (2021)	CP-ANN, XY-Fs, SKNs, SVM, XGBoost, ReLu	Maize	ROC, Sensitivity, Accuracy
Pant et al. (2021)	GBR, RFR, SVR, DTR	Maize, Potatoes, Rice, Wheat	R <sup>2</sup>
Singh Boori et al. (2022)	LR, DT, RF	Wheat	R <sup>2</sup> , RMSE
Prasad et al. (2021)	RF	Cotton	R <sup>2</sup> , RMSE, MAPE, IA
Joshua et al. (2021)	SVM, RBFNN, GRNN, BPNN	Rice	R <sup>2</sup> , RMSE, MAE, MSE, MAPE, CV, NSME
Batool et al. (2022)	SVR, AdaBoost Regressor, ARDR, DTR, MLPR, MLR, RANSACR, SLR, XGBoost, SVMR	Tea	MAE, MSE, RMSE
Burdett and Wellen (2022)	MLR, ANN, DT, RF	Corn, Soyabean	R <sup>2</sup> , MAE, RMSE
Jeevaganesh et al. (2022)	AdaBoost, RF	Rice, Maize, Blackgram, Lentil, Banana, Mango, Grapes, Apple, Orange, Papaya	Precision, Recall, F1-score
Choudhary et al. (2022)	DT, LR, RF	Rice	RMSE, R <sup>2</sup>
Jain and Choudhary (2022)	SVM, RF, NB, LR	Wheat, Maize	Precision, Recall, F1-score, Accuracy
Cedric et al. (2022)	DT, MLR, KNN	Rice, Maize, Cassava, Seed Cotton, Yams, Banana	R <sup>2</sup> , MAE
Croci et al. (2022)	KNN, RF,GPR,SVMr, SVMl, NNET, CUB	Maize	R <sup>2</sup> , MAE, RMSE, MAPE, Nrmse

Table Cont....



Authors	Machine Learning Algorithms	Crops	Performance Evaluation Metrics
Gopi and Karthikeyan (2022)	MMML-CRYP	Groundnut, Maize, Moong, Rice, Urad	Accuracy, Precision, Recall, Specificity, PR-Score, ROC-Score, F1-Score, MCC
Rahman and Aktar (2022)	LR, PR, SVR	Rice	MSE, MAE, MedAE, R <sup>2</sup>
Joshua et al. (2022)	BPNN, SVM, GRNN	Rice	R <sup>2</sup> , MAE, RMSE, MAPE, NMSE, CV, ME
Torsoni et al. (2023)	MLR, MLP, SVM, RF, XGBOOSTING, GradBOOSTING	Soyabean	R <sup>2</sup> , RMSE, MSE, MAE, MAPE
Wu et al. (2023)	RF, XGBOOST, LSTM	Rice	R <sup>2</sup> , RMSE
Iniyar et al. (2023)	MLR, DT, GBR, ENet, Lasso Regression, Ridge Regression, PLS Regression, LSTM	Bajra, Wheat, Jowar	R <sup>2</sup> , MAE, RMSE
Islam et al. (2023)	RF, XGBOOST, LightGBM, GradientBoost, LR	Rice	RMSE, MAE
Ed-Daoudi et al. (2023)	DT, RF, NN	Wheat, Apples, Dates, Almonds, Olives	MSE, R <sup>2</sup>
Sathya and Gnanasekaran (2023)	MLR-LSTM(Hybrid), LSTM, SVM, RF	Rice	R <sup>2</sup> , RMSE, MAE, MSE, F1-Score, Recall, Precision, Accuracy
Wang et al. (2023)	LR, DT, SVM, EL, GPR	Wheat	RMSE, MAE, MSE, R <sup>2</sup>

The articles were analyzed to answer Performance evaluation metrics (RQ5), presenting the ML algorithms and various evaluation approaches used in Table 2.

## CONCLUSIONS

The objective of this systematic literature review is to identify areas where further research is needed in machine learning, deep learning, hybrid, and optimization for crop yield prediction. It also offers valuable insights into how vegetation indices and environmental factors impact the prediction of crop yield. The studies were conducted on various crops with different temperatures, rainfall levels, and other factors. Ultimately, the machine learning deep learning and hybrid approaches outperform in predicting crop yield with the highest accuracy. The surveyed models are all equally capable of predicting crop yields based on the model's parameters and factors. However, the most effective approaches for crop yield prediction are RF, CatBoost, CNN, and LSTM, with Optimization. As per the survey, the RF algorithm can provide better results and insights depending on the specific parameters and problem at hand. CNN has the capability to identify significant features that could impact the prediction of crop yield. In addition, LSTM identifies the variation pattern of interdependence time-series data. RMSE is the evaluation metric most commonly used in the reviewed articles. It is followed by MAE, R<sup>2</sup>, MAPE, and MSE. Future investigation will be carried out on implementing crop yield prediction using the proposed RF-CatBoost hybrid model with Horse Herd optimization.

## REFERENCES

- Aghighi, H., Azadbakht, M., Ashourloo, D., Shahrabi, H.S. and Radiom, S., 2018. Machine learning regression techniques for the silage maize yield prediction using time-series images of Landsat 8 OLI. *IEEE Journal of Selected Topics in Applied Earth Observations and Remote Sensing*, 11(12), pp.4563-4577.
- Alagurajan, M. and Vijayakumaran, C., 2020. ML methods for crop yield prediction and estimation: An exploration. *International Journal of Engineering and Advanced Technology*, 9(3), pp.3506-3508.
- Amani, M., Kakooei, M., Moghimi, A., Ghorbanian, A., Ranjgar, B., Mahdavi, S., Davidson, A., Fiset, T., Rollin, P., Brisco, B. and Mohammadzadeh, A., 2020. Application of Google Earth Engine cloud computing platform, Sentinel imagery, and neural networks for crop mapping in Canada. *Remote Sensing*, 12(21), pp.1-18.
- Amudha, M. and Brindha, K., 2022. Multi techniques for agricultural image disease classification and detection: A review. *Nature Environment and Pollution Technology*, 21(5), pp.2165-2175.
- Ang, Y., Shafri, H.Z.M., Lee, Y.P., Bakar, S.A., Abidin, H., Mohd Junaidi, M.U.U., Hashim, S.J., Che'Ya, N.N., Hassan, M.R., Lim, H.S., Abdullah, R., Yusup, Y., Muhammad, S.A., Teh, S.Y. and Samad, M.N., 2022. Oil palm yield prediction across blocks from multi-source data using machine learning and deep learning. *Earth Science Informatics*, 15(4), pp.2349-2367.
- Batool, D., Shahbaz, M., Shahzad Asif, H., Shaukat, K., Alam, T.M., Hameed, I.A. and Luo, S., 2022. A hybrid approach to tea crop yield prediction using simulation models and machine learning. *Plants*, 11(15), p.1925.
- Bondre, D.A. and Mahagaonkar, S., 2019. Prediction of crop yield and fertilizer recommendation using machine learning algorithms. *International Journal of Engineering Applied Sciences and Technology*, 4(5), pp.371-376.
- Burdett, H. and Wellen, C., 2022. Statistical and machine learning methods for crop yield prediction in the context of precision agriculture. *Precision Agriculture*, 23(5), pp.1553-1574.
- Cai, Y.P., Guan, K.Y., Lobell, D., Potgieter, A.B., Wang, S.W., Peng,

- J., Xu, T.F., Asseng, S., Zhang, Y.G., You, L.Z. and Peng, B., 2019. Integrating satellite and climate data to predict wheat yield in Australia using machine learning approaches. *Agricultural and Forest Meteorology*, 274, pp.144-159.
- Cedric, L.S., Adoni, W.Y.H., Aworka, R., Zoueu, J.T., Mutombo, F.K., Krichen, M. and Kimpolo, C.L.M., 2022. Crops yield prediction based on machine learning models: Case of West African countries. *Smart Agricultural Technology*, 2, p.100049.
- Choudhary, K., Shi, W., Dong, Y. and Paringer, R., 2022. Random forest for rice yield mapping and prediction using Sentinel-2 data with Google Earth Engine. *Advances in Space Research*, 70(8), pp.2443-2457.
- Cravero, A., Pardo, S., Sepúlveda, S. and Muñoz, L., 2022. Challenges to use machine learning in agricultural big data: A systematic literature review. *Agronomy*, 12(3), pp. 114-124.
- Croci, M., Impollonia, G., Meroni, M. and Amaducci, S., 2022. Dynamic maize yields predictions using machine learning on multi-source data. *Remote Sensing*, 15(1), p. 178.
- Deepa, N. and Ganesan, K., 2019. Hybrid rough fuzzy soft classifier based multi-class classification model for agriculture crop selection. *Soft Computing*, 23(21), pp.10793-10809.
- Durai, S.K.S. and Shamili, M.D., 2022. Smart farming using machine learning and deep learning techniques. *Decision Analytics Journal*, 3, p.100041.
- Ed-Daoudi, R., Alaoui, A., Ettaki, B. and Zerouaoui, J., 2023. Improving crop yield predictions in Morocco using machine learning algorithms. *Journal of Ecological Engineering*, 24(6), pp.392-400.
- Elavarasan, D. and Vincent, P.D., 2020a. Crop yield prediction using deep reinforcement learning model for sustainable agrarian applications. *IEEE Access*, 8, pp.86886-86901.
- Elavarasan, D. and Vincent, D.R., 2020b. Reinforced XGBoost machine learning model for sustainable, intelligent agrarian applications. *Journal of Intelligent and Fuzzy Systems*, 39(5), pp.7605-7620.
- Elavarasan, D. and Vincent, P.M.D.R., 2021. A reinforced random forest model for enhanced crop yield prediction by integrating agrarian parameters. *Journal of Ambient Intelligence and Humanized Computing*, 12(11), pp.10009-10022.
- Elavarasan, D., Durai Raj Vincent, P.M., Srinivasan, K. and Chang, C.Y., 2020. A hybrid CFS filter and RF-RFE wrapper-based feature extraction for enhanced agricultural crop yield prediction modeling. *Agriculture (Switzerland)*, 10(9), pp.1-27.
- Elavarasan, D., Vincent, P.M.D.R., Sharma, V., Zomaya, A.Y. and Srinivasan, K., 2018. Forecasting yield by integrating agrarian factors and machine learning models: A survey. *Computers and Electronics in Agriculture*, 155(August), pp.257-282.
- Filippi, P., Jones, E.J., Wimalathunge, N.S., Somarathna, P.D.S.N., Pozza, L.E., Ugbaje, S.U., Jephcott, T.G., Paterson, S.E., Whelan, B.M. and Bishop, T.F.A., 2019. An approach to forecasting grain crop yield using multi-layered, multi-farm data sets and machine learning. *Precision Agriculture*, 20(5), pp.1015-1029.
- Goldstein, A., Fink, L., Meitin, A., Bohadana, S., Lutenberg, O. and Ravid, G., 2018. Applying machine learning on sensor data for irrigation recommendations: revealing the agronomist's tacit knowledge. *Precision Agriculture*, 19(3), pp.421-444.
- Gopi, P.S.S. and Karthikeyan, M., 2023. Multimodal machine learning-based crop recommendation and yield prediction model. *Intelligent Automation and Soft Computing*, 36(1), pp.313-326.
- Guo, Y., Fu, Y., Hao, F., Zhang, X., Wu, W., Jin, X., Bryant, C.R. and Senthilnath, J., 2021. Integrated phenology and climate in rice yield prediction using machine learning methods. *Ecological Indicators*, 120, p.106935.
- Hazra, S., Karforma, S., Bandyopadhyay, A., Chakraborty, S. and Chakraborty, D., 2023. Prediction of crop yield using machine learning approaches for agricultural data. *TechRxiv. Preprint*, pp.0-10.
- Iniyani, S., Varma, V.A. and Naidu, C.T., 2023. Crop yield prediction using machine learning techniques. *Advances in Engineering Software*, 175(August 2022), p.103326.
- Ip, R.H.L., Ang, L.M., Seng, K.P., Broster, J.C. and Pratley, J.E., 2018. Big data and machine learning for crop protection. *Computers and Electronics in Agriculture*, 151(November 2017), pp.376-383.
- Islam, M.D., Di, L., Qamer, F.M., Shrestha, S., Guo, L., Lin, L., Mayer, T.J. and Phalke, A.R., 2023. Rapid rice yield estimation using integrated remote sensing meteorological data and machine learning. *Remote Sensing*, 15(9).
- Jain, K. and Choudhary, N., 2022. Comparative analysis of machine learning techniques for predicting production capability of crop yield. *International Journal of System Assurance Engineering and Management*, 13(s1), pp.583-593.
- Jeevaganesh, R., Harish, D. and Priya, B., 2022. A machine learning-based approach for crop yield prediction and fertilizer recommendation. *2022 6th International Conference on Trends in Electronics and Informatics (ICOEI)*, pp.1330-1334.
- Joshua, S.V., Priyadharsan, A.S.M., Kannadasan, R., Khan, A.A., Lawanont, W., Khan, F.A., Rehman, A.U. and Ali, M.J., 2022. Crop yield prediction using machine learning approaches on a wide spectrum. *Computers, Materials and Continua*, 72(3), pp.5663-5679.
- Joshua, V., Priyadharsan, S.M. and Kannadasan, R., 2021. Exploration of machine learning approaches for paddy yield prediction in the eastern part of Tamil Nadu. *Agronomy*, 11(10), pp.1-19.
- Kalaifarasi, E. and Anbarasi, A., 2022. Multi-parametric multiple kernel deep neural networks for crop yield prediction. *Materials Today: Proceedings*, 62, pp.4635-4642.
- Kalaivanan, K. and Vellingiri, J., 2022. Survival study on different water quality prediction methods using machine learning. *Nature Environment and Pollution Technology*, 21(3), pp.1259-1267.
- Kamir, E., Waldner, F. and Hochman, Z., 2020. Estimating wheat yields in Australia using climate records, satellite image time series and machine learning methods. *ISPRS Journal of Photogrammetry and Remote Sensing*, 160(9), pp.124-135.
- Kaur Dhaliwal, J., Panday, D., Saha, D., Lee, J., Jagadamma, S., Schaeffer, S. and Mengistu, A., 2022. Predicting and interpreting cotton yield and its determinants under long-term conservation management practices using machine learning. *Computers and Electronics in Agriculture*, 199(6), p.107107.
- Khaki, S. and Archontoulis, S.V., 2020. A CNN-RNN framework for crop yield prediction. *Frontiers in Plant Science*, 10, p.1750.
- Khaki, S. and Wang, L., 2019. Crop yield prediction using deep neural networks. *Frontiers in Plant Science*, 10(6), pp.1-10.
- Khosla, E., Dharavath, R. and Priya, R., 2019. Crop yield prediction using aggregated rainfall-based modular artificial neural networks and support vector regression. *Environment, Development and Sustainability*, 22(6), pp.5687-5708.
- Klompenburg, T., Kassahun, A. and Catal, C., 2020. Crop yield prediction using machine learning: A systematic literature review. *Computers and Electronics in Agriculture*, 177(01), p.105709.
- Kouadio, L., Deo, R.C., Byrareddy, V., Adamowski, J.F., Mushtaq, S. and Phuong Nguyen, V., 2018. Artificial intelligence approach for the prediction of Robusta coffee yield using soil fertility properties. *Computers and Electronics in Agriculture*, 155(8), pp.324-338.
- Krishna, M.V., Swaroopa, K., Swarna Latha, G. and Yasaswani, V., 2023. Crop yield prediction in India based on mayfly optimization empowered attention-bi-directional long short-term memory (LSTM). *Multimedia Tools and Applications*, 13, p.789.
- Kumar Nagothu, S., Anitha, G., Siranthini, B., Anandi, V. and Siva Prasad, P., 2023. Weed detection in agriculture crop using unmanned

- aerial vehicle and machine learning. *Materials Today: Proceedings*, 16, pp.412-418.
- Kumari, P., Rathore, S., Kalamkar, A., Kumari, P., Rathore, S., Kalamkar, P.A. and Kambale, T., 2020. Prediction of crop yield using SVM approach with the facility of E-MART system. *Easychair*, 17, p.318-339.
- Leroux, L., Castets, M., Baron, C., Escorihuela, M.-J., Bégue, A. and Lo Seen, D., 2019. Maize yield estimation in West Africa from crop process-induced combinations of multi-domain remote sensing indices. *European Journal of Agronomy*, 108, pp.11-26.
- Liang, J., Li, H., Li, N., Yang, Q. and Li, L., 2023. Analysis and prediction of the impact of socio-economic and meteorological factors on rapeseed yield based on machine learning. *Agronomy*, 13(7), pp.1-17.
- Liu, Y., Wang, S., Wang, X., Chen, B., Chen, J., Wang, J. and Zhu, K., 2022. Exploring the superiority of solar-induced chlorophyll fluorescence data in predicting wheat yield using machine learning and deep learning methods. *Computers and Electronics in Agriculture*, 192, p.106612.
- Maya Gopal, P.S. and Bhargavi, R., 2019a. A novel approach for efficient crop yield prediction. *Computers and Electronics in Agriculture*, 165(6), p.104968.
- Maya Gopal, P.S. and Bhargavi, R., 2019b. Performance evaluation of best feature subsets for crop yield prediction using machine learning algorithms. *Applied Artificial Intelligence*, 33(7), pp.621-642.
- Moussaid, A., El Fkihi, S., Zennayi, Y., Lahlou, O., Kassou, I., Bourzeix, F., El Mansouri, L. and Imani, Y., 2022. Machine learning applied to tree crop yield prediction using field data and satellite imagery: A case study in a citrus orchard. *Informatics*, 9(4), pp.111-121.
- Muruganantham, P., Wibowo, S., Grandhi, S., Samrat, N.H. and Islam, N., 2022. A systematic literature review on crop yield prediction with deep learning and remote sensing. *Remote Sensing*, 14(9), pp.17-30.
- Ndehedehe, C.E., Agutu, N.O. and Okwuashi, O., 2018. Is terrestrial water storage a useful indicator in assessing the impacts of climate variability on crop yield in semi-arid ecosystems? *Ecological Indicators*, 88(January), pp.51-62.
- Nevavuori, P., Narra, N. and Lipping, T., 2019. Crop yield prediction with deep convolutional neural networks. *Computers and Electronics in Agriculture*, 163, p.104859.
- Nihar, A., Patel, N.R. and Danodia, A., 2022. Machine-learning-based regional yield forecasting for sugarcane crop in Uttar Pradesh, India. *Journal of the Indian Society of Remote Sensing*, 50(8), pp.1519-1530.
- Nyéki, A., Kerepesi, C., Daróczy, B., Benczúr, A., Milics, G., Nagy, J., Harsányi, E., Kovács, A.J. and Neményi, M., 2021. Application of spatio-temporal data in site-specific maize yield prediction with machine learning methods. *Precision Agriculture*, 22(5), pp.1397-1415.
- Panigrahi, B., Kathala, K.C.R. and Sujatha, M., 2022. A machine learning-based comparative approach to predict the crop yield using supervised learning with regression models. *Procedia Computer Science*, 218, pp.2684-2693.
- Pant, J., Pant, R.P., Kumar Singh, M., Pratap Singh, D. and Pant, H., 2021. Analysis of agricultural crop yield prediction using statistical techniques of machine learning. *Materials Today: Proceedings*, 46, pp.10922-10926.
- Paudel, D., Boogaard, H., de Wit, A., Janssen, S., Osinga, S., Pylaniadis, C. and Athanasiadis, I.N., 2021. Machine learning for large-scale crop yield forecasting. *Agricultural Systems*, 187(October), p.103016.
- Prasad, N.R., Patel, N.R. and Danodia, A., 2021. Crop yield prediction in cotton for regional level using random forest approach. *Spatial Information Research*, 29(2), pp.195-206.
- Rahman, T. and Aktar, S., 2022. Machine learning approaches to predict rice yield of Bangladesh. *2022 International Conference on Innovations in Science, Engineering and Technology*, ICISSET 2022, February, pp.329-333.
- Raut, J. and Mittal, S., 2020. Soil fertility and crop recommendation using machine learning and deep learning techniques: A review. *Turkish Journal of Computer and Mathematics Education*, 11(02), pp.1119-1127.
- Reddy, D.J. and Kumar, M.R., 2021. Crop yield prediction using machine learning algorithm. *Proceedings - 5th International Conference on Intelligent Computing and Control Systems*, ICICCS 2021, pp.1466-1470.
- Sathya, P. and Gnanasekaran, P., 2023. Paddy yield prediction in Tamilnadu Delta region using MLR-LSTM model. *Applied Artificial Intelligence*, 37(1).
- Satpathi, A., Setiya, P., Das, B., Nain, A.S., Jha, P.K., Singh, S. and Singh, S., 2023. Comparative analysis of statistical and machine learning techniques for rice yield forecasting for Chhattisgarh, India. *Sustainability*, 15(3), p.2786.
- Serra, A. and Tagliaferri, R., 2018. Unsupervised learning: Clustering. *Encyclopedia of Bioinformatics and Computational Biology: ABC of Bioinformatics*, 1-3, pp.350-357.
- Shiu, Y.S. and Chuang, Y.C., 2019. Yield estimation of paddy rice based on satellite imagery: Comparison of global and local regression models. *Remote Sensing*, 11(2), pp.1-18.
- Singh Boori, M., Choudhary, K., Paringer, R. and Kupriyanov, A., 2023. Machine learning for yield prediction in Fergana Valley, Central Asia. *Journal of the Saudi Society of Agricultural Sciences*, 22(2), pp.107-120.
- Su, Y.X., Xu, H. and Yan, L.J., 2017. Support vector machine-based open crop model (SBOCM): Case of rice production in China. *Saudi Journal of Biological Sciences*, 24(3), pp.537-547.
- Sun, F., Meng, X., Zhang, Y., Wang, Y., Jiang, H. and Liu, P., 2023. Agricultural product price forecasting methods: A review. *Agriculture*, 13(9), p.1671.
- Taherei Ghazvinei, P., Darvishi, H.H., Mosavi, A., Bin Wan Yusof, K., Alizamir, M., Shamshirband, S. and Chau, K.W., 2018. Sugarcane growth prediction based on meteorological parameters using extreme learning machine and artificial neural network. *Engineering Applications of Computational Fluid Mechanics*, 12(1), pp.738-749.
- Tian, H., Wang, P., Tansey, K., Han, D., Zhang, J., Zhang, S. and Li, H., 2021a. A deep learning framework under attention mechanism for wheat yield estimation using remotely sensed indices in the Guanzhong Plain, PR China. *International Journal of Applied Earth Observation and Geoinformation*, 102, p.102375.
- Tian, H., Wang, P., Tansey, K., Zhang, J., Zhang, S. and Li, H., 2021b. An LSTM neural network for improving wheat yield estimates by integrating remote sensing data and meteorological data in the Guanzhong Plain, PR China. *Agricultural and Forest Meteorology*, 310, p.108629.
- Torsoni, G.B., de Oliveira Aparecido, L.E., dos Santos, G.M., Chiquitto, A.G., da Silva Cabral Moraes, J.R. and de Souza Rolim, G., 2023. Soybean yield prediction by machine learning and climate. *Theoretical and Applied Climatology*, 151(3-4), pp.1709-1725.
- Tseng, F.H., Cho, H.H. and Wu, H.T., 2019. Applying big data for intelligent agriculture-based crop selection analysis. *IEEE Access*, 7, pp.116965-116974.
- Verma, R., 2022. Crop analysis and prediction. *2022 5th Multimedia, Signal Processing and Communication Technologies (IMPACT)*, 44, pp.1-5.
- Wang, J., Tian, G., Tao, Y. and Lu, C., 2023. Prediction of Chongqing's grain output based on support vector machine. *Frontiers in Sustainable Food Systems*, 7.
- Wang, X., Huang, J., Feng, Q. and Yin, D., 2020. Winter wheat yield prediction at the county level and uncertainty analysis in main wheat-producing regions of China with deep learning approaches. *Remote Sensing*, 12(11), p.1744.

Wang, Y., Shi, W. and Wen, T., 2023. Prediction of winter wheat yield and dry matter in North China Plain using machine learning algorithms for optimal water and nitrogen application. *Agricultural Water Management*, 277(January), p.108140.

Wu, H., Zhang, J., Zhang, Z., Han, J., Cao, J., Zhang, L., Luo, Y., Mei, Q., Xu, J. and Tao, F., 2023. AsiaRiceYield4km: Seasonal rice yield in Asia from 1995 to 2015. *Earth System Science Data*, 15(2), pp.791-808.

Zhong, H., Li, X., Lobell, D., Ermon, S. and Brandeau, M.L., 2018. Hierarchical modeling of seed variety yields and decision making for future planting plans. *Environment Systems and Decisions*, 38(4), pp.458-470.

---

#### ORCID DETAILS OF THE AUTHORS

P. Kumaresan: <https://orcid.org/0000-0001-5563-8325>



# Anaerobic Co-digestion of Palm Oil Sludge, Cassava Peels, Cow Dung and Ground Eggshells: Process Optimization and Biogas Generation

D. O. Olukanni<sup>1</sup>, M. J. Kamlenga<sup>2†</sup>, C. N. Ojukwu<sup>1</sup> and T. Mkandawire<sup>3</sup>

<sup>1</sup>Department of Civil Engineering, College of Engineering, Covenant University, Ota, Nigeria

<sup>2</sup>Department of Civil Engineering, Arusha Technical College, Arusha, Tanzania

<sup>3</sup>Department of Civil Engineering, Malawi University of Business and Applied Sciences, Blantyre, Malawi

†Corresponding author: M.J. Kamlenga; mwigine.kamlenpags@stu.cu.edu.ng

Nat. Env. & Poll. Tech.  
Website: [www.neptjournal.com](http://www.neptjournal.com)

Received: 13-03-2024

Revised: 16-04-2024

Accepted: 26-04-2024

## Key Words:

Anaerobic digestion

Biogas

Co-digestion

Crop waste

Environmental pollution

Environmental sustainability

Organic wastes

## ABSTRACT

Indiscriminate disposal of crop and animal wastes has grown in acceptance across the globe as an environmentally hazardous practice. This study used a 225L polyethylene digester that was specially made to produce biogas from anaerobic co-digestion of palm oil sludge, cassava peels, and cow dung using ground eggshells for pH stabilization and a greenhouse for temperature control. Cassava peels, palm oil sludge, cow dung, and water were combined in a ratio of 1:1:2:5.3, respectively, and 1.3 kilograms of crushed eggshells were added. The bio-digestion system generated 650.60 L of cumulative biogas throughout the 30-day sludge retention period. The pH averaged 6.0, and the slurry temperature averaged 34.76°C during digestion, which is favorable for the production of biogas since microbial populations thrive under hospitable conditions. The biogas produced after a hydraulic retention time (HRT) of over 20 days had the highest methane concentration of 60%, while days under 10 HRT had the lowest methane content of 45.5%. On the 13<sup>th</sup> day of anaerobic digestion, biogas output peaked at 34.90L, and pH and temperature were maintained at 6.5 and 35.0°C, respectively, the ideal ranges for a healthy process. An efficient technique for producing energy in the form of biogas was shown by optimized anaerobic co-digestion of animal and crop waste utilizing ground eggshells and a greenhouse for pH and temperature control. Future research should focus on developing more efficient, cheaper microbial agents, such as enzymes for biological pre-treatment of palm oil sludge to reduce lignin, which negatively impacts biogas generation.

## INTRODUCTION

The world's rising population has been linked to an increase in energy demand since more agricultural goods need to be processed to meet food demand, which leads to tremendous waste generation and environmental pollution. According to Olukanni et al. (2018), the generation of solid waste is rising faster than waste management programs put in place by organizations with sound financial and technical standing. Municipal waste, agricultural waste, and animal waste, all of which contain organic materials, are examples of solid wastes created (Giwa et al. 2017). The tropical climate favors the growth of crops such as cassava, palm oil, maize, cocoyam, yam groundnut, sorghum, cocoa, and cotton (Anh et al. 2022). When these crops are processed, wastewater, sediments, and peels are produced. All of these waste products are disposed of, and some are even eaten by cattle (Olukanni & Olatunji 2018). The peels and sludge that are discarded damage the atmosphere by giving off unpleasant odors. In addition, these wastes can contaminate the soil and

surface water when rain washes them away because they contain acid (Omilani et al. 2019).

Appropriate handling and treatment of crop wastes (CW) have emerged as a global trend in many nations because they pollute the environment (Pramanik et al. 2019). In accordance with a study by De Clercq et al. (2017), the disposal of agricultural waste in landfills causes the production of large volumes of greenhouse gases (GHGs), such as carbon dioxide (CO<sub>2</sub>) and methane (CH<sub>4</sub>). The release of GHGs into the atmosphere, where CH<sub>4</sub> is 25 times more hazardous than CO<sub>2</sub>, is thought to be the primary contributor to global warming (Slorach et al. 2019). Developing a proper management system of organic waste to recover biogas can be a breakthrough for developing nations that have a deficit in clean cooking energy, which leads to continuous deforestation and hence releases over 50 million tons of carbon dioxide emissions (Nwafor 2021). Due to inadequate energy sources, people are forced to rely on wood and charcoal as a source of energy for cooking, which leads to

indoor air pollution and a variety of health problems, such as lower respiratory tract infections and chronic obstructive pulmonary disorders (US EPA 2013).

Appropriate handling of agricultural and animal wastes is one that Nations must address (Fagbenle & Olukanni 2022). The adequate management of cow dung (CD) has not been established recently, it has either been used without treatment, neglecting the expected implications on groundwater and soil contamination (Almomani & Bhosale 2020). Numerous techniques, such as anaerobic digestion (AD) (Almomani et al. 2017, 2019), composting (Guerra-Rodríguez et al. 2001), incineration (Demirer & Chen 2004), and soil application (Araji et al. 2001) were utilized to handle organic wastes. Up to a certain point, incineration is convenient, but it still has low productivity, poor energy value, and significant environmental problems in addition to greenhouse gas (GHG) emissions (Almomani & Bhosale 2020). Application to soil results in a significant loss of biomass, high carbon dioxide (CO<sub>2</sub>) levels, and unpleasant odors that attract fungi and viruses that propagate disease (Xiao et al. 2013). Furthermore, composting emits greenhouse gases (GHG), results in the loss of nitrogen that is already present, and necessitates a suitable site with adequate protection from rainfall (Jacobs et al. 2019, Ren et al. 2019). To benefit the environment and take environmentally beneficial actions, it is necessary to find the appropriate conditions for using the energy value of cow dung and crop wastes.

Since 1870, AD has been one of the traditional methods used to treat a variety of wastes, including cow dung (CD) and crop wastes (CW) (LoraGrando et al. 2017). While other developed nations like Germany, the United States of America (USA), and Switzerland are pioneering with biogas plants supplied by anaerobic digestion systems, households living in villages in Asia have been using miniature anaerobic digesters to generate energy for use in cooking and lighting (Parthiba Karthikeyan et al. 2018, Vasco-Correa et al. 2018). As a result, it is vital to highlight the use of AD among the various biomass processes to satisfy the rising demand for energy worldwide (Khalid et al. 2011). The utilization of AD technology to process organic wastes with lower GHG emissions and produce renewable energy is a proven engineering principle (Zhang et al. 2019). Biogas is frequently formed as a result of the anaerobic breakdown of organic waste and other materials by a wide variety of bacterial species in the absence of oxygen (Chuichulcherm et al. 2017).

To maintain the mesophilic condition while enhancing the production of methane (CH<sub>4</sub>) in the solid-state anaerobic co-digestion, cucumber wastes, and dairy manure were added at a feedstock-to-inoculum ratio of 1:1 (Li et al. 2021).

Additionally, Dima et al. (2020) carried out anaerobic co-digestion of sugar beetroot root waste, cow dung, and chicken manure under mesophilic conditions in 30 days HRT, and the greatest output of methane was obtained ranging from 105.32 mL.g<sup>-1</sup> VS to 356.10 mL.g<sup>-1</sup> VS. Furthermore, the anaerobic digestion of rice straw in a reactor with a capacity of 300,000 liters resulted in the volumetric biogas of 323,000 liters per ton of dry rice straw (Zhou et al. 2017). Aside from lighting and cooking, manufactured biogas may also be used as gasoline for internal combustion engines and as a source of heat or power through the use of boilers and generators, among other things (Kadam & Panwar 2017). The biogas produced by anaerobic digestion contains a variety of different elements, depending on the type of organic wastes used as feedstock, with the majority being from 50 to 75% methane (CH<sub>4</sub>), 25 to 50% carbon dioxide (CO<sub>2</sub>), and other gases like 0 to 3% hydrogen sulfide (H<sub>2</sub>S), 0 to 2% oxygen (O<sub>2</sub>), 0 to 1% hydrogen (H), and 0 to 10% nitrogen (N<sub>2</sub>) (Fagbenle & Olukanni 2022, Oladejo et al. 2020).

It has been shown that anaerobic co-digestion of biodegradable waste, such as crop wastes and cow dung, is an effective technique that might increase the production of biogas by over 80% (Braun et al. 2003). Because they contain a variety of nutrients, including the nitrogen that methanogens need, as well as a significant amount of buffering capacity, cow dung and other livestock manures are considered to be potential co-substrates (Moral et al. 2008). Anaerobic co-digestion provides the perfect environment for digestion by resolving a variety of practical difficulties such as pH, inhibition, carbon-to-nitrogen ratio (C: N) limits, substrate breakdown, and moisture content (MC) (Alkaya & Demirer 2011, Xu et al. 2018). Moreover, the ratios of CW and CD to be mixed, the makeup of the feedstocks to be blended, and the presence of low inert organic matter are additional key factors for the beneficial outcomes of anaerobic co-digestion (Almomani & Bhosale 2020). The purpose of this study was to investigate the anaerobic co-digestion of cow dung, cassava peels, and palm oil sludge to produce biogas while utilizing ground eggshells to maintain the pH and a specially-made reactor housed in a greenhouse to regulate the temperature.

## MATERIALS AND METHODS

### Description of the Anaerobic Bio-digester

As shown in Fig. 1, the 225L Polyethylene (PE) digester served as a single-stage anaerobic bio-digester for thirty days, during which sludge was retained. The design included one inlet (1) for loading feedstock and three outlets: the top outlet, the center outlet, and the bottom outlet. The first outlet

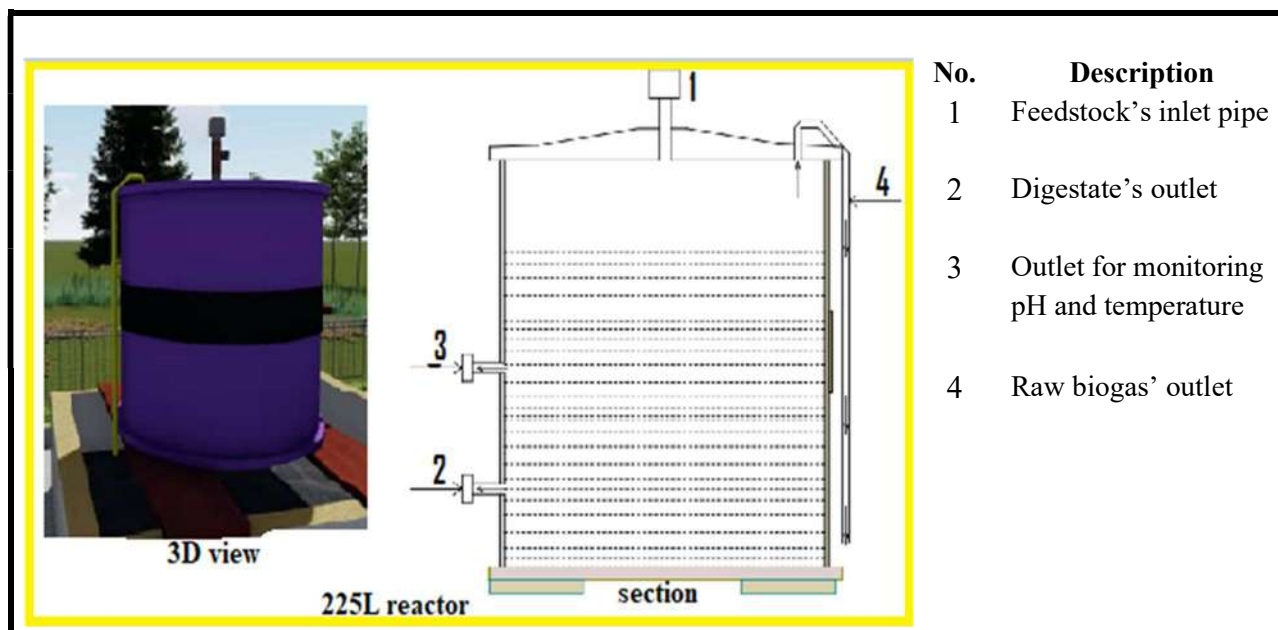


Fig. 1: The anaerobic bio-digesters schematic diagram.

(4) was connected to a gas pipe to collect the digester's raw biogas; the second outlet assisted (3) with daily monitoring by providing a location to collect slurry samples to determine pH and temperature; and the third outlet (2) was utilized to discharge the digestate once the digestion process was finished.

### Substrates and Inoculum

Crop wastes, including cassava peels and palm oil sludge produced during the pressing of palm tree fruits to produce palm oil, were used as substrates. This experiment used cow dung from an abattoir in Ota, Ogun State, Nigeria, as the inoculum. Cassava peels were collected in Owode, Ogun State, while palm oil sludge was acquired from a mill at Covenant University in Canaanland, Ogun State, Nigeria. Before and following the anaerobic digestion (AD) procedure, samples of the substrates and inoculum were collected and examined, and their compositions were determined.

### Methods of Analysis and Optimization of Process-Affecting Variables

15 kg of cassava peels and 15 kg of palm oil sludge were thoroughly combined in a weight-based ratio of 1:1. As an inoculum, 30 kg of cow dung was added to the substrate mixture in a weight-based ratio of 1:2. After that, the mixture of substrates and inoculum was combined with the freshwater volume of 80 liters. This created the ideal ratio of 1:1:2:5.3 for the corresponding amounts of cassava peels, palm oil

sludge, cow dung, and water. 1.3 kg of ground eggshell was added to the slurry to regulate the pH value since they stop affecting the anaerobic digestion process when the pH value reaches 6.8, which is within the permitted range of 6.5 to 8.5 (Jain et al. 2015, Kumar & Samadder 2020). The physiochemical parameters including carbohydrates, proteins, lipids, total solids (TS), volatile solids (VS), total carbon (TC), total nitrogen (TN), total phosphorus (TP), total potassium (TK), volatile fatty acids (VFAs) of sludge before and after digestion were measured using AOAC 931.02, AOAC 930.25, AOAC 922.06, APHA 4500-1, APHA 4500-1, ASTM D5907-04, AOAC 930.25, Spectrophotometry, AOAC 977.29, and IS 548:2010 respectively (Pramanik et al. 2019). The substrate sludge was manually mixed during the digestion phase, and a multimeter (HI 9813-5) was used to measure the pH and temperature of the slurry every day. The mesophilic state, which is between 30°C and 45°C (Zhang et al. 2017), was maintained as the optimal temperature for the anaerobic digestion process at about 34.76°C. To maintain this interior temperature range, the anaerobic bio-digester was erected in a greenhouse made of clear plastic sheets, as illustrated in Fig. 2.

### Biogas Collection and its Purification Strategy

Fig. 3 illustrates the method used to collect and store the raw biogas produced during the anaerobic digestion phase using 175/65 R14 tire tubes.

Methane (CH<sub>4</sub>), carbon dioxide (CO<sub>2</sub>), and hydrogen sulfide (H<sub>2</sub>S) concentrations in the collected biogas were



Fig. 2: Greenhouse for raising an anaerobic bio-digester.



Fig. 3: Biogas-filled 175/65 R14 tyre tube.

measured both before and after the purification procedure using the biogas analyzer (GFM Series). The quantity of these components was measured and compared to limits provided in the literature to provide recommendations for the usage of such biogas in daily life.

The purification protocol that was used to extract biogas with greater methane concentrations used the coupled adsorption and absorption technique (Zhang et al. 2019). Powdered activated carbon and calcium hydroxide were the materials utilized in the experiment because of how



reasonably priced they were. Calcium hydroxide was ground into a powder to increase the surface area. The calcium hydroxide was mixed with water, resulting in the formation of an aqueous solution of the substance. The initial calcium hydroxide flask was put to use in the process of extracting CO<sub>2</sub> from the raw biogas. To get rid of the H<sub>2</sub>S, the biogas from the first flask was transferred into the second one using a connecting hose that contained powdered activated carbon.

## RESULTS AND DISCUSSION

### Physical and Chemical Characteristics of the Mixture of Substrates and Inoculum

The undigested and digested slurry was used to ascertain the physicochemical properties of the combined mixture of substrates and inoculum used for this experiment. The laboratory test findings, which were obtained at a temperature of 25°C and a humidity of 51%, explain the contents of the sludge before and after the anaerobic digestion process.

**Carbohydrates, fat and protein:** Large amounts of proteins and carbohydrates in the sludge may make it possible for more biogas to be produced during anaerobic digestion (Xu et al. 2018). Proteins and carbohydrates break down during the hydrolysis phase of digestion more quickly than lipids. Before digestion, the amount of carbohydrates in the sludge was higher than the amount of protein and fat, which

helped to produce biogas. As shown in Fig. 4, hydrolysis, which lowered the quantity of the three macronutrients; carbohydrates, proteins, and lipids into smaller, more soluble molecules known as monomers, resulted in an average reduction of the three macronutrients by 45% after thirty (30) days of anaerobic digestion. As reported by Lohani (2020), this decrease in their contents shows that anaerobic co-digestion with eggshell added to control pH stabilized the digestion process inside the reactor and improved the biogas production due to the mixed feedstock’s diverse composition.

**Total solids (TS) and volatile solids (VS):** After thirty days of anaerobic sludge retention time, there was a 25% reduction in the concentration of total solids (TS). Due to their ability to remove volatile solids (VS), which lowers the cost of pre-treating and dewatering digestate, the reactor’s dry digestion phase with a considerable quantity of biogas generation is made possible by the percentage drop in total solids to 14.25% (Yi et al. 2014). The mixture of substrates and inoculum exhibited higher amounts of organic matter before and after digestion, as evidenced by the volatile solids (VS) content, with VS/TS ratios of 91.09% and 91.02%, respectively, as shown in Fig. 5. In the single-stage anaerobic bio-digester used in this research, biogas with increased methane (CH<sub>4</sub>) concentration is produced due to quick stabilization during digestion when volatile solids (VS) are reduced during the anaerobic digestion process. The amount

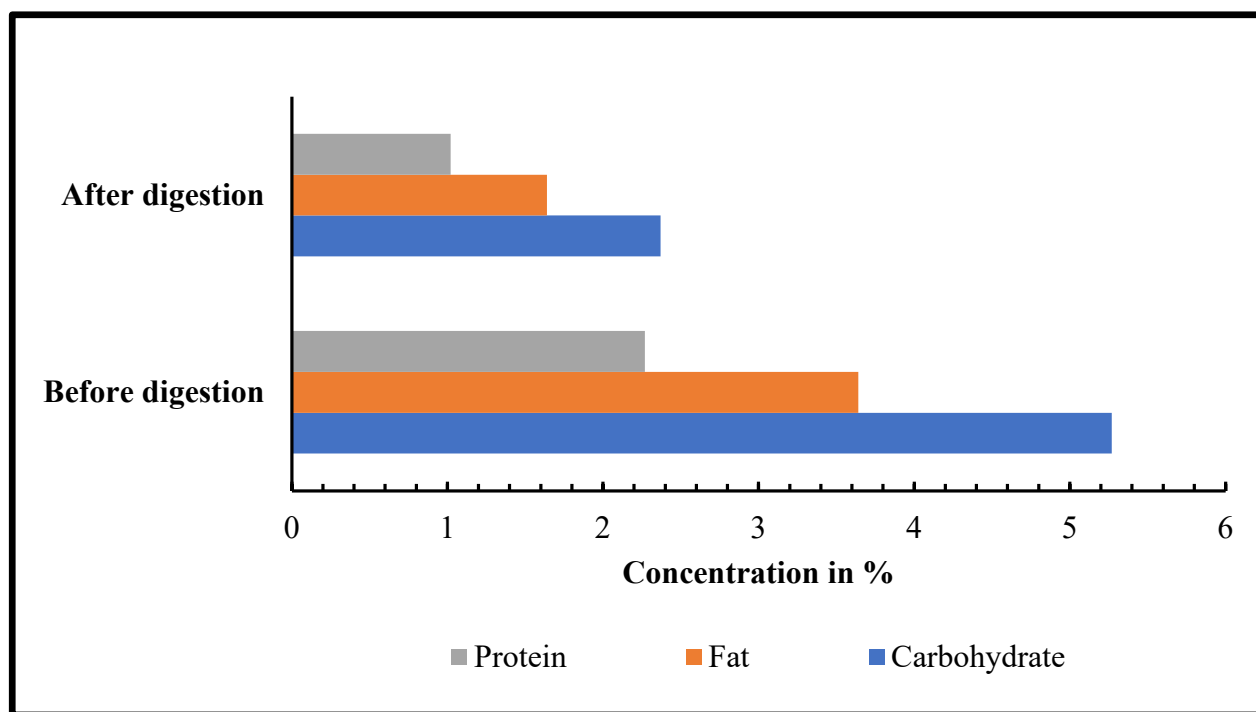


Fig. 4: Concentrations of carbohydrate, fat, and protein in slurry.

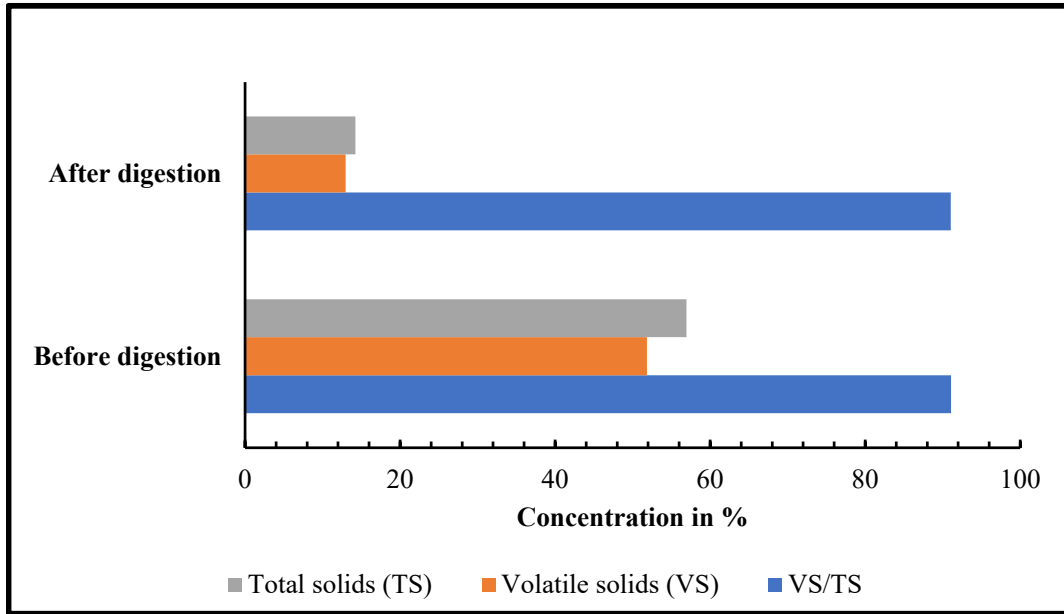


Fig. 5: Variation in the contents of total solids (TS) and volatile solids (VS).

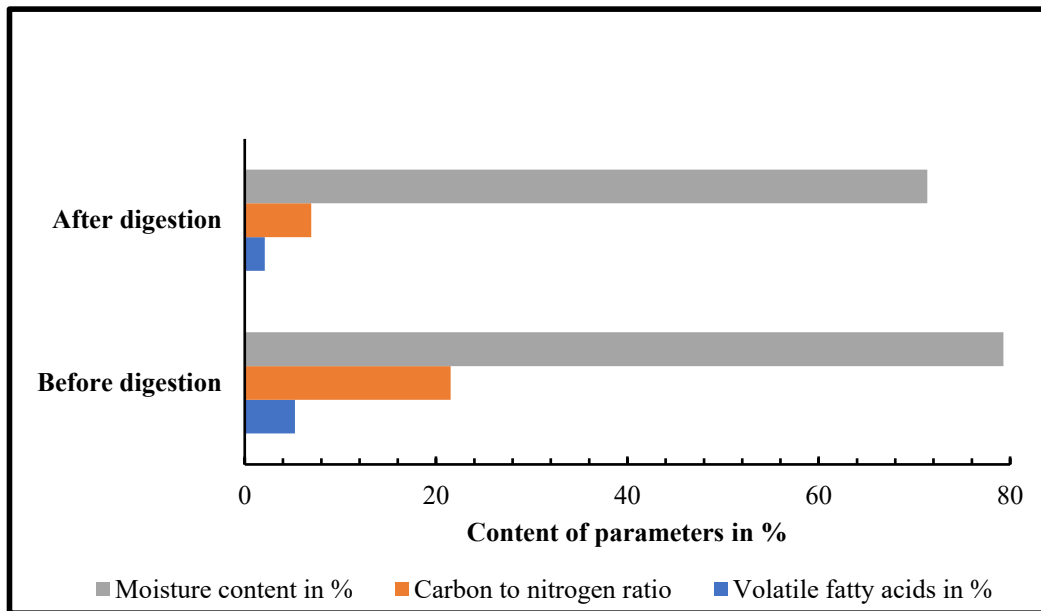


Fig. 6: Variation of volatile fatty acids (VFA), moisture content (MC), and carbon to nitrogen ratio (C:N) in the slurry.

of volatile solids (VS) in the slurry was reduced by 25% after 30 days of anaerobic digestion, with hydraulic retention time (HRT) being the deciding factor.

**Volatile fatty acids (VFAs), moisture content (MC), and carbon-to-nitrogen ratio (C:N):** Proteins in substrates degrade because the pH of slurry rises when the level of ammonia does, and it decreases when the amount of

volatile fatty acids (VFA) increases (Kumar & Samadder, 2020). Volatile fatty acid (VFA) concentration dropped by 40% after digestion took thirty (30) days, which helped to maintain the pH to an average of 6.0 and sped up the breakdown procedure. As advised by Zhang et al. (2019), before digestion, the sludge's carbon to nitrogen (C:N) ratio was 21.53, which is in the range between 20 and 30. This

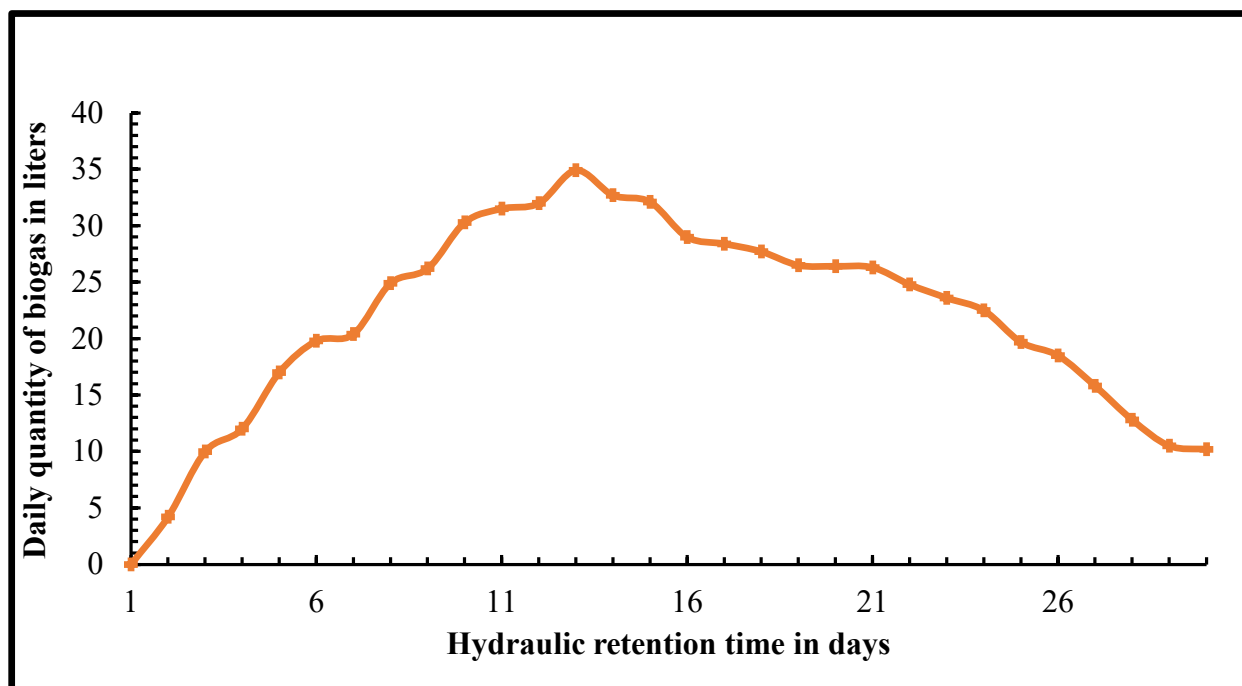


Fig. 7: Daily production of biogas from the anaerobic digester.

C:N ratio measurement demonstrated that the digestion method used to produce biogas was successful. Following the digestion process, the total carbon content decreased, and the C:N ratio subsequently exceeded the permissible threshold. In addition, the moisture level of 79.29%, as in Fig. 6, showed that there was room for microorganisms to move around freely and develop during the digestive process.

### Generation of Biogas

The anaerobic co-digestion of cow dung, cassava peels, and palm oil sludge in this investigation resulted in a total of 650.6 liters of biogas from a 225L bio-digester, which is about 138% of the projected capacity in the design. More lignin content in palm oil sludge, which had a negative biogas contribution of roughly 34.24 percent, was a major factor in the inability to fulfill the predicted biogas for partial satisfaction of a single household. According to Fagbenle and Olukanni (2022), more biogas was produced through anaerobic co-digestion using cassava peels and cow dung as inoculum, both of which have high hemicellulose and low lignin concentrations. By successfully adjusting the pH using eggshells and the temperature to the mesophilic range using a greenhouse, a favorable habitat was established for the microorganisms that reacted with the sludge, increasing the production of biogas. According to Fig. 7, the maximum volume of biogas produced at the 13<sup>th</sup> day of retention time was 34.90 liters while that generated at the 20<sup>th</sup> day was 26.40 liters.

Fig. 8 shows the total volume of biogas generated by anaerobic digestion over the course of the hydraulic retention time, which was 30 days. The 225L PE digester used for the anaerobic co-digestion process started producing biogas in detectable levels on day two, at 4.20 liters. On day three, the biogas produced increased to 10.0 liters, and on day four, that amount grew to 12.0 liters. It was evident that the biogas generation had improved up to the 13<sup>th</sup> day of anaerobic digestion due to the favorable conditions for microorganisms generated by adding eggshells and a greenhouse for pH and temperature management, respectively. As in a comparable investigation carried out by Fagbenle & Olukanni (2022), the biogas was not created on the first day. The anaerobic co-digestion of cassava peels, palm oil sludge, and cow dung required a longer start-up time because of the oily content of palm oil sludge, which was also discovered by Aziz et al. (2020). The reactor's anaerobic digestion for 20 days of sludge retention revealed the best time that can be employed in batch digestion systems because the data indicate that biogas output started to decrease more after the 20<sup>th</sup> day.

### pH Optimization and Biogas Generation

The pH value, which can be acidic when below 7.0 or alkaline when over 7.0, might affect how well the anaerobic digestion process works. The high acidity of the cassava peels and the palm oil sludge, both of which are similarly depicted by Fagbenle & Olukanni (2022), led to the sludge's

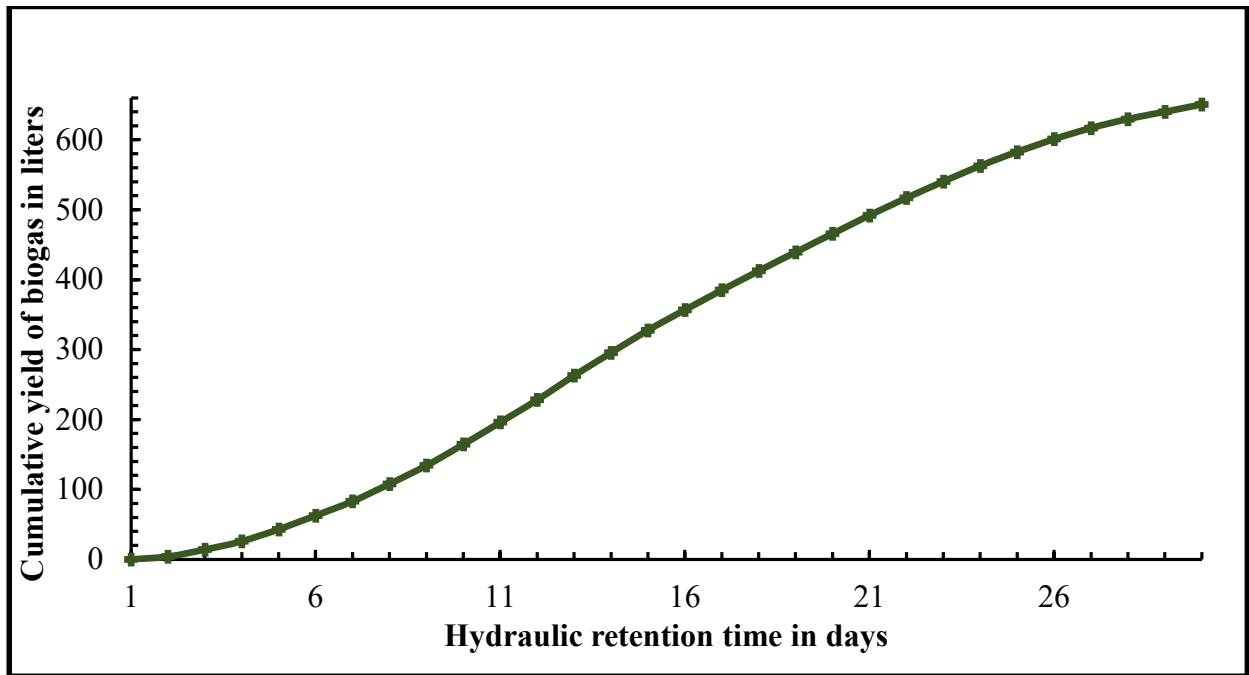


Fig. 8: Cumulative generation of biogas from the anaerobic digester.

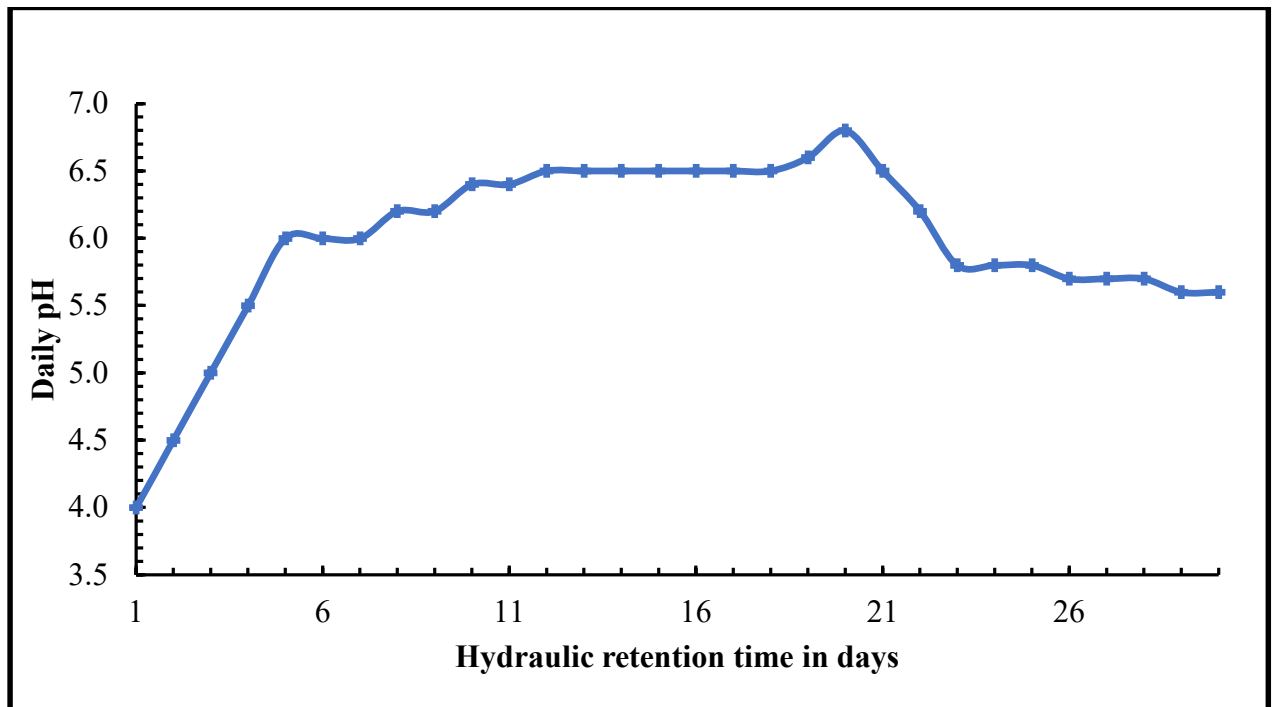


Fig. 9: Daily pH fluctuations.

pH value being high before digestion, as seen in Fig. 9. An average pH of 6.0 was found for the digestion period, which is within the range that is ideal for increased biogas

since the microbial population may thrive in a hospitable environment, according to Zhang et al. (2019). The addition of green buffer material comprised of ground eggshells on

the fifth day caused the pH value to begin rising toward the neutral range. On the thirteenth day, the digester system's biogas production reached its peak, with a pH value of 6.5 (within the ideal range of 6 and 8). The pH was able to be stabilized by the eggshells used as a buffer up to a value of 6.8, after which it returned to the acidic range and stayed there until the 30<sup>th</sup> day of the anaerobic digestion process when it reached a value of 5.6.

### Temperature Optimization and Generation of Biogas

The anaerobic co-digestion process was carried out inside a greenhouse that had been built to regulate the temperature. Daily measurements were made for the ambient, greenhouse, and slurry temperatures. An average slurry temperature of 34.76°C was found for the hydraulic retention period of 30 days, which is within the mesophilic range of between 30°C and 45°C, according to Zhang et al. (2019). While the surrounding air temperature was 28.18°C, the anaerobic digester's temperature was measured to have a mean of 33.58°C, which still fell within the mesophilic range. According to Oladejo et al. (2020), at mesophilic temperatures, anaerobic microorganisms function well to facilitate a mean catalytic efficiency of enzymes, enhancing

the generation of biogas by stabilizing the AD process. The use of a greenhouse as a mesophilic refuge for an anaerobic digester has proven to be effective. The greenhouse that was built for the privacy of the digester during the anaerobic co-digestion process ensured the safety of the reactor against strong winds, heavy rain, and destructive objects. When the slurry temperature reached 35.83°C, which is ideal for mesophilic conditions, while it was 35.33°C in the greenhouse, 34.90 liters of biogas were produced at their highest rate. Fig. 10 depicts the average daily temperature for the ambient air, the greenhouse, and the reactor's slurry, respectively.

### Components in Generated Biogas

As shown in Fig. 11, the amount of methane (CH<sub>4</sub>), carbon dioxide (CO<sub>2</sub>), and hydrogen sulfide (H<sub>2</sub>S) in a sample of biogas produced by the reactor was measured after being collected and analyzed every ten days during the digestion period. The biogas is more combustible when there is more methane in it. The biogas produced in the first ten days had percentage concentrations of CH<sub>4</sub>, CO<sub>2</sub>, and H<sub>2</sub>S that were out of the range recommended by Oladejo et al. (2020): 45.5, 51.5, and 3.5, respectively. As also observed by Oladejo et

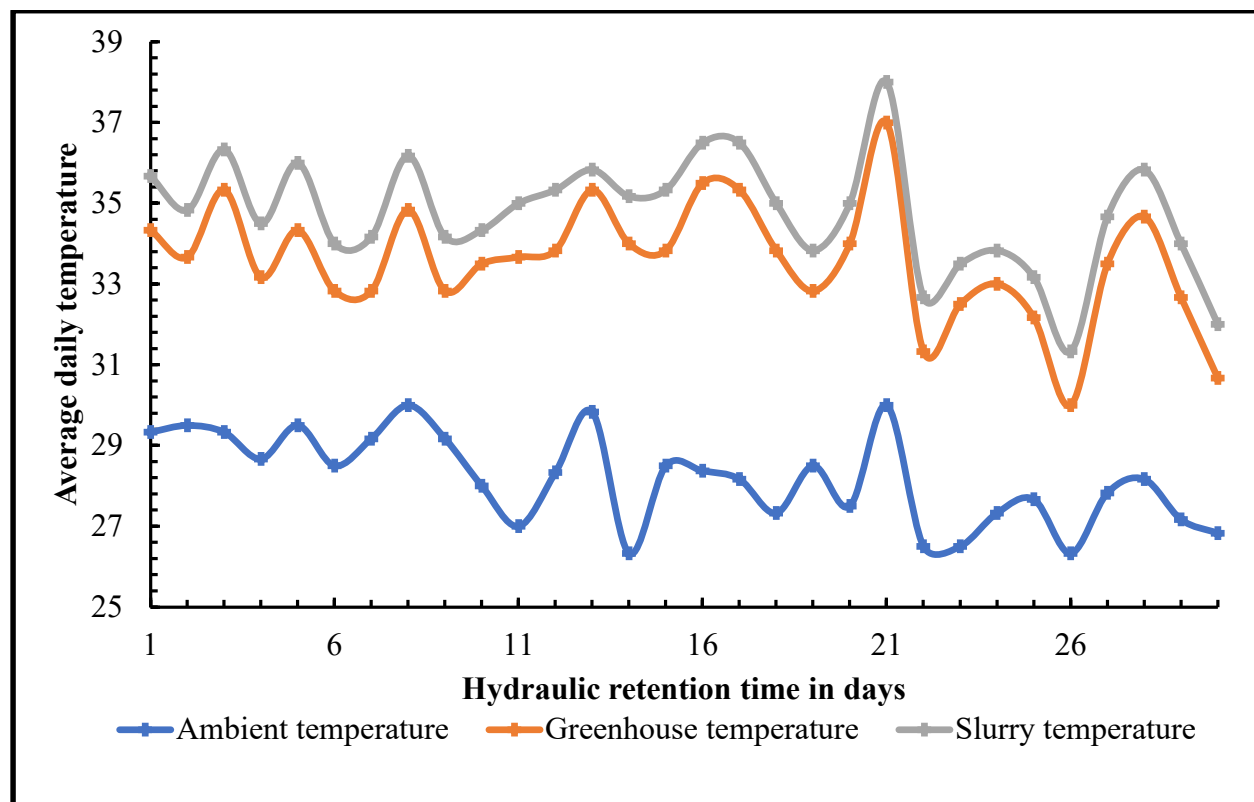


Fig. 10: Average daily ambient, greenhouse, and slurry temperatures.

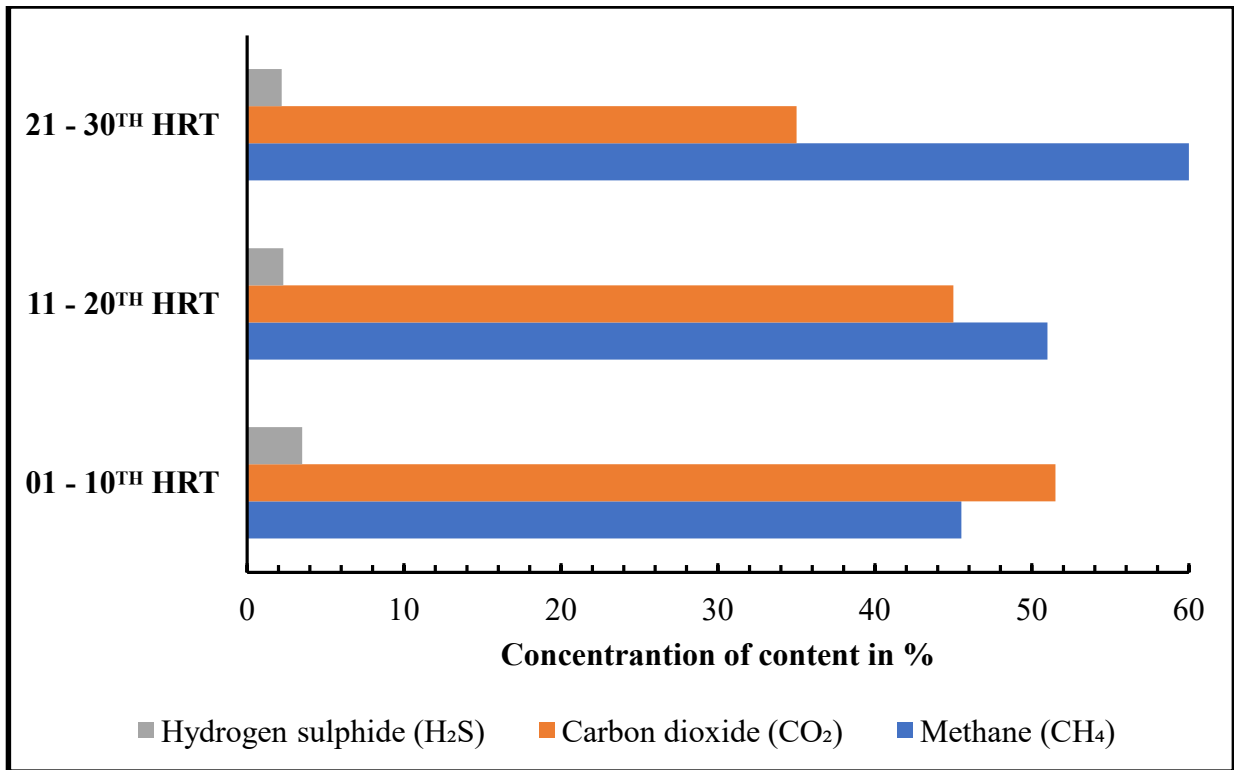


Fig. 11: Contents of the generated biogas

al. (2020), the concentration of methane (CH<sub>4</sub>) grew to 51% in the second ten days, which is between 50% and 75%. The concentrations of CO<sub>2</sub> and H<sub>2</sub>S reduced to 35% and 2.2%, respectively, over the third 10 days of the anaerobic co-digestion process, whereas CH<sub>4</sub> content increased to 60%. The amount of methane (CH<sub>4</sub>) found through testing in laboratories from hydraulic retention durations of 20 days to 30 days showed that the biogas is combustible when it catches fire and can be utilized for cooking and lighting in homes.

### Purification of Biogas

The removal of pollutants, including carbon dioxide (CO<sub>2</sub>) and hydrogen sulfide (H<sub>2</sub>S), was undertaken to produce biogas high in methane (CH<sub>4</sub>). An efficiency of around 92% was achieved in removing CO<sub>2</sub> contamination, which was higher than other contaminants from the biogas produced. This elimination efficiency was also noted in the research mentioned by Fagbenle & Olukanni (2022). After 240 minutes of the absorption process, employing an aqueous solution of calcium hydroxide (Ca(OH)<sub>2</sub>), the CO<sub>2</sub> extracted from the created biogas was finally stripped into liquid condition. As shown in Fig. 12, there was only a very tiny variation in the amount of CO<sub>2</sub> that had been lowered

between 180 minutes and 240 minutes, with the difference being less than or equal to 4.7%.

However, it was discovered that the efficacy of the reduction in hydrogen sulfide (H<sub>2</sub>S) concentration was around 85%. For biogas to be used in engine combustion, Fagbenle & Olukanni (2022) states that the H<sub>2</sub>S concentration in the gas cannot be more than 0.5%. As demonstrated in Fig. 13, after a single-phase treatment with activated carbon for 240 minutes, the amount of H<sub>2</sub>S in the produced biogas was reduced to 0.39 percent, making it appropriate for engine combustion. According to Oladejo et al. (2020), the final output of treated biogas has a concentration of less than 3%, which permits the storage of purified biogas in storage tanks without producing corrosion for household uses like cooking and lighting.

### CONCLUSION

The findings of this study demonstrate that the anaerobic co-digestion of ground eggshells, cow manure, cassava peels, and palm oil sludge is a feasible and environmentally beneficial approach for obtaining energy in the form of biogas. A pH level that is within the range advised for the anaerobic digestion process was maintained in the mixture of

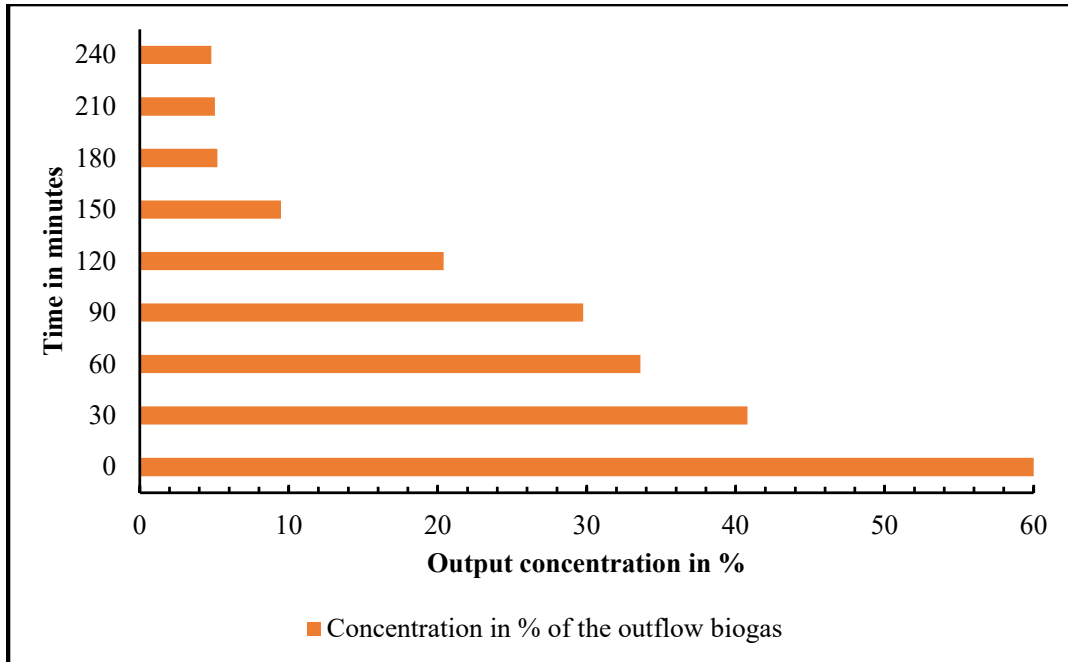


Fig. 12: Concentration of output biogas during CO<sub>2</sub> removal.

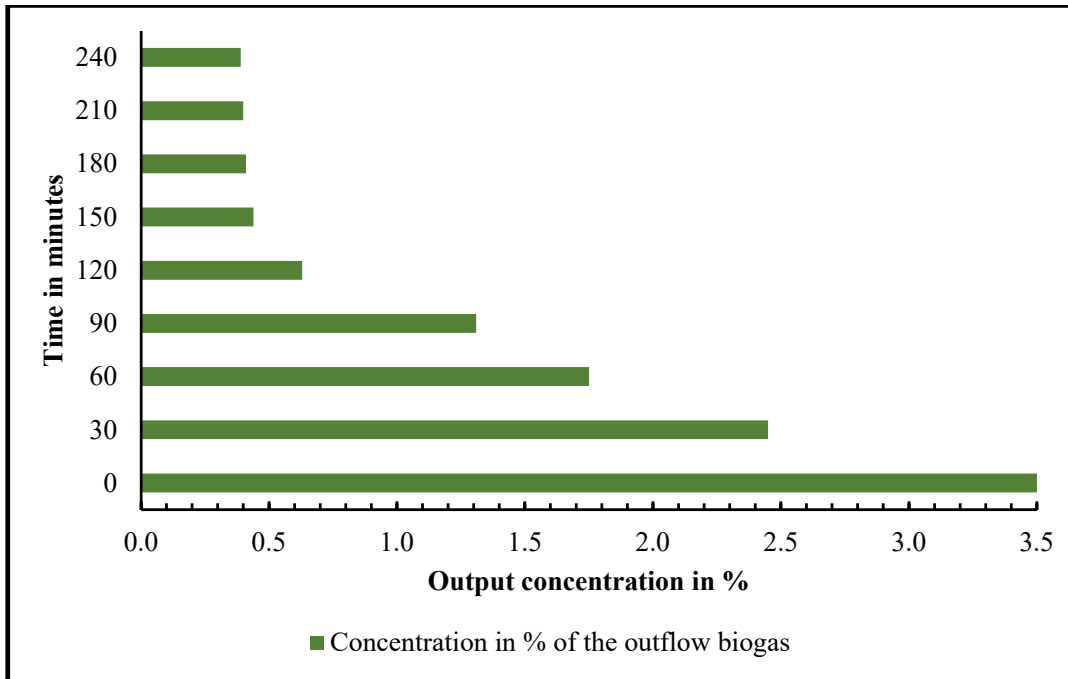


Fig. 13: Concentration of output biogas during H<sub>2</sub>S removal.

substrates and inoculum with powdered eggshells added as a buffer material. The use of greenhouses to adjust temperature has shown to be a viable method for maintaining mesophilic conditions during anaerobic co-digestion for increased biogas

production. The 225L digester used for the anaerobic co-digestion process produced 650.60L of cumulative biogas for the 30-day sludge retention period. From the biogas produced on days over 20 HRT, the greatest methane

concentration of 60% was found, while on days under 10 HRT, the lowest methane content of 45.5%. On the 13<sup>th</sup> day of anaerobic digestion, the production of biogas reached its peak at 34.90L, while pH and temperature were kept at optimal levels for a healthy anaerobic digestion process with 6.5 and 35.83°C, respectively, on that same day. With an efficiency of 92% and 85% for the removal of CO<sub>2</sub> and H<sub>2</sub>S, respectively, the purification strategy using combined absorption and adsorption has shown to be a successful way of treating biogas produced in 20 days or more of hydraulic retention time. Future research should focus on the discovery and development of more effective, less expensive microbial agents, such as enzymes for biological pre-treatment and more environmentally friendly chemical solvents for chemical pre-treatment of palm oil sludge, to reduce a significant amount of lignin that has a negative impact on biogas generation.

## ACKNOWLEDGEMENT

The authors would like to express their gratitude to the administration of Covenant University and the Project Supervision Board of the African Sustainable Infrastructure Mobility (ASIM) Scholarship for providing the funding and resources required for this research.

## REFERENCES

- Alkaya, E. and Demirel, G.N., 2011. Anaerobic mesophilic co-digestion of sugar-beet processing wastewater and beet-pulp in batch reactors. *Renewable Energy*, 36(3), pp.971-975. <https://doi.org/10.1016/j.renene.2010.08.040>
- Almomani, F. and Bhosale, R.R., 2020. Enhancing the production of biogas through anaerobic co-digestion of agricultural waste and chemical pre-treatments. *Chemosphere*, 255, p.126805. <https://doi.org/10.1016/j.chemosphere.2020.126805>
- Almomani, F., Bhosale, R.R., Khraisheh, M.A.M. and Shawaqfeh, M., 2019. Enhancement of biogas production from agricultural wastes via pre-treatment with advanced oxidation processes. *Fuel*, 253, pp.964-974. <https://doi.org/10.1016/j.fuel.2019.05.057>
- Almomani, F., Shawaqfeh, M., Bhosale, R.R., Kumar, A. and Khraisheh, M.A.M., 2017. Intermediate ozonation to enhance biogas production in batch and continuous systems using animal dung and agricultural waste. *International Biodeterioration & Biodegradation*, 119, pp.176-187. <https://doi.org/10.1016/j.ibiod.2016.11.008>
- Anh, N.M., Cheng, W., Yu, C. and Yuen, T., 2022. Universal anaerobic digester for biogas production in rural communities. 44.
- Araji, A.A., Abdo, Z.O. and Joyce, P., 2001. Efficient use of animal manure on cropland—economic analysis. *Bioresource Technology*, 79(2), pp.179-191. [https://doi.org/10.1016/S0960-8524\(01\)00042-6](https://doi.org/10.1016/S0960-8524(01)00042-6)
- Aziz, A., Md Maniruzzaman, Kassim, K.A., ElSergany, M., Anuar, S., Jorat, M. E., Yaacob, H., Ahsan, A., Imteaz, M. A. and Arifuzzaman, 2020. Recent advances in palm oil mill effluent (POME) pretreatment and anaerobic reactor for sustainable biogas production. *Renewable and Sustainable Energy Reviews*, 119, p.109603. <https://doi.org/10.1016/j.rser.2019.109603>
- Braun, R., Brachtel, E. and Grasmug, M., 2003. Codigestion of proteinaceous industrial waste. *Applied Biochemistry and Biotechnology*, 109(1), pp.139-153. <https://doi.org/10.1385/ABAB:109:1-3:139>
- Chuichulcherm, S., Kasichan, N., Srinophakun, P., Saisriyoot, M. and Thanapimmetha, A., 2017. The use of ozone in a continuous cyclical swing mode regeneration of Fe-EDTA for a clean biogas process from a swine farm waste. *Journal of Cleaner Production*, 142, pp.1267-1273. <https://doi.org/10.1016/j.jclepro.2016.06.181>
- De Clercq, D., Wen, Z., Gottfried, O., Schmidt, F. and Fei, F., 2017. A review of global strategies promoting the conversion of food waste to bioenergy via anaerobic digestion. *Renewable and Sustainable Energy Reviews*, 79, pp.204-221. <https://doi.org/10.1016/j.rser.2017.05.047>
- Demirel, G. N. and Chen, S., 2004. Effect of retention time and organic loading rate on anaerobic acidification and biogasification of dairy manure. *Journal of Chemical Technology & Biotechnology*. <https://onlinelibrary.wiley.com/doi/abs/10.1002/jctb.1138>
- Dima, A.D., Părvulescu, O.C., Mateescu, C. and Dobre, T., 2020. Optimization of substrate composition in anaerobic co-digestion of agricultural waste using central composite design. *Biomass and Bioenergy*, 138, p.105602. <https://doi.org/10.1016/j.biombioe.2020.105602>
- Fagbenle, E.O. and Olukanni, D.O., 2022. Production and purification of biogas from cassava peel using cow dung as inoculum. *IOP Conference Series: Earth and Environmental Science*, 993(1), p.012012. <https://doi.org/10.1088/1755-1315/993/1/012012>
- Giwa, A., Alabi, A., Yusuf, A. and Olukan, T., 2017. A comprehensive review on biomass and solar energy for sustainable energy generation in Nigeria. *Renewable and Sustainable Energy Reviews*, 69, pp.620-641. <https://doi.org/10.1016/j.rser.2016.11.160>
- Guerra-Rodriguez, E., Diaz-Raviña, M. and Vázquez, M., 2001. Co-composting of chestnut burr and leaf litter with solid poultry manure. *Bioresource Technology*, 78(1), pp.107-109. [https://doi.org/10.1016/S0960-8524\(00\)00159-0](https://doi.org/10.1016/S0960-8524(00)00159-0)
- Jacobs, K., Wind, L., Krometis, L.A., Hession, W.C. and Pruden, A., 2019. Fecal Indicator Bacteria and Antibiotic Resistance Genes in Storm Runoff from Dairy Manure and Compost-Amended Vegetable Plots. *Journal of Environmental Quality*. <https://access.onlinelibrary.wiley.com/doi/abs/10.2134/jeq2018.12.0441>
- Jain, S., Jain, S., Wolf, I.T., Lee, J. and Tong, Y.W., 2015. A comprehensive review on operating parameters and different pretreatment methodologies for anaerobic digestion of municipal solid waste. *Renewable and Sustainable Energy Reviews*, 52, pp.142-154. <https://doi.org/10.1016/j.rser.2015.07.091>
- Kadam, R. and Panwar, N.L., 2017. Recent advancement in biogas enrichment and its applications. *Renewable and Sustainable Energy Reviews*, 73, pp.892-903. <https://doi.org/10.1016/j.rser.2017.01.167>
- Khalid, A., Arshad, M., Anjum, M., Mahmood, T. and Dawson, L., 2011. The anaerobic digestion of solid organic waste. *Waste Management*, 31(8), pp.1737-1744. <https://doi.org/10.1016/j.wasman.2011.03.021>
- Kumar, A. and Samadder, S.R., 2020. Performance evaluation of anaerobic digestion technology for energy recovery from organic fraction of municipal solid waste: A review. *Energy*, 197, p.117253. <https://doi.org/10.1016/j.energy.2020.117253>
- Li, Y., Qi, C., Zhang, Y., Li, Y., Wang, Y., Li, G. and Luo, W., 2021. Anaerobic digestion of agricultural wastes from liquid to solid state: Performance and environ-economic comparison. *Bioresource Technology*, 332, p.125080. <https://doi.org/10.1016/j.biortech.2021.125080>
- Lohani, S.P., 2020. Anaerobic co-digestion of food waste, goat and chicken manure for sustainable biogas production. *International Journal of Energy Applications and Technologies*, 7(4), pp.120-125. <https://doi.org/10.31593/ijeat.748982>
- Lora Grando, R., de Souza Antune, A.M., da Fonseca, F.V., Sánchez, A., Barrera, R. and Font, X., 2017. Technology overview of biogas production in anaerobic digestion plants: A European evaluation of research and development. *Renewable and Sustainable Energy Reviews*, 80, pp.44-53. <https://doi.org/10.1016/j.rser.2017.05.079>



- Moral, R., Perez-Murcia, M. D., Perez-Espinosa, A., Moreno-Caselles, J., Paredes, C. and Rufete, B., 2008. Salinity, organic content, micronutrients and heavy metals in pig slurries from South-eastern Spain. *Waste Management*, 28(2), pp.367-371. <https://doi.org/10.1016/j.wasman.2007.01.009>
- Nwafor, J., 2021. How to clean cooking helps the climate. *BBC*. Available at <https://www.bbc.com/future/article/20211103-nigeria-how-clean-cooking-helps-the-climate>
- Oladejo, O.S., Dahunsi, S.O., Adesulu-Dahunsi, A.T., Ojo, S.O., Lawal, A.I., Idowu, E.O., Olanipekun, A.A., Ibikunle, R.A., Osueke, C.O., Ajayi, O.E., Osueke, N. and Egbuomwan, I., 2020. Energy generation from anaerobic co-digestion of food waste, cow dung and piggery dung. *Bioresource Technology*, 313, p.123694. <https://doi.org/10.1016/j.biortech.2020.123694>
- Olukanni, D. and Olatunji, T., 2018. Cassava Waste Management and Biogas Generation Potential in Selected Local Government Areas in Ogun State, Nigeria. *Recycling*, 3(4), p.58. <https://doi.org/10.3390/recycling3040058>
- Olukanni, D., Aipoh, A. and Kalabo, I., 2018. Recycling and Reuse Technology: Waste to Wealth Initiative in a Private Tertiary Institution, Nigeria. *Recycling*, 3(3), p.44. <https://doi.org/10.3390/recycling3030044>
- Omilani, O., Abass, A.B. and Okoruwa, V.O., 2019. Smallholder Agroprocessors' Willingness to Pay for Value-Added Solid-Waste Management Solutions. *Sustainability*, 11(6), p.6. <https://doi.org/10.3390/su11061759>
- Parthiba Karthikeyan, O., Trably, E., Mehariya, S., Bernet, N., Wong, J.W.C. and Carrere, H., 2018. Pretreatment of food waste for methane and hydrogen recovery: A review. *Bioresource Technology*, 249, pp.1025-1039. <https://doi.org/10.1016/j.biortech.2017.09.105>
- Pramanik, S.K., Suja, F.B., Zain, S.M. and Pramanik, B.K., 2019. The anaerobic digestion process of biogas production from food waste: Prospects and constraints. *Bioresource Technology Reports*, 8, p.100310. <https://doi.org/10.1016/j.biteb.2019.100310>
- Ren, X., Wang, Q., Awasthi, M.K., Zhao, J., Wang, J., Liu, T., Li, R. and Zhang, Z., 2019. Improvement of cleaner composting production by adding Diatomite: From the nitrogen conservation and greenhouse gas emission. *Bioresource Technology*, 286, p.121377. <https://doi.org/10.1016/j.biortech.2019.121377>
- Slorach, P.C., Jeswani, H.K., Cuéllar-Franca, R. and Azapagic, A., 2019. Environmental sustainability of anaerobic digestion of household food waste. *Journal of Environmental Management*, 236, pp.798-814. <https://doi.org/10.1016/j.jenvman.2019.02.001>
- US EPA, 2013. Wood Smoke and Your Health [Overviews and Factsheets]. Available at <https://www.epa.gov/burnwise/wood-smoke-and-your-health>
- Vasco-Correa, J., Khanal, S., Manandhar, A. and Shah, A., 2018. Anaerobic digestion for bioenergy production: Global status, environmental and techno-economic implications, and government policies. *Bioresource Technology*, 247, pp.1015-1026. <https://doi.org/10.1016/j.biortech.2017.09.004>
- Xiao, R.F., Zhu, Y.-J., Li, Y.-D. and Liu, B., 2013. Studies on Vascular Infection of *Fusarium oxysporum* f. sp. *cubense* Race 4 in Banana by Field Survey and Green Fluorescent Protein Reporter. *International Journal of Phytopathology*. Available at: <https://esciencepress.net/journals/index.php/phytopath/article/view/64>
- Xu, F., Li, Y., Ge, X., Yang, L. and Li, Y., 2018. Anaerobic digestion of food waste – Challenges and opportunities. *Bioresource Technology*, 247, pp.1047-1058. <https://doi.org/10.1016/j.biortech.2017.09.020>
- Yi, J., Dong, B., Jin, J. and Dai, X., 2014. Effect of increasing total solids contents on anaerobic digestion of food waste under mesophilic conditions: Performance and microbial characteristics analysis. *PLOS ONE*, 9(7), p.e102548. <https://doi.org/10.1371/journal.pone.0102548>
- Zhang, J., Loh, K.C., Li, W., Lim, J.W., Dai, Y. and Tong, Y.W., 2017. Three-stage anaerobic digester for food waste. *Applied Energy*, 194, pp.287-295. <https://doi.org/10.1016/j.apenergy.2016.10.116>
- Zhang, L., Loh, K.C. and Zhang, J., 2019. Enhanced biogas production from anaerobic digestion of solid organic wastes: Current status and prospects. *Bioresource Technology Reports*, 5, pp.280-296. <https://doi.org/10.1016/j.biteb.2018.07.005>
- Zhou, J., Yang, J., Yu, Q., Yong, X., Xie, X., Zhang, L., Wei, P. and Jia, H., 2017. Different organic loading rates on the biogas production during the anaerobic digestion of rice straw: A pilot study. *Bioresource Technology*, 244, pp.865-871. <https://doi.org/10.1016/j.biortech.2017.07.146>





# Plant Leaf Disease Detection Using Integrated Color and Texture Features

Jayamala Kumar Patil<sup>†</sup> and Vinay Sampatrao Mandlik

Department of Electronics and Telecommunication Engineering, Bharati Vidyapeeth's College of Engineering, Kolhapur, Maharashtra, India

<sup>†</sup>Corresponding author: Jayamala Kumar Patil; jayamala.p@rediffmail.com

Nat. Env. & Poll. Tech.  
Website: [www.neptjournal.com](http://www.neptjournal.com)

Received: 06-03-2024

Revised: 18-04-2024

Accepted: 03-05-2024

## Key Words:

Plant disease detection  
Content-based image retrieval  
CBIR  
YCbCr histogram  
LGGP histogram  
Advanced image analysis  
Maize leaf rust

## ABSTRACT

In the realm of precision agriculture, a pivotal challenge lies in the detection, identification, and grading of crop diseases. This multifaceted task necessitates the involvement of expert human resources and time-sensitive actions aimed at mitigating the risks of production losses and the rapid spread of diseases. The effectiveness of the majority of developed systems in this domain hinges on the quality of image features and disease segmentation accuracy. This paper presents a comprehensive research endeavor in the domain of Content-Based Image Retrieval (CBIR), specifically tailored to detect and classify leaf diseases. The proposed system integrates both color and texture features to underpin its functionality, providing a robust framework for accurate disease detection. By leveraging advanced image processing techniques, the system enhances the precision of disease identification, which is crucial for timely and effective intervention in agricultural practices. To evaluate the system's performance, maize leaves afflicted by rust and blight serve as prime candidates for testing. These diseases were chosen due to their prevalence and significant impact on crop yield. The experimental results demonstrate that the developed system consistently excels in its disease detection and identification tasks, boasting an impressive efficiency rate of 98.33%. This high level of accuracy underscores the potential of the system to be a valuable tool in precision agriculture, aiding farmers and agricultural experts in maintaining healthy crops and optimizing production. The integration of color and texture features not only improves the detection accuracy but also provides a comprehensive understanding of the disease characteristics. This dual-feature approach ensures that the system can distinguish between different types of diseases with high precision, making it a versatile solution for various agricultural applications. The findings of this research highlight the importance of advanced image analysis techniques in enhancing the capabilities of disease detection systems, paving the way for more efficient and effective agricultural practices.

## INTRODUCTION

Agricultural growth plays a pivotal role in the economies of countries primarily reliant on agro-based industries. The quality and yield of crops are profoundly influenced by factors such as weather patterns and the prevalence of crop diseases. Notably, research by Kannan (2014) underscores the global impact of these diseases. In the context of India, the statistics are no less concerning, with crop loss estimates of 25% in rice and maize. The economic implications of such losses are substantial, with farmers expending millions of dollars annually to combat crop diseases.

The key strategy for enhancing crop yields lies in the early detection of diseases through vigilant crop monitoring and timely interventions. A study by Prasann Kumar (2012) revealed a survey conducted by the International Crops Research Institute indicates that 93% of Indian farmers

heavily depend on pesticides to manage crop diseases and pests, with pesticide application occurring anywhere from 1 to 15 times before harvesting. Unfortunately, this overreliance on pesticides translates into significant losses, ranging from 11% to 40%. Beyond the economic repercussions, the extensive use of pesticides introduces several adverse consequences, including disruptions in the food chain, the potential for secondary pest infestations, heightened human health risks, and the possibility of acute or long-term health issues. Early disease diagnosis not only opens doors to timely remediation but also serves as a fundamental strategy for controlling disease propagation through various trajectories, including time, wind, water, birds, and insects. This approach facilitates the implementation of protective measures, including the application of pesticides, and biological control agents, and the adoption of Integrated Pest Management (IPM) practices.

The process of disease diagnosis in plants is a complex one, typically relying on experts with a profound understanding of plants and their associated diseases. These experts possess the ability to recognize diseases, estimate the extent of damage through visual observation, and recommend suitable treatment options. However, this traditional approach has inherent limitations, marked by subjectivity and relatively low throughput. To address these shortcomings, electronic or computer-based expert systems have emerged as viable alternatives. These systems can encapsulate the knowledge and experience of expert farmers or agricultural advisors, effectively constituting what is termed an “Expert System,” as stated by Patil & Kumar (2017).

Electronic expert systems rely on image pattern recognition and understanding to identify and diagnose plant diseases and pests. Developing precise and sophisticated image pattern algorithms is essential for their accuracy. These systems compare input images of diseased plants with stored images to make informed decisions, similar to how human experts use their knowledge and experience. Content-Based Image Retrieval (CBIR) systems work with the same principles as human experts and hence can be employed in electronic expert systems to analyse image content, such as color, shape, and texture, and quickly retrieve similar images. As a result, electronic expert systems are a successful approach for assisting users in diagnosing plant diseases when their knowledge is limited.

The impetus for this research is drawn from the aforementioned considerations. The current investigation aims to conduct a comprehensive exploration of computer vision and image processing algorithms specifically tailored for disease detection based on the principle of image retrieval. These algorithms will be employed for the analysis of plant leaf images, primarily in color, to identify plant diseases and improve both diagnostic accuracy and throughput.

## RELATED WORK

The realm of plant disease detection has witnessed substantial growth with the adoption of diverse techniques and methodologies that draw from fields such as Image Processing, Artificial Neural Networks (ANN), genetic algorithms, and wireless technology. These technologies have played a pivotal role in the development of systems capable of not only detecting but also classifying plant diseases, thus facilitating expedited disease diagnosis. Several notable research studies have significantly contributed to this area.

Naik et al. (2014) introduced a plant disease diagnosis system. In their research, they utilized pomegranate leaves with foliar disease spots for experimentation. The acquired images underwent resizing and noise reduction through the

application of the Gaussian Low Pass filter. The segmented diseased images using K-means clustering were thresholded to extract Regions of Interest (ROIs), with Haar wavelet used for feature extraction. A Mamdani-type fuzzy classifier was then employed, taking these features as input to classify the disease.

Singh et al. (2015) developed an image-processing-based method for the classification of rice diseases. In their approach, leaf images exhibiting diseased blights were subjected to noise removal through pre-processing. Further processing involved the application of the Wiener filter and adaptive histogram equalization. The use of K-means clustering facilitated image segmentation, while texture features like entropy and standard deviation were extracted. These features were subsequently utilized for classification through a Support Vector Machine (SVM) classifier. The authors acknowledged the potential for enhancing both segmentation and classification by exploring alternative classifiers.

Karmokar et al. (2015) developed a neural network-based approach for the recognition of diseases in tea leaves. The images of tea leaves afflicted by five distinct diseases were subjected to appropriate pre-processing steps involving cropping and resizing. The process included thresholding for the segmentation of diseased leaf portions and feature extraction. These features were harnessed for training neural networks. The authors reported an accuracy rate of 91% in their developed recognizer and highlighted the possibility of creating a real-time leaf disease recognition system using mobile platforms.

Ahmad et al. (2015) proposed an algorithm rooted in Artificial Bee Colony (ABC) for leaf lesion classification. In the filtration phase, healthy and dying leaf images were filtered out from three categories of leaf images (healthy, unhealthy, and dying). Recognition and detection algorithms were designed leveraging Artificial Bee Colony, Fuzzy Logic, Otsu’s thresholding, and geometric formulas. The algorithm’s performance was evaluated using leaf images with varying lesion severities and compared against Otsu, Canny, Robert, and Sobel algorithms, yielding an average accuracy of 96.83%.

Another approach, reliant on thresholding, was adopted for disease spot detection on plant leaves by Revathy & Chennakesavan (2015). The approach encompassed the conversion of diseased color leaf images from the RGB color space to other color spaces, including Gray, HSV, YCbCr, YIQ, and CIELAB. The median filter was utilized for noise removal and image smoothing. Disease spot segmentation was realized through Otsu’s thresholding and histogram-based methods, specifically focusing on a particular channel

from various color spaces. The research revealed that the 'I' component of YIQ and the 'A' component of CIELAB color spaces exhibited enhanced disease spot detection capabilities in comparison to other color models.

Notably, the aforementioned research efforts have presented diverse methods in the detection and classification of various leaf diseases. These methodologies primarily rely on image processing and ANN, often necessitating significant training time. In light of these observations, there is a notable scarcity of research leveraging Content-Based Image Retrieval systems, which offer promising potential for disease detection. CBIR systems, mirroring the working principles of human agricultural experts, hold the potential to address multifaceted challenges in plant disease detection and classification while enhancing accuracy.

## MATERIALS AND METHODS

In the conventional tactics within plant science, plant scientists typically rely on visual observation and their expertise to subjectively assess leaf damage without the aid of photographic documentation. This approach suffers from inherent limitations, characterized by subjectivity and low throughput. This research endeavors to introduce an innovative disease detection and classification system based on Content-Based Image Retrieval, as illustrated in Fig. 1.

Any CBIR system comprises two fundamental steps: Feature Extraction and Feature Matching. In the Feature Extraction step, image characteristics, including color and texture, are extracted and subsequently stored within a dedicated Feature Database. Upon presentation of a query image, its feature vector is extracted and subsequently compared with the feature vectors archived in the database during the ensuing feature-matching phase. The retrieval of similar images hinges on the relative value of the comparison threshold. The ultimate determination of leaf health status is contingent on the precision of the retrieved images.

The cornerstone of CBIR's effectiveness lies in the robustness and relevance of the image features used. An assortment of image features, encompassing color, shape, and texture, can be systematically extracted and applied in CBIR systems. The system presented in this research is specifically tailored to exploit color and texture features, optimizing its performance for the given application.

### Color Feature

The human visual system is naturally attuned to color images, exhibiting a heightened sensitivity compared to grayscale images. This inherent quality has led to the widespread utilization of color features as the predominant image feature in retrieval processes. In their study, Singh & Hemachandran (2012) noted that color features are notably straightforward to extract, robust against variations in background conditions, and self-sufficient. The choice of a color space or model is a critical aspect of color image processing, significantly influencing the outcomes. Within any color space, color features can be extracted using diverse techniques, including methods such as color histograms as used by Choras (2007), Suhasini et al. (2009), correlograms, moments by Huang et al. (2010), Maheswary & Srivastav (2008), Shih & Chen (2002), and color structure descriptors, among others.

Human perception is inherently more responsive to luminance than chrominance. In this context, the YCbCr color space capitalizes on this attribute to achieve an effective representation of images. YCbCr color space uncouples the luminance and chrominance of an image, offering advantages over conventional color spaces like RGB and HSV, as found by Patil & Kumar (2017). The transformation from RGB space to YCbCr space is accomplished using the following equations used by Phatale et al. (2020)

$$Y = 0.299(R - G) + G + 0.114(B - G) \quad \dots(1)$$

$$Cb = 0.564(B - Y) \quad \dots(2)$$

$$Cr = 0.713(R - Y) \quad \dots(3)$$

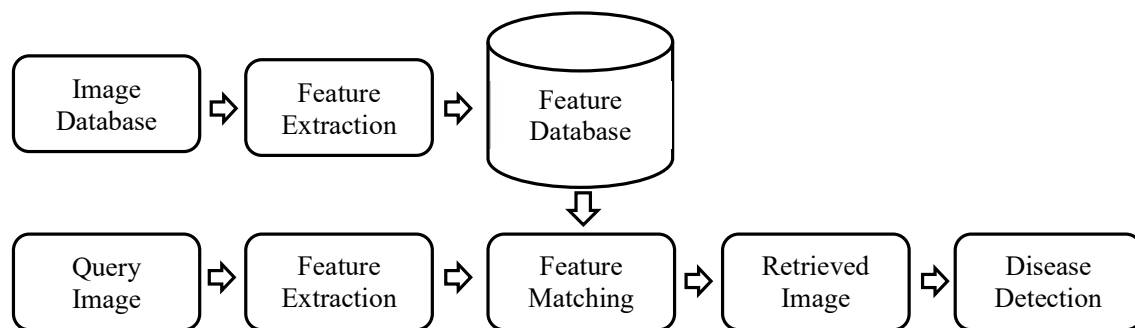


Fig. 1: Block diagram of CBIR system for disease detection.

Among the diverse color features enumerated earlier, the Histogram stands out as an easily computed attribute, displaying robustness against minor image variations. Comparing the histograms of two images employing appropriate similarity measures establishes a solid foundation for the classification or recognition of objects. The Histogram, in this context, is defined as a graphical representation illustrating the distribution of image pixel counts across various light intensities within an image. An image histogram is a discrete function, as stated in equation (4) by Gonzalez & Woods (2008).

$$P(r_k) = \frac{n_k}{N} \quad \dots(4)$$

Where,

$r_k$  is the  $k^{\text{th}}$  gray level, N is the total number of pixels in the image,  $n_k$  is the number of pixels in the image with that gray level,

### Texture Feature

The definition of image texture is inherently elusive, as it encompasses recurring patterns of variations in intensity and color, manifesting as complex visual patterns. These encompass sub-patterns that are associated with the perception of attributes such as lightness, uniformity, density, roughness, regularity, linearity, and frequency. These attributes are intricately linked to image brightness and color, as specified in research by Grigorescu et. al. (2002). Textures are a rich source of visual information, rendering texture feature extraction a pivotal function in a myriad of image processing applications, including but not limited to medical imaging, face recognition, and Content-Based Image Retrieval (CBIR).

Among the multitude of texture feature extractors, Gabor filters, as described by et al. (2004), and Local Binary Pattern (LBP), as described by Vatamanu et al. (2015), emerge as particularly significant for this research. The human visual system exhibits characteristics associated with image decomposition, wherein an image formed on the retina is deconstructed into several filtered images. Each of these filtered images conveys variations in intensity within specific ranges of frequencies and orientations. Gabor filters are adept at simulating these characteristics, as they are orientation-sensitive.

LBP effectively describes local structures within an image and is computationally efficient while demonstrating resilience to illumination variations. Consequently, LBP finds applications in various image processing tasks, encompassing the analysis of biomedical images, facial images, aerial imagery, and image and video retrieval, as listed by Ahonen et al. (2006), among others. Senechal et

al. (2011) found that the fusion of Gabor and LBP, denoted as Local Gabor Binary Pattern (LGBP), further enhances the effectiveness of texture feature extraction.

In the proposed experimentation, a modified version of LGBP, referred to as Local Gray Gabor Pattern (LGGP), is developed to extract texture features as researched by Patil & Kumar (2016). It extracts texture features from diseased leaves that exhibit pronounced textural characteristics owing to the manifestation of disease symptoms. The procedure employed for the extraction of LGGP features from the image is elucidated in the flowchart depicted in Fig. 2.

To derive LGGP values from LBP and LGBP images, the mathematical computation described in equation (5) is employed. This computation involves the comparison of each pixel within the LBP and LGBP images using a (3x3) neighborhood, as outlined in equation (5).

$$LGGP(x, y) =$$

$$\begin{cases} LBP(x, y) & \text{if } LBP(x, y) = LGBP(x, y) \\ 1 & \text{if } [A \cup B] \text{ have more number of 1's than number of 0's} \\ 0 & \text{otherwise} \end{cases} \quad \dots(5)$$

Where A and B represent adjacent neighbors of LBP(x,y) and LGBP(x,y), respectively.

### Proposed Method

In the proposed methodology, features extracted from both the color and texture of an image, in the form of the YCbCr histogram and the LGGP histogram, are extracted and subsequently stored in a feature database. Upon presentation of a query image, its features are extracted using a method similar to the feature extraction process applied to the database images. To measure similarity, correlations between the color histograms and correlations between the LGGP texture histograms are utilized. Fig. 3 illustrates the CBIR System employing the YCbCr Histogram and LGGP Histogram.

The algorithm utilized for the development of CBIR, incorporating a combination of the YCbCr histogram and LGGP histogram, is presented as follows.

#### Algorithm: CBIR using YCbCr histogram and LGGP histogram

Step 1: The RGB leaf image is provided as input for the query.

Step 2: Transform the RGB image into the YCbCr image.

Step 3: Calculate the histogram of each plane, i.e., Y, Cb, and Cr- plane.

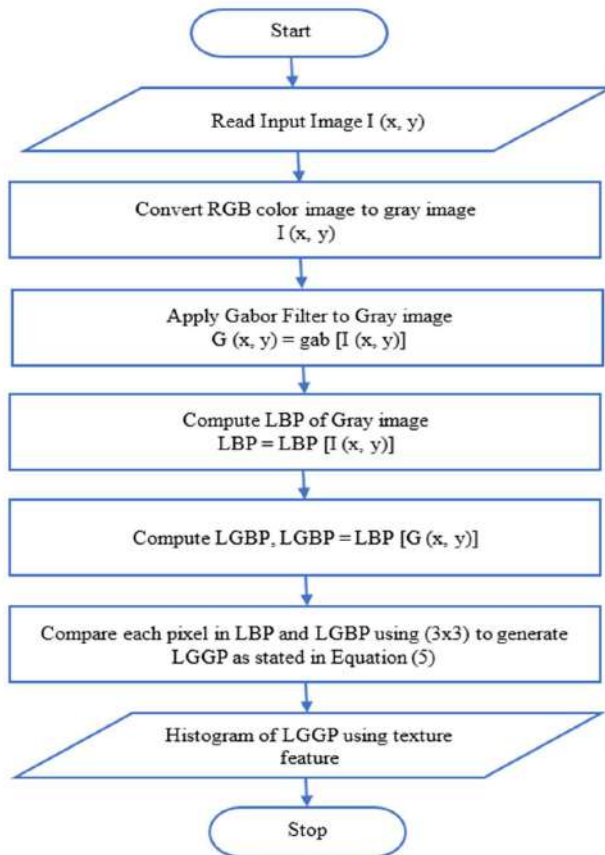


Fig. 2: Flowchart for extracting LGGP features.

Step 4: Combine the histograms of Y, Cb, and Cr components to generate a query color histogram, denoted as  $H_Q$ .

Step 5: Convert the input image to a gray image

Step 6: Compute LGGP histogram ( $L_Q$ ).

Step 7: Extract the YCbCr histogram ( $H_D$ ) and LGGP histogram ( $L_D$ ) of database images from the feature database.

Step 8: Formulate a final feature vector for retrieval by uniting the correlation of  $H_Q$  and  $H_D$ , and  $L_Q$  and  $L_D$

Step 9: Determine the mean value of the feature vector obtained in Step 8 for all database images.

Step 10: Organize mean values in descending order and retrieve images that are similar.

Step 11: Based on the top N retrieval results, the disease of the query image is deduced to match that of the maximum-retrieved image.

## RESULTS AND DISCUSSION

### Database

The leaves of Maize, one of the most widely distributed crops globally, have been selected as candidates for testing the developed methods. Maize is renowned for its richness in carbohydrates, proteins, iron, vitamin B, and minerals, rendering it a valuable resource for the production of a diverse range of food and non-food products, including

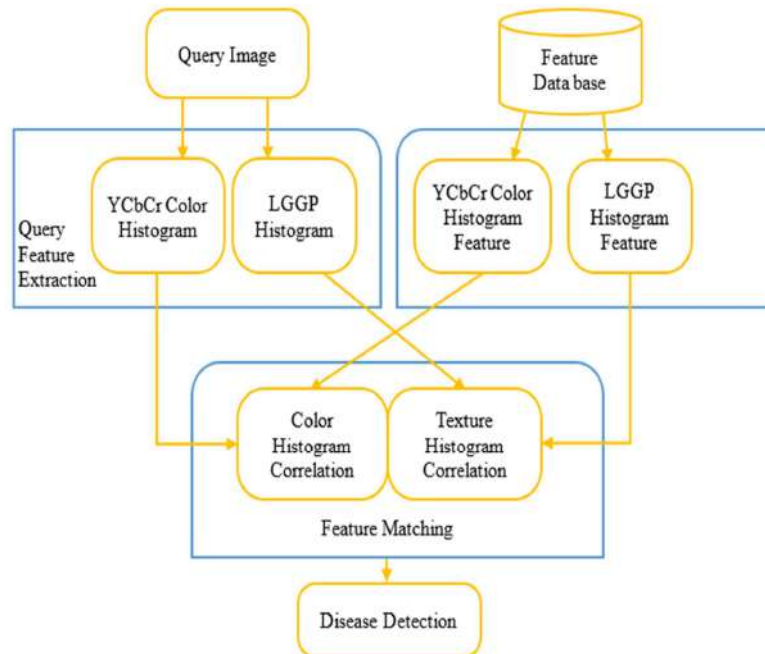


Fig. 3: CBIR System using YCbCr Histogram and LGGP Histogram.

cornmeal, oil, starch, and ethanol. With over 70 countries engaged in maize production, India secures the fifth position globally in maize production, as reported by Corn (2008).

To facilitate experimentation, a maize database has been curated, incorporating samples of diseased leaves affected by maize rust, leaf blight, and healthy leaves. These samples have been collected from fields located in the Sangli and Kolhapur districts of the state of Maharashtra, India, as well as from internet sources. For training purposes, 100 images of each disease type and healthy condition are utilized, along with an additional set of 365 images designated for testing.

**Performance Parameters**

Precision measures exactness according to equation (6), while recall assesses completeness as per equation (7), which is employed to evaluate the performance of the developed system. The % of retrieval precision is called retrieval efficiency defined by Wang & Qin (2009).

$$\text{Precision}(p) = \frac{N_{rr}}{N_{tr}} \quad \dots(6)$$

$$\text{Recall}(r) = \frac{N_{rr}}{N_{tri}} \quad \dots(7)$$

Where,  $N_{rr}$ : number of relevant images retrieved,  $N_{tr}$ : total number of images retrieved and

$N_{tri}$ : total number of relevant images.

The efficiency of disease detection is calculated using

equation (8) as the ratio of correctly detected diseased leaf images to the total number of leaf images tested during experimentation.

$$\text{Disease Detection Efficiency (e)} = \frac{Ic}{It} \times 100 \quad \dots(8)$$

Where  $Ic$  is the number of correctly detected images, and  $It$  is the total number of tested images.

**Sample Result of the Developed System**

To assess the effectiveness of the developed system, it is essential to carry out a thorough examination of the CBIR system, analyzing individual features such as the YCbCr color histogram and the LGGP histogram separately. The evaluation concentrates on the top 40 retrieved images, with disease detection determinations relying on the precision of the top 10 images.

When using the YCbCr color histogram as a standalone feature, the approach involves utilizing three image planes: Y (Luminance), Cr, and Cb (Chrominance). The histogram of the query image is calculated for each of these planes and then compared with the histograms stored in the feature database using correlation analysis. Subsequently, based on the correlation values between the query image and all the images in the database, the top 40 similar images are retrieved for performance analysis, as illustrated in Fig. 4.

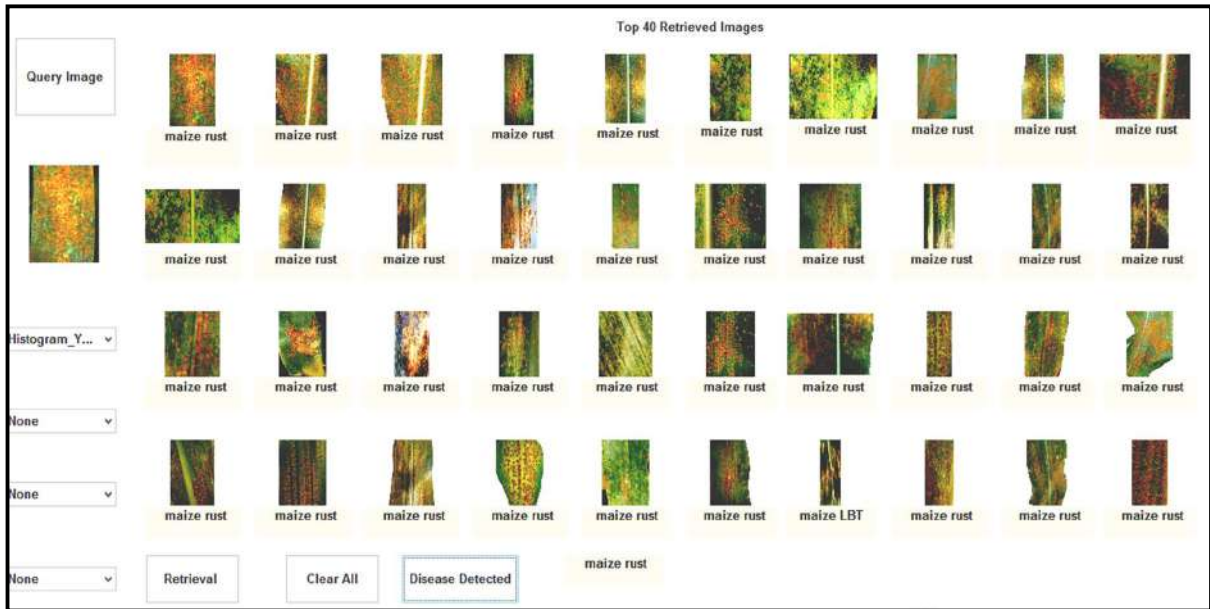
For instance, in the case of a query about maize leaf blight, Fig. 4(a) demonstrates that the YCbCr histogram



(a) Leaf Blight

Figure Cont....





(b) Leaf Rust



(c) Healthy Leaf

Fig. 4: CBIR for maize leaf using YCbCr histogram.

method yields a precision of 70% within the top 10 retrieved images, leading to accurate disease detection. Similarly, when dealing with maize rust, as depicted in Fig. 4(b), a precision

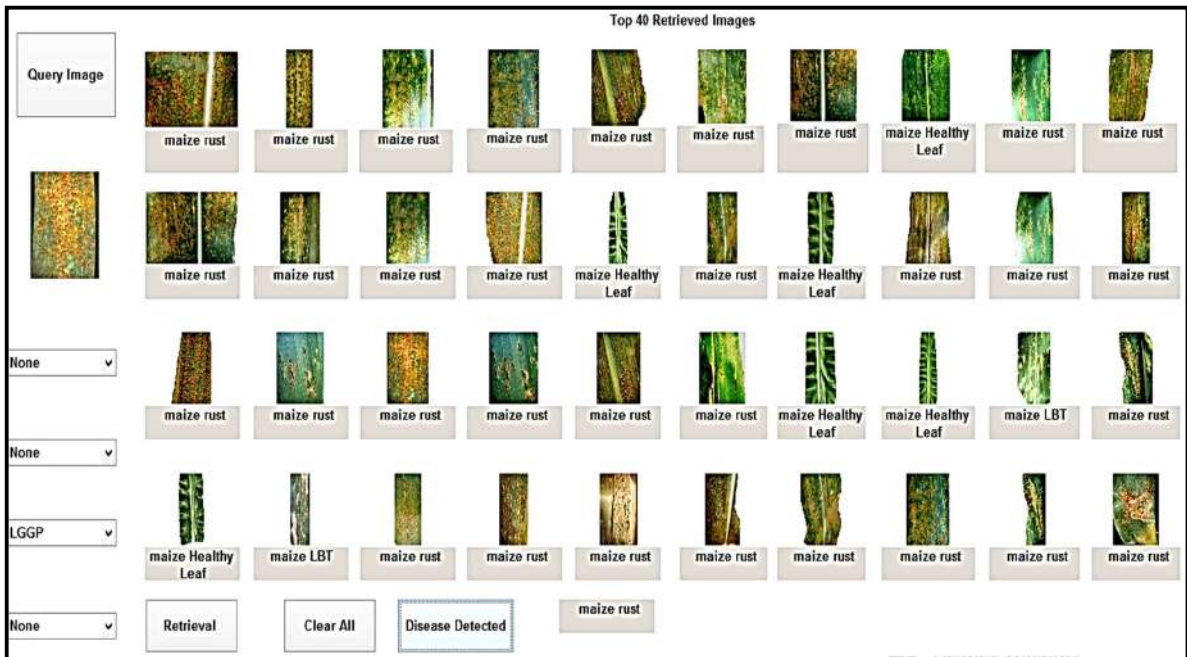
of 100% is achieved within the top 10 retrievals, resulting in precise disease detection. Even in the case of a healthy leaf query, a precision of 80% is maintained within the top 10

retrievals, as illustrated in Fig. 4(c). These findings underscore the system's ability to effectively and accurately detect diseases in plant leaves using the CBIR approach, particularly when employing the YCbCr color histogram feature.

The study assesses the performance of Local Gray Gabor Pattern (LGGP) for disease retrieval and detection, maintaining consistency by comparing LGGP histograms of database and query images using the

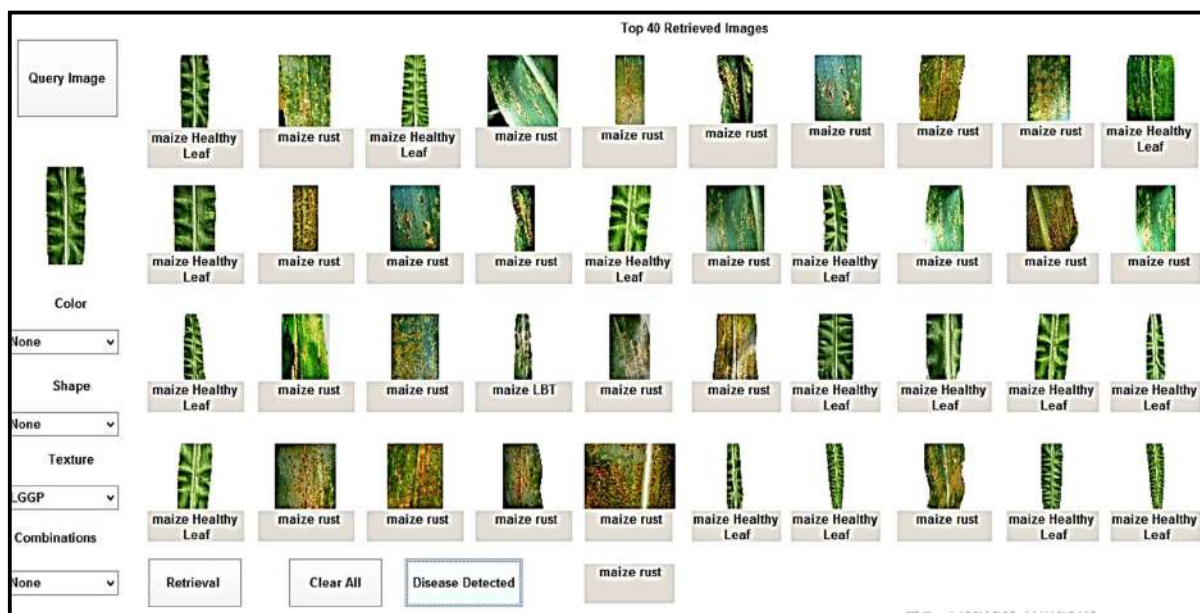


(a) Leaf Blight



(b) Leaf Rust

Figure Cont....



(c) Healthy Leaf

Fig. 5: CBIR for maize leaf using LGGP.

methodology outlined in the texture feature. Fig. 5 illustrates the outcomes.

Fig. 5(a) reveals that for the query on leaf blight, most retrieved images correspond to healthy leaves, with relevant images appearing only at the 8th and 9th positions, resulting in a modest precision of 20%. In contrast, Fig. 5(b) displays a remarkable precision of 90% in correctly detecting maize rust disease due to its distinctive textural features, highlighting LGGP's efficacy in texture-based disease detection. This texture-sensitivity feature of LGGP proves invaluable in identifying objects with rich textures across various image recognition and computer vision applications regardless of color. Additionally, Fig. 5(c) demonstrates a 60% precision in correctly identifying healthy leaves.

Now, observe the results obtained from the Content-Based Image Retrieval (CBIR) system, integrating both the YCbCr color histogram and the Local Gradient Binary Pattern (LGGP) histogram, as illustrated in Fig. 3. Integration at the classification stage produces better identification results as experimented by Dhole et al. (2023). A feature vector is constructed according to the algorithm outlined in the proposed method, and the findings are presented in Fig. 6.

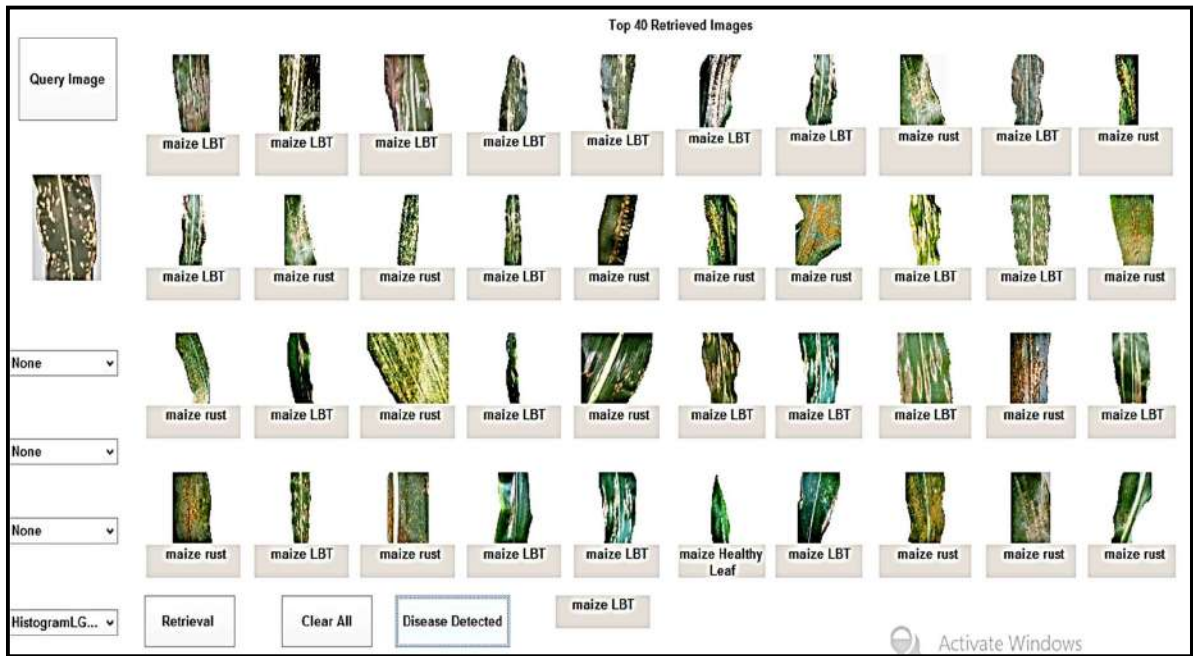
For leaf blight, a precision of 80% within the top 10 retrievals is achieved (Fig. 6(a)). This is an improvement compared to the individual YCbCr color histogram method,

which retrieved 22 leaf blight images within the top 40 retrievals (Fig. 4(a)). Furthermore, the integrated method outperforms the individual YCbCr histogram (Fig. 4(b)) and LGGP histogram (Fig. 5(b)) methods when dealing with maize rust, delivering 100% precision in both top 10 and top 40 retrievals. As depicted in Fig. 6(c), healthy leaves are correctly identified with a precision of 70%. The performance of this integrated approach surpasses individual texture-based methods (Fig. 5(c)) but lags behind the individual color-based performance (Fig. 4(c)), primarily due to leaf blight's retrieval at the 7<sup>th</sup> position.

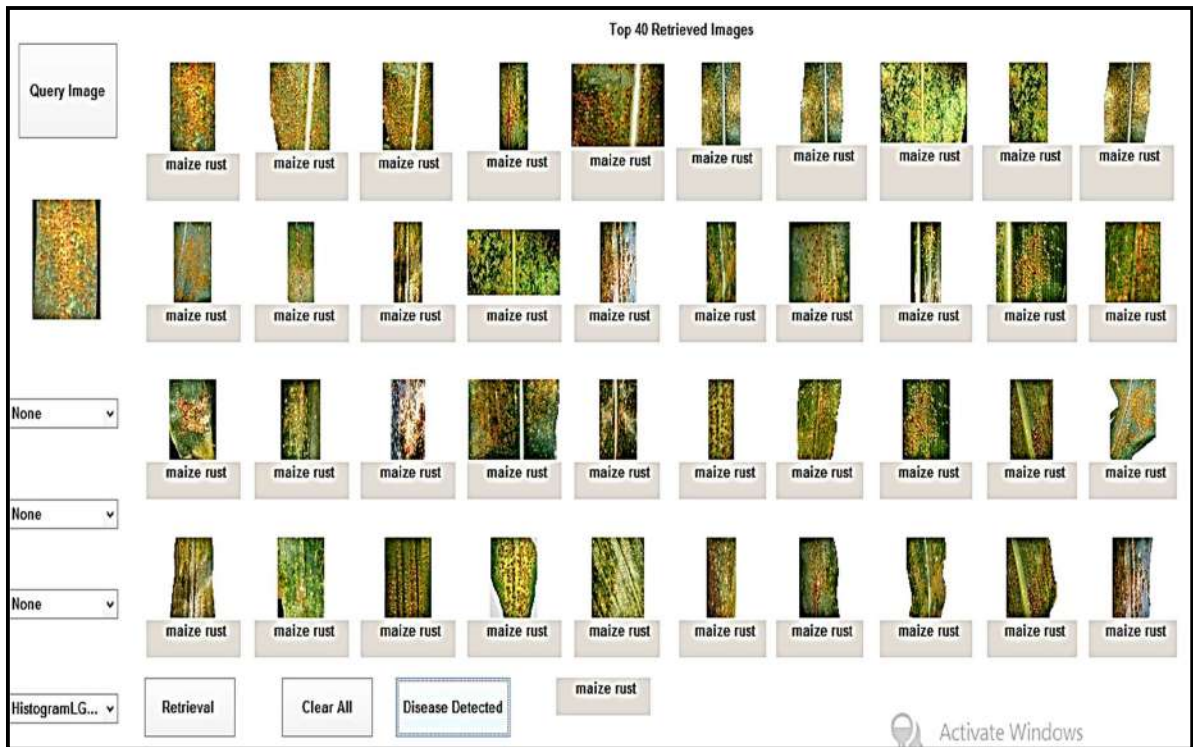
This integrated approach demonstrates significant promise, particularly for scenarios such as maize rust detection.

The experiment is replicated for a set of randomly chosen images. Fig. (7) shows a performance comparison of all tested methods for all candidate maize diseases concerning disease detection precision, recall, and efficiency.

The individual performance of the color histogram exhibits commendable results, with a disease detection efficiency of 96.66%. However, it is essential to acknowledge its limitations that when two distinct images exhibit a similar color distribution, their histograms can be indistinguishable. Consequently, relying solely on histograms cannot guarantee accurate object detection or recognition. Conversely, texture features yield favorable outcomes when images are texture-



(a) Leaf Blight



(b) Leaf Rust

Figure Cont...



(c) Healthy Leaf

Fig. 6: CBIR for maize leaf using YCbCr histogram and LGGP histogram.

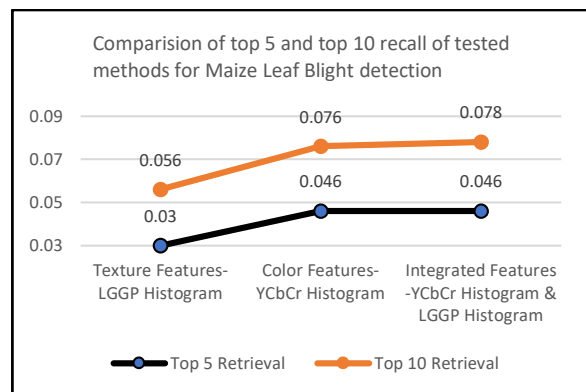
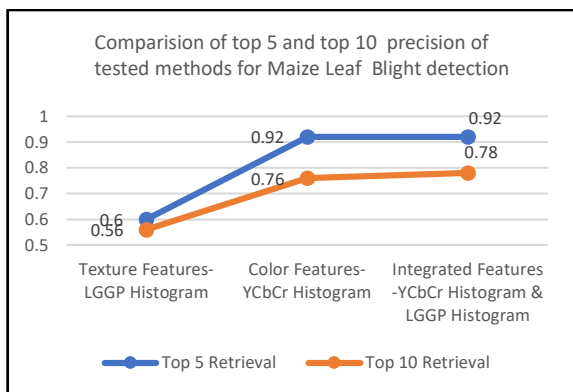
rich, but their individual use results in an average efficiency of 63.33%. Therefore, it is evident that the integration of both color and texture features is pivotal to achieving the highest efficiency, amounting to 98.33%.

Fig. 8 offers a comparative illustration of disease detection efficiency within the developed CBIR system, evaluated using individual color and texture features, as

well as their integrated approach. This visual representation underscores the significant performance improvements achieved through feature integration.

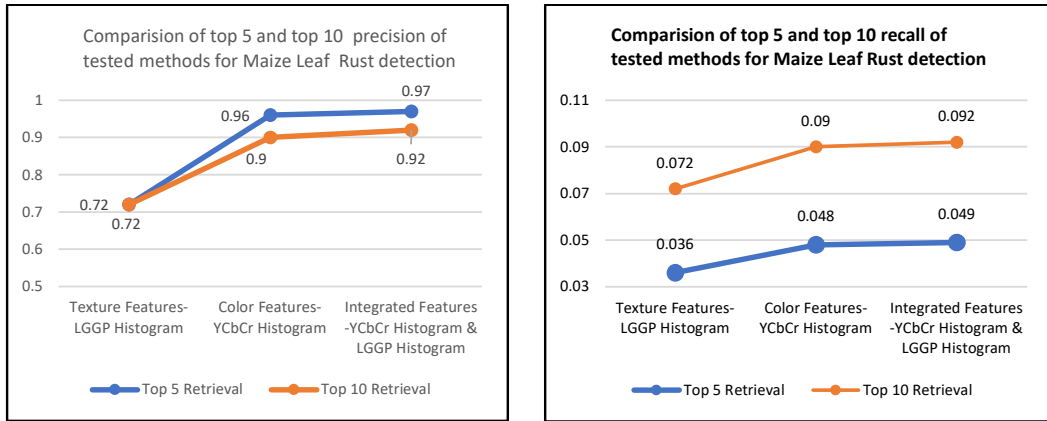
**CONCLUSION**

A system is developed to detect and identify plant leaf diseases through the analysis of leaf image features using

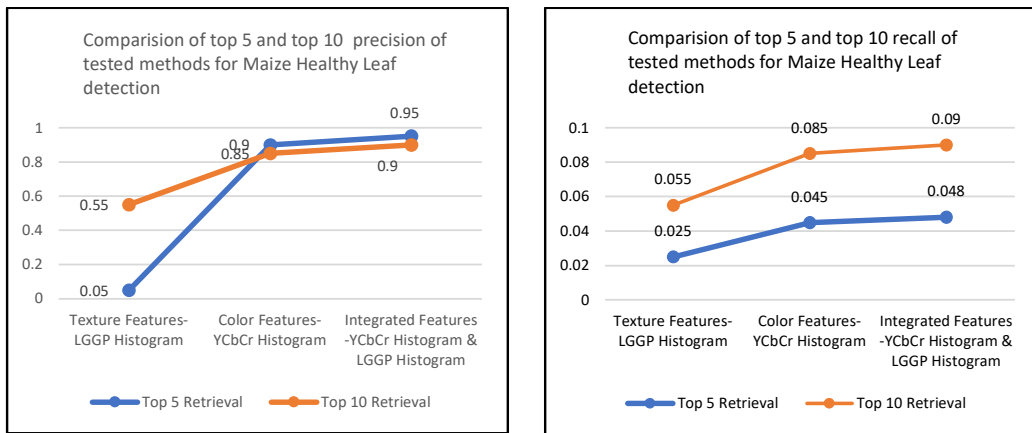


a) Leaf Blight

Figure Cont...



b) Leaf Rust



c) Healthy

Fig. 7: Top 5 and Top 10 average precision and recall for maize leaf disease.

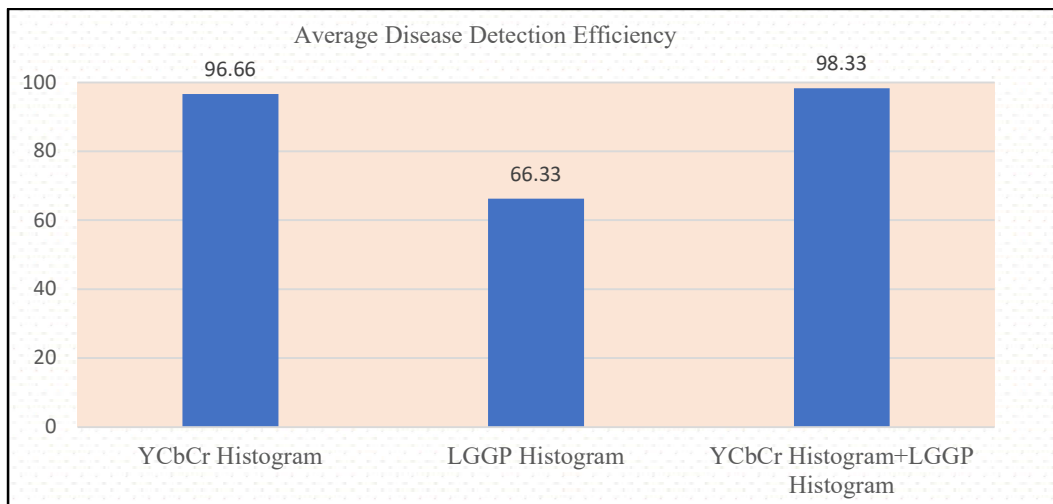


Fig. 8: Disease detection efficiency.

Content-Based Image Retrieval (CBIR). The system's performance is assessed individually using YCbCr color histograms and Local Gradient Binary Pattern (LGGP) texture histograms. To harness the collective power of color and texture features, they are harmoniously integrated to construct a comprehensive feature vector for retrieval purposes. This integration significantly surpasses the individual performance of these two features when considering precision, recall, and the efficiency of disease detection and identification. The integration of features achieves a remarkable disease detection efficiency of 98.33%. To enhance the system's versatility, it can be further evaluated with additional color, texture, and shape features, thus extending its capabilities to detect various diseases across different crop types. This expansion has the potential to bring about the application of CBIR in the realm of precision agriculture.

## ACKNOWLEDGMENT

This research is funded by Shivaji University, Kolhapur, Maharashtra, India under the scheme 'Diamond Jubilee Research Grant To College Teachers' Scheme 2022-2023 for Non 2(f) 12(b) Colleges.

## REFERENCES

- Ahmad, F., Ku-Mahamud, K.R., Sainin, M.S. and Airuddin, A., 2015. Leaf lesion classification (LLC) algorithm based on artificial bee colony (ABC). *ARPN Journal of Engineering and Applied Sciences*, 10(3), pp.1311-1315. ISSN: 1819-6608.
- Ahonen, T., Hadid, A. and Pietikainen, M., 2006. Face description with local binary patterns: Application to face recognition. *IEEE Transactions on Pattern Analysis and Machine Intelligence*, 28(12), pp.2037-2041.
- Choras, R.S., 2007. Image feature extraction techniques and their applications for CBIR and biometrics systems. *International Journal of Biology and Biomedical Engineering*, 1(1), pp.6-16.
- Corn, D., 2008. Importance and utilization of maize. *cornindia.com*. Available at <http://cornindia.com/importance-and-utilization-of-maize/>.
- Dhole, S.A., Patil, J.K., Jagdale, S.M., Govardhana Reddy, H.G. and Gowda, V.D., 2023. Multimodal biometric identification system using a random selection of biometrics. *SSRG International Journal of Electrical and Electronics Engineering*, 10(1), pp.63-73.
- Gonzalez, R.C. and Woods, R.E., 2008. *Color Image Processing*. 3rd ed. Pearson Education, Inc.
- Grigorescu, S.E., Petkov, N. and Kruijzinga, P., 2002. Comparison of texture features based on Gabor filters. *IEEE Transactions on Image Processing*, 11(10), pp.1160-1167.
- Huang, Z.C., Chan, P.P.K., Ng, W.W.Y. and Yeung, D.S., 2010. Content-based image retrieval using color moment and Gabor texture feature. In: *International Conference on Machine Learning and Cybernetics (ICMLC)*, pp.719-724.
- Kannan, E., 2014. Assessment of pre and post-harvest losses of important crops in India. *Agricultural Development and Rural Transformation Centre Institute for Social and Economic Change Bangalore*, Research Report: IX/ADRTC/153A.
- Karmokar, B.C., Ullah, M.S., Siddiquee, Md.K. and Alam, K.M.R., 2015. Tea leaf disease recognition using neural network ensemble. *International Journal of Computer Applications*, 114(17), pp.27-30. ISSN: 0975-8887.
- Kumar, P., 2012. Feeding the future: Crop protection today. *Acta Chim. Pharm. Indica*, 2(4), pp.231-236.
- Maheswary, P. and Srivastav, N., 2008. Retrieving similar images using color moment feature detector and K-means clustering of remote sensing images. *International Conference on Computer and Electrical Engineering*, pp.821-824.
- Naik, S.I., Reddy, V. and Sannakki, S.S., 2014. Plant disease diagnosis system for improved crop yield. *International Journal of Innovations in Engineering and Technology (IJIET)*, 4(1), pp.198-204.
- Patil, J. and Kumar, R., 2016. Comparative analysis of content-based image retrieval using texture features for plant leaf diseases. *International Journal of Applied Engineering Research*, 11(9), pp.6244-6249. ISSN: 0973-4562.
- Patil, J. and Kumar, R., 2017. Analysis of content-based image retrieval plant leaf diseases using color, shape, and texture features. *Engineering in Agriculture, Environment, and Food*, 10(2), pp.69-78. ISSN: 1881-8366.
- Phatale, A., Malode, V. and Mulay, M., 2020. Skin segmentation of Indian sign language recognition system for differently-abled people. *International Journal of Advances in Science Engineering and Technology*, 8(2), pp.6-11. ISSN(e): 2321-9009.
- Revathy, R. and Chennakesavan, S.A., 2015. Threshold-based approach for disease spot detection on plant leaf. *Transactions on Engineering and Sciences*, 3(5), pp.72-75.
- Ruiz, L.A., Fdez-Sarría, A. and Recio, J.A., 2004. Texture feature extraction for classification of remote sensing data using wavelet decomposition: A comparative study. *20th ISPRS Congress*, 35(part B), pp.1109-1114.
- Senechal, T., Rapp, V., Salam, H., Seguiet, R., Bailly, K. and Prevost, L., 2011. Combining AAM coefficients with LGBP histograms in the multikernel SVM framework to detect facial action units. In: *IEEE International Conference on Automatic Face and Gesture Recognition*, pp.860-865.
- Shih, J.L. and Chen, L.H., 2002. Color image retrieval based on primitives of color moments. *International Conference on Advances in Visual Information Systems*, Springer Berlin Heidelberg, pp.88-94.
- Singh, A.K., Rubiya, A. and Raja, B.S., 2015. Classification of rice disease using digital image processing and SVM classifier. *International Journal of Electrical and Electronics Engineers*, 7(1), pp.294-299.
- Singh, S.M. and Hemachandran, K., 2012. Content-based image retrieval using color moment and Gabor texture feature. *International Journal of Computer Science*, 9(5), pp.299-309.
- Suhasini, P.S., Krishna, K.S.R. and Krishna, I.V.M., 2009. CBIR using color histogram processing. *Journal of Theoretical and Applied Information Technology*, 6(1), pp.116-122.
- Vatamanu, O.A., Frande, M., Lungeanu, D. and Mihala, G.I., 2015. Content-based image retrieval using local binary pattern operator and data mining techniques. *Digital Healthcare Empowering Europeans*, pp.75-79.
- Wang, S. and Qin, H., 2009. A study of order-based block color feature image retrieval compared with cumulative color histogram method. In: *Sixth International Conference on Fuzzy Systems and Knowledge Discovery*. IEEE Computer Society, pp.81-84.

---

## ORCID DETAILS OF THE AUTHORS

Jayamala Kumar Patil: <https://orcid.org/0000-0002-7063-8275>

Vinay Sampatrao Mandlik: <https://orcid.org/0000-0002-5656-3502>







# Optimization and Thermodynamic Analysis of CO<sub>2</sub> Refrigeration Cycle for Energy Efficiency and Environmental Control

Manish Hassani† and Kamlesh Purohit

Department of Mechanical Engineering, MBM University, Jodhpur-342011, Rajasthan, India

†Corresponding author: Manish Hassani; manish.hassani@gmail.com

Nat. Env. & Poll. Tech.  
Website: [www.neptjournal.com](http://www.neptjournal.com)

Received: 22-03-2024

Revised: 07-05-2024

Accepted: 17-05-2024

## Key Words:

Carbon dioxide  
Refrigeration system  
Coefficient of performance  
Greenhouse gas emissions  
Carbon footprints  
Environmental control

## ABSTRACT

Supermarket applications are significant contributors to greenhouse gas emissions, necessitating efforts to reduce carbon footprints in the food retail sector. Carbon dioxide (R744) is recognized as a viable long-term refrigerant choice due to its favorable properties, including low Global Warming Potential, non-toxicity, non-flammability, affordability, and widespread availability. However, enhancing the energy efficiency of pure CO<sub>2</sub> systems in basic architecture units, particularly in warm regions like India, remains a challenge. To address this, modern refrigeration systems must prioritize low energy consumption and high coefficient of performance (COP) while meeting environmental standards. This study investigates different operating conditions to determine the optimal parameter range for maximizing COP and improving the efficiency of conventional CO<sub>2</sub> refrigeration configurations. It examines both subcritical and transcritical refrigeration cycles under varying parameters, emphasizing the importance of understanding COP's relationship with factors such as subcooling, superheating, ambient temperature, and evaporator temperature. The study advises against superheating in CO<sub>2</sub> systems but highlights the substantial COP increase with higher degrees of subcooling, leading to enhanced system performance. Additionally, it provides a comprehensive theoretical comparison between advanced pure CO<sub>2</sub> supermarket applications and commonly used hydrofluorocarbons-based systems, offering insights into energy efficiency and environmental impacts for informed decision-making in the industry.

## INTRODUCTION

Modern refrigeration systems face multiple demands, including performance, reliability, controllability, compactness, and environmental sustainability. Pollution in compression systems arises mainly from refrigerant leakage and energy consumption for system operation, making it crucial to use an environmentally friendly refrigerant, particularly in mobile applications like automotive air-conditioning (Prabakaran et al. 2022). Carbon dioxide (CO<sub>2</sub>) has emerged as a suitable refrigerant that meets these criteria when combined with optimized system components (Yuan et al. 2021).

CO<sub>2</sub> (R744) was widely used as a refrigerant in the 19th century (Ciconkov 2018). However, in the 1930s, it was gradually replaced by newly developed synthetic refrigerants (HCFCs) due to their lower system pressures and simpler technology (Riffat et al. 1997). The shift in refrigerants was driven by the desire for more efficient and easier-to-handle refrigeration systems.

Moulina & Rowland (1974) brought attention to the damaging effects of chlorine emissions on the ozone layer,

leading to the introduction of HFCs like R-134a, which are currently used in many refrigeration applications. R-134a, a commonly used refrigerant, does not contribute to ozone depletion as it has an ozone-depleting potential (ODP) of zero. However, it does have a substantial impact on global warming potential (GWP) compared to CO<sub>2</sub>. In fact, the GWP of R134a is approximately 1,300 times higher than that of CO<sub>2</sub> (Bolaji & Huan 2013).

The consideration of global warming potential has become increasingly important in recent years, as there is a growing awareness of the environmental impact of greenhouse gas emissions (Shirmohammadi et al. 2018). As a result, there has been a renewed interest in utilizing CO<sub>2</sub> as a refrigerant due to its negligible global warming potential and other favorable thermophysical properties. CO<sub>2</sub> is non-flammable, inexpensive, non-toxic, and readily available, making it an attractive long-term working fluid for refrigeration systems (Lorentzen & Pettersen 1993). The CO<sub>2</sub> (R744) is compared with R-12, R-22, R-134a, and R717 refrigerants in Table 1 (Kim et al. 2004).

Table 1: Comparison of R744 with other refrigerants (Kim et al. 2004).

	R-12	R-22	R-134a	R717	R744
GWP	8500	1700	1300	0	1
ODP	1	0.05	0	0	0
Flammability	No	No	No	Yes	No
Toxicity	No	No	No	Yes	No
Mass [kg.kmol <sup>-1</sup> ]	120.9	86.5	102	17	44
Critical Temperature [°C]	112	96	101.1	133	31.1
Critical Pressure [MPa]	4.11	4.97	4.07	11.42	7.38
Refrigeration Capacity [kJ.m <sup>-3</sup> ]	2734	4356	2868	4382	22545
First commercial use	1931	1936	1990	1859	1869

By transitioning back to CO<sub>2</sub> as a refrigerant, it is possible to significantly reduce the carbon footprint associated with the refrigeration industry. However, further research and development are needed to advance the energy efficiency of pure CO<sub>2</sub> systems, particularly in units with basic architectures operating in warm regions (Kauf 1999). These efforts aim to maximize the performance of CO<sub>2</sub> refrigeration systems and make them even more environmentally friendly alternatives to synthetic refrigerants like R134a.

The resurgence of CO<sub>2</sub> as a refrigerant sheds light on the development of air conditioning and refrigeration systems. Initially, efforts concentrated on enhancing compressors to address cost and efficiency concerns. The introduction of CFCs brought advantages like low-pressure operation, improved thermodynamic efficiency, and enhanced safety. This led to cost reductions, enabling widespread production. As energy prices decreased, the industry focused on the simplified vapor-compression cycle and optimized components to maximize efficiency by utilizing the specific transport properties of the refrigerant (Bose & Saini 2022).

Carbon dioxide serves as the working fluid in a refrigeration system through the thermodynamic CO<sub>2</sub> refrigeration cycle. To produce cooling effects, CO<sub>2</sub> is compressed, condensed (making the gas cooler), expanded, and evaporated. The CO<sub>2</sub> gas is compressed by a compressor during the CO<sub>2</sub> refrigeration cycle, raising its pressure and temperature (Javadpour et al. 2024). The high-pressure CO<sub>2</sub> then travels through a condenser, where it undergoes a phase transition into a liquid and emits heat to the environment. The high-pressure liquid CO<sub>2</sub> then passes through an expansion valve (Ejector), where it rapidly expands, resulting in a decrease in pressure and temperature. The use of an ejector in a transcritical CO<sub>2</sub> cycle has several benefits, including a higher performance coefficient and easier management of the gas cooler pressure (Manjili & Yavari 2012). This is accomplished by adjusting the ejector nozzle's throat region. After entering an evaporator, the low-pressure CO<sub>2</sub> liquid or

mixture of liquid and gas absorbs heat from its surroundings, such as a refrigerated area or product. As a result, the CO<sub>2</sub> evaporates and turns back into a gas, completing the cycle.

Brown et al. (2005) investigated the thermodynamic analysis of the transcritical refrigeration system theoretically. It was concluded that CO<sub>2</sub> exhibits promise as a natural refrigerant in refrigeration and air-conditioning, particularly in compact automobile systems with high operating pressures. Unlike R134a, which contributes to global warming, CO<sub>2</sub> is environmentally friendly. However, additional research is necessary to enhance the safety and efficiency of CO<sub>2</sub> systems. While current performance may not be on par with existing systems, CO<sub>2</sub> and similar refrigerants hold potential as realistic alternatives in the future.

Silva et al. (2012) conducted a comparative study between R744 cascade, R404A, and R22 refrigeration systems. Their findings indicated that carbon dioxide cascade systems offer significant advantages in refrigeration applications. These advantages include reduced electric energy consumption (13-24%), increased compressor lifespan due to lower compression ratio, high CO<sub>2</sub> density and pressure in the low-pressure stage, reduced piping diameter, lower refrigerant charge, affordability, improved enthalpy and cooling capacity, lower Global Warming Potential (GWP) and carbon taxes, compact compressors with reduced displacement, streamlined installation with fewer compressors and a compact refrigeration rack, efficient evaporator coils, and reduced installation and maintenance costs.

Getu & Bansal (2008) investigated the thermodynamics of an R744-R717 cascade refrigeration system at -50°C evaporator temperature and 40°C condensing temperature. It observed that increasing superheat decreased COP but increased mass flow ratio while increasing subcooling improved both. Additionally, higher condensing temperatures reduced COP but increased mass flow ratios, whereas higher evaporating temperatures enhanced COP while reducing mass flow ratios.

Kauf (1999) investigated the impact of high pressure in transcritical refrigeration systems on the COP. However, the graphical method was found to be time-consuming for determining the optimal high pressure. Kauf proposed a linear correlation suggesting that the optimal high pressure should be 0.26 times the ambient temperature to achieve maximum COP.

Sun et al. (2020) conducted a comprehensive analysis to evaluate the operational efficacy of the supermarket refrigeration system in varying climate zones across China, employing both R134a and R744 (CO<sub>2</sub>) as working fluids. Their study focused on the examination of cascade and double-stage compression configurations. The findings of their investigation unequivocally demonstrated that the CO<sub>2</sub> refrigeration system featuring the cascade and double-stage compression designs exhibited remarkable promise for deployment in supermarket refrigeration applications.

Zhang et al. (2015) conducted an in-depth investigation into the transcritical carbon dioxide refrigeration cycle with double-stage compression, incorporating an expander. The study focused on the analysis of four distinct double-compression CO<sub>2</sub> transcritical refrigeration cycles: the double-compression external intercooler cycle (DCEI), double-compression external intercooler cycle with an expander (DCEIE), double-compression flash intercooler cycle (DCFI), and double-compression flash intercooler cycle with an expander (DCFIE). The key findings of their research concluded that the replacement of the throttle valve with an expander in the DCEI cycle resulted in a decrease in the optimal gas cooler pressure, with minimal variation observed in the optimal intermediate pressure.

Perez-Garcia et al. (2013) conducted simulations on a single-stage transcritical CO<sub>2</sub> refrigeration cycle. The study concluded that the implementation of an internal heat exchanger (IHE) for subcooling the refrigerant exiting the gas cooler proved to be the most effective configuration for enhancing the COP. For gas cooler outlet temperatures below 31 °C, the inclusion of an IHE was not advised as it resulted in slightly lower cycle performance compared to the basic cycle. The degree of superheating in the Dual Expansion Cycle (DEC) and DEC + IHE configurations proved to be beneficial in both cases. However, in the DEC, the influence of this parameter was particularly significant in the first two Celsius degrees, as it led to a noteworthy increase in COP within this range.

Singh et al. (2016) conducted a comparative analysis of various configurations of CO<sub>2</sub> refrigeration cycles specifically designed for warm climate conditions. The study yielded important conclusions, notably that systems incorporating internal heat exchangers demonstrated reduced

mass flow rates at elevated ambient temperatures. This finding implies that such systems can operate effectively with lower gas cooler pressures. Additionally, the performance of systems equipped with internal heat exchangers was observed to be comparatively superior under higher ambient temperature conditions. However, for applications involving refrigeration and air cooling, the performance of multi-stage systems was found to be similar to that of the basic system, rendering them less effective. Among the real-time constraints considered, compressor efficiency emerged as the most influential factor affecting the system's COP. Furthermore, the gas cooler capacity exhibited rapid growth with increasing ambient temperature.

One of the primary goals in the design of refrigeration systems is to achieve elevated energy efficiency while minimizing energy consumption. In transcritical CO<sub>2</sub> refrigeration cycles, the system's high pressure and desired cabin temperature exert significant influence on the COP, which directly impacts energy efficiency. This study focuses on calculating the optimal COP under various operating conditions and determining the ideal high pressure based on the ambient temperature. Additionally, the analysis in this study examines the impact of superheating on the system's COP and compressor work. Furthermore, the subcooling effect achieved through the use of an internal heat exchanger to reduce the refrigerant temperature emerging from the gas cooler is analyzed at different ambient and evaporator temperatures.

To optimize the COP of the refrigeration system, careful examination of operating parameters is necessary. By adjusting these parameters, the COP can be maximized, leading to enhanced overall performance and energy efficiency. This study showcases the utilization of CO<sub>2</sub> as a refrigerant in modern refrigeration systems, highlighting the importance of optimized components. Specifically, the study investigates the impact of superheating after the evaporator outlet and subcooling after the gas cooler. In this study, MATLAB simulation is employed to investigate the impact of different operating parameters on both subcritical and transcritical refrigeration cycles, facilitating a thorough examination of system performance.

## MATERIALS AND METHODS

### CO<sub>2</sub> Refrigeration System

A CO<sub>2</sub> compression cycle comprises several essential components, including the compressor, gas cooler (which replaces the conventional condenser to handle supercritical heat rejection), expansion unit, and evaporator, as depicted in Fig. 1. Ideally, the refrigerant is drawn from the evaporator

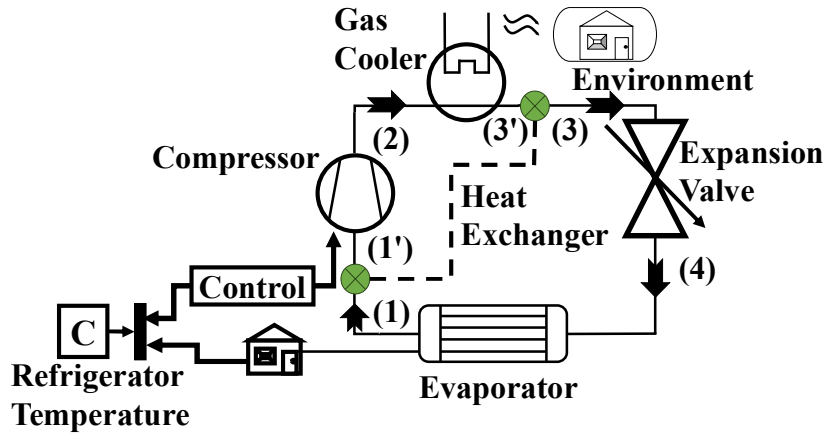


Fig. 1: CO<sub>2</sub> Refrigeration system.

as saturated vapor (point 1) and undergoes an isentropic compression process to reach a higher pressure (point 2). At this higher pressure, the hot CO<sub>2</sub> is cooled in the gas cooler by transferring heat ( $Q_{amb}$ ) to the surrounding ambient air (point 3). Subsequently, the refrigerant is throttled to a lower pressure (point 4). Within the evaporator, the refrigerant extracts heat ( $Q_{evap}$ ), also referred to as the refrigerating capacity, from the ambient air, thereby providing a cooling effect.

The subcritical cycle having CO<sub>2</sub> as refrigerant is depicted in Fig. 2(A). Subcritical cycles are a type of refrigeration system where the refrigerant can undergo the condensation process. This implies that the pressure at the discharge of the compressor is maintained at a level below the critical pressure of the refrigerant. In subcritical cycles, the refrigerant transitions from a high-pressure, high-temperature vapor state to a lower-pressure liquid state during the condensation process (Yaakop et al. 2023).

Currently, the management of high system pressures in CO<sub>2</sub> refrigeration cycles has become more manageable

through effective regulation. The critical point of CO<sub>2</sub>, which occurs at 7.38 bar and 31°C, often necessitates the operation of refrigeration cycles in a transcritical mode. This is particularly prominent in automotive air-conditioning systems and supermarket refrigeration systems that operate in environments with high ambient temperatures. In such systems, the evaporation process occurs at pressures and temperatures below the critical point, referred to as subcritical conditions, while heat rejection takes place at pressures and temperatures above the critical point, known as supercritical conditions. The supercritical (Transcritical) cycle having CO<sub>2</sub> as refrigerant is depicted in Fig. 2(B).

In the subcritical cycle, the refrigerant is evaporated and condensed below the critical point of CO<sub>2</sub>, which is 31.1°C and 7.38 MPa. In this cycle, the CO<sub>2</sub> goes through a phase transition from a liquid to a vapor in the evaporator and then condenses back into a liquid form in the condenser. In applications needing moderate cooling temperatures, including commercial refrigeration

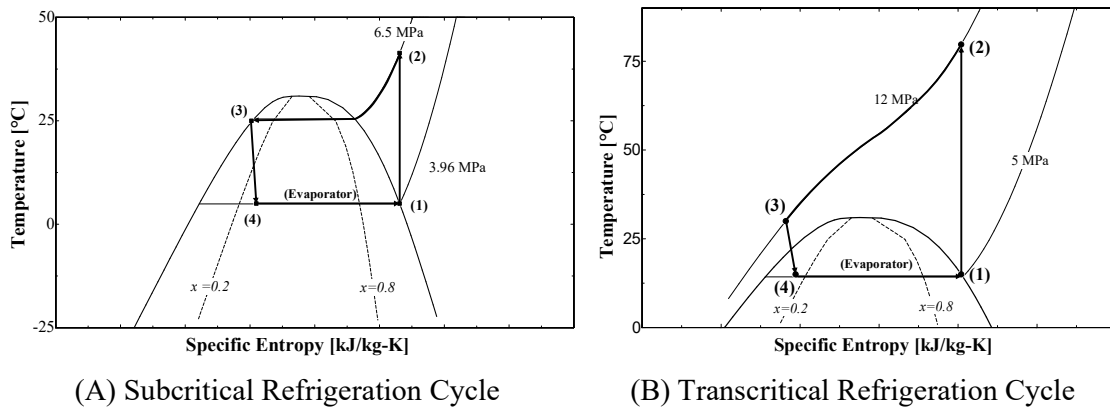


Fig. 2: CO<sub>2</sub> Refrigeration cycles on T-S diagrams.

and air conditioning, the subcritical cycle is frequently employed.

The transcritical cycle, on the other hand, functions at pressures and temperatures higher than the CO<sub>2</sub> critical point. During the heat rejection phase of this cycle, the refrigerant does not change phases. Instead, a supercritical process where the characteristics of a liquid and a gas coexist is used to release the heat. The transcritical cycle is appropriate for operations like heat pumps and some industrial ones that need cooling at higher temperatures.

Superheating after the evaporator occurs when the temperature of the refrigerant exceeds its saturation temperature after completing the evaporation process within the evaporator. Initially, in the refrigeration cycle, the refrigerant enters the evaporator as a saturated mixture of liquid and vapor. As heat is absorbed from the surroundings, the liquid component of the refrigerant evaporates, transforming into a fully saturated vapor state. However, if the refrigerant temperature continues to rise beyond the saturation temperature, it becomes superheated. The presence of superheating is typically desirable in specific applications to prevent any potential for liquid refrigerant entering the compressor, which can result in system damage and reduced efficiency. To visually illustrate the phenomenon of superheating, a schematic representation of the process (1-1') is presented in Fig. 3.

Subcooling in a CO<sub>2</sub> refrigeration system involves an additional reduction in temperature that occurs after the refrigerant has passed through the gas cooler. The gas cooler's main purpose is to lower the refrigerant's temperature, and subcooling builds upon this process by further decreasing the temperature of the refrigerant. To accomplish subcooling, an internal heat exchanger is utilized.

This heat exchanger facilitates the transfer of heat from the refrigerant as it exits the evaporator. The heat extracted by the internal heat exchanger is then utilized to superheat the refrigerant that is leaving the evaporator.

Consequently, the temperature of the refrigerant that exits the gas cooler is effectively reduced. The subcooling process plays a vital role in optimizing the performance and efficiency of the refrigeration system. To visually illustrate the phenomenon of subcooling, a representation of the process (3-3') is presented in Fig. 3.

Currently, the management of high system pressures in CO<sub>2</sub> refrigeration cycles has become more manageable through effective regulation. The critical point of CO<sub>2</sub>, which occurs at 7.38 bar and 31°C, often necessitates the operation of refrigeration cycles in a transcritical mode. This is particularly prominent in automotive air-conditioning systems and supermarket refrigeration systems that operate in environments with high ambient temperatures. In such systems, the evaporation process occurs at pressures and temperatures below the critical point, referred to as subcritical conditions, while heat rejection takes place at pressures and temperatures above the critical point, known as supercritical conditions. Fig. 3(A) presents the transcritical system configuration that includes superheating, as depicted by the process (1-1') shown in the figure. On the other hand, Fig. 3(B) showcases the transcritical system with both superheating and subcooling, with the process (3-3') representing the subcooling in the figure.

This paper focuses on using carbon dioxide as the refrigerant and examines subcritical and transcritical cycles with subcooling and superheating in great detail. A thorough understanding of these cycles, their performance traits, and their applicability for various applications are the goals of

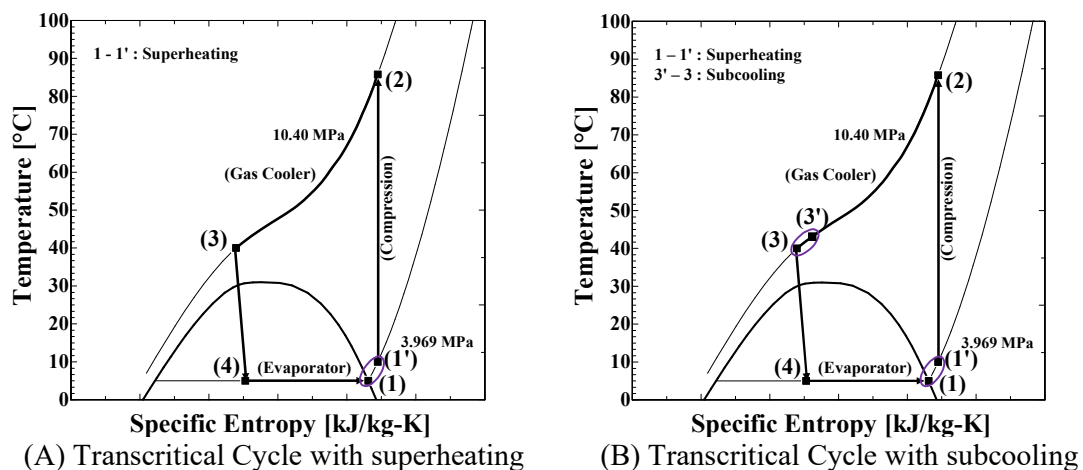


Fig. 3: CO<sub>2</sub> Transcritical refrigeration cycles on T-S diagrams.

the analysis. These cycles are used in a range of cooling applications, including small-scale industrial processes and home freezers. The intended temperature range, needed energy efficiency levels, and environmental concerns all play a role in which the cycle is selected.

This study's analysis includes a thorough assessment of the thermodynamic efficiency of subcritical and transcritical cycles with superheating and subcooling using an internal heat exchanger. Considerations are made for variables such as system complexity, cooling capacity, pressure effect, and energy efficiency. When employing CO<sub>2</sub> as the refrigerant, the researchers want to be able to determine the benefits and drawbacks of each cycle.

### Data Reduction

This study's major goal was to evaluate the effectiveness of transcritical refrigeration systems with subcooling and superheating. Determining the rate at which heat is removed from the refrigerated room, which is described by equation (1), was a significant component of the investigation. It was supposed that all of the refrigerant that leaves the evaporator is vapor.

$$Q_{evp} = h_1 - h_4 \quad \dots(1)$$

The heat exchanger plays a pivotal role in elevating the temperature of the refrigerant after its evaporation process. This augmentation in temperature beyond the point of saturated vapor is commonly referred to as the degree of superheat.

Entropy at the compressor's input and exit is assumed to be constant in this analysis under the assumption that the compressor is isentropic. The analysis and calculations can be made simpler due to this supposition. The compressor work without superheating, a crucial factor in evaluating the performance of the refrigeration system, is calculated using equation (2). The calculation of compressor work following the superheating of the refrigerant is determined utilizing equation (3).

$$\text{Without superheat} \quad W_c = h_2 - h_1 \quad \dots(2)$$

$$\text{With superheat} \quad W_c = h_2 - h_1' \quad \dots(3)$$

The quantity of heat rejected by the heat exchanger, sometimes referred to as the gas cooler, is calculated using equation (4).

$$Q_{amb} = h_2 - h_3 \quad \dots(4)$$

A refrigeration system's COP is greatly influenced by equation (5). The system's effectiveness at converting energy input into practical cooling output is determined by the COP. Equation (4) can be used to calculate the COP based on the ratio of the intended cooling effect (heat removed from the

refrigerated space) to the energy input (compressor effort).

$$COP = Q_{evp} / W_c \quad \dots(5)$$

The degree of superheating is calculated using equation (6)

$$\text{Degree of superheat} = T_{1'} - T_1 \quad \dots(6)$$

The degree of subcooling is calculated using equation (7)

$$\text{Degree of subcooling} = T_{3'} - T_3 \quad \dots(7)$$

In the refrigeration system, the refrigerant is assumed to undergo subcooling by superheating it after the evaporator, resulting in a reduction of its temperature. The heat that is lost by the refrigerant after passing through the gas cooler is then gained by the refrigerant coming out from the evaporator. The degree of subcooling can be determined by utilizing equation (8), which takes into account the degree of superheating. In this equation,  $C_{p,H}$  represents the specific heat at higher pressure, while  $C_{p,L}$  represents the specific heat at the evaporator pressure, which is the lower pressure in this context. For this analysis, a mass flow rate of 1 (unity) is considered.

$$C_{p,H}(T_{3'} - T_3) = C_{p,L}(T_{1'} - T_1) \quad \dots(8)$$

The higher pressure ( $P_2$ ), which corresponds to the refrigerant pressure after compression, is determined based on the ambient temperature. The optimal value for the higher pressure (MPa) is calculated as 0.26 multiplied by the ambient temperature ( $T_{amb}$ ) in degrees Celsius (Kauf 1999).

To make the analysis of the refrigeration system simpler, certain assumptions are used in this study. The gas cooler's pressure drop is regarded as insignificant, which reduces how much it affects system performance. The expansion process in the ejector is also thought to be isenthalpic, which implies that there is no enthalpy change. These presumptions make the study simpler by assuming that losses and energy changes during expansion are eliminated.

## RESULTS AND DISCUSSION

The study sheds light on how refrigeration systems function under various circumstances by analyzing the performance and behavior of these systems. In particular, it looks into the COP and how different operational factors affect it in subcritical and transcritical refrigeration systems with superheating and subcooling. The study improves our comprehension of system performance by examining the effects of variables like pressure, evaporator temperature, and ambient temperature on COP. The results and discussions offer insightful information for supporting energy conservation, increasing system performance, and enhancing efficiency in transcritical refrigeration systems.

### Effect of Evaporator Temperature on COP of Subcritical CO<sub>2</sub> Refrigeration System at Constant Higher Pressure

In Fig. 4, the link between evaporator temperature and COP is shown, highlighting significant results. The findings provide important light on how fluctuations in evaporator temperature affect the energy efficiency of the subcritical refrigeration system. This information helps with system optimization and encourages energy efficiency. By illuminating the system's behavior under various operating circumstances, the research helps us get a greater knowledge of how well it performs. In the research, the compressor's output pressure is referred to as "higher pressure" ( $P_2$ ).

The main objective of the inquiry is to determine how the COP in a subcritical refrigeration system is impacted by the evaporator temperature. While the evaporator temperature is adjusted between  $-5^{\circ}\text{C}$  and  $12^{\circ}\text{C}$ , three constant high pressures, i.e., 6 MPa, 6.5 MPa, and 7 MPa, are taken into consideration. The findings show a clear relationship between evaporator temperature and COP, with higher temperatures translating into greater COP numbers. The greater temperature difference between the evaporator and its surroundings, which improves heat transfer and increases refrigeration capacity, is the likely cause of this link. By requiring less compression work, lower compressor pressures also help increase COP values. Notably, the study finds that the COP increases more significantly at 6 MPa as a result of the interaction between lower compressor pressures and higher evaporator temperatures. The diminishing returns and limited gains in heat transfer at higher pressures, on the other hand, may be the cause of the COP increment being less noticeable at 7 MPa.

A greater COP is related to a higher evaporator temperature in a refrigeration system. This is because there

is less temperature disparity, which lowers heat transfer losses and boosts system effectiveness. A higher COP is also the result of higher evaporator temperatures because they necessitate less compression effort and permit greater refrigeration capacity. To maximize system effectiveness and achieve a higher COP, evaporator temperature optimization is essential.

### Effect of Superheating after Evaporator and Subcooling after Gas Cooler on COP

The objective is to examine the impact of the degree of superheat on the COP in a transcritical refrigeration system with a fixed high pressure. By investigating this relationship, the research aims to gain a better understanding of how varying degrees of superheat influence the system's energy efficiency. The determination of the optimal high pressure after the compressor is investigated by Kauf (Kauf 1999), providing insight into the appropriate operating conditions for the system. In Fig. 5(A), the link between the degree of superheating and COP is shown, highlighting significant results. The findings provide important light on how variations in the degree of superheat affect the energy efficiency of the transcritical CO<sub>2</sub> refrigeration system. The subcooling is not considered for this analysis in Fig. 5(A). This information helps with system optimization and energy efficiency while using the system with superheating. By illuminating the system's behavior under various operating circumstances, the research would help to get a greater knowledge of how well it performs.

Fig. 5(B) presents a comparison between the degree of superheating and subcooling and their respective impacts on the COP. These findings contribute valuable insights into the influence of variations in the degree of superheat on the energy efficiency of transcritical CO<sub>2</sub> refrigeration

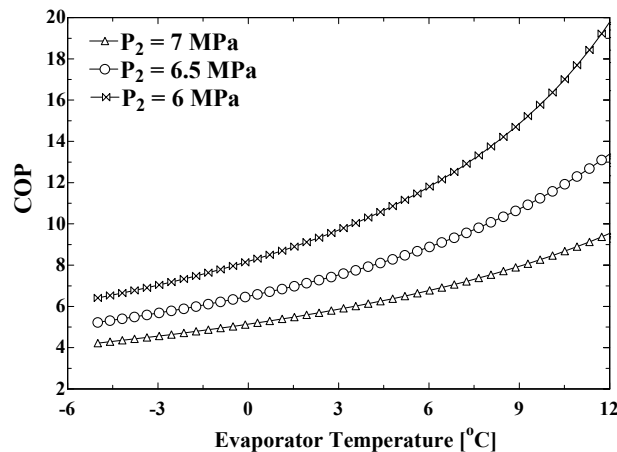


Fig. 4: Effect of evaporator temperature on COP of subcritical CO<sub>2</sub> refrigeration system.

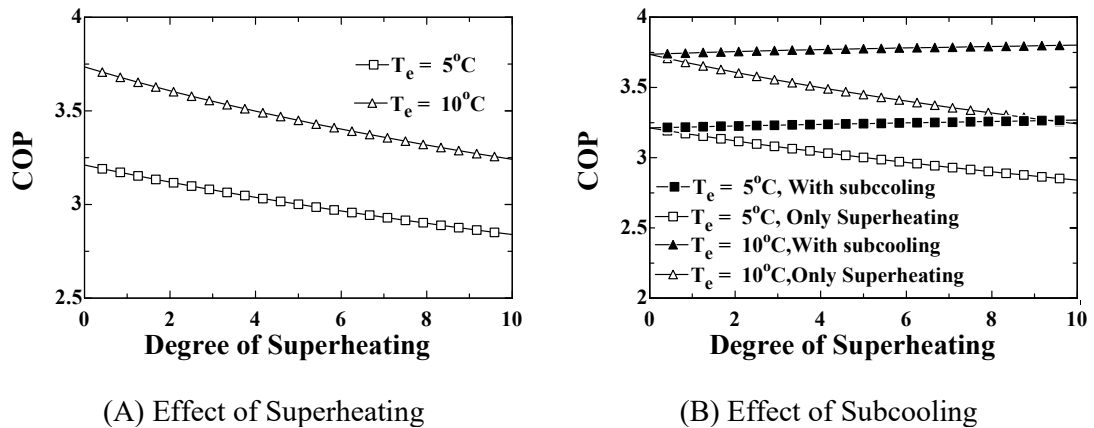


Fig. 5: Effect of superheating and subcooling on COP and compressor work.

systems, particularly in relation to the subcooling process. By examining the system's behavior under different subcooling and superheating conditions, this research enhances our understanding of its performance characteristics.

The primary aim of this investigation is to assess the impact of evaporator temperature resulting from superheating on the COP in a transcritical refrigeration system. By gradually increasing the evaporator temperature after reaching saturated vapor, the effects on COP are examined. The evaporator temperature is adjusted at two specific values, namely  $5^\circ\text{C}$  and  $10^\circ\text{C}$ , to obtain the corresponding results. To investigate the relationship between superheating and COP, the degree of superheating after the evaporator temperature is varied from 0 to 10. Additionally, the higher pressure maintained throughout this simulation is 10.4 MPa, while the ambient temperature remains constant at  $40^\circ\text{C}$ .

The results reveal a distinct correlation between the degree of superheat and the coefficient of performance (COP), indicating that higher temperatures lead to lower COP values. Particularly noteworthy is the finding that the COP experiences a more pronounced reduction with an increase in the degree of superheat. Comparing identical boundary conditions, the COP is higher at a  $10^\circ\text{C}$  evaporator temperature than at a  $5^\circ\text{C}$  evaporator temperature. Fig. 5(A) further illustrates that superheating is not recommended for use in  $\text{CO}_2$  refrigeration systems.

Fig. 5(B) displays the impact of subcooling in the  $\text{CO}_2$  refrigeration system. Subcooling significantly affects the coefficient of performance of the system, with COP increasing as the degree of subcooling increases. The degree of subcooling also influences the degree of superheating. Greater subcooling results in higher degrees of superheating. The heat released during subcooling is subsequently absorbed by the refrigerant during superheating.

The findings in Fig. 5(B) indicate that the COP increases with an increase in superheating at both  $5^\circ\text{C}$  and  $10^\circ\text{C}$  of subcooling. However, it is important to note that superheating is only advisable when used in conjunction with subcooling of the refrigerant. This relationship between subcooling and superheating plays a crucial role in optimizing the system's performance and efficiency in  $\text{CO}_2$  refrigeration systems.

### Gas Cooler Subcooling Effects on Evaporator Inlet Vapor Quality

The degree of subcooling is dependent on the degree of superheating, as illustrated in Fig. 6. Increasing the degree of superheating influences the degree of subcooling, and this relationship is analyzed. The investigation is conducted under a constant ambient temperature of  $40^\circ\text{C}$ .

At a constant evaporator temperature of  $5^\circ\text{C}$ , when the degree of superheating increases from 0 to  $10^\circ\text{C}$ , the degree of subcooling also increases from 0 to  $4.284^\circ\text{C}$ , as depicted in Fig. 6. As a result of this increase in subcooling, the vapor quality at the evaporator inlet decreases from 0.4426 to 0.3585. This reduction in vapor quality has a positive impact on the performance of the refrigeration system, as a lower inlet vapor quality leads to a higher refrigeration effect, thus improving the COP.

Similarly, at a constant evaporator temperature of  $10^\circ\text{C}$ , an increase in the degree of superheating from 0 to  $10^\circ\text{C}$  results in an increase in the degree of subcooling from 0 to  $4.781^\circ\text{C}$ , as shown in Fig. 5. Consequently, the vapor quality at the evaporator inlet decreases from 0.4155 to 0.3144. This decline in vapor quality again leads to an improvement in the performance of the refrigeration system, enhancing the COP. Overall, the findings from Fig. 6 demonstrate the interplay between the degree of superheating and subcooling and their effects on the refrigeration system's performance, ultimately positively influencing the COP.



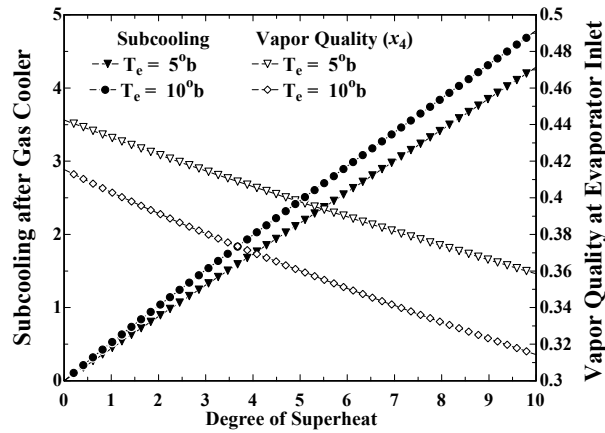
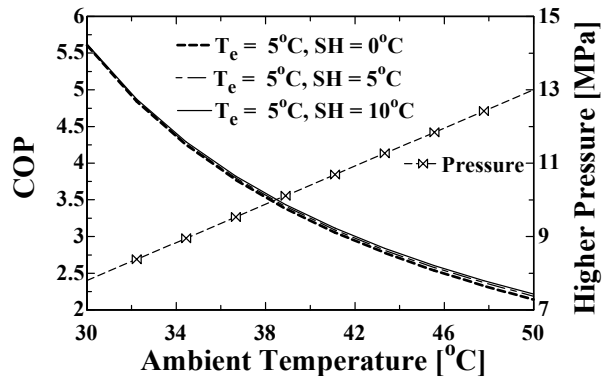


Fig. 6: Effect of subcooling on evaporator inlet and gas cooler temperature.

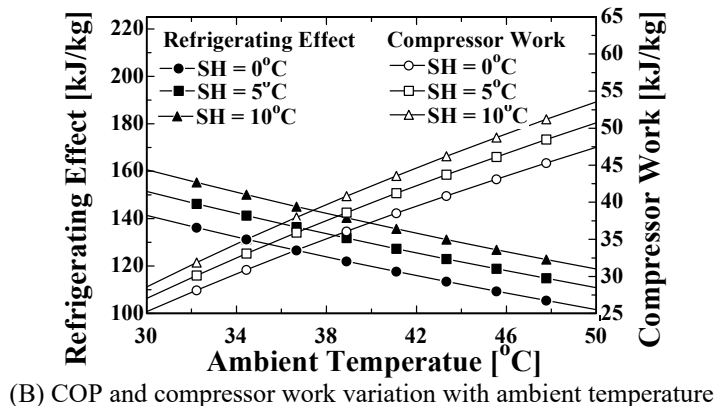
### Effect of Ambient Temperature on the COP of Refrigeration System with Subcooling

Fig. 7 presents an investigation into the combined effect of ambient temperature and degree of subcooling. The ambient temperature is varied from 30 to 50°C to observe its impact. For this analysis, a constant evaporator temperature of 5°C

is maintained, and three different degrees of superheating, namely 0°C, 5°C, and 10°C, are considered. The system's optimum pressure is determined based on the ambient temperature. Understanding the relationship between ambient temperature and the coefficient of performance is essential for optimizing energy efficiency and overall system performance in transcritical refrigeration systems.



(A) COP and pressure variation with ambient temperature



(B) COP and compressor work variation with ambient temperature

Fig. 7: Effect of ambient temperature on COP with superheating.

Engineers can make informed decisions regarding energy efficiency improvements and energy consumption reductions based on this understanding. Moreover, the refrigeration system's capability is significantly influenced by the ambient temperature.

In Fig. 7(A), the optimal higher pressure ( $P_2$ ) is displayed on the secondary y-axis, which is selected based on the surrounding temperature range from 30°C to 50°C. The primary y-axis shows the resulting COP values, providing valuable information on the connection between system performance and ambient temperature.

The results from Fig. 7(A) reveal that the COP of the transcritical refrigeration system decreases as the ambient temperature rises. Without superheating, the COP varies from 5.605 to 2.14 when the ambient temperature is changed from 30°C to 50°C. Concurrently, the compressor work increases from 25.22 to 47.44 kJ.kg<sup>-1</sup> under the same ambient temperature range. With 5°C of superheating, the COP changes from 5.609 to 2.186 as the ambient temperature varies from 30°C to 50°C. The compressor work increases from 27.01 to 50.71 kJ.kg<sup>-1</sup> during this temperature change. Similarly, with 10°C of superheating, the COP varies from 5.623 to 2.216 when the ambient temperature is changed from 30°C to 50°C. The compressor work increases from 28.57 to 53.57 kJ.kg<sup>-1</sup> for the same range of ambient temperatures.

Fig. 7(B) provides an analysis of the refrigerating effect and compressor work in response to changes in ambient temperature. The refrigerating effect varies from 141.4 kJ.kg<sup>-1</sup> to 101.6 kJ.kg<sup>-1</sup> when the ambient temperature is varied from 30°C to 50°C without superheating. With 5°C of superheating, the refrigerating effect ranges from 151.5 kJ.kg<sup>-1</sup> to 110.9 kJ.kg<sup>-1</sup> for the same variation in ambient temperature. Additionally, with 10°C of superheating, the refrigerating effect varies from 160.6 kJ.kg<sup>-1</sup> to 118.7 kJ.kg<sup>-1</sup> as the ambient temperature is changed from 30°C to 50°C. It

is important to note that the evaporator temperature for this analysis is maintained at 5°C.

Furthermore, it is observed from Fig. 6 and Fig. 7 that the COP decreases as the ambient temperature increases. However, there is only a minimal increase in COP at 10°C superheating. These findings provide valuable insights into the impact of ambient temperature and superheating on the performance of the refrigeration system. There are many reasons for the decrease in COP with rising ambient temperature observed in Fig. 7. First of all, greater ambient temperatures result in a smaller temperature difference between the condenser and the environment, which reduces heat rejection and lowers system efficiency. As a result, the system is less able to effectively remove heat. Second, greater ambient temperatures put the compressor under more strain, which raises energy costs and lowers COP. Increased system losses and decreased refrigeration capacity may also result from higher ambient temperatures. These elements work together to explain the transcritical refrigeration system's reported decline in COP with rising ambient temperature.

#### Effect of Evaporator Temperature on COP with Subcooling

Fig. 8 provides an analysis of the effect of evaporator temperature with superheating in a transcritical refrigeration system. The evaporator temperature is varied from 0 to 10°C to observe its impact on the coefficient of performance. Three different degrees of superheating, namely 0°C, 5°C, and 10°C, are considered for this analysis, with the ambient temperature set at 40°C.

Optimizing energy efficiency and overall system performance requires a thorough investigation into how the evaporator temperature affects the COP in a transcritical refrigeration system. Additionally, the refrigeration system's capacity is significantly influenced by the evaporator temperature.

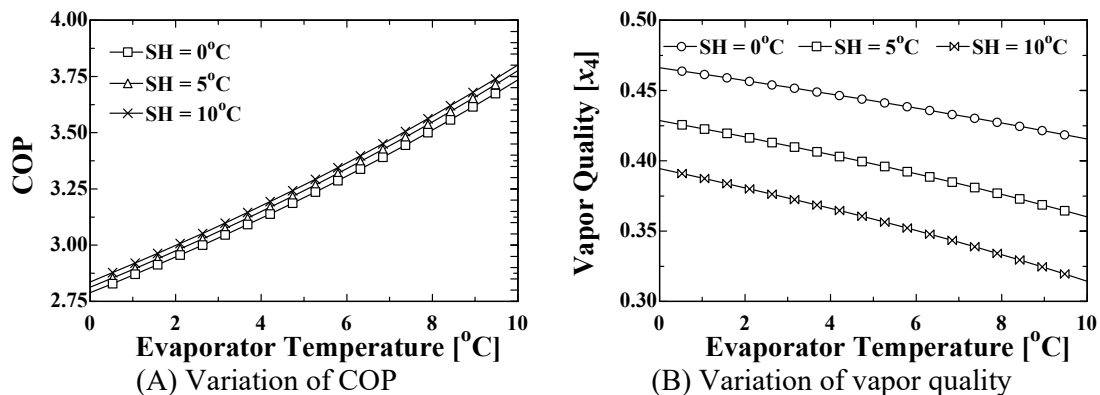


Fig. 8: Effect of evaporator temperature on COP with subcooling.

In Fig. 8(A), it is evident that the transcritical refrigeration system's COP increases with an increase in the evaporator temperature. Moreover, the COP shows a consistent rise with the increase in superheating. Notably, at 10°C of superheating, the COP is higher at higher evaporator temperatures. Specifically, the COP varies from 2.789 to 3.735 when the evaporator temperature is changed from 0 to 10°C without superheating. With 5°C of superheating, the COP ranges from 2.814 to 3.776 for the same range of evaporator temperatures. Furthermore, with 10°C of superheating, the COP varies from 2.837 to 3.801 as the evaporator temperature is changed from 0 to 10°C.

In Fig. 8(B), the inlet vapor quality at the evaporator is presented for the variation of evaporator temperature from 0 to 10°C. Without superheating, the inlet vapor quality at the evaporator varies from 0.4662 to 0.4155 as the evaporator temperature changes from 0 to 10°C. With 5°C of superheating, the inlet vapor quality at the evaporator ranges from 0.4287 to 0.3601 for the same range of evaporator temperatures. Similarly, with 10°C of superheating, the inlet vapor quality at the evaporator varies from 0.3944 to 0.3144 as the evaporator temperature is changed from 0 to 10°C.

The findings from Fig. 8 indicate that the COP is higher at higher evaporator temperatures and increases with the increase in the degree of superheating. Additionally, the inlet vapor quality at the evaporator is decreased due to subcooling. Increasing the evaporator temperature results in a larger temperature difference between the evaporator and the surroundings, leading to improved heat transfer rates and increased refrigeration capacity. These observations offer valuable insights into the factors affecting the performance and efficiency of the transcritical refrigeration system.

### Effect of Higher Pressure on COP of Transcritical Refrigeration System

Fig. 9(A) shows how increased pressure affects a transcritical refrigeration system's COP at constant evaporator temperatures. The study's goal was to evaluate the impact of various higher pressures ( $P_2$ ) on the system's COP. At constant evaporator temperatures of 10°C and 15°C, the ideal higher pressure of a transcritical refrigeration system is examined. There are three different ambient temperatures: 35°C, 40°C, and 45°C. The ideal higher pressure is determined by the maximal COP at various higher pressures.

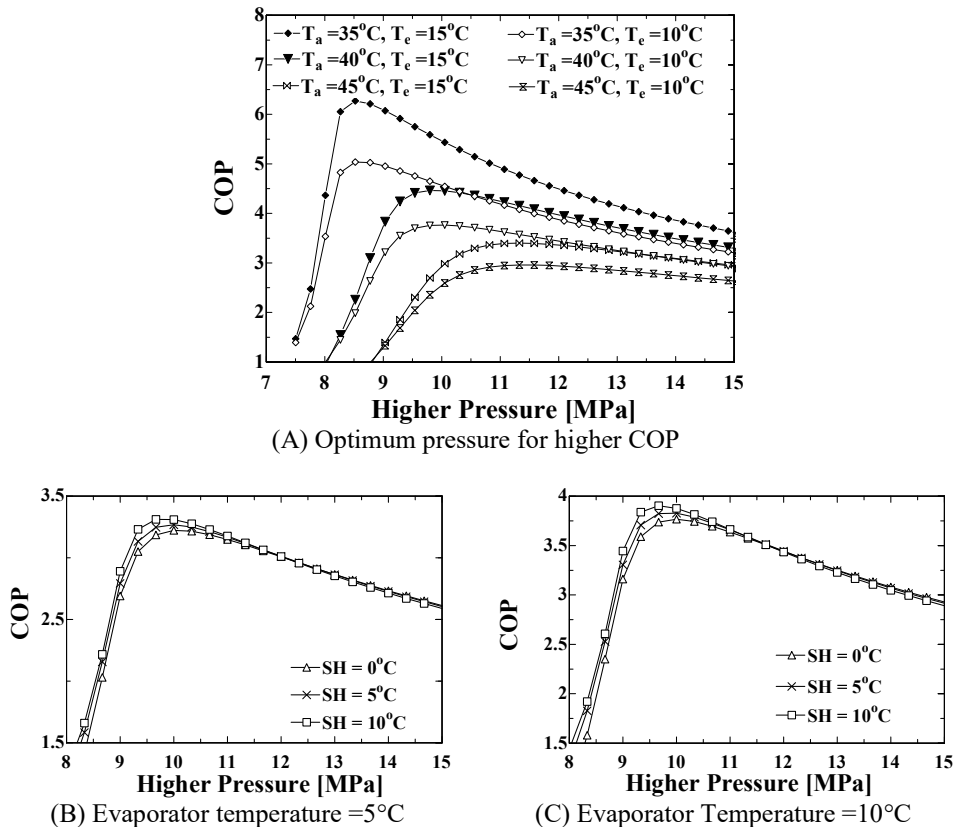


Fig. 9: Effect of compressor pressure on COP.

The ideal higher pressure at 35°C ambient temperature is 8.52MPa at both the 10°C and 15°C evaporator temperatures. The ideal higher pressure for both evaporator temperatures is 9.8MPa at 40°C ambient temperature. The ideal higher pressure at both evaporator temperatures is 11.33MPa at 45°C ambient temperature.

An ambient temperature of 35°C produced an ideal higher pressure of 8.52 MPa for both evaporator temperatures. Similar to this, at 40°C and 45°C, respectively, the optimal higher pressure was 9.8 MPa and 11.33 MPa. Lower evaporator temperatures result in decreased heat transfer rates and refrigeration capacity, which lowers COP. The smaller temperature differential has an impact on the system's capacity to extract heat.

Fig. 9 presents the effect of increased pressure on the coefficient of performance of a transcritical refrigeration system with superheating while keeping the evaporator temperatures constant. The primary goal of this study was to assess the influence of various higher pressures ( $P_2$ ) on the system's COP. For this analysis, constant evaporator temperatures of 5°C and 10°C were considered, with an ambient temperature of 40°C. Three different degrees of superheating, namely 0°C, 5°C, and 10°C, were also taken into account. The ideal higher pressure ( $P_2$ ) was determined by identifying the maximum COP at various higher pressures.

In Fig. 9(B), the ideal higher pressure values for a 5°C evaporator temperature are 3.233 MPa, 3.249 MPa, and 3.268 MPa for superheating values of 0°C, 5°C, and 10°C, respectively. Similarly, in Fig. 9(C), the ideal higher pressure values for a 10°C evaporator temperature are 3.766 MPa, 3.827 MPa, and 3.904 MPa for the same superheating values.

One important observation from Fig. 9 is that the optimum higher pressure is dependent on ambient temperature. However, evaporator temperature and superheating do not have a significant effect on the optimum higher pressure. Lower evaporator temperatures lead to decreased heat transfer rates and refrigeration capacity, which subsequently lower the COP. The reduced temperature differential affects the system's ability to extract heat effectively. Additionally, the compressor experiences higher stress in lower temperatures, resulting in increased energy consumption and decreased performance. System losses also increase at lower evaporator temperatures, further reducing the COP. These factors collectively explain why the COP decreases with decreasing evaporator temperature.

## CONCLUSION

This study provides a comprehensive analysis of subcritical and transcritical refrigeration systems using CO<sub>2</sub> as the refrigerant, with a primary focus on the coefficient of performance and its

relationship with various operating parameters. The effects of subcooling and superheating on the COP have been thoroughly investigated. Understanding the interplay between the COP and operating parameters, such as subcooling, superheating, ambient temperature, and evaporator temperature, is critical in optimizing the performance and energy efficiency of CO<sub>2</sub> refrigeration systems.

The findings underscore that superheating is not advisable for CO<sub>2</sub> refrigeration systems. Conversely, the COP experiences a significant increase with greater degrees of subcooling. Subcooling results in a decrease in vapor quality, leading to enhanced system performance and an elevated COP.

Furthermore, as the ambient temperature rises, the COP decreases, with only minimal improvements observed at 10°C superheating. Higher evaporator temperatures correspond to higher COP values, and the COP further increases with increasing degrees of superheating. Additionally, subcooling reduces the inlet vapor quality at the evaporator. The study also highlights that the optimum higher pressure depends on ambient temperature, while evaporator temperature and superheating have negligible effects on the optimal higher pressure.

## NOMENCLATURE

### Definitions

$T$	Temperature [°C]
$C_p$	Specific heat [J.kgK <sup>-1</sup> ]
$Q_{amb}$	Heat transfer to ambient [kW]
$Q_{evap}$	Evaporator heat [kW]
$W_c$	Compressor work [kJ.kg <sup>-1</sup> ]
$h$	Enthalpy [kJ.kg <sup>-1</sup> ]
$P$	Pressure [MPa]

### Abbreviations

CO <sub>2</sub>	Carbon Dioxide
COP	Coefficient of Performance
ODP	Ozone Depleting Potential
GWP	Global Warming Potential
THE	Internal Heat Exchanger
DEC	Dual Expansion Cycle

### Subscripts

$L$	Lower (Evaporator)
$H$	Higher (Condenser)
$c$	Compressor
$amb$	Ambient
$evp$	Evaporator

## REFERENCES

- Bolaji, B.O. and Huan, Z., 2013. Ozone depletion and global warming: The case for the use of natural refrigerant – a review. *Renewable and Sustainable Energy Reviews*, 18, pp.49–54. <https://doi.org/10.1016/j.rser.2012.10.008>
- Bose, A. and Saini, D.K., 2022. Biomass-fired thermal power generation technology - a route to meet growing energy demand and sustainable development. *Nature Environment and Pollution Technology*, 21(3), pp.1307–1315. <https://doi.org/10.46488/nept.2022.v21i03.037>
- Brown, M., Rosario, L. and Rahman, M.M., 2008. Thermodynamic analysis of transcritical carbon dioxide cycles. *ASME International Mechanical Engineering Congress and Exposition (AES) Conf. Proc.*, 45, pp.59–70. <https://doi.org/10.1115/imece2005-82097>
- Ciconkov, R., 2018. Refrigerants: there is still no vision for sustainable solutions. *International Journal of Refrigeration*, 86, pp.441–448. <https://doi.org/10.1016/j.ijrefrig.2017.12.006>
- Getu, H.M. and Bansal, P.K., 2008. Thermodynamic analysis of an R744–R717 cascade refrigeration system. *International Journal of Refrigeration*, 31(1), pp.45–54. <https://doi.org/10.1016/j.ijrefrig.2007.06.014>
- Javadpour, S.M., Naserian, M.M. and Ashkezari, A.Z., 2023. A new multi-objective optimization of refrigeration cycles (case study: 'optimization of transcritical carbon dioxide cycle'). *Environmental Progress & Sustainable Energy*, 43(1), p.e14284. <https://doi.org/10.1002/EP.14284>
- Kauf, F., 1999. Determination of the optimum high pressure for transcritical CO<sub>2</sub>-refrigeration cycles. *International Journal of Thermal Sciences*, 38(4), pp.325–330. [https://doi.org/10.1016/S1290-0729\(99\)80098-2](https://doi.org/10.1016/S1290-0729(99)80098-2)
- Kim, M.H., Pettersen, J. and Bullard, C.W., 2004. Fundamental process and system design issues in CO<sub>2</sub> vapor compression systems. *Progress in Energy and Combustion Science*, 30(2), pp.119–174. <https://doi.org/10.1016/J.PECS.2003.09.002>
- Lorentzen, G. and Pettersen, J., 1993. A new, efficient, and environmentally benign system for car air-conditioning. *International Journal of Refrigeration*, 16(1), pp.4–12. [https://doi.org/10.1016/0140-7007\(93\)90014-Y](https://doi.org/10.1016/0140-7007(93)90014-Y)
- Manjili, F.E. and Yavari, M.A., 2012. Performance of a new two-stage multi-intercooling transcritical CO<sub>2</sub> ejector refrigeration cycle. *Applied Thermal Engineering*, 40, pp.202–209. <https://doi.org/10.1016/j.applthermaleng.2012.02.014>
- Molina, M.J. and Rowland, F.S., 1974. Stratospheric sink for chlorofluoromethanes: chlorine atomic-catalyzed destruction of ozone. *Nature*, 249, pp.810–812. <https://doi.org/10.1038/249810A0>
- Perez-Garcia, V., Belman-Flores, J.M., Navarro-Esbrí, J. and Rubio-Maya, C., 2013. Comparative study of transcritical vapor compression configurations using CO<sub>2</sub> as refrigeration mode based on simulation. *Applied Thermal Engineering*, 51, pp.1038–1046. <https://doi.org/10.1016/j.applthermaleng.2012.10.018>
- Prabakaran, R., Lal, D.M. and Kim, S.C., 2022. A state-of-the-art review on future low global warming potential refrigerants and performance augmentation methods for vapor compression-based mobile air conditioning system. *Journal of Thermal Analysis and Calorimetry*, 148(2), pp.417–449. <https://doi.org/10.1007/S10973-022-11485-3>
- Riffat, S.B., Afonso, C.F., Oliveira, A.C. and Reay, D.A., 1997. Natural refrigerants for refrigeration and air-conditioning systems. *Applied Thermal Engineering*, 17(1), pp.33–42. [https://doi.org/10.1016/1359-4311\(96\)00030-0](https://doi.org/10.1016/1359-4311(96)00030-0)
- Shirmohammadi, R., Soltanieh, M. and Romeo, L.M., 2018. Thermoeconomic analysis and optimization of post-combustion CO<sub>2</sub> recovery unit utilizing absorption refrigeration system for a natural-gas-fired power plant. *Environmental Progress & Sustainable Energy*, 37(3), pp.1075–1084. <https://doi.org/10.1002/EP.12866>
- Silva, A.D., Filho, E.P.B. and Antunes, A.H.P., 2012. Comparison of an R744 cascade refrigeration system with R404A and R22 conventional systems for supermarkets. *Applied Thermal Engineering*, 41, pp.30–35. <https://doi.org/10.1016/j.applthermaleng.2011.12.019>
- Singh, S., Purohit, N. and Dasgupta, M.S., 2016. Comparative study of cycle modification strategies for trans-critical CO<sub>2</sub> refrigeration cycle for warm climatic conditions. *Case Studies in Thermal Engineering*, 7, pp.78–91. <https://doi.org/10.1016/j.csite.2016.03.002>
- Sun, Z., Li, J., Liang, Y., Sun, H., Liu, S., Yang, L., Wang, C. and Dai, B., 2020. Performance assessment of CO<sub>2</sub> supermarket refrigeration system in different climate zones of China. *Energy Conversion and Management*, 208, 112572. <https://doi.org/10.1016/j.enconman.2020.112572>
- Yaakop, S.N., Fauadi, M.H.F. and Damanhuri, A.A.M., 2023. Experimental study on heat recovery of air dryer from waste heat energy of condensing unit from VCRS air conditioner. *Nature Environment and Pollution Technology*, 22(1), pp.149–157. <https://doi.org/10.46488/nept.2023.v22i01.013>
- Yuan, J., Wu, C., Xu, X. and Liu, C., 2021. Multi-mode analysis and comparison of four different carbon dioxide-based combined cooling and power cycles for the distributed energy system. *Energy Conversion and Management*, 244, 114476. <https://doi.org/10.1016/j.enconman.2021.114476>
- Zhang, Z., Tong, L. and Wang, X., 2015. Thermodynamic analysis of double-stage compression transcritical CO<sub>2</sub> refrigeration cycles with an expander. *Entropy*, 17(4), pp.2544–2555. <https://doi.org/10.3390/e17042544>

## ORCID DETAILS OF THE AUTHORS

Manish Hassani: <https://orcid.org/0009-0000-1830-7172>





# Enhancing Smart Grids for Sustainable Energy Transition and Emission Reduction with Advanced Forecasting Techniques

Farah Rania<sup>†</sup>, Farou Brahim, Kouahla Zineddine and Seridi Hamid

Department of Computer Science, LabStic Laboratory, University 8 Mai 1945, Guelma, 24000, Algeria

<sup>†</sup>Corresponding author: Farah Rania; farah.rania@univ-guelma.dz

Nat. Env. & Poll. Tech.  
Website: [www.neptjournal.com](http://www.neptjournal.com)

Received: 07-02-2024

Revised: 13-03-2024

Accepted: 10-04-2024

## Key Words:

Smart grid  
Short-term load forecasting  
Carbon dioxide  
Electrical consumption  
Deep learning model  
Harmful energy

## ABSTRACT

Smart grids are modernized, intelligent electricity distribution systems that integrate information and communication technologies to improve the efficiency, reliability, and sustainability of the electricity network. However, existing smart grids only integrate renewable energies when it comes to active demand management without taking into consideration the reduction of greenhouse gas emissions. This paper addresses this problem by forecasting CO<sub>2</sub> emissions based on electricity consumption, making it possible to transition to renewable energies and thereby reduce CO<sub>2</sub> emissions generated by fossil fuels. This approach contributes to the mitigation of climate change and the preservation of air quality, both of which are essential for a healthy and sustainable environment. To achieve this goal, we propose a transformer-based encoder architecture for load forecasting by modifying the transformer workflow and designing a novel technique for handling contextual features. The proposed solution is tested on real electricity consumption data over a long period. Results show that the proposed approach successfully handles time series data to detect future CO<sub>2</sub> emissions excess and outperforms state-of-the-art techniques.

## INTRODUCTION

The load demand for electrical energy is gradually increasing as the number of Electrical appliances in different fields such as Heating, lighting, washing, and many more vital daily life activities is rising (Hernandez et al. 2014). However, the misuse of this energy resource makes it a double-edged sword. How people generate electricity is a crucial issue at a time when environmental issues and the struggle against climate change are taking on more and more importance in our daily lives (Harper & Snowden 2017). Many countries, such as the United States, China, and Russia, rely heavily on fossil fuels for electricity generation, mainly due to the availability of fossil resources on their territory and the existing capacity of their power stations (Schulz & AQAL Group 2019). Power generation from fossil fuels such as natural gas or coal has long been an important source of energy but is now coming under scrutiny due to its environmental implications (Zou et al. 2016). It is essential to keep in mind that although this method of generating electricity from natural gas is efficient in terms of energy output, it still has a major negative impact on the environment and significantly increases carbon dioxide (CO<sub>2</sub>) emissions, which are one of the main causes of global environmental problems. Rising sea levels, more extreme weather

conditions, and the devastation of ecosystems are just some of the effects of climate change caused by CO<sub>2</sub> emissions related to electricity generation (Slingo & Slingo 2024). In addition to CO<sub>2</sub>, the combustion of fossil fuels releases other atmospheric pollutants such as nitrogen oxides (NO<sub>x</sub>), sulfur dioxide (SO<sub>2</sub>), and fine particles. These pollutants have adverse effects on air quality and can cause serious health problems for local populations. The use of fossil fuels also leads to the destruction of ecosystems, deforestation, water pollution, and the disruption of biodiversity. Cooling fossil fuel power plants requires large quantities of water, which can lead to conflicts over water use and the disruption of aquatic ecosystems (Wu et al. 2023). Furthermore, in 2022, global CO<sub>2</sub> emissions from energy combustion and industrial processes reached a new historical record of 36.8 billion metric tons (Gt) (Wang & He 2023). This represents an increase of 0.9%, equivalent to 321 million metric tons (Mt) in the previous year (Scott et al. 2000).

Smart grids are an emerging technology aiming to optimize energy usage by enabling precise management of electricity production, distribution, and consumption. This can reduce energy losses and maximize system efficiency (Mishra & Singh 2023). Additionally, smart grids facilitate the efficient integration of renewable energy sources, such as

solar and wind, into the electricity grid (Kataray et al. 2023). However, existing smart grids transition to renewable energy to address fluctuations in demand, environmental constraints, and seasonal variations without adequately considering air pollution. Consequently, it has become essential to develop accurate forecasting systems to anticipate future demand and effectively manage these energies, ultimately leading to a reduction in CO<sub>2</sub> emissions.

This study presents a novel adaptation of the transformer architecture specifically tailored for load forecasting. The focus of this research is on improving forecast accuracy for real-time data streams by incorporating modifications to the encoder component. In contrast to many charge forecasting studies that assess proposed solutions based on short-term data, our investigation delves into the adaptability and performance of our solution across extended periods of data flow.

Introducing a 4-space transformation module with a revamped workflow, this approach aims to bolster the efficiency of load forecasting tasks. The evaluation of the proposed method utilizes real data streams, demonstrating that the adapted transformer consistently outperforms existing state-of-the-art methods.

## RELATED WORKS

Forecasting is a very important challenge for electricity providers and has received considerable attention in the existing literature. The ability to accurately forecast electricity demand is crucial for efficient resource planning, grid management, and ensuring a reliable and sustainable electricity supply, which automatically implies a reduction in CO<sub>2</sub> emissions in order to preserve society's health and its environment. By managing electricity demand more effectively, it is possible to reduce the use of fossil fuel power stations. This translates into lower CO<sub>2</sub> emissions, helping to fight climate change and its harmful effects. Many studies have focused on developing forecasting models and techniques specifically tailored to the unique characteristics of electricity consumption. These models have been developed to capture the complex and dynamic nature of electricity demand, taking into account factors such as temporal patterns, seasonality, weather conditions, economic indicators, and consumer behavior.

Researchers have used a wide range of approaches to forecast electricity demand, including statistical methods, machine learning algorithms, time series analysis, artificial neural networks, and hybrid models. These techniques continue to evolve and improve with advances in data availability, computing power, and predictive analysis. The studies on electricity demand forecasting offer valuable

perspectives, methodologies, and empirical results that help to understand the complexities of the problem. This knowledge forms the basis for the development of accurate and robust forecasting models, which support decision-making processes within the electricity industry.

Recent studies in electrical process management include several techniques in an attempt to analyze, understand, and predict electrical consumption, ranging from conventional ones such as CNN (Kim & Cho 2019), to statistical approaches to modern machine learning (Solyali 2020, Ahmad & Chen 2018) and deep learning methods [Bedi & Toshniwal 2019, Rahman et al. 2018] such as Long Short Term Memory (LSTM) based deep framework and deep Recurrent Neural Network (RNN). Process analysis, which is an evaluation of time series (Singh & Yassine 2018) by taking into account historical relationships between occurrences of electrical data, is used in a substantial part of the aforementioned methodologies.

The most traditional electrical consumption predictions are Artificial neural networks (ANN) (Deo & Şahin 2017, Jetcheva et al. 2014), which have determined that ANN is a high-performance model that generates good results in the case of energy prediction, whether for an entire region or a single building., Support vector machine (SVM) (Guo et al. 2006, Daut et al. 2017), which has proven its effectiveness in various fields, regression that offers a modeling of the relationships between the independent variables and the dependent variable (Yildiz et al. 2017, Kavousi-Fard et al. 2014), random forest (RF) known to reduce overfitting (Dudek 2015) that uses the seasonal cycles of time series to simplify the forecasting problem. The use of Convolution neural networks (CNN) architecture for their performance of feature extraction (Levi & Hassner 2015, He 2017) by using more than one feature to estimate electrical demand, including temperature (Deo & Şahin 2017), weather (Chow & Leung 1996), and many other exogenous variables (Jetcheva et al.2014, Roldán-Blay et al. 2013). In the aforementioned related works, as well as the recent advancement architectures: Support vector regression with modified firefly algorithm (SVR-MFA) (Kavousi-Fard & Marzbani 2014) and Support vector regression (SVR) combined with swarm optimization algorithms (SVR-PSO) (Jiang et al. 2016). In various traditional modeling approaches, the processing analysis of input data is handled independently, without taking into account the temporal nature of the data. This implies that each data point is used as separate information, regardless of its relationship to all the other occurrences of the data. However, considering time-series data, as in this paper, energy consumption, the temporal aspect plays a crucial role. Values are interdependent, interconnected, and influenced by previous or subsequent



ones. The most important information to use are patterns, trends, and dependencies, which are essential for an accurate analysis and prediction.

To address this issue, (RNN) (Huang et al. 2021, Elsaraiti & Merabet 2021) and (LSTM) architecture can catch temporal dependencies in energy consumption data (Memarzadeh & Keynia 2021, Le et al. 2019) are frequently employed in the prediction of nonlinear time series as a neural network that integrates time dependency, and their usefulness has been demonstrated in the field of building energy consumption. The use of RNN in the field of building energy consumption prediction has been expanded to more complex LSTM (Chen et al. 2018) and generative adversarial networks (GAN) which are an advanced deep learning method (Zhang & Guo 2020). Baasch et al. (2021) and Bendaoud et al. (2021) demonstrated that GAN offers an innovative approach to electric charge prediction by generating new realistic electric charge time series and improving prediction despite their complexity. One way to explore the Attention Mechanism and Transformer Model power in comparison to the classic machine-learning (ML) approach is to identify the processing mode for previously known information and forecast future known or unknown information. Encoders and decoders are extensively employed in natural language processing and were originally utilized for sequence-to-sequence encoding and processing (Wu et al. 2021, Giuliani et al. 2021), with the use of historical data.

Traditionally, machine learning algorithms are the root of artificial intelligence techniques that have been used in electrical forecasting for decades, exploiting their capacity to capture complicated non-linear data correlations. The advancement of deep learning techniques is used to address a wide range of more complex applications, especially applied to electricity usage.

From these models, Recurrent neural networks (RNN), Long Short-Term Memory (LSTM), and Convolutional Neural Networks (CNN), in particular, have demonstrated their usefulness in dealing with time series (Fu et al. 2022).

Due to the irregular nature of the market, forecasting electricity consumption has shown to be a tricky task; it may be classified as a non-linear time series problem (Clements et al. 2004) since future values cannot be represented as linear combinations of previous ones. Several researchers employed statistical or machine learning-based time series forecasting models to anticipate the near future electrical load to solve this issue. However, extracting important features from the large quantities of data collected from different sources is a difficult task that remains largely unsolved. To this end, processing and analyzing these data represents a major

challenge that still requires significant advances to achieve complete resolution (Bello-Orgaz et al. 2016).

The most recent studies underline the need to accurately forecast energy demand, a key element in optimizing power grid management and reducing CO<sub>2</sub> emissions. This research takes place in a global context where the transition to renewable energies is becoming an imperative in the fight for a healthier environment.

ve in the fight for a healthier environment. Focusing on consumption forecasting, the researchers aim to facilitate the efficient integration of renewable energies, such as solar and wind power (Kamani & Ardehali 2023), into the power grid. To achieve their goals, various research projects have focused on the Internet of Things (IoT), and a number of studies have focused on connected sensors to observe load, temperature, humidity, or energy consumption in real-time. To observe changes and decide whether they should be shifted towards renewable energies (Raju & Laxmi 2020). Venkatesan et al. (2022) provided an effective solution for managing agricultural energy. The smart farm system described in this study is based on the ability to regulate the growing environment with sensors, which are designed to regulate their internal power levels according to the temperatures they observe. A prediction model based on the Internet of Things (IoT) and artificial intelligence (AI) to monitor IAQ in real time using CO<sub>2</sub> measurement data has been modeled (Zhu et al. 2022). It highlights the importance of monitoring indoor air quality (IAQ), particularly in response to the COVID-19 pandemic, as poor IAQ can have an impact on health.

This research will not only optimize the use of clean energy but also reduce CO<sub>2</sub> emissions into the air by comparing several ML approaches such as Transformer, CNN, LSTM, and RNN. A more precise and accurate prediction of electricity consumption will lead to a significant reduction in power losses, particularly by limiting the overproduction of electricity, which is the source of pollution due to CO<sub>2</sub> emissions. In addition, this prediction will alert us to consumption peaks before they occur, enabling us to switch quickly to renewable energies.

## PROPOSED APPROACH

This section is divided into two parts. First, the theoretical background was introduced, including numerous essential time-series concepts and the deep learning models used in this work. The proposed approach is then presented following the suggested transformer model validation technique.

### Theoretical Background

This section highlights the importance of deep learning in predicting power generation to reduce CO<sub>2</sub> emissions. Deep

learning neural networks, in particular the transformer, are proving effective in processing indexed temporal data. These networks are capable of learning complex correspondences between inputs and outputs and excel in the automatic processing of a wide range of temporal data. In the context of this study, the processor is considered a forecaster. Unlike traditional approaches such as CNN, RNN, and LSTM, which encounter difficulties in modeling complex long-term relationships in data sequences due to problems such as “gradient disappearance and explosion” in RNNs and the limitations of convolutional filters, the transformer offers a novel solution. It introduces a revolutionary model of long-term memory, as described in the article Attention Is All You Need (Vaswani et al. 2017). The practical application of this technology lies in the accurate prediction of electricity demand. Once the prediction reaches a certain threshold, the system automatically switches to using renewable energies rather than more polluting sources such as gas for power generation. This proactive strategy optimizes the use of renewable energies and significantly reduces CO<sub>2</sub> emissions, thus contributing to a more sustainable and environmentally friendly transition in the power generation sector. In a nutshell, transformers represent a cutting-edge approach to Natural Language Processing (NLP). They leverage the Multi-head Self-Attention (MSA) mechanism to gather information and build dynamic contextual understanding by comparing each token in an input sequence to every other token. The Transformer model establishes an information-passing graph among its inputs. Unlike sequential processing, transformers circumvent the issue of vanishing gradients commonly encountered by RNNs during long-term predictions. As a result, transformers have been successfully employed in datasets containing extensive historical data to derive optimal models for time-series forecasting (Zeng et al. 2023).

### Encoder-Decoder Transformer-Based Prediction Model

The Transformer-based forecasting model (Vaswani et al. 2017) is based on the original Transformer architecture, which consists of encoder and decoder layers. The architecture of an encoder-decoder transformer is made up of many significant components and steps.

The principal element of the model is the encoder, which is in charge of processing inputs and transforming them into representations helpful for prediction. A number of encoder layers are stacked on top of one another. The two primary sub-modules that compose up each encoder layer are the forward propagation neural network and the multi-headed attention. The input layer transforms the time series data into a vector of dimension  $d$  using a fully connected network, as shown in Fig. 1.

Transforms the time series data into a vector of dimension using a fully connected network, as shown in Fig. 1. The usage of a multi-head attention mechanism requires this transition. The multi-head attention assists the model in identifying the relations between various elements of the input sequence. The positional encoding helps the model to identify temporal dependencies and the relationship between the various values across time. The position vectors can be added to electrical charge value embedding using position encoding using sine and cosine functions. Then, the four encoder layers receive the generated vector. A  $d$ -dimensional model vector created by the encoder is then supplied to the decoder.

The decoder inputs are created using the last data point of the encoder outputs. A decoder input layer is employed to process these inputs, converting them into a  $d$ -dimensional vector representation suitable for further processing. Multi-

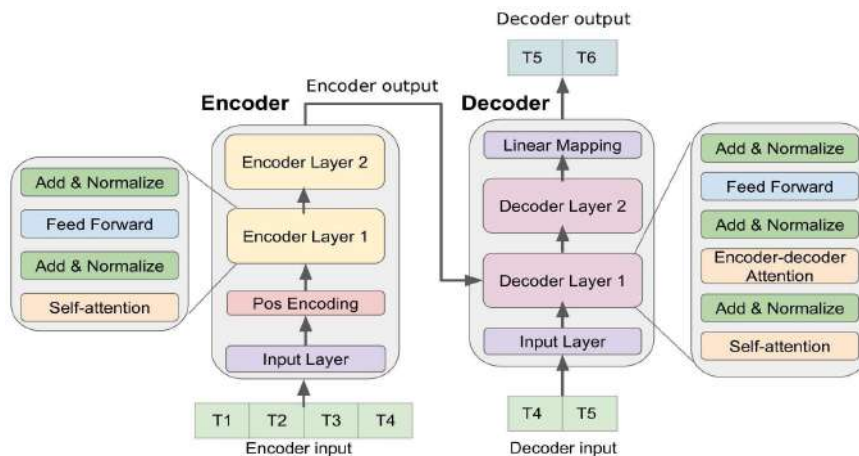


Fig. 1: Encoder-decoder transformer-based prediction model (Vaswani et al. 2017).

head attention is also employed in the decoder; however, it differs slightly from the attention used in the encoder. Multi-head attention considers both the outputs from the encoder and the outputs from the previous decoders for each place in the decoder. This enables the decoder to focus on both the information coming from the encoder that is pertinent and the data that the decoder has already produced. The output layer is responsible for generating the target time sequence based on the results of the preceding decoding layers. It combines the data from earlier layers to create the desired output. A method known as look-ahead masking is used to ensure that decoder predictions only depend on previous positions. This masking forces the decoder to rely solely on historical data by preventing access to future data throughout the prediction process. Additionally, the decoding module introduces a one-position offset between the decoder input and the target output.

**Encoder Transformer-Based Prediction Model**

Transformers have often been developed as encoder-decoder neural networks. The encoder-decoder configuration is frequently used in a variety of unsupervised tasks, including anomaly detection (Huang et al. 2020), translation (Vaswani et al. 2017), language and vision (Zhu et al. 2021), and more, which is necessary for this specific usage of transformer topology. The basic structure has been modified in the suggested modeling approach to use only the Encoder module. The global complexity of the model is reduced when the model is limited to the encoder, which facilitates learning and inference.

The main goal of these prediction tasks is to produce output that reflects the input data. However, consumption prediction is a supervised activity in which the model is trained using known inputs and corresponding outputs. Identifying the complicated, non-linear relationship between inputs (such as historical consumption habits, time of day,

and weather conditions) and outputs (future consumption) is challenging. Transformers have proved effective in detecting these relationships in a variety of tasks, but their direct use for supervised prediction problems can be challenging. The considered approach focuses on obtaining the most pertinent information from the input data using only the encoder part of the transformer.

**SYSTEM ARCHITECTURE**

The study used a dataset of 4,380 days of quarter-hourly electricity consumption from Algerian electricity supplier “Sonalgaz,” covering the years 2008 to 2020. (Bendaoud et al. 2021) The survey showed that a number of variables, such as climate and seasonal fluctuations, have a significant impact on electricity consumption. The Min-Max normalization procedure was used to ensure data stability for the analysis of daily consumption. This normalization method improves data stability, which facilitates model learning and convergence. The model aimed to meet the challenge of forecasting daily electrical energy consumption using multivariate data collected at 24-hour intervals in order to switch to renewable energies during periods of high consumption and reduce CO<sub>2</sub> emissions, as shown in Fig. 2. The figure describes the impact of electricity consumption prediction on CO<sub>2</sub> emissions, renewable energy use, and intelligent grid management, which relies on a complex symbiosis between different players in the energy system. Initially, the gas-fired power plant generates electricity while emitting CO<sub>2</sub>, revealing the environmental implications associated with this traditional production method. Electricity consumption prediction is emerging as a key enabler of this process. It draws on historical data and sophisticated predictive models to anticipate future electricity demand. This forecast guides Prediction Response, triggering adjustments in generation and prompting a transition to renewable energy sources. This last aspect is essential, as it marks a turning point

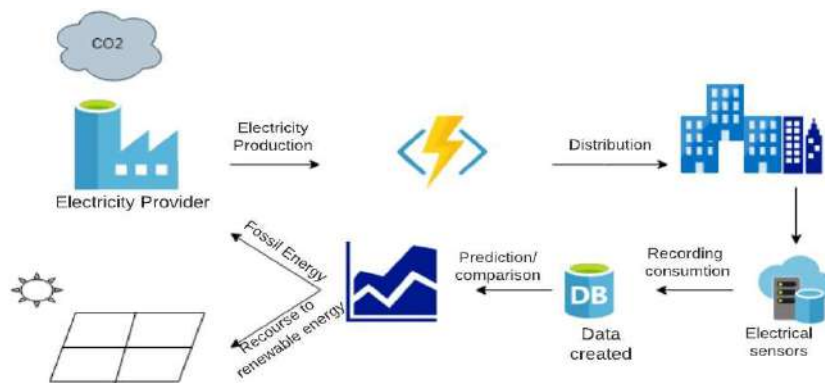


Fig. 2: Architecture of the proposed system.

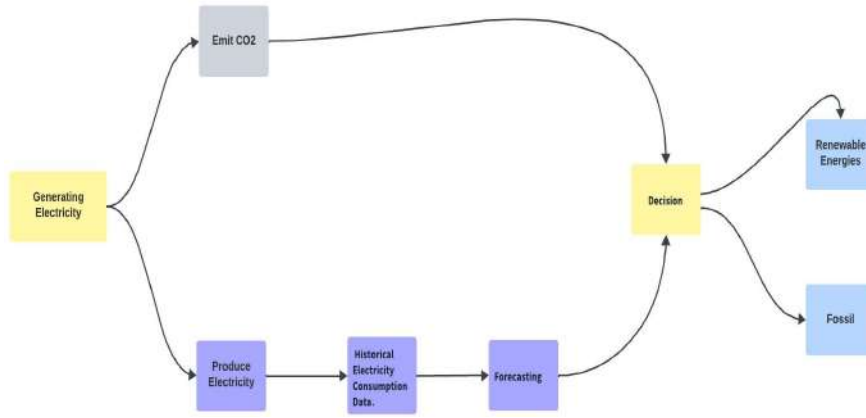


Fig. 3: Conceptual chart of the proposed system.

towards cleaner production and a consequent reduction in CO<sub>2</sub> emissions.

**System Planning Proposed**

The process of converting gas into electricity in a power plant is usually handled by a gas-fired power station. In a gas-fired power plant, gas (often natural gas) is burned in a combustion chamber to produce heat. This heat is used to vaporize a heat-transfer fluid, usually water, creating high-pressure steam that is directed toward a turbine, causing it to rotate. The rotation of the turbine drives a generator that converts mechanical energy into electricity. The electricity generated is then distributed via the power grid to homes or housing estates, which are equipped with electrical sensors that measure electricity consumption in real-time, recording consumption data and creating a dynamic database containing information on consumption patterns as shown in Fig. 3. From these data, different prediction models are tested and compared in order to choose the best possible predictor. First of all, the results of these predictions are of crucial importance, as they offer valuable insights to guide electricity suppliers in their strategic decisions. In particular, if the forecasts indicate an excessively high CO<sub>2</sub> emission rate, this can guide the supplier towards greater integration of renewable energies. These results can be used as a compass

to take proactive measures to reduce the carbon footprint, adjusting power generation for more sustainable sources where necessary. Using this data, several prediction models are rigorously tested and compared to select the best-performing predictor. The results of these predictions are of crucial importance, as they offer valuable insights to guide electricity suppliers in their strategic decisions. In particular, if the forecasts indicate an excessively high CO<sub>2</sub> emission rate, this can guide the supplier towards greater integration of renewable energies. These results can be used as a compass to take proactive measures to reduce the carbon footprint, adjusting power generation in favor of more sustainable sources where necessary. In addition, prediction results provide crucial indications for optimal power generation planning. With an understanding of expected demand trends, the supplier can adjust production accordingly, optimizing available resources and improving operational efficiency. This iterative process of prediction, model evaluation and strategic adjustment helps to establish proactive management of power generation, aligned with environmental sustainability objectives, while ensuring efficient planning and agile response to changing energy needs.

**Transformer-Based Encoder**

The basic Transformer encoder architecture and a number of additional models were trained and compared to predict

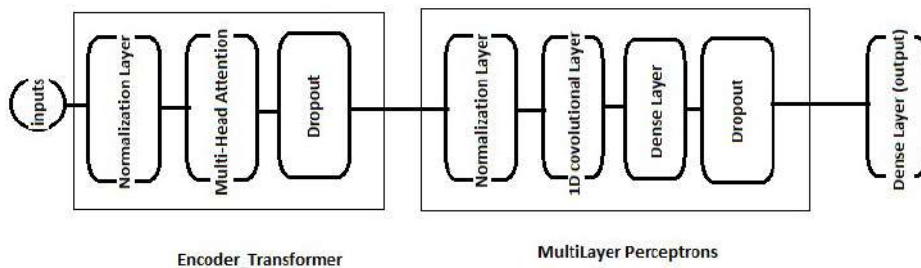


Fig. 4: The Transformer-Encoder framework.

load data for the next day using data divided into 24-hour intervals. The encoder presented in this research paper is based on the Transformer architecture and will be compared with other models in the following section, as shown in Fig. 4.

The Transformer model is a neural network design that is frequently employed in Natural language processing. Nevertheless, its applications are not limited to language-related tasks. One such application is electrical load prediction, where the Transformer model can be effectively utilized. The Transformer Encoder design is a stack of residual encoder blocks in a more formal sense. During training, the transformer-based encoder maps the input sequence to a contextualized encoding sequence.

The encoder block begins with a bidirectional self-attention layer, followed by two feedback layers. Various implementations have been explored to optimize performance on time-series data, each customizing its methods to meet specific needs. A crucial adaptation has been introduced to the attention map to effectively capture short-term patterns. This adjustment involves incorporating a window that confines backward attention, allowing focused analysis on nearby time sequences. Following a normalization step, the input sequence is transformed into a fixed-dimension vector for each element, ensuring uniform data preparation for consistent analysis. In the instance of electric charge prediction, each element represents a specific temporal value of electric charge, contributing to a meaningful representation for a more nuanced understanding of temporal patterns. Maintaining the chronological order of power consumption times is facilitated by positional encoding. Assigning a specific value to each element in the time sequence based on its relative position is essential for the model to capture temporal dynamics and accurately interpret variations in power consumption over time. Position-dependent cyclic patterns are made using the sin in eq. 1 and cos functions eq. 2. The embedding of the sequence elements is then enhanced using these cyclic patterns. In doing so, it is possible for each element to have a distinct vector representation that includes both information and position.

$$PE(pos2i) = \sin(pos/2i/(10000d_{model})) \dots(1)$$

$$PE(pos2i + 1) = \cos(pos/2i/(10000d_{model})) \dots(2)$$

with *PE*: the calculated positional encoding.

Once the position vectors have been generated, they are combined with their respective elements in the sequence. This step involves summing the position vectors with the existing embedding. This allows position information to be combined with the characteristics of each element with the eq. 3. The addition of position vectors enables the model to distinguish elements according to their relative position in the sequence, which is essential for understanding the

temporal order of electric charge values and capturing the dependencies between them.

$$PE = PV + EV \dots(3)$$

with *PV*: the positional vector and

*EV*: the embedding vector.

Each data point in the electric charge sequence will be converted by the encoding process of the Transformer into a context-dependent vector representation, taking into account any previous and potential future data points. The complex interactions between the numerous electric charge features are subsequently captured by the encoding blocks, which further enhance this contextual representation. This procedure is repeated until the last encoding block generates the contextual coding, which contains the crucial data required to make precise projections regarding future electric charges. Consequently, the model can identify the temporal correlations and patterns in the electrical charge data and then can make predictions of the future electrical charge demand.

After merging the inputs with the positional encoding eq. (3), the model will utilize a linear layer to create a collection of query vectors (key/value) for these features. Multi-headed attention employs a particular attention process known as self-attention.

*V*, *K*, and *Q* will just be identical copies of the embedding vector in the encoder case (plus positional encoding).

*Batchsize \* seq<sub>en</sub> \* d<sub>model</sub>* will be the sequence length. The integration vector is divided into *N* heads in multihead attention; giving them the dimensions *batch* and *d<sub>k</sub>* will be the dimension of the queries and keys of the attention Eq.(4)

$$Size * N * seq_{en} * (d_{model}/N) \dots(4)$$

After the scalar product between the queries and the keys, a score matrix is formed to determine the significance and the relevance of various input sequence elements Eq. (5)

$$Q * K = Scorematrix \dots(5)$$

Then, the scalar products are subjected to a softmax function eq. (6) to generate the score matrix. In order to create a weighting distribution over the keys in the sequence, the softmax function normalizes the scores so that the sum of all scores for each query is equal to 1.

$$softmax(Q * K/sqrt(d_k)) = attention(q,k,v) * V \dots(6)$$

where *Softmax* is a function that normalizes attention scores, and *sqrt(d<sub>k</sub>)* is the square root of the dimension.

After this, all attention head outputs are concatenated and multiplied by a projection weight matrix *W<sub>o</sub>* of size (*d<sub>model</sub> \* d<sub>model</sub>*) to obtain the final multi-head attention output

$$Attention_i = Concatenate(O_1, O_2, \dots, O_h) * W_o \dots(7)$$

Where *i<sub>o</sub>* is the output of the head attention *i*.

The neural network layer can learn to combine and transform input features to capture the complex patterns and non-linear relationships that influence target values. During model training, weights are iteratively adjusted using optimization techniques, such as gradient backpropagation, to minimize the gap between model predictions and actual target values. The representation that results from this contextual encoding will then be run through a fully linked layer to calculate the amount of electricity used.

## MATERIALS AND METHODS

### Settings

It is essential to introduce in this subsection the setting parameters that lead to the experimental results of the paper.

### Event-Cause Analysis

Different events show that consumption is not a linear and constant process; it can range from a political speech, a football match, an abrupt climate change, or simply a change of seasons. It is essential to find which are the most influencing factors and to understand them, and this allows our prediction system to be as efficient as possible. Accurate forecasts of electricity consumption enable service providers to better manage energy resources, savings, and maintenance operations and guarantee a stable, reliable power supply. Anticipating the demand will avoid a lack of production and subsequent load shedding since overproduction is simply a huge economic loss and a major source of pollution. Maintenance operations will be easier to do, and distribution will be more efficient. Good forecasting will have a positive effect on the environment and, therefore, on human health.

Anticipating and effectively controlling these fluctuations in electricity consumption not only ensures reliable service but also contributes to energy efficiency and sustainable development while keeping CO<sub>2</sub> levels acceptable enough to protect air quality. This enables service providers to choose wisely and deploy resources more effectively, which ultimately benefits suppliers, customers, and the environment.

An inventive strategy was used to achieve the objectives of forecasting energy consumption and maximizing the use of renewable energy sources and battery storage. To achieve this, the data were divided into 24-hour segments to represent days. This division allows a comprehensive examination of the correlations between energy consumption and various important factors. In order to give a clear picture of the temporal relationships and patterns present in the data, the aim is to assess the influence of past values in the time series on current or future values. Prediction plays a central role in the process of managing electricity consumption. Using machine learning algorithms, the system analyzes historical data to accurately anticipate electricity demand. A critical threshold is determined, which triggers a transition to renewable energy sources, such as solar or wind power, as soon as the prediction indicates that electricity consumption is close to or exceeds this threshold. This proactive strategy minimizes the use of polluting sources and reduces the CO<sub>2</sub> emissions associated with electricity production. In addition, in the event of excess production from renewable sources, excess electricity is efficiently stored in batteries. These batteries act as energy stores, enabling demand to be satisfied during periods of insufficient renewable production or peak consumption. In this way, the system ensures optimal use of

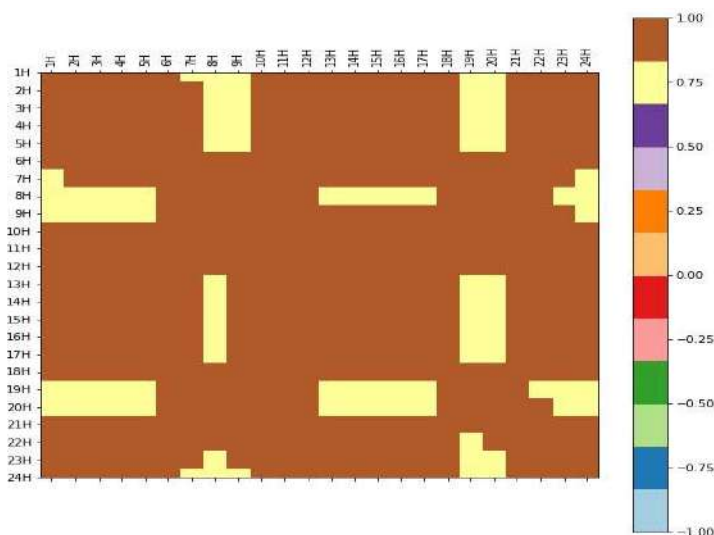


Fig. 5: The correlation results.

renewable energies, avoiding overproduction and responding dynamically to fluctuations in demand. Integrating prediction, transition to renewable energies, and electricity storage, this process offers a comprehensive approach to reducing CO<sub>2</sub> emissions from electrical consumption while guaranteeing a reliable and sustainable energy supply.

The outcome in Fig. 5 amply demonstrates that there is a very strong correlation between the database's variables. A linear link and a strong relationship between the variables were discovered through this statistical investigation, which can be used to reduce the amount of data needed for future research and make forecasting easier. Electricity consumption patterns vary according to the day, season, and year. In summer, when temperatures rise, demand increases in the afternoon, as residential and commercial spaces rely heavily on air conditioning. This translates into a higher overall hourly electrical load.

Conversely, during the winter months, the hourly electrical load is relatively stable but peaks in the morning and evening. These distinct patterns reflect the fluctuation in electricity consumption across different time periods, driven by factors such as climatic conditions and consumer usage habits. Understanding these dynamics is essential for effectively managing energy resources and implementing strategies to optimize power generation and distribution.

In addition, electricity consumption follows a daily cycle, with peak demand occurring at a given time of day (*depending on the season*) and then declining in the late evening. This fluctuation in electricity demand is due to daily habits of energy use by households and companies but is also influenced by weather conditions. Due to variations in weather conditions and the types of electrical equipment used, the overall quantity and trend of total electricity demand fluctuates from year to year.

Here are some curves of average consumption during the seasons to back up these claims.

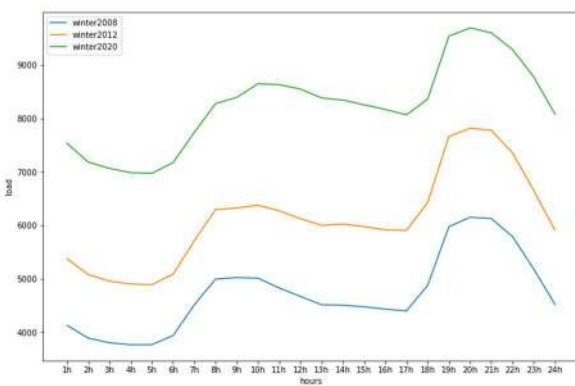


Fig. 6: The average consumption curve in winter.

**Winter:** The Fig. 6 shows the consumption trends during the winter months. This season is characterized by lower daylight hours and longer evenings. Consequently, the peak in electricity use happens around 8 p.m., reflecting the higher demand in the evening.

**Summer:** Fig. 7 represents the summer consumption pattern, which is characterized by the habits and life routines of Algerian citizens compared to other seasons. As a result, consumption curves show significant variations. In the morning, there is a significant drop in electricity consumption, probably due to reduced activity in the early hours of the day. However, around 12 o'clock, consumption rises significantly, probably because it is too hot. Another interesting observation is a minor shift in the peak, which occurs at 10 p.m., indicating a higher demand for electricity during the evening hours. These variations highlight the unique consumption behavior during the summer season, reflecting the specific needs and routines of Algerian citizens during this period.

**Spring:** With more daylight hours than in winter, spring brings a remarkable change in peak electricity consumption. This change is illustrated by Fig. 8, which shows that the peak is at 10 p.m. This change in peak time reflects the shift in energy consumption trends due to the lengthening of the day and the beginning of night-time activities. Spring's longer days allow for more outdoor activities and later working hours, shifting the peak consumption period to later in the day.

**Autumn:** In autumn, electricity consumption peaks at 8 pm. This is because the days gradually resemble those of winter, as illustrated in Fig. 9. Shorter daylight hours and colder temperatures lead to changes in consumer behavior, resulting in higher electricity consumption during the evening hours. The combination of winter and summer factors influences the consumption profile during autumn, resulting in a peak at 8 pm.

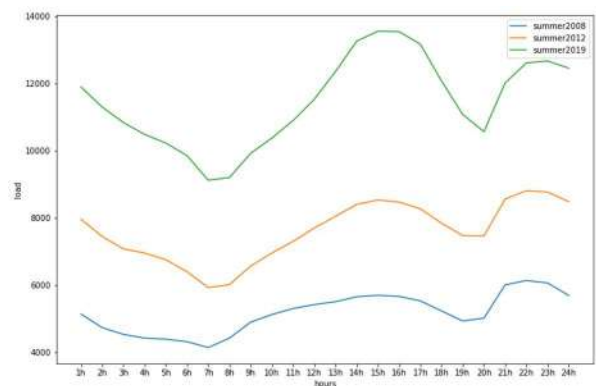


Fig. 7: The average consumption curve in summer.

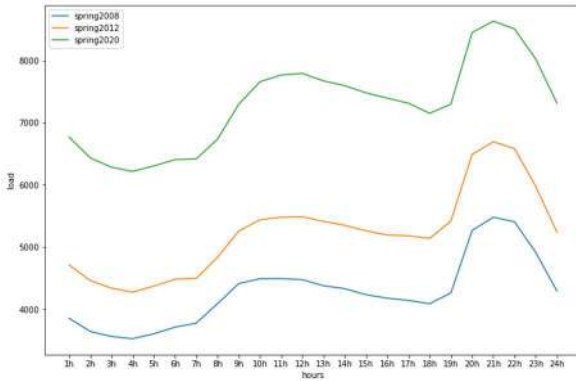


Fig. 8: The average consumption curve in spring.

As a result, seasonal influence becomes a key element to consider. Detailed observation of electricity consumption profiles for each season demonstrates the significant impact of seasonal variations. These seasonal differences, clearly visible in electricity consumption patterns, are crucial for refining predictive models. Taking these seasonal variations into account, the models can more accurately anticipate fluctuations in demand, enabling more efficient energy management and a consequent reduction in the CO<sub>2</sub> emissions associated with electricity generation.

## RESULTS AND DISCUSSION

The Transformer-Encoder model is compared to many other models in this study to evaluate its performance, particularly in predicting electricity consumption while using and considering the influence of historical data. The models were evaluated using metrics frequently used in time series analysis, including mean absolute error (MAE), mean square error (MSE), root mean square error (RMSE), and accuracy (100- (mean absolute percentage error (MAPE) (Boylan 2011))). These parameters serve as standard metrics for estimating model performance in catching and predicting

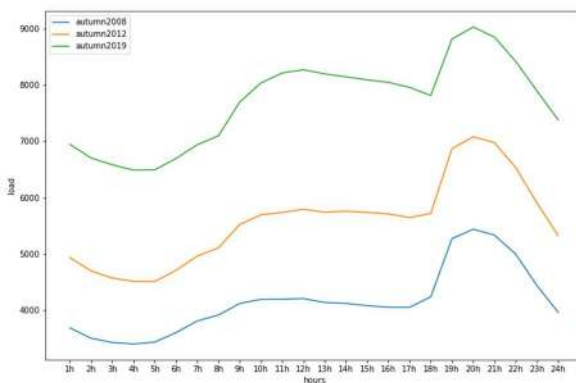


Fig. 9: The average consumption curve in autumn.

Table 1: Obtained model results.

Models	Accuracy	MAE	MSE	RMSE
RNN	0.89	1.34	3.20	1.72
Transformer-Encoder	0.98	0.71	0.26	0.53
CNN	0.98	0.09	0.09	0.099
LSTM	0.98	0.28	0.62	0.8

the patterns of time series data. MAPE measures the average percentage deviation between predicted and actual values. Subtracting MAPE from 100 gives the precision measure, which represents the proportion of accurate predictions in percentage terms. This formulation enables a better interpretation of accuracy. The results are resumed in Table 1 and Fig. 10, respectively.

The comparison presented in Table 1 and Fig. 10 highlights the significant relationship between accurate power consumption forecasts and the use of appropriate forecasting models. As with any deep learning model, various factors, such as data quality and quantity, as well as model parameters, contribute to model performance and results. It is important to note that the Transformer-Encoder model achieves a remarkably high level of accuracy during training. Consequently, it highlights the potential for the Transformer model to be applied and adapted to meet such forecasting challenges.

Comparing this time series model with other architectures, it is interesting to note that transformers and CNNs achieved similar results. While CNNs are reputed for their ability to extract relevant features, transformers performed equally well in predicting power consumption. This finding highlights the ability of transformers to capture the complex temporal relationships inherent in time series.

On the other hand, when comparing RNNs with transformers, the main differentiating factor is the presence of parallelism in RNNs. Transformers may process several input sequences at once in contrast to RNNs, which only process one input sequence at a time in a sequential fashion. Transformers have more ability to recognize and represent complicated relationships due to this parallelism. In RNNs, the learned representation of the input sequence must be compressed into a single state vector before processing subsequent sequences. The model may not be able to accurately capture long-term dependencies due to this compression. RNNs can also experience gradient explosion issues, which further limits their capacity to manage long-term dependencies, even when using cutting-edge methods like LSTMs. Transformers, on the other hand, have a much wider bandwidth, enabling them to efficiently capture long-term dependencies and model relationships across the entire sequence. When it comes to managing long-



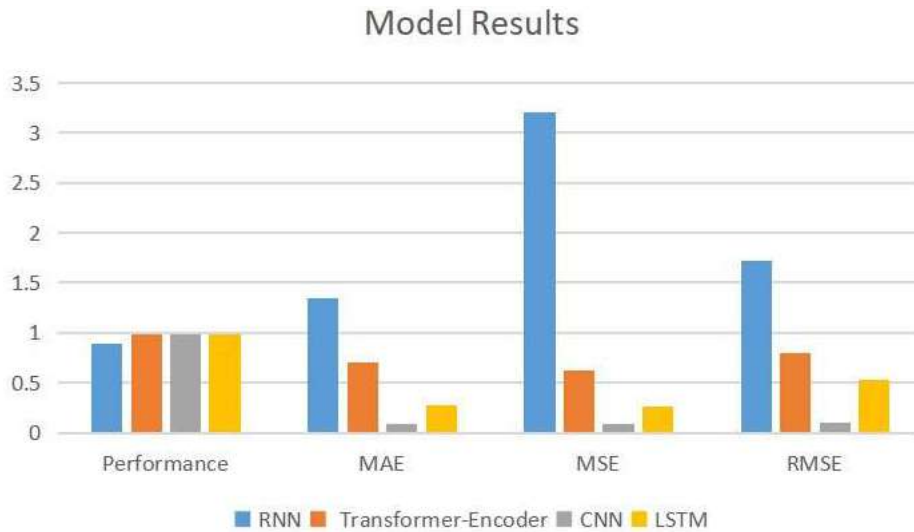


Fig. 10: Representation of the Model's results.

term dependencies and processing information effectively, transformers clearly outperform RNNs due to their parallel processing and capacity to handle all tokens directly. Transformers can effectively model complicated patterns and relationships within sequences, making them a powerful alternative for applications involving time-series data.

According to all that has been discussed, it becomes evident that transformers, both in their general form and through customized architectures, have a profound impact on the forecast of electrical consumption. Their attention and parallel processing mechanisms enable them to effectively understand the overall context and interrelationships within time series. This enables processors to make accurate forecasts and provide valuable information on future consumer trends. Overall, transformers are emerging as a transformational method for predicting energy use. Their ability to take advantage of the temporal aspect of the problem and their global modeling capabilities make them an effective tool for correctly forecasting future consumption patterns and supporting informed decision-making in the energy sector. This capability becomes crucial in the context of reducing CO<sub>2</sub> emissions linked to electricity production. Accurate forecasting of electricity consumption enables more precise planning of energy activities. The electricity production process has a significant impact on the relationship between electricity consumption forecasts and CO<sub>2</sub> emissions. In other words, accurate forecasting of energy needs has a direct impact on carbon dioxide emissions by improving the production, delivery, and use of electricity. Table 2 shows the CO<sub>2</sub> emission results, illustrating predicted values of the Transformer over a few hours of a day, as an example.

A significant observation emerges regarding the direct link between calculated CO<sub>2</sub> emissions and predicted values: an increase in consumption is directly correlated with an increase in CO<sub>2</sub> emissions. To illustrate this mathematically, the relationship between electricity consumption (E), CO<sub>2</sub> emissions (CO<sub>2</sub>), and greenhouse gases can be represented by the following equation:

$$CO_2 = E * EF \quad \dots(8)$$

where CO<sub>2</sub> represents carbon dioxide emissions, E represents electricity consumption, and EF (Emission Factor) represents the emissions conversion factor specific to the electricity source.

The EF depends on the source of electricity used to produce the energy. For example, if the electricity is mainly produced from gas, the emission factor will be high due to the high CO<sub>2</sub> emissions associated with gas combustion. On the other hand, if the electricity comes from renewable sources, the emission factor will be close to zero. Focusing on Algeria, the EF for gas use in the country was set at 548 gCO<sub>2</sub>/kWh for this study. Although this value seems modest on a global scale, it is of significant importance for the country's environmental health. It is essential to recognize that all production has an impact on the global environment, as evidenced by global pollution reaching 32,252 Mt in 2020, according to the International Energy Agency (IEA) (Palaian Premalalitha & Balraj 2024). Even if these values are

Table 2: CO<sub>2</sub> Emission results.

Hours	1h	6h	12h	17h	21h
Predicted Values	7250	6250	6877	7145	7840
CO <sub>2</sub> Emission	3973	3768	3916	3739	4296

expressed in grams, the commitment to reducing greenhouse gas emissions is crucial, particularly through the increased integration of renewable energies. It is important to note, however, that countries are not isolated entities. Without the exceptional growth in renewable energies, electric vehicles, heat pumps, and energy efficiency technologies, the increase in CO<sub>2</sub> emissions would have been almost three times higher. These advances, therefore, play a crucial role in the fight against rising global emissions, demonstrating the importance of sustainable initiatives. Awareness of these emissions specific to Algeria provides a crucial basis for developing more sustainable energy policies aimed at minimizing environmental impact while improving health on a national scale.

## CONCLUSIONS

Energy is the most important resource in the economy. There can be no economic development without energy control, and wasting energy is a disaster for the economy and the environment. One of the ways of controlling electrical energy is to forecast its consumption, which not only optimizes production and allows us to anticipate equipment maintenance but also helps us to move towards a more sustainable energy future. To achieve these objectives, it is necessary to apply statistical processing techniques to consumption data, enabling historical trends to be understood and interpreted. These findings enable a range of models, including linear and non-linear approaches, to be used to accurately explain and predict electricity consumption patterns that will play a fundamental role in reducing CO<sub>2</sub> emissions and promoting renewable energies. Through statistical processing, companies can gain a better understanding of their energy consumption patterns, enabling them to make informed decisions about energy management strategies. Accurate prediction of electricity demand enables production to be adapted in real-time, consequently reducing the use of CO<sub>2</sub>-emitting energy sources, particularly during peak hours. This method will encourage more efficient management of energy resources and will also directly reduce greenhouse gas emissions, thus making an active contribution to the fight against climate change. The proposed models are deep learning models such as CNN, RNN, LSTM, and the transformer. The different used profiles are known as well as daily, seasonal, and yearly can catch the Algerian behavior. However, the obtained results are very promising, with up to 98 percent of good prediction for CNN, 98% for RNN, 98% for LSTM, and 98% for Transformers. The integration of renewable energies into the energy mix is a crucial step towards a sustainable future. By anticipating energy needs, accurate prediction of electricity consumption makes it possible to optimize the use of these clean sources. A deeper

transition to renewable energies becomes feasible when forecast reliability reaches a defined threshold. The transition is accompanied by a significant reduction in dependence on fossil fuels. Intelligent management of surplus energy is another essential pillar. The use of batteries to store surplus electricity during periods of low demand offers a practical solution for smoothing out variations in production. This approach guarantees a stable supply of clean energy. This fusion of capabilities enables a more comprehensive and powerful approach to forecast electricity consumption, enabling informed decisions to optimize this energy, reduce costs, and contribute to a greener, more sustainable future.

## REFERENCES

- Ahmad, T. and Chen, H., 2018. Utility companies strategy for short-term energy demand forecasting using machine learning-based models. *Sustainable Cities and Society*, 39, pp.401-417.
- Baasch, G., Rousseau, G. and Evins, R., 2021. A Conditional Generative Adversarial Network for energy use in multiple buildings using scarce data. *Energy and AI*, 5, p.100087.
- Bedi, J. and Toshniwal, D., 2019. Deep learning framework to forecast electricity demand. *Applied Energy*, 238, pp.1312-1326.
- Bello-Orgaz, G., Jung, J. J. and Camacho, D., 2016. Social big data: Recent achievements and new challenges. *Information Fusion*, 28, pp.45-59.
- Bendaoud, N. M. M., Farah, N. and Ahmed, S. B., 2021. Comparing Generative Adversarial Networks architectures for electricity demand forecasting. *Energy and Buildings*, 247, p.111152.
- Boylan, J., 2011. A "Softer" Approach to the Measurement of Forecast Accuracy. *Foresight: The International Journal of Applied Forecasting*, (23).
- Chen, Y., Wang, Y., Kirschen, D. and Zhang, B., 2018. Model-free renewable scenario generation using generative adversarial networks. *IEEE Transactions on Power Systems*, 33(3), pp.3265-3275.
- Chow, T. W. and Leung, C. T., 1996. Neural network based short-term load forecasting using weather compensation. *IEEE Transactions on Power Systems*, 11(4), pp.1736-1742.
- Clements, M. P., Franses, P. H. and Swanson, N. R., 2004. Forecasting economic and financial time series with non-linear models. *International Journal of Forecasting*, 20(2), pp.169-183.
- Daut, M. A. M., Hassan, M. Y., Abdullah, H., Rahman, H. A., Abdullah, M. P. and Hussin, F., 2017. Building electrical energy consumption forecasting analysis using conventional and artificial intelligence methods: A review. *Renewable and Sustainable Energy Reviews*, 70, pp.1108-1118.
- Deo, R. C. and Şahin, M., 2017. Forecasting long-term global solar radiation with an ANN algorithm coupled with satellite-derived (MODIS) land surface temperature (LST) for regional locations in Queensland. *Renewable and Sustainable Energy Reviews*, 72, pp.828-848.
- Dudek, G., 2015. Short-term load forecasting using random forests. In: *Intelligent Systems' 2014: Proceedings of the 7th IEEE International Conference Intelligent Systems IS'2014*, September 24-26, 2014, Warsaw, Poland, Springer International Publishing, pp.821-828.
- Elsaraiti, M. and Merabet, A., 2021. Application of long-short-term-memory recurrent neural networks to forecast wind speed. *Applied Sciences*, 11(5), p.2387.
- Fu, Y., Wang, H. and Virani, N., 2022. Masked multi-step multivariate time series forecasting with future information. *arXiv*, 9, p.14413.
- Giuliani, F., Hasan, I., Cristani, M. and Galasso, F., 2021. Transformer networks for trajectory forecasting. *Pattern Recognition*, 601, pp.10335-10342.

- Guo, Y. C., Niu, D. X. and Chen, Y. X., 2006. Support vector machine model in electricity load forecasting. In: 2006 International Conference on Machine Learning and Cybernetics. IEEE, pp.2892-2896.
- Harper, C. and Snowden, M., 2017. *Environment and Society: Human Perspectives on Environmental Issues*. Routledge.
- He, W., 2017. Load forecasting via deep neural networks. *Procedia Computer Science*, 122, pp.308-314
- Hernandez, L., Baladron, C., Aguiar, J. M., Carro, B., Sanchez-Esguevillas, A. J., Lloret, J. and Massana, J., 2014. A survey on electric power demand forecasting: Future trends in smart grids, microgrids, and smart buildings. *IEEE Communications Surveys & Tutorials*, 16(3), pp.1460-1495.
- Huang, B., Zheng, H., Guo, X., Yang, Y. and Liu, X., 2021. A Novel Model Based on DA-RNN Network and Skip Gated Recurrent Neural Network for Periodic Time Series Forecasting. *Sustainability*, 14(1), p.326.
- Huang, S., Liu, Y., Fung, C., He, R., Zhao, Y., Yang, H. and Luan, Z., 2020. Hitanomaly: Hierarchical transformers for anomaly detection in the system log. *IEEE Transactions on Network and Service Management*, 17(4), pp.2064-2076.
- Jetcheva, J. G., Majidpour, M. and Chen, W. P., 2014. Neural network model ensembles for building-level electricity load forecasts. *Energy and Buildings*, 84, pp.214-223.
- Jiang, H., Zhang, Y., Muljadi, E., Zhang, J. J. and Gao, D. W., 2016. A short-term and high-resolution distribution system load forecasting approach using support vector regression with hybrid parameters optimization. *IEEE Transactions on Smart Grid*, 9(4), pp.3341-3350.
- Kamani, D. and Ardehali, M. M., 2023. Long-term forecast of electrical energy consumption with considerations for solar and wind energy sources. *Energy*, 268, p.126617.
- Kataray, T., Nitesh, B., Yarram, B., Sinha, S., Cuce, E., Shaik, S. and Roy, A., 2023. Integration of smart grid with renewable energy sources: Opportunities and challenges – A comprehensive review. *Sustainable Energy Technologies and Assessments*, 58, p.103363.
- Kavousi-Fard, A., Samet, H. and Marzbani, F., 2014. A new hybrid modified firefly algorithm and support vector regression model for accurate short-term load forecasting. *Expert Systems with Applications*, 41(13), pp.6047-6056.
- Kim, T. Y. and Cho, S. B., 2019. Predicting residential energy consumption using CNN-LSTM neural networks. *Energy*, 182, pp.72-81.
- Le, T., Vo, M. T., Vo, B., Hwang, E., Rho, S. and Baik, S. W., 2019. Improving electric energy consumption prediction using CNN and Bi-LSTM. *Applied Sciences*, 9(20), p.4237.
- Levi, G. and Hassner, T., 2015. Age and gender classification using convolutional neural networks. *Computer Vision and Pattern Recognition*, 14, pp.34-42.
- Memarzadeh, G. and Keynia, F., 2021. Short-term electricity load and price forecasting by a new optimal LSTM-NN-based prediction algorithm. *Electric Power Systems Research*, 192, p.106995.
- Mishra, P. and Singh, G., 2023. Energy management systems in sustainable smart cities based on the internet of energy: A technical review. *Energies*, 16(19), p.6903.
- Palaian Premalalitha, P. and Balraj, A., 2024. Low-temperature dielectric heating-assisted CO<sub>2</sub> stripping/solvent regeneration of aqueous carbon-rich monoethanolamine, piperazine, and 2-amino-2-methyl-1-propanol solvents. *Industrial & Engineering Chemistry Research*, 142, pp.883-896.
- Rahman, A., Srikumar, V. and Smith, A. D., 2018. Predicting electricity consumption for commercial and residential buildings using deep recurrent neural networks. *Applied Energy*, 212, pp.372-385.
- Raju, M. P. and Laxmi, A. J., 2020. IOT based online load forecasting using machine learning algorithms. *Procedia Computer Science*, 171, pp.551-560.
- Roldán-Blay, C., Escrivá-Escrivá, G., Álvarez-Bel, C., Roldán-Porta, C. and Rodríguez-García, J., 2013. Upgrade of an artificial neural network prediction method for electrical consumption forecasting using an hourly temperature curve model. *Energy and Buildings*, 60, pp.38-46.
- Scott, G. J., Rosegrant, M. W. and Ringler, C., 2000. Global projections for root and tuber crops to the year 2020. *Food Policy*, 25(5), pp.561-597.
- Singh, S. and Yassine, A., 2018. Big data mining of energy time series for behavioral analytics and energy consumption forecasting. *Energies*, 11(2), p.452.
- Slingo, J. M. and Slingo, M. E., 2024. The science of climate change and the effect of anaesthetic gas emissions. *Anaesthesia*, 11(5), p. 22-36.
- Solyali, D., 2020. A comparative analysis of machine learning approaches for short-/long-term electricity load forecasting in Cyprus. *Sustainability*, 12(9), p.3612.
- Vaswani, A., Shazeer, N., Parmar, N., Uszkoreit, J., Jones, L., Gomez, A. N. and Polosukhin, I., 2017. Attention is all you need. *Advances in Neural Information Processing Systems*, 30, p.771.
- Venkatesan, S., Lim, J., Ko, H. and Cho, Y., 2022. A machine learning based model for energy usage peak prediction in smart farms. *Electronics*, 11(2), p.218.
- Wang, J. and He, Q. P., 2023. Methane removal from the air: Challenges and opportunities. *Methane*, 2(4), pp.404-414.
- Wu, H., Shen, G. Q., Lin, X., Li, M. and Li, C. Z., 2021. A transformer-based deep learning model for recognizing communication-oriented entities from patents of ICT in construction. *Automation in Construction*, 125, p.103608.
- Wu, Z., Zhai, H., Grol, E. J., Able, C. M. and Siefert, N. S., 2023. Treatment of brackish water for fossil power plant cooling. *Nature Water*, pp.1-13.
- Yildiz, B., Bilbao, J. I. and Sproul, A. B., 2017. A review and analysis of regression and machine learning models on commercial building electricity load forecasting. *Renewable and Sustainable Energy Reviews*, 73, pp.1104-1122.
- Zeng, A., Chen, M., Zhang, L. and Xu, Q., 2023. Are transformers effective for time series forecasting?. *Artificial Intelligence*, 37(9), pp.11121-11128.
- Zhang, G. and Guo, J., 2020. A novel ensemble method for residential electricity demand forecasting based on a novel sample simulation strategy. *Energy*, 207, p.118265.
- Zhu, C., Ping, W., Xiao, C., Shoybi, M., Goldstein, T., Anandkumar, A. and Catanzaro, B., 2021. Long-short transformer: Efficient transformers for language and vision. *Advances in Neural Information Processing Systems*, 34, pp.17723-17736.
- Zhu, Y., Al-Ahmed, S. A., Shakir, M. Z. and Olszewska, J. I., 2022. LSTM-based IoT-enabled CO<sub>2</sub> steady-state forecasting for indoor air quality monitoring. *Electronics*, 12(1), p.107.
- Zou, C., Zhao, Q., Zhang, G. and Xiong, B., 2016. Energy revolution: From a fossil energy era to a new energy era. *Natural Gas Industry B*, 3(1), pp.1-11.

---

## ORCID DETAILS OF THE AUTHORS

Rania Farah: <https://orcid.org/0000-0003-3067-6231>  
 Brahim Farou: <https://orcid.org/0000-0002-1609-6006>  
 Zineddine Kouahla: <https://orcid.org/0000-0001-8105-9810>  
 Hamid Seridi: <https://orcid.org/0000-0002-0236-8541>





# Microplastics in Agricultural Soil and Their Impact: A Review

P. Solanki<sup>1†</sup>, S. Jain<sup>1</sup>, R. Mehrotra<sup>2</sup>, P. Mago<sup>2</sup> and S. Dagar<sup>3</sup>

<sup>1</sup>IGNOU, Dyal Singh College, Delhi, India

<sup>2</sup>Shaheed Rajguru College of Applied Science for Women, University of Delhi, Delhi, India

<sup>3</sup>Department of Environmental Engineering, Delhi Technological University, Delhi, India

†Corresponding author: Pooja Solanki; solankipooja8@gmail.com

Nat. Env. & Poll. Tech.  
Website: [www.neptjournal.com](http://www.neptjournal.com)

Received: 19-03-2024

Revised: 07-05-2024

Accepted: 18-05-2024

## Key Words:

Microplastics  
Agricultural soil  
Sludge  
Sewage  
Microbes  
Soil health

## ABSTRACT

The rapid global plastic production of 348 million tonnes in 2018 has led to widespread environmental pollution, especially in terrestrial ecosystems. This study examines microplastics in agricultural soils, coming alarmingly. Particles  $\leq 5$  mm, which are defined as microplastics, have detrimental effects on the earth's environment. Because of its ecological importance, soil acts as an important microplastic sink, affecting soil and plant health and microbial activity. A variety of factors contribute to microplastic pollution in agricultural soils, including plastic mulching, manure, agricultural products (silage nets, twine), sewage sludge, weathering, and other indirect processes. These microplastics migrate, threatening soil integrity and biodiversity. Soil microplastics are analyzed for size, volume fraction, and polymer. Common materials include polyethylene, polypropylene, polyamide, polystyrene, polyvinyl chloride, and polyesters. Techniques, including optical microscopy and spectroscopy, extract and analyze microplastics. This comprehensive review calls for increased concern about the ecological effects of microplastics in agricultural soils. It emphasizes the importance of managing plastics to solve environmental challenges. The integrated environmental assessment highlights the complex relationship between microplastics and soil ecosystems, providing insights into potential risks and suggesting strategies to combat this looming environmental threat.

## INTRODUCTION

Plastic is a flexible, long-lasting, and cost-effective material used in a variety of important industries such as packaging, electronics, agricultural production, etc. (Plastic Europe 2018). The widespread use of these synthetic materials increased manufacturing, resulting in a huge amount of plastic litter in the environment (Geyer et al. 2017). In 2018, the anticipated global plastic production was 348 million tonnes (Plastic Europe 2018). Around  $\geq 6000$  Mt of plastic garbage was generated in 2015, with around 80% of the material ending up being dumped directly into the environment that finds its way to landfills (Geyer et al. 2017). It is also observed that around 8078 Mt of Plastic has been generated in the last 50 years between 1950 and 2020 (Plastic Europe 2021). Plastic waste is ubiquitous and has been discovered in a variety of environmental compartments (de Souza Machado et al. 2018a), where it is subjected to increasing fragmentation caused mostly by thermo-oxidation, photo-oxidation, UV light, and mechanical abrasion (Wang et al. 2019, Hayes 2019 & Da Costa et al. 2019). Unfortunately, the fragmentation process does not entirely disintegrate

the plastic waste but instead transforms it into a plethora of fine-sized plastic particles, encompassing Microplastics defined as 5 mm in diameter (Arthur et al. 2009, Thompson et al. 2004).

## CHARACTERISTIC FEATURES OF MICROPLASTICS

The sink of Microplastics discovered in the soil can indicate localized usage, adjacent artificial activities, or atmospheric deposition, but the soil is a potential sink for Microplastics from different sources (Forster et al.2020). The capacity to understand the formation of Microplastics in soil, where the distribution distance on both temporal and spatial scales, among the point of origin and the sampling site, may be shorter than that in atmospheric transfer, is made possible by correlations among different kinds and occurrences of Microplastics discovered and regional human activities (Eerkes-Medrano et al. 2018, Luo et al. 2020). Additionally, the effects of different types of Microplastics on terrestrial systems vary (de Souza Machado et al. 2019, Lozano et al. 2020).

## Shape

According to researchers (Xu et al. 2020, Yang et al. 2021), the Microplastics seen may be divided into numerous shapes, including pellets, fragments, foam, fiber, and film. According to a laboratory weathering experiment, PP pellets may create  $6084 \pm 1061$  particles after being subjected to UV light for 12 months and mechanical abrasion for 2 months (Yang et al. 2021).

In addition to being the master batch for products like industrial pellets, pellet particles are also connected to personal care items like cosmetics and cleaning supplies (Xu et al. 2020). Additionally, a new class called “fiber balls” is created since fibers frequently tangle and form balls. Such a fiber ball often comes in bundles and is made up of fibers in various colors (Weber & Opp 2020).

## Size Fractions

The definition of Microplastics by researchers, as well as the sensitivity of the extraction and analytical techniques utilized, makes determining the size of Microplastics fairly challenging. The concept of Microplastics has become clearer as a result of an early study that focused on their presence in aquatic ecosystems. Microplastics are known to have a size of less than 5 mm. However, the sampling, pretreatment, and identification procedures directly affect the minimum particle size (Yang et al. 2021, Weber & Opp. 2020). In soil environments, Microplastics with minute particle sizes ( $\leq 1$  mm) have been commonly reported.

## Polymer Identification

According to the study of Yang et al. (2021), the presence of Microplastics is crucial for determining the source of contamination. Polyethylene, polypropylene, polyvinyl chloride, polyamide, polystyrene, and polyester are the most prevalent polymers found in soil. Polyethylene and polypropylene are the most commonly found in soil.

Microplastic pollution has recently received a lot of attention both from the general public as well as scientific communities all over the world, with a focus on aquatic settings, particularly the marine environment (Hidalgo-Ruz et al. 2012, Auta et al. 2017). The availability of Microplastics in the oceans has been linked mostly to ongoing inputs and also the degradation and fragmentation of large plastic litter (Hidalgo-Ruz et al. 2012), the vast majority of which are emitted from land (Rezania et al. 2018).

Microplastics in aquatic conditions may be consumed by Oligochaeta, crustacea, mollusks, nematodes, and vertebrates (Jambeck et al. 2015, Desforges et al. 2015, Hurley et al. 2007, Lei et al. 2018b). Microplastics and

plastic-derivative compounds, such as plastic additives and adhered contaminants, have been linked to diversified toxicological effects that include inflammatory responses, metabolic disorders, stunted growth and reproduction issues, and other lethal issues (Hurley et al. 2007). Such circumstances are also likely for soil biota. Microplastics have been a research-intensive subject in aquatic environments for over a decade (Van Cauwenberghe et al. 2015, Akdogan & Guven et al. 2019, Rillig 2018, Cole et al. 2014, Riilig & Bonkowski 2018, Cozar et al. 2014, Ivleva et al. 2017).

Microplastics accumulate more in terrestrial soil than in aquatic habitats (Zhao et al. 2018). As per UNEP reports, substantial amounts of particle plastics observed in the marine environment worldwide originate from land-based sources (UNEP, 2016). According to Rezania (2018), around 4.8 - 12.7 Mt of terrestrial plastic garbage is found entering the ocean every year, accounting for approximately 1.7-4.6% of total plastic waste generated globally. Sediment transmission during soil erosion is an event that permits particle plastics to be transported from terrestrial to aquatic habitats. Despite this connection to terrestrial resources, numerous scientific studies on the particles of plastic have overlooked the consequences of these synthetic materials (Bolan & Bradney 2019). Given that the majority of plastic waste is generated and discharged on land, it is surprising that Microplastics research has only recently begun to focus on terrestrial systems, where soil appears as a long-term sink for Microplastics debris (Kumar et al. 2020, Moller et al. 2020, Rochman 2018). Terrestrial domains, such as soils, are more vulnerable to plastic contamination than the oceans. According to Nizzetto et al. (2016), the annual input of Microplastics from sewage and wastewater treatment sludge on agricultural fields could exceed the total amount of Microplastics currently floating in the global oceans. Although the underlying mechanisms are unknown, preliminary data suggest that the presence of Microplastics in soils may impact the soil properties, plant performance, and microbial activity (de Souza Machado et al. 2019).

Recent research has discovered a considerable amount of filamentous and fragmented Microplastics in soils all around the world (Zhao et al. 2018). For example, recently discovered fragmented-dominated Microplastics in agricultural soils, where sewage sludge application promotes a Microplastics buildup (van den Berg et al. 2020). Microplastics accumulated in the soil can be easily taken up by plants and transferred through the food chain (Guo et al. 2020).

Although the genesis and potential translocation pathways of Microplastics in soil are varied, including the use of sewage-generated sludge and organic compost (Huerta

Lwanga et al. 2017), irrigation (Blasing & Amelung 2018), plastic mulching (Yang et al. 2021), littering (Akdogan & Given 2019), and atmospheric deposition (Allen et al. 2019), urban soil used for agriculture is more prone to Microplastics pollution since they are often exposed to Microplastics (Moller et al. 2020, Chase et al. 2018).

Microplastics have been shown to harm soil health and function (de Souza Machado et al. 2018b, Liu et al. 2018), as well as in marine environments. Contamination will certainly result in inadvertent Microplastics ingestion by soil fauna. Worms, including Earthworms and ringworms, have been shown to consume Microplastics, with the rate increasing substantially as the amount of Microplastics rises; for example, Huerta Lwanga et al. (2017) detected around 14.8-28.8 Microplastics particles/gram of earthworm casts and 129.8- 82.3 particles/grams of chicken feces in home garden soils. Panebianco et al. (2019) discovered Microplastics in the majority of the snails (a total of 425 specimens), with an average of 0.92-1.21 particles/5 snails.

Plastic trash, particularly biodegradable plastics, is more prone to physical fragmentation than decay by mineralization, resulting in smaller plastic sizes. Natural disintegration and degradation of Microplastics can produce plastic particles as small as 0.1 mm in diameter, known as nano-plastics (NPs)(de Souza Machado et al. 2018a, 2018b). The plastics gradually weather and accumulate in the soil, contaminating the soil with Microplastics fragments. Furthermore, the recent increase in the number of waste sites has made soil huge Microplastics sink. Microplastics migration in soil happens both vertically as well as horizontally, i.e., they are conveyed to people and animals horizontally via the terrestrial food chain and drain down vertically into groundwater with run-off. Microplastics have also been identified in sheep faces, which were most likely biomagnified by feed and the surrounding environment (Beriot et al. 2021).

In agricultural fields, plastic mulching is widely used across the world to boost yields, improve fruit quality, and improve water usage efficiency (Ashrafuzzamann et al. 2011). Furthermore, due to their specific optical and material properties, plastic mulches are employed globally (Chalker-Scott et al. 2007). Besides this, the use of organic fertilizers and films made up of plastic in agricultural operations is the primary cause of Microplastics (MP) buildup in farms (Weithmann et al. 2018).

A study by Kumar et al. (2021) shows that plastic mulching has been detected in four locations for producing vegetables viz tomatoes and beans in different regions of Tamil Naidu, India. The soil from the Sular region had more plastic residues than the soil compared to the other areas. At a depth of 0-10 cm, the plastic content of the soil taken from

Sular varied from  $0.092 \pm 0.02$  to  $4.96 \pm 0.08$  g kg<sup>-1</sup> soils. The plastic content varied from  $0.075 \pm 0.01$  to  $3.45 \pm 0.01$  at a depth of 11-20 cm. At a depth of around 21-30 cm, the plastic content was determined to be in a range of  $0.01 \pm 0.02$  to  $2.81 \pm 0.01$  g kg<sup>-1</sup> soils.

## SOURCES OF MICROPLASTICS IN AGRICULTURAL SOIL

Microplastic sources are primarily characterized as either primary or secondary (Cole et al. 2011, Thompson & Richard 2015). Primary Microplastics are designed with specific applications in mind, such as cosmetic harsh chemicals, drug vectors, and engineering-related uses such as air blasting (Auta et al. 2017, Hays et al. 1974). Microplastics are difficult to eliminate utilizing sewage disposal systems, and once they enter the wastewater, they eventually accumulate in the environment (Van Cauwenberghes et al. 2015).

Secondary Microplastics are formed when bigger plastics are gradually shattered into smaller bits by a variety of complicated environmental factors, including wave action, temperature of wind, and UV radiation (Andrady 2011, Rocha-Santos & Duarte 2015). Repeated usage of products made of plastics can induce fragmentation and the development of additional Microplastics (Hartline et al. 2016). Furthermore, plastic emissions from vehicle transportation, such as wearing and tearing of tires, brakes, and road markings, are major contributors to Microplastics in the natural environment (Gieré et al. 2018). The World average of Microplastics emissions from road vehicle tire abrasion was calculated to be  $0.81$  kg.year<sup>-1</sup>.capita<sup>-1</sup> (Kole et al. 2016). Aside from Vehicles, abrasion from aircraft tires accounts for around 2% of total tire disintegration emissions in the Netherlands (Kole et al. 2016).

Furthermore, artificial grass is a major secondary source of Microplastics, with estimates ranging from 760-4500 t.y<sup>-1</sup> (Kole et al. 2016, Lassen et al. 2015, Magnusson et al. 2016) result, many types of Microplastics are discharged into natural environments and ecosystems. Compared to the sources of Microplastics in the ocean, which primarily include land-based sources (80%), tourism on the coast, recreational and commercial fishing gear contributing 18%, shipping and marine industries (e.g., aquaculture, oil rigs, etc.) (Cole et al. 2011, Hays & Cormons 1974, Kole et al. 2016). Microplastics enter soil through a variety of pathways, including landfills (He et al. 2019), amendments of the soil (Zubris et al. 2005), sewage sludge land application (Corradini et al. 2019, Mintenig et al. 2017, Ziajahromi et al. 2017), wastewater irrigation. Furthermore, plastic debris in soil also fragments into Microplastics by the actions of soil fauna, such as feeding, digesting, and excretion (Chae et al. 2018).

## Direct Sources/Primary Sources of Microplastics in Agricultural Oils

### Plastic Mulching

Massive but undetectable sources of plastics are continually flooding the soil, causing Microplastics deposition, but with no obvious ability to stop or disrupt them. Mulch film, which is made of polyvinyl chloride and polyethylene, has become a popular technique in worldwide agriculture because of its numerous economic benefits, including increased harvest, enhanced quality of fruits, and water use efficiency (Yang et al. 2021). In 2016, the worldwide market for agricultural films made of plastic was 4 million tonnes, and it is predicted to rise at a pace of 5.6 percent per year by 2030 (Jambeck 2015).

Large chunks of plastic mulch debris lying on the farm land's surface are naturally exposed to UV light, producing photo-degradation and becoming brittle (Astner et al. 2019). Shear pressures on plastic trash in farmland will also be felt when agricultural soils are plowed and cultivated, potentially fragmenting already fragile polymers (Piehl et al. 2018).

According to the study by Kumar et al. (2021), Microplastics are found in the 3 regions of India in the amount of 37.97%, 35.07%, and 36.99% of the tomato fields that use the process of Plastic Mulching in Fig. 1.

### Littering

The excessive growth of plastics and unplanned or poor management procedures have increased the presence of a large variety and range of Microplastics waste in the soil

(Akdogan & Given 2019, Kumar et al. 2020). Microplastics in aquatic environments can emerge from a substantial volume of plastic trash (Blasing et al. 2018). From the 1950s till 2015, roughly 6.3 Bt of plastic rubbish was created globally, with 4.97 Bt ending up in landfills and natural habitats (Geyer et al. 2017).

### Silage and Bale Nets

In the first research addressing the issue of the presence of Microplastics in soils at an agricultural scale, (Piehl et al. 2018) indicated the pollution of livestock feeds due to the use of plastics in the form of wrapped grass bales and silage after intake, may enter the soil through excretion.

### Twine

The twine composed of Polypropylene (PP) is used for various agricultural uses (Guerrini et al. 2017). Twine helps to secure plants to stakes for significant crops, including tomatoes, crucifers, sweet peppers, etc. It is utilized in the cultivation of bananas to connect plants and keep them from toppling over (Hernandez & Witter 2016). During harvesting, the twine is cut and frequently dumped carelessly in the fields only, where it ends up in the form of Microplastics in the soil. There are initiatives to promote the use of biodegradable twine, which may be gathered along with plant leftovers and composted (Guerrini et al. 2017, Biothop 2019).

### Plastics Used for Plant Protection

Plastic films, along with non-woven textiles made of plastic, such as those utilized in greenhouses, polytunnels, shade

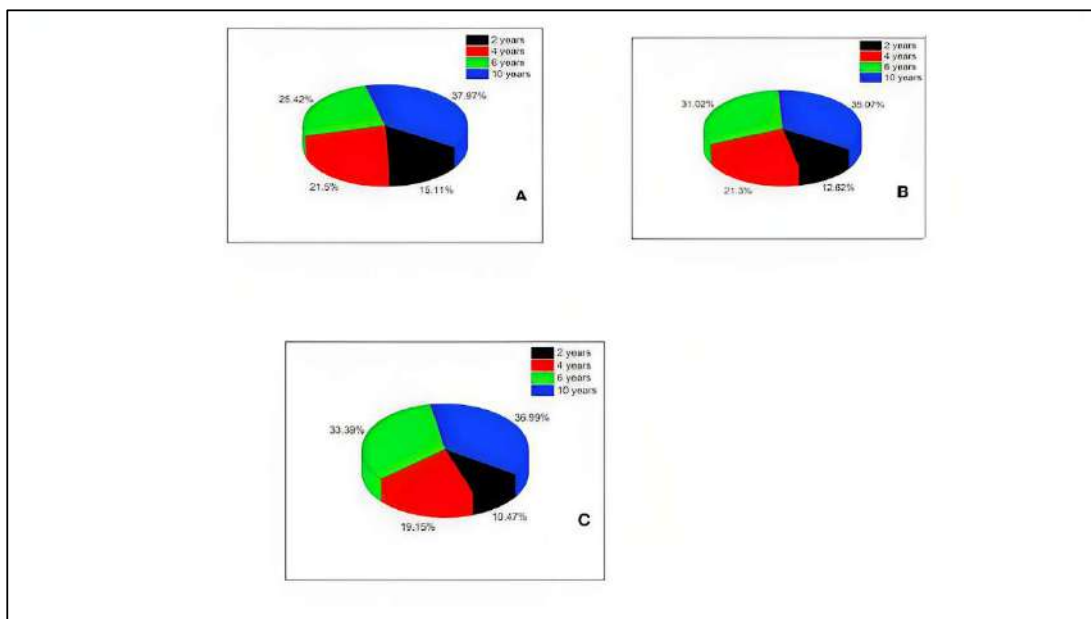


Fig. 1: Effect of the duration of plastic film mulching on percent distribution of plastic residues at different soil depths (A) 0-10 cm (B) 11-20 cm (C) 21-30 cm by Kumar et al. (2021).



nets, and also as wind barriers, enhance the presence of Microplastics in soil samples. Liu (2021) reported that for an identical productive area, samples of soil collected from farms without greenhouses contained fewer Microplastics compared to soil samples collected from farms with greenhouses. At fields where greenhouses were initially utilized in the 1980s, the authors recorded a range of 1000 - 3786 particles of MP kg<sup>-1</sup>. Liu (2021) also observed an average of 2110 MP kg<sup>-1</sup> in soil samples collected within greenhouses compared to 310/kg Microplastics in soil samples collected outdoors.

### Improper Storage

According to Svensk Ensilageplast Retur, Plastic may be found in abundance on an agricultural farm. Farmers have to put additional efforts into collecting and storing old plastics since they frequently lack the time or technical competence to securely clean and preserve the used ones. To keep plastic garbage clean and avoid it from blowing away, it must be deposited in a dry spot that is shielded from the wind. Plastic waste management in agricultural regions is a major problem, which can be ascribed in part to inappropriate plastic storage on farms.

### Indirect Sources/Secondary Sources of Microplastics

#### Sewage Sludge

Sludge from sewage and wastewater treatment plants causes Microplastics contamination, and Microplastics can build in soil with repeated sludge use (Xu et al. 2021). Microplastics enter wastewater treatment facilities via a variety of routes (Gao 2018). Micro beads from personal cleaning and care products, polymer fibers released from washing textiles, plastic masterbatches seeped from the plastic production facility, and Microplastics from automobile tires are all transmitted to sewage. These tiny particles flow and settle throughout the sewage treatment process. A portion of them is released from the sewage system, while the majority is segregated during the sewage treatment sedimentation process and eventually enters the wastewater sludge (Gao 2018).

#### Compost

Compost soil addition can potentially provide a conduit for Microplastics to enter the soil. Organic waste is often placed in fields as nutrients after it has been composted and fermented for reuse nutrients, minerals, trace elements, and humus. Composts made from biological waste, for example, have been shown to include plastics as a result of improper disposal and insufficient waste categorization (Blasing & Amelung 2018). The concentration of plastic pieces detectable to the human eye in a composting factory in Bonn is 2.38 to 180 mg kg<sup>-1</sup>, confirming the presence of Microplastics in organic compost (Blasing & Amelung

2018). Weithmann et al. (2018) discovered that the compost from municipal organic waste and green clipping in German contained 24MP particles/kg ranging in size from 1mm to 5mm. Furthermore, according to (Crossman 2020), despite compliance with current regulations, biosolid applications may result in significant rates of Microplastics export. Liu (2021) discovered that total Microplastics concentrations in soils are 545.9 and 87.6 items/kg after yearly launch with 30 and 15 t ha<sup>-1</sup> of sludge composts, respectively, which is considerably higher than soil lacking compost application.

### Irrigation

The presence of Microplastics in agricultural irrigation water resources has been widely verified (Jian et al. 2020). Rivers, lakes, reservoirs, and aquifers are the primary irrigation water sources worldwide. Sewage is also utilized for irrigation in some locations when water resources are restricted (Blasing & Amelung 2018). Despite the fact that a substantial number of Microplastics may be eliminated during the sewage treatment process, high quantities of Microplastics remain in the purified wastewater (Ziajahromi 2017). Several studies have shown significant amounts of Microplastics in rivers, lakes, reservoirs, and aquifers (Koelmans et al. 2019). Microplastics contained within water reservoirs will be transported to the soil by irrigation, creating a pedigree of Microplastics in the soil.

### Flooding and Street Runoff

Street runoff and floods, in addition to purposeful irrigation, are key channels for the transfer and accumulation of Microplastics into the soil (Blasing & Amelung 2018). Street runoff and floods can introduce unmanaged rubbish dumping near roadways, as well as rubber tire abrasion into soils. Some of them already constitute Microplastics, while others are progressively changed into Microplastics as a result of numerous environmental encounters.

### Input From the Atmosphere

Atmospheric transmission is a significant mode of Microplastics deposition to land. A study (Liu et al. 2019) quantified and recorded the first to record and quantify the accumulation of fibrous Microplastics both indoors and outdoors, with the settled flux of atmospheric Microplastics outside reaching 0.3-1.5 fibers m<sup>-3</sup> (Liu et al. 2019). Every day, relative averages of around 249 fragments, 74 pieces of film, and 43 fibers might be deposited in a distant mountainous catchment region (Allen et al. 2019).

## TRANSPORTATION OF MICROPLASTICS TO AGRICULTURAL SOILS

Migration, which includes horizontal and vertical movement as well as biological and non-biological transportation, is

a critical link for extending the effect of Microplastics in soil (Xu et al. 2021). Surface runoff or wind can transport Microplastics in surface soil (Koelmans et al. 2019, Qi et al. 2018). The presence of Microplastics in deep soil indicates that Microplastics migrate downhill (Liu et al. 2018). Since Soil is porous, Microplastics in the micrometer ( $\mu\text{m}$ ) range can be percolated through soil pores via leaching. External pressures such as biological disturbance by the fauna and flora and agricultural operations cause bigger Microplastics to move in the soil.

Also, the bioturbation of plant roots in soil may influence Microplastics translocation through root growth and movement, root water extraction, and furthermore. Soil fauna may help to move Microplastics vertically and horizontally in the soil (Xu et al. 2020). Microplastics have been discovered to be transferred and dispersed by earthworms and collembola species, either by adhesion or excretion (de Souza Machado et al. 2019, Maaß et al. 2017). Furthermore, the formation of fractures in the soil produced by the dry environment allows Microplastics to enter deep soil (Koelmans et al. 2019, Qi et al. 2018).

## METHODS TO EXTRACT MICROPLASTICS FROM THE SOIL

### Density Separation

The technique of density separation is one of the most often used techniques for separating soil Microplastics. To ensure every particle in the bulk sample sinks or floats, the soil is first treated with ultrasonics (Liu et al. 2018). Sodium chloride is a low-cost, ecologically friendly salt that is commonly used in suspension solutions (Zhou et al. 2018). Yet, the density of a saturated solution of NaCl is  $1.2 \text{ g cm}^{-3}$ , implying that high-density polymers such as polyvinyl chloride (PVC,  $1.35 \text{ g cm}^{-3}$ ), polyethylene terephthalate (PET,  $1.38 \text{ g cm}^{-3}$ ), and others cannot be separated in this method (Ruggero et al. 2020). As a result, for the suspension medium, several researchers employ a saturated solution of zinc chloride ( $\text{ZnCl}_2$ ), sodium iodide (NaI), sodium bromide (NaBr), calcium chloride ( $\text{CaCl}_2$ ), and zinc bromide ( $\text{ZnBr}_2$ ) (Imhof et al. 2017, Scheurer & Bigalke 2018).

### Electrostatic Separation

Plastics are not electrically conductive, unlike soil minerals and other particles. An external electric field can be used to separate the two because of the difference in electrostatic characteristics. Electrostatic separation is a dry processing technology that uses electric forces working on charged particles to separate main and secondary raw materials (Deotterl et al. 2000). It was investigated that plastic

particle's electrostatic behavior can be improved before separation from sediment samples using a tiny electrostatic separation apparatus. Without sacrificing Microplastics, up to 99% of the original sample mass might be eliminated (Felsing et al. 2018).

### Oil Separation

The lipophilic characteristics of microplastics are used as an alternative to density-based oil recovery technologies in a new, cost-effective oil extraction process (OEP) (Crichton et al. 2017). For seven polymers, the OEP exhibited a recovery ratio of 90-100%, showing a better efficiency than density separation in a salt solution. OEP is less complicated, easier, and less expensive than salt solution separation. However, oil interferes with Fourier Transform Infrared Spectroscopy (FTIR) for identification; thus, a wash with 90% ethanol is required following extraction. Using castor oil, Mani et al. (2019) separated MPs from fluvial suspended surface solids, marine suspended surface solids, marine beach sediments, and agricultural soil substrates. In this investigation, 0.3-1 mm MP particles were extracted utilizing four virgin polymers [polypropylene (PP), polystyrene (PS), polymethyl-methacrylate (PMMA), and glycol-modified polyethylene terephthalate (PETG)]. The average SD MPs spike recovery percentage was 99.4%, with a 95.4% matrix decrease (dry weight,  $n = 16$ ). This process is less expensive, less risky, and more rapid than salt solution isolation.

### Froth Flotation

Froth flotation takes the use of the material's density and the hydrophilic nature of its surface. It is widely employed in the recycling sector. Froth preferentially binds to hydrophobic particles and lifts them upward, segregating them from hydrophilic molecules. To remove plastics from dirt, this approach employs various hydrophilic properties. Plastic flotation techniques include gamma flotation, reagent adsorption, and surface modification (Fraunholz 2014, Huang et al. 2017) attained a 95% recovery rate for PVC and PMMA by using pinacol (97.71% pure) as the foaming agent and potassium permanganate as the surface modification. In study conducted by Imhof et al. (2017) extracted MPs from sediments using froth flotation but observed low observed found low efficiency and substantial variance across various polymers.

### Magnetic Extraction

Grbic et al. (2019) created a magnetic plastic extraction technique in which Magnetized hydrophobic iron nanoparticles are bonded to plastic particles. Iron nanoparticles bond to the surface of Microplastics after being treated with hydrophobic hydrocarbons using cetyl

trimethyl silane (HDTMS) and may be retrieved using a magnetic field. Microplastics (polyethylene, polystyrene, polyurethane, PVC, and polypropylene) recovered from fresh water and sediment were 84% and 78%, respectively, spanning particle sizes ranging from 200 m to 1 mm.

## ANALYTICAL TECHNIQUES FOR ANALYSIS OF MICROPLASTICS

Identification and quantification of Microplastics from the ambient matrix are required after separation and purification (Kumar et al. 2020). The common strategy is to first identify obvious/possible Microplastics using a microscope, followed by confirmation using spectroscopy and thermodynamic methods such as Fourier Transform infrared spectroscopy (FTIR) or Raman spectroscopies, and Pyrolysis gas chromatography-mass spectrometry (Yang et al. 2021). Optical microscopes, particularly stereomicroscopes, are essential tools for documenting the physical features of Microplastics (Wang et al. 2018a, 2018b)

By using the microscope, the micron ( $\mu\text{m}$ ) range of the particles can be analyzed. This approach can swiftly identify Microplastics and record their physical properties and abundance. However, Microplastics with diameters of 1 mm are difficult to detect. As a result, only visible Microplastics are easily identified. Furthermore, in order to avoid inaccurate results and other misinterpretations, the technique necessitates labor-intensive pre-concentration and laboratory hygiene. Integrating high-resolution digital cameras into microscopes, on the other hand, allows for the identification of smaller particles as well as the determination of particle size. This approach has the advantage of being non-destructive (Zhang et al. 2019). Unfortunately, visual detection of Microplastics can be occasionally inaccurate (David et al. 2018, David et al. 2019). Additionally, without the assistance of FTIR and Raman spectroscopies, which use their distinctive absorption spectrum to identify the associated functional groups, the microscope can't determine the detailed chemical composition of Microplastics.

Furthermore, without the support of FTIR and Raman spectroscopies, which employ distinctive absorption spectra to identify the relevant functional groups, the microscope cannot detect the exact chemical composition of Microplastics. Optical microscopes, particularly stereomicroscopes, are essential tools for documenting the physical features of Microplastics ((Wang et al. 2018a, Wang et al. 2018b). However, visual assessment alone might result in a large number of false positives, particularly for small fibers. FTIR and its optimization technologies, such as micro-FTIR (- FTIR), attenuated total reflectance FTIR (ATR-FTIR), and focal plane arrays FTIR (FPA-FTIR),

thereby demonstrate significantly increased Microplastics characterization capabilities (Wang et al. 2018a, 2018b). These infrared spectroscopic sensors have a detection limit of 5-10 m for Microplastics (Mintenig et al. 2017, Yang et al. 2021). FTIR can identify Microplastics with a particular thickness and has a detection limit of 10 m. The use of ATR-FTIR can benefit from the high signal-to-noise ratio and the extensive literature spectrum (Yang et al. 2021). Focal plane array FTIR can be employed in precision equipment to automatically identify the Microplastics in the sample filter of the preliminary polymer types allocated (Mintenig et al. 2017).

Raman spectroscopy is a further technique for identifying Microplastics. When used in conjunction with a microscope, it can identify Microplastics as tiny as 1 m in size, with spatial resolution reaching as low as 500 nm in some situations (Elert et al. 2017). Another significant benefit of Raman spectroscopy is its ability to analyze wet materials while also identifying fillers or pigments (Dumichen et al. 2017).

Three mass spectrometry analysis methods offer novel approaches for identifying Microplastics (Pual et al. 2019). Pyrolysis-gas chromatography-mass spectrometry (Pyr-GC-MS) (Nuelle et al. 2014), thermo-gravimetric analysis-mass spectrometry (TGA-MS) (Majewsky et al. 2016), as well as thermal extraction desorption-gas chromatography-mass spectrometry (TED-GC-MS) (Pual et al. 2019) have also been demonstrated to be in useful identifying and quantifying Microplastics (Wang et al. 2018). Thermo analytical methods do not need sample pretreatment, and the processed particle size that may be analyzed is limited only by the ability to manually place them into the pyrolysis tube (Zhao et al. 2018). Unfortunately, these procedures remove the Microplastics' color, size, and shape information, which is critical for assessing the potential hazards of Microplastics.

A new approach for size-independent Microplastics analysis has developed (Piehl et al. 2018). Polycarbonate (PC) and polyethylene terephthalate (PET) Microplastics were effectively quantified using the alkali-assisted heating depolymerization technique (Wang et al. 2018). This technology represents a significant advancement in the painstaking separation, recognition, and counting of Microplastics. However, for polymers containing a wide range of important structural components, this technique e requires further validation.

Several technologies, including NIR spectroscopy (Du et al. 2020a), quantitative H-NMR spectroscopy, and hyperspectral imaging technology, offer alternative options for high-throughput Microplastics investigation (Shan et al. 2018). Although these methods need minimum sample preparation, they do have certain intrinsic limitations that

may limit their use (Wang et al. 2018a, 2018b). So far, the sensitivity and specificity trials of the integrated NIR spectroscopic chemometric method have failed (Du et al. 2020a). To reduce signal variations, the best setting for the  $^1\text{H-NMR}$  approach is to remove any organic debris from the sample (Moller et al. 2020). It is now hard to entirely remove organic materials from environmental samples without destroying the Microplastics, and the application of  $^1\text{H-NMR}$  for the examination of soil Microplastics samples is dubious (Moller et al. 2020).

(TOF-SIMS) Time-of-flight secondary ion mass spectrometry might offer information on the Microplastic's size distribution and chemical components (Rillig et al. 2017a). This approach, however, can only be utilized to analyze Microplastics with known composition.

## IMPACT AND POTENTIAL RISK OF MICROPLASTICS IN AGRICULTURAL SOIL ECOSYSTEM

Soil nature influences Microplastics migration, and Microplastics change soil properties such as soil structure and functioning as well as the diversity of microbes (Rillig et al. 2017b, Zhang et al. 2018), which may have implications for plant and animal health and pose possible risks for the safety and quality of food, ultimately jeopardizing human health (Rillig et al. 2018). The presence of substantial residual plastic films in soil has been found to reduce soil-saturated hydraulic conductivity and influence soil microbial activity and abundance, thereby influencing soil fertility (Wan et al. 2018).

### Impact on Soil Structure

Because Microplastics can interact with different soil features, soil nature may be the fundamental metric for assessing the dangers presented to terrestrial ecosystems by Microplastics (de Souza Machado et al. 2018a). To variable degrees, Microplastics particles may penetrate soil aggregations and clumps: loosely in fragment types and more firmly in linear types (Liu et al. 2018). Furthermore, de Souza Machado et al. (2018b) discovered that polyester fibers may significantly boost capacity while decreasing bulk density and water-stable aggregation; yet, the impacts of polyethylene (PE) and polyacrylic acid on water-holding capacity show no clear trends. As a result, Microplastics of various materials have varying impacts on soil. Microplastics have also been demonstrated to influence soil permeability and water retention, which affects the evaporation of water (de Souza Machado et al. 2018a, Wang et al. 2018). Wan evaluated how the addition of Microplastics affects the evaporation of water and desiccation cracking in two clay soils and found that

both are significant and rise with increasing Microplastics concentration (Allison & Jastrow et al. 2006). According to these findings, Microplastics can change the water cycle in soils, increase soil water shortages, and influence pollutant migration into deep soil layers through fissures (Rillig 2018).

### Soil Fertility and Nutrient

Soil enzymes with high catalytic capacity are closely associated with a variety of soil biochemical processes; these enzymes serve as an indicator for assessing soil fertility and play an important role in regulating the process of soil nutrient cycling for nutrients like C, N, and P (Trasar-Cepeda et al. 2008, Arthur et al. 2012). Since Microplastics include polymer chains, Microplastics -Carbon may be disguised as a significant caused by human components of the soil organic carbon pool (Rillig 2018). Therefore, according to de Souza Machado et al. (2018b), the impacts of Microplastics on soil are largely dependent on Microplastics content as well as the exposure period.

### Soil Microorganisms

According to researchers ((Rillig 2018, Girvan et al. 2003, Naveed et al. 2016, and Rubol et al. 2013), soil characteristics and nutrients are highly linked with soil microbial activity. Changes in the physical environment of the soil, particularly soil aggregation, which has been shown to include linear microfibers (de Souza Machado et al. 2018a, Zhang et al. 2019), are likely to affect microbial development more significantly than non-microfiber-structured soils (Rillig et al. 2017b, Zhang et al. 2018). Furthermore, Microplastics-induced changes in soil porosity and wetness may affect the flow of oxygen in the soil, altering the proportions of anaerobic and aerobic microbes (Veresoglou et al. 2015). Changes in pore spaces induced by Microplastics may also result in the extinction of indigenous microorganisms (Judy et al. 2019). Furthermore, DeForest et al. (2004a) discovered that the addition of Microplastics considerably interacted with the microbial community composition, and the substrate-induced respiration (SIR) levels dramatically dropped, showing that Microplastics generated alterations in soil microbial function. Because Dissolved organic matter (DOM) serves as a substrate and an important source of carbon for microorganisms, it has been linked to both water eutrophication and the greenhouse effect (DeForest et al. 2004b, Marschner & Kalbitz 2003, Alimi et al. 2018). Thus, changes in DOM caused by Microplastics could impact soil function and microbial communities (Judy et al. 2019).

### Soil Contamination

The growing prominence of Microplastics as an ecosystem stressor impacts not only soil health and function but also soil

biophysical characteristics, resulting in complicated changes in the environmental behavior of other soil contaminants (Wang et al. 2018a, 2018b, Yang et al. 2021, Hahladakis et al. 2018). Due to their high specific surface area and elevated adsorption capacity, Microplastics not only contain additives like diethylhexyl phthalate (DEHP), a common organic pollutant used during the manufacture of plastic (Groh et al. 2019, Brennecke et al. 2016), but they also adsorb dangerous contaminants, such as heavy metals like zinc, copper, and lead, antibiotics, toxic organic chemicals like polybrominated diphenyl ether (PBDE) and perfluorochemicals (PFOS), and PFOS (Gaylor et al. 2013, Li et al. 2018, Lagana et al. 2018, He et al. 2018).

### Transfer Along Food Chains

The most alarming findings in the research on Microplastics in soil come from the ecological and health concerns posed by Microplastics exposure (Guo et al. 2020, Sarker et al. 2020, Kumar et al. 2020, Schwabl et al. 2019). The concept that Microplastics can be transported from prey (at a lower nutritional level) to a predator (at a higher nutritional level) in the food chain is supported by food chain modeling and field experiments (Guo et al. 2020). Evidence of macro- and Microplastics transmission from soils to chickens in traditional Mayan household gardens in Southeast Mexico is well documented by Huerta Lwanga et al. (2017). Microplastics have recently been found in human feces and adult colectomy tissues, demonstrating their presence in the human digestive system (Ibrahim et al. 2021, Jiang et al. 2019).

### Uptake of Microplastics by Plants

According to Zhou et al. (2018), the presence of Microplastics would alter the physical and chemical properties of the soil, which will alter the root system and the vegetative phase and thus impair plant growth. Certain Present studies showed significant effects of Microplastics on plants, including wheat (*Triticum aestivum*) (Qi et al. 2018), perennial ryegrass (*Lolium perenne*), *Vicia faba* (Khalid et al. 2020), Polystyrene Microplastics (PS-MPs) were shown to cause evident growth suppression, genotoxic and oxidative damage to hydroponic *Vicia faba*, and a substantial number of 100 nm PS-MPs were found to collect in root tips using laser confocal scanning microscopy (Khalid et al. 2020).

### Agricultural Production

Soil Microplastics can cause direct crop harm in the early stages by physically blocking the seed capsule openings or roots (Pignattelli et al. 2020). Indeed, with Microplastics exposure, extremely short-term unfavorable impacts on edible plant development may show as early as 6 days after

sowing (Napper & Thompson 2019). Furthermore, the extreme durability of polymeric plastic particles hinders breakdown processes; even biodegradable plastic bags stay unchanged after 27 months in soil (Kumari et al. 2022, Silva et al. 2021). The direct absorption of Microplastics from soils through apoplastic and symplastic routes, and by distribution to the plant as a whole through the vascular system, is well documented to affect the development of agriculturally important plants. According to Bouaicha et al. (2022), from the perspective of agricultural output, Microplastics generally have a detrimental influence on crop productivity.

### FUTURE CHALLENGES

There are several future challenges associated with Microplastics contamination in the agricultural soil -

- **Widespread Soil Contamination:** The proliferation of microplastics in soil poses an ongoing challenge, as current levels continue to rise due to persistent plastic use and inadequate waste management.
- **Ecosystem Disruption:** Microplastics impact soil ecosystems, potentially altering microbial communities, nutrient cycling, and overall soil health, leading to cascading effects on plant and animal life.
- **Agricultural Concerns:** The use of plastic mulching in agriculture, a primary source of microplastics in soil, presents a dilemma, as alternatives must be developed and adopted to reduce environmental harm without compromising crop productivity.
- **Human Health Risks:** The potential transfer of microplastics through the food chain raises concerns regarding human health impacts. Research is needed to figure out the extent of these risks and implement strategies to minimize exposure.
- **Lack of Comprehensive Regulation:** The absence of strict regulations governing plastic production, use, and disposal contributes to the persistence of microplastic pollution. A coordinated global effort is necessary to address these gaps.
- **Limited Biodegradation:** The slow degradation of plastics exacerbates the persistence of microplastics in the environment. Developing and adopting more biodegradable alternatives is essential for reducing long-term environmental impacts.

### REFERENCES

- Akdogan, Z. and Guven, B., 2019. Microplastics in the environment: A critical review of current understanding and identification of future research needs. *Environmental Pollution*, 254, p.113011.

- Alimi, O.S., Farner Budarzi, J., Hernandez, L.M. and Tufenkji, N., 2018. Microplastics and nanoplastics in aquatic environments: aggregation, deposition, and enhanced contaminant transport. *Environmental Science & Technology*, 52(4), pp.1704-1724.
- Allen, S., Allen, D., Phoenix, V.R., Le Roux, G., Jimenez, P.D., Simonneau, A., Binet, S. and Galop, D., 2019. Author Correction: Atmospheric transport and deposition of microplastics in a remote mountain catchment. *Nature Geoscience*, 12, pp.339-344.
- Allison, S.D. and Jastrow, J.D., 2006. Activities of extracellular enzymes in physically isolated fractions of restored grassland soils. *Soil Biology & Biochemistry*, 38, pp.3245-3256.
- Andrady, A.L., 2011. Microplastics in the marine environment. *Marine Pollution Bulletin*, 62, pp.1596-1605.
- Arthur, C., Baker, J. and Bamford, H., 2009. The occurrence, effects, and fate of microplastic marine debris. *NOAA*, 11, p.30.
- Arthur, E., Moldrup, P., Holmstrup, M., Schjonning, P., Winding, A., Mayer, P. and de Jonge, L.W., 2012. Soil microbial and physical properties and their relations along a steep copper gradient. *Agriculture, Ecosystems & Environment*, 159, pp.9-18.
- Ashrafuzzaman, M., Halim, M.A., Ismail, M.R., Shahidullah, S.M. and Hossain, M.A., 2011. Effect of plastic mulch on growth and yield of chili (*Capsicum annum* L.). *Brazilian Archives of Biology and Technology*, 54(2), pp.321-330.
- Astner, A.F., Hayes, D.G., O'Neill, H., Evans, B.R., Pingali, S.V., Urban, V.S. and Young, T.M., 2019. Mechanical formation of micro- and nanoplastic materials for environmental studies in agricultural ecosystems. *Science of the Total Environment*, 685, pp.1097-1106.
- Auta, H.S., Emenike, C.U. and Fauziah, S.H., 2017. Distribution and ecological impact of marine microplastics: A review of scientific evidence. *Environment International*, 102, pp.165-176.
- Beriot, N., Peek, J., Zornoza, R., Geissen, V. and Lwanga, E.H., 2021. Low-density microplastics detected in sheep feces and soil: A case study from intensive vegetable farming in southeast Spain. *Science of the Total Environment*, 755, p.142653.
- Biothop, 2019. *Biotwine Hop Waste Transformation Into Novel Product Assortments for Packaging and Horticulture Sector*. Biothop.
- Blasing, M. and Amelung, W., 2018. Plastics in soil: Analytical methods and possible sources. *Science of the Total Environment*, 612, pp.422-435.
- Bolan, N. and Bradney, L., 2019. Particulate plastics in soils. *Chemistry in Australia*, 18.
- Bouaicha, O., Mimmo, T., Tiziani, R., Praeg, N., Polidori, C., Lucini, L., Vigani, G., Terzano, R., Sanchez-Hernandez, J.C., Illmer, P. et al., 2022. Microplastics make their way into the soil and rhizosphere: A review of the ecological consequences. *Rhizosphere*, 22, p.100542.
- Brennecke, D., Duarte, B., Paiva, F., Cacador, I. and Canning-Clode, J., 2016. Microplastics as vectors for heavy metal contamination from the marine environment. *Estuarine, Coastal and Shelf Science*, 175, pp.189-195.
- Chae, Y. and An, Y.J., 2018. Current research trends on plastic pollution and ecological impacts on the soil ecosystem: A review. *Environmental Pollution*, 240, pp.387-395.
- Chalker-Scott, L., 2007. Impacts of mulches on landscape plants and the environment - A review. *Journal of Horticulture and Forestry*, 25, p.239.
- Cole, M., Lindeque, P., Halsband, C. and Galloway, T.S., 2011. Microplastics as contaminants in the marine environment: A review. *Marine Pollution Bulletin*, 62, pp.2588-2597.
- Cole, M., Webb, H., Lindeque, P.K., Fileman, E.S., Halsband, C. and Galloway, T.S., 2014. Isolation of microplastic in biota-rich seawater samples and marine organisms. *Scientific Reports*, 4, p.4528.
- Corradini, F., Meza, P., Eguiluz, R., Casado, F., Huerta-Lwanga, E. and Geissen, V., 2019. Evidence of microplastic accumulation in agricultural soils from sewage sludge disposal. *Science of the Total Environment*, 671, pp.411-420.
- Cozar, A., Echevarria, F., Gonzalez-Gordillo, J.I., Irigoien, X., Ubeda, B., Hernandez-Leon, S., Palma, A.T., Navarro, S., Garcia-de-Lomas, J., Ruiz, A., Fernandez-de-Puelles, M.L. and Duarte, C.M., 2014. Plastic debris in the open ocean. *Proceedings of the National Academy of Sciences of the United States of America*, 111, pp.10239-10244.
- Crichton, E.M., Noel, M., Gies, E.A. and Ross, P.S., 2017. A novel, density-independent, and FTIR-compatible approach for the rapid extraction of microplastics from aquatic sediments. *Analytical Methods*, 9(9), pp.1419-1428.
- Crossman, J., Hurley, R.R., Futter, M. and Nizzetto, L., 2020. Transfer and transport of microplastics from biosolids to agricultural soils and the wider environment. *Science of the Total Environment*, 724, p.138334.
- Da Costa, J.P., Paço, A., Santos, P., Duarte, A.C. and Rocha-Santos, T., 2019. Microplastics in the environment: Challenges in analytical chemistry - A review. *Environmental Chemistry*, 16, pp.145-156.
- David, J., Steinmetz, Z., Kučerik, J. and Schaumann, G.E., 2018. Quantitative analysis of poly(ethylene terephthalate) microplastics in soil via thermogravimetry-mass spectrometry. *Analytical Chemistry*, 90, pp.8793-8799.
- David, J., Weissmannová, H.D., Steinmetz, Z., Kabelíková, L., Demyan, M.S. and Šimečková, J., 2019. Introducing a soil universal model method (SUMM) and its application for the qualitative and quantitative determination of poly(ethylene), poly(styrene), poly(vinyl chloride), and poly(ethylene terephthalate) microplastics in a model soil. *Chemosphere*, 225, pp.810-819.
- de Souza Machado, A.A., Kloas, W., Zarfl, C., Hempel, S. and Rillig, M.C., 2018a. Microplastics as an emerging threat to terrestrial ecosystems. *Global Change Biology*, 24(4), pp.1405-1416.
- de Souza Machado, A.A., Lau, C.W., Kloas, W., Bergmann, J., Bachelier, J.B., Faltin, E., Becker, R., Gorlich, A.S. and Rillig, M.C., 2019. Microplastics can change soil properties and affect plant performance. *Environmental Science & Technology*, 53(10), pp.6044-6052.
- de Souza Machado, A.A., Lau, C.W., Till, J., Kloas, W., Lehmann, A., Becker, R. and Rillig, M.C., 2018b. Impacts of microplastics on the soil biophysical environment. *Biology*, 24, pp.1405-1416.
- DeForest, J.L., Zak, D.R., Pregitzer, K.S. and Burton, A.J., 2004a. Atmospheric nitrate deposition and the microbial degradation of cellobiose and vanillin in a northern hardwood forest. *Soil Biology and Biochemistry*, 36, pp.965-971.
- DeForest, J.L., Zak, D.R., Pregitzer, K.S. and Burton, A.J., 2004b. Atmospheric nitrate deposition, microbial community composition, and enzyme activity in northern hardwood forests. *Soil Science Society of America Journal*, 68, pp.132-138.
- Deotterl, M., Wachsmuth, U., Waldmann, L., Flachberger, H., Mirkowska, M., Brands, L., Beier, P.-M. and Stahl, I., 2000. Extraction and identification methods of microplastics and nanoplastics in agricultural soil: A review. *Journal of Environmental Management*, 294.
- Desforges, J.P., Galbraith, M. and Ross, P.S., 2015. Ingestion of microplastics by zooplankton in the Northeast Pacific Ocean. *Environmental Contamination and Toxicology*, 69, pp.320-330.
- Doyle, M.J., Watson, W., Bowlin, N.M. and Sheavly, S.B., 2011. Plastic particles in coastal aquatic ecosystems of the Northeast Pacific Ocean. *Marine Environmental Research*, 71(1), pp.41-52.
- Du, C., Liang, H., Li, Z. and Gong, J., 2020a. Pollution characteristics of microplastics in soils in southeastern suburbs of Baoding City, China. *International Journal of Environmental Research and Public Health*, 17, p.845.
- Dumichen, E., Eisentraut, P., Bannick, C.G., Barthel, A.K., Senz, R. and Braun, U., 2017. Fast identification of microplastics in complex environmental samples by a thermal degradation method. *Chemosphere*, 174, pp.572-584.
- Eerkes-Medrano, D. and Thompson, R., 2018. Occurrence, fate, and effect of microplastics in freshwater systems. *Environmental Pollution*, pp.95-132.

- Elert, A.M., Becker, R., Duemichen, E., Eisentraut, P., Falkenhagen, J., Sturm, H. and Braun, U., 2017. Comparison of different methods for microplastic detection: What can we learn from them, and why asking the right question before measurements matters? *Environmental Pollution*, 231, pp.1256-1264.
- Felsing, S., Kochleus, C., Buchinger, S., Brennholt, N., Stock, F. and Reifferscheid, G., 2018. A new approach in separating microplastics from environmental samples based on their electrostatic behavior. *Environmental Pollution*, 234, pp.20-28.
- Forster, N.A., Tighe, M.K. and Wilson, S.C., 2020. Microplastics in soils of wilderness areas: What is the significance of outdoor clothing and footwear? *Geoderma*, 378, p.114612.
- Fraunholz, N., 2014. Separation of waste plastics by froth flotation - A review, Part 1. *Minerals Engineering*, 17(2), pp.261-268.
- Gao, H., Yan, C., Liu, Q., Ding, W., Chen, B. and Li, Z., 2018. Effects of plastic mulching and plastic residue on agricultural production: A meta-analysis. *Science of the Total Environment*, 651, pp.484-492.
- Gaylor, M.O., Harvey, E. and Hale, R.C., 2013. Polybrominated diphenyl ether (PBDE) accumulation by earthworms (*Eisenia fetida*) exposed to biosolids-, polyurethane foam microparticle-, and penta-BDE-amended soils. *Environmental Science and Technology*, 47, pp.13831-13839.
- Geyer, R., Jambeck, J.R. and Law, K.L., 2017. Production, use, and fate of all plastics ever made. *Science Advances*, 3, pp.1-5.
- Gieré, R., Sommer, F., Dietze, V., Baum, A., Gilge, S., Sauer, J. and Maschowski, C., 2018. Tire abrasion is a major source of microplastics in the environment. *Geological Society of America*, 50, p.6.
- Girvan, M.S., Bullimore, J., Pretty, J.N., Osborn, A.M. and Ball, A.S., 2003. Soil type is the primary determinant of the composition of the total and active bacterial communities in arable soils. *Applied and Environmental Microbiology*, 69, pp.1800-1809.
- Grbic, J., Nguyen, B., Guo, E., You, J.B., Sinton, D. and Rochman, C.M., 2019. Magnetic extraction of microplastics from environmental samples. *Environmental Science & Technology Letters*, 6(2), pp.68.
- Groh, K.J., Backhaus, T., Carney-Almroth, B., Geueke, B., Inostroza, P.A., Lennquist, A., Leslie, H.A., Maffini, M., Slunge, D., Trasande, L., Warhurst, A.M. and Muncke, J., 2019. Overview of known plastic packaging-associated chemicals and their hazards. *Science of the Total Environment*, 651, pp.3253-3268.
- Guerrini, S., Borreani, G. and Voojjs, H., 2017. Biodegradable materials in agriculture: Case histories and perspectives. In: Malinconico, M. (Ed.), *Soil Degradable Bioplastics for Sustainable Agriculture*. Springer, Berlin Heidelberg, pp.35-65.
- Guo, J.J., Huang, X.P., Xiang, L., Wang, Y.Z., Li, Y.W., Li, H., Cai, Q.Y., Mo, C.H. and Wong, M.H., 2020. Source, migration, and toxicology of microplastic in soil. *Environmental International*, 137, p.105263.
- Hahladakis, J.N., Velis, C.A., Weber, R., Iacovidou, E. and Purnell, P., 2018. An overview of chemical additives present in plastics: Migration, release, fate and environmental impact during their use, disposal, and recycling. *Journal of Hazardous Materials*, 344, pp.179-199.
- Hartline, N.L., Bruce, N.J., Karba, S.N., Ruff, E.O., Sonar, S.U. and Holden, P.A., 2016. Microfiber masses recovered from conventional machine washing of new or aged garments. *Environmental Science & Technology*, 50(21), pp.11532-11538.
- Hayes, D., 2019. Biodegradable mulch performance and adoption in sustainable agriculture: A review. *Biodegradable Mulch Performance and Adoption*, 124, pp.1-6.
- Hays, H. and Cormons, G., 1974. Plastic particles are found in tern pellets on coastal beaches and at factory sites. *Marine Pollution Bulletin*, 5, pp.44-46.
- He, L., Wu, D., Rong, H.F., Li, M., Tong, M.P. and Kim, H., 2018. Influence of nano- and microplastic particles on the transport and deposition behaviors of bacteria in quartz sand. *Environmental Science and Technology*, 52, pp.11555-11563.
- Hernandez, C.E. and Witter, S., 2016. Evaluating and managing the environmental impact of banana production in Costa Rica: A systems approach. *Ambio*, 25(3), pp.171-178.
- Hidalgo-Ruz, V., Gutow, L., Thompson, R.C. and Thiel, M., 2012. Microplastics in the marine environment: A review of methods, occurrence, and effects. *Environmental Science & Technology*, 46, pp.3060-3075.
- Huang, L., Wang, H., Wang, C., Zhao, J. and Zhang, B., 2017. Microwave-assisted surface modification for the separation of polycarbonate from polymethylmethacrylate and polyvinyl chloride waste plastics by flotation. *Waste Management & Research*, 35(3), pp.294-300.
- Huerta Lwanga, E., Mendoza Vega, J., Ku Quej, V., Chi, J.L.A., Sanchez Del Cid, L., Chi, C., Escalona Segura, G., Gertsen, H., Salanki, T., van der Ploeg, M., Koelmans, A.A. and Geissen, V., 2017. Field evidence for transfer of plastic debris along a terrestrial food chain. *Scientific Reports*, 7, p.14071.
- Hurley, R.R., Woodward, J.C. and Rothwell, J.J., 2007. Ingestion of microplastics by freshwater tubifex worms. *Environmental Science & Technology*, 51, pp.12844-12851.
- Ibrahim, Y.S., Tuan Anuar, S., Azmi, A.A., Wan Mohd Khalik, W.M.A., Lehata, S., Hamzah, S.R., Ismail, D., Ma, Z.F., Dzulkarnaen, A., Zakaria, Z., Mustaffa, N., Tuan Sharif, S.E. and Lee, Y.Y., 2021. Detection of microplastics in human colectomy specimens. *JGH Open*, 5, pp.116-121.
- Imhof, H.K., Sigl, R., Brauer, E., Feyl, S., Giesemann, P., Klink, S., Leupolz, K., Löder, M.G., Löschel, L.A., Missun, J. and Muszynski, S., 2017. Spatial and temporal variation of macro, meso, and microplastic abundance on a remote coral island of the Maldives, Indian Ocean. *Marine Pollution Bulletin*, 116(1-2), pp.340-347.
- Ivleva, N.P., Wiesheu, A.C. and Niessner, R., 2017. Microplastics in aquatic environments. *Angewandte Chemie International Edition*, 56, pp.1720-1739.
- Jambeck, J.R., Geyer, R., Wilcox, C., Siegler, T.R., Perryman, M., Andrade, A., Narayan, R. and Law, K.L., 2015. Plastic waste inputs from land into the ocean. *Science*, 347, pp.768-771.
- Jian, M., Zhang, Y., Yang, W., Zhou, L., Liu, S. and Xu, E.G., 2020. Occurrence and distribution of microplastic in China's largest freshwater lake system. *Chemosphere*, 261, p.128186.
- Jiang, X., Chen, H., Liao, Y., Ye, Z., Li, M. and Klobučar, G., 2019. Ecotoxicity and genotoxicity of polystyrene microplastics on higher plant *Vicia faba*. *Environmental Pollution*, 250, pp.831-838.
- Judy, J.D., Williams, M., Gregg, A., Oliver, D., Kumar, A., Kookana, R. and Kirby, J.K., 2019. Microplastics in soil: Microplastics in municipal mixed-waste organic outputs induce minimal short to long-term toxicity in key terrestrial biota. *Environmental Pollution*, 252, pp.522-531.
- Khalid, N., Aqeel, M. and Noman, A., 2020. Microplastics could be a threat to plants in terrestrial systems directly or indirectly. *Environmental Pollution*, 267, p.115653.
- Koelmans, A.A., Mohamed Nor, N.H., Hermesen, E., Kooi, M., Mintenig, S.M. and De France, J., 2019. Microplastics in fresh and drinking water: Critical review and assessment of data quality. *Water Research*, 155, pp.410-422.
- Kole, P.J., Löhr, A.J., Van Belleghem, F. and Ragas, A., 2017. Wear and tear of tires: A stealthy source of microplastic in the environment. *International Journal of Environmental Research and Public Health*, 14(10), p.1265.
- Kumar, M., Xiong, X., He, M., Tsang, D.C.W., Gupta, J. and Khan, E., 2020. Microplastics as pollutants in agricultural soils. *Environmental Pollution*, 265, p.114980.
- Kumar, M., Xiong, X., He, M., Tsang, D.C.W., Gupta, J., Khan, E., Harrad, S., Hou, D., Ok, Y.S. and Bolan, N.S., 2020. Microplastics as pollutants in agricultural soils. *Environmental Pollution*, 265, p.114980.
- Kumar, M.V. and Sheela, A.M., 2021. Effect of plastic film mulching on the distribution of plastic residues in agricultural fields. *Chemosphere*, 273, pp.128590.

- Kumari, A., Rajput, V.D., Mandzhieva, S.S., Rajput, S., Minkina, T., Kaur, R., Sushkova, S., Kumari, P., Ranjan, A. and Kalinitchenko, V.P., 2022. Microplastic pollution: An emerging threat to terrestrial plants and insights into its remediation strategies. *Plants*, 11, p.340.
- Laganà, P., Caruso, G., Corsi, I., Bergami, E., Venuti, V., Majolino, D., Ferla, R.L., Azzaro, M. and Cappello, S., 2018. Do plastics serve as a possible vector for the spread of antibiotic resistance? First insights from bacteria associated with a polystyrene piece from King George Island (Antarctica). *International Journal of Hygiene and Environmental Health*, 222, pp.89-100.
- Lassen, C., Hansen, S.F., Magnusson, K., Hartmann, N.B., Rehne Jensen, P., Nielsen, T.G. and Brinch, A., 2015. Microplastics: Occurrence, effects, and sources of releases to the environment in Denmark. *Danish Environmental Protection Agency*, 1793, p.206.
- Lei, L., Wu, S., Lu, S., Liu, M., Song, Y., Fu, Z., Shi, H., Raley-Susman, K.M. and He, D., 2018b. Microplastic particles cause intestinal damage and other adverse effects in zebrafish *Danio rerio* and nematode *Caenorhabditis elegans*. *Science of the Total Environment*, 619, pp.1-8.
- Li, J., Zhang, K. and Zhang, H., 2018. Adsorption of antibiotics on microplastics. *Environmental Pollution*, 237, pp.460-467.
- Liu, M., Lu, S., Song, Y., Lei, L., Hu, J., Lv, W., Zhou, W., Cao, C., Shi, H., Yang, X. and He, D., 2018. Microplastic and mesoplastic pollution in farmland soils in suburbs of Shanghai, China. *Environmental Pollution*, 242, pp.855-862.
- Liu, M., Song, Y., Lu, S., Qiu, R., Hu, J., Li, X., Bigalke, M., Shi, H. and He, D., 2019. A method for extracting soil microplastics through the circulation of sodium bromide solutions. *Science of the Total Environment*, 691, pp.341-347.
- Liu, Y., Zhang, J., Tang, Y., He, Y., Li, Y., You, J., Breider, F., Tao, S. and Liu, W., 2021. Effects of anthropogenic discharge and hydraulic deposition on the distribution and accumulation of microplastics in surface sediments of a typical seagoing river: The Haihe River. *Journal of Hazardous Materials*, 404, p.124180.
- Lozano, Y.M. and Rillig, M.C., 2020. Effects of microplastic fibers and drought on plant communities. *Environmental Science & Technology*, 54, pp.6166-6173. <https://doi.org/10.1021/acs.est.0c01051>.
- Luo, Y., Zhang, Y., Xu, Y., Guo, X. and Zhu, L., 2020. Distribution characteristics and mechanism of microplastics mediated by soil physicochemical properties. *Science of the Total Environment*, 726, p.138389.
- Maaß, S., Daphi, D., Lehmann, A. and Rillig, M.C., 2017. Transport of microplastics by two collembolan species. *Environmental Pollution*, 225, pp.456-459.
- Magnusson, K., Eliasson, K., Fråne, A., Haikonen, K., Hultén, J., Olshammar, M., Stadmark, J. and Voisin, A., 2016. *Swedish sources and pathways for microplastics to the marine environment*. IVL Svenska Miljöinstitutet
- Mani, T., Frehland, S., Kalberer, A. and Burkhardt-Holm, P., 2019. Using castor oil to separate microplastics from four different environmental matrices. *Analytical Methods*, 11 (13), pp.1788-1794.
- Marschner, B. and Kalbitz, K., 2003. Controls of bioavailability and biodegradability of dissolved organic matter in soils. *Geoderma*, 113, pp.211-235.
- Minteni, S.M., Int-Veen, I., Loder, M.G.J., Primpke, S. and Gerdt, G., 2017. Identification of microplastic in effluents of wastewater treatment plants using focal plane array-based micro-Fourier-transform infrared imaging. *Water Research*, 108, pp.365-372.
- Moller, J.N., Loder, M.G.J. and Laforsch, C., 2020. Finding microplastic in soils: A review of analytical methods. *Environmental Science & Technology*, 54, pp.2078-2090.
- Napper, I.E. and Thompson, R.C., 2019. Environmental deterioration of biodegradable, oxo-biodegradable, compostable, and conventional plastic carrier bags in the sea, soil, and open air over a 3-year period. *Environmental Science & Technology*, 53, pp.4775-4783.
- Naveed, M., Herath, L., Moldrup, P., Arthur, E., Nicolaisen, M., Norgaard, T., Ferre, T.P.A. and de Jonge, L.W., 2016. Spatial variability of microbial richness and diversity and relationships with soil organic carbon, texture, and structure across an agricultural field. *Applied Soil Ecology*, 103, pp.44-55.
- Nizzetto, L., Futter, M. and Langaas, S., 2016. Are agricultural soils dumps for microplastics of urban origins? *Environmental Science & Technology*, 50, pp.10777-10779.
- Panbianco, A., Nalbone, L., Giarratana, F. and Ziino, G., 2019. First discoveries of microplastics in terrestrial snails. *Science of the Total Environment*, 106722, pp.1-7.
- Paul, A., Wander, L., Becker, R., Goedecke, C. and Braun, U., 2019. High-throughput NIR spectroscopic (NIRS) detection of microplastics in soil. *Environmental Science and Pollution Research International*, 26, pp.7364-7374.
- Piehl, S., Leibner, A., Löder, M.G.J., Dris, R., Bogner, C. and Laforsch, C., 2018. Identification and quantification of macro-and microplastic on agricultural farmland. *Scientific Reports*, 8, p.17950.
- Pignattelli, S., Broccoli, A. and Renzi, M., 2020. Physiological responses of garden cress (*Lepidium sativum*) to different types of microplastics. *Science of the Total Environment*, 727, p.138609.
- Plastics Europe, 2018. *Plastics - The Facts 2018: An analysis of European plastic production, demand, and waste data for 2018*. EUA
- PlasticsEurope, 2021. *Plastics - The Facts 2021: An analysis of European plastics production, demand and waste data*. Retrieved from: <https://plasticseurope.org/knowledge-hub/plastics-the-facts-2021/>.
- Qi, Y., Yang, X., Pelaez, A.M., Lwanga, E.H., Beriot, N., Gertsen, H., Garbeva, P. and Geissen, V., 2018. Macro-and microplastics in soil-plant system: Effects of plastic mulch film residues on wheat (*Triticum aestivum*) growth. *Science of the Total Environment*, 645, pp.1048-1056.
- Rezania, S., Park, J., Md Din, M.F., Mat Taib, S., Talaiekhazani, A., Kumar Yadav, K. and Kamyab, H., 2018. Microplastics pollution in different aquatic environments and biota: A review of recent studies. *Marine Pollution Bulletin*, 133, pp.191-208.
- Rillig, M.C., 2018. Microplastics disguising as soil carbon storage. *Environmental Science & Technology*, 52, pp.6079-6080.
- Rillig, M.C. and Bonkowski, M., 2018. Microplastic and soil protists: A call for research. *Environmental Pollution*, 241, pp.1128-1131.
- Rillig, M.C., Ingrassia, R., de Souza, M. and Anderson, A., 2017. Microplastic incorporation into soil in agroecosystems. *Frontiers in Plant Science*, 8, pp.305719.
- Rillig, M.C., Muller, L.A.H. and Lehmann, A., 2017. Soil aggregates as massively concurrent evolutionary incubators. *ISME Journal*, 11, pp.1943-1948.
- Rocha-Santos, T. and Duarte, A.C., 2015. A critical overview of the analytical approaches to the occurrence, the fate, and the behavior of microplastics in the environment. *Trends in Analytical Chemistry*, 65, pp.47-53.
- Rochman, C.M., 2018. Microplastic research: From sink to source. *Science*, 360, pp.28-29.
- Rubol, S., Manzoni, S., Bellin, A. and Porporato, A., 2013. Modeling soil moisture and oxygen effects on soil biogeochemical cycles, including dissimilatory nitrate reduction to ammonium (DNRA). *Advances in Water Resources*, 62, pp.106-124.
- Sarker, A., Deepo, D.M., Nandi, R., Rana, J., Islam, S., Rahman, S., Hossain, M.N., Islam, M.S., Baroi, A. and Kim, J.E., 2020. A review of microplastic pollution in the soil and terrestrial ecosystems: A global and Bangladesh perspective. *Science of the Total Environment*, 733, p.139296.
- Scheurer, M. and Bigalke, M., 2018. Microplastics in Swiss floodplain soils. *Environmental Science & Technology*, 52, pp.3591-3598.
- Schwabl, P., Koppel, S., Königshofer, P., Bucsis, T., Trauner, M., Reiberger, T. and Liebmann, B., 2019. Detection of various



- microplastics in human stool: A prospective case series. *Annals of Internal Medicine*, 171, pp.453-457.
- Silva, G., Madrid, F.G., Hernández, D., Pincheira, G., Peralta, A., Gavilán, M.U., Vergara-Carmona, V. and Fuentes-Peñailillo, F., 2021. Microplastics and their effect on horticultural crops: Food safety and plant stress. *Agronomy*, 11, pp.1528.
- Thompson, R.C., Olsen, Y., Mitchell, R.P., Davis, A., Rowland, S.J., John, A.W.G., McGonigle, D. and Russell, A.E., 2004. Lost at sea: Where is all the plastic? *Science*, 304, pp.838.
- Thompson, Richard C., 2015. Microplastics in the Marine Environment: Sources, Consequences, and Solutions. In: Bergmann, M., Gutow, L. and Klages, M. (Eds.), *Marine Anthropogenic Litter*. Springer International Publishing, Cham, pp.185-200.
- Trasar-Cepeda, C., Leiros, M.C. and Gil-Sotres, F., 2008. Hydrolytic enzyme activities in agricultural and forest soils: Some implications for their use as indicators of soil quality. *Soil Biology and Biochemistry*, 40, pp.2146-2155.
- Van Cauwenberghe, L., Claessens, M., Vandegehuchte, M.B. and Janssen, C.R., 2015. Microplastics are taken up by mussels (*Mytilus edulis*) and lugworms (*Arenicola marina*) living in natural habitats. *Environmental Pollution*, 199, pp.10-17.
- van den Berg, P., Huerta-Lwanga, E., Corradini, F. and Geissen, V., 2020. Sewage sludge application as a vehicle for microplastics in eastern Spanish agricultural soils. *Environmental Pollution*, 261, p.114198.
- Veresoglou, S.D., Halley, J.M. and Rillig, M.C., 2015. Extinction risk of soil biota. *Nature Communications*, 6, p.8862.
- Wan, Y., Wu, C., Xue, Q. and Hui, X., 2018. Effects of plastic contamination on water evaporation and desiccation cracking in soil. *Science of the Total Environment*, 654, 576-582.
- Wang, F., Wong, C.S., Chen, D., Lu, X., Wang, F. and Zeng, E.Y., 2018. Interaction of toxic chemicals and microplastics: A critical review. *Water Research*, 139, pp.208-219.
- Wang, J., Liu, X., Li, Y., Powell, T., Wang, X., Wang, G. and Zhang, H., 2019. Microplastics as contaminants in the environment: A review focusing on effects to organisms. *Science of the Total Environment*, 691, pp.848-857.
- Wang, J., Taylor, A., Xu, C.Y., Schlenk, D. and Gan, J., 2018. Evaluation of different methods for assessing bioavailability of DDT residues during soil remediation. *Environmental Pollution*, 238, pp.462-470.
- Weber, C.J. and Opp, C., 2020. An overview of the potential risks, sources, and analytical methods for microplastics in soil. *Environmental Pollution*, 267, p.115390.
- Weithmann, N., Möller, J.N., Löder, M.G.J., Piehl, S., Laforsch, C. and Freitag, R., 2018. Organic fertilizer is a vehicle for the entry of microplastic into the environment. *Science Advances*, 4, p.8060.
- Weithmann, N., Möller, U.N., Löder, M.G.J., Piehl, S., Laforsch, C. and Freitag, R., 2018. Organic fertilizer as a vehicle for the entry of microplastic into the environment: A critical review. *Science Advances*, 4, eaap8060.
- Xu, C., Zhang, B., Gu, C., Shen, C., Yin, S., Aamir, M. and Li, F., 2020. Are we underestimating the sources of microplastic pollution in terrestrial environments? *Journal of Hazardous Materials*, 400, p.123228.
- Xu, C., Zhang, B., Gu, C., Shen, C., Yin, S., Aamir, M. and Li, F., 2020. Environmental impacts of microplastics: A critical review of the literature. *Journal of Hazardous Materials*, 400, p.123228.
- Xu, G., Liu, Y. and Yu, Y., 2021. Effects of polystyrene microplastics on uptake and toxicity of phenanthrene in soybean. *Science of the Total Environment*, 783, 147016.
- Yang, L., Zhang, Y., Kang, S., Wang, Z. and Wu, C., 2021. Microplastics in freshwater sediment: A review on methods, occurrence, and sources. *Science of the Total Environment*, 780, p.146546.
- Yang, L., Zhang, Y., Kang, S., Wang, Z. and Wu, C., 2021. Corrigendum to Microplastics in soil: A review on methods, occurrence, sources, and potential risk. *Science of the Total Environment*, 780, pp.146546.
- Zhang, G.S., Zhang, F.X. and Li, X.T., 2019. Effects of polyester microfibers on soil physical properties: Perception from a field and a pot experiment. *Science of the Total Environment*, 670, pp.1-7.
- Zhang, S., Yang, X., Gertsen, H.N., Peters, P., Salánki, Y. and Geissen, V., 2018. A simple method for the extraction and identification of light-density microplastics from soil. *Science of the Total Environment*, 616-617, pp.1056-1065.
- Zhao, S., Zhu, L., Gao, L. and Li, D., 2018. Limitations for microplastic quantification in the ocean and recommendations for improvement and standardization. *Marine Pollution Bulletin*, 127, pp.27-49.
- Zhou, Q., Zhang, H., Fu, C., Zhou, Y., Dai, Z., Li, Y., Tu, C. and Luo, Y., 2018. The distribution and morphology of microplastics in coastal soils adjacent to the Bohai Sea and Yellow Sea. *Geoderma*, 322, pp.201-208.
- Ziajahromi, S., Neale, P.A., Rintoul, L. and Leusch, F.D., 2017. Plastic pollutants in the water environment. *Water Research*, 112, pp.93-99.
- Zubris, K.A.V. and Richards, B.K., 2005. Synthetic fibers as an indicator of land application of sludge. *Environmental Pollution*, 138(2), pp.201-211.





# Numerical Modeling of Instantaneous Spills in One-dimensional River Systems

Fatima M. A. Al-khafaji<sup>1</sup> and Hussein A. M. Al-Zubaidi<sup>2</sup>

Department of Environmental Engineering, College of Engineering, University of Babylon, Babylon, Iraq

†Corresponding author: Hussein A. M. Al-Zubaidi; hussein.alzubaidi@uobabylon.edu.iq; alzubaidih10@gmail.com

Nat. Env. & Poll. Tech.  
Website: [www.neptjournal.com](http://www.neptjournal.com)

Received: 04-03-2024

Revised: 16-04-2024

Accepted: 27-04-2024

## Key Words:

Advection dispersion equation  
Instantaneous spills  
Numerical methods  
One-dimensional river system  
Shallow water equations

## ABSTRACT

Modeling the fate and transport of spills in rivers is critical for risk assessment and instantaneous spill response. In this research, a one-dimensional model for instantaneous spills in river systems was built by solving the advection-dispersion equation (ADE) numerically along with the shallow water equations (SWEs) within the MATLAB environment. To run the model, the Ohio River's well-known accidental spill in 1988 was used as a field case study. The verification process revealed the model's robustness with very low statistic errors. The mean absolute error (MAE) and root mean squared error (RMSE) relative to the absorbed record were 0.0626 ppm and 0.2255 ppm, respectively. Results showed the spill mass distribution is a function of the longitudinal dispersion coefficient and the mass decay rate. Increasing the longitudinal dispersion coefficient reduces the spill impact widely, for instance after four days from the mass spill the maximum concentration decreased from 0.846789 to 0.486623 ppm, and after five days it decreased from 0.332485 to 0.186094 ppm by increasing the coefficient from 15 to 175 m<sup>2</sup>/sec. A similar reduction was achieved by increasing the decay rate from 0.8 to 1.2 day<sup>-1</sup> (from 0.846789 to 0.254274 ppm and from 0.332485 to 0.0662202 ppm after four and five days, respectively). Thus, field measurements of these two factors must be taken into account to know the spill fate in river systems.

## INTRODUCTION

Many rivers especially populated ones are exposed to instantaneous spills of pollutants due to increasing industrialization and urbanization. Predicting the movement of pollutants in rivers is one area where water quality management is supported. Numerous things can poison rivers. Diffusion and advection transport processes have caused these pollutants to spread longitudinally, laterally, and vertically, resulting in a decline in the river's water quality (Ramezani et al. 2016, Ukpaka & Agunwamba 2023, Yip et al. 2021). In addition to instantaneous spills, the most frequent oil spills can have substantial, long-term detrimental effects on the ecosystem and river systems. Throughout the world in recent decades, there have been thousands of unintentional and intentional unlawful releases of pollutants into surface water. Large spatial distributions, limited capacities for dilution and dispersion, and a high potential for the formation of pollutant droplets and their interaction with suspended particles and sediments make spills in medium- and small-sized rivers more detrimental than spills in seas. The main factors influencing the river spill modeling are pollutant density, river movement, hydraulic structures, vegetation, and interaction with sediments. Also, the transport, spread, and fate of river spills are subject to complex physical and chemical processes that depend on the characteristics of

the river, river hydraulics, and environmental conditions. The main instantaneous spill transport processes include the following: (i) advection brought induced by wind and river currents, (ii) Surface spreading is caused by the equilibrium of surface forces, gravitational forces, inertia, and viscous forces, and it results from both mechanical and turbulent diffusion. (iii) weathering mechanisms like oxidation, dissolution, emulsification, and evaporation, (iv) tumultuous mixing across the river's depth, (v) the way in which contaminants mix with river sediment and particle matter (vi) contact of pollutants with coastline (Kvočka et al. 2021, Kwon et al. 2021, Li et al. 2018, Zeunert & Meon 2020, Antonopoulos et al. 2015, Kargar et al. 2020, Tenebe et al. 2016, Al-Dalimy & Al-Zubaidi 2023).

There are different approaches for modeling pollutant spills in rivers. Ramezani et al. (2019) developed a one-dimensional model that simulates the fate of pollutant transport by solving the effect of several formulas for the longitudinal dispersion coefficient on ADE. The numerical solution was used to predict the transport of pollutants using MATLAB and Excel. The model used the finite differences to discretize the ADE explicitly. Results showed that the longitudinal dispersion coefficient is very essential and can impact the numerical solution accuracy extensively. In addition, the model results were close to the observations;

however, an inconsistent match with data was noticed in one of the case studies. Milišić et al. (2020) employed the MIKE11 model as a robust and successful numerical model in addition to the one-dimensional ADE model to compute the longitudinal dispersion coefficient mathematically and numerically. The results and the experimental data from the Neretva River (in the northern region of Bosnia and Herzegovina) were found to be fairly consistent. The temporal and spatial variations of pollutants might also be predicted using this model. Thus, for calculating solute distribution in big rivers, one-dimensional modeling, and single-point measurement techniques are straightforward and reasonably reliable instruments that should be taken into consideration. Ritta et al. (2020) calculated the longitudinal dispersion coefficient for the ADE utilizing an analytical and numerical one-dimensional linear technique. The longitudinal dispersion coefficient was calculated utilizing a large number of parametric equations that can be predicted using partial differential equations. By comparing the analytical and numerical results, it was found that there was good agreement between them. They advanced from the top together, and suddenly they decreased sharply to almost zero. It was also observed that as the distance increased the concentration decreased. Camacho Suarez et al. (2019) investigated how concentration dynamics and adherence to river rules were affected by uncertainty in the longitudinal dispersion coefficient. To do this, six longitudinal dispersion

regression equations were evaluated using the one-dimensional ADE and an analytical solution. The results showed that the Disley et al. equation (Disley et al. 2015) utilized efficiency metrics to determine which equation best described the dispersion coefficient. The results also showed that the effect of uncertainty varies greatly depending on the different characteristics of the rivers. Andallah & Khatun (2019) used numerical simulation by the one-dimensional ADE. Numerical and analytical solutions were used for the ADE. The Crank-Nicolson scheme was used in the numerical analysis and the relative error of three finite differences between FTBSCS and FTSCCS was compared. It was found that the Crank-Nicolson scheme was more accurate and the CNS and FTSCCS schemes were at a good rate of closeness. Thereby, many of these models try simplifying the solution to get results without linking the river flow continuity and momentums. In this research, the target numerical solution approach is to build a one-dimensional numerical model that simulates the fate of transport instantaneous pollutants spilled in rivers within the MATLAB environment using the analytical and numerical solution of the ADE simultaneously with SWEs to provide instant water depth and velocity at every numerical time step.

## MATERIALS AND METHODS

Fig. 1 displays the general numerical development approach

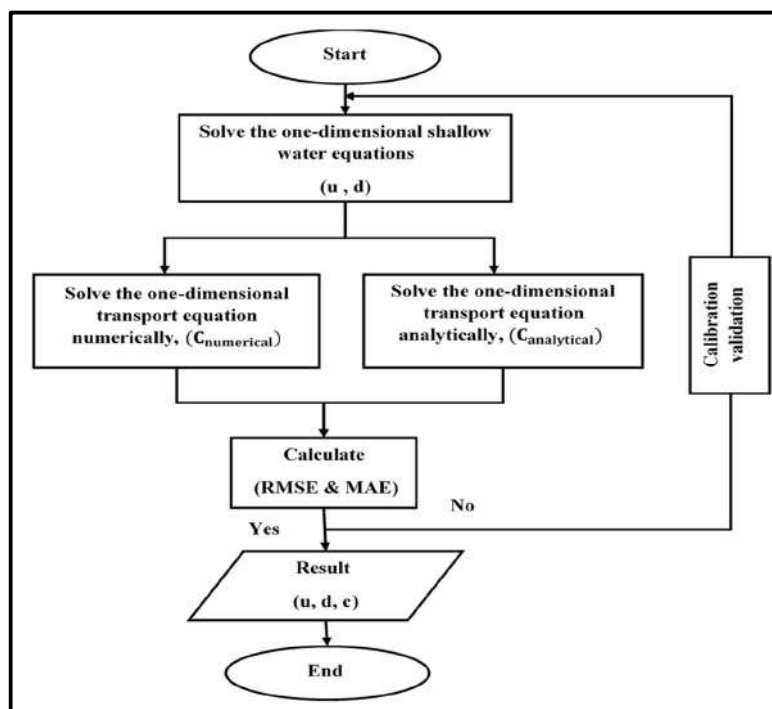


Fig. 1: Model development flow chart.

used in the present model. The model starts by solving the SWEs to get the river longitudinal velocity (u) and the propagated water surface wave height (d) along the river length. Then, the ADE is solved analytically and numerically for the pollutant concentration (c) longitudinally and temporally. These solutions are repeated every numerical time step until the best calibrated and validated results are achieved with fewer statistical errors.

**Numerical Solutions of the One-dimensional SWEs**

SWEs consist of two fundamental equations of continuity equation (Eq.1) and momentum equation (Eq.2). The numerical solutions are found using the finite difference method by characterizing space and time as shown in Fig. 2. Accurate numerical solutions are obtained by relocating the grid points efficiently to reduce linearity error (Al-Zubaidi & Wells 2020, Delis & Nikolos 2021, Guinot 2013, Morel et al. 1996, Welahettige et al. 2018).

$$\frac{\partial d}{\partial t} + D \frac{\partial u}{\partial x} = 0 \text{ (continuity equation)} \quad \dots(1)$$

$$\frac{\partial u}{\partial t} + G \frac{\partial d}{\partial x} + \frac{cf \cdot u|u|}{D} = 0 \text{ (momentum equation)} \quad \dots(2)$$

Where  $D = d \pm d'$  as in Fig. 2, G is the acceleration of gravity (m/s<sup>2</sup>), d is the height (m), u is the velocity (m/s), and cf is the friction coefficient.

A sequence of time-stepped numerical solutions for the unknown height and velocity of a wave propagating through an incompressible medium with a given constant density is obtained using the initial and boundary conditions can

be computed numerically in the form of Eq.4 and 5 based on the grid discretization in Fig. 3 in which  $\Delta x$  is the space increment and  $\Delta t$  is the time steps (Li & Chen 2019, Zhou et al. 2018):

$$\frac{d_j^{i+1} - d_j^i}{\Delta t} + \beta D^i \frac{u_{j+1}^{i+1} - u_{j-1}^{i+1}}{2\Delta x} + (1 - \beta) D^i \frac{u_{j+1}^i - u_{j-1}^i}{2\Delta x} = 0 \quad \dots(3)$$

$$\begin{aligned} \frac{u_{j-1}^{i+1} - u_{j-1}^i}{\Delta t} + \beta G \frac{d_j^{i+1} - d_{j-1}^{i+1}}{2\Delta x} + (1 - \beta) G \frac{d_j^i - d_{j-1}^i}{2\Delta x} \\ + \frac{cf \cdot |u^i|}{D^i} (\beta u_{j-1}^{i+1} + (1 - \beta) u_{j-1}^i) = 0 \end{aligned} \quad \dots(4)$$

If the  $\beta$  is between ( $0 > \beta > 1$ ), the solution is semi-implicit, and If the  $\beta = 0$ , the solution is fully explicit, and the solution will be fully implicit when  $\beta = 1$ .

**Numerical Solution of the One-dimensional ADE**

To account for a variable cross-sectional area of the river, the one-dimensional ADE (Eq. 5) is discretized as shown in Eqs. 6 and 7 First-order forward difference method for the temporal derivative, Second-order Central Difference Scheme for the second spatial derivative, and First-order Upwind Strategy for the first spatial derivative are used.

$$\frac{\partial C}{\partial t} + \frac{1}{A} \frac{\partial uAC}{\partial x} = \frac{E}{A} \frac{\partial^2 AC}{\partial x^2} - kC \quad \dots(5)$$

Where C is the pollutant cross-sectional average concentration (ppm), E is the longitudinal dispersion

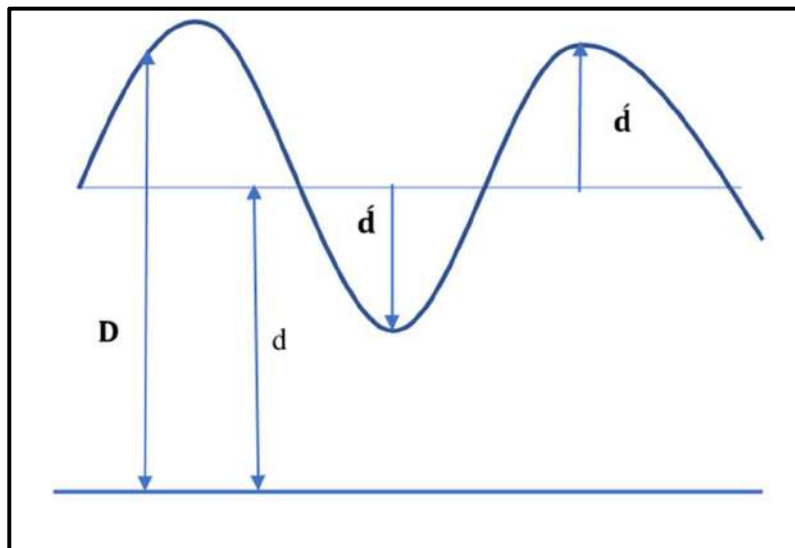


Fig. 2: Water depth presentation in the SWEs.

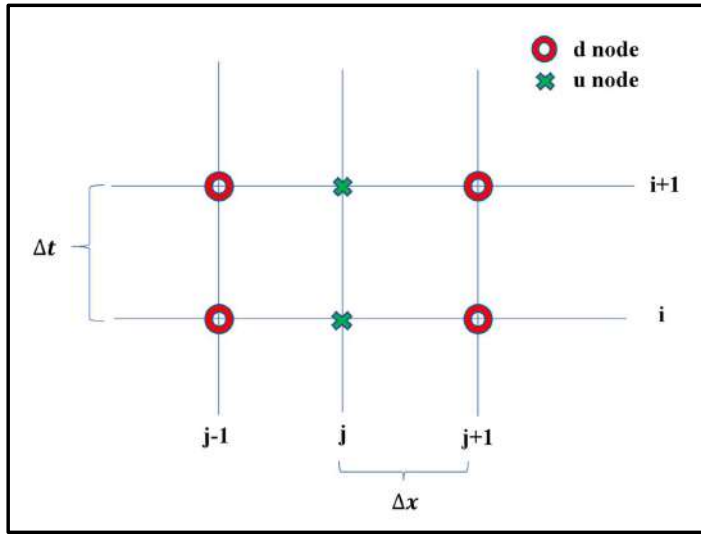


Fig. 3: Grid discretization of SWEs numerical solution.

coefficient (m<sup>2</sup>/s), k is the chemical degradation or decay rate (1/s), and A is the river cross-section area (m<sup>2</sup>).

$$C_j^{i+1} = C_j^i - \Delta t[\text{UPWIND}] + \frac{E\Delta t}{\Delta x^2 A_j^i}$$

$$\left[ A_{i+\frac{1}{2}}^i (C_{j+1}^i - C_j^i) - A_{i-\frac{1}{2}}^i (C_j^i - C_{i-\frac{1}{2}}^i) \right] - KC_j^i \Delta t \quad \dots(6)$$

$$\text{UPWIND} = \begin{cases} (uAC|_j^i - uAC|_{j-1}^i)/(A_j^i \Delta x) \\ (uAC|_j^i - uAC|_{j+1}^i)/(A_j^i \Delta x) \end{cases}$$

$$\begin{cases} u_j^i \geq 0 \\ u_j^i < 0 \end{cases} \quad \dots(7)$$

**Model Verification**

Analytically, reactive pollutants instantaneously leaked into rivers by the advection and dispersion processes, passing through the first mixing zone can be described according to Eq.8 (Chin, 2006) which is the analytical solution of Eq. 5:

$$C = \frac{M}{A\sqrt{4\pi Et}} \exp - \left[ \frac{[x - ut]^2}{4Et} + kt \right] \quad \dots(8)$$

Where M is the spill mass (g).

The model was validated by comparing the one-dimensional ADE numerical solution with the analytical solution and calculating statistical errors. MAE and RMSE were used as statistical measures to measure and evaluate

model performance in research studies. The RMSE and the MAE are calculated for model results as shown in Eqs. 9 and 10 (Al-Zubaidi & Wells 2018, Al-Zubaidi & Wells 2017, Chai & Draxler 2014, Chicco et al. 2021, Hodson 2022, Robeson & Willmott 2023, Wang & Lu 2018):

$$\text{MAE} = \frac{\sum_1^N |C_{\text{numerical}} - C_{\text{analytical}}|}{N} \quad \dots(9)$$

$$\text{RMSE} = \sqrt{\frac{\sum_1^N (C_{\text{numerical}} - C_{\text{analytical}})^2}{N}} \quad \dots(10)$$

Where N is the number of comparisons.

**Case Study**

The Ohio River in the eastern United States of America as in Fig. 4 was chosen as a case study to test the performance of the established model. The Allegheny and Monongahela Rivers meet here, forming the Ohio River, a little below Pittsburgh (Clark et al. 1990). The river dimensions are (an average length of 480000 m, average width of 800 m, and average depth of the river 10 m) with an average discharge of 1500 m<sup>3</sup>/s. Many intricate processes, like as mixing, exchange with storage zones, shearing advection, lateral mixing, hyporheic exchange, and effective diffusion in bottom sediment, affect the transport of pollutants in large rivers. On Saturday, January 2, 1988, over 3.8 million gallons of diesel oil collapsed in a storage tank in Pittsburgh. About 800,000 gallons spilled into the river at that time. This accident was chosen as a field case study to run the model based on. The river length was discretized using

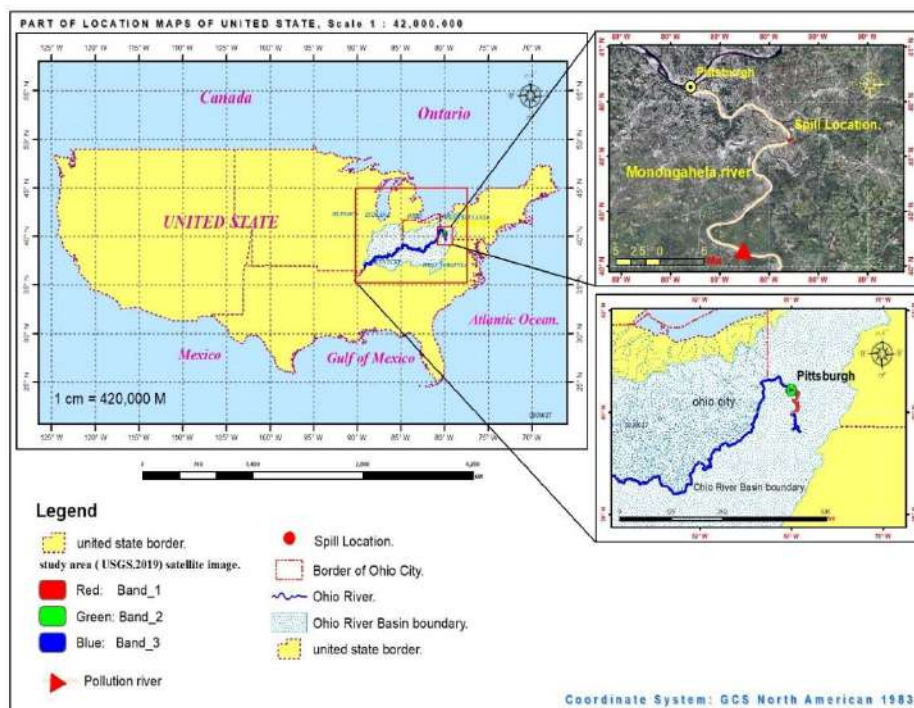


Fig. 4: Ohio River study area, US.

longitudinal increments ( $\Delta x$ ) of 3000 m and time steps ( $\Delta t$ ) of 303 s to ensure the model stability. The spill location is located at  $i = 2$  and that happened on day 2 from the start of the simulation. In addition, a first-order decay rate ( $k$ ) of 0.8 1/day and dispersion coefficient ( $E$ ) of 15  $m^2/s$  were known for the river.

## RESULTS AND DISCUSSION

The model was run using the available input data of the Ohio River spill to simulate and predict the pollutant fate and transport along the river. Fig. 5 displays the model simulation results after different days from the mass spill initial date. The model shows that the highest concentrations occur within the mixing zone at the source of the instantaneous spill and decrease with river distance. Also as travel time increases, the maximum pollutant concentration decreases as the instantaneous spill flows downstream the river length. This means that the relationship between pollutant travel distance and time with concentration is opposite. The pollutant plume moves with distance taking the bell shape, and as it travels along the river distance its amplitude decreases and becomes wider similar to the model behavior developed (Ramezani et al. 2019). A comparison was made between the analytical and numerical solutions for the presented case study of the Ohio River to verify the model performance. Fig. 6 shows the comparison results of the model predictions compared to the

analytical solution. Very good agreement was accomplished by the model based on the same case study in which the MAE value was 0.0626 ppm and the RMSE value was 0.2255 ppm. In addition, another comparison was made to check the differences at various selected locations along the river length as shown in Fig. 7. The statistical errors were very good reflecting the model's robustness. For example, at a river distance of 45 miles, the RMSE=0.3959 ppm and the MAE=0.021 ppm, at a river distance of 56.25 miles, the RMSE=0.1907 ppm, and the MAE=0.0077 ppm, and at a river distance of 65.625 miles, the RMSE=0.0984 ppm and MAE=0.0034 ppm.

Two parameters are responsible for the pollutant's final fate within the river, the longitudinal dispersion coefficient and the pollutant decay rate. In other words, how the plume amplitude and width decay and vanish eventually. Fig. 8 shows the evaluation of the model sensitivity to longitudinal dispersion coefficient variation. Several values of the longitudinal dispersion coefficient were selected ( $E=15,55,95,135$ , and 175  $m^2/s$ ) on two different days ( $t=4$  and 5 days) to run the model for the same Ohio River hydraulic and geometric properties along the river. The impact is very clear. A gradual decrease in the pollutant concentrations happens as the longitudinal dispersion coefficient increases. For example, on day number 4, the maximum pollutant concentration decreased from 0.846789

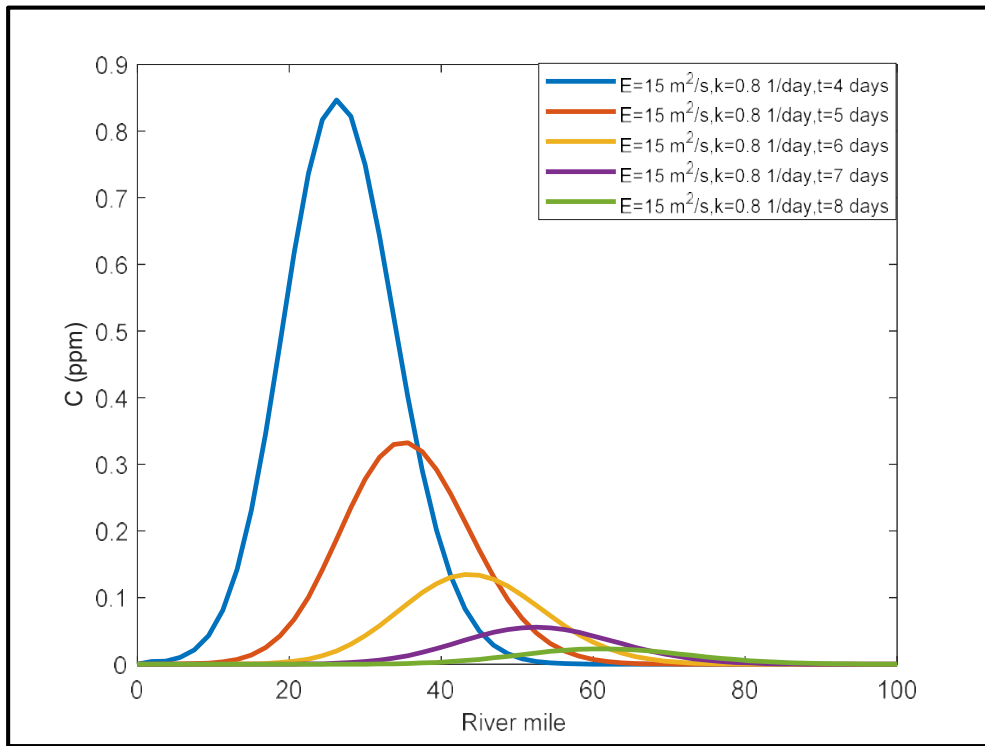


Fig. 5: Model simulation results at different days along the river.

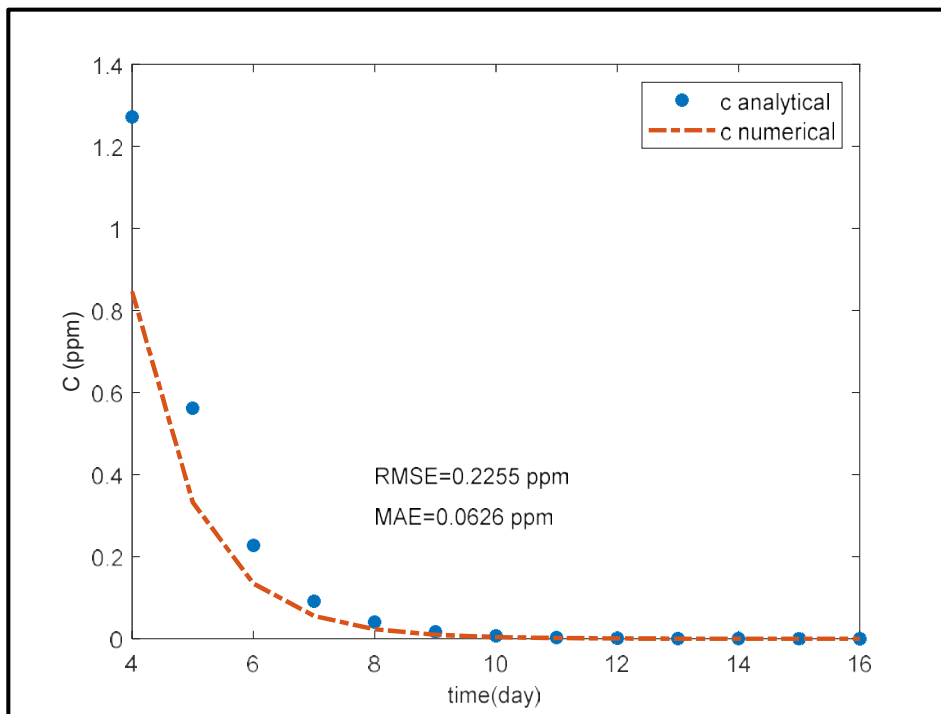


Fig. 6: Comparison between analytical and numerical solution results on different days after the initial spill date along the river.



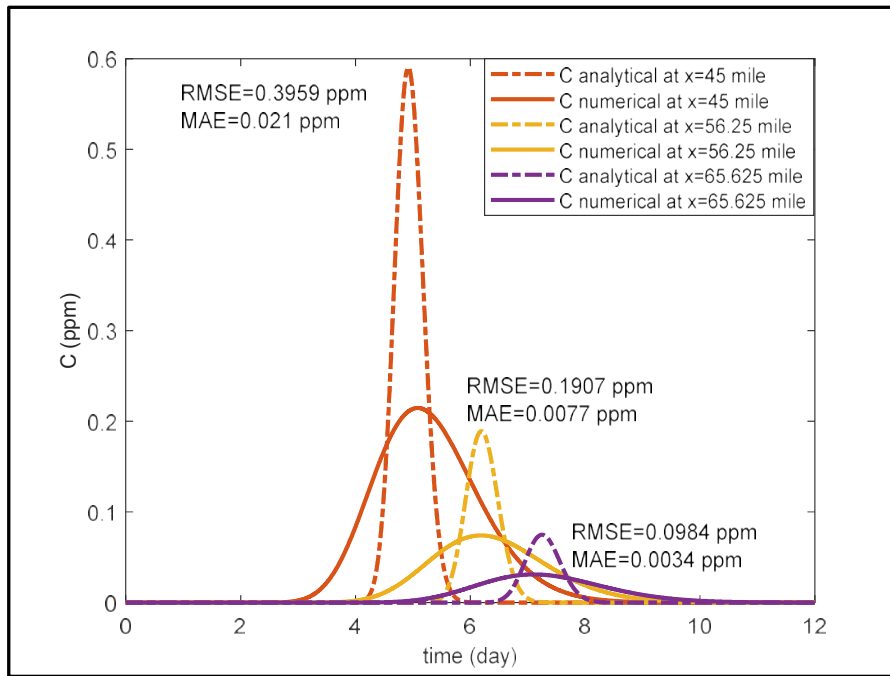


Fig. 7: Analytical solution plume of concentration compared to the numerical solution results of the model at different distances along the river.

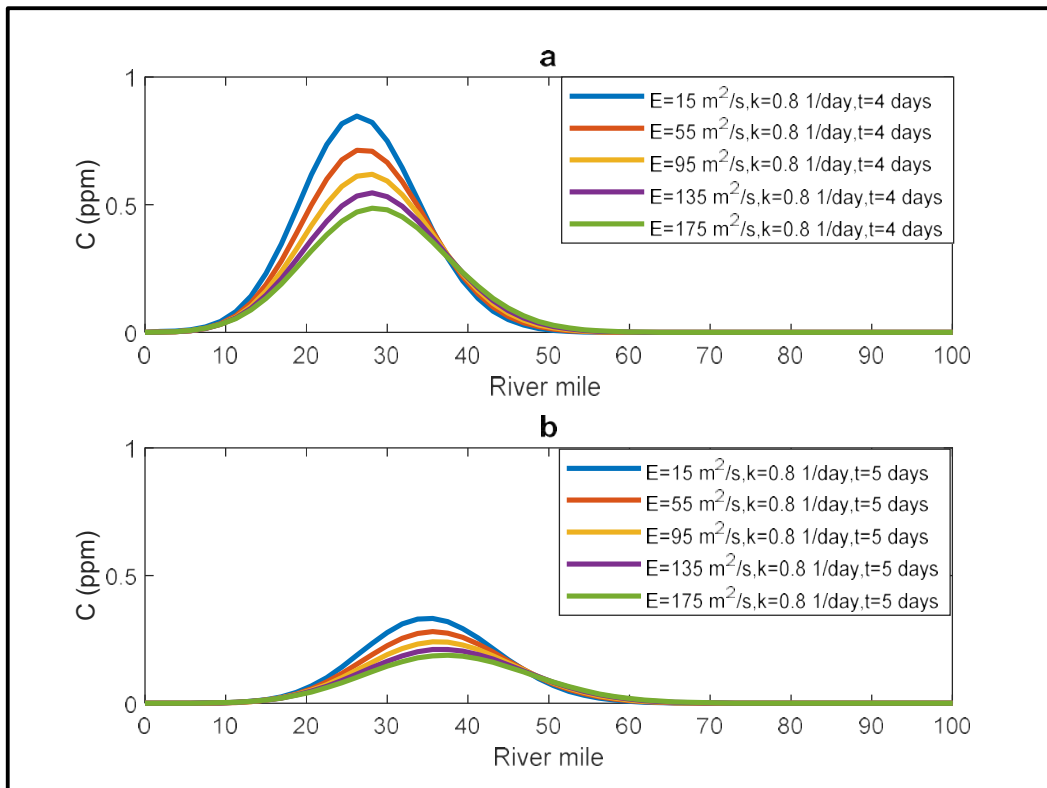


Fig. 8: Pollutant concentration distribution based on different longitudinal dispersion coefficients (a) at a time of 4 days and (b) at a time of 5 days from the spill date.

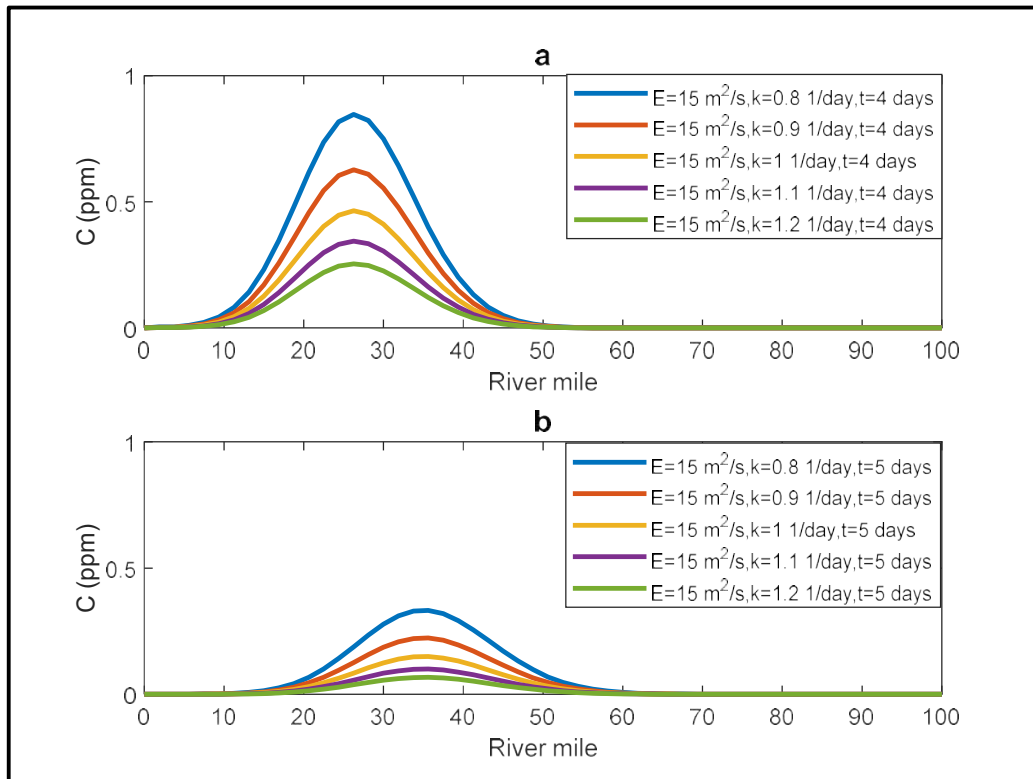


Fig. 9: Pollutant concentration distribution based on different decay rates (a) at the time of 4 days and (b) at the time of 5 days from the spill date.

to 0.486623 ppm, and on day number 5 day, the maximum pollutant concentration decreased from 0.332485 to 0.186094 ppm. Implying that there is an inverse association between them. Therefore, the longitudinal dispersion coefficient is very important and greatly affects the accuracy of the numerical solution. As conducted by Andallah & Khatum (2020), it is the main parameter that determines the transport of pollutants in one-dimensional river systems.

The latter parameter depends on the mass type itself. In general, the decay coefficient has the opposite impact on the pollutant residence time. Accordingly, different values of the decay rate were taken to determine the influence on the pollutant concentration distribution to assess the model capability of the decay rate variation. The decay rate values were taken on two different days too. The range for the chosen decay rate was from 0.8 to 1.2 1/day. At day number 4, the maximum pollutant concentration decreased from 0.846789 to 0.254274 ppm, and at day number 5, the maximum pollutant concentration decreased from 0.332485 to 0.0662202 ppm. Similar plume concentration reduction behavior compared to the longitudinal dispersion coefficient effect in which increasing the rate of decay with time reduces the concentration distribution longitudinally and temporally. Comparing the results in Fig. 8 and 9 leads to conclude that

the effect of the longitudinal dispersion coefficient is very small compared to the decay rate. Also, the plume takes a bell shape as it travels from the source of the instantaneous mass spill. Consequently, the pollutant concentration distribution around the plume center decreases and its amplitude becomes lower and wider as the plume moves away from the spill source. Finally, by constructing a one-dimensional model including the numerical and analytical solution of ADE based on the available data to simulate the fate and transport of pollutants in the rivers, it was found it is necessary to model the case numerically rather than solving the case analytically only for better representation and realistic predictions (Fry et al. 1993).

## CONCLUSION

In this study, a one-dimensional numerical model was developed to simulate the fate and transport of instantaneous spills in rivers by solving the ADE in conjugate with SWEs. It was found that the maximum pollutant concentrations occur within the mixing zone and decrease with increasing distance from the spill location. Also, as travel time increases the maximum concentration decreases as the pollutant plume flows downstream the river, spreading

the pollutant distribution with less concentration until vanishing. In addition, it was concluded that whenever either the longitudinal dispersion coefficient or the decay rate increases during the model run, the pollutant concentration plume distribution decreases with distance. This property plays a major role in the pollutant fate and transport in the river, impacting the pollutant residence time. Furthermore, the numerical modeling along with the analytical solution gave the case study more applicability since it can control the river characteristics broadly.

## ACKNOWLEDGMENTS

The authors thank the Department of Environmental Engineering at the University of Babylon for their support in doing this research.

## REFERENCES

- Al-Dalimy, S. Z. and Al-Zubaidi, H. A. M., 2023. One-dimensional model predictions of carbonaceous biological oxygen demand and dissolved oxygen for Hilla river water quality, Iraq. *Ecological Engineering and Environmental Technology*, 24(7). <https://doi.org/10.12912/27197050/170100>
- Al-Zubaidi, H. A. M. and Wells, S. A., 2018. Comparison of a 2D and 3D hydrodynamic and water quality model for lake systems. In *World Environmental and Water Resources Congress 2018* (pp. 84-74). Reston, VA: American Society of Civil Engineers. <https://doi.org/10.1061/9780784481400.007>
- Al-Zubaidi, H. A. and Wells, S. A., 2017. 3D numerical temperature model development and calibration for lakes and reservoirs: A case study. In *World Environmental and Water Resources Congress 2017*, pp.595-610. <https://doi.org/10.1061/9780784480601.051>
- Al-Zubaidi, H. A. M. and Wells, S. A., 2020. Analytical and field verification of a 3D hydrodynamic and water quality numerical scheme based on the 2D formulation in CE-QUAL-W2. *Journal of Hydraulic Research*, 58(1). <https://doi.org/10.1080/00221686.2018.1499051>
- Andallah, L. and Khatun, M., 2020. Numerical solution of advection-diffusion equation using finite difference schemes. *Bangladesh Journal of Scientific and Industrial Research*, 55(1), pp.15–22. <https://doi.org/10.3329/bjsir.v55i1.46728>
- Antonopoulos, V. Z., Georgiou, P. E. and Antonopoulos, Z. V., 2015. Dispersion coefficient prediction using empirical models and ANNs. *Environmental Processes*, 2(2), pp.379–394. <https://doi.org/10.1007/s40710-015-0074-6>
- Camacho Suarez, V. V., Schellart, A. N. A., Brevis, W. and Shucksmith, J. D., 2019. Quantifying the impact of uncertainty within the longitudinal dispersion coefficient on concentration dynamics and regulatory compliance in rivers. *Water Resources Research*, 55(5), pp.4393–4409. <https://doi.org/10.1029/2018WR023417>
- Chai, T. and Draxler, R. R., 2014. Root mean square error (RMSE) or mean absolute error (MAE)? *Geosci. Model Dev. Discuss.*, 7, pp.1525–1534. <https://doi.org/10.5194/gmdd-7-1525-2014>
- Chicco, D., Warrens, M. J. and Jurman, G., 2021. The coefficient of determination R-squared is more informative than SMAPE, MAE, MAPE, MSE and RMSE in regression analysis evaluation. *PeerJ Computer Science*, 7, pp.1–24. <https://doi.org/10.7717/PEERJ-CS.623>
- Chin, D. A., 2006. Water-quality engineering in natural systems. In *Water-Quality Engineering in Natural Systems*. <https://doi.org/10.1002/0471784559>
- Clark, R. M., Vicory, A. H. and Goodrich, J. A., 1990. The Ohio river oil spill: a case study. *Journal AWWA*, 82(3). <https://doi.org/10.1002/j.1551-8833.1990.tb06934.x>
- Delis, A. I. and Nikolos, I. K., 2021. Shallow water equations in hydraulics: Modeling, numerics and applications. In *Water (Switzerland)*, 13(24). <https://doi.org/10.3390/w13243598>
- Disley, T., Gharabaghi, B., Mahboubi, A. A. and Mcbean, E. A., 2015. Predictive equation for longitudinal dispersion coefficient. *Hydrological Processes*, 29(2). <https://doi.org/10.1002/hyp.10139>
- Fry, V. A., Istok, J. D. and Guenther, R. B., 1993. An analytical solution to the solute transport equation with rate-limited desorption and decay. *Water Resources Research*, 29(9). <https://doi.org/10.1029/93WR01394>
- Guinot, V., 2013. *Wave Propagation in Fluids: Models and Numerical Techniques: Second Edition*. <https://doi.org/10.1002/9781118558034>
- Hodson, T. O., 2022. Root-mean-square error (RMSE) or mean absolute error (MAE): when to use them or not. *Geoscientific Model Development*, 15(14), pp.5481–5487. <https://doi.org/10.5194/gmd-15-5481-2022>
- Kargar, K., Samadianfard, S., Parsa, J., Nabipour, N., Shamshirband, S., Mosavi, A. and Chau, K. W., 2020. Estimating longitudinal dispersion coefficient in natural streams using empirical models and machine learning algorithms. *Engineering Applications of Computational Fluid Mechanics*, 14(1), pp.311–322. <https://doi.org/10.1080/19942060.2020.1712260>
- Kvočka, D., Žagar, D. and Banovec, P., 2021. A review of river oil spill modeling. In *Water (Switzerland)*, 13(12). <https://doi.org/10.3390/w13121620>
- Kwon, S., Noh, H., Seo, I. W., Jung, S. H. and Baek, D., 2021. Identification framework of contaminant spill in rivers using machine learning with breakthrough curve analysis. *International Journal of Environmental Research and Public Health*, 18(3). <https://doi.org/10.3390/ijerph18031023>
- Li, D., Tang, X., Li, Y., Wang, X. and Zhang, H., 2018. Mathematical modeling of marine oil spills in the Luanjiakou District, near the Port of Yantai. *Discrete Dynamics in Nature and Society*. <https://doi.org/10.1155/2018/2736102>
- Li, J. and Chen, Y. T., 2019. *Computational Partial Differential Equations Using MATLAB®*. <https://doi.org/10.1201/9780429266027>
- Milišić, H., Hadžić, E. and Jusić, S., 2020. Estimation of longitudinal dispersion coefficient using field experimental data and 1D numerical model of solute transport. In *Lecture Notes in Networks and Systems*, 83, pp.305–323. [https://doi.org/10.1007/978-3-030-24986-1\\_24](https://doi.org/10.1007/978-3-030-24986-1_24)
- Morel, A. T., Fey, M. and Maurer, J., 1996. Multidimensional High Order Method of Transport for the Shallow Water Equations. *SAM Research Report* <https://doi.org/10.3929/ethz-a-004284555>
- Ramezani, M., Karami, M. and Sarang, A., 2016. One-dimensional transport simulation of pollutants in natural streams. *Ambient Science*, 3(02 / Sp1). <https://doi.org/10.21276/ambi.2016.03.2.ta04>
- Ramezani, M., Noori, R., Hooshyaripor, F., Deng, Z. and Sarang, A., 2019. Numerical modelling-based comparison of longitudinal dispersion coefficient formulas for solute transport in rivers. *Hydrological Sciences Journal*, 64(7), pp.808–819. <https://doi.org/10.1080/02626667.2019.1605240>
- Ritta, A. G. S. L., Almeida, T. R., Chacaltana, J. T. A. and Moreira, R. M., 2020. Numerical analysis of the effluent dispersion in rivers with different longitudinal diffusion coefficients. *Journal of Applied Fluid Mechanics*, 13(5), pp.1551–1559. <https://doi.org/10.36884/JAFM.13.05.31015>
- Robeson, S. M. and Willmott, C. J., 2023. Decomposition of the mean absolute error (MAE) into systematic and unsystematic components. *PLoS ONE*, 18(2). <https://doi.org/10.1371/journal.pone.0279774>
- Tenebe, I. T., Ogiye, A., Omole, D. O. and Emenike, P. C., 2016. Estimation of longitudinal dispersion co-efficient: A review. *Cogent Engineering*, 3(1). <https://doi.org/10.1080/23311916.2016.1216244>

- Ukpaka, C. and Agunwamba, J. C., 2023. Performance of equations for the longitudinal dispersion coefficient: a case study in the Orashi River. *Water Practice & Technology*. <https://doi.org/10.2166/wpt.2023.177>
- Wang, W. and Lu, Y., 2018. Analysis of the mean absolute error (MAE) and the root mean square error (RMSE) in assessing rounding model. *IOP Conference Series: Materials Science and Engineering*, 324(1). <https://doi.org/10.1088/1757-899X/324/1/012049>
- Welahettige, P., Vaagsaether, K. and Lie, B., 2018. A solution method for one-dimensional shallow water equations using flux limiter centered scheme for open Venturi channels. *Journal of Computational Multiphase Flows*, 10(4), pp.228–238. <https://doi.org/10.1177/1757482X18791895>
- Yip, B. F., Alias, N. A. F. and Kasiman, E. H., 2021. Numerical modelling of pollutant transport in a straight narrow channel using upwind finite difference method. *IOP Conference Series: Materials Science and Engineering*, 1153(1), 012003. <https://doi.org/10.1088/1757-899x/1153/1/012003>
- Zeunert, S. and Meon, G., 2020. Influence of the spatial and temporal monitoring design on the identification of an instantaneous pollutant release in a river. *Advances in Water Resources*, 146. <https://doi.org/10.1016/j.advwatres.2020.103788>
- Zhou, J., Bao, W., Li, Y., Cheng, L. and Bao, M., 2018. The modified one-dimensional hydrodynamic model based on the extended Chezy formula. *Water (Switzerland)*, 10(12). <https://doi.org/10.3390/w10121743>

---

#### ORCID DETAILS OF THE AUTHORS

Fatima M. A. Al-khafaji: <https://orcid.org/0009-0008-0616-9604>

Hussein A. M. Al-Zubaidi: <https://orcid.org/0000-0001-8746-8543>



# Assessment of Water Poverty Index (WPI) Under Changing Land Use/Land Cover in a Riverine Ecosystem of Central India

Girish Kumar<sup>1†</sup>, M. M. Singh<sup>1</sup>, Dheeraj Kumar Singh<sup>1</sup>, Bal Krishan Choudhary<sup>2</sup>, Vijay Kumar Singh Rathore<sup>3</sup> and Pramod Kumar<sup>1</sup>

<sup>1</sup>Institute of Earth Sciences, Bundelkhand University, Jhansi, Uttar Pradesh, India

<sup>2</sup>Department of Environmental Science, Women's College, Agartala, Tripura, India

<sup>3</sup>K.S. Saket P.G. College, Ayodhya, Uttar Pradesh, India

†Corresponding author: Girish Kumar; yadavgirish317@gmail.com

Nat. Env. & Poll. Tech.  
Website: [www.neptjournal.com](http://www.neptjournal.com)

Received: 13-12-2023

Revised: 10-02-2024

Accepted: 12-02-2024

## Key Words:

Land use/Land cover  
Water poverty index  
Watershed development  
Geographical Information System

## ABSTRACT

Watershed Development is a very common phenomenon in the river basins in India due to its dynamic and continuously changing nature, which are interconnected via. Land use/land cover (LULC) change and water poverty scenario over time. In the present study, the samples were chosen from seven sampled villages for the Water Poverty Index (WPI) in the upper Tons River Basin. Among them, Ghunwara and Maihar Village exhibit the highest and lowest WPI, i.e., 98.1 and 62.91 out of 100, respectively. This indicates that villages with a high WPI face challenges in their water requirements, regardless of the seasonal river serving the basin area. Conversely, villages with a low WPI can satisfy their water needs solely from the basin. The present analysis of the Upper Tons River Basin suggests that Land Use and Land Cover (LULC) will undergo influences or adjustments at various stages, ultimately affecting agricultural land in the impact region. It also becomes evident that areas with limited land use and land cover (LULC) extensions exhibit lower Water Productivity Index (WPI), primarily due to their reliance on agricultural land. It is observed that alterations, reductions, or modifications in LULC lead to changes in multiple aspects of agricultural land, resulting in noticeable variations in various metrics. The present paper not only evaluates the land use in the Upper Tons River Basin spanning from 2001 to 2021 but also highlights the changing patterns that impact water resources and their utilization capacity. Furthermore, the study estimates the influence of reducing specific features on the distribution of WPI and other LULC parameters. The Upper Tons River Basin faces challenges such as unfavorable rainfall patterns and inadequate planning for irrigation at the fundamental and local levels. Additionally, its geographical location in a rainfed area negatively affects the WPI.

## INTRODUCTION

The term "land cover" refers to the different types of natural and man-made features that can be found on the surface of the earth. This can include both natural and man-made buildings. Land usage refers to how humans use the land and its resources for a variety of reasons. Land usage and land cover have always been subject to change wherever there has been population growth, technical advancement, or economic expansion. This has always been the case (Biswas et al. 1999). Human actions have had a direct or indirect impact on the natural environment. Human production demands cannot be satisfied without modifying or converting land cover. It is anticipated that the most significant problems that the world will face in the coming century will be caused by significant shifts in the usage and coverage of land (Cox 1994). Forest, woodland, and grassland on a global scale

have been converted to varied purposes in one way or another over the last three centuries to suit society's and economy's expanding demands (Bhatt & Ahmed 2014). The most significant aspects of world change at the moment are the intensification of agriculture, the urbanization of previously rural areas, and the clearing of land, all of which are the result of human activity (Grohmann 2004). Thematic layers for morphometric analysis are created via Remote Sensing (Patel et al. 2022, Barman et al. 2021, Bhatt et al. 2021, 2023). Land use maps, on the other hand, are renowned for better and more specific analysis within basins and changes, allowing for a better understanding of the basin's present Land use (Ganas et al. 2005). This project's main objectives were to conduct a LULC investigation of the Upper Tons River Basin and determine various parameters using various parameters such as The study of land use in the present context is the

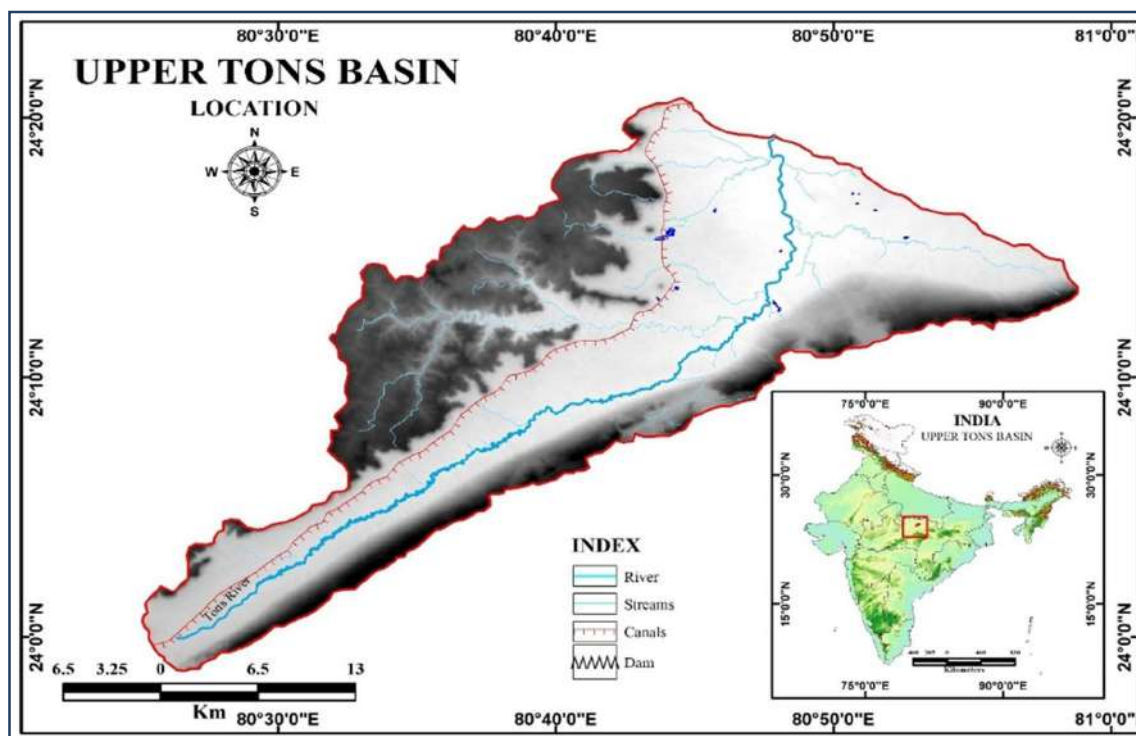
distribution of Northern Jharkhand's surface area with all of its natural environment and human circumstances to evaluate its socio-economic development (Stamp 1960).

Due to increased urbanization and commercialization of land in both urban and rural areas, the changing forest area and diminishing agricultural land have been offset by an increase in non-agricultural land. Changing rural morphology and rising concretization have been the formal process in recent years, where individuals have become much more competent and awarded to earning chances and modifying the various locations in which they are. Land use change may be seen over 20 years when it will be considerably more obvious. Land use is an essential component of geographical studies, and the way a region's land is utilized and maintained may be used to gauge its progress to some extent (Choudhary 2002). The practice of investigating the land use for a certain goal is known as land utilization. Land use affects the natural and human environment, which is inextricably linked to physical, climatic, and educational factors, as well as human activities that alter those variables to achieve certain aims (Al Saud 2009). The geographical distribution of sunlight, rainfall, the topography of the land, drainage quality, mineral availability, and the position of human settlement in relation to market centers and transportation lines all influence Land use. The aim and nature of land use are influenced by the geographical differentiation of these aspects. Although the area suitable for anyone's use is frequently relatively limited, the land on the earth's surface has potential value for some use or combination of purposes. Land use is a notion that has been devised to suit practical reasons and refers to the interplay of land and the environment. The primary goal of a Land-use Survey is to document the distribution of land under diverse uses in varied socioeconomic and environmental situations and to allocate resources to enhance those uses using scientific principles while avoiding environmental deterioration. As a result, LULC planning is required to meet the changing demands of the population.

LULC planning's purpose is to guide LULC decisions in such a manner that all available environmental resources are put to the best possible use while also being conserved for the future. LULC planners have the primary responsibility of analyzing diverse land features in terms of various natural aspects and recommending the optimal use under prescribed management techniques for long-term utilization. Any alternate land use should be recommended without disrupting the area's natural equilibrium. The purpose of this study is to investigate the alterations that took place in Northern Ethiopia's land use and land cover as a direct result of the implementation of integrated watershed management. Alterations to land use and plant cover are among the

alternatives for watershed management. These alterations are made to rehabilitate degraded areas and protect soil and water systems. Integrated watershed management seeks to enhance people's living conditions by reducing population pressure, increasing land productivity, and ensuring sustainable livelihoods and land use practices. These goals can be accomplished through enhancing land production and lowering population pressure. If the intervention strategy and its results are carefully analyzed and researched, it may be possible to foster the replicability of land resource management. As a consequence of this, the primary concerns of the research are the implications of integrated watershed management and the shifts in the dynamics of land use and land cover.

The idea of poverty used in the WPI's framework is based on research by Townsend (1979) and Sen (1983, 1985, 1995, 1999), and it has been expanded by Desai (1995). It is recognized that poverty is a state brought on by a lack of capabilities. Building on the fundamental needs method that was initially proposed by Pigou (1920), Sen has shown that poverty is the result of a lack of at least one of the fundamental conditions (or talents) that are necessary for a productive living. In this sense, we are linking an absence of water with a shortage of one of these essential necessities; nevertheless, an absence of water will also have a variety of additional repercussions. For instance, it can be demonstrated that a lack of water has a direct impact on health since personal and food cleanliness would be compromised. Additionally, bad water quality or polluted water can cause a variety of diseases. As a consequence of this, having limited access to it will affect the functioning of the economy, and the obvious but occasionally neglected time that will be spent harvesting water will be time that cannot be used for other purposes. It is expected that a lack of water will have a severe impact on the ecology of the area by either hastening the process of desertification and wind-driven soil erosion or reducing the rate at which biomass may develop. To better understand the many ways in which this impacts people's lives, we can look to the Sustainable Livelihoods Framework (Scoones 1998, Carney 1998), which donor organizations frequently use to measure the success of development efforts. The framework examines the impacts of development in terms of a number of qualities, which are referred to as capitals or assets for maintaining lifestyles and are described as natural, physical, financial, social, and human assets. The framework also evaluates the effects of development in terms of a number of other characteristics. We use a mix of some or all of these to maintain our lifestyles. Poor communities, by definition, lack some or all of the resources needed for a living. The objectives of this paper are (i) to assess the LULC changes from 2001 to 2020. (ii) To Estimate the Impact of LULC



(Source: SRTM-DEM 30m resolution)

Fig. 1: Location map of the study area.

change during the Watershed Development of the Upper Tons River Basin and (iii) to evaluate the Water Poverty Index (WPI) in the rain fade Tons River basin due to rapid urbanization and agricultural demands.

**MATERIALS AND METHODS**

**Study Area**

The Tons River Basin is located in the north-eastern part of Madhya Pradesh. The area of this basin falls in the districts of Satna, Panna, and Katni between the latitudes of 23°58'36.14"N and 24°20'41.38" N and the longitudes of 80°25'7.32"E and 80°58'47.07" E. (Fig. 1). The total area of Upper Tons River Basin is 797.93 km<sup>2</sup>. The Upper Tons River Basin is divided into five sub-basins. The perimeter of the River Basin is 171 kilometers, and the total number of streams found in the basin is 59, having a total length of 303.97 kilometers (Yadav 2018).

**Data and Methodology**

The study has been conducted using secondary data from sources. Toposheets and various satellite imageries have been used in the research. The Toposheets were downloaded from the Survey of India Portal, while the Landsat 4-5

(TM) and Landsat 8 (OLI/TIRS) satellite images were downloaded from the USGS Earth Explorer Portal. The Land use-Landcover Map for the years 2001 and 2021 was created utilizing topographical maps that were georeferenced spatially and masked, along with Supervised Classification of satellite pictures using ArcGIS software.

The five essential components of the water poverty index are combined to form the broad statement shown below in Equation (1):

$$WPI = \frac{\sum_{i=1}^N w_i X_i}{\sum_{i=1}^N w_i} \dots(1)$$

'Xi' denotes the structure for the WPI component, whereas 'wi' denotes the weight given to that component, and WPI is the water poverty index value for that site. Each component is composed of several subcomponents, which are then merged using the same method to produce the components. Equation (1) may be rewritten to account for the parts mentioned above.

$$WPI = \frac{w_r R + w_a A + w_c C + w_u U + w_e E}{w_r + w_a + w_c + w_u + w_e} \dots(2)$$

Equation (ii) represents the five components' weighted average (R, A, C, U, and E): resources (R), access (A),

Table 1: Comparison of water poverty index and sustainable livelihood capitals.

WPI Components	Livelihood Capitals
Resources	Natural capital, as well as physical and financial capital, represents infrastructure.
Access	Social capital, financial capital
Capacity	Human and social capital, including institutional issues and financial capital for investment
Use	Physical capital, financial capital
Environment	Natural capital

capacity (C), use (U), and environment (E). Each component is first standardized to have a value between 0 and 100. As a result, the final WPI value likewise falls within this range. The best scenario (or the lowest level of water poverty) is considered to be 100, while the worst situation (or 0) is considered to be. Other methods of integrating the data to get the WPI were taken into consideration, but it was determined that this method produced the desired results while maintaining the benefits of simplicity and clarity (Sullivan et al. 2003).

### Water Poverty Index

Complex and adaptable, the Water Poverty Index (WPI) measures how severely people are affected by water scarcity. Several measures of water and human well-being are linked to reach this conclusion. This index's primary purpose is to draw attention to people who are poor and lack access to clean water. The Water Poverty Index (WPI) collaborates with other groups to study the environmental, social, and economic factors that contribute to water scarcity and the inability to put this resource to good use. Consultation with many stakeholders, politicians, and scientists establishes the five most important criteria in calculating WPI: resource (R), access (A), capacity (C), use (U), and environment (E). The WPI components and how they support themselves are listed in Table 1.

(U), and environment (E). The WPI components and how they support themselves are listed in Table 1.

The Resource (R) factor considers the variability, quality, and quantity of available water while making an assessment (Table 2). The Access (A) factor, on the other hand, assesses how easy it is to get water by considering criteria like how far it is from homes and how long it takes for each individual to gather it. Similarly, the Capacity (C) component assesses people's abilities to manage water, which includes the amount of money individuals have available to spend on improving their water quality, education, and health. Use (U), the fourth component assesses the many uses of water, including those in the home, agricultural, and industrial settings, among others. Last but not least, the Environment (E) component analyzes the environmental quality of the water as well as an evaluation of the ecological benefits and services offered by the aquatic ecosystems in the region.

### WPI Structure

The Water Poverty Index for a certain site can be determined using the method proposed by Sullivan et al. (2003), which is shown below.

$$WPI = \frac{W1 \times R + W2 \times A + W3 \times U + W4 \times C + W5 \times E}{W1 + W2 + W3 + W4 + W5}$$

Where,

Wi = is the Weight applied to each of the five components  
R – Resource, A – Access, U – Use, C – Capacity, E – Environment.

These weights (Wi) cannot have a negative value, and their sum must equal one. To ensure that the WPI value falls somewhere between 0 and 100, each component has been standardized. The maximum possible score of 100 indicates

Table 2: WPI component variables for study sites.

WPI Components	Variables/Sub-components
Resources (R)	<ul style="list-style-type: none"> <li>• Runoff potential</li> <li>• Ran potential</li> <li>• Variability of rainfall</li> </ul>
Access (A)	<ul style="list-style-type: none"> <li>• Time required to carry water</li> <li>• Reliability of pipe water supply</li> <li>• Percentage of agricultural land with access to the river for irrigation</li> </ul>
Capacity (C)	<ul style="list-style-type: none"> <li>• Percentage of households with economic activities</li> </ul>
Use (U)	<ul style="list-style-type: none"> <li>• Total percentage of households owning only agricultural land</li> <li>• Total percentage of households with agricultural land and livestock</li> <li>• Water required per household (domestic water demand including cattle demand)</li> </ul>
Environment (E)	<ul style="list-style-type: none"> <li>• Quality index of water sources with percentage of people dependent on similar water quality.</li> <li>• Percentage of area with natural vegetation.</li> </ul>

Source: Thakur et al. (2017)



Table 3: Calculation for Resource (R) Component.

S. No.	Sample Villages	Rain Index (Ir)	Perennial river benefit factor (B)	Runoff Index (R)	Corrected Runoff Index (Ik) = (R*(1-B)+B)	Resources (R)=(Ir+Ik)/2*20
1.	Maihar	1	0.35	0.22	0.493	14.93
2.	Sarlanagar	1	0.32	0.29	0.5172	15.17
3.	Bharauli	1	0.28	0.32	0.5104	15.10
4.	Mohania	1	0.31	0.26	0.4894	14.89
5.	Ghunwara	1	0.14	0.37	0.4582	14.58
6.	Gagdi	1	0.16	0.41	0.5044	15.04
7.	Nainiya	1	0.21	0.31	0.4549	14.55

the best possible circumstance, while the lowest possible score of 0 indicates the worst possible circumstance.

### Calculation of Components

Tables 4–8 describe how to calculate five components according to Coppin (1990):

#### Resource (R)

The Resource component is computed as follows:

$$R = \frac{Ir + Ik}{2} \times 20$$

Where,

The rain index is Ir, while the runoff index is Ik. Table 3 depicts the computation of the Resource component. The main source is excess if yearly rainfall exceeds water requirements for annual crop rotation in the area, i.e., Rain index (IR) = 1.

If annual precipitation falls 'p' percent short of what is required for agricultural production, the Rain sub-index (IR) is given a rating of 1 (p/100). The fluctuation of the climate contributes to the unpredictability of rainfall. To calculate adjusted rainfall, rainfall is multiplied by the variability of rainfall. The runoff index, denoted by the letter 'k,' is arrived at by deducting the present runoff from the sufficient perennial runoff, with the number '1' serving as the highest possible benchmark. The surface water rating is, if there is plenty of water available for domestic use, livestock, and crop irrigation, or if the water supply from a nearby source or tap reliably and indefinitely satisfies all needs. These rivers will be of assistance to many communities located along the larger rivers that are fed by snow. Using the perennial river benefit factor 'B' (benefit for all settlements = 1), one may determine what percentage of Sample Villages are comprised of such settlements. For the purpose of calculating the corrected runoff index, the factor is multiplied by the value '1' of the perennial runoff index, and the non-beneficial value (1-B) is multiplied by the runoff index that is produced by rainfall.

#### Access (A)

The access (A) component is computed as follows:

$$A = \frac{Id + Ii}{\gamma} \times 20$$

Where,

The index of the amount of time that households are able to carry water is denoted by Id, and the indicator of irrigation access is denoted by Ii. The Access componentize computation is illustrated in Table 4. As a direct consequence of this, the water carrying time index is as follows:

$$R = 1 - \frac{T}{480}$$

Where,

T represents the amount of time that must be spent collecting and storing the water. According to the results of the field tests, the longest amount of time necessary to transport water is 480 minutes, while the least amount of time necessary with a direct pipe supply in the house is zero minutes. It is possible to determine it at the scale of the sample village as

$$Id = \frac{w1X Id1 + w2X Id2}{w1 + w2}$$

Where,

homes W1 and W2 are the ones who get their water from a well out in the country, whereas homes W3 and W4 get their water from a municipal pipe system. The time indexes for remote water collection are Id1 and Id2, while the time index for pipe water collection is Id2. The following is included in the irrigation accessibility index:

$$Ii = \frac{Ti}{Ta}$$

Where,

Table 4: Calculation for Access (A) Component.

S. No.	Sample Villages	Households that depend upon distant water resources (w1)	Households that depend on pipe water resources (w2)	Water carrying time index for distant water source (Id1) = 1 – T/maximum time required	Water carrying time index for a pipe water source (Id2)	Water carrying Index (Id) = (w1 × Id1 + w2 × Id2)/(w1 + w2)	Irrigation access index (Ii)	Access Index (A) = (Id + Ii)/2*20
1.	Maihar	5022	8047	0.69	1	0.89	0.37	12.67
2.	Sarlanagar	153	191	0.65	1	0.86	0.38	12.45
3.	Bharauli	641	852	0.69	1	0.88	0.66	15.43
4.	Mohania	52	77	0.66	1	0.88	1.32	22.00
5.	Ghunwara	762	952	0.64	1	0.85	1.05	19.04
6.	Gaddi	137	157	0.56	1	0.81	0.95	17.69
7.	Nainiya	214	257	0.55	1	0.82	1.43	22.50

Ti is the total area in km<sup>2</sup> with access to irrigation, while Ta is the total arable land in km<sup>2</sup>.

### Capacity (C)

As the education component of capacity, the literacy rate is employed, while the percentage of households with economic activity is used as the economic component. Consequently, the following formula is used to compute the capacity component:

$$C = \frac{Ic + Iic}{2} \times 20S$$

Where,

Ic stands for education capacity index, while Iic stands for income capacity index.

Education capacity index

$$Ic = \frac{L}{100}$$

Income capacity index

$$Iic = \frac{Tc}{Th}$$

Where,

The letter L stands for the literacy rate, the letter Te represents the number of households in the sample villages that are involved in economic activities, and the letter N stands for the total number of households in the sample villages. The computation of the Capacity component is shown in Table 5.

### Use (U)

The value of the Use component is determined by a household's average daily water use measured in liters per person. It is generally agreed that one liter per person per day constitutes the bare minimum water usage. The value of the Use component is determined by a household's average daily water use measured in liters per person. It is generally agreed that one liter per person per day constitutes the bare minimum water usage.

$$U = \frac{S + Smin}{Sr - Smin} \times 20$$

Where,

S is the quantity of water that a home uses (measured in liters per cubic meter per day), Smin is the predicted minimal

Table 5: Calculation for Capacity (C) Component.

S. No.	Sample Villages	Literacy rate (%) (L)	Education capacity Index (Ic) = (L/100)	Number of households which has economic activities (Te)	Total number of households (Th)	Income capacity index (Iic) = (Te/Th)	Capacity (C) = ((Ic + Iic)/2)*20
1.	Maihar	59.14	0.59	4328	8047	0.54	11.29
2.	Sarlanagar	64.17	0.64	121	191	0.63	12.75
3.	Bharauli	61.49	0.61	581	852	0.68	12.97
4.	Mohania	80.80	0.81	43	77	0.56	13.66
5.	Ghunwara	64.16	0.64	685	952	0.72	13.61
6.	Gaddi	74.90	0.75	102	157	0.65	13.99
7.	Nainiya	69.83	0.70	193	257	0.75	14.49

water demand (measured in liters per cubic meter per day), and SR is the amount of water that is required in a home (measured in liters per cubic meter per day). The calculation of the Use component is shown in Table 6.

Again,

$$S = \frac{K}{Hs}$$

Where,

Hs is household size and

$$K = \frac{La \times Ha \times Lb \times Hb}{Ht}$$

Where,

A household (Ha) with exclusively agricultural land collects La liters of water per day, while a family (Hb) with both agricultural land and animals collects L liters per day. Ht is the total number of homes. Ht is the total number of homes in a certain area.

$$WQI = \sum_{i=1}^7 Wi \times I$$

**Environment (E)**

The Environment component is a weighted average of the water quality index (WQI) and the natural vegetation coverage index. WQI computation entails collecting water from the field, analyzing it in the laboratory, and ultimately calculating it as described below. The evaluation of natural vegetation is carried out by using Google Earth pictures. The Environment (E) component is computed as follows:

$$E = \frac{Iw + Iv}{2} \times 2$$

Where,

Both the Water Quality Index (WQI) and the Natural Vegetation Coverage Index (NVCI) are denoted by the letters

Iw and Iv,, respectively. The results of the computation for the Environment component are presented in Table 8. According to the Natural Sanitation Foundation (NSF), the Water Quality Index (WQI) is the weighted linear sum of the sub-indices (I) that are as follows:

$$WQI = \sum_{i=1}^7 Wi \times I$$

The weights of the nine constituents are shown as follows:

$$Iv = \frac{V}{A}$$

Where,

The natural vegetation index is denoted by Iv. V represents the natural vegetation-covered area, while A represents the Village's entire area.

**RESULTS AND DISCUSSION**

**LULC Analysis**

Changing LULC patterns are a global and regional phenomenon that affects people all over the world. Changes in LULC are influenced by changes in certain natural characteristics over a period of time. Since 2001, changes in LULC have been noticed, as seen in Fig. 2 and 3, created using the supervised classification approach in ArcGIS software, where we can see changes in all parameters. The main parts of landing have been created in the Landsat data evaluation and mapping methodologies, as shown in Table 7, where fluctuation in LULC over 20 years may be shown.

Table 7 and Fig. 2 show where vegetation cover has increased to 195.54 km<sup>2</sup> in 2021 as compared to 2001, where Vegetation cover was 176.32 km<sup>2</sup> which includes Shrubs, grasslands, Plantation crops, and forest regions from Bhandar Plateau and Kaimur Hills. The built-up area has also increased by 574.8% in 2021, 17.41 km<sup>2</sup> which was

Table 6: Calculation for Use (U) Component.

S. No.	Sample Villages	No. of households	Total water demand (Tw)	Total population (Tp)	Water use S = (Tw/Tp)	Use component U = (S - Smin)/(SR - Smin)*20
1.	Maihar	8047	4278589.9	40235	106.34	17.22
2.	Sarlanagar	191	138299.28	1337	103.44	16.23
3.	Bharauli	852	331359.84	3408	97.23	14.12
4.	Mohania	77	204803.88	2316	88.43	11.13
5.	Ghunwara	952	540545.6	4760	113.56	19.67
6.	Gaddi	157	76890.75	785	97.95	14.13
7.	Nainiya	257	118078.65	1285	91.89	12.31

Table 7: LULC Assessment, 2001-2021.

S.No.	LULC	Area (km <sup>2</sup> )		Change	
		2001	2021	km <sup>2</sup>	%
1.	Built-up	2.58	17.41	14.83	574.8
2.	Vegetation	176.32	195.54	19.22	10.9
3.	Agricultural Land	425.68	434.84	9.16	2.1
4.	Fallow Land	148.62	93.32	-55.3	-37.2
5.	Barren Land	33.21	52.61	19.4	58.4
6.	Waterbodies	11.52	4.21	-7.31	-63.4
Total		797.93	797.93	0	0

(Source: Supervised Image Classification, Landsat 05 and 08, 2001-2021)

2.58 km<sup>2</sup> only. The area under the Agricultural land was 434.84 km<sup>2</sup> in 2021, which was 425.68 km<sup>2</sup> with an increase of 2.1%. Area under Fallow and Barren Land is 93.32 km<sup>2</sup> and 52.61 km<sup>2</sup> in 2021 which was 148.62 km<sup>2</sup> and 33.21 km<sup>2</sup> out of which fallow land has decreased by -37.2% and barren land increased by 58.4%, whereas waterbodies with the total area of 4.21 km<sup>2</sup> in 2021 have recorded decrease of -63.4% with compared to 2001 where it was 11.52 km<sup>2</sup>.

Table 7 also shows the land use evaluation from 2001 to 2020, showing that the vegetation cover rose by 21.41 km<sup>2</sup> or 22.49%, which is a very good number. 33.12% increase in grassland has also been noted. It's also worth mentioning that the district's 15.86 percent rise in the built-up area has been a key influence in the Land use shift. Map 2 depicts the shift in land use from 2001 to 2020. The changes in the LULC components, particularly in Vegetation, Agriculture, and Plantation, are vividly visible on the map.

Further from Fig. 2 itself, we can infer that the vegetation level has subsequently increased on account of the decrease in the fallow land with respect to the conversion of traditional agriculture. Area Underwater bodies have also decreased with the increase in agricultural land and built-up areas.

An increase in the barren land on account of fallow land has a major impact on the river basin and the agricultural practices for the future perspectives. From Fig.3, it can be inferred clearly that subsequent changes in LULC and its components have been recorded. The agriculturally induced LULC change is the main factor of change, which has further transferred into all other land use components. We all know that land use change is influenced by economic and social activities, as well as temporal variations based on ground observations, departmental assessments, and remote sensing surveys, which may be used to detect land use change and compute the Change Matrix.

According to the study topic, the decadal Land Use Change Matrix has an influence on the landscape owing to shifts in economic activity. It is used during the transition of agricultural methods from traditional to plantation crops. The ensuing shift in land use patterns has been a widespread and natural process that has been documented and a matrix created.

The decadal shift is also subject to a behavioral and social baseline, which has developed during the district's land use change journey's several transitional phases. In terms of demographics, the transition from rural to urban

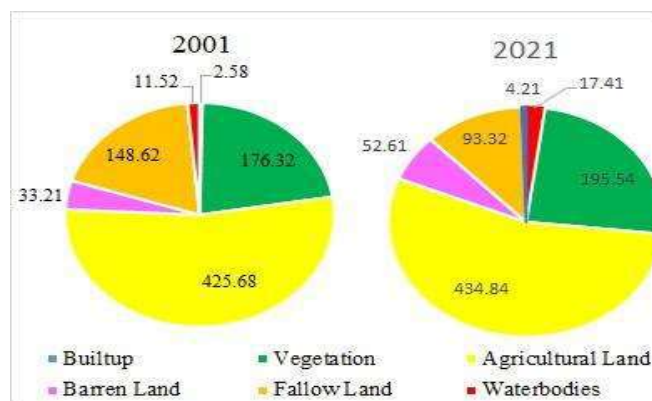
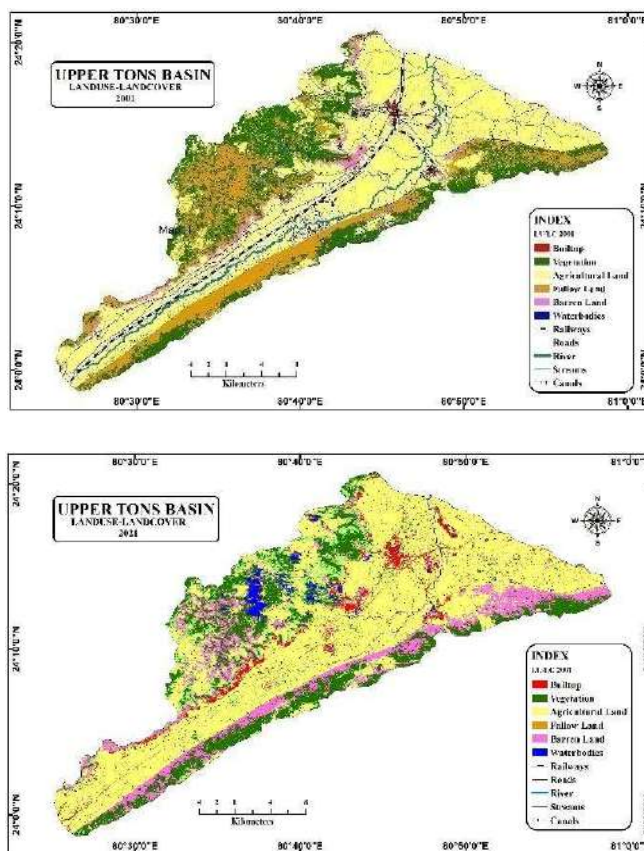


Fig. 2: LULC Assessment, 2001-2021 and Change.



(Source: Landsat 05, USGS Earth Explorer, Path-143, Row-043, taken on 08.06.2001)

Fig. 3: LULC Map of Upper Tons River Basin, 2001 and 2021.

causes a shift in economic activity behavior to improve their living standards. As a result, the fundamentals of land use have changed, both on the ground and through mapping and statistical methods. It's also worth noting that between 2001 and 2010, the biggest shift in the temporal land use pattern was evident based on vegetation, cash crop planting, and shrinking Barren land limitations.

The change in Land use has also been the pull factor around the urban centers and induced rural-to-urban

migration in the purview of the district boundary and away from it to neighboring urban centers. The demographic increase has created new settlements around and nearby to an urban and leaner extent along the Roads and other types of transportation.

Any number that is larger than 75 will be considered extremely low, and any number that is less than 25 will be considered extremely high. Any Figure that is greater than 100 or less than zero will be adjusted to 100 or zero. It was

Table 8: Calculation for Environment (E) Component.

S. No.	Sample Villages	Vegetation area (Iv)	WQI for various sections			eWQI (Iw)	Environment (E) = (Iw + Iv)/2*20
			Western	Central	Eastern		
1.	Maihar	0.17	-	-	100	0.51	6.8
2.	Sarlanagar	0.31	-	-	50	0.93	12.8
3.	Bharauli	0.44	-	50	-	1.32	17.6
4.	Mohania	0.21	-	50	-	0.63	8.4
5.	Ghunwara	0.78	50	-	-	2.34	31.2
6.	Gaddi	0.16	50	-	-	0.48	6.4
7.	Nainiya	0.28	50	-	-	0.84	11.2

Table 9: WPI for upper tons river basin.

S. No.	Sample Villages	Resource (R)	Access (A)	Capacity (C)	Use (U)	Environment (E)	WPI
1.	Maihar	14.93	12.67	11.29	17.22	6.8	62.91
2.	Sarlanagar	15.17	12.45	12.75	16.23	12.8	69.4
3.	Bharauli	15.10	15.43	12.97	14.12	17.6	75.22
4.	Mohania	14.89	22.00	13.66	11.13	8.4	70.08
5.	Ghunwara	14.58	19.04	13.61	19.67	31.2	98.1
6.	Gaddi	15.04	17.69	13.99	14.13	6.4	67.25
7.	Nainiya	14.55	22.50	14.49	12.31	11.2	75.05

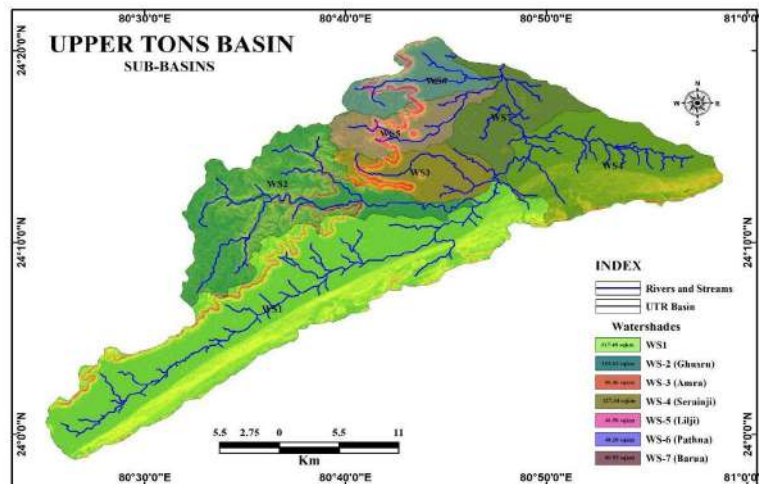
decided to give each component of the WPI framework the same amount of weight. Hence,  $W = 1$  was entered into equation 1. After multiplying each factor by 20, the resulting score, which ranges from 0 to 100, is then tallied. The average WPI for the upper Tons River basin is shown in Fig. 4, with the Environment Component having the lowest score and the Access Component having the highest score. The final WPI score for each of the 7 Sample Villages in the research region, as well as the scores for each component, can be found in Table 9 which can be found below.

The outcomes shown here are the product of the WPI's initial development and use at the local level. It is obvious that a thorough examination of the claim that the index values accurately reflect the extent of water poverty is not practicable. Instead, we used a consultative approach. Participants at workshops from a variety of national and local government agencies learned about and contributed to the index as well as compared the findings to their in-depth local knowledge. Participants in each case concurred that the WPI and its underlying elements accurately reflected the state of the communities.

## Watershed Development

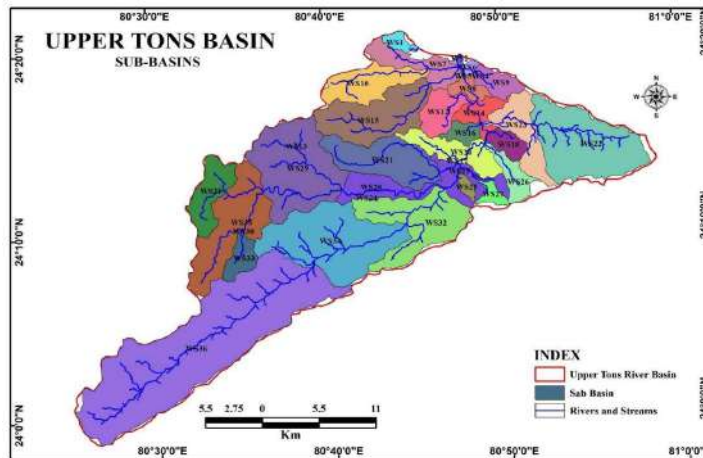
Watershed development is a gradual process that occurs as a result of several natural and regional forces that affect any river basin area over time. The growth of the Basin and the watershed are inextricably interwoven. The Tons River Basin is located at an elevation of 610 m in the Kaimur Range (Upper Vindhyan), with a linear length of 264 km and an area of 16,860 km<sup>2</sup>. The morphometric features were utilized to build a quantitative approach to the development of the Tons River basin. The drainage network was created using SRTM, DEM, and Landsat8 data.

Upstream, the trellis pattern dominates the drainage basin, while the center and downstream are dominated by the dendritic pattern. The drainage density indicates a permeable subsurface and dense plant cover in the basin. For a smaller drainage area, greater form factor values suggest a bigger flow peak. The Tons River Basin is prone to soil erosion, as evidenced by its high roughness number and relief ratio. The Tons River Basin is less prone to flooding and soil erosion and has a great supply of surface water, according



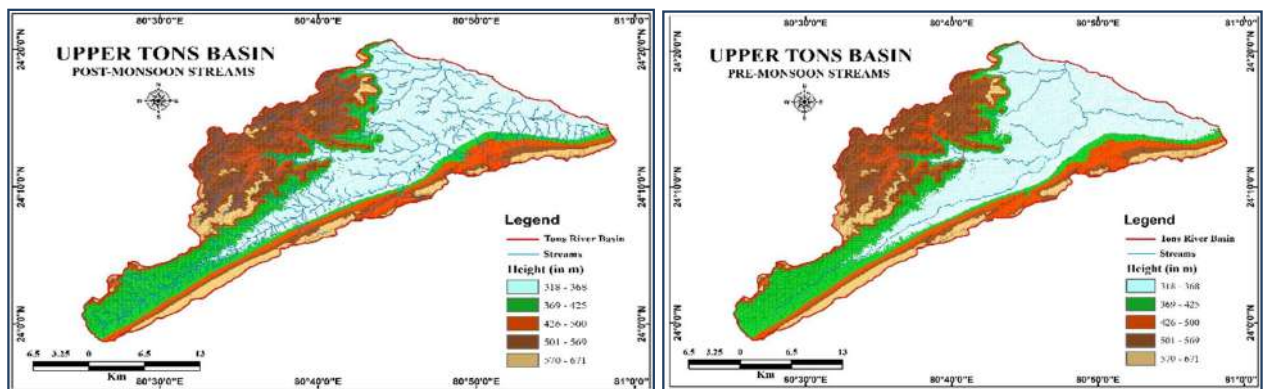
(Source: DEM and SRTM-30m, 2001-2021)

Fig. 4: Watersheds of Upper Tons River Basin.



(Source: DEM and SRTM-30m, (March) 2021)

Fig. 5: Sub-Basins in UTB.



(Source: DEM and SRTM-30m, (May and October) 2021)

Fig. 6: Pre and Post Monsoon Streams in the Upper Tons River Basin, 2021.

to the present study. This research would help with water resource utilization and would be enhanced for the long-term development of the Tons River basin area.

These studies aimed to establish a relationship between morphometric drainage parameters and basin hydrologic features using GIS. As a result, the current study's purpose is to quantify the Tons River Basin's morphometric properties (linear, areal, and relief aspects) as well as hydrologically characterize them. Fig. 4 shows an overview of watersheds in the UTB, with 7 separate watersheds retrieved using DEM and Hydrology tools in ArcGIS 10.4.1 for key rivers such as the Ghusru, Amra, Serainji, Lilji, Pathna, Barua, and Tons, as well as their lower (WS-1) and upper (WS-2) courses (WS-7). WS-1 is the largest, covering 317.48 km<sup>2</sup>, while WS-5 is the smallest, at 46.56 km<sup>2</sup>.

In the Upper Tons River Basin, the watershed division in Fig. 5 is further broken into 36 minor sub-basins.

Sub-basin SW-36 is the biggest, whereas Sub-basin SW-25 is the smallest, as seen in Fig. 5. The pre and post-monsoon stream in the Upper Ton's river basin is shown in Fig. 6. The river basin's watershed development is influenced by spatial configurations and locational significance. The development of the watershed is governed by an accessibility index and a penetration scale, through which every project may scale and identify its core objectives, ensuring the watershed's consistency with current developmental matrixes.

## CONCLUSIONS

The Water Poverty Index (WPI) is a phenomenon and subject to change due to components like LULC pattern and watershed area of the river basin, which are closely proportional and interlinked according to the research conducted in this paper. It is evident from the above research that WPI remains lower in the southwestern part as compared

to the north-eastern part of the river basin. Results show the WPI of 7 sample villages in the River Basin, out of which Ghunwara and Maihar Village have the maximum and minimum WPI which is 98.1 and 62.91, respectively, out of 100, which shows that with high WPI, villages face challenges in fulfilling its water needs irrespective of river which serves the basin area seasonally and with low WPI village fulfill all its water need from the basin. In our analysis of the Upper Tons River Basin, LULC will be influenced or adjusted at various stages, and agricultural land is in the impact region at the end. From all the above discussions, it is clear that the WPI is lower in the areas of fewer LULC extensions due to dependency on agricultural land and that when LULC is influenced, lessened, or altered, multiple components of agricultural land will change, and various metrics will be noted. In addition, the report provides an assessment of land use in the Upper Tons River Basin from 2001 to 2021, as well as its shifting patterns which have also impacted the water resources and its access with use capacity. The impact of decreasing certain features on the distribution of WPI and other LULC parameters has also been estimated. The Upper Tons River Basin suffers from unfavorable rainfall patterns, as well as negligence in irrigation planning at the basic and local levels. Its geographical location in a rainfed area also acts negatively on the WPI.

## ACKNOWLEDGEMENTS

The first author (Girish Kumar) is grateful to the University Grants Commission (UGC), New Delhi, India, for providing the NET-JRF scholarship. We are extremely thankful to the Head of the Department, Institute of Earth Sciences, Bundelkhand University, for providing us with laboratory facilities.

## REFERENCES

- Al Saud, M., 2009. Morphometric analysis of Wadi Aurnah drainage system, western Arabian Peninsula. *The Open Hydrology Journal*, 3(1), pp. 69-73.
- Barman, B.K., Rao, C.U.B., Rao, K.S., Patel, A., Kushwaha, K. and Singh, S.K., 2021. Geomorphologic analysis, morphometric-based prioritization and tectonic implications in Chite Lui river, Northeast India. *Journal of the Geological Society of India*, 97, pp. 385-395.
- Bhatt, S. and Ahmed, S.A., 2014. Morphometric analysis to determine floods in the Upper Krishna basin using Cartosat DEM. *Geocarto International*, 29(8), pp. 878-894.
- Bhatt, S.C., Patel, A., Pradhan, S.R., Singh, S.K., Singh, V.K., Tripathi, G.P. and Kishor, K., 2023. Morphometric and Morphotectonic Attributes of Ken Basin, Central India: Depicting Status of Soil Erosion, and Tectonic Activities. *Total Environment Advances*, 200088.
- Bhatt, S.C., Singh, R., Singh, R., Singh, V.K. and Patel, A., 2021. Morphometric and morphotectonic studies of Sindh Basin, Central India, using advanced techniques of remote sensing and GIS. In *Geological and Geo-Environmental Processes on Earth* (pp. 259-275). Springer, Singapore.
- Biswas, S., Sudhakar, S. and Desai, V.R., 1999. Prioritisation of subwatersheds based on morphometric analysis of drainage basin: A remote sensing and GIS approach. *Journal of the Indian Society of Remote Sensing*, 27, pp. 155-166.
- Carney, D. (ed.), 1998. *Sustainable rural livelihoods: What contribution can we make?* London: Department for International Development.
- Choudhary, A., 2002. Morpho-Lithological analysis and groundwater resource management through GIS modeling and DIP: a case study of Bata River, Himachal Pradesh (Doctoral dissertation, University of Allahabad).
- Coppin, N.J., 1990. Use of vegetation in civil engineering. In I.G. Richards (Ed.), *Butterworths: Ciria* (pp. 23-36).
- Cox, R.T., 1994. Analysis of drainage-basin symmetry as a rapid technique to identify areas of possible Quaternary tilt-block tectonics: an example from the Mississippi Embayment. *Geological Society of America Bulletin*, 106(5), pp. 571-581.
- Desai, M., 1995. *Poverty, Famine and Economic Development: The Selected Essays of Meghnad Desai, Volume II*. Edward Elgar Publishing Ltd.
- Ganas, A., Pavlides, S. and Karastathis, V., 2005. DEM-based morphometry of range-front escarpments in Attica, central Greece, and its relation to fault slip rates. *Geomorphology*, 65(3-4), pp. 301-319.
- Grohmann, C.H., 2004. Morphometric analysis in geographic information systems: applications of free software GRASS and R. *Computers & Geosciences*, 30(9-10), pp. 1055-1067.
- Patel, A., Singh, M.M., Singh, S.K., Kushwaha, K. and Singh, R., 2022. AHP and TOPSIS-based sub-watershed prioritization and tectonic analysis of Ami River Basin, Uttar Pradesh. *Journal of the Geological Society of India*, 98(3), pp. 423-430.
- Pigou, A.C., 1924. *The Economics of Welfare*. Macmillan.
- Scoones, I., 1998. *Sustainable Rural Livelihoods: a Framework for Analysis*. Blackwell Publishing Ltd.
- Sen, A., 1983., Poor, relatively speaking. *Oxford Economic Papers*, 35(2), pp. 153-169.
- Sen, A.K., 1985. *Commodities and Capabilities*. North-Holland
- Sen, A.K., 1995. *Mortality as an Indicator of Economic Success and Failure*. Discussion Paper 66. London School of Economics and Political Science, London.
- Sen, A.K., 1999. *Development as Freedom*. Clarendon.
- Stamp, L.D., 1960. *Applied Geography*. Pelican Books, p. 38.
- Sullivan, C.A., Meigh, J.R. and Giacomello, A.M., 2003. The water poverty index: development and application at the community scale. *Natural Resources Forum*, 27(3), pp. 189-199
- Thakur, J.K., Neupane, M. and Mohanan, A.A., 2017. Water poverty in upper Bagmati River basin in Nepal. *Water Science*, 31(1), pp.93-108.
- Townsend, P., 1979. *Poverty in the UK*. Penguin
- Yadav, S.K., 2018. *Impact of Morpho-tectonics on drainage network of Upper Tons Basin*. Doctoral Thesis. University of Allahabad, Prayagraj.





# Assessment of Physicochemical Properties of Water and Public Perceptions of Water Quality in Tasik Chini, Pahang, Malaysia

M. S. Islam<sup>1†</sup>, T. M. Ekhwan<sup>2</sup>, F. N. Rasli<sup>3</sup> and C. T. Goh<sup>1</sup>

<sup>1</sup>Institute for Environment and Development (LESTARI), Universiti Kebangsaan Malaysia (UKM), Bangi, 43600, Selangor, Malaysia

<sup>2</sup>Faculty of Social Sciences and Humanities, Universiti Kebangsaan Malaysia (UKM), Bangi 43600, Selangor, Malaysia

<sup>3</sup>Centre for Research in Development, Social and Environment (SEEDS), Faculty of Social Sciences and Humanities, Universiti Kebangsaan Malaysia (UKM), Bangi 43600, Selangor, Malaysia

†Corresponding author: M. S. Islam; [sujaul@ukm.edu.my](mailto:sujaul@ukm.edu.my)

Nat. Env. & Poll. Tech.

Website: [www.neptjournal.com](http://www.neptjournal.com)

Received: 27-12-2023

Revised: 13-02-2024

Accepted: 09-03-2024

## Key Words:

Physicochemical parameters

Water Quality Index

Water quality perception

Tasik Chini

## ABSTRACT

The study was conducted to evaluate the physicochemical parameters of water and assess the public perception of the water quality status in the Tasik Chini watershed based on a community survey. The water sample was analyzed based on standard methods and categorized according to WQI (Water Quality Index). Multivariate statistical analysis was adopted to find spatial variations in water quality, determining the pollution level and sources of contamination. The study results were compared with NWQS (National Water Quality Standard for Malaysia). The results showed that the value of dissolved oxygen (DO) was low ( $4.68 \text{ mg.L}^{-1}$ ), while the level of biological oxygen demand (BOD), chemical oxygen demand (COD), and total dissolved solids (TDS) was found to be high,  $2.92 \text{ mg.L}^{-1}$ ,  $26.10 \text{ mg.L}^{-1}$  and  $22.93 \text{ mg.L}^{-1}$  respectively. High turbidity was recorded in a mining area in the rainy season ( $35.76 \text{ NTU}$ ). The DOE-WQI value categorized the lake under class II and class III. The Principal Component Analysis (PCA) revealed that the major sources of contamination were due to anthropogenic activities, especially settlement, mining, agriculture, and illegal activities. Overall, Tasik Chini's water quality status was classified as slightly polluted to highly polluted based on hierarchical cluster analysis (CA) results. The survey showed that 55% of the local community reported that the water quality was poor. The knowledge and attitude level of the local people was medium category, while community practice was low. The Pearson correlation coefficient test showed a strong significant relationship at 0.01 level between knowledge and attitude and knowledge and practices. The scientific findings with public perceptions might be useful for policymakers and the general public to improve the management system for a desirable future.

## INTRODUCTION

Water resources are important for human beings as well as for industrial and agricultural purposes. One of the most important concerns of the twenty-first century is to ensure that everyone has access to safe and secure drinking water. However, the water demand is always increasing across the globe, and the quality of the world's water resources is worsening as a result of human activities (Phong et al. 2023). Various industries, wastewater treatment facilities, mining sites, excessive use of fertilizers and pesticides in agriculture, and other anthropogenic activities produce effluents containing physical and chemical contaminants, among other things. The degradation of water quality as a result of these toxins may lead to certain major environmental issues, posing a hazard to aquatic communities' general health

(Islam et al. 2022). The quality of the surface water system changes based on multiple factors from natural variations and anthropogenic activities. The anthropogenic processes such as industrial untreated effluents, domestic waste, and agricultural discharge are the prime contributors to surface water pollution and water quality deterioration (Madilonga et al. 2021). The direct release of improperly disposed domestic waste, industrial wastewater, and agricultural runoff in watersheds leads to an increase in freshwater pollution and depletion of clean water resources (Sujaul et al. 2015). As a result, public awareness of the relevance of surface water quality to human health and the environment has grown, and numerous researches have been focused on assessing surface water quality and mitigating its environmental contamination impacts (Caputo et al. 2022).

Public awareness about surface water quality plays an important role in successful pollution prevention. Local communities that live close to nature have significant and long-standing relationships with it. However, they build up an intimate and intuitive understanding of the environment over long periods. Local perceptions of natural resources are derived from daily interactions with the environment. Therefore, the experiences and knowledge of local people can help to reduce the pollution load into surface water. Perception research plays a very important part in global change and sustainable development (Mahler 2021, Khalid et al. 2018). Public perception of environmental issues has been of interest to many researchers and policymakers for several years. These have been obtained through a range of different methods, primarily quantitative social surveys and, more recently, in-depth qualitative studies. Several studies have argued that people's perceptions and attitudes toward the depletion of natural resources are influential to the wise use and management of natural resources (Caputo et al. 2022, Akter et al. 2017).

In this situation, an attempt was made to look into the current status of water quality using water quality standards. Pearson regression and correlation, principal component analysis (PCA), and cluster analysis (CA) have all been frequently done for the assessment and evaluation of lake water quality. Keeping the view in consideration, a social survey (very similar to the KAP survey) was conducted to evaluate the knowledge, perception, and awareness of the local communities on changes in water quality in the Tasik Chini watershed. The study was done to generate quantitative information about the water quality using scientific findings and communities' knowledge and perceptions. Therefore, the purpose of this study is to assess the characteristics of

physicochemical parameters and sources of pollutants and to determine public awareness regarding the water quality in Tasik Chini.

## MATERIALS AND METHODS

### Study Area

Tasik means Lake in Malay. Tasik Chini (Chini Lake) is the second-largest natural freshwater lake in Malaysia. The lake system lies between 3°22'30" to 3°28'00" N and 102°52'40" to 102°58'10" E. The Chini is located in the southeastern region of the state of Pahang (Ali & Lee 1995) and around 100 kilometers away from Kuantan, the capital city. Tasik Chini covers 202 hectares of open water and 700 ha of Riparian, Peat, Mountain, and Lowland Dipterocarp forests (Fig. 1). Three hills, namely Bt. Ketaya (209 m), Bt. Tebakang (210 m), and Bt. Chini (210 m) surrounds the gazetted Tasik Chini Park and its watershed (641 m). Only Butit Chini has certain endemic environments (Marimuthu & Zakariah 2020). In this tropical, hot, and humid environment, annual rainfall ranges from 1,488 to 3,071 mm. Twelve different reservoirs create a finger-like structure known as "Laut" locally. Indigenous dipterocarp forest is heavily inhabited in the riparian zones and neighboring lowlands. There are only two seasons in the studied region: dry season and wet season (Islam et al. 2012).

### Water Sampling

Water quality varies depending on geographic location, weather, human activities, and site-specific conditions. While point sources of pollution, such as domestic or industrial discharge, are relatively easy to identify and control, non-point sources of pollution, such as urban or agricultural

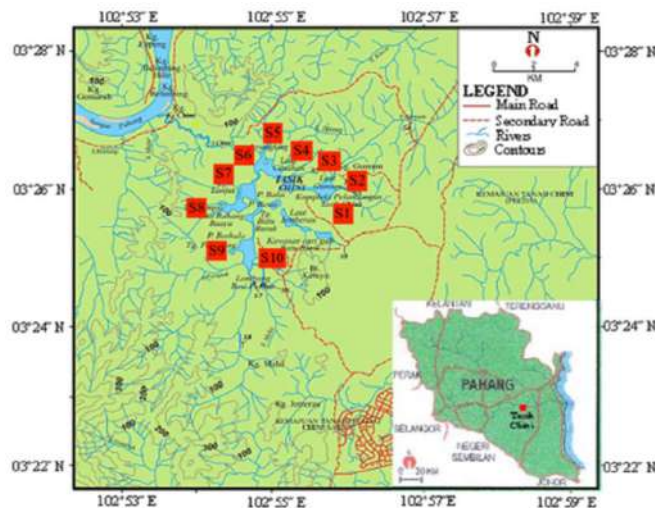


Fig. 1: Location of the study area and sampling stations.

Table 1: Description of the sampling station and surrounding area.

Stations	Grid References	Location	Source of pollution
S1	03°25'331" 102°55'662"	Laut Jemberau, near to the Jemberau River	Mining and forest area
S2	03°25'413" 102°55'385"	Laut Batu Busuk	National service training camp, primary forest and logging area
S3	03°24'877" 102°54'727"	Laut Melai, near the Melai River	Logging, agricultural, and mining area
S4	03°24'970" 102°54'642"	Laut Serodong	Agricultural and mining area
S5	03°25'940" 102°54'653"	Laut Kenawar	Forest and rubber plantation area
S6	03°26'283" 102°54'726"	Laut Gt. Teratai	Rubber plantation and upland primary forest area
S7	03°26'512" 102°54'773"	Draining point of the lake at the initiation of the Chini River	Draining end point of Tasik Chini at Chini River
S8	03°26'248" 102°55'89"	Laut Cenahan, near the jetty	Cenahan Village and agricultural area
S9	03°25'986" 102°55'334"	Laut Pulau Balai, near the tourist main jetty	Tourist settlement zone, secondary forest, and rubber plantation area
S10	03°26'131" 102°55'707"	Laut Gumum, near the jetty	Gumum village, agriculture, shifting cultivation, and oil palm plantation area

sources, are more difficult to identify and control (Haldar et al. 2020). The monitoring stations were chosen based on the probable sources of pollution (Fig. 1), which included urban, agricultural discharges, settlement, and forest areas. Water samples were taken from 10 chosen sites and 10-15 cm below the surface using 1000 mL HDPE bottles. According to (Baird 2017), water sampling for BOD analysis was obtained using dark BOD vials (300 mL) bottles. For subsequent examination, the collected samples were kept in the laboratory cold room in a cool and dry environment below 4°C. Fig. 1 shows the locations of both types of water samples in the study area. The latitude and longitude coordinates and the surrounding area of the monitoring stations are shown in Table 1.

### Water Quality Assessment

Temperature, pH, turbidity, DO, EC (electrical conductivity), and salinity were monitored in situ using a portable YSI multisensory instrument (model 6600-M). A spectrophotometer was used to measure ammoniacal nitrogen (AN), Phosphate (PO<sub>4</sub>), Sulfate (SO<sub>4</sub>), Nitrate (NO<sub>3</sub>), and COD (HACH DR5000 model and HACH 2010). TSS and TDS were measured in the laboratory using the Gravimetric technique, whereas BOD was determined using a DO meter.

The assessment of the water quality of the Tasik Chini Lake was done using the Water Quality Index (WQI). Six parameters were obtained to calculate WQI (DOE 2014). The following equation (1), developed by the Department

of Environment; in Malaysia, based on six water quality parameters (Naubi et al. 2016), was used to calculate DOE-WQI. WQI is the sum of weighted subindices for six variables (DO, BOD, COD, NH<sub>3</sub>-N, TSS, and pH). The subindices values are derived based on segmented nonlinear functions. The value of the weighted subindices is a score between 0 and 100 that is categorized into five classes (I - V) to suggest the uses of water. The equation (1) is illustrated below:

$$WQI = 0.22 \times SIDO + 0.19 \times SIBOD + 0.16 \times SICOD + 0.15 \times SIAN + 0.16 \times SITSS + 0.12 \times SIPH \quad \dots (1)$$

Where the SI indicates the sub-index function and the coefficients are the weights for the corresponding parameters with a total value of unity.

### Questionnaire Survey

A well-structured, closed-ended questionnaire was designed to better understand the local people's knowledge, perception, environmental awareness, and attitudes to water quality. The questionnaire consisted of 36 closed-ended questions and was designed with four categories covering respondents' demographic information, knowledge and perception of water quality, source of information, as well as awareness and willingness to participate as a volunteer in a watershed management program. To make the survey easier for responders, the questionnaires consisted of six parts. The first part was designed to obtain general information on age, gender, race, educational qualification, occupation, family members, and place of residence. The second part contained

4 different types of questions, which are related to the water quality of the Tasik Chini area. The third, fourth, and fifth parts are related to local people's knowledge, attitudes, and practice of local people to pollution issues and management. The last part was done to know the portability of the local community to participate in a collaborative project with authorities for the management of the study area. The questionnaire surveys were conducted in the watershed area using Equation (2) to get the demographic information of the respondents, knowledge about water quality and sources of pollutants. The questionnaire surveys were conducted using the following Equation 2 (Ahmed et al. 2018).

$$n = N/1+N(e)^2 \quad \dots(2)$$

Where,  $n$  = sample size;  $N$  = population size;  $e$  = level of perception, 0.05 at 95%

### Statistical Analysis

A descriptive statistical analysis was performed to show the range (minimum-maximum), mean value, and standard deviation for the physicochemical variables in water samples. For social survey data, a descriptive analysis of respondents' demographic characteristics was conducted. The frequencies procedure was applied to summarize the measures of demographic information and presented under the study. The analysis was also performed for communities' knowledge and perceptions of water quality (Nagaraju et al. 2016, Tanjung et al. 2020). The relationship among the physicochemical parameters was measured using Pearson correlation (two-tailed) analysis. The regression and correlation were calculated using IBM SPSS software (version 22) to determine significant differences among the physicochemical water quality parameters. The Principal Component Analysis was used to identify potential pollution sources, while the Cluster Analysis was used to organize the monitoring stations by contamination level (Arafat et al. 2017).

### Non-Parametric Test

Before statistical analysis, water quality parameters were examined for normality of distribution using the Shapiro-Wilk's test ( $p > 0.05$ ) (Razali & Wah 2010). All the parameters showed a violation of the normal distribution and equal variance assumptions of the parametric tests. Hence, a nonparametric test was performed to compare significance differences. Non-parametric tests were carried out in the statistical analyses due to non-normal distributions of the parameters. A non-parametric Lavene's test was used to verify the equality of variances ( $p > 0.05$ ) (Martin & Bridgmon 2012). The nonparametric Kruskal-Wallis test was performed to estimate the significant differences in

water quality parameters under different sampling stations and seasons ( $p$ -value  $< 0.05$ ) (Ling et al. 2017).

## RESULTS AND DISCUSSION

### Physicochemical Assessment of Water

Table 2 shows the water quality and standard deviation of parameters at different sampling stations. The average temperature measured along the Tasik Chini was  $29.88 \pm 2.01^\circ\text{C}$ , which ranged from  $26.70^\circ\text{C}$  to  $32.05^\circ\text{C}$ . The highest temperature value was recorded in July ( $32.05^\circ\text{C}$ ) at station S5, while the lowest in December ( $26.70^\circ\text{C}$ ) at station S10. The temperature readings showed little regional variation but did exhibit temporal variation. Moreover, most of the stations showed higher temperatures in the dry season than in the rainy season. The average temperature in the study area was found to be within the threshold level of the Malaysian standard. The highest turbidity was recorded at station S1 during the rainy season ( $35.76$  NTU), while the lowest was recorded at station S10 during the dry season ( $17.20$  NTU). Turbidity showed a positive relationship (Table 3) with  $\text{SO}_4$  ( $r=0.295$ ,  $P<0.01$ ), according to a correlation study. The average value of turbidity at all stations was classified as class II based on NWQS, Malaysia (EQR 2016). The mean concentration of TSS was  $9.11 \pm 3.42$   $\text{mg.L}^{-1}$ ; the highest value was recorded at station S6 ( $18.70$   $\text{mg.L}^{-1}$ ) during the wet season (December) and the lowest at station S10 ( $4.08$   $\text{mg.L}^{-1}$ ) during the dry period (July). The mean total dissolved solid in Tasik Chini was  $22.93 \pm 1.96$   $\text{mg.L}^{-1}$ , ranging from  $15.66$  to  $34.66$   $\text{mg.L}^{-1}$ . The lowest TDS value was found to be at Station S8 ( $10.20$   $\text{mg.L}^{-1}$ ), whereas the highest concentration was recorded at Station S3. The values of TDS were found to be higher than expected in the mining zone due to illicit deforestation. TDS value has only a positive relationship with electrical conductivity EC ( $r=0.535$ ,  $P<0.01$ ), according to correlation analysis. The TDS levels increased in general when the season changed from dry to rainy.

The average value of pH measured along the Tasik Chini was 6.26. Station S10 reported the highest pH value (7.91), while station S1 recorded the lowest (5.65). The majority of the stations were found to be mildly acidic. In natural waterways, a low pH value implies the presence of a lot of organic matter (Matilainen et al. 2011). The salinity results ranged from 0.00 to 3.00%. The highest concentration of salinity (2.80%) was observed at station S7 in April, and the lowest was recorded at station S4 (0.03%) in December. An average of  $31.46$   $\mu\text{S.cm}^{-1}$  electrical conductivity was recorded in the lake during the study period. The concentration of DO value varied from 4.83 to 6.11  $\text{mg.L}^{-1}$ , with a mean of  $5.19$   $0.41 \pm$   $\text{mg.L}^{-1}$ . The DO value in Chini Lake water

was shown to be positively correlated with temperature ( $r=0.435$ ,  $P<0.01$ ). The DO value near the settlement area was recorded as low. Most of the stations along the water body were acidic due to a shortage of DO. The average value of BOD in Chini Lake was  $2.92\pm 0.52$  mg.L<sup>-1</sup>; it ranged from 2.58 to 3.07 mg.L<sup>-1</sup>. BOD value was positively correlated with DO ( $r=0.200$ ,  $P<0.01$ ), pH ( $r=0.404$ ,  $P<0.01$ ), SO<sub>4</sub> ( $r=0.173$ ,  $p>0.01$ ) and negatively correlated with EC ( $r=-0.232$ ,  $P<0.01$ ) and TDS ( $r=-0.362$ ,  $P<0.01$ ). The mean COD value was  $26.10\pm 4.50$  mg.L<sup>-1</sup>, ranging from 17.23 to 32.24 mg.L<sup>-1</sup>. The COD value was positively correlated with DO ( $r=0.213$ ,  $P<0.01$ ) and AN ( $r=0.263$ ,  $P<0.01$ ) and negatively correlated with pH ( $r=-0.219$ ,  $P<0.01$ ). The maximum value (42.24 mg.L<sup>-1</sup>) of COD was recorded at station S3 in June, and the lowest value (14.23 mg.L<sup>-1</sup>) was recorded at station S10 in August. The threshold level of COD for surface water in Malaysia (NWQS) is 60.00 mg.L<sup>-1</sup> (EQR 2016).

The average ammoniacal nitrogen (NH<sub>3</sub>-N) (AN) content in Tasik Chini was  $0.66\pm 0.22$  mg.L<sup>-1</sup>, which ranged from 0.14 to 1.31 mg.L<sup>-1</sup>. All samples collected during dry and wet seasons were lower than the threshold level of the Malaysian standard (EQR 2016). The value of NH<sub>3</sub>-N showed a positive correlation with COD ( $r=0.263$ ,  $P<0.01$ ) and a negative with pH ( $r=-0.294$ ,  $P<0.01$ ). The average NO<sub>3</sub> value in Tasik

Chini was 0.38 mg.L<sup>-1</sup>, ranging from 0.12 to 0.80 mg.L<sup>-1</sup>. NO<sub>3</sub> showed a positive relationship with turbidity ( $r=0.159$ ,  $p>0.05$ ) and BOD ( $r=0.154$ ,  $p=0.05$ ). The PO<sub>4</sub> levels of water samples measured across the seasons varied from 0.08 to 0.19 mg.L<sup>-1</sup>. The average concentration was recorded at 0.13 mg.L<sup>-1</sup>. The highest value (0.19 mg.L<sup>-1</sup>) was recorded at station S3 during the wet season, and the lowest (0.08 mg.L<sup>-1</sup>) was recorded at station S10 during the dry season. The PO<sub>4</sub> value was positively correlated with ammoniacal nitrogen ( $r=0.398$ ,  $P<0.01$ ). The SO<sub>4</sub> content in water samples ranged from 0.32 to 2.00 mg.L<sup>-1</sup>, on average of  $0.79\pm 0.04$  mg.L<sup>-1</sup>. The highest SO<sub>4</sub> concentrations were recorded at station S4 ( $2.00\pm 0.17$  mg.L<sup>-1</sup>) and the lowest at station S5 (0.32 mg.L<sup>-1</sup>). All the samples collected during the dry and wet seasons were far below the maximum permissible limit (250.00 mg.L<sup>-1</sup>) set by NWQS, Malaysia (EQR 2016).

### Water Quality Index

The water quality index value of different stations in Tasik Chini water body was calculated based on six parameters, namely DO, BOD, COD, TSS, NH<sub>3</sub>-N, and pH, and their sub-index value. The calculated WQI values for the 10 stations varied from 51 to 86 (Table 4). Based on the WQI score, stations S1, S2, S5, S6, S7, S8, S9, and S10 were classified

Table 2: Water quality parameters of the Tasik Chini at different stations.

Station	Temp	EC	TDS	DO	PH	Turbidity	BOD	COD	TSS	Salinity	AN	PO <sub>4</sub>	SO <sub>4</sub>	NO <sub>3</sub>
	°C	µS.cm <sup>-1</sup>	mg.L <sup>-1</sup>	mg.L <sup>-1</sup>		NTU	mg.L <sup>-1</sup>	mg.L <sup>-1</sup>	mg.L <sup>-1</sup>	%	mg.L <sup>-1</sup>	mg.L <sup>-1</sup>	mg.L <sup>-1</sup>	mg.L <sup>-1</sup>
S1	30.06	30.31	23.33	5.83	5.74	35.76	2.24	26.75	7.17	0.04	0.14	0.18	1.06	0.20
	±0.60	±1.45	±0.56	±0.12	±0.06	±1.10	±0.04	±0.21	±0.30	±0.01	±0.05	±0.03	±0.24	±0.11
S2	30.81	29.65	22.00	5.86	6.17	16.06	2.70	27.18	11.10	0.23	0.19	0.12	0.33	0.26
	±0.30	±2.09	±1.53	±0.08	±0.02	±3.09	±0.04	±0.18	±0.15	±0.20	±0.03	±0.03	±0.21	±0.13
S3	30.62	31.68	27.33	4.96	6.41	22.88	3.07	29.15	7.08	0.026	0.28	0.21	0.66	0.29
	±0.51	±0.58	±0.34	±0.05	±0.01	±2.15	±0.01	±0.09	±0.32	±0.01	±0.02	±0.01	±0.31	±0.14
S4	30.50	31.31	21.33	4.68	6.39	27.33	2.80	22.33	11.10	0.03	0.54	0.19	2.00	0.14
	0.75±	±0.54	±1.67	±0.04	±0.01	±0.95	±0.04	±0.25	±0.27	±0.01	±0.01	±0.02	±0.19	±0.08
S5	31.90	30.66	17.33	5.77	6.31	13.14	2.57	23.14	9.60	0.14	0.47	0.09	0.32	0.20
	±0.45	±1.67	±2.58	±0.09	±0.03	±3.90	±0.04	±0.20	±0.25	±0.20	±0.01	±0.04	±0.16	±0.09
S6	31.47	30.32	18.33	5.62	6.27	16.10	2.21	20.2	18.70	0.05	0.64	0.16	0.90	0.25
	±0.60	±1.87	±2.52	±0.04	±0.02	±2.25	±0.05	±0.35	±0.08	±0.01	±0.01	±0.01	±0.35	±0.10
S7	32.02	30.65	18.33	4.99	6.41	25.84	2.61	24.09	11.04	2.80	0.74	0.11	0.42	0.12
	±0.35	±1.65	±2.26	±0.11	±0.01	±1.15	±0.03	±0.15	±0.21	±0.07	±0.01	±0.01	±0.28	±0.04
S8	31.72	28.67	18.00	4.90	6.19	34.20	2.41	20.16	9.94	0.04	1.31	0.09	0.66	0.14
	±0.26	±3.06	±1.98	±0.11	±0.03	±0.25	±0.02	±0.30	±0.26	±0.01	±0.01	±0.01	±0.32	±0.05
S9	31.36	32.62	18.67	6.08	6.32	26.81	2.33	24.73	9.16	0.09	0.90	0.13	0.61	0.41
	±0.55	±1.05	±1.67	±0.02	±0.04	±0.85	±0.04	±0.09	±0.20	±0.02	±0.01	±0.02	±0.25	±0.08
S10	29.75	34.68	19.33	5.79	6.24	17.20	2.33	18.53	4.08	2.60	0.49	0.08	0.83	0.80
	±0.45	±0.35	±1.12	±0.01	±0.01	±2.10	±0.05	±0.11	±1.25	±0.19	±0.01	±0.03	±0.37	0.13±

Table 3: Pearson correlation coefficient among the parameters of water quality at Tasik Chini.

	Temp	EC	TDS	DO	PH	Turbidity	BOD	COD	TSS	Salinity	AN	PO <sub>4</sub>	SO <sub>4</sub>	NO <sub>3</sub>
Temp	1													
EC	-0.271**	1												
TDS	-0.366**	0.535**	1											
DO	0.435**	-0.210**	-0.161*	1										
PH	0.285**	-0.079	-0.178*	0.196**	1									
Turbidity	0.044	-0.073	-0.043	-0.008	0.052	1								
BOD	0.407**	-0.232**	-0.362**	0.200**	0.404**	0.050	1							
COD	0.161*	0.184*	-0.044	0.213**	-0.219**	-0.037	-0.003	1						
TSS	0.012	0.069	-0.262**	-0.382**	0.183*	-0.021	0.006	-0.076	1					
Salinity	-0.108	-0.086	0.075	-0.084	0.033	0.193**	-0.023	-0.128	-0.083	1				
AN	0.105	0.064	0.045	0.143	-0.294**	0.001	-0.078	0.263**	-0.127	-0.095	1			
PO <sub>4</sub>	0.092	-0.019	-0.052	0.098	0.101	-0.103	0.002	0.106	-0.042	-0.040	0.398**	1		
SO <sub>4</sub>	0.073	-0.075	-0.147*	-0.043	-0.104	0.295**	0.173**	0.039	0.044	-0.119	0.219**	0.051	1	
NO <sub>3</sub>	0.053	0.031	-0.077	-0.031	-0.003	0.159*	0.154*	-0.027	0.048	-0.004	-0.108	-0.067	-0.046	1

\*\* Correlation is significant at the 0.01 level (2-tailed).

\* Correlation is significant at the 0.05 level (2-tailed).

as Class II (slightly polluted), whereas stations S3 and S4 were classified as Class III (polluted). The WQI scores for stations S3 and S4 were the lowest among the stations. The calculated DO value at the two stations (S3 and S4) was the lowest due to the flooding area. The results showed that the concentration of organic matter and nutrients, particularly phosphate, affected the water quality status of Stations S3 and S4. These stations are close to an indigenous peoples' community in the Gumum region, an agricultural area, as well as a resort and a National Service Centre camp, all of which might contribute to organic loading. Improper treatment of sanitation in local communities, resorts, and camps areas may introduce additional biological loadings into the lake, raising BOD levels. On the other hand, the lake

surrounding the forest area was almost clean. In the study area, the water quality index value agreed with the study conducted by Sujaul et al. (2013).

However, Tasik Chini water quality was classified as class II overall. WQI fluctuates depending on the location of stations in the lake. Table 4 demonstrates the WQI values and status during the study period. According to DOE-WQI, the water quality in the study area is sensitive to aquatic species and only suitable for recreational use with body contact (DOE 2014).

### Water Quality Based on Principal Component Analysis

PCA is a multivariate analysis technique that has been used to discover new variables characterized by a linear combination of variables with correlations via the variance-covariance matrix of several multivariate variables; it clarifies the majority of the total variations with some important principal components (Jung et al. 2016). PCA may classify contaminants into multiple categories based on their loading, with the highest loading component describing the whole data set's characteristics (Ebrahimi et al. 2017). Five principal components were extracted from PCA. The PC1 explained 20.64% of the total variation, which was strongly loaded on electrical conductivity (0.903) and TDS being heavily loaded (0.905). The second PC2, which comprises three parameters: DO (0.433), NH<sub>3</sub>-N (AN) (0.403), and SO<sub>4</sub> (0.738), explained 11.46% of total variability, whereas the other three PC3, PC4, and PC5 explained 10.64%, 8.28%, and 7.78% of total variability, respectively (Table 5). PC1 was significantly loaded (>0.75), according to the

Table 4: Water quality classification based on DOE-WQI.

Sampling Stations	WQI	CLASS	WQ STATUS
S1	84	II	SP
S2	83	II	SP
S3	51	III	P
S4	53	III	P
S5	83	II	SP
S6	86	II	SP
S7	83	II	SP
S8	84	II	SP
S9	83	II	SL
S10	83	II	SP

P = Poluted and SP = Slightly Polluted, Class I = >92.7, Class II = 76.5 – 92.7, Class III = 51.9 – 76.5, Class IV = < 51.9

Table 5: Rotated component matrix for physicochemical parameters in water.

	PC1	PC2	PC3	PC4	PC5
TEMP	0.129	-0.243	0.115	0.555	-0.269
PH	0.025	-0.152	-0.091	0.143	0.174
DO	-0.059	0.433	0.350	0.120	0.357
EC	0.903	0.141	0.226	-0.132	-0.036
TDS	0.905	0.092	0.183	-0.087	-0.093
TUR	-0.532	0.215	0.643	0.169	0.122
TSS	-0.293	-0.556	0.418	0.225	-0.214
BOD	-0.616	0.278	0.099	-0.213	-0.151
COD	0.497	-0.166	0.143	0.559	0.120
NH <sub>3</sub> -N	-0.131	0.403	-0.247	0.196	-0.519
Salinity	-0.380	-0.370	0.162	-0.011	0.292
PO <sub>4</sub>	0.102	0.043	-0.346	0.135	0.629
SO <sub>4</sub>	-0.046	0.738	0.119	0.376	0.036
NO <sub>3</sub>	0.251	-0.014	0.649	-0.395	-0.010
Eigenvalues	2.889	1.605	1.489	1.159	1.089
% of variance	20.635%	11.464%	10.635%	8.276%	7.781%

factor loading categorization by Low et al. (2016). PC2 and PC3 were characterized as moderated loading. In PC4, the COD was described as somewhat loaded. Finally, PC5 was also mildly loaded on PO<sub>4</sub>. The component plot (Fig. 2) supported all classifications. The Strong loading parameters indicate similar effects that affect negatively on surface water quality and cause pollution of it. The components of the same group are originated from similar sources, and strong loading indicates significant anthropogenic activities such as agriculture, mining, logging, building, etc.

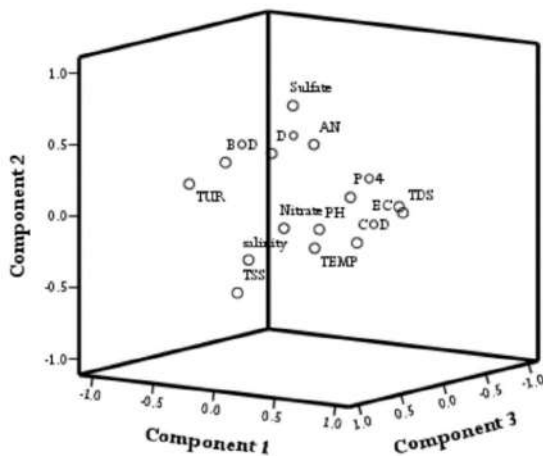


Fig. 2: Component plot in rotated shape for the physicochemical parameters of water.

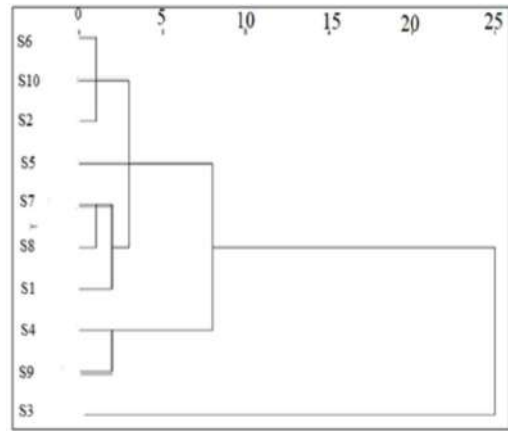


Fig. 3: Dendrogram showing different clusters of sampling sites located in the study area.

### Cluster Analysis

Cluster analysis (CA) is commonly used to examine both temporal and spatial variations in water quality information (Hajigholizadeh & Melesse 2017). Hierarchical cluster analysis (HCA) was used to classify the sampling station based on pollutant similarities. This analysis was done based on the pollution status of all physicochemical parameters, where 10 stations were categorized into similar groups of pollution. Temperature, pH, EC, turbidity, salinity, DO, BOD, COD, TSS, TDS, SO<sub>4</sub>, PO<sub>4</sub>, AN (NH<sub>3</sub>-H), and NO<sub>3</sub> were taken into consideration. The pollution level of sampling stations was categorized using cluster analysis based on their degree of similarity (Samsudin et al. 2011). Station S3 was under Cluster 1, which was highly polluted, whereas Cluster 2 (S9, S4, and S5) was assigned as a moderate pollution source (MPS). Cluster 3 (S1, S8, S7, S2, S10, and S6) was eventually designated as a low pollution source (LPS) (Fig. 3). This technology can complement future spatial sampling efforts by providing dependable clustering of water quality in any location (Juahir et al. 2010). Based on hierarchical cluster analysis results, the order of all stations is as follows: S3> S9> S4> S5> S1> S8> S7> S2> S10> S6.

### Perception of Water Quality

**Community perception about the water quality:** There are two quantitative variables in this demographic section of the community survey for the community (Table 6). The questions were about the family members and duration of stay in the studied area (Tasik Chini Lake). The results showed that the size of the family varied from 2 to 12 members, with an average of 6 members, and this variable also had a variation of approximately 2 members. On the other hand, the average duration of permanent residence in this area was 15 years, and the stay range was

Table 6: The minimum, maximum, average, and standard deviation of family members and years of living for the local community.

	N	Minimum	Maximum	Mean	St. Deviation
How many members of your family?	100	2	12.00	6.1100	2.1022
How long have you been here?	100	2	50.00	15.020	10.1120

Table 7: The minimum, maximum, average, and standard deviation of years of work and total work experience for employees in the agricultural sector.

	N	Minimum	Maximum	Mean	St. Deviation
Your total working experience as a professional	100	2	35.00	15.1920	9.00810
How long have you been working here?	100	2	30	9.0110	6.5870

from 2 years to 50 years with a standard deviation of 10 years. The average family size and stay in the community showed that the people from the community had sufficient stakes and concerns regarding the environment because they had a moderate quantity of their families and spent enough time observing the environmental changes in the water quality.

The majority of the community (55%) reported that the quality of Tasik Chini water was poor. However, the remaining people (45%) said that it was good. The first group of local communities (24%) reported that it was difficult to use the lake water in their routine work like before. About 23% of total people agree that the water quality has been degraded, and 15% strongly agree that the quality of water has been degraded over time. However, 22% of people showed a neutral to this question. Only 19% of the people disagreed, and almost the same percentage strongly disagreed (19%) with this statement.

#### Agricultural respondents' perception of water quality:

There are two quantitative variables in this section which are total working experience and experience with a current employer (Table 7). Results have shown that the employees have sufficient working experience, and the mean total experience was 15 years with 9 years of standard deviation. On the other hand, employees had almost 9 years of average experience with their current employer with a standard deviation of 6 years. The results indicated that the majority of agricultural representatives knew about the current employment policies and practices regarding the environment control plan because they had almost 10 years of experience with their current employer.

The majority of agricultural workers shared that the water quality of the Tasik Chini was poor. But more importantly, this percentage was 75% higher than the community people survey. It gave little idea about the knowledge difference between community and agricultural employees regarding the water quality and their true observation. 75% of the total workers collectively agreed that water has deteriorated over time. Half of them strongly agreed, and the other half just agreed with this change. 25% of participants showed a neutral

attitude about water degradation. Only 5% did not agree with the water quality change over time.

#### Community Knowledge, Attitude, and Practice Toward Water Quality

The correlation based on the Pearson correlation coefficient for community data is given in Table 8. The range of correlation values is from -1 to +1. A correlation value of zero indicates that there is no association, but a value close to 1 indicates that there is a substantial relationship. The significance of the link is characterized by a sign of (\*\*) in the table of correlation coefficients. Knowledge and attitude of local people have a correlation coefficient of 0.450\*\*, which showed a positive correlation. The correlation between practices and knowledge has a strong relationship (0.540\*\*), medium relationship is between practice and attitude (0.475\*\*). Moreover, \*\* showing this relationship was highly significant means the relationship was significant at 0.01 level significance. The table highlighted that all components were positively correlated to each other with high significance. The relationships can lead to more positive practices and attitudes for managing and protecting the environment and vice versa. Knowledge systems influence community people's better attitudes and practices toward environmental management systems (Al Amin et al. 2021).

Agricultural respondents' knowledge, attitude, and practice toward water quality: The knowledge and attitude of agricultural respondents have a strong positive correlation with a value of 0.580\*\*, showing that both components have positively correlated with each other. \*\* showed a high significance, which means this relationship was significant at a 0.01 level of significance (Table 9). Attitude and knowledge

Table 8: The correlation test results between knowledge, attitude, and practice aspects of community respondents.

	Knowledge	Attitude	Practices
Knowledge	1		
Attitude	0.450**	1	
Practices	0.540**	0.475**	1

\*\* . Pearson correlation is significant at 0.01 level (2-tailed); N = 100



Table 9: The correlation test results between knowledge, attitude, and practice aspects of agricultural respondents.

	Knowledge	Attitude	Practices
Knowledge	1		
Attitude	0.580**	1	
Practices	0.920**	0.880**	1

\*\*Pearson correlation is significant at 0.01 level (2-tailed); N = 100

also highlighted the strongest relationship (0.920). The relationship between attitude and practices also has a strong significant correlation with practices (0.880). This finding indicated that the agricultural respondents have sufficient knowledge and a positive attitude toward environmental protection plans. However, they do not practice as per the given standard practices regarding the protection of the environment. Better Knowledge, human attitudes, and practices by the local community greatly influence the conservation and management system of the watershed (Sridhar et al. 2020).

### Public Authorities' Perception of Water Quality

Only eight people were working in the Department of Environment around the concerned area. They have a high level of education, experience, and sufficient knowledge about the area and the status of Tasik Chini water quality. The employees of the Department of Environment rate the quality of water in the clean category. However, the majority of local community and agricultural workers shared that the water quality of the Tasik Chini was poor. This contradiction was possible because it was the primary duty to reduce environmental degradation and maintain the balance of the environment. If they reported that water quality was not good, they would create a problem for themselves.

### CONCLUSIONS

Tasik Chini is invaluable for its presence and function as a wetland and for biodiversity in the environment. Temperature, DO, BOD, and COD values were found to increase in the dry season, whereas turbidity, TSS, TDS, NH<sub>3</sub>-N, NO<sub>3</sub>, PO<sub>4</sub>, and SO<sub>4</sub> increased in the wet season. From the study, it could be recommended that the main reasons behind the contamination of Tasik Chini are anthropogenic activities such as agriculture, illegal logging, and unhygienic defecation. Flood flash from the Pahang River during the rainy season increased the TDS and nutrient value in the Tasik Chini water body. Overall, the water of the lake system stands in class II based on WQI, which could be used after conventional treatment. This study also found that the knowledge and attitude of the local community about the water quality of the lake was at a medium level, while

the management practices were low. This study attempted to find out some factors influencing public perception of water quality and better public knowledge regarding the pollution sources. Survey results also revealed that the level of knowledge influenced public awareness behavior and human practices in nature conservation management. The policymaker may use the results and better understanding of public perception subsequently to improve the water quality system and protect the local community.

### ACKNOWLEDGMENTS

The authors are very much thankful to Universiti Kebangsaan Malaysia (UKM), 43600 Bangi, Selangor Malaysia for financial support through the project SK-2018-013 and KRA-2023-002.

### REFERENCES

- Ahmed, M.F., Alam, L., Mohamed, C.A.R., Mokhtar, M.B. and Ta, G.C., 2018. Health risk of polonium 210 ingestion via drinking water: An experience of Malaysia. *International Journal of Environmental Research and Public Health*, 15, 2056. doi:10.3390/ijerph15102056.
- Akter, K.S., Kurisu, K. and Hanaki, K., 2017. Water use and pollution recognition from the viewpoint of local residents in Dhaka, Bangladesh. *Water*, 9(5), 331. doi:10.3390/w9050331.
- Al Amin, M.A., Adrianto, L., Kusumastanto, T. and Imran, Z., 2021. Community knowledge, attitudes and practices towards environmental conservation: Assessing influencing factors in Jor Bay Lombok, Indonesia. *Marine Policy*, 129, 104521.
- Ali, A.B. and Lee, K.Y., 1995. Chenderoh Reservoir, Malaysia: A characterization of a small-scale, multigear, and multispecies artisanal fishery in the tropics. *Fisheries Research*, 23(3-4), pp.267-281.
- Arafat, M.Y., Mir, S.I., Md, A.K., Zularisam, A.W. and Edriyana, A.A., 2017. Characterization of Chini Lake water quality with Malaysian WQI using multivariate statistical analysis. *Bangladesh Journal of Botany*, 46(2), pp.691-699.
- Baird, R.B., 2017. *Standard Methods for the Examination of Water and Wastewater*. Water Environment Federation, American Public Health Association, American Water Works Association.
- Caputo, A., Tomai, M., Lai, C., Desideri, A., Pomoni, E., Méndez, H.C., Castellanos, B.A., Longa, F.L., Crescimbeni, M., Consortium, A.F. and Langher, V., 2022. The perception of water contamination and risky consumption in El Salvador from a community clinical psychology perspective. *International Journal of Environmental Research and Public Health*, 19, 1109.
- DOE, 2014. *Environmental Quality Report 2013*. Retrieved from <https://enviro.doe.gov.my/view.php?id=15791>.
- Ebrahimi, M., Gerber, E.L. and Rockaway, T.D., 2017. Temporal performance assessment of wastewater treatment plants by using multivariate statistical analysis. *Journal of Environmental Management*, 193, pp.234-246.
- EQR, 2016. *Environmental Quality Report 2015*. Retrieved from <http://enviro.doe.gov.my/ekmc/digital-content/environmental-quality-report-2015/>.
- Haldar, K., Kujawa-Roeleveld, K., Dey, P., Bosu, S., Datta, D.K. and Rijnaarts, H.H., 2020. Spatio-temporal variations in chemical-physical water quality parameters influencing water reuse for irrigated agriculture in tropical urbanized deltas. *Science of the Total Environment*, 708, p.134559.

- Hajigholizadeh, M. and Melesse, A.M., 2017. Assortment and spatiotemporal analysis of surface water quality using cluster and discriminant analyses. *Catena*, 151, pp.247-258.
- Islam, M.S., Ismail, B.S., Barzani, G.M., Sahibin, A.R. and Ekhwan, T.M., 2012. Hydrological assessment and water quality characteristics of Chini Lake, Pahang, Malaysia. *American-Eurasian Journal of Agriculture & Environmental Science*, 12(6), pp.737-749.
- Islam, M.S., Khalid, Z.B., Gabar, S.M. and Yahaya, F.M., 2022. Heavy metals pollution sources of the surface water of the Tunggak and Balok River in the Gebeng industrial area, Pahang, Malaysia. *International Journal of Energy and Water Resources*, 21, p.171.
- Juahir, H., Zain, S.M., Aris, A.Z., Yusoff, M.K. and Mokhtar, M.B., 2010. Spatial assessment of Langat River water quality using chemometrics. *Journal of Environmental Monitoring*, 12(1), pp.287-295.
- Jung, K.Y., Lee, K.L., Im, T.H., Lee, I.J., Kim, S., Han, K.Y. and Ahn, J.M., 2016. Evaluation of water quality for the Nakdong River watershed using multivariate analysis. *Environmental Technology & Innovation*, 5, pp.67-82.
- Khalid, S., Murtaza, B., Shaheen, I., Ahmad, I., Ullah, M.I., Abbas, T., Rehman, F., Ashraf, M.R., Khalid, S., Abbas, S. and Imran, M., 2018. Assessment and public perception of drinking water quality and safety in district Vehari, Punjab, Pakistan. *Journal of Cleaner Production*, 181, pp.224-234. <https://doi.org/10.1016/j.jclepro.2018.01.178>.
- Ling, T.Y., Soo, C.L., Phan, T.P., Nyanti, L., Sim, S.F. and Grinang, J., 2017. Assessment of water quality of Batang Rajang at Pelagus Area, Sarawak, Malaysia. *Sains Malaysiana*, 46(3), pp.401-411. doi:10.17576/jsm-2017-4603-07.
- Low, K.H., Koki, I.B., Juahir, H., Azid, A., Behkami, S., Ikram, R., Mohammed, H.A. and Zain, S.M., 2016. Evaluation of water quality variation in lakes, rivers, and ex-mining ponds in Malaysia. *Desalination and Water Treatment*, 57(58), pp.28215-28239.
- Madilonga, R.T., Edokpayi, J.N., Volenzo, E.T., Durowoju, O.S. and Odiyo, J.O., 2021. Water quality assessment and evaluation of human health risk in Mutangwi River, Limpopo Province, South Africa. *International Journal of Environmental Research and Public Health*, 18(13), 6765.
- Mahler, R.L., 2021. Public perception trends of drinking water quality over a 32-year period in the Pacific Northwest, USA. *International Journal of Environmental Impacts*, 4(2), pp.186-196.
- Marimuthu, S.B. and Zakariah, A.A., 2020. The sufficiency of Malaysia's environmental laws for the protection of the Tasik Chini UNESCO Biosphere Reserve. *Australian Journal of Asian Law*, 21(1), pp. 451-4633.
- Martin, W.E. and Bridgmon, K.D., 2012. *Quantitative and Statistical Research Methods: From Hypothesis to Results*. John Wiley & Sons.
- Matilainen, A., Gjessing, E.T., Lahtinen, T., Hed, L., Bhatnagar, A. and Sillanpää, M., 2011. An overview of the methods used in the characterization of natural organic matter (NOM) in relation to drinking water treatment. *Chemosphere*, 83(11), pp.1431-1442.
- Nagaraju, A., Sreedhar, Y., Thejaswi, A. and Sayadi, M.H., 2016. Water quality analysis of the Rapur area, Andhra Pradesh, South India using multivariate techniques. *Applied Water Science*. doi:10.1007/s13201-016-0504-2.
- Naubi, I., Zardari, N.H., Shirazi, S.M., Ibrahim, N.F.B. and Baloo, L., 2016. Effectiveness of water quality index for monitoring Malaysian river water quality. *Polish Journal of Environmental Studies*, 25(1), pp.231-239. <https://doi.org/10.15244/pjoes/60109>.
- Phong, N.T., Vinh, P.T., Luan, N.D., Dung, P.H., Tanim, A.H., Gagnon, A.S., Lohpaisankrit, W.P.T., Hoa, P.T., Truong, P.N. and Vuong, N.D., 2023. Assessment of water quality during 2018–2022 in the Yam Co River Basin, Vietnam. *Nature Environment and Pollution Technology*, 22(4), pp.1747-1763.
- Razali, N.M. and Wah, Y.B., 2010. Power comparisons of some selected normality tests. *Paper presented at the Regional Conference on Statistical Sciences*, Malaysia.
- Samsudin, M.S., Juahir, H., Zain, S.M. and Adnan, N.H., 2011. Surface river water quality interpretation using environmetric techniques: Case study at Perlis River Basin, Malaysia. *International Journal of Environmental Protection*, 1(5), pp.1–8.
- Sridhar, M.K.C., Okareh, O.T. and Mustapha, M., 2020. Assessment of knowledge, attitudes, and practices on water, sanitation, and hygiene in some selected LGAs in Kaduna State, Northwestern Nigeria. *Journal of Environmental and Public Health*, Article ID 6532512. <https://doi.org/10.1155/2020/6532512>.
- Sujaul, I., Hossain, M., Nasly, M.A. and Sobahan, M.A., 2013. Effect of industrial pollution on the spatial variation of surface water quality. *American Journal of Environmental Science*, 9, pp.120-129.
- Sujaul, I.M., Sobahan, M.A., Edriyana, A.A., Yahaya, F.M. and Yunus, R.M., 2015. Adverse impacts of poor wastewater quality in the Gebeng industrial area, Pahang, Malaysia. *The London United Kingdom*, 17(5), Part XIX.
- Tanjung, M., Syahreza, S. and Rusdi, M., 2020. Comparison of interpolation methods based on geographic information system (GIS) in the spatial distribution of seawater intrusion. *Jurnal Natur Indonesia*, 20, pp.24-30.



# Environmental Monitoring and Assessment for Sustainable Construction Projects: Leveraging Lean Techniques

Ardra Suseelan† and Senthil Vadivel. T.

Department of Civil Engineering, School of Engineering and Technology, Manav Rachna International Institute of Research and Studies, Faridabad, Haryana-121004, India

†Corresponding author: Ardra Suseelan; ardras24@gmail.com

Nat. Env. & Poll. Tech.  
Website: [www.neptjournal.com](http://www.neptjournal.com)

Received: 21-03-2024

Revised: 09-05-2024

Accepted: 18-05-2024

### Key Words:

Construction management

Lean construction

Lean tools

Last planner system

Sustainable project delivery

## ABSTRACT

To increase productivity and avoid waste, the construction industry has started implementing Lean ideas and methodologies in construction projects. Due to a lack of awareness of lean practices in the preparation, design, and execution of building and infrastructure projects, lean practices are not very familiar among construction projects, which are most commonly used in the manufacturing industry. Hence, an effort has been made in this paper to provide a comprehensive review of the literature and case studies to analyze the suitability of lean practice in sustainable waste management, increased productivity, and on-time project delivery. It aims to explore the effect of improving communication and fostering collaboration among stakeholders on time, costs, and resource management. The review identified the most commonly applied lean practices, Just in Time (JIT) and Last Planner System (LPS), and linked the adoption of lean techniques within the construction sector to a total of sixteen distinct benefits for the economy, society, and the environment. According to this study, lean techniques have a strong chance of boosting productivity in the construction industry and developing a sustainable built environment, but they also need to be used widely and continuously to achieve these goals.

## INTRODUCTION

One of the industries in India with the highest rate of growth is building, which is crucial to the continued growth and development of the nation. It contributes about 8.7% of GDP. Despite the use of several cutting-edge technologies still, the efficiency of the construction sector is relatively very low. In 2015, over 430 million people were living in cities; by 2030, that number is projected to rise to about 600 million, or about 40% of India's population. The Indian government's "Housing for All by 2022" mission is a large-scale initiative that calls for the completion of 20 million reasonable housing in cities by that year. India currently has a shortage of 19 million dwellings in urban areas and 44 million in rural regions, and the number is predicted to reach 114 million by 2022, according to the National Real Estate Development Council, despite our present supply.

The principles of lean are all about maximizing value and minimizing waste. Although it may seem easy, doing so is rather challenging. That is because a variety of waste can sneak into any process, whether it's software development, manufacturing, or something else different. Lean construction helps to reduce waste, maximize the

benefits, and deliver a sustainable project at the end of the construction. JIT and Automation, the two pillars of Toyota's manufacturing system, are shown in Fig. 1.

For the design of the Lean Production System, a set of goals was established for the design of the production system influenced by Total Quality Management (TQM). These goals help to maintain Lean Principles and to deliver a product that satisfies consumer needs without keeping any inventory upon request shown in Fig. 2.

Lean is built on a set of guiding principles intended to get rid of waste and help businesses do better at what they do. Five lean principles were outlined by Womack & Jones (1996) as a means of reducing waste in businesses. According to Womack & Jones (1996), one strategy for enhancing organizational performance in terms of value creation is lean thinking. The primary objective is "optimizing the total value," not "minimizing the cost." The literature study helps to identify Lean Principles and their application in the construction sector, identifying the imperatives that bound the application of Lean in the construction sector, the framework assessment process of Lean Principles, model creation, and evaluation of the model. The two sides of the

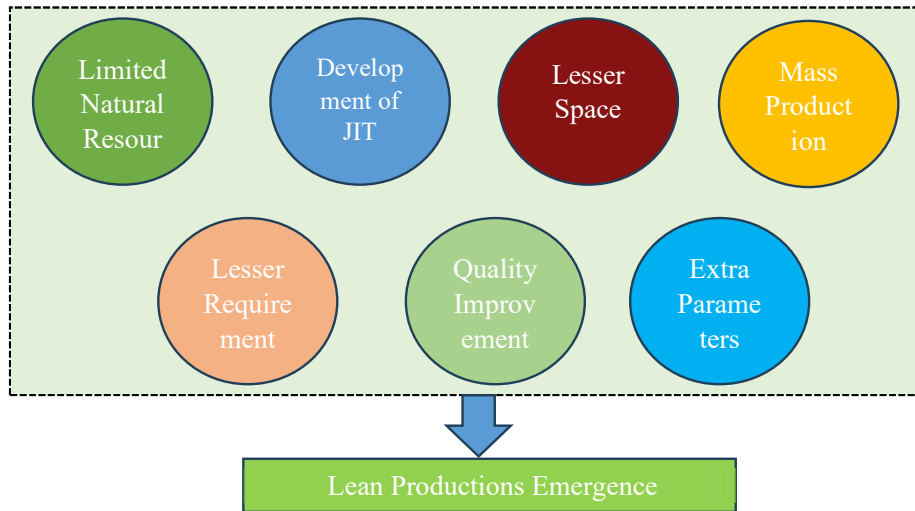


Fig. 1: Lean productions origins (Aziz & Hafez 2013).

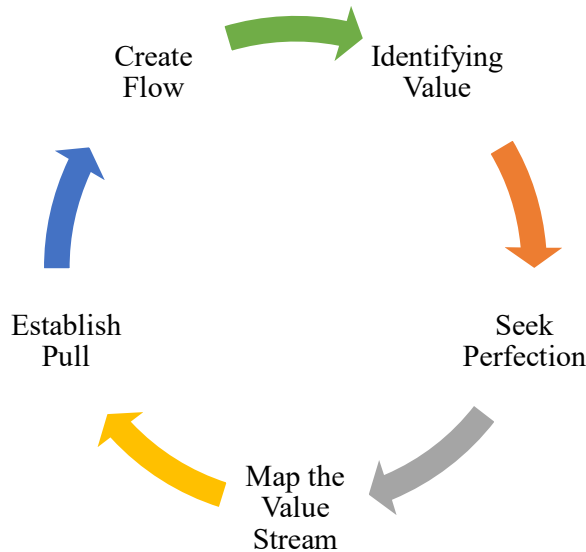


Fig. 2: Fundamentals of Lean.

lean construction coin that keep rotating during a project are (1) Planning and (2) Control. A detailed literature study has been conducted to identify Lean Principles and their application in the construction sector, identifying the imperatives that bound the application of Lean in the construction sector, the framework assessment process of Lean Principles, model creation, and evaluation of the model (Green 2005).

## LEAN TOOLS

Adopting a lean strategy inside an organization has the potential to have an impact on productivity, service delivery, and quality, which eventually leads to significant

cost savings. Lean construction tools like LPS, improved visualization, and daily huddles were evaluated by "Site Implementation and Assessment of Lean Construction Techniques." Most of the lean tools selected are easily accessible or proposed with slight modifications. The Lean construction methodology and the tools are gives in Tables 2 & 3 respectively.

## MATERIALS AND METHODS

A proper systematic literature review of 118 articles was carried out in this study. The following five questions should be considered for a proper literature study, which includes identifying good quality papers, proper research

Table 1: Lean principles' applications.

Lean principles	Applications	Ideas for a deeper and sustainable application of lean principles
Value	Cost-saving enhancements to the construction process. Value, as seen by the client, is not routinely taken into account as a rule.	Recognizing value from the viewpoint of the client. Reviewing the construction process to improve additional willed features while also providing the client with greater value.
Value Stream	Process mapping software	Material and information value stream mapping. Creating a future value stream map and suggesting necessary upgrades
Flow	Applications for specific tools include pokayoke and visual controls. Utilizing work structuring, the last planner identified and reduced process wastes while stabilizing the working flow.	Creating a continuous flow environment by changing how teams and employees divide up their work. Adopting standardized work by specifying rhythm, inventory, and sequence.
Pull	Applications for the supply of specific supplies or tradespeople.	Imagine a vast direct communications system for bringing in services, parts, and supplies just as required.
Perfection	Utilization of Quality Systems, with a primary emphasis on process traits influencing product performance.	Designing procedures for quick problem detection. When differences in standardized work processes are found, establishing systematic procedures for ongoing learning and improvements on the functional hierarchy base are important.

Table 2: Lean construction methodology and levels.

Stages	Lean Construction Approaches	Related Lean Manufacturing Methodology
Stage One	Cards for resources Kanban	Kanban system
Stage Two	Visual inspection Tools for monitoring quality	Visual inspection (Poka-Yoke devices) Multifunctional layout TQM Standard operations Single-minute exchange of dies (SMED)
Stage Three	Daily huddle meetings for the last planner's plan conditions of work environment (PCWE)	Kanban system Production leveling Toyota verification of assembly line (TVAL)

Table 3: Lean tools and their benefits in the literature study.

Lean Tools	Benefits	References
LPS, 5S, Poke Yoke	Waste Reduction, Mistake Correction,	Dineshkumar & Kathirvel 2015, Banawi & Bilec 2014, Li et al. 2019, Ngowtanawan 2013, Agrawal et al. 2024, Hossain & Purdy 2023)
Continuous Improvement	The drive of the workforce, prompt project completion, and little rework	(Pamfilie et al. 2012, Rahim et al. 2012), (Dunlop & Smith 2004), (Khodeir & Othman 2018), (Dombrowski & Mielke 2013)
Daily huddle meetings, VSM	Minimum Rework, Regular Schedule, and Workplace Cleanliness	(Dombrowski & Mielke 2013), (Martens & Carvalho 2017), (Musa et al. 2016), (Batwara et al. 2023).
Visual inspection, LPS, BIM	Proper site management, prompt project completion	(Singh & Kumar 2016), (Lopez et al. 2021), (Molavi & Barral 2016), (Issa 2013), ( Li et al. 2019).

questions, identifying relevant papers, identifying papers with accurate findings and summaries, and interpreting the results, discussions, and conclusions. Papers are identified using the keywords "Lean Construction, Lean tool, Lean Principles" to identify the articles between 1993 and 2024. The databases selected should be among one of the largest online collections of content that have undergone both peer-review and un-reviewed. Fig. 3 represents the methodology used in this study.

Databases include research papers, articles, conference proceedings, books, and reports. About 150 journals, conferences, articles, and books were identified at the initial screening. The second step included the screening and

sorting of articles based on their abstract and content and how they are relevant to Lean. The second selection criteria were based on the citations; papers with more citations had given more preferences. After proper screening and sorting, a total of 118 journals were selected over the last 21 years. Among these 118 journals, 33 articles from Scopus, 53 from Science Direct, 16 from Google Scholar, 5 from books, and 11 from conferences. After the chosen articles are examined, the results are presented in the form of charts, tables, Figs, etc. Fig. 4 gives a detailed representation of the total number of articles published and the year. The result identified that 81% of the material was from 2010 to 2024, and most of the studies were conducted in countries such as the USA and

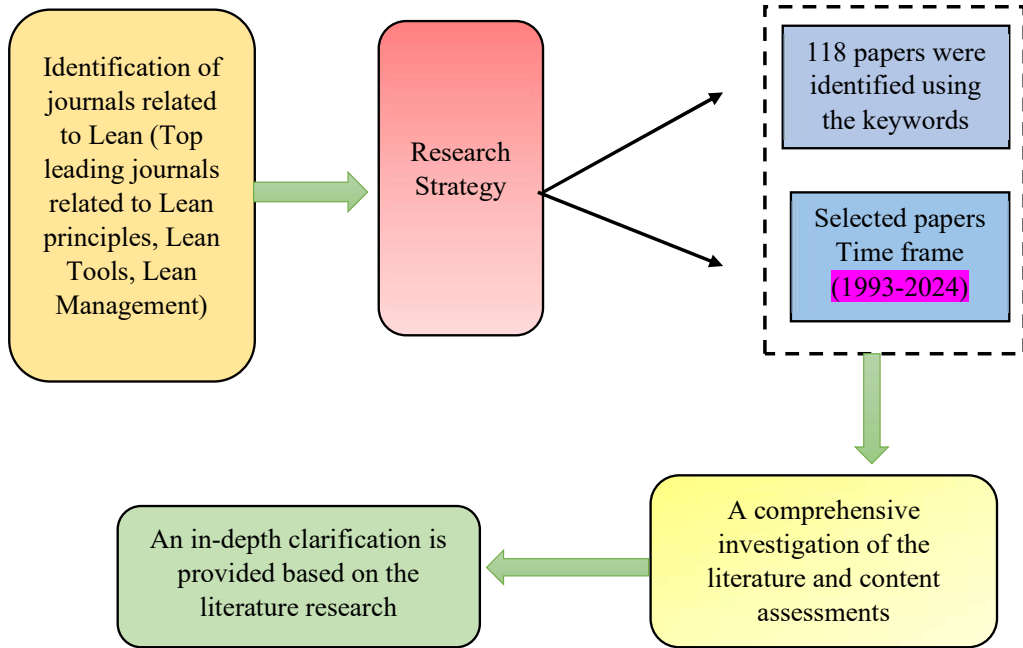


Fig. 3: Flow chart of methodology.

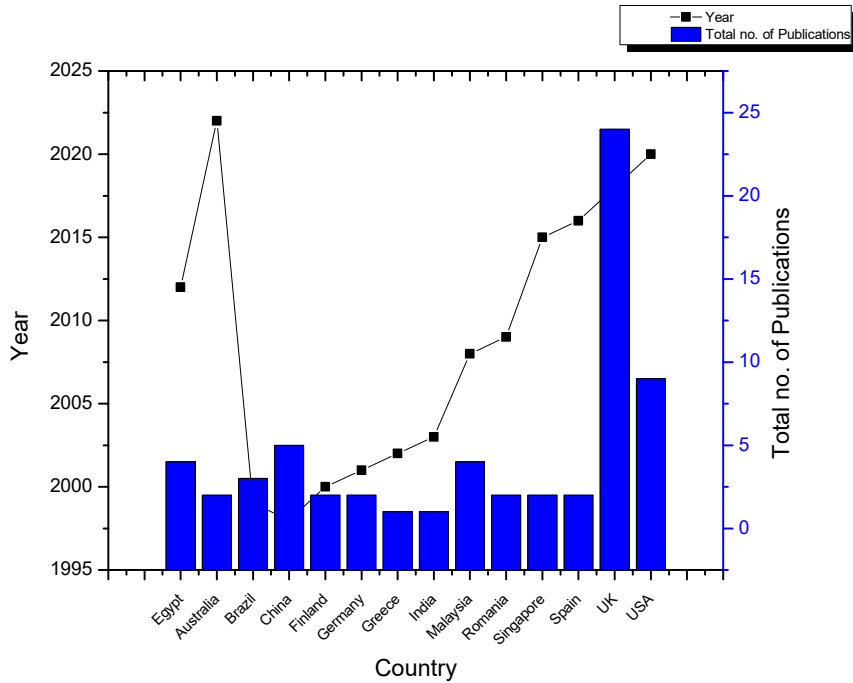


Fig. 4: Total no. of articles referred from different Countries.

the UK, reflecting the dire need for implementation of Lean Principles in the construction sector.

**Sustainable Lean Construction Practices**

There is a ton of evidence in the literature related to LCPs that makes it possible to achieve lean construction goals. The list of LCPs found in the papers analyzed is given in Table 1. These lean methodologies are based on verifiable proof

of their use at various phases of planning, designing, and building projects for buildings and physical infrastructure in distinct nations. The JIT was the most prevalent JIT discovered in this analysis, as evidenced by the reporting of its application in 108 distinct papers from 14 various countries (sources are included in Fig. 4). The LPS is mentioned adjacent to JIT and has been documented in ten different papers. Integrated project delivery (IPD) and thorough briefing are the two LCPs that have received the least amount of implementation.

## CASE STUDY ON LEAN TOOLS

Phaniraj (2015) conducted a case study at the Brigade Orchards Precast Plant near Devanahalli, Bangalore. This project is conducted on 130 Acres of land, which contains small villas, hospitals, stadiums, schools, etc. Various steps included in this case study are recording the current procedure, recognizing wastes, Creating Lean alternatives, and Recording the changes. Kaizen recording is carried out before and after the changes. The output is generated using one of the Lean methods, Kaizen, which helps to reduce non-value-added materials and costs and increase customer satisfaction. The study also gives a brief discussion on employee involvement; labor cooperation is a crucial component of successful Lean Implementation. This study also discusses the barriers to implementing Lean. The Kaizen method helps to maximize the output and minimize the waste.

Gupta & Jain (2014) conducted a case study on 5S and Kaizen and identified that it helps increase process effectiveness and efficiency, better process visibility, improve employee morale and safety and reduce delays and searching time. In this study, company XYZ, a producer of quartz glassware, is selected, which is a small-scale industry in Ambala, Haryana, and recorded observations such as turnover, employees, marketing network, and quality systems. In this study, problem identification is carried out, and training to employees and identified the changes in 1<sup>st</sup> S, 2<sup>nd</sup> S, and so on. Both Kaizen and 5S can be used in any organization and any industry, whether it be small or large. Unwanted items are removed by putting the first S into practice. When the second S is used, the working environment is enhanced, and space utilization can be done. Maintaining a safe and cleaner environment can be done with 3<sup>rd</sup> S. Better workplace and visual control systems by fourth S, foster discipline and team spirit by fifth S.

Eldeep et al. (2022) conducted a case study at Dammam University, which had 48 classrooms and 8 laboratories, with a total cost of 36 million SAR. The technology used was the standard design-build procurement process. The project took 2 months for the bidding procedure, 4 months

for the design stage, and 22 months for execution. The project usually followed a two-dimensional method. In this project, Revit and Navisworks (BIM Software) have been used to redesign the work. With the help of BIM software, the model is prepared within two months and also gives a detailed view of the comparison of 2D works and BIM in detail, which includes increased visual clarity, streamlined process, and information flow.

Rahman et al. (2013) conducted a case study on one of the Malaysian manufacturing Companies that produced a variety of cars, parts, and services and identified that slow staff involvement and less commitment from upper management are the reasons. The study uses a Lean tool known as Kanban. The persons included in this study are employees and management staff from different departments such as store, production, logistics, etc. Data collection is done through structured interviews and observation. A structured interview with the managers of the manufacturing organization was undertaken to comprehend the manufacturing processes and acquire precise data on the facility's existing use of the Kanban system.

Vargas et al. (2018) identified defects are one of the major wastes in the manufacturing sector, which affects delivery time, cost, quality, etc. A case study is carried out in a manufacturing company in Tijuana, Mexico. The main aim of this case study is to reduce waste by 20%, and the PDCA (Plan Do Check Act) method is applied. The three product models were examined. Auxiliary tools such as Pareto charts and Flowcharts were used. Hence, faults dropped by 65%, 79%, and 77%. As a result, the case study concluded that PDCA, Pareto Charts, and Flow Charts are the top-quality tools that aid in lowering the proportion of defective components.

Desai & Shelat (2014) conducted a case using VSM to identify the waste and flow of information among people. The study was conducted in a Steel Yard in Mumbai. VSM helps in creating a roadmap to address problem areas and to reduce the gap between the current state and the desired state of various construction operations. For Mapping, the information is collected from contractors, engineers, supervisors, etc. All the data, like types of activities and quantities, are gathered. And the graphical representation helps to identify the data more easily and reduce waste.

Ryan et al. (2019) conducted a case study on Irish case study organization on LPS. The information was gathered using a qualitative online survey, and the secondary data was collected using an examination of a pilot project within the client organization in 2015. For a better understanding of the advantages and difficulties of the LPS in the context of Ireland, the survey included both open-ended and

closed-ended questions. Lack of standardization and lack of customization to a particular client sector were two issues raised by the case study. The study's shortcomings, which include the use of part-time researchers and application to just one case study organization, are acknowledged. It is advised to conduct more research on the Irish background as well as on ways to address the issues raised by the case study.

## BENEFITS OF ADOPTING LEAN CONSTRUCTION TECHNIQUES

Lean Construction techniques offer a wide range of benefits in terms of economics, environmental sustainability, and social impact. The review paper identified 16 benefits in the construction industry related to Lean Construction Im-

plementation. Based on their nature, these identified benefits were grouped into three groups, mainly social, economic, and environmental, as shown in Table 4.

## INTEGRATION OF DIGITAL TOOLS IN LEAN FOR SUSTAINABLE CONSTRUCTION

Integration of digital tools in Lean Construction practices can significantly enhance project efficiency, reduce waste, improve collaboration, and better project outcomes. BIM and the Internet of Things (IoT) are the two advanced technologies that are widely used in the construction of buildings and infrastructure (Lee et al. 2020, Xu et al. 2018), (Woodhead et al. 2018, Kanan et al. 2018). Lean Construction can benefit from Industry 4.0 in the construction

Table 4: Advantages of Lean principles.

Advantages of Lean Principles	Description	References
Economic	Cost Reduction	Samaila & Hamid 2012, Babalola et al. 2019, Ahiakwo et al. 2013, Ansah & Sorooshian 2017, Bansal et al. 2019
	Improved Profit Margins	Babalola et al. 2019, Ballard & Howell 1998, Alhuraish et al. 2016, Banawi & Bilec 2014, Bansal et al. 2017
	Faster Project Delivery	Bynum et al. 2013, Abdelhamid & Salem 2005, Ansah & Sorooshian 2017, Babalola et al. 2019, Ahiakwo et al. 2013, Brioso 2015, Carvalho & Rabechini 2017
	Higher Return on Investment	Dineshkumar & Kathirvel 2015, Aziz & Hafez 2013, Anvari et al. 2016, Babalola et al. 2019, Eldeep et al. 2022, Gil et al. 2000, Tommelein & Koskela 2002
	Competitive Advantage	Ansah & Sorooshian 2017, Ballard & Howell 1998, Forbes & Ahmed 2003, Dombrowski & Mielke 2013, Tam et al. 2007, Eldeep et al. 2022, Ding et al. 2019
Environmental	Reduced Resource Consumption	Abdelhamid & Salem 2005, Sepasgozar 2020, Singh & Kumar 2016, Zhang & Chen 2016, Rahim et al. 2012, Womack & Jones 1996, Pamfilie et al. 2012
	Lower Carbon Footprint	Anvari et al. 2016, Tam et al. 2007, Lee et al. 2020, Babalola et al. 2019, Jiang et al. 2016, Kamara 2003, Jamil & Fathi 2016
	Sustainable Practices	Ansah & Sorooshian 2017, Li & Froese 2016, Forbes & Ahmed 2003, Kelly & Male 1992, Lakmal 2014, Koskela 1992, Eldeep et al. 2022, Lakmal 2014, Lodgaard et al. 2016
	Waste Reduction	Andelin et al. 2015, Alhuraish et al. 2016, Babalola et al. 2019, Shirowzhan et al. 2020, Issa 2013, Marhani et al. 2012, Kazaz et al. 2015, Moser & Santos 2003
	Energy efficiency	Andelin et al. 2015, Kanan et al. 2018, Phaniraj et al. 2015, Ministry of Finance 2022, Martens & Carvalho 2017, Kumar et al. 2022,
Social Benefits	Safe Work Environment	Pheng & Hui 1999, Sepasgozar 2020, Picchi & Granja 2004, Sapuay 2016, Ryan et al. 2019, Kanan et al. 2018
	Job Creation	Alhuraish et al. 2016, Rahman et al. 2013, Mohammad et al. 2016, Sarhan et al. 2018, Rahman et al. 2013, Mossman 2009, Li et al. 2019, Lakmal 2014
	Enhanced Collaboration	Abdelhamid & Salem 2005, Alhuraish et al. 2016, Babalola et al. 2019, Ballard & Howell 1998, Anvari et al. 2016, Carvalho & Jr 2017, Dulaimi & Tanamas 2001, Eldeep et al. 2022, Gran & Picchi 2004
	Community Engagement	Zhang & Chen 2016, Abdelhamid & Salem 2005, Alhuraish et al. 2016, Anvari et al. 2016, Aziz & Hafez 2013, Babalola et al. 2019, Ballard & Howell 1998, Banawi & Bilec 2014, Brioso 2015
	Improved living and working spaces	Rahim et al. 2012, Zhang & Chen 2016, Zhang et al. 2020, Womack & Jones 1996, Xu et al. 2018, Ying, et al. 2020, Woodhead et al. 2018
	Stakeholder Satisfaction	Paez et al. 2005, Salem et al. 2006, Picchi & Granja 2004, Molavi & Barral 2016, Vargas et al. 2018, Ballard & Howell 1998



Table 5: Digital tools.

Digital Tools	Advantages	References
BIM	It allows for better visualization and coordination of construction projects. BIM can detect clashes and conflicts in design early on, reducing rework and waste.	Abdelhamid & Salem 2005, Abiakwo et al. 2013, Ansah & Sorooshian 2017, Babalola et al. 2019, Ballard & Howell 1998, Anvari et al. 2016
Lean Construction Software	Specialized Lean Construction software can help teams implement Lean principles more effectively. Helps to facilitate pull planning, production control, and the LPS enabling better collaboration and task scheduling.	Li et al. 2019, Banawi & Bilec 2014, Banawi & Bilec 2014, Bynum et al. 2013, Alhuraish et al. 2016
Kanban Cards	Helps in visualizing team workflow, tracking progress, and managing tasks efficiently.	Mostafa et al. 2017, Issa 2013, Jamil & Fathi 2016, Jiang et al. 2016, Jørgensen & Emmitt 2008,
Cloud- Based Platforms	Cloud-based platforms enable real-time collaboration and information sharing among project teams. Field workers can access up-to-date project data, drawings, and documents from anywhere, reducing delays and errors.	Rahman et al. 2013, Ngowtanasuwan 2013, Koskela 1992, Mostafa et al. 2017, Lopez et al. 2021, Pheng & Hui 1999
Digital Documentation	Tools like project management software, document management systems, and collaboration platforms enhance communication and information sharing among team members.	Abdelhamid & Salem 2005, Martens & Carvalho 2017, Molavi & Barral 2016, Lopez et al. 2021, Gatell & Avella 2024, Bag et al. 2024, Frank et al. 2024
Supply Chain Management Software	Digital Tools can optimize the supply chain by providing real-time visibility into material availability, tracking deliveries, and managing inventory efficiency.	Tam et al. 2007, Rahim et al. 2012, Ying et al. 2020, Woodhead et al. 2018, Womack & Jones 1996,
Predictive Analytics	This technology can analyze historical project data to identify patterns and predict potential issues. By using predictive analysis, teams can make data-driven decisions to optimize resource allocation and avoid potential delays.	Molavi & Barral 2016, Shirowzhan et al. 2020, Singh et al. 2014, Womack & Jones 1996, Moser & Santos 2003, Mostafa et al. 2017, Moser & Santos 2003

sector, which includes essential technology for Cyber-Physical Construction Systems (CPCS), (Shirowzhan et al. 2020). The integration of BIM and CPCS helps to improve information exchange and provide real-time data (Ying et al. 2020, Sepasgozar et al. 2018). Digital solutions that translate policies into the system in a language that is accessible to all project stakeholders may lead to improvements in performance. To monitor performance in real-time, sensors are also necessary. BIM and IoT are robust technologies with a wide range of untapped uses that may enhance the use of lean. Scholars want to connect other innovations and tools to BIM to take advantage of its capability for a variety of uses, including safety, life cycle cost optimization, quality control, and shared communication channels among stakeholders. The industry's deliverables, connections, and roles are affected by the innovative technology, procedures, and policies that make up BIM. BIM enables the improvement of project quality, and rework and, as a result, shortens the design process time.

## INTEGRATED PROJECT DELIVERY IN SUSTAINABLE CONSTRUCTION

The construction industry uses Integrated Project Delivery (IPD), an open-ended project delivery strategy, to enhance efficiency, reduce waste, and improve cooperation. IPD brings together key point stakeholders, including the owner,

architect, contractor, and sometimes other consultants, in a highly collaborative and integrated manner. IPD represents a departure from the traditional Construction Project Delivery System to the most modern integrated method (Abdelhamid & Salem 2005). Fig. 5 shows a brief description of Integrated Project Delivery and its advantages. Some benefits of using IPD in construction are enhanced collaboration, early involvement, risk management, improved communication, optimized design, streamlined decision-making, cost control, improved risk management, faster project delivery, higher quality, team building, sustainability, transparency, owner satisfaction, and innovation. While IPD offers numerous benefits, it is essential to note that successful implementation depends on the commitment and collaboration of all project stakeholders. It may not be suitable for every project or organization, but when applied effectively, it can lead to more efficient, cost-effective, and successful completion of projects.

## DISCUSSION

Lean construction is the application of an efficient management process that helps in waste reduction and increases efficiency. This is one of the new management techniques that help in reducing time, money, and environment.

Lean Construction methods help in limited misuse of materials and time and produce the most extreme conceivable

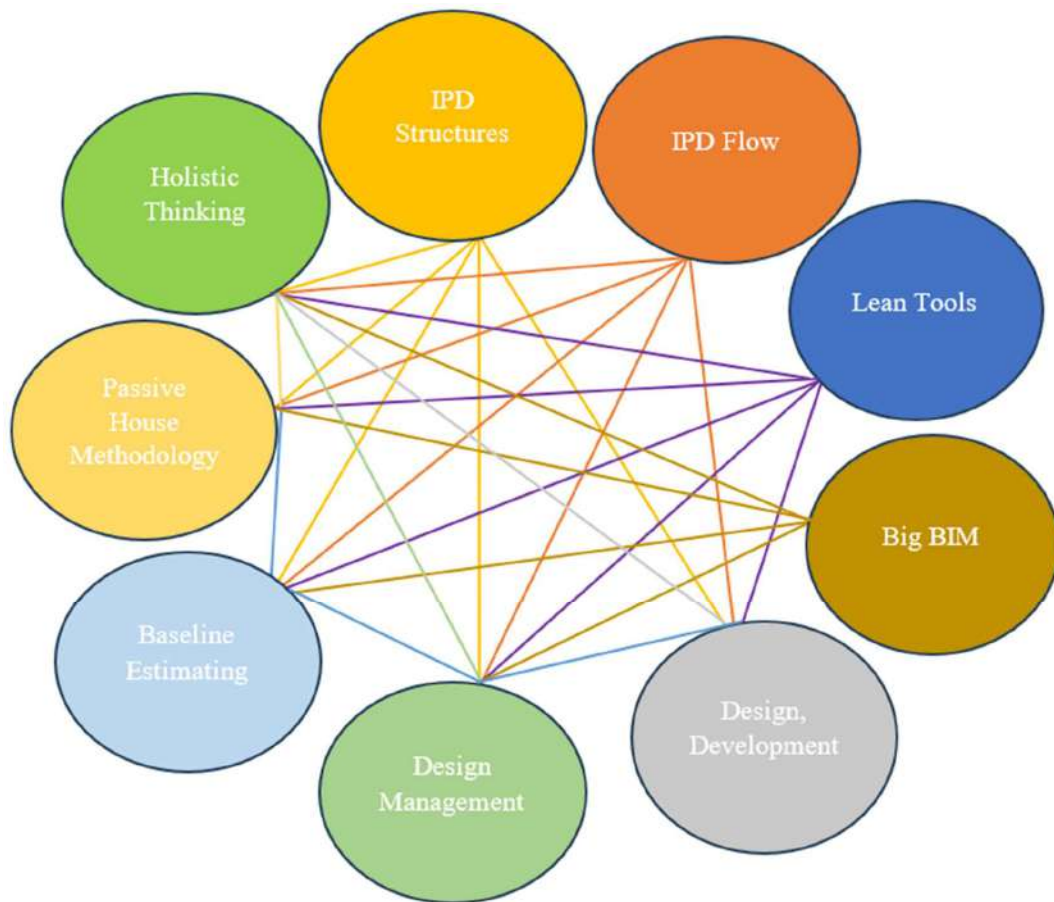


Fig. 5: Integrated Project Delivery (Ngowtanasuwan 2013).

measure of significance. This method helps to provide a general framework of work among contractors, clients, and customers. A systematic review was conducted on papers on Lean tools and Principles and their acceptance in the Indian Construction Industry. The outcome also demonstrates that the JIT, one of the 15 LCPs found in the study literature, is the most widely used. Notably, the JIT includes several lean construction planning concepts that facilitate efficient project planning, making it both a lean construction tool and a conduit for lean construction implementation. It has been referred to as a widespread, ecologically friendly, and lean construction and site management approach that has been incorporated into conventional construction procedures. The most commonly used Digital Methods are BIM, A3, Esteem Chain Mapping, 5s, and Visual Site. Fig. 1 gives a detailed description of the beginnings of Lean Production.

During the 1950s, Toyota Motor Company used the method of Lean Production. Toyota's framework has both the idea JIT and Automation. To meet exceptional customer requirements, Lean creation refers to the planning and

production of items that are differentiated from mass and art types of generations by the destinations and strategy. Koskela (1992) proved how Lean Manufacturing Concepts make changes in the manufacturing sector and conceptualized them in three complementary ways, specifically as transformation, flow, and value. Lean Project Management is different from other management tools, which have a clear set of objectives for the delivery process, help in enhancing client execution at the project level, and help to control the project throughout the life span.

The LPS is the one that has been used the second most. Notably, the LPS includes several lean construction planning concepts that facilitate efficient project planning; as a result, it may function as both a lean construction tool and a conduit for lean construction implementation. LPS is a crucial component of a new production management system for production based on one-off projects, such as design and building, and it enables project managers to greatly increase efficiency and client/end-user satisfaction. Additionally, LPS is a potent strategy that managers use

when formulating work schedules, planning strategies, and operations since it encourages the development of new explicit knowledge inside a project. Consequently, it is viewed as a genuine improvement in planning and control. Tables 2 & 3 give a brief description of different levels of Lean methodologies and Lean Tools. LPS is the most well-known and widely used lean construction technique because it makes use of a variety of planning techniques, including continuous improvement, daily huddle meetings, etc. This makes it particularly well-suited for the construction industry. Table 4 identifies 16 different benefits of Lean Principles in this review. In conclusion, the benefits of lean principles are multifaceted and extend across various dimensions of an organization, from operational efficiency and cost reduction to quality enhancement and employee engagement. Embracing lean principles can position an organization for sustainable growth and competitiveness in an ever-changing business landscape.

Table 5 gives a brief description of 7 different digital tools in lean and their advantages in implementation in the construction sector. Digital tools play a significant role in enhancing the implementation of lean construction principles. These tools leverage technology to streamline processes, improve communication, and increase efficiency. This research paper gives a brief description of some of the common digital tools used in lean construction and their associated benefits. In conclusion, digital tools play a crucial role in modernizing and optimizing the construction industry in line with lean principles. These tools offer numerous benefits, including improved collaboration, efficiency, communication, and decision-making, ultimately leading to reduced waste, enhanced productivity, and more successful lean construction projects.

This review has highlighted the importance of Lean Principles and its importance in organizations to improve their operations, deliver value to customers, and foster a culture of continuous improvement. Fig. 2 gives a brief description of lean principles. It helps in reducing waste by focusing on identifying and eliminating waste in the process. This includes the elimination of overproduction, excess inventory, unnecessary transportation, and other forms of waste. Fig. 4 gives a detailed picture of the total number of articles referred to in this literature and countries. India leads among the smaller number of studies regarding Lean Principles and its implementation. Fig. 5 gives a detailed description of Integrated Project Delivery in construction, which helps to make projects more successful and efficient construction projects. It helps in enhanced collaboration, early involvement of stakeholders, helps in improving decision-making, cost saving, quality improvement, and enhanced productivity.

## CONCLUSIONS

Through an organized review of the literature, this paper has discovered, classified, and analyzed the many lean methods used in the construction sector and their advantages in the sustainability agenda. The extensive body of literature leads to the following conclusions:

1. The application of lean practices to increase the construction industry's sustainability and productivity is demonstrated in this study.
2. According to the lean philosophy, to increase productivity, from design to the executive stage, the inventory network requires meticulous organization so that value is increased and waste is minimized.
3. Lean Construction Practices offer numerous advantages over traditional construction methods. These advantages contribute to increasing the efficiency of project performance and productivity, cost-effectiveness, waste minimization, and successful completion of the project.
4. The LPS, TVD, and the Lean Manufacturing Method are the three outstanding tools and methodologies that were particularly taken into consideration for sustainable construction.
5. Further, this paper discusses the Implementation of Digital Tools into Lean Construction Practices to enhance the efficiency, transparency, and overall success of construction projects.

## Credit Authorship Contribution Statement

**Ardra Suseelan:** Conceptualization, Methodology, Reviewing, Writing, Investigation and Visualization. **Senthil Vadivel T:** Conceptualization, Methodology, Reviewing, Investigation, Visualization, Editing and Supervision.

## Declaration Of Competing Interest

The study's authors so acknowledge that no third-party money was received from any organization to conduct the research stated in this publication. The writers further declare that none of them has any financial or non-financial interests that might jeopardize the accuracy of the work presented in this publication. No conflicts of interest are disclosed.

## REFERENCES

- Abdelhamid, T.S. and Salem, O.M., 2005. *Lean Construction: A New Paradigm for Managing Construction*. The International Workshop on Innovations in Materials and Design of Civil Infrastructure.
- Abdelhamid, T.S. and Salem, O.M., 2005. Lean construction: a new paradigm for managing construction. *The International Workshop on Innovations in Materials and Design of Civil Infrastructure*, Cairo, Egypt.

- Agrawal, A.K., 2024. Moving toward lean construction through automation of planning and control in last planner system: A systematic literature review. *Developments in the Built Environment*, 18, p.100419.
- Ahiakwo, O., Oloke, D., Suresh, S. and Khatib, J., 2013. A case study of last planner system implementation in Nigeria. *Lean Construction*, 112, pp.699-707.
- Alhuraish, I., Robledo, C. and Kobi, A., 2016. Assessment of lean manufacturing and Six Sigma operation with decision-making based on the analytic hierarchy process. *IFAC-PapersOnLine*, 49(12), pp.59-64.
- Alhuraish, I., Robledo, C. and Kobi, A., 2016. Assessment of lean manufacturing and Six Sigma operation with decision-making based on the analytic hierarchy process. *IFAC-PapersOnLine*, 49(12), pp.59-64.
- Andelin, M., Karhu, J. and Junnila, S., 2015. Creating shared value in a construction project: A case study. *Procedia Economics and Finance*, 21, pp.446-453.
- Andelin, M., Karhu, J. and Junnila, S., 2015. Creating shared value in a construction project – A case study. *Procedia Economics and Finance*, 21, pp.446-453.
- Ansah, R.H. and Sorooshian, S., 2017. Effect of lean tools to control external environment risks of construction projects. *Sustainable Cities and Society*, 32, pp.348-356.
- Ansah, R.H. and Sorooshian, S., 2017. Effect of lean tools to control external environment risks of construction projects. *Sustainable cities and society*, 32, pp.348-356.
- Anvari, B., Angeloudis, P. and Ochieng, W.Y., 2016. A multi-objective GA-based optimization for holistic manufacturing, transportation, and assembly of precast construction. *Automation in Construction*, 71(2), pp.226-241.
- Anvari, B., Angeloudis, P. and Ochieng, W.Y., 2016. A multi-objective GA-based optimization for holistic manufacturing, transportation, and assembly of precast construction. *Automation in Construction*, 71(2), pp.226-241.
- Aziz, R.F. and Hafez, S.M., 2013. Applying lean thinking in construction and performance improvement. *Alexandria Engineering Journal*, 52, pp.679-695.
- Babalola, O., Ibem, E.O. and Ezema, I.C., 2019. Implementation of lean practices in the construction industry: A systematic review. *Building and Environment*, 148, pp.34-43.
- Bag, S. et al., 2024. Building digital technology and innovative lean management capabilities for enhancing operational performance: An empirical study. *Production Planning & Control*, pp.1-20.
- Ballard, G. and Howell, G., 1998. Shielding Production: Essential Step in Production Control. *Journal of Construction Engineering and Management*, 1(11), pp.11-17.
- Banawi, A. and Bilec, M.M., 2014. A framework to improve construction processes: Integrating lean, green and Six Sigma. *International Journal of Construction Management*, 14(1), pp.45-55.
- Bansal, S., Biswas, S. and Singh, S., 2017. Fuzzy decision approach for selection of most suitable construction method of green buildings. *International Journal of Sustainable Built Environment*, 6(1), pp.122-132.
- Bansal, S., Biswas, S. and Singh, S., 2019. Review of green building movement and appraisal of rating systems in the Indian context. *International Journal of Technology Management & Sustainable Development*, 18(1), pp.55-74.
- Batwara, A., Sharma, V., Makkar, M. and Giallanza, A., 2023. Towards smart, sustainable development through value stream mapping: A systematic literature review. *Heliyon*, 9(5), p.15852.
- Brioso, X., 2015. Teaching Lean Construction: Pontifical Catholic University of Peru Training Course in Lean Project & Construction Management. *Procedia Engineering*, 123, pp.85-93.
- Bynum, P., Issa, R.R.A. and Olbina, S., 2013. Building information modeling in support of sustainable design and construction. *Journal of Construction Engineering and Management*, 139, pp.24-34.
- Carvalho, M.M. and Rabechini, R., 2017. Can project sustainability management impact project success? An empirical study applying a contingent approach. *International Journal of Project Management*, 35(6), pp.1120-1132.
- Carvalho, M.M. and Rabechini, R.R., 2017. Can project sustainability management impact project success? An empirical study applying a contingent approach. *International Journal of Project Management*, 35(6), pp.1120-1132.
- Dave, B., Buda, A., Nurminen, A. and Främling, K., 2018. A framework for integrating BIM and IoT through open standards. *Automation in Construction*, 95, pp.35-45.
- Desai, A.E. and Shelat, M.J., 2014. Value stream mapping as a lean construction tool – A case study. *International Journal of Engineering Research & Technology (IJERT)*, 3(12), pp.354-358.
- Dineshkumar, K., Ramanathan, P. and Ramasamy, S., 2015. Comparative study on prefabrication construction with cast in-situ construction of residential buildings. *IJISSET – International Journal of Innovative Science Engineering Technology*, 2(4), pp.1-6.
- Ding, K., 2019. Defining a digital twin-based cyber-physical production system for autonomous manufacturing in smart shop floors. *International Journal of Production Research*, 57, pp.6315-633.
- Dombrowski, U. and Mielke, T., 2013. Lean leadership – Fundamental principles and their application. *Procedia CIRP*, 7, pp.569-574.
- Dulaimi, M. and Tanamas, C., 2001. The principles and applications of lean construction in Singapore. *Lean Construction Journal*, 54, pp.712-721.
- Dunlop, P. and Smith, S.D., 2004. Planning, estimation, and productivity in the lean concrete pour. *Engineering, Construction, and Architectural Management*, 11(1), pp.55-64.
- Eldeep, A.M., Farag, M.A. and El-hafez, L.A., 2022. Using BIM as a lean management tool in construction processes – A case study. *Ain Shams Engineering Journal*, 13(2), p.68.
- Forbes, L. and Ahmed, S.M., 2003. *Construction Integration and Innovation through Lean Methods and E-Business Applications*. American Society of Civil Engineers, pp. 1-10.
- Frank, A.G., Thüerer, M., Filho, M.G. and Marodin, G.A., 2024. Beyond Industry 4.0 – Integrating lean, digital technologies and people. *International Journal Of Operations & Production Management*, 19, 1121-1130.
- Gatelli, I.S. and Avella, L., 2024. Impact of Industry 4.0 and circular economy on lean culture and leadership: Assessing digital green lean as a new concept. *European Research On Management And Business Economics*, 30(1), p.100232.
- Gil, N., Tommelein, I., Kirkendall, R. and Ballard, G., 2000. Contribution of specialty contractor knowledge to early design. *Lean Construction*, 17-19, pp.641-652.
- Gran, A.D. and Picchi, F., 2004. Construction Sites: Using Lean Principles to Seek Broader Implementations. In: *12th Annual Conference of the International Group for Lean Construction*. Helsingor.
- Green, S.E., 2005. Systematic review and meta-analysis. *Singapore Medical Journal*, 46(6), pp. 270-274.
- Gupta, S. and Jain, S.K., 2014. The 5S and kaizen concept for overall improvement of the organization: a case study. *International Journal of Lean Enterprise Research*, 1(1), pp. 23-40.
- Hossain, M.M. and Purdy, G., 2023. Integration of Industry 4.0 into Lean production systems: A systematic literature review. *Manufacturing Letters*, 35, pp. 1347-1357.
- Issa, U.H., 2013. Implementation of lean construction techniques for minimizing the effect of the risk on project construction time. *Alexandria Engineering Journal*, 52(4), pp.697-704.
- Issa, U.H., 2013. Implementation of lean construction techniques for minimizing the effect of the risk on project construction time. *Alexandria Engineering Journal*, 52(4), pp. 697-704.
- Jamil, A.H.A. and Fathi, M.S., 2016. The integration of lean construction and sustainable construction: A stakeholder perspective in analyzing

- sustainable lean construction strategies in Malaysia. *Procedia Computer Science*, 100, pp.634-643.
- Jiang, R., Wu, C., Mao, C. and Shrestha, A., 2016. Ecosystem Visualization and Analysis of the Chinese Prefabricated Housing Industry. *Procedia Engineering*, 145, pp.436-443.
- Jørgensen, B. and Emmitt, S., 2008. Lost in transition: the transfer of lean manufacturing to construction. *Engineering Construction and Architectural Management*, 15(4), pp.383-398.
- Kamara, J., 2003. Enablers for Concurrent Engineering in Construction. In: *Proceedings of the 11th Annual Conference of the International Group for Lean Construction*. University of Salford, Salford, UK.
- Kanan, R., Elhassan, O. and Bensalem, R., 2018. An IoT-based autonomous system for workers' safety in construction sites with real-time alarming, monitoring, and positioning strategies. *Automation in Construction*, 88, pp.73-86.
- Kazaz, A., 2015. Fresh ready-mixed concrete waste in construction projects: A planning Approach. *Procedia Engineering*, 123, pp.268-275.
- Kelly, J. and Male, S., 1992. *Value Management in Design and Construction*. Springer, p. 196.
- Khodeir, L.M. and Othman, R., 2018. Examining the interaction between lean and sustainability principles in the management process of the AEC industry. *Ain Shams Engineering Journal*, 9(4), pp.1627-1634.
- Koskela, L., 1992. *Application of the new production philosophy to construction*. Stanford University.
- Kumar, K.S., 2022. Implementation of 5S practices in small-scale manufacturing industries. *Materials Today Proceedings*, 62(4), pp.1913-1916.
- Lakmal, D., 2014. Managing the challenge of generational diversity in the workplace. *SSRN*, 110, pp.1-11.
- Lee, J.H., Ostwald, M.J. and Gu, N., 2020. *Design Thinking and Building Information Modelling*. Springer, pp.147-163.
- Li, P. and Froese, T.M., 2016. Life-cycle assessment of high-performance, low-cost homes. *Procedia Engineering*, 145, pp.1322-1329.
- Li, X., Shen, G.Q., Wu, P. and Teng, Y., 2019. Integrating building information modeling and prefabrication housing production. *Automation in Construction*, 100, pp.46-60.
- Lodgaard, E., Ingvaldsen, J.A., Gamme, I. and Aschehoug, S., 2016. Barriers to Lean Implementation: Perceptions of Top Managers, Middle Managers and Workers. *Procedia CIRP*, 57, pp.595-600.
- Lopez, S., Gardoki, O.A. and Lizundia, E., 2021. Comparative life cycle assessment of high-performance lithium-sulfur battery cathodes. *Journal of Cleaner Production*, 282.
- Marhani, M.A., Jaapar, A. and Bari, N.A.A., 2012. Lean construction: Towards enhancing sustainable construction in Malaysia. *Procedia - Social and Behavioral Sciences*, 68, pp.87-98.
- Martens, M.L. and Carvalho, M.M., 2017. Key factors of sustainability in project management context: A survey exploring the project managers' perspective. *International Journal of Project Management*, 35(6), pp.1084-1102.
- Ministry of Finance, 2022. Real GDP growth in 2021-22 stands at 8.7 percent, 1.5 percent higher than the real GDP of 2019-20. PIB Delhi.
- Mohammad, M.F., Sham, A.B., Musa, M.F. and Yusof, M.R., 2016. The potential application of IBS modular system in the construction of housing scheme in Malaysia. *Procedia - Social and Behavioral Sciences*, 222, pp.75-82.
- Molavi, J. and Barral, D.L., 2016. A Construction Procurement Method to Achieve Sustainability in Modular Construction. *Procedia Engineering*, 145, pp.1362-1369.
- Moser, L. and Santos, A.d., 2003. Exploring the role of visual controls on mobile cell manufacturing: a case study on drywall technology. In: *Proceedings of the Eleventh Annual Conference of the International Group for Lean Construction*, Blacksburg, pp.418-426.
- Mossman, A., 2009. Why isn't the UK construction industry going lean with gusto? *International Journal of Construction Management*, 5(1), pp.24-36.
- Mostafa, S., Chileshe, N. and Jr, R.R., 2017. Can project sustainability management impact project success? An empirical study applying a contingent approach. *International Journal of Project Management*, 35(6), pp.1120-1132.
- Musa, M.F., Mohammad, M.F., Yusof, M.R. and Ahmad, R., 2016. Industrialised Building System Modular System (IBSMS) Organisational Readiness Framework. *Procedia - Social and Behavioral Sciences*, 222, pp.83-92.
- Ngowtanasuwan, G., 2013. Mathematical model for optimization of construction contracting in housing development project. *Procedia - Social and Behavioral Sciences*, 105, pp.94-105.
- Ngowtanasuwan, G., 2013. Mathematical model for optimization of construction contracting in housing development project. *Procedia - Social and Behavioral Sciences*, 105, pp.94-105.
- Paez, O., Salem, O.M., Solomon, J. and Genaidy, A.M., 2005. Moving from lean manufacturing to lean construction: Toward a common sociotechnological framework. *Human Factors and Ergonomics in Manufacturing*, 15(2), pp.233-245.
- Paez, O., Salem, O.M., Solomon, J. and M, A.G., 2005. Moving from lean manufacturing to lean construction: Toward a common sociotechnological framework. *Human Factors and Ergonomics in Manufacturing*, 15(2), pp.233-245.
- Pamfilie, R., Petcu, A.J. and Draghici, M., 2012. The Importance of Leadership in Driving a Strategic Lean Six Sigma Management. *Procedia - Social and Behavioral Sciences*, 58, pp.187-196.
- Phaniraj, K., 2015. Lean construction: A case study at Precast Plant. *International Journal of Engineering Research & Technology (IJERT)*, 4(5), pp.823-827.
- Pheng, L.S. and Hui, M.S., 1999. The application of JIT philosophy to construction: a case study in site layout. *Construction Management and Economics*, 17(5), pp.657-688.
- Picchi, F. and Granja, A.D., 2004. Construction Sites: Using Lean Principles to Seek Broader Implementations. In: *12th Annual Conference of the International Group for Lean Construction*, Helsingor, Denmark.
- Rahim, A.A., Zen, I., Hamid, Z.A. and Ismail, Z., 2012. Adaptable Housing of Precast Panel System in Malaysia. *Procedia - Social and Behavioral Sciences*, 50, pp.369-382.
- Rahman, N.A.A., Sharif, S.M. and Esa, M.M., 2013. Lean manufacturing case study with Kanban System. *Procedia Economics and Finance*, 7, pp.174-180.
- Ryan, M., Murphy, C. and Casey, J., 2019. Case Study in the Application of the Last Planner® System. In: *Proceedings of 27th Annual Conference of the International Group for Lean Construction (IGLC)*, pp.215-226.
- Salem, O.M., Solomon, J., Genaidy, A.M. and Minkarah, I., 2006. Lean Construction: From Theory to Implementation. *Journal of Management in Engineering*, 22(4), pp.168-175.
- Samaila, A. and Hamid, R.A., 2012. Lean construction techniques implementation in Nigeria's construction industry. *International Journal of Scientific & Engineering Research*, 3(12), pp.1-11.
- Sapauy, S.E., 2016. Construction waste: Potentials and constraints. *Procedia Environmental Sciences*, 35, pp.714-722.
- Sarhan, J., Xia, B., Karim, A. and Fawzia, S., 2018. Barriers to implementing lean construction practices in the Kingdom of Saudi Arabia (KSA) construction industry. *Construction Innovation*, 18(2), pp.246-272.
- Sepasgozar, S., Forsythe, P. and Shirowzhan, S., 2018. Evaluation of Terrestrial and Mobile Scanner Technologies for Part-Built Information Modeling. *Journal of Construction Engineering and Management*, 144, p.1051.
- Sepasgozar, S.M., 2020. Digital technology utilisation decisions for facilitating the implementation of Industry 4.0 technologies. *Construction Innovation*, 3, p.12.
- Shirowzhan, S., Tan, W. and Sepasgozar, S., 2020. Digital twin and

- CyberGIS for Improving Connectivity and Measuring the Impact of Infrastructure Construction Planning in Smart Cities. *International Journal of Geo-Information*, 9(4).
- Singh, J., Vikas, R. and Sharma, R., 2014. Implementation of 5S practices: A review. *Uncertain Supply Chain Management*, 2(3), pp.155-162.
- Singh, S. and Kumar, K., 2016. Review of literature of lean construction and lean tools using systematic literature review technique (2008–2018). *Ain Shams Engineering Journal*, 11(2), pp.465-471.
- Singh, S. and Kumar, K., 2016. the integration of lean construction and sustainable construction: A stakeholder perspective in analyzing sustainable lean construction strategies in Malaysia. *Procedia Computer Science*, 121, pp.634-643.
- Tam, V.W., Tam, C.M., Zeng, S.X. and Ng, W.C., 2007. Towards adoption of prefabrication in construction. *Building and Environment*, 42(10), pp.3642-3654.
- Tommelein, I.D. and Koskela, L., 2002. Lean construction tools and techniques. *Des Constrme*, 18, p.504.
- Vargas, A. R., Arredondo-Soto, K. C., Gutiérrez, T. C. and Ravelo, G., 2018. Applying the plan-do-check-act (PDCA) cycle to reduce the defects in the manufacturing industry: A case study. *Applied Sciences*.
- Womack, J. P. and Jones, D. T., 1996. Lean thinking: Banish waste and create wealth in your corporation. *Journal of the Operational Research Society*, 48(11), pp.24-39.
- Woodhead, R., Stephenson, P. and Morrey, D., 2018. Digital construction: From point solutions to IoT ecosystem. *Automation in Construction*, 93, pp.35-46.
- Xu, G., Li, M., Chen, C.H. and Wei, Y., 2018. Cloud asset-enabled integrated IoT platform for lean prefabricated construction. *Automation in Construction*, 93, pp.123-134.
- Ying, L., Yongping, R., Jiamin, W. and Hsiu, L. C., 2020. BIM-based cyber-physical systems for intelligent disaster prevention. *Journal of Industrial Information Integration*, 20, p. 114.
- Zhang, H., Yan, Q. and Wen, Z., 2020. Information modeling for cyber-physical production system based on digital twin and automation. *The International Journal of Advanced Manufacturing Technology*, 107, pp.1927-1945.
- Zhang, L. and Chen, X., 2016. Role of lean tools in supporting knowledge creation and performance in lean construction. *Procedia Engineering*, 145, pp.1267-1274.

---

#### ORCID DETAILS OF THE AUTHORS

Senthil Vadivel. T.: <https://orcid.org/0000-0001-5979-718X>



# Forecasting Precipitation Using a Markov Chain Model in the Coastal Region in Bangladesh

Al Mamun Pranto<sup>1</sup>, Usama Ibn Aziz<sup>1</sup>, Lipon Chandra Das<sup>1†</sup> , Sanjib Ghosh<sup>2</sup> and Anisul Islam<sup>3</sup>

<sup>1</sup>Department of Mathematics, University of Chittagong, Chittagong-4331, Bangladesh

<sup>2</sup>Department of Statistics, University of Chittagong, Chittagong-4331, Bangladesh

<sup>3</sup>Computer and Information Sciences, University of Northumbria, Newcastle, UK

†Corresponding author: Lipon Chandra Das; liponbgc@gmail.com

Nat. Env. & Poll. Tech.  
Website: [www.neptjournal.com](http://www.neptjournal.com)

Received: 04-04-2024

Revised: 30-05-2024

Accepted: 02-06-2024

## Key Words:

Markov chain  
Rainfall forecasting  
Stationary test statistic  
Climate  
Bangladesh

## ABSTRACT

This work explores the detailed study of Bangladeshi precipitation patterns, with a particular emphasis on modeling annual rainfall changes in six coastal cities using Markov chains. To create a robust Markov chain model with four distinct precipitation states and provide insight into the transition probabilities between these states, the study integrates historical rainfall data spanning nearly three decades (1994–2023). The stationary test statistic ( $\chi^2$ ) was computed for a selected number of coastal stations, and transition probabilities between distinct rainfall states were predicted using this historical data. The findings reveal that the observed values of the test statistic,  $\chi^2$ , are significant for all coastal stations, indicating a reliable model fit. These results underscore the importance of understanding the temporal evolution of precipitation patterns, which is crucial for effective water resource management, agricultural planning, and disaster preparedness in the region. The study highlights the dynamic nature of rainfall patterns and the necessity for adaptive strategies to mitigate the impacts of climate variability. Furthermore, this research emphasizes the interconnectedness of climate studies and the critical need for enhanced data-gathering methods and international collaboration to bridge knowledge gaps regarding climate variability. By referencing a comprehensive range of scholarly works on climate change, extreme rainfall events, and variability in precipitation patterns, the study provides a thorough overview of the current research landscape in this field. In conclusion, this study not only contributes to the understanding of precipitation dynamics in Bangladeshi coastal cities but also offers valuable insights for policymakers and stakeholders involved in climate adaptation and resilience planning. The integration of Markov chain models with extensive historical data sets serves as a powerful tool for predicting future rainfall trends and developing informed strategies to address the challenges posed by changing precipitation patterns.

## INTRODUCTION

Bangladesh, located in South Asia, stands as the world's largest deltaic nation, characterized by heavy precipitation owing to its distinctive geographical attributes. The climate is changing both the global (Lambert et al. 2003, Dore 2005) and regional levels (Gemmer et al. 2004) as a result of global warming. In recent years, several research studies have examined precipitation patterns in Bangladesh. The majority of the studies focused on precipitation (Shahid 2011), especially the regional and temporal distribution of monsoon rainfall (Das et al. 2024). The study also examined the fluctuations in yearly rainfall (Shamsuddin & Ahmed 1974), as well as the timing of the entrance and withdrawal of the summer monsoon season (Ahmed & Karmakar 1993), and the variations in rainfall within and between

different areas of Bangladesh (Debsarma 2003). Das et al. (2022) carried out research to identify the temporal trends of rainfall in Bangladesh, revealing that the highest rainfall occurs during the monsoon months through nonparametric methodologies. Various probability models have been developed in several studies to depict the distribution of rainfall patterns. From 1989 to 2018, there's been an annual average rainfall decline of  $0.014 \text{ mm.y}^{-1}$ , with increased rainy season rainfall and decreased winter rainfall observed across multiple meteorological stations (Das & Zhang 2021). Most current research relies on analyzing patterns in extreme weather conditions (Khan et al. 2020). For instance, there are differences in the distribution and timing of rainfall along the southwest coast (Hossain et al. 2014) and in other regions of Bangladesh (Sarker & Bigg 2010). The majority of reports were derived from either anecdotal accounts or computer

models rather than direct observation. A significant challenge faced by academics is the absence of precise and extensive historical rainfall data from many locations worldwide, which would allow them to differentiate between localized or periodic fluctuations in rainfall trends (Ibeje et al. 2018).

The Markov Chain was used to study the modeling and simulation of various weather phenomena (Gringorten 1996) as well as the development of lengthy time series of weather data (Racsko et al. 1991). The initial stochastic model of temporal precipitation, utilizing a two-state first-order Markov chain, was developed by (Gabriel & Neuman 1962). In 1981, Richardson utilized a first-order Markov chain combined with an exponential distribution to characterize the distribution of daily rainfall in the United States. Akaike (1974) employed a Markov chain model to simulate the daily incidence of rainfall. In addition, the work cited in reference (Sujatmoko & Bambang 2012) employed the methodology of “Statistical Modelling of Daily Rainfall Occurrence”. These investigations have demonstrated that by applying the Markov chain combined with an appropriate probability distribution, the produced data accurately maintains the seasonal and statistical properties of historical rainfall data. Several studies have shown that the Markov Chain model is suitable for generating rainfall time series data. A stochastic process is simply a probability process; that is, any process in nature whose evolution we can analyze successfully in terms of probability (Doob 1942). A stochastic process is said to incorporate a Markov chain if it satisfies the characteristics of Markov, often known as the Markovian property. The Markov properties imply that the probability of a future occurrence, given knowledge of past and current events, is independent of previous events and relies on present events (Tovler 2016). The Markov chain is often categorized into two types: The Markov chain with a discrete parameter index and the Markov chain with a continuous parameter index. A Markov chain is considered to have a discrete parameter index when the transition between states happens at specified, discrete time intervals. The Markov chain is said to have a continuous parameter index when the shift state happens within a continuous time interval (Ross 1996). Rainfall data is a temporal dataset that represents the progression of precipitation in a certain region across regular and distinct time intervals.

This research examines a discrete-time four-state model to forecast yearly rainfall patterns and compare them among six coastal cities in Bangladesh. Estimating the probability of rainfall based on current time series data allows us to forecast statistical characteristics such as the mean, standard deviation, and first-order correlation coefficient of rainfall. Accurate assessment of transition probabilities between states

at consecutive time occurrences is essential for constructing a model. Theoretical Weibull, Gamma, and Extreme Value Distribution functions are commonly employed in practice and for forecasting rainfall intensity (Villarini et al. 2010). When modeling accounting dependence in a time series, it is common to apply a first-order Markov Chain. Accurate forecasting of future precipitation is necessary to proactively prepare for prolonged periods of high rainfall intensity. In addition, it suggests that we must take into account other factors that might greatly contribute to the escalation of rainfall intensity (Hermawan et al. 2017). A finite Markov chain, a stochastic process with discrete time parameters, was employed in this study to model the yearly rainfall patterns in six coastal cities of Bangladesh. The Markov chain is characterized by the property that the future state of the system depends solely on the present state and is independent of the previous history. The number of states in the process, as defined by Bracken and Croke (2007), can be either limited or countably infinite. The daily precipitation data served as the foundational input for constructing the Markov model, which aimed to simulate the transition of rainfall intensity levels over time. Understanding the intricate variations in rainfall patterns is crucial for multiple sectors in Bangladesh, particularly in coastal areas where the ecology and way of life are significantly influenced by precipitation. Historical rainfall data spanning from 1994 to 2023 were collected for the six coastal cities under investigation: Chittagong, Barishal, Bhola, Cox’s Bazar, Khulna, and Patuakhali. The data were meticulously sourced from reputable meteorological databases, governmental archives, and scholarly publications to ensure accuracy and reliability. While previous studies have acknowledged the effectiveness of the Markov model in predicting rainfall, there is a scarcity of research comparing the results of forecasting rainfall using different rainfall states through Markov probability matrices with the outcomes of Markov chain models for future periods. To fill the gaps in past studies, this study establishes the following objectives: (1) To offer further elucidation on modifications in precipitation patterns; (2) To determine the duration required for obtaining limiting state probabilities in rain forecasting; (3) To predict and project rainfall in upcoming periods; (4) To demonstrate the application of the first-order Markov chain model in generating annual rainfall data for future instances. This study proposes an innovative approach for developing prediction models by using various rainfall states derived from the Markov model. The effectiveness of the Markov model in predicting and generating time series data is displayed. The technique employed in this study is transferable to other locations within coastal regions of Bangladesh, as well as to other countries.



**MATERIALS AND METHODS**

Bangladesh is geographically located in the zone of subtropical climate with the eastern longitude from 88.68°E to 92.97°E and the northern latitude from 20.87°N to 25.78°N (Fig. 1). The country is located in south Asia, which is bordered on the south by the Bay of Bengal, on the southeast by Myanmar, and the remaining by India. Bangladesh is a low plain land comprised of 64 districts. This country is almost entirely flat on a deltaic plain with low elevation and without some hills alongside the Burmese border. This country has a humid subtropical climate; throughout the year, the majority of the country’s monsoon weather prevails. As a result, the country’s river is, in many instances, flooded with the aid of the tropical cyclones off the Bay of Bengal and with the aid of tidal bores because of its location just south of the foothills of the Himalayas, where monsoon winds turn west, and northwest, the region of Sylhet in eastern Bangladesh receives the greatest average precipitation. From 1994 to 2023, annual rainfall in that

region ranged between 3101 and 5944 millimeters per year. The average annual rainfall is 2200 mm. The southwest monsoon is the principal source of rainfall in the districts. About 80% of the total rainfall is received during the period from June to September. From year to year, the variation in the annual rainfall and temperature is not large. In the present study, a series of annual precipitations were analyzed. Most Bangladeshi coastal cities are on riverbanks in low-lying tidal zones at 1.0–1.5 m above sea level. Different coastal regions of Bangladesh house these cities, offering a diversified geographical representation. Including cities from diverse places helps reflect coastal rainfall variability. Rainfall datasets from six weather stations covering the period 1994–2023 were obtained from the Bangladesh Meteorological Department (BMD) in Agargaon, Dhaka. Data is available for the coastal cities of Cox’s Bazar, Chittagong, Patuakhali, Bhola, Khulna, and Barishal. The geographical characteristics and locations of all 34 stations in Bangladesh are shown in Fig. 1.

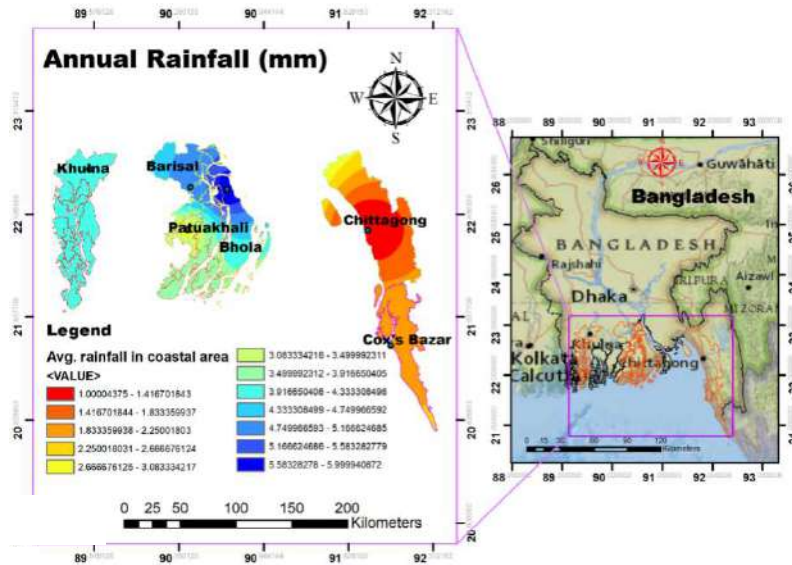


Fig.1: Study region of rainfall stations in Bangladesh.

Table 1: Statistics of the annual rainfall data for the six stations.

Stations	Descriptive Measure					
	Maximum	Minimum	Mean	CV[%]	Skewness	Kurtosis
Chittagong	3833	2208	2953	16.79	0.178	-1.102
Barisal	2858	1418	2057.581	18.23	0.156	-0.842
Bhola	3080	1493	2156.453	17.704	0.296	-0.441
Cox’s Bazar	4716	2483	3728.903	14.178	-0.268	-0.159
Khulna	2594	1073	1806.226	19.578	-0.188	-0.196
Patuakhali	3098	1847	2547.419	13.962	-0.499	-0.823

Table 1 provides an analysis of annual rainfall data from six meteorological stations: Chittagong, Barishal, Bhola, Cox's Bazar, Khulna, and Patuakhali. Statistical summaries include maximum, minimum, and mean annual rainfall levels, coefficient of variation (CV %), skewness, and kurtosis for each station. For instance, Chittagong's maximum annual rainfall is 3833mm, with a mean of 2953mm and a coefficient of variation of 16.79%. Barishal has a maximum of 2858mm, a mean of 2057.581mm, and a slightly higher coefficient of variation at 18.23%. These insights offer valuable data for meteorological and climate research.

## Methodology

### Markov Chain Modeling

The study's methodology is rooted in the theoretical framework of Markov chains, with a focus on transition probabilities, steady-state probabilities, and limiting-state probabilities. The analysis relies on the following definitions, theorems, and equations:

A Markov chain is characterized as a random sequence  $(X_n, n \in N)$  where each state  $X_n$  is dependent solely on the preceding state  $X_{n-1}$ . This Markov property asserts that the future state is conditionally independent of past states, given the present state.

**Transition probabilities:** In a consistent Markov chain  $(J_n, n \geq 0)$ , transition probabilities from state  $i$  to state  $j$  are denoted as  $P_{ij}$ . The transition matrix  $P = [P_{ij}]$  encapsulates all transition probabilities between states  $i$  and  $j$ .

**Steady-state transition probabilities:** Steady-state transition probabilities are observed in the Markov process  $X$  when the  $n$ -step transition probability  $P_{ij}^n$  satisfies the condition  $P_{ij}^n = P \{X_{n+m} = j / X_m = i\}$  for all  $n, m \geq 0$ , and all states  $i, j \geq 0$ .

$$P_{ij}^{n+m} = \sum_{k=0}^{\infty} P_{ik}^n P_{kj}^m = 0 \text{ for all } n, m \geq 0 \dots(1)$$

for all  $n, m \geq 0$ , establishes the relationship between  $n$ -step and  $m$ -step transition probabilities in a Markov chain.

**Induction and limiting state probability:** Through induction, it is shown that  $P^n = P^0 P^n$ , where  $P^0$  represents the initial state vector of the transition matrix. The limiting state probability is denoted as  $P^n = [P_1^n \ P_2^n \ P_3^n \ P_4^n]$ , indicating the probabilities of reaching each state after  $n$  steps.

A dataset was compiled for each city to define four rainfall states in a Markov chain model. These states were categorized as follows: State 1 represents low rainfall, State 2 denotes moderate rainfall that is evenly distributed, State 3 indicates heavy rainfall, and State 4 represents moderate rainfall that is not evenly distributed. Transition probabilities

were depicted in a diagram and matrix, strategically incorporating zeros to represent no direct transitions between certain states. Regional climate variability, ecological impacts, historical data, sector-specific factors, and modeling objectives influenced the state definitions. This methodology aimed to capture nuanced rainfall variations and their implications for coastal cities. The transition diagram in Fig. 2 and the probability matrix  $P$  depict the transition between states.

$$P = \begin{bmatrix} P_{11} & P_{12} & P_{13} & P_{14} \\ 0 & P_{22} & P_{23} & P_{24} \\ P_{31} & P_{32} & P_{33} & 0 \\ P_{41} & P_{42} & 0 & 0 \end{bmatrix}$$

Zeros in the probability matrix denote impossible transitions between certain rainfall states. For example, State 4 doesn't transition directly to State 3 or State 1, reflecting the constraints of realistic rainfall patterns observed in coastal cities. These zeros shape the Markov model, ensuring meaningful state transitions based on observed rainfall characteristics.

## RESULTS AND DISCUSSION

In this study, we analyze the patterns of rainfall distribution in key coastal cities of Bangladesh, namely Chittagong, Barishal, Bhola, Cox's Bazar, Khulna, and Patuakhali (Table 2). Utilizing data on rainfall measurements and frequency of occurrences, the study unveils distinctive precipitation trends across these urban centers. Findings indicate varying ranges of rainfall, with Chittagong experiencing a broad spectrum of precipitation, while Cox's Bazar demonstrates a more concentrated pattern. Barishal and Bhola exhibit similar rainfall tendencies, with notable peaks in specific ranges. Khulna showcases a diversified rainfall regime, reflecting its adaptive capacity, while Patuakhali witnesses substantial precipitation occurrences. These insights underscore the importance of tailored urban planning and disaster preparedness strategies to address climatic vulnerabilities in Bangladesh's coastal regions.

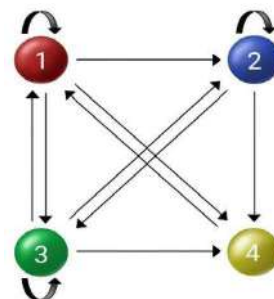


Fig. 2: Transition Diagram.

**Limiting State Probabilities**

The Markov chain model provides a succinct and probabilistic framework for comprehending and perhaps forecasting rainfall patterns. To simulate more intricate rainfall dynamics and align with specific research goals, the model may be adjusted by integrating more states or altering transition probabilities.

**Chittagong:** The assumed model for annual rainfall in the Chittagong area is State-1: (2200-2745) mm, State-2: (2746-3290) mm, State-3: (3291-3845) mm, State-4: (2746-3290) mm. Therefore, the transition matrix

$$M = \begin{bmatrix} 5 & 3 & 2 & 3 \\ 0 & 1 & 5 & 0 \\ 6 & 1 & 1 & 0 \\ 2 & 1 & 0 & 0 \end{bmatrix}$$

i.e.,  $P_{ij} = \frac{f_{ij}}{\sum f_{ij}}$   $i, j = 1, 2, 3, 4$ . (Arumugam & Karthik

2018) Where  $f_{ij} \rightarrow$  transition frequency from state to state  $j$ ,  $0 \leq P_{ij} \leq 1$ . We get the probability matrix

$$P = \begin{bmatrix} 0.38 & 0.23 & 0.16 & 0.23 \\ 0 & 0.16 & 0.84 & 0 \\ 0.75 & 0.125 & 0.125 & 0 \\ 0.67 & 0.33 & 0 & 0 \end{bmatrix} \dots(2)$$

N-step transition probability, we have

$$P^2 = \begin{bmatrix} 0.419 & 0.220 & 0.274 & 0.087 \\ 0.63 & 0.131 & 0.239 & 0 \\ 0.378 & 0.208 & 0.241 & 0.173 \\ 0.255 & 0.207 & 0.384 & 0.154 \end{bmatrix}$$

$$P^4 = \begin{bmatrix} 0.439 & 0.196 & 0.267 & 0.097 \\ 0.437 & 0.206 & 0.261 & 0.964 \\ 0.425 & 0.196 & 0.277 & 0.1 \\ 0.422 & 0.195 & 0.271 & 0.112 \end{bmatrix}$$

$$P^6 = \begin{bmatrix} 0.433 & 0.198 & 0.269 & 0.099 \\ 0.434 & 0.197 & 0.268 & 0.098 \\ 0.432 & 0.198 & 0.269 & 0.100 \\ 0.431 & 0.198 & 0.270 & 0.101 \end{bmatrix}$$

And

$$p^8 = \begin{bmatrix} 0.433 & 0.198 & 0.269 & 0.1 \\ 0.433 & 0.198 & 0.269 & 0.1 \\ 0.433 & 0.198 & 0.269 & 0.1 \\ 0.433 & 0.198 & 0.269 & 0.1 \end{bmatrix}$$

In a Markov chain method, here, two successive iterations yield identical results, which signifies convergence toward the limiting state. This indicates stable probabilities of transitioning between states, suggesting further iterations are unlikely to alter the state distribution significantly. The system has reached a consistent state, implying its long-term behavior has been established, regardless of additional iterations. After  $n$  steps,  $P^0$  gets the fixed value (3), i.e.,  $n \geq 6$

Let us take  $P^0 = (1 \ 0 \ 0 \ 0)$

$$P^0 P^n = (1 \ 0 \ 0 \ 0) \begin{bmatrix} 0.433 & 0.198 & 0.269 & 0.1 \\ 0.433 & 0.198 & 0.269 & 0.1 \\ 0.433 & 0.198 & 0.269 & 0.1 \\ 0.433 & 0.198 & 0.269 & 0.1 \end{bmatrix} = (0.433 \ 0.198 \ 0.269 \ 0.1)$$

Thus,  $n = nP = (0.433 \ 0.198 \ 0.269 \ 0.1)$  These results show the yearly rainfall probability after 6 years. In the first year, the likelihood is (0.433 0.198 0.269 0.1). When the odds were compared, state 4 declined steadily while the likelihood of states 1 and 2 increased, exceeding six years. This means that 43% of the yearly rainfall in Chittagong will fall on State 1, 20% on State 2, 27% on State 3, and 10% on State 4. Similarly, we have five coastal cities: Barishal, Bhola, Cox’s Bazar, Khulna, and Patuakhali, and their probability matrices are  $P_B, P_{Bh}, P_{CB}, P_K, P_P$ .

**Barishal:** Let the model for yearly rainfall for the Barishal region be State-1: (1415-1900) mm, State-2: (1901-2385) mm, State-3: (2386-2870) mm, State-4: (1901-2385) mm. Therefore, the transition matrix

$$M = \begin{bmatrix} 4 & 5 & 4 & 3 \\ 0 & 1 & 2 & 2 \\ 3 & 2 & 0 & 1 \\ 6 & 0 & 0 & 0 \end{bmatrix}$$

Table 2: Frequency of annual rainfall in six coastal cities between 1994-2023.

State	Chittagong		Barishal		Bhola		Cox’s Bazar		Khulna		Patuakhali	
	Rainfall [mm]	Frequency	Rainfall [mm]	Frequency	Rainfall [mm]	Frequency	Rainfall [mm]	Frequency	Rainfall [mm]	Frequency	Rainfall [mm]	Frequency
1	2200-2745	13	1415-1900	13	1490-2025	14	2480-3230	5	1130-1620	10	2100-2435	10
2	2746-3290	6	1901-2385	5	2026-2560	6	3231-3980	11	1621-2111	10	2436-2770	8
3	3291-3845	8	2386-2870	6	2561-3095	4	3981-4730	10	2112-2602	3	2771-3105	9
4	2746-3290	3	1901-2385	6	2026-2560	6	3231-3980	4	1621-2111	7	2436-2770	3

And get the probability matrix.

$$P_B = \begin{bmatrix} 0.25 & 0.313 & 0.25 & 0.188 \\ 0 & 0.2 & 0.4 & 0.4 \\ 0.5 & 0.34 & 0 & 0.16 \\ 1 & 0 & 0 & 0 \end{bmatrix} \quad \dots (3)$$

After  $n$  steps,  $P^0$  gets the fixed value i.e.,  $n \geq 4$  also gets (0.39 0.23 0.19 0.19) four stages are limiting stage probabilities. The resultant values show the 4 years annual probability distribution of rainfall. The odds for each state in the first year are spread as (0.39 0.23 0.19 0.19). A comparison study shows that the chance of State 4 has consistently decreased over the decade, while the probability of States 1 and 2 has increased. As a result, after ten years, 39% of yearly rainfall in Barishal is expected to fall in State 1, 23% in State 2, 19% in State 3, and 19% in State 4.

**Bhola:** Let the model for yearly rainfall for the Bhola region be State-1: (1490-2025) mm, State-2: (2026-2560) mm, State-3: (2561-3095) mm, State-4: (2026-2560) mm. Consequently, the transition matrix

$$M = \begin{bmatrix} 7 & 1 & 3 & 3 \\ 0 & 2 & 1 & 2 \\ 1 & 3 & 0 & 0 \\ 6 & 0 & 0 & 0 \end{bmatrix}$$

And probability matrix

$$P_{Bh} = \begin{bmatrix} 0.5 & 0.08 & 0.21 & 0.21 \\ 0 & 0.4 & 0.2 & 0.4 \\ 0.25 & 0.75 & 0 & 0 \\ 1 & 0 & 0 & 0 \end{bmatrix} \quad \dots(4)$$

After  $n$  steps,  $P^0$  receives the fixed value i.e.,  $n \geq 4$  also obtains the four-stage limiting stage probability The expression (0.44 0.23 0.14 0.19) is the solution to equation (4), which represents the yearly probability distribution of rainfall after four years. The probability in the first year is (0.44 0.23 0.14 0.19). When the probability is compared, State 4 shows a continuous reduction, but States 1 and 2 show an increase during the four years. As a result, the Bhola projection suggests that 44% of the yearly rainfall will fall in State 1, 23% in State 2, 14% in State 3, and 19% in State 4.

**Cox's Bazar:** In the Cox's Bazar region, the yearly rainfall model is State-1: (2480-3230) mm, State-2: (3231-3980) mm, State-3: (3981-4730) mm, State-4: (3231-3980) mm. Consequently, the transition matrix

$$M = \begin{bmatrix} 1 & 1 & 1 & 2 \\ 0 & 6 & 4 & 1 \\ 1 & 4 & 5 & 0 \\ 3 & 1 & 0 & 0 \end{bmatrix}$$

and probability matrix

$$P_{CB} = \begin{bmatrix} 0.2 & 0.2 & 0.2 & 0.4 \\ 0 & 0.54 & 0.36 & 0.1 \\ 0.1 & 0.4 & 0.5 & 0 \\ 0.75 & 0.25 & 0 & 0 \end{bmatrix} \quad \dots(5)$$

After the  $n$  steps,  $P^0$  receives the fixed value, i.e.,  $n \geq 8$ , also obtains the four-stage limiting stage probability (0.13 0.42 0.35 0.1). The probability distribution (0.1334 0.4175 0.354 0.0951) for Cox's Bazar over eight years is obtained by solving equation (5). An eight-year comparison demonstrates a consistent reduction in State 4, with a rise in odds for States 2 and 3. As a result, Cox's Bazar expects 13% of its annual rainfall to fall in State 1, 42% in State 2, 45% in State 3, and 10% in State 4.

**Khulna:** The annual rainfall model for the Khulna area is State-1: (2200-2745) mm, State-2: (2746-3290) mm, State-3: (3291-3845) mm, State-4: (2746-3290) mm. Thus, the transition matrix

$$M = \begin{bmatrix} 1 & 7 & 1 & 5 \\ 0 & 7 & 1 & 2 \\ 2 & 0 & 1 & 0 \\ 7 & 0 & 0 & 0 \end{bmatrix}$$

and probability matrix

$$P_K = \begin{bmatrix} 0.1 & 0.3 & 0.1 & 0.5 \\ 0 & 0.7 & 0.1 & 0.2 \\ 0.67 & 0 & 0.33 & 0 \\ 1 & 0 & 0 & 0 \end{bmatrix} \quad \dots(6)$$

The fixed value of (6) is obtained after  $n$  steps, and the four-stage limiting stage probabilities (0.33 0.33 0.11 0.23) are obtained as well when  $n \geq 12$ . The solution of equation (6) can be expressed as the expression. (0.33 0.33 0.11 0.23), reflecting Khulna's yearly rainfall probabilities over twelve years. Probabilities correspond with this solution in the twelfth year. A comparison study reveals that State 4 has been steadily declining throughout the decade, while States 1 and 2 have maintained equal odds. As a result, Khulna predicts that 33% of yearly rainfall will fall in State 1, 33% in State 2, 11% in State 3, and 23% in State.

**Patuakhali:** For the Patuakhali region, the yearly rainfall model is State-1: (2200-2745) mm, State-2: (2746-3290) mm, State-3: (3291-3845) mm, State-4: (2746-3290) mm. Thus, the transition matrix

$$M = \begin{bmatrix} 4 & 1 & 4 & 1 \\ 0 & 3 & 4 & 1 \\ 3 & 4 & 1 & 1 \\ 3 & 0 & 0 & 0 \end{bmatrix}$$

and probability matrix

$$P_P = \begin{bmatrix} 0.4 & 0.1 & 0.4 & 0.1 \\ 0 & 0.375 & 0.5 & 0.125 \\ 0.34 & 0.44 & 0.11 & 0.11 \\ 1 & 0 & 0 & 0 \end{bmatrix} \dots(7)$$

When n is greater than or equal to 4, not only is the fixed value (7) reached after n steps, but the four-stage limiting stage probability. (0.34 0.26 0.3 0.1) is also acquired. Finally, solving equation (7) produces the probability distribution. (0.34 0.26 0.3 0.1) For Patuakhali s yearly rainfall over four years. A comparison analysis shows a consistent reduction in State 4, whereas States 1 and 3 see an increase in probability during the ten years. As a result, Patuakhali predicts that 34% of yearly rainfall will fall in State 1, 26% in State 2, 30% in State 3, and 10% in State 4.

Fig. 3 illustrates the probability distribution of each state (state-1, state-2, state-3, and state-4) among six distinct study areas. The likelihood of each state is depicted by distinct bars. By comparing the heights of these bars for each district, we may gain insight into the probability distribution of states in each coastal city. The graph illustrates four discrete situations of rainfall limitation, which may be classified according to the magnitude of rainfall. Let us designate them as State 1, State 2, State 3, and State 4. The graph represents six districts: Chittagong, Barishal, Bhola, Cox’s Bazar, Khulna, and Patuakhali. These districts are probably coastal areas, as previously noted. The figures depicted in the graph denote the odds of transitioning between states within each district. Each row corresponds to a certain district, while each column represents an individual state. For instance, the number in the initial row and second column (State 2) represents the chance

of moving from State 1 to State 2 in the Chittagong area. The percentages displayed in each cell of the graph indicate the probability of shifting from one state to another within a certain district. For example, examining the number in the third row and fourth column (State 4) reveals the chance of moving from State 3 to State 4, specifically in the Bhola area. The Markov chain model is applicable for the analysis and prediction of rainfall patterns in specified areas. By analyzing the transition probabilities, it is possible to determine the probability of distinct rainfall conditions happening in each district. This information holds significant value for many applications, including agricultural planning, water resource management, infrastructure building, and disaster preparedness. To summarize, the above graph depicts a Markov chain model that showcases the odds of transitioning between different states of rainfall limitation across six districts. It offers valuable information on the probability of distinct rainfall conditions happening in each district, assisting in decision-making processes for sectors affected by rainfall patterns.

In summary, this section elucidates the foundational principles of Markov chains, emphasizing the importance of transition probabilities, steady-state probabilities, and limiting-state probabilities in analyzing the behavior and stability of dynamic systems. These theoretical constructs serve as the cornerstone for our subsequent application of Markov models in investigating complex processes and phenomena.

**Stationary Test for Rainfall Occurrences**

Since satisfactory crop yields mainly depend on the pattern of rainfall occurrences, it is necessary to know whether the

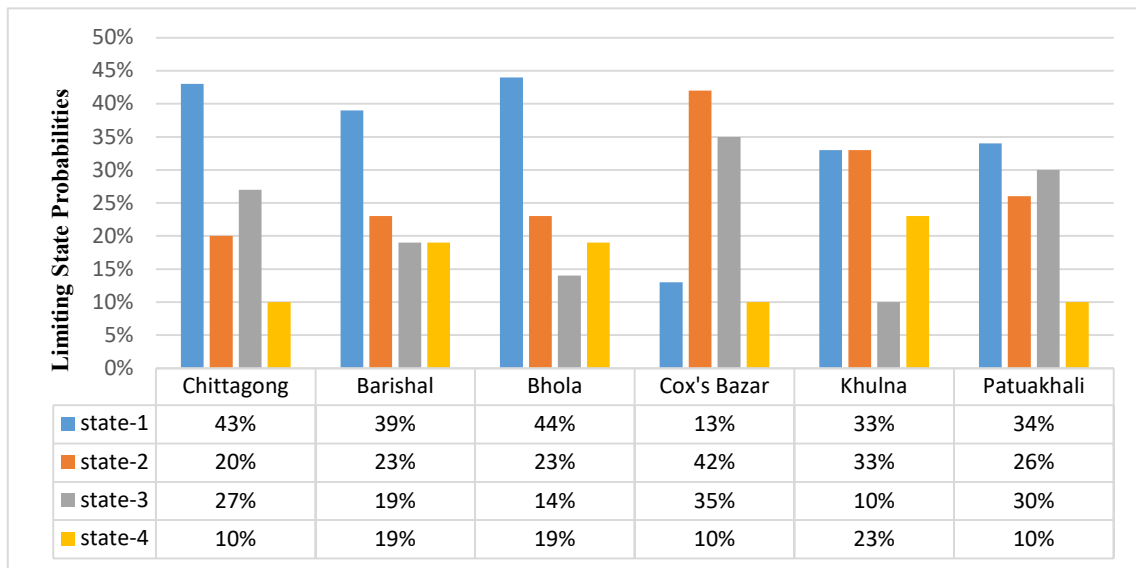


Fig. 3: Observed state probabilities for six coastal regions of Bangladesh.

rainfall occurrences are stationary or not to estimate the crop yields for later periods. Thus the stationary test has been employed on rainfall data to test the null hypothesis that rainfall occurrences are stationary against the alternative that rainfall occurrences are not stationary.

$$\text{i.e., } H_0: P_{ij}(t) = P_{ij}$$

$$H_1: P_{ij}(t) \neq P_{ij}$$

For all selected stations, let us consider the transition probabilities.  $\widehat{P}_{ij}$  and  $\widehat{P}_{ij}(t)$  which are estimated from the rainfall data for 30 years (1994-2023). Using these probabilities, the values of stationary test statistic  $\chi^2$  have been calculated for the selected stations, which are shown in Table 3. The  $\chi^2$  values are found to be insignificant for coastal stations. Thus we may conclude that rainfall occurrences are stationary for all the stations.

Table 3: Values of Stationary Test Statistic,  $\chi^2$  for Selected Stations.

Stations	Observed values of $\chi^2$	Degrees of Freedom	P value
Chittagong	18.66**	9	0.028
Barishal	16.91	9	0.050
Bhola	20.76**	9	0.014
Cox's Bazar	19.98**	9	0.018
Khulna	31.31**	9	0.00026
Patuakhali	21.65**	9	0.01
** Insignificant at 0.05 level.			

The stationary test was conducted to examine the null hypothesis () that the rainfall occurrences are stationary against the alternative hypothesis () that the rainfall occurrences are not stationary. This test is crucial for estimating crop yields in later periods, as the pattern of rainfall occurrences is a key factor influencing agricultural productivity. The results show that the observed values of the test statistic,  $\chi^2$ , are found to be significant for all coastal stations except Barishal at a 5% level of significance with 7 degrees of freedom.

## CONCLUSIONS

To sum up, the investigation of Bangladesh's precipitation patterns using finite Markov chains has provided insight into the complicated mechanisms of the region's rainfall variability. Through the use of advanced modeling tools and historical data, this work has yielded useful data about the temporal history of rainfall patterns, providing a detailed understanding of the fluctuations in precipitation that occur in various states and regions. The statistical studies

carried out in this study highlight the complicated nature of Bangladesh's rainfall patterns by identifying lighter-tailed distributions and leftward skewness in the data. The results of the stationary show that the observed values of the test statistic,  $\chi^2$ , are found to be significant for all coastal stations except Barishal. We conclude that the rainfall occurrences are stationary for Barishal stations and other stations; the rainfall occurrences are non-stationary.

By filling data gaps and fostering international collaborations, scientists can enhance predictive models, shedding light on how climate change will impact rainfall patterns. This study enhances understanding of Bangladeshi precipitation dynamics, underscoring the importance of data-driven insights and advanced modeling in navigating climate complexity. With ongoing innovation and collaboration, we can pursue sustainable solutions, fostering a more adaptable and stable society amidst environmental shifts.

## REFERENCES

- Ahmed, R. and Karmakar, S., 1993. Arrival and withdrawal dates of the summer monsoon in Bangladesh. *International Journal of Climatology*, 13, pp.727-740.
- Akaike, H., 1974. A new look at the statistical model identification. *IEEE transactions on automatic control*, 19(6), pp.716-723.
- Arumugam, P. and Karthik, S.M., 2018. Stochastic modelling in yearly rainfall at Tirunelveli District, Tamil Nadu, India. *Materials Today: Proceedings*, 5(1), pp.1852-1858.
- Bracken, L.J. and Croke, J., 2007. The concept of hydrological connectivity and its contribution to understanding runoff-dominated geomorphic systems. *Hydrological Processes: An International Journal*, 21(13), pp.1749-1763.
- Das, L.C. and Zhang, Z., 2021. Annual and seasonal variations in temperature extremes and rainfall in Bangladesh, 1989–2018. *International Journal of Big Data Mining for Global Warming*, 3(01), p.2150004.
- Das, L.C., Islam, A.S.M.M. and Ghosh, S., 2022. Mann–Kendall trend detection for precipitation and temperature in Bangladesh. *International Journal of Big Data Mining for Global Warming*, 4(1), p.2250001.
- Das, L.C., Zhang, Z., Crabbe, M.J.C. and Liu, A., 2024. Spatio-temporal patterns of rainfall variability in Bangladesh. *International Journal of Global Warming*, 33(2), pp.206–221. <https://doi.org/10.1504/IJGW.2024.10063123>
- Debsarma, S.K., 2002. Intra-annual and inter-annual variation of rainfall over different regions of Bangladesh. In *Proceedings of SAARC Seminar on Climate Variability in the South Asian Region and its Impacts*. SMRC.
- Dore, M.H., 2005. Climate change and changes in global precipitation patterns: What do we know? *Environment International*, 31(8), pp.1167-1181.
- Gemmer, M., Becker, S. and Jiang, T., 2004. Observed monthly precipitation trends in China, 1951–2002. *Theoretical and Applied Climatology*, 77, pp.39-45.
- Gabriel, K.R. and Neumann, J., 1962. A Markov chain model for daily rainfall occurrence at Tel Aviv. *Quarterly Journal of the Royal Meteorological Society*, 88, pp.90-95.
- Gringorten, I.I., 1996. A stochastic model of the frequency and duration of weather events. *Journal of Climate and Applied Meteorology*, 5, pp.606-624.
- Hossain, S., Roy, K. and Datta, D.K., 2014. Spatial and temporal variability

- of rainfall over the southwest coast of Bangladesh. *Climate*, 2(2), pp. 28–46. <https://doi.org/10.3390/cli2020028>
- Hermawan, E., Ruchjana, B.N., Abdullah, A.S., Jaya, I.G.N.M., Sipayung, S.B. and Rustiana, S., 2017. Development of the statistical ARIMA model: An application for predicting the upcoming of MJO index. *Journal of Physics: Conference Series*, 893, p. 012019. <https://doi.org/10.1088/1742-596/893/1/012019>
- Ibeje, A.O., Osuagwu, J.C. and Onosakponome, O.R., 2018. A Markov model for prediction of annual rainfall. *International Journal of Scientific Engineering and Applied Science (IJSEAS)*, 3(11), pp.1-5.
- Doob, J.L. 1942. What is a stochastic process? *The American Mathematical Monthly*, 49(10), pp.648-653.
- Khan, M.J.U., Islam, A.K.M., Das, M., Mohammed, K., Bala, S. and Islam, G.M., 2019. Observed trends in climate extremes over Bangladesh from 1981 to 2010. *Climate Research*, 77, pp.45-61.
- Lambert, F., Stott, P. and Allen, M., 2003. Detection and attribution of changes in global terrestrial precipitation. *EGS-AGU-EUG Journal*, 121, p.6140).
- Racsko, P.L., Szeidl, L. and Semenov, M., 1991. A series approach to local stochastic weather models. *Ecological Modelling*, 57, pp.27-41.
- Ross, S.M., 1996. *Stochastic Processes* (2nd ed.). University of California
- Shahid, S., 2011. Trends in extreme rainfall events of Bangladesh. *Theoretical and Applied Climatology*, 104, pp.489-499.
- Shamsuddin, S.D. and Ahmed, R., 1974. Variability of annual rainfall in Bangladesh. *Journal of Bangladesh National Geographical Association*, 2, pp.13-20.
- Sarker, M.S.H. and Bigg, G., 2010. The consequences of climate change for precipitation trends in Bangladesh. In *Proceedings of the 1st International Seminar: Climate Change, Environmental Challenges in the 21st Century*. Rajshahi, Bangladesh.
- Sujatmoko, M. and Bambang, C. 2012. Markov chain stochastic reliability analysis for simulating daily rainfall data in the Kampar watershed. *Jurnal Sains dan Teknologi*, 11(1), pp.65-76.
- Tovler, A. 2016. *An Introduction to Markov Chains*. Department of Mathematical Sciences, University of Copenhagen, Denmark.
- Villarini, G., Smith, J.A. and Napolitano, F. 2010. Nonstationary modeling of a long record of rainfall and temperature over Rome. *Advances in Water Resources*, 33(10), pp. 1256-126.

---

**ORCID DETAILS OF THE AUTHORS**


Lipon Chandra Das: <https://orcid.org/0000-0001-8150-8057>







# An Assessment of Land Use Land Cover Using Machine Learning Technique

V. Pushpalatha<sup>1</sup>, H. N. Mahendra<sup>2†</sup> , A. M. Prasad<sup>3</sup>, N. Sharmila<sup>4</sup>, D. Mahesh Kumar<sup>2</sup>, N. M. Basavaraju<sup>2</sup>, G. S. Pavithra<sup>5</sup> and S. Mallikarjunaswamy<sup>2</sup>

<sup>1</sup>Department of Information Science and Engineering, JSS Academy of Technical Education (Affiliated to Visvesvaraya Technological University, Belagavi), Bengaluru-560060, Karnataka, India

<sup>2</sup>Department of Electronics and Communication Engineering, JSS Academy of Technical Education (Affiliated to Visvesvaraya Technological University, Belagavi), Bengaluru-560060, Karnataka, India

<sup>3</sup>Department of Computer Science and Engineering, Dayananda Sagar College of Engineering, Bengaluru-560078, Karnataka, India

<sup>4</sup>Department of Electrical and Electronics Engineering, JSS Science and Technology University, Mysuru- 570015, Karnataka, India

<sup>5</sup>Department of Computer Science and Engineering (AI-ML), RNS Institute of Technology (Affiliated to Visvesvaraya Technological University, Belagavi), Bengaluru- 560098, Karnataka, India

†Corresponding author: H. N. Mahendra; mahendrah@jssateb.ac.in

Nat. Env. & Poll. Tech.  
Website: [www.neptjournal.com](http://www.neptjournal.com)

Received: 02-02-2024  
Revised: 13-03-2024  
Accepted: 27-03-2024

## Key Words:

Remote sensing  
Geographic information system  
Multispectral data  
Support vector machine  
LISS-III  
Land use land cover

## ABSTRACT

This research paper presents a comprehensive assessment of the built-up area in Mysuru City over the decade spanning from 2010 to 2020, employing advanced geospatial techniques. The study aims to analyze the spatiotemporal patterns of urban expansion, land-use dynamics, and associated factors influencing the city's built environment. Remote sensing imagery, Geographic Information System (GIS) tools, and machine learning algorithms are leveraged to process and interpret satellite data for accurate land-cover classification. The methodology involves the acquisition and preprocessing of multi-temporal satellite imagery to delineate and map the built-up areas at different time intervals. Land-use change detection techniques are employed to identify and quantify alterations in urban morphology over the specified period. Additionally, socio-economic and environmental variables are integrated into the analysis to discern the drivers of urban growth. The outcomes of this research contribute valuable insights into urbanization dynamics and land-use planning strategies, facilitating informed decision-making for sustainable urban development.

## INTRODUCTION

Urbanization is an unequivocal global phenomenon, transforming landscapes and shaping the dynamics of human habitation (Aithal et al. 2012, Hosseiny et al. 2022, Mahendra et al. 2023c). The rapid expansion of built-up areas within cities has become a critical facet of this transformative process, necessitating a comprehensive understanding of its implications on the environment, society, and urban planning (Dash et al. 2015, Mahendra et al. 2023a). This research paper embarks on a meticulous investigation, employing advanced geospatial techniques, to assess the evolution of the built-up area in Mysuru City over the critical decade spanning 2010 to 2020.

Mysuru, a city steeped in historical and cultural significance, has undergone significant urbanization in recent years. The burgeoning population, economic activities,

and infrastructural developments have played pivotal roles in altering the city's physical fabric (Kanga et al. 2022, Mahendra et al. 2023d). The utilization of geospatial technologies, including satellite imagery, remote sensing, and Geographic Information Systems (GIS), provides an unprecedented opportunity to scrutinize and quantify the spatial and temporal dynamics of urban expansion (Mahendra et al. 2023, Firoz et al. 2016). This research endeavors to unravel the patterns, drivers, and consequences of the built-up area expansion in Mysuru, offering valuable insights for sustainable urban development strategies.

The significance of this study extends beyond the confines of Mysuru, as urbanization challenges are pervasive and multifaceted. By delving into the specific case of Mysuru, this research aims to contribute to the broader discourse on urban growth, aiding policymakers, urban planners, and researchers in formulating evidence-based

strategies for managing and mitigating the impacts of rapid urbanization. The integration of geospatial techniques allows for a nuanced analysis, enabling the identification of hotspots of development, encroachments, and potential areas for conservation or redevelopment (Kumar Jat et al. 2008, Mahendra et al. 2019).

As the world grapples with the repercussions of unchecked urbanization, understanding the dynamics of built-up area expansion becomes imperative for achieving sustainable and resilient cities. The insights garnered from this case study on Mysuru City serve as a microcosm, illustrating the intricate interplay between historical, cultural, economic, and environmental factors influencing urban growth. Through this research, we aim to provide a foundation for informed decision-making and policy formulation, fostering a balance between urban development and environmental preservation in the face of escalating urban challenges.

### SIMILAR STUDIES IN THE PAST

In the literature, several studies have utilized geospatial techniques to assess the LULC classes of the study area. Dash et al. (2015) have to estimate the urban built-up area of Bangalore city and the latter quantifying urban expansion over 19 years. Ramachandra et al. (2012) applied remote sensing and spatial metrics to study the urbanization process in Mysuru, identifying a significant increase in built-up area. Usha et al. (2014) also used remote sensing and GIS technology to evaluate the growth of built-up areas in Udupi Taluk, highlighting the environmental impact of urbanization. Kanga et al. (2022) linked urban growth in Bangalore to changes in land surface temperature, revealing a significant increase in built-up areas. Shahfahad et al. (2020), in a study of Surat, found a rapid increase in both population and built-up area, with a strong positive relationship between population density and built-up area.

Prakash & Bharath (2020) conducted a case study of Bangalore for assessment of urban built-up using geospatial methods. The study results show that the eastern part of the city has urban volume development compared to the central business district. Aithal (2012) presented a dynamics assessment of LULC classes in Mysuru city between the years 1973 to 2009. The coalescence of urban areas occurred during the rapid urban growth from 2000 to 2009. Santosh et al. (2018) conducted a case study in Chikodi Taluk, Belagavi District, Karnataka, using a GIS-based multicriteria evaluation technique for urban development. Suribabu et al. (2014) conducted a case study on Thanjavur City, Tamil Nadu, India using remote sensing and GIS tools for evaluation of urban growth. The leapfrog sprawl dominates the study area in the study area.

Shahfahad et al. (2020) presented a case study of Surat City using multi-temporal Landsat data sets for the assessment of built-up density and urban expansion of fast-growing. The study results show that the growth rate of population and urban area are not identical to each other. Sharma et al. (2012) presented an urban dynamics change using geospatial techniques for the assessment of land consumption. The results show that land consumption is increasing rapidly with the exponential growth of the population. These studies collectively underscore the importance of geospatial techniques in understanding, and managing urban growth and highlight the need for ongoing assessment and planning to manage the impacts of urbanization in Indian cities.

### STUDY AREA

Mysuru, also known as Mysore, is a city located in the southern part of the Indian state of Karnataka. Renowned for its rich cultural heritage and historical significance, Mysuru stands as a testament to the grandeur of the Wodeyar dynasty that ruled the region for centuries. The city is celebrated for its majestic Mysuru Palace, a stunning example of Indo-Saracenic architecture that attracts visitors from around the world. The palace, illuminated with thousands of lights during the annual Dasara festival, is a symbol of the city's royal past. Mysuru is also famous for its well-preserved heritage buildings, including the Jaganmohan Palace and the Chamundi Hills, which offer panoramic views of the city and house the Chamundeshwari Temple, a revered pilgrimage site.

Apart from its historical and cultural significance, Mysuru is recognized as an educational hub with a thriving academic environment. The city is home to prestigious institutions like the University of Mysore, which has played a pivotal role in shaping the educational landscape of the region. The serene surroundings and pleasant climate make Mysuru an ideal destination for students seeking a conducive learning environment. Additionally, the city is known for its yoga centers and wellness retreats, attracting enthusiasts from all over the world. Mysuru's unique blend of heritage, education, and wellness makes it a captivating study area that offers a holistic experience for residents and visitors alike. The map of the Mysuru city is shown in Fig. 1.

### DATA USED

LISS-III (Linear Imaging Self-Scanning Sensor-III) is an advanced remote sensing sensor designed and developed by the Indian Space Research Organization (ISRO). It is part of the payload on board the Indian Remote Sensing (IRS) satellites, specifically designed for Earth observation.

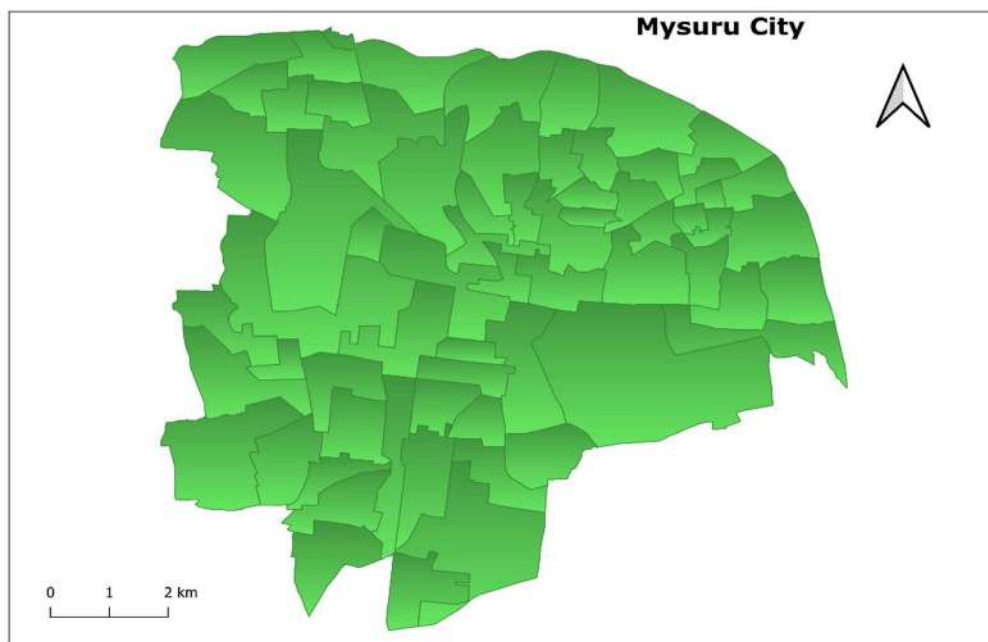


Fig. 1: Map of the Mysuru City.

LISS-III operates in the visible and near-infrared spectral bands, capturing imagery with a spatial resolution of 23.5 meters. The sensor's ability to acquire multispectral data makes it a valuable tool for land use and land cover (LULC) classification, as it can distinguish between different surface features based on their spectral characteristics.

In the context of LULC classification, LISS-III data proves instrumental due to its high spatial resolution, enabling the identification and mapping of various land cover types with greater detail. The multispectral capabilities allow for the extraction of valuable information about vegetation, urban areas, water bodies, and other land features. This data is particularly useful for monitoring changes in land cover, assessing environmental impacts, and supporting land management and planning initiatives. Researchers and decision-makers leverage LISS-III imagery to enhance their understanding of the Earth's surface, contributing to more effective land-use planning, resource management, and environmental conservation efforts.

## MATERIALS AND METHODS

The research aimed to assess the built-up area in Mysuru City over a decade (2010-2020) using advanced geospatial techniques. The urban landscape is constantly evolving due to factors like population growth, urbanization, and infrastructure development. Understanding the temporal changes in built-up areas is crucial for effective urban

planning and sustainable development. The methodology followed in this work is shown in Fig. 2.

**Study area and data collection:** The study focused on Mysuru City, a rapidly growing urban center in India. Various geospatial datasets, including satellite imagery, aerial photographs, and land-use maps from 2010 and 2020, were collected. High-resolution images, acquired at regular intervals, formed the basis for the analysis, ensuring a comprehensive representation of land cover changes.

**Image preprocessing:** To enhance the accuracy of the analysis, the collected satellite imagery underwent rigorous preprocessing. This included radiometric and atmospheric corrections, image registration, and mosaicking. These steps aimed to standardize the data, reducing potential errors and ensuring consistency across the temporal dataset.

**Land cover classification:** A supervised classification approach was employed to categorize land cover types. Machine learning algorithms, such as Support Vector Machines (SVM), were utilized to train the classifier. Training samples were selected based on ground truth data, and the algorithm was fine-tuned to accurately identify built-up areas, distinguishing them from other land cover classes.

**Change detection analysis:** Change detection analysis was conducted to identify and quantify alterations in the built-up area between 2010 and 2020. This involved overlaying the classified land cover maps for the two time periods and extracting areas where changes occurred. The analysis aimed

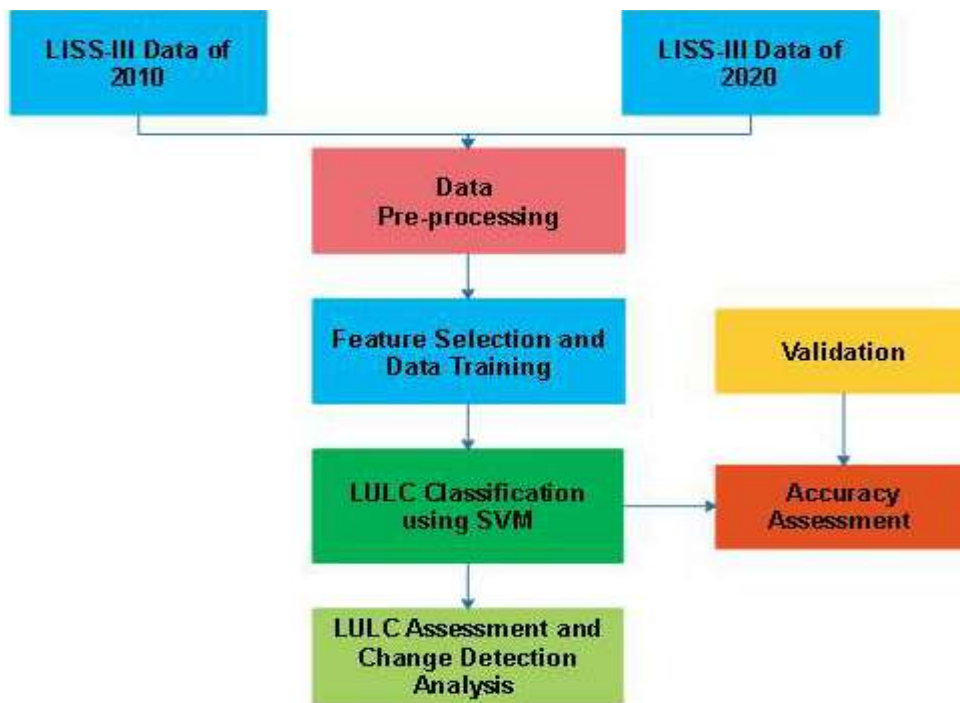


Fig. 2: Methodology followed in this work.

to identify expansion, contraction, and spatial shifts in the built-up zones.

**Accuracy assessment:** To validate the accuracy of the classification results, a rigorous accuracy assessment was carried out using ground truth data. This involved comparing the classified maps with independently collected reference data, assessing overall accuracy, producer's accuracy, and user's accuracy. The assessment ensured the reliability of the geospatial techniques employed in the study.

**Spatial-temporal analysis:** Spatial and temporal patterns of built-up area changes were analyzed to identify hotspots of urban expansion or decline. Geographic Information System (GIS) tools were employed to visualize and interpret the results, providing valuable insights into the dynamics of urban growth within Mysuru City.

### SUPPORT VECTOR MACHINE (SVM)

Support Vector Machine (SVM) is a powerful machine learning algorithm widely employed in land use and land cover (LULC) classification tasks. LULC classification involves categorizing different types of land and surface cover, such as urban areas, water bodies, vegetation, and agricultural land, based on remotely sensed data (Mahendra et al. 2022). SVMs are particularly well-suited for this task due to their ability to handle high-dimensional data

and non-linear relationships between features (Davis et al. 2002).

One key strength of SVMs in LULC classification is their capability to find optimal hyperplanes that effectively separate different classes in the feature space. The algorithm aims to maximize the margin between classes, enhancing its generalization performance. In the context of LULC, this means SVM can delineate distinct land cover types with minimal overlap, resulting in more accurate classification maps. SVMs are robust in handling both binary and multi-class classification problems, making them versatile for LULC applications where multiple land cover classes need to be identified. The algorithm's ability to work with various kernel functions, such as linear, polynomial, and radial basis functions (RBF), allows it to capture complex patterns in the data. This flexibility is crucial when dealing with diverse and intricate LULC patterns across different landscapes.

SVMs are effective in handling imbalanced datasets commonly encountered in LULC classification. Land cover types may not be evenly distributed in remote sensing datasets, and SVMs can adapt to this by assigning appropriate weights to different classes, ensuring a balanced and accurate classification outcome. In comparison to some other machine learning algorithms, SVMs exhibit good generalization performance, meaning they can maintain their classification accuracy on new, unseen data. This is essential in LULC classification, where accurate predictions

on new satellite images or time-series data are crucial for monitoring land cover changes over time. SVMs may face challenges in handling very large datasets or those with high dimensionality. Additionally, parameter tuning is important for optimizing performance, and selecting the right kernel and regularization parameters requires careful consideration. Overall, Support Vector Machines remain a valuable tool in LULC classification, offering robustness, versatility, and the ability to discern complex patterns in remotely sensed data.

Support vector machines offer a robust and versatile approach to LULC image classification. Their ability to handle high-dimensional data, accommodate non-linear relationships, and provide interpretability makes them a valuable tool in extracting meaningful information from remote sensing imagery. As technology advances and the demand for accurate and timely land cover information grows, SVMs continue to be a relevant and effective choice for researchers and practitioners engaged in LULC mapping and monitoring. The classification function of the SVM is shown in Fig. 3 and represented in Equation (1)

$$f(x_i) = \begin{cases} 1 & \text{if } w \cdot x_i + b \geq 1 \\ -1 & \text{if } w \cdot x_i + b \leq -1 \end{cases} \quad \dots(1)$$

## RESULTS AND DISCUSSION

### LULC Classification

In this study, we employed geospatial techniques to assess the built-up area in Mysuru, focusing on LULC classes such as built-up, vegetation, water bodies, and others. The classification was performed using LISS-III satellite images for the years 2010 and 2020. The results reveal significant changes in the built-up area over the decade, providing valuable insights into urbanization trends in the region. The

classified map of the years 2010 and 2020 are shown in Fig. 4 and Fig. 5 respectively.

The analysis of the classified LISS-III images from 2010 and 2020 indicated a substantial increase in the built-up area within Mysuru city. The urban expansion is particularly pronounced, signifying the rapid growth and development experienced by the city over the studied period. Concurrently, a decline in vegetation cover and alterations in water bodies were observed, underscoring the dynamic nature of land use changes. These findings contribute to a comprehensive understanding of the urban landscape evolution in Mysuru.

Furthermore, the classification accuracy assessment demonstrated the reliability of the geospatial techniques employed in delineating LULC classes. The overall accuracy and kappa coefficient were calculated to validate the classification results for both years. The high accuracy values validate the robustness of the classification methodology and highlight its applicability for monitoring changes in built-up areas using remote sensing data.

### LULC Assessment

The assessment of LULC in the city of Mysuru was conducted through the classified images of the years 2010 and 2020. The primary LULC classes considered for this study included built-up areas, vegetation cover, water bodies, and other land cover types. The results of the classification process revealed significant changes in the built-up area over the decade under consideration.

In the year 2010, the analysis indicated a notable extent of built-up areas concentrated in specific regions of Mysuru, with distinct patterns of urban development. The classification highlighted the distribution and density of infrastructure, residential, and commercial zones. In contrast, the 2020 LISS-III imagery exhibited a discernible

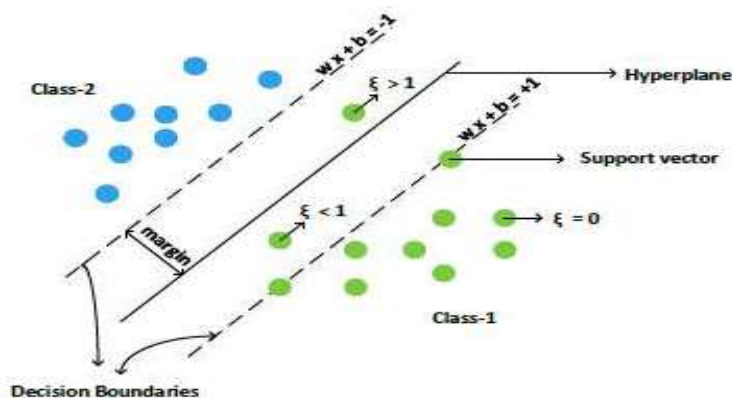


Fig. 3: Illustration of SVM classification function.

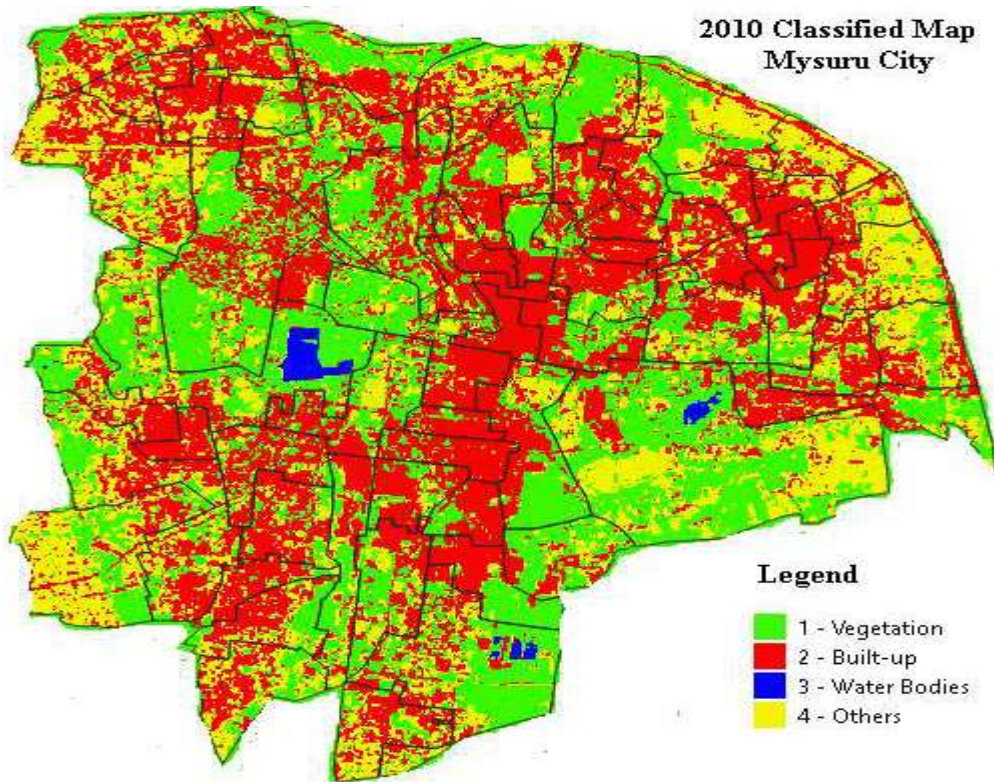


Fig. 4: Classified map of Mysuru city for the year 2010.

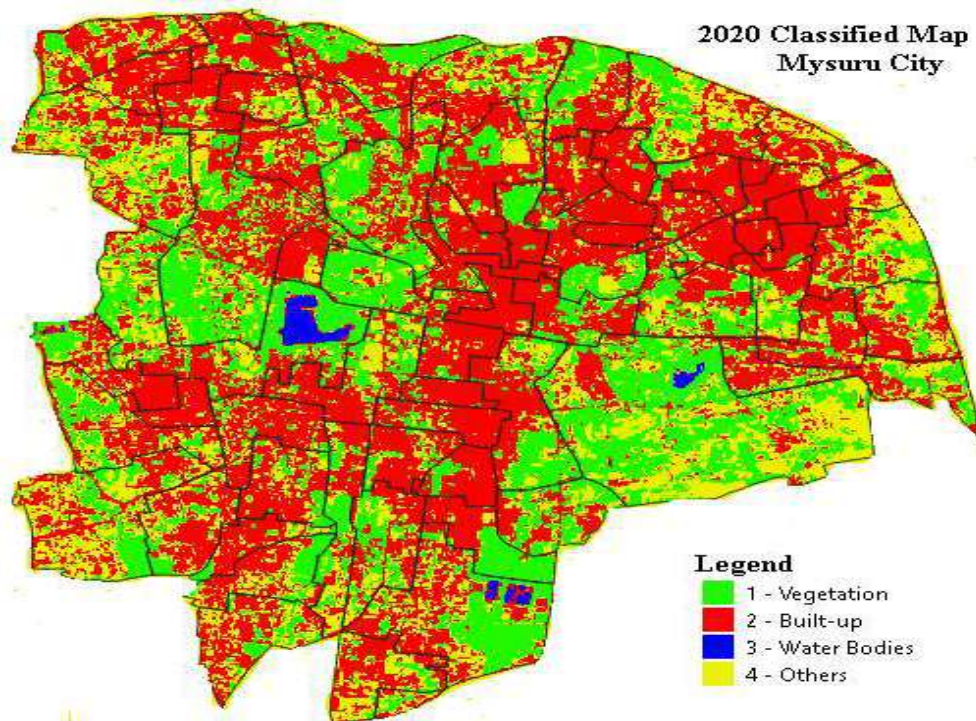


Fig. 5: Classified map of Mysuru city for the year 2020.

Table 1: LULC assessment of Mysuru city.

Class Name	2010		2020		Area difference (in Sq. km)	Change of Area in %
	Area (in Sq. km)	% Area	Area (in sq. km)	% Area		
Built-up	49.75	38.53	70.08	54.27	20.33	15.74
Vegetation	45.37	35.13	37.04	28.68	-8.33	-6.45
Water bodies	0.744	0.576	0.808	0.625	0.064	0.049
Others	33.25	25.75	20.38	15.78	-12.87	-9.97

increase in the built-up area, signifying urban expansion and potential changes in land-use policies. The results further underscored the need for sustainable urban planning to manage growth and maintain a balance between development and environmental preservation.

Furthermore, the LULC assessment demonstrated fluctuations in vegetation cover and water bodies. Changes in green cover were observed, reflecting alterations in the city's landscape due to factors such as deforestation, urbanization, or afforestation initiatives. Similarly, alterations in the extent and distribution of water bodies provided insights into the impact of urban development on hydrological patterns. The LULC assessment for the years 2010 and 2020 is shown in Table 1. The LULC assessment results of the year 2010 show the built-up area of 38.53%, vegetation of 45.37%, water bodies of 0.576%, and others of 25.75%. Similarly, the assessment results of the year 2020 show the built-up area of 54.2%, vegetation of 28.68%, water bodies of 0.625%, and others of 15.78%.

### Change Detection Analysis

In this study, we conducted a comprehensive change detection analysis to assess the dynamics of the built-up area in Mysuru city over a decade (2010-2020) using a post-classification comparison technique. The change detection analysis between the years 2010 and 2020 is shown in Table 1.

Our analysis revealed significant changes in the built-up area of 15.74% of Mysuru city between 2010 and 2020. The built-up class exhibited a noticeable expansion, indicating urbanization and infrastructural development within the region. The expansion of built-up areas was spatially mapped and quantified, providing insights into the extent and distribution of urban growth over the decade. Concurrently, changes in vegetation cover of -6.45%, water bodies of 0.049%, and other land cover types of -9.97% were also identified and analyzed. These findings contribute to a comprehensive understanding of the urbanization dynamics and associated environmental impacts in Mysuru.

Furthermore, the change detection analysis facilitated the identification of specific areas undergoing rapid

transformation. Hotspot analysis was employed to pinpoint regions with the most pronounced changes in land cover, offering valuable information for urban planning and resource management. The results highlight the necessity of sustainable urban development strategies to mitigate the environmental implications of rapid urban expansion observed in Mysuru. Overall, the change detection analysis presented in this study serves as a valuable tool for policymakers, urban planners, and environmental researchers seeking to comprehend and address the evolving landscape of Mysuru city.

### Accuracy Assessment

In comparing the classified maps with ground truth data, the overall accuracy of the built-up area classification for the year 2010 was determined to be 89.84% using confusion matrix, indicating a high level of precision in identifying urban and developed regions. Additionally, the kappa coefficient, a measure of classification accuracy that accounts for chance agreement, was found to be 0.878, further substantiating the reliability of the geospatial techniques employed. Similar accuracy assessment metrics were applied to the LISS-III images from 2020, revealing an overall accuracy of 88.28% and a kappa coefficient of 0.865. These results highlight the effectiveness of the geospatial techniques in consistently identifying built-up areas over the temporal span of the study. The confusion matrix constructed for a classified map for the years 2010 and 2020 is shown in Table 2 and Table 3 respectively.

Furthermore, individual class accuracies were examined to understand the performance of the classification across various land cover categories. The built-up class exhibited a high level of accuracy of 93.23%, demonstrating the robustness of the geospatial techniques in delineating urban environments. Additionally, accuracies for vegetation and water bodies were also assessed at 89.51% and 86.66% respectively for the 2010 classified map, providing insights into the reliability of the classification across diverse land cover types. The comparative analysis between the years 2010 and 2020 allowed for an assessment of changes in the built-up area over the study period, providing valuable information for urban planning and environmental monitoring.

Table 2: Confusion matrix for a classified map of 2010.

Classified Data	Class	Number of samples	Reference Data			
			Built-up	Vegetation	Water Bodies	Others
	Built-up	355	331	6	7	11
	Vegetation	410	10	367	14	19
	Water Bodies	240	8	13	208	11
	Others	275	10	12	9	244
Overall Accuracy: 89.84%			Kappa Coefficient: 0.878			

Table 3: Confusion matrix for a classified map of 2020.

Classified Data	Class	Number of samples	Reference Data			
			Built-up	Vegetation	Water Bodies	Others
	Built-up	355	326	8	9	12
	Vegetation	410	12	362	15	21
	Water Bodies	240	10	14	203	13
	Others	275	12	14	10	239
Overall Accuracy: 88.28 %			Kappa Coefficient: 0.865			

## CONCLUSION

This research paper presents a comprehensive assessment of the built-up area in Mysuru City, Karnataka State, India, employing advanced geospatial techniques. Through meticulous analysis and application of remote sensing and GIS technologies, the study has yielded significant insights into the urban expansion dynamics over the past decade. The obtained results showcase an impressive overall accuracy of 89.84% for the year 2010 and 88.28% for 2020, underscoring the reliability and effectiveness of the employed methodologies. The research not only contributes to the understanding of urbanization patterns but also highlights the potential of geospatial techniques in urban planning and management, providing valuable data for policymakers, city planners, and researchers aiming to address the challenges associated with rapid urban growth.

## REFERENCES

- Aithal, B.H., 2012. Spatial metrics based landscape structure and dynamics assessment for an emerging Indian megalopolis. *International Journal of Advanced Research in Artificial Intelligence*, 1.
- Dash, P.P., Kakkar, R., Shreenivas, V., Prakash, P., Mythri, D., Kumar, K.H., Singh, V.V. and Sahai, R., 2015. Quantification of urban expansion using geospatial technology-A case study in Bangalore. *ARS*, 4, pp.330-342.
- Davis, L.S. and Townshend, J.R.G., 2002. An assessment of support vector machines for land cover classification. *International Journal of Remote Sensing*, 23(4), pp.725-749. DOI: 10.1080/01431160110040323.
- Firoz, A. and Laxmi, G., 2016. Analysis of urban sprawl dynamics using geospatial technology in Ranchi city, Jharkhand, India. *Journal of Environmental Geography*, 9(1-2), pp.7-13.
- Hosseiny, B., Abdi, A.M. and Jamali, S., 2022. Urban land use and land cover classification with interpretable machine learning-A case study using Sentinel-2 and auxiliary data. *Remote Sensing Applications: Society and Environment*, 28, p.100843.
- Kanga, S., Meraj, G., Johnson, B.A., Singh, S.K., Muhammed Naseef, P., Farooq, M., Kumar, P., Marazi, A. and Sahu, N., 2022. Understanding the linkage between urban growth and land surface temperature - A case study of Bangalore City, India. *Remote Sensing*, 14, p.4241.
- Kumar Jat, M., Garg, P.K. and Khare, D., 2008. Monitoring and modeling of urban sprawl using remote sensing and GIS techniques. *International Journal of Applied Earth Observation and Geoinformation*, 10, pp.26-43.
- Mahendra, H.N. and Mallikarjunaswamy, S., 2022. An efficient classification of hyperspectral remotely sensed data using a support vector machine. *International Journal of Electronics and Telecommunications*, 68(3), pp.609-617.
- Mahendra, H.N. and Mallikarjunaswamy, S., 2023c. An analysis of change detection in land use land cover area of remotely sensed data using supervised classifier. *International Journal of Environmental Technology and Management*, 26.
- Mahendra, H.N., Mallikarjunaswamy, S. and Rama Subramoniam, S., 2023a. An assessment of vegetation cover of Mysuru City, Karnataka State, India, using deep convolutional neural networks. *Environmental Monitoring and Assessment*, 195, p.526. <https://doi.org/10.1007/s10661-023-11140-w>.
- Mahendra, H.N., Mallikarjunaswamy, S. and Rama Subramoniam, S., 2023b. An assessment of built-up cover using geospatial techniques - A case study on Mysuru district, Karnataka state, India. *International Journal of Environmental Technology and Management*. DOI: <http://dx.doi.org/10.1504/IJETM.2022.10048734>.
- Mahendra, H.N., Mallikarjunaswamy, S., Kumar, D.M., Kumari, S., Kashyap, S., Fulwani, S. and Chatterjee, A., 2023d. Assessment and prediction of air quality level using ARIMA model: A case study of Surat City, Gujarat State, India. *Nature Environment and Pollution Technology*, 22(1).
- Mahendra, H.N., Mallikarjunaswamy, S., Rekha, V., Puspapalatha, V. and Sharmila, N., 2019. Performance analysis of different classifiers for remote sensing application. *International Journal of Engineering and Advanced Technology*, 9, pp.2249-8958. DOI: 10.35940/ijeat.A1879.109119.
- Prakash, P.S. and Bharath, H.A., 2020, September. Assessment of Urban Built-Up Volume Using Geospatial Methods: A Case Study of



- Bangalore. In *IGARSS 2020-2020 IEEE International Geoscience and Remote Sensing Symposium* (pp. 4242-4239). IEEE.
- Raj, K.G., Trivedi, S., Ramesh, K.S., Sudha, R., Subramoniam, S.R., Ravishankar, H.M. and Vidya, A., 2021. Assessment of vegetation cover of Bengaluru city, India, using geospatial techniques. *Journal of the Indian Society of Remote Sensing*, 49, pp.747-758. <https://doi.org/10.1007/s12524-020-01259-5>.
- Ramachandra, T.V., Aithal, B.H. and Sanna, D.D., 2012. Insights to urban dynamics through landscape spatial pattern analysis. *International Journal of Applied Earth Observation and Geoinformation*, 18, pp.329-343.
- Santosh, C., Krishnaiah, C. and Deshbhandari, P.G., 2018. Site suitability analysis for urban development using GIS based multicriteria evaluation technique: A case study in Chikodi Taluk, Belagavi District, Karnataka, India. *IOP Conference Series: Earth and Environmental Science*, 169.
- Sharma, L.K., Pandey, P.C. and Nathawat, M.S., 2012. Assessment of land consumption rate with urban dynamics change using geospatial techniques. *Journal of Land Use Science*, 7, pp.135-148.
- Suribabu, C.R. and Bhaskar, J., 2014. Evaluation of urban growth using remote sensing and GIS tools: Case study on Thanjavur City, Tamil Nadu, India. *Jordan Journal of Civil Engineering*, 8.
- Usha, N., 2014. Urbanization study with land use/land cover change detection for the environmental impact on climate change using remote sensing and GIS technology: A case study of Udupi Taluk, Karnataka State, India. *International Journal of Geoinformatics*, 10.

---

#### ORCID DETAILS OF THE AUTHORS

H. N. Mahendra: <https://orcid.org/0000-0003-3854-5500>





# Evaluating the Association Between Ambient Pollutants and Climate Conditions in Chiangmai, Thailand

S. Piyavadee<sup>1†</sup> , R. Chumaporn<sup>2</sup> and V. Patipat<sup>3</sup>

<sup>1</sup>Program in Environmental Health, School of Public Health, University of Phayao, Phayao 56000, Thailand

<sup>2</sup>Program in Occupational Health and Safety, School of Public Health, University of Phayao, Phayao 56000, Thailand

<sup>3</sup>Atmospheric Pollution and Climate Change Research Unit, School of Energy and Environment, University of Phayao, Phayao 56000, Thailand

†Corresponding author: S. Piyavadee; piyavadee.sr@up.ac.th

## Nat. Env. & Poll. Tech.

Website: [www.neptjournal.com](http://www.neptjournal.com)

Received: 22-04-2024

Revised: 03-06-2024

Accepted: 04-06-2024

### Key Words:

Climate change  
Ambient pollutants  
PM10  
Particulate matter

## ABSTRACT

The most significant air pollutant is particulate matter of less than 10 microns (PM10), followed by ozone (O<sub>3</sub>) during the monitoring period from 2006 to 2022 in Chiangmai. The association between ambient pollutants and climate conditions in Chiangmai was assessed using regression analysis and analysis of variance (ANOVA). The ANOVA analysis indicated that the average temperature was associated significantly with the nitrogen dioxide (NO<sub>2</sub>) concentration in the ambient, but the average rainfall volume was associated significantly with most pollutants except only sulfur dioxide (SO<sub>2</sub>). From the prediction models, the rise in average temperature affected to increase in the concentrations of PM10 and O<sub>3</sub>. Interestingly, the increase in rainfall will be advantageous to compromise the severity of all pollutants. Meanwhile, on hotter days should be careful of the rise of PM10 and O<sub>3</sub> concentrations. Therefore, the vital meteorological variables associated with air pollution are very useful for forecasting the harmful and severity level of each air pollutant.

## INTRODUCTION

Chiangmai is the seventh best city in the world for workcation and vacation. Unfortunately, Chiangmai has been facing a serious air pollution crisis for a long time. The severity of the air pollution crisis has increased continuously over the last ten years (Pardthaisonga et al. 2018). The main causes of air pollution consisted of forest fires, and agricultural waste open burning, often known as human-made. It is noteworthy that more than 90% of hot spots (approximately 934 hot spots) occurred in forest areas (both reserved forest and conserved forest) between January and March 2019 (Chiangmai Provincial Smog and Forest Fire Problem Solving Command Center 2019). It impacted a lot of people's well-being, causing health risks, bad environments, economic losses, etc. Thao et al. (2022) conducted research found that the impacts on public health and the economy within the mainland Southeast Asia (MSEA) region. This area encompasses Chiangmai province, which harbors the largest population and is most significantly affected by the particulate matter less than 10 microns (PM10) issue. Interestingly, air pollution can be intensified directly through adverse temperatures and changes in rainfall patterns. The temperature plays a pivotal role in altering the concentration levels of air pollutants

in atmospheric physicochemical processes. Temperature influences of the air pollution transported in the horizontal direction by wind and in the vertical direction by turbulent diffusion are determinants of atmospheric stability (Lee et al. 2021). Additionally, temperature significantly impacts the intensity of air pollution in chemical processes, contributing to the formation of secondary air pollutants (Ebi et al. 2021). Rainfall significantly contributes to the reduction of air pollutants through a crucial process known as wet deposition, effectively washing the pollution down from the atmosphere (Pan et al. 2017).

However, there are small studies about Chiangmai air pollution. Nowadays, extreme climate variations occur very rapidly and more frequently due to climate change and global warming. Moreover, Chiangmai has developed dramatically and grown to become an economically powerful city. All resulted in large changes in the land use of Chiangmai (Pardthaisonga et al. 2018). The forest area continues to reduce to 69.84% (15,458 km<sup>2</sup>) in 2018 as compared with 82.61% (16,609 km<sup>2</sup>) in 2008 (Royal Forest Department 2023) resulting from forest fire, deforestation, etc. In addition, the geography of Chiangmai is like a pan basin, which is surrounded by high mountains. Consequently,

it risks accumulated air pollution for a longer time easily. Making it difficult to dilute or clean air pollution. The complex topography of Chiangmai significantly influences its meteorology and particulate matter (Solanki et al. 2019). Mountain and valley winds impact particulate matter distribution (Song & Min 2023). Additionally, factors like temperature stratification, mountain boundary layer height, strong and weak synoptic forcing, and thermally induced flows impact how particulate matter spreads across diverse terrain (Giovannini et al. 2020). In summary, the terrain's obstruction can lead to haze accumulation over plains and the lifting of pollution along mountainous regions. These processes contribute to the concentration of particulate matter in specific areas, exacerbating air pollution.

This work aimed to evaluate the association between the four important air pollutants and the climate conditions in Chiangmai, Thailand. The results help to forecast the severity of air pollution. These are beneficial to manage and mitigate air pollution in Chiangmai.

## MATERIALS AND METHODS

The selected ambient air quality monitoring station (35T)

by the Pollution Control Department (PCD) is located in Chang Phueak, Muang, Chiangmai Province, Thailand. The monthly average value was used to describe the datasets of air pollutants: PM<sub>10</sub>, ozone (O<sub>3</sub>), sulfur dioxide (SO<sub>2</sub>), and nitrogen dioxide (NO<sub>2</sub>) between 2006 and 2022. Meanwhile, the climate conditions consisted of two variables (average monthly temperature and average monthly rainfall), which were obtained from the Thai Meteorological Department (TMD), Ministry of Digital Economy and Society. The association between ambient pollutants and climate conditions in Chiangmai was assessed using regression analysis and analysis of variance (ANOVA).

## RESULTS AND DISCUSSION

### Chiangmai Background

The land is surrounded by a lot of mountains. The area feature is like a pan basin (Fig.1). Therefore, when air pollution occurs, it has higher adverse impacts. This is because of easy accumulation and difficult dispersion (Amnuaylojaroen & Kreasuwun 2012). The period between mid-February and late May marks the transition from the Northeast monsoon (which occurs in December-January) to the Southwest

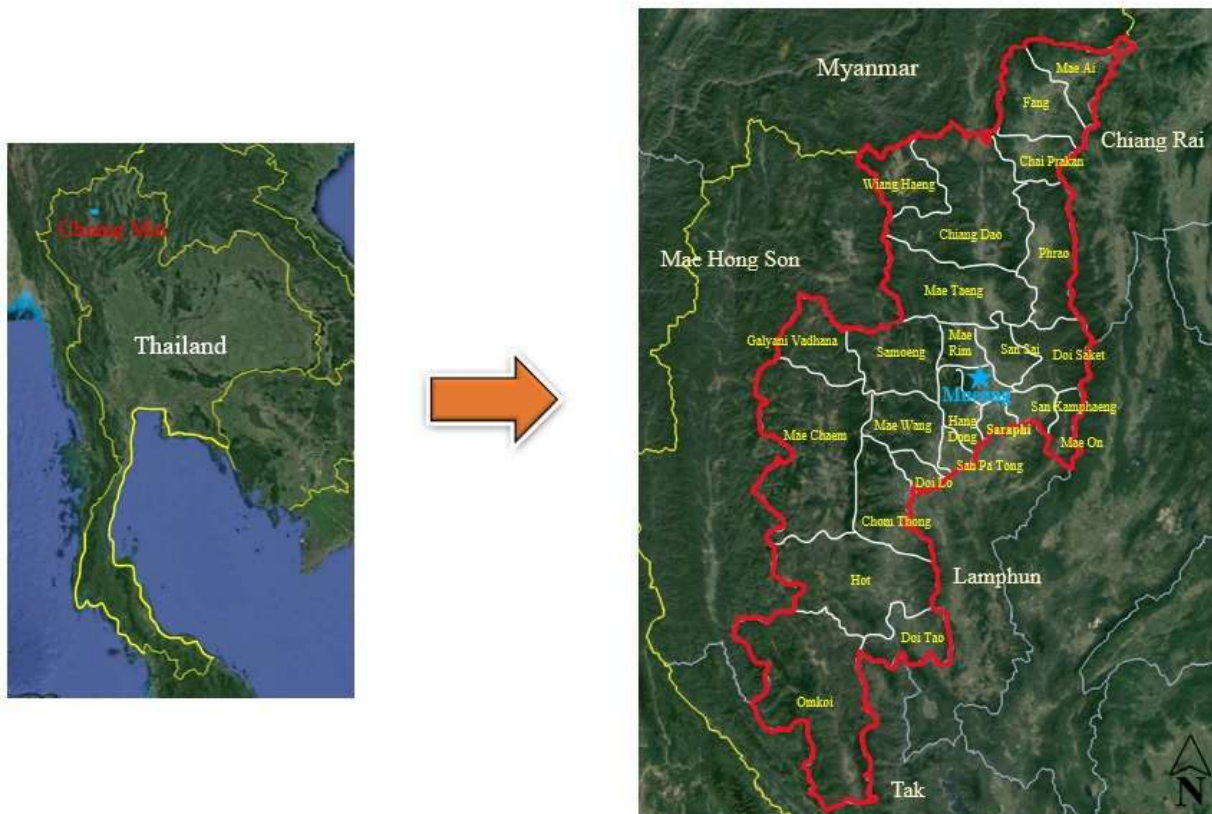


Fig. 1: The topography and ambient air monitoring station location in Chiangmai.

monsoon (commonly observed in July-August). The hottest weather, typically occurring in March-April, coincides with the presence of intense thermal lows in the region. Both meteorology and emissions are interconnected and play pivotal roles in the formation of haze episodes. The Chiangmai land area covers approximately 20,107 km<sup>2</sup>. Most land use is forest area within 13,717 km<sup>2</sup> (68%), followed by an agricultural area of 5,005 km<sup>2</sup> (25%), and community and construction of 850 km<sup>2</sup> (4%), respectively (Fig. 2). The main water resources of Chiangmai is Ping River which flows through the center of the province from north to south. Especially, it is an important water resource for air pollution mitigation and safe zone building. For instance, on 21 February 2020, the Chiangmai Provincial Administrative Organization used up to 32 cars to spray

water to reduce smog in the commercial zone (Manager Online 2019).

The biggest source of gross provincial products (GPP) per capita is the service section approximately 69.40% (Fig. 3). Importantly, Chiangmai is the central cultural and natural city of upper northern Thailand, which makes the province more attractive to a lot of tourists and investors. It is well known as a UNESCO Creative City of Craft and Folk Art (Yodsurang et al. 2022). The high air pollutant concentration in Chiangmai is affecting tourists because of the need to avert outdoor activities. The tourism income in 2020 (between February and March as the high season) extremely dropped by an average of 65.71% as compared to 2019 (Chiangmai Provincial Office 2020). Importantly, it is related significantly to the supply and demand of workers in the job market.

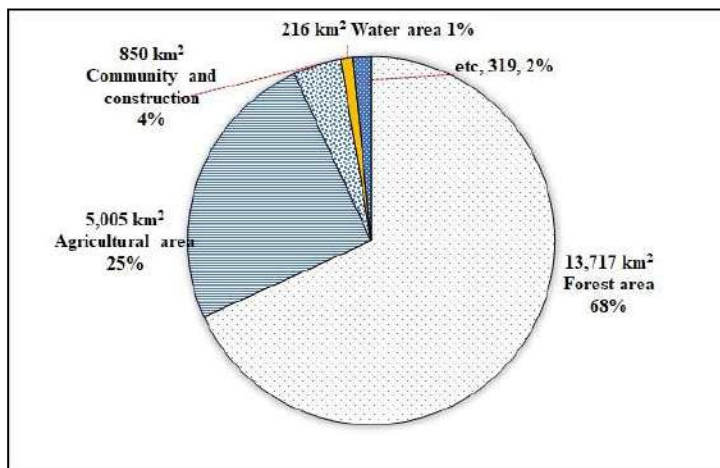


Fig. 2: The proportion of land use (Chiangmai Provincial Office 2020).

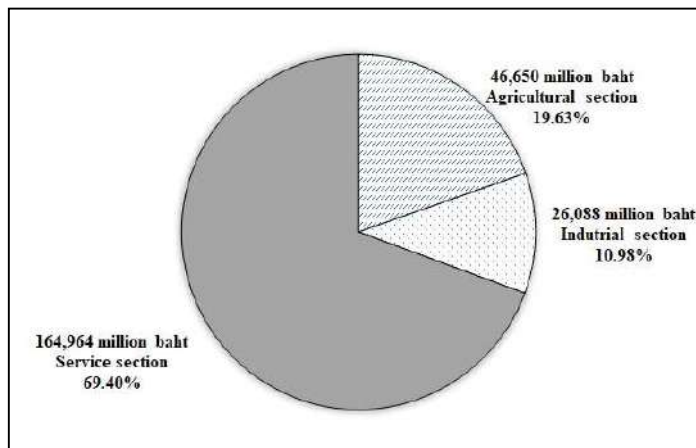


Fig. 3: The proportion of GPP.  
(Chiangmai Provincial Office 2020)

**Climate Conditions**

The average temperature of Chiangmai province in the period 2006 to 2022 is shown in Fig. 4. The average temperature presented high fluctuation during a year. In some years (2010, 2013, 2015) had a large variation, which may be an initial sign of climate change. There was a slight increase in the average temperature over the period. The created linear

equation indicates the province’s temperature has increased trend by an average of 0.0002°C per month (0.024°C per decade).

Fig. 5 presents the highest volume at 470.6 mm in August 2010. Generally, Thailand’s rainy season is from mid-May to mid-October (The Public Relations Department 2023). The monthly rainfall volume was around 106.4 mm in the

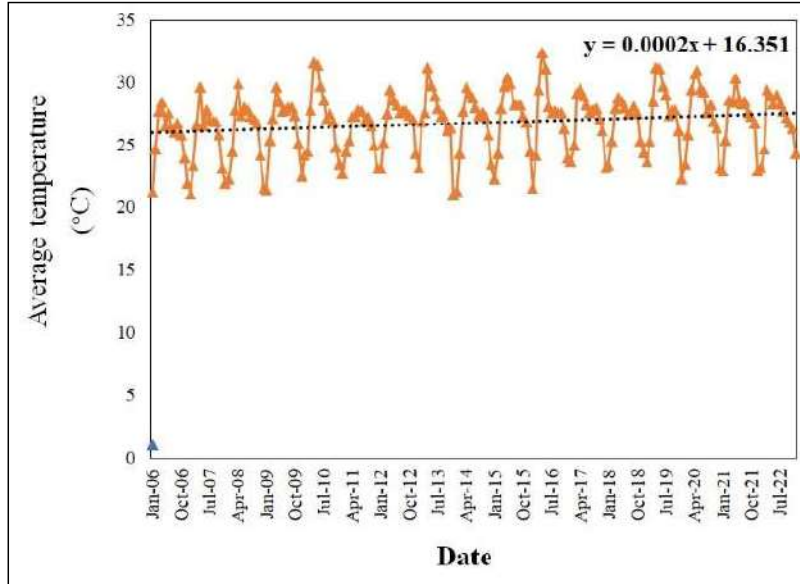


Fig. 4: The average temperature between 2006 and 2022 (The Meteorological Department 2023).

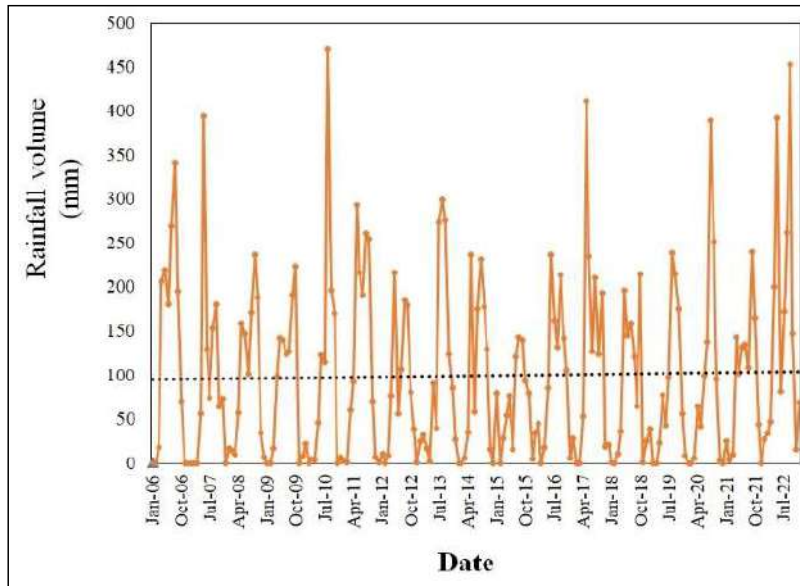


Fig. 5: The rainfall volume between 2006 and 2022 (The Meteorological Department 2023).

monitoring period. On average, there was 1,276.8 mm a year, as compared with Thailand's average rainfall volume of 1,622.9 mm between 1991 and 2020 (Office of Natural Resources and Environmental Policy and Planning 2023). This indicated that Chiangmai a low rainfall area resulted in negative impacts on air pollution control. Moreover, rainfall is so difficult to precipitate lately due to climate change, El Nino, etc. For example, in 2019 (El Nino) had particulate matter less than 2.5 microns (PM<sub>2.5</sub>) much higher than in 2017 (La Nina) (Kraisitnitikul et al. 2024). The governor is very aware of this obstacle. Therefore, the Department of Royal Rainmaking and Agricultural

Aviation is assigned to making artificial rainfall in Chiangmai.

### Ambient Air Quality Monitoring

The trends in the concentrations of PM<sub>10</sub> exceeded or were close to the 24-hour National Ambient Air Quality Standards (NAAQS) (less than 120  $\mu\text{g}/\text{m}^3$ ) between 2012 and 2022 (Fig. 6). Especially, March had the highest PM<sub>10</sub> concentration during the summer season, which is the biomass open-burning period (February to April) after harvesting (Kawichai et al. 2022). There was an increase in the number of hospital outpatient department visitors

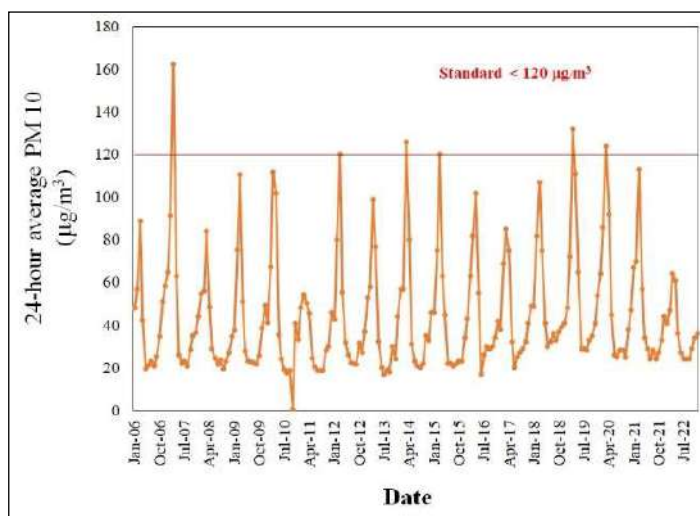


Fig. 6: The 24-hour average PM<sub>10</sub> concentration (Pollution Control Department 2023).

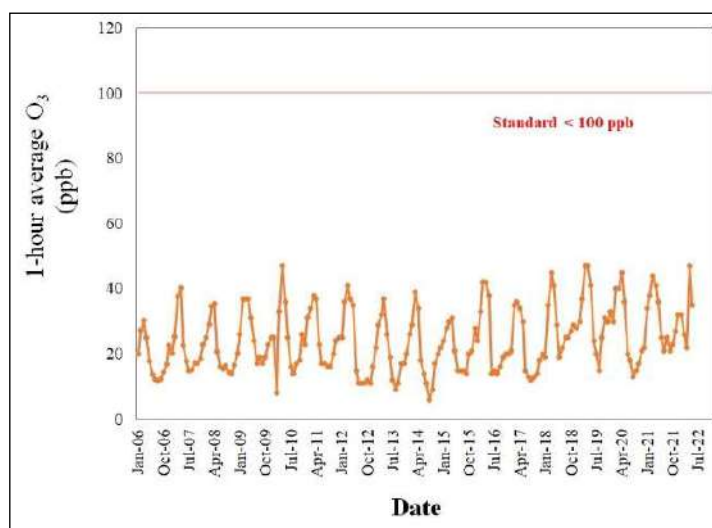


Fig. 7: The 1-hour average O<sub>3</sub> concentration (Pollution Control Department 2023).

because of respiratory disease in the period of January-March from 209,413 visitors in 2006 to 237,348 visitors in 2007. This period had the highest record of PM10 level (Bank of Thailand 2007). Additionally, it was confirmed that the increase in PM10 concentration was related to asthma and chronic obstructive pulmonary disease in Chiangmai. This appearance of emergency exacerbations was after around one week (Pothirat et al. 2016). Because the PM10 can be inhaled into and deposited in the respiratory tract system and lungs. Moreover, Jeensoon et al. (2018) found that fine particle matter has a high effect on visibility at low altitudes in Chiangmai.

Meanwhile, other pollutants ( $O_3$ ,  $SO_2$ ,  $NO_2$ ) spread far from their standards very much.  $O_3$  likes to lift in January of every year, which is the last period of the winter season (Fig. 7). This is starting to warm up and give more sunlight. Accordingly,  $O_3$  formation is more accelerated in warm and sunny weather (EPA 2023). As well known that  $O_3$  is a secondary pollutant that occurs through photochemical reactions linking to other pollutants (nitrogen oxides and volatile organic compounds). Considering the threshold  $O_3$  concentration of 50 ppb is harmful to human health with long-term exposure. Anxiously, the air pollution crisis will drive it close to the threshold of toxic concentration recently

(UK Air Pollution Information System 2023). In Thailand, a small group of people know that  $O_3$  is an air toxicant on the ground level. For example, the misunderstanding of some tourist attractions presented the slogan “visiting to inhale  $O_3$  pollution for longevity” (Bavonkiti 2012). This resulted in less concern and awareness about  $O_3$ .

Normally,  $SO_2$  and  $NO_2$  are used to be the cause of acid rain. Their concentrations are very low with a small spreading variation (Fig. 8 and Fig. 9). Mostly, this resulted from biomass burning in the forest, emitting lower  $NO_2$  and  $SO_2$  than in rice fields (Acharya et al. 2018). The study by Brassard et al. 2014 indicated that  $SO_2$  and  $NO_2$  were released from agricultural waste burning significantly higher than forest biomass burning in Quebec, Canada. Typically,  $SO_2$  was produced from oil and coal burning but  $NO_2$  was generated from fossil fuels such as gasoline (Brassard et al. 2014). Accordingly, their emissions depend on the fuel's nitrogen and sulfur content (South Carolina Department of Health and Environmental Control 2023).

Interestingly, all pollutants are likely to rise to the highest concentration at the same interval between February and April. Therefore, this interval is a critical time, which needs a special monitor for air pollution as well as an effective early warning and controlling system.

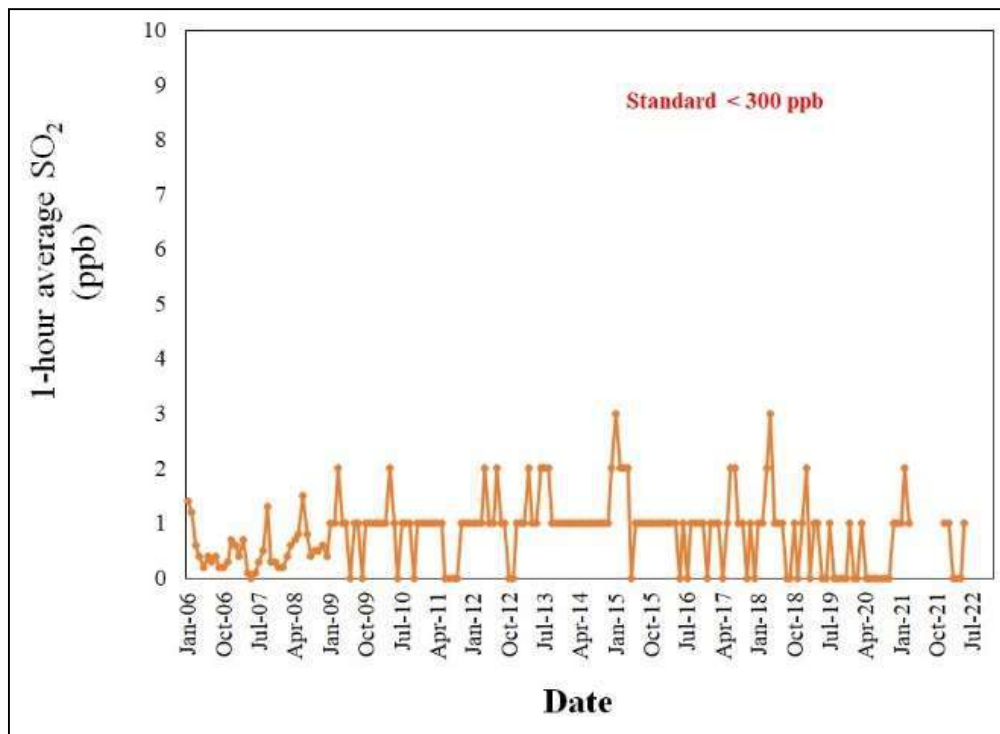


Fig. 8: The 1-hour average  $SO_2$  concentration (Pollution Control Department 2023).



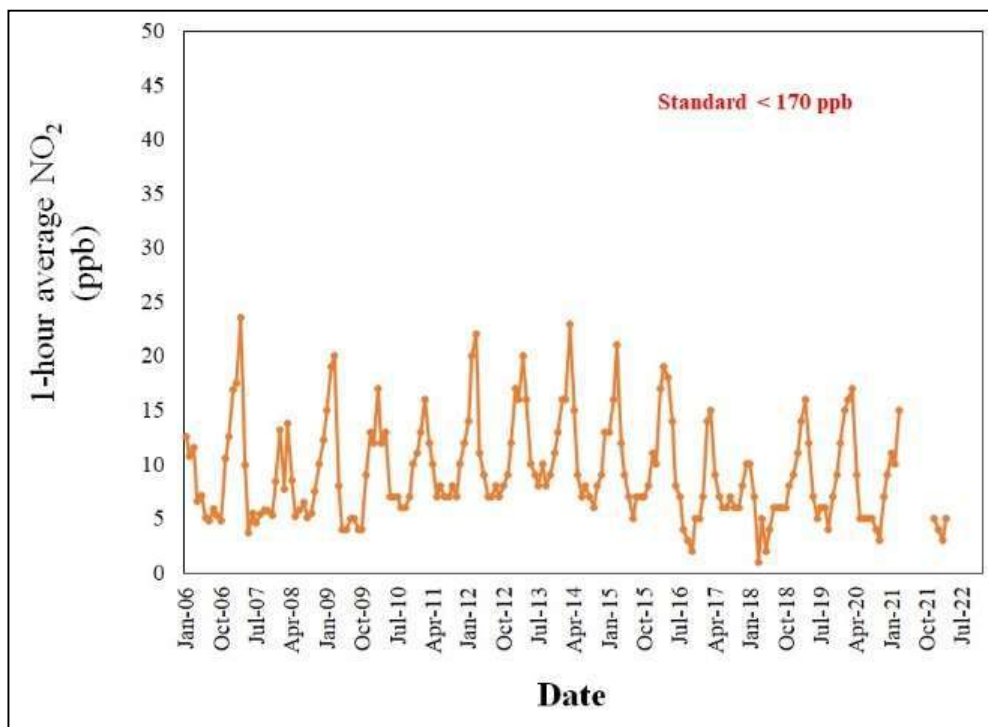


Fig. 9: The 1-hour average NO<sub>2</sub> concentration (Pollution Control Department 2023).

Table 1: The regression of analysis and ANOVA results.

Independent variable	Dependent variable	F-value	P-value	R <sup>2</sup>	Predictive model
Average temperature	PM10	0.055	0.814	0.000	PM10 = 39.241 + 0.188 (Temp)
	O <sub>3</sub>	5.400	0.021	0.027	O <sub>3</sub> = 6.890 + 0.652 (Temp)
	SO <sub>2</sub>	0.645	0.423	0.003	SO <sub>2</sub> = 1.206 – 0.0015 (Temp)
	NO <sub>2</sub>	10.943	0.001	0.056	NO <sub>2</sub> = 21.128 – 0.443 (Temp)
Average rainfall	PM10	73.873	0.000	0.282	PM10 = 56.991 – 0.138 (Rainfall)
	O <sub>3</sub>	37.865	0.000	0.173	O <sub>3</sub> = 27.834 – 0.04 (Rainfall)
	SO <sub>2</sub>	4.112	0.044	0.023	SO <sub>2</sub> = 0.899 – 0.001 (Rainfall)
	NO <sub>2</sub>	66.376	0.000	0.280	NO <sub>2</sub> = 11.363 – 0.024 (Rainfall)

Remark: A P-value less than 0.001 is statistically highly significant.

**ANOVA Results**

According to the ANOVA results in Table 1. The average temperature associated with only NO<sub>2</sub> by P-value is less than 0.001. Because NO<sub>2</sub> is photochemical smog, its degradation is related directly to the presence of sunlight and relatively high temperature (Han et al. 2011) as shown in Equation 1.



On the other hand, the rainfall volume is associated

significantly with the most pollutants (PM10, O<sub>3</sub>, NO<sub>2</sub>), except only SO<sub>2</sub>.

Noteworthy, the increase in average temperature resulted in the decrease of SO<sub>2</sub> and NO<sub>2</sub> concentrations. The higher average temperature may accelerate the degradation of SO<sub>2</sub> and NO<sub>2</sub> converting to other intermediates (NASA 1997). Conversely, this encourages the occurrences of PM10 and O<sub>3</sub>. Similarly, the concentrations of O<sub>3</sub> were found to rise with the increases in temperature during heatwaves in Birmingham,

UK (Kalisa et al. 2018). Differently, the PM10 concentration tends to be higher during wintertime with small rainfall and low temperature in Hanoi, Vietnam (Dung et al 2019). This is because the PM10 emission sources are different from Chiangmai, which most PM10 from biomass and forest fires in summer.

Meanwhile, the rainfall increase affected to reduction of all pollutants. Same as the particulate matter less than 2.5 microns (PM2.5) is less in the rainy season because rain has a wet deposition effect on PM2.5 in Chiangmai and no open burning which constitutes a significant source of emissions in this period (Anusasanana et al. 2022). At 896 monitoring stations in China between 2014 and 2019, Liu et al. (2020) found that the concentrations of all air pollutants (PM2.5, PM10, SO<sub>2</sub>, carbon monoxide (CO), NO<sub>2</sub>, and O<sub>3</sub>) were positively associated with ambient pressure, but significantly negatively associated with wind speed, rainfall, and relative humidity.

Lastly, the Thai government can use these results for artificial rainmaking and planning to mitigate the air pollution crisis in Chiangmai. Haleem et al. (2023) stated that artificial rain is a promising defense method for air pollution management. However, field measurements are necessary to further evaluate the cost-effectiveness of the method, including the other benefits or challenges. Moreover, the predictive models are very useful for forecasting the harmful and severity level of each air pollutant according to the average temperature and rainfall volume.

## CONCLUSION

The rainfall volume can significantly reduce all air pollutants in the ambient, especially PM10 in Chiangmai. Therefore, we should help to increase the rainfall volume. Admittedly, the increasing average temperature may reflect to rise of PM10 and O<sub>3</sub>. Climate change monitoring by using the average temperature is vital for preparing and preventing the harmful effects of both pollutants. Finally, further research should study more meteorological variables associated with air pollution such as relative humidity, wind speed, solar radiation, etc.

## ACKNOWLEDGMENT

The authors would like to acknowledge Mr. Sirichai Suwanlamai for all his support. This research was supported by the University of Phayao and Thailand Science Research and Innovation Fund (Fundamental Fund 2024).

## REFERENCES

- Acharya, P., Sreelesh, S., Kulshrestha, U. and Gupta, G., 2018. Characterisation of emission from open-field burning of crop residue during harvesting period in north-west India. *Environmental Monitoring and Assessment*, 190: 1-19.
- Anusasanana, P., Morasum, D., Suwanarat, S. and Thangprasert, N., 2022. Correlation between PM2.5 and meteorological variables in Chiang Mai, Thailand. *Journal of Physics: Conference Series*, 2145(2022): 1-9.
- Bank of Thailand, 2007. The smog situation on the upper northern of Thailand. Retrieved February 22, 2023, from: <https://www.tei.or.th/thaicityclimate/public/document-36.pdf>
- Bavonkiti, S., 2012. To inhale pure ozone or not? For what. *Thammasat Medical Journal*, 12(1): 198-200.
- Brassard, P., Palacios, J.H., Godbout, S., Bussieres, D., Lagace, R., Larouche, J.P. and Pelletier, F., 2014. Comparison of the gaseous and particulate matter emissions from the combustion of agricultural and forest biomasses. *Bioresource Technology*, 155(March 2014): 300-306.
- Chiangmai Provincial Office, 2020. Report on the results of driving Thailand together. Retrieved March 8, 2023, from: [https://www.chiangmai.go.th/thaitogether/assets/pdf/3\\_3.pdf](https://www.chiangmai.go.th/thaitogether/assets/pdf/3_3.pdf)
- Chiangmai Provincial Office, 2020. Summary of Chiangmai province 2020. Retrieved February 27, 2023, from <http://chiangmai.go.th/managing/public/D8/8D17Jan2022133138.pdf>
- Chiangmai Provincial Smog and Forest Fire Problem Solving Command Center, 2019. Report on work to solve smog and forest fire problems in Chiang Mai Province. Retrieved January 20, 2023, from <https://chiangmai.mnre.go.th/>
- Duan, Y., Duan, L., Wang, J. and Anthony, E.J., 2019. Observation on simultaneously low CO, NOx and SO<sub>2</sub> emission during Oxy-coal combustion in a pressurized fluidized bed. *Fuel*, 242: 374-381.
- Dung, N.A., Son, D.H., Hanh, N.T.D. and Tri, D.Q., 2019. Effect of meteorological factors on PM10 concentration in Hanoi, Vietnam. *Journal of Geoscience and Environment Protection*, 7(11): 138-150.
- Ebi, K.L., Vanos, J., Baldwin, J.W., Bell, J.E., Hondula, D.M., Errett, N.A., Hayes, K., Reid, C.E., Saha, S., Spector, J. and Berry, P., 2021. Extreme weather and climate change: Population health and health system implications. *Annual Review of Public Health*, 42(1): 293-315.
- EPA, 2023. Trends in ozone adjusted for weather conditions. Retrieved February 2, 2023, from <https://www.epa.gov/air-trends/trends-ozone-adjusted-weather-conditions>
- Giovannini, L., Ferrero, E., Karl, T., Rotach, M.W., Staquet, C., Castelli, S.T. and Zardi, D., 2020. Atmospheric pollutant dispersion over complex terrain: Challenges and needs for improving air quality measurements and modeling. *Atmosphere*, 11(6): 1-32.
- Haleem, N., Kumar, P., Uguz, S., Jamal, Y., McMaine, J. and Yang, X., 2023. Viability of artificial rain for air pollution control: insights from natural rains and roadside sprinkling. *Atmosphere*, 14(1714): 1-18.
- Han, S., 2011. Analysis of the relationship between O<sub>3</sub>, NO and NO<sub>2</sub> in Tianjin, China. *Aerosol and Air Quality Research*, 11(2): 128-139.
- Jeensorn, T., Apichartwivat, P. and Jinsart, W., 2018. PM10 and PM2.5 from haze smog and visibility effect in Chiang Mai province Thailand. *Applied Environmental Research*, 40(3): 1-10.
- Kalisa, E., Fadlallah, S., Amani, M., Nahayo, L. and Habiyaemye, G., 2018. Temperature and air pollution relationship during heat waves in Birmingham, UK. *Sustainable Cities and Society*, 43: 111-120.
- Kawichai, S., Prapamontol, T., Cao, F., Song, W. and Zhang, Y., 2022. Source identification of PM2.5 during a smoke haze period in Chiang Mai, Thailand, using stable carbon and nitrogen isotopes. *Atmosphere*, 13(7): 1-12.
- Kraisitititkul, P., Thepnuan, D., Chansuebsri, S., Yabueng, N., Wirinya, W., Saksakulkrai, S., Shi, Z. and Chantara, S., 2024. Contrasting compositions of PM2.5 in Northern Thailand during La Niña (2017) and El Niño (2019) years. *Journal of Environmental Sciences*, 135: 585-599.
- Lee, S., Lee, S.J., Kang, J.H. and Jang, E.S., 2021. Spatial and temporal variations in atmospheric ventilation index coupled with particulate matter concentration in South Korea. *Sustainability*, 13(16): 1-13.

- Liu, Y., Zhou, Y. and Lu, J., 2020. Exploring the relationship between air pollution and meteorological conditions in China under environmental governance. *Scientific Reports*, 10(14518): 1-11.
- Manager online, 2019. Increasing mobilize vehicles to spray water all over Chiang Mai for moisture increasing to reduce smog and dust. Retrieved February 25, 2023, from <https://mgronline.com/local/detail/9620000018351>
- NASA, 1997. Chemical kinetics and photochemical data for use in stratospheric modeling. Jet Propulsion Laboratory, California Institute of Technology, Pasadena, California.
- Office of Natural Resources and Environmental Policy and Planning, 2023. Report on average rainfall volume indicator (2556-2565). Retrieved February 26, 2023, from [http://env\\_data.onep.go.th/reports/subject/view/167](http://env_data.onep.go.th/reports/subject/view/167)
- Pan, Y.P., Zhu, X.Y., Tian, S.L., Wang, L.L., Zhang, G.Z. and Zhou, Y.B., 2017. Wet deposition and scavenging ratio of air pollutants during an extreme rainstorm in the North China Plain. *Atmospheric and Oceanic Science Letters*, 10(5): 348-353.
- Pardthaisonga, L., Sin-ampol, P., Suwanpravit, C. and Charoenpanyanet, A., 2018. Haze pollution in Chiang Mai, Thailand: A road to resilience. *Procedia Engineering*, 212: 85-92.
- Pollution Control Department, 2023. Ministry of Natural Resources and Environment. Retrieved February 22, 2023, from <http://air4thai.pcd.go.th/webV2/download.php>
- Pothirat, C., 2016. Effects of seasonal smog on asthma and COPD exacerbations requiring emergency visits in Chiang Mai, Thailand. *Asian Pacific Journal of Allergy and Immunology*, 34(4): 1-6.
- Royal Forest Department, 2023. Forest area by type and province between 2008 and 2018. Retrieved February 2, 2023, from <https://forestinfo.forest.go.th/Content.aspx?id=80>
- Solanki, R., Macatangay, R., Sakulsupich, V., Sonkaew, T. and Mahapatra, P.S., 2019. Mixing layer height retrievals from mini MPL measurements in the Chiang Mai valley: Implications for particulate matter pollution. *Frontiers in Earth Science*, 7(308): 1-12.
- Song, Y. and Min, S., 2023. Impacts of complex terrain features on local wind field and PM<sub>2.5</sub> concentration. *Atmosphere*, 14(5): 1-14.
- South Carolina Department of Health and Environmental Control, 2023. Retrieved January 5, 2023, from <https://scdhec.gov/sites/default/files/Library/CR-008071.pdf>
- Thai Meteorological Department, 2023. The average temperature and rainfall volume 2006 - 2022. Retrieved February 23, 2023, from <https://www.tmd.go.th/service/tmdData>
- Thao, N.N.L., Pimonsree, S., Prueksakorn, K., Thao, P.T.B. and Vongruang, P., 2022. Public health and economic impact assessment of PM<sub>2.5</sub> from open biomass burning over countries in mainland Southeast Asia during the smog episode. *Atmospheric Pollution Research*, 13(6): 101418.
- The Public Relations Department, 2023. The seasons of Thailand. Retrieved February 2, 2023, from [https://thailand.go.th/issue-focus-detail/009\\_142](https://thailand.go.th/issue-focus-detail/009_142)
- UK Air Pollution Information System, 2023. Retrieved February 22, 2023, from [https://www.apis.ac.uk/overview/pollutants/overview\\_o3.htm](https://www.apis.ac.uk/overview/pollutants/overview_o3.htm)
- Yodsurang, P., Kiatthanawat, A., Sanoamuang, P., Kraseain, A. and Pinijvarasin, 2022. Community-based tourism and heritage consumption in Thailand: An upside-down classification based on heritage consumption. *Cogent Social Sciences*, 8(1): 1-20.

---

#### ORCID DETAILS OF THE AUTHORS

- Piyavadee Srivichai: <https://orcid.org/0000-0002-6762-5465>  
Chumaporn Rodsrida: <https://orcid.org/0000-0002-2752-3245>  
Patipat Vongruang: <https://orcid.org/0000-0002-7628-7285>







# Environmental Awareness Toward Issues and Challenges of Sustainable Consumerism in the Indian Apparel Industry

Shivani Jadhav† and Asha Verma

Gujarat National Law University, Gandhinagar, Gujarat, India

†Corresponding author: Shivani Jadhav; shivaniphd202017@gnlu.ac.in

**Nat. Env. & Poll. Tech.**  
Website: [www.neptjournal.com](http://www.neptjournal.com)

Received: 23-02-2024  
Revised: 01-04-2024  
Accepted: 03-04-2024

## Key Words:

Environmental awareness  
Sustainable consumption  
Apparel industry  
Consumerism  
Green supply chain

## ABSTRACT

This confirmatory study focused on studying the attitude and behavior as well as environmental awareness towards sustainable consumerism. The study also aimed to check if accountability on the part of brands and the government could enhance sustainability in the apparel industry. An empirical inquiry was conducted with 396 respondents, considering they are consumers with purchasing power. The collected data were analyzed using correlation and descriptive analysis. Based on the findings, consumers' apparel use and brand accountability are positively associated. At the same time, it was found that the attitude and behavior of consumers are the least essential determinants for sustainable apparel consumption. This might imply that their optimistic outlook may not always translate into real purchase behavior, which is consistent with earlier studies. The results of this research provide a foundation for a better comprehension of the many factors, including the sustainability of a clothing brand or product, which may affect consumer behavior. This approach could help the fashion industry develop practical strategies and alter how people think about and utilize apparel in the future.

## INTRODUCTION

Environmental degradation is one of the key global concerns that has gained importance over recent years. It is a direct and indirect consequence of human activities such as industrialization and urbanization. The media repeatedly covers news of pollution, deforestation, and depletion of natural resources. Sufficient evidence shows that human intervention causes pollution, depletion of natural resources, and environmental change (Jäger 2001). The primary contribution is done through capitalism and overconsumption. For capitalism to flourish, consumers need to keep buying more (Rogers 2007). The economic growth of any given society is linked to consumption, which results in waste generation. It wouldn't be inaccurate to state that the rapid pace of economic expansion is not sustainable (Crane 2015). It is imperative to note here that the Sustainable Development Goals were formulated by the collaborative efforts of the United Nations Department of Economic and Social Affairs to improve health, education, and economic growth while tackling climate change (The 17 Goals | Sustainable Development, n.d.). The latest step in that direction is the Conference of the Parties (COP27) 2022 to the United Nations Framework Convention on Climate Change (UNFCCC), where deliberations were made on what can be done to slow down climate change (United Nations Climate Change n.d.).

The climate crisis is getting worse by the day. Ignoring the crisis is no longer an option for the global community. However, the global community is not treating the climate catastrophe as seriously as it should be since it is developing gradually (Lawrenz et al. 2021). Management of the garbage accumulating as a result of consumerism, population increase, and the existing linear economic paradigm. The linear economic model is based on the formula of take, make, and dispose (Nadazdi et al. 2022). It essentially means manufacturing products and discarding them at the end of their life cycle, where there is negligible or no scope to recycle or reuse. This directly leads to the rapid depletion of natural resources. However, as opposed to this model, the circular economy has an environmentally friendly approach to maximize the use of natural resources. The circular economy is a model that is more resource-efficient and an economic model that should be given greater importance (Didenko et al. 2018).

The linear model entails introducing and pushing products in the consumer market through the means of hypermarketing. This is done to constantly change market trends as well as to drive new trends. Marketing-driven consumer behavior and buying patterns lead to consumerism, where consumers buy more than needed. The primary victims are urban, environmentally unaware consumers who, when it comes to waste management, believe in out of sight and out of

mind (Hojnik et al. 2020). The urban population is detached and blinded from the realities of the effects of their buying patterns, which are highly unsustainable. However, there has been an increase in green initiatives directly proportional to the increasing evidence of environmental degradation. Overconsumption and its negative effects, like huge volumes of waste generation, make a strong case for moving towards a circular economy. The fundamental characteristics of a circular economy are based on sustainability in both its consumption and production patterns. However, there continues to be no empirical evidence to back up the notion that moving from a linear model to a circular economy will have positive economic effects (Lobova & Tyryshkin 2021).

Traditionally, societies did not face the problem of dealing with oversupply as is witnessed currently. But at present, it is prevalent in modern societies. A dissection of the concept of Sustainable Consumerism can help extract its true meaning. It is notably the current topic of discussion for policymakers at both national and international levels, by news agencies, and even in academic research (Diprose et al. 2017). At the same time, numerous meanings and definitions are attributed to the concept. The development of the concept can be traced back to the year 1987 when the Brundtland Report was published. One of the first definitions was given in 1983 by the Brundtland Commission or the World Commission on Environment and Development (WCED), United Nations. It was defined as the development that meets the needs of the present generation without compromising the ability of future generations to meet their needs (Thomsen 2013). Sustainability can be achieved when economic growth, environmental protection, and social justice operate harmoniously (Diprose et al. 2017). This is aimed to be achieved through a global partnership using the 17 sustainable development goals.

The pattern where consumers are fixated on buying and owning more than necessary can be understood as consumerism (Cooper 2000). When such practices are prevalent, it leads to mindless mass production, thereby necessitating extraction of resources which then ends up harming the environment seriously. As rightly asserted by Rothman (1998), consumption patterns drive and dictate the quantum of production. Therefore, if the demand for unsustainable apparel reduces, it will directly affect and reduce mass production (Jain & Jain 2019). Sustainable consumption is meeting demands with high-quality goods without endangering the environment. In other words, the least hazardous and least harmful products are those that emit the least amount of carbon dioxide or other pollutants. These products are made mostly of natural materials and have the least negative effects on the environment. Sustainable consumption is often referred to as “green

consumption” (Khalil et al. 2021). Consumerism as a concept, on the other hand, has been attributed to more than one and contrasting meanings that have evolved over a long period. The original definition given by Nelson (2008) talks about manipulative advertising and marketing encouraging consumers to consume more. In 2008 scholars defined it as a consumer movement to protect their rights against excessive marketing (Diprose et al. 2017). Lastly, Murphy (2000) interpreted consumerism as a consumer ideology through which customers may obtain happiness and well-being via purchases. One meaning can be seen as being in favor of the rights and interests of consumers. In contrast, the other is seen as being advantageous for companies while being against both those of consumers and society at large (Idowu et al. 2013). It is essential to realize that the notion of sustainability and the long-term repercussions of consumption are in direct opposition to one another (Jones et al. 2005).

The article aims to investigate the necessity of sustainable consumption on a global scale and its operation in the Indian context. The researcher wants to learn more about how selected consumers perceive and are aware of sustainable consumerism. To further understand their consumerism, ecological awareness, and business expectations, their replies will be analyzed. The framework of the paper has covered the introductory comments and an extensive review of the literature first, followed by a doctrinal inquiry. The research will be anchored on the empirical study conducted. The paper concludes with conclusive comments, suggestions based on data analysis, and a discussion of the scope of further research.

## MATERIALS AND METHODS

### Environmental Awareness

The degree of widespread knowledge of the advantages of green products can influence consumer purchase behavior. Consumers’ view of the value they obtain from a product rises as environmental issues become more widely known. A “green product” is typically made from natural components, recyclable materials, and permitted chemicals. Additionally, it often isn’t toxic, can be recycled or used again, isn’t subjected to animal testing, doesn’t cause pollution, and isn’t excessively packed. Companies started creating environmentally friendly or “green” items as well as green product policies to sway customers’ purchasing decisions as the hazardous substance of products started to be a problem. When choosing a green product, shoppers base their selection on price. Cost increases on green items deter consumers from buying them. All products supplied should be ecologically sustainable without sacrificing quality or paying more for it.

Consumers who practice ethical consumerism have recently raised many concerns about social and ethical issues, including labor legislation, environmental development, and human rights (Anderson & Cunningham 1972). Customers exercise ethical consumerism, or the act of taking into account interests other than their immediate self-interest, when making purchases (Grand et al. 2021). The topic of environmental deterioration has drawn more attention and discussion. The issue has attracted traction from stakeholders like governments, companies, consumers, researchers, and so on. The awareness of environmental problems around and globally impacts an individual's life in multifarious ways. One such impact can be felt in the buying patterns of an individual. An environmentally concerned consumer will ascertain the effect that their consumption will have, as opposed to an unaware consumer. Green knowledge involves what a consumer knows about environmental degradation and has an awareness of what can be possible ways or solutions to resolve it (Apaydin & Szczepaniak 2017). Initiatives to spread awareness about the harmful effects of the apparel industry on the environment play a significant role in promoting sustainable development. It also promotes the approach of diverting society from sustainable consumerism to sustainable consumption. Celebration of days as a tool is used to enhance environmental awareness among consumers, where each year, a theme is celebrated worldwide. Sustainable fashion is one of the agendas under the Earth Day celebration across the world to spread awareness about the destructive effects of the apparel industry (Earth Day 2023). Water pollution from textile factories, lack of expert collaboration for innovation and technology, wastewater generated from chemicals and microfibers, apparel industry-induced water scarcity, and waste generation from a linear economy are concerns that require urgent attention. Like-minded and socially driven individuals often come together to form advocacy groups or environmental non-governmental organizations to draw attention to these pressing issues. Advocacy groups such as Cotton Diaries, Conscious Fashion and Lifestyle Network, Drip by Drip, Earth Logic, and Ellen MacArthur Foundation work in multiple lanes of the apparel industry to highlight concerns. Another impactful awareness tool is social media. Brands communicate, influence, and interact with their consumers through social media on sustainability aspects of apparel. They educate the consumers on the benefits of sustainable clothing, share consumption practices, and build trust based on brand reviews (Son et al. 2022). Hence, the researcher proposes:

### **Positive Impact of Environmental Awareness on Consumer Intentions**

**Attitude and behavior:** A consumer's attitude impacts their

behavior directly, especially so in the case of environmental behavior (Ertz et al. 2016). Attitude toward sustainable purchasing is defined as "the consumer's cognitive evaluation of sustainable purchase behavior; it includes consumer attitude toward green and fair purchasing" (Lee 2014). Pro-environmental behavior has been defined as "behavior that harms the environment as little as possible or even benefits the environment" (Steg & Vlek 2009). The attitude and behavior of a consumer can be assessed through multiple indicators such as frequency of purchasing apparel, placing importance on the sustainability of clothes being bought, and recycling or reusing habits. Literature on the topic reflects that inquiries have been made to understand the economic factors involved in consuming sustainably. As eco-friendly apparel is more expensive than its polluting counterpart, consumers willing to buy a sustainable item have to shell out an additional amount. Thus, attracting younger, more educated, and wealthier consumers. Consumers buying more than is required and their higher frequency has been seen as one of the reasons for numerous environmental problems. Consumers are choosing greener options as they grow more environmentally conscious every day. They frequently wear clothing that can be recycled and used repeatedly. At the same time, literature shows that there is a high prevalence of consumers buying fast fashion apparel. Consumers accept the changing trends in the market and so India has seen a surge in the fast fashion industry (Bhattacharjee & Chanda 2022). Buying behavior, like checking whether a particular apparel is made or produced from a sustainable material before buying, also determines the consumer's attitude towards sustainable consumption.

### **Impact of Sustainable Attitudes and Behaviors on Consumer Intentions**

**Accountability:** Instead of placing the onus on consumers to reduce their consumption, the approach for promoting sustainable consumption should be shifted towards the power-possessing stakeholders. Multinational corporations, governments, and retailers are seen to be held accountable for their carbon footprints. Their carbon footprint is evaluated by looking at the shipping, packaging, and raw material sourcing processes (Carbone & Moatti 2011). The question of whether the supply chains are sustainable and green has also been raised. The term "greenwashing" or "misleading marketing of the actions taken and alleged by garment firms" is used to describe this behavior (Marcatajo 2021). Having a sustainable supply chain is considered to be a sort of green communication without any significant or genuine green activity. When it comes specifically to the Indian jurisdiction, certain quality assurance labels have been in place, like the Indian Standards Institution (ISI), Bureau of Indian Standards

(BIS), and Agmark. The Government of India has set these out. These have been successfully adopted into the consumer consciousness through sufficient promotion by government-led advertisements. A step in the same direction was taken by the government by introducing the Eco mark, which has not been adequately promoted, leading to no awareness about it among consumers (Jaiswal et al. 2021). Such labeling can make apparel companies accountable as well as simultaneously increase market demand for sustainable clothing. From the government's perspective, a suggested model is to intensify punitive measures for entities that violate environmental policies as well as frequently check compliance and supervise. Thinking from the corporations' perspective, extended access to the latest science, technology, and innovation can help in addition to maintaining a top-to-bottom green supply chain (Awaga et al. 2020). Sustainable Fashion Brands is another way the corporations can be held accountable. They can do this through the use of eco-friendly raw materials, have a low or less carbon footprint, and quality production of apparel. However, 'sustainable fashion' as a term is seen as an oxymoron by scholars. This is due to the preliminary meaning attributed to fashion, which is in and out frequently. Nature in itself is not being long-term. Sustainability is synonymous with long-term use. And so, despite the huge environmental impacts of the industry, it keeps growing in the form of fast fashion as it offers clothing that is produced cheaply, used frequently, and only in trend for a brief time (Mandarić et al. 2022).

### **Brand Accountability and Its Influence on Sustainable Consumption Intentions**

**Consumption intention:** Purchase intention can be defined as a person's location on a subjective probability dimension involving a relationship between himself and some action, as researched by Fishbein & Ajzen (1975). However, there are plenty of papers that established that a person's buying behavior might change depending upon the brand, alternatives, environment of the store, etc., as observed by Jing. One of the crucial topics covered in the marketing sector of a company is the choice to buy. The strongest association is with purchasing habits. A variety of brand attributes significantly influences the customer's intention to buy.

Nominated subjective standards (beliefs about what others consider to be right or wrong), behavioral patterns (beliefs about the results of a behavior), and perceived behavioral control (beliefs about one's ability to control one's behavior) all have an impact on one's intention to consume (Ajzen 1985). As previously said, a consumer's mindset will affect whether they plan to buy sustainable clothing. This intention can be said to cause damage or harm as minimal as possible to the environment, which culminates

in sustainable consumption after the consumer buys the product. The consumer's desire to buy eco-friendly goods is a strong indicator of how they feel about the items and how much they respect the environment (Vazifehdoust et al. 2013). Consumption intention determines a consumer's ability to choose eco-friendly apparel over its polluting and cheap counterparts.

### **Significant Impact of Consumer Intentions on Sustainable Consumption**

**Sustainable consumption:** Consumer behavior needs to be observed to extract the reason behind it. The values and ethics of consumers play a major role when they make sustainable choices. The association of the term sustainable consumption with apparel has been a recent phenomenon (Kim & Damhorst 1998). The association has been a result of discussions on the harmful effects of the apparel industry on the environment. Sustainable consumption has been attributed numerous meanings, such as societal, environmental, responsible business practices, and even financial (Ha-Brookshire & Norum 2011). Commitment by the apparel industry and showcasing the same in the right way can thus result in short-term and long-term success. If done skillfully, these sustainability-related messages can help establish a positive brand name. This would, in turn, contribute to the decision-making of the consumer. It, therefore, becomes imperative to understand the consumption intention behind a consumer's choices to advocate sustainable consumption.

### **Consumer Product Choices Driving Sustainable Consumption Intentions**

The research approach employed in this study is quantitative, combining both doctrinal and non-doctrinal research methods. Primary data were collected through empirical means, while secondary data were reviewed from scholarly articles, reports, and reliable internet sources to supplement the primary data. The research is exploratory and aimed at studying a new and emerging phenomenon (Khalil et al. 2021). The scope of this research in the doctrinal as well as non-doctrinal aspects has been demarcated. The scope of the non-doctrinal study is focused firstly on evaluating the awareness of the respondents about the environmental impacts of their buying patterns and choices. Secondly, it analyses the general attitude and behavior of the consumers towards their apparel consumption and if the same are sustainable in nature. Thirdly, the study seeks to understand if accountability on the part of the government and apparel industry would promote sustainable buying practices. Fourthly, the study seeks to understand consumers' consumption intentions. Lastly, to check the respondents' general understanding of what constitutes sustainable consumerism.

As the study is conducted to understand the determinants



of the consumption intention of consumers at large and if their buying practices are sustainable, the respondents are consumers above the age of 18. Respondents have been categorized into students, employed individuals, businesspersons, and an 'other' category, which includes homemakers, unemployed persons, and so on. Due to time and budget constraints, and given the topic's public relevance and everyday significance, the researcher opted for a convenience non-probability sampling method. The study focuses on individuals as the sampling unit rather than institutions or groups. The sampling universe consists of consumers who purchase clothing items and have at least a high school education. The sample size collected was 396, which is suitable for behavioral studies (Roscoe 1975). The sampling error has been decided to be of 95% confidence with a 5% variation. The respondents were part of the research by circulating a questionnaire among consumers. A questionnaire in the form of a Google Form was used as the tool for data collection to ensure higher participation. The questionnaire method was used to reach the maximum number of respondents. The method of sampling was chosen keeping in mind the accessibility of respondents. It was administered to respondents through electronic means. No personal information was collected. This made it easier for both the researcher and the respondent to collect data.

## RESULTS AND DISCUSSION

The data collected in this study was statistically tested and analyzed with the help of the Statistical Program for Social Sciences (SPSS) and Amos software. The questionnaire used for the research was standardized, as has been evidenced in Table 1 which elaborates in detail with respect to individual variables.

The sampling demographic included both males and females from age 18 to 56 and above. The majority, i.e., 64 percent of the respondents, were female, while 46 percent of respondents were from the age group of 26 to 35. 50 percent of the respondents were employed. The selected respondents were essential to the study as they are consumers of apparel. The respondents were consumers with the buying capacity in the mentioned age bracket (Table 2).

In the first step, confirmatory factor analysis was conducted to evaluate whether respondents answered according to the intended questions and to check if the items measured the constructs they were meant to assess. In other words, the analysis confirmed the reliability and validity of the standardized instrument adopted by the researcher. The means of the items ranged from 2 to 4, with standard deviations ranging from 0.7 to 1.4. The relatively low standard deviations indicate that the responses are closely

Table 1: Measurement Constructs.

Items	Variable	Author
	<i>Environmental Awareness</i>	Lin Zhang et al. (2018)
EA1	The apparel (clothing) industry generates tonnes of waste, which harms the environment.	
EA2	Water pollution is caused because of the dyeing and manufacturing process of clothes.	
EA3	Apparel manufacturing is responsible for a high carbon footprint.	
	<i>Attitude and Behavior</i>	Al-Kumaim, N.H. et al. (2021)
AB1	How often do you buy clothes?	
AB2	How often do you check whether the clothing item you buy is eco-friendly?	
AB3	How often do you donate clothes?	
	<i>Accountability</i>	Khalil (2021)
AC1	Will you buy clothing items that have Eco-friendly Labels?	
AC2	Will you buy clothing items that have the same price as eco-friendly and unsustainable items?	
AC3	Will you buy clothing items that have been produced by a sustainable clothing brand?	
	<i>Consumption Intention</i>	Omar (2022)
CI1	Do you buy clothing materials that are less polluting for the environment?	
CI2	Do you switch from your current brand to a sustainable clothing brand?	
CI3	Do you use second-hand clothing or thrift shops?	
	<i>Sustainable Consumerism</i>	Deepak Jaiswala & Rishi Kant (2018)
SC1	Sustainable Consumerism is rejecting apparel that is not sustainably produced.	
SC2	Sustainable Consumerism is reducing the frequency of buying apparel.	
SC3	Sustainable Consumerism is reusing apparel rather than using it once and dumping it.	

Table 2: Demographics.

S. No.	Classification	Category	Frequency	[%]
1.	Age	18 – 25	178	44.9
		26 – 35	182	46.0
		36 – 45	16	4.0
		46 – 55	18	4.5
		56 and above	2	0.5
2.	Gender	Female	254	64.1
		Male	142	35.9
3.	Designation	Student	158	39.9
		Employed	200	50.5
		Unemployed	8	2.0
		Business	28	7.1
		Other	2	0.5

clustered, suggesting the collected data is reliable. The average variance extracted (AVE) is benchmarked at 0.5, while 0.7 is regarded as considerably good (Hair et al. 2010). The average variance extracted (AVE) for the variables ranges between 0.5 to 0.6, and hence, the reliability can be said to be as per the benchmark. Composite reliability (CR) has a minimum benchmark of 0.7. Each of the variables is above the specified value, so we can consider them valid according to the thumb rule of at least 0.5 and 0.7, respectively. The benchmark for Cronbach's  $\alpha$  is 0.7, and all the collected responses indicated values higher than this benchmark. Hence, it can be concluded that all the variables

Table 3: Psychometric properties of measures.

Constructs	Items	Factor Loading	Mean	SD	Average variance extracted (AVE)	Composite reliability (CR)
Environmental Awareness	EA1	0.573	3.41	1.281	0.533	0.799
	EA2	0.553	3.70	1.252		
	EA3	0.604	3.16	1.396		
Attitude and Behavior	AB1	0.566	3.38	0.762	0.654	0.716
	AB2	0.522	2.20	1.074		
	AB3	0.686	3.67	1.055		
Accountability	AC1	0.681	3.90	0.866	0.641	0.702
	AC2	0.696	3.94	1.004		
	AC3	0.614	4.09	0.876		
Consumption Intention	CI1	0.553	3.58	1.037	0.522	0.765
	CI2	0.685	3.82	0.935		
	CI3	0.653	2.76	1.317		
Sustainable Consumerism	SC1	0.614	3.48	0.910	0.548	0.722
	SC2	0.604	3.16	1.396		
	SC3	0.553	3.58	1.037		

possess a good degree of internal consistency, and hence, the collected data analysis is reliable (Table 3).

The Kaiser-Meyer-Olkin (KMO) test helps the researcher measure and understand if the data collected is suitable for factor analysis. In other words, it indicates sampling adequacy. Where the test reflects a value less than 0.5, it is considered that the sample is inadequate for factor analysis. For the data collected in the current study, the values reflected are more than the benchmark and are suitable for factor analysis (Table 4).

Lastly, the structural model (Fig. 1) was created and analyzed using Amos software which indicated the model to be valid and whether the hypotheses were supported. Hypothesis 1, 3, and 4 were found to be supported according to analysis, while hypothesis 2 was rejected.

## CONCLUSIONS

The effects of the apparel industry's supply chain operations on the environment are being examined more and more closely. The apparel sector is perpetually growing even after its well-known detrimental impacts on the environment. Reasons range from the emergence of fast fashion, which involves low-cost production from developing countries, frequent consumption, and apparel usage as per constantly changing trends. Sustainable consumption is more than simply a fad; it requires accountability from apparel manufacturers and considers the "price" paid for it in terms of social, environmental, and economic factors. The opposite

Table 4: Discriminant validity.

Constructs	KMO	EA	AB	CI	AC
EA	0.727	0.730			
AB	0.749	0.239**	0.809		
CI	0.735	0.260**	0.345**	0.722	
AC	0.735	0.176**	0.208**	0.382**	0.838
SC	0.742	0.236**	0.129*	0.374**	0.314**

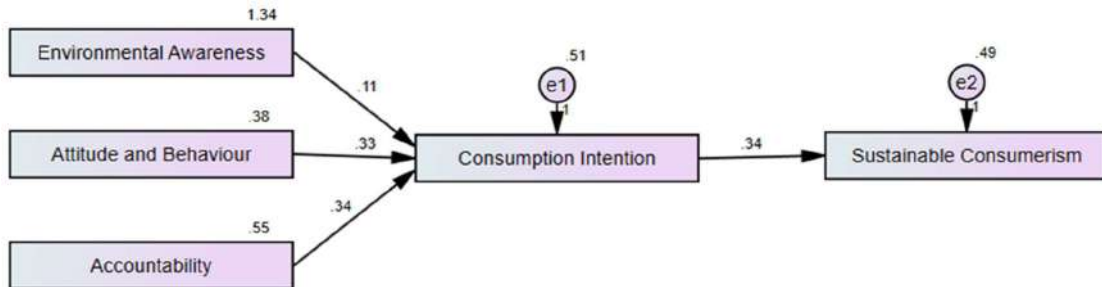


Fig. 1: Structural equation modeling.

of sustainable or slow fashion is fast fashion, which is a predominant production strategy in the fashion industry. Fast fashion retailers harm the planet by, among other things, using plastic fibers in a large percentage of the clothing they produce. Additionally, it has been stated that one garbage truck's worth of clothing is thrown away or burned every second. When textiles are washed, microfibers are created, and these microfibers end up in the ocean. These facts indicate that the apparel sector significantly contributes to environmental degradation. The influence of the industry is anticipated to increase as well since it is expanding, evolving, and responding to both market demand and fashion trends. Due to this, it is important to reduce how badly supply chains influence society and the environment, boost the dedication of garment companies to ethical business practices, and increase customer awareness of the repercussions of excessive purchases. In addition to harming the environment, the emergence of fast fashion, which is associated with low-cost production and the procurement of materials from overseas industrial markets, has changed consumer views on the purchase of clothing. As a result, the fashion industry has developed a culture of impulsive purchasing because the typical customer may purchase new clothing every week. Consumers need to understand the differences between the negative consequences of fast and affordable fashion and the positive concerns for environmental sustainability. This is the trick to altering consumer habits and behavior. The same has been mirrored in the current study's hypotheses. The current study confirms that brand accountability has a positive impact on furthering sustainable consumerism.

It adds to the existing literature which can help fashion brands see the financial benefits of a green supply chain and accordingly develop action plans.

The current study's findings are in line with other studies which have concluded that generally speaking, consumers make purchases without giving much thought and attention to how their choices would affect the environment. According to consumer responses, they place little to no importance on environmental considerations while shopping. However, respondents showed a willingness to buy sustainable apparel if labels indicate a carbon footprint or eco-friendly material. This can be further accelerated through advertising by sustainable fashion brands, increasing awareness among consumers as well as their profits. Willingness to pay for sustainable apparel was also found to be higher when the price was lesser or equivalent to its unsustainable counterpart. Further, it may be deduced that consumers who use sustainable apparel frequently do not have favorable opinions about sustainable fashion. To meet these demands, the apparel industry should identify additional customer priorities like pricing, durability, and quality to modify their advertising strategy. A new viewpoint and understanding are needed for the entire system to adopt a sustainable business model, which necessitates innovation and engagement between designers, manufacturers, relevant parties, and end users. To determine how to support sustainable behavior, extensive research is needed. To recapitulate, increasing customer awareness of the benefits of buying sustainable apparel and changing consumer behavior is crucial to promoting the adoption of sustainable practices, consumer

behavior, and the market share of sustainable fashion brands.

## REFERENCES

- Ajzen, I., 1985. From intentions to actions: a theory of planned behavior. In *Springer eBooks*, pp.11-39. [https://doi.org/10.1007/978-3-642-69746-3\\_2](https://doi.org/10.1007/978-3-642-69746-3_2)
- Al-Kumaim, N.H., Alhazmi, A.K., Mohammed, F., Gazem, N.A., Shabbir, M.S. and Fazea, Y., 2021. Exploring the impact of the COVID-19 pandemic on university students' learning life: An integrated conceptual motivational model for sustainable and healthy online learning. *Sustainability*, 13(5), p.2546. doi:10.3390/su13052546
- Anderson, W.T. and Cunningham, W.H., 1972. The socially conscious consumer. *Journal of Marketing*, 36(3), pp.23. <https://doi.org/10.2307/1251036>
- Apaydin, F. and Szczepaniak, M., 2017. Analyzing the profile and purchase intentions of green consumers in Poland. *Ekonomika*, 96(1), pp.93-112. <https://doi.org/10.15388/ekon.2017.1.10666>
- Awaga, A., Xu, W., Liu, L. and Zhang, Y., 2020. Evolutionary game of green manufacturing mode of enterprises under the influence of government reward and punishment. *Advances in Production Engineering & Management*, 15(4), pp.416-430. <https://doi.org/10.14743/apem2020.4.375>
- Bhattacharjee, A. and Chanda, R., 2022. Psychology of consumer: study of factors influencing buying behavior of millennials towards fast-fashion brands. *CARDIOMETRY*, 23, pp.360-368. <https://doi.org/10.18137/cardiometry.2022.23.360-368>
- Carbone, V. and Moatti, V., 2011. Towards greener supply chains: an institutional perspective. *International Journal of Logistics*, 14(3), pp.179-197. <https://doi.org/10.1080/13675567.2011.609160>
- Cooper, T., 2000. Product development implications of sustainable consumption. *Design Journal*, 3(2), pp.46-57. <https://doi.org/10.2752/146069200789390150>
- Crane, D., 2015. Environmental change and the future of consumption: implications for consumer identity. *Anuario Filosófico*, 353, pp.1394. <https://doi.org/10.15581/009.43.1394>
- Didenko, N.I., Klochkov, Y.S. and Skripnuk, D.F., 2018. Ecological criteria for comparing linear and circular economies. *Resources*, 7(3), p.48. <https://doi.org/10.3390/resources7030048>
- Diprose, K., Fern, R., Vanderbeck, R.M., Chen, L., Valentine, G., Liu, C. and McQuaid, K., 2017. Corporations, consumerism and culpability: sustainability in the British press. *Environmental Communication-a Journal of Nature and Culture*, 12(5), pp.672-685. <https://doi.org/10.1080/17524032.2017.1400455>
- Earth Day, 2023. Earth Day 2023 - Earth Day. *Earth Day*. <https://www.earthday.org/earth-day-2023/>
- Ertz, M., Karakas, F. and Sarigöllü, E., 2016. Exploring pro-environmental behaviors of consumers: an analysis of contextual factors, attitude, and behaviors. *Journal of Business Research*, 69(10), pp.3971-3980. <https://doi.org/10.1016/j.jbusres.2016.06.010>
- Fishbein, M. and Ajzen, I., 1977. Belief, attitude, intention, and behavior: An introduction to theory and research.
- Grand, J.L., Roberts, J. and Chandra, G., 2021. Buying for good: altruism, ethical consumerism and social policy. *Social Policy & Administration*, 55(7), pp.1341-1355. <https://doi.org/10.1111/spol.12729>
- Ha-Brookshire, J. and Norum, P.S., 2011. Willingness to pay for socially responsible products: case of cotton apparel. *Journal of Consumer Marketing*, 28(5), pp.344-353. <https://doi.org/10.1108/07363761111149992c>
- Hair, J.F., Black, W., Babin, B.J. and Anderson, R.E., 2010. *Multivariate Data Analysis: A Global Perspective*. Pearson
- Hojnik, J., Ruzzier, M. and Manolova, T.S., 2020. Sustainable development: Predictors of green consumerism in Slovenia. *Corporate Social Responsibility and Environmental Management*, 27(4), pp.1695-1708. <https://doi.org/10.1002/csr.1917>
- Idowu, S.O., Capaldi, N., Zu, L. and Das Gupta, A., 2013. *Encyclopedia of corporate social responsibility*. Springer. <https://doi.org/10.1007/978-3-642-28036-8>
- Jäger, J., 2001. Global Environmental Change: human dimensions. *Elsevier eBooks*, pp.6227-6232. <https://doi.org/10.1016/b0-08-043076-7/04137-1>
- Jain, P. and Jain, P., 2019. Ensuring sustainable development by curbing consumerism: An eco-spiritual perspective. *Sustainable Development*, 27(3), pp.474-480. <https://doi.org/10.1002/sd.1935>
- Jaiswal, D. and Kant, R., 2018. Green purchasing behaviour: A conceptual framework and empirical investigation of Indian consumers. *Journal of Retailing and Consumer Services*, 41, pp.60-69.
- Jaiswal, D., Singh, B., Kant, R. and Biswas, A., 2021. Towards green product consumption: effect of green marketing stimuli and perceived environmental knowledge in Indian consumer market. *Society and Business Review*, 17(1), pp.45-65. <https://doi.org/10.1108/sbr-05-2021-0081>
- Jones, P., Hillier, D., Comfort, D. and Eastwood, I., 2005. Sustainable retailing and consumerism. *Management Research News*, 28(1), pp.34-44. <https://doi.org/10.1108/01409170510784760>
- Khalil, S., Ismail, A. and Ghalwash, S., 2021. The rise of sustainable consumerism: evidence from the Egyptian generation Z. *Sustainability*, 13(24), pp.13804. <https://doi.org/10.3390/su132413804>
- Kim, H. and Damhorst, M.L., 1998. Environmental concern and apparel consumption. *Clothing and Textiles Research Journal*, 16(3), pp.126-133. <https://doi.org/10.1177/0887302x9801600303>
- Lawrenz, S., Leiding, B., Mathiszig, M.E.A., Rausch, A., Schindler, M. and Sharma, P., 2021. Implementing the Circular Economy by Tracing the Sustainable Impact. *International Journal of Environmental Research and Public Health*, 18(21), pp.11316. <http://dx.doi.org/10.3390/ijerph182111316>
- Lee, K., 2014. Predictors of sustainable consumption among young educated consumers in Hong Kong. *Journal of International Consumer Marketing*, 26(3), pp.217-238. <https://doi.org/10.1080/08961530.2014.900249>
- Lobova, S.V. and Tyryshkin, V.V., 2021. Is it possible to change to a circular economy based on waste recycling? An overview of the situation, opportunities, and barriers for the Altai Krai. *IOP Conference Series: Earth and Environmental Science*, 670(1), p.12060. <https://doi.org/10.1088/1755-1315/670/1/012060>
- Mandarić, D., Hunjet, A. and Vuković, D., 2022. The impact of fashion brand sustainability on consumer purchasing decisions. *Journal of Risk and Financial Management*, 15(4), pp.176. <https://doi.org/10.3390/jrfm15040176>
- Marcatajo, G., 2021. Green claims, green washing, and consumer protection in the European Union. *Journal of Financial Crime*, 30(1), pp.143-153. <https://doi.org/10.1108/jfc-11-2021-0240>
- Murphy, P.L., 2000. The Commodified Self in Consumer Culture: A Cross-Cultural Perspective. *The Journal of social psychology*, 140(5), pp.636-647. doi: <https://doi.org/10.1080/00224540009600504>
- Nadazdi, A., Naunovic, Z. and Ivanisevic, N., 2022. Circular economy in construction and demolition waste management in the Western Balkans: A sustainability assessment framework. *Sustainability*, 14(2), p.871. <https://doi.org/10.3390/su14020871>
- Nelson, M.R., 2008. The hidden persuaders: Then and now. *Journal of Advertising*, 37(1), pp.113-126. doi: <http://dx.doi.org/10.2753/JOA0091-3367370109>
- Omar, Al-Dubai 2022. Green Marketing and Its Impact on Consumer Buying Behavior. *Journal of International Trade, Logistics and Law*, 8(1), <https://www.jital.org/index.php/jital/article/view/282>

- Rogers, H., 2007. Garbage Capitalism's Green Commerce. Retrieved January 15, 2023 from <https://socialistregister.com/index.php/srv/article/view/5866>
- Roscoe, J.T. 1975. *Fundamental Research Statistics for the Behavioural Sciences*, 2<sup>nd</sup> edition. New York: Holt Rinehart & Winston.
- Rothman, D.S. 1998. Environmental kuznets curves—real progress or passing the buck? *Ecological Economics*, 25(2), pp. 177–194. doi: [https://doi.org/10.1016/S0921-8009\(97\)00179-1](https://doi.org/10.1016/S0921-8009(97)00179-1)
- Son, J., Nam, C. and Diddi, S., 2022. Emotion or information: what makes consumers communicate about sustainable apparel products on social media? *Sustainability*, 14(5), pp.2849. <https://doi.org/10.3390/su14052849>
- Steg, L. and Vlek, C., 2009. Encouraging pro-environmental behavior: an integrative review and research agenda. *Journal of Environmental Psychology*, 29(3), pp.309-317. <https://doi.org/10.1016/j.jenvp.2008.10.004>
- The 17 Goals | Sustainable Development. (n.d.). <https://sdgs.un.org/goals>
- Thomsen, C., 2013. *Sustainability*. Springer, pp.2358-2363. [https://doi.org/10.1007/978-3-642-28036-8\\_531](https://doi.org/10.1007/978-3-642-28036-8_531)
- United Nations Climate Change. (n.d.). Five Key Takeaways from COP27. Retrieved January 15, 2023, from <https://unfccc.int/process-and-meetings/conferences/sharm-el-sheikh-climate-change-conference-november-2022/five-key-takeaways-from-cop27>
- Vazifehdoust, H., Taleghani, M., Esmaeilpour, F., Nazari, K. and Khadang, M., 2013. Purchasing green to become greener: factors influence consumers' green purchasing behavior. *Management Science Letters*, pp.2489-2500. <https://doi.org/10.5267/j.msl.2013.08.013>
- Zhang, L., Chen, L., Wu, Z., Zhang, S. and Song, H., 2018. Investigating young consumers' purchasing intention of green housing in China. *Sustainability*, 10(4), p.1044. doi:10.3390/su10041044





# Evaluation of the Drought Situation Using Remote Sensing Technology, an Applied Study on a Part of North Wasit Governorate in Iraq

A. J. Dakhil<sup>1</sup>, E. K. Hussain<sup>2</sup> and F. F. Aziz<sup>2†</sup>

<sup>1</sup>Department of Road and Transport Engineering, University of Al-Qadisiyah, Collage of Engineering, Al-Diwaniyah, Iraq

<sup>2</sup>Department of Civil Engineering, University of Al-Qadisiyah, Collage of Engineering, Al-Diwaniyah, Iraq

†Corresponding author: F. F. Aziz; fatinalkhuzaai@gmail.com

Nat. Env. & Poll. Tech.  
Website: [www.neptjournal.com](http://www.neptjournal.com)

Received: 21-03-2024

Revised: 07-05-2024

Accepted: 17-05-2024

## Key Words:

Drought  
GIS  
NDVI  
VCI  
Remote Sensing

## ABSTRACT

Drought presents a substantial threat to both ecological and agricultural systems. Agriculture in Iraq is predicated on precipitation, which is a major contributor to the likelihood of drought resulting from even marginal fluctuations in precipitation. Furthermore, research suggests that Iraq suffers an approximate annual loss of 100,000 acres of arable land due to drought. NDVI and VCI, two significant indices, were utilized in this research to assess and monitor the severity of the drought in the northern region of Wasit province in Iraq. For the period from 1993 to 2023, drought intensity maps were generated utilizing NDVI-based VCI and the Geographic Information System (GIS), an extremely effective spatial data management instrument. NDVI results evidenced that the vegetation cover area was the highest in 1993 and 1998 and declined until it reached the lowest levels in 2023. The vegetation area was concentrated in the southwest parts. In contrast, VCI results demonstrated the extreme drought through the years from 2003 to 2023, which can be attributed to higher temperatures, evaporation, and lower amounts of rainfall. Throughout the thirty-year analysis period, extreme drought conditions were prevalent, especially in the last two decades. Furthermore, this drought should prompt the government to implement preventative measures to avert it. Implementing soil and water conservation measures, such as the establishment of percolation basins, contour bunds, and check dams, can also enhance drought management.

## INTRODUCTION

Drought is a costly natural peril that has extensive consequences for the socioeconomic, agricultural, ecological, and water supply sectors. Drought transforms into various forms as it circulates through the water cycle; its effects extend to the human society and biological system (Zhang et al. 2022). Vegetation cover and its type significantly impact the climate in dry regions (Wang et al. 2023, Omuto et al. 2010), it influences the weather and environmental conditions as well as the exchange of energy, water, and carbon between plants, lowering the concentration of carbon in the atmosphere because plants use carbon dioxide and energy in the process of photosynthesis, lowering the concentration of carbon in the atmosphere. This also helps to minimize the consequences of anthropological carbon emissions.

Although vegetation occupies 20% of the earth's surface, growing levels of desertification are having a detrimental influence on climate by interfering with the phenomena mentioned previously (Jones 2013, Pachauri et al. 2014).

Because vegetation cover growing has a significant impact on the ecosystem, with an important consideration

in contemporary climate change debates (Jones 2013, Pachauri et al. 2014). By comprehending the correlation between climate change and vegetation, the extent to which vegetation reacts to climate change can be inspected. This knowledge, in turn, furnishes crucial and useful insights for adapting to climate change (Afuye et al. 2021). The proliferation of remote sensing satellites has high accuracy and rapid progress of quantitative remote sensing technology has facilitated the acquisition of various categories of feature information from long-time series and large-scale remote sensing image data (Kattenborn et al. 2021, Pan et al. 2023). Scientists employ remote sensing techniques to observe and quantify vegetation changes at the regional level, which are influenced by both natural climate variability and human activities (Rousvel et al. 2013). Gao et al. (2020) state that dynamic monitoring models that derive changes in vegetation cover from remote sensing image data are crucial to assess and monitor environmental functions and regional ecological quality, including the Normalized Difference Vegetation Index (NDVI) and Vegetation Condition Index (VCI). Nevertheless, the application of NDVI for such investigations may not be prevalent in other regions of the globe due to

the complexity of the growth and distribution of vegetation and the distinctive attributes of various arid regions (Kumar et al. 2022). NDVI is a highly effective technique utilized for the surveillance of ground vegetation conditions, as it genuinely accounts for vegetation biomass, ground cover, and vegetation growth. Monitoring the dynamic alterations of vegetation cover and land use on a regional and global scale is a common application of this technique (Huang et al. 2022). Numerous research on the spatiotemporal distribution of regional vegetation have been conducted, as determined by NDVI values, and have been undertaken by academicians from around the world over the past few decades (Huang et al. 2022). On the other hand, the effectiveness of the VCI derived from the NDVI in monitoring drought conditions has been investigated in numerous regions across the globe. In Kazakhstan, the VCI derived from NDVI has also been compared to measurements of vegetation density, biomass, and field reflectance; this comparison has demonstrated that the VCI is an accurate predictor of the weather's effect on vegetation health (Gitelson et al. 1998). The evaluation of the VCI focuses on monitoring drought during the period of maximum vegetation conditions and the growing season (Tran et al. 2017).

According to NASA and the USGS, vegetation change observations can be reliably conducted using MOD13Q1 products, provided that cloud interference is minimal (source: <https://lpdaac.usgs.gov>). Given that the majority of the year in Iraq is devoid of clouds, this product is appropriate for this research. So, any part of Iraq serves as a compelling subject of study.

Based on the findings of the Global Environment Outlook 1 by the United Nations Environment Program, Iraq is identified as the fifth most susceptible nation globally in relation to the decline in the availability of food and water, adverse climatic conditions, and associated health concerns. Moreover, it is estimated that Iraq experiences an annual loss of around 100,000 acres of agricultural land. Furthermore, it has been highlighted that Iraq has the greatest population growth rate among all countries in West Asia. This demographic trend is expected to exacerbate the aforementioned predicaments to a greater extent. Iraq ranks 39th globally in terms of water stress and is among the top five countries experiencing significant adverse effects from climate change. In 2021, the annual precipitation reached a historically minimal level, mostly attributed to unsustainable farming methods, a reduction in vegetative coverage, and the occurrence of the second-most arid season during the preceding four decades. The insufficiency of rainfall throughout the annual cycle, in conjunction with these ecological elements, has resulted in the occurrence of water scarcity, desertification, and soil degradation.

The protracted battle in Iraq has resulted in detrimental effects on the nation's water and land resources, leading to an exacerbation of soil erosion and pollution. The study aims to assess and monitor the spatial and temporal drought conditions and variation in vegetation cover in the northern part of Wasit Governorate, Iraq, using drought indices such as NDVI and VCI based on Landsat 5, 7 and 8 satellite images of agricultural drought and determine the extent to which it is affected by rainfall rates and temperature changes. Study results can help government planners formulate and manage drought impacts.

## MATERIALS AND METHODS

### Describing the Study Area

Wasit Governorate is located within a central part of Iraq, occupying the northeastern part of the alluvial plain. It is bordered to the east by Iran, to the north by Diyala and Baghdad governorates, to the west by Babel and Diwaniyah governorates, to the southwest by Nasiriyah Governorate, and to the southeast by Maysan governorate. The area of Wasit Governorate is (17,153) km<sup>2</sup>, which constitutes 3.94% of the total area of Iraq, which amounts to (435,052) km<sup>2</sup> (Central Bureau of Statistics, 7162, p. 6). The study area is located astronomically between latitudes 32°30' N and longitudes 44°46' E, as indicated in Fig. 1. The governorate is considered one of the agricultural governorates; its agricultural arable land is about 4 km<sup>2</sup>. This investigation focused on the northern part of Wasit Governorate in Iraq, which covered an area of approximately 10196.94 km<sup>2</sup> and lies between latitudes 32°30' N and longitudes 44°46' E. Fig. 1. The climatic conditions of the study region are characterized by a spectrum from arid to semiarid. The climate in this region is characterized by extremely cold winters and arid, scorching summers. In this particular geographic area, the onset of precipitation often occurs in October and lasts until May, as the annual rainfall amounts range between 103 and 195 mm, and the evaporation-transpiration amounts range between 1669 and 2235 mm.

### Datasets

To monitor the status of agricultural distress in the area of study, the particular agricultural drought indices were developed using satellite images of Landsat 5, Landsat 7, and Landsat OLI 8 and 9. Fig. 2 shows how one Landsat image completely encapsulates the research area (Path 168, Row 37). In the scope of the study, satellite images of Landsat-5 and Landsat-8 for January and February of 1993 1998, 2003, 2013, 2018, and 2013 were obtained when plants were in their growing season. Table 1 lists the attributes of the satellite images utilized. A remotely sensed data set with visible and near-infrared bands and a 30-meter spatial resolution was



utilized to analyze the drought conditions in the study area. The study utilized annual precipitation data obtained from the General Directorate of Meteorology and satellite images obtained from the USGS.

**Normalized Difference**

Both agricultural drought indices, which utilize spectral analysis, were employed in the study.

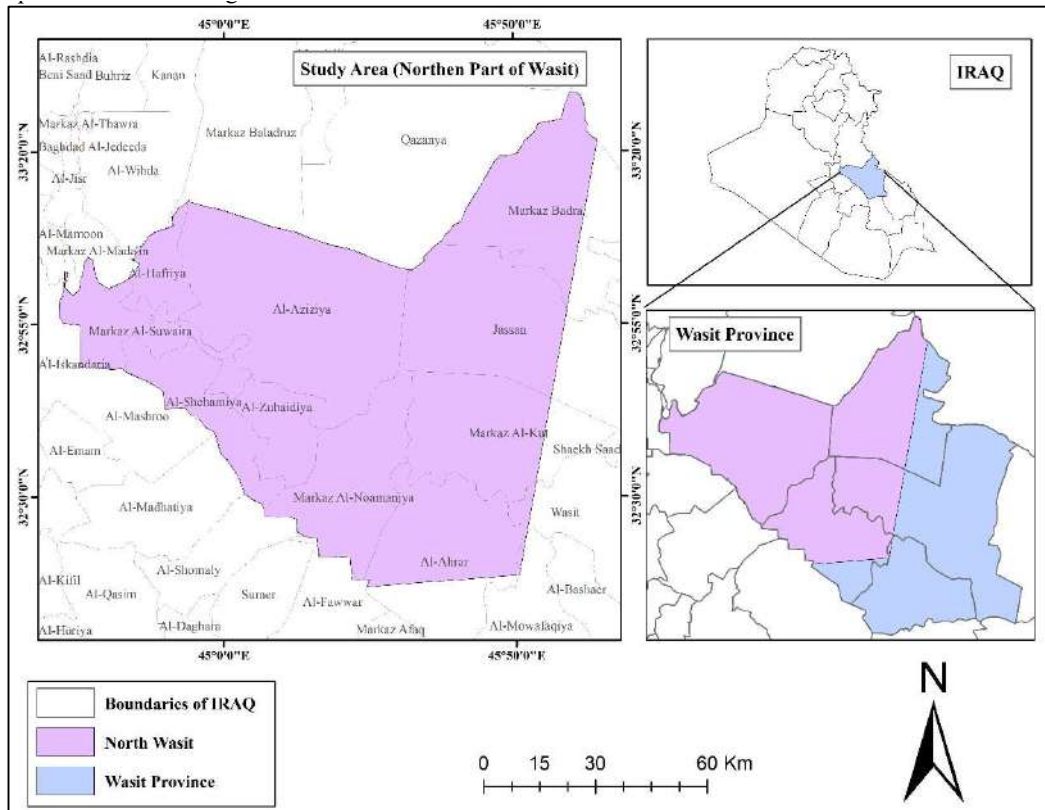


Fig. 1: Geographical map of study area showing Wasit Province and studied area.

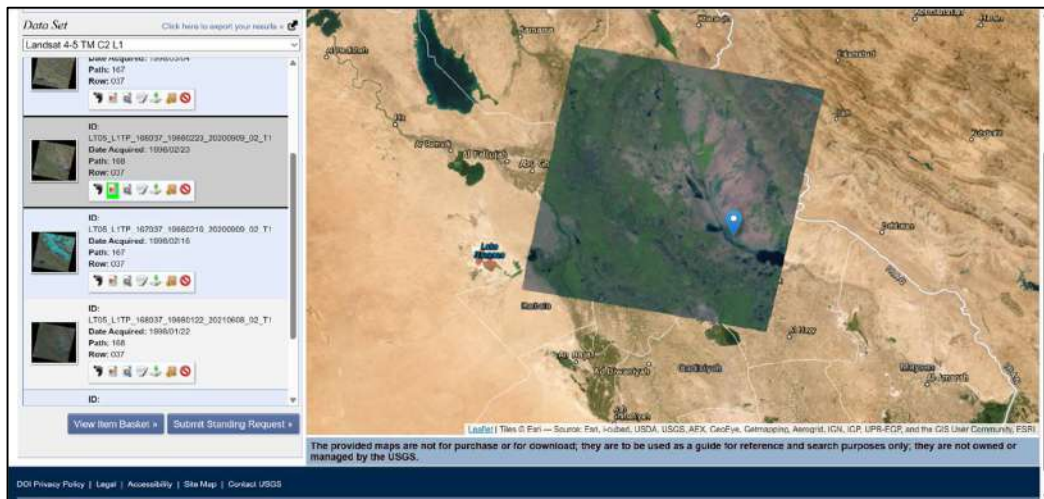


Fig. 2: Landsat images of the study area.

Table 1: Satellite data specifications.

Landsat	Path/Row	Date	Bands	Resolution (m)
LT05 ETM	168/37	1993/01/24	Multispectral	30
LT05 ETM	168/37	1998/03/11	Multispectral	30
LT07 ETM	168/37	2003/01/3	Multispectral	30
LT07 ETM	168/37	2013/02/24	Multispectral	30
LT08 OLI	167/37	2018/01/29	Multispectral	30
LT08 OLI	167/37	2023/02/05	Multispectral	30

\*Data Source (USGS website) <https://www.usgs.gov/>

### Normalized Difference Vegetation Index (NDVI)

Normalized Difference Vegetation Index (NDVI) is a vegetation index widely used in environmental research. The calculation involves the use of wavelengths throughout the red and near-infrared spectrums. The formula utilized in the determination procedure is as follows (Borowik et al. 2013).

The Normalized Difference Vegetation Index (NDVI) is a widely used remote sensing index that quantifies:

$$NDVI = ((\rho_{Nir} - \rho_{Red}) / ((\rho_{Nir} + \rho_{Red}))) \quad \dots(1)$$

Where:

Nir: used to denote the near-infrared reflectance.

Rid: used to denote the red reflectance band.

The non-dimensional vegetation index, commonly referred to as NDVI is a radiometric measurement used to assess the differential response of various plant species to radiation in the red and near-infrared (NIR) spectra. The use of the Normalized Difference Vegetation Index (NDVI) has been widely employed in agricultural and drought-related research due to its ability to establish a correlation between the index and the proportion as well as the overall health of green vegetation. This phenomenon can be attributed to the significant utility of the Normalized Difference Vegetation Index (NDVI). Examples of studies falling under this area include the computation of seasonal variations, the categorization of land cover types, and the evaluation of plant conditions (Jurecka et al. 2016), The NDVI values can vary within a range from negative to positive. A decrease in the Normalized Difference Vegetation Index (NDVI) signifies a reduced presence of vegetation within the given region, while an increase in the NDVI value suggests a larger concentration of vegetation in the area (Singh et al. 2016). The NDVI values utilized in this study were obtained through the analysis of photos acquired by the Landsat satellite throughout January for each respective year.

### Vegetation Condition Index (VCI)

The Vegetation Condition Index (VCI) is a method utilized

to evaluate the spatial attributes, duration, and intensity of drought. Furthermore, it exhibits a strong correlation with precipitation patterns and compares the present range of values of the Normalized Difference Vegetation Index (NDVI) for the same period in previous years to determine the health of the vegetation (Ainembabazi 2022). It is denoted in percentage form and indicates the observed value's position relative to the minimum and maximum values from the preceding years. Decreased and increased values correspond to unfavorable and favorable conditions of vegetation, respectively.

VCI can be classified into five categories, according to (Bhuiyan et al. 2006) as shown in Table 2.

According to Kogan (1995), the Vegetation Condition Index (VCI) can be calculated as follows:

$$VCI = ((NDVI_j - NDVI_{min}) / ((NDVI_{max} - NDVI_{min})) * 100. \quad \dots(2)$$

Where:

NDVI<sub>i</sub>: the NDVI of the current year.

NDVI max: the maximum NDVI of multiyear studied.

NDVI min: the minimum NDVI of multiyear studied.

## RESULTS AND DISCUSSION

### Variation in Normalized Difference Vegetation Index (NDVI)

The NDVI for the period 1993-2023 was calculated every

Table 2: Drought classification by VCI according to (Bhuiyan et al. 2006) definition.

VCI Level	Drought -Severity
<10%	Extreme Drought
10% - 20%	Severe Drought
20%-30%	Moderate Drought
30%-40%	No Drought
40%-100%	Wet

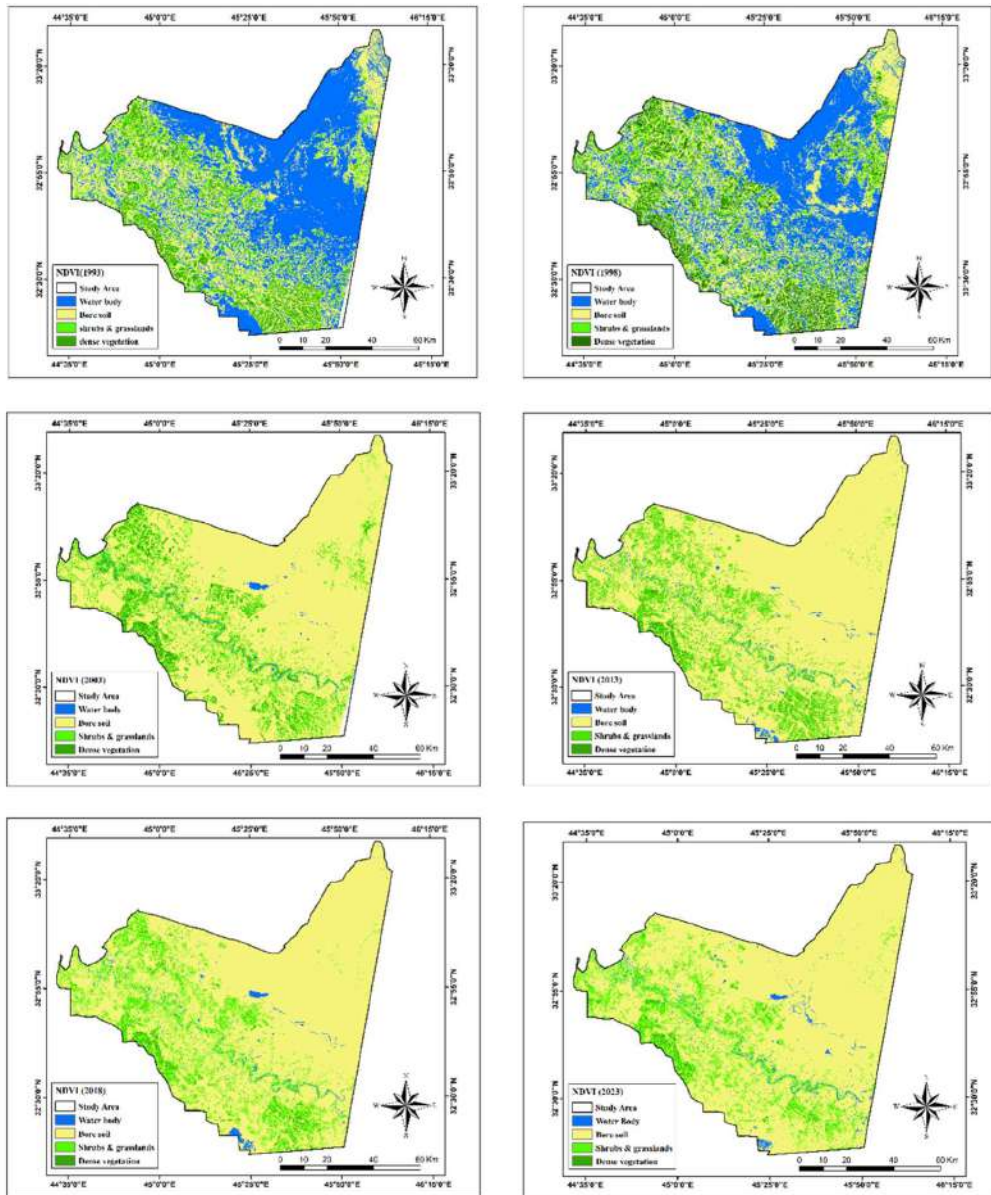


Fig. 3: NDVI raster for the years (A) 1993; (B) 1998; (C) 2003; (D) 2013; (E) 2018; and (F) 2023.

three years. This was done using Landsat-5, Landsat-7 and Landsat-8 satellite images acquired from the USGS for January and Feb. Then the Difference Vegetation Index (NDVI) was calculated via Arc Map 10.8 software. Fig. 3 shows the NDVI raster class distribution for the six years studied. These images were analyzed to determine how drought and vegetation cover have changed in the study area. Spatiotemporal analysis showed a significant change due to drought for NDVI images; yellow areas were unhealthy, areas with buildings, or bore soil, while green showed healthy, moist vegetated areas; in addition, blue

areas demonstrate marshes and swamps (water bodies) (Rousta et al. 2020). In general, NDVI values for green parts ranged between 15.443% and 21.976% in 2023 and 1998, respectively. Extract vegetation coverage data as shown in Table 3 and calculate the area and vegetation layer percentage in each year.

The vegetation condition increased between 1993 and 1998 by 3.6%. The values returned to decrease in subsequent years until 2023 to some extent in the plant area. The spatiotemporal of the NDVI plot for the northern part of Wasit shown in Fig. 3 also indicated a similar evolution

Table 3: The area and percentage of vegetation for the study area over the period 1993 to 2023.

Year	Vegetation Area (km <sup>2</sup> )	Percent (%)	Variation (±)
1993	1813.437	18.371	-0.011
1998	2169.226	21.976	3.594
2003	1922.537	19.477	1.095
2013	1720.794	17.433	-0.949
2018	1736.517	17.592	-0.790
2023	1524.371	15.443	-2.939
Average (6 years)	1814.480	18.382	
Total study Area 9871 km <sup>2</sup>			

and a tendency for a decrease in the NDVI during the years 2003 to 2013 and a return to increase in 2018 and then a decrease in 2023, due to severe or extreme drought years that hit the region, the highest percentage of vegetation cover was recorded in 1998. On the other hand, the NDVI results showed that the northern Badra district recorded the highest decline. The area located in the southwest of the study area has the densest vegetation coverage, as shown in Fig. 3. Fig. 4 shows the relationship of vegetation cover percentage (NDVI) with precipitation.

#### Variation in Vegetation Condition Index (VCI)

The VCI-based agricultural drought intensity maps from 1993 to 2023 are shown in Fig. 5 during January and February. VCI varies considerably in vegetation phenology is 0 -100 in the study area over the period 1993-2023 (Fig. 6).

For example, in 1993 and 1998, larger parts of the agricultural land recorded a low VCI (VCI<20), reaching 67% of the total studied area. From Fig. 5, it can be observed that the highest VCI in 2003 may be affected by the low precipitation in this year. The following years 2013, 2018, and 2023 recorded high VCI values, which occupied an area larger than the study area which gradually decreased with the increase in the amount of rainfall, as can be seen in Figs. 5 and 6.

This increasing level of drought can be attributed to the fact that Wasit Governorate, like other regions in central and southern Iraq, is now suffering from water shortages as a result of a combination of factors, including historically low levels of rainfall, and inadequate water resource management practices and reduced water inflow from upstream regions that share borders with the Tigris and Euphrates rivers. The decrease in water flow from upstream is the primary factor contributing to this shortage. In addition to the enormous urban sprawl that exists in the study region and the governorates that are located nearby.

The wetted area occupied around 5690.98 km<sup>2</sup>, 4500.728 km<sup>2</sup>, 471.32 km<sup>2</sup>, 1084.44 km<sup>2</sup>, 1132.21 km<sup>2</sup> and 1359.4 km<sup>2</sup> for the years 1993, 1998, 2003, 2013, 2018, and 2023, respectively, from the total area (9871 km<sup>2</sup>).

#### CONCLUSION

In this investigation, Mapper (TM) photos and operational images (OLI) were used to identify changes in vegetation

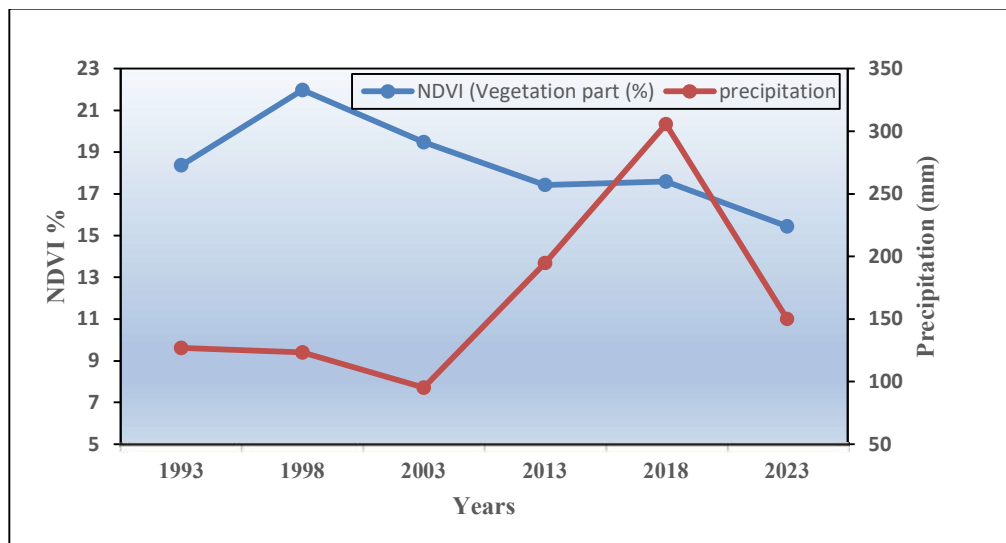


Fig. 4: Relationship of vegetation cover percentage (NDVI) with precipitation.

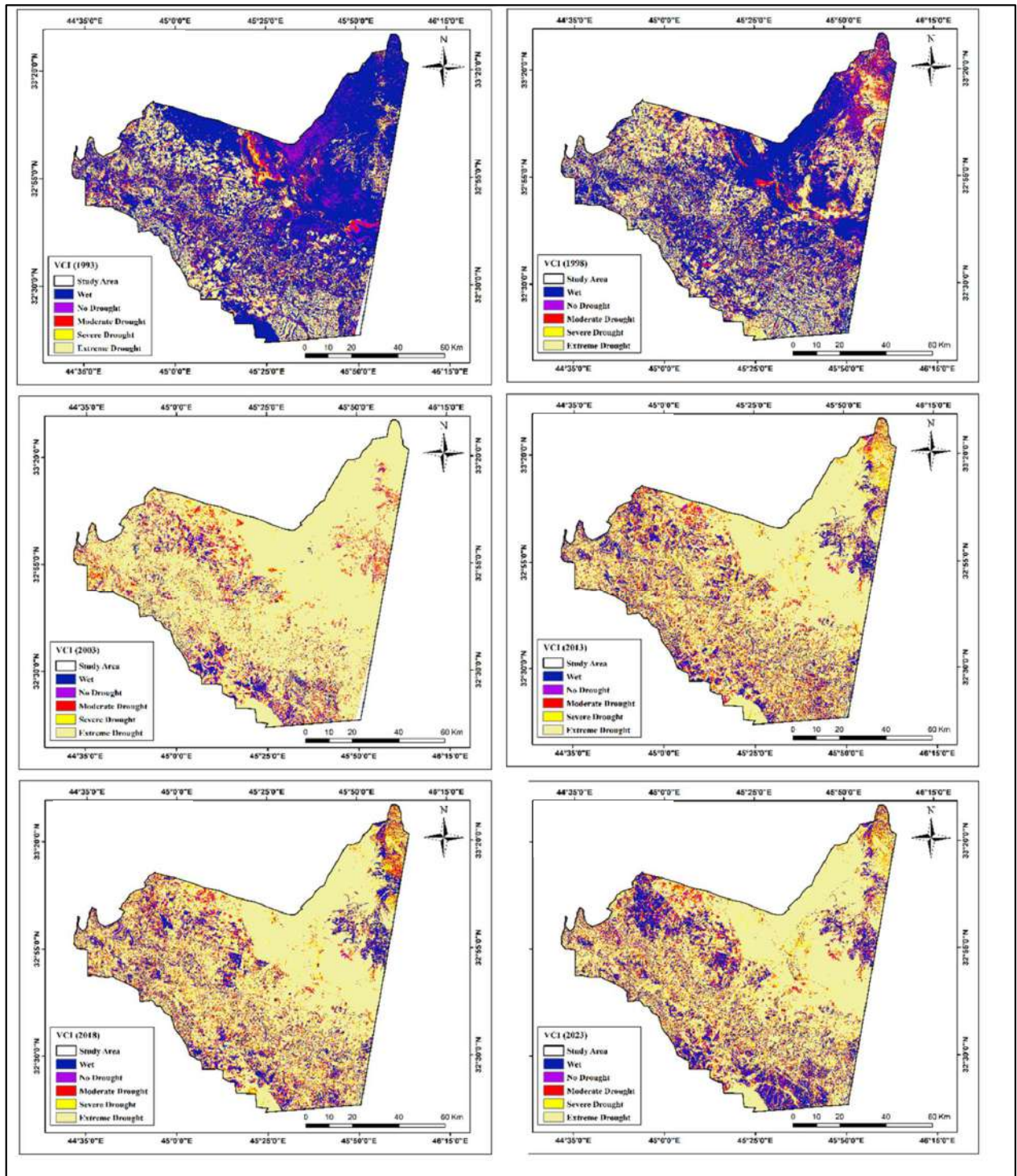


Fig. 5: VCI raster for the years (A) 1993; (B) 1998; (C) 2003; (D) 2013; (E) 2018; and (F) 2023.

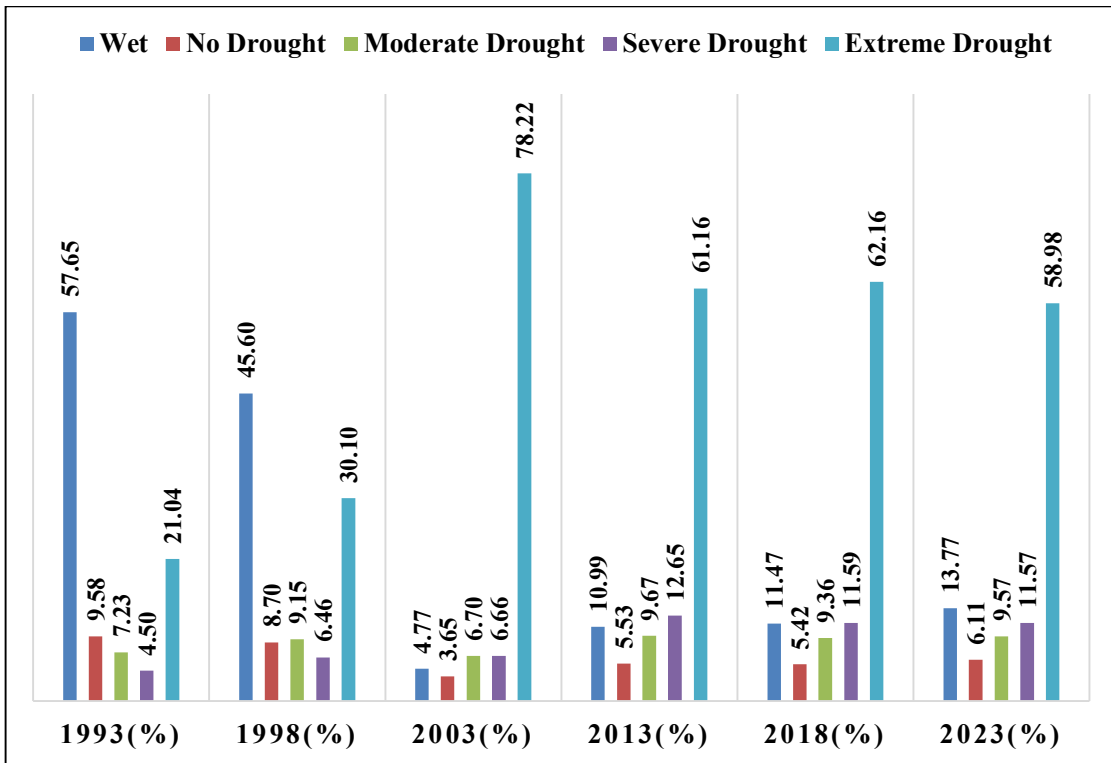


Fig. 6: Variation in Drought Severity Level (VCI) in the Northern Part of Wasit for the study years.

and drought conditions via GIS 10.8, which led finally to the following facts:

1. During this period, the vegetation pattern was continuously declining. According to the NDVI, the peak vegetation cover was 2,169.22 km<sup>2</sup> in 1998, and it reached 1,524.37 km<sup>2</sup> in 2023. The reduction accounted for 6.5% of the total area. While the overall rate of decreasing vegetation cover is 1,814.48 km<sup>2</sup>.
2. For the variation in vegetation condition index (VCI), extreme drought areas in 2003 were the largest with an area of about 7721 km<sup>2</sup>. It found that the wet area was large in most of the districts in 1993 and 1998, as noticed in the districts of Badra, Al-Aziziya, and Jassan.
3. The reductions in vegetation cover during periods of drought can be ascribed to the scarcity of water resources and irrigation water. In addition to the extensive urban development that encompasses the study area and the neighboring governorates. Conversely, the scarcity of precipitation throughout the study period contributed to the severe drought in the area. Following this, the reduction in precipitation caused a substantial depletion of the studied area's surface and groundwater resources, including lakes, rivers, and groundwater; as a result, the soil moisture content decreased.

4. Finally, it can be concluded that the utilization of geographic information systems (GIS) and remote sensing data can be instrumental in the investigation and surveillance of land cover changes. They can provide information that is more precise, economical, and timely.

## REFERENCES

- Afuye, G. A., Kalumba, A. M. and Orimoloye, I. R., 2021. Characterisation of vegetation response to climate change: A review. *Sustainability*, 13(13), pp.7265. <https://doi.org/10.3390/su13137265>
- Ainembabazi, S., 2022. Comparison of standardized precipitation index (SPI) and vegetation health index (VHI) in drought monitoring in Insingiro District (Doctoral dissertation). <http://hdl.handle.net/20.500.12281/14299>
- Bhuiyan, C., Singh, R. P. and Kogan, F. N., 2006. Monitoring drought dynamics in the Aravalli region (India) using different indices based on ground and remote sensing data. *International Journal of Applied Earth Observation and Geoinformation*, 8(4), pp.289-302. <https://doi.org/10.1016/j.jag.2006.03.002>
- Borowik, T., Pettorelli, N., Sönnichsen, L. and Jędrzejewska, B., 2013. Normalized difference vegetation index (NDVI) as a predictor of forage availability for ungulates in forest and field habitats. *European Journal of Wildlife Research*, 59, pp.675-682. <https://doi.org/10.1016/j.jag.2006.03.002>
- Gao, L., Wang, X., Johnson, B.A., Tian, Q., Wang, Y., Verrelst, J., Mu, X. and Gu, X., 2020. Remote sensing algorithms for estimation of fractional vegetation cover using pure vegetation index values: A review. *ISPRS Journal of Photogrammetry and Remote Sensing*, 159, pp.364-377.

- Gitelson, A.A., Kogan, F., Zakarin, E., Spivak, L. and Lebed, L., 1998. Using AVHRR data for quantitative estimation of vegetation conditions: Calibration and validation. *Advances in Space Research*, 22(5), pp.673-676. <https://doi.org/10.1016/j.isprsjprs.2019.11.018>
- Huang, J., Ge, Z., Huang, Y., Tang, X., Shi, Z., Lai, P., Song, Z., Hao, B., Yang, H. and Ma, M., 2022. Climate change and ecological engineering jointly induced vegetation greening in global karst regions from 2001 to 2020. *Plant and Soil*, pp.1-20.
- Jones, H. G., 1992. *Plants and microclimate: A quantitative approach to environmental plant physiology*.
- Jurecka, F., Hlavinka, P., Lukas, V., Trnka, M. and Zalud, Z., 2016. Crop yield estimation at the field level using vegetation indices. In: *Proceedings of International PhD Students Conference. Czech Republic Phd MENDELNET*, pp.90-95.
- Kattenborn, T., Leitloff, J., Schiefer, F. and Hinz, S., 2021. Review on Convolutional Neural Networks (CNN) in vegetation remote sensing. *ISPRS Journal of Photogrammetry and Remote Sensing*, 173, pp.24-49. <https://doi.org/10.1016/j.isprsjprs.2020.12.010>
- Kogan, F. N., 1995. Application of vegetation index and brightness temperature for drought detection. *Advances in Space Research*, 15(11), pp.91-100. [https://doi.org/10.1016/0273-1177\(95\)00079-T](https://doi.org/10.1016/0273-1177(95)00079-T)
- Kumar, B. P., Babu, K. R., Anusha, B. N. and Rajasekhar, M., 2022. Geo-environmental monitoring and assessment of land degradation and desertification in the semi-arid regions using Landsat 8 OLI/TIRS, LST, and NDVI approach. *Environmental Challenges*, 8, 100578. <https://doi.org/10.1016/j.envc.2022.100578>
- Omuto, C. T., Vargas, R. R., Alim, M. S. and Paron, P., 2010. Mixed-effects modelling of time series NDVI-rainfall relationship for detecting human-induced loss of vegetation cover in drylands. *Journal of Arid Environments*, 74(11), pp.1552-1563. <https://doi.org/10.1016/j.jaridenv.2010.04.001>
- Pachauri, R.K., Allen, M.R., Barros, V.R., Broome, J., Cramer, W., Christ, R., Church, J.A., Clarke, L., Dahe, Q., Dasgupta, P. and Dubash, N.K., 2014. *Climate change 2014: synthesis report. Contribution of Working Groups I, II and III to the fifth assessment report of the Intergovernmental Panel on Climate Change: 151*. IPCC. <https://hdl.handle.net/10013/epic.45156>
- Pachauri, R.K., Allen, M.R., Barros, V.R., Broome, J., Cramer, W., Christ, R., Church, J.A., Clarke, L., Dahe, Q., Dasgupta, P. and Dubash, N.K., 2014. *Climate Change*.
- Pan, J., Chen, L., Shu, Q., Zhao, Q., Yang, J. and Jin, S., 2023. Spatiotemporal imagery selection for full coverage image generation over a large area with HFA-Net based quality grading. *Geo-spatial Information Science*, pp.1-18. <https://doi.org/10.1080/10095020.2023.2270641>
- Rousta, I., Olafsson, H., Moniruzzaman, M., Zhang, H., Liou, Y. A., Mushore, T. D. and Gupta, A., 2020. Impacts of drought on vegetation assessed by vegetation indices and meteorological factors in Afghanistan. *Remote Sensing*, 12(15), 2433. <https://doi.org/10.3390/rs12152433>
- Rousvel, S., Armand, N., Andre, L., Tengeleng, S., Alain, T. S. and Armel, K., 2013. Comparison between vegetation and rainfall of bioclimatic ecoregions in central Africa. *Atmosphere*, 4(4), pp.411-427. <https://doi.org/10.3390/atmos4040411>
- Singh, R. P., Singh, N., Singh, S. and Mukherjee, S., 2016. Normalized difference vegetation index (NDVI) based classification to assess the change in land use/land cover (LULC) in Lower Assam, India. *International Journal of Advanced Remote Sensing and GIS*, 5(10), pp.1963-1970. <https://doi.org/10.23953/cloud.ijarsg.74>
- Tran, H. T., Campbell, J. B., Tran, T. D. and Tran, H. T., 2017. Monitoring drought vulnerability using multispectral indices observed from sequential remote sensing (Case Study: Tuy Phong, Binh Thuan, Vietnam). *GIScience & Remote Sensing*, 54(2), pp.167-184. <https://doi.org/10.1080/15481603.2017.1287838>
- Wang, X., Liu, G., Xiang, A., Xiao, S., Lin, D., Lin, Y. and Lu, Y., 2023. Terrain gradient response of landscape ecological environment to land use and land cover change in the hilly watershed in South China. *Ecological Indicators*, 146, 109797. <https://doi.org/10.1016/j.ecolind.2022.109797>
- Zhang, X., Hao, Z., Singh, V. P., Zhang, Y., Feng, S., Xu, Y. and Hao, F., 2022. Drought propagation under global warming: Characteristics, approaches, processes, and controlling factors. *Science of the Total Environment*, 838, 156021. <https://doi.org/10.1016/j.scitotenv.2022.156021>

---

#### ORCID DETAILS OF THE AUTHORS

- A. J. Dakhil: <https://orcid.org/0000-0002-3598-261X>  
 E. K. Hussain: <https://orcid.org/0000-0002-2228-2817>  
 F. F. Aziz: <https://orcid.org/0009-0002-7744-1712>







# Testing the Validity of Environmental Kuznets Curve for Carbon Emission: A Cross-Section Analysis

Punam Chanda<sup>†</sup> , Pintu Majhi and Salina Akther

Department of Economics, Tripura University (A Central University), Suryamaninagar, Tripura 799022, India

<sup>†</sup>Corresponding author: Punam Chanda; punamchanda123@gmail.com

Nat. Env. & Poll. Tech.  
Website: [www.neptjournal.com](http://www.neptjournal.com)

Received: 12-07-2023

Revised: 27-08-2023

Accepted: 21-09-2023

## Key Words:

Environmental Kuznets Curve  
Economic growth  
Carbon emission  
Environmental sustainability

## ABSTRACT

Global warming and its consequences have heightened the urgency of reducing emissions of carbon dioxide globally. The concern arises from countries' relentless efforts to achieve economic development at the expense of the environment. In this context, the paper examines the Environmental Kuznets Curve (EKC) hypothesis at the world level using carbon emission as an indicator of environmental degradation. The EKC hypothesis postulates an inverted U-shaped curve between economic development and environmental degradation; degrading environmental quality at the initial stages of development and, after a threshold level, environmental degradation lowers. The study investigates the validity of the EKC hypothesis for carbon emission with an analysis of 158 countries in the world, with population, urbanization, forest cover, and tourist inflow as the control variables. The study is based on secondary data collected from the World Bank. A regression analysis is used for the study. To ensure environmental sustainability, it is important to identify the determinants of carbon emissions across countries with varying levels of economic development. The findings of the study support the hypothesized inverse U-shaped association between Gross Domestic Product per capita and carbon emission per capita at the world level. Out of the four control variables, urbanization and tourist inflow were found statistically significant. Urbanization was positively correlated with carbon emission per capita while forest area was negatively correlated. Carbon emission per capita initially increases with rising GDP per capita and declines after GDP per capita reaches a certain level. The estimated turning point of GDP per capita occurs at a high level and therefore, most of the countries are anticipated to emit carbon dioxide.

## INTRODUCTION

In recent times, issues on global warming and economic development have drawn the attention of the intellectual world towards sustainable development strategies. The countries towards accelerating economic growth often neglect environmental degradation which if not addressed can cause irreparable environmental damage and divert away from sustainability. Therefore, attempts to combat carbon emissions are one of the important challenges for countries across the globe. There are many facets to environmental quality. The air we breathe, the water we drink, the natural beauty we experience, and the variety of species we interact with all have an impact on how we live. Climatic conditions, rainfall patterns, and the nutrient content in the soil all have an impact on how productively our resources produce goods and services. These and other aspects of environmental quality may all react differently to economic growth (Grossman & Kruger 1995).

At the global level, the need to reduce environmental harms by mitigating carbon dioxide emissions the major contributor to greenhouse gas has been realized. The Kyoto Protocol in 1997 under the United Nations Convention on Climate Change (UNCCC) stressed countries to limit and curb their carbon emissions. The United Nations' 2030 Agenda for Sustainable Development Goals (SDGs) and Paris Climate Change Conference, 2015 also allow countries to take up the resolution of cutting their greenhouse gas emissions. The Paris Agreement directs the countries to cut their emission of greenhouse gases to keep the rise in global temperature of this century within 2 degrees Celsius and lower it to 1 degree Celsius. Despite several strategies, the global emission levels are higher to control global warming to 2 degrees Celsius and 1 degree Celsius (UNEP 2019).

Worldwide emission of carbon dioxide, one of the major greenhouse gases is approximately 4.47 metric tons per capita (World Bank 2019). The amount of carbon emission varies over time and across countries. Therefore, identifying

the determinants of carbon emission, and the relationship between GDP and carbon emission assumes importance. Carbon emissions have been associated with economic growth which can be explained by the Environmental Kuznets Curve (EKC). According to the EKC hypothesis, in the early stages of economic growth environmental degradation increases which after attaining the threshold level of economic growth reduces gradually. The inverse U shape of carbon emission-induced EKC can be illustrated due to agricultural activities and subsequent shift towards industries leading to more emission of carbon dioxide (Gokmenoglu & Taspinar 2018, Opoku & Boachie 2020). This is called the scale effect and composition effects of economic growth (Murshed et al. 2020). In the later stages of economic growth, improvement in technology, and infrastructure along with environmental consciousness lowers the emission of carbon dioxide. This is called the technique effect.

The Environmental Kuznets Curve (EKC) hypothesis has been largely discussed in the field of environmental economics over the past years. The Environmental Kuznets Curve (EKC) hypothesis has been coined from the Kuznets Curve forwarded by Simon Kuznet that proposed that income inequality widens along the path of economic development in the early stage and improves in the later stages (Kuznet 1955). A seminal work investigated the environmental repercussions of the North American Free Trade Association (NAFTA) taking sulfur dioxide, dark matter, and suspended particulate matter as indicators; and observed that environmental quality does not degrade steadily with economic growth. The study holds that economic growth results in degradation in the early phase but after a certain level of economic growth, environmental quality improves (Grossman & Krueger 1991). Shafik & Bandyopadhyay (1992) observed the relationship between economic growth and environmental quality by assessing the patterns of environmental transformation for countries at different levels of income taking eight indicators of environmental quality. These studies developed the ground for the Kuznets curve hypothesis and the term “Environmental Kuznets Curve hypothesis” was used for the first time by Panayotou in 1993. Several studies establish the validity of the inverse U-shaped relationship between economic growth and environmental degradation. A cross section study of 68 countries both developed and developing with deforestation as an indicator of environmental degradation validated an inverse U-shaped EKC. The turning point for deforestation was estimated between USD800-USD1200 per capita (Panayotou1993). A similar study found an inverse U-shaped relationship between economic development and carbon dioxide emission on a panel of 130 countries from 1951-1986 with USD35428 as the turning point (Holtz Eakin & Selden 1995). EKC

for carbon emission was also obtained for OECD countries from 1980-2002 using a fixed effect and random effect approach. The estimated turning point in the study is between USD11152 and USD15949 (Halkos Tzeremes 2009). An inverted U-shaped relationship between tourism and CO<sub>2</sub> emissions was found implying that a nation's emissions initially increase with the tourism industry's growth and decline after reaching the threshold (Jiaqi et al. 2022). Apart from testing the validity of EKC with respect to carbon emission, studies regarding the evidence of EKC across other variables are ample. EKC hypothesis was also evidenced in the rate of water utilization in a cross-section study of 163 countries for the year 2000 (Barbier 2004). Similarly, EKC in case export quality was observed for Bangladesh and India of the five South Asian countries from 1972 to 2014 (Murshed & Dao 2020). A strong relationship between GDP per capita and e-waste generation per capita in the cross-section of 174 countries was observed at the world level and continent level (year 2016). It found the validity of EKC for e-waste at the continent levels for all except for Asia and a turning point at USD 70, 000 (Boubellouta & Kusch-Brandt 2021).

Although several works support the validity of EKC for carbon emission, however some studies do not. For instance, EKC for carbon emissions of 149 countries was not observed from 1960 to 1990 (Shafik & Bandyopadhyay 1992). Another study observed that environmental degradation measured in CO<sub>2</sub> emissions increased with economic growth (Shafik 1994). In a cross-country panel data for 13 OECD countries also did not observe EKC for solid waste (Cole et al. 1997). Similarly, in the panel of 152 countries from 1970-1990 EKC for carbon emission was not established (Magnani 2001). On the other hand, N shaped relationship was observed between economic growth and environmental degradation in Nigeria (Usenobong & Chukwu 2011). A similar observation was found in a study that examined how the per capita water footprint varies with per capita income at both aggregated and disaggregated levels of water footprint using cross-section data. The estimation results give rise, in most cases, to evolution into an N-shaped relationship but provide no support for an inverted U environmental Kuznets curve. The turning point is estimated at USD17,700 and USD40,434 (Sebri 2015). Therefore, the EKC hypothesis for carbon emission remains inconclusive. In addition, the volume of carbon emissions varies across countries and over time. It is unlikely that different volumes of carbon emission are emitted from sources unrelated to Gross Domestic Product if such large differences in growth to development gap between countries. Therefore, in examining the determinants of carbon emission the association between Gross Domestic Product and carbon emission assumes importance. This paper attempts to find the validity of EKC in carbon dioxide

emissions of 158 countries. In this study, carbon dioxide emission is conceptualized as an indicator of environmental degradation, and Gross Domestic Product (GDP) as an indicator of economic development. Apart from the cross-country analyses it also incorporates explanatory variables namely, population, urban population, forest cover, and tourist inflow. The EKC hypothesis has been used in several studies to examine the association between environmental quality and economic development. The main purpose of the paper is to identify the factors of carbon emission across countries with different stages of economic development. The paper will be an addition to the literature in the field of an empirical study of the test for the Kuznets curve for carbon emission around the world. The rest of the paper is arranged as follows. Section 2 provides the literature review followed by methodology in section 3. The results are explained in section 4 and conclusions in section 5.

## MATERIALS AND METHODS

To fulfill the objectives, the regression model is used to examine the nature of the association between GDP and carbon emission and the factors of carbon emission. To study this at the global level, the sample comprises 158 countries of the world for 2019 based on secondary information for which full data was available. The reference year of the study is 2019 since it is a recent dataset and contains the maximum countries of in the world.

For testing the EKC in the case of South Asian countries (excluding Afghanistan due to insufficient data), data have been obtained for a period between 1990 to 2019 except for Maldives i.e. between 1995 and 2019. All data are obtained from the official database of the World Bank.

### Econometric Model

For examining the inverse U-shaped EKC, several studies have incorporated a quadratic term of GDP per capita in the model (Murshed et al. 2020, Boubellouta & Brandt 2021, Mehmood et al. 2022). To examine the inverse U-shaped relationship between GDP and CO<sub>2</sub> emission, the following empirical model is used:

$$\ln\text{CO}_2\text{-em. per capita}_i = \beta_0 + \beta_1 \ln(\text{GDP per capita}_i) + \beta_2 \ln(\text{GDP per capita}_i)^2 + \beta_3 \ln(Z) + u_i \quad \dots(1)$$

Where, CO<sub>2</sub>-em. per capita<sub>i</sub> refers to carbon dioxide emission measured in terms of metric tons of carbon dioxide equivalents, GDP per capita<sub>i</sub> and GDP per capita<sub>i</sub><sup>2</sup> refer to per capita gross domestic product and its squared term respectively measured in constant 2015 US dollar prices. Z is a vector of variables which includes population, urban population, forest cover, and tourist inflow. The population

is the total population of the country, urbanization is the percentage of the total population living in urban areas, forest cover is measured as the percentage of land under forest area, and tourist inflow is expressed as the number of tourists arriving in the country.

The coefficients  $\beta_1$  and  $\beta_2$  capture the linear and non-linear relationship respectively,  $i$  refers to the country and  $u_i$  is the error term. For the EKC hypothesis to be valid, the coefficients of  $\beta_1$  and  $\beta_2$  should be significantly positive and negative simultaneously. This will indicate the existing inverted U-shaped EKC; carbon dioxide emission increases with GDP per capita and after the threshold level, carbon emission lowers. Thus, to examine this, regression analysis is used. The variables used are in natural logarithms.

The turning point GDP level where further economic growth will not increase carbon emission is calculated as (Cole et al. 1997):

$$\exp - \beta_1 / 2 \beta_2 \quad \dots(2)$$

The econometric software SPSS 22 was used. Ordinary Least Squares regression was used to examine the model. This study uses cross-section data (the year 2019); panel data over several years are not available for countries worldwide. The OLS method has been widely used in previous studies and is a standard method of choice to analyze cross-section data.

### Dependent, Independent and Control Variables

This work takes carbon emission per capita as the dependent variable calculated by dividing total carbon emission per year by the total population in each country. Independent variables contain GDP per capita. To test the EKC, i.e., to check whether the relationship between GDP per capita and carbon emission per capita is inverse U shaped, GDP per capita (linear term) and GDP per capita squared (non-linear term) in the econometric model. The association between dependent and independent variables is inverted U-shaped if the estimates of the linear and non-linear terms have positive and negative signs respectively. This will imply that the validity of EKC, which states that carbon emission initially increases with GDP per capita and after reaching the threshold level (turning point), it decreases.

A set of control variables that could influence carbon emission have been included. For instance, population growth is found to be responsible for increasing air pollutants. Population causes pollution as it is associated with the rise in the consumption of energy due to rising industries, transport services, and power demand. It further escalates pollution by large-scale clearing of forests. Population is expected to have a positive relation with carbon emissions. Similarly,

urbanization is also anticipated to positively affect carbon emissions. Another factor that is expected to positively affect carbon emissions is tourism. Around 5 percent of global carbon emissions are generated by tourism (Jiaqi et al. 2021). Tourism leads to an increase in demand for transportation, hotels, consumption, and shopping activities which can contribute to carbon emissions. On the other hand, forest cover is expected to be negatively related to carbon emissions. Forests play a vital role in regulating global warming as it acts as a sink of carbon dioxide, the prime pollutant of greenhouse gas emission. Forests in UNESCO World Heritage sites absorb approximately 190 million tonnes of net carbon dioxide emission annually.

## RESULTS AND DISCUSSION

For several decades environmental repercussions of carbon emissions have been widely debated. Global warming and climate change are the important consequences of carbon dioxide emission which constitutes the major portion of the greenhouse gas emission. During the last decade, the global surface average for carbon dioxide rose by 2.15 parts per million (NOAA 2023). One of the ways to find the drivers of carbon emissions is to look at GDP values and population figures. Table 1 presents carbon emissions around the world in 2019, fragmented into 7 regions (a list of countries is given in Appendix I). The absolute quantities of carbon emission (metric tons) show that Europe and Central Asia generate the highest carbon emission, followed by North America, while South Asia, and Middle East, and North Africa emit less carbon emission than Europe and Central Asia but more than Latin America and Caribbean and East Asia and Pacific. Sub-Saharan Africa has the lowest carbon emission among all the regions

Table 1 further reveals that the population figures do not have an impact on carbon emissions, in East Asia and Pacific, South Asia, and Sub-Saharan Africa, the populated regions have low emissions of carbon dioxide compared with North America (the least populated region). However, the average carbon emission is higher for regions with high per capita GDP except for Latin America and the Caribbean region. The highest GDP per capita is observed in North America coupled with the highest carbon emission per capita i.e., 14.75 Mt followed by Europe and Central Asia (6.59 Mt), East Asia and Pacific (6.37 Mt), Middle East and North Africa (7841.2394 kg/inh). This reflects that GDP per capita has an impact on the amount of carbon emission per capita and the link between the two has been reported in literature for sets of countries. This may be because increased output requires more input and hence more natural resources resulting in increased pollution.

In the South Asian region, Maldives (3.97 Mt), and India (1.80 Mt) emit carbon dioxide higher than the average of the region as a whole (Table 2). It can be observed that Maldives, the highest GDP per capita in the region generates maximum carbon emission per capita while Afghanistan, the lowest GDP per capita emits less carbon dioxide per capita in 2019. The energy and waste sectors are the prime emitters of greenhouse gases in Maldives (Second National Communication of Maldives to the United Nations Framework Convention on Climate Change 2016).

Table 3 shows the descriptive statistics of the variables- carbon emission, GDP per capita, population, urbanization, forest cover, and tourist inflow. All the variables are for the year 2019. Table 4 gives the correlation coefficients among the variables. This shows that there is a modest positive correlation between GDP per capita and carbon emission per capita. A moderately high correlation exists between GDP per capita and carbon emission per capita with urbanization. A positive correlation exists between GDP per capita, carbon emission, population, and urbanization with tourism. There is no multicollinearity problem as no strong correlation is present among the variables.

Table 5 presents the regression results. The relationship between carbon emission and GDP per capita is studied without control variables in Model 1 and with control variables (population, urbanization, tourist inflow, and forest cover) in the regression model for robust results. Model 1 (excluding the explanatory variables) and Model 2 analyze carbon dioxide emission per capita as the dependent variable. For each model, the turning point is calculated, and since the turning point depends on the estimation method and model specifications, the turning point under model 1 may not be the same as model 2 (extended model). In Model 1, the coefficient of GDP per capita and its squared shows are positive and negative values significant at 1 percent. This implies the presence inverted U-shaped EKC in case of carbon emission. Further, model 2 includes explanatory variables- population, urbanization, forest cover, and tourist inflow to ensure the robustness of model 1. The coefficients of GDP per capita and its square value justify the non-linear EKC for carbon emission. This implies that carbon emission per capita initially increases with GDP per capita and after a certain level of GDP per capita it falls.

The adjusted  $R^2$  of model 2 shows that 84.5 percent variation in carbon emission per capita is explained by population, urbanization, forest cover, and tourist inflow. It is further observed that urbanization and forest cover are significant factors of carbon emission while population and tourist inflow is insignificant. The positive sign of urbanization implies that urbanization leads to more carbon

Table 1: Carbon emissions generated around the world and different regions in 2019.

Indicators	South Asia	Europe and Central Asia	North America	Latin America & Caribbean	Middle East and North Africa	East Asia and Pacific	Sub Saharan Africa	World
Number of countries with sufficient data availability	8	48	2	32	19	29	46	158
Population	1835776769	915718285	365931183	614138933	434954058	2292892002	1092398639	6769930892
Total CO <sub>2</sub> emission (metric ton)	2784080	6033360	5397930	1515650	2518340	14602910	821190	32788560
CO <sub>2</sub> emission per capita (Mt/inh)	1.52	6.59	14.75	2.47	5.79	6.37	0.75	4.84
GDP total (2015 USD)	3419823615667	22277926765204.30	21621599192026.10	5210710532862.06	3410578892388.07	25320593651684.80	1828341243913.62	80149650103828.20
GDP per capita (USD/inh)	1862.88	24328.36	59086.52	8484.58	7841.24	11043.08	1673.69	11839.06

Source: Own calculation using data from the World Bank (2019)

Table 2: Carbon emission among the South Asian countries in 2019.

Country	CO <sub>2</sub> emission per capita(Mt)	GDP per capita (USD/inh)
Afghanistan	0.16	555.14
Bangladesh	0.56	1581.57
Bhutan	1.38	3238.06
India	1.80	1965.54
Maldives	3.97	10197.09
Nepal	0.47	1069.79
Pakistan	0.88	1497.99
Sri Lanka	1.09	4228.15
Total	1.52	1862.88

Source: World Bank (2019)

emissions. The negative sign of forest cover indicates the beneficial role of forests with respect to curbing carbon emissions across the world.

Although the estimated coefficients of GDP per capita and GDP per capita square on carbon emission per capita slightly reduced after including population, urbanization, forest area, and tourist inflow, there is still a quadratic relationship between and strong relationship between GDP per capita and carbon emission per capita at 1 percent level of significance. This implies that carbon emission per capita initially increases with the rise in GDP per capita and declines after GDP per capita attains a certain level. This

Table 3: Descriptive statistics of 158 countries.

Variables	Mean	Maximum	Minimum	Standard Deviation	N
lnGDP per capita	8.79	11.59	6.04	1.31	158
lnCO <sub>2</sub> emission per capita (in metric tons)	0.84	3.09	-2.98	1.30	158
lnPopulation	15.65	21.07	9.36	2.20	158
lnUrbanization (in % of urban population)	3.99	4.61	2.58	0.46	158
lnTourist inflow	14.82	19.20	8.19	2.07	158
lnForest cover (in % of land)	14.82	4.58	-4.82	1.41	158

Note: Figures are rounded to the nearest hundred

Table 4: Correlation Matrix.

Variables	lngdp_percapita	lnco <sub>2</sub> _percapita	lnpopulation	lnurbanisation	lntourist	lnforest
lngdp_percapita	1					
lnco <sub>2</sub> _percapita	0.87*	1				
lnpopulation	-0.11	-0.06	1			
lnurbanisation	0.64*	0.63*	0.12	1		
lntourist	0.55*	0.56*	0.56*	0.48*	1	
lnforest	-0.00	-0.07	-0.10	-0.09	-0.07	1

Note: \* denotes significance at 1 percent level.

validates the hypothesis that EKC between carbon emission per capita and GDP per capita. In addition, this relationship appears robust since similar results are obtained from both models.

The EKC turning points vary from USD69831.9 GDP per capita and USD56499.61 GDP per capita for model 1 and model 2 respectively. In the sample of 158 countries, three countries have exceeded the turning point GDP per capita of USD69831.9 (Ireland, Luxembourg, and Norway) while eight countries have exceeded the turning point of USD56499.61 (Australia, Czechia, Iceland, Ireland, Luxembourg, Norway, Singapore and USA).

Moreover, two diagnostic tests were applied to ensure the appropriateness of the model. First, Durbin-Watson statistics have been used to check the possibility of autocorrelation. It is observed that the value is closer to 2 in both the models which reject the presence of autocorrelation. Secondly, the Bruesch-Pagan test is used to check for heteroskedasticity. The result of the Bruesch-Pagan test is insignificant; therefore there is no heteroskedasticity in both the models. The high adjusted R<sup>2</sup> and significant F-statistics justify the overall goodness of the models.

## CONCLUSION

During the last few decades, there has been growing concern about the impact of carbon dioxide on the environment

Table 5: Results of OLS regression with lnCO<sub>2</sub> emission per capita (metric ton) as dependent variable.

Variables	Model 1	Model 2
Intercept	-20.486*	-20.726*
lnGDP per capita	4.060*	3.961*
lnGDP per capita <sup>2</sup>	-0.182*	-0.181*
lnPopulation		0.033
lnUrbanization		0.228***
Lnforest area		-0.101***
Intouristinflow		-0.047
R <sup>2</sup>	0.834	0.852
Adjusted R <sup>2</sup>	0.832	0.845
F-statistics	389.711*	123.348*
Turning point	69831.9	56499.61
N	158	158
DW statistics	1.9	2.1

Note: \*, \*\* and \*\*\* denote statistical significance at 1%, 5%, and 10% respectively.

and human health. The paper examined the validity of CO<sub>2</sub>-induced EKC at the world level and in seven South Asian countries along with the drivers of carbon emission at the world level. To analyze the relationship between carbon emission and GDP with respect to EKC, by adding variables like population, urbanization, forest cover, and tourist inflow were assessed. The findings show that EKC for carbon emission is valid at the world level implying that initially, carbon emission per capita increases with rising GDP per capita, and eventually falls after reaching the threshold level. The turning point of GDP per capita (for the world sample) is high for most of the countries. Only eight countries have surpassed the estimated turning point GDP per capita Australia, Czechia, Iceland, Ireland, Luxemburg, Norway, Singapore and the USA. A strong relationship between GDP per capita and carbon emission was found at the world level. It is observed that urbanization and forest cover influence the link between GDP per capita and carbon emissions. Urbanization has a positive effect on carbon emissions which is due to the fact of increasing consumption of goods and services, infrastructure development, and land use ultimately degrading the environmental quality. On the other hand, the forest was negatively associated with carbon emissions implying that countries with larger forest areas have lower carbon emissions. Therefore, it throws light on the need for urban planning to build a sustainable environment for the cities. A negative sign effect of forest cover on carbon emission directs the significant role of trees in reducing carbon emissions and combating the problem of global warming.

Based on the empirical findings of this study, the following are a few recommendations:

1. The study establishes the validity of EKC for carbon emission across the world and turning points at high GDP per capita levels. Carbon emissions will continue for many years before any decoupling of carbon mission and economic growth is likely to occur. This emphasizes the need for effective implementation of policy to fasten the decoupling. Thus, it would be unjustified to rely on reducing the amount of carbon emission as like EKC effect.
2. The results show that urbanization and forest cover are important determinants of carbon emissions. Therefore, policy directions for curbing carbon emissions for improving environmental quality should consider these two factors in policy measures. This calls for the need for the countries to concentrate on green economies and designing a sustainable plan for urban development. Growth strategies need to align with the environmental welfare policies whereby the macroeconomic factors resulting in carbon emission are taken care of for instance energy diversification in a way of shift towards alternative renewable energy resources.
3. The study found a negative correlation between forest area and carbon emission which signifies the crucial role of forest in combating global warming. Forests absorb huge amounts of carbon dioxide which if destroyed can be a source of greenhouse gas. Countries should take incentives to check on deforestation. Recently, as a part of the Paris Agreement countries have established the 'REDD+' (Reducing Emissions from Deforestation and Forest Degradation in developing countries) framework to protect the forests.

## REFERENCES

- Barbier, E.B., 2004. Water and economic growth. *Economic Record*, 80(248), pp.1-16.
- Boubellouta, B. and Kusch-Brandt, S., 2021. Cross-country evidence on environmental Kuznets curve in waste electrical and electronic equipment for 174 countries. *Sustainable Production and Consumption*, 25, pp.136-151.
- Kuznets, S., 1955. Economic growth and income inequality. *The American Economic Review*, 45(1), pp.1-28.
- Cole, M.A., Rayner, A.J. and Bates, J.M., 1997. The environmental Kuznets curve: an empirical analysis. *Environment and Development Economics*, 2(4), pp.401-416.
- Gokmenoglu, K.K. and Taspinar, N., 2018. Testing the agriculture-induced EKC hypothesis: the case of Pakistan. *Environmental Science and Pollution Research*, 25, pp.22829-22841.
- Grossman, G.M. and Krueger, A.B., 1991. Environmental impacts of a North American free trade agreement.
- Grossman, G.M. and Krueger, A.B., 1995. Economic growth and the environment. *The Quarterly Journal of Economics*, 110(2), pp.353-377.

- Halkos, G.E. and Tzeremes, N.G., 2009. Exploring the existence of Kuznets curve in countries' environmental efficiency using DEA window analysis. *Ecological Economics*, 68(7), pp.2168-2176.
- Holtz-Eakin, D. and Selden, T.M., 1995. Stoking the fires? CO2 emissions and economic growth. *Journal of Public Economics*, 57(1), pp.85-101.
- Jiaqi, Y., Yang, S., Ziqi, Y., Tingting, L. and Teo, B.S.X., 2022. The spillover of tourism development on CO2 emissions: A spatial econometric analysis. *Environmental Science and Pollution Research*, pp.1-16.
- Magnani, E., 2001. The Environmental Kuznets Curve: development path or policy result? *Environmental Modelling & Software*, 16(2), pp.157-165.
- Mehmood, U., Tariq, S., Ul Haq, Z., Azhar, A. and Mariam, A., 2022. The role of tourism and renewable energy towards EKC in South Asian countries: fresh insights from the ARDL approach. *Cogent Social Sciences*, 8(1), p.2073669.
- Ministry of Environment and Energy, 2016. Second National Communication of Maldives to the United Nations Framework Convention on Climate Change.
- Murshed, M. and Dao, N.T.T., 2022. Revisiting the CO2 emission-induced EKC hypothesis in South Asia: the role of Export Quality Improvement. *GeoJournal*, 87(2), pp.535-563.
- NOAA, 2023. Greenhouse gases continued to increase rapidly in 2022. Available at: <https://www.noaa.gov/news-release/greenhouse-gases-continued-to-increase-rapidly-in-2022#:~:text=The global surface average for,higher than pre-industrial levels> [Accessed 27 Sep. 2024].
- Opoku, E.E.O. and Boachie, M.K., 2020. The environmental impact of industrialization and foreign direct investment. *Energy Policy*, 137, p.111178.
- Panayotou, T., 1993. Empirical tests and policy analysis of environmental degradation at different stages of economic development.
- Sebri, M., 2015. Testing the environmental Kuznets curve hypothesis for water footprint indicator: a cross-sectional study. *Journal of Environmental Planning and Management*, 59(11), pp.1933-1956.
- Shafik, N. and Bandyopadhyay, S., 1992. Economic growth and environmental quality: time-series and cross-country evidence. *World Bank Publications*.
- UNEP, 2019. Emissions Gap Report 2019. United Nations Environment Programme, Nairobi. Available at: <https://www.unep.org/resources/emissions-gap-report> [Accessed 27 Sep. 2024].
- Usenobong, E.A. and Chukwu, A.C., 2011. Economic growth and environmental degradation in Nigeria: beyond the environmental Kuznets curve. In: *Proceedings of the NAEF conference on green energy and energy security option for Africa*, pp.212-234.
- World Bank, 2019. World Development Indicators. Available at: <https://databank.worldbank.org/source/world-development-indicators> [Accessed 27 Sep. 2024].

---

#### ORCID DETAILS OF THE AUTHORS

Punam Chanda : <https://orcid.org/0009-0002-7381-6759>





# Environmental Education Model Based on Local Wisdom of the Dayak Paramasan Tribe Indonesia

D. F. Wardhani<sup>1</sup>, D. Arisanty<sup>2†</sup>, A. Nugroho<sup>3</sup> and U. B. L. Utami<sup>4</sup>

<sup>1</sup>Doctoral Program of Environmental Science, Lambung Mangkurat University, South Kalimantan, Indonesia

<sup>2</sup>Department of Geography Education, Lambung Mangkurat University, South Kalimantan, Indonesia

<sup>3</sup>Department of Agricultural Industrial Technology, Lambung Mangkurat University, South Kalimantan, Indonesia

<sup>4</sup>Department of Chemistry, Lambung Mangkurat University, South Kalimantan, Indonesia

†Corresponding author: D. Arisanty; deasyarisanty@ulm.ac.id

**Nat. Env. & Poll. Tech.**  
Website: [www.neptjournal.com](http://www.neptjournal.com)

Received: 14-02-2024

Revised: 27-03-2024

Accepted: 11-04-2024

## Key Words:

Dayak local wisdom  
Environmental education model  
Structural equation modelling  
Sustainability  
Dayak Paramasan tribe

## ABSTRACT

The indigenous knowledge of the Dayak Paramasan in Indonesia holds the potential for environmental sustainability. This study aims to assess an environmental education framework grounded in the local wisdom of the Paramasan Dayak tribe. A survey was conducted among 300 individuals, including traditional leaders and members of indigenous communities residing in the Paramasan Subdistrict, Indonesia. Data collection occurred from May 2023 to July 2023 and was analyzed using Structural Equation Modelling (SEM). The findings indicate a significant association between indigenous values, local expertise, and community cohesion concerning environmental education. Local wisdom includes local skills, values, and community solidarity, which are crucial for environmental education. Local skills, like farming and hunting, have a significant impact on environmental protection. Passing down knowledge to younger generations needs improvement. Limited local resources create a gap between generations, but some believe traditional leaders can safeguard nature without formal education. Further exploration of implementing environmental education models within school settings will offer valuable insights for Indigenous communities and society, fostering environmentally conscious behaviors.

## INTRODUCTION

The dimensions of local wisdom of the Dayak tribe include the preservation of cultural values and practices, sustainable management of the environment, and the use of traditional architecture and spaces for cultural activities. The Dayak tribes have a rich cultural heritage passed down from generation to generation, including traditional practices such as Dayak Binatur (Purba et al. 2021). They also have local wisdom in managing forest areas, such as the Bahuma Batahun system, which involves correctly burning forests at the right time to prevent disasters (Wahyu 2021). The Dayak Jangkang Bokidoh tribe has tangible and intangible architectural values, with traditional houses and spaces used for cultural activities like the “Gawai” ceremony (Fajarwati & Masruri 2019). The local wisdom of the Dayak tribe in Central Kalimantan has been diminishing, but it offers unique opportunities for researchers to explore their cultures, traditions, and biodiversity (Setyabudi et al. 2021).

Local wisdom plays a crucial role in environmental sustainability. It encompasses the values and practices passed down through generations and aimed at maintaining the natural environment. The implementation of local wisdom

can be seen in various aspects, such as river preservation, entrepreneurship development, water resource conservation, and ecological guidelines. For example, the Kali Loji Festival in Pekalongan City, Indonesia, teaches the community to preserve the river and increases public awareness of river sustainability (Santoso et al. 2020). In Kulonprogo, Indonesia, sustainable entrepreneurship is developed to harmonize economic development with environmental preservation, and local wisdom is recognized as one of the domains for sustainable entrepreneurial development (Kartika et al. 2020). Similarly, in Lempur, the local wisdom of society is essential in conserving water resources and ensuring their proper conservation (Ferry 2019). Furthermore, the people of Kampung Naga in Tasikmalaya implement local wisdom to preserve the environment and sustain natural resources (Asteria et al. 2021). Lastly, integrating STEM education and character-based local wisdom in Indonesia enhances sustainability literacy and empowers local wisdom as an approach to invention (Akbar et al. 2020).

Environmental sustainability is paramount in ensuring our planet's and future generations' long-term well-being. It involves preserving the ecological system's structure and functions, assessing the ecosystem's state, and aligning

business operations with sustainable practices (Sulimin et al. 2021). Current diets and agricultural practices contribute to environmental problems such as climate change, biodiversity loss, and water shortages, emphasizing the need to change food systems and dietary choices (Rose et al. 2019). Shifting towards more sustainable dietary patterns and adopting new food analogs with lower environmental impacts can help reduce the global environmental impact of food production (Cottrell et al. 2021). However, ensuring that these new foods effectively drive the disadoption of existing high-impact alternatives is crucial to prevent exacerbating the environmental impact of human diets. Environmental sustainability is essential for maintaining a healthy planet and achieving a sustainable future.

Local wisdom refers to the ideas, values, and views that are wise, valuable, and inherent to a local community. It encompasses cultural, economic, communication, and ecological aspects and attitudes that are naturally created and passed down through customs or ancestral teachings (Limba et al. 2023). Local wisdom is the heritage of cultural values and norms that are strategically reformed and developed in the era of Information Technology (Ezir et al. 2023). It is a characteristic or culture that develops locally and is passed down from generation to generation, embodying cultural values (Sari et al. 2023). Local wisdom is seen as relevant to learning mathematics and can include various aspects of culture, such as philosophy, values, norms, ethics, rituals, beliefs, habits, and customs (Messy et al. 2023). Additionally, local wisdom serves as a means of social control and shared values that guide the lives of local people, preserving the environment and maintaining a balance between the needs of local life and ecological sustainability (Handayani & Suparno 2023).

Local wisdom positively correlates with environmental education (Duriani et al. 2019, Kurniasari et al. 2020, Mahendra 2021, Susanti et al. 2018). Local wisdom is believed to instill students' awareness and love for the environment (Hilman & Sunaedi 2018). The challenges of applying local wisdom in the educational environment include the impact of technological development, changes in the physical environment, contact with other communities and the culture of the community replacing local culture, and the perception that local wisdom is complicated and slow compared to modernity (Munawwarah & Astuti 2019). However, efforts to conserve local wisdom and integrate it into education can effectively function in promoting cultural education and advocating for social-cultural equality (Chaer et al. 2021). The massive use of technology poses a threat to local wisdom, but when combined with technology, local wisdom can increase people's understanding of its values

and importance in education (Komariah & Asyahidda 2020). The need for instructional materials incorporating local wisdom is evident, as existing materials often fail to fulfill students' needs and implement character values (Yuniyati 2017). Integrating local wisdom values, such as tolerance and cooperation, into the national curriculum can contribute to maintaining national unity and diversity (Yamin & Wahyu 2018).

Spirituality and connectedness with nature are closely linked. Research has shown that spirituality can be part of well-being and influence well-being (Ryff 2021). Additionally, individuals with a strong sense of connectedness with nature, known as human-nature connectedness (HNC), tend to have higher levels of well-being and engage in pro-nature behaviors (Barragan-Jason et al. 2022). Indigenous worldviews also emphasize the importance of relationships with the environment for well-being (Keaulana et al. 2021). Furthermore, studies have found that connectedness to nature positively relates to sustainable behavior (Navarro et al. 2020). Parents' self-efficacy in engaging their children in nature-related activities, known as nature connectedness parental self-efficacy (NCPSE), is also associated with greater nature connectedness and well-being (Barnes et al. 2021). These findings suggest that spirituality, connectedness with nature, and well-being are interconnected and can positively affect individuals and their engagement with the natural world.

Local wisdom plays a significant role in the management of natural resources. It involves utilizing traditional knowledge and practices to support sustainable nature management and biodiversity conservation (Sonbait et al. 2021). Local wisdom is often embedded in communities' cultural and social systems, guiding their interactions with the environment and shaping their livelihoods (Intem et al. 2021). This includes accumulating, transferring, and inheriting knowledge from generation to generation, contributing to self-reliance, and preserving local identity (Setiawan et al. 2021). Local wisdom also informs the management of forest areas, with communities adhering to traditions, rules, and restrictions passed down through the years (Nurhayati et al. 2021). In fisheries resource conservation, local wisdom is valuable for tourism education and protecting fisheries resources (Rozaki et al. 2020). By incorporating local wisdom into natural resource management, communities can maximize the benefits of these resources while ensuring long-term sustainability.

The tradition of Gotong Royong, a form of cooperation and collaboration, is still actively practiced in Indonesian society in rural and urban areas (Simarmata et al. 2020). This tradition has been observed in various contexts, such as

disaster response in Palu Valley, where ethnic and religious communities and non-governmental organizations played a significant role in the emergency response phase (Alamsyah et al. 2020). Cooperation has also been observed in the face of the COVID-19 pandemic, where communities have come together to provide mutual help and support, contributing to societal resilience (Bahagia et al. 2020). Gotong Royong is deeply rooted in Indonesian culture and has been recognized as crucial for community development and poverty reduction (Slikkerveer 2019). However, there is evidence of a decline in social trust and cooperation among different generations, indicating a change in societal values (Tomo et al. 2020). Overall, the tradition of Gotong Royong and collaboration continues to play a significant role in Indonesian society, fostering community resilience and unity.

Indigenous roles and Indigenous leadership are essential aspects in various contexts. The crucial role played by a solid local Aboriginal workforce in health care delivery emphasizes the importance of collaboration in developing effective prevention programs at a community level (Stroud et al. 2021). Indigenous research leadership can enhance

research benefits to Indigenous communities (Kiatkoski Kim et al. 2021). The scholarly upbringing of Indigenous leaders from the Krikati (western Maranhão area, Central Brazil) people highlights the determination of native leaders to appropriate Western knowledge, contributing to the strengthening of their leaderships and the realization of projects in their territories (de Oliveira Silva et al. 2021). Indigenous leadership operates from the connected place of family and community, striving for better conditions and outcomes for all Indigenous peoples (Ryan & Evans 2020).

Environmental sustainability is an integral part of the Dayak tribal identity. The Dayak Ngaju community views the forest as sacred, communally owned, protected based on customary law rules, and passed down through generations (Ahmad 2020). The Central Borneo Dayak Tribe uses singers and jipen as ethical punishments to maintain environmental conditions and reduce ecological change (Azhari 2019). The Dayak Jalai community utilizes environmental history to reduce disaster risk and increase awareness of natural disasters (Wibowo et al. 2019). The indigenous peoples of Borneo have appropriate

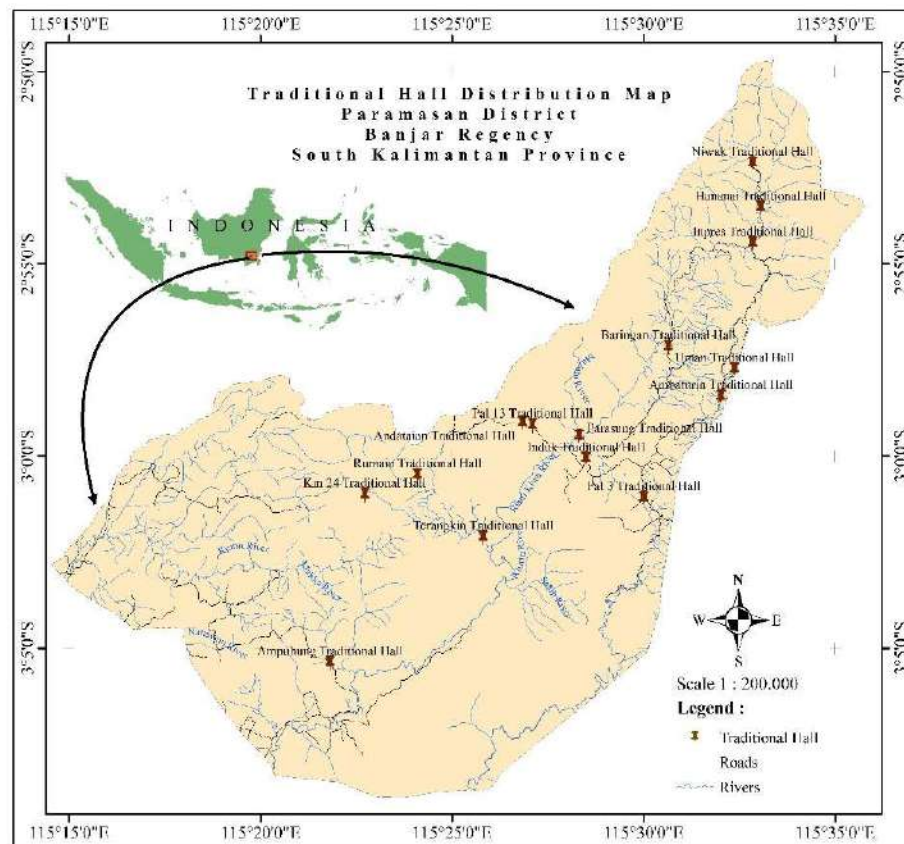


Fig. 1: Map of the research location.

images of their close connection to nature to address economic, cultural, and ecological challenges (Duile 2017). Sustainable development is essential for businesses in global markets, and companies should respect and apply sustainability principles (Paurova & Chlebkova 2020).

## MATERIALS AND METHODS

### Research Location

This study was conducted in Paramasan, South Kalimantan, Indonesia. The map of the study site is shown in Fig. 1.

### Data Collection

The data were collected using questionnaires distributed to a total of 300 respondents. They live as indigenous peoples in Angkipih Village, Paramasan Atas Village, and Paramasan Bawah Village, Indonesia. The data collection was carried out from Mei 2023 to July 2023. The variables used to analyze the environmental education model of the Dayak Paramasan tribe are local knowledge (LK), local values (LV), local skills (LS), local sources (LSo), Mechanism of local decision-making (MLDC), Local Society Solidarity (LSS) and Environmental Education (EE). We asked 35 questions on the questionnaire. The 35 items employed a Likert scale (1-5, strongly disagree-strongly agree).

### Data Analysis

The data were analyzed using Structural Equation Modeling (SEM). Factors loading was used to assess discriminant validity, where only items with factors that outperformed 0.50 would remain in the model (Hair Jr et al. 2017). The hypotheses in this study are: Dimensions of Local Wisdom of the Paramasan Dayak Tribe (1-6) have a positive influence on Environmental Education (EE)

1. Local Knowledge (LC) has a positive influence on Environmental Education (EE)
2. Local Value (LV) has a positive influence on Environmental Education (EE)
3. Local Skill (LS) has a positive influence on Environmental Education (EE)
4. Local Source (LSo) has a positive influence on Environmental Education (EE)
5. Mechanism of local decision-making (MLDC) has a positive influence on Environmental Education (EE)
6. Local Society Solidarity (LSS) has a positive influence on Environmental Education (EE)

## RESULTS AND DISCUSSION

### Local Knowledge of The Dayak Paramasan

The local knowledge of indigenous people can be used in environmental education by integrating it into the curriculum and teaching practices. This can be achieved by incorporating indigenous practices, traditional ecological knowledge (TEK), and indigenous storytelling (Brondo et al. 2023, Matsekoleng & Mapotse 2023). By including indigenous knowledge, environmental education can provide a fresh perspective on environmental issues and offer solutions grounded in indigenous practices (Rosemary A. Kinch 2016). Integrating indigenous and local knowledge into sustainability and environmental education can promote epistemological justice and enhance students' identity and learning outcomes (Druker-Ibáñez & Cáceres-Jensen 2022). However, challenges are associated with incorporating Indigenous knowledge, such as the need for resources and support and the need for actors to navigate different frames of reference (Njoh et al. 2022). Despite these challenges, incorporating indigenous knowledge into environmental education can contribute to a more inclusive and holistic approach to sustainability.

The Dayak Paramasan people possess a profound knowledge of natural phenomena and signs that indicate shifts in seasonal cycles, including the transitions between dry and rainy seasons. They comprehensively understand the types and names of animals and plants in their village, including wild and domesticated species. However, only a limited number of these were mentioned in interviews due to their frequent encounters or protection within the area (Wardhani et al. 2023).

### Local Value of the Dayak Paramasan

Indigenous peoples' values in environmental education emphasize interculturality, transversal, flexible approaches to education, and a connection to the natural world (Damas da Silveira & Aily Franco de Camargo 2015). They aim to promote environmental learning and reconnection with the natural world while also rebuilding and strengthening Indigenous identities, cultures, and ways of life (Nesterova 2020). Indigenous education models have long recognized the interconnectedness of humans and the environment and incorporate concepts of transformation, holism, caring, and responsibility (Mckee 2012). Indigenous pedagogies and environmental education can complement each other in transformative endeavors, providing alternative pedagogies that value and harness the diversity of students' backgrounds and experiences (Biermann 2008). Indigenous peoples' knowledge about the environment and sustainability,



Fig. 2: Ritual of Dayak Paramasan Indonesia.

particularly regarding the cultural role of ethnicity, is considered in designing educational materials for environmental education (Cebrián-de-la-Serna & Noguera-Valdemar 2010). The Paramasan community adheres to strict regulations during their traditional environmental protection rituals (Fig. 2), which include restrictions on logging, hunting, and other activities that harm nature (Wardhani et al. 2023).

#### Local Skill of the Dayak Paramasan

The local skill of the Dayak Paramasan indigenous people in environmental education is an essential aspect of their cultural heritage. They deeply understand their natural surroundings and have developed sustainable practices to conserve the environment (Tajibu 2020). The Dayak Paramasan people have traditional knowledge and practices that contribute to disaster risk reduction and environmental change management (Damas da Silveira & Aily Franco de Camargo 2015). They utilize their local indigenous knowledge in various ways, such as emergency evacuation and post-disaster relocation, food and livelihood security strategies, and weather forecasting from animals and celestial bodies (Surtikanti et al. 2017). The elders are crucial as local hazard forecasters and are dedicated to transmitting and preserving their local indigenous knowledge to the younger generation (Cuaton & Su 2020). This local skill is not only valuable for the Dayak Paramasan people but also has the potential to contribute to broader environmental education efforts (Gunawan & Dharman 2017).

The Paramasan Dayak community possesses a range of indigenous expertise in hunting, agriculture, and collecting resources from the forest, with hunting being primarily conducted for cultural rituals and employing a combination

of traditional and contemporary tools while prioritizing minimal harm to terrestrial, aquatic, and avian fauna (Wardhani et al. 2023).

#### Local Source of the Dayak Paramasan

Indigenous peoples have been actively involved in environmental education, incorporating their knowledge systems and ways of knowing (Nesterova 2020). This involvement supports environmental learning, reconnecting with the natural world, and rebuilding and strengthening Indigenous identities, cultures, and ways of life (Damas da Silveira & Aily Franco de Camargo 2015). Indigenous schools in Brazil also emphasize the importance of environmental education and promote interculturality, transversal, and flexible approaches to education in their syllabuses (Cebrián-de-la-Serna & Noguera-Valdemar 2010). In the sub-region of Amazonia-Orinoquia in Venezuela, research was conducted to analyze indigenous peoples' knowledge about the environment and sustainability, particularly regarding the cultural role of ethnicity (Verma et al. 2016). The study also aimed to design and elaborate educational materials that address environmental education related to the cultural role that ethnic groups play in species preservation. These objectives were achieved through collaboration with indigenous communities and using various data collection techniques.

Local resources found in the forest, such as *Durio dulcis*, *Durio oxleyanus* Griff, *Nephelium ramboutanake* Lennh, and others, contribute to the biodiversity and ecological balance of the area. Similarly, local resources in the garden and water, including *Mystacoleucus padangensis* and *Barbonymus gonionotus* Bleeker, play a significant role in sustaining the local ecosystem (Wardhani et al. 2023).

## **A Mechanism of Local Decision of The Dayak Paramasan**

Indigenous peoples have been actively engaged in collaborative research projects and environmental education programs to address climate change and ecological degradation. These initiatives aim to incorporate Indigenous knowledge systems and ways of knowing, promote reconnection with the natural world, and strengthen Indigenous identities and cultures (Damas da Silveira & Aily Franco de Camargo 2015, Nesterova 2020). In the context of indigenous schools, environmental education should be rooted in interculturality, transversally, and flexible approaches that are linked to the natural world and the social dynamics of indigenous children and young natives (Cebrián-de-la-Serna & Noguera-Valdemar 2010). Research conducted in the Amazonia-Orinoquia sub-region involved indigenous communities as subjects and objects of analysis, focusing on analyzing their knowledge about the environment and sustainability. The study also aimed to design educational materials that address environmental education related to the cultural role of ethnic groups in species preservation (Magni 2017). Indigenous knowledge systems can contribute to sustainable practices, land and resource management, climate change adaptation, and disaster risk reduction strategies. Ensuring Indigenous peoples' full access to land and justice to realize their rights and foster an integrated knowledge system involving Indigenous groups in decision-making is essential.

All villages in the Paramasan Sub District possess customary institutions, although they need legal provisions on a national scale. The customary law in Paramasan District is being effectively implemented, adhering to government regulations. Local communities are granted the right to utilize their natural surroundings responsibly and abide by regional regulations, allowing them to cultivate their land (Wardhani et al. 2023).

### **Local Society Solidarity of The Dayak Paramasan**

Local society solidarity in environmental education is crucial for achieving effective environmental outcomes and promoting community empowerment. Studies have shown that community environmental education, which includes public participation, environmental adult education, and environmental communication, can lead to collaborative efforts between organizations and local communities, resulting in improved local environments (Blair 2008). However, community participation in environmental management and activities is often limited and symbolic rather than effective or collaborative (Bilar & De Mendonça Pimentel 2020). It is essential to incorporate social

participation and environmental education into protected areas to promote community empowerment and raise citizen participation (Malone 1996). Additionally, community participation significantly stimulates pro-environmental behaviors and place attachment, which is essential for achieving eco-environmental protection goals (Zhang et al. 2020). Factors such as lower income inequality, more businesses, and democratic political participation can contribute to higher levels of within-community cooperation for a shared green reputation (Rivera et al. 2017).

Cooperation in nature activities is well-executed due to mutual assistance and adherence to a predetermined schedule. Residents from different villages also contribute, particularly in land clearing, planting, and harvesting. When the work area is extensive and the workforce is inadequate, wage labor is employed for 8 hours with a wage of 120,000. Community cooperation is evident in various activities scheduled for each village or customary area, such as bridge repairs and road cleaning on Sundays for the Balai Matang Lahung indigenous community. The Balai 24 customary community conducts road and bridge construction every Wednesday (Wardhani et al. 2023).

Environmental education models based on local wisdom have been explored in several studies. These models aim to integrate local knowledge and practices into educational strategies to promote sustainable thinking and behaviors (Chaer et al. 2021). One study focused on developing an environmental education model beyond cognitive learning and addressing affective and psychomotor aspects (Dudung et al. 2019). Another study examined the relationships between community contexts and the application of local wisdom in school management of education, suggesting that the involvement of community members and experts is crucial for the successful implementation of local wisdom in schools (Lander 2017). Additionally, a study proposed a model of education suitable for underdeveloped areas, prioritizing local wisdom and improving the quality of education in lagging regions (Jahja 2016). These studies highlight the importance of incorporating local wisdom into environmental education models to enhance sustainability education and promote local knowledge and conservation practices.

Environmental education models based on local wisdom are seen from various aspects, including local knowledge, local values, local skills, local sources, mechanism of local decision-making mechanisms, and local societal solidarity. There are around 35 questions regarding the dimensions of local wisdom of the Paramasan Dayak tribe to obtain an environmental education model. The loading factor value is relatively high, with a value of > 0.5 and Cronbach's Alpha

Table 1: Summary of measurement models.

Construct	Item	Loading Factor	Cronbach's Alpha
Local Knowledge (LC)	LC1	0.710	0.833
	LC2	0.755	
	LC3	0.657	
	LC4	0.796	
	LC5	0.806	
	LC6	0.699	
Local Value (LV)	LV1	0.617	0.848
	LV2	0.765	
	LV3	0.660	
	LV4	0.653	
	LV5	0.763	
	LV6	0.786	
	LV7	0.818	
Local Skill (LS)	LS1	0.721	0.872
	LS2	0.681	
	LS3	0.711	
	LS4	0.720	
	LS5	0.679	
	LS6	0.624	
	LS7	0.678	
	LS8	0.737	
	LS9	0.763	
Local Source (LSo)	LSo1	0.940	0.865
	LSo2	0.937	
Mechanism of Local Decision Making (MLDC)	MLDC1	0.892	0.745
	MLDC2	0.893	
Local Society Solidarity (LSS)	LSS1	0.882	0.761
	LSS2	0.914	
Environmental Education (EE)	EE1	0.665	0.887
	EE2	0.667	
	EE3	0.817	
	EE4	0.795	
	EE5	0.747	
	EE6	0.865	
	EE7	0.845	

Source: Questionnaire Results (2023)

> 0.7. In Table 1, a summary of the measurement model is presented.

The correlation between local knowledge, local value, local source, local society solidarity, and environmental education ranges from 0.6 to 0.7. The lowest correlation value is between the Mechanism of Local Decision Making in environmental education and other correlation values, namely 0.584. The highest correlation value is between

local skills in environmental education compared to other correlation values, namely 0.741. It indicates that the relationship between local skill and environmental education is closer than the relationship between other local wisdom variables (Table 2).

The influence of local skills on environmental education is more significant than that of other local wisdom. This shows that farming, hunting, and forest product-gathering

Table 2: Correlation between local wisdom on environmental education.

Variable	Environmental Education
Local Knowledge	0.671
Local Value	0.715
Local Skill	0.741
Local Source	0.694
Mechanism of Local Decision-Making	0.584
Local Society Solidarity	0.682

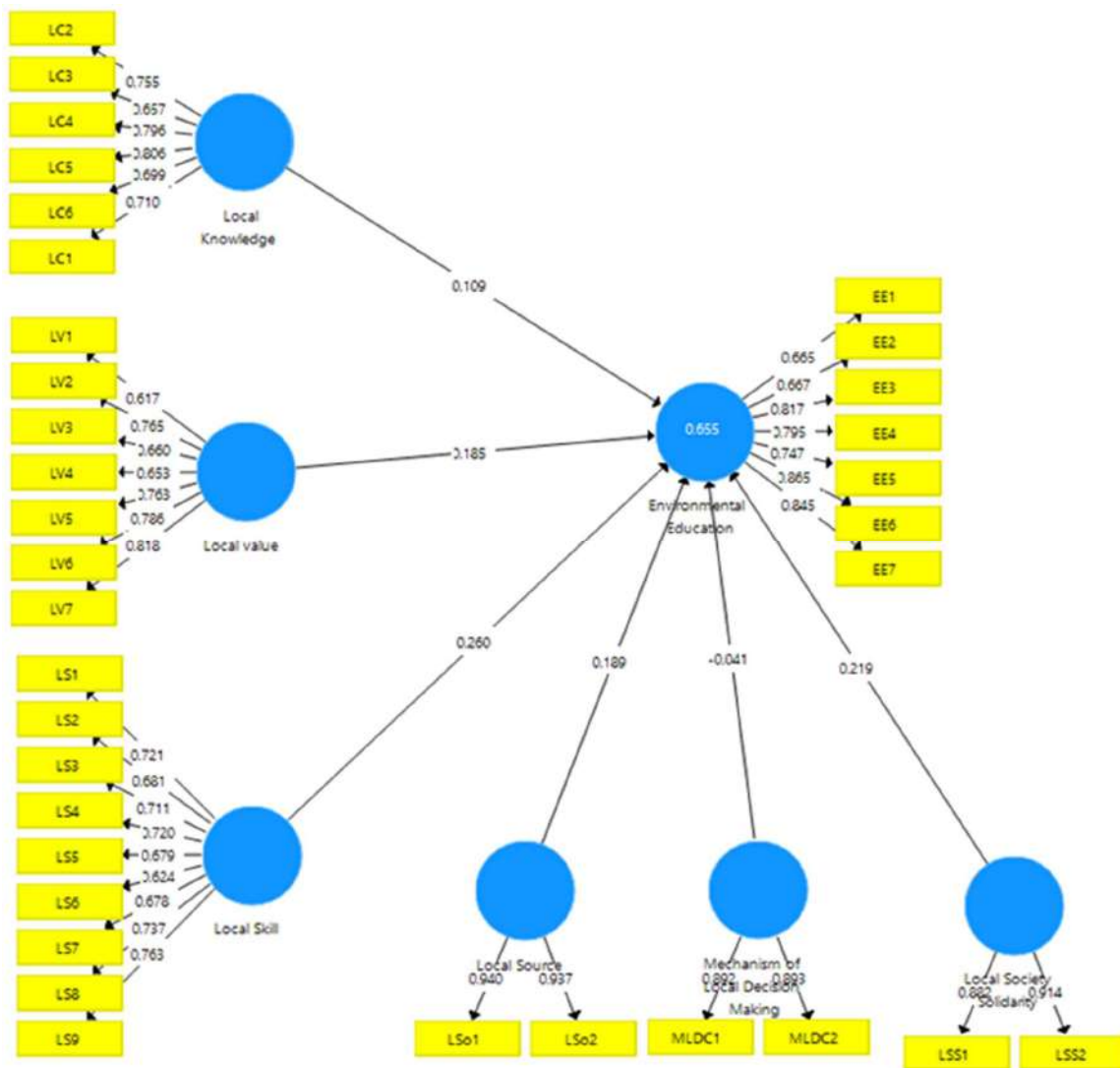
Source: data processing with SEM (2023)

skills significantly influence environmental education compared to different aspects.

The Environmental Education Model Based on the Local Wisdom of the Paramasan Dayak Tribe is shown in Fig. 3 and Table 3.

The p-value shows <0.05, causing the influence of the variable's local values, local skills, and local community solidarity with environmental education to be significant, while the variable's local knowledge, local resources, and regional decision-making mechanisms on environmental education are not significant.

Based on the data above, local skills have the highest significance value for environmental education, namely 0.260. The local skills of the Paramasan Dayak tribe include



(Source: data processing with SEM 2023).

Fig. 3: Environmental Education Model Based on Local Wisdom of the Paramasan Dayak Tribe.



Table 3: Model summary.

Model Summary	Original Sample (O)	Sample Mean (M)	Standard Deviation (STDEV)	T Statistics ( O/STDEV )	P Values	Conclusion
Local Knowledge -> Environmental Education	0.109	0.115	0.082	1.326	0.185	Not Significant
Local Value -> Environmental Education	0.185	0.185	0.074	2.502	0.013	Significant
Local Skill -> Environmental Education	0.260	0.265	0.092	2.825	0.005	Significant
Local Source -> Environmental Education	0.189	0.175	0.107	1.766	0.078	Not Significant
Mechanism of Local Decision Making -> Environmental Education	-0.041	-0.036	0.075	0.542	0.588	Not Significant
Local Society Solidarity -> Environmental Education	0.219	0.221	0.086	2.560	0.011	Significant

Source: Data Processing with SEM (2023)

animal hunting techniques (water, land, and air), farming techniques, techniques for gathering forest products, and ways to preserve natural products to be utilized by the next generation.

Local skills have the highest significance value for environmental education. Using local examples and skills in environmental education can provide a sensible and necessary approach to fostering a sense of informed stewardship in students (Dale & Carlisle, 2008). Locality in environmental education is essential, and local and contextual activities can contribute to a better understanding of ecological problems (Robottom 2004). Integrating environmental issues based on local wisdom into the elementary school curriculum can help create awareness and knowledge among students (Gündüz et al. 2019). The effectiveness of environmental education relies heavily on educators' knowledge, skills, and attitudes, emphasizing the importance of education and awareness among teachers (Sarbaini et al. 2022). Therefore, local skills are critical in environmental education because they contribute to a deeper understanding of environmental problems and enhance sustainable development

Local community solidarity also significantly influences environmental education, which can be seen at a value of 0.219. This value shows a more significant influence compared to the local value. The strong solidarity of the local Dayak Paramasan tribe can be seen from the existence of cooperation activities in various stages of farming, community activities, and various ritual or ceremonial activities carried out by indigenous communities.

Local community solidarity plays an essential role in environmental education (do Amaral et al. 2020, Gallay et al. 2021, Grúňová et al. 2017, Salazar et al. 2022, Schmitz et al. 2010). Collaborative educational models that link environmental sustainability with community engagement and social justice effectively promote

sustainable communities. Environmental education programs for school children in local communities have been found to increase knowledge and support conservation activities. Engaging students in environmental projects in their urban communities fosters an appreciation for nature and promotes pro-environmental leadership and behavior. Regional/municipal governments can facilitate school participation in environmental education programs, especially in communes where local authorities can promote voluntary initiatives. Environmental education programs that involve schools and communities in joint planning and implementation processes strengthen ties between schools and local communities and promote environmental awareness.

Local values provide a significant influence on environmental education worth 0.185. This value is among the lowest of the other two dimensions of local wisdom: local skills and community solidarity. The local values of the Paramasan Dayak tribe consist of carrying out traditional ritual/ceremonial processes to respect nature, obedience in avoiding various prohibitions or restrictions related to environmental management, application of local wisdom values that support the sustainable development of the village, and awareness of the importance of passing on local values to the next generation.

Local values provide a significant influence in the field of environmental education. Studies have shown that environmental education can effectively change students' environmental attitudes and behavior, which depends on their relationship with the natural world and their ecological worldview (Ma et al. 2021). Additionally, utilizing local examples in environmental education is a logical and indispensable approach, as it helps cultivate an enlightened sense of stewardship in students and builds social capital in society (Robottom 2004). In addition, research has confirmed that environmental education can result in the cultivation

of ecological values and the formation of students' environmental experiences, both essential for promoting environmental sustainability and resolving environmental difficulties (Liu et al. 2018). Therefore, incorporating local values and experiences into environmental education can increase its efficacy and positively impact environmental outcomes.

Local knowledge, local resources, and regional decision-making mechanisms on environmental education may not be significant due to various factors. One possible reason is the lack of teaching materials and limitations on teachers' capabilities, which hinder the successful implementation of environmental education programs (Mendoza Jr et al. 2023). Additionally, neoliberal capitalism's constraints placed on conservation NGOs can limit the incorporation of local experiences, memories, and knowledge in environmental education programming (Brondo et al. 2023). Furthermore, the involvement of local stakeholders in adaptive ecosystem management choices can play a crucial role in influencing knowledge retention and pro-environmental behavior intentions (Krogman 2017). It is also essential to consider the influence of social capital and cognitive dimensions on individual environmental knowledge and behavior (Sechi et al. 2018). Lastly, capturing and sharing local ecological knowledge in a digital format can be challenging, especially in communities with limited technical skills or no formal education (Vitos 2018).

## Discussion

The local wisdom of the indigenous Dayak Paramasan people in preserving the environment is based on their deep connection and respect for nature. They view the forest as more than just an economic asset, it is a part of their life and belief system (Suswandari et al. 2022). The Dayak Paramasan people practice sustainable behaviors, such as conserving land and resources and utilizing traditional rules and customs to guide their ecological behavior (Rachmat Effendi et al. 2020). They treat the forest with the same care and respect as they would, understanding that nature's well-being is interconnected with their well-being (Fahrianoor et al. 2016). This local wisdom is reflected in their livelihoods, social values, knowledge, and beliefs centered around maintaining a harmonious relationship with the environment (Rahmawati 2015). The Dayak Paramasan people's preservation efforts are crucial in the face of deforestation and forest degradation, as they recognize the importance of protecting and conserving plant diversity for their sustenance and future generations (Herianto et al. 2018).

A local wisdom-based environmental education model can potentially increase pro-environmental activity. This model

integrates environmental education with existing subjects in schools, allowing for applying environmental knowledge in daily life (Lyesmaya et al. 2020), by incorporating local wisdom and culture into education policies, character education based on local knowledge can be implemented, leading to better cultural education and advocating for social-cultural equality (Lander 2017). Additionally, the proposed model for education for sustainability based on wisdom provides a theoretical framework that connects educators to existing education and developmental theories, supporting curricular design and assessment (Jahja 2016). When implemented effectively, education for sustainability can encourage the development of wisdom and promote sustainable thinking and behaviors among students (Chaer et al. 2021). Therefore, a local wisdom-based environmental education model can potentially foster pro-environmental attitudes and actions among individuals (Filipović 2018).

The Dayak Paramasan community has six dimensions of local knowledge in managing the environment that must be maintained. These dimensions include togetherness, obedience, consensus, fairness, and caring (Utomo et al. 2020). Norms play a role in utilizing natural resources, including prohibitions/taboo and suggestions (Chaiphar et al. 2013). Beliefs are also important, with practices such as providing *labuhan*/offerings and *Selamat/ritual* (Dirhamsyah et al. 2020). The community's knowledge management is divided into internal and external knowledge exchange (Wibowo et al. 2019). Additionally, the community participates in specific activities through group formation, such as saving money and handicraft production (Himawan et al. 2014). Therefore, the six dimensions of local knowledge the Dayak Paramasan community must maintain in managing the environment are values, norms, beliefs, internal knowledge exchange, external knowledge exchange, and active participation in environmental preservation.

Local wisdom plays a significant role in environmental education in Indonesia (Fatmawati 2021)(Hanafie Das et al. 2022). It is evidence of the behaviors and values of local people that are mutually agreed upon in a particular place (Parker & Prabawa-Sear 2020). However, there are shortcomings in environmental education in Indonesia, including underqualified teachers and outdated pedagogy (Parker 2018). The Indonesian government has recognized the need for environmental awareness in schools and has implemented the Adiwiyata program, but its influence has been low. To address these issues, education in Indonesia needs to undergo a cultural transformation and be expanded to reach various sectors. Overall, local wisdom can contribute to environmental education in Indonesia, but there is a need for improvement in the current educational system.

Local science-based environmental education models play an essential role in safeguarding the environment into the future. These models provide guidelines for educators and managers to better understand and manage the learning environment in which environmental education programs occur (Buchan 2004). They also help promote innovative and engaging activities that underline the scientific aspect of environmental education, provoking interest in green sciences among students and increasing the number of students choosing science-related subjects (Lichtveld 2010). Environmental education is a lifelong interdisciplinary field of study that helps inculcate awareness, skills, attitudes, knowledge, and participatory potential in people to adjust their activities in a way that does not clash with the environment (Markaki 2014). Teacher training programs in environmental education and adequate funding for conservation research and resources are necessary for the future development of environmental education (Mushtaq et al. 2020).

## CONCLUSIONS

Local wisdom encompasses various aspects, including local skills, local values, and local community solidarity, and these elements play a significant role in environmental education. Among these, local skills have the most substantial impact on environmental education. This is evident in the fact that farming, hunting, and forest product-gathering skills are more effective in environmental protection than other aspects of local wisdom. Local values also influence environmental education, although there is room for improvement, particularly in transmitting knowledge and traditions, especially during rituals, to younger generations. The limited availability of local knowledge, local decision-making processes, and local resources highlights a knowledge gap between older and younger generations. Some believe that as long as traditional leaders exist, there's no need for formal study, but they continue to safeguard nature based on the knowledge they possess.

## ACKNOWLEDGMENTS

We thank the experts for their appropriate and constructive suggestions to improve this manuscript. We thank Indonesia's Ministry of Education, Culture, Research, and Technology for research funding and Lambung Mangkurat University for research permission.

## REFERENCES

- Ahmad, A., 2020. Dayak Ngaju forest sustainability Sharia Maqashid analysis. *Proceedings of the 1st International Conference on Islamic Civilization, ICIC 2020*, 27th August 2020, Semarang, Indonesia, pp. 1-8.
- Akbar, N., Abubakar, I.R. and Bouregh, A.S., 2020. Fostering urban sustainability through the ecological wisdom of traditional settlements. *Sustainability*, 12(23), pp. 1-19.
- Alamsyah, M.N., Nawawi, M. and Syamsiah, M.Z., 2020. Gotong Royong of civil society: The identity struggle in handling the Palu Valley disaster response. *International Journal of Progressive Sciences and Technologies*, 20(2), pp. 219-228.
- Asteria, D., Brotosusilo, A., Soedrajad, M.R. and Nugraha, F.N., 2021. Environmental preservation and sustainability of natural resources through traditional adat value (Study case Kampung Naga, West Java). *IOP Conference Series: Earth and Environmental Science*, 716(1), pp. 12051.
- Azhari, M., 2019. The impact Singer & Jipen of Dayak tribe on environmental sustainability in Central Borneo. *International Journal of Architecture and Urbanism*, 3(1), pp. 43-50.
- Bahagia, B., Rahmadanti, R. and Indriya, I., 2020. Societies resilience for confronting Covid-19 based on Gotong Royong tradition (Mutual cooperation). *Tunas Geografi*, 9(2), pp. 119-128.
- Barnes, C., Harvey, C., Holland, F. and Wall, S., 2021. Development and testing of the Nature Connectedness Parental Self-Efficacy (NCPSE) scale. *Urban Forestry & Urban Greening*, 65, p. 127343.
- Barragan-Jason, G., de Mazancourt, C., Parmesan, C., Singer, M.C. and Loreau, M., 2022. Human-nature connectedness as a pathway to sustainability: A global meta-analysis. *Conservation Letters*, 15(1), p. e12852.
- Biermann, S., 2008. Indigenous pedagogies and environmental education: Starting a conversation. *International Journal of Pedagogical and Learning*, 4(3), pp. 27-38.
- Bilar, A.B.C. and De Mendonça Pimentel, R.M., 2020. Community participation in the management and protection actions of plant biodiversity in protected areas. *Desenvolvimento e Meio Ambiente*, 53, pp. 151-166.
- Blair, M., 2008. Community environmental education as a model for effective environmental programmes. *Australian Journal of Environmental Education*, 24, pp. 45-53.
- Brondo, K.V., Kent, S., Turcios, J., Robinson, K. and Nadeem, A., 2023. Local knowledge and environmental education in Utila, Bay Islands, Honduras. *Human Organization*, 82(2), pp. 95-106.
- Buchan, J., 2004. Successful environmental education: Adapting to the educational habitat. *Australian Journal of Environmental Education*, 20(1), pp. 45-55.
- Cebrián-de-la-Serna, M. and Noguera-Valdemar, J., 2010. Conocimiento indígena sobre el medio ambiente y diseño de materiales educativos. *Comunicar*, 17(34), pp. 115-124.
- Chaer, M.T., Rochmah, E.Y. and Sukatin, S., 2021. Education based on local wisdom. *Journal of Islamic Education*, 6(2), pp. 1-13.
- Chaiphaph, W., Promsaka Na Sakolnakorn, T. and Naipinit, A., 2013. Local wisdom in the environmental management of a community: Analysis of local knowledge in Tha Pong Village, Thailand. *Journal of Sustainable Development*, 6(8), pp. 16-25.
- Cottrell, R.S., Maier, J., Ferraro, D.M., Blasco, G.D., Geyer, R., Froehlich, H.E. and Halpern, B.S., 2021. The overlooked importance of food disadoption for the environmental sustainability of new foods. *Environmental Research Letters*, 16(10), p. 104022.
- Cuatón, G.P. and Su, Y., 2020. Local-indigenous knowledge on disaster risk reduction: Insights from the Mamanwa indigenous peoples in Basey, Samar after Typhoon Haiyan in the Philippines. *International Journal of Disaster Risk Reduction*, 48, p. 101596.
- Dale, M. and Carlisle, M., 2008. Familiarity breeds context - delivering environmental education through local awareness. In: 15th Biennial Australian Association for Environmental Education Conference - Environmental Education up Track Hot Topics Our Community, 15, pp. 1-8.

- Damas da Silveira, E. and Aily Franco de Camargo, S., 2015. Environmental education in the indigenous schools of Brazil. *Holos Environment*, 15(1), pp. 10-18.
- de Oliveira Silva, I.M., da Silveira, F.M., de Almada, F.de A.C. and Zaquieu, L.da C.C., 2021. Indigenous leaderships beyond the tangle of concepts and their functions in the tracks of history: An exercise in listening. *International Journal of English Literature and Social Sciences*, 6(2), pp. 099-111.
- Dirhamsyah, D., Utama, D.B., Widyaningrum, N. and Widana, I.D.K., 2020. Kearifan lokal dan partisipasi persekutuan Dayak Kalimantan Timur dalam menghadapi bencana kebakaran hutan dan lahan. *Perspektif*, 9(2), pp. 314-321.
- do Amaral, J.A.A., da Cunha, F.M. and Dias, B.de M.M., 2020. The systemic impacts of a large-scale socio-environmental educational program. *Journal of Social Technology and Environmental Science*, 9(3), pp. 09-32.
- Druker-Ibáñez, S. and Cáceres-Jensen, L., 2022. Integration of indigenous and local knowledge into sustainability education: A systematic literature review. *Environmental Education Research*, 28(8), pp. 1209-1236.
- Dudung, A., Hasanah, U. and Silitonga, M., 2019. The education model for authorized, outdoor and terrible areas concerning the diversity of environmental, social and cultural conditions (Based on local wisdom). *KnE Social Sciences*, 3(12), pp. 189-201.
- Duile, T., 2017. Being Dayak in West Kalimantan: Constructing indigenous identity as a political and cultural resource. In: C. Arenz, M. Haug, S. Seitz & O. Venz (eds.), *Continuity under Change in Dayak Societies*, pp. 123-140. Springer Fachmedien Wiesbaden.
- Duriani, I., Halim, I., Batlajery, S. and Raf, N., 2019. The implementation of integrated local wisdom based curriculum in enhancing environmental education. *IOP Conference Series: Earth and Environmental Science*, 343(1), pp. 1-6.
- Ezir, E., Lidiana Permata Sari, P., Aryni, Y., Supiatman, L. and R., 2023. Strategic role and function of local wisdom of Melayu Asahan in the era of information technology on anthropolinguistic perspectiveness. *KnE Social Sciences*, 2023, pp. 172-179.
- Fahrianoor, F., Windari, T., Taharuddin, T., Ruslimar'i, R. and Maryono, M., 2016. The practice of local wisdom of Dayak people in forest conservation in South Kalimantan. *Journal of Wetlands Environmental Management*, 1(1), pp. 33-41.
- Fajarwati, N. and Masruri, M.S., 2019. Role of local wisdom community Dayak Kanayatin in the fire disaster prevention (forest fires for the opening of farming fields in West Kalimantan). *IOP Conference Series: Earth and Environmental Science*, 271(1), p. 12022.
- Fatmawati, D., 2021. Islam and local wisdom in Indonesia. *Journal of Social Sciences*, 2(1), pp. 20-28.
- Ferry, D., 2019. Local wisdom based water resources conservation for environmental sustainability. *Science Education Journal of Science Education*, 8(2), pp. 220-230.
- Filipović, M., 2018. Environmental education in the function of pro-environmental behavior as a prerequisite for environmental security. *Bezbednost*, Beograd, 60(1), pp. 99-111.
- Gallay, E., Pykett, A. and Flanagan, C., 2021. "We make our community": Youth forging environmental identities in urban landscapes. *Sustainability*, 13(14), pp. 1-18.
- Grůňová, M., Brandlová, K., Svitálek, J. and Hejčmanová, P., 2017. Environmental education supports conservation action by increasing the immediate and long-term environmental knowledge of children in West Africa. *Applied Environmental Education and Communication*, 16(1), pp. 3-16.
- Gunawan, I.G.D. and Dharman, G., 2017. Character education through education media of Dayak and Balinese local culture. In: *Dafis Proceeding, Darma Acarya Faculty International Seminar October 2016*, pp. 293-295.
- Gündüz, Ş., Laama, I.F. and Erdoğan, M., 2019. The significance of international higher education in environmental issues. In: *Policies and Initiatives for the Internationalization of Higher Education*, pp. 1-11. IGI Global.
- Hair Jr, J.F., Matthews, L.M., Matthews, R.L. and Sarstedt, M., 2017. PLS-SEM or CB-SEM: Updated guidelines on which method to use. *International Journal of Multivariate Data Analysis*, 1(2), pp. 107-123.
- Hanafie Das, S.W., Halik, A., Ahdar and Iman, B., 2022. Prenatal education process based on local wisdom in Indonesia. *Education Research International*, 2022, p. 6500362.
- Handayani, E. and Suparno, S., 2023. The role of customary law in the governance of sustainable agrarian culture in local communities. *Corporate Law and Governance Review*, 5(1), pp. 29-37.
- Herianto, H., Kusuma, Z., Nihayati, E. and Prayogo, C., 2018. The plant wisdom of Dayak Ot Danum, Central Kalimantan. *Journal of Tropical Life Sciences*, 8(2), pp. 130-143.
- Hilman, I. and Sunaedi, N., 2018. Revitalization of local wisdom for the environmental education. *Geosfera Indones.*, 2(1), pp. 19-28.
- Himawan, W., Sjarkowie, F. and Alfitri, A., 2014. Local wisdom from the socio-ecological perspectives: Managing former mine lands in achieving green era. *IOSR Journal of Humanities and Social Science*, 19(12), pp. 52-57.
- Intem, N., Phuwanatwicht, T., Sarobol, A. and Wannapaisan, C., 2021. The local wisdom management "Mohom" for stable inherit and lifelong learning. *Journal of Education and Learning*, 10(5), pp. 38-50.
- Jahja, R.S., 2016. Developing environmental education model based on local wisdom. *KOMUNITAS: International Journal of Indonesian Society and Culture*, 8(1), pp. 135-144.
- Kartika, N., Iwan, P. and Nuryasman, M.N., 2020. Ensuring local wisdom environmental sustainability through sustainable entrepreneurial development: A conceptual framework for Kulonprogo, Yogyakarta. In: *Proceedings of the Tarumanagara International Conference on the Applications of Social Sciences and*, pp. 182-187.
- Keaulana, S., Kahili-Heede, M., Riley, L., Park, M.L.N., Makua, K.L., Vegas, J.K. and Antonio, M.C.K., 2021. A scoping review of nature, land, and environmental connectedness and relatedness. *International Journal of Environmental Research and Public Health*, 18(11), p. 5897.
- Kiatkoski Kim, M., Watkin Lui, F., Ah Mat, L., Cadet-James, Y., Bainbridge, R. and McCalman, J., 2021. Indigenous leadership in research in Australia. *Journal of Higher Education Policy and Management*, 43(4), pp. 353-368.
- Komariah, S. and Asyahidda, F.N., 2020. Decrease or increase: Analysis of the existence of local wisdom as the core of education in the technology era. In: *Proceedings of the 4th Asian Education Symposium (AES 2019)*, pp. 207-210.
- Krogman, N., 2017. Engaging local stakeholders. *Science*, 356(6343), pp. 1134-1135.
- Kurniasari, N.D.R., Sigit, D.V. and Komala, R., 2020. Correlation between local wisdom knowledge with ecoliteracy and green behavior of students of Adiwiyata School, Bandung, West Java. *International Journal of Multicultural and Multireligious Understanding*, 7(4), pp. 411-416.
- Lander, L., 2017. Education for sustainability: A wisdom model. In: *Handbook of Theory and Practice of Sustainable Development in Higher Education: Volume 3* (W. Leal Filho, M. Mifsud, C. Shiel, & R. Pretorius, eds.), pp. 47-58. Springer International Publishing.
- Lichtveld, M.Y., 2010. Education for environmental protection: Successes, challenges, and opportunities for USEPA's environmental education program. *Human Ecology Risk Assessment: An International Journal*, 16(6), pp. 1242-1248.
- Limba, A., Tamaela, E.S., Sopacua, F., Manuhutu, L. and Huwae, I.V., 2023. Identification of science-physics concepts in the traditional game of bambu gila and its implementation in learning. *Edu Science Journal*, 4(1), pp. 1-10.

- Liu, S., Hou, Q. and Guo, L., 2018. Based on environmental experience to discuss the effect of environmental education on environmental value. *Ekoloji Dergisi*, 1(106), p. 991.
- Lyesmaya, D., Musthafa, B. and Sunendar, D., 2020. Local wisdom value's-based literacy education learning model in elementary school. In: *7th South East Asia Design Research International Conference (SEADRIC 2019)*, 1470(1), pp. 1-7.
- Ma, H., Chen, W., Ma, H. and Yang, H., 2021. Influence of publicity and education and environmental values on the green consumption behavior of urban residents in Tibet. *International Journal of Environmental Research and Public Health*, 18(20), p.10808.
- Magni, G., 2017. Indigenous knowledge and implications for the sustainable development agenda. *European Journal of Education*, 52(4), pp.437-447.
- Mahendra, P.R.A., 2021. Conception of local wisdom Nangun Sad Kerthi Loka Bali in character education. *SHEs Conference Series*, pp.78-84.
- Malone, K., 1996. School and community partnerships in socially critical environmental education: Research as environmental activism. *Deakin University*.
- Markaki, V., 2014. Environmental education through inquiry and technology. *Science Education International*, 25(1), pp.86-92.
- Matsekoleng, T.K. and Mapotse, T.A., 2023. Technology teachers' use of indigenous knowledge to integrate environmental education into technology education. In: Gumbo, M.T. and Williams, P.J. (Eds.), *Indigenous Technology Knowledge Systems: Decolonizing the Technology Education Curriculum*, Springer Nature Singapore, pp.283-295.
- Mckeon, M., 2012. Two-eyed seeing into environmental education: Revealing its "natural" readiness to indigenize. *Canadian Journal of Environmental Education*, 17(1762), pp.131-147.
- Mendoza Jr, A.B., Bernadas, M.B., Rances, A.B., Borejon, M.C., Tango, M.L.U. and Bradecina, R.G., 2023. Knowledge and awareness on the fishery resources of elementary and high school students. *Aquademia*, 7(1), ep23002.
- Messy, R., Samuel, U., Jakobus, N., Yoseph, W., Jakobus, D., Elisabeth, L., Regina, N. and Erna, Grace, O., 2023. Mathematical learning based on Tanimbar culture. *Journal of Community Service*, 4(2), pp.123-133.
- Munawwarah, M. and Astuti, S., 2019. Early childhood character education practices based on local wisdom in Aceh: Challenges and efforts made in globalization era. *Gender Equality International Journal of Child and Gender Studies*, 5(2), pp.71-82.
- Mushtaq, B., Bandh, S.A. and Shafi, S., 2020. Environmental education and environmental impact assessment. In: Mushtaq, B., Bandh, S.A. and Shafi, S. (Eds.), *Environmental Management: Environmental Issues, Awareness and Abatement*, Springer, pp.95-148.
- Navarro, O., Tapia-Fonllem, C., Fraijo-Sing, B., Roussiau, N., Ortiz-Valdez, A., Guillard, M., Wittenberg, I. and Fleury-Bahi, G., 2020. Connectedness to nature and its relationship with spirituality, wellbeing and sustainable behaviour (Conectividad con la naturaleza y su relación con la espiritualidad, el bienestar y la conducta sustentable). *PsyEcology*, 11(1), pp.37-48.
- Nesterova, Y., 2020. Rethinking environmental education with the help of indigenous ways of knowing and traditional ecological knowledge. *Journal of Philosophy of Education*, 54(4), pp.1047-1052.
- Njoh, A.J., Esongo, N.M., Ayuk-Etang, E.N.M., Soh-Agwetang, F.C., Ngyah-Etchutambe, I.B., Asah, F.J., Fomukong, E.B. and Tabrey, H.T., 2022. Challenges to indigenous knowledge incorporation in basic environmental education in Anglophone Cameroon. *Journal of Asian and African Studies*, 1(1), pp.1-6.
- Nurhayati, A., Pratiwi, D.Y., Putra, P.K.D.N.Y., Nurruhwati, I., Riyanti, I. and Herawati, T., 2021. Relevance of local wisdom to tourism education for fisheries resources conservation: The case study in West Java Province, Indonesia. *ECISOJIM (Economic Social of Fisheries and Marine Journal)*, 8(2), pp.295-309.
- Parker, L., 2018. Environmentalism and education for sustainability in Indonesia. *Indonesia and the Malay World*, 46(136), pp.235-240.
- Parker, L. and Prabawa-Sear, K., 2020. Environmental education in Indonesia: Creating responsible citizens in the global south? *Taylor & Francis*.
- Paurova, V. and Chlebkikova, D., 2020. Sustainability as part of corporate identity in conditions of globalization. *19th International Scientific Conference on Globalization and its Socio-Economic Consequences 2019 - Sustainability of Global Economy*, 74, pp.1-8. <https://doi.org/10.1051/shsconf/20207406023>.
- Purba, D.A., Suhadi, J. and Purwarno, P., 2021. Local wisdom of Dayak Binatur in the Simalungun community. *KnE Social Sciences*, 5(4), pp.1-8.
- Rachmat Effendi, M., Setiadi, E. and Ahmad Nasir, M., 2020. The local wisdom based on religious values: A case of indigenous people in Indonesia. *Humanities and Social Sciences Reviews*, 8(3), pp.1395-1404.
- Rahmawati, H., 2015. Local wisdom dan perilaku ekologis masyarakat Dayak Benuaq. *Jurnal Indigena*, 13(1), pp.72-78.
- Rivera, J., Naranjo, M.A., Robalino, J., Alpizar, F. and Blackman, A., 2017. Local community characteristics and cooperation for shared green reputation. *Policy Studies Journal*, 45(4), pp.613-632.
- Robottom, I., 2004. Environmental education and local initiatives: A rationale, international examples, and an issue for research. *Applied Environmental Education & Communication*, 3(1), pp.21-28.
- Rose, D., Heller, M.C. and Roberto, C.A., 2019. Position of the Society for Nutrition Education and Behavior: The importance of including environmental sustainability in dietary guidance. *Journal of Nutrition Education and Behavior*, 51(1), pp.3-15.
- Kinch, R.A., 2016. Indigenous storytelling, Cherokee traditional ecological knowledge, and place-based education. *March Issue*.
- Rozaki, Z., Wijaya, O., Keothoumma, K. and Salim, E., 2020. A review: Farmers' local wisdom on natural resources. *Andalasian International Journal of Agriculture and Natural Sciences*, 1(1), pp.25-32.
- Ryan, T. and Evans, M., 2020. The wisdom of differentiating between Indigenous leader and Indigenous leadership. In: *Practical Wisdom, Leadership, and Culture*, Routledge, pp.46-62.
- Ryff, C.D., 2021. Spirituality and well-being: Theory, science, and the nature connection. *Religions*, 12(11), p.914.
- Salazar, C., Leiva, M., Jaime, M. and González, N., 2022. Environmental educational programs in Chile: Do the characteristics of local governments affect school participation? *Environmental Education Research*, 28(12), pp.1755-1776.
- Santoso, I., Setyowati, D.L. and Priyanto, A.S., 2020. The local culture wisdom of the Kali Loji Festival in maintaining the sustainability of the river in Pekalongan. *Proceedings of the International Conference on Science and Education and Technology (ISET 2019)*, pp.682-685.
- Sarbaini, S., Hernawan, A.H., Darmawan, D. and Ali, M., 2022. Environmental education based on local values: its integration in the Indonesian elementary school curriculum. *International Journal of Educational Practice*, 10(4), pp.322-333.
- Sari, E.P.D.N., Amiruddin, M.Z.B., Admoko, S., Suprpto, N. and Suliyannah, S., 2023. Exploration concept of physics on local wisdom in traditional game Angkle (Engklek) as student teaching material. *Berkala Ilmiah Pendidikan Fisika*, 11(1), p.40.
- Schmitz, C.L., Stinson, C.H. and James, C.D., 2010. Community and environmental sustainability: Collaboration and interdisciplinary education. *Critical Social Work*, 11(3), pp.83-100.
- Sechi, G., Borri, D., De Lucia, C. and Celmins, V., 2018. Environmental learning in regions: A social capital based approach. The case of Latvia. *Environmental Education Research*, 24(3), pp.343-364.
- Setiawan, E., Sukesi, K., Hidayat, K. and Yulianti, Y., 2021. Conservation of natural resource management in the buffer village community of Alas Purwo Banyuwangi National Park East Java Indonesia based on local wisdom. *Local Wisdom*, 13(1), pp.100-111.

- Setyabudi, I., Santoso, D.K. and Albina, K., 2021. "Gawai": Cultural activities in the shroud of Jangkang Bokidoh Dayak tribe traditional architecture in Balai Sebut Village. *Local Wisdom*, 13(1), pp.36-50.
- Simarmata, N., Yuniarti, K.W., Riyono, B. and Patria, B., 2020. Gotong Royong in the millennial era. *Digital Press Social Sciences and Humanities*, 5, p.7.
- Slikkerveer, L.J., 2019. Gotong royong: An indigenous institution of communality and mutual assistance in Indonesia. In *Integrated Community-Managed Development Strategies: Indigenous Knowledge Institutions and Poverty Reduction for Sustainable Community Development in Indonesia* (pp.307-320).
- Sonbait, L.Y., Manik, H., Warmetan, H., Wambrauw, Y.L.S., Sagrim, M., Djitmau, D.A., Wanggai, J., Rettob, B. and Murdjoko, A., 2021. The natural resource management to support tourism: A traditional knowledge approach in Pegunungan Arfak Nature Reserve, West Papua, Indonesia.
- Stroud, V., Adams, J., Champion, D., Hogarth, G., Mahony, A., Monck, R., Pinnegar, T., Sprigg dos Santos, N. and Watson, C., 2021. The role of Aboriginal leadership in community health programmes. *Primary Health Care Research & Development*, 22, e58.
- Sulimin, V., Shvedov, V. and Lvova, M., 2021. Environmental sustainability: Quality assessment criteria. In *International Scientific Forum on Sustainable Development and Innovations (WFSDI 2021)*, 295, pp.1-4.
- Surtikanti, H.K., Syulasma, A. and Ramdhani, N., 2017. Traditional knowledge of local wisdom of Ammatoa Kajang Tribe (South Sulawesi) about environmental conservation. In *International Conference on Mathematics and Science Education* (pp.895-904).
- Susanti, S., Sukaesih, S. and Koswara, I., 2018. Forms of communication in local wisdom-based environmental education at Eco Camp. In *International Conference on Media and Communication Studies (ICOMACS 2018)* (pp.103-105).
- Suswandari, S., Armiyati, L. and Azid, N., 2022. Local wisdom of Dayak ethnic groups in Central Kalimantan, Indonesia. *ETNOSIA: Jurnal Etnografi Indonesia*, 7(1), pp.67-85.
- Tajibu, K., 2020. Pasang Ri Kajang in developing youth character of environmental love in Tana Toa Kajang. *Jurnal Adab*, 20(1), pp.131-152.
- Tomo, S.W., Wardana, A., Indrahadi, D., Zummi, N.Q.A. and Sulistyosari, Y., 2020. The waning gotong-royong: Assessing the intergenerational decline of social trust in the contemporary Indonesian society. *Proceedings of the 2nd International Conference on Social Science and Character Educations (ICoSSCE 2019)*, pp.255-259.
- Utomo, A.P., Al Muhdhar, M.H.I., Syamsuri, I. and Indriwati, S.E., 2020. Local knowledge of the using tribe farmers in environmental conservation in Kemiren Village, Banyuwangi, Indonesia. *Biosfer*, 13(1), pp.14-27.
- Verma, P., Vaughan, K., Martin, K., Pulitano, E., Garrett, J. and Piirto, D.D., 2016. Integrating indigenous knowledge and Western science into forestry, natural resources, and environmental programs. *Journal of Forestry*, 114(6), pp.648-655.
- Vitos, M., 2018. Making local knowledge matter: Exploring the appropriateness of pictorial decision trees as interaction style for non-literate communities to capture their traditional ecological knowledge. *UCL (University College London)*.
- Wahyu, 2021. Local wisdom in Banjar cultural perspective. *Proceedings of the 2nd International Conference on Social Sciences Education (ICSSE 2020)*, pp.11-15.
- Wardhani, D.F., Arisanty, D., Nugroho, A. and Utami, U.B.L., 2023. The local wisdom of the Paramasan Dayak tribe in environmental management. *Environmental Ecology Research*, 11(5), pp.859-872.
- Wibowo, B., Setyowati, D.L., Wasino, M. and Joebagio, H., 2019. Environmental history of Dayak Jalai community as an effort towards disaster risk reduction. *Proceedings of the International Conference on Rural Studies in Asia (ICoRSIA 2018)*, pp.275-278.
- Yamin, M. and Wahyu, 2018. Repositioning the local wisdom towards the national curriculum. *Proceedings of the First Indonesian Communication Forum of Teacher Training and Education Faculty Leaders International Conference on Education 2017 (ICE 2017)*, pp.535-540.
- Yuniyati, S., 2017. The implementation of local wisdom-based learning in elementary school: The analysis of instructional materials for 2013 curriculum. *Journal of Educational Issues*, 9(2), p.768
- Zhang, Y., Xiao, X., Cao, R., Zheng, C., Guo, Y., Gong, W. and Wei, Z., 2020. How important is community participation to eco-environmental conservation in protected areas? From the perspective of predicting locals' pro-environmental behaviours. *Science of the Total Environment*, 739, p.139889.



# Effectiveness of Different Artificial Neural Network Models in Establishing the Suitable Dosages of Coagulant and Chlorine in Water Treatment Works

Dnyaneshwar V. Wadkar<sup>1</sup>, Ganesh C. Chikute<sup>1</sup>, Pravin S. Patil<sup>2</sup>, Pallavi D. Wadkar<sup>3</sup>  
and Manasi G. Chikute<sup>4†</sup>

<sup>1</sup>Department of Civil Engineering, AISSM'S College of Engineering, Pune, Maharashtra, India

<sup>2</sup>Department of Civil Engineering, DY Patil University, Ambi, Pune, India

<sup>3</sup>Department of Electronics and Telecommunication Engineering, Marathwada Mitra Mandal's College of Engineering, Pune, Maharashtra, India

<sup>4</sup>Secondary Division, Muktangan English School, Pune India

†Corresponding author: Ganesh Chikute; [chikute.ganesh@gmail.com](mailto:chikute.ganesh@gmail.com)

Nat. Env. & Poll. Tech.  
Website: [www.neptjournal.com](http://www.neptjournal.com)

Received: 08-02-2024

Revised: 19-03-2024

Accepted: 29-03-2024

## Key Words:

Urban plants  
Xenobiotics  
Mycorrhiza  
Heavy metals  
Pollution

## ABSTRACT

Generally, in India, determining the chlorine and coagulant dosage in a WTP depends on the proficiency of operators, which may lead to overdosing or underdosing of coagulants and chlorine. Nevertheless, the determination of both coagulant and chlorine dosages frequently changes as inlet water quality varies which demands extensive laboratory analyses, leading to prolonged experimentation periods in water treatment plants. So objective of the study is to develop the precise relationship between coagulant dose and chlorine dose in a water treatment plant by using an artificial neural network (ANN). As a result, ANN models were developed to predict chlorine dose using coagulant dose by comparing the performance of the number of ANN models. It has been found that radial basis function neural networks (RBFNN) and generalized regression neural networks (GRNN) modeling provide better prediction. In RBFNN and GRNN modeling, the spread factor is varied from 0.1 to 15 to establish a stable and accurate model with high predictive accuracy. It is observed that the RBFNN model showed good prediction ( $R^2 = 0.999$ ). The application of a soft computing model for defining doses of coagulant and chlorine that are inextricably linked at a Water treatment plant (WTP) will be highly beneficial for WTP Managers.

## INTRODUCTION

In WTP, there are various treatment processes but the most important nonlinear and complex treatment processes are coagulation and disinfection because they ensure safe and clear water. Generally, chlorine is the most commonly used disinfectant, and aluminum sulfate (alum) is a coagulant due to its ease of application, monitoring, low cost, and effectiveness. The effectiveness of the chlorination and coagulation process mainly depends upon three major parameters, namely turbidity of water, pH of water, and applied dosages (Bello et al. 2014, Bowden et al. 2006). Traditionally, optimum coagulant doses are determined using jar tests. However, jar tests are conducted periodically, which means that they are reactive rather than proactive, whereas coagulant doses need to change continuously with turbidity (Bobadilla et al. 2019, Chan Moon 2017). In India, generally, in WTP coagulant dose is kept constant for specific periods due to a time delay of the jar test, which leads to the production of a dose or overdose of coagulant

sometimes. Chlorine emerges as the dominant disinfectant due to its ease of application and monitoring, low cost, and strong bactericidal capabilities. The efficacy of chlorination is heavily dependent on three key parameters: water turbidity, pH levels, and the amount of chlorine applied (Constans et al. 2003, Librantz et al. 2018).

Turbidity plays a vital role in both coagulation and disinfection processes, facilitating particle settlement and acting as a shield against microbes (Kennedy et al. 2018). However, the relationship between turbidity, chlorination, and coagulation demonstrates nonlinear behavior, proving challenging to capture through linear mathematical models (Kim & Kim 2014). Hence, there arises a necessity to devise prediction models for residual chlorine utilizing Artificial Neural Networks (ANNs).

Traditionally, in India, determining chlorine dosage in a WTP relies on operators' expertise, while coagulant dosage is assessed through jar tests (Haghiri et al. 2017). However, the determination of both coagulant and chlorine

dosages typically involves labor-intensive laboratory analyses, leading to prolonged experimental times in field water treatment plants (Kejiang et al. 2013). Consequently, there is a pressing need to develop predictive models for chlorine dosage based on coagulant dosage at WTPs. Such models would streamline the dosage determination process, enhancing efficiency and ensuring optimal water treatment outcomes.

In this study, many ANN models for the establishment of the relationship between the Coagulant and Chlorine Dose are developed. It is necessary to test and compare various ANN and training algorithms to develop a network that can perform satisfactorily in a reasonable amount of time (Jayaweera & Aziz 2018). Each model is trained many times, and the best performance is evaluated.

## MATERIALS AND METHODS

For Coagulant and chlorine dose neural network (CCDNN) modeling, 1849 data samples of input variables (Turbidity of the outlet water, residual chlorine, and coagulant dose) and target variable (chlorine dose) were collected from WTP. The variables examined in this study are inextricably linked to the coagulation and chlorination processes. Data were collected from the WTP laboratory for four years for inlet and outlet water quality daily (2012-2016). MATLAB version 16 was used to develop ANN models. ANN models such as RBFNN, FFNN, CFNN, and GRNN have been developed with a trial run that allows modification of the input variables, hidden nodes, training function, and the spread factor (SF). It is always a difficult task to create an optimal number of hidden nodes in ANN applications (Reilly et al. 2018, Salim & Noureddine 2015, Loc et al. 2020). The optimum number of nodes in each layer is not possible precisely and easily. In this study, information from both input and output nodes is used for building hidden neurons in a hidden layer. The training and test data are divided between 75:30 and 80:20, respectively, during the development of the ANN models. Diverse training functions, such as Bayesian Regularization (BR), Levenberg-Marquardt (LM), Resilient Back Propagation (RP), BFGS Quasi-Newton (BFG), One-Step Secant (OSS) Conjugated Gradient Back Propagation (CGB), Cluster-Powell (CGF), and Gradient Back Propagation (VLRB) are used. It was reported that the RBFNN and the GRNN models have the best test performance, respectively, with SF of 1 and 0.1 (Heddad et al. 2011). Thus, RBFNN and GRNN models ranging from 0.1 to 15 have been tested in this study. Standard statistics (JK), a standard deviation (L), skewness (M1), kurtosis (M2), and error statistics like regression coefficient (R), mean square error (MSE) and mean absolute error are used to quantify the percentage performance of these ANN

models (MAE) (Alka & Dnyaneshwar 2019). For its highest R and lowest MSE and MAE values, the best-performing ANN model is chosen. In addition, standard statistics, time series plots, and scatterplots are checked for the mapping with the observed series. For the best model in each category, GUIs for chlorine prediction and coagulant dosage were developed.

## RESULTS AND DISCUSSION

### Neural Network Model for Coagulant and Chlorine Dose 1

Sixteen models are developed for the coagulant and chlorine dose neural network 1 (CCDNN1) model. To establish the optimal networks, coagulant dose as the input parameter and chlorine dose as the output parameter are examined with various training functions and ANN. Based on numerous performance criteria, the behavior of ANNs is evaluated which is shown in Table 1.

For ANN prediction with FFNN and CFNN, different training functions were tried with varying hidden nodes from 15 to 90 (Alka & Dnyaneshwar 2019), and for RBFNN and GRNN, the value of SF varied from 0.1 to 20 during training to achieve the best-performing network. It is observed during the training period that minimum MSE = 0.019 and minimum MAE = 0.078 whereas maximum value of  $R^2 = 0.753$  is found. Similarly, standard statistics  $\sigma = 0.137$  to 0.873,  $\gamma_1 = -2.058$  to 0.635, and  $\gamma_2 = 1.978$  to 15.718. During training, it is observed that as SF value decreases in GRNN and RBFNN models, the values of R increase and values of MSE decrease. On the other hand, predictions are highly comparable RBFNN 1 model with SF = 0.1.

Similarly, it is observed during the testing period the minimum MSE = 0.014 and minimum MAE = 0.068, whereas the maximum value of  $R^2 = 0.715$  is found. Similarly, standard statistics such as  $\sigma = 0.12$  to 0.608,  $\gamma_1 = -2.461$  to -0.762, and  $\gamma_2 = 3.184$  to 12.287.

Prediction accuracy is higher for the RBFNN1 model with SF = 0.1 obtained. Further performance measures of all models are compared and observed that all the models resulted in poor performance, only the RBFNN1 model produced a good result ( $R = 0.72$ ). Fig.1. shows the plot of observed and predicted series of best FFNN, CFNN, RBFNN, and GRNN models during the testing period.

### Neural Network Model for Coagulant and Chlorine Dose 2

In the coagulant and chlorine dose neural network 2 (CCDNN2) model, sixteen models are developed for the



Table 1: Performance indices of CCDNN1 models during the testing period.

Type of ANN Model	SF/Training algorithm	Error statistics			Standard statistics			
		R <sup>2</sup>	MSE	MAE	$\bar{x}$ (1.954)	$\sigma$ (0.171)	$\gamma_1$ (2.53)	$\gamma_2$ (12.39)
RBFNN1	0.1	0.753	0.018	0.077	1.962	0.120	-2.438	12.287
	1	0.504	0.033	0.113	1.926	0.180	-2.023	15.283
	5	0.285	0.040	0.133	1.916	0.200	-2.058	13.280
	10	0.443	0.617	0.647	1.890	0.786	0.374	2.183
	15	0.421	0.631	0.661	1.913	0.795	0.414	2.147
GRNN1	0.1	0.554	0.534	0.584	1.885	0.731	0.352	2.431
	1	0.451	0.611	0.642	1.888	0.782	0.401	2.177
	5	0.424	0.633	0.663	1.980	0.796	0.506	2.134
	10	0.385	0.660	0.699	1.929	0.812	0.593	2.073
	15	0.342	0.684	0.720	1.888	0.827	0.619	2.024
FFNN	LM	0.427	0.628	0.651	1.903	0.792	0.392	2.181
	BR	0.400	0.648	0.646	1.910	0.803	0.473	2.288
	BFG	0.396	0.649	0.672	1.9064	0.805	0.386	2.298
	RP	0.384	0.655	0.677	1.8063	0.809	0.475	2.100
	CGF	0.398	0.657	0.684	1.8038	0.810	0.406	2.191
	CGM	0.302	0.715	0.702	1.921	0.844	0.516	2.171
	OSS	0.197	0.763	0.753	1.908	0.873	0.403	2.258
CFNN	LM	0.407	0.640	0.654	1.962	0.800	0.463	2.249
	BR	0.411	0.638	0.665	1.934	0.799	0.449	2.147
	BFG	0.219	0.731	0.742	1.879	0.855	0.6351	1.980
	RP	0.237	0.724	0.732	1.914	0.851	0.631	1.978
	CGF	0.256	0.717	0.731	1.862	0.847	0.623	1.983
	CGM	0.373	0.665	0.689	1.880	0.815	0.586	2.088
	OSS	0.405	0.642	0.666	1.985	0.801	0.452	2.165

coagulant and chlorine dose neural network 2 (CCDNN1) model. To establish the optimal networks, coagulant dose, and residual chlorine as input parameters and chlorine dose as output parameters are examined with various training functions and ANN. Based on numerous performance criteria, the behavior of ANNs is evaluated. It is observed that during the training period, MSE = 0.002 to 0.028 and MAE = 0.013 to 0.104, whereas R<sup>2</sup> varies from 0.197 to 0.978. Similarly, standard statistics such as  $\sigma$  = 0.044 to 0.184,  $\gamma_1$  = -2.713 to -4.286, and  $\gamma_2$  = 19.83 to 62.15 Prediction accuracy is higher for the RBFNN2 model with SF = 0.1 obtained.

Similarly, it is observed during the testing period that minimum MSE = 0.001, and minimum MAE = 0.015, whereas the maximum value of R<sup>2</sup> = 0.97 is found. Similarly, standard statistics such as  $\sigma$  = 0.036 to 0.128,  $\gamma_1$  = -1.713 to -8.717, and  $\gamma_2$  = 17.667 to 89.15. It is seen from the results of the training and testing period that the RBFNN2 model with SF = 0.1 resulted consistently better than the FFNN, CFNN, and GRNN models. Fig. 2 shows the plot of the observed and

predicted series of best FFNN, CFNN, RBFNN, and GRNN models during the testing period.

### Neural Network Model for Coagulant and Chlorine Dose 3

In the coagulant and chlorine dose neural network 3 (CCDNN3) model, sixteen models were developed. To establish the optimal networks, turbidity of the outlet water, residual chlorine, and coagulant dose as input parameters and chlorine dose as output parameters are examined with FFNN, CFNN, RBFNN, and GRNN. The developed models were tested to get an appropriate network that provided satisfactory performance. The important performance indices of all ANN models are displayed in Table 2, indicating standard statistics and error statistics during the testing period. From Table 2, it has been observed that during the testing period, standard statistics, for example,  $\sigma$  (Min) = 0.026,  $\gamma_1$  (Max) = 1.032, and  $\gamma_2$  (Min) = 5.309. Similarly, error statistics such as MSE (min) = 0.001 and MAE (min) = 0.009, whereas the

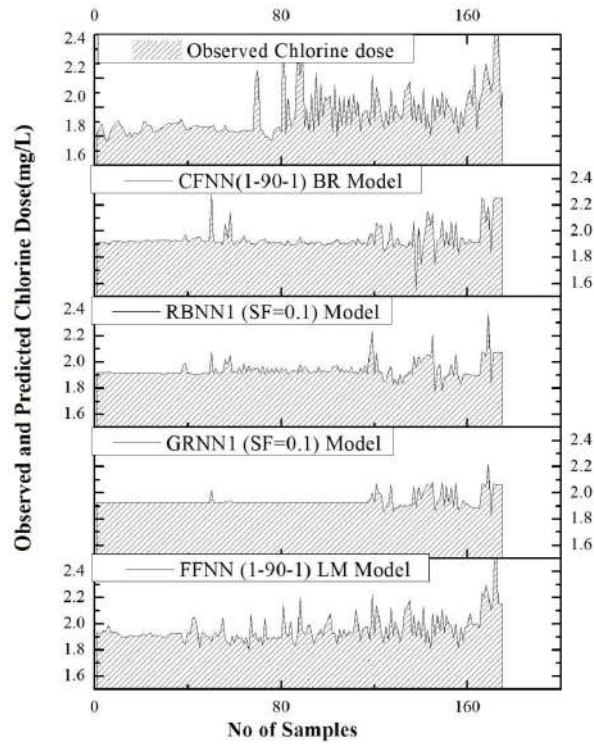


Fig. 1: Comparison of best CCDNN1 models during the testing period.

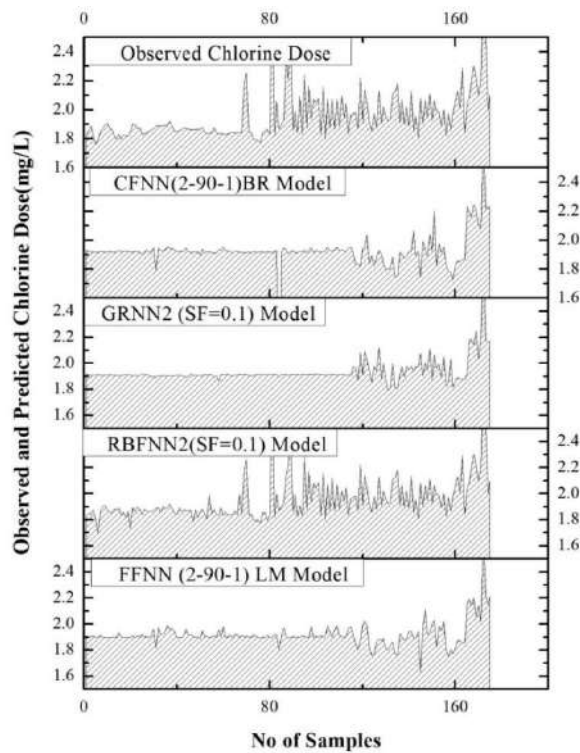


Fig. 2: Comparison of best CCDNN2 models during the testing period.

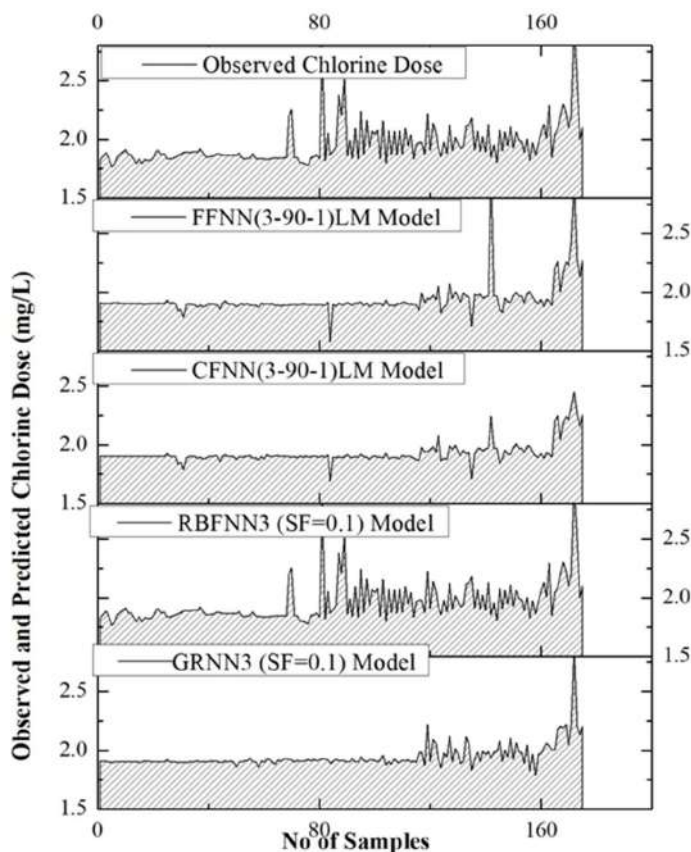


Fig. 3: Comparison of best CCDNN3 models during the testing period.

maximum value of  $R^2=0.99$  is found. In RBFNN and GRNN models, as SF increases, prediction efficiency decreases. In the RBFNN model, however, there is clear superiority in prediction with SF = 0.1.

Fig. 3 shows a comparison of the best CCDNN3 models in the test period, where the plot of RBFNN3 almost coincides with the plot of observed values. Compared to all other ANN models, the RBFNN3 model with SF 0.1 produced the highest R. It is found that the prediction efficiency has increased in RBFNN and GRNN models, with a decrease in SF value. Furthermore, compared to all other training algorithms, FFNN and CFNN models with BR training function produced good predictions. These models, however, are less efficient.

RBFNN models, on the other hand, have a noticeable advantage in prediction. It also demonstrates that models with three inputs perform better than models with various input variations to the networks. Tables 2 show a summary of standard statistics for the best RBFNN models in Class I, II, and III during the training and testing period. Standard statistics for all ANN models were evaluated and displayed in Table 3 during the training and testing periods. During

training and testing, the RBFNN 3 model exhibited the least  $\sigma$  and  $\gamma_2$ . Most of the best ANN models produced a positive kurtosis, where heavier tails are associated with a higher peak.

The  $\sigma$  (least) of the RBFNN 3 model suggests that the data points tend to be close to the set's predicted value, whereas the  $\sigma$  (Max) of the RBFNN 1 model indicates that data points are dispersed throughout a larger range of values.

The results of model simulation indicate that the lower the absolute value of  $\gamma_1$  (1.032), and the larger the  $\gamma_2$  (21.046) lies with RBFNN3 models, which indicate higher the accuracy of the prediction. Compared to other ANN models from Class I, II, and III, the RBFNN3 model performed the best with MSE = 0.001 and R = 0.999 over the testing period shown in Fig. 4. Time series plots and scatter plots of the RBFNN3 model during the testing period are shown in Fig. 4.a) and b), respectively. The observed and predicted chlorine dose series is seen to closely map indicating the best model. Due to better non-linear approximation, the RBFNN model showed excellent predictive results.

In most developing countries, the chlorine dose in a WTP is usually calculated by the operator's knowledge, while a

Table 2: Performance indices of CCDNN3 models during the testing period.

Type of ANN Model	SF/ Training algorithm	Error statistics			Standard statistics			
		R <sup>2</sup>	MSE	MAE	$\bar{x}$ (1.954)	$\sigma$ (0.171)	$\gamma_1$ (2.53)	$\gamma_2$ (12.39)
RBFNN3	0.1	0.999	0.001	0.009	1.953	0.026	1.032	21.046
	1	0.812	0.01	0.047	1.949	0.1	-3.014	20.019
	5	0.012	1.069	0.298	1.853	1.005	-10.24	15.45
	10	-0.175	0.091	0.272	1.782	0.181	-2.265	12.225
	15	-0.237	0.181	0.391	1.771	0.22	-1.608	7.813
GRNN3	0.1	0.477	0.023	0.099	1.91	0.151	-2.324	11.231
	1	0.053	0.051	0.199	1.851	0.138	-3.786	28.395
	5	0.053	0.051	0.199	1.851	0.138	-3.786	28.395
	10	0.246	0.028	0.113	1.894	0.166	-2.539	12.257
	15	0.053	0.051	0.199	1.852	0.138	-3.786	28.395
FFNN	LM	0.444	0.025	0.1	1.911	0.154	-1.963	10.019
	BR	0.271	0.037	0.108	1.867	0.188	-3.107	20.4
	BFG	0.392	1.028	0.982	1.889	0.519	-1.922	6.269
	RP	0.349	0.046	0.145	1.901	0.184	-1.337	6.873
	CGF	0.407	0.033	0.119	1.918	0.166	-1.122	8.197
	CGB	0.239	0.063	0.177	1.889	0.192	-1.035	5.309
	OSS	0.262	0.037	0.117	1.899	0.186	-2.306	11.735
CFNN	LM	0.277	0.125	0.324	1.878	0.193	-2.178	10.786
	BR	0.314	0.099	0.287	1.898	0.182	-2.263	12.078
	BFG	0.32	0.143	0.344	1.888	0.212	-1.681	8.283
	RP	0.249	0.074	0.187	1.889	0.234	-1.003	4.76
	CGF	0.433	0.035	0.124	1.896	0.164	-1.133	8.628
	CGB	0.378	0.041	0.135	1.898	0.194	-0.51	9.123
	OSS	0.376	0.052	0.157	1.882	0.19	-1.136	9.387

Table 3: Standard statistics of RBFNN models during the training and testing period.

ANN Model	Training period				Testing period			
	$\bar{x}$	$\sigma$	$\gamma_1$	$\gamma_2$	$\bar{x}$	$\sigma$	$\gamma_1$	$\gamma_2$
Observed values	1.909	0.2088	2.0978	12.314	1.954	0.171	2.533	12.390
RBFNN1 SF = 0.1	1.910	0.137	-1.967	15.718	1.962	0.120	-2.438	12.287
RBFNN2 SF = 0.1	1.910	0.044	-4.286	62.155	1.954	0.036	-1.713	17.667
RBFNN3 SF = 0.1	1.910	0.026	3.027	98.898	1.953	0.026	2.032	21.046

jar test measures the coagulant dose. Laboratory analysis is usually used to determine the coagulant and chlorine dosage, which takes a long time in WTP. As a result, at WTP, a link between chlorine dose and coagulant dose must be established. Operators of WTP will be able to use the developed relationship to select the optimum dose.

Similarly, the relation between chlorine dose and coagulant dose is quite simplified by various  $n^{\text{th}}$  degree

expressions, as shown in eq. 1, 2 and 3.

$$y = -0.00046 \times z + 1.6 \quad \dots(1)$$

$$y = 3.5 \times 10^{-6} \times z^2 - 0.001 \times z + 1.9. \quad \dots(2)$$

$$y = -3.5 \times 10^{-8} \times z^3 + 1.4 \times 10^{-5} \times z^2 - 0.0017 \times z + 1.9. \quad \dots(3)$$

Where  $y$  = chlorine dose and  $z$  = coagulant dose in mg/L.

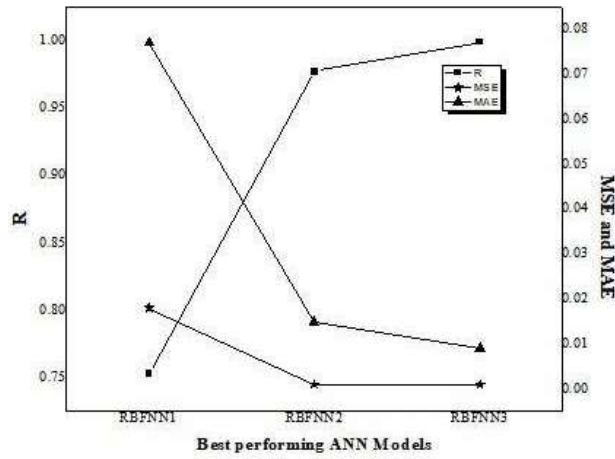


Fig. 4: Error statistics of RBFNN models during the testing period.

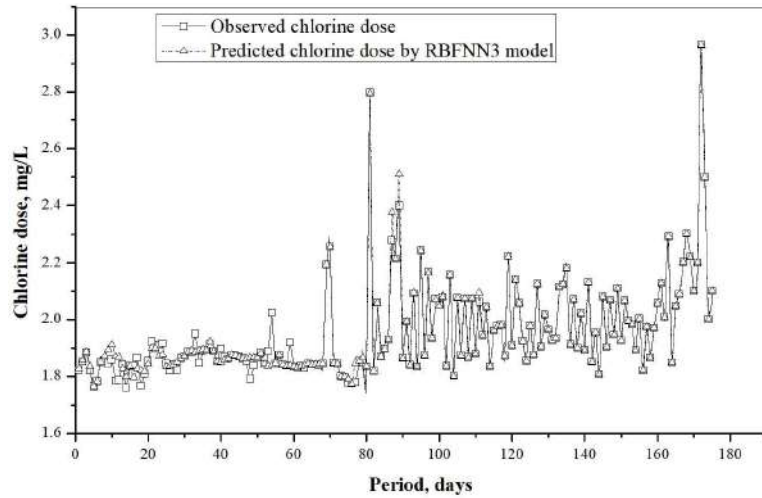


Fig. 4a: Time series of RBFNN3 model during the testing period.

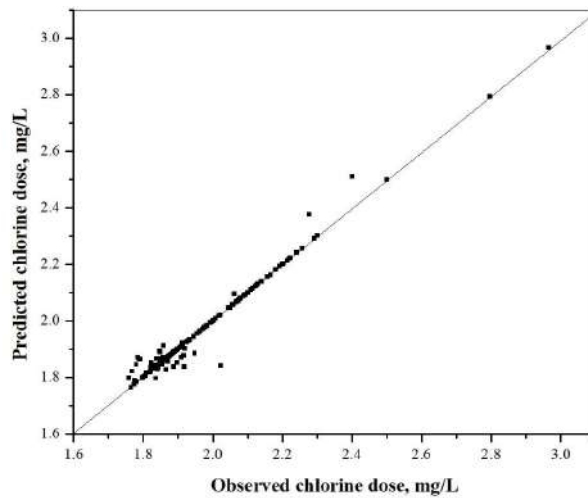


Fig. 4b: Scatter plot of RBFNN3 model during the testing period.

## Development of Graphical User Interface

To transfer the modeling knowledge to the field, GUI software has been developed. The developed GUI will provide a useful tool to plant operators and managers for deciding the required chlorine and coagulant dose. GUIs for predicting chlorine dose in WTP were developed using the best model. The GUI was developed in MATLAB software. Determination of chlorine dose is an essential aspect of WTP. It decides the concentration of residual chlorine in the outgoing water of WTP. In India, most WTP operators provide higher chlorine doses for maintaining a high level of residual chlorine in WDN. The more chlorine consumption creates many health problems. Hence, there is a need to apply optimum chlorine dose. The GUI will be useful for the determination of chlorine dose at WTP.

1. Run the CCDNN model.
2. Enter the value of the coagulant dose applied at WTP in mg/L
3. Enter the value of outlet water turbidity (NTU)
4. Enter the value of desirable residual chlorine at the outlet of WTP so that minimum residual chlorine is maintained at the end of WDN.
5. After entering all data, click on the 'Chlorine Dose' button.
6. Within a few seconds, the chlorine dose value will be displayed in the output window (Fig 5).

Developed GUIs was helpful for WTP operators and managers to plan the short-term and long-term activities

## CONCLUSION

Several CCDNN models have been developed to predict chlorine dosage, utilizing input parameters such as the outlet water's turbidity, residual chlorine, and coagulant dose for ANN modeling. These selected parameters are closely associated with chlorination and coagulation processes. As the concentration of suspended solids (SF) increases, the prediction efficiency of RBFNN and GRNN models decreases. However, within the RBFNN model, there is a noticeable superiority in prediction when SF ranges from 0.1 to 1. Such correlations prove valuable in determining the optimal chlorine or coagulant dosage. Additionally, it's observed that the range of chlorine dosage is narrower compared to that of the coagulant dosage. The relationship between them is established by the CCDNN model, wherein the prediction of chlorine dosage based on coagulant dosage demonstrated an impressive correlation ( $R = 0.99$ ) according to RBFNN.

## REFERENCES

- Alka, S.K. and Dnyaneshwar, V.W., 2019. Application of feed forward neural network for prediction of optimum coagulant dose in water treatment plant. *International Journal of Innovative Technology and Exploring Engineering*, 8(12), pp.1853-1856.
- Bello, O., Hamam, Y. and Djouani, K., 2014. Coagulation process control in water treatment plants using multiple model predictive control. *Alexandria Engineering Journal*, 71, pp.420-435.

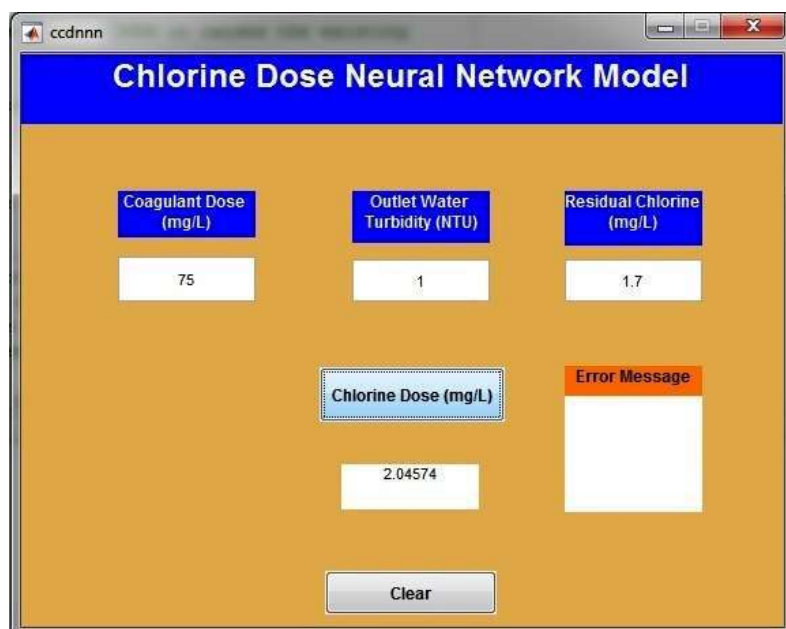


Fig. 5: Screen Shot of GUI for CCDNN (RBNN3 (SF = 0.1)) model.

## NOMENCLATURE

Symbol	Description
ANN	Artificial neural networks
ANFIS	Adaptive neural fuzzy inference system
BFGS	Broyden–Fletcher–Goldfarb–Shanno (BFGS) algorithm
BR	Bayesian regularization
CFNN	Cascade feed forward neural network.
CDNN	Coagulant dose neural network
CCDNN	Coagulant and chlorine dose neural network
CGB	Conjugate gradient back propagation
FFNN	Feed forward neural network
GUI	Graphical user interface
GRNN	Generalized regression neural networks
GD	Gradient descent
GDM	Gradient descent with momentum
GCF	Conjugate gradient back propagation with Fletcher-Powell
LM	Levenberg-Marquardt
MAE	Mean absolute error
MSE	Mean square error
PCMC	Pimpri Chinchwad Municipal Corporation
RBFNN	Radial basis function neural network
RP	Resilient back propagation
RMSE	Root mean square error
R <sup>2</sup>	Coefficient of determination
SF	Spread factor
WTP	Water treatment plant
WWTP	Wastewater treatment plant
WDN	Water distribution network
WQI	Water quality index

- Bowden, G.J., Nixon, J.B. and Dandy, G.C., 2006. Forecasting chlorine residuals in a water distribution system using a general regression neural network. *Mathematical and Computer Modelling*, 44, pp.469–484.
- Bobadilla, M.C., Lorza, R.L., Garcia, R.E., Gomez, F.S. and Gozalez, E.V., 2019. Coagulation: determination of key operating parameters by multi-response surface methodology using desirability functions. *Water*, 11, pp.1-21.
- Chan Moon, K.M.P., 2017. Prediction of settled water turbidity and optimal coagulant dosage in drinking water treatment plant using a hybrid

model of k-means clustering and adaptive neuro-fuzzy inference system. *Applied Water Science*, 17, pp.541-549. DOI: 10.1007/s13201-017-0541-5.

- Constans, S., Bremond, B. and Morel, P., 2003. Simulation and Control of Chlorine Levels in Water Distribution Networks. *Journal of Water Resources Planning and Management*, 129, pp.135-145.
- Haghiri, S., Sina, M.A. and Daghighi, A., 2017. Optimum Coagulant Forecasting with Modeling the Jar Test Experiments Using ANN. *Journal of Drinking Water Engineering and Science*, 51, pp.1-12.
- Heddham, S., Abdelmalek, B. and Dechemi, N., 2011. Applications of Radial-Basis Function and Generalized Regression Neural Networks for Modeling of Coagulant Dosage in a Drinking Water-Treatment Plant Comparative Study. *Journal of Environmental Engineering*, 137, pp.1209-1214.
- Heddham, S., Bermad, A. and Dechemi, N., 2011. ANFIS-based modelling for coagulant dosage in drinking water treatment plant: a case study. *Environmental Monitoring and Assessment*, 184(4), pp.1953–1971. DOI: 10.1007/s10661-011-2091-x.
- Jayaweera, C.D. and Aziz, N., 2018. Development and comparison of Extreme Learning machine and multi-layer perceptron neural network models for predicting optimum coagulant dosage for water treatment. *Journal of Physics: Conference Series*, 11, pp.1-8.
- Kim, H.S. and Kim, J.C., 2014. Prediction of chlorine concentration in various hydraulic conditions for a pilot scale water distribution system. *Procedia Engineering*, 70, pp.934 – 942.
- Kejiang, Z., Achari, G., Li, H., Zargar, A. and Sadiq, R., 2013. Machine learning approaches to predict coagulant dosage in water treatment plants. *International Journal of Systems Assurance Engineering and Management*, 4(2), pp.205–214.
- Kennedy, M.J., Gandomia, A.H. and Miller, C.M., 2015. Coagulation modelling using ANN to predict both turbidity and dom-parafac component removal. *Journal of Environmental Chemical Engineering*, 3(4), pp.2829-2838.
- Librantz, A.F., Santos, F.C. and Dias, C.G., 2018. Artificial neural networks to control chlorine dosing in a water treatment plant. *Acta Scientiarum. Technology*, 40, pp.1-9.
- Loc, H.H., Do, Q.H., Cokro, A.A. and Irvine, K.N., 2020. Deep neural network analyses of water quality time series associated with water sensitive urban design (WSUD) features. *Journal of Applied Water Engineering and Research*, 16, pp.1–20. DOI: 10.1080/23249676.2020.1831976.
- Reilly, G.O., Bezuidenhout, C.C. and Bezuidenhout, J.J., 2018. Artificial neural networks: applications in the drinking water sector. *Water Supply*, 18(6), pp.1869-1887.
- Salim, H. and Nouredine, D., 2015. A new approach based on the dynamic evolving neural-fuzzy inference system (DENFIS) for modelling coagulant dosage (Dos): case study of water treatment plant of Algeria. *Desalination and Water Treatment*, 53, pp.1045–1053.

## ORCID DETAILS OF THE AUTHORS

Ganesh C. Chikute: <https://orcid.org/0000-0003-3590-466X>







# A Comparative Study on India's Green Tax Policies Vis-a-Vis China with Reference to Environmental Justice in the Automobile Industry

Naresh Anguralia<sup>1†</sup>  and Shamsher Singh<sup>2</sup> 

<sup>1</sup>University Institute of Legal Studies, Chandigarh University, Mohali-140413, Punjab, India

<sup>2</sup>Department of Law, Regional Campus, Gurdaspur (Guru Nanak Dev University, Amritsar), Punjab, India

†Corresponding author: Naresh Anguralia; nareshanguralia3@gmail.com

Nat. Env. & Poll. Tech.

Website: [www.neptjournal.com](http://www.neptjournal.com)

Received: 31-03-2024

Revised: 10-05-2024

Accepted: 19-05-2024

## Key Words:

Green taxation

Energy

Automobile industry

Environmental justice

Green economics

Sustainable resource use

Environmental sustainability

## ABSTRACT

As part of green economics, taxes are imposed on emissions of pollutants that adversely impact the environment and public health to reward more innovative, environmentally sustainable, and low-carbon resource use. There are still many nation-states testing the concept of green taxation. Many environmental performance indicators place India low on the list of countries with the worst pollution. One of the main sources of pollution is vehicle exhaust. Green taxes will be imposed on older motor vehicles under guidelines released by the Indian government in 2021. The United Nations Framework Convention on Climate Change received the Indian Nationally Determined Contribution Report in 2022. Taxonomies and low-carbon transport systems were prioritized in India, and incentives and tax breaks were offered to encourage the manufacture and use of vehicles that consume more ethanol. Academic discussions and literature on the subject are still lacking among the masses. Researchers intend to analyze the legal and economic measures taken by the Indian Government to curb vehicular pollution against this background. Due to its significant contribution to air and water pollution, as well as greenhouse gas emissions, the automobile industry has come under increasing scrutiny in recent years. India and China, for instance, have implemented green tax policies to reduce the automotive sector's environmental footprint and promote environmental sustainability. These policies are effective, but not all of them address the disproportionate impact of environmental injustice on vulnerable populations. Specifically, this study examines the impact of Indian green tax policies on environmental justice in the automobile industry as compared to those in China. A key aim of this study is to provide insights into the strengths and weaknesses of the green taxation policies adopted by each country in the automotive sector, as well as their implications for achieving environmental justice, by analyzing the scope, enforcement, impact on vulnerable communities, industry implications, and alignment with international commitments.

## INTRODUCTION

Producers/polluters do not bear the cost of pollution associated with the creation of their products. In addition to climate change, impaired health, and noxious odors, we are all responsible for pollution's negative effects. There is a potential to reduce pollution with indirect taxes, such as taxes on alternative policies or related goods like authorized technology standards, but the costs may be quite high (Lehmann 2012).

It would be ineffective for drivers to make sure the pollution control equipment in their cars is maintained if the gasoline tax was raised to reduce environmental damage caused by automobile emissions. Increasing pollution control equipment taxes on direct emissions is a cost-effective way to make sure those who need to work towards reducing pollution start doing so. Those who find pollution reduction

expensive will continue to pollute and pay more taxes as a result, while those who find it less expensive can reduce their pollution and, therefore, pay less taxes. Green taxes are not the only alternative to tradable permits (Carattini et al. 2017).

Due to the issuance of a certain number of emission permits, it is as cost-effective as levying direct taxes. As a result, polluters can trade these permits. Permit prices are similar to taxes in that polluters who find it expensive to lower their emissions purchase permits that allow them to keep emitting pollutants instead. Before selling their unused permits, those who can reduce emissions at a lower price can reduce emissions.

## THE RESEARCH PROBLEM

The rapid industrialization, urbanization, and economic growth of India and China have created environmental

challenges. To counteract environmental degradation, both countries have implemented green tax policies. The effectiveness of these policies, however, remains to be evaluated in terms of their effectiveness in addressing environmental justice concerns. Green tax policies in the automobile industry are explored and compared in this research problem.

## RESEARCH OBJECTIVES

1. To assess the environmental justice implications of green tax policies in India and China, focusing on their impact on different socio-economic groups and vulnerable populations in the automobile industry.
2. To explore the institutional and governance factors influencing the implementation and effectiveness of green tax policies in India and China, including issues of transparency, accountability, and stakeholder engagement in the automobile industry.
3. To synthesize the findings into policy recommendations aimed at enhancing the environmental justice outcomes of green tax policies in India and China, considering the unique contexts and challenges faced by each country.

## SIGNIFICANCE OF THE STUDY

Environmental justice in India and China is a topic of utmost importance in this study, which examines the effects of green tax policy on environmental justice. Using the automobile industry in both countries as a case study, we examine green tax policies to identify their strengths and weaknesses and to identify opportunities for enhancing environmental justice outcomes. Researchers will develop policy recommendations based on the findings of the study to support the development of more equitable and sustainable environmental governance in India, China, and other similar cases.

## GREEN TAX POLICIES IN INDIA

Environmental pollution varies significantly among Indian states in terms of its extent and source. The Supreme Court of India recognized the right to a pollution-free environment as part of the fundamental right to life underlying Article 21 of the Indian Constitution in *Mehta v. Union of India 1986*. This method of reducing carbon emissions and their impacts on the environment is referred to as the carbon tax on fossil fuels. Even though driving does not pose any inherent danger or danger, drivers and other polluters are responsible for any pollution and health risks resulting from their actions. Ecosystem management policies that combine multiple methods and instruments are hybrid policies. Regulations such as environmental taxes, saleable emission permits,

and minimum environmental standards are key, as well as incentives for renewable technology enhancements in the manufacturing sector (Rissman et al. 2020).

Environmental concerns in the automobile sector have been addressed by India through policies and initiatives, including green taxation measures. These policies encourage clean and fuel-efficient vehicles, along with discouraging pollution-generating vehicles. Indian automobile policy on green tax includes the following aspects (Sulkowski et al. 2016):

**Vehicle scrappage policy:** As part of its voluntary vehicle scrappage policy, the Indian government proposed retiring old and inefficient vehicles from the road. Old vehicles were to be scrapped voluntarily at authorized scrappage centers under this policy. To encourage participation in the scrappage program, incentives were offered, including discounts on new vehicles, road tax rebates, and scrap value for old vehicles. A green tax was also proposed to be imposed on old vehicles as part of the scrappage policy. Depending on the age, type of fuel, and emissions of a vehicle, a green tax would be imposed. Essentially, the green tax disincentivizes the use of older, more polluting vehicles and encourages the use of cleaner, newer ones. In addition to reducing emissions, improving air quality, and conserving natural resources, the vehicle scrappage policy and green tax were intended to reduce vehicular emissions and improve air quality. To combat air pollution and mitigate climate change, the policy encouraged the retirement of old vehicles and the adoption of newer, greener vehicles (James et al. 2023).

**Goods and Services Tax (GST):** GST replaced multiple indirect taxes in 2017 by the Indian government. Various goods and services, including automobiles, are taxable according to different tax slabs in the GST regime. EVs are more affordable and more widely adopted due to lower GST rates compared with conventional vehicles (Revathi & Aithal 2019).

**FAME India scheme:** To promote the adoption of electric and hybrid vehicles, the Indian government launched the Faster Adoption and Manufacturing of Hybrid and Electric Vehicles (FAME) India scheme. The purpose of this scheme is to make electric and hybrid vehicles more affordable by providing incentives to manufacturers and buyers. Tax benefits and subsidies are among these incentives (Sangodkar 2021).

**Green cess:** Vehicles with high pollution levels are subject to a green cess or pollution tax in some Indian states to discourage their use. Engine capacity, age, and emissions are usually factors that determine the amount of cess. A fuel-efficient and cleaner vehicle is encouraged by this additional tax (Singh & Gahlot 2023).

**BS-VI emission standards:** In April 2020, Bharat Stage VI (BS-VI) emission norms were implemented across the country to reduce vehicular emissions. To comply with these stricter emission standards, automobile manufacturers must produce vehicles that emit fewer pollutants and have cleaner engines. Pollution reduction has been achieved by adopting advanced emission control technologies in vehicles as a result of BS-VI compliance (Gajbhiye et al. 2023).

**Incentives for scrappage:** To phase out old and polluting vehicles, the Indian government implemented a vehicle scrappage policy. By offering discounts on vehicle purchases and reducing registration fees for new vehicles, this policy encourages owners of old vehicles to scrap them and purchase new ones (Singh et al. 2021).

**Research and Development incentives:** R&D incentives and grants are provided by the government to encourage the development of hybrid and electric vehicle technologies in the automobile sector (Wu et al. 2021).

Incentives like these are intended to encourage innovation and the development of cleaner, more sustainable transportation solutions. India's green tax policies aim to reduce pollution and greenhouse gas emissions from the transportation sector and encourage the adoption of environmentally friendly vehicles. In order to achieve India's sustainability goals, these policies are crucial. In order for green tax policies to be successful in the long term, it is important to monitor their effectiveness and make necessary adjustments. India has a number of green tax policies that apply to automobiles. As a result of these laws, pollution levels are expected to be reduced, fuel-efficient vehicles will be adopted, and sustainable transportation practices will be promoted. Green tax policy in the automobile sector in India is governed by the following laws and regulations:

- 1. Motor Vehicles Act, 1988:** India's Motor Vehicles Act governs road transport and vehicles. Regulations provide for the registration and taxation of vehicles, as well as safety and environmental standards. It has been amended over the years in order to incorporate provisions related to green taxation and emission standards (Bansal & Bandivadekar 2013).
- 2. Central Motor Vehicles Rules, 1989:** In addition to detailed provisions regarding vehicle standards, specifications, and registration procedures, these rules are based on the Motor Vehicles Act. Vehicle fuel efficiency standards, emissions regulations, and pollution control devices are also covered in the rules (Freund 2007).
- 3. Bharat Stage Emission Standards:** There are a series of emission standards known as Bharat Stage (BS)

norms that regulate what is allowed as far as pollution is concerned from vehicles in India. Carbon monoxide (CO) is one of the pollutants that are included in these standards, as well as hydrocarbons (HC), nitrogen oxides (NOx), Sulfur oxides (SOx), and particulate matter (PM). Vehicle emissions have been reduced, and air quality has improved thanks to stricter BS norms (Anchan 2018).

- 4. Goods and Services Tax (GST) Act, 2017:** Taxes on goods and services in India are governed by the GST Act. Automobile taxes, including those on electric and hybrid vehicles, are included in the act. EVs are more affordable and are incentivized to be adopted because GST rates are lower than for conventional vehicles (Stephens et al. 2018).
- 5. Finance Act:** Various taxation and incentive provisions may be included in the annual Finance Act as part of the Union Budget. Automobile and automotive component excise duties, customs duties, and other tax changes may affect these changes (Cnossen 2001).
- 6. State Motor Vehicles Taxation Laws:** State laws and rules concerning motor vehicle taxation in India are in addition to the central laws. In addition to road tax, registration fees, and pollution taxes, states have the authority to charge vehicles a variety of fees and taxes. Polluting vehicles are being discouraged in some states by green cesses or pollution taxes. Green tax policies in the automobile industry in India are governed by these laws and regulations. In this way, environmental concerns and public health goals are balanced with the economic interests of the automotive industry. To reduce vehicular pollution and promote sustainable mobility solutions, stakeholders must obey these laws (Singh & Gahlot 2023).

## IMPACT OF GREEN TAX POLICIES ON VARIOUS SOCIO-ECONOMIC GROUPS IN INDIA

Socio-economic groups in India may be affected differently by automobile green taxes based on factors such as income levels, access to alternative transportation, and geographic location. Various socioeconomic groups may be affected differently. People who use older and more polluting vehicles due to affordability constraints may face additional financial hardships if a green tax is imposed. A higher tax or upgrading to a cleaner vehicle may be too expensive for them. It may be difficult for low-income people to switch to greener modes of transportation due to limited access to public transportation. The green tax may be levied without viable alternatives, putting them at risk. Older vehicles subject to higher tax

rates may also be affected by the green tax, particularly if they belong to a middle-income family. To accommodate the increased tax burden, they might have to reevaluate their budgets (Gupta & Köhlin 2006).

Although middle-income individuals may be more able to afford cleaner vehicles than low-income individuals, they may still face difficulty purchasing electric or hybrid vehicles if the upfront costs are high. There is a possibility that individuals with high incomes may be in a better position to absorb the costs. Vehicle owners may even see it as an incentive to upgrade to cleaner and more fuel-efficient vehicles due to the environmental impact of the green tax. Investing in electric or hybrid vehicles may be more appealing to them since they often come with tax benefits. Market trends can also be influenced by high-income individuals' purchasing decisions, which can lead to increased demand for eco-friendly vehicles and technological advances. Often, people in rural areas are dependent on their own vehicles for transportation because public transportation is limited. Rural communities may be disproportionately affected by the green tax since they typically lack access to cleaner vehicles and alternative modes of transportation. Green taxes may have a lesser impact in urban areas that have better access to public transportation and rideshare services. For some segments of the population, affordability remains a concern when it comes to investing in cleaner vehicles or switching to greener modes of transportation (Lusk et al. 2023).

The green tax may present some short-term challenges in terms of economic growth, but the long-term benefits of reducing air pollution, improving public health, and mitigating climate change can be positive for all groups of society. By improving the quality of air and living environment, productivity can be improved, healthcare costs can be reduced, and overall quality of life can improve. As a result of the impact of the green tax on socio-economic groups in India, policy measures should be designed to ensure equitable access to cleaner transportation alternatives, especially for marginalized groups, while also considering affordability constraints. A smoother transition to greener mobility solutions may require subsidies, incentives, and support mechanisms (Alvarez et al. 1997).

## FACTORS RESPONSIBLE FOR THE IMPLEMENTATION OF GREEN TAX POLICIES

Green tax policies in India are influenced by the following factors:

- **Environmental challenges:** Deforestation, pollution, and resource depletion are among the significant environmental issues facing India. By encouraging environmentally friendly practices and reducing

pollution, green tax policies aim to address these challenges (Barbier 2011).

- **Public health Concerns:** Public health risks in Indian cities are mainly caused by poor air quality caused by vehicular emissions. By encouraging cleaner technologies and alternative transportation modes, green tax policies aim to improve air quality.
- **Climate change mitigation:** As part of its commitment to addressing climate change, India is reducing its carbon footprint. Through the promotion of energy-efficient technologies, renewable energy sources, and the reduction of greenhouse gas emissions, green tax policies play a crucial role in achieving these goals.
- **International commitments:** Indian green tax policies align with global environmental objectives as a signatory to international agreements like the Paris Agreement.
- **Technological advancements:** The advancement of technology enables us to develop cleaner, more sustainable solutions. As a result of green tax policies, these technologies are adopted, resulting in innovation and a transition to a greener economy.
- **Public awareness and support:** Environmental issues are becoming more popular, and governments are being pressured to take action. The public usually supports green tax policies, particularly when the funds are invested in environmentally friendly infrastructure and conservation.
- **Revenue generation:** Environmental conservation, infrastructure development, and public welfare programs can be funded with revenue from green taxes (De Serres et al. 2010).
- **Policy stability:** Long-term investments in green technologies must be encouraged by stable and predictable policy frameworks. Businesses and consumers can transition to sustainable practices with confidence if green tax policies are clear and consistent.
- **Industry collaboration:** To implement green tax policies successfully, collaboration with industry stakeholders is crucial. Maintaining compliance with regulations and promoting innovation in sustainable practices can be accomplished by working with automobile manufacturers, energy companies, and transportation providers.

## CHALLENGES FACED BY INDIA IN IMPLEMENTING GREEN TAX POLICIES

Green taxes in India face multiple challenges, including:

1. **Inadequate infrastructure and financial mechanisms:** Large-scale scrapping is hampered by limited registered scrapping facilities and malfunctioning automated testing stations. Due to land constraints and a lack of access to business finance, the informal sector cannot handle increasing volumes of End-of-Life Vehicles (ELVs) with crude methods and slow processing. Incentives for scrapping ELVs rely solely on state governments and Original Equipment Manufacturers (OEMs) since on-road emissions inspections are time-consuming. Since owners have a strong attachment to their vehicles, higher compensation is needed to convince them to scrap (Naik 2018).
2. **Criteria for fleet renewal/scrappage policies:** The lack of centralized databases hinders monitoring emissions and retesting vehicles, which should be prioritized in vehicle-renewal policies.
3. **Viability for OEMs to set up ELV scrappage units:** For dismantling to be economically viable, large volumes of ELV are necessary. It is imperative to optimize the entire chain from fitness testing to recycling units for both economic and environmental benefits. In addition, OEMs lack Extended Producer Responsibility (EPR) because of a lack of regulation regarding aftermarket parts (Wong et al. 2018).
4. **Usage and disposal of hazardous materials in vehicles:** Hazardous materials must be properly disposed of, but informal dismantlers lack modern equipment, contaminating the environment. The ozone layer can be negatively affected by escaping. The ozone layer can be harmed by refrigerants such as Freon, making regulation essential. The circular economy does not integrate recycled materials, and Freon gas accumulates at de-pollution stages, which requires authorized vendors to collect it. The quality of recycled products is affected by challenges in plastic recycling, including segregation issues. To ensure the effective implementation of the scrappage policy and minimize environmental impacts, comprehensive measures, including infrastructure development, regulatory reforms, and compliance with environmental regulations, are essential (Zorpas & Inglezakis 2012).

## GREEN TAX POLICIES IN CHINA

To address environmental concerns and promote the adoption of cleaner vehicles, China has implemented several green tax policies in the automobile industry. As a result of these policies, emissions have been reduced, air quality has been improved, and environmentally friendly technologies have been developed and adopted. In China, the automobile

industry is governed by the following green taxes and laws (Zhang & Bai 2017):

1. **Vehicle Emission Standards (China VI):** With China VI being the most stringent standard, China has been progressively tightening its vehicle emission standards. In addition to nitrogen oxides (NO<sub>x</sub>), particulates (PM), and hydrocarbons (HC), these standards mandate lower levels of pollutants emitted by vehicles. To register and operate a vehicle, these standards must be met.
2. **New Energy Vehicle (NEV) Subsidies and Incentives:** Electric vehicles (EVs) and plug-in hybrid vehicles (PHEVs) are among the new energy vehicles (NEVs) that China promotes with subsidies and incentives. It is possible to provide incentives for NEVs in the form of subsidies, tax exemptions or reductions, as well as preferential registration.
3. **Fuel Efficiency Standards:** China has set fuel efficiency standards for automobiles in order to reduce fuel consumption and greenhouse gas emissions. Getting their fleets to meet these standards requires manufacturers to improve their fuel efficiency.
4. **Vehicle Purchase Tax:** Depending on automobile type, engine displacement, and emissions, China imposes a vehicle purchase tax on its automobile sales. NEVs, for instance, may be eligible for lower tax rates in some cases to encourage their adoption.
5. **Carbon Emissions Trading System (ETS):** Several industries, including the automobile sector, are participating in China's nationwide carbon emissions trading system. Carbon emission allowances are assigned to companies, and those who exceed their allowances are required to purchase additional allowances (Meckling & Nahm 2019).
6. **Green Vehicle Registration Policies:** Green vehicle registration policies have been implemented in some Chinese cities, which provide preferential parking and access to restricted areas for low-emission vehicles.
7. **Environmental Protection Laws and Regulations:** In China, there are numerous laws and regulations related to environmental protection. These laws and regulations govern emissions, pollution control, and environmental standards related to the automobile industry. Regulations on vehicle emissions and pollution control measures are included in the Environmental Protection Law as well as the Air Pollution Prevention and Control Law.
8. **Industry Development Plans:** Clean and energy-efficient vehicles are being developed and manufactured by the Chinese government through development plans

and policies. In order to shift to greener technologies, these plans outline targets, incentives, and support measures. Its commitment to environmental protection, sustainable development, and a transition to a low-carbon economy is reflected in the green tax policies and regulations in the auto industry. Environmental challenges are addressed by these policies, pollution is reduced, and cleaner vehicles and technologies are developed and adopted (Zhang et al. 2014).

## CHALLENGES FACED BY CHINA IN IMPLEMENTING GREEN TAX POLICIES

Several challenges face China's automobile industry when implementing green tax policies, including (Hu et al. 2010):

**Complex Regulatory Framework:** There are multiple government agencies and overlapping regulations in China's automobile regulatory framework. Inconsistencies and loopholes in enforcement may result from a lack of coordination between these agencies when implementing and enforcing green tax policies.

- **Resistance from Industry Stakeholders:** A green tax policy that imposes additional costs or requirements on auto manufacturers and related industries may be objected to by these industries. Green tax policies could be weakened by resistance from powerful industry stakeholders.
- **Lack of Consumer Awareness and Demand:** It is possible that many Chinese consumers are unaware of the environmental benefits of green vehicles or the implications of green tax policies. Green tax policies may not work well if there is not sufficient consumer demand for eco-friendly vehicles.
- **Infrastructure Challenges:** Investing in infrastructure, such as charging stations, battery swapping plants, and hydrogen refueling stations, is crucial to making the switch to green vehicles, such as electric or hydrogen-powered vehicles. Adoption of green vehicles may be hindered by insufficient infrastructure, while green tax policies may be less effective.
- **Technological Barriers:** The Chinese automobile industry may not have the expertise or technologies needed to develop and produce green vehicles. In order to accelerate the adoption of green vehicles and maximize the benefits of green tax policies, technological barriers should be overcome, such as battery performance and range limitations.
- **Enforcement and Compliance Challenges:** A robust enforcement strategy and monitoring system are needed to ensure auto industry compliance with green

tax policies and emission standards. In the event of corruption, insufficient resources, or administrative capacity limitations hampering enforcement, green tax policies may lose their effectiveness and be rendered ineffective.

- **Social Equity Considerations:** Certain segments of the population may be disproportionately affected by green tax policies, particularly low-income individuals who may be unable to afford green vehicle upfront costs or have difficulty accessing alternative transportation options. In order to garner public support and minimize social resistance, green tax policies must ensure social equity and address potential disparities in distributional impacts.
- **International Trade and Competition:** There is fierce competition from foreign manufacturers in both domestic and international markets for the Chinese automobile industry due to its profound integration into global supply chains. Chinese automakers' competitiveness could be affected by green tax policies, resulting in trade imbalances and market access concerns.

## COMPARISON BETWEEN INDIA AND CHINA GREEN TAX POLICIES

There are differences in approach and outcomes between India and China's green taxes on automobiles with respect to environmental justice. In India, green tax policies, such as vehicle scrappage, focus primarily on phasing out old and polluting vehicles, with little treatment of fuel efficiency and emissions standards. A larger number of policies are in place in China, including strict vehicle emission standards, fuel quality regulations, and incentives for the use of clean vehicles. Environmental benefits are greater as a result of this broader scope. Consequently, India's policies may unfairly affect the low-income community, as they may lack access to alternative transportation options or are unable to afford newer, cleaner vehicles. In addition to affecting low-income groups, China's policies may promote environmental justice more effectively due to measures such as subsidies for electric vehicles and public transportation investments. Inadequate infrastructure, limited compliance mechanisms, and regulatory loopholes make it difficult for India to enforce its green tax policies. In China, emission standards and pollution control measures are strictly enforced due to a more robust regulatory framework and enforcement mechanisms (Pucher et al. 2007).

The automotive industry may oppose India's policies and face economic consequences such as job losses in the informal sector and disruption of the automotive value

chain. China's policies have fostered economic growth and job creation in the green automotive sector by investing in clean technology and innovation. There is an international agreement called the Paris Agreement, which commits both India and China to reduce greenhouse gas emissions and combat climate change to reduce greenhouse gas emissions. China's green tax policies demonstrate greater leadership in addressing environmental challenges and align closely with international commitments. As a result, although India and China have instituted policies to promote environmental justice through green taxes on automobiles, China's policies appear to be more comprehensive, effective, and aligned with international commitments. It may be difficult for India to achieve environmental justice through green tax policies due to challenges in enforcement, coverage, and industry acceptance. While both countries have opportunities to learn from one another's experiences and improve their policies, environmental and social equity issues still need to be addressed effectively (Lam & Mercure 2021).

## RECOMMENDATIONS AND CONCLUSIONS

A comprehensive approach to implementing green tax policies in the automobile industry is required to take into account the interests of various stakeholders, economic factors, and environmental objectives. Focus on reducing emissions and encouraging fuel efficiency in the automobile sector by implementing green tax policies that encourage the adoption of electric and hybrid vehicles. Adapt tax rates based on vehicle emissions, fuel efficiency, and carbon footprint to account for the environmental performance of vehicles. For eco-friendly vehicles, lower taxes or incentives should be provided, while higher taxes or incentives should be imposed on vehicles with higher emissions and lower fuel efficiency. Fund the development of infrastructure associated with green mobility, such as charging stations for electric and hydrogen vehicles and public transportation. Cleaner transportation options will be made possible by this infrastructure investment. Promoting green vehicles and green tax policies through public awareness campaigns. Consumers will be encouraged to purchase eco-friendly vehicles if they receive tax rebates, subsidies, or discounts. Contribute to the development of advanced clean and sustainable transportation technologies, such as electric vehicles, hydrogen fuel cells, and alternative fuels, by supporting research and development (R&D) initiatives. Incentives are available to promote innovation in the automotive industry, such as grants, tax credits, and other incentives.

Setting industry-wide environmental performance standards with automobile manufacturers and encouraging

the development of greener vehicles should be a priority. Investing in green technology and adopting sustainable manufacturing practices can earn companies incentives or tax breaks. Compliance with green tax policies and emission standards needs to be enforced through strict regulations and monitoring mechanisms. To promote accountability among automobile manufacturers and deter violations, implement fines and penalties for non-compliance. Identify, share, and harmonize environmental standards with international organizations, governments, and stakeholders. It is possible to accelerate the transition towards sustainable transportation by participating in global initiatives that leverage resources and expertise. Provide investors and businesses with stability and predictability by developing long-term strategies and policies. Coordinate and align green tax policies with broader environmental objectives and goals. In addition to monitoring and evaluating a green tax policy's effectiveness, it should also identify ways to improve economic and environmental outcomes. Ensure continuous improvement by reviewing and updating policies based on performance data. In implementing these recommendations, governments can encourage a cleaner and healthier future for society by driving sustainable transformation in the automobile industry, reducing environmental impact, and promoting sustainable transformation.

## REFERENCES

- Alvarez, X.C., Gago, A. and Labandeira, X., 1997. Green tax reform: facts and experiences. *Australia Tax Journal*, 14, p.361.
- Anchan, A., 2018. Challenges & emission control technologies for heavy-duty commercial vehicles to meet Bharat Stage VI Norms: A review. *International Research Journal of Engineering and Technology*, 5(12), pp.993-1001.
- Bansal, G. and Bandivadekar, A., 2013. Overview of India's vehicle emissions control program. *ICCT, Beijing, Berlin, Brussels, San Francisco, Washington*.
- Barbier, E., 2011. *The Policy Challenges for Green Economy and Sustainable Economic Development*. Blackwell Publishing Ltd.
- Carattini, S., Baranzini, A., Thalmann, P., Varone, F. and Vöhringer, F., 2017. Green taxes in a post-Paris world: are millions of nays inevitable? *Environmental and Resource Economics*, 68, pp.97-128.
- Cnossen, S., 2001. Tax policy in the European Union: A review of issues and options. *FinanzArchiv/Public Finance Analysis*, 58(4), pp.466-558.
- De Serres, A., Murtin, F. and Nicoletti, G., 2010. A framework for assessing green growth policies.
- Freund, D.M., 2007. *Foundations of Commercial Vehicle Safety: Laws, Regulations, and Standards*. Springer
- Gajbhiye, M.D., Lakshmanan, S., Aggarwal, R., Kumar, N. and Bhattacharya, S., 2023. Evolution and mitigation of vehicular emissions due to India's Bharat Stage Emission Standards—A case study from Delhi. *Environmental Development*, 45, p.100803.
- Gupta, G. and Köhlin, G., 2006. Preferences for domestic fuel: analysis with socio-economic factors and rankings in Kolkata, India. *Ecological Economics*, 57(1), pp.107-121.
- Hu, X., Chang, S., Li, J. and Qin, Y., 2010. Energy for sustainable road transportation in China: Challenges, initiatives, and policy implications. *Energy*, 35(11), pp.4289-4301.

- James, A.T., Asjad, M., Kumar, G., Shukla, V.C. and Arya, V., 2023. Analyzing barriers to implementing new vehicle scrap policy in India. *Transportation Research Part D: Transport and Environment*, 114, p.103568.
- Lam, A. and Mercure, J.F., 2021. Which policy mixes are best for decarbonizing passenger cars? Simulating interactions among taxes, subsidies, and regulations for the United Kingdom, the United States, Japan, China, and India. *Energy Research & Social Science*, 75, p.101951.
- Lehmann, P., 2012. Justifying a policy mix for pollution control: a review of economic literature. *Journal of Economic Surveys*, 26(1), pp.71-97.
- Lusk, A.C., Li, X. and Liu, Q., 2023. If the government pays for full home charger installation, would affordable housing and middle-income residents buy electric vehicles? *Sustainability*, 15(5), p.4436.
- Meckling, J. and Nahm, J., 2019. The politics of technology bans: Industrial policy competition and green goals for the auto industry. *Energy Policy*, 126, pp.470-479.
- Naik, T.S., 2018. *End of Life Vehicles Management at Indian Automotive System*. Jonkoping University
- Pucher, J., Peng, Z.R., Mittal, N., Zhu, Y. and Korattyswaroopam, N., 2007. Urban transport trends and policies in China and India: impacts of rapid economic growth. *Transport Reviews*, 27(4), pp.379-410.
- Revathi, R. and Aithal, P.S., 2019. Review on global implications of goods and service tax and its Indian scenario. *Saudi Journal of Business and Management Studies*, 4(4), pp.337-358.
- Rissman, J., Bataille, C., Masanet, E., Aden, N., Morrow III, W.R., Zhou, N., Elliott, N., Dell, R., Heeren, N., Huckestein, B. and Cresko, J., 2020. Technologies and policies to decarbonize global industry: Review and assessment of mitigation drivers through 2070. *Applied Energy*, 266, p.114848.
- Sangodkar, M.R.V., 2021. Faster adoption and manufacturing of hybrid & electric vehicles (fame India) scheme overview. *The GCCE Peer Reviewed Journal of Multi-Disciplinary Research*, 11, p.27.
- Singh, K.D. and Gahlot, S., 2023. Policy framework of green taxation on motor vehicles: A comparative perspective. *European Journal of Sustainable Development*, 12(3), pp.49-49.
- Singh, N., Mishra, T. and Banerjee, R., 2021. Analysis of retrofit and scrappage policies for the Indian road transport sector in 2030. *Transportation Research Record*, 2675(12), pp.233-246.
- Stephens, T., Zhou, Y., Burnham, A. and Wang, M., 2018. Incentivizing Adoption of Plug-In Electric Vehicles: A Review of Global Policies and Markets. Argonne National Laboratory
- Sulkowski, A.J., Alexander, M. and Wiggins, W., 2016. Sustainability & Tax Policy: Fixing a Patchwork of Policies with a Coherent Federal Framework. *Virginia Environmental Law Journal*, *Forthcoming*.
- Wong, Y.C., Al-Obaidi, K.M. and Mahyuddin, N., 2018. Recycling of end-of-life vehicles (ELVs) for building products: Concept of processing framework from automotive to construction industries in Malaysia. *Journal of Cleaner Production*, 190, pp.285-302.
- Wu, Y.A., Ng, A.W., Yu, Z., Huang, J., Meng, K. and Dong, Z.Y., 2021. A review of evolutionary policy incentives for sustainable development of electric vehicles in China: Strategic implications. *Energy Policy*, 148, p.111983.
- Zhang, X. and Bai, X., 2017. Incentive policies from 2006 to 2016 and new energy vehicle adoption in 2010–2020 in China. *Renewable and Sustainable Energy Reviews*, 70, pp.24-43.
- Zhang, X., Xie, J., Rao, R. and Liang, Y., 2014. Policy incentives for the adoption of electric vehicles across countries. *Sustainability*, 6(11), pp.8056-8078.
- Zorpas, A.A. and Inglezakis, V.J., 2012. Automotive industry challenges in meeting EU 2015 environmental standard. *Technology in Society*, 34(1), pp.55-83.

---

#### ORCID DETAILS OF THE AUTHORS

Shamsher Singh: <https://orcid.org/0009-0007-8909-1613>  
 Naresh Anguralia: <https://orcid.org/0009-0002-1374-4626>





# Investigations on Photodegradation and Antibacterial Activity of Mixed Oxide Nanocrystalline Materials

P. P. Shinde<sup>1</sup>, R. J. Sayyad<sup>1</sup>, S. S. Shukla<sup>1</sup>, S. A. Waghmode<sup>2</sup> and S. R. Gadale<sup>1†</sup>

<sup>1</sup>Yashwantrao Mohite College of Art, Science and Commerce, Bharati Vidyapeeth Deemed to be University, Pune, India

<sup>2</sup>MES, Garware College, Pune, India

†Corresponding author: S. R. Gadale; [dagade@rediffmail.com](mailto:dagade@rediffmail.com)

Nat. Env. & Poll. Tech.  
Website: [www.neptjournal.com](http://www.neptjournal.com)

Received: 20-02-2024

Revised: 26-03-2024

Accepted: 29-04-2024

## Key Words:

Mixed oxide  
Cobalt doped molybdenum  
Catalytic activity  
Methyl orange  
Methylene blue  
Microbial analysis

## ABSTRACT

In this study, we synthesized cobalt-doped molybdenum supported on silica (Co/MS) nanocomposites with varying concentrations of cobalt (1, 5, 10, 15, and 20 wt%) using the sol-gel method. We investigated their physico-chemical properties, photocatalytic activity, and antimicrobial efficacy. The synthesized nanocomposites were characterized using a range of techniques, including X-ray powder diffraction (XRD) to determine crystal structure, UV-vis spectroscopy for optical properties, Fourier transform infrared spectroscopy (FT-IR) for functional group analysis, and scanning electron microscopy coupled with energy-dispersive X-ray microanalysis (SEM-EDX) for morphological and elemental composition analysis. The photocatalytic performance of these catalysts was assessed by their ability to degrade organic dyes, specifically methyl orange and methylene blue, under visible light irradiation. Our results demonstrated that the photocatalytic efficiency increased with higher cobalt content, with the 20 wt% Co/MS nanocomposite showing the highest degradation rates. Additionally, we evaluated the antibacterial activity of the nanocomposites against a range of microorganisms, including Gram-positive and Gram-negative bacteria, as well as fungal species. The 20 wt% Co/MS nanocomposite exhibited superior antimicrobial activity compared to the other samples, indicating its potential for applications in environmental remediation and antimicrobial treatments.

## INTRODUCTION

The world population is growing faster in this era. Hence, to satisfy the demands of the people, newer industries and medical laboratories are being established all over the world. When such places release their wastewater into freshwater systems without first treating it, it adversely affects the natural ecosystem, including aquatic life (Gita et al. 2017, Kant 2015). These industries' harmful byproducts contain a variety of dangerous dyes that represent a significant danger to aquatic life and ecosystems (Manzoor & Sharma 2020, Lellis et al. 2019) Worldwide, many factories are responsible for water and air pollution, which can be seen from the disturbed ecosystem and climate (Zhang et al. 2010). It is clear that reducing population is significantly more challenging than improving industrial plant safety and pollution control (Weber & Sciubba 2019). Rather than employing traditional water purification techniques, one should discover more practical and environmentally beneficial wastewater treatment methods (Pandit et al. 2015). These techniques utilize physical, chemical, and biological techniques, including membrane separation, ozonation, adsorption, biological digestion, and clay minerals (Buonomenna 2013, Putatunda et al. 2015). While each

of these methods has advantages and disadvantages, the scientific community is searching for more efficient water purification techniques. (Bian et al. 2015, Kou et al. 2014). The textile sector is a big contributor to water pollution because it needs vibrant dyes and pigments to produce garments more effectively (Isik & Sponza 2005). Methyl red, methyl orange, methylene blue, rhodamine 6B, rose Bengal, congo red, and crystal violet have been used consistently in the textile industry up until now. Nearly all of the dyes mentioned above have been thoroughly examined for both their benefits and drawbacks; several of them are poisonous to people when they come into touch with them (Lan et al. 2014). Finding an alternative or alternative procedure for the treatment of dirty waste water is required because this is a very important problem. Recently, the environmental remediation process has successfully used the heterogeneous photocatalysis approach (Fang et al. 2013). Typically, semiconductor oxides are used as a catalyst in photocatalysis techniques in the presence of light. The electron from the semiconductor's valence band (VB) reaches the conduction band (CB) in the presence of light of the right wavelength, producing electron-hole pairs (Mills et al. 1993). Superoxide anion radicals are produced when the CB electron reacts with

oxygen molecules that were adsorbed on the surface, while OH radicals are produced when the VB hole reacts with water molecules. These freshly formed superoxide anions and OH radicals have enhanced reducing and oxidizing capacities and, therefore, can reduce or oxidize a wide variety of substances (Lu et al. 2013). Herein, we have prepared the Co-doped MoO<sub>3</sub>/SiO<sub>2</sub> nanocomposite with different concentrations using the sol-gel reaction technique, calcined at temperatures of 500°C, and studied its photocatalytic activity towards methyl orange degradation.

Global public health is seriously threatened by the spread of infectious illnesses, especially as antibiotic-resistant bacterial species proliferate. Bacterial species, both Gram-positive and Gram-negative, are generally regarded as major hazards to public health. Over the years, Antibiotics have been used to treat infections caused by environments observed in both hospitals and the community (Komolafe 2003, Hawkey 2008). New antibacterial medications are likely to be developed as a result of recent developments in nanobiotechnology, specifically the capacity to generate metal oxide nanoparticles of a particular size and shape. The primary factor affecting the functional activity of the nanomaterials is their particle size. Because of their exceptional physical, chemical, and biological qualities, nanomaterials have drawn a lot of interest from a variety of industries, and medicine is no exception.

Additionally, it has been noted that nanoparticles with lower particle sizes exhibit good antibacterial action (Jones et al. 2008). There is very little information available on the antibacterial characteristics of metal oxide nanoparticles compared to published publications on their physical and chemical properties. Realizing the potential antimicrobial applications of metal oxide nanoparticles and taking these characteristics into account, we employed Co-doped MoO<sub>3</sub>/SiO<sub>2</sub> nanocomposite at varying concentrations to study their antifungal and antibacterial properties against Gram-positive (*S. aureus*) bacteria and Gram-negative (*Pseudomonas aeruginosa* and *E. coli*). Also, two fungal strains were used, i.e., *Candida albicans* and *Aspergillus niger*.

## MATERIALS AND METHODS

### Materials

The chemicals used for the preparation of nanocatalysts were analytical grade (A.R.) All the reagents viz. Ammonium heptamolybdate, tetra ethyl orthosilicate (Chemplast, Chennai, CAS register no. 18945-71-7), isopropyl alcohol (IPA), and Cobalt nitrate were AR grade (99.8%) and acquired from S.D. Fine, Thomas Baker, LOBA, and Merck

Chemicals India. Distilled water was used as a solvent as well as for catalyst synthesis.

### Methods

Using a Rigaku Miniflex G-600 diffractometer set to scan at a rate of 10°/min, an X-ray diffraction (XRD) study was conducted at room temperature to record the pattern in the 2θ range of 10-80. Measurements using a scanning electron microscope (SEM) were made using a Nova Nano SEM (NPEP303). Using a 15 k beam energy, SEM-associated energy-dispersed X-ray microanalysis (EDX) was used to examine the elemental compositions. Thermo Nicolet iS5 IR device was used to perform Fourier Transfer InfraRed spectroscopy at room temperature with KBr pellets at a resolution of 4 cm<sup>-1</sup> in the 4000-400 cm<sup>-1</sup> range and 32 scans. Using a Shimadzu UV-3600 model UV-Vis-NIR spectrophotometer, the optical investigation was conducted between 200 and 800 nm in wavelength. The absorption spectra of UV-visible were noted.

### Synthesis of Co/Mo/SiO<sub>2</sub> Catalysts

Co-doped on Mo/SiO<sub>2</sub> nanomaterial was prepared by simple sol-gel method to obtain the material with high surface area as well as for uniform distribution of Co/Mo on silica support tetraethyl orthosilicate was used as a silica source. In this work, nanocatalyst was synthesized with different wt.% cobalt oxide concentrations (1, 5, 10, 15, and 20 wt. %). A suitable amount of cobalt nitrate was dissolved in distilled water for the synthesis of Co-doped on a MoO<sub>3</sub>/SiO<sub>2</sub> nanomaterial. This cobalt nitrate aqueous solution was added dropwise to a mixture of AHM and TEOS solution. After that, the sol formed was stirred for 5 h at room temperature. The resultant bluish gel was further dried overnight at room temperature. The gel was kept in an oven at 100°C for 12 h while xerogel powder was obtained, which was calcined at 500°C temperatures for 4 h.

## RESULTS AND DISCUSSION

### Fourier Transfer Infrared Spectroscopy (FT-IR)

The bending and stretching vibrations of the functional groups present in the samples were obtained by FTIR studies. Fig. 1 displays the FTIR spectra of a Co-doped Mo/SiO<sub>2</sub> (Co/MS) nanomaterial that was calcined at 500°C for 4 h. A moderate absorption band, produced by the O-H bond's bending vibration, appeared at 1631.40 cm<sup>-1</sup>. These absorption bands are a result of hydroxyl and water absorbed on the sample surface (Fig. 1). A strong absorption band present at approximately 1072.54 cm<sup>-1</sup> was due to the vibration of the chemical bond of Si-O-Si which confirms

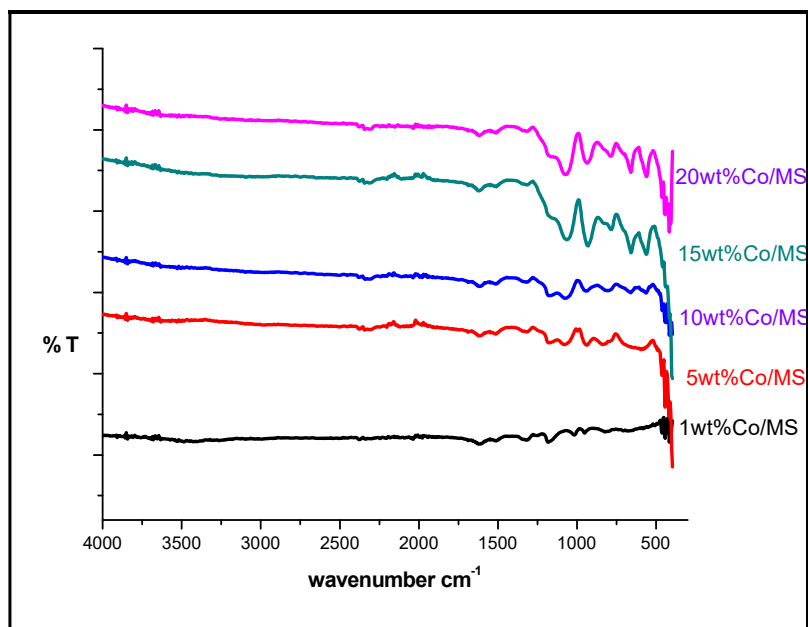


Fig. 1: FT-IR Spectra of 1-20 wt % Co/MS nanocatalysts.

the interaction between molybdenum and supported matrix. Additionally, the new peaks for the 1, 5, 10, 15, and 20 wt % Co-doped MS are located at around  $556.41\text{ cm}^{-1}$ , and these correspond to the Co-O stretching mode in the tetrahedral site and octahedral environment (Rahman et al. 2021). The peaks at  $778.32$  and  $809.55\text{ cm}^{-1}$  can be assigned to  $\nu\text{Mo-O}$  vibrations. The peaks at  $936.11\text{ cm}^{-1}$  were attributed to the Mo-O-Mo of  $\text{Mo}^{6+}$  (Chiang & Yeh 2014, Dong & Dunn 1998, Muhammad et al. 2021).

### Uv-Visible Spectroscopy

Understanding the electronic structure of the material for the optical study, especially the band gap study, was done with the analysis of the UV-Vis absorption spectrum. Fig. 2(a) illustrates the UV-visible absorbance spectrum of synthesized Co/MS (1-20wt%), which was measured in diffuse reflectance mode between 200 and 800 nm. The UV-visible absorbance spectrum showed a band edge around 255 nm. Strong absorption band in the UV-light region is noticed, and the corresponding band gap observed to be 3.98 eV for 1wt% Co/MS, which is gradually decreased as the concentration of material increased, i.e., 3.69eV for 20wt% which is seen in Fig. 2(b).

A crucial component of catalytic activity is the produced materials' optical absorption wavelength. The catalyst's photocatalytic activity will be maximal when enough electrons are stimulated from the valence band to the conduction band. The catalyst that is supplying incident light energy is equal to or greater than the band gap energy of the

photocatalyst. Fig. 2(b) depicts the results of the Tauc plot. Using the Tauc equation,  $(h\nu)^{1/n} = A(h E_g)$ , the energy band gap was calculated. The extrapolation in the linear region of the plot gives an energy band gap,  $E_g$ .

Where,

$\alpha$  is the absorption coefficient

$h$  is Planck's constant

$\nu$  is the vibration frequency

$n$  is a sample transition, and

'A' is a proportionality constant

The results of the UV-visible absorption demonstrated that the mixed oxide nanomaterials are capable of producing more electrons and holes when exposed to UV light. The holes and electrons produced during catalytic reactions will actively take part in the oxidation and reduction process. These findings revealed that the Co/MS nanomaterial had a greater photocatalytic efficiency.

### X-Ray Diffraction Analysis

The prepared Co/MS nanostructures were subjected to X-ray analysis in order to identify the phase and crystalline size of nanomaterials; various amounts of (1, 5, 10, 15, and 20 wt.%) Co-doped on  $\text{MoO}_3$  supported on  $\text{SiO}_2$  were investigated by X-ray diffraction studies over the  $2\theta$  values in the range of  $10\text{-}80^\circ$ . The intense XRD peaks confirm the formation of highly crystalline materials with mainly two phases, i.e.,  $\alpha\text{-MoO}_3$  and  $\text{CoMoO}_4$  (Fig. 3).

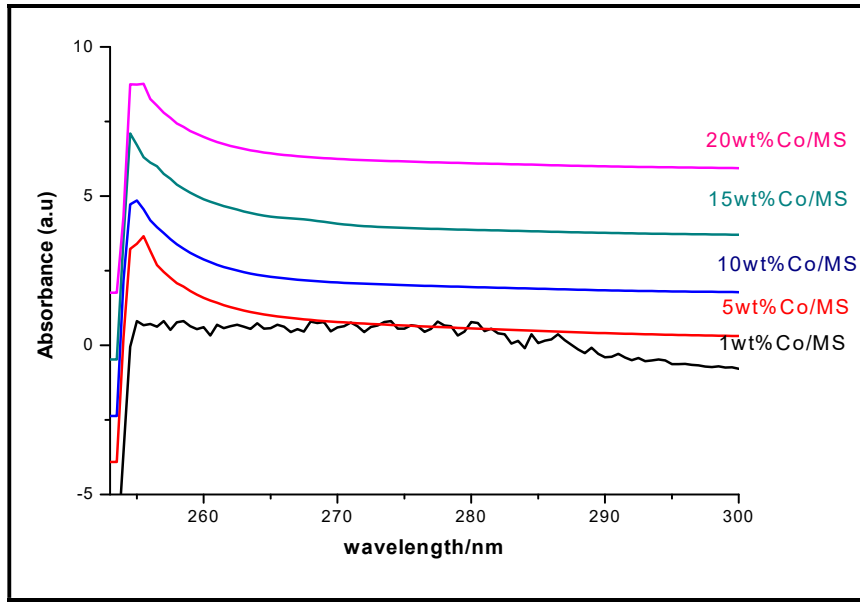


Fig. 2(a): UV Spectra of 1-20wt% Co/MS nanomaterials.

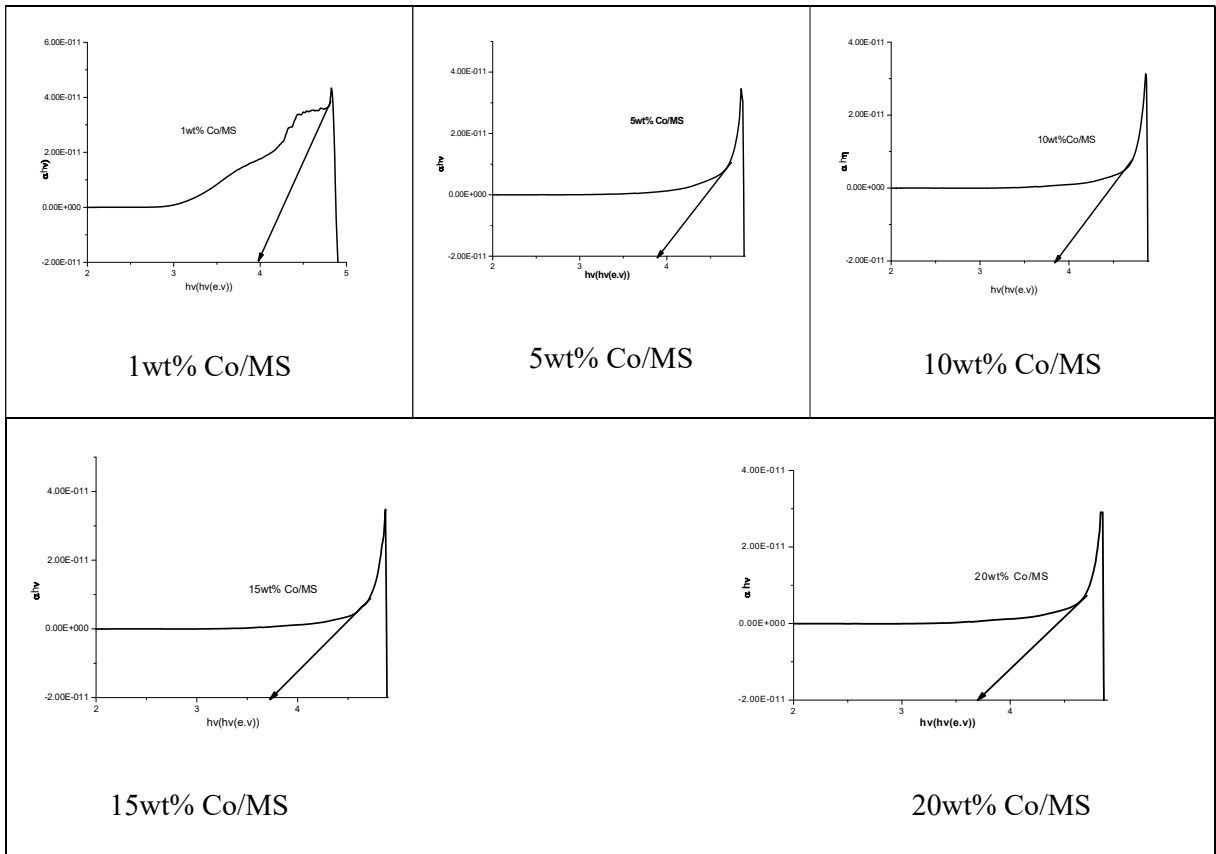


Fig. 2(b): Band gap graph for 1-20wt% Co/MS.

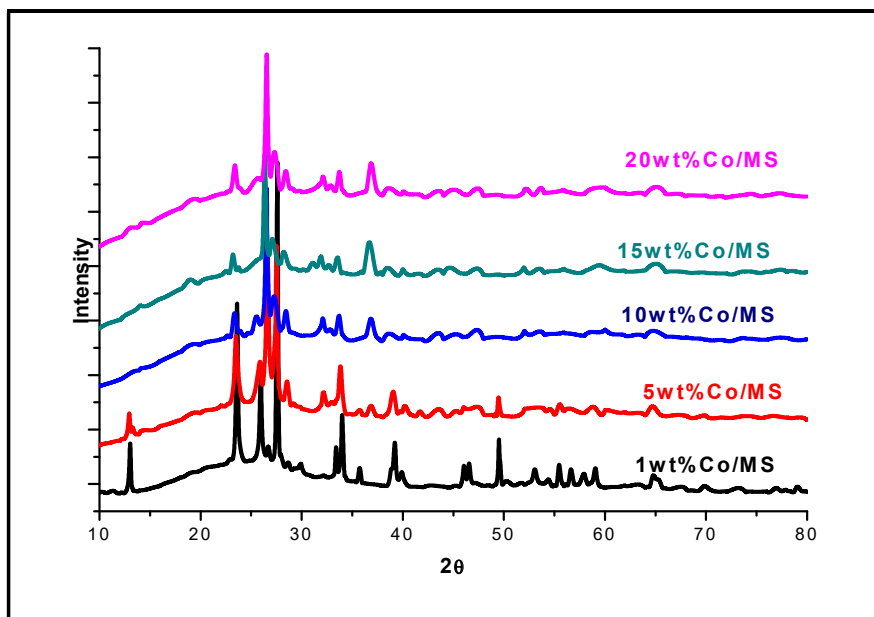


Fig. 3: XRD Spectra of Co/Mo/SiO<sub>2</sub> nanomaterials.

The diffraction peak for  $\alpha$ -MoO<sub>3</sub> can be assigned to 12.98°, 25.87°, 27.51°, 33.86°, 35.67° and 49.52° indexed as (020), (040), (021), (111), (041) and (002). CoMoO<sub>4</sub> indicated 2 $\theta$  at 23.44°, 27.61°, 28.46°, 45.75° and 59.43° indexed as (021), (22-1), (220), (420) and (35-1). Which exactly matches with (JCPDS NO-01-073-6497) and (JCPDS NO-00-25-1434), respectively. The crystallite size in the range of 10 nm to 70 nm was calculated from the Debye Scherrer equation ( $D=0.9\lambda/\beta \cos \theta$ ), where

D is the crystal size

$\lambda$  is the wavelength of X-ray

$\theta$  is the Bragg's angle in radians and

$\beta$  is the full width at half maximum of the peak in radians

### SEM and EDX Analysis

Based on SEM images that were captured, the surface morphology of the as-prepared samples was examined, and an EDX analysis of the created nanomaterials was done, and the results are shown in Fig. 4 (a, b, c, d, and e). In 1-20wt% Co/MS showed global and uniform particles with spherical shapes that are coherent together.

Using energy dispersive X-ray spectroscopy analysis, the chemical makeup of samples 1 and 20 wt% Co/MS oxide particle was examined. The spectra are displayed in Fig. 5(a) and 5(b), with the peaks indicating the components present in the samples. The representative EDX data in Fig. 5(a) and 5(b) shows two intense and prominent peaks of molybdenum and silica and other comparatively smaller peaks of cobalt.

These results confirmed the existence of Co atoms in the nanomaterials. Consequently, it may be concluded that Co ions are evenly distributed throughout the molybdenum and silica oxide crystallites.

### Photodegradation Studies

The effect of the presence of the nanomaterials on the photodegradation of MO dye was evaluated under visible light irradiation. For the degradation, a 100 mL solution containing 10 ppm methyl orange (MO) dye was chosen for the study of the photocatalytic activity of prepared samples. The 1-liter stock solution of 10 ppm dyes was prepared by dissolving 10 mg of MO in deionized water. For the evaluation of photocatalytic activity, 100 mL, 10 ppm of each dye solution was taken in a 250 mL conical flask. About 100mg of Co/Mo/SiO<sub>2</sub> nanomaterials was added.

This reaction was carried out in a closed box fitted with the lamp was 200W, and the distance between the lamp and the reaction mixture was fixed throughout the study (10 cm). Before being exposed to light, the suspension was agitated for 30 min in the dark to create equilibrium between the catalyst and substrate. Subsequently, the suspension was continuously stirred while exposed to visible light. At various intervals during the irradiation process, 2 mL of the suspension was routinely removed from the reactor. For MO in aqueous heterogeneous solution suspensions, the absorption peak at 470 nm was used to quantitatively assess the catalyst's catalytic activity. The % of dye degradation was computed using the following formula.

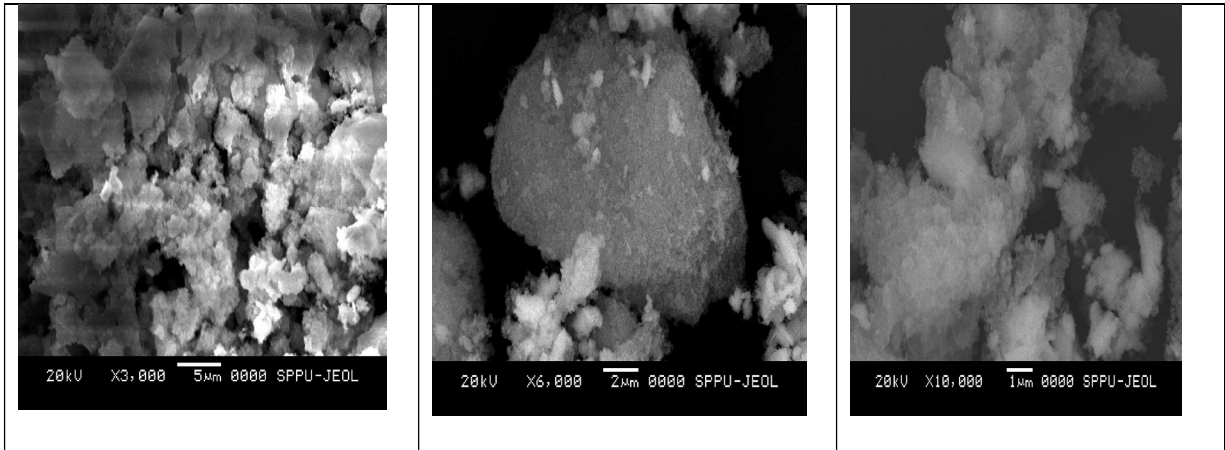


Fig. 4(a). 1wt% Co/MS.

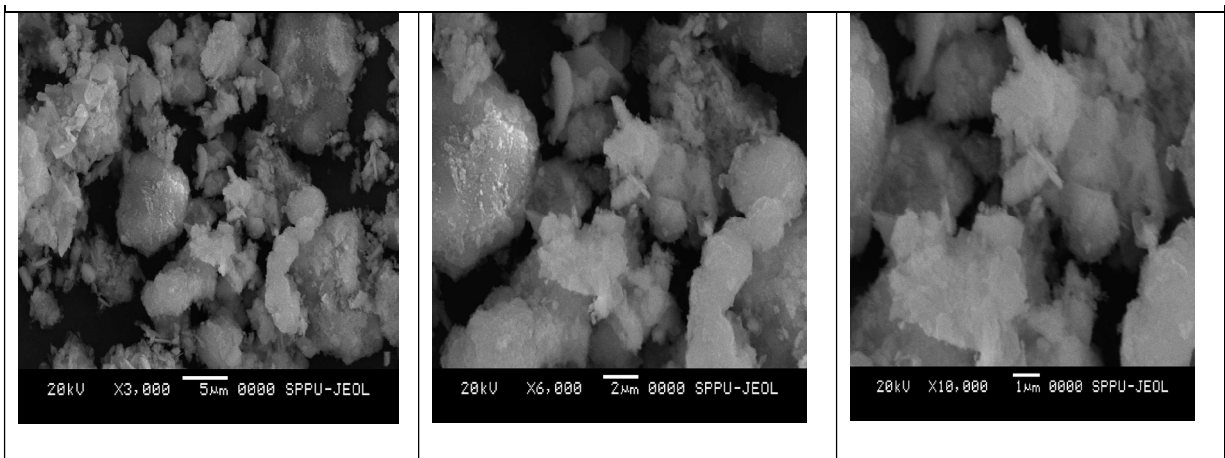


Fig. 4(b): 5wt% Co/MS.

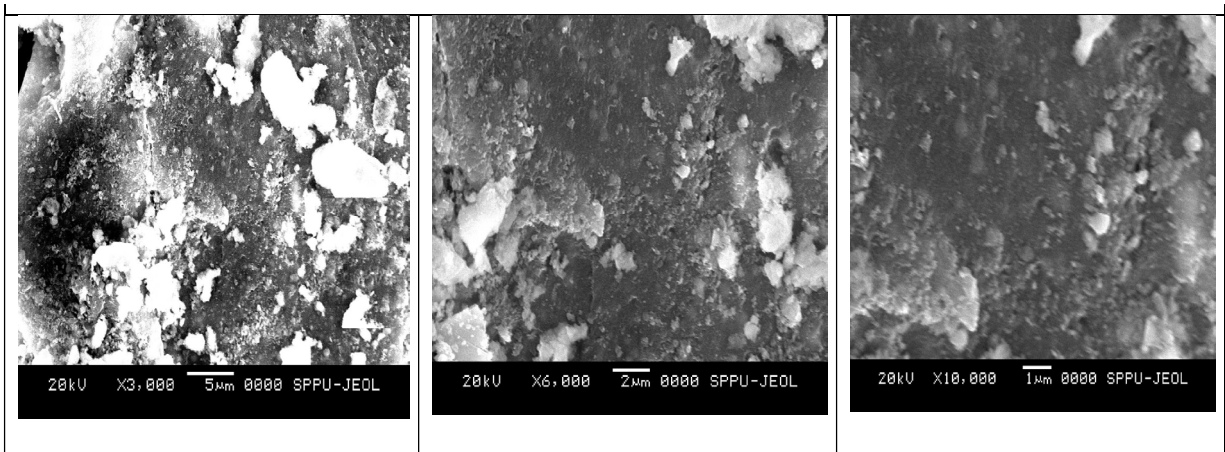


Fig. 4(c): 10wt% Co/MS.

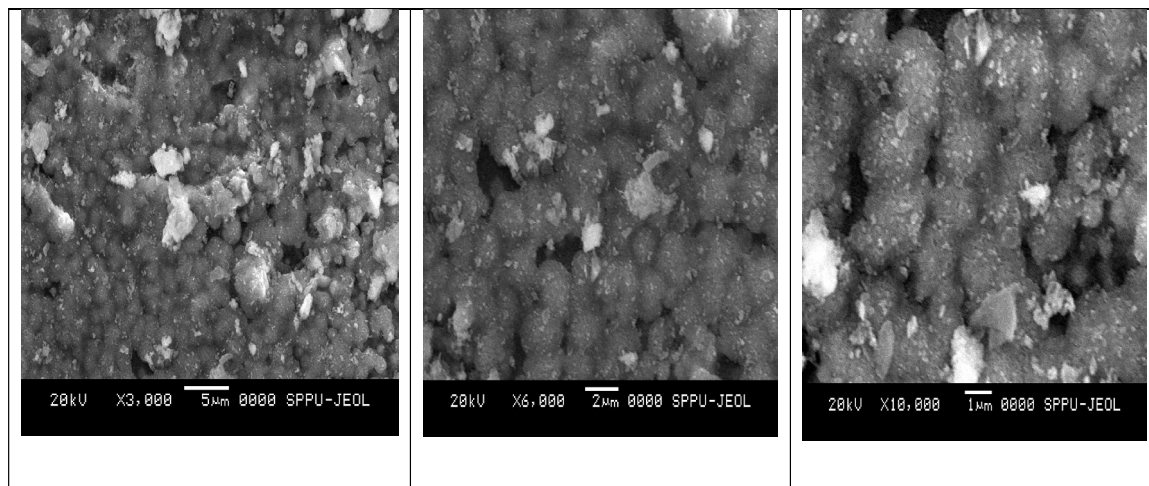


Fig. 4(d): 15wt% Co/MS.

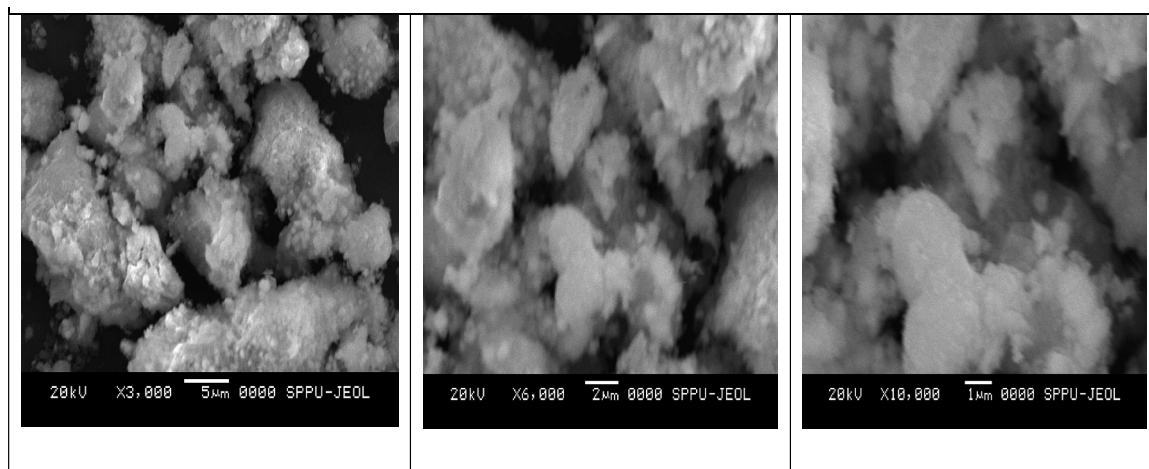


Fig. 4(e): 20wt% Co/MS.

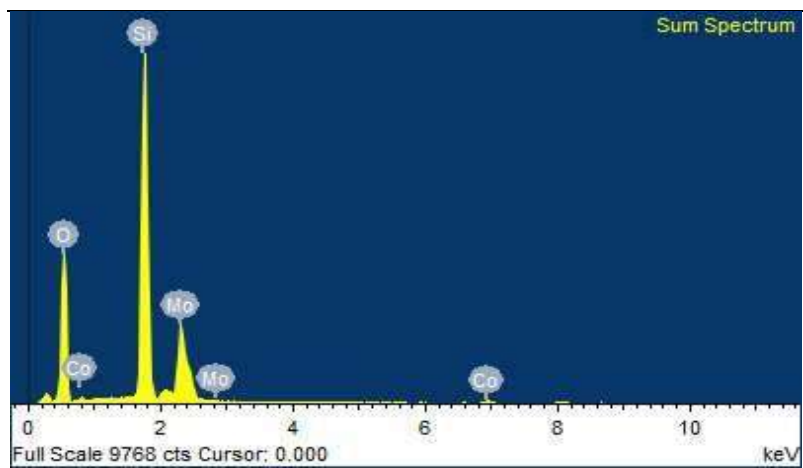


Fig. 5(a): EDX graph of 1wt% Co/MS.

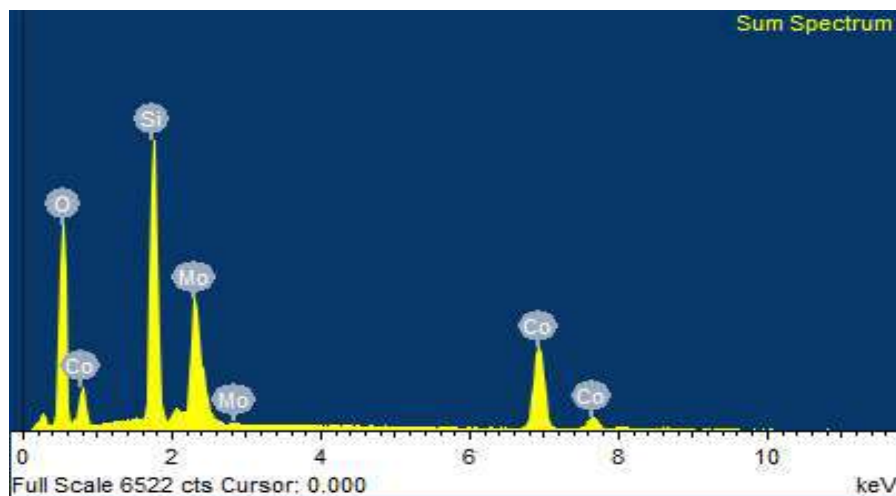


Fig. 5(b): EDX graph of 20wt% Co/MS.

$$\text{Degradation Efficiency} = \left\{ \frac{C_0 - C_t}{C_0} \times 100 \right. \quad \dots(1)$$

Where  $C_0$  is the initial concentration of the dye solution,

$C_t$  is the concentration of the dye solution after photoirradiation in a selected time interval.

### Photodegradation of Cobalt Doped MS Nanostructures

Following thorough structural and optical characterization, the degradation of MO dye under a 200W lamp was used to assess the photocatalytic activity of the 1, 5, 10, 15, and 20wt% Co/MS nanomaterials. The step-by-step instructions are listed below. The main purpose of stirring the solution in the dark was to monitor the adsorption-desorption equilibrium. The MO solution sample was taken out of the reaction mixture at prearranged intervals, and its absorption spectra were recorded to track the rate of degradation and removal effectiveness. Fig. 6 shows the representative absorption spectra of MO solution following the degradation experiment in the presence of 1–20% Co/MS samples. After 180 minutes of irradiation, it was evident that the absorption peak of the MO solution isolated from the 20wt% sample (Fig. 6(e)) had a greater reduction in peak intensity. Thereby indicating its superior dye-removal efficiency compared to the other four samples (Fig. 6 (a-d)).

More precisely, 38.50%, 54.15%, 56.84%, 61.94%, and 71.23% of MO dye was degraded by 1wt%, 5wt%, 10wt%, 15wt% and 20wt% Co/MS samples, respectively (Fig. 6 d).

The presence of larger cobalt concentrations in the host lattice-possibly because of a lower band gap energy-can be the reason for the 20wt% sample's improved photocatalytic performance when compared to the 1–15wt% sample.

### Degradation Mechanism

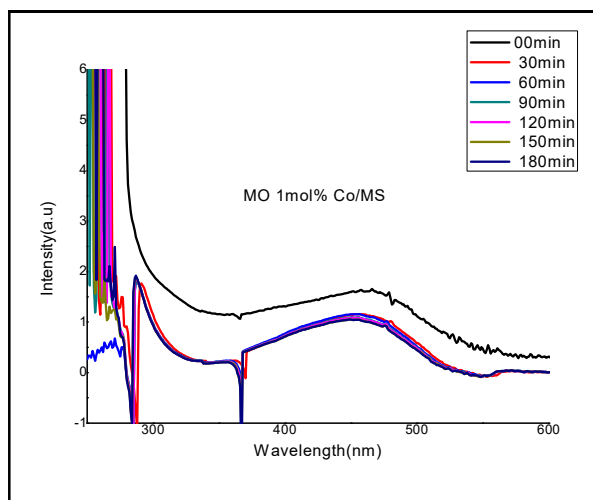
Because of its lower bandgap, the Co/MS sample absorbs UV-visible radiation from solar radiation, which causes its valence electrons to move from the valence band (VB) to the conductive band (CB). The valence electron was excited, resulting in the creation of a positively charged ( $h^+$ ) hole in the VB. By acting as a trapping agent for the excited electrons, the Co/MS sample decreased the likelihood of electron-hole recombination (Fig. 7). Acting as an intermediary, the Co and Mo contents first captured excited electrons, which they then utilized to convert molecular oxygen ( $O_2$ ) into the superoxide radical  $O_2^-$  (free radical). After being excited by electrons, the positively charged hole ( $h^+$ ) created in the VB further interacted with  $H_2O$  or OH to form the hydroxyl free radical  $OH^\cdot$ .

Thus, in brief, molecular oxygen and water were transformed into secondary active free radicals ( $O_2^-/OH^\cdot$ ) via oxidation/reduction reactions involving the primary active species, free electrons, and holes. Ultimately, the organic MO dye was broken down into straightforward, non-toxic metabolites by the highly active free radicals' interaction with it. The following diagram summarizes the mechanism of the entire degradation process.

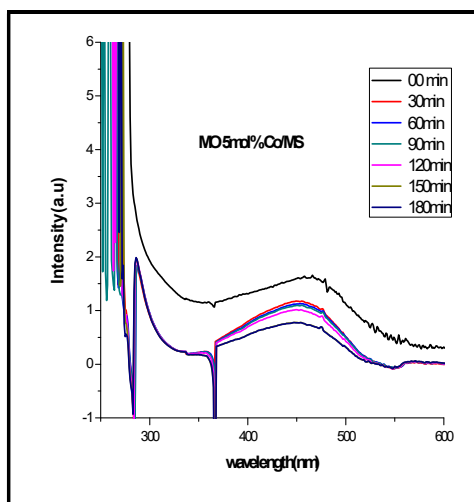
### Antibacterial Activity

The antibacterial activity of all compositions (1wt%, 5wt%, 10wt%, 15wt%, and 20wt%) of Co/MS samples against Gram-positive (*Bacillus subtilis*, *Staphylococcus aureus*), Gram-negative (*Escherichia coli*, *Klebsiella pneumoniae*) and fungal (*Aspergillus niger*, *Candida albicans*) was examined by using well diffusion method as shown in

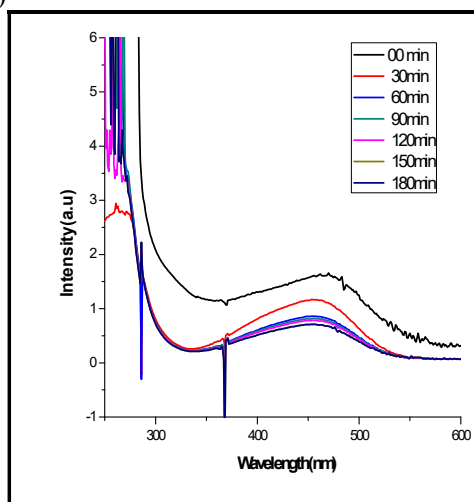




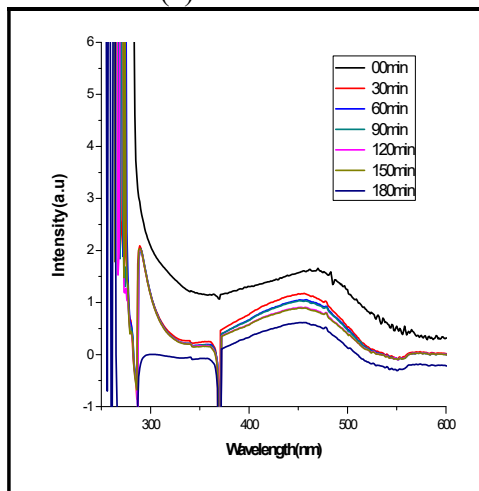
(a)



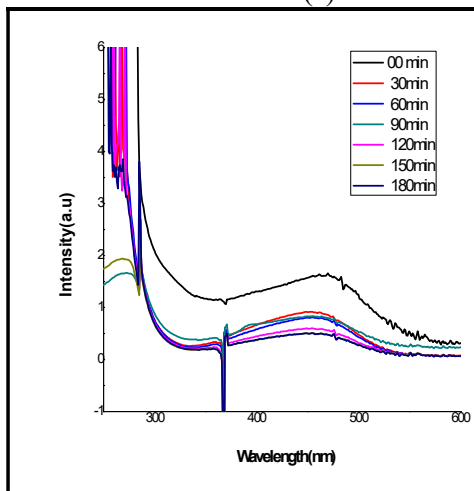
(b)



(c)



(d)



(e)

Fig. 6: Absorption spectra for the degradation of MO dye over (a) 1wt%, (b) 5wt%, (c) 10wt%, (d) 15wt% and (e) 20wt%Co/MS.

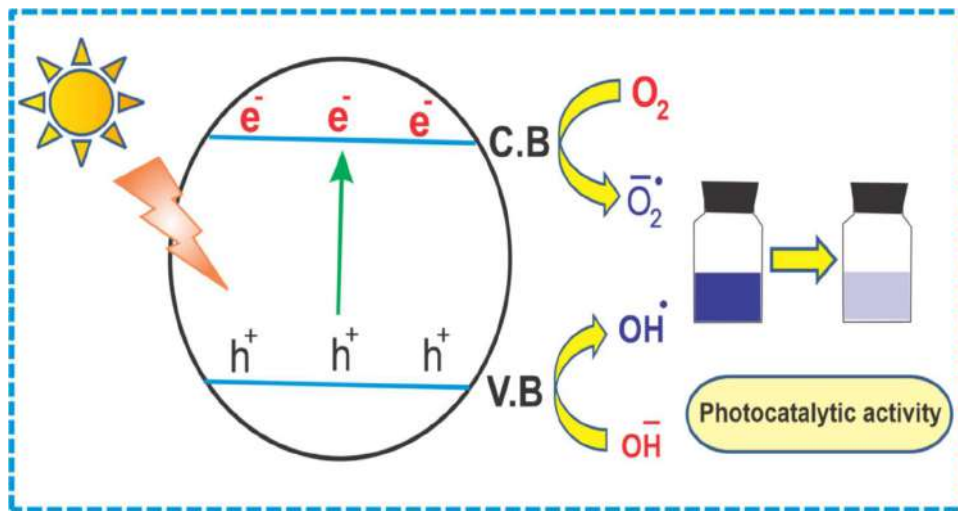


Fig. 7: Mechanism of the degradation process (Zhang et al. 2010).

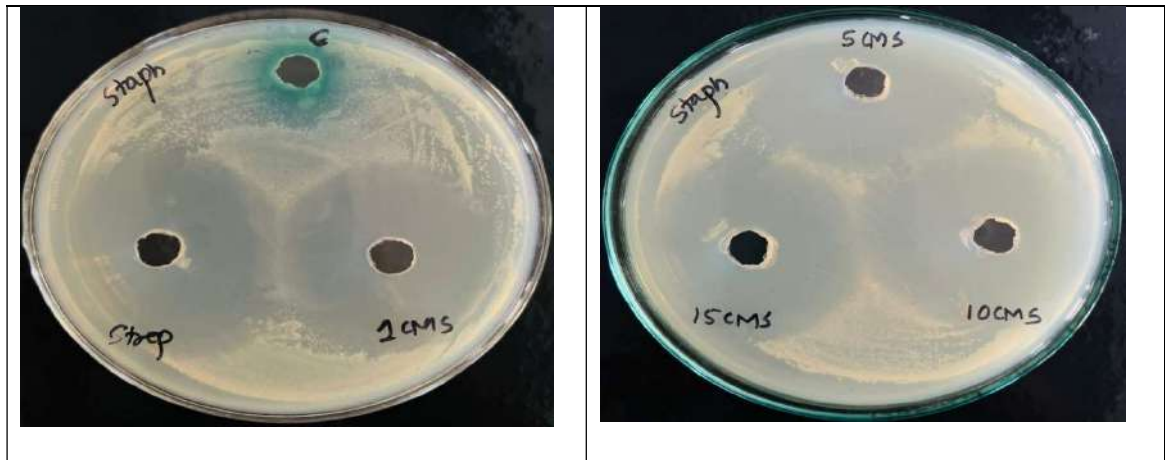


Fig. 8(a): Antimicrobial activity of Co/MS catalyst against *Staphylococcus aureus*.

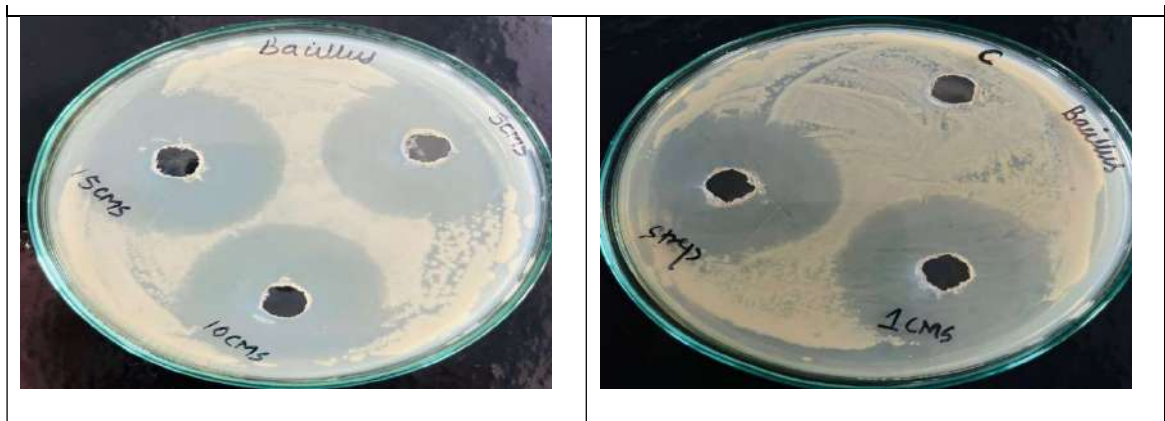


Fig. 8(b): Antimicrobial activity of Co/MS catalyst against *Bacillus subtilis*.

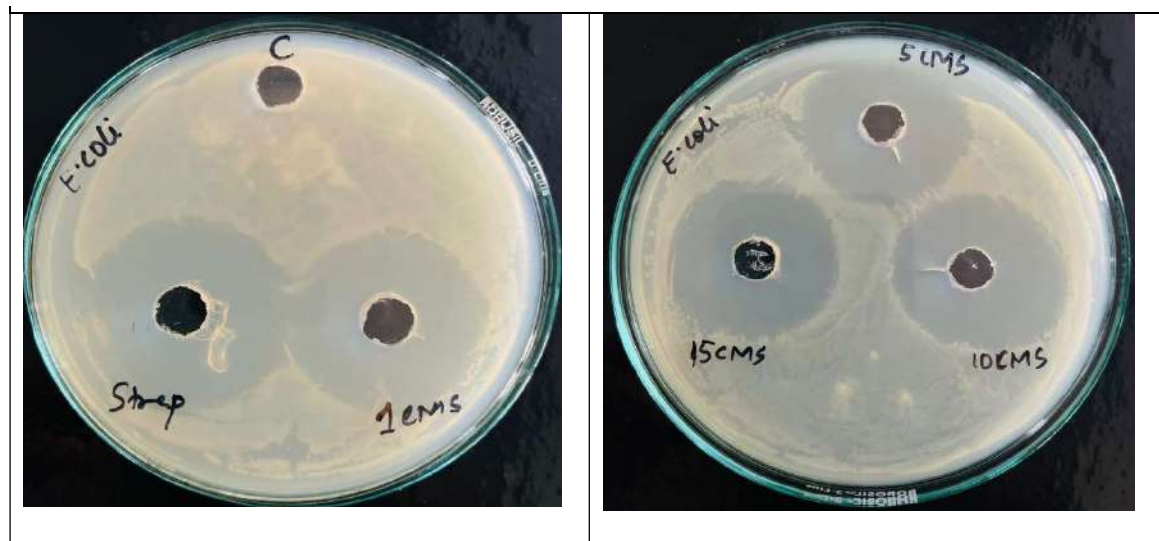


Fig. 8(c): Antimicrobial activity of Co/MS catalyst against *E. coli*.

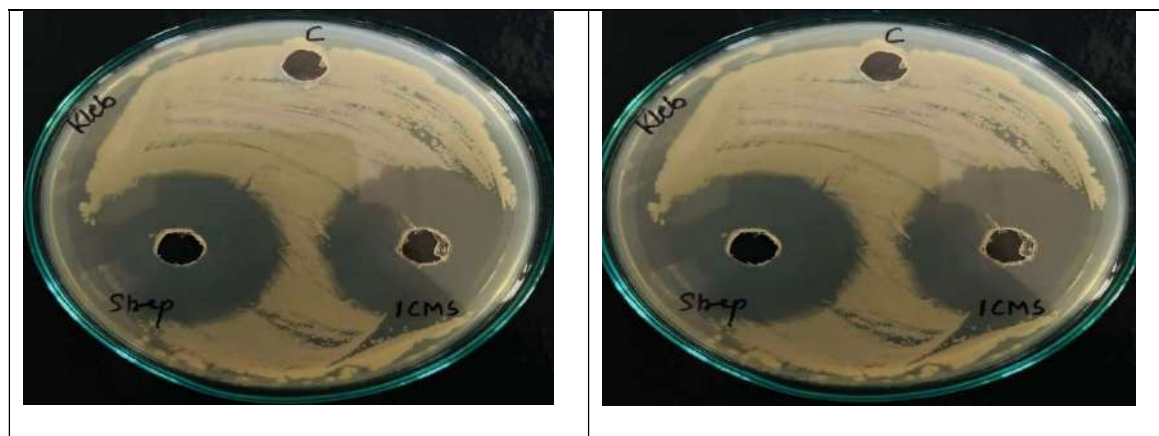


Fig. 8(d): Antimicrobial activity of Co/MS catalyst against *Klebsiella pneumoniae*.

Table 1(a): Zone of inhibition in mm for Co/MS materials for microbial strains.

Catalyst %	Zone of inhibition in mm			
	<i>S. aureus</i>	<i>B. subtilis</i>	<i>E.coli</i>	<i>K.pneumoniae</i>
1wt% Co/MS	27 ± 0.02	23 ± 0.02	21 ± 0.01	27 ± 0.02
5wt% Co/MS	28 ± 0.03	24 ± 0.01	22 ± 0.02	28 ± 0.03
10wt% Co/MS	32 ± 0.02	27 ± 0.02	20 ± 0.04	32 ± 0.02
15wt% Co/MS	33 ± 0.01	28 ± 0.03	18 ± 0.01	33 ± 0.01
20wt% Co/MS	35 ± 0.02	32 ± 0.02	22 ± 0.02	35 ± 0.02
Std. Streptomycin	23 ± 0.02	22 ± 0.02	19 ± 0.01	23 ± 0.02
Control (DMSO)	00	00	00	00

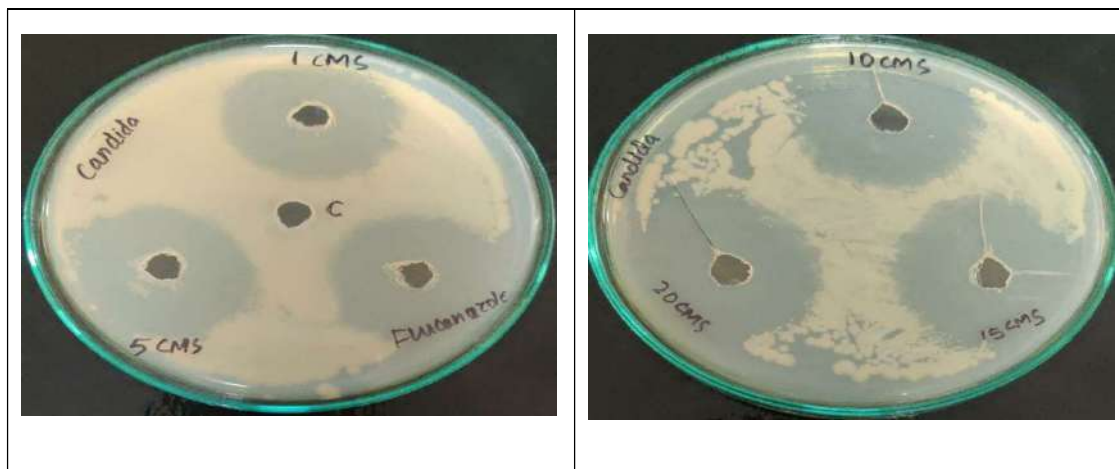


Fig. 9(a): Antimicrobial activity of Co/MS catalyst against *Candida albicans*.

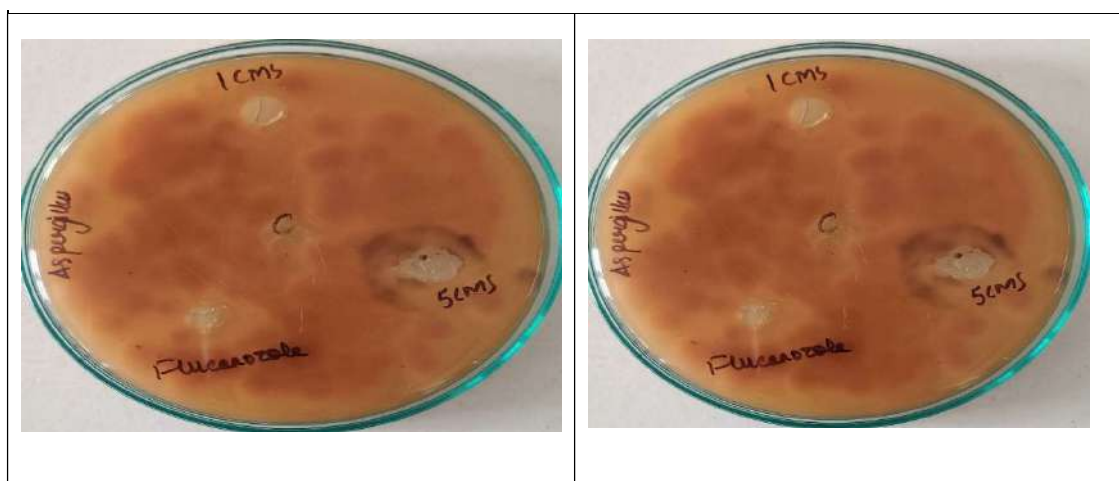


Fig. 9(b): Antimicrobial activity of Co/MS catalyst against *Aspergillus niger*.

Table 1(b): Zone of inhibition in mm for Co/MS materials for fungal strains.

Catalyst %	<i>Candida albicans</i>	<i>Aspergillus niger</i>
1wt% Co/MS	21 ± 0.02	05 ± 0.01
5wt% Co/MS	24 ± 0.03	10 ± 0.03
10wt% Co/MS	27 ± 0.03	09 ± 0.03
15wt% Co/MS	29 ± 0.01	08 ± 0.02
20wt% Co/MS	32 ± 0.02	10 ± 0.01
Std. Fluconazole	22 ± 0.02	01 ± 0.03
Control (DMSO)	00	00

Figs. 8(a-d) and 9(a and b), all prepared samples illustrated good antibacterial activity against both Gram-positive and Gram-negative bacterial and fungal strains, respectively. Table 1(a and b) summarises the comparative results of measuring inhibition areas in all samples.

It is evident from the antibacterial results that the 20wt% Co/MS sample exhibited a superior antibacterial aptitude than that of a 1-15% Co/MS and standard against Gram-positive and Gram-negative bacteria as well as fungal strains. There was a continuous increase in the inhibition zone as the concentration of Co/MS catalysts increased from 1wt%–20wt%. 20wt% concentrations are more crystalline, which is the reason they have shown more inhibition of microorganisms because the activity of Co/MS catalysts depended on the size and structure responsible for the inhibition of microbe. Nanomaterial incorporation inhibits phagocytosis, inhibits oxidative stress, limits cell development, lowers cell viability, and eventually compromises cell integrity. The production of reactive oxygen species (ROS), which can harm cellular proteins, lipids, and the cell wall membrane and ultimately destroy the bacteria's cell, is one of the crucial steps in increasing toxicity.

The antifungal activities of Co/MS catalysts are carried out towards two fungal strains, *Candida albicans*, and *Aspergillus niger*, and their activity was referred to standard antifungal agent fluconazole. The results are brief in Tables 1(a) and 1(b). Among the two fungus species, *Candida albicans* and *Aspergillus niger* have been observed with good antifungal effects. From Table 1(b), it is seen that *Candida albicans* showed more antifungal activity than *Aspergillus niger* for all Co/MS catalysts.

## CONCLUSION

The cobalt-doped molybdenum-supported silica oxide nanocatalysts were synthesized by the Sol-gel method. The powder X-ray diffraction analysis confirmed the good crystalline nature. The presence of functional groups was established by FTIR analysis. Results of the UV-Vis spectrum indirect transition band gap shifted from  $E_g = 3.98$  eV to 3.69 eV. SEM-EDX data showed that all materials in Co/MS were agglomerated with spherical shape and materials were prepared in good composition. A photodegradation study of MO dye stated that 20wt% Co/MS gave higher degradation efficiency for methyl orange dye as compared to 1-15 wt% Co/MS. From the antibacterial and antifungal study, it is concluded that 20% Co/MS nanocatalyst showed the highest zone of inhibition for both microbial as well as fungal species, and nanocomposite material is suitable for antibiotic applications.

## REFERENCES

- Bian, Z., Cao, F., Zhu, J. and Li, H., 2015. Plant uptake-assisted round-the-clock photocatalysis for complete purification of aquaculture wastewater using sunlight. *Environmental Science & Technology*, 49, pp.2418.
- Buonomenna, M., 2013. Membrane processes for a sustainable industrial growth. *RSC Advances*, 3, pp.5694.
- Chiang, T.H. and Yeh, H.C., 2014. A novel synthesis of  $\beta$ -MoO<sub>3</sub> nanobelts and the characterization. *Journal of Alloys and Compounds*, 585, pp.535–541.
- Dong, W. and Dunn, B., 1998. Sol-gel synthesis of monolithic molybdenum oxide aerogels and xerogels. *Journal of Materials Chemistry*, 8, pp.665–670.
- Fang, G., Wu, Y., Dong, X., Liu, C., He, S. and Wang, S., 2013. Synthesis, characterization, and photocatalytic activity of tungsten oxide nanostructures. *Journal of Agricultural and Food Chemistry*, 61, pp.3834.
- Gita, S., Hussan, A. and Choudhury, T.G., 2017. Impact of textile dyes waste on aquatic environments and its treatment. *Environment & Ecology*, 35(3C), pp.2349-2353.
- Hawkey, P.M., 2008. The growing burden of antimicrobial resistance. *Journal of Antimicrobial Chemotherapy*, 62(Suppl 1), pp.1–9.
- Isik, M. and Sponza, D.T., 2005. Characterization of sulfate-reducing bacteria anaerobic granular sludge and granulometric analysis with grey relation. *Bioresource Technology*, 96, pp.633.
- Jones, N., Ray, B., Ranjit, K.T. and Manna, A.C., 2008. Antibacterial activity of ZnO nanoparticles suspensions on a broad spectrum of microorganisms. *FEMS Microbiology Letters*, 279, pp.71–76.
- Kant, R., 2015. Textile dyeing industry an environmental hazard. *Natural Science*, 4(1), Article ID:17027, pp.5.
- Komolafe, O.O., 2003. Antibiotic resistance in bacteria – an emerging public health problem. *Malawi Medical Journal*, 15, pp.63–67.
- Kou, J., Zhou, X., Lu, H., Wu, F. and Fan, J., 2014. The effect of temperature on water desalination through two-dimensional nanopores. *Nanoscale*, 6, pp.1865.
- Lan, S., Liu, L., Li, R., Leng, Z. and Gan, S., 2014. Preparation of ZnO photocatalyst for the efficient and rapid photocatalytic degradation of azo dyes. *Industrial & Engineering Chemistry Research*, 53, pp.3131.
- Lellis, C., Zani, F. and João, A.P., 2019. Effects of textile dyes on health and the environment and bioremediation potential of living organisms. *Biotechnology Research and Innovation*, 3(2), pp.275-290.
- Lu, J., Zhang, P., Li, A., Su, F., Wang, T., Liu, Y. and Gong, J., 2013. Mesoporous N-doped TiO<sub>2</sub> with enhanced adsorption and visible light photocatalytic activity. *Chemical Communications*, 49, pp.5817.
- Manzoor, J. and Sharma, M., 2020. *Impact Of Textile Dyes on Human Health and Environment*. IGI Global Publishing
- Mills, A., Davies, R. and Worsley, D., 1993. Water purification by semiconductor photocatalysis. *Journal of the Chemical Society, Reviews*, 22, pp.417.
- Muhammad, A., Rahman, A., Zulfiqar, S., Alsafari, I.A. and Shahid, M., 2021. Facile synthesis of binary metal substituted copper oxide as a solar light-driven photocatalyst and antibacterial substitute. *Advanced Powder Technology*, 32, pp.940–950.
- Pandit, V.U., Ambekar, J., Arbuji, S.S. and Rane, S.B., 2015. Synthesis of hierarchical ZnO nanostructure and its photocatalytic performance study. *Journal of Nanoengineering and Nanomanufacturing*, 5, pp.1-5.
- Putatunda, S., Sen, D. and Bhattacharjee, C., 2015. Microbial production of phenol via salicylate decarboxylation. *RSC Advances*, 5, pp.52676.
- Rahman, R., Samanta, D., Pathak, A. and Nath, T.K., 2021. Tuning of structural and optical properties with enhanced catalytic activity in chemically synthesized Co-doped MoS<sub>2</sub> nanosheets. *RSC Advances*, 11, pp.1303.
- Weber, H. and Sciubba, J.D., 2019. The effect of population growth on the environment: evidence from European regions. *European Journal of Population*, 35(2), pp.379–402.
- Zhang, Y., Singh, S. and Bakshi, B., 2010. Accounting for ecosystem services in life cycle assessment, Part I: A critical review. *Environmental Science & Technology*, 44, pp.2232.

## ORCID DETAILS OF THE AUTHORS

S. R. Gadale: <https://orcid.org/0000-0002-2872-505X>





# Potential Low-cost Treatment of Tannery Effluents from Industry by Adsorption on Activated Charcoal Derived from Olive Pomace

I. Alouiz, M. Benhadj, D. Elmouassir, M. Sennoune, M.Y. Amarouch and D. Mazouzi†

R.N.E Laboratory, Multidisciplinary Faculty of Taza, University Sidi Mohamed Ben Abdellah, Fez, Morocco

†Corresponding author: D. Mazouzi; driss.mazouzi@usmba.ac.ma

Nat. Env. & Poll. Tech.  
Website: [www.neptjournal.com](http://www.neptjournal.com)

Received: 28-02-2024

Revised: 26-03-2024

Accepted: 11-04-2024

## Key Words:

Tannery effluent  
Toxicity  
Activated charcoal  
Adsorption  
Treatment  
Chromium

## ABSTRACT

Tannery wastewater contains a significant amount of chemical compounds, including toxic substances. Due to the toxicity and negative environmental effects of these tannery effluents, mandatory treatment is necessary. The main objective of this study was to treat effluent from an artisanal tannery in the city of Fez (Morocco) using the adsorption process with activated charcoal derived from olive pomace. The physicochemical characterization of tanning water included several parameters, such as chemical oxygen demand (COD), total Kjeldahl nitrogen (TKN), suspended solids (SS), sulfate ions ( $\text{SO}_4^{2-}$ ), nitrate, and chromium Cr(VI). The analyses show that the adsorption process reduced nitrate by 57.54%, sulfate by 94.08%, TKN by 74.84%, COD by 68.18%, Cr by 91.27%, and Cr (VI) by 89.78%. The activated charcoal was characterized before and after tannery effluent treatment using various techniques, including FT-IR, SEM, and EDX. From the above, it can be inferred that using activated carbon made from olive pomace has the potential to reduce tannery effluent pollution parameters. This innovative approach demonstrates that competitive results can be achieved without sacrificing economic viability, thereby promoting sustainable practices in the treatment of industrial liquid waste and wastewater treatment plants.

## INTRODUCTION

Environmental pollution is a global issue that is on the rise due to human activities such as urbanization and industrialization (Tadesse et al. 2017, Deghles et al. 2016). Industrial activities disrupt the natural flow of materials and introduce new chemicals into the environment, including bodies of water, soil, plants, vegetables, humans, and other living organisms (Islam et al. 2013, Shaibur et al. 2022). In this sense, water pollution is a significant global issue, primarily caused by the increase in industrialization (Asaduzzaman et al. 2016, Hassan et al. 2020). Indeed, industries produce toxic organic and inorganic substances that lower treatment performance and make reuse impossible (Naushad 2018, Linares-Hernández et al. 2009). Therefore, rational management of water resources become a major challenge worldwide, and wastewater treatment and reuse are considered the best solutions for coping with water scarcity.

Tanneries, or leather manufacturing industries, play a significant role in the economy by generating income and creating jobs. Despite their positive impacts, these industries have a negative image due to the pollution they produce (Elkarrach et al. 2018). In this sense, tanneries are perceived as resource-intensive and polluting. Indeed, during

the process of transforming hides into leather goods, several operations generate a considerable amount of waste (Elmagd et al. 2014). At different stages of processing, liquid and solid pollutants are produced (Patel et al. 2021 & Leta et al. 2003). The extent of pollution caused by tanning depends on the methods used. Chromium tanning is the most commonly used method in modern tanneries worldwide (Onukak et al. 2017, Dargo et al. 2014). It is used to enhance the leather's water resistance, flexibility, and high shrinkage temperature. However, the chromium salts are not entirely fixed by the hides, and 70% of them join the spent tanning liquor (Mella et al. 2015, Cooman et al. 2003). Tannery effluents are also known for their high production of wastewater. Processing one ton of raw hide produces 200 kg of final leather product, along with 250 kg of untanned waste, 200 kg of tanned waste (containing 3 kg of chromium), and 50,000 kg of wastewater (containing 5 kg of chromium) (Mella et al. 2017, Sundar et al. 2022). This means that only 20% of the raw material's weight is converted into leather (Tahiri et al. 2009).

During the tanning process, chromium salts produce hexavalent chromium and trivalent chromium. Hexavalent chromium is a well-known toxic substance that can cause teratogenic, carcinogenic, and mutagenic effects on living organisms, even at low concentrations. This is why many

countries have designated it as a priority contaminant (Elmagd et al. 2014, Harboul et al. 2022, Sandana Mala et al. 2015). Cr (III) is an essential component of human metabolism and homeostasis. It has low mobility and toxicity and is insoluble in water (Shaibur et al. 2022, Chojnacka et al. 2010, Wang et al. 2020). Cr (III) can be oxidized to Cr (VI) under uncontrollable conditions (Popiolski et al. 2022). The removal of Cr (VI) from industrial wastewater is a long-standing scientific and technological problem. The rapid pace of industrialization has led to an expansion in manufacturing and environmental contamination, mainly by heavy metals, particularly in developing countries (Sandhya et al. 2016). Therefore, it is crucial to note that the process of tanning requires a significant amount of water (Popiolski et al. 2022). As a result, the leftover tanned leather and effluent can be categorized as hazardous waste, posing a significant technological and environmental challenge that necessitates proper treatment and disposal in an industrial landfill.

According to recent literature on tannery wastewater treatment, a variety of physical-chemical, biological, and combined treatment processes have been studied for the treatment of these effluents. These processes include chemical precipitation (Sun et al. 2007, Xu et al. 2011), ion exchange (Pakzadeh & Batista 2011), reverse osmosis (Ranganathan et al. 2011), electrodialysis (Deghles et al. 2016), membrane filtration, photocatalysis (Elahi et al. 2020), and adsorption (Pradhan et al. 2017, Tahir et al. 2007), and ultrafiltration, microfiltration, nanofiltration (Kanamrapudi et al. 2018), flotation, coagulation/flocculation (Cheballah et al. 2015, Espinoza-Quiñones et al. 2009), methanation (Mekonnen et al. 2016), the combination of ozone oxidation and membrane bioreactor (Di Iaconi et al. 2002), and the sequential batch reactor (Elkarrach et al. 2020). The performance of each process is highly dependent on the nature of the effluent, the flow rate to be treated, and the treatment objective. Physicochemical treatments are known for their high performance, but they are very expensive and can generate other, more serious pollution. Biological treatments are also effective and ecological, but the presence of toxic substances, such as heavy metals like chromium, is one of their major constraints (Mella et al. 2017). The challenge is to select a treatment process that is environmentally friendly, efficient, and economical while providing sustainable waste management. To this end, the current study aims to find an effective, ecological, and low-cost treatment for tannery effluents.

Therefore, the present study aims to investigate the effectiveness of our recently prepared olive pomace-derived activated charcoal for the treatment of tannery effluents in Fez. The activated charcoal is synthesized by a simple, efficient, and economical process using  $H_3PO_4$

as the activating agent, followed by calcination under the atmosphere at  $500^\circ C$  to develop the porous structure (Alouiz et al. 2022). The analyses indicate that the adsorption process achieved significant reductions in nitrate (57.54%), sulfate (94.08%), TKN (74.84%), COD (68.18%), Cr (91.27%), and Cr (VI) (89.78%). The activated carbon was characterized before and after effluent treatment using various techniques, including FT-IR, SEM, and EDX. This study aims to demonstrate that activated carbon derived from olive pomace can be a sustainable, viable, and environmentally friendly solution for mitigating the adverse consequences and reducing the pollution parameters of tannery effluents.

## MATERIALS AND METHODS

### Synthesis of Activated Charcoal ACp

The preparation of activated charcoal (ACp) from olive pomace (OP) was carried out in two steps: chemical activation of olive pomace followed by calcination of impregnated OP (Fig. 1). Olive pomace was crushed and washed to remove the adhering impurities, then oven-dried at  $100^\circ C$ , followed by chemical activation with  $H_3PO_4$  as the activating agent (22 vol%) for 2h. Finally, the chemically activated OP was heat-treated in the air at temperatures ranging from room temperature to  $500^\circ C$  using a programmable muffle furnace with a calcination time set within 1h, as described by Alouiz et al. (2022). The main physical and chemical properties of the activated carbon are summarized in Table 1.

### Sampling of Tannery Effluent

Tannery effluent samples were collected aseptically from the Ain Nokbi industrial zone in the city of Fez-Morocco (Fig. 1), located at 34.0659915 Lat. North and -4.950160 West-Morocco, in March 2022. Samples were transported to the laboratory in a cool box at  $4^\circ C$ . Sampling and storage were carried out by ISO 5667-2 (Rodier et al. 2009).

### Physico-chemical Characterization of Tannery Effluent

The collected tannery effluent samples were analyzed to

Table 1: The main physical and chemical properties of the ACp adsorbent.

ACp properties	
Moisture [%]	1.71
Ash [%]	4.15
Fixed carbon [%]	87.77
Density [ $g \cdot cm^{-3}$ ]	1.768
Iodine number [ $mg \cdot g^{-1}$ ]	923
SBET [ $m^2 \cdot g^{-1}$ ]	1400
$pH_{pzc}$	8.8



Table 2: Analytical methods for physico-chemical parameters of tannery effluents.

Parameters	Analytical methods and equipment	Unit	Standard
pH	Measured by a multi-parameter (type CONSORT C535, Turnhout, Belgium)	1-12	
EC	Measured by a multi-parameter (type CONSORT C535, Turnhout, Belgium)	$\mu\text{S.cm}^{-1}$	
SS	Filtration of a volume of effluent on a 0.45 $\mu\text{m}$ membrane	$\text{mg.L}^{-1}$	Standard NF T90.105
COD	Acid oxidation by excess potassium dichromate in the presence of ammonium iron sulfate at 148°C	$\text{mg of O}_2.\text{L}^{-1}$	AFNOR T90-101
$\text{SO}_4^{2-}$	Precipitation of sulfates in hydrochloric acid in the form of barium sulfates. Colorimetric determination by spectrophotometry. (Specuvisi UV/VIS Spectrophotometer, n° RE1701008)	$\text{mg.L}^{-1}$	Standard NF T 60-203
$\text{NO}_3^-$	Sodium salicylate. Colorimetric determination by spectrophotometry (Specuvisi UV/VIS Spectrophotometer, n° RE1701008)	$\text{mg.L}^{-1}$	AFNOR T90-012, T90-015
TKN	Measured by mineralization followed by distillation	$\text{mg.L}^{-1}$	AFNOR T90-110
Cr (VI)	DPC colorimetric method, Spectrophotometric assay (Specuvisi UV/VIS Spectrophotometer, No. RE1701008)	$\text{mg.L}^{-1}$	AFNOR NF T 90-043
Metallic elements	Inductively Coupled Plasma Atomic Emission Spectrometer (ICP-AES)	$\text{mg.L}^{-1}$	

determine the intensity and degree of organic and inorganic pollution. Several physicochemical parameters were measured: pH, electrical conductivity (EC), suspended solids (SS), chemical oxygen demand (COD), sulfate ( $\text{SO}_4^{2-}$ ), nitrate ( $\text{NO}_3^-$ ), and Kjeldahl nitrogen (TKN). Concentrations of metallic elements were analyzed by inductively coupled plasma atomic emission spectroscopy (ICP-AES) using Jobin-Yvon-Horriba spectroscopy. Table 2 summarizes the analytical methods and equipment used in these measurements according to the protocols described by Rodier (2009). These parameters were measured before and after treatment of the effluent with activated charcoal ACp derived from olive pomace.

**Description of Tannery Effluent Treatment Protocol**

To evaluate the efficacy of ACp-activated charcoal, 2 g of charcoal was added to 500 mL of tannery effluent contaminated with 50 mg/L Cr (VI). The mixture was stirred at room temperature for up to 48 hours. It was then centrifuged at 6500 rpm for 15 minutes (Fig. 1). The concentration of hexavalent chromium (Cr (VI)) in the filtrate was measured according to AFNOR standard NF T 90-043, using a spectrophotometer colorimetric assay method. Cr (VI) ions were complexed with 1-5 diphenyl carbazide in an acidic medium, forming a complex that could be quantified using a UV-visible spectrophotometer (Specuvisi UV/VIS Spectrophotometer, RE1701008) at a wavelength of 540

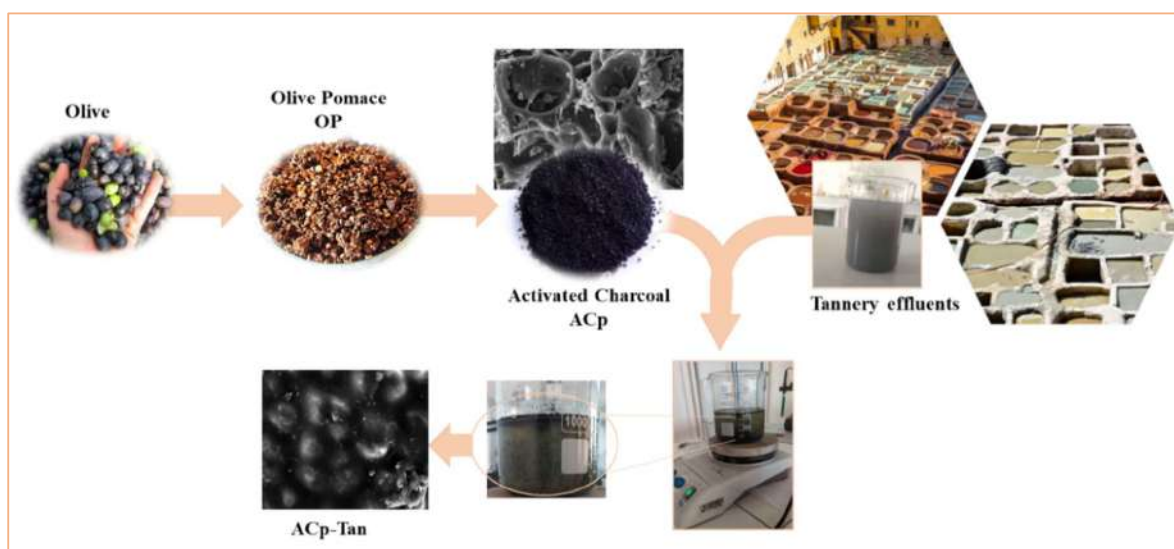


Fig. 1: Set-up of treatment of tannery effluents process.

nm. The removal efficiency of Cr (VI), COD, and TKN by ACp-activated charcoal was calculated from the following equation:

$$R(\%) = \frac{C_i - C}{C_i} \times 100 \quad \dots(1)$$

C<sub>i</sub>: initial Cr (VI) concentration in mg/L

C: after-treatment Cr (VI) concentration in mg/L

## Materials Characterizations

Determination of the functional groups present in the activated charcoal surface before and after Fourier carried out tannery effluent treatment transform infrared spectroscopy (FT-IR), using an FTIR spectrum recorded with a resolution of 1 cm<sup>-1</sup> and 10 scans between 400 and 4000 cm<sup>-1</sup> using an FTR-Vertex 70-Bruker spectrometer. The morphology of the activated charcoal obtained from olive pomace was studied using a JEOL model SEM, JEOL-IT500HR, equipped with an EDX analyzer with an acceleration voltage of 15 kV in high vacuum mode.

## RESULTS AND DISCUSSION

### Characterization of the Adsorbents

#### Scanning electron microscopy SEM and EDX analysis:

The morphological characteristics of the samples were analyzed using the SEM technique. Fig. 2 shows the different morphologies and microscopic appearance of ACp-activated carbon before and after tannery effluent treatment. The surface morphology of ACp before treatment showed a large number of irregular voids and fine open pores (Fig. 2a). The high porosity resulted in a large surface area (Solgi et al. 2017), which was also confirmed by iodine number analysis (greater than 923 mg.g<sup>-1</sup>) and BET specific surface area (greater than 1400 m<sup>2</sup>.g<sup>-1</sup>). Regarding the ACp-Tan sample after the adsorption process and treatment of tannery rejects, the morphology of the carbon surface was significantly modified after the adsorption process due to the precipitation of Cr (VI) on the adsorbent surface (Fig. 2b). The absence of pores on the surface can also be observed, indicating that the Cr adheres to the pore hole and cavity. Consequently, the image of the ACp-Tan surface after treatment indicates the effectiveness of the adsorption process and also confirms the very high values obtained for the de-pollution of tannery effluents. Similar results have been obtained by other researchers using different precursors to show the adsorbent surface modification after chromium adsorption (Benmahdi et al. 2022, Fito et al. 2023). In addition, Fig. 2c.d shows EDX spectra showing that activated carbon is a carbon-enriched material containing about 88.33% carbon. After the wastewater treatment, the carbon content decreased, and

the oxygen content increased, resulting in the appearance of a new Cr peak in the ACp-Tan surface (Fig. 2d). Overall, these results confirm the good treatment of tannery effluents by activated carbon.

**FT-IR spectroscopy:** The surface chemistry of the adsorbent and its effect on the adsorption process is usually studied by Fourier transform infrared spectroscopy (FTIR). The prepared activated carbon had a high carbon content and a low oxygen content. The functional groups on ACp are determined by pHpzc, which was measured at 8.8 (Table 1). However, FTIR analysis provides more information about the nature of these functional groups. The IR spectra of activated carbon before and after treatment of tannery rejects are shown in Fig. 3. The spectra show the shift of some peaks and the appearance of others. The spectrum of activated carbon before ACp treatment (in black) shows the following bands: A band around 1580 cm<sup>-1</sup> attributed to the stretching vibration of the lactone C=O and carbonyl groups by the C=C groups conjugated to the aromatic rings. The band observed between 1100-1180 cm<sup>-1</sup> is generally found with oxidized carbons and has been attributed to C-O stretching in acids or ester groups (Yakout et al. 2016, Ozbay et al. 2016). The bands between 1250 and 1300 cm<sup>-1</sup> may be related to angular deformation in the plane of C-H bonds of aromatic rings.

After treatment, analysis of the FTIR spectrum of ACp-Tan shows changes in the intensity and position of peaks and the appearance of others. A more intense band appears in the region of 3200-3600 cm<sup>-1</sup>, corresponding to O-H (hydroxyl group) stretching vibrations in alcohols, phenols, and carboxylic acids (Solgi et al. 2017). The peak at 2900 cm<sup>-1</sup> has been attributed to asymmetric (C-H) stretching vibrations of the methyl group (Fito et al. 2023, Labied et al. 2018). The peaks at 1615 and 1430 cm<sup>-1</sup> represent the presence of an average stretching vibration C=C and C=O carbonyl group (Abatan et al. 2020). The peak intensity increases from 1000 to 1180 cm<sup>-1</sup>, corresponding to C-O stretching vibrations (Pradhan et al. 2017, Rahman et al. 2017). Finally, the 700-900 cm<sup>-1</sup> peaks became more prominent, attributed to C-H stretching vibrations for out-of-plane aromatic deformations (Shakya et al. 2019, Dhanakumar et al. 2007). The different peaks observed before and after wastewater treatment could be due to the presence of different functional groups. The binding of Cr ions in the activated carbon site could be the reason for the increased peaks in the FT-IR spectrum. The adsorption of Cr-O ions in activated carbon derived from olive pomace indicates that ACp has the potential to interact with other metal elements present in tannery rejects (Fito et al. 2023, Abatan et al. 2020). Similar results have been found in previous studies with biochar based on pine apple peels, rapeseed stalks, and medlar seeds (Solgi et al. 2017, Shakya et al. 2019, Zhao et al. 2018).

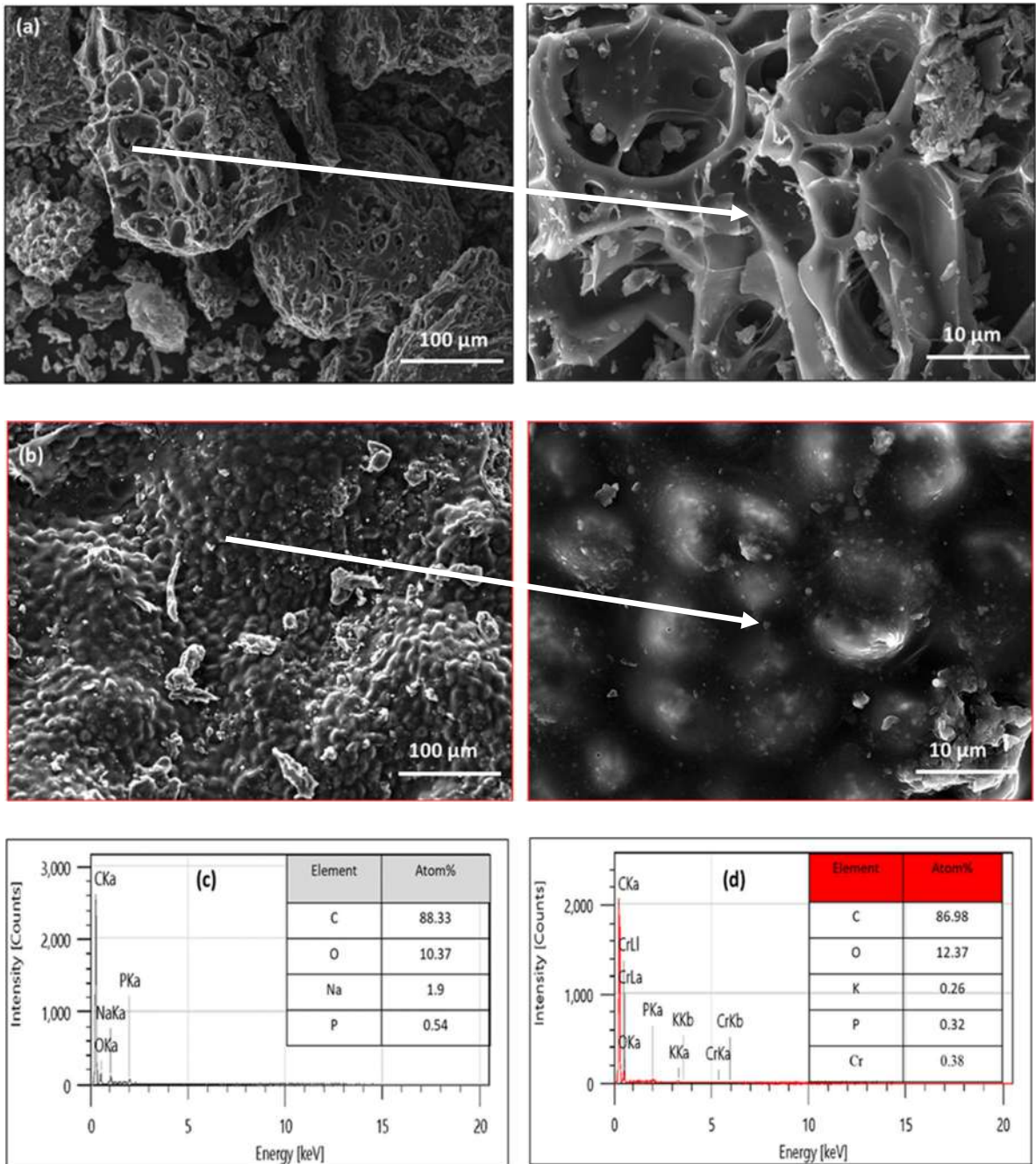


Fig. 2: SEM images of activated charcoal before (a) and after (b) the tannery effluent treatment process, (c) EDX before and (d) EDX after treatment.

**Physico-chemical characterization of tannery effluent:**

To evaluate the physicochemical and metallic quality of the studied tannery effluent, we analyzed the pollution indicator parameters. The results presented in Table 3 show that this effluent is highly polluted and does not meet the Moroccan discharge standard for several parameters, including pH, electrical conductivity, COD, TKN, sulfate ions, suspended solids, chromium, and other metallic elements.

According to Table 3, the pH of this effluent is basic due to the use of sodium carbonate and sodium bicarbonate in the tanning process. These neutralize the sulfides and sulfuric acid used, thus increasing the pH of the effluent. The literature has shown that this parameter is influenced by the type of process used in each tannery. Moreover, the pH value obtained is consistent with that found in other studies by Elkarrach et al. (2021). Other studies, such as those of

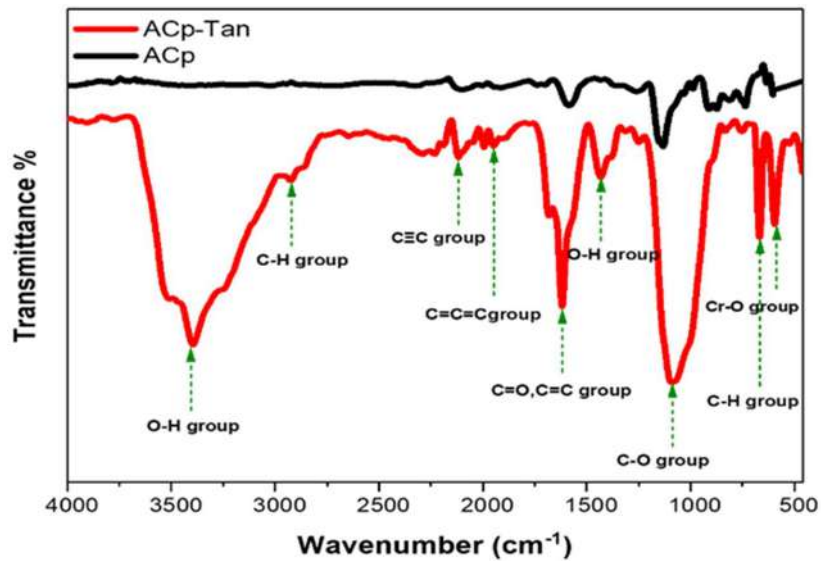


Fig. 3: FT-IR spectrum of activated charcoal before (black-ACp) and after (red-ACp-Tan) the treatment of tannery effluent.

Kurdekar et al. (2015), find a value of  $\text{pH}=2.7$  acid. The electrical conductivity, which reflects the ionic concentration of the medium, is in the order of  $\text{mS/cm}$  for the raw effluent and exceeds the norm with a concentration of about  $11.24 \text{ mS/cm}$ . This high conductivity is mainly due to the natural salt content of the hides and the preservative salts used by the tanners before tanning (Cooman et al. 2003). Research has shown that high conductivity above  $3000 \mu\text{S/cm}$  can upset the ecological balance and inhibit microbial growth (Merimi et al. 2017).

COD, SS, and sulfate ions are also present in very high concentrations, far from the values set by the Moroccan discharge standards, with values around  $14065.92 \text{ mg O}_2\cdot\text{L}^{-1}$ ,  $5280 \text{ mg}\cdot\text{L}^{-1}$  and  $4919.06 \text{ mg/L}$ , respectively. These high concentrations are due to the amount of chemicals used in the tanning process (Leta et al. 2003). TKN is also far from the norm. The TKN concentration is high at  $162.624 \text{ mg}\cdot\text{L}^{-1}$ . This concentration represents the amount of organic and ammoniacal nitrogen present in this tannery effluent. As for the analysis of metallic elements, chromium reached a high concentration of  $127.04 \text{ mg}\cdot\text{L}^{-1}$ ; this high amount was found to be due to the chromium used in the leather manufacturing process (Sundar et al. 2022). The other elements, Al, Fe, and Zn, are present in low concentrations (Table 3). Consequently, the results of the physicochemical characterization of the tannery effluents show that all the parameters analyzed far exceed the discharge standards established in Morocco. This situation is because workers do not use adequate quantities of products and the quality of the hides processed. Chemicals are used excessively to ensure their penetration into the hides (Scholz et al. 2003). Consequently, it is imperative to pre-treat these tannic

effluents before discharging them into the environment to comply with current environmental regulations.

### Performance of the ACp Tannery Effluent Treatment Process

To evaluate the effectiveness of activated charcoal derived

Table 3: Physicochemical characterization before and after treatment of tannery effluent.

Parameters	Values		
	Raw effluent	Treated effluent	Moroccan Standards of Rejects
Color	Dark blue	-	-
pH	8.67	8.91	5.5-9.5
EC [ $\text{mS}\cdot\text{cm}^{-1}$ ]	11.24	5.86	2.7
SS [ $\text{mg}\cdot\text{L}^{-1}$ ]	5280	-	30
$\text{NO}_3^-$ [ $\text{mg}\cdot\text{L}^{-1}$ ]	19.69	8.36	40
$\text{SO}_4^{2-}$ [ $\text{mg}\cdot\text{L}^{-1}$ ]	4919.06	290.81	600
TKN [ $\text{mg}\cdot\text{L}^{-1}$ ]	162.62	41.74	40
COD [ $\text{mg}\cdot\text{L}^{-1}$ ]	14065.92	4479.59	500
Ca [ $\text{mg}\cdot\text{L}^{-1}$ ]	211.08	213.39	-
K [ $\text{mg}\cdot\text{L}^{-1}$ ]	56.514	56.33	-
Mg [ $\text{mg}\cdot\text{L}^{-1}$ ]	171.05	56.53	-
Na [ $\text{mg}\cdot\text{L}^{-1}$ ]	705.72	718.74	-
Zn [ $\text{mg}\cdot\text{L}^{-1}$ ]	0.880	0.924	5
Fe [ $\text{mg}\cdot\text{L}^{-1}$ ]	< 0.01	< 0.01	5
Al [ $\text{mg}\cdot\text{L}^{-1}$ ]	3.13	< 0.01	10
Cr [ $\text{mg}\cdot\text{L}^{-1}$ ]	127.04	11.08	2
Cr (VI) [ $\text{mg}\cdot\text{L}^{-1}$ ]	50	5.11	0.2

from olive pomace for the treatment of tannery effluents, physicochemical analyses were carried out on the raw effluent and after charcoal treatment, as shown in Table 3. The reduction rates were then calculated for each parameter after 48 h of treatment. The results of the physicochemical analyses showed a significant reduction in conductivity from 11.24 to 3.86  $\text{mS}\cdot\text{cm}^{-1}$ . In addition, the reduction rate was about 66%. In terms of pH, a stabilization was observed at 8.91 in the basic medium, which was attributed to the pH<sub>pzc</sub> of the carbon, which is intrinsically basic. This result is in agreement with that obtained by EL Fadel et al. (2013), who attributed the increase in pH to the basicity of the ash used as an adsorbent. The final levels of sulfate and nitrate were less than 290.812 and 8.36  $\text{mg}\cdot\text{L}^{-1}$ , respectively. The treated effluent more than met the Moroccan discharge standards with a sulfate removal efficiency of 94.08%. This removal efficiency is higher than those found by Omor et al., who used the precipitation process (Omor et al. 2017), and Elkarrach et al. (2018), who used a process combining precipitation and a sequential batch reactor to treat tannery effluent. Fig. 4, which illustrates the evolution of COD and TKN over time, shows a decrease in both tannery effluent pollutants during the first 30 h. After this period, COD and TKN concentrations remained constant. COD finally reached a concentration of 4479  $\text{mg}\cdot\text{O}_2\cdot\text{L}^{-1}$  and the treated effluent did not comply with the Moroccan discharge standards. On the other hand, the TKN concentration decreased from 163  $\text{mg}\cdot\text{L}^{-1}$  to 41  $\text{mg}\cdot\text{L}^{-1}$ , giving a reduction rate of 74.84%. This reduction in TKN is also accompanied by a reduction in nitrates. The effluent treatment thus enabled compliance with Moroccan effluent standards. Comparatively, our removal rates exceed those obtained by the activated carbon adsorption process of Kanawade et al. (2014) and are in line with those obtained by Song et al. (2004) on the physicochemical treatment

of tannery effluents by the chemical coagulation process. Thus, it appears that biomass-based activated carbon is very efficient and can replace more costly techniques. The results of metal analysis after treatment with AC<sub>p</sub> are presented in Table 3. Aluminum, iron, and zinc were reduced so that the treated effluent met the Moroccan discharge standards. The evolution and monitoring of hexavalent chromium (Cr (VI)) is shown in Fig. 4. During the treatment, a decrease in Cr (VI) content was observed. This decrease reached up to 5.11  $\text{mg}\cdot\text{L}^{-1}$  after 48 h of tannery effluent treatment.

The efficiency of activated carbon produced from olive pomace for the treatment of tannery effluents and the reduction of pollutant parameters in these effluents are shown in Fig. 5. We can see that the removal rates for nitrate, sulfate, TKN, COD, total Cr, and Cr (VI) were 57.54%, 94.08%, 74.84%, 68.18%, 91.27%, and 89.78%, respectively. These results indicate that activated carbon from olive pomace effectively reduces several pollutant parameters in tannery effluents. This suggests that this treatment method can significantly contribute to the improvement of tannery effluent quality.

#### Comparison of Results with Previous Studies

Table 4 compares the results obtained in our study with the literature, highlighting the remarkable performance of our tannery effluent treatment process using olive pomace-derived activated carbon. Our results show that our activated carbon has a good abatement and reduction rate for tannery effluent pollution parameters such as chemical oxygen demand (COD), TKN, sulfate, nitrate, and hexavalent chromium. What sets our approach apart is the simplicity and effectiveness of our method, which uses only activated carbon derived from olive pomace, a locally available biomass, without the need for complex

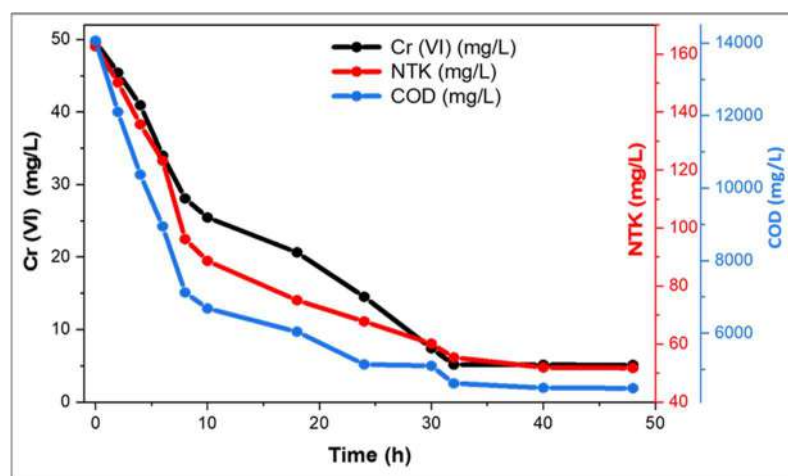


Fig. 4: Evolution of COD, TKN, and Cr (VI) during tannery effluent treatment with AC<sub>p</sub>.

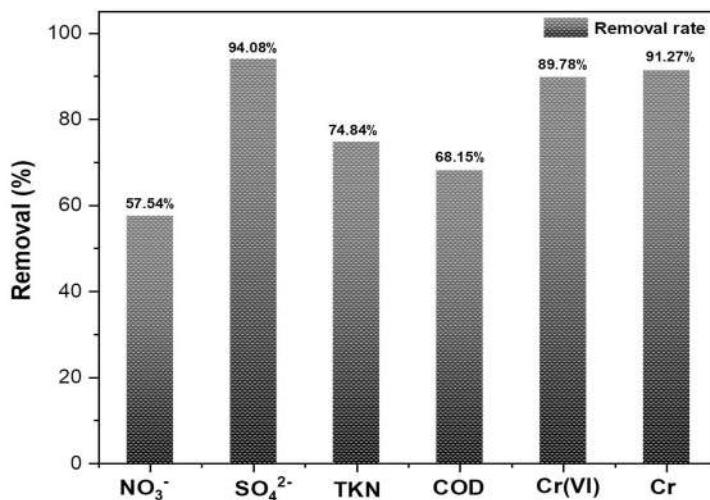


Fig. 5: Activated charcoal abatement rates for different tannery effluent pollution parameters.

Table 4: Comparison of AC<sub>p</sub> results with other previous studies.

EC	SO <sub>4</sub> <sup>-</sup>	TKN	COD	Cr (VI)	Process used	Ref
NR	78	21	49	NR	Membrane filtration	Scholz et al. (2003)
36 %	57%	NR	71%	99.7%	Coagulation and adsorption	Song et al. (2004)
NR	98.5%	66.6%	64.3%	80.7%	Treatment anaerobic and reactor.	Ayoub et al. (2011)
48%	NR	NR	40%	74.4%	Coagulation and adsorption	Kanawade (2014)
82%	99.57%	95.45%	98.17%	96.1%	Precipitation and the sequential batch reactor	Elkarrach et al. (2021)
NR	NR	NR	60.9	99.4%	Chemically enhanced primary treatment	Roš et al. (1998)
66%	94.08%	74.84%	66.18%	89.79 %	Adsorption	present study

NR: not reported

processes or additional costs. Compared to other research studies, some of which are close to our removal rates and others that have achieved better results, it is important to note that these improved performances were often the result of the joint use of two separate processes (Song et al. 2004, Ayoub et al. 2011). This approach, while potentially efficient, is associated with higher processing costs (Scholz et al. 2003), which underscores the economics of our method. The main advantage of our method is its simplicity and accessibility. By focusing solely on the use of activated charcoal derived from olive pomace, we have developed a sustainable and economical solution for the treatment of tannery effluent that meets environmental standards while minimizing the environmental footprint. This innovative approach demonstrates the possibility of achieving competitive results without sacrificing economic viability, thus contributing to the promotion of sustainable practices in the field of industrial liquid effluent treatment.

## CONCLUSIONS

This study highlights the importance of treating tannery effluents through the innovative use of activated carbon derived from olive pomace. The results show that this approach is highly effective in reducing effluent pollution parameters, particularly nitrate, sulfate, TKN, COD, Cr, and hexavalent chromium (Cr (VI)). The effectiveness demonstrated by activated carbon in adsorbing and reducing these pollutants is remarkable, achieving competitive removal rates while highlighting the simplicity and accessibility of this treatment method. The in-depth physico-chemical characterization of the tanning water has allowed us to understand the composition of the effluents, underlining the crucial importance of such a step in the environmental management of industrial waste. In addition, the economic advantage of our method is characterized by the use of an adsorbent derived from locally available biomass. This approach offers a promising perspective for the sustainable management of tannery effluents.

## ACKNOWLEDGEMENT

The work was financially supported by the VGOLIVES Project, the authors would like to thank the support from the Ministry of Energy, Mining, Water and Environment, Morocco. The findings achieved herein are solely the responsibility of the authors.

## REFERENCES

- Abatan, O.G., Alaba, P.A., Oni, B.A., Akpojevwe, K., Efevbokhan, V. and Abnisa, F., 2020. Performance of eggshells powder as an adsorbent for adsorption of hexavalent chromium and cadmium from wastewater. *SN Applied Sciences*, 2, pp.1996.
- Alouiz, I., Amarouch, M.Y. and Mazouzi, D., 2022. Process for the elaboration of porous activated carbon reinforced with a fibrous texture from olive pomace. *Morocco Patent*, 55, p.339.
- Asaduzzaman, M., Hasan, I., Rajia, S., Khan, N. and Kabir, K.A., 2016. Impact of tannery effluents on the aquatic environment of the Buriganga River in Dhaka, Bangladesh. *Toxicology and Industrial Health*, 32(6), pp.1106–1113.
- Ayoub, G.M., Hamzeh, A. and Semerjian, L., 2011. Post treatment of tannery wastewater using lime/bittern coagulation and activated carbon adsorption. *Desalination*, 273(2–3), pp.359–365.
- Benmahdi, F., Khettaf, S. and Kolli, M., 2022. Efficient removal of Cr(VI) from aqueous solution using activated carbon synthesized from silver berry seeds: Modeling and optimization using central composite design. *Biomass Conversion and Biorefinery*, 11, p.545.
- Cheballah, K., Sahmoune, A., Messaoudi, K., Drouiche, N. and Lounici, H., 2011. Utilization of natural materials for the removal of chromium from tannery wastewater. *Desalination and Water Treatment*, 27, pp.1–8.
- Chojnacka, K., 2010. Biosorption and bioaccumulation—the prospects for practical applications. *Environmental International*, 36(3), pp.299–307.
- Cooman, K., Gajardo, M., Nieto, J., Bornhardt, C. and Vidal, G., 2003. Tannery wastewater characterization and toxicity effects on *Daphnia* spp. *Environmental Toxicology*, 18(1), pp.45–51.
- Dargo, H. and Ayalew, A., 2014. Tannery wastewater treatment: A review. *International Journal of Emerging Trends in Science and Technology*, 1(9), pp.1488–1494.
- Deghles, A. and Kurt, U., 2016. Treatment of tannery wastewater by a hybrid electrocoagulation/electrodialysis process. *Chemical Engineering & Processing: Process Intensification*, 104, pp.43–50.
- Dhanakumar, S., Salaraj, G., Mohanraj, R. and Pattabhi, S., 2007. Removal of Cr (VI) from aqueous solution by adsorption using cooked tea dust. *Indian Journal of Science and Technology*, 1(2), pp.1–6.
- Di Iaconi, C., Lopez, A., Ramadori, R., Di Pinto, A.C. and Passino, R., 2002. Combined chemical and biological degradation of tannery wastewater by a periodic submerged filter (SBBR). *Water Research*, 36(9), pp.2205–2214.
- El Fadel, H., Merzouki, M., Faouzi, M., Laamayem, A., Najem, M. and Benlemlih, M., 2013. Purification performance of filtration process for leachate in Morocco by marine sands, clays, and fly ash. *Journal of Biotechnology Letters*, 4(1), pp.51–59.
- Elahi, A., Arooj, I., Bukhari, D.A. and Rehman, A., 2020. Successive use of microorganisms to remove chromium from wastewater. *Applied Microbiology and Biotechnology*, 104(9), pp.3729–3743.
- Elkarrach, K., Merzouki, M., Laidi, O., Biyada, S., Omor, A. and Benlemlih, M., 2020. Sequencing batch reactor: Inexpensive and efficient treatment for tannery effluents of Fez city in Morocco. *Desalination and Water Treatment*, 202, pp.71–77.
- Elkarrach, K., Merzouki, M., Laidi, O., Omor, A. and Benlemlih, M., 2018. Treatment of tannery effluents of Fez City by the sequential batch reactor. *European Journal of Scientific Research*, 150(3), pp.334–348.
- Elkarrach, K., Merzouki, M., Laidi, O., Omor, A., Biyada, S. and Benlemlih, M., 2021. Combination of chemical and biological processes for the treatment of tannery effluent of Fez city in Morocco. *Desalination and Water Treatment*, 220(12), pp.109–115.
- Elmagd, A.M.A. and Mahmoud, M.S., 2014. Tannery wastewater treatment using activated sludge process system (Lab scale modeling). *International Journal of Engineering Technology Research*, 2(5), pp.21–28.
- Espinoza-Quñones, F.R., Fornari, M.M.T., Módenes, A.N., Palácio, S. M., da Silva, F.G., Szymanski, N., Kroumov, A.D. and Trigueros, D.E.G., 2009. Pollutant removal from tannery effluent by electrocoagulation. *Chemical Engineering Journal*, 151(1–3), pp.59–65.
- Fito, J., Tibebe, S. and Nkambule, T.T.I., 2023. Optimization of Cr (VI) removal from aqueous solution with activated carbon derived from *Eichhornia crassipes* under response surface methodology. *BMC Chemistry*, 17(1), pp.1–20.
- Harboul, K., Alouiz, I., Hammani, J. and El-Karkouri, A., 2022. Isotherm and kinetics modeling of biosorption and bioreduction of Cr(VI) by *Brachybacterium paraconglomeratum* ER41. *Extremophiles*, 26(3), pp.30.
- Hassan, E.S.R.E., Rostom, M., Farghaly, F.E. and Abdel Khalek, M.A., 2020. Bio-sorption for tannery effluent treatment using eggshell wastes, kinetics, isotherm, and thermodynamic study. *Egyptian Journal of Petroleum*, 29(4), pp.273–278.
- Islam, S., Islam, F., Bakar, M.A., Das, S. and Bhuiyan, H.R., 2013. Heavy metals concentration at different tannery wastewater canals of Chittagong city in Bangladesh. *International Journal of Agriculture and Environmental Biotechnology*, 6(3), pp.355.
- Kanamarlupudi, S., Chintalupudi, V.K. and Muddada, S., 2018. Application of biosorption for the removal of heavy metals from wastewater. *Biosorption*, 18(69), pp.70–116.
- Kanawade, S.M., 2014. Treatment of dye industrial wastewater by using adsorption. *International Journal of Chemical and Material Sciences*, 2(3), pp.059–067.
- Kurdekar, P. and Shivayogimath, C., 2015. Treatment of tannery effluent using electrocoagulation. *International Journal of Innovative Research in Science, Engineering and Technology*, 4(7), pp.6554–6560.
- Labied, R., Benturki, O. and Hamitouche, A.Y.E., Donnot, A., 2018. Adsorption of hexavalent chromium by activated carbon obtained from a waste lignocellulosic material (*Ziziphus jujuba* cores): Kinetic, equilibrium, and thermodynamic study. *Adsorption Science & Technology*, 36(3–4), pp.1066–1099.
- Leta, S., Assefa, F. and Dalhammar, G., 2003. Characterization of tannery wastewater and assessment of downstream pollution profiles along Modjo River in Ethiopia. *Ethiopian Journal of Biological Sciences*, 2(2), pp.157–168.
- Linares-Hernández, I., Barrera-Díaz, C., Roa-Morales, G., Bilyeu, B. and Ureña-Núñez, F., 2009. Influence of the anodic material on electrocoagulation performance. *Chemical Engineering Journal*, 148(1), pp.97–105.
- Mekonnen, A., Leta, S. and Njau, K.N., 2016. Co-digestion of tannery wastewater and *Phragmites karka* using a laboratory scale anaerobic sequencing batch reactor. *Modern Applied Science*, 9(1), pp.9–14, doi: 10.7537/marsnys09011602.
- Mella, B., Glanert, A. C. and Gutterres, M., 2015. Removal of chromium from tanning wastewater and its reuse. *Proceedings of the Institution of Mechanical Engineers, Part B: Journal of Engineering Manufacture*, 95, pp.195–201.
- Mella, B., Puchana-Rosero, M.J., Costa, D.E.S. and Gutterres, M., 2017. Utilization of tannery solid waste as an alternative biosorbent for acid dyes in wastewater treatment. *Journal of Molecular Liquids*, 242, pp.137–145.
- Merimi, I., Oudda, H. and Hammouti, B., 2017. Characterization of the quality of the polluting load of an industrial zone. *Journal of Chemical and Pharmaceutical Research*, 9(4), pp.165–170.

- Naushad, M., 2018. A new generation material graphene: Applications in water technology. *Springer International Publishing*.
- Omor, A., Rais, Z., El Rhazi, K., Merzouki, M., El Karrach, K., Elallaoui, N. and Taleb, M., 2017. Optimization of the method wastewater treatment of unit bovine hides' unhairing liming. *Journal of Materials and Environmental Science*, 8(4), pp.1235–1246.
- Onukak, I.E., Mohammed-Dabo, I.A., Ameh, A.O., Okoduwa, S.I.R. and Fasanya, O.O., 2017. Production and characterization of biomass briquettes from tannery solid waste. *Recycling*, 2, pp.17.
- Ozbay, N. and Yargic, A.S., 2016. Comparison of surface and structural properties of carbonaceous materials prepared by chemical activation of tomato paste waste: The effects of activator type and impregnation ratio. *Journal of Applied Chemistry*, 16(3), pp.1–10.
- Pakzadeh, B. and Batista, J.R., 2011. Chromium removal from ion-exchange waste brines with calcium polysulfide. *Water Research*, 45, pp.3055–3064.
- Patel, N., Shahane, S., Chauhan, D., Rai, D., Khan, Z.A. and Bhunia, M.B., 2021. Environmental impact and treatment of tannery waste. *Water Pollution and Remediation: Organic Pollutants*, 54, pp.577–592.
- Popiolski, A.S., Demaman Oro, C.E., Dallago, R.M., Steffens, J., Bizzi, C.A., Santos, D., Alessio, K.O., Flores, E.M. and Duarte, F. A., 2022. Microwave-assisted extraction of Cr from residual tanned leather: A promising alternative for waste treatment from tannery industry. *Journal of Environmental Chemical Engineering*, 10(1), pp.6–11.
- Pradhan, D., Sukla, L.B., Sawyer, M. and Rahman, P.K.S.M., 2017. Recent bioreduction of hexavalent chromium in wastewater treatment: A review. *Journal of Industrial and Engineering Chemistry*, 55, pp.1–20.
- Rahman, M.W., Ali, M.Y., Saha, I., Al Raihan, M., Moniruzzaman, M., Alam, M.J. and Deb, A., Khan, M.M.R., 2017. Date palm fiber as a potential low-cost adsorbent to uptake chromium (VI) from industrial wastewater. *Desalination and Water Treatment*, 88(11), pp.169–178.
- Ranganathan, K. and Kabadgi, S.D., 2011. Studies on the feasibility of reverse osmosis (membrane) technology for treatment of tannery wastewater. *Journal of Environmental Protection (Irvine, Calif.)*, 2(1), pp.37–46.
- Rodier, J., 2009. *Analysis of Water – Fresh Water, Wastewater, Seawater*. Dunod, pp.1475.
- Roš, M. and Gantar, A., 1998. Possibilities of reduction of recipient loading of tannery wastewater in Slovenia. *Water Science and Technology*, 37(8), pp.45–52.
- Sandana Mala, J. G., Sujatha, D. and Rose, C., 2015. Inducible chromate reductase exhibiting extracellular activity in *Bacillus methylotrophicus* for chromium bioremediation. *Microbiological Research*, 170, pp.235–241.
- Sandhya, M. and Bharagava, R.N., 2016. Toxic and genotoxic effects of hexavalent chromium in the environment and its bioremediation strategies. *Journal of Environmental Science and Health, Part C*, 34(1), pp.1–32.
- Scholz, W. and Lucas, M., 2003. Techno-economic evaluation of membrane filtration for the recovery and re-use of tanning chemicals. *Water Research*, 37(8), pp.1859–1867.
- Shaibur, M.R., Tanzia, F.K.S., Nishi, S., Nahar, N., Parvin, S. and Adjadeh, T.A., 2022. Removal of Cr (VI) and Cu (II) from tannery effluent with water hyacinth and arum shoot powders: A study from Jashore, Bangladesh. *Journal of Hazardous Materials Advances*, 7(2), pp.100102.
- Shakya, A. and Agarwal, T., 2019. Removal of Cr(VI) from water using pineapple peel derived biochars: Adsorption potential and re-usability assessment. *Journal of Molecular Liquids*, 293, pp.111497.
- Solgi, M., Najib, T., Ahmadnejad, S. and Nasernejad, B., 2017. Synthesis and characterization of novel activated carbon from Medlar seed for chromium removal: Experimental analysis and modeling with artificial neural network and support vector regression. *Resources Technology*, 3(3), pp.236–248.
- Song, Z., Williams, C.J. and Edyvean, R.G.J., 2004. Treatment of tannery wastewater by chemical coagulation. *Desalination*, 164(3), pp.249–259.
- Sun, J.M., Chang, S.Y., Li, R. and Huang, J.C., 2007. Factors affecting co-removal of chromium through copper precipitation. *Separation and Purification Technology*, 56(1), pp.57–62.
- Sundar, V.J., Rao, J.R. and Muralidharan, C., 2022. Cleaner chrome tanning emerging options. *Journal of Cleaner Production*, 10, pp.69–74.
- Tadesse, G.L. and Kasa, T.G., 2017. Impacts of tannery effluent on environments and human health. *Journal of Environmental and Earth Sciences*, 7(3), pp.88–97.
- Tahir, S.S. and Naseem, R., 2007. Removal of Cr(III) from tannery wastewater by adsorption onto bentonite clay. *Separation and Purification Technology*, 53(3), pp.312–321.
- Tahiri, S. and Miguel, D., 2009. Treatment and valorization of leather industry solid wastes: A review. *Journal of the American Leather Chemists Association*, 104(2), pp.52–67.
- Wang, Q., Zhou, C., Kuang, Y.J., Jiang, Z.H. and Yang, M., 2020. Removal of hexavalent chromium in aquatic solutions by pomelo peel. *Water Science and Engineering*, 13(1), pp.65–73.
- Xu, X., Gao, B. Y., Tan, X., Yue, Q.Y., Zhong, Q. and Li, Q., 2011. Characteristics of amine-crosslinked wheat straw and its adsorption mechanisms for phosphate and chromium (VI) removal from aqueous solution. *Carbohydrate Polymers*, 84(3), pp.1054–1060.
- Yakout, S.M. and Sharaf El-Deen, G., 2016. Characterization of activated carbon prepared by phosphoric acid activation of olive stones. *Arabian Journal of Chemistry*, 9, pp.S1155–S1162.
- Zhao, B., O'Connor, D., Zhang, J., Peng, T., Shen, Z., Tsang, D.C.W. and Hou, D., 2018. Effect of pyrolysis temperature, heating rate, and residence time on rapeseed stem derived biochar. *Journal of Cleaner Production*, 174, pp.977–987.





# Contribution of Organic Carbon, Moisture Content, Microbial Biomass-Carbon, and Basal Soil Respiration Affecting Microbial Population in Chronosequence Manganese Mine Spoil

S. Dash and M. Kujur

Department of Biotechnology, Gangadhar Meher University, Sambalpur, Odisha, 768001, India

†Corresponding author: M. Kujur; mkujur@gmuniversity.ac.in

Nat. Env. & Poll. Tech.

Website: [www.neptjournal.com](http://www.neptjournal.com)

Received: 29-02-2024

Revised: 20-04-2024

Accepted: 29-04-2024

## Key Words:

Microbial population

Chronosequence

Organic carbon

Microbial metabolic quotients

Microbial biomass carbon

## ABSTRACT

The research was carried out to determine the potential effect of microbiota, organic carbon, percentage of moisture content, and microbial biomass concentration as an evaluator of variation in basal soil respiration rate. Relative distribution and composition of the microbial population were estimated from six different chronosequence manganese mine spoil (MBO0, MBO2, MBO4, MBO6, MBO8, MBO10) and forest soil (FS). The variation was seen in moisture content ( $6.494 \pm 0.210$ - $11.535 \pm 0.072$ )%, organic carbon ( $0.126 \pm 0.001$ - $3.469 \pm 0.099$ )%, MB-C ( $5.519 \pm 1.371$ - $646.969 \pm 11.428$ )  $\mu\text{g}\cdot\text{g}^{-1}$  of soil. A positive correlation was shown between OC with MB-C ( $r = 0.938$ ;  $p < 0.01$ ) and moisture content (MC) ( $r = 0.962$ ;  $p < 0.01$ ). Variation in the basal soil respiration (BSR) and microbial metabolic quotients (MMQ) was shown to range between  $0.352 \pm 0.007$ - $0.958 \pm 0.014$   $\mu\text{g CO}_2\cdot\text{C}\cdot\text{g}^{-1}$  and  $6.5 \times 10^{-3}$  -  $1.481 \times 10^{-3}$   $\mu\text{g CO}_2\cdot\text{C}\cdot\text{g}^{-1}$  microbial-C $\cdot\text{h}^{-1}$  with BSR: OC from (2.793-0.276)% respectively. This result shows that there is a gradual increase in OC, MC, MB-C, and BSR across seven different sites due to progressive enhancement in soil fertility that leads to the initialization of succession. Stepwise multiple regression analysis further confirms the degree of variability added by microbial biomass C, moisture content, organic carbon, and microbial population on basal soil respiration in microbes. Principal component analysis enables the differentiation of seven different soil profiles into independent clusters based on cumulative variance given by physico-chemical and microbial attributes that indicate the level of degradation of land and act as an index to restore soil fertility.

## INTRODUCTION

The soil is a composite, highly porous, and dynamic form of earth components that bears metabolically active microorganisms from major kingdoms of life. In the current decades, the diversified microbiota of soil plays an essential role in many biological interactions that may be crucial for the cycling of organic carbon, nitrogen, and phosphorus and introduced soil as a multifunctional system that does lots of functions at the same time (Kopittke et al. 2022, Evangelista et al. 2023) Emancipation and assimilation of nutrients from biomass is readily absorbed by growing plants (Sivaranjani & Panwar 2023) and in this regards the microbial biomass reflects as both source and sink of nutrients (Smith et al. 1986).

Respiration in the ecosystem provides energy that is primarily contributed by different functional elements of the ecosystem. Soil carbon is released to the atmosphere through respiration by activities of heterotrophic organisms present in the soil that regulates  $\text{CO}_2$  level in the environment (Sáez-

Sandino et al. 2023). Besides, microbial respiration is the ultimate measure of microbial activity, and its contribution to the process of soil genesis in degraded land generally complies with the determination of microbial biomass but is somehow more variable. Respiration in terms of microbial biomass (i.e., respiration occurs per unit microbial biomass) commonly decreases with respect to increasing microbial biomass (Helingerova et al. 2010), as has been observed from overburdened mine spoil along with all soil types (Santruckova & Straskraba 1991). Thus, with increasing microbial biomass, respiration might stagnate (Helingerova et al. 2010). Microbial respiration can be directly measured by conducting field experiments in soil or from soil taken into the lab for in-vitro analysis. The respiration at the ecosystem level must depend on both environmental and biological components such as structural constituents, microbial action in soil, qualitative and quantitative measurement of organic carbon, available moisture content, and nutrients (Amundson 2001). Besides, MB-C and basal soil respiration are also used to analyze the changes in microbial community

distribution and action among different overburdened mine spoil.

The areas after mining activities serve as an admissible opportunity to explore the study of soil microbial community development during the processes of pedogenesis. Microorganisms first colonized excavated soil and these microbes undergo significant changes in successional pattern during the process of soil formation. Microbial community configurations in soil play a primary role in the organization of nutrient cycles as well as the transfiguration of organic matter and regulate soil habitat by catalyzing numerous biochemical and biophysical reactions (Philipot et al. 2024). Physico-chemical and biological attributes of soil are affected by the activity and interaction of microorganisms (Tangjang & Arunachalam 2009), and community dynamics of microbes are also transformed by land utilization patterns and the availability of minerals in soil that measure the existence of microbial community by providing nutrients for growth and habitats to live (Kourtev et al. 2003). Further, the accessibility of microbes in different overburden spoil is largely influenced by variations in the concentration of organic carbon, which has a direct correlation with nitrogen cycling (Griffiths et al. 2012).

The rate of respiration in different microbial populations has been measured in various ecosystems to assess microbial interactions in soil, nutrient turnover and cycling of carbon and another organic solute. This metabolic process is also helpful in analyzing the soil contaminated with heavy metals because microbes are highly sensitive to heavy metal concentrations above critical levels (Kubat et al. 1999). Besides, the factors that possess a major impact on respiration include physical-chemical and biochemical ease of access to the substrate by microbes (Davidson et al. 2006), availability of water and diffusion of a substrate (Davidson & Janssens 2006), dynamics of microbial communities (Monson et al. 2006). Additionally, soil moisture is recognized as one of the efficacious environmental factors regulating soil respiration (Xu & Qi 2001).

As responsive indicators of the restoration process, mine spoil genesis converges on the gradual shifting of the composition of microbial population and inter and intra-specific relationships (Harris 2003). Though the restoration of mine spoil is a relatively longer process, it is necessary to traverse the shifting of microbial community distribution using highly responsive soil quality biomarkers.

Thus, a comprehensive study of microbial respiration rates in various mine spoil and the factors majorly affecting the respiration rate in microbes give further knowledge about the understanding of microbial distribution. Based on the above information, the current investigation was

formulated to examine the relative abundance, composition, and action of microbial communities in different manganese overburden spoil collected in a chronosequence manner (fresh mine spoil: FMS; 2-year dump: MBO2; 4-year dump: MBO 4; 6-year dump: MBO 6; 8-year dump: MBO8; 10-year dump: MBO10; Forest soil: FS) across the sites.

## MATERIALS AND METHODS

### Study Site

The study was carried out at Kanther Manganese mines, Koira, Sundargarh, Odisha (geographical location: between 85A°20'09.67" east longitude and 21°53'45.34" north latitude) maintained by Rangta mine PVT Ltd. Out of the total geographical area about 73,653 ha area 14,796 ha are the mineralized area of Koira.

### Sampling

Sampling was done by following the soil microbiological methods of Parkinson et al. 1971. For sampling, each over-dump site was divided into 5 blocks, and five soil samples were collected randomly from 0-15 cm soil depth by spading pits of (15 x 15 x 15) cm<sup>3</sup> size in each block and referred to as sub-samples, forming composite sample by mixing thoroughly. These samples were obtained from each site in January for analysis and subjected to sieving (2 mm mesh size) for further characterization.

### Moisture Content (MC)

The moisture content from seven different soil profiles was estimated by the methods proposed by Mishra 1968. A freshly collected soil sample of about 10g (W1) was taken and kept oven-dried at 105°C for 24 h up to a constant dry weight (W2) was achieved.

$$\text{Soil moisture (\%)} = [(W1 - W2)/10] \times 100$$

### Organic Carbon Content (OC)

A partial oxidation method was used to determine soil organic carbon (Walkly & Black 1934).

### Microbial Biomass-C (MB-C)

For stability of respiration and further analysis, freshly collected soil samples were stored at (28 ± 2)°C. The fumigation extraction method was used to determine microbial biomass carbon from seven different soil samples by using the methods of Vance et al. (1987).

### Basal Soil Respiration (BSR)

Methods of Witkamp (1966) followed by Ohya et al. (1988) are used to calculate basal soil respiration, measured by

calculating the concentration of CO<sub>2</sub> released from the soil through the alkali absorption technique.

### Microbial Metabolic Quotient

Microbial metabolic quotient (CO<sub>2</sub>-C.g<sup>-1</sup> microbial carbon.h<sup>-1</sup>) is defined as the amount of CO<sub>2</sub>-C respired per unit MB-C per unit time, and the calculation was done from the ratio of the mean value of MB-C and basal soil respiration (BSR) from seven different overburden spoils.

### Enumeration of Microbes

Relative distribution of microbes in soil was performed using serial dilution techniques. Colonies were isolated using selective media by standard spread plate dilution technique. Relative distribution of *Azotobacter* populations (AZB) was analyzed using *Azotobacter* mannitol agar media and kept for incubation in 48 h incubated for 48 h at 25-30°C (ATCC 1992). *Arthrobacter* (ARB) isolating media was used to isolate the *Arthrobacter* population (Hagedorn & Holt 1975). Yeast extract mannitol agar (Vincent 1970) was used for rhizobial count (RZB) containing Congo red dye to differentiate them from other bacteria from seven different soil samples. Sulphur-reducing bacteria (SRB) population counted by using medium (Hi-Media); (Eaton et al. 2005). Enumeration of actinomycetes populations (ACM) was done using (CSA) starch-casein agar (Hunter-Cevera & Eveleigh 1990). The fungal population (FUN) was enumerated using rose Bengal agar media supplemented with streptomycin (50 µL.mL<sup>-1</sup>) to inhibit bacterial contaminants (Alef & Nannipieri 1995). Yeast count (YES) was determined using potato sucrose agar [500 mL potato extract; 20 g.L<sup>-1</sup> sucrose; 1mL trace metal solution; 500 mL distilled water; pH 6.7] (Krishna et al. 2001).

### Statistical Analysis

To examine the test of significance among different physico-chemical parameters like OC, MC MB-C with BSR, and

microbial populations from different chronosequence mine spoil, a simple correlation analysis was performed using SPSS (Version 16.0). To quantify the role and contribution of microbial populations towards variability in BSR, stepwise multiple regression analysis was performed using STATA 15X-64 software. The principal component analysis (PCA) was performed to summarize the large data tables collected from the above calculations using Past 4.06 software.

## RESULTS AND DISCUSSION

### Estimation of MC, OC, MB-C and BSR

In the current investigation, moisture content was estimated from seven different soil samples that resulted in an increasing pattern from fresh mine spoil (MBO 0; 6.494±0.210) to native forest soil (FS; 11.535±0.072). Organic carbon was estimated from overburden dump soil freshly collected, and the percentage of organic carbon increased from MBO (0.126±0.001) to native forest soil (3.469±0.099). The same increasing pattern was followed in the case of an amount of microbial biomass carbon (MB-C). The rate of basal soil respiration was estimated from seven chronosequence manganese mine spoil and represented in Table 1 along with other attributes which were increasing from fresh mine spoil (MBO0, 0.352 ± 0.007 µg CO<sub>2</sub>-C.g<sup>-1</sup> soil.h<sup>-1</sup>) to relatively higher in ten-year dump soil (MBO10, 0.921 ± 0.012 µg CO<sub>2</sub>-C.g<sup>-1</sup> soil.h<sup>-1</sup>) and further increasing in case of FS (0.958 ± 0.014 µgCO<sub>2</sub>-C.g<sup>-1</sup> soil.h<sup>-1</sup>).

### Enumeration of Microbes

In the current study, enumeration of microbial communities and their relative availability was denoted in terms of colony-forming unit (CFU.g<sup>-1</sup> soil) (Table 2). The variations that occur in terms of their relative abundance of microbiota among seven different chronosequence manganese mine spoil were shown in terms of log<sub>10</sub> transformed of CFU.g<sup>-1</sup> soil (Table 2). The current study specified the increasing pattern of *Azotobacter* count (AZB) from fresh mine spoil

Table 1: Table showing moisture content, organic carbon content, microbial biomass -C and BSR in chronosequence manganese mine spoil.

Soil types	MC %	OC%	MB-C [µg.g <sup>-1</sup> soil]	BSR [µ g CO <sub>2</sub> -C.g <sup>-1</sup> soil.h <sup>-1</sup> ]
MBO0	6.494±0.210	0.126±0.001	5.519±1.371	0.352 ± 0.007
MBO2	7.496±0.127	0.312±0.013	124.911±2.587	0.392 ± 0.011
MBO4	7.72±0.101	0.626±0.1	244.401±5.392	0.594 ± 0.016
MBO6	8.819±0.129	1.247± 0.031	431.163±8.378	0.842 ± 0.013
MBO8	9.928± 0.8	1.687± 0.0431	498.359± 13.126	0.914 ± 0.015
MBO10	10.72±0.18	2.048±0.083	540.942± 6.025	0.921 ± 0.012
FS	11.535±0.072	3.469± 0.099	646.969± 11.428	0.958 ± 0.014

± denotes the standard deviation

Table 2: Relative distribution of microbial community and their abundance among seven different manganese mine spoil.

Microbial populations	CFU.g <sup>-1</sup> dry wt. soil in (0-15) cm soil depth						
	MBO 0	MBO 2	MBO 4	MBO 6	MBO 8	MBO 10	FS
Azotobacter	12×10 <sup>-1</sup>	29×10 <sup>-1</sup>	26.0×10 <sup>-2</sup>	52×10 <sup>-3</sup>	46.2×10 <sup>-4</sup>	58.2×10 <sup>-4</sup>	61×10 <sup>-4</sup>
Arthrobacter	25×10 <sup>-2</sup>	29×10 <sup>-2</sup>	79×10 <sup>-2</sup>	10.2×10 <sup>-3</sup>	21.5×10 <sup>-4</sup>	31.2×10 <sup>-4</sup>	36.5×10 <sup>-4</sup>
Rhizobia	28×10 <sup>-1</sup>	39×10 <sup>-1</sup>	51×10 <sup>-2</sup>	8.6×10 <sup>-3</sup>	13.3×10 <sup>-4</sup>	17.8×10 <sup>-4</sup>	20.8×10 <sup>-4</sup>
Heterotrophic Aerobes	28×10 <sup>-2</sup>	58×10 <sup>-2</sup>	85×10 <sup>-4</sup>	98×10 <sup>-6</sup>	17.1×10 <sup>-8</sup>	21.5×10 <sup>-8</sup>	24.2×10 <sup>-8</sup>
Sulfur reducing bacteria	30.4 ×10 <sup>-3</sup>	34×10 <sup>-3</sup>	7.9×10 <sup>-2</sup>	66×10 <sup>-1</sup>	46×10 <sup>-1</sup>	15.6×10 <sup>-1</sup>	0.8×10 <sup>-1</sup>
Actinomycetes	6×10 <sup>-2</sup>	15×10 <sup>-2</sup>	29×10 <sup>-2</sup>	12.8×10 <sup>-3</sup>	36×10 <sup>-3</sup>	42×10 <sup>-3</sup>	55×10 <sup>-3</sup>
Yeast	7×10 <sup>-1</sup>	16×10 <sup>-1</sup>	10×10 <sup>-2</sup>	23×10 <sup>-2</sup>	43×10 <sup>-2</sup>	67×10 <sup>-2</sup>	85×10 <sup>-3</sup>
Fungi	9×10 <sup>-1</sup>	13×10 <sup>-2</sup>	19×10 <sup>-2</sup>	25×10 <sup>-2</sup>	11.5×10 <sup>-3</sup>	23×10 <sup>-3</sup>	45×10 <sup>-3</sup>

(FMS) (MBO 0: 12×10<sup>-1</sup>) to forest soil (FS) (61×10<sup>-4</sup>) (Table 2). From FMS (12×10<sup>-1</sup>) *Azotobacter* colony showed an effective increment (MBO6, 52×10<sup>-3</sup>), and then further the pattern continued up to MBO10(58.2×10<sup>-4</sup>). In the case of relative availability of *Arthrobacter* (ARB), the count increased from fresh mine spoil (MBO0, 25×10<sup>-2</sup>) to native forest soil (FS, 36.5×10<sup>-4</sup>) at an increasing rate. Further, the rhizobial count (RZB) followed a similar trend with significant variation from 28×10<sup>-1</sup> (FMS) to 20.8×10<sup>-4</sup> (FS). The population of heterotrophic aerobes (HAB) increases from FMS 28×10<sup>-2</sup> to MBO 10(21.5×10<sup>-8</sup>) at an increasing rate as compared to FS (24.2×10<sup>-8</sup>). The highest sulfur-reducing bacterial count (SRB) was found in MBO0 (30.4 ×10<sup>-3</sup>) and decreased towards MBO 10 (15.6×10<sup>-1</sup>) and the population was found less in FS (0.8×10<sup>-1</sup>). Further, actinomycetes count (AMC) varies from 6×10<sup>-2</sup> (FMS) to 55×10<sup>-3</sup> (FS). Relative distribution of yeast (YES) count showed progressive increment from fresh mine spoil(7×10<sup>-1</sup>) to ten-year dump soil MBO 10 (67×10<sup>-2</sup>) and highest at forest soil FS (85×10<sup>-3</sup>). Fungal count was found to be higher in the case of ten-year dump soil MBO10 (23×10<sup>-3</sup>) as compared to fresh mine spoil MBO0 (9×10<sup>-1</sup>) favors a suitable environment for microbial growth and action (Table 2).

## Discussion

Basal soil respiration depicts the availability of steady and slow-flowing carbon for nurturing microbial populations and determines the basic turnover rate in soil. BSR from different manganese overburden dump soil has shown significant variation from fresh mine spoil (MBO0) to natural forest soil (FS) ranging from 0.352 ± 0.007 µg CO<sub>2</sub>-C.g<sup>-1</sup> soil.h<sup>-1</sup> to 0.958 ± 0.014 µg CO<sub>2</sub>-C.g<sup>-1</sup> soil.h<sup>-1</sup>. The rate of basal soil respiration is slow in microbes present in fresh mine spoil, substantiates the minimum turnover rate of microbes, which may be due to low accessibility nutrients present in the soil for the growth of microbes as well as the susceptibility of mine spoil to various environmental

adversities. However, the gradual investment of organic C forms the vegetation remains led to an increase in BSR across different overburden dump sites (Yuste et al. 2007). The BSR: OC ratio represents an increasing pattern with higher FMS (2.793%) and minimum FS (0.276%) across the areas (Table 3). The study actualized the fact that a high BSR: OC ratio validates the greater use of the native organic C by the existing microflora in soil colonizing fresh mine spoil as compared to other soil profiles efficiently that are ultimately responsible for increasing adversities of the habitat (Killham & Firestone 1984).

## Microbial Metabolic Quotient

The ratio between microbial respiration per unit biomass per unit time primarily regulates the heterotrophic respiration is known as microbial metabolic quotient qCO<sub>2</sub> (Xu et al. 2017), which also refers to the ratio between the release of CO<sub>2</sub>-C to CO<sub>2</sub> consumed (Insam & Domsch 1988). The microbial metabolic quotient tells about the adequacy of soil microbial communities in terms of utilization of substrate/energy (Insam & Haselwandter 1989, Insam 1990). Besides, the respiratory process is affected by microbial community composition, microbial biomass and basal soil respiration, ultimately affecting microbial metabolic quotient (Jiang et al. 2013).

Table 3: Percentage of organic C released as CO<sub>2</sub>-C (BSR: OC) and microbial metabolic quotients (qCO<sub>2</sub>) from seven different manganese mine spoil.

Soil profiles	BSR/OC [%]	Microbial metabolic quotients CO <sub>2</sub> -C.g <sup>-1</sup> microbial – C.h <sup>-1</sup>
MBO0	2.793	6.5×10 <sup>-3</sup>
MBO2	1.263	3.1×10 <sup>-3</sup>
MBO4	0.948	2.43×10 <sup>-3</sup>
MBO6	0.675	1.953×10 <sup>-3</sup>
MBO8	0.541	1.834×10 <sup>-3</sup>
MBO10	0.449	1.703×10 <sup>-3</sup>
FS	0.276	1.481×10 <sup>-3</sup>

In the current study, the microbial metabolic quotient was shown to follow a decreasing pattern across sites from fresh mine spoil to natural forest soil. In FMS, microbial metabolic quotient was found to be higher ( $6.5 \times 10^3$ ) as compared to the minimum in FS ( $1.481 \times 10^{-3}$ ) (Table 3). Generally, more qualitative and nutrient-rich soil responsible for the release of less  $\text{CO}_2\text{-C}$  per unit microbial biomass gives a lower metabolic quotient (Insam & Domsch 1988, Insam & Haselwandter 1989). Detritus is lacking in mine-operated soil, leading towards less decomposition and an almost small amount of organic substrate and the microbial population is anticipated to follow the ecotype of r- a strategy that acquires more  $\text{CO}_2\text{-C}$  per unit of substrate availability. Whereas in FS, due to the presence of a good amount of residue, the soil is predominated by decomposers that are expected to follow the ecotype of k strategy that is responsible for the respiration of comparatively less  $\text{CO}_2\text{-C}$  per unit decomposed organic substrate (Lynch & Panting 1982), known as economic metabolism given by Insam 1990. Additionally, greater the inconstant C that easily disintegrates would favor more opportunistic and unstable r"-strategy ecotype as compared to k"-strategy ecotype (Yuste et al. 2007), which are predominately enzyme producers. This variation in  $q\text{CO}_2$  between fresh mine spoil (MBO0) and FS can be elaborated with respect to qualitative substitution in microbial populations. Thus, the study supports the areas exposed to more stress responsible for the release of  $q\text{CO}_2$  as compared to fertile land due to the lack of action of microorganisms efficiently.

### Enumeration of Microbes

In the current study, the relative availability of *Azotobacter*, *Arthrobacter*, rhizobia, heterotrophic aerobic bacteria, actinomycetes, yeast, and fungi are increased at an increasing rate (Table 2) that rely upon the level of accessibility of quality substrate, OC content, variations in microclimatic factors and intensity of vegetation cover with heterogeneity. *Azotobacter* is chemoheterotrophic, a gram-negative, free-living microbe that belongs to the family Azotobacteriaceae, which is an obligate aerobic, nitrogen-fixing bacteria. In fresh mine spoil, due to deficiency of available nutrients, *Azotobacter* count was less and showed an increasing trend up to forest soil. *Arthrobacter* genus belongs to the family Micrococcaceae (Paul et al. 2011) and is a non-spore-forming gram-positive bacteria that functions as a valuable dinitrogen-fixing organism. *Arthrobacter* colony count was increasing from fresh mine spoil to forest soil and decreasing towards acidity that prevails microbial growth that resulted in a minimal count of *Arthrobacter* population in fresh mine spoil (Hagedorn & Holt 1975).

*Rhizobium* genus belongs to the family Rhizobiaceae and possesses a remarkable feature because of its symbiotic relationship with legumes located in a wide range of tropical and subtropical regions and enables the growth of plants in nitrogen-deficient soils. This association has a major quantitative impact on the global nitrogen cycle and is also important ecologically and agriculturally because it contributes a considerable amount of nitrogen from the atmosphere to fix essential forms like ammonia, nitrate, and organic  $\text{N}_2$  and is important for the stability and functioning of the ecosystem (Nakade 2013) that might be the possible reason for exhibiting less RHB count in FMS as compare to highly fertile FS. Heterotrophic aerobic bacteria count (HAB) was much higher in nutrient-rich contamination-free native forest soil as compared to MBO0 because of lacking ecological balance and equilibrium due to the continuous degradation of surface soil because of mining. Microbial communities exposed to high environmental stress were less diverse, with a low network of stability as compared to microbes with less stress (Hernandez et al. 2021). However, the relative count of sulphur-reducing bacteria (SRB) showed a decreasing pattern from MBO0 to nearby native forest soil. During the surface mining process, textural properties and geomorphic features are lost in low OC content, but the availability of pyrite from  $\text{FeS}_2$  enables the growth of SRB in degraded soil. Actinomycetes are saprophytes that have both features of bacteria and fungi widely distributed in soil and belong to the order Actinomycetales. Distribution of this non-spore-forming positive bacteria is majorly influenced by factors like temperature, OC content, moisture content, and aeration and moisture content of soil (Arifuzzaman et al. 2010) and this may be the probable reason for high actinomycetes (ACM) count in MBO as compare to FS. Yeast (YES) is an artificial group of fungi with the unicellular form of life cycle widespread in soil across the world. Yeast has an effective impact on an aggregation of soil (Bab'eva & Moawad 1973), assists in the regeneration of nutrients (Botha 2011) but also influences ground vegetation (Cloete et al. 2009) and other organisms in soil (Yurkov et al. 2012). This might be the possible reason for the highest yeast count in fresh mine spoil (MBO0) as compared to FS, which favors the microenvironment for the existence of microbes. Fungi are microscopic cells that act like natural cycling mediums and reabsorb essential nutrients from the soil. The filamentous hyphal structure of these microorganisms forms macro-aggregates in soil by binding soil particles together, improving the infiltration of water and water-holding capacity of the soil. The fungal hyphae form a network that expands the surface area of plant roots and helps in the translocation of deficient nutrients across the plants. Additionally, this might be the possible explanation

Table 4: Table showing simple correlation coefficients of microbial population and properties of soil.

	AZB	ARB	RZB	HAB	SRB	AMC	YES	FUN	MC	OC	MBC	BSR
MC	.950**	.959**	.936**	.932**	-.893**	.939**	.958**	.910**	1			
OC	.872*	.899**	.872*	.859*	-.864*	.847*	.972**	.824*	.962**	1		
MBC	.982**	.928**	.919**	.979**	-.944**	.960**	.970**	.899**	.976**	.938**	1	
BSR	.992**	.900**	.900**	.997**	-.945**	.955**	.923**	.866*	.928**	.864*	.983**	1

\*\* Correlation significant at > 0.01 level; \* Correlation significant at > 0.05 level

for the highest fungal count in native forest soil due to the presence of a high amount of utilizable substrate, adequate OC content, favorable moisture, and pH content. Fungi populations are also being reported in some acidic soil like fresh mine spoil (Domsch et al.1980).

In soil, microbes as a whole interact with each other, and the fundamental properties of these soil habitats are heterogenic and diversified. The structural arrangement of each soil type develops its own physico-chemical properties and microbial habitats and, at the same time, gives a definite living space for inhabitants of microorganisms to take space in a particular niche. Besides, variations in characteristics of soil due to addition, loss transformation, and transfer of energy regulate the exhibition of microhabitats in soil. The variations occur between microbial population and MC, OC, MB-C, and BSR determined by simple correlation analysis (Table 4)

According to the data provided, not only variable number of microbes are inhabitants in different overburden dumps but also diversity occurs in their metabolic activities in terms of soil respiration rate. Initialization of pioneering microbial colonies and their distribution was less in fresh mine spoil as compared to native forest soil because variation occurs due capacity of soil microorganisms to adsorb onto soil aggregates containing organo-mineral supplements and not get protected against heavy metals present in effectively high concentration. Microorganisms are highly sensitive and negatively impacted due to high concentrations of heavy metals (Gogoi & Das 2024). It may be possible that microbes and toxic heavy metals bind to the same binding site by formation of complex and spatial separation between the two did not occur (Kandeler et al. 2000). Heavy metal concentration above critical limit affect metabolic functions, and functions related to carbon and nitrogen cycle and contamination status of soil affected by heavy metals (Li et al. 2020). The variations in microbial communities positively correlated to the OC content of different overburden mine spoil (Fierer et al. 2003). The large population of fungi, bacteria, and other microbes enzymes like cellulolytic, hemicellulolytic, nitrifying, and denitrifying present in soil organic carbon make it more conducive for microbial growth and also act as a source and sink of nutrients as well as maintenance of soil fertility (Khatoun et al. 2021).

Respiration mostly relies on the moisture content (Silva et al. 2015). Soil with well adequate moisture can sustain more diverse microbial communities, and optimum soil moisture maintains the microflora of soil that is responsible for the transformation of organic compounds and the detoxification of toxic metals (Borowik & Wyszowska 2016). Among these seven overburden mines, spoil microbial community composition and action solely depend on available moisture, thus showing a positive correlation.

Step-wise multiple regression analysis from seven overburdened mine spoils by taking microbial communities as a dependent variable was summarized (Table 5). Azotobacter (AZB) and actinomycetes (AMC) contribute about 98.48% and 91.25% of the variability in basal soil respiration. Additionally, AZB, as a first variable, 0.37% contributed by SRB and MC gave a marginal effect by contributing 0.26% to microbial respiration. Arthrobacter (ARB), as the first variable, contributed 81.02% independently and explained 15.71% and 2.97% as MBC as the first variable and AZB as the second variable. The marginal effect explained by MC by contributing 0.28% to the variability of BSR that denotes optimum moisture may favor a good number of microbial communities with adequate BSR (Borowik & Wyszowska 2016). In BSR, rhizobia (RZB) explained 81.03% variability and 15.60% contribution explained by MB-C. Heterotrophic aerobic bacteria (HAB) and sulfate-reducing bacteria (SRB) added 99.48% and 89.31% variation to the BSR independently (Table 5). 85.14% variability contributed by yeast (YES) independently, with 13.07% explained by MB-C as the first variable. The marginal effect is shown as 0.03% by Fungi ((FUN). As eukaryotes, Fungi contribute 75.04% variability to BSR and play a major role in nutrient storage as well as release (Yurkov et al. 2011). 7.04% variation is explained by organic carbon (OC), with 7.93% contributed by SRB. 76.44% contribution explained by organic carbon as the first variable that favors more microbial activity and favors more microbes to colonize with 7.42% variation. To regulate the carbon cycle in the terrestrial ecosystem, microbial biomass C plays a major role and contributes 96.62% variation to BSR. Soil moisture is a primary factor in improving soil physico-chemical properties and contributes 82.20% with 16.45% variation incorporated by MB-C to make the soil more fertile for vegetation.

Table 5: Step wise multiple regression analysis by using microbial composition as a dependent variable influencing the variability in BSR in seven different sites.

	Equations	R <sup>2</sup>
Microbial BSR	0.021248+ 0.16159AZB	98.48
	-0.26598+0.25559AMC	91.25
	0.25921+0.13852AZB-0.4132SRB	98.85
	0.3712+0.16060AZB-0.04423SRB-0.0362MC	99.11
	-0.36109+0.2408ARB	81.02
	0.36609-0.02355ARB+0.001237MBC	96.73
	0.25144-0.0804ARB+0.0003MBC+0.1654AZB	99.70
	0.5377-0.1633ARB+0.00092MBC+0.1144AZB-0.00645MC	99.98
	-0.03026+0.1867RZB	81.03
	0.30411-0.0039RZB+0.001163MBC	96.63
	021423-0.00648RZB+0.001MBC+0.0412AMC	96.81
	0.0158+0.09907HAB	99.48
	1.4359-0.2363SRB	89.31
	0.4791-0.0393SRB+0.00097MBC	96.89
	-0.04576+0.232185YES	85.14
	0.50839-0.13036YES +0.00172MBC	98.21
	0.51667-0.1272YES+0.00175YES-0.007865 FUN	98.24
	0.05863+0.19102FUN	75.04
	0.2097+01059FUN+0.10441OC	82.08
	1.0674+0.0377FUN+0.2929OC-0.1712SRB	90.91
0.44851+0.19268OC	74.66	
0.206971+0.1044OC+0.1059FUN	82.08	
0.29577+0.00114MB-C	96.62	
-0.4642+0.1311MC	82.20	
0.85375-0.9232MC+0.00188MBC	98.65	
0.8598-0.09498MC+0.001877MBC-0.005922	98.66	

\*All R2 - values are significant at p< 0.001

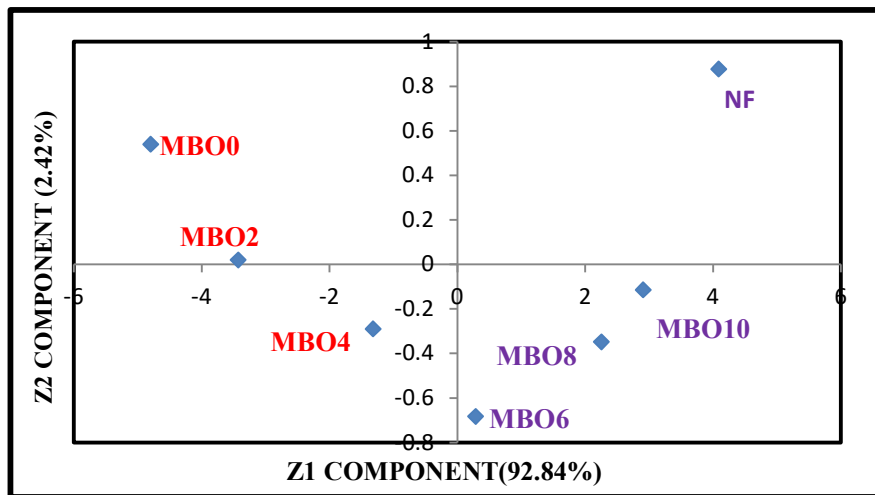


Fig. 1: PCA based on MC, OC, MB-C, basal soil respiration, and microbial population parameters in six different manganese mine spoil and nearby forests.

To acquire a clear understanding of variations among different sites based on MC, OC, MB-C, BSR, as well as microbial populations, principal component analysis was performed (Ludwig & Reynolds 1988). Principal component analysis denotes the Z1 and Z2 components that represent

maximum variance with respect to soil physico-chemical and microbial parameters, contributing a maximum cumulative variance percentage of about 95.26%, which discriminates seven different soil profiles into independent clusters (Fig.1).

## CONCLUSION

The present investigation was accomplished to examine the intensity of variation among soil parameters like organic carbon, moisture content with microbial biomass carbon, microbial community distribution, and basal soil respiration in different manganese mine spoil. The variation in basal soil respiration in different sites may be due to microbial action that is greatly influenced by OC and MC of different chronosequence mine spoil. The significance of microbial flora in the functioning of the ecosystem is absorbing major attention to increasing research in microbial biomass pools that work as both a source and sink of major plant available nutrients and enhance the fertility of the soil. Thus, analysis of microbial biomass and microbial metabolic quotients signifies an index for regular surveillance of the genesis of mine spoil. The diverse results of basal soil respiration rate are due to the transformation of microbial community structure over time, and the increase in respiration rate is also encouraged by the accumulation of organic carbon and suitable moisture. The study also signifies the sudden response of microbes to the disturbed soil physico-chemical properties of overburdened mine spoil and it is shifting towards highly fertile soil with vegetation. Hence, evaluation of microbial biomass, community structure, and basal soil respiration rate used as highly responsive indicators of the genesis of mine spoil and their role in the transformation of microbe deficient infertile to microbial enriched, productive land due to their contribution towards nutrient cycling in an ecosystem, turnover of organic carbon, structural and functional stability of soil towards restoration.

## ACKNOWLEDGEMENT

The authors are thankful to the Head of the School of Biotechnology, Gangadhar Meher University, Sambalpur, Odisha, India, for the necessary guidance and support. The investigation was made possible through the support provided by Soil Testing Lab, Sambalpur. The authors remain grateful to Mr. Soujatya Sarangi for his assistance during the entire field survey. We are also thankful to Dr. Jitesh Kumar Maharana for his contribution to the sample collection.

## REFERENCES

Alef, K. and Nannipieri, P., 1995. *Methods in Applied Soil Microbiology and Biochemistry*. Academic Press.

Amundson, R., 2001. The carbon budget in soils. *Annual Review of Earth and Planetary Sciences*, 29, pp.535-562.

Arifuzzaman, M., Khatun, M.R. and Rahman, H., 2010. Isolation and screening of actinomycetes from Sundarbans soil for antibacterial activity. *African Journal of Biotechnology*, 9(29), pp.4615-4619.

ATCC, 1992. *Catalog of Bacteria and Bacteriophages*. American Type Culture Collection.

Bab'eva, I.P. and Moawad, H., 1973. Soil yeasts of the genus *Lipomyces* as soil-conditioning agents. *Eurasian Soil Science*, 8, pp.430-432.

Borowik, A. and Wyzkowska, J., 2016. Soil moisture is a factor affecting the microbiological and biochemical activity of soil.

Botha, A., 2011. The importance and ecology of yeasts in soil. *Soil Biology and Biochemistry*, 43, pp.1-8.

Cloete, K.J., Valentine, A.J., Stander, M.A., Blomerus, L.M. and Botha, A., 2009. Evidence of symbiosis between the soil yeast *Cryptococcus laurentii* and a sclerophyllous medicinal shrub, *Agathosma betulina* (Berg.) Pillans. *Microbial Ecology*, 57, pp.624-632.

Davidson, E.A. and Janssens, I.A., 2006. Temperature sensitivity of soil carbon decomposition and feedback to climate change. *Nature*, 440(7081), pp.165-173.

Davidson, E.A., Janssens, I.A. and Luo, Y., 2006. On the variability of respiration in terrestrial ecosystems: moving beyond Q10. *Global Change Biology*, 12, pp.154-164.

Domsch, K.H., Gams, W. and Anderson, T.H., 1980. *Compendium of soil fungi. Volume 1*. Academic Press, London.

Eaton, A.D., Clesceri, L.S. and Greenberg, A.W., 2005. *Standard Methods for the Examination of Water and Wastewater*. APHA, Washington, D.C.

Evangelista, S.J., Field, D.J., McBratney, A.B., Minasny, B., Ng, W., Padarian, J., Dobarco, M.R. and Wadoux, A.M.C., 2023. A proposal for the assessment of soil security: soil functions, soil services and threats to soil. *Soil Security*, 10, 100086.

Fierer, N., Schimel, J.P. and Holden, P.A., 2003. Variations in microbial community composition through two soil depth profiles. *Soil Biology and Biochemistry*, 35(1), pp.167-176.

Gogoi, I. and Das, K., 2024. Heavy Metal Resistant Bacteria in Rhizospheric Soil: A Review. *Ecology Environment and Conservation*, 30, pp.S202-S205.

Griffiths, M.L., Fohlmeister, J., Drysdale, R.N., Hua, Q., Johnson, K.R., Hellstrom, J.C., Gagan, M.K. and Zhao, J.X., 2012. Hydrological control of the dead carbon fraction in a Holocene tropical speleothem. *Quaternary Geochronology*, 14, pp.81-93.

Hagedorn, C. and Holt, J.G., 1975. Differentiation of *Arthrobacter* soil isolates and named strains from other bacteria by reactions on dye-containing media. *Canadian Journal of Microbiology*, 21(5), pp.688-693.

Harris, J.A., 2003. Measurements of the soil microbial community for estimating the success of restoration. *European Journal of Soil Science*, 54(4), pp.801-808.

Helingerova, M., Frouz, J. and Šantrůčková, H., 2010. Microbial activity in reclaimed and unreclaimed post-mining sites near Sokolov (Czech Republic). *Ecological Engineering*, 36(6), pp.768-776.

Hernandez, D.J., David, A.S., Menges, E.S., Searcy, C.A. and Afkhami, M.E., 2021. Environmental stress destabilizes microbial networks. *The ISME Journal*, 15(6), pp.1722-1734.

Hunter-Cevera, J.C. and Eveleigh, D.E., 1990. *Actinomycetes Soil Biology Guide*. John Wiley and Sons, New York.

Insam, H., 1990. Are the soil microbial biomass and the basal respiration governed by the climatic regime? *Soil Biology and Biochemistry*, 22(4), pp.525-532.

Insam, H. and Domsch, K.H., 1988. Relationship between soil organic carbon and microbial biomass on chronosequences of reclamation sites. *Microbial Ecology*, 15, pp.177-188.

Insam, H. and Haselwandter, K., 1989. Metabolic quotient of the soil microflora in relation to plant succession. *Oecologia*, 79, pp.174-178.

Jiang, Y., Sun, B., Jin, C. and Wang, F., 2013. Soil aggregate stratification of nematodes and microbial communities affects the metabolic quotient in an acid soil. *Soil Biology and Biochemistry*, 60, pp.1-9.



- Kandeler, E., Tschirko, D., Bruce, K.D., Stemmer, M., Hobbs, P.J., Bardgett, R.D. and Amelung, W., 2000. Structure and function of the soil microbial community in microhabitats of a heavy metal polluted soil. *Biology and Fertility of Soils*, 32, pp.390-400.
- Kopittke, P.M., Berhe, A.A., Carrillo, Y., Cavagnaro, T.R., Chen, D., Chen, Q.L., Román Dobarco, M., Dijkstra, F.A., Field, D.J., Grundy, M.J. and He, J.Z., 2022. Ensuring planetary survival: the centrality of organic carbon in balancing the multifunctional nature of soils. *Critical Reviews in Environmental Science and Technology*, 52(23), pp.4308-4324.
- Khatoun, K., Anas, M., Siddiqui, Z. and Malik, A., 2021. Role of soil microbial flora in remediation of hydrocarbon stressed soils. *Microbiome and Global Climate Change*, pp.295-319.
- Killham, K. and Firestone, M., 1984. Salt stress control of intracellular solutes in Streptomycetes indigenous to saline soils. *Applied and Environmental Microbiology*, 47, pp.301-306.
- Kourtev, P.S., Ehrenfeld, J.G. and Häggblom, M., 2003. Experimental analysis of the effect of exotic and native plant species on the structure and function of soil microbial communities. *Soil Biology and Biochemistry*, 35(7), pp.895-905.
- Krishna, H., Carpenter, A. and Potter, F., 2001. Effect of washing additives on the incidence of rots and an enumeration of surface microbes in stored squash. *New Zealand Plant Protection*, 54, pp.76-79.
- Kubat, J., Nováková, J., Mikanová, O. and Šimon, T., 1999. Selection of microbial methods for the bioindication of soil pollution. *Pathways and Consequences of the Dissemination of Pollutants in the Biosphere II Symposium*, Praha, pp.61-75.
- Li, S., Wu, J., Huo, Y., Zhao, X., and Xue, L., 2020. Profiling multiple heavy metal contamination and bacterial communities surrounding an iron tailing pond in Northwest China. *Science of the Total Environment*, 752, 141827.
- Ludwig, J.A. and Reynolds, J.F., 1988. *Statistical Ecology: A Primer in Method and Computing*. John Wiley and Sons, pp. 337.
- Lynch, J.M. and Panting, L.M., 1982. Effect of season, cultivation, and nitrogen fertilizer on the size of the soil microbial biomass. *Journal of the Science of Food and Agriculture*, 33, pp.249-252.
- Mishra, R., 1968. *Ecology Workbook*. Oxford & IBH Publishing Co., New Delhi.
- Monson, R.K., Lipson, D.L., Burns, S.P., Turnipseed, A.A., Delany, A.C., Williams, M.W. and Schmidt, S.K., 2006. Winter forest soil respiration is controlled by climate and microbial community composition. *Nature*, 439(7077), pp.711-714.
- Nakade, B., 2013. Bacterial diversity in sugarcane (*Saccharum officinarum*) rhizosphere of saline soil. *International Research Journal of Biological Sciences*, 2(2), pp.60-64.
- Ohya, H., Fujiwara, S., Komai, Y. and Yamaguchi, M., 1988. Microbial biomass and activity in urban soils contaminated with Zn and Pb. *Biology and Fertility of Soils*, 6, pp.9-13.
- Parkinson, D., Gray, T.R.G. and Williams, S.T., 1971. *Methods to Study Ecology of Soil Microorganisms*. IBP Handbook No. 19, Blackwell Scientific Publications, Oxford, pp. 116.
- Paul, S., Singh Rathi, M. and Prakash Tyagi, S., 2011. Interactive effect with AM fungi and Azotobacter inoculated seed on germination, plant growth, and yield in cotton (*Gossypium hirsutum*). *Indian Journal of Agricultural Sciences*, 81(11), pp.1041.
- Philippot, L., Chenu, C., Kappler, A., Rillig, M.C. and Fierer, N., 2024. The interplay between microbial communities and soil properties. *Nature Reviews Microbiology*, 22(4), pp.226-239.
- Sáez-Sandino, T., García-Palacios, P., Maestre, F.T., Plaza, C., Guirado, E., Singh, B.K., Wang, J., Cano-Díaz, C., Eisenhauer, N., Gallardo, A. and Delgado-Baquerizo, M., 2023. The soil microbiome governs the response of microbial respiration to warming across the globe. *Nature Climate Change*, 13(12), pp.1382-1387.
- Santruckova, H. and Straskraba, M., 1991. On the relationship between specific respiration activity and microbial biomass in soils. *Soil Biology and Biochemistry*, 23, pp.525-532.
- Silva, B.M., Santos, W.J.R.D., Oliveira, G.C.D., Lima, J.M.D., Curi, N. and Marques, J.J., 2015. Soil moisture space-time analysis to support improved crop management. *Ciência e Agrotecnologia*, 39, pp.39-47.
- Sivaranjani, S. and Panwar, V.P., 2023. Soil nutrient dynamics under mountainous landscape: issues and challenges. In *Understanding Soils of Mountainous Landscapes*, pp. 131-149.
- Smith, G.A., Nickels, J.S., Kerger, B.D., Davis, J.D., Collins, S.P. and White, D.C., 1986. Quantitative characterization of microbial biomass and community structure in subsurface material: a prokaryotic consortium responsive to organic contamination. *Canadian Journal of Microbiology*, 32, pp.104-111.
- Tangjang, S. and Arunachalam, A., 2009. Role of traditional home garden systems in Northeast India. *Research Journal of Soil Biology*, 1, pp.1-7.
- Vance, E.D., Brookes, P.C. and Jenkinson, D.S., 1987. An extraction method for measuring soil microbial biomass C. *Soil Biology and Biochemistry*, 19, pp.703-707.
- Vincent, J.M., 1970. *A Manual for the Practical Study of Root-Nodule Bacteria*. IBP Handbook of Methods No. 15. Blackwell Scientific Publications, Oxford.
- Walkley, A. and Black, I.A., 1934. An examination of the Degtjareff method for determining soil organic matter and a proposed modification of the chromic acid titration method. *Soil Science*, 37(1), pp.29-38.
- Witkamp, M., 1966. Rate of CO<sub>2</sub> evolution from the forest floor. *Ecology*, 47, pp.492-494.
- Xu, M. and Qi, Y., 2001. Spatial and seasonal variations of Q10 determined by soil respiration measurements at a Sierra Nevada Forest. *Global Biogeochemical Cycles*, 15(3), pp.687-696.
- Xu, X., Schimel, J.P., Janssens, I.A., Song, X., Song, C., Yu, G., Sinsabaugh, R.L., Tang, D., Zhang, X. and Thornton, P.E., 2017. Global pattern and controls of soil microbial metabolic quotient. *Ecological Monographs*, 87(3), pp.429-441.
- Yurkov, A.M., Kemler, M. and Begerow, D., 2011. Species accumulation curves and incidence-based species richness estimators to appraise the diversity of cultivable yeasts from beech forest soils. *PLoS One*, 6(8), 23671.
- Yurkov, A.M., Kemler, M. and Begerow, D., 2012. Assessment of yeast diversity in soils under different management regimes. *Fungal Ecology*, 5(1), pp.24-35.
- Yuste, J.C., Baldocchi, D.D., Gershensoni, A., Goldstein, A., Misson, L. and Wong, S., 2007. Microbial soil respiration and its dependency on carbon inputs, soil temperature, and moisture. *Global Change Biology*, 13, pp.1-18.

---

#### ORCID DETAILS OF THE AUTHORS

S. Dash: <https://orcid.org/0000-0001-8098-6161>

M. Kujur: <https://orcid.org/0000-0001-7973-3087>





# Community Perception on the Effect of Cultural Livelihoods on the Environment in Kogi State, Nigeria

G. O. Chukwurah<sup>1</sup>, N. M. Aguome<sup>2</sup>, M. O. Isimah<sup>3†</sup>, E. C. Enoguanbhor<sup>4</sup>, N. E. Obi-Aso<sup>5</sup>, N. U. Azani<sup>6</sup>  
and O. C. Nnamani<sup>7</sup>

<sup>1</sup>Department of Urban and Regional Planning, University of Nigeria, Nsukka, Nigeria

<sup>2</sup>Department of Architecture and Planning, University of Botswana Gaborone, Botswana

<sup>3</sup>Departments of Geography and Environmental Sustainability, University of Nigeria, Nigeria

<sup>4</sup>Department of Geography (Applied Geoinformation Science Lab), Humboldt University of Berlin, Germany

<sup>5</sup>Department of Estate Management, Nnamdi Azikiwe University Awka, Nigeria

<sup>6</sup>Department of Urban and Regional Planning, University of Delta, Delta State, Nigeria

<sup>7</sup>Department of Estate Management, University of Nigeria, Nsukka, Nigeria

†Corresponding author: M. O. Isimah; matthew.isimah@unn.edu.ng

Nat. Env. & Poll. Tech.  
Website: [www.neptjournal.com](http://www.neptjournal.com)

Received: 04-02-2024

Revised: 16-04-2024

Accepted: 25-04-2024

## Key Words:

Community perception  
Cultural livelihood  
Environment  
Kogi State

## ABSTRACT

This study examines the cultural livelihood of Kogi State and its effects on the environment. The study describes some of the cultural livelihood practices found in Kogi State, considering the contemporary condition of cultural livelihood and its effects on the environment. Secondary and primary data were employed, which include archives and internet search engines. Using a 4-stage sampling procedure, data were collected from a 120-person sample through an interview, field observation, a focus group discussion, and a questionnaire. Descriptive statistics using frequencies, percentages, and charts were used for the analyses. The results were compiled using the Statistical Package for Social Sciences (SPSS). Findings show that about 85% of the participants discovered crop farming, arable farming, weaving, blacksmithing, fishing, and festivals of harvest, such as the New Yam Festival, among others, as the predominant cultural livelihoods. The local farming implements were made of local materials, like stones and wood. They have indigenous crop production, protection, and harvest techniques. The farming tools were economical in terms of labor, affordability, and time savings in the subsistence farming system. The study discovered that cultural livelihoods are 4% very efficient and 56% on the verge of extinction. Analyses of the effect of cultural livelihood show that 78% have a high negative effect on the economic environment, 57% have a moderate negative effect on the social environment, 51% hurt the political environment, and 22% have a low negative effect on the political environment. The intervention of the various tiers of government with the cooperation of the various communities is needed for the provision of a conducive environment for the practice of cultural livelihood, particularly in the aspect of insecurity. Adequate provision of modern equipment, funding, and social welfare services is also recommended to enhance cultural livelihoods.

## INTRODUCTION

Nigeria is a nation endowed with rich cultural heritage sourced from its multicultural communities (Onyima 2016). A new paradigm of urban development is necessary to solve the current urban problems, such as joblessness and food insecurity, among others. Urban environments should foster a sense of belonging, promote social cohesion, and counter segregation and wealth inequality to foster greater integration and connection among residents. Cultural livelihood comprises a society's philosophies, arts, customs, inventions, language, institutions, technology, and tenets. Cultural livelihoods are relics of the present that unify

us with the past, as they provide the contemporary world with insight into the past. Cultural livelihood includes both tangible and intangible heritage. The tangible heritages are monuments, buildings, historic areas, and artifacts, among others, that safeguard the future. These tangible objects are vital in the context of archaeology, architecture, science, and technology in a particular culture. Intangible heritages are living expressions and inherited traditions from their ancestors that are transferred to their offspring (AIC 2005).

Cultural livelihood is where individuals earn a living through particular skills, resources, and pursuits (Ellis 1999, Carney 1998, Chambers & Conway 1992, Onyekwere &

Nworgu 2020). There is an increasing realization that culture and environment play major roles in tourism, and cultural livelihood has contributed immensely to the development of many communities and states. Several developing countries are redirecting policies on the preservation of cultural livelihoods and environmental resources. Nigeria is a nation endowed with a rich culture, which also serves as a means of livelihood (Sarfo-Mensah & Oduro 2007, Chukwurah 2022).

Kogi State is known for its diverse cultural livelihood. Beyond the fundamental needs of living, the cultural livelihoods of the Kogi state incorporate identity, social connection management, and tourism attractions (Wallman 1984). Cultural livelihood has added value to development and primary economic opportunities for the people (Chukwurah & Onyekwere 2020), particularly the indigenes of Kogi. Some of the cultural livelihoods of Kogi serve as a tourist attraction and generate huge income, especially in the early days. It also serves as job creation; however, the sustainability of the cultural livelihood is under severe threat (Sarfo-Mensah & Oduro 2007, Beier 1980, Feldman 2000), despite studies done by some experts, including Chukwurah (2022), Onyekwere & Nworgu (2020), Njoku & Nwaogwugwu (2014), and Akinwale (2011) on cultural livelihood. It, therefore, implies that there are limited studies on cultural livelihoods for sustainable development, particularly in developing countries, of which this current study tends to fill the lacuna. This study examines the community's perception of the effect of cultural livelihoods in Kogi state. The objectives of this study, therefore, are to (i) identify some major cultural livelihoods of the state, (ii) examine the contemporary state of cultural livelihoods, and (iii) examine the effects of the contemporary state of cultural livelihoods in Nigeria, particularly in Kogi State.

## SIMILAR STUDIES

Cultural livelihood, developed by any society, is passed down from generation to generation. According to George (2010), this gives young people a feeling of identity and continuity, fostering an appreciation for the cultural variety and the works of the human mind. UNESCO (2015:3) defines intangible attributes of society as inherited, maintained, and preserved, including tangible cultural heritage, physical representations, and artifacts for future preservation. It is imperative to express that cultural livelihood is as old as man's, and development cannot be sustained without it. Onyekwere & Nworgu (2020) identified the threat indicators to sustainable rural livelihood, ascertaining the threat outcomes and the vulnerable groups. Flooding of compounds and farms, herdsman attacks, and government impunity, among others, are acute threats to rural livelihoods.

The outcomes include insecurity, food crises, loss of lives and property, hunger, loss of shelter, and suicide. A study by Njoku & Nwaogwugwu (2014) discovered that cultural issues significantly influence rural household economies. Their study analyses the cultural factors affecting the livelihood strategies of rural households in southeast Nigeria. The predominant agricultural livelihood strategies discovered include crop farming, livestock farming, and farm produce processing; the non-predominant agricultural livelihoods include petty trading and civil service. The report by UNESCO (2015) recognizes that cultural livelihood has historically been a driving force behind regional sustainable development. The practices to integrate cultural heritage into regional sustainable development strategies are currently being observed in such a way that cultural heritage is now recognized by the international community as a major component and innovation of strategic regional planning for sustainable development. Hari (2020) observed that conserving cultural heritage is of less priority compared to other important issues like social amenities, the creation of employment opportunities, and poverty alleviation; however, conservation will help to safeguard the resources, revitalize local economies, and bring about a sense of identity and pride among the residents. Cultural livelihoods have experienced a decline in productivity (Raven 2003).

Cobbinah's study on informal culture and urban planning in Africa analyzed the influence of the culture of informality on urban planning and development in Kumasi, Ghana (Cobbinah 2021). He bolstered how local people perceive and consider their culture as a tool for urban planning and development. Their findings indicate that four out of five identified values of the culture of informality have a statistically significant influence on urban planning and development. Though other studies have looked at cultural livelihood, it is less productive despite the challenges of a harsh economy, food insecurity, and the poverty rate. It, therefore, means there are areas of cultural livelihood that are yet to be addressed, which this study is aimed at addressing.

## THE STUDY AREA

Kogi State is the study area. Kogi State lies in the north-central region of Nigeria. It was carved out of Kwara and Benue States in 1991, with a land area of 29,833 square kilometers. It has 21 local government areas (thirteen local government areas from the former Kwara and eight from Benue States) and comprises the Igala, Ebira, Kabba, Yoruba, and Kogi divisions of the former Kabba province. It shares common boundaries with Niger, Kwara, Nassarawa States, and the Federal Capital Territory to the north. To the east,

the state is bounded by Benue State, to the south by Enugu and Anambra States, and to the west by Ondo, Ekiti, and Edo States. There are three main ethnic groups and languages in Kogi State: Igala, Ebira, and Okun (similar to Yoruba), with other minorities like Bassa, a small fraction of Nupe mainly in Lokoja, Gwari, Kakanda, Oworo people (like Yoruba), Ogori, Magongo, and the Eggan community. Lokoja Local Government Area, Kogi State, is popularly called the confluence state because the confluence of Rivers Niger and Benue occurs close to its capital, Lokoja. The majority of the people are farmers. Kogi State enjoys a favorable climate and fertile soil. Kogi State, rich in limestone and coal, has a population of 3,278,487, according to the 2006 census.

## MATERIALS AND METHODS

### Research Design

The study adopted a survey-based application of contingent valuation design based on research questions. The three research questions used included: What are the predominant cultural livelihoods in the area? What is the contemporary condition of cultural livelihood? What is the extent of the effect of cultural livelihoods on the environment? Therefore, the questionnaire, interview, and focus group discussion (FGD) were designed to identify the predominant cultural livelihood of the state, the contemporary condition of the cultural livelihood and to determine the effects of the cultural livelihood on the environment. The mixed research approach, which is the use of a questionnaire survey combined with focus group discussion for data collection and analysis integrated into the study, is to elaborate on specific findings from the focus group analysis and to cross-check the data against the questionnaire data on the extent of the effect of cultural livelihoods on the environment.

### Population, Sample, and Response Rate

Four-stage random sampling techniques were used. Using multi-stage and simple random sampling techniques, six communities were randomly selected from the local government headquarters of the three major ethnic languages such as Igala (dominant in the East Senatorial District), Okun (dominant in the West Senatorial District), and Ebira (dominant in the Central Senatorial District). Two communities each were randomly chosen from the three major ethnic groups making it a total of six communities. Among them are Idah, Lokoja, Ajaokuta, OkeneAgbaja, and Iyara. Due to a lack of reliable data about the total population of those engaged in cultural livelihood in the study area, the authors decided on a sample size of 240 participants who are engaged in cultural livelihood activities (20 males

and 20 females from each community) for the distribution of questionnaires; 210 were retrieved and were valid to analyze. This shows a response rate of 87.5%, which is valid; built-environment survey response rates vary between 7% and 40% (Moyo & Crafford 2010: 68, John-Nsa 2021: 33, Enoguanbhor et al. 2023: 45). Since the questionnaire data was to complement the secondary data and authors plan to utilize descriptive statistics with the questionnaire data, analyzing 210 questionnaires is valid for the current study. Table 1 presents the sampled population and questionnaires retrieved from key information participants.

### Data Collection

The study employs both primary and secondary sources of data. Primary data came from twenty-four FGD with young people and adults who are also community leaders within six communities. The participants were from the three local government areas in Kogi State. Gender, age, status, and availability were considered factors in the selection of the volunteers. A list of the selected Kogi State communities and participants is in Table 1.

The study adheres closely to social science research ethical guidelines. Eight to ten people participated in each FGD. In each community, 24 focus group discussions were conducted, with youth and adult/community leaders as participants. Age and gender distribution were the same in every FGD. Table 1 displays the overall sample size of 210 people from the selected communities. In addition to community leaders 40 years of age and older, the participants included male and female youngsters in the 18–35 age range. Purposive and stratified random sampling methods were adopted in this study. The essence was to select eligible participants across the communities in the study area. Three major ethnic groups in local government areas (LGAs) in Kogi State were categorized into identified cultural livelihoods. Subsequently, six (6) communities in three LGAs were purposively selected. The study utilized a focus group discussion guide to investigate participants' perspectives on cultural livelihoods and the impact of contemporary livelihoods in the study area. Each FGD comprised same-sex participants to protect participants from unnecessary constraints. Each FGD consists of people of the same gender to protect participants from unnecessary distractions. Theoddeven product-moment correlation statistics were used to test the reliability of the instrument. The co-efficient index was calculated, and the score obtained was 0.87. The reason behind the choice of respondents is because they are involved and knowledgeable about the cultural livelihoods of the people. The research participants were interviewed during FGD, which took place during

Table 1: List of Respondents in the Focus Group Discussion (FGDs).

Community (LGA Headquarters)	Adults/Community Leaders		Youths		Total FGDs N= 24
	Males FGDs N=10	Female FGDs (N=10)	Male FGDs N=10	Female FGDs N=10	
Idah	8	10	8	9	35
Lokoja	10	10	10	10	40
Ajaokuta,	8	8	9	8	34
Okene	9	8	8	10	35
Agbaja	8	9	7	8	32
Iyara	8	9	8	9	34
Total	51	54	50	54	210

Source: Researcher's survey on cultural Livelihoods in Kogi State, 2023.

the morning hours of the meeting in the various selected communities. The questionnaire was administered by the first and three other authors who reside in the community. The questionnaire administration and interview were done within 2 months.

### Data Analysis and Interpretation of the Findings

The analysis of the FGDs involved a combination of different models of content analysis, systematic coding, and categorization of textual information to ascertain the trends and patterns of words used, the frequency, relationships, structures, and discourses of communication, Grbich (2007). Data was also analyzed descriptively.

## RESULTS AND DISCUSSION

The following presentation of the study outcomes follows the research questions. The cultural livelihood framework's primary concerns and discussions serve as a foundation for interpreting the findings of 24 focus group discussions held in Kogi State.

### Cultural Livelihoods of Kogi State

Participants in all the focus group discussions identified crop and arable farming, fishing, weaving, Iron Smiting, and festival of harvest as the major Cultural livelihoods of Kogi State among other identified cultural livelihoods.

### Farming

Farming is one of the major cultural livelihoods of the people. It is the most common occupation of residents in the study area because of its vast agricultural land area. The state is known for farming coffee, cocoa, palm oil, cashews, groundnuts, maize, cassava, yam, rice, and melon. Local farmers use traditional farming implements in land preparation, planting, and harvesting a wide variety of crops. In rural communities, agriculture and farming practices

are regarded as the primary occupations of individuals. The livelihood of about two-thirds of rural families is subsistence agriculture, through either small-scale farming or working on farms for little pay. The remaining one-third of rural households are involved in minor services. It is well established that most rural households, particularly those in developing nations, reside in rural areas and depend on agriculture for their sustenance. There are indigenous tools and implements that are well-designed and used for farming. The farming implements are made of metal, copper, brass, bronze, iron, and wood.

### Festival of Harvest

During the harvest season, the people showcase their farm produce in a way of the festival, for example, rice. Rice (Ucholoohikapa) is highly valued. It is part of the culture and tradition of the people (Fig. 1). The harvest season is a joyous one because it marks the end of the season's work. A successful harvest means farmers and their families have enough food for the next season. The rice crop is harvested by cutting stalks with sharp hand tools. Some farmers only cut the panicles, while others cut the stalks directly from the base. Early rice farmers would use sharp objects to find suitable cutting tools. Indigenous farmers used mollusk shells for harvesting, especially giant African snails. Both men and women are involved in farming, but most tools are used exclusively by women. The rice display is held in Aganepoje, Idah. The event is dedicated to the rice goddess in a time of joyous celebration that was held a long time ago. This event is also designed to tell the story of the people's brand of rice to the world and generations to come. Other ethnic groups are invited to display their various types of rice to depict the real cultural representation. Participants enjoy tasting various recipes of Ochikapa. The traditional drummers are on the ground to add color to the event, while the farmers are also on the ground to educate and sell their brand at affordable prices. Unfortunately, the tradition has



Source: Artsandculture.com

Fig. 1: Festival of Harvest.

not been held for some time now. This culture is gradually fading away.

### Weaving Industry

The weaving of clothes is one of the major livelihoods of the people of Kogi State. About 97% of the research respondents revealed that the three major senatorial districts are known for weaving clothes (Fig. 2). Although women are more involved in clothing weaving, it is done on a small scale using local materials. The people of Kogi weave different types of cultural attire, known as Ebira, Igala, Owe, and Idoma, among others. It is said to be as old as humanity. Even though the necessity to conceal one's nakedness led to the development of cloth weaving, the fabric may be seen from a socio-cultural point of view in addition to serving as a body covering and protector. The type of attire someone is wearing conveys both their social status and the event or

occasion. The various types of clothes produced by the people describe their pasts and traditions. Both men and women worked on weaving fabric, but in Owe Land, the women's contribution was greater than that of the men. The output of raw cotton in Owe land was significantly increased by the presence of ideal climatic conditions, rich soil for cotton cultivation, and other communities where clothing is woven. The majority of the families are involved in cloth weaving. There are also industries where clothing and the weaving of clothing are produced. Cloth weaving was prominent in Owe-land because of the availability of the raw materials. Men and women both participated in the weaving process, which was one of the major occupations of the people in the area, using different looms. Women utilized the vertical loom, while men worked on the horizontal one. Before its downfall, the Owe woven fabric was the most sought-after in the area due to its high popularity and exquisite aesthetic



Source: ukomuigala.wordpress.com

Fig. 2: Weaving Industry.

patterns. From the beginning, cloth weaving was one of the main human vocations within and outside Owe Land, with high demand inside. The artistic genius of the people is expressed in the Owe-woven textile, which is the engine of economic development in Owe Land.

About 86% of the research participants revealed that the gold color shows the richness of the land and is connected with the minerals and fertility of the land, which symbolize the wealth and prosperity of the people. The black color represents their skin color, yellow symbolizes the beauty of the land, a touch of blue represents the waters and rivers in the land, green symbolizes the vegetation, and the white color stands for purity.

### Fish Farming

Fish farming was identified as one of the major cultural livelihoods of Kogi State. The two major rivers in Nigeria, the Niger and the Benue, meet in Lokoja, along with other water bodies in the state where fishing is done (Fig. 3). 96% of the research respondents revealed that the Igu-Koton-Karfe Kingdom in the Kogi local government area of Kogi State holds an annual fishing and cultural festival. It is an event known for the display of boat regattas, symposiums, exhibitions, and cultural displays. The fishing festival usually has no fewer than 3,000 fishermen, which comprises elders, middle-aged men, and youths from different ethnic backgrounds, such as Ganagana, Bassa, Igala, Agatu, Gwari, and the Egbira. Various cultural troupes usually converge in front of the palace of Ohimegye of Igu-koton-kafe, Alhaji Abdulrazakisa Koto, to display their dancing steps and masquerades in different attire to entertain the people till dawn, while the biggest catch of the day is given a prize. This is a means of preserving and encouraging fish

farming; however, this cultural fish festival is also fading away.

### Iron Smiting Industry

The research respondents (98%) confirm that Kogi natives are renowned for their blacksmithing. The Igala people are skilled in producing farming tools, kitchen appliances, and military equipment locally. The process of creating iron items from blooms or iron scraps is known as blacksmithing (Fig. 4). A pair of bellows, a fire point, an anvil, and a buried water bowl or pot are common items in a blacksmith's workplace. The fire point, where metal bits are implanted and heated to a red-hot iron, uses the bellows to speed up the combustion of charcoal. The communities' smiths make a variety of items required for basic subsistence needs and beyond, using essentially the same basic equipment. Smiting takes place in some of the villages in an open, rectangular hut with thatched roofs. The people in the villages that practice blacksmithing do not use any metal to till or hit the earth during the period of their ritual, which happens once a year. They believe they are bonded by the spirit of their forefathers, who were blacksmiths.

The contemporary state of cultural livelihood was examined. About 56% of the respondents revealed that the cultural livelihood of Kogi State is on the verge of extinction; 23% of the research respondents believe that cultural livelihood is less efficient; 9% revealed that it is efficient; and 4% opined that cultural livelihood is still efficient in Kogi State (Fig. 5). This finding summarizes that cultural livelihood is going extinct. This finding is consistent with the findings of Sarfo-Mensah & Oduro (2007) and Beier (1980), who found that cultural values are on the verge of extinction in Nigeria. The participants revealed that cultural livelihood



Source: National Museum, Lokoja

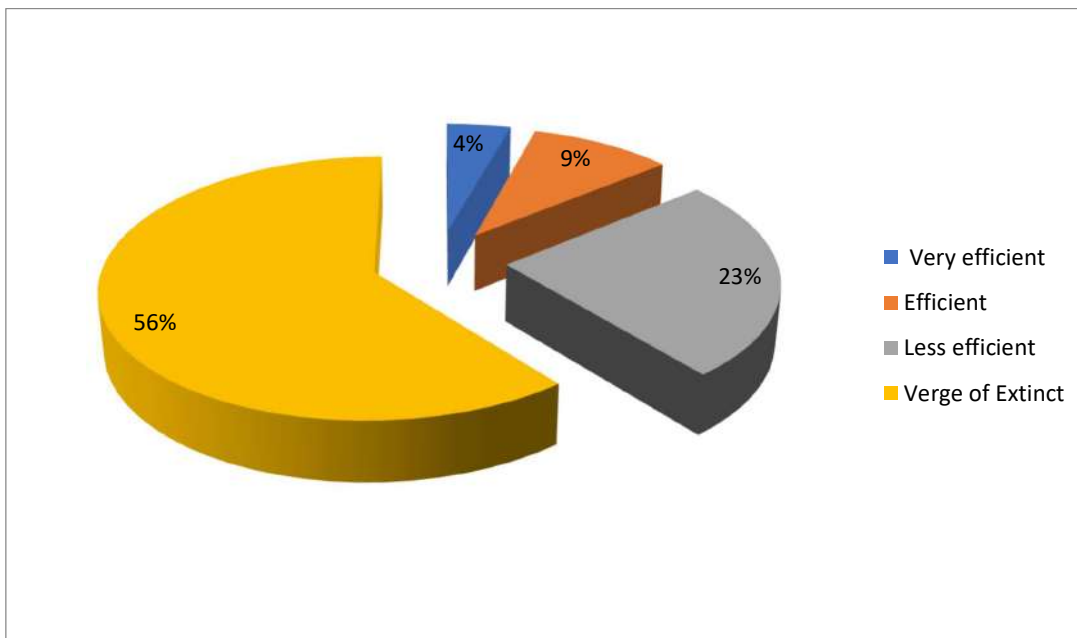
Fig. 3: Donkwo, Fishing Festival, Lokoja.





Source: National Museum, Lokoja.

Fig. 4: Iron Smiting Industry.

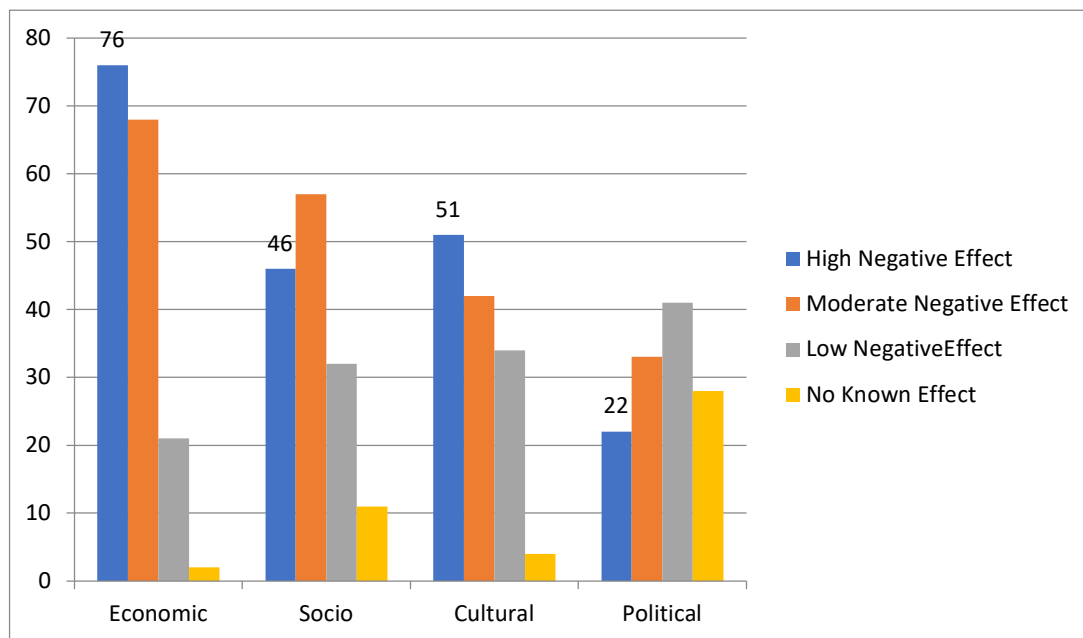


Source: Researchers Field Survey, 2023

Fig. 5: The Contemporary State of Cultural Livelihood in Kogi State.

has served as a means of income generation for communities, states, and individuals. Many people survive by practicing their cultural livelihood. It has also served as a means of additional income for families, as many civil servants are also involved in some of the cultural livelihoods like fishing, farming, and garment making. It brings about communal living and a show of identity. It had also been a contributing factor that affected the competitiveness and viability of the overall tourism product in some communities in the state.

The effects of the contemporary state of the cultural livelihood were assessed as shown in Fig. 6. About 76% of the participants revealed that the contemporary state of the cultural livelihood has a high negative effect, particularly on the economic environment, with Moderate negative effect (57%) on the social environment, High negative effect (51%) on the cultural environment and 22% High Negative effect on the political environment. Most participants, including men and women (youth and adults), display the



Source: Researchers' survey 2023

Fig. 6: The Effects of the Contemporary State of Cultural Livelihood on the Environment.

effects of the contemporary state of cultural livelihoods on the environment. Many cultural livelihoods, like farming, weaving, and harvest festivals, have significant effects. The following remarks are the consensus reached in one of the FGDs.

We find it difficult to go to the farm now. Many of us have large farms where we cultivate things like yam, rice, and other local foods, but some of us cannot go to such farms because of insecurity challenges. Many of us opted to get land close to the neighborhoods', and you cannot get such massive land close by. Money is another challenge. As farmers, you pay some people to work on the farms, as you cannot do it alone, particularly the elders. The majority of us do farming as our job, and it serves as a means of livelihood, but now we are finding it difficult to make a living out of it. Many have lost interest in this job and are searching for other means of livelihood. (Male and female youth, FGD 2023).

#### Another Remark Reaches by One FGD

Fishing is our primary occupation. Both the youth and adults do fishing, particularly the males. Even though some do fish as a part-time job to substitute for the circular job, many adults and youth take up fishing occupations and make a living out of it. However, incessant flooding and security challenges have also been an impending factor for the fishing industry. People come from various states to buy fish from us; we no longer get markets as usual. As a result, the fishing industry dwindled. We also display our produce

in the "festival of harvest," where people come around to patronize us. But for a long time, we have not done that.

The "festival of harvest" is an opportunity to see friends and relatives and enjoy ourselves together, and the hardest-working farmers, such as big yam producers, rice producers, and the biggest fish catch, get awards, but this has not been done for some period now (Male and Female Adult FGD 2023). Many of our youth are losing interest in some of our cultural livelihoods, like farming, in search of white-collar jobs. The crime rate is increasing as youths lose interest in farming activities due to insecurity and flooding in particular.

Summary analyses in Fig. 6 show that the contemporary state of cultural livelihoods affects every aspect of the country but more adversely on the socio-economic development of Nigeria. This finding is inconsistent with the opinion of Ekundayo (2022) and Chukwurah & Onyekwelu (2022) that cultural livelihood could boost economic development by way of generating substantial economic returns from investments made to safeguard cultural heritage, which can, in turn, be used to support conservation, local employment, and the socio-cultural development of the community.

#### Implications of the Findings

The implication of the findings can be deduced from the qualitative analyses of the questionnaire survey and FGDs on the perception effect of cultural livelihood on the environment. The contraction between the questionnaire

survey and FGDs shows that the findings support each other. For example, the questionnaire survey on the predominant cultural livelihood and contemporary state of cultural livelihood supports the respondents' opinion of the FGDs' findings that the contemporary state of the cultural livelihood is on the verge of extinction. Also, the findings from the data analyses of the respondent's perception of the effects of the contemporary state of the cultural livelihood on the environment support the FGD discussion that the contemporary state of cultural livelihood has a high negative effect on the economy, moderate negative effect on the social and cultural environment, and low effect on the political environment. Further implication of the findings can be deduced from the predominant cultural livelihood, considering that no previous study was conducted at this level in the study area.

### Limitations and Recommendations

The lack of reliable data about the total population of people involved in cultural livelihood at the grass root level in the state is a limitation, as only some whose cultural livelihood is their major source of income and are in associations are willing to participate and respond to the questionnaires, and it made it difficult to identify participant who was willing to response to questionnaires. However, 210 out of 240 questionnaires retrieved are very useful for the analysis, considering no inferential statistics were performed on the questionnaires in the current study. The study focuses on some of the major cultural livelihoods, but there may still be other areas of cultural livelihood that may be significant to the development of the state that this study did not consider. Also, the effects of the contemporary state of cultural livelihood on the environment may be broad and not have been covered in detail in the study.

Based on the limitations and research findings, the study, therefore, makes some recommendations, such as the conservation and preservation of cultural livelihood. The study discovered that cultural livelihood is on the verge of extinction. For example, the festival of harvest, where farmers display and market their produce like yam, fish, and rice in their different produce, attains affordable prices, has not been held for some time. This culture is gradually fading away. The people are encouraged during the festival of harvest as the largest farmer. For example, the largest fish producers are awarded a prize. This serves as a means of encouraging the farmers and it also encourages communal life. Therefore, the community leaders with the assistance of the state governments, should find a means of reviving the culture of harvest as one of the ways of conserving and preserving cultural livelihood in Nigeria, particularly in the study area. The three fundamental levels of administration,

such as federal, state, and local governments, should create a conducive environment for the practice of cultural livelihood, particularly in the aspect of insecurity. The provision of modern equipment and funds to the grassroots, the provision of adequate social welfare services, and the enhancement of cultural livelihood activities are also very necessary.

### CONCLUSIONS

The study shows that cultural livelihood has been affected, and the effects are high on the socio-economic lives of the people in the study area. The downturns in livelihoods can be traced to poor administration and climate change. Therefore, concerted efforts are paramount to providing leadership and modalities to mitigate climate challenges. Fundamentally, state interventions should be geared towards improving the deplorable livelihood conditions in the state. The study created awareness of the cultural livelihood in Nigeria, particularly in Kogi state, which may be similar to other cities in Africa. The information provided in the current study is very crucial for decision-makers, and it also contributes to urban and regional planning as a strategic action for improving and achieving urban and regional sustainability by integrating conservation and preservation into the urban and regional planning process. Future research should consider a detailed study of specific areas of the effect (such as cultural or socio-economic) of cultural livelihood on the physical environment for sustainable development. Also, a detailed study of cultural livelihood can be broken down to a particular community or local government area.

### REFERENCES

- AIC, 2005. *American Institute for Conservation (AIC) Foundation for Advancement in Conservation*. AIC
- Akinwale, A.A., 2011. Livelihoods and environmental challenges in coastal communities of Nigeria. *Journal of Sustainable Development in Africa*, 12, pp. 79-88.
- Beier, B., 1980. *Health Culture in the Heartland*. Springer
- Carney, D., 1998. *Sustainable Rural Livelihoods: What Contributions Can We Make?* London Department for International Development.
- Chambers, R. and Conway, G., 1992. *Sustainable Rural Livelihoods: Practical Concepts for the 21st Century*. Brighton Institute of Development Studies.
- Chukwurah, G.O., 2022. Preservation of urban historic and cultural heritage site in Delta State, Nigeria. *International Journal of Science and Management Studies (IJSMS)*, 5(2), p.105. <https://doi.org/10.51386/25815946/ijsms-v5i2p105>.
- Chukwurah, G.O. and Onyekwelu, E., 2020. Conservation of eco-tourism sites in Nigeria. *Journal of Environmental Engineering and Studies*, 6(1), p.395. <http://doi.org/10.5281/zenodo.3740395>.
- Cobbinah, P.B., 2021. Urban resilience in climate change hotspot. *Land Use Policy*, 100, p.104948.
- Ellis, F., 1999. *Rural livelihoods and diversity in developing countries*. Oxford University Press.
- Enoguanbhor, E.C., Chukwurah, G.O., Enoguanbhor, E., John-Nsa, C., Isimah, M.O., Edo, I., Achenui, R., Matemilola, S., Cheforfotang, U.I. and Ibrahim, E., 2023. Evaluating urban land-use demarcation and

- implementation for various urban functions using GIS and survey-based data: The case of Abuja City, Nigeria. *Town and Regional Planning*, 83, pp. 45-56.
- Feldman, R., 2000. The ethics of belief. *Philosophy and Phenomenological Research*, 60(3), pp. 667-695.
- George, W., 2010. *Co-Modifying Local Culture for Tourism Development and Community Sustainability*. Library Congress Press.
- Grbich, C., 2007. *Qualitative data analysis: An introduction*. London: Sage.
- Hari, S., 2020. Heritage and conservation strategies: understanding the justifications and implications. *Policy Analysis Series*, 2, p.100.
- John-Nsa, C.A., 2021. Understanding the factors influencing the spatial dynamics of informal settlements: The case of Enugu City, Nigeria. *Town and Regional Planning*, 79, pp. 29-43. <http://dx.doi.org/10.18820/2415-0495/trp79i1.5>
- Moyo, T. and Crafford, G., 2010. The impact of hyperinflation on the Zimbabwean construction industry. *Acta Structilia*, 17(2), pp. 53-83.
- Njoku, M. and Nwaogwugwu, O., 2014. Cultural factors affecting livelihood strategies of rural households in Southeast Nigeria: Implication for agricultural agenda. *Russian Journal of Agricultural and Socio-Economic Science*, 47(6), pp.530-541.
- Onyekwere, A. and Nworgu, K.O., 2020. Threats to rural livelihoods in Nigeria: Implications for social order and crisis management. *Advances in Applied Sociology*, 10(3), p.4. <http://doi.org/10.4236/aasoci.2020.103004>.
- Onyima, B.N., 2016. Cultural heritage: preservation, challenges, and prospects. *A New Journal of African Studies*, 12, pp. 274–292.
- Raven, P.H., 2003. *The Environmental Challenge*. England Natural History Museum
- Sarfo-Mensah, P. and Oduro, W., 2007. Traditional natural resources management practices and biodiversity conservation in Ghana: A review of local concepts and issues on change and sustainability. *Fondazione Eni Enrico Mattei*, 17, p.149
- UNESCO, 2015. International Conference on “Culture for Sustainable Cities” held in New York on 25-27.
- Wallman, S., 1984. *Eight London Households*. London: Tavistock.

---

#### ORCID DETAILS OF THE AUTHORS

- G. O. Chukwurah: <https://orcid.org/0000-0002-2356-0591>
- N. M. Aguome: <https://orcid.org/0000-0002-6668-9731>
- M. O. Isimah: <https://orcid.org/0000-0003-4679-5788>
- E. C. Enoguanbhor: <https://orcid.org/0000-0003-4752-3063>
- N. E. Obi-Aso: <https://orcid.org/0000-0001-7421-3912>
- O. C. Nnamani: <https://orcid.org/0000-0001-5729-3922>



# Process Optimization for *Madhuca indica* Seed Kernel Oil Extraction and Evaluation of its Potential for Biodiesel Production

S. Sudalai<sup>1</sup>, S. Prabakaran<sup>2</sup>, M. G. Devanesan<sup>1</sup> and A. Arumugam<sup>2†</sup>

<sup>1</sup>Department of Chemical Engineering, Annamalai University, Chidambaram, Tamil Nadu, India

<sup>2</sup>Bioprocess Intensification Laboratory, Centre for Bioenergy, School of Chemical & Biotechnology, SASTRA Deemed University, Thirumalaisamudram, Tamil Nadu, Thanjavur, India

†Corresponding author: A. Arumugam; aruchemxl@sabt.sastra.edu

Nat. Env. & Poll. Tech.  
Website: [www.neptjournal.com](http://www.neptjournal.com)

Received: 11-03-2024

Revised: 22-04-2024

Accepted: 01-05-2024

## Key Words:

Solvent extraction

Cu@dolomite

*Madhuca indica* oil

Response surface methodology

Biodiesel

## ABSTRACT

The current research aims to optimize the solvent-based oil extraction process from Mahua (*Madhuca indica*) seed using response surface methodology and biodiesel production using heterogeneous catalysts. The oil extraction was varied through the levels of process parameters including extraction temperature (60 to 80 °C), solvent-to-seed ratio (3 to 9 wt/wt), and time (2 to 4 h). The experiments were designed following the Central Composite model. The regression model provided optimal values for the selected process parameters based on the extraction yield percentage. To ensure the model's reliability, it was experimentally validated. Maximum experimental oil yields of 50.9% were obtained at an optimized extraction scenario of 70 °C extraction temperature, solvent-to-seed ratio of 6 wt/wt, and time 4 h. The extracted oil's physicochemical properties and fatty acid composition were tested. Also, using copper-coated dolomite as a catalyst, the extracted oil was transformed into biodiesel via transesterification. The FAME (94.31%) content of the prepared biodiesel was determined via gas chromatography. As a result, the findings of this study will be useful in further research into the use of *Madhuca indica* as a potential feedstock for biodiesel production.

## INTRODUCTION

Fast economic growth around the world has caused an increase in unusual energy demand. The majority of energy requirements are met by fossil fuels such as petroleum and coal (Hong et al. 2023). As a result, the fuel reserves are gradually depleted. Beyond that, greenhouse emissions from fossil fuels harm global weather. In addition, the use of fossil fuels contributed to up to 62% of the worldwide emissions of greenhouse gases (Mathiarasi & Partha 2016, Cako et al. 2022, Mukhtar et al. 2022). Likewise, the transport industry alone accounted for approximately 16% of total emissions. As a result, there is a quick need to look into sustainable and alternate forms of energy for worldwide use while attempting to reduce the environmental impact of growth (Borges & Díaz 2012, Keneni & Marchetti 2017, Krishnamoorthy et al. 2023).

A circular bioeconomy concept for biomass entails the sustainable, effective use of biological resources in a way that decreases waste and improves value for the resources' entire lifecycle. This strategy is consistent with the principles of the circular economy, which seeks to reduce, reuse, recycle,

and regenerate resources to develop a more resilient and environmentally friendly economy. Furthermore, future strategies for decarbonization are required to grow and establish renewables to reduce dependence on fossil fuels and safeguard the environment from climate change and air pollution (Jan et al. 2023). As an alternative to diesel, biodiesel is considered a promising option that can be used to address both the challenges of fossil fuel depletion and greenhouse gas emissions at the same time. Biodiesel's global popularity has grown in the past decade (Baskar et al. 2018, Milano et al. 2022, Mulyatun et al. 2022).

Biodiesel research has progressed, with an increasing focus on sustainability, lowering transportation fuel's carbon footprint, and energy security. Furthermore, technological advancements and greater awareness of feedstock options could have opened up new avenues for biodiesel production. Government policies promoting renewable fuels influenced both national and international research efforts. Researchers were investigating the efficacy of these policies as well as their effects on the biodiesel industry (Osman et al. 2021, Al-Muhtaseb et al. 2022). Biodiesel is made from renewable sources such as plant and animal waste, and a few plants,

such as *Jatropha* and *Calophyllum*, are specifically grown to produce biodiesel. *Madhuca indica* belongs to the Sapotaceae family, commonly known as Mahua or Indian Butter Tree, and has been considered a potential biofuel feedstock due to its oil-rich seeds and sustainability. *Madhuca indica* is found primarily in India's tropical and subtropical regions, as well as in parts of Southeast Asia. It grows in deciduous forests, tropical and subtropical regions, and is adaptable to a wide range of soil types. However, its successful use as a biofuel source would require addressing challenges related to yield variability, processing, infrastructure, and environmental impact (Tirkey et al. 2022).

As a result, biodiesel is viewed as an environmentally friendly, renewable source of energy that is less hazardous to the ecosystem than conventional energy derived from petroleum or diesel (Sá et al. 2021). Bio-oil can be extracted from biomasses in several ways, including solvent extraction, mechanical press, and enzymatic. While the extraction technique used by Soxhlet has several benefits, it also comes with some drawbacks (Salehzadeh et al. 2014, Jayakumar et al. 2021, Aparamarta et al. 2022). Long extraction times, the need for large solvent volumes, and the risk of thermal degradation for thermally sensitive compounds are among them. As a result, for effective bio-oil extraction, it is critical to consider these factors and optimize the extraction conditions in accordance. Abdi Sharma et al. examined the ultrasound amplitude level (20-40%), extraction time (30-60 min), and solvent-to-seed ratio (10-20 mL g<sup>-1</sup>) were the process parameters considered. The regression model provided optimal values for these process parameters, along with the related extraction yield (Thanikodi et al. 2023).

Following our comprehensive literature review, no optimization study regarding the extraction of oil from *Madhuca indica* has been reported. The findings contribute to filling a significant gap in the literature by providing a detailed and optimized approach to oil extraction from mahua seeds, followed by its conversion into biodiesel. Using RSM along with the central composite experimental designs, an optimized condition for solvent-based oil extraction from *Madhuca indica* was obtained. The objective of this research is to determine the effect of process parameters, including extraction time, temperature, and solvent-to-seed ratio, on the bio-oil yield from *Madhuca indica* seed. The obtained optimum process parameter levels from the regression model were validated through experimental results. The extracted oil was then characterized before being transformed into biodiesel via transesterification. Followed by the prepared biodiesel, also characterized by ASTM D6751 regulations.

## MATERIALS AND METHODS

### Oil Extraction

Soxhlet extraction was used for the extraction of mahua seed kernel oil. When compared to other procedures, the constant cycling of solvent through the sample facilitates an effective extraction of the oil and produces larger yields. Choosing the right solvent based on the type of substance to be extracted can be flexible when using Soxhlet extraction. Depending on the polarity and other characteristics of the oil, several solvents can be utilized. The seeds are collected from the ripe stage fruits fallen from the mahua tree, and the seeds were spread out to dry in an area with adequate ventilation. The drying process removes moisture in the seeds and sets them up for extraction.

After drying, the seeds' outer husk was removed, and afterwards the seeds were finely powdered. The ground seed powder is then used for oil extraction. The Soxhlet extraction method was followed for oil extraction using hexane as solvent. The thimble is filled with biomass, and the hot solvent extracts the desired compound from the powdered seeds. The chemical reaction continues to cycle with the system after extracting the compound from the sample. The desired compound gradually collects through the continuous boil and condensation of solvents. This process is repeated several times to ensure complete extraction.

The levels of influencing process parameters for the oil extraction process, including temperature (60 to 80°C), time (2 to 4 h), and solvent-to-oil ratio (3 to 9 wt/wt) were followed from previous studies (Rodríguez-Solana et al. 2014, Mujeeb et al. 2021, Mehdi et al. 2023). The experimental model with a total of twenty experiments was developed using RSM with the central composite approach. The obtained yield value from each test was entered into the model developed by the Design Expert to forecast the optimum values of each process parameter. A maximum of 50.9 % oil was extracted for the conditions of temperature (70 °C), time (4 h), and solvent-to-oil ratio (6 wt/wt). To remove any impurities or solid particles, the extracted oil is filtered. Fig. 1 shows the seeds are extracted by removing the skin and husk from the seed shell used for bio-oil extraction, kernel powder, and deoiled cake.

### Transesterification

The reaction rate and biodiesel yields are influenced by several factors, including the reaction duration, reaction temperature, methanol-to-oil molar ratio, and the weight percentage of the catalyst (Rocha-Meneses et al. 2023). Nanoparticle-doped catalysts have the potential to improve the efficiency and sustainability of biodiesel production.



Fig. 1: *Madhuca indica* Linn (a) Tree (b) (i) seed (ii) seed husk (iii) kernel (c) *Madhuca indica* oil (d) *Madhuca indica* deoiled cake.

They provide benefits such as increased catalytic activity, decreased waste, and potentially higher-quality biodiesel (Gurunathan & Ravi 2015).

The Teflon-coated reactor with a temperature-controlled magnetic stirrer was used for the biodiesel preparation from *Madhuca indica* oil. The condenser is positioned over the reactor to prevent methanol leakage through boiling. The suggested optimal reaction was run for 6 h at 75°C with a methanol to oil molar ratio of 20:1 and copper-coated dolomite catalyst of 5 wt.%. For the synthesis of biodiesel, copper-coated dolomite is preferred due to its catalytic activity, stability, reusability, and potential for enhanced transesterification process efficiency. This catalyst is a viable way to improve the biodiesel production processes' cost-effectiveness and sustainability.

Following the end of the reaction time, due to the difference in density, the reactants were allowed to settle with the layers of biodiesel, glycerol, and catalyst at the bottom. The glycerol was removed by gravity separation, followed by the catalyst being recovered from the mixture through a centrifuge process for the next reaction. In the end, to obtain pure biodiesel, the contaminants are removed by water wash and the suspended water particles are heated to evaporate. Fig. 2 represents the full process layout for oil extraction and biodiesel production.

### Response Surface Methodology

RSM is a statistical technique that helps in the understanding of the relationship between input variables and the output response of the model. Design Expert Version 12.0 was

employed to model the extraction's process parameters and optimize the operating conditions. The experimental model was designed through central composite design (CCD) because it offers an abundance of details with a minimum experiment. CCD is used to generate a sequence of experimental runs, each with its own set of factor levels, including the central point, factorial points, and axial points. Experiments are carried out using the CCD matrix, and the results are recorded. Regression analysis is used to fit a second-order polynomial model to the experimental data. The response surface is represented by this model. The response surface model is examined to determine factor effects, interactions, and surface curvature. Numerical optimization techniques can be used to find the optimal factor settings that maximize the output response. Once the optimal conditions have been determined, additional experiments may be carried out to confirm the predicted results. In this experimental work, A: temperature (h), B: solvent-to-seed ratio (wt/wt), and C: time (h) are the three selected independent variables based on previous literature. The table shows how each parameter in the experiment was coded to levels -1, 0, and +1. The optimized process parameter levels were identified through a regression model.

### FAME Analysis

The fatty acid composition of the extracted *Madhuca indica* oil was determined using gas chromatography (Shimadzu, SH-Rxi-5Sil Ms). It was further employed to determine the linolenic methyl ester percentage and fatty acid methyl ester (FAME) content of the produced biodiesel following the EN 14103:2011 standard.

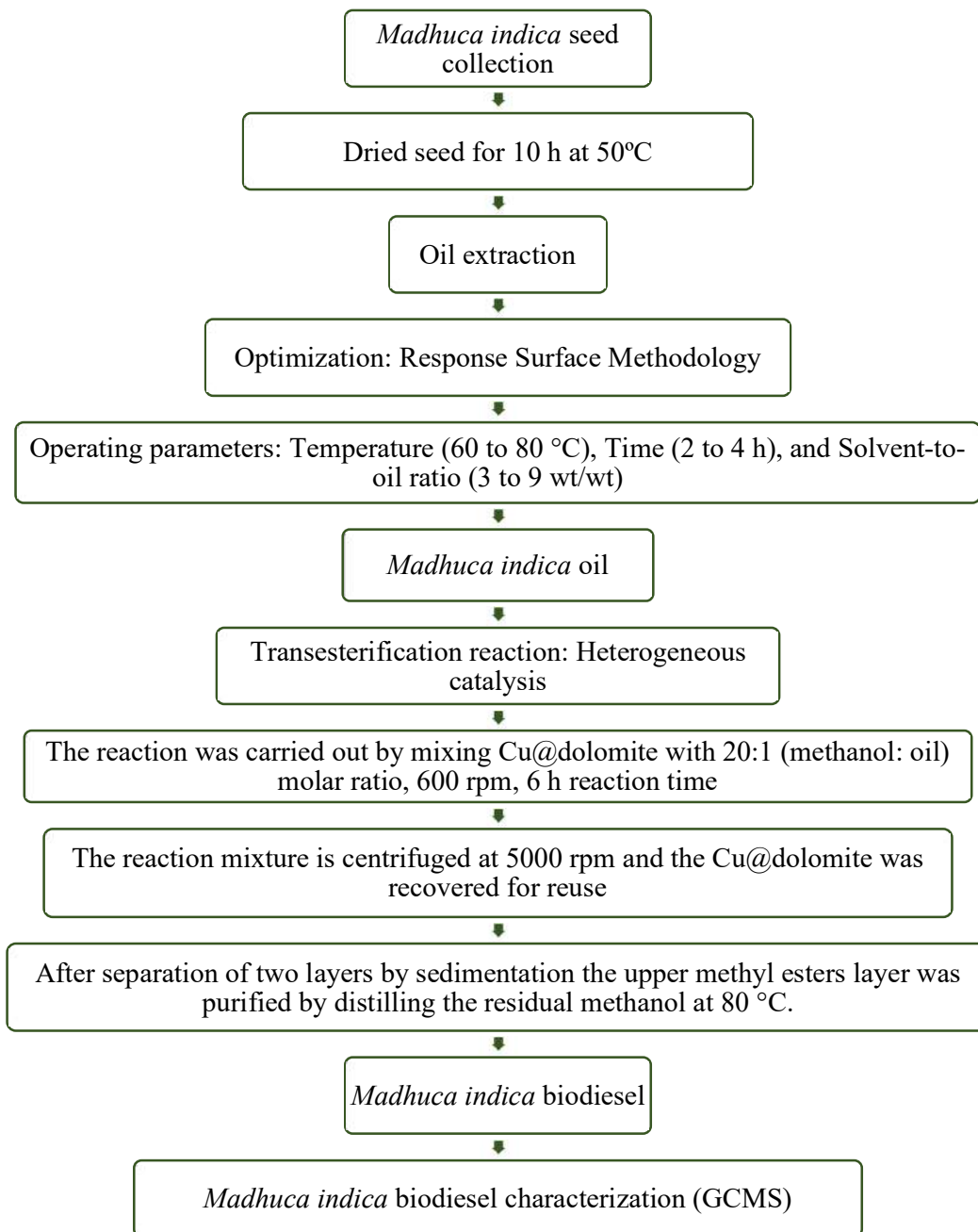


Fig. 2: Process layout for *Madhuca indica* oil extraction and biodiesel production.

## RESULTS AND DISCUSSION

### Response Surface Methodology for Oil Extraction

The Central Composite experimental model was used in the optimization work to investigate the effect of different variables, including temperature, time, and solvent-to-seed ratio, on *Madhuca indica* oil extraction yield. By

applying the previously mentioned coded levels, the central composite experimental model developed a total of 20 experiments shown in Table 1. The obtained yield value from each test was entered into the model developed by the Design Expert to forecast the optimum values of each process parameter. The *Maduca indica* oil yield was predicted by the second-order regression model equation (2). The regression



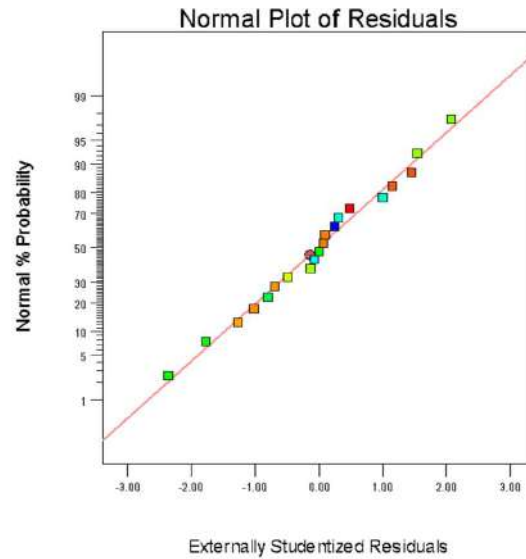


Fig. 3: Statistical analysis of the response surface quadratic model for a plot of normal % probability to externally studentized residual.

Table 1: Central composite design matrix and the responses of the dependent variable-biodiesel yield from *Madhuca indica* oil.

StdOrder	RunOrder	PtType	Blocks	T	S <sub>R</sub>	Time	Yield (wt%)	
							Experimental	Predicted
1	1	1	1	60	3	2	12.6	12.4
2	2	1	1	80	3	2	29.2	29.7
3	3	1	1	60	9	2	23.7	23.5
4	4	1	1	80	9	2	36.7	35.6
5	5	1	1	60	3	4	32.1	33
6	6	1	1	80	3	4	37.7	37.8
7	7	1	1	60	9	4	23.9	23.3
8	8	1	1	80	9	4	22.9	22.9
9	9	-1	1	60	6	3	31.8	31.8
10	10	-1	1	80	6	3	39.8	40.2
11	11	-1	1	70	3	3	37.3	35.9
12	12	-1	1	70	9	3	32.3	34.1
13	13	-1	1	70	6	2	45.5	46.5
14	14	-1	1	70	6	4	50.9	50.4
15	15	0	1	70	6	3	46.2	46.1
16	16	0	1	70	6	3	47.5	46.1
17	17	0	1	70	6	3	44.6	46.1
18	18	0	1	70	6	3	46.2	46.1
19	19	0	1	70	6	3	47.8	46.1
20	20	0	1	70	6	3	45.2	46.1

T (°C) - Extraction temperature; S<sub>R</sub>- solvent to seed ratio (wt/wt); θ (h)- Extraction time.

model provides optimal values for independent variables and their impact on the output by iteratively adjusting the model's coefficients during the training process to minimize the error between predicted and actual values. The final coefficients represent the model's estimate of the relationship between each independent variable and the output variable. The significance of regression model coefficients was analyzed using ANOVA, which is shown in Table 2.

According to the ANOVA results, the model's p-value is very low (less than 0.005), implying that the developed model is significant in predicting *Madhuca indica* oil yield (Kodgire et al. 2023). In addition, the p-value for the lack of fit is 0.419, which is regarded as insignificant. To determine how well the model fits the data, its coefficients and goodness-of-fit statistics were examined. In this way, it demonstrates that the developed regression model fits the experimental results well. The obtained  $R^2$  (0.9918) value depicts that the regression model describes over 99.18% of the variability in *Madhuca indica* oil extraction (Liu et al. 2023). The significant  $R^2$  value additionally suggests that data points were very close to the regression line, indicating that the experimental and predicted results agreed well, as shown in Fig. 3. The predicted values for the optimal conditions of temperature, time, and solvent-to-seed ratio were noted as 50.4%.

Meanwhile, to validate the model, the experiment was conducted at the optimum data points, and the

experimental yield was obtained as 50.9%. Nonetheless, the variation between the two values is relatively low (0.5%), demonstrating that the regression model is good at predicting *Madhuca indica* seed extraction yield (Sundaramahalingam et al. 2021, Dharmalingam et al. 2023).

#### % oil extraction

$$= 15.74 T + 22.68 S_R + 20.18 \theta - 0.10 T^2 - 1.23 S_R^2 + 2.36 \theta^2 - 0.043 T \times S_R - 0.31 T \times \theta - 1.734 S_R \times \theta - 619.8$$

Fig. 4 shows, Three-dimensional plots to examine the effect of process parameters (extraction temperature, extraction time, and solvent-to-seed ratio) in the *Madhuca indica* oil extraction yield. Overall, it has been discovered that a specific range of values for each variable leads to a rise in oil yield. When the parametric values crossed the specified range, the extraction yield decreased, resulting in non-optimal operating conditions.

Fig. (4. a) shows the combined effect between solvent-to-seed ratio and temperature on oil yield. The convex pattern shows that the central points play the dominant role. Oil yield improves significantly as seed to seed-to-solvent ratio and extraction temperature increase until the central data point is reached. After this point, the oil yield begins to fall. When the seed-to-solvent ratio is from 3 to 6 wt/wt, the extracted oil yield increases, whereas a similar case is observed when the extraction temperature is varied from 60 to 70°C.

Table 2: Analysis of Variance for biodiesel yield from *Madhuca indica* oil.

Source	DF	Adj SS	Adj MS	F-Value	P-Value
Model	9	2058.25	228.694	133.72	0.000
Linear	3	226.21	75.404	44.09	0.000
T	1	178.51	178.506	104.37	0.000
$S_R$	1	8.78	8.780	5.13	0.047
$\theta$	1	38.93	38.927	22.76	0.001
Square	3	1523.85	507.949	296.99	0.000
T*T	1	279.69	279.695	163.54	0.000
$S_R * S_R$	1	338.52	338.522	197.93	0.000
$\theta * \theta$	1	15.25	15.252	8.92	0.014
2-Way Interaction	3	308.19	102.729	60.06	0.000
T* $S_R$	1	13.16	13.158	7.69	0.020
T* $\theta$	1	78.50	78.500	45.90	0.000
$S_R * \theta$	1	216.53	216.528	126.60	0.000
Error	10	17.10	1.710		
Lack-of-Fit	5	9.37	1.875	1.21	0.419
Pure Error	5	7.73	1.546		
Total	19	2075.35			

$R^2 = 98.18\%$ ;  $R^2$  (pred) = 95.23%;  $R^2$  (adj) = 98.43%

T (°C) - Reaction temperature;  $S_R$  - solvent to seed ratio (wt/wt);  $\theta$  (h)- Reaction time.

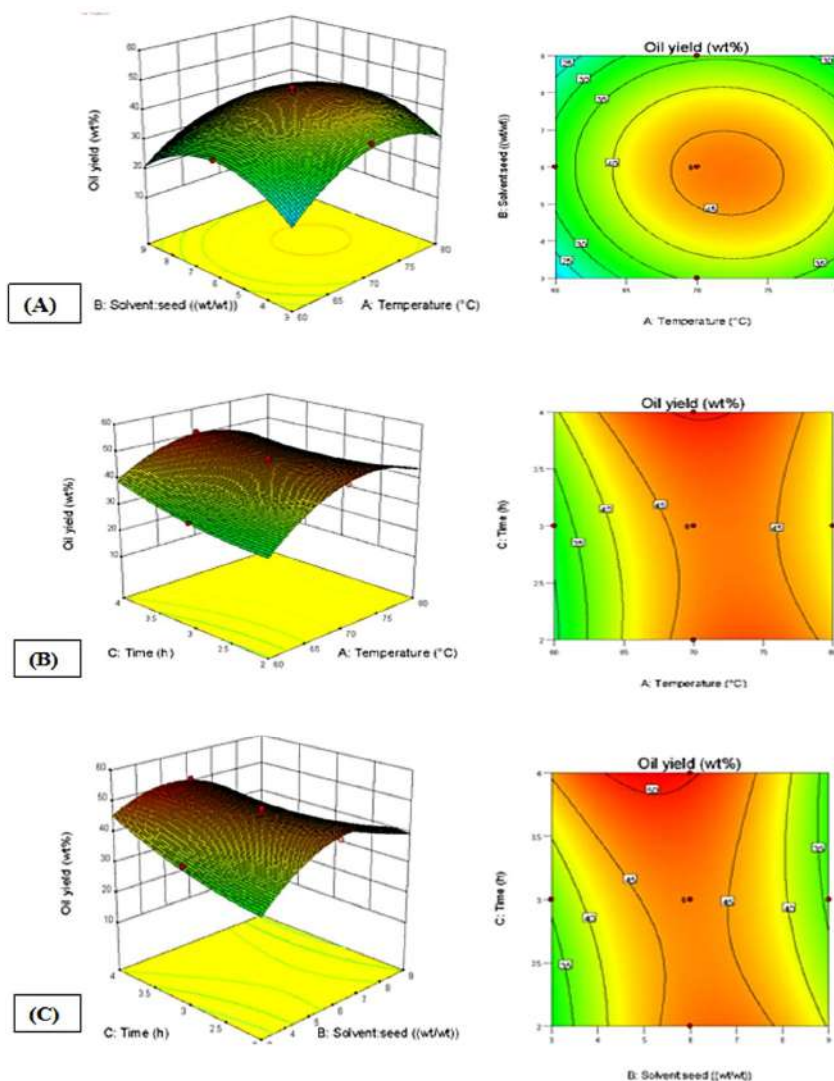


Fig. 4: Response surface graph showing interaction effects between solvent: seed ratio and temperature (A), temperature and time (B), and solvent: seed ratio and time (C).

Fig. (4. b) shows oil yield rises as extraction time increases. The reaction goes for a longer period as time increases. As a result of this phenomenon, more amount of heat is produced (Prabakaran et al. 2021, Sebyang et al. 2023). This could lead to the breaking down of the cell wall, allowing the solvent molecule to penetrate the cell. Fig. (4. c) demonstrates a 3D plot of the interaction between solvent-to-seed ratio and extraction time. The catalyst weight (%) increased to 6wt%, which marked a considerable rise in the percentage output of biodiesel. Still, because of the high rate of mass transfer resistance in the transesterification process using the excess catalyst, increasing the catalyst content further reduces the output of biodiesel. While the solvent-to-seed ratio ranges from 3 to 6 % wt/wt,

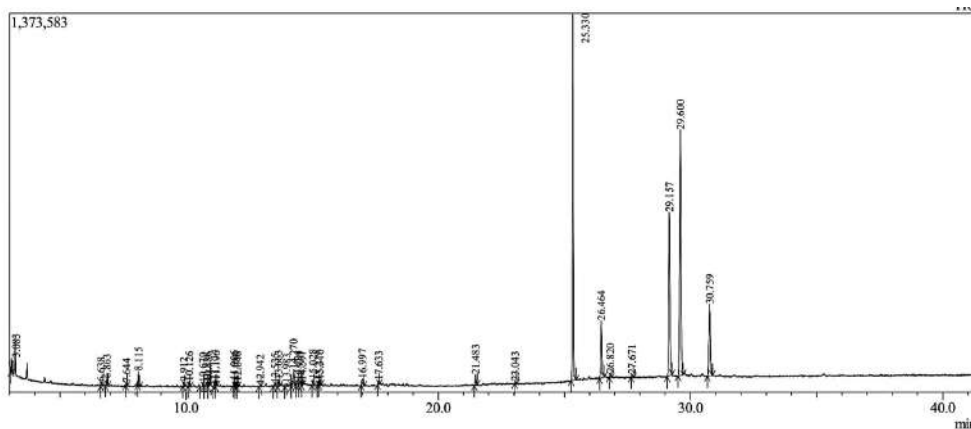
the oil yield increases, resulting in a maximum yield of 50.9%.

### Quality Analysis of Biodiesel

Individual FAMES in a biodiesel sample can be separated and identified using GC-MS. Table 3 illustrates the FAME amount in *Madhuca indica* biodiesel as estimated by gas chromatography. Fig. 5 represents the overall GC-MS result of *Madhuca indica* biodiesel. EN 14103:2011 suggests a minimal FAME level of 90 %wt/wt, with linolenic acid methyl ester (C18:3) linolenic ranging between 1 and 15 (wt/wt). The FAME percentage of *Madhuca* biodiesel is 94.31 %wt/wt, which is significantly higher than the EN 14103:2011 recommended value.

Table 3: GC-MS result of *Madhuca indica* biodiesel.

Peak#	Retention time	Area %	Name
1	3.083	0.77	2-Butene, 1-chloro-2-methyl-
2	6.638	0.32	3-Hydroxy-3-methyl-2-butanone
3	6.863	0.63	Nonane, 5-(2-methyl propyl)-
4	7.644	0.16	1,1-Dimethyl-3-chloropropanol
8	10.67	0.28	Heptadecane, 2,6,10,15-tetramethyl-
9	10.126	0.61	Pentadecane
11	11.134	0.47	Eicosane
17	13.535	0.34	Tetradecanoic acid, 12-methyl-, methyl ester
18	13.663	0.49	Nonadecane
27	16.997	0.78	Pentadecanoic acid, 14-methyl-, methyl ester
28	17.633	0.27	2-Methyltriacontane
29	21.483	1.02	Methyl tetradecanoate
30	23.043	0.14	2-Butenedioic acid (Z)-, dibutyl ester
31	25.33	31.81	Hexadecanoic acid, methyl ester
33	26.82	0.39	Phenol, 3,5-bis(1,1-dimethyl ethyl)-
34	27.671	0.28	Benzoic acid, 2-methyl-, (2-isopropyl-5-methyl
35	29.157	20.04	Methyl stearate
36	36 29.600	30.96	9-Octadecenoic acid (Z)-, methyl ester
37	37 30.759	10.24	9,12-Octadecadienoic acid (Z, Z)-, methyl ester

Fig. 5: Overall GC-MS result of *Madhuca indica* biodiesel.

The physicochemical properties of *Madhuca indica* bio-oil and biodiesel are shown in Table 4. The density of biodiesel may be measured at a temperature of 15°C, which makes it possible to characterize its mass per unit volume in relation to storage and transit conditions. Density at room temperature is frequently used to evaluate the quality and suitability of biodiesel to requirements. As this temperature is more indicative of the conditions under which biodiesel is typically utilized, particularly in diesel engines, the kinematic viscosity of biodiesel is evaluated at 40°C. Diesel engines run at high temperatures; thus, biodiesel is usually mixed with diesel to be used as fuel. It is possible to evaluate how well the biodiesel flows and lubricates under operating circumstances by measuring the kinematic viscosity at 40°C.

Table 4: Physicochemical properties of *Madhuca indica* bio-oil and biodiesel.

Properties	Diesel	<i>Madhuca indica</i> bio-oil	<i>Madhuca indica</i> Biodiesel
Density @ 15°C [g.cc <sup>-1</sup> ]	0.834	0.960	0.870
Kinematic viscosity @ 40°C [cSt]	2.5	24.7	5.2
Calorific value [MJ.kg <sup>-1</sup> ]	43.5	36.5	35.0
Cetane number	45	46	52
Flashpoint [°C]	51	232	148
Pour point [°C]	-21.2	8	2.67
Iodine Number [gI <sub>2</sub> ,100g <sup>-1</sup> ]	38.3	88	70
Water Content [%]	-	0.02	-

Table 5: A comparison of current investigations with earlier studies

Biomass	Operating Conditions	Yield	Reference
<i>Madhuca indica</i>	Soxhlet technique: Temperature - 70°C; reaction time 4 h and Solvent-to-seed ratio of 6 wt/wt, Solvent – n-hexane; Transesterification: Reaction time 6 h at 75 °C with a methanol to oil molar ratio of 20:1 and copper-coated dolomite catalyst 5 wt.%	Bio-oil Yield 50.9% Biodiesel Yield 94.31%	Present
<i>Madhuca indica</i>	Ultrasonication technique: temperature 50°C, Contact time 20 min, seed to solvent ratio (diethyl ether:ethanol) 1:10 (3:1)	Bio-oil Yield 82%	(Baskar et al. 2018)
<i>Stoechospermum marginatum</i>	Soxhlet technique; Temperature - 45°C; reaction period – 72 h; Solvent – n-hexane;	Bio-oil Yield 24.4%	(Venkatesan et al. 2017)
<i>Sargassum wightii</i>	Soxhlet technique; reaction period – 12 h; solvent-to-solid ratio – 6:1	Bio-oil yield – 25%	(Kumar et al. 2015)
<i>Azolla microphylla</i>	Soxhlet technique; Solvent - chloroform and methanol (2:1); Reaction temperature 65°C; Reaction time 12 h	Bio-oil yield – 17%	(Thiruvengkatachari et al. 2021)
<i>Cladophora</i> sp.	Soxhlet technique; Reaction time 18 h; Solvent – Trichloethylene [1:10 g.mL <sup>-1</sup> ]	Bio-oil yield – 31.1%	(Firemichael et al. 2020)
<i>Madhuca indica</i>	Transesterification: Reaction temperature 60 °C; Methanol-to-oil ratio (6:1 molar ratio) and 0.7% w/v KOH as an alkaline catalyst to produce biodiesel	Biodiesel yield – 98%	(Ghadge & Raheman 2006)
Ulva lactuca	Transesterification: Oil to methanol molar ratio 1:12; Catalyst loading 1.5 wt%; Reaction temperature 63°C; Reaction time 1.7 h	Biodiesel yield – 88.77%	(Binhweel et al. 2023)
Azolla pinnata	Transesterification: Methanol to oil molar ratio 30:1; heterogeneous catalyst weight 4%; operation temperature 70°C	Biodiesel yield – 88.7%	(Prabakaran et al. 2021)
Waste and crude vegetable oils	Heterogonous acid Catalysts (Activated Carbon supported-SO <sub>3</sub> H, SBA-15, HPA); Solvent – Methanol.	Biodiesel yield – 90%	(Hara 2010)
Canola oil, rapeseed oil, waste cooking oil	Hydroxyapatite catalyst from waste quail beaks (7 wt %); reaction time (4 h); oil to methanol molar ratio (1:12);	Biodiesel yield – 89.4, 96.7 and 91.7%	(Khan et al. 2020)
Triacetin	Base supported carbon catalysts CaO supported on nanoporous carbon (NC-2); reaction time (4 h); oil to methanol molar ratio (1:6); Temperature 60°C.	Biodiesel yield – 99%	(Zu et al. 2010)

The methodology, process parameters, and output responses of the present experimental study for both bio-oil extraction and biodiesel production were compared with the previous studies in Table 5. When evaluating the potential of mahua oil for biodiesel production, a number of critical metrics, including fatty acid composition, viscosity, and cold flow qualities, can be used to compare the quality of the oil to other feedstocks. Every feedstock has a distinct composition and set of characteristics that affect the final biodiesel's applicability and quality.

## CONCLUSION

In summary, *Madhuca indica* has the potential to be a valuable biofuel feedstock due to its high oil content and sustainability. The present research aimed to optimize oil extraction from *Madhuca indica* seed via RSM with a central composite experimental design. The optimal values for the independent variables analyzed for the solvent extraction were 70 °C, 6 %wt/wt, and 4 h for extraction temperature, solvent-to-seed ratio, and time, respectively. Under this optimized scenario, the forecasted and experimental oil yields were 50.4% and 50.9%, respectively, which demonstrates

the regression model's reliability. The physicochemical properties were measured as per ASTM D6751 regulations. The biodiesel was produced from the extracted oil with a 94.31% yield through transesterification. The measured physicochemical properties of biodiesel were within the specified ranges of ASTM D6751. As a result, *Madhuca indica* seeds can be considered a viable feedstock for the production of biodiesel. Future research direction for this experimental work is to improve extraction efficiency and consider using innovative technologies such as ultrasound-assisted extraction or microwave-assisted extraction. Furthermore, a life cycle analysis (LCA) has to be conducted to assess the environmental sustainability of *Madhuca indica* seed kernel oil-derived biodiesel production and use.

## REFERENCES

- Al-Muhtaseb, A.H., Jamil, F., Osman, A.I., Tay Zar Myint, M., Htet Kyaw, H., Al-Hajri, R., Hussain, M., Ahmad, M.N. and Naushad, M., 2022. State-of-the-art novel catalyzed synthesized from waste glassware and eggshells for cleaner fuel production. *Fuel*, 330, p.125526.
- Aparamarta, H.W., Gunawan, S., Ihsanpuro, S.I., Safawi, I., Bhuana, D.S., Mochtar, A.F. and Yusril Izhar Noer, M., 2022. Optimization and kinetic study of biodiesel production from nyamplung oil with microwave-assisted extraction (MAE) technique. *Heliyon*, 8 (8).
- Baskar, G., Naveenkumar, R., Mohanapriya, N., Nivetha, S.R. and Aiswarya, R., 2018. Optimization and kinetics of ultrasonic assisted bio-oil extraction from *Madhuca indica* seeds. *Industrial Crops & Products*, 124 (February), pp.954-959.
- Binhweel, F., Pyar, H., Senusi, W., Shaah, M.A., Hossain, M.S. and Ahmad, M.I., 2023. Utilization of marine ulva lactuca seaweed and freshwater *Azolla filiculoides* macroalgae feedstocks toward biodiesel production: Kinetics, thermodynamics, and optimization studies. *Renewable Energy*, 205, pp.717-730.
- Borges, M.E. and Díaz, L., 2012. Recent developments on heterogeneous catalysts for biodiesel production by oil esterification and transesterification reactions: A review. *Renewable and Sustainable Energy Reviews*, 16(5), pp.2839-2849.
- Cako, E., Wang, Z., Castro-Muñoz, R., Rayaroth, M.P. and Boczkaj, G., 2022. Cavitation based cleaner technologies for biodiesel production and processing of hydrocarbon streams: A perspective on key fundamentals, missing process data and economic feasibility – A review. *Ultrasonics Sonochemistry*, 88, p. 978.
- Dharmalingam, B., Balamurugan, S., Wetwatana, U., Tongnan, V., Sekhar, C., Paramasivam, B., Cheenkachorn, K., Tawai, A. and Sriariyanun, M., 2023. Comparison of neural network and response surface methodology techniques on optimization of biodiesel production from mixed waste cooking oil using heterogeneous biocatalyst. *Fuel*, 340, p.127503.
- Firemichael, D., Hussen, A. and Abebe, W., 2020. Production and characterization of biodiesel and glycerine pellet from macroalgae strain: *Cladophora glomerata*. *Bulletin of the Chemical Society of Ethiopia*, 34 (2), pp.249-258.
- Ghadge, S.V. and Raheman, H., 2006. Process optimization for biodiesel production from mahua (*Madhuca indica*) oil using response surface methodology. *Bioresource Technology*, 97, pp.379-384.
- Gurunathan, B. and Ravi, A., 2015. Process optimization and kinetics of biodiesel production from neem oil using copper-doped zinc oxide heterogeneous nanocatalyst. *Bioresource Technology*, 190, pp.424-428.
- Hara, M., 2010. Biodiesel production by amorphous carbon bearing SO<sub>3</sub>H, COOH, and phenolic OH groups, a solid Brønsted acid catalyst. *Topics in Catalysis*, 53(11-12), pp.805-810.
- Hong, Z., Chu, J., Zhang, L.L. and Wang, N., 2023. Recycling channel selection for a manufacturer involving consumers' green-return behavior. *IEEE Transactions on Engineering Management*, 6162, p. 121415.
- Jan, H.A., Osman, A.I., Al-Fatesh, A.S., Almutairi, G., Surina, I., Al-Otaibi, R.L., Al-Zaqri, N., Kumar, R. and Rooney, D.W., 2023. Biodiesel production from *Sisymbrium irio* as a potential novel biomass waste feedstock using homemade titania catalyst. *Scientific Reports*, 13(1), p.11282.
- Jayakumar, S., Bhuyar, P., Pugazhendhi, A., Rahim, M.H.A., Maniam, G.P. and Govindan, N., 2021. Effects of light intensity and nutrients on the lipid content of marine microalga (diatom) *Amphiprora* sp. for promising biodiesel production. *Science of the Total Environment*, 768, p.145471.
- Keneni, Y.G. and Marchetti, J.M., 2017. Oil extraction from plant seeds for biodiesel production. *AIMS Energy*, 5 (2), pp.316-340.
- Khan, H.M., Iqbal, T., Ali, C.H., Yasin, S. and Jamil, F., 2020. Waste quail beaks as a renewable source for synthesizing novel catalysts for biodiesel production. *Renewable Energy*, 154, pp.1035-1043.
- Kodgire, P., Sharma, A. and Kachhwaha, S.S., 2023. Optimization and kinetics of biodiesel production of *Ricinus communis* oil and used cottonseed cooking oil employing synchronized 'ultrasound + microwave' and heterogeneous CaO catalyst. *Renewable Energy*, 212, pp.320-332.
- Krishnamoorthy, N., Pathy, A., Kapoor, A. and Paramasivan, B., 2023. Exploring the evolution, trends, and scope of microalgal biochar through scientometrics. *Algal Research*, p.102944.
- Kumar, P.S., Pavithra, J., Suriya, S., Ramesh, M. and Kumar, K.A., 2015. *Sargassum wightii*, a marine alga, is the source for the production of algal oil, bio-oil, and application in dye wastewater treatment. *Desalination and Water Treatment*, 55 (5), pp.1342-1358.
- Liu, Y., Sayed, B.T., Sivaraman, R., Alshahrani, S.M., Venkatesan, K., Thajudeen, K.Y., Al-Bahrani, M., Hadrawi, S.K. and Yasin, G., 2023. Novel and robust machine learning model to optimize biodiesel production from algal oil using CaO and CaO/Al<sub>2</sub>O<sub>3</sub> as catalyst: Sustainable green energy. *Environmental Technology and Innovation*, 30, p.103018.
- Mathiarasi, R. and Partha, N., 2016. Optimization, kinetics, and thermodynamic studies on oil extraction from *Daturametel* Linn oil seed for biodiesel production. *Renewable Energy*, 96, pp.583-590.
- Mehdi, R., Naqvi, S.R., Khan, A.A. and Mirani, A.A., 2023. Optimization of olive oil extraction from olive pomace using solvent extraction and response surface methodology analysis of oil yield. *Fuel*, 348, p.128633.
- Milano, J., Shamsuddin, A.H., Silitonga, A.S., Sebayang, A.H., Siregar, M.A., Masjuki, H.H., Pulongan, M.A., Chia, S.R. and Zamri, M.F.M.A., 2022. Tribological study on the biodiesel produced from waste cooking oil, waste cooking oil blends with *Calophyllum inophyllum*, and its diesel blends on lubricant oil. *Energy Reports*, 8, pp.1578-1590.
- Mujeeb, O.K., Anjali, A.E. and Sathiyarayanan, K., 2021. Extraction, characterization, and optimization of high-quality bio-oil derived from waste date seeds. *Chemical Engineering Communications*, 208 (6), pp.801-811.
- Mukhtar, A., Saqib, S., Lin, H., Ul, M., Shah, H., Ullah, S., Younas, M., Rezakazemi, M., Ibrahim, M., Mahmood, A., Asif, S. and Bokhari, A., 2022. Current status and challenges in the heterogeneous catalysis for biodiesel production. *Chemical Engineering Journal*, 157 (May 2021).
- Mulyatun, M., Prameswari, J., Istadi, I. and Widayat, W., 2022. Production of non-food feedstock based biodiesel using acid-base bifunctional heterogeneous catalysts: A review. *Fuel*, 314, p.122749.
- Osman, A.I., Qasim, U., Jamil, F., Al-Muhtaseb, A.H., Jrai, A.A., Al-Riyami, M., Al-Maawali, S., Al-Haj, L., Al-Hinai, A., Al-Abri, M., Inayat, A., Waris, A. and Farrell, C., 2022. *Renewable and Sustainable Energy Reviews*, 152, p.111677.

- Prabakaran, S., Mohanraj, T. and Arumugam, A., 2021. Azolla pinnata methyl ester production and process optimization using a novel heterogeneous catalyst. *Renewable Energy*, 180, pp. 353-371.
- Rocha-Meneses, L., Hari, A., Inayat, A., Yousef, L.A., Alarab, S., Abdallah, M., Shanableh, A., Ghenai, C., Shanmugam, S. and Kikas, T., 2023. Recent advances on biodiesel production from waste cooking oil (WCO): A review of reactors, catalysts, and optimization techniques impacting the production. *Fuel*, 348, p.128514.
- Rodríguez-Solana, R., Salgado, J.M., Domínguez, J.M. and Cortés-Diéguez, S., 2014. Characterization of fennel extracts and quantification of estragole: Optimization and comparison of accelerated solvent extraction and Soxhlet techniques. *Industrial Crops and Products*, 52, pp.528-536.
- Sá, A.G.A., Silva, D.C. da, Pacheco, M.T.B., Moreno, Y.M.F. and Carciofi, B.A.M., 2021. Oilseed by-products as plant-based protein sources: Amino acid profile and digestibility. *Future Foods*, 3, p.100023.
- Salehzadeh, A., Naemi, A.S. and Arasteh, A., 2014. Biodiesel production from Azolla filiculoides (Water Fern). *Tropical Journal of Pharmaceutical Research*, 13(6), pp.957-960.
- Sebayang, A.H., Kusumo, F., Milano, J., Shamsuddin, A.H., Silitonga, A.S., Ideris, F., Siswantoro, J., Veza, I., Mofijur, M. and Reen Chia, S., 2023. Optimization of biodiesel production from rice bran oil by ultrasound and infrared radiation using ANN-GWO. *Fuel*, 346, p.128404.
- Sundaramahalingam, M.A., Karthikumar, S., Shyam Kumar, R., Samuel, K.J., Shajahan, S., Sivasubramanian, V., Sivashanmugam, P., Varalakshmi, P., Syed, A., Marraiki, N., Elgorban, A.M., Vinoth Kumar, R. and Ganesh Moorthy, I., 2021. An intensified approach for transesterification of biodiesel from Annona squamosa seed oil using ultrasound-assisted homogeneous catalysis reaction and its process optimization. *Fuel*, 291, p.2612.
- Thanikodi, S., Milano, J., Sebayang, A.H., Shamsuddin, A.H., Rangappa, S.M., Siengchin, S., Silitonga, A.S., Bahar, A.H., Ibrahim, H. and Benu, S.M., 2023. Enhancing the engine performance using multi fruits peel (exocarp) ash with nanoparticles in biodiesel production. *Energy Sources, Part A: Recovery, Utilization and Environmental Effects*, 45(1), pp.2122-2143.
- Thiruvengkatachari, S., Saravanan, C.G., Edwin Geo, V., Vikneswaran, M., Udayakumar, R. and Aloui, F., 2021. Experimental investigations on the production and testing of Azolla methyl esters from *Azolla microphylla* in a compression ignition engine. *Fuel*, 287, p.119448.
- Tirkey, J.V., Kumar, A. and Singh, D.K., 2022. Energy consumption, greenhouse gas emissions, and economic feasibility studies of biodiesel production from Mahua (*Madhuca longifolia*) in India. *Energy*, 249, p.123690.
- Venkatesan, H., Godwin, J.J. and Sivamani, S., 2017. Data set for extraction and transesterification of bio-oil from *Stoechospermum marginatum*, a brown marine algae. *Data in Brief*, 14, pp.623-628.
- Zu, Y., Liu, G., Wang, Z., Shi, J., Zhang, M., Zhang, W. and Jia, M., 2010. CaO is supported on porous carbon as a highly efficient heterogeneous catalysts for the transesterification of triacetin with methanol. *Energy and Fuels*, 24 (7), pp.3810-3816.







# Revolutionizing Education: Harnessing Graph Machine Learning for Enhanced Problem-Solving in Environmental Science and Pollution Technology

R. Krishna Kumari<sup>†</sup>

Department of Mathematics, College of Engineering and Technology, SRM Institute of Science and Technology, Kattankulathur, Chennai-603203, Tamilnadu, India

<sup>†</sup>Corresponding author: R. Krishna Kumari; krishrengan@gmail.com

## ABSTRACT

Amidst the shifting tides of the educational landscape, this research article embarks on a transformative journey delving into the fusion of theoretical principles and pragmatic implementations within the realm of Graph Machine Learning (GML), particularly accentuated within the sphere of nature, environment, and pollution technology. GML emerges as a potent and indispensable tool, adeptly leveraging the intrinsic interconnectedness embedded within environmental datasets. Its application extends far beyond mere analysis towards the profound ability to forecast ecological patterns, prescribe sustainable interventions, and tailor pollution mitigation strategies with precision and efficacy. This article does not merely scratch the surface of GML's applications but dives deep into its tangible implementations, unraveling its potential to revolutionize environmental science and pollution technology. It endeavors to bridge the gap between theory and practice, weaving together relevant ecological theories and empirical evidence that underpin the theoretical foundations supporting GML's practical utility in environmental domains. By synthesizing theoretical insights with real-world applications, this research elucidates the profound transformative potential of GML, paving the way for proactive and data-driven approaches toward addressing pressing environmental challenges. In essence, this harmonization of theory and application catalyzes advancing the adoption of GML in environmental science and pollution technology. It not only illuminates the path towards sustainable practices but also lays the groundwork for fostering a holistic understanding of our ecosystem. Through this integration, GML emerges as a beacon guiding us toward a future where environmental stewardship is informed by data-driven insights, leading to more effective and sustainable solutions for the benefit of our planet and future generations.

**Nat. Env. & Poll. Tech.**  
Website: [www.neptjournal.com](http://www.neptjournal.com)

Received: 27-03-2024

Revised: 09-05-2024

Accepted: 19-05-2024

### Key Words:

Graph machine learning  
Environmental science  
Environmental data analysis  
Graph theory  
Pollution technology  
Sustainable practices

## INTRODUCTION

The traditional challenges within the domain of environmental science and pollution technology mirror those encountered in education—struggling to adapt to the diverse intricacies of the natural world. As methodologies evolve, the limitations of standardized approaches in addressing environmental issues become increasingly apparent, urging exploration into innovative technologies to overcome these barriers (Ying et al. 2020, Zhang et al. 2021, 2023, Li et al. 2020). In this pursuit of transformative solutions, Graph Machine Learning (GML) emerges as a beacon of hope, offering a fresh perspective to revolutionize environmental practices (Lozano et al. 2017, Shen 2020, Nguyen et al. 2020, Li et al. 2022). The core issue lies in acknowledging that a uniform approach often fails to accommodate the unique dynamics and complexities of ecosystems. This recognition fuels a growing interest in technologies capable of adapting to the

nuanced nature of environmental challenges. GML, among these technologies, stands out as particularly promising, positioning itself as a versatile tool poised to reshape the landscape of environmental science and pollution technology (Liu et al. 2020, Romero & Peña-Casas 2010).

This research article embarks on a comprehensive exploration of GML, not solely as a technological innovation but as a solution deeply rooted in theoretical foundations. The focus extends beyond the practical applications of GML in environmental science to delve into the theoretical frameworks that underpin its effectiveness (Wang & Rajagopalan 2020). At the heart of GML's transformative potential lies its ability to leverage the intricate network structures inherent in environmental data. By deciphering and navigating the complex interconnections within ecosystems, GML aims to facilitate tailored solutions that transcend the limitations of conventional methodologies (Li et al. 2023, Liu et al. 2023).

As we embark on this journey into the theoretical underpinnings supporting GML, the goal is not merely to showcase its potential but to unveil a deeper understanding of how this technology can catalyze personalized solutions for environmental challenges (Sun et al. 2021). By harnessing the network structures within environmental data, GML endeavors to offer customized interventions that align with the unique characteristics of each ecosystem (Luo et al. 2023). This exploration transcends superficial applications and delves into the theoretical frameworks that drive its practical implementations. Essentially, this research article serves as a conduit between theory and application, shedding light on the symbiotic relationship that defines GML's role in environmental science and pollution technology. Through a nuanced examination of its theoretical foundations, we aim to uncover the mechanisms that empower GML to transcend traditional constraints within environmental research. As we navigate this intersection of theory and practice, the overarching objective is to contribute to the discourse on personalized environmental solutions, advocating for approaches that embrace the diversity and complexity of the natural world.

Expanding upon this narrative, future research could delve deeper into specific case studies where GML has been successfully applied to address environmental challenges, providing empirical evidence to support the theoretical assertions presented in this article. Additionally, exploring the ethical implications and potential biases associated with the adoption of GML in environmental decision-making processes could offer valuable insights into ensuring equitable and sustainable outcomes. Overall, this research sets the stage for a more holistic understanding of GML's role in shaping the future of environmental science and pollution technology, paving the way for innovative and adaptive solutions to safeguard our planet's health and resilience.

## THEORETICAL UNDERPINNINGS OF GML IN ENVIRONMENTAL SCIENCE

### Foundational Graph Theory Concepts

**Graph structures in environmental science:** In the realm of environmental science, the utilization of graph theory serves as a foundational framework, guiding our comprehension of the intricate relationships embedded within environmental datasets. At its essence, a graph comprises nodes representing diverse components within the environmental landscape and edges denoting the connections between these components. This fundamental structure offers both a visual and mathematical abstraction of the intricate web of interactions

that define environmental systems.

**Nodes as Environmental components:** Within this graph, nodes encapsulate a myriad of environmental components, spanning from individual species and specific habitats to broader ecological concepts and environmental variables. Each node embodies a distinct aspect of the environment, and their arrangement within the graph reflects the interconnections present in the natural world.

**Edges as interactions:** Edges, serving as the links between nodes, encapsulate the interactions that govern environmental dynamics. These interactions can manifest in various forms, such as predator-prey relationships, habitat connectivity, and nutrient flows within ecosystems. The graph thus evolves into a dynamic representation of the interdependencies and interactions that characterize environmental systems.

**Complex graph structures:** The resultant graph structure is far from simplistic, portraying a complex network that mirrors the intricate web of interactions in nature. As species interact within ecosystems, habitat connectivity shapes biodiversity patterns, and nutrient cycles influence ecosystem functions. Grasping and deciphering these intricate structures become essential for effective environmental management and conservation efforts.

**Graph algorithms for environmental insights:** The theoretical frameworks of graph theory extend beyond their representation to practical application through the utilization of advanced graph algorithms. These algorithms, tailored to extract meaningful insights from environmental graphs, play a pivotal role in informing decision-making processes and optimizing conservation efforts.

**PageRank algorithm:** One such significant algorithm is PageRank, initially developed for ranking web pages but finding relevance in environmental contexts. Within environmental graphs, PageRank serves as a guiding light, spotlighting nodes of importance. Species, habitats, or ecological concepts with higher PageRank scores emerge as influential nodes, indicating their centrality within the environmental network. Grounded in mathematical rigor, this algorithm provides a quantitative lens to the qualitative intricacies of ecological relationships.

The algorithm in Fig. 1 iteratively calculates the PageRank scores for each node in the environmental graph until convergence or until reaching the maximum number of iterations specified. The damping factor adjusts the influence of incoming edges, while the tolerance determines the level of convergence. The algorithm returns the final PageRank scores for each node in the environmental graph.

**Community detection algorithms:** Similar to their role in educational contexts, community detection algorithms

**Algorithm 1** PageRank Algorithm for Environmental Network Analysis

```

1: function PAGERANK(EnvironmentalGraph, dampingFactor, tolerance, maxIterations)
2:   // Initialize PageRank scores for all nodes
3:   for each node in EnvironmentalGraph do
4:      $PageRankScores[node] \leftarrow \frac{1}{NumberOfNodes(EnvironmentalGraph)}$ 
5:   end for
6:   // Initialize variables
7:   iterations  $\leftarrow 0$ 
8:   diff  $\leftarrow tolerance + 1$ 
9:   // Main iteration loop
10:  while diff > tolerance and iterations < maxIterations do
11:    diff  $\leftarrow 0$ 
12:    // Create a copy of PageRank scores for the previous iteration
13:    previousPageRankScores  $\leftarrow copy(PageRankScores)$ 
14:    // Update PageRank scores for each node
15:    for each node in EnvironmentalGraph do
16:      newPageRankScore  $\leftarrow 0$ 
17:      // Calculate contributions from incoming edges
18:      for each incomingEdge in node.incomingEdges do
19:        contributingNode  $\leftarrow incomingEdge.sourceNode$ 
20:        contributingNodePageRank  $\leftarrow previousPageRankScores[contributingNode]$ 
21:        totalOutgoingEdges  $\leftarrow NumberOfOutgoingEdges(contributingNode)$ 
22:        if totalOutgoingEdges > 0 then
23:           $contribution \leftarrow \frac{contributingNodePageRank}{totalOutgoingEdges}$ 
24:          newPageRankScore  $\leftarrow newPageRankScore + contribution$ 
25:        end if
26:      end for
27:      // Apply damping factor and add teleportation probability
28:       $newPageRankScore \leftarrow (1 - dampingFactor) / NumberOfNodes(EnvironmentalGraph) + dampingFactor \times newPageRankScore$ 
29:      // Update difference between current and previous PageRank scores
30:      diff  $\leftarrow diff + |newPageRankScore - previousPageRankScores[node]|$ 
31:      // Update PageRank score for the current node
32:      PageRankScores[node]  $\leftarrow newPageRankScore$ 
33:    end for
34:    // Increment iteration counter
35:    iterations  $\leftarrow iterations + 1$ 
36:  end while
37:  return PageRankScores
38: end function

```

Fig. 1: PageRank algorithm for environmental network analysis.

illuminate cohesive clusters within environmental graphs. These algorithms identify subsets of nodes with stronger internal connections than external ones. In the environmental context, these communities may represent interconnected

ecosystems, habitat clusters, or species associations. By unveiling these natural groupings, community detection algorithms enhance our understanding of the underlying structure of environmental networks.

**Algorithm 2** Community Detection Algorithm for Environmental Networks

```

1: function DETECTCOMMUNITIES(EnvironmentalGraph)
2:   // Initialize variables
3:   communities ← []
4:   visited ← set()
5:   // Main loop to traverse nodes
6:   for each node in EnvironmentalGraph do
7:     if node not in visited then
8:       community ← []
9:       // Depth-first search to find connected component
10:      DFS(node, community, visited)
11:      communities.append(community)
12:    end if
13:  end for
14:  return communities
15: end function
16:
17: function DFS(currentNode, community, visited)
18:   // Add current node to the community and mark as visited
19:   community.append(currentNode)
20:   visited.add(currentNode)
21:   // Recursively traverse neighboring nodes
22:   for each neighbor of currentNode do
23:     if neighbor not in visited then
24:       DFS(neighbor, community, visited)
25:     end if
26:   end for
27: end function

```

Fig. 2: Community detection algorithm for environmental network.

The output of the Community Detection Algorithm for Environmental Networks program (Fig. 2) is a set of communities or cohesive clusters identified within the environmental graph. Here's an explanation of the output:

- **Data Structure:** The algorithm utilizes a list of communities to store the detected communities or clusters found in the environmental graph. Each community is represented as a list containing the nodes belonging to that community.
- **Traversal and Detection:** The algorithm traverses each node in the environmental graph. For each unvisited node encountered during traversal, it initiates a depth-first search (DFS) to identify the connected component or community to which the node belongs. The DFS recursively explores neighboring nodes connected to the current node until all nodes within the same community are visited.
- **Appending Communities:** Once a community is fully explored, it is appended to the communities list. This

process continues until all nodes in the environmental graph are visited and assigned to their respective communities.

- **Returned Output:** Finally, the algorithm returns the communities list containing all the identified communities or cohesive clusters within the environmental graph.
- The output of the program, therefore, consists of a list of communities, where each community is represented as a list of nodes. This output provides valuable insights into the underlying structure of the environmental network by highlighting the interconnected groups or clusters of nodes within it.

**Optimal conservation strategies and ecological clusters:** Beyond identification, these algorithms offer insights into optimal conservation strategies and clusters of interconnected ecological components. They inform the formulation of tailored conservation plans, suggesting the most effective sequences of actions or highlighting areas where deeper

exploration may be necessary. Consequently, the theoretical basis of these algorithms extends beyond computation, directly influencing the practical implementation of conservation strategies.

Overall, the fusion of graph theory and advanced algorithms not only reveals the complex structures within environmental data but also provides a theoretical framework for deriving actionable insights. By comprehending the intricacies of graph structures and strategically deploying algorithms, GML harnesses the potential of these foundational concepts to capture and optimize the dynamic interactions that define environmental systems.

## MACHINE LEARNING THEOREMS SUPPORTING GML

### Universal Approximation Theorem

**Neural networks as function approximators:** The Universal Approximation Theorem establishes the capability of neural networks to approximate any continuous function on a bounded input space, provided they possess a non-constant, bounded activation function and a single hidden layer with a sufficient number of neurons. Mathematically, this is expressed as:

$$f(x) \approx \sum_{i=1}^N w_i \cdot \sigma(b_i + W_i \cdot x)$$

Where,

$N$  is the number of neurons in the hidden layer,

$w_i$  are the weights,

$b_i$  is the bias,

$W_i$  is the weight vector,

$x$  is the input vector

$\sigma$  is the activation function.

**Applicability to environmental dynamics:** Let's consider the applicability of neural networks in the realm of environmental dynamics. Suppose we employ a neural network with adaptable weights ( $w_i$ ) and biases ( $b_i$ ), updated iteratively using backpropagation during training. This model adapts to the complexities of environmental data by fine-tuning these parameters to minimize the disparity between predicted and observed outcomes, effectively learning the intricate relationships within the data.

**Accurate predictions in environmental modeling:** In scenarios where precise predictions are essential, such as environmental modeling, the Universal Approximation Theorem assures us of the neural network's ability to approximate complex environmental functions. In this scenario, the model might take the form:

$$\text{Prediction} = \sum_{j=1}^N w_{ij} \cdot \sigma(b_{ij} + W_{ij} \cdot X_i)$$

Here,  $i$  indexes the student,  $j$  indexes the neurons in the hidden layer,  $w_{ij}$  are the weights,  $b_{ij}$  are the biases,  $W_{ij}$  is the weight vectors, and  $X_i$  is the input vector for student  $i$ .

Example Calculation:

Let's consider a simplified scenario where we aim to predict student performance (Prediction) based on two features (Feature<sub>1</sub> and Feature<sub>2</sub>) using a sigmoid activation function ( $\sigma$ ):

$$\text{Prediction} = \sigma(w_1 \cdot \text{Feature}_1 + w_2 \cdot \text{Feature}_2 + b)$$

Here,  $w_1$  and  $w_2$  are the weights, and  $b$  is the bias. The Universal Approximation Theorem assures us that, with a sufficiently complex neural network, this structure can effectively approximate the underlying function mapping environmental factors to pollutant concentrations.

### No Free Lunch Theorem

**Tailoring models to environmental complexity:** The No Free Lunch Theorem posits that no single machine learning algorithm universally outperforms others across all possible problem scenarios. This theorem emphasizes the need to tailor models to the specific nuances of environmental data, which can vary widely in terms of spatial and temporal dynamics, non-linear interactions, and heterogeneous structures.

**Understanding environmental data complexity:** Environmental datasets often exhibit diverse characteristics, including non-linear relationships between variables, spatial and temporal dependencies, and heterogeneous data structures. The No Free Lunch Theorem underscores the importance of comprehending these complexities. For example, in the context of analyzing pollution patterns, algorithm A, which excels in capturing spatial dependencies, may outperform algorithm B, which is better suited for modeling temporal variations, depending on the specific characteristics of the environmental data distribution.

**Optimizing GML for environmental insight:** Optimization strategies in GML, guided by the No Free Lunch Theorem, involve iterative refinement based on insights gained from the unique characteristics of environmental data. If algorithm C proves effective in capturing certain types of environmental interactions, it would be prioritized over other algorithms in those specific environmental contexts.

Example Calculation:

Consider the scenario where GML practitioners aim to optimize a model for predicting air quality. Let A represent a neural network-based algorithm and B represent a decision tree-based algorithm. Depending on the spatial and temporal

dynamics of pollution sources and meteorological factors, one algorithm may outperform the other in different environmental contexts.

In summary, the No Free Lunch Theorem highlights the importance of adapting machine learning algorithms to the specific complexities of environmental data, ensuring that GML approaches are optimized for addressing the diverse challenges within the realm of nature, environment, and pollution technology.

## TRANSLATING THEORY INTO PRACTICE

### Theoretical Frameworks for Environmental Predictions

**Graph theory foundation:** GML's efficacy in environmental science stems from its grounding in graph theory, where nodes represent entities such as species, habitats, and environmental variables, while edges depict interactions like predator-prey relationships and nutrient flows. This structured framework facilitates a comprehensive understanding of complex environmental systems.

**Machine learning theorems in action:** The Universal Approximation Theorem serves as a cornerstone, empowering GML models to adapt and predict environmental outcomes. Neural networks, as powerful function approximators, accommodate the intricate interplay of environmental factors, surpassing linear models' limitations.

**Predictive Analytics in Environmental Networks:** Leveraging historical environmental data, GML models utilize predictive analytics to anticipate ecological patterns and pollution trends. The wealth of historical context, coupled with the flexibility offered by machine learning theorems, enables these models to navigate the dynamic environmental landscape with precision.

### Theoretical Underpinnings of Recommending Environmental Solutions

**Algorithmic empowerment:** GML's effectiveness stems from its strategic utilization of graph algorithms rooted in theoretical frameworks. These algorithms, such as PageRank, offer a systematic approach to identifying influential nodes

### Theoretical Advances in Data Quality and Privacy

Research Direction	Key Theoretical Insights
<b>Advancements in Graph Theory and Privacy-Preserving ML</b>	<ul style="list-style-type: none"> <li>• <b>Refining Graph Theory Models:</b> Enhance data quality by refining models that represent educational networks using graph theory.</li> <li>• <b>Cryptographic Techniques:</b> Develop cryptographic techniques to ensure privacy in handling sensitive educational data.</li> <li>• <b>Secure Multi-Party Computation:</b> Implement secure multi-party computation to build robust GML models while preserving data integrity and privacy.</li> </ul>

and optimal intervention pathways within environmental networks.

**Personalized environmental solution recommendations:** Graph algorithms empower GML to recommend tailored environmental solutions precisely aligned with the unique characteristics of each ecosystem. By identifying influential nodes, GML ensures personalized and contextually relevant suggestions, surpassing generic approaches.

**Practical intervention strategies:** The theoretical underpinnings of GML, combined with graph algorithms, extend beyond theoretical realms to practical intervention strategies. These recommendations are not only informed by historical data but are also deeply rooted in ecological principles, guaranteeing meaningful and effective environmental interventions.

In this context, the integration of graph theory foundations and machine learning theorems in GML unfolds as a dynamic force in environmental science. By seamlessly translating theoretical concepts into actionable strategies, GML emerges as a transformative tool, predicting environmental patterns and delivering personalized solutions with practical efficacy.

## RESEARCH DIRECTIONS

While GML in education benefits from theoretical foundations, ongoing research is crucial to address challenges and refine theoretical frameworks.

In these research directions, the emphasis is on the key theoretical insights driving advancements in GML for Environmental science. This section provided a structured overview of theoretical frameworks addressing data quality, privacy, model interpretability, and ethical considerations.

## FUTURE POTENTIAL OF GML IN ENVIRONMENTAL SCIENCE: EXPANDING HORIZONS

### Fostering Collaborative Environmental Research

- **In-depth collaborator identification:** GML's detailed analysis of environmental data allows for the identification of potential collaborators. ii. Considers

### Theoretical Frameworks for Model Interpretability

Research Direction	Key Theoretical Insights
<b>Theoretical Advances in Explainable AI</b>	<ul style="list-style-type: none"> <li>• <b>Model Interpretability Frameworks:</b> Develop theoretical frameworks to enhance model interpretability in GML.</li> <li>• <b>Clear Explanations:</b> Provide clear explanations for GML predictions, ensuring transparency and understanding.</li> <li>• <b>Building Trust:</b> Enhance trust among educators and students by establishing transparent and interpretable models.</li> </ul>

### Theoretical Approaches to Address Ethical Considerations

Research Direction	Key Theoretical Insights
<b>Theoretical Frameworks for Bias and Fairness in ML</b>	<ul style="list-style-type: none"> <li>• <b>Addressing Biases:</b> Develop theoretical frameworks to identify and address biases in GML models.</li> <li>• <b>Equitable Access:</b> Ensure equitable access to personalized learning opportunities by mitigating bias.</li> <li>• <b>Embedding Ethical Considerations:</b> Embed ethical considerations into the core of GML theoretical foundations to guide algorithmic development.</li> </ul>

### Theoretical Foundations for Integration with Existing Environmental Systems

Research Direction	Key Theoretical Insights
<b>Theoretical Advances in System Integration Models</b>	<ul style="list-style-type: none"> <li>• <b>Seamless Integration Models:</b> Develop theoretical models for the seamless integration of GML tools into existing environmental systems.</li> <li>• <b>Collaborative Frameworks:</b> Establish collaborative frameworks between environmental scientists, policymakers, and technologists for harmonious integration.</li> <li>• <b>Harmony with Educational Frameworks:</b> Ensure theoretical advances align with and complement existing environmental frameworks and regulations, promoting sustainable practices and conservation efforts.</li> </ul>

factors such as expertise in specific ecological domains, past collaboration success, and compatibility in research methodologies.

- **Optimized team formation:** Recommends collaborative projects and research teams that capitalize on each member’s expertise and strengths. ii. Enhances interdisciplinary collaboration and fosters a holistic approach to addressing complex environmental challenges.
- **Real-world application:** Prepares environmental scientists for collaborative research environments by simulating real-world interdisciplinary collaborations. ii. Aligns with the growing trend of interdisciplinary approaches in tackling environmental issues, reflecting the interconnected nature of ecological systems.

#### Adapting to Individual Learning Styles in Environmental Research

- **Dynamic research environment:** GML’s real-time analysis enables the dynamic adaptation of research methodologies and approaches. ii. Adjusts research methodologies and data analysis techniques to accommodate the evolving preferences and strengths of individual researchers.

- **Tailoring environmental research approaches:** Ensures that research methodologies remain effective by accommodating individual researchers’ preferred approaches and techniques. ii. Incorporates diverse research methods, such as fieldwork, remote sensing, and modeling, to cater to varying research styles.
- **Continuous optimization:** Reflects a commitment to continuous improvement by adapting to emerging trends in environmental research methodologies. ii. Utilizes ongoing feedback loops to refine and enhance research methodologies and approaches based on individual researcher feedback and performance.

#### Promoting Self-Directed Environmental Research

- **Empowering researchers:** GML empowers environmental scientists by providing personalized research recommendations tailored to their unique research interests and goals. ii. Enables researchers to take an active role in shaping their research agendas and methodologies, fostering a sense of ownership and autonomy.
- **Tools for self-assessment:** Equips researchers with tools for self-assessment, allowing them to evaluate their research progress and methodology effectiveness.

ii. Facilitates a reflective research process, encouraging researchers to identify areas for improvement and refine their research approaches accordingly.

- **Autonomy in research path:** Promotes autonomy by offering a range of supplementary resources aligned with individual research objectives and interests. ii. Encourages researchers to set personalized research goals, explore new research avenues, and track their research achievements autonomously.

## CONCLUSIONS

Graph Machine Learning (GML), rooted in foundational theories from graph theory and machine learning, emerges as a powerful tool for revolutionizing environmental science and pollution technology. The synergy between theory and practical application underpins GML's effectiveness in predicting environmental patterns, recommending mitigation strategies, and tailoring solutions to address complex environmental challenges. As theoretical advancements progress, GML stands poised to unleash the full potential of personalized and sustainable environmental management. The future outlook for GML in environmental science transcends predictive analytics, encompassing collaborative problem-solving, real-time adaptation to changing environmental dynamics, and the empowerment of self-directed environmental research. As GML evolves, these expanded applications signify a paradigm shift towards a more adaptive, collaborative, and environmentally conscious approach to addressing the complexities of our natural world.

Expanding upon this narrative, future research could explore the specific applications of GML in various environmental domains, such as biodiversity conservation, climate change mitigation, and pollution control. Case studies demonstrating the successful implementation of GML algorithms in real-world environmental scenarios would provide valuable insights into its potential impact. Additionally, interdisciplinary collaborations between environmental scientists, data scientists, and policymakers could further enhance the development and deployment of GML solutions for environmental management. Furthermore, ethical considerations surrounding the use of GML in environmental decision-making processes, including issues of data privacy, algorithmic bias, and equity, warrant careful examination. Addressing these concerns is crucial to ensure that GML technologies are deployed responsibly and equitably to benefit both human societies and the natural environment.

In conclusion, GML holds immense promise for revolutionizing environmental science and pollution technology, offering innovative solutions to address pressing environmental challenges. By embracing the principles of collaboration, adaptability, and sustainability, GML has the potential to usher in a new era of environmental stewardship, where data-driven insights inform proactive and holistic approaches to safeguarding our planet's health and resilience.

## REFERENCES

- Li, J., Wu, Y., Liu, Y., Zhao, Y. and Wang, X., 2023. Applications of machine learning in environmental science and management: A review. *Environmental Science and Pollution Research*, 31, pp.1-23.
- Li, S., Liu, W., Zhao, L. and Zhu, X., 2020. A survey of environmental science education research in the context of sustainability. *Sustainability*, 12(11), p.4338.
- Li, Y., Luo, F., Xu, C. and Lu, W., 2022. Applications of graph neural networks in environmental science: A review. *Environmental Science and Ecotechnology*, 6(1), p.100134.
- Liu, W., Yao, X. and Wu, J., 2020. A survey on applications of graph neural networks. *Journal of Computer Science and Technology*, 35(6), pp.1021-1033.
- Liu, Y., Wu, J., Wang, X. and Zhao, Y., 2023. A review of machine learning for environmental risk assessment. *Journal of Environmental Management*, 223, p.116225.
- Lozano, R., Lozano-García, F.M. and Herrera-Giraldez, M.D., 2017. A decade of educational technology research in environmental education: A bibliometric analysis. *Journal of Cleaner Production*, 149, pp.674-688.
- Luo, J., Shang, Y. and Liu, Z., 2023. Graph machine learning for environmental knowledge graph construction: A survey. *Environmental Science and Pollution Research*, pp.1-17.
- Nguyen, T.T., Ngo, H.L. and Hoang, V.M., 2020. A survey on deep learning for pollution forecasting. *Neurocomputing*, 418, pp.122-142.
- Romero, C. and Peña-Casas, R., 2010. Environmental education in engineering education for sustainable development. *Sustainable Development*, 18(7), pp.450-455.
- Shen, Y., 2020. A review of graph convolutional networks for semantic segmentation. *IEEE Access*, 8, pp.168030-168045.
- Sun, Y., Liu, Y., Li, J. and Wang, X., 2021. Machine learning for soil environmental science: A review. *Environmental Pollution*, 289, p.117824.
- Wang, J. and Rajagopalan, R., 2020. A survey on deep learning for environmental remote sensing. *IEEE Geoscience and Remote Sensing Magazine*, 8(4), pp.1-22.
- Ying, R., He, R. and Fan, J., 2020. Graph neural network for semi-supervised learning on labeled and unlabeled graphs. *IEEE Transactions on Knowledge and Data Engineering*, 33(1), pp.109-121.
- Zhang, Y., Cheng, S. and Zhou, K., 2021. Recent advances in environmental informatics: A bibliometric analysis. *Environmental Science and Pollution Research*, 28(12), pp.10023-10040.
- Zhang, Z., Liu, X., Sun, Y., Li, P. and Li, J., 2023. Applications of deep learning in environmental science. *Environmental Science and Pollution Research*, 14(2), pp.1-22.

## ORCID DETAILS OF THE AUTHORS

R. Krishna Kumari: <https://orcid.org/0000-0002-1802-628X>





# An Intelligent Crow Search Optimization and Bi-GRU for Forest Fire Detection System Using Internet of Things

Syed Abdul Moeed<sup>1</sup>, Bellam Surendra Babu<sup>2</sup>, M. Sreevani<sup>3</sup>, B. V. Devendra Rao<sup>4</sup>, R. Raja Kumar<sup>5</sup> and Gouse Baig Mohammed<sup>6†</sup>

<sup>1</sup>Department of Computer Science and Engineering, Kakatiya Institute of Technology and Science, Warangal, Telangana, India

<sup>2</sup>Department of Computer Science and Engineering, KLEF (Koneru Lakshmaiah Education Foundation (Deemed to be University), Vaddeswaram, Andhra Pradesh, India

<sup>3</sup>Department of Computer Science and Engineering, BVRIT Hyderabad College of Engineering for Women, Hyderabad, India

<sup>4</sup>PTO & Associate Professor (AcSIR), CSIR-IICT, Tarnaka, Hyderabad, India

<sup>5</sup>Department of Computer Science and Engineering, Rajeev Gandhi Memorial College of Engineering and Technology, Nanadyal, Andhra Pradesh, India

<sup>6</sup>Department of Computer Science and Engineering, Vardhaman College of Engineering, Shamshabad, Hyderabad, India

†Corresponding author: Gouse Baig Mohammed; gousebaig@vardhaman.org

Nat. Env. & Poll. Tech.  
Website: [www.neptjournal.com](http://www.neptjournal.com)

Received: 03-03-2024

Revised: 16-04-2024

Accepted: 03-05-2024

## Key Words:

Internet of things  
Artificial intelligence  
Forest fire detection  
EfficientDet  
Bi-GRU  
Crow search optimization

## ABSTRACT

Natural ecosystems have been facing a major threat due to deforestation and forest fires for the past decade. These environmental challenges have led to significant biodiversity loss, disruption of natural habitats, and adverse effects on climate change. The integration of Artificial Intelligence (AI) and Optimization techniques has made a revolutionary impact in disaster management, offering new avenues for early detection and prevention strategies. Therefore, to prevent the outbreak of a forest fire, an efficient forest fire diagnosis and aversion system is needed. To address this problem, an IoT-based Artificial Intelligence (AI) technique for forest fire detection has been proposed. This system leverages the Internet of Things (IoT) to collect real-time data from various sensors deployed in forest areas, providing continuous monitoring and early warning capabilities. Several researchers have contributed different techniques to predict forest fires at various remote locations, highlighting the importance of innovative approaches in this field. The proposed work involves object detection, which is facilitated by EfficientDet, a state-of-the-art object detection model known for its accuracy and efficiency. EfficientDet enables the system to accurately identify potential fire outbreaks by analyzing visual data from the sensors. To facilitate efficient detection at the outbreak of forest fires, a bi-directional gated recurrent neural network (Bi-GRU-NN) is needed. This neural network architecture is capable of processing sequential data from multiple directions, enhancing the system's ability to predict the spread and intensity of fires. Crow Search Optimization (CSO) and fractional calculus are used to create an optimal solution in the proposed crow search fractional calculus optimization (CSFCO) algorithm for deep learning. CSO is inspired by the intelligent foraging behavior of crows, and when combined with fractional calculus, it provides a robust optimization framework that improves the accuracy and efficiency of the AI model. Experimental analysis shows that the proposed technique outperformed the other existing traditional approaches with an accuracy of 99.32% and an error rate of 0.12%. These results demonstrate the effectiveness of the integrated AI and optimization techniques in enhancing forest fire detection and prevention. The high accuracy and low error rate underscore the potential of this system to be a valuable tool in mitigating the risks associated with forest fires, ultimately contributing to the preservation of natural ecosystems.

## INTRODUCTION

The world is facing a major threat of climatic change. This is mainly due to rapid industrialization and globalization efforts made during the past decade. Forest fires are more prevalent

among many nations of the world due to the alarming rise of global warming and deforestation. Forest fires result in increased economic loss and ecosystem damage, resulting in an unprecedented catastrophe to human lives. Forest fires are usually induced by man-made activities and

environmental disasters. Due to these factors, forest fires are rapid and tough to subdue. Utilization of sensor-based forest fire detection systems performs efficiently, but the deployment and coverage become enormously difficult (Chen et al. 2007, Zhang et al. 2020, 2018, Yu et al. 2005, Zhang et al. 2009). The rapid spread of forest fires not only affects the nearby community, it also causes health hazards and fatalities. This also results in environmental pollution that would harm the entire city. In addition, even the firemen cannot be able to access and calculate the amount of damage caused by forest fires. It is also evident that due to environmental speculation, limited coverage of infrared and ultraviolet detectors (Kang et al. 2013, Lee et al. 2001) will not provide any support in remote areas. Forest fires of long-range can be easily detected by using satellite remote sensing (Botta et al. 2016). However, the detection of lesser fires is much tougher to diagnose at remote locations. Due to greenhouse emissions, global warming, and climatic change, hydrological patterns get altered, resulting in unforeseen greenhouse gas concentrations.

Technological advancements in image processing and computer vision have a critical impact on addressing the problem of forest fires which attracts several researchers. Especially the Internet of Things (IoT) and information and communication technology (ICT) spurn remote sensing capabilities using VANETs, UAVs, and drones (Rathore et al. 2016, Rajkumar & Kumar 2024a, 2024b). Since IoT devices are resource-constrained and dynamic, they are capable of forming a network by making their own decisions. These devices can be disintegrated at remote locations possessing limited storage and energy. IoT supports a wide variety of applications pertaining to security, machine vision, image processing, etc. (Fernandes et al. 2004). IoT unleashed the birth of smart cities by connecting sensors, detectors, transportation systems, home appliances, and every indoor and outdoor object via the internet to make dynamic decision-making and learning potential on its own. Therefore, appropriate conceptions and rules are supposed to be made in terms of objects and participants (Kyriazis et al. 2013). This will generate a new arena by providing various research opportunities in case of heterogeneous situations. Several policies relating to energy, infrastructure environment, and society are supposed to be enacted utilizing IoT (Bui et al. 2012). IoT devices also capture a large amount of information which contains hidden insights to make decisions by finding patterns using data analytics. Smart cities coagulate smart services, welfare programs, and digitization by shifting access to objects remotely. Therefore, these advancements are facilitated with the help of the smart city operating systems, which capture a huge amount of data about the physical location of where the IoT devices are installed. The

data gets stored on a public cloud (Farrell et al. 2018). This amounts to a large amount of big data, and with the help of AI, real-time simulation models to study human behavior and decision-making can be enacted. This leads to sensitive policy-making by private as well as government institutions. Several case studies have been adapted to counter the effect of forest fires, and bushfires have been investigated (Lai et al. 2018). Models of deep learning find a wide application in the arena of forest fire detection and management study.

## MOTIVATION

Forest Fires cause huge destruction to the livelihood of the people, environment, climate, animals, and other living beings on the planet. Since forest fires possess a global economic significance, several technologies and techniques are being put forth for their diagnosis and aversion. Advancements made in Computer Vision (CV), Artificial Intelligence (AI), and the Internet of Things (IoT) (Tandon & Tandon 2019) invoke its use for collecting data and predicting forest fires. This provokes the thought to develop a deep learning-based real-time object detection model for forest fire detection. Since AI performs much better at feature learning and attributes, they perceive a higher amount of semantic information than human capabilities. Hence deep learning finds a wide use even in the field of disaster and fire detection industry.

## MAJOR CONTRIBUTIONS

Several applications and technologies have been proposed by various researchers to detect and prevent forest fires using AI and IoT. The proposed work involves the following major contributions, which are defined as follows:

- This study emphasizes the detection and prediction of outbreaks of forest fires with the help of deep learning techniques. The proposed work involves the use of the real-time object detection model called EfficientDet (Tan et al. 2020).
- Bi-GRU-NN for fire detection (Başarslan & Kayaalp 2023) and Crow Search (Thawkar & Shankar 2022). Fractional Calculus Optimization (Mahaveerakannan et al. 2023), techniques are utilized for optimizing the training parameters to obtain optimal performance.
- The proposed work involves the use of four different sets of forest fire datasets such as BowFire (BowFire 2019), FD-Dataset (FD-Dataset 2019), Forestry Images (ForestryImages 2018) and VisiFire (VisiFire 2003).
- Evaluation results obtained achieve a 99.32% accuracy rate with an error rate of 0.12%. Table 1 provides the list of abbreviations utilized in our study.

Table 1: Abbreviations utilized.

Abbreviations	Description
Bi-GRU	Bi-directional Gated Recurrent Unit
GRU	Gated Recurrent Unit
LSTM	Long Short-Term Memory Networks
Bi-LSTM	Bi-Directional Long Short Term Memory Networks
DL	Deep Learning
ML	Machine Learning
IoTs	Internet of Things
AI	Artificial Intelligence
NN	Neural Network
Bi-GRU-NN	Bi-directional Gated Recurrent Unit based Neural Network
CSO	Crow Search Optimization
CSFCO	Crow Search-based Fractional Calculus Optimization
ICT	Information and Communication Technology
VANETs	Vehicular Adhoc Networks
UAVs	Unmanned Aerial Vehicles
CV	Computer Vision
FD, ReLu	Fire Detection, Rectified Linear Unit
WSN	Wireless Sensor Networks
FFDNet	Forest Fire Detection Network
RMSProp	Root Mean Square Propagation
FN	Fog-Node
KELM	Kernel Extreme Learning Machine
EPO	Emperor Penguin Optimizer
MCU	Micro-controller Unit
DTF	Decreasing total flying time algorithm
TSA	Tunicate Swarm Algorithm
ITF	Increasing total flying time algorithm
HRA	Half regions assignment algorithm
QRA	Quarter regions assignment algorithm
TRA	Tier regions assignment algorithm
RID	Randomly-iteratively drone algorithm
SEOF	Sleep Scheduling and Energy Optimized Framework
MATLAB, TSHO	Maths Laboratory, Taylor Spotted Hyena Optimization
ANN	Artificial Neural Network
CNN	Convolutional Neural Network
RNN	Recurrent Neural Network
WMSNs	Wireless Multimedia Sensor Networks
IMAGENet	Image Network
VGG	Visual Geometry Group
RLSTM-NN	Recurrent Long Short Term Memory Networks based Neural Networks
OPCNN	Optimal Convolutional Neural Network
NAS	Neural Architectural Search
Bi-FPN	Bi-directional Feature Pyramid Network
PANets	Path Aggregation Networks
CIFAR	Canadian Institute for Advanced Research

## PAST STUDIES OF RELEVANCE

Several Researchers have put forth various works on the detection, managing, predicting, and forecasting of forest fires. This section provides a clear-cut overview of various techniques catering to the need for forest fires, along with their benefits and limitations.

In the Chinese province of Jiangsu, a fuzzy inference-based prediction system for forest fires has been proposed (Lin et al. 2018). Their technique works based on accessing and quantifying the consequences using fuzzy inference. Fuzzification and output rating levels are utilized to deliver these parameters into a triangular fuzzy number. Their technique has been carried out by using rechargeable WSNs. Their technology successfully identified the likelihood of a forest fire with a high degree of accuracy. A Fog-assisted hierarchical data routing strategy for IoT-enabled WSN for forest fire detection has been developed by (Moussa et al. 2022), making use of an energy-efficient multi-fog node (FN) based clustered network model. By reducing communication costs, their technique preserves the energy of the sensor nodes. High efficiency of 8.23% of network lifetime and 19.02% of response time are achieved by their suggested system. However, their work has not focused on real-world sensor nodes. A WSN-based automated system for the detection of forest fires has been proposed by utilizing the FFDNet deep learning framework, which combines a modified Xception network for feature extraction with an optimizer for root mean square propagation (RMSProp) and guided filter for noise removal (Paidipatti et al. 2023). The EPO algorithm has been applied to choose the ideal parameters, and the kernel extreme learning machine (KELM) model has been used to identify forest fires. Their proposed work used FFD Dataset implemented using Python thereby achieving a high accuracy rate of 99.17%. However, their technique has to be combined with the deep ensemble fusion model to assess its performance. Using a dynamic convolutional neural network, (Zheng et al. 2023) created an application for monitoring forest fires and providing early warnings. Their proposed technique put forth a back propagation neural network fire algorithm. The forest fire image dataset has been used and is classified for feature extraction. According to a performance investigation, 84.37% accuracy is achieved in low frame rate forest fire recognition. However, their model is complex, and optimization is essential. IoT-based forest fire monitoring and early warning system was proposed (Divya et al. 2019) utilizing uses sensor- and microcontroller-based technology to identify forest fires. However, their technique has not been evaluated with the machine and deep learning algorithms. A forest fire prediction model using IoT and deep learning techniques using an MCU microcontroller node in

conjunction with sensor technology (Ananthi et al. 2022). Though their system performs the prediction of forest fires, it cannot handle large amounts of big data.

A surveillance system based on drones utilizing an optimization algorithm for forest fire prevention using Decreasing total flying time algorithm (DTF), Increasing total flying time algorithm (ITF), Half regions assignment algorithm (HRA), Quarter regions assignment algorithm (QRA), Tier regions assignment algorithm (TRA), Randomly-iteratively drone algorithm (RID) has been proposed (Jemmali et al. 2023). According to experimental data, the RID algorithm performs optimally, achieving 90.03% accuracy in 0.08 seconds. A deep learning architecture based on long short-term memory networks was used to develop a fire alert forecasting model has been developed (Jamshed et al. 2022). Their technique utilized the Pakistan forest fire dataset and achieved a prediction performance of 95% accuracy. However, the performance of the model has to be improved to handle big data. To optimize the fitness parameters (Verma et al. 2021), The Tunicate Swarm Algorithm (TSA), which is based on sleep scheduling and an energy-optimized framework (SEOF), has been developed for the detection of forest fires. The experiment was conducted by using MATLAB thereby achieving a network stability of 35.3%. However, the optimization of sink placement and mobility scenarios are to be tested to enhance the performance. An early forest fire detection system utilizing machine learning, image processing, and sensor fusion technology has been proposed (Nassar et al. 2022). Their technique chose ANN, RNN, and CNN models with the IMAGENet dataset. They have achieved an accuracy of 99.5%. Nonetheless, maximizing solar energy and node energy consumption extends the network's lifespan. By creating a lightweight deep learning model, A novel hierarchical method for detecting forest fires in diverse wireless multimedia sensor networks (WMSNs) has been investigated (Kizilkaya et al. 2022). Between the sink and the edge, their suggested work increases detection accuracy and traffic efficiency by 98.28% and saves 29.94% of energy.

Nevertheless, the proposed algorithm has to be tested for E-Health platforms. An early warning classification of forest fires using bird sounds has been investigated by using a CNN model (Permana et al. 2022). The model has been chosen to classify the bird sounds and achieved an accuracy of forest fire detection of 96.43%. IMAGENet dataset has been utilized for the forest fire detection system. Using additional animal sounds can further increase accuracy. For hazy IoT environments, a convolutional neural network solution based on smoke detection has been investigated (Khan et al. 2019). VGG-16, Googlenet and Alexnet models have been utilized

for their study. ImageNet dataset with their proposed model achieved an accuracy of 97.72%. The model must be made less expensive, though, because it is rather sophisticated.

A forest fire monitoring system utilizing IoT in conjunction with the Catswarm Fractional Calculus Optimization (CSFCO) algorithm was proposed (Mahaveerakannan et al. 2023). EfficientDet, an object detection model, has been chosen for the implementation where the forest fire has to be detected by using RLSTM-NN. With an error rate of 0.14%, their recommended method produced results with a precision of 98.6%. Furthermore, a smoke detection model can be developed to reduce optimization approach errors. An optimization technique based on surveillance towers, monitoring balloons, and drone technology to develop an

integrated forest fire detection system has been investigated (Fuente et al. 2024). They created a mixed linear integer algorithm model to handle routing, coverage, and location decisions.

Further improvement can be made by using a meta-heuristic algorithm. An emergency adaptive routing scheme for WSN to monitor the fire hazard in emergencies has been investigated utilizing the Jacobson algorithm to achieve less end-to-end delay and average load energy (Zeng et al. 2011). The future work can be tested on industries and building fires. Gomez et al. have come up with a novel application for the early detection of forest fires using overhead power lines of WSNs. They have utilized sensor technology for the detection of forest fires. However, their work lacked novelty

Table 2: Comparative analysis of works on forest fire detection.

References	Problem Addressed	Technique Utilized	Benefits	Limitations
Moussa et al. (2022)	Detection of Forest Fires	Hierarchical Data Routing Strategy	Network Lifetime is increased by 8.23%	Real-time implementation has to be tested
Paidipatti et al. (2023)	Detection of Forest Fires	Guided Filtering, Modified Xception Network, Root mean square propagation (RMSProp) optimizer, Kernel Extreme Learning Machine (KELM), EPO algorithm	Accuracy 99.59%	The technique has to be tested across various scenarios
Zheng et al. (2023)	Monitoring of Fire Hazards	Emergency-Adaptive Routing Scheme	Energy Consumption is increased	The routing hole problem is yet to be addressed
Ananthi et al. (2022)	Prediction of Forest Fires	NodeMCU controller	Accuracy 97%	Training the dataset has not been considered
Jemmali et al. (2023)	Prevention of Forest Fires	Increasing total flying time algorithm (DTF, ITF), Half regions assignment algorithm (HRA), Quarter regions assignment algorithm (QRA), Randomly iteratively Drone Algorithm (RID)	Accuracy 90.3%	Dataset instances are very low, which needs to be considered
Jamshed et al. (2022)	Forecasting of Forest Fires	Long Short Term Memory Networks (LSTM)	Accuracy 95%	Several parameters concerning forests have not been considered
Verma et al. (2021)	Detection of Wild Fires	Sleep scheduling-based Energy Optimized Framework (SEOF), Tunicate Swarm Algorithm (TSA)	-	Physical obstacle between sensor nodes to withstand high temperatures during wildfires has to be improved.
Kizilkaya et al. (2022)	Detection of Forest Fires	Convolutional Neural Networks	Accuracy 98.28%, Energy saving 29.94%	The proposed work has not considered edge computing devices, Accuracy needs to be improved.
Mahaveerakannan et al. (2023)	Detection of Forest Fires	Cat Swarm Optimization, Recurrent Long Short Term Memory Networks (RLSTM)	Precision 98.6% Error Rate 0.14%	The smoke area has been left, which needs to be taken into consideration
Fuente et al. (2024)	Monitoring of Forest Fires	Mixed-integer linear programming model	Energy Cost, Distance	-
Zeng et al. (2011)	Recognition of Forest Fires	Back propagation neural network fire (BPNNFire) Algorithm	Accuracy 84.37%	Detection and performance have to be improved by using optimization algorithms.
Jayasingh et al. (2024)	Detection of Forest Fires	Optimal convolution neural networks (OPCNN) Models: CNN & J48	Accuracy 95.11%	Still, the accuracy needs to be improved

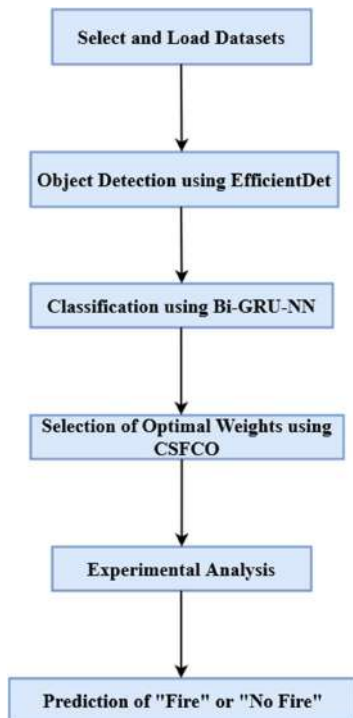


Fig. 1: Methodology of forest fire detection system.

and dataset training. An experimental method for forest fire detection employing an optimum convolutional neural network has been developed and investigated (Jayasingh et al. 2024). Their proposed model utilized a forest fire dataset implemented using Python, achieving an accuracy of 93.45%. In addition, optimal parameter selection and hybrid soft computing models provide better accuracy. Table 2 provides a comparative analysis of various works on forest fire outbreak detection, along with their advantages and limitations.

From Table 2, it is evident that the works proposed by the researchers attempted for forest fire detection achieved

an accuracy of up to 99%. However, the error rate has to be minimized to a greater extent. Additionally, object detection models have to be developed to adapt to the natural ecosystem under various illumination conditions. Hence, there is a strong need to increase the optimization technique to achieve optimum performance. To achieve high detection accuracy of forest fires, our proposed work involves the use of a crow search-based fractional calculus optimization technique.

## MATERIALS AND METHODS

The proposed methodology involves the use of IoT and AI for forest fire detection. To facilitate object detection remotely, the deep learning-based bi-directional gated recurrent neural network has been developed, designed, and implemented. The framework involves the use of fractional calculus-based optimization to improve the performance of the optimal parameters chosen for detection. Fig. 1 provides a depiction of the methodology involved in the Forest fire detection strategy.

### Datasets Utilized

The proposed methodology used publically available datasets, which involved a combination of ground fires, trunk fires, and canopy fire images. The publicly available datasets like Bow fire, FD-Dataset, Forestry images, and Visifire are involved in our proposed work. Fig. 2 represents the datasets utilized for our proposed work. A flame, like a peat wildfire, burns the organic components that cover the ground beneath the covering. Trunks normally have one branch, but they can also possess several stems. The primary responsibilities include transportation and support for supplies. The bark's major job is to protect the basal layer, which is a live cell. A canopy is an open-sided, extending roof structure. It may be used for decorative reasons or to attract interest to a direction or part of a structure, in addition to its primary function of

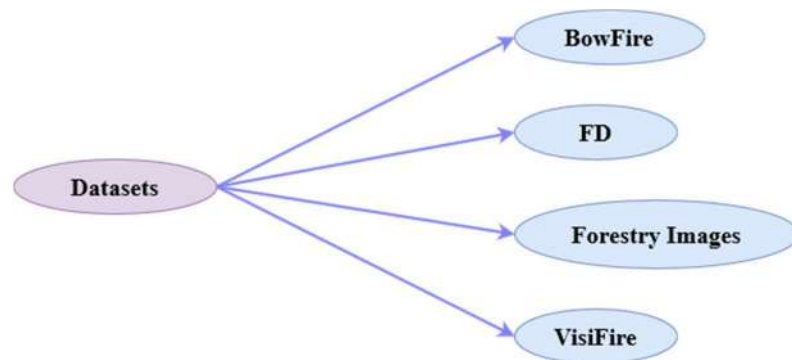


Fig. 2: Datasets utilized in our proposed work.



a. Groundfire-1

b. Groundfire-2



c. Trunk Enthusiasm

d. Canopy Fire

Fig. 3 (a-d): An overview of forest fire images of the datasets.



a. Normal Forest scene-1.

b. Normal Forest Division 2.



c. Normal Forest Division 3.

4. Normal Forest Division 4.

Fig. 4 (a-d): Represents the list of non-fire forestry images from the chosen datasets without any fire substances.



Fig. 5 (a-d): Represents the list of non-unit sections of forestry images with the sun from the chosen datasets incorporated with the fiery nature of a sun.

protecting from heat and moisture. Manually, the forest fire dataset has been assembled, which is combined with 10,581 photographs (2976 fire images and 7605 non-fire images) for the evaluation of our proposed work. Figs. 3-5 provide an overview of the different scenarios of our datasets.

### Object Detection

The performance and accuracy of the Convolutional neural networks can be improved by the method of larger compound scaling. Since an image contains detailed information about objects it is necessary to be captured to increase the precision. In the case of larger images, deeper networks are highly required this can be induced by receptor neurons and channels to capture minute details of objects. Researchers discovered that the performance of the deeper networks from model scaling is stationed upon the baseline network. This gives rise to the development of Neural Architecture Search (NAS) to find an optimum baseline network (Datascience 2019). In summary, the NAS algorithm detects the best structures by employing Reinforcement Learning when the fitness function is provided. This leads to a new category of models of deepNets called EfficientNets. To address the challenges of multi-scale feature fusion and model scaling EfficientNets in coagulation with Bi-directional Feature Pyramid Network (BiFPN) a new object detection model has been built called EfficientDets. EfficientDet makes use of BiFPN for a compounded model scaling strategy that adapts frameworks, depth, width, and resolution. EfficientNet models showed high accuracy with ImageNet

and CIFAR-100 datasets. Figs. 3-5 provide the model of the EfficientDet architecture. EfficientDet is backed by the high-performance EfficientNets, which provides the model with the capabilities it needs to comprehend the subtle differences between various kinds of forest fires. All the fragments of the developed framework calculate a variety of attributes such as warmth, lighting, movement, moisture, and altitude. One characteristic that sets forest fires apart is that they occur in open spaces with strong winds. Conversely, they are fueled by highly combustible compounds such as flammable lignocellulose, which is a dried leaf. Sometimes perilous chemicals, fire, and air induce forest fires.

Secondly, EfficientDets utilize PANet (Wang et al. 2019) variant such as Bi-FPN for fusing the feature maps with various resolutions and receptive fields outputted by the last three stages of the backbone network to enhance the process of feature extraction (Liu et al. 2018). Bi-FPN provides quick and multi-scale feature fusion. From a single view of any dimension, a learning technique called a Feature Pyramid Network, or FPN, generates proportionately scaled image features at several levels in a fully performing fashion. This process is independent of the layered patterns that underlie it. There are several more layers situated behind the skull and vertebrae. They are employed to acquire different feature maps constructed on prior phases. Among other options, the cervical part could be an FPN, PANet, or Bi-FPN. With the aid of learnable weights that enable the net to determine the relative importance of different input features, the Bi-FPN regularly uses multi-scale feature fusion. In addition to class



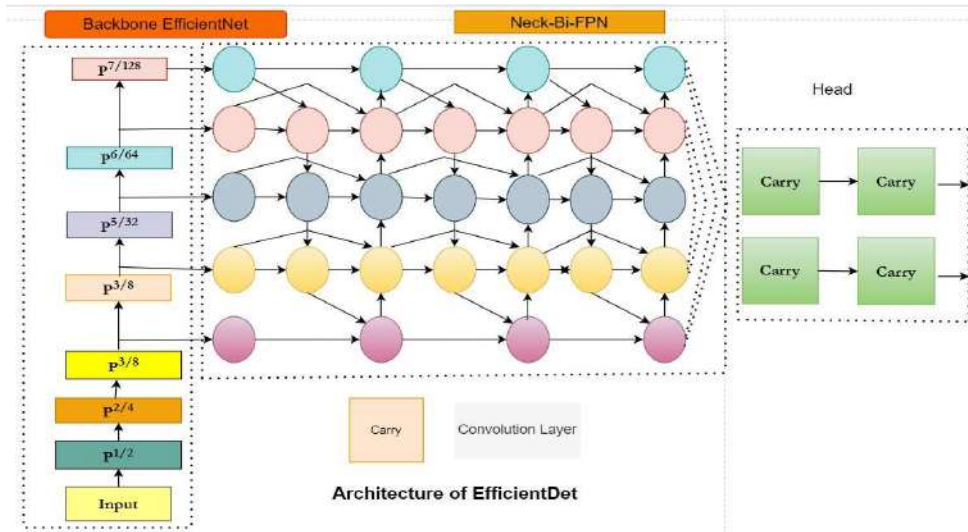


Fig. 6: Architectural structure of EfficientDet.

recognition, perceptron learning seeks to alter weighting. With fewer parameters and FLOPS, Bi-FPN surpasses Yolov50's neck PANet. Feature extraction usually happens through blending pertinent data from a collection of testing and training images, which is called feature fusion. Pixel-level fusion models such as DU, UD-Fusion, RL, and LR-Fusion are used for our proposed work. The objects detected vary with respect to the type of the fusion model, which detects different classes of semantic data. Finally, the compounded scaling strategy involves scaling in terms of precision, depth, width, and resolution of all backbones and feature networks. This is mainly responsible for achieving high performance

and accuracy in the case of resource-constrained devices. To perform this, compounded coefficients are utilized. Every component is incremented to a possible range of flexibility in contrast to random increases in parameters. To achieve high precision, more resources are needed (Tan et al. 2020). Fig. 6 provides the architectural structure of EfficientDet.

### Classification Using Bi-Directional Gated Recurrent Neural Network

Bi-GRU, being a recurrent neural network, possesses the ability to train the long-term provinces. The disappearing

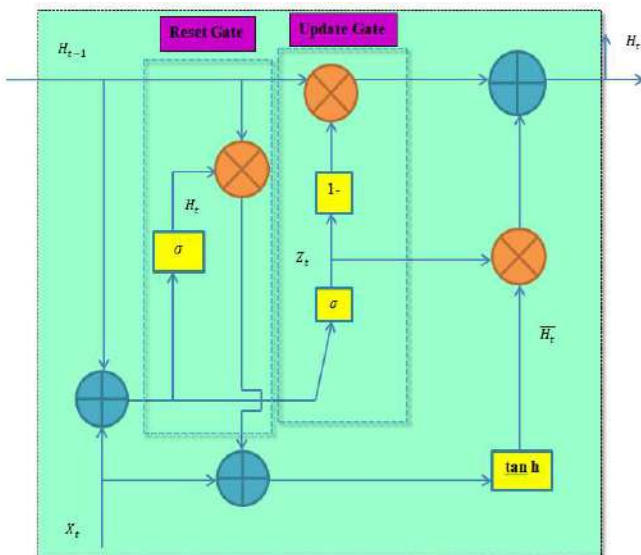


Fig. 7a: Structure of GRU.

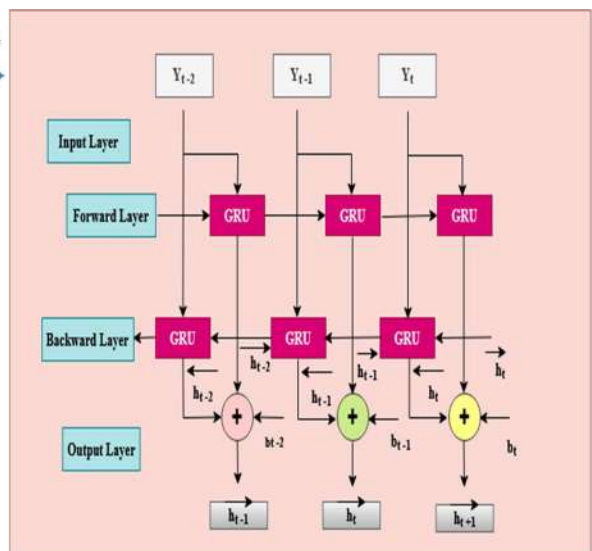


Fig. 7b: Structure of Bi-GRU.

slope problem arising from the derivation of the input signal is fed as input to the construction of the neural net. To overcome this problem, the learning algorithm has to be changed. For instance, in the input layer, Gaussian has to be replaced by ReLu. The slope, which is computed across T time steps, is used to update the connection weights. The conditional variance velocity is equal to the average of T slopes, identical to RNNs. Every one of these T sub-gradients ought to vanish for the standard deviation slope to do so as well. Both training and prediction will make use of the composite features, which include motion, spatial, and deep data. GRU receives the combined feature vector pairs of the detections and predictions, and the output is the feature pair's similarity. In particular, we use GRU networks to encapsulate long-term dependencies in the sequence of data (Lit et al. 2021).

An empirical analysis using a gated recurrent unit, which yields the same performance as that of LSTM, has been chosen in our proposed work (Chung et al. 2014). The simplified version of long short-term memory networks (LSTM) is called Gated Recurrent Units (GRUs). GRU is also a type of the recurrent neural network (RNN). The major difference between LSTM and the GRU is that GRU couples the input and output gate into the update gate. A simple structure of a GRU is depicted using Fig. 7a. The structure of a Bi-directional GRU is depicted in Fig. 7b.

Let us assume that the  $h$  is the hidden layer,  $X_t \in R^{n \times d}$ . Where  $n$  is the number of samples and  $d$  is the number of units, the hidden state at the previous time  $t-1$  is  $H_{t-1} \in R^{n \times h}$ .  $\Sigma$  is the sigmoid activation function. The output hidden state  $h$  of a single GRU at the current time step  $t$  can be given as follows:

$$R_t = \sigma(X_t W_{rx} + H_{t-1} W_{hr} + b_r) \quad \dots(1)$$

$$Z_t = \sigma(X_t W_{zx} + H_{t-1} W_{hz} + b_z) \quad \dots(2)$$

$$\bar{H}_t = \tanh(X_t W_{xh} + (R_t \odot H_{t-1}) W_{hh} + b_h) \quad \dots(3)$$

$$H_t = (1 - Z_t) \odot H_{t-1} + Z_t \odot \bar{H}_t \quad \dots(4)$$

$$\sigma(x) = \frac{1}{1 + e^{-x}} \quad \dots(5)$$

From the equations (1), (2) and (3)  $W_{rx}$ ,  $W_{hr}$ ,  $W_{zx}$ ,  $W_{hz}$  defines the weights of the connecting layers between the input layer and reset gate, hidden layer and reset gate, input layer and update gate, hidden layer and reset gate. Similarly,  $b_r$  and  $b_z$  define the bias of the reset and update gates.  $\bar{H}_t$  is the candidate hidden state of the current time step  $t$ ,  $\odot$  represents the multiplication of matrices of two elements,  $\tanh$  being the hyperbolic activation function, then the formula can be given as:

$$\tanh(x) = 1 - \frac{2}{1 + e^{-2x}} \quad \dots(6)$$

This indicates that the parameters necessary for the outbreak of forest fires get predicted, the current value is relatively closer to that of the previous time and the value of the next time.

Bi-GRU (Yan et al. 2021) consists of two units of GRUs comprising forward propagating GRU and backward propagating GRU.

$$\vec{H}_t = GRU(X_t, \vec{H}_{t-1}) \quad \dots(7)$$

$$\overleftarrow{H}_t = GRU(X_t, \overleftarrow{H}_{t-1}) \quad \dots(8)$$

$$H_t = w_t \vec{H}_t + v_t \overleftarrow{H}_t + b_t \quad \dots(9)$$

From the equations (7), (8), (9)  $X_t$ -current input decides the hidden layer state of Bi-GRU, the output of  $\vec{H}_t$  the forward hidden layer and the output  $\overleftarrow{H}_t$  of the backward hidden layer at time step  $t-1$ , then  $GRU(\cdot)$  indicates the GRU network performs the non-linear transformation of the forest fire input image. The input vector is fed into the corresponding GRU hidden state.  $w_t, v_t$ -defines the weights of the state  $\vec{H}_t$  of the forward hidden layer and  $\overleftarrow{H}_t$  of the backward hidden layer at a time  $t$ ,  $b_t$  defines the bias of the state of the hidden layer at time  $t$ . With Adam's gradient descent optimization approach, the GRU network is trained to predict similarity using the cross-entropy loss function. In the case of sporadic data, optimization techniques provide an active learning performance. Min-batch learning technique has been applied to the gradient descent method. Two gates are inserted into the GRU-NN to control of flow of information, as shown in the equations from (1)-(9). Since our proposed technique heavily relies on the weights, which can be controlled efficiently by the utilization of optimization technique. Fractional calculus is incorporated along with the Crow Search and Taylor Spotted Hyena optimization (CSFCO).

### Solution Encoding

GRU network should be given the optimal weights, which are fed to encode the solution of the CSFCO procedure. Several possible solutions support any length of input or destination. The optimal weights for the Bi-GRU-NN network must be established to encode the CSFCO process solution. The space of potential solutions has  $[1Z]$  items. It supports any length as an input or destination. Random input variables are processed by RNN by using its memory space. As a result, RNNs are the best at predicting the actual phrase within a string of sentences. If there are no microorganisms in a GRU level but  $n_i$  in the level before, then each component of the cell will have  $n_i + 1 + n_i$  components.

### Fitness Evaluation

The proposed CSFCO technique utilizes the minimization

function obtained as the GRU-error NN's function to decide the fitness. The fitness function can be expressed as

$$Z = 1/N \sum_{n=1}^N (O^n - D^n)^2 \quad \dots(10)$$

Equation (10)  $O^n$  defines the GRU-NN's output and  $D^n$  defines the expected output. The optimization process, also known as the inference engine, establishes how closely a given resolution conforms to the optimum option toward the desired issue. It determines the suitability of optimizers. The preceding sentence defines the fitness measure for the optimization process. Optimization-derived weights need to provide minimal classification mistakes.

**Algorithm for CSFCO Procedure**

The proposed work incorporates the swarm intelligence approach to crow search (Askarzadeh et al. 2016) and the fractional calculus technique. The actions of crows, like the intelligence of stealing and hiding food, are mimicked. The mirror test proved that they exhibit self-awareness. Crows provide alerts by recognizing faces in case of an unfriendly one. Even after several months, they remember the place where they hide their food (Corvus 2024, Hooded Crow 2024, Prior et al. 2008, Rincon 2005). In their method, though the first-order derivative solution yields peculiar results for the periodic system, the second-order derivative incorporates previous solutions. This second order-based derivative solution yields either a maxima or minima value. The slope becomes upward if the partial derivative number is a favorable string if the partial derivative number is negligible. Crow search provides faster solutions at the local search in a speedy manner. The attributes utilized for the execution of the crow search algorithm are Nmax, representing the maximum number of iterations; Psize, indicating the size of the population; Pa being the probability of awareness, which provides a trade-off between the exploration and exploitation phase, flen is the flight length and mem being the memory value of the food hiding places of each crow (Crepinsek 2013). The crows operate in the exploration and exploitation phase, which can be described as follows:

**Step 1: Population Initialization**

The number of crows in the current CSO is chosen as random. Let us assume that there are n possible solutions where the space of solutions can be defined as

$$Cr = \{Cr_1, Cr_2, Cr_3, \dots, Cr_n\} \forall 1 \leq i \leq N \quad \dots(11)$$

Where  $Cr_i$  defines the ith solution in the answer space.

**Step 2: Fitness Evaluation and position update:** To find the optimal weights for the GRU network, it is used for optimization.

**Case 1:** When a single crow finds food, the population gets updated, which can be defined by the equation (12)

$$Cr_{new,i} = rand, \forall 0 \leq rand \leq 1 \quad \dots(12)$$

Equation (12) shows that the crow is followed.

**Case 2:** When a crow does not know that it is being followed. The population gets updated, which can be defined by equation (13) as follows:

$$Cr_{new,i} = Cr_i + rand * flen * (mem_i - Cr_i) \text{ If } rand > pa \quad \dots(13)$$

The position update of the

$$Cr_{i,j}(t + 1) = Cr_{i,j}(t) + v_i(t) + rand * flen * (mem_{i_{best}} - Cr_{i,j}) \quad \dots(14)$$

Rearranging the equation (14)

$$Cr_{i,j}(t + 1) - Cr_{i,j}(t) = v_i(t) + rand * flen * (mem_{i_{best}} - Cr_{i,j}) \quad \dots(15)$$

**Step 3:** Using fractional calculus, the second-order derivative can be given as

$$D^n (Cr_{i,j}(t + 1) - Cr_{i,j}(t)) = v_i(t) + rand * flen * (mem_{i_{best}} - Cr_{i,j}) \quad \dots(16)$$

To solve equation (16) by taking the second-order derivative, we have

$$Cr_{i,j}(t + 1) - \alpha Cr_{i,j}(t) - \frac{1}{2} \alpha Cr_{i,j}(t - 2) - \frac{1}{6} \alpha (1 - \alpha) (Cr_{i,j}(t - 2) - \frac{1}{24} \alpha (1 - \alpha) (2 - \alpha) Cr_{i,j}(t - 3)) = v_i(t) + rand * flen * (mem_{i_{best}} - Cr_{i,j}) \quad \dots(17)$$

From equation (17), the full appearance of the position update can be defined by equation (18)

$$Cr_{i,j}(t + 1) = \alpha Cr_{i,j}(t) - \frac{1}{2} \alpha Cr_{i,j}(t - 2) - \frac{1}{6} \alpha (1 - \alpha) (Cr_{i,j}(t - 2) - \frac{1}{24} \alpha (1 - \alpha) (2 - \alpha) Cr_{i,j}(t - 3)) + v_i(t) + rand * flen * (mem_{i_{best}} - Cr_{i,j}) \quad \dots(17)$$

**Step 4:** After the best optimal value is found, it will be swapped from best to j, which will be the perfect fitness value.

**Step 5:** When the ideal weight gets obtained, it will be fed as input to the GRU

**RESULTS AND DISCUSSION**

The proposed work aims to identify and classify the outbreak of fire by fire alerts using the Crow search fractional calculus optimization technique. Identification of smoke, for in a

Table 3: Comparison of TPR on various techniques with respect to different datasets.

Technique	Bow Fire Dataset	FD-Dataset	Forestry Images	VisiFire Dataset
FL	94.70%	94.00%	90.50%	91.30%
EE-DCNN	93.80%	91.70%	92.50%	93.50%
LWDL	90.40%	89.80%	93.70%	95.80%
DBN-RLSTM-NN	89%	92.60%	95.60%	95.30%
CSO-RLSTM-NN	98.60%	96.80%	97.40%	96.60%
CS-Bi-GRU-NN	97.89%	97.20%	97.60%	97.80%

Table 4: Comparison of FPR on various techniques with respect to different datasets.

Technique	BowFire Dataset	FD-Dataset	Forestry Images	VisiFire Dataset
FL	3.90%	3.60%	4.20%	5.90%
EE-DCNN	4.20%	4.10%	3.70%	5.30%
LWDL	5.60%	5.30%	3.10%	4.80%
DBN-RLSTM-NN	7%	4.50%	2.50%	4.30%
CSO-RLSTM-NN	1.40%	2.50%	1.30%	3.60%
CS-Bi-GRU-NN	1.30%	2.30%	1.20%	3.40%

hostile environment happens using IoT devices. IoT devices once deployed, sense, capture, and transmit the captured information for further processing. Huge data will be obtained which will be of the data set, out of which 70% has been utilized for training and 30% for testing.

**Performance Metrics**

The proposed work has been evaluated by utilizing performance metrics, namely True Positive Rate (TPR), False Positive Rate (FPR), Error\_Rate, and Accuracy. These metrics facilitate efficient prediction before the Outbreak of fire – The formula to calculate the performance metric is as follows:

$$TPR = \frac{True\ Positive}{False\ negative + True\ Positive} \dots(18)$$

$$FPR = \frac{False\ Positive}{True\ Negative + False\ Positive} \dots(19)$$

$$Precision = \frac{True\ Positive}{True\ Positive + False\ Positive} \dots(20)$$

$$Error\_Rate = \frac{False\ Positive + False\ Negative}{False\ Negative} \dots(21)$$

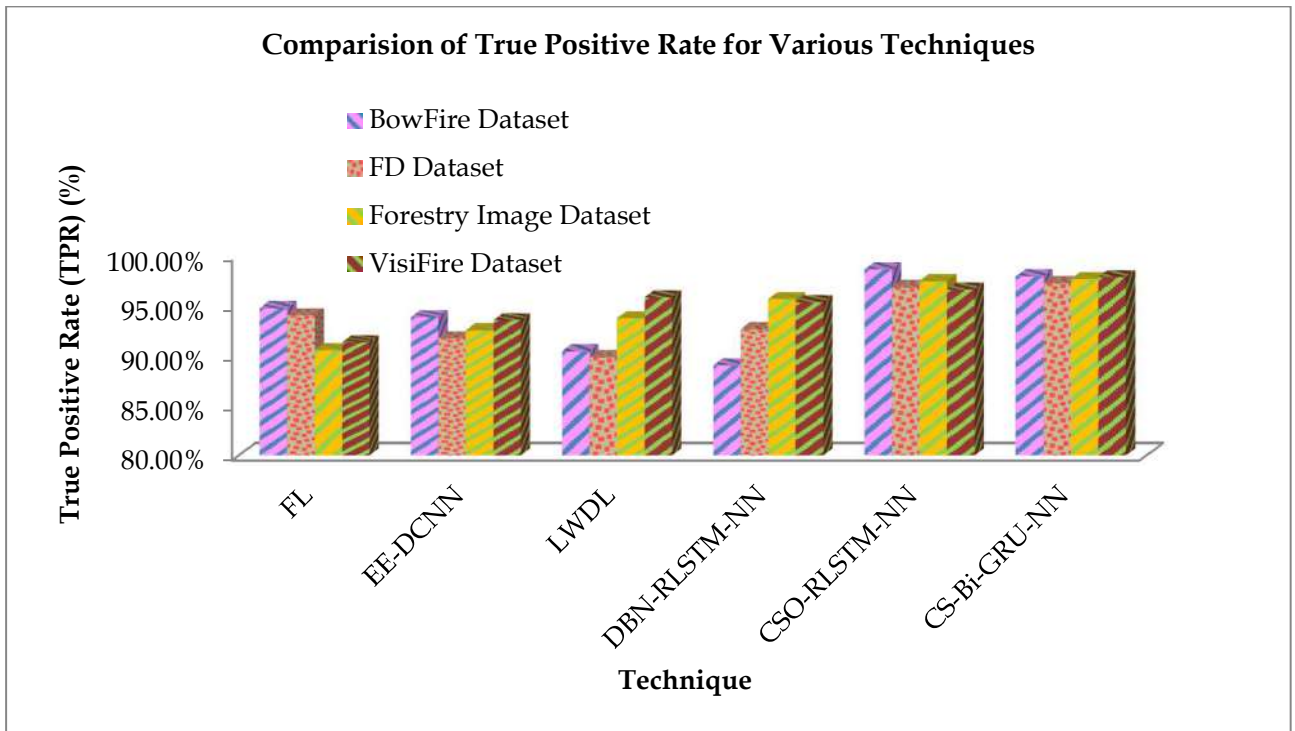


Fig. 8: Comparison graph of TPR for various techniques on different datasets.

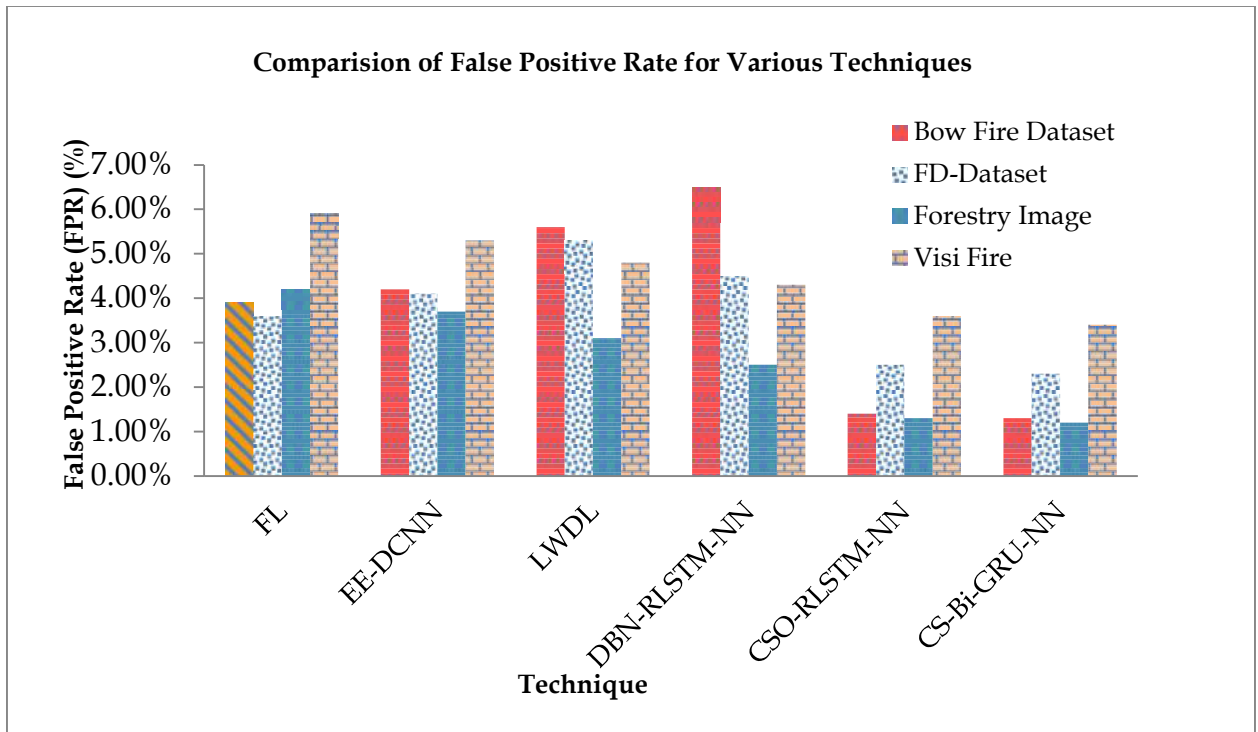


Fig. 9: Comparison graph of FPR for various techniques on different datasets.

Table 5: Comparison of Accuracy of various techniques with respect to different datasets.

Accuracy (%)				
Technique	Bow Fire Dataset	FD-Dataset	Forestry Images	VisiFire Dataset
FL	95.2%	94.2%	90.1%	91.2%
EE-DCNN	94.1%	91.5%	92.4%	93.2%
LWDL	91.2%	89.6%	93.6%	94.6%
DBN-RLSTM-NN	89.4%	92.3%	95.3%	95.2%
CSO-RLSTM-NN	98.4%	96.4%	97.3%	96.7%
CS-Bi-GRU-NN	98.9%	97.5%	97.6%	97.4%

**Comparative Analysis based on True Positive Rate (TPR)**

Table 3 provides the experimental analysis of the TPR of the proposed work compared with the existing technique with respect to different datasets. Fig. 8 provides the comparison graph on TPR of the proposed work compared with the existing technique with respect to different datasets.

**Comparative Analysis Based on False Positive Rate (FPR)**

Table 4 provides the experimental analysis of the FPR of the proposed work compared with the existing technique with respect to different datasets. Fig. 9 provides the comparison

Table 6: Comparison of error rate on various techniques with respect to different datasets.

Technique	Bow Fire Dataset	FD-Dataset	Forestry Images	VisiFire Dataset
FL	0.38	0.35	0.43	0.61
EE-DCNN	0.42	0.43	0.38	0.52
LWDL	0.63	0.53	0.31	0.46
DBN-RLSTM-NN	0.75	0.42	0.25	0.42
CSO-RLSTM-NN	0.14	0.26	0.13	0.37
CS-Bi-GRU-NN	0.12	0.23	0.1	0.35

graph on the FPR of the proposed work compared with the existing technique with respect to different datasets.

**Comparative Analysis Based on Accuracy**

Table 5 provides the experimental analysis of the accuracy of the proposed work compared with the existing technique with respect to different datasets. Fig. 10 provides the comparison graph on the accuracy of the proposed work compared with the existing technique with respect to different datasets.

**Comparative Analysis based on Error\_Rate**

Table 6 provides the experimental analysis of the error rate

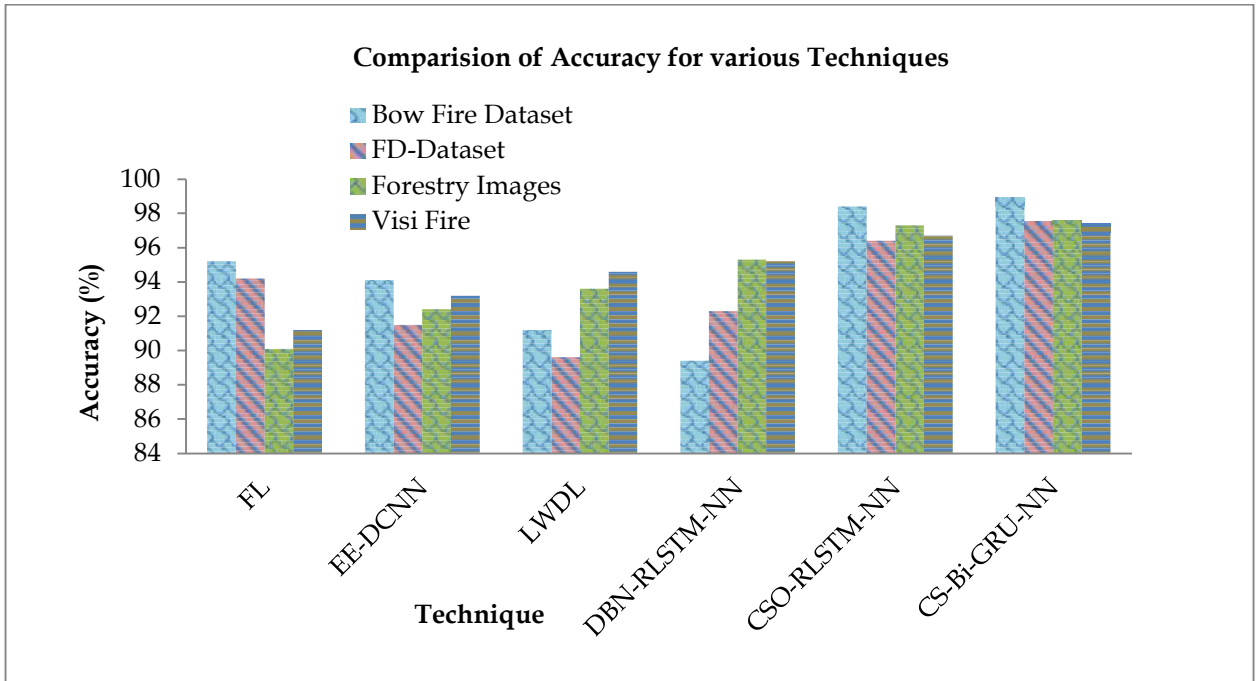


Fig. 10: Comparison graph of accuracy for various techniques on different datasets.

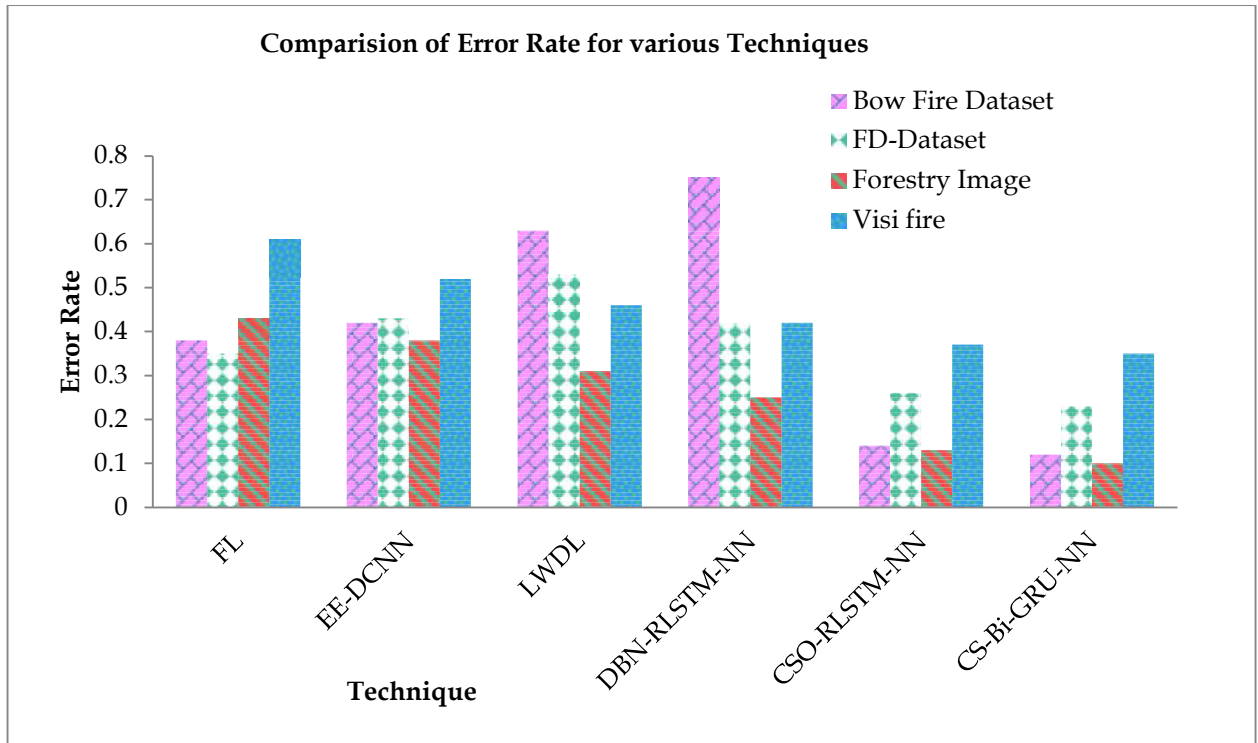


Fig. 11: Comparison graph of error rate for various techniques on different datasets.

of the proposed work compared with the existing technique with respect to different datasets. Fig. 11 provides the comparison graph on the error rate of the proposed work compared with the existing technique with respect to different datasets.

## CONCLUSIONS

Our proposed work has been based on a forest fire detection system by coagulating Crow Search with a Bi-GRU-NN model. Forest fires can be detected efficiently by object detection models. To assist this, CNN performs efficiently. Nevertheless, it is difficult for an individual object detection to detect forest fires in a hostile environment like forests. Additionally, object detectors cannot be able to distinguish between chimney smoke and clouds. This induces the fake positive rate owing to the narrow range of object detectors. Since our proposed work utilized a Crow search-based optimization algorithm, it exhibits high efficiency.

Further work can be extended by the use of LSTM & its variants for other emergency scenarios. In addition, to prevent unwanted false negatives, smoke detection models have to be built. Different optimization techniques can be adopted to assess the comparative performance for efficient use in forest fire detection.

## REFERENCES

- Ananthi, J., Sengottaiyan, N., Anbukaruppusamy, S., Upreti, K. and Dubey, A.K., 2022. Forest fire prediction using IoT and deep learning. *International Journal of Advanced Technology and Engineering Exploration*, 9(87), pp.246-256.
- Askarzadeh, A., 2016. A novel meta-heuristic method for solving constrained engineering optimization problems: Crow Search Algorithm. *Computers & Structures*, 169, pp.1-12.
- Başarslan, M.S. and Kayaalp, F., 2023. MBi-GRUMCONV: A novel Multi Bi-GRU and Multi CNN-Based deep learning model for social media sentiment analysis. *Journal of Cloud Computing*, 12(5), p.386. <https://doi.org/10.1186/s13677-022-00386-3>.
- Botta, A., De Donato, W., Persico, V. and Pescapè, A., 2016. Integration of cloud computing and internet of things: a survey. *Future Generation Computer Systems*, 56, pp.684-700.
- BoWFire dataset, 2019. Datasets. Available online: <https://bitbucket.org/gbdi/bowfire-dataset/downloads/>.
- Bui, N., Castellán, A.P., Casar, P. and Zorz, M., 2012. The internet of energy: a web-enabled smart grid system. *IEEE Network*, 26(4), pp.39-45.
- Chen, S.J., Hovde, D.C., Peterson, K.A. and Marshall, A.W., 2007. Fire detection using smoke and gas sensors. *Fire Safety Journal*, 42, pp.507-515.
- Chung, J., Gulcehre, C., Cho, K. and Bengio, Y., 2014. Empirical evaluation of gated recurrent neural networks on sequence modeling. *arXiv*, 14(12), p.3555.
- Crepinsek, M., Liu, S.H. and Mernik, M., 2013. Exploration and exploitation in evolutionary algorithms: A survey. *ACM Computing Surveys (CSUR)*, 45(3), pp.1-33. <https://doi.org/10.1145/2480741.2480752>.
- De la Fuente, R., Aguayo, M.M. and Contreras-Bolton, C., 2024. An optimization-based approach for an integrated forest fire monitoring system with multiple technologies and surveillance drones. *European Journal of Operational Research*, 313(2), pp.435-451.
- Divya, A., Kavithanjali, T. and Dharshini, P., 2019. IoT-enabled forest fire detection and early warning system. In *2019 IEEE International Conference on System, Computation, Automation and Networking (ICSCAN)*, pp.1-5. IEEE. Doi: 10.1109/CVPR42600.2020.01079.
- Farrell, F., Soyer, O.S. and Quince, C., 2018. Machine learning-based prediction of functional capabilities in metagenomically assembled microbial genomes. *BioRxiv*, 30, p.157.
- FD-Dataset, 2019. FD-Dataset. Available online: <http://www.nnmtl.cn/EFDNet/>.
- Fernandes, A.M., Utkin, A.B., Lavrov, A.V. and Vilar, R.M., 2004. Development of neural network committee machines for automatic forest fire detection using lidar. *Pattern Recognition*, 37, pp.2039-2047.
- ForestryImages, 2018. Forestry Images Available online: <https://www.forestryimages.org/browse/subthumb.cfm?sub=740>.
- Haifeng, L., Xiaoyu, L., Xinyue, W. and Yunfei, L., 2018. A fuzzy inference and big data analysis algorithm for the prediction of forest fire based on rechargeable wireless sensor networks. *Sustainable Computing: Informatics and Systems*, 18, pp.101-111. <https://doi.org/10.1016/j.suscom.2017.05.004>.
- Hooded Crow, 2024. Hooded crow. Available online: [https://en.wikipedia.org/wiki/Hooded\\_crow](https://en.wikipedia.org/wiki/Hooded_crow).
- Jamshed, M.A., Theodorou, C., Kalsoom, T., Anjum, N., Abbasi, Q.H. and Ur-Rehman, M., 2022. Intelligent computing based forecasting of deforestation using fire alerts: A deep learning approach. *Physical Communication*, 55, p.101941.
- Jayasingh, S.K., Swain, S., Patra, K.J. and Gountia, D., 2024. An experimental approach to detect forest fire using machine learning mathematical models and IoT. *SN Computer Science*, 5(1), p.148.
- Jemmali, M., Kayed, B.M.L., Boulila, W., Amdouni, H. and Alharbi, M.T., 2023. Optimizing forest fire prevention: intelligent scheduling algorithms for the drone-based surveillance system. *Procedia Computer Science*, 225, pp.1562-1571.
- Kalburgi, S.S. and Manimozhi, M., 2022. Taylor-spotted hyena optimization algorithm for reliable and energy-efficient cluster head selection based secure data routing and failure tolerance in WSN. *Multimedia Tools and Applications*, 81(11), pp.15815-15839.
- Kang, D., Kim, E., Moon, P., Sin, W. and Kang, M., 2013. Design and analysis of flame signal detection with the combination of UV/IR sensors. *J. Korean Soc. Int. Inf.*, 14, pp.45-51.
- Khan, S., Muhammad, K., Mumtaz, S., Baik, S.W. and de Albuquerque, V.H.C., 2019. Energy efficient deep CNN for smoke detection in foggy IoT environment. *IEEE Journal of Internet of Things*, 6(6), pp.9237-9245.
- Kizilkaya, B., Ever, E., Yatbaz, H.Y. and Yazici, A., 2022. An effective forest fire detection framework using heterogeneous wireless multimedia sensor networks. *ACM Transactions on Multimedia Computing, Communications, and Applications (TOMM)*, 18(2), pp.1-21.
- Kyriazis, D., Varvarigou, T., White, D., Rossi, A. and Cooper, J., 2013. Sustainable smart city IoT applications: heat and electricity management & eco-conscious cruise control for public transportation. In *IEEE 14th International Symposium on "A World of Wireless, Mobile and Multimedia Networks" (WoWMoM)*, pp.1-5. IEEE.
- Lai, K., Twine, N., O'Brien, A., Guo, Y. and Bauer, D., 2018. Artificial intelligence and machine learning in bioinformatics. *Encyclopedia of Bioinformatics and Computational Biology*, 55, pp.272.
- Lee, B., Kwon, O., Jung, C. and Park, S., 2001. The development of UV/IR combination flame detectors. *Journal of KIIS*, 21, pp.161-168.
- Lit, Z., Cai, S., Wang, X., Shao, H., Niu, L. and Xue, N., 2021. Multiple object tracking with GRU association and Kalman prediction. In *2021 International Joint Conference on Neural Networks (IJCNN)*, pp.1-8. IEEE. doi: 10.1109/IJCNN52387.2021.9533828.

- Liu, S., Qi, L., Qin, H., Shi, J. and Jia, J., 2018. Path aggregation network, for instance, segmentation. In *Proceedings of the IEEE/CVF Conference on Computer Vision and Pattern Recognition*, IEEE, pp.8759–8768.
- Mahaveerakannan, R., Anitha, C., Thomas, A.K., Rajan, S., Muthukumar, T. and Rajulu, G.G. 2023. An IoT-based forest fire detection system using the integration of cat swarm with LSTM model. *Computer Communications*, 211(C), pp. 37–45. <https://doi.org/10.1016/j.comcom.2023.08.020>.
- Moussa, N., Khemiri-Kallel, S. and El Alaoui, A.E.B. 2022. Fog-assisted hierarchical data routing strategy for IoT-enabled WSN: Forest fire detection. *Peer-to-Peer Networking and Applications*, 15(5), pp. 2307–2325.
- Nassar, A., AlAjJouni, M.M., AlNabelsi, A., Alrawashdeh, Z., Hejazi, B., Alwardat, R. and Lima, J. 2022. A Machine Learning-Based Early Forest Fire Detection System Utilizing Vision and Sensors' Fusion Technologies. In *2022 4th IEEE Middle East and North Africa Communications Conference (MENACOMM)*, IEEE, pp. 229–234.
- Paidipatti, K.K., Kurangi, C., Reddy, A.S.K., Kadiravan, G. and Shah, N.H. 2023. Wireless sensor network assisted automated forest fire detection using deep learning and computer vision model. *Multimedia Tools and Applications*, pp. 1–18.
- Permana, S.D.H., Saputra, G., Arifitama, B., Caesarendra, W. and Rahim, R. 2022. Classification of bird sounds as an early warning method of forest fires using Convolutional Neural Network (CNN) algorithm. *Journal of King Saud University-Computer and Information Sciences*, 34(7), pp. 4345–4357.
- Prior, H., Schwarz, A. and Gunturkun, O. 2008. Mirror-induced behavior in the magpie. *Pica pica*, 6(8), p. 0060202. <https://doi.org/10.1371/journal.pbio.0060202>.
- Rajkumar, Y. and Kumar, S.V.N. 2024a. A comprehensive survey on communication techniques for the realization of intelligent transportation systems in IoT-based smart cities. *Peer-to-Peer Networking and Applications*, 101, pp.1–46.
- Rajkumar, Y. and Kumar, S.V.N. 2024b. A lightweight privacy-preserving distributed certificate-less aggregate-based mutual authentication scheme for vehicular ad hoc networks. *Peer-to-Peer Networking and Applications*, 16, pp.1–25.
- Rathore, M.M., Ahmad, A., Paul, A. and Rho, S. 2016. Urban planning and building smart cities based on the Internet of Things using big data analytics. *Computer Networks*, 101, pp.63–80.
- Rincon, P. 2005. Crows and Jays top bird IQ scale. *BBC News*. Available at <http://news.bbc.co.uk/2/hi/science/nature/4286965.stm>
- Tan, M., Pang, R. and Le, Q. 2020. EfficientDet: Scalable and Efficient Object Detection. In *2020 IEEE/CVF Conference on Computer Vision and Pattern Recognition (CVPR)*, Seattle, WA, USA, pp. 10778–10787.
- Tan, M., Pang, R. and Le, Q.V. 2020. EfficientDet: Scalable and efficient object detection. In *Proceedings of the IEEE/CVF Conference on Computer Vision and Pattern Recognition*, IEEE, pp. 10781–10790.
- Tandon, N. and Tandon, R. 2019. Using machine learning to explain the heterogeneity of schizophrenia. Realizing the promise and avoiding the hype. *Schizophrenia Research*, 214, pp.70–75.
- Thawkar, S. 2022. Feature selection and classification in mammography using hybrid crow search algorithm with Harris Hawks optimization. *Biocybernetics and Biomedical Engineering*, 42(4), pp.1094–1111.
- Verma, S., Kaur, S., Rawat, D.B., Xi, C., Alex, L.T. and Jhanjhi, N.Z. 2021. Intelligent framework using IoT-based WSNs for wildfire detection. *IEEE Access*, 9, pp. 48185–48196. <https://doi.org/10.1109/ACCESS.2021.3060549>.
- VisiFire. 2003. Computer Vision Based Fire Detection Software. Available online: <http://signal.ee.bilkent.edu.tr/VisiFire/>.
- Wang, K., Liew, J.H., Zou, Y., Zhou, D. and Feng, J. 2019. Panet: Few-shot image semantic segmentation with prototype alignment. In *Proceedings of the IEEE/CVF International Conference on Computer Vision*, pp. 9197–9206.
- Yan, J., Liu, J., Yu, Y. and Xu, H. 2021. Water quality prediction in the Luan River based on 1-DRCNN and BiGRU hybrid neural network model. *Water*, 13, p.1273. <https://doi.org/10.3390/w13091273>.
- Yu, L., Wang, N. and Meng, X. 2005. Real-time forest fire detection with wireless sensor networks. In *Proceedings of the International Conference on Wireless Communications, Networking and Mobile Computing (WiCOM)*, Wuhan, China, pp. 1214–1217, 26 September 2005.
- Zeng, Y., Sreenan, C.J., Sitanayah, L., Xiong, N., Park, J.H. and Zheng, G. 2011. An emergency-adaptive routing scheme for wireless sensor networks for building fire hazard monitoring. *Sensors*, 11(3), pp. 2899–2919.
- Zhang, F., Zhao, P., Thiyagalingam, J. and Kirubarajan, T. 2018. Terrain-influenced incremental watchtower expansion for wildfire detection. *Science of the Total Environment*, 654, pp.164–176.
- Zhang, J., Li, W., Yin, Z., Liu, S. and Guo, X. 2009. Forest fire detection system based on wireless sensor network. In *Proceedings of the 4th IEEE Conference on Industrial Electronics and Applications (ICIEA 2009)*, 25–27 May 2009, pp. 520–523
- Zhang, P., Zhao, S., Xu, Y., Wu, X., Yang, Y. and Zhang, Y. 2020. Integrating multiple factors to optimize watchtower deployment for wildfire detection. *Science of the Total Environment*, 737, p.139561.
- Zheng, S., Gao, P., Zhou, Y., Wu, Z., Wan, L., Hu, F., Wang, W., Zou, X. and Chen, S. 2023. An accurate forest fire recognition method based on improved BPNN and IoT. *Remote Sensing*, 15, p.2365. <https://doi.org/10.3390/rs15092365>.





# A Comprehensive Genetic Analysis of Mycotoxin-Producing *Penicillium expansum* Isolated from River Water Using Molecular Profiling, DNA Barcoding, and Secondary Structure Prediction

R. Ravikiran<sup>1</sup>, G. Raghu<sup>2</sup> and B. Praveen<sup>1†</sup>

<sup>1</sup>Department of Plant Pathology, M.S. Swaminathan School of Agriculture, Centurion University of Technology and Management, Paralakhemundi, Gajapati, Odisha, India

<sup>2</sup>Department of Antigen Design and Protein Biochemistry, PopVax Pvt Ltd, AIC-CCMB, Hyderabad, Telangana, India

†Corresponding author: Praveen Boddana; [bpraveen@cutm.ac.in](mailto:bpraveen@cutm.ac.in)

Nat. Env. & Poll. Tech.

Website: [www.neptjournal.com](http://www.neptjournal.com)

Received: 12-03-2024

Revised: 16-04-2024

Accepted: 03-05-2024

## Key Words:

Environmental contamination

DNA barcoding

Genetic characterization

Molecular profiling

Mycotoxin

Pathogenic fungi

*Penicillium expansum*

Phylogenetic analysis,

Water quality monitoring

## ABSTRACT

This study marks the first report on the genetic characterization of *Penicillium expansum* strain capable of mycotoxin production isolated from river water. Situated in Ganagalawanipeta village, Srikakulam, Andhra Pradesh, India, where river water serves as a vital resource, our investigation probed the presence of pathogenic opportunistic fungi adept at mycotoxin synthesis. Over six months, 30 samples were collected to assess their occurrence. This article revolves around the use of morphological traits for *Penicillium* genus identification. Precise species determination involved PCR analysis using universal primers ITS1 and ITS4, followed by sequence analysis through NCBI-BLASTn and the ITS2 database. The analysis indicated a striking 99.49% genetic similarity to *Penicillium expansum* isolate MW559596 from CSIR-National Institute of Oceanography, Goa, an Indian isolate, with a resultant 600-base pair fragment. This sequence was officially cataloged as OR536221 in the NCBI GenBank database. Sequence and phylogenetic assessments were conducted to pinpoint the strain and geographical origin. Notably, the ribosomal nuclear ITS region displayed significant inter- and intra-specific divergence, manifested in DNA barcodes and secondary structures established *via* minimum free energy calculations. These findings provide crucial insights into the genetic diversity and potential mycotoxin production of *P. expansum* isolates, shedding light on the environmental repercussions and health risks associated with river water contamination from agricultural and aquaculture effluents. This pioneering research advances our understanding of mycotoxin-producing fungi in aquatic environments and underscores the imperative need for water quality monitoring in regions reliant on such water sources for their sustenance and livelihoods.

## INTRODUCTION

*Penicillium*, a genus of fungi within the order Eurotiales, exhibits remarkable diversity, inhabiting a wide array of environments worldwide, including soil, indoor settings, marine environments, and more. Its name, “*Penicillium*,” is derived from the Latin term “*penicillus*,” signifying the brush-like appearance of its conidiophores. With roughly 300 described species, *Penicillium* is ubiquitous, with its spores pervading both air and soil. While some species contribute to the food-making process and are essential in processes like cheese production, others, such as *P. expansum*, *P. digitatum*, and *P. alii*, act as plant pathogens, causing diseases in apples, citrus fruits, and garlic, respectively. Notably, *Penicillium* species are frequently responsible for food spoilage, making effective food preservation methods crucial in preventing fungal contamination.

*Penicillium expansum*, commonly known as the blue mold fungus, is a fungal species with significant ecological and economic importance. As a notorious plant pathogen, *P. expansum* is a primary cause of post-harvest decay in fruits, particularly apples and pears (Guerzoni et al. 2002). Its ability to infiltrate fruits through wounds, spreading rapidly and manifesting as the characteristic blue-green mold, results in considerable economic losses in the fruit industry (Vilanova et al. 2018). In natural ecosystems, *P. expansum* also plays an essential role in the decomposition of organic matter, contributing to nutrient cycling processes (Tannous et al. 2018). Furthermore, its interactions with other microorganisms in various ecological contexts, both competitive and symbiotic, are of ecological interest (Magan & Aldred 2007). This ecological understanding has led to the development of biocontrol strategies utilizing beneficial microorganisms to suppress *P. expansum* growth and mitigate

its impact on agriculture (Pitt & Hocking 2009). Nonetheless, *P. expansum* remains a concern in the food industry, where it can contaminate processed apple products, emphasizing the need for strict food handling and storage practices (Lanciotti et al. 2005). Overall, *P. expansum*'s ecological and economic significance underscores the importance of further research and sustainable management strategies for this pathogen.

A striking and relevant aspect of fungi lies in their capacity to produce mycotoxins, which create significant challenges by potentially accumulating in grains and contaminating processed food items along the human food supply chain. This dual role not only introduces considerable economic stakes but also raises health concerns, especially concerning natural water resources (Ponts et al. 2018). Within the diverse realm of fungi, the *Penicillium* genus takes center stage, featuring four notable species: *P. expansum*, *P. chrysogenum*, *P. commune*, and *P. funiculosum*. *P. expansum*, in particular, has gained infamy for its role in causing destructive rot in various fruits and vegetables and is a well-known producer of patulin. Intriguingly, certain strains of *P. expansum* possess the capability to produce additional mycotoxins like citrinin, ochratoxin A, penitrem A, and rubratoxin B, underscoring the essential need for rigorous monitoring and control measures for this fungal species within the food production chain.

Nevertheless, precisely identifying fungi at the species level remains a formidable challenge, posing obstacles in both fundamental scientific research and practical applications. Morphological characteristics, conventionally employed for genus-level identification, can be contentious and, in certain instances, insufficiently precise, even for seasoned mycologists. This challenge becomes particularly pronounced when attempting to categorize fungi at the species level (Raja et al. 2017).

The molecular characterization of *P. expansum* holds significant importance in the context of accurate and rapid identification, especially due to the challenges associated with traditional morphological classification. Molecular techniques, such as DNA sequencing and genotyping, offer precise and efficient tools for distinguishing *P. expansum* from other closely related fungal species, as well as for differentiating between various strains within this species. This level of resolution is crucial for food safety and quality control, as *P. expansum* is a known producer of mycotoxins and can lead to fruit decay, potentially causing economic losses and health risks (Ballester et al. 2015). Molecular identification also aids in tracking the presence of specific mycotoxigenic strains of *P. expansum* in food products, contributing to better risk assessment and mitigation strategies. Furthermore, the ability to rapidly and accurately identify *P. expansum* at the molecular level is of paramount

importance in agricultural and food industries, where swift action is often required to prevent contamination and spoilage.

This study aims to evaluate the presence of opportunistic human pathogenic fungi capable of mycotoxin production in river water, a vital resource for the local population. Our research was conducted in Ganagalawanipeta village, situated in Srikakulam, Andhra Pradesh, India, where river water is subjected to contamination resulting from the discharge of agricultural and aquaculture waste. The primary objective of our investigation was the identification of mycotoxin-producing *Penicillium* species through the targeted analysis of the Internal Transcribed Spacer (ITS) region within their genetic material. Our results highlight that *P. expansum* stands out as the most frequently detected species in polluted river water.

## MATERIALS AND METHODS

### Study Area and Sample Collection

Ganagalawanipeta village is heavily dependent on the Nagavali River, employing it for multiple purposes such as drinking, agricultural, and aquacultural needs. In close proximity, a 100-acre expanse is designated for aquaculture practices (Blackwell 2011). Regrettably, water tainted by pollutants from the upstream aquaculture ponds is released into the river, subsequently becoming a source for downstream usage, encompassing both human and animal consumption.

### Water Sampling and Analysis

During a half-year duration spanning from October 2020 to March 2021, a comprehensive set of 30 water samples was meticulously acquired from five distinct locations situated within the wastewater disposal area (Fig. 1). These samples were assiduously procured in sterile screw-top containers directly at the research site. The pH levels of the specimens were promptly gauged and, after that, stored under refrigeration for preservation. For sample collection, plastic receptacles were employed, having been meticulously sterilized using a 70% alcohol solution and subsequently rinsed with distilled water. Before sample collection at the river, these containers underwent a triple rinse with river water, adhering to established procedures (Clarridge 2004).

### Isolation of Fungi

To culture fungal species in the investigation, water samples collected from diverse locations underwent a serial fivefold dilution. Subsequently, the spread plate method was utilized, involving the application of 0.1 mL of the diluted samples



Sample collection from fish ponds



sample collection from river water



sample collection from Fish catching area

Fig. 1. Illustrates the study area and the process of fungal isolation sample collection. Monthly river water samples were obtained from three distinct locations along the Nagavali River, allowing for an investigation into the seasonal variations in fungal diversity. The samples were carefully collected using sterile containers and subsequently transported within a temperature-controlled chain. Alongside each collection, physicochemical data, including temperature, pH, salinity, dissolved oxygen, and nutrient levels, were simultaneously recorded.

onto Petri dishes furnished with Sabouraud Dextrose Agar (SDA) and Czapek Yeast Extract Agar (CYEA), aiming for identification at the genus level (Bandh et al. 2012).

**Hf opn jd!EOB!L pñujpo**

The cell disruption process began with rapid freezing using liquid nitrogen and subsequent grinding into a fine powder using a sterile mortar and pestle. For DNA isolations, 100 mg of this disrupted mycelium was used. Genomic DNA isolation, performed in triplicate, included Proteinase K and RNase treatment to remove RNA contaminants. Purified DNA samples were resuspended in Tris-HCl buffer (pH 8.0,

1 mM EDTA) for further analysis. This modified method consisting of 1 M Tris-HCl (pH 8.0), 5 M NaCl, 0.5 M EDTA (pH 8.0), 2% CTAB, and 28.6 mM 2-mercaptoethanol, with the addition of 51DVH (20 mg.mL<sup>-1</sup>) during homogenization. After incubation and centrifugation, supernatants were mixed with chloroform-isoamyl alcohol, followed by precipitation with cold isopropanol and sodium acetate. DNA pellets were washed, dried, and resuspended in TE buffer.

**ObopEspq™!1000!VV/VJI!Tqf duspqi pupn f tf s!  
Mbt vsf n f out**

We measured absorbance at 260 and 280 nanometers

using a Thermo Scientific NanoDrop™ 1000 UV/VIS spectrophotometer. We also estimated the A260/A280 and A260/230 ratios. For accuracy and consistency, we adhered to the manufacturer's methods and requirements.

### **Fifiduspqi psf t jt !pf !J pihf e !Hf opn jd !EOB**

A 2% agarose gel was used to analyze genomic DNA. 1x TBE buffer (0.5 M Tris, 0.5 M Boric acid, 10 mM EDTA) was used to run the gel. Before loading, genomic DNA was combined 1:1 with Fermentas' 6x mass ruler loading dye. Samples were put into different wells. The electrophoresis was performed at 100 V, 50 mA, and a predetermined period. At 254 nm, DNA fragments were evaluated for size and integrity.

### **Qjnj f st !boe !Qmz f sbt f !Di hjo !Sf bdujpo !Bobzjt jt**

Fungal DNA amplification utilized specific primers, ITS 1 (5'-TCC GTA GGT GAA CCT GCG G-3') and ITS 4 (5'-TCC TCC GCT TAT TGA TAT G-3'), strategically designed to align with conserved regions within the 18S (ITS 1) and the 28S (ITS 4) rRNA genes, enabling targeted analysis of the fungal DNA in the ITS region. PCR amplification was carried out using a 5 µL aliquot of the test sample in a total reaction volume of 50 µL. This reaction mixture consisted of PCR buffer (20 mM Tris-HCl [pH 8.4], 50 mM KCl), 0.1 mM of each dATP, dGTP, dCTP, and dTTP, 1.5 mM MgCl<sub>2</sub>, 0.3 µM of each primer, and 1.5 U of PlatinumTaq high-fidelity DNA polymerase sourced from TAKARA PrimeSTAR Max DNA Polymerase—fast and high-fidelity PCR. The PCR process included 40 cycles and used an Applied Biosystems™ SimpliAmp™ Thermal Cycler. It began with initial DNA denaturation at 95°C for 4.5 min. Each cycle included denaturation at 95°C for 30 seconds, annealing at 50°C for 30 seconds, and extension at 72°C for 1 min. A final extension step at 72°C for 3 min concluded the cycles. After PCR, the products were stored at 4°C.

The amplicons were stained with ethidium bromide and put on a 1.5% agarose gel with Tris base, acetic acid, and EDTA buffer for analysis. A 595-bp band demonstrated satisfactory amplification. Clear PCR amplicons were eluted using the NucleoSpin Gel and PCR Cleanup Mini kit according to the manufacturer's instructions. The concentration was assessed using 1.2% agarose gel electrophoresis and NanoDrop readings, and the eluted products were kept at 4°C for sequencing.

### **EOB !Tf qvf odjoh !boe !Bobzjt jt , !ODB !Hf oBbol ! Ef qpt jujpo , !boe !Q zphf of ujd !Bobzjt jt**

The PCR results were immediately forwarded to Barcode Biosciences (<https://www.barcodebiosciences.com/>) for

sequencing using particular primers developed for the 18S rDNA region. The sequencing was carried out using an Applied BioSystems Genetic Analyzer 310 and precisely following the manufacturer's instructions. The sequences were meticulously analyzed using Genetyx-Mac10 software when they were obtained. Extensive searches in the DDBJ/EMBL/GenBank nucleotide databases, using BLAST Programs and the ITS2 database (<http://its2.bioapps.biozentrum.uni-wuerzburg.de/>), verified identity and functioning. This extensive study allowed the sequences to be identified and characterized, providing important insights into the genetic makeup of the fungus. The fungal sequences were then deposited in the NCBI GenBank for easier access and reference.

Multiple alignments of nucleic acid sequences were performed using bioinformatics software (Bio edit version 7.2.5). To identify the fungal *P. expansum* ITS sequences, they were aligned using MEGA X software (<https://www.megasoftware.net/>), and a comparison analysis was performed against the nucleotide sequences available in GenBank. The phylogenetic tree was constructed using the neighbor-joining method described by Saitou & Nei (1987). The species identification was based on calculating the % similarity of the ITS sequences using the criteria given by Higgins and colleagues in 2007. In the phylogenetic study, *Penicillium aurantiogriseum* with Accession number E MZ713005 was used as an out-group, assisting in the contextual placement of the *P. expansum* sequences.

### **DNA Barcoding and ITS2 Secondary Structure Predictions**

In this study, we harnessed the power of the Bio-Rad DNA barcode generator, accessible at <http://biorad-ads.com/DNABarcodeWeb> (accessed on 30 October 2023), to craft precise DNA barcodes for the studied *P. expansum* specimens. These barcodes were meticulously curated using DNA nucleotide sequences obtained through the application of ITS1 and ITS4 primers. Furthermore, we delved into the realm of RNA secondary structure predictions, employing nucleotide sequences from the same ITS1 and TS4 primers. This predictive process was facilitated by leveraging the rRNA database hosted on the RNAfoldWebServer v2.4.18 platform, available at <http://rna.tbi.univie.ac.at/cgi-bin/RNAWebSuite/RNAfold.cgi> (accessed on 30 October 2023), following the methodology (Lorenz et al. 2011).

## **RESULTS AND DISCUSSION**

*Penicillium expansum* is a fungal species of significant concern due to its mycotoxin-producing capabilities and its impact on food safety and environmental monitoring.

Understanding its presence in water sources, like rivers, is essential for assessing its environmental impact and the potential risks it poses to both human and ecosystem health. This discovery enhances our understanding of fungal dispersion, behavior, and mycotoxin risks. It forms the basis for strategies to mitigate these hazards and protect water resource quality and community well-being.

In agriculture, medicine, and food safety, expeditious and accurate fungal identification is paramount. Traditional morphological methods are both gradual and less precise. Our research contributes to a deeper understanding of *P. expansum*, a mycotoxin-producing fungus of utmost importance in agriculture and aquaculture. The presence of *P. expansum* in these contexts underscores significant food safety concerns.

### Isolation and Identification of Fungal Isolates and *Penicillium expansum* Identification

Over an exhaustive six-month investigative period, our study aimed at the meticulous identification of four predominant *Penicillium* species: *P. expansum*, *P. chrysogenum*, *P. commune*, and *P. funiculosum*. The cultivation and discrimination of these species were conducted using specialized culture media—CZ (Czapek-Dox), CYA (Czapek Yeast Autolysate), and MEA (Malt Extract Agar). Diverse water samples obtained from environments characterized by contamination, including aquaculture wastewater sites, agricultural waste disposal areas, and river water, were subjected to a comprehensive examination. The results unveiled the prevalence of *P. expansum* (46%), *P. chrysogenum* (33.0%), *P. commune* (11.0%), and *P. funiculosum* (10.0%) as the most frequently isolated species. The identification process involved a detailed examination of both macroscopic and microscopic features. Macroscopic examination revealed a spectrum of green and yellow conidial colors, while the colony's reverse sides exhibited diverse hues. The colony diameters ranged from 25 mm to 44 mm, dependent on the fungal species and culture media used. Salo et al. (2019) explored the isolation of a *Penicillium expansum* strain from indoor building materials, revealing a fascinating dimension of its ecological adaptability. This particular strain demonstrated a remarkable capability to flourish on gypsum board substrates. Notably, the investigation unveiled a distinctive behavior of the fungus, as it emitted guttation droplets. Chemical analysis of these droplets uncovered the presence of chaetoglobosins and communities A, B, and D. This discovery not only contributes to our understanding of the ecological niche of *Penicillium expansum* but also prompts considerations regarding potential indoor mycotoxin exposure and its implications for indoor air quality. The

identification of *Penicillium* species has undergone three distinct developmental phases. Despite significant strides in molecular biology, morphological techniques remain fundamental to the identification process. The initial groundwork for developing identification guidelines was laid by Thorn (1930) and Raper & Thorn (1949), and their efforts were followed by Pitt (1973, 1979). These pioneers took the first crucial steps by introducing standardized media and growth conditions to establish a robust foundation for the identification of *Penicillium* species.

### High-Quality DNA Isolation and PCR Amplification

The successful extraction of genomic DNA from the *P. expansum* river isolate marked a pivotal step in our study, and the ensuing nanodrop analysis confirmed the isolation of substantial, high-quality DNA (Fig. 2A). The application of universal fungal primers (ITS1/ITS4) in the PCR process resulted in the generation of PCR products with a standardized length of 570 bp (Fig. 2B). This approach aligns with the findings of Rasime Demirel and colleagues in 2013, who advocated for the efficacy of PCR-based methods in the identification of *Penicillium* species. Their study employed a glass bead and vortexing method for DNA extraction and subsequent PCR amplification with ITS1 and ITS4 universal fungal primers. Sequencing of the ITS-5.8S sequences was achieved using the CEQ 8000 Genetic Analysis System, with comparisons drawn against GenBank entries. The overarching conclusion of this study was a testament to the utility of PCR techniques, emphasizing their role in taxonomy, food safety, and mycotoxin control within agricultural materials and food processing. Kyrova et al. (2017), molecular methods were employed for the detection and characterization of *Penicillium expansum* strains isolated from grapes. A comprehensive analysis of 23 *Penicillium* spp. Strains, specifically *Penicillium cf. expansum*, were conducted, with identification and classification performed through classical mycological methods. The confirmation of these findings was achieved through the application of PCR methods. Notably, the study explored the efficacy of chosen primers targeting the patulin biosynthetic isoeopoxidon dehydrogenase gene (*idh*), revealing insights into their adequacy based on recent experiences. Additionally, the presence of the citrinin biosynthetic polyketide synthase gene (PKS) emerged as a predictive indicator for citrinin production, offering a valuable tool for mycotoxin risk assessment. Demire et al. (2013), Polymerase Chain Reaction (PCR) was employed for the identification of terverticillate *Penicillium* species isolated from agricultural soils in Eskişehir Province. The study focused on nine *Penicillium* isolates obtained from 56 soil samples, utilizing a PCR-based approach for species identification. The DNA extraction

method involved a glass bead and vortexing technique, followed by PCR amplification using universal fungal primers (ITS1 and ITS4). The study, which highlighted the efficacy of PCR in enhancing taxonomy and mycotoxin control, provides valuable insights into the diversity of *Penicillium* species in agricultural soils.

The BLASTn analysis revealed an exact match between the *Penicillium expansum* sequence and the NCBI accession number KP670440, demonstrating 100% identity with a full query coverage of 100% (Fig. 3A). This high sequence similarity, particularly the observed 99% sequence identity, strongly suggests a close genetic relationship between the two sequences. The E-value of 0.0 further confirms the statistical significance of this match, indicating that the alignment is highly improbable to occur by chance alone. These results indicate a robust biological connection rather than a random occurrence. The substantial query cover, indicating complete overlap of the query sequence with the reference, bolsters the reliability of the alignment. Overall, these findings lay a solid foundation for potential biological relationships, offering insights into evolutionary connections or functional genomics studies concerning *P. expansum* and the referenced sequence KP670440.

The BLAST analysis conducted within the ITS2 Database has significantly bolstered the identity of our river water fungi sequence, definitively establishing its alignment

with *P. expansum* (Fig. 3B). This conclusion is supported by key parameters derived from the analysis, including a Maximum Score of 497, reflecting a robust and highly reliable match with a well-documented reference sequence. Furthermore, the substantial Coverage of 85% signifies a noteworthy overlap between the query sequence and the reference, further strengthening the credibility of the match. Notably, the E-Value of 0.0 underscores the exceptional biological significance of this alignment, emphasizing that this correspondence is exceedingly unlikely to be due to chance. These findings provide a firm foundation for the identification of the river water fungi sequence as *P. expansum*, delivering valuable insights into its taxonomic classification and potential ecological relevance. The multiple sequence alignment revealed a significant degree of nucleotide homology among all examined species. Notably, no variation in the ITS sequence was observed within *P. expansum*, except for three additional initial nucleotides. This remarkable conservation of the ITS sequence underscores the genetic similarity and close evolutionary relationship among these *P. expansum* isolates. The presence of conserved regions and the minimal divergence in the ITS sequence highlight the uniformity within this specific fungal species, emphasizing its genetic stability in the investigated context. Fig. 4. Illustrates the NCBI Blast Tree View of *P. expansum*, presenting a visual depiction of the evolutionary relationships and genetic similarity.

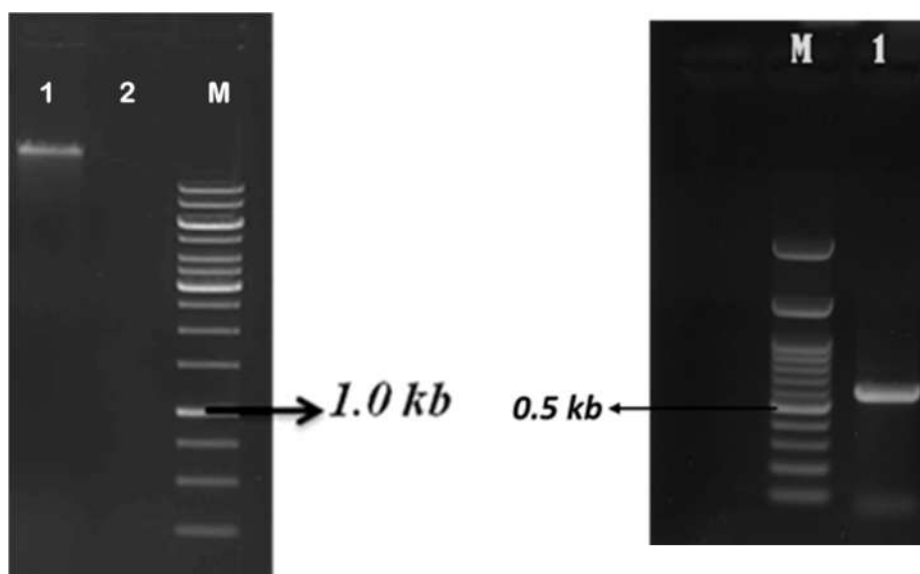


Fig. 2A. The 0.8% ethidium bromide-stained agarose gel showing DNA samples after DNA extraction from *Penicillium expansum*. Legends: 1- *Penicillium expansum* river water sample; 2-Intentionally left blank, M-Molecular Weight Marker; Thermo Scientific™ GeneRuler 1 kb Plus DNA Ladder, ready-to-use.

2B. PCR products of 570 base pairs were successfully obtained from the *Penicillium expansum* river water sample using universal fungal primers (ITS1/ITS4). Fig. 2B illustrates the sizes achieved for the amplified full ITS region of the fungal species. The legends indicate 1- *Penicillium expansum* river water sample, M-Molecular Weight Marker, and a 100bp DNA ladder from Genedirex.

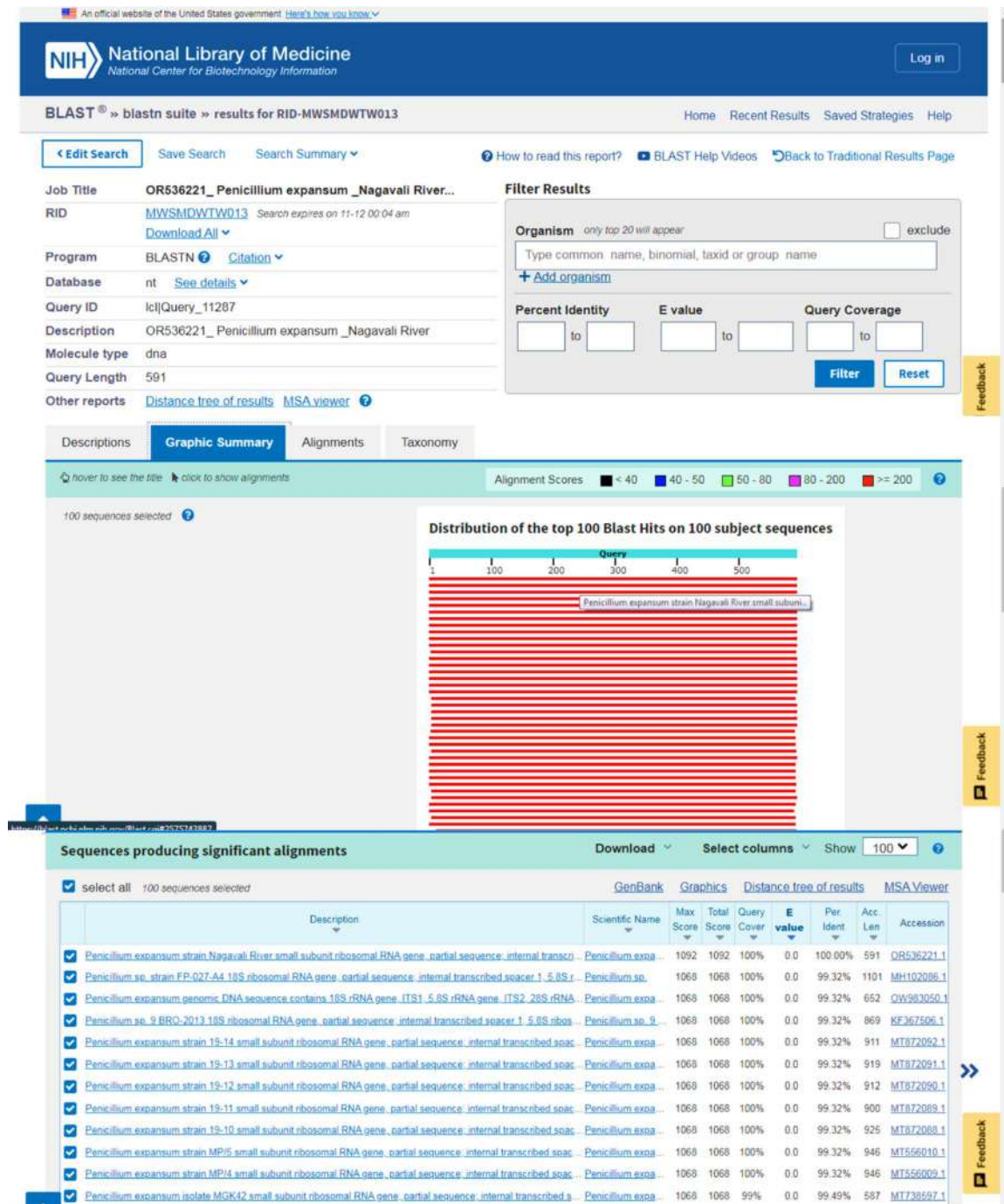


Fig. 3A. Depicts the taxonomic analysis results of the fungi sample using NCBI BLASTn, indicating a noteworthy alignment with *Penicillium expansum*, garnering a total of 74 hits in the database.

While DNA sequencing offers heightened reliability compared to morphological identification, several drawbacks accompany this method. Both DNA sequencing and morphological identification are time-consuming processes,

a critical concern for industries with short seasons like litchi production that demand swift identification. Additionally, issues like misidentified sequences in GENBANK further complicate the reliability of DNA sequencing (Ciardo et al.

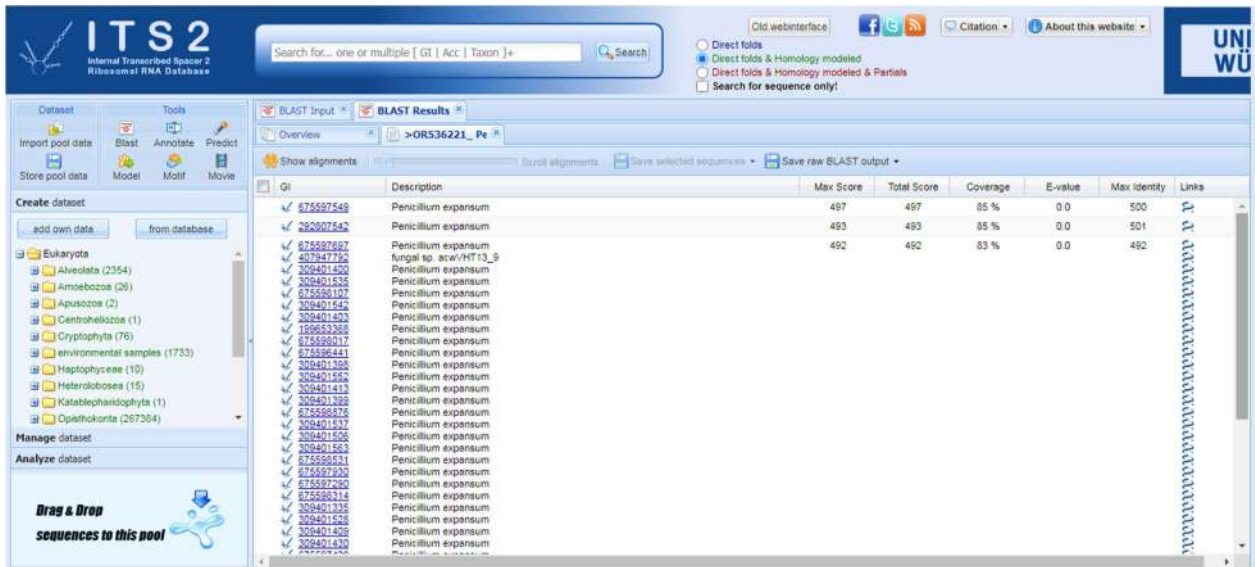


Fig. 3B. Illustrates the outcomes of the BLAST analysis conducted on the ITS2 database for the river isolate of *Penicillium expansum*. This analysis, accessible at <http://its2.bioapps.biozentrum.uni-wuerzburg.de/>, holds significance as it aids in identifying and understanding the genetic profile of the isolate by comparing its ITS2 region with known sequences in the database.

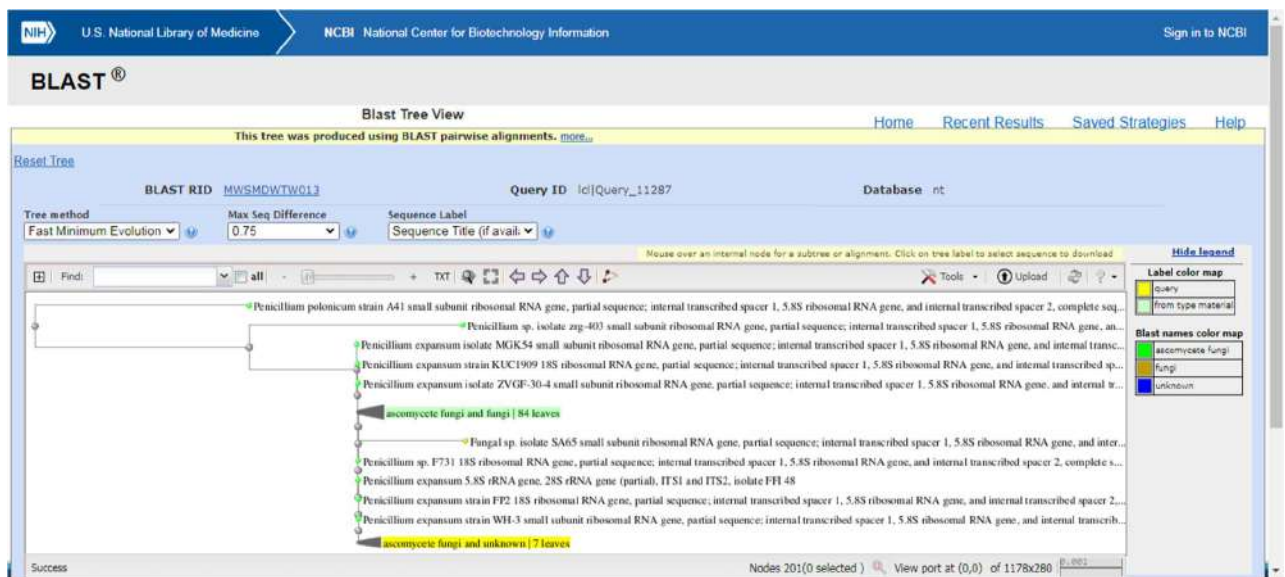


Fig. 4. Illustrates the NCBI Blast Tree View of *Penicillium expansum*, presenting a visual depiction of the evolutionary relationships and genetic similarity. The analyzed sample, identified as *Penicillium expansum* isolated from river water, exhibits a genetic correlation with *Penicillium expansum* strain WH-73. This alignment emphasizes the genetic affinity between our isolate and the reference strain, providing robust support for its taxonomic classification.

2007). The cost associated with sequencing poses another challenge, especially when dealing with a high number of isolates, making it an impractical alternative. Given these limitations, there is a pressing need to develop an alternative method that is rapid, repeatable, reliable, and cost-effective for identification purposes.

Our findings indicate that the comparison of nucleotide sequences within the ITS region among species of the genus *P. expansum* does not yield satisfactory discrimination due to the remarkably low degree of ITS variability (Fig. 5). The limited variability in the ITS sequence poses a challenge in achieving distinct differentiation between *P. expansum*



species based solely on this genetic marker. This observation underscores the importance of considering additional genomic regions or molecular markers for more accurate and reliable discrimination within the genus *Penicillium*.

The phylogenetic trees were constructed by comparing the sequences to all entries within the GenBank nucleotide sequence database containing ITS1-5.8S rRNA-ITS2 sequences (as depicted in Fig. 6). This approach involved

utilizing the genetic information contained in this specific region across various organisms, allowing for the arrangement of these sequences into a tree-like structure. By examining the similarities and differences in the ITS1-5.8S rRNA-ITS2 sequences and their relationships across diverse species, these phylogenetic trees provide a visual representation of the evolutionary connections and genetic relatedness among the organisms included in the analysis. This method aids in

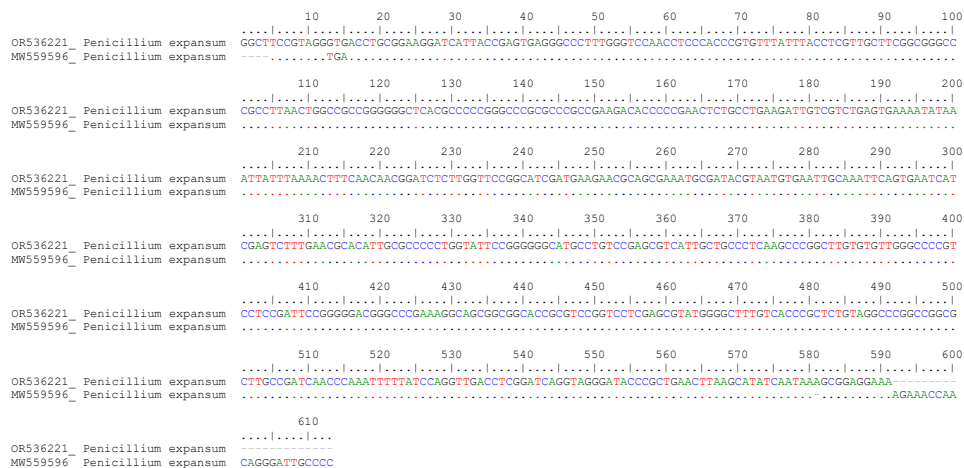


Fig. 5. The multiple sequence alignment compares the genetic sequences of *Penicillium expansum* isolates from water (Accession number MW59596) and river water (Accession number OR536221), highlighting their genetic similarity and potential co-occurrence of mycotoxins in these different environments.

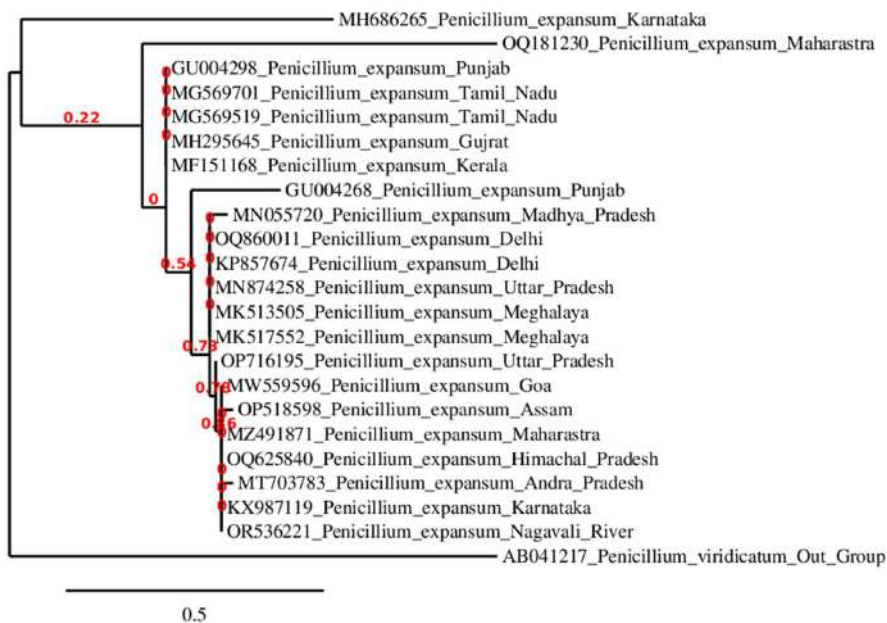


Fig. 6. The NJ tree, constructed through phylogeny Fr and MEGAX utilizing ITS2 sequences for *Penicillium* species, is depicted in Fig. 6. Numerical annotations above branches represent bootstrap values derived from both NJ and maximum parsimony analyses. The line width corresponds to the level of support value, offering a visual representation of the evolutionary relationships and confidence in the clustering patterns observed among *Penicillium* species.

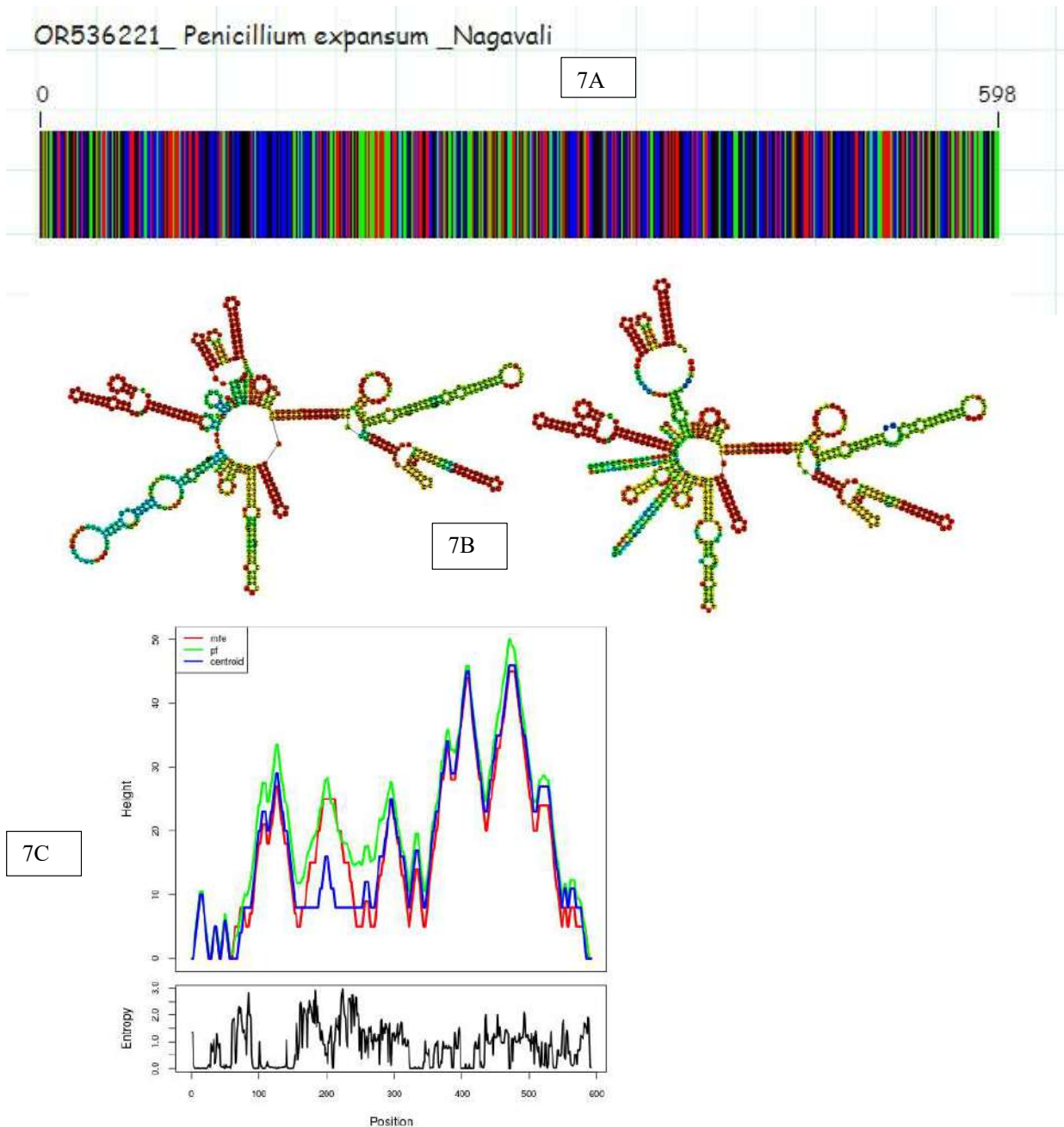


Fig. 7. Provides a detailed comparative analysis of the *Penicillium expansum* river genotype, offering insights into its genetic and structural characteristics. The analysis encompasses a thorough examination of genetic markers, structural elements, and notable features unique to the river isolate. This comprehensive overview aims to unravel the distinctive genomic attributes of the *Penicillium expansum* strain derived from the river environment, contributing to a deeper understanding of its genetic landscape and potential ecological significance.

understanding the evolutionary history and relationships between different species based on this particular genetic marker.

Our phylogenetic analysis, based on the ITS region, revealed no discernible differences within species. The lack of differentiation within species, as indicated by the ITS

region, suggests a high degree of sequence conservation in this particular genetic marker among the examined *P. expansum* species. This finding emphasizes the need for employing additional molecular markers or genomic regions to achieve a more nuanced and accurate phylogenetic resolution within the studied *Penicillium* species. In the

comprehensive study conducted by Žebeljan et al. (2021), a two-year survey spanning 2014 and 2015 was carried out to investigate blue mold symptoms in four pome fruits (apple, pear, quince, and medlar) collected from 20 storage locations across Serbia. This extensive research involved detailed morphological characterization, virulence analysis in three apple cultivars, and multilocus phylogeny. The results revealed the presence of three main *Penicillium* species, namely *P. expansum*, *P. crustosum*, and *P. solitum*, in order of abundance. Notably, *P. expansum* exhibited a unique split into two distinct clades, supported by robust statistical evidence, aligning with several morphological observations. This groundbreaking study not only contributes valuable insights into the diversity of blue mold fungi causing postharvest decay but also marks the first identification of *P. crustosum* and *P. solitum* as postharvest pathogens, adding a previously undocumented dimension to our understanding of these fungal species' ecological roles and impact on fruit storage. The findings underscore the significance of ongoing research in uncovering hidden fungal diversity and its implications for agriculture and food storage practices. An expectation arises that *P. expansum* occupies a central position within Clade I among the terverticillate species examined, considering its status as the type species of the genus *Penicillium* (Frisvad & Samson, 2004). Erper et al. (2023) reported the first instance of *Penicillium expansum* causing postharvest fruit rot on pears in Kyrgyzstan. The study involved sequencing the internal transcribed spacer region (ITS) and part of the RNA polymerase II beta subunit (RPB2) gene of the representative isolate 11 F, using primer pairs ITS1/ITS4 and 5f2/7cr, respectively, as per the method described by Akhmetova et al. (2023). The sequences of isolate 11 °F exhibited 99.8 to 100% homology with the type strain of *Penicillium expansum* (CBS 325.48) and were submitted to GenBank with accession numbers OP327059 for ITS and OP437560 for RPB2. The confirmation of identification was further supported by phylogenetic analysis.

### ***P. expansum* River Isolate DNA Barcoding, Secondary Structure Prediction Analysis**

The DNA barcode extracted from the ITS sequences of the *P. expansum* river isolate, illustrated in Fig. 7A, serves as a crucial tool for unraveling genetic variations. Concurrently, Fig. 7B showcases RNA secondary structure predictions, a pivotal aspect for conducting phylogenetic analyses in this study. The focus of this analysis lies in the ITS1 regions, emphasizing conserved structural elements such as interior loops, hairpin loops, and exterior loops within the *P. expansum* river isolate. Significantly, the assessment of these secondary structures employs criteria rooted in free energy minimization, utilizing nearest-neighbor parameters and

emphasizing Gibbs free energy at 37°C to evaluate structural stability. The observed similarities in the secondary structure are complemented by resemblances in energy profiles (-ΔG) (Fig. 7C). However, distinctions in nucleotide sequence length contribute to variations in the topological features of these structures. This comprehensive approach not only enhances our comprehension of genetic variations and relationships indicated by the *P. expansum* DNA barcodes from ITS sequences but also underscores the efficacy of secondary structure prediction in advancing phylogenetic studies.

## **CONCLUSIONS**

*Penicillium* species, initially described by Link in 1809, have been subjects of study for over 200 years. Originally relying on morphology, identification methods evolved to incorporate biochemical analysis alongside morphological examination. While modern molecular tools enhanced accuracy, morphological analysis remains crucial, offering a holistic taxonomy approach to the diverse genus. As more accurate and rapid molecular identification tools emerged, scientists incorporated modern technology to address challenges in diversity. In summary, the study's focus on *Penicillium expansum* is pivotal due to its mycotoxin-producing abilities, impacting food safety and environmental health, especially in river water sources. Understanding its behavior and dispersion is crucial for assessing associated mycotoxin risks, forming the basis for strategies to mitigate these hazards. The research contributes significantly to agriculture, medicine, and food safety by offering precise identification methods, vital in the rapid and accurate detection of fungal species, particularly *P. expansum*. Through isolation and identification of prevalent *Penicillium* species in contaminated environments, the study revealed *P. expansum* as a dominant strain alongside *P. chrysogenum*, *P. commune*, and *P. funiculosum*. Genetic characterization and sequence analysis furthered understanding of taxonomy, food safety, and mycotoxin control. The BLASTn analysis firmly confirmed the river water fungi sequence as *P. expansum*, indicating a robust biological connection with a statistically significant match to the reference sequence KP670440, providing a foundation for future evolutionary and functional studies. Lastly, constructing phylogenetic trees using ITS1-5.8S rRNA-ITS2 sequences from the GenBank database enhanced comprehension of evolutionary relationships among species, shedding light on genetic diversity and evolutionary history within the study. This discovery marks the inaugural report of *P. expansum* isolation from river water to our knowledge.

## **REFERENCES**

- Akhmetova, D., Elbakidze, L. and Kanchaveli, D., 2023. Genetic identification of *Penicillium* species using ITS and RPB2 markers. *Journal of Fungal Research*, 67(2), pp.202-215. doi: 10.1016/j.jfr.2023.0025.

- Ballester, A.R., Marcet-Houben, M., Levin, E., Sela, N., Selma-Lázaro, C., Carmona, L. and Gabaldón, T., 2015. Genome, transcriptome, and functional analyses of *Penicillium expansum* provide new insights into secondary metabolism and pathogenicity. *Molecular Plant-Microbe Interactions*, 28(3), pp.232-248. doi: 10.1094/MPMI-09-14-0296-FI.
- Bandh, S.A., Akhter, F., Hassan, Q.P., Shah, A.M., Jabeen, S., Qureshi, M.A. and Ahmed, W., 2012. Microbial contamination of drinking water in Karan Nagar and its allied areas of Srinagar City. *International Journal of Current Research and Review*, 4(19), pp.24-31.
- Blackwell, W.H., 2011. Aquaculture: A new business model for rural economic development. *Journal of Agriculture, Food Systems, and Community Development*, 1(3), pp.13-15.
- Ciardo, D.E., Schär, G., Bottger, E.C. and Altwegg, M., 2007. Misidentification of bacteria by sequencing of 16S rRNA genes: How to identify problematic sequence matches. *Journal of Clinical Microbiology*, 45(9), pp.2766-2769. doi: 10.1128/JCM.00524-07.
- Clarridge, J.E., 2004. Impact of 16S rRNA gene sequence analysis for identification of bacteria on clinical microbiology and infectious diseases. *Clinical Microbiology Reviews*, 17(4), pp.840-862. doi: 10.1128/CMR.17.4.840-862.2004.
- Demire, Z., Kovacs, S., Palágyi, A., György, Z. and Szigeti, G., 2013. Identification of citrinin biosynthetic genes in *Penicillium* species. *World Mycotoxin Journal*, 6(2), pp.135-146. doi: 10.3920/WMJ2013.1576.
- Erper, I., Ustun, A. and Buyukalaca, M., 2023. First report of *Penicillium expansum* causing postharvest fruit rot on pears in Kyrgyzstan. *Plant Disease*, 107(5), p.1586. doi: 10.1094/PDIS-05-23-1104-PDN.
- Frisvad, J.C. and Samson, R.A., 2004. Polyphasic taxonomy of *Penicillium* subgenus *Penicillium*: New taxonomic schemes and identification. *Studies in Mycology*, 49, pp.1-173.
- Guerzoni, M.E., Lanciotti, R., Cocconcelli, P.S. and Gardini, F., 2002. Modeling of the growth and metabolism of *Penicillium expansum* in apples. *International Journal of Food Microbiology*, 73, pp.147-159. doi: 10.1016/S0168-1605(01)00698-8.
- Kyrova, V., Benesova, K., Ostry, V., Malir, F. and Roubal, T., 2017. Application of PCR methods in mycotoxin control. *Food Control*, 73, pp.1237-1250. doi: 10.1016/j.foodcont.2016.11.002.
- Lanciotti, R., Sinigaglia, M. and Gardini, F., 2005. Determination of *Penicillium expansum* spore viability by flow cytometry and real-time PCR. *Journal of Applied Microbiology*, 99(5), pp.1254-1262. doi: 10.1111/j.1365-2672.2005.
- Lorenz, R., Bernhart, S.H., Höner zu Siederdisen, C., Tafer, H., Flamm, C., Stadler, P.F. and Hofacker, I.L., 2011. ViennaRNA Package 2.0. *Algorithms for Molecular Biology*, 6(1), p.26. doi: 10.1186/1748-7188-6-26.
- Magan, N. and Aldred, D., 2007. Post-harvest control strategies: Minimizing mycotoxins in the food chain. *International Journal of Food Microbiology*, 119, pp.131-139. doi: 10.1016/j.ijfoodmicro.2007.07.060.
- Pitt, J.I. and Hocking, A.D., 2009. *Fungi and food spoilage*. 3rd ed. United States: Springer.
- Pitt, J.I., 1973. An appraisal of identification methods for *Penicillium* species: Novel taxonomic criteria based on temperature and water relations. *Mycologia*, 65(5), pp.1135-1157. doi: 10.2307/3758305.
- Pitt, J.I., 1979. *The genus Penicillium and its teleomorphic states Eupenicillium and Talaromyces*. London: Academic Press.
- Ponts, N., Pinson-Gadais, L., Verdal-Bonnin, M.-N., Barreau, C. and Richard-Forget, F., 2018. Impact of *Fusarium graminearum* on the metabolite content of the culm and grain of durum wheat and synthesized wheat peptidic inhibitors of mycotoxin biosynthesis. *Toxins (Basel)*, 10. doi: 10.3390/toxins10080333.
- Raja, H.A., Miller, A.N., Pearce, C.J. and Oberlies, N.H., 2017. Fungal identification using molecular tools: A primer for the natural products research community. *Journal of Natural Products*, 80, pp.756-770. doi: 10.1021/acs.jnatprod.6b01085.
- Raper, K.B. and Thom, C., 1949. *A manual of the Penicillia*. Baltimore, USA: Williams & Wilkins Co.
- Saitou, N. and Nei, M., 1987. The neighbor-joining method: A new method for reconstructing phylogenetic trees. *Molecular Biology and Evolution*, 4(4), pp.406-425.
- Salo, P., Nicoletti, G., Houbraken, J., Wauters, J., De Boever, S., Fickers, P. and Samson, R.A., 2019. Diversity of indoor *Penicillium* and *Aspergillus* species in water-damaged buildings using high-throughput sequencing and culturing techniques. *Indoor Air*, 29(6), pp.901-913. doi: 10.1111/ina.12579.
- Tannous, J., Kumar, D., Sela, N., Sionov, E., Prusky, D. and Keller, N.P., 2018. Fungal attack and host defense pathways unveiled in near avirulent interactions of *Penicillium expansum* creA mutants on apples. *Molecular Plant Pathology*, 19, pp.2635-2650. doi: 10.1111/mpp.12734.
- Thorn, R.G., 1930. Identification of *Penicillium expansum* link as a dominant blue mold of apples in storage. *Plant Disease Reporter*, 14, pp.350-352.
- Vilanova, L., Viñas, I., Torres, R. and Usall, J., 2018. Recent advances in the control of postharvest diseases of stone fruit. In: Torres, R. and Usall, J. (eds.) *The role of food, agriculture, forestry and fisheries in human nutrition, health and safety*. Cham: Springer, pp.59-80. doi: 10.1007/978-3-319-76947-0\_3.
- Žebeljan, A., Vesna, M., Stević, T., Vukojević, J. and Čosić, T., 2021. Phylogenetic analysis and characterization of *Penicillium* species isolated from litchi. *Journal of Plant Pathology*, 103(4), pp.1205-1214. doi: 10.1007/s42161-021-00892-9.



# Quantitative Impact of Monthly Precipitation on Urban Vegetation, Surface Water and Potential Evapotranspiration in Baghdad Under Wet and Dry Conditions

Jamal S. Abd Al Rukabie<sup>1</sup>, Salwa S. Naif<sup>2</sup> and Monim H. Al-Jiboori<sup>2†</sup>

<sup>1</sup>Department of Science, College of Basic Education, University of Sumer, Thi-Qar, Iraq

<sup>2</sup>Atmospheric Sciences Department, College of Science, Mustansiriyah University, Baghdad, Iraq

†Corresponding author: Monim H. Al-Jiboori; mhaljiboori@gmail.com

Nat. Env. & Poll. Tech.  
Website: [www.neptjournal.com](http://www.neptjournal.com)

Received: 25-01-2024

Revised: 13-03-2024

Accepted: 20-04-2024

## Key Words:

Precipitation

Aridity index

MNDWI

NDVI

Potential evapotranspiration

## ABSTRACT

Precipitation is a fundamental variable that is widely used in the organization of water resources and has a great influence on hydrological processes and ecological assessment. This study investigated the quantitative effect of monthly precipitation on surface water area (denoted by the Modified Normalized Difference Water Index, MNDWI), vegetation area (denoted by Normalized Difference Vegetation Index, NDVI), and potential evapotranspiration (PET) during two years (2018 and 2021) in the city of Baghdad, Iraq. Using the Thornthwaite aridity index, the annual aridity was first assessed to quantify the climate category of these years. The result shows that they were semi-arid and very arid, respectively. The empirical relationships between precipitation and areas of MNDWI and NDVI, and between rainfall and PET, were also examined. Due to less precipitation in 2021, no relationship was found in arid climates, while in 2018 for semi-arid climates, precipitation had a positive non-linear correlation with MNDWI and NDVI areas and a negative correlation with PET.

## INTRODUCTION

Baghdad, the federal administrative capital of Iraq, is one of the world's megacities characterized by high rainfall variability during only eight months of the year (from October to May) (Muter et al. 2024) and sparse natural surface water bodies, including the Tigris River and small ponds (Mahdi et al. 2024). It is therefore highly sensitive to anthropogenic activities, including high continuous population, urbanization, and land use change. However, climate change could affect the intensity and frequency of precipitation in any region, especially in continental regions such as Baghdad. Therefore, the city was subjected to severe warming effects (Al-Jiboori et al. 2020, Wahab et al. 2022) and the continuous increase in air temperature exacerbates the drought event, so the aridity (or dryness) index is used to quantify the degree of dryness of a climate at a given space and time.

Precipitation is the fall of water in any form (rain, fog, snow, etc.) to the earth's surface in all weather conditions. Precipitation is the main source of soil and surface water, and is a major hydrological factor and an important meteorological metric for determining vegetation growth, maintaining surface flows and groundwater resources, and linking atmospheric and land surface processes (Zeppel et

al. 2014, Shi et al. 2016, Naqi et al. 2021). Precipitation also plays a key role in water resources, soil moisture, and potential evapotranspiration (PET). Most aridity index (AI) calculation methods rely mainly on precipitation as an active driver. Highly variable precipitation may not only have direct effects on vegetation growth and water body size but also on local climate conditions (Fay et al. 2011, Halos et al. 2017). Consequently, precipitation may also affect PET, which represents water lost to the atmosphere from different surfaces composed of water and vegetation through evaporation and transpiration (Zhang & Wang 2021). Reductions in vegetation and water areas often lead to increased rates of PET, especially in months with clear skies. This leads to complex relationships between vegetation, surface water, and PET (Adams et al. 2011). However, few researchers have investigated monthly variations across the year, and even fewer have considered the effect of precipitation on vegetation, water, and PET in the same months. This study provides detailed knowledge on these issues for ecosystem resilience to precipitation variability in arid and semi-arid environments.

Water scarcity and vegetation degradation are likely to threaten natural ecosystems and have caused adverse problems for agriculture and industry (Ingrao et al. 2023). Therefore, it is essential to study the quantitative

relationships between precipitation, vegetation cover, surface water, and PET, especially their correlation with precipitation variability. Many researchers have investigated these issues for some water bodies. For example, Yan et al. (2017) investigated the response of vegetation growth to precipitation patterns in the Huang-Huai-Hai River basin, in China. They showed that vegetation cover and precipitation have a similar spatial distribution in arid and semi-arid areas, which are characterized by sparse vegetation. When there is less precipitation, surface water areas and vegetation cover are limited. Therefore, the expansion of surface water and vegetation growth can be considered an important reflection of changes in precipitation. Seasonal changes in accumulative precipitation during the year: winter, spring, summer, and autumn were investigated by Zeppel et al. (2014) who found that precipitation had a more dramatic effect on plants in summer than in winter. However, these changes in warm or dry seasons may have greater effects than changes in cool or wet seasons. Based on the Landsat satellite imagery, the seasonal effects of precipitation on the spectral values of the vegetation pixel were investigated by Jaber et al. (2020) for four seasons of 2019 for the same site. Finally, Salwa et al. (2020) also investigated this effect on vegetated areas, but only for two seasons (winter and summer) of three years: 2008, 2013 and 2019. Overall, the last two studies showed that vegetation growth was highly

correlated with their monitoring during the current seasons. More recently, Olivares et al. (2021) studied the relationship between normalized difference vegetation index (NDVI), rainfall, and PET in banana plantations in Venezuela for the period January/2016 to December/2017. They showed that there was a delay of 1 month in plant growth response to changes in rainfall and drought conditions, but the low spatial resolution (i.e. 250 m) NDVI derived from MODIS Terra product is not sufficient to identify plant activity. Here, we describe the quantitative impact of highly variable monthly precipitation on surface water and NDVI derived from high resolution (i.e. 10 m) satellite Sentinel-2 and PET under quite different weather conditions, addressing a key research gap in this paper of deeper understanding to derive their empirical relationships. The main objectives of this study were to 1) classify the type of the two years 2018 and 2021 as dry or wet according to AI, 2) analyze the monthly values of vegetation cover area, surface water area and PET in these years, and finally 3) investigate the statistical relationships describing the effects of precipitation on vegetation, surface water and PET under wet and dry conditions.

## STUDY SITE AND DATA

Baghdad is located in the center of Iraq, on the Tigris River at the confluence with the Euphrates River, 40 km away. It

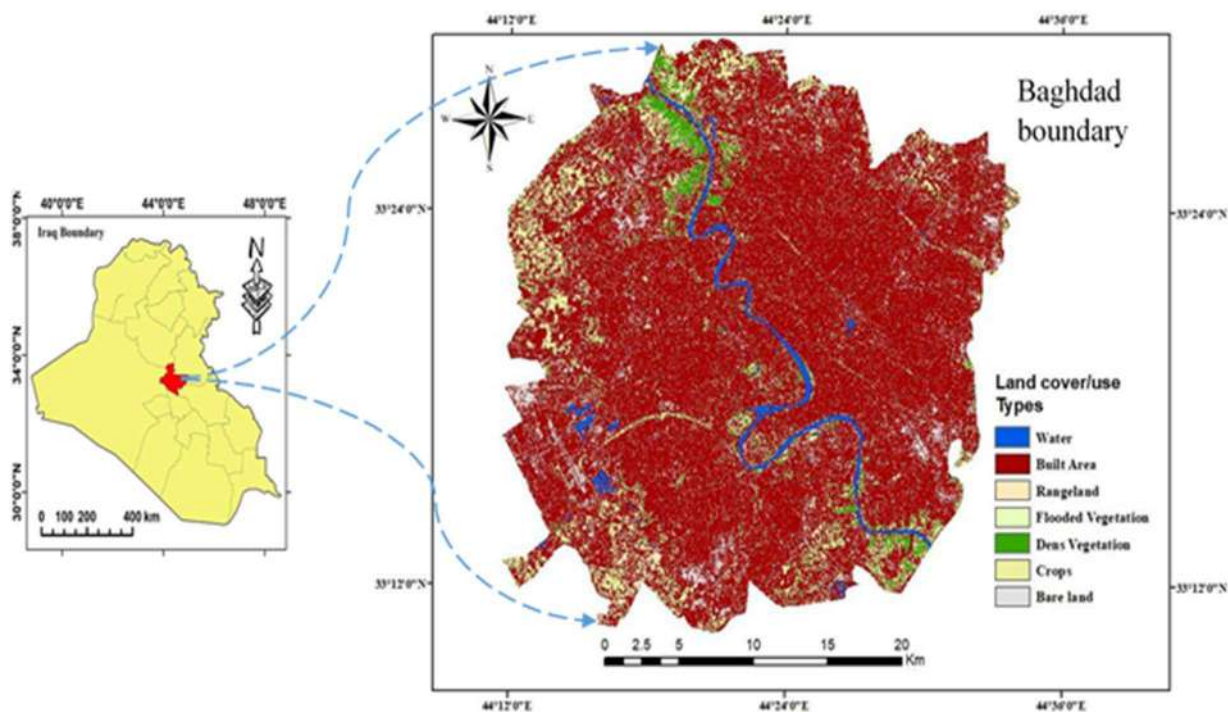


Fig. 1: Map of Iraq (left) and the study area of this study (right).

covers an area of 894.3 km<sup>2</sup>, which is 0.2% of the total area of Iraq (see Fig. 1). It extends from 33°12' to 33°29' N and from 44°1' to 44°36' E, with an average elevation of 34 m above sea level. The city stretches along two banks of the Tigris River with a length of about 60 km. The eastern side (called Rusafa) has a high population density but with small and low (1-2 stores) residential buildings, while the western side (called Karkh) has a low population and high buildings. There are also seven bridges connecting the two sides. Due to Baghdad's land being flat with low-lying plains, groundwater with an average depth of 5 m and some small surface water are found within the city as shown in Fig. 1, where urban vegetation is composed of forest of tall trees (like palm) in the north and green areas such as parks, household gardens, sparse shading trees (like eucalyptus, buckthorn, etc.). The city's climate is hot and dry in summer and cool and wet in winter. The spring and autumn seasons are short but pleasant. The average annual temperature, relative humidity, and wind speed reach 27°C, 40%, and 3.5 m/s respectively. Rainfall is scarce with an average of 140 mm per year and falls mainly between December and April, with no summer rainfall.

Precipitation data obtained through direct measurement from weather stations is the most accurate and widely used data. Monthly meteorological data of both air temperature and accumulated precipitation from the Iraqi Meteorological Organization and Seismological (IMOS) for two years, 2018 and 2021, were used. In addition, based on Sentinel-2 images for the same location and period, results of PET, surface water bodies, and vegetation cover from the references (Mahdi et al. 2024, Ahmed et al. 2024) were used to achieve the objectives of this study.

## MATERIALS AND METHODS

### Aridity Index

To distinguish the type of climate, whether dry or wet, for the two years 2018 and 2021, the aridity index was calculated using the Thornthwaite aridity index, which is based on the monthly temperature and precipitation during each year, defined by the following expression (Mendez 2006, Mustafa et al. 2018).

$$AI = \sum_i^n 1.65 * \left(\frac{P}{Ta - 10}\right)^{10/9} \dots(1)$$

where P and Ta are precipitation and air temperature, respectively. n is the number of months. Table 1 shows the classifications of AI used to quantify aridity degree.

Table 1: Climate classifications of Thornthwaite aridity index.

AI	<16	16-31	32-63	64-127	>127
Climate type	Arid	Semi-arid	Sub-humid	Humid	Wet

### Surface Water, Vegetation and Potential Evapotranspiration

The spectral indices for spatial monitoring of urban surface water and vegetation are modified normalized difference water index (MNDWI) and normalized difference vegetation index (NDVI), which are expressed by

$$MNDWI = \frac{\text{Green (band 3)} - \text{SWIR (band 11)}}{\text{Green (band 3)} + \text{SWIR (band 11)}} \dots(3)$$

$$NDVI = \frac{\text{NIR (band 8)} - \text{Red (band 4)}}{\text{NIR (band 8)} + \text{Red (band 4)}} \dots(4)$$

Both indices have values between -1 and +1. The spatial areas of water and vegetation were calculated using a raster calculator in the OGIS program after classifying the results of MNDWI and NDVI. For more details, we could refer to the references of Mahdi et al. (2024) and Ahemd et al. (2024) for the extraction of MNDWI and NDVI, respectively.

Finally, the potential evapotranspiration results reported by Ahemd et al. (2024) were also used in the present paper, which was calculated using the Truc method based on solar radiation (RS), air temperature (Ta), and relative humidity (RH) data.

$$PET = 0.01333((239000 * RS) + 50) \left(\frac{Ta}{Ta+15}\right)$$

for RH > 50% ... (5)

$$0.01333((239000 * RS) + 50) \left(\frac{Ta}{Ta+15}\right) \left(1 + \left(\frac{50 - RH}{70}\right)\right)$$

for RH < 50% ... (6)

where RS, Ta, and RH are expressed in MJ.m<sup>-2</sup>.day<sup>-1</sup>, °C, and % respectively.

## RESULTS AND DISCUSSION

### Aridity Index

Using monthly cumulative precipitation and mean temperatures, the aridity index was calculated separately by Eq. 1 for each of the years 2018 and 2021. Table 2 shows the values of the annual means for P, Ta, AI and climate type. According to the standard classifications given in Table 1, the AI values are 16.9 in 2018 with semi-arid climate type due to high annual precipitation and 1.3 in 2021 with severe arid (or hyperarid) climate due to very limiting precipitation, as shown in Table 2. The inter-annual distribution of precipitation for both years is shown in the histogram bars in

Table 2: Annual means of (mean, minimum, and highest temperature), precipitation, and aridity Index.

Year	Lowest Ta (°C)	Highest Ta (°C)	Range (°C)	Mean Ta (°C)	P (mm)	Aridity Index	Climate type
2018	12.1	35.4	23.3	24.3±8.8	284.2	16.9	Semi-arid
2021	11.5	37.8	26.3	24.5±9.9	25	1.3	Arid

Fig. 2, where the difference between monthly precipitation amounts is visible. The annual precipitation amounts reached 284.2 mm in 2018 and 25 mm in 2021.

The interesting point can be explained by discussing the inter-annual variations. Although the annual mean temperatures of both years are approximately the same, the standard deviation (SD), denoted by the symbol ( $\pm$ ), is quite different. In the dry year (2021) the inter-annual variations of the monthly mean temperature were larger ( $SD=9.9^{\circ}C$ ) than in the wet year 2018 ( $SD=8.8^{\circ}C$ ). Also, the annual heat range, defined as the difference between maximum and minimum mean temperature, was larger in the dry year than in the wet year.

Owing to a sharp deficit in the amounts of precipitation in 2021, several environmental impacts were produced such as human discomfort (Al Rukabie et al. 2024), fed-rain plants, high evaporation rates (Trenberth 2011), and changes in hydrodynamic and water environment (Limonos 2021). The dry year (2021) recorded the highest monthly temperature ( $37.8^{\circ}C$ ), while the wet year (2018) recorded the lowest values of the highest temperature ( $35.4^{\circ}C$ ).

### Inter-Annual Variations of Urban Water, Vegetation and Evapotranspiration

Fig. 3 shows monthly variations of quantitative areas for both surface water and vegetation represented by the calculation of MNDWI and NDVI respectively. Monthly PET results

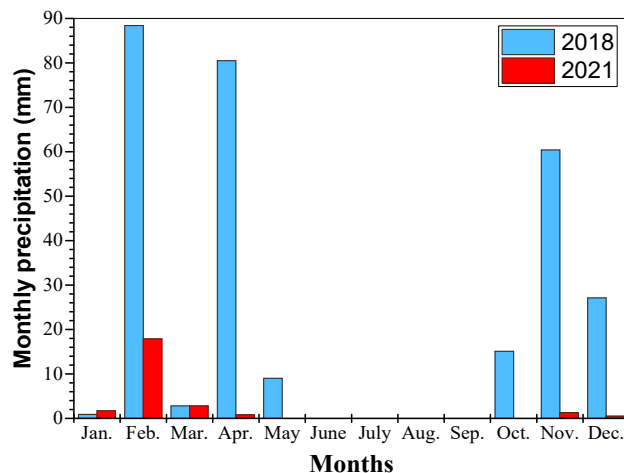


Fig. 2: Histogram bars of monthly precipitation recorded in weather Baghdad station in two years 2018 and 2021.

for these years are also added at the bottom of the figure. The green dotted lines are for these quantitative areas in semi-arid conditions (2018), while the red dotted lines are for arid conditions (2021). In general, the surface water areas in 2018 are relatively larger than those in 2021, especially in the six months (i.e. February, March, April, May, June and November). In summer (i.e. July, August and September) the areas are about the same with an average value of  $18 \text{ km}^2$ . The only exception is January and December, where more water areas were recorded, especially in January. This distribution of water areas was mostly reflected in the growth of vegetation in Baghdad, where the total area of pixels for vegetation (NDVI) in January, March, April, June, October, and December of 2018 was larger than those of 2021. The remaining months have almost the same NDVI areas, especially in May.

Due to large amounts of solar radiation falling on the surface of Baghdad for six months from May to September, a lot of water is lost through evaporation and transpiration, so high PET values were also associated with these months, as shown in Fig. 3. Furthermore, in these months, PET values in the arid year (2021) were expected to be higher than those in the semi-arid year (2018). In the winter months (i.e. December and January) no difference was observed.

### Relation Between Precipitation and Water, Vegetation and Potential Evapotranspiration

Here we try to study the effect of monthly precipitation

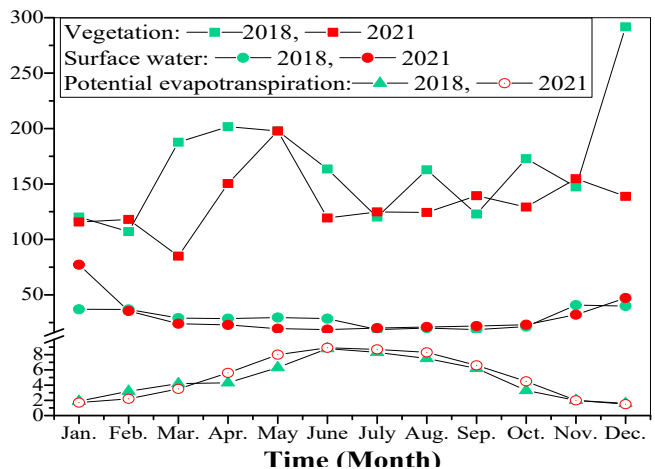


Fig. 3: Monthly variation of areas of surface water and vegetation, and of PET within Baghdad.



on the derived environmental quantities: surface water, vegetation cover, and potential evapotranspiration in an urban environment. For comparison purposes and because precipitation is a spatial distribution phenomenon, the precipitation observed by IMOS can represent a spatial distribution of the city of Baghdad because it is almost produced by extratropical low-pressure systems, mostly from the Mediterranean, Arabian and Red Sea regions (Babu

et al. 2011). For a deeper understanding, investigate the relationships between the above parameters, Figs. 4a, 4b, and 4c show the scatter plots between precipitation versus surface water (or MNDWI) area, precipitation versus vegetated (or NDVI) area, and precipitation versus PET, respectively, with precipitation on the x-axis and other quantities on the y-axis. If there was a good relationship, the best-fitting line was drawn through the data points, and the statistical parameter

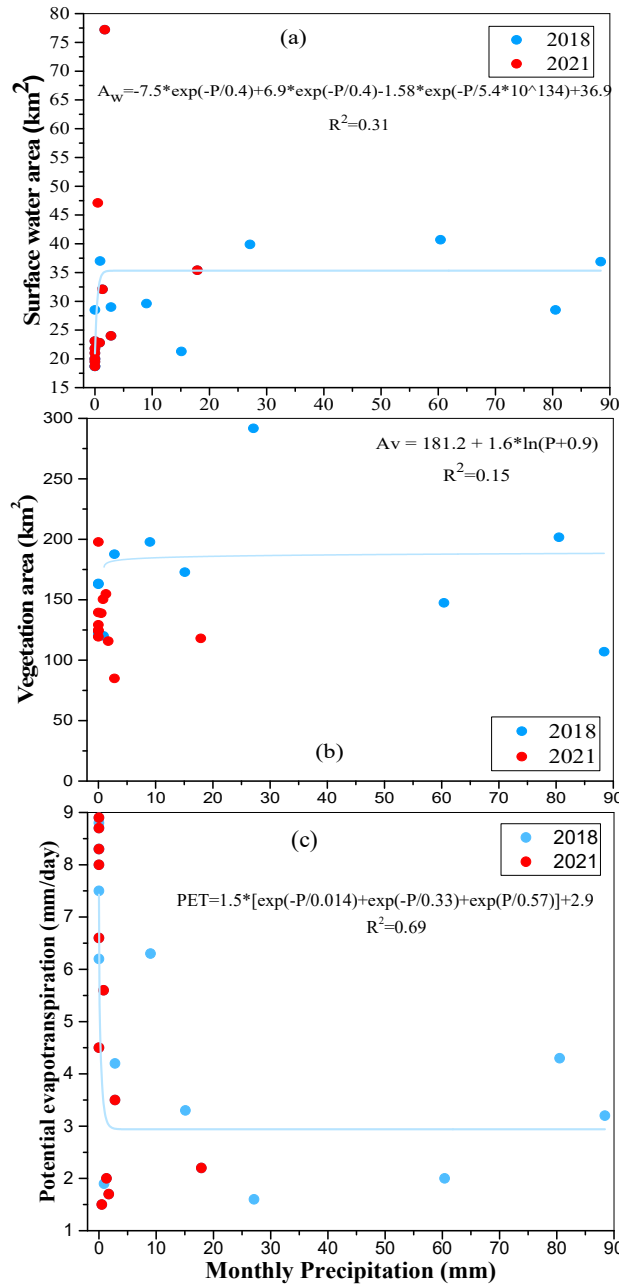


Fig. 4: Relationship of monthly precipitation with (a) surface water area ( $A_w$ ), (b) vegetation area ( $A_v$ ), and (c) potential evapotranspiration.

of goodness of fit ( $R^2$ ) was also determined. In addition, due to a sharp lack of precipitation in the dry year (2021), these relationships could not be concluded as shown in Fig. 4 for red points, so during the semi-arid year of 2018, the relationships were discussed below.

Fig. 4a shows monthly precipitation and urban surface water areas over arid and semi-arid periods. In 2018, water areas increased sharply only when there was precipitation of 2 mm, and then increased slowly with high precipitation, resulting in a positive correlation. The best line drawn through the data points obeys the exponential expression written on the panel of the figure with  $R^2=0.36$ . The relationship between precipitation and urban vegetation cover is clear in the semi-arid year, which shows a positive non-linear correlation as shown in Fig. 4b. The fitted line could pass through the data points that obeyed the logarithmic equation reported in the panel of the figure with  $R^2=0.15$ . This weak correlation is not suppressing, because the high fluctuation of precipitation, as well as NDVI areas in each month, responds slowly to the moisture activities of the previous month produced by precipitation irrigation. Monthly PET results estimated by the Truc method (Eqs. 5 and 6) were plotted against precipitation as shown in Fig. 4c. In the semi-arid period of 2018, when precipitation increased during the winter and spring rainy seasons, PET values decreased dramatically. These quantities are negatively correlated and the best-fitting line could pass through the data points followed by the decay exponential function written in the panel of the figure with moderate strength ( $R^2=0.69$ ).

## CONCLUSIONS

Precipitation is a very important factor in natural ecosystems and plays a key role in the hydrological cycle. By combining precipitation data with surface water bodies, vegetation, and potential evapotranspiration, we have explored the impact of precipitation on these quantities, which can improve better tools and strategies for water resources management and drought risk mitigation. This study presents monthly precipitation and air temperature observations from the Baghdad Ground Meteorological Station for two years, 2018 and 2021. We chose these years for a detailed analysis of the effects of precipitation under different climatic conditions. Using the Thornthwaite aridity index, the year 2018 was found to be in the semi-arid climate class with a value of 16.9, which is between 16 and 31, while the year 2021 was in the very arid class with a very small value of 1.3, which was far from the limit (16). Based on the published results of surface water areas, vegetation cover areas, and PET (Ahmed et al. 2024) for the same years and site, the quantitative effect of precipitation on these quantities in terms of MNDWI

for water and NDVI for vegetation, has been examined. In most of the rainy months of 2018, MNDWI areas were larger than in 2021, except for January. The annual mean NDVI area was 166.3 km<sup>2</sup> in 2018, which is larger than the area of 133.1 km<sup>2</sup> monitored in 2021. Also, vegetation degradation with the lowest value of 85 km<sup>2</sup> was found with the lowest precipitation in March 2021. In the warm months (March to October) of 2021, PET estimates were larger than those of 2018. Through quantitative analyses discussed in this paper, the non-linear increased relationship between precipitation and water area was shown, it was also non-linear with vegetation area, and finally, precipitation was inversely correlated with PET values. These results would be valuable for researchers to better understand the changing characteristics of precipitation and for managers to make better decisions in the future.

## ACKNOWLEDGMENTS

The authors are grateful to Mustansiriyah University for accepting this work. Finally, the authors thank anonymous reviewers especially the Editor-in-Chief for constructive comments for improvement of the paper.

## REFERENCES

- Adams, H.D., Luce, C.H., Breshears, D.D., Allen, C.D., Weiler, M., Hale, V.C., Smith, A.M.S. and Huxman, T.E., 2011. Ecohydrological consequences of drought- and infestation-triggered tree die-off: insights and hypotheses. *Ecohydrology*, 5, pp.145-159.
- Ahmed, M.H., Mahdi, Z.S., Al-Jiboori, M.H. and Mahmood, D.A., 2024. Interannual variations of normalized difference vegetation index and potential evapotranspiration and their relationship in the Baghdad area. *Open Agriculture*, 9. doi: 10.1515/opag-2022-0386.
- Al Rukabie, J.S.A., M.H., Mahmood, Al-Jiboori, D.A. and Srayyih, M.S., 2024. Assessing of monthly surface water changes impact on thermal human discomfort in Baghdad. *Journal of Environmental Engineering and Landscape Management*, 23(4), pp. 283–291. doi: 10.3846/jeelm.2024.22353.
- Al-Jiboori, M.H., Abu-Alshaer, M.J. and Ahmed, M.M., 2020. Impact of land surface changes on air temperatures in Baghdad. *Kuwait Journal of Science*, 47(4), pp.118-126.
- Babu, C.A., Samah, A.A. and Varikoden, H., 2011. Rainfall climatology over Middle East region and its variability. *International Journal of Water Resources and Arid Environments*, 1, pp.180-192.
- Fay, P.A., Blair, J.M., Smith, M.D., Nippert, J.B., Carlisle, J.D. and Knapp, A.K., 2011. Relative effects of precipitation variability and warming on tallgrass prairie ecosystem function. *Biogeoscience*, 8, pp.3053-3068. doi:10.5194/bg-8-3053-2011
- Halos, S.H., Al-Taai, U.T. and Al-Jiboori, M.H., 2017. Impact of dust events on aerosol optical properties over Iraq. *Arabian Journal of Geoscience*, 10, p.263. doi:10.1007/s12517-017-3020-2
- Ingrao, C., Strippoli, R., Lagiolia, G. and Huisinigh, D., 2023. Water scarcity in agriculture: An overview of causes, impacts and approaches for reducing the risks. *Heliyon*, 9(8). doi:10.1016/j.heliyon.2023.e18507
- Jaber, S.H., Al-Saadi, L.M. and Al-Jiboori, M.H., 2020. Spatial vegetation growth and its relation to seasonal temperature and precipitation in Baghdad. *International Journal of Agricultural and Statistical*

- Sciences*, 16(Supplement 1). Available at: <https://connectjournals.com/03899.2020.16.2021>
- Limones, N., 2021. A global-scale overview of precipitation-deficit flash droughts. *Terrestrial, Atmospheric and Oceanic Sciences*, 32, pp.597-611. doi:10.3319/TAO.2021.09.16.01
- Mahdi, Z.S., Tawfeek, Y.Q. and Al-Jiboori, M.H., 2024. Monthly urban surface water assessment at Baghdad and their environmental effects. *Water Practice and Technology*, 9(5): pp. 1794–1809. doi:10.2166/wpt.2024.098.
- Mendez, F.H., 2006. Assessment of climate indices in drylands of Colombia. Universiteit Gent.
- Mustafa, N.F., Rashid, H.M. and Ibrahim, H.A., 2018. Aridity index based on temperature and rainfall data for Kurdistan region-Iraq. *Journal of University of Duhok*, 21(1), pp.65-85. doi:10.26682/sjuod.2018.21.1.6
- Muter, A.S., Al-Jiboori, M.H. and Al-Timimi, Y.K., 2024. Assessment of spatial and temporal monthly rainfall trend over Iraq. *Baghdad Journal of Science*, 22(4). doi: 10.21123/bsj.2024.10367.
- Naqi, N.M., Al-Jiboori, M.H. and Al-Madhhach, A.T., 2021. Statistical analysis of extreme weather events in the Diyala River basin, Iraq. *Journal of Water and Climate Change*, 12(8), pp.3770-3785. doi:10.2166/wcc.2021.217
- Olivares, B.O., Paredes, F., Rey, J.C., Lobo, D. and Galvis-Causil, S., 2021. The relationship between the normalized difference vegetation index, rainfall, and potential evapotranspiration in a banana plantation of Venezuela. *Sanis Tanah-Journal of Soil Science and Agroclimatology*, 18(1), pp.58-64. doi:10.20961/stjssa.v18i1.50379
- Salwa, N., Dalia, A. and Al-Jiboori, M.H., 2020. Seasonal NDVI responses to air temperature and precipitation in Baghdad. *Open Agriculture*, 5, pp.631-637. doi:10.1515/opag-2020-0065
- Shi, H., Li, T., Wei, J., Fu, W. and Wang, G., 2016. Spatial and temporal characteristics of precipitation over the three-river headwaters region during 1980-2014. *Journal of Hydrology: Regional Studies*, 6, pp.52-65. doi:10.1016/j.ejrh.2016.03.001
- Trenberth, K.E., 2011. Changes in precipitation with climate change. *Climatic Research*, 47, pp.123-138. doi:10.3354/cr00953
- Wahab, B.I., Naif, S.S. and Al-Jiboori, M.H., 2022. Development of annual urban heat island in Baghdad under climate change. *Journal of Environmental Engineering and Landscape Management*, 30(1), pp.179-187. doi:10.3846/jeelm.2022.16374
- Yan, D., Xu, T., Grima, A., Yuan, Z., Weng, B., Qin, T., Do, P. and Yong, Y., 2017. Regional correlation between precipitation and vegetation in the Huang-Huai-Hai River Basin, China. *Water*, 9. doi:10.3390/w9080557
- Zeppel, M.J.B., Wilks, J.V. and Lewis, J., 2014. Impacts of extreme precipitation and seasonal changes in precipitation on plants. *Biogeosciences*, 11, pp.3083-3093. doi:10.5194/bg-11-3083-2014
- Zhang, H. and Wang, L., 2021. Analysis of the variation in potential evapotranspiration and surface wet conditions in the Hancang River Basin, China. *Scientific Reports*, 11. doi:10.1038/s41598-021-88162-2





# Dolomite as A Potential Source of Heterogenous Catalyst for Biodiesel Production from *Pongamia pinnata*

S. Sudalai<sup>1</sup>, M. G. Devanesan<sup>1</sup> and A. Arumugam<sup>2†</sup>

<sup>1</sup>Department of Chemical Engineering, Annamalai University, Chidambaram, Tamilnadu, India

<sup>2</sup>Bioprocess Intensification Laboratory, Centre for Bioenergy, School of Chemical & Biotechnology, SASTRA Deemed University, Thirumalaisamudram, Tamil Nadu, Thanjavur, India

†Corresponding author: A. Arumugam; aruchemxl@sbt.sastra.edu

Nat. Env. & Poll. Tech.  
Website: [www.neptjournal.com](http://www.neptjournal.com)

Received: 02-02-2024

Revised: 13-03-2024

Accepted: 29-03-2024

## Key Words:

*Pongamia pinnata*

Biodiesel

Transesterification

Dolomite

Heterogenous catalyst

## ABSTRACT

Biodiesel production from *Pongamia pinnata*, a tree-based oil using healthcare industrial waste dolomite as a catalyst, was studied. The studies aimed to establish the ideal parameters for producing biodiesel, such as temperature, the ratio of methanol to oil, and the weight percentage of the catalyst. The healthcare industrial waste was procured and characterized. With the operating conditions, temperature maintained at 75°C, methanol to oil molar ratio of about 20:1, and a catalyst weight of 5%, the optimum yield of 92.3% was obtained. The tree-based nonedible oil source for biodiesel production was suggested widely due to its ability to achieve sustainable development goals (SDGs). The *Pongamia Pinnata* cultivation on barren land supports the afforestation projects with economic and environmental values; further biodiesel from renewable bioresources reduces emissions, and livelihood development to eradicate unemployment are the primary objectives for achieving the SDGs. The tree-based biodiesel production and adaptation of dolomite as a heterogeneous catalyst have proven to be a recent attraction among scientists. The present study is the first report on *Pongamia pinnata* for biodiesel production catalyzed by dolomite.

## INTRODUCTION

The ability to produce energy scales the development of the nation. Resource depletion, pollution due to emissions, and global governance's commitment to climate change are pushing to shift the fossil fuel-based energy production process into renewable energy sources (Dey et al. 2022). The capital investment toward infrastructure, time consumption, inconsistency in power generation, and other parameters limit energy production from renewable sources like wind, solar, and tide. Locally produced biofuel from domestic resources mitigates transboundary emissions and favors social welfare. Biodiesel from vegetative sources is widely investigated and adopted as an alternative to fossil fuels. As evidenced by the performance and emission studies, biodiesel significantly reduces air pollution in the production and operation processes (Mac Kinnon et al. 2018).

Positive socioeconomic effects from the production and use of biodiesel as an alternative fuel may eventually result in sustainable development. Developing biodiesel can yield socioeconomic benefits for rural communities and agricultural sectors, and this livelihood development significantly contributes to achieving the SDG, among

other sustainability credits (Brinkman et al. 2020). However, the large-scale production of fuel-yielding crops seriously threatens food security due to the land use pattern. Accordingly, the search for biodiesel feedstock shifted toward non-edible sources.

As a sustainable energy source, biodiesel helps reduce greenhouse gas emissions, which is part of the REDD+ (Reducing Emissions from Deforestation and Forest Degradation) program. Through REDD+, developing countries will be encouraged to manage their forests responsibly and prevent further global warming. In comparison to fossil fuels, biodiesel is a greener fuel that can be generated from renewable resources like plant or animal fats, which lowers emissions from vehicles. Biodiesel production from wild vegetation sources further strengthens the implementation of REDD+, and this further facilitates the climate financing from developed countries to develop forest regions in developing countries (Kuh 2018). The potential of various tree-based oils from *Azadirachta indica*, *Jatropha curcas*, *Madhuca longifolia*, *Pongamia glabra*, *Calophyllum inophyllum*, *Pongamia pinnata*, *Hevea brasiliensis*, *Simmondsia chinensis*, *Linum usitatissimum* were studied (Chimezie et al. 2022).

The monotypic genus *Karanja* is a known species native to Southeast Asia and the Indian subcontinent. *Pongamia* is a nitrogen-fixing, self-pollinating tree that grows well in humid, subtropical climates with minimum mean monthly temperatures between 10 and 50°C. It may also be grown easily in wastelands and infertile areas where temperatures range from 16 to 40°C for ideal growth (Sharma et al. 2020).

The United States and other regions with humid tropical climates have adopted this plant. *Pongamia* trees can generally attain a height of 15-25 m, begin to flower at 3-4 years old, achieve maturity in 4-5 years, and yield up to 90 kg of seeds annually. The wood, seeds, and leaves from *Pongamia* trees have various value-added applications. For alternative biomass sources, *Pongamia pinnata* has numerous benefits. Primarily, it is a resilient and drought-tolerant tree that can flourish in a variety of soil conditions, such as marginal and degraded areas, making it appropriate for cultivation in drought-prone regions where other crops could find it difficult. The second reason is that *Pongamia pinnata* is a nitrogen-fixing plant. It works in symbiotic partnerships with bacteria to enrich the soil with nitrogen, which lowers the demand for external fertilizers and increases soil fertility. Some of these applications include fuel, livestock feed, and medicinal uses (Degani et al. 2022).

The most common biodiesel production from bio-oil involves the transesterification process; a catalyst facilitates the reaction between the feedstock of vegetable oil and short-chain alcohol during the transesterification process. Sodium hydroxide (NaOH) and potassium hydroxide (KOH) are two homogeneous base catalysts that are frequently employed to catalyze the transesterification of refined vegetable oil (Amirthavalli et al. 2022). When employing crude vegetable oil feedstock with a high free fatty acid (FFA) content, soap production is unavoidable with the base catalyst, and this limitation mandates the pretreatment of high FFA content feedstock using homogenous acid catalysts like phosphoric acid (H<sub>3</sub>PO<sub>4</sub>) and sulfuric acid (H<sub>2</sub>SO<sub>4</sub>) to lower the FFA concentration (Baskar et al. 2019).

However, using a homogenous catalyst has always been linked with drawbacks, including the inability to separate homogeneous phase products, the fact that they are non-recyclable, and the significant increase in the cost of using a wastewater treatment system to neutralize the catalyst before discharging. The enzyme catalyst is expensive to replace the homogeneous. Recyclable and readily separable, heterogeneous catalysts have emerged as a viable substitute for homogeneous catalysts, offering better performance (Brahma et al. 2022).

Dolomite is a sedimentary rock that occurs naturally and includes carbonates of magnesium and calcium. To make

biodiesel, transesterification is a process that it catalyzes. Initially, the ions calcium and magnesium function as Lewis acid sites to accelerate the reaction and act as catalysts. Due to its broad availability, dolomite is also less expensive than the other catalytic substitutes (Maroa & Inmbao 2021).

It uses less energy to make and generates less waste because of its capacity to regenerate and reuse itself. Furthermore, studies show that dolomite catalysts outperform other catalysts in terms of yield and reaction kinetics. Dolomite from industrial waste in the healthcare sector has special advantages for the manufacture of biodiesel since it may be used for both environmental remediation and catalysis. When dolomite from medical waste is used, resource usage is streamlined, lessening the impact on the environment and solving disposal issues. Moreover, the inherent catalytic activity of dolomite promotes effective transesterification processes, increasing the yield of biodiesel. This strategy adheres to the circular economy principles by reducing waste and promoting the creation of renewable energy.

The present study is the first work investigating the use of dolomite in the transesterification of *Karanja* oil with a higher yield of biodiesel. The current work uses Response Surface Methodology (RSM) to optimize the transesterification parameters for the methyl ester synthesis from *Pongamia pinnata* seed oil. This study examined how process variables, including catalyst weight, temperature, and the ratio of methanol to oil, affected the amount of biodiesel produced. The ASTM technique was used to determine the characteristics of *Pongamia pinnata* biodiesel.

## MATERIALS AND METHODS

### Materials

*Pongamia pinnata* oil was obtained from the highway road of Bahour main road, Puducherry (11°48.56.5"N, 79°4501.4"E) (Fig. 1). The seed extracted *Pongamia pinnata* oil was found to have the density of 906 kg/m<sup>3</sup>. At 40°C, the oil's viscosity was estimated as 26.5 mm<sup>2</sup>/s. The oil had an acid value of 7 mg KOH/g. Stearic acid (18.36%), linolenic acid (14.87%), oleic acid (54.22%), and palmitic acid (12.55%) make up the fatty acid makeup of *Pongamia pinnata* oil. The dolomite was obtained from Puducherry, the healthcare sector of TTK, Puducherry.

### Transesterification Process

Every transesterification experiment was carried out in a 50 ml vial. 20 grams of *Karanja* oil were combined with a 3:1 methanol to oil ratio, 1 weight percent catalyst, and a temperature of 70°C sustained for 9 h at 400 rpm. To

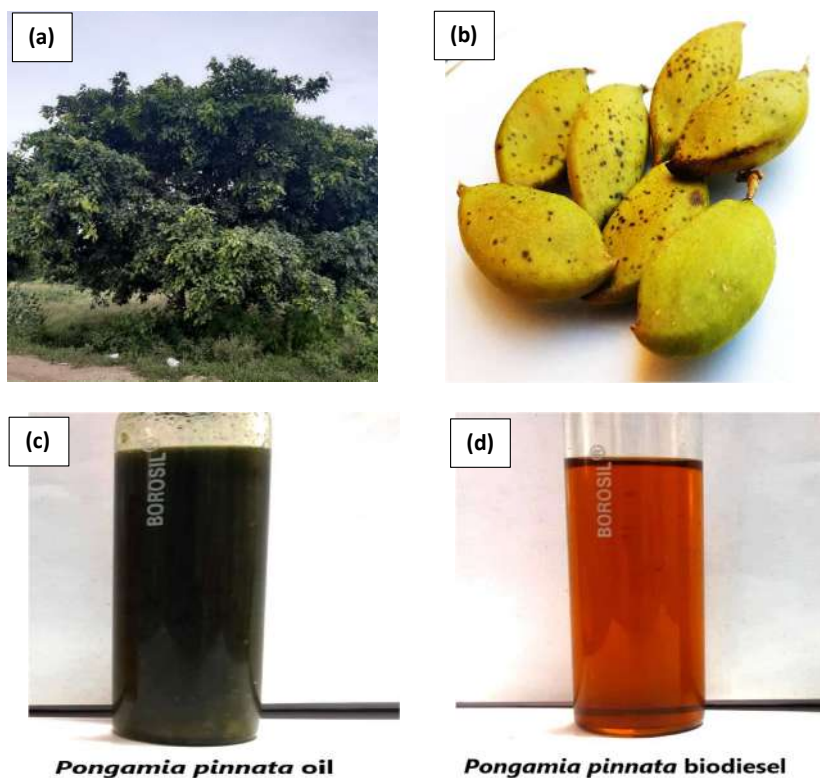


Fig. 1: *Pongamia pinnata* Linn (a) Tree (b) Seed (c) *Pongamia pinnata* oil (d) *Pongamia pinnata* biodiesel.

eliminate any remaining methanol in the combination, the sample was centrifuged at 4000 rpm after 9 h. Methanol to oil ratio of 15:1 to 25:1, a temperature range of 65°C to 85°C, a catalyst weight of 1 to 3 wt%, and methyl esters yield measured by GC-MS were all adjusted to maximize

production (Fig. 2). Gas chromatography-mass spectroscopy (CLARUS 500, PerkinElmer, USA) was used to analyze the biodiesel made from the Karanja oil (*Pongamia pinnata*). Every experiment was carried out in triplicates (Vishali et al. 2023).

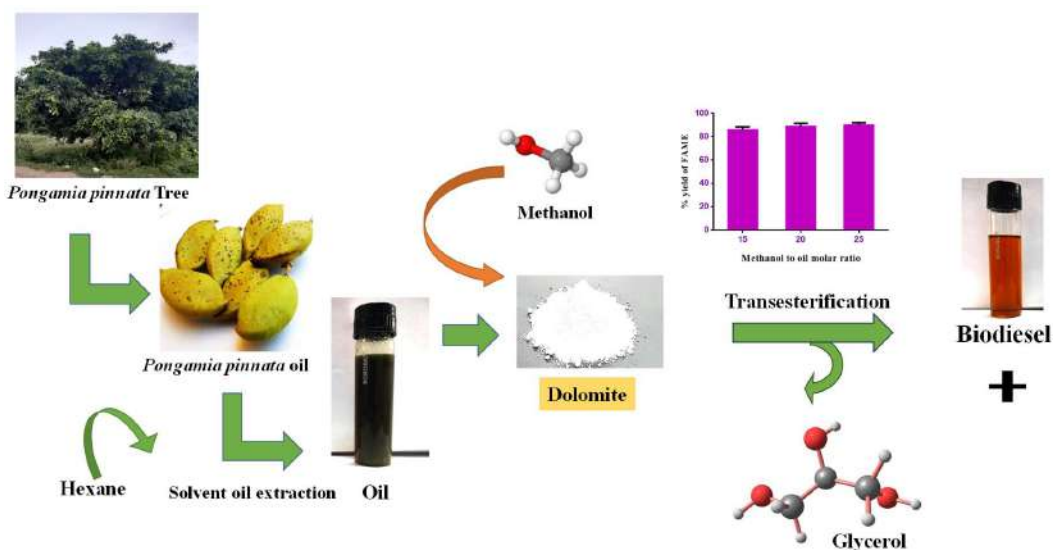


Fig. 2: Process flow for biodiesel production from *Pongamia pinnata* oil.

**Biodiesel yield = (Mass of biodiesel produced/ Mass of oil used) × Area % of FAME × 100**

### Characterization

*Pongamia pinnata* biodiesel produced using a dolomite catalyst has been subjected to GC-MS analysis. A potent method for characterizing biodiesel is gas chromatography-mass spectrometry (GC-MS) analysis, which yields comprehensive data on the composition and quality of biodiesel fuels. Gas chromatography is used in this analytical approach to separate the components of biodiesel according to their volatility and affinity for the stationary phase. Mass spectrometry is used to identify and quantify these components by examining their mass-to-charge ratios.

## RESULTS AND DISCUSSION

### Effect of Methanol Content

Stoichiometry indicated that three moles of methanol were needed for the transesterification reaction to yield methyl esters from one mole of triglyceride. Excessive addition of alcohol can be used to adjust the rate of reaction. The stoichiometric molar ratio of alcohol to oil in the generation of biodiesel is 1:3; however, to shift the chemical equilibrium in favor of the generation of biodiesel, more excellent molar ratios are a convenient solution. Furthermore, developing the three phases (oil, alcohol, and catalyst) at the start of the reaction may limit the contact between the reactive mixes; still, in this scenario, the excess alcohol in the reaction reduces the issue (Hoda 2010). As shown in Fig. 3, biodiesel yield improves with increased methanol-to-oil ratio up to a certain point when the yield declines from the highest possible biodiesel production. Therefore, it is essential to carefully optimize the methanol-to-oil ratio to achieve

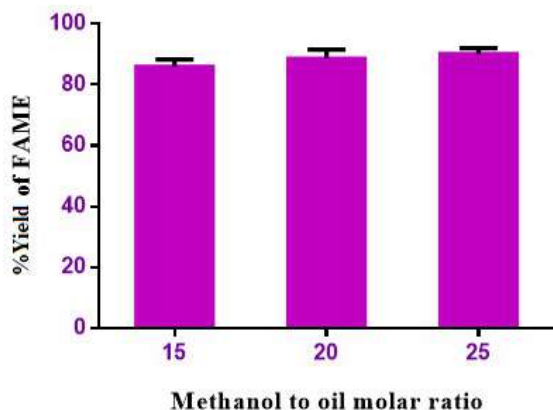


Fig. 3: Effect of methanol to oil molar ratio (15:1, 20:1, 25:1) on *Pongamia pinnata* biodiesel production.

maximum biodiesel yield without compromising efficiency and cost-effectiveness (Kedir et al. 2023). The highest yield of 90.7% was obtained at a 20:1 methanol to oil molar ratio.

### Effect of Temperature

The temperature significantly influences biodiesel production via transesterification since the intrinsic rate constants strongly depend on temperature. Therefore, to get the highest yield, it is crucial to adjust the operating temperature. The trials were performed with a temperature range of 65°C to 85°C to obtain the optimum yield (Takase 2022). The data shown in Fig. 4 indicates that biodiesel yields rise as the temperature rises, peaking at 75°C, after which it begins to fall. After 75°C, the conversion percentage decreased. As the temperature rises, the methanol vaporizes at a greater temperature, shifting the balance to the reactant side and decreasing the biodiesel output (Ezekannagha et al. 2017).

### Catalyst Concentration

The impact of catalyst amount (range of 3-5 wt%) in the transesterification reaction as catalyst was shown in Fig. 5. The percentage yield of 84.6% was obtained at 3wt% catalyst concentration. Further increased the catalyst concentration to 4 wt% the maximum yield of 92.3 was obtained. When the amount of catalyst is increased beyond 4 wt%, the yield of biodiesel decreases to 88.3%. This may be due to too high concentration of catalyst reduces the reactant interaction and also favors high glycerin concentration which in turn reduces the biodiesel yield (Jan et al. 2023).

### Reusability of Dolomite

Dolomite catalyst's reusability was also looked at since it can lower process costs. Following the reaction, the dolomite catalyst was filtered out and reused for a new reaction

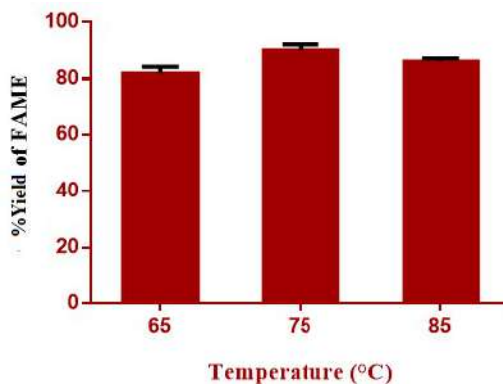


Fig. 4: Effect of temperature (T = 65, 75, and 85°C) on *Pongamia pinnata* biodiesel production.



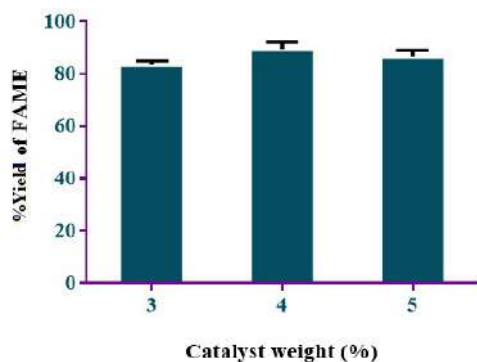


Fig. 5: Effect of catalyst concentration (3, 4, and 5 wt%) on *Pongamia pinnata* biodiesel production.

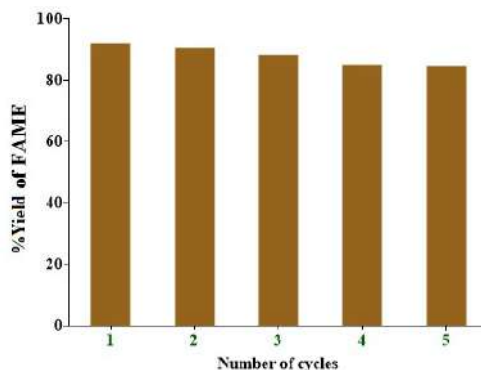


Fig. 6: Reusability studies of dolomite catalysis on *Pongamia pinnata* biodiesel production.

(Fig. 6). With a 4 weight percent catalyst quantity and a 20:1 molar ratio of methanol to oil, the transesterification process was conducted at methanol reflux. From Fig. 4 there was no appreciable reduction in the biodiesel yield. The reduction in the yield after the five cycles of recycling of the catalyst was found to be 7.79% (Ilgen 2011).

### Characterization of Biodiesel

GC-MS analysis of the product revealed the presence of several significant compounds (Fig.7). Octadecenoic acid (Z)-, methyl ester was discovered with a retention duration of 54.98 minutes, indicating its presence in the sample. In addition, it was found that methyl stearate had a retention duration of 3.96 minutes, but the methyl ester of hexadecanoic acid had a retention time of 2.54 minutes. These compounds are significant because feedstock used to produce biodiesel typically includes them and because they are critical to the fuel's quality and properties. Accurate identification and measurement of these components provide crucial information for determining the sample's general composition and suitability for biodiesel production.

### CONCLUSIONS

The findings of the research emphasize the significant effects of temperature, catalyst concentration, and methanol to molar ratio on the production of biodiesel from *Pongamia pinnata* oil. To produce biodiesel with improved quality and yields and to support environmentally friendly and sustainable energy production, the study emphasizes the importance of optimizing these factors. An industrial waste dolomite heterogeneous catalyst is used for biodiesel production. Maximum biodiesel yield of 92.3% was observed at 20:1 methanol to oil ratio, temperature of 75°C, and catalyst weight of about 5 wt%. Additionally, research has been done on the catalyst's reusability. Even after five cycles, it has been discovered that dolomite still exhibits superior catalytic activity. The characteristics of the biodiesel made from *Pongamia pinnata* and diesel appear to be comparable.

### REFERENCES

Amirthavalli, V., Warriar, A.R. and Gurunathan, B., 2022. Various methods of biodiesel production and types of catalysts. In *Biofuels and bioenergy* (pp. 132-111). Elsevier.

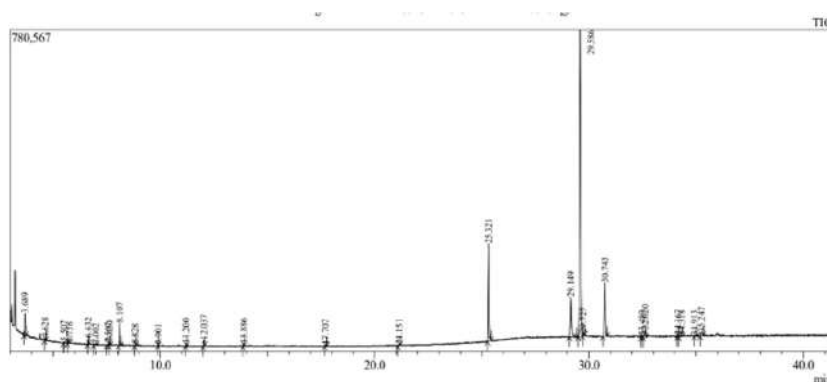


Fig. 7: GC-MS analysis for the produced *Pongamia pinnata* biodiesel.

- Baskar, G., Kalavathy, G., Aiswarya, R. and Abarnaebenezer Selvakumari, I., 2019. Advances in bio-oil extraction from nonedible oil seeds and algal biomass. *Advances in Eco-Fuels for a Sustainable Environment*, pp.187-210.
- Brahma, S., Nath, B., Basumatary, B., Das, B., Saikia, P., Patir, K. and Basumatary, S., 2022. Biodiesel production from mixed oils: A sustainable approach towards industrial biofuel production. *Chemical Engineering Journal Advances*, 10, 100284.
- Brinkman, M., Levin-Koopman, J., Wicke, B., Shutes, L., Kuiper, M., Faaij, A. and van der Hilst, F., 2020. The distribution of food security impacts of biofuels, a Ghana case study. *Biomass and Bioenergy*, 141, 105695.
- Chimezie, E.C., Zhang, X., Djandja, O.S., Nonso, U.C. and Duan, P.-G., 2022. Biodiesel production from nonedible feedstocks catalyzed by nanocatalysts: A review. *Biomass and Bioenergy*, 163, 106509.
- Degani, E., Prasad, M.V.R., Paradkar, A., Pena, R., Soltangheisi, A., Ullah, I., Warr, B. and Tibbett, M., 2022. A critical review of *Pongamia pinnata* multiple applications: From land remediation and carbon sequestration to socioeconomic benefits. *Journal of Environmental Management*, 324, 116297.
- Dey, S., Sreenivasulu, A., Veerendra, G.T.N., Rao, K.V. and Babu, P.S.S.A., 2022. Renewable energy present status and future potentials in India: An overview. *Innovation and Green Development*, 1(1), 100006.
- Ezekannagha, C.B., Ude, C.N. and Onukwuli, O.D., 2017. Optimization of the methanolysis of lard oil in the production of biodiesel with response surface methodology. *Egyptian Journal of Petroleum*, 26(4), pp.1001-1011.
- Hoda, N., 2010. Optimization of biodiesel production from cottonseed oil by transesterification using NaOH and Methanol. *Energy Sources, Part A: Recovery, Utilization, and Environmental Effects*, 32(5), pp. 434-441.
- Ilgen, O., 2011. Dolomite as a heterogeneous catalyst for transesterification of canola oil. *Fuel Processing Technology*, 92(3), pp.452-455.
- Jan, H.A., Osman, A.I., Al-Fatesh, A.S., Almutairi, G., Surina, I., Al-Otaibi, R.L., Al-Zaqri, N., Kumar, R. and Rooney, D.W., 2023. Biodiesel production from *Sisymbrium irio* as a potential novel biomass waste feedstock using homemade titania catalyst. *Scientific Reports*, 13(1), 11282.
- Kedir, W.M., Wondimu, K.T. and Weldegrum, G.S., 2023. Optimization and characterization of biodiesel from waste cooking oil using modified CaO catalyst derived from snail shell. *Heliyon*, 9(5), e16475.
- Kuh, K.F., 2018. The law of climate change mitigation: an overview. In: D.A. Dellasala and M.I.B.T.-E. of the A. Goldstein, eds. Oxford: Elsevier, pp.505-510.
- Mac Kinnon, M.A., Brouwer, J. and Samuelsen, S., 2018. The role of natural gas and its infrastructure in mitigating greenhouse gas emissions, improving regional air quality, and renewable resource integration. *Progress in Energy and Combustion Science*, 64, pp.62-92.
- Maroa, S. and Inambao, F., 2021. A review of sustainable biodiesel production using biomass derived heterogeneous catalysts. *Engineering in Life Sciences*, 21(12), pp.790-824.
- Sharma, A., Kaushik, N. and Rathore, H., 2020. Karanja (*Milletia pinnata* (L.) Panigrahi): a tropical tree with varied applications. *Phytochemistry Reviews*, 19(3), pp.643-658.
- Takase, M., 2022. Biodiesel yield and conversion percentage from waste frying oil using fish shell at Elmina as a heterogeneous catalyst and the kinetics of the reaction. *International Journal of Chemical Engineering*, 2022, 8718638.
- Vishali, K., Rupesh, K.J., Prabakaran, S., Sudalai, S., Babu, K. and Arumugam, A., 2023. Development and techno-economic analysis of *Calophyllum inophyllum* biorefinery for the production of biodiesel, biohydrogen, bio-oil, and biochar: Waste to energy approach. *Bioresource Technology*, 218, pp.212-222.



# Aquatic Macroinvertebrate Diversity and Water Quality, La Gallega-Morropón Creek, Piura, Peru

Mónica Santa María Paredes-Agurto<sup>1</sup>, Armando Fortunato Ugaz Cherre<sup>1,2</sup>, José Manuel Marchena Diones<sup>1,2†</sup> and Robert Barrionuevo García<sup>1,2</sup>

<sup>1</sup>Laboratorio de Investigación en Zoología, Facultad de Ciencias, Universidad Nacional de Piura, Urb. Miraflores S/N, Castilla, Perú

<sup>2</sup>Laboratorio de Hidrobiología, Centro de Investigación en Biología Tropical y Conservación-CINBIOTYC, Piura, Peru

†Corresponding author: José Manuel Marchena Diones; [jmarchenad@unp.edu.pe](mailto:jmarchenad@unp.edu.pe)

Nat. Env. & Poll. Tech.  
Website: [www.neptjournal.com](http://www.neptjournal.com)

Received: 05-02-2024

Revised: 14-03-2024

Accepted: 04-04-2024

## Key Words:

Macroinvertebrate diversity  
Aquatic invertebrates  
Bioindicators  
Water quality

## ABSTRACT

Freshwater systems are one of the most important natural resources for life. Despite their value, these ecosystems have suffered great impacts caused by human activities, which directly affect the aquatic biota and the quality of water sources. Considering the value of aquatic macroinvertebrates as bioindicators of water quality, the richness, composition, and water quality of La Gallega-Morropón stream, Piura-Peru, were compared. Two field trips were conducted between November 2018 and May 2019 (contemplated wet and dry periods, respectively), performing 4 sampling stations. A total of 1772 individuals of macroinvertebrates were recorded, distributed in 22 families. Psychodidae had an abundance of 670 individuals, followed by morphospecies (Gasteropoda) with 379 individuals, Chironomidae with 275 individuals, and Elmidae with 136 individuals (all indicators of water quality). Finally, the water quality index method: 1) BMWP/Col, presented one station with good (HB1), acceptable (HB2), and critical (HB3 and HB4) quality, while 2) EPT exhibited two stations with good quality (HB3 and HB4), HB1 regular quality and HB2 poor (HB3 and HB4), HB1 regular quality and HB2 poor quality.

## INTRODUCTION

The biological component has always been used as an alternative to understanding the quality of aquatic environments; throughout history, algae, protozoa, bacteria (perhaps the most used group), fish, macrophytes, fungi, and aquatic macroinvertebrates have been used (Roldán 2003, Coayla-Peñaloza et al. 2023).

For example, temperate regions were among the first to use these indices, and if they want to use them in tropical areas, they need to analyze the general processes and disturbances that exist (Álvarez & Pérez 2007, Bonada et al. 2006). Likewise, these must be flexible, selective, and broad to be used to indicate not only water quality but also human economic impacts (de la Lanza et al. 2000), furthermore, they constitute the animal biomass in rivers playing a vital role in the transfer of energy from primary resources to the main consumers in food webs (Medina & Yasmy 2011, Custodio & Chávez 2019).

The advantages are ease of sampling, rapid changes in trophic structure, and composition and occurrence of some groups due to various types of natural and anthropogenic

disturbances and their sedentary character, giving a good idea of what happens in each sampled habitat (Bailey et al. 2003), these communities are sensitive to small increases in temperature, variations in hydrogen potential (Bergkamp & Orlando 1999, Durance & Ormerod 2007, Roldán 2003).

Freshwater bodies are always subject to various changes related to agriculture (pesticides, herbicides, fertilizers that settle in the water), livestock, or deforestation (Martínez et al. 2022). Fernández et al. (2004) stated that these compounds can be released into water from sewers and industrial effluents if they are close to the human population.

The pollution of the Piura River in recent years, is increasingly serious, which is due to discharges of domestic and hospital wastewater discharged without or poor treatment, agriculture, solid waste, and heavy metals due to illegal mining.

Aware of the essential role played by macroinvertebrates in freshwater aquaculture systems, the objective was to analyze the richness, composition, and water quality of the La Gallega-Morropón stream, Piura.

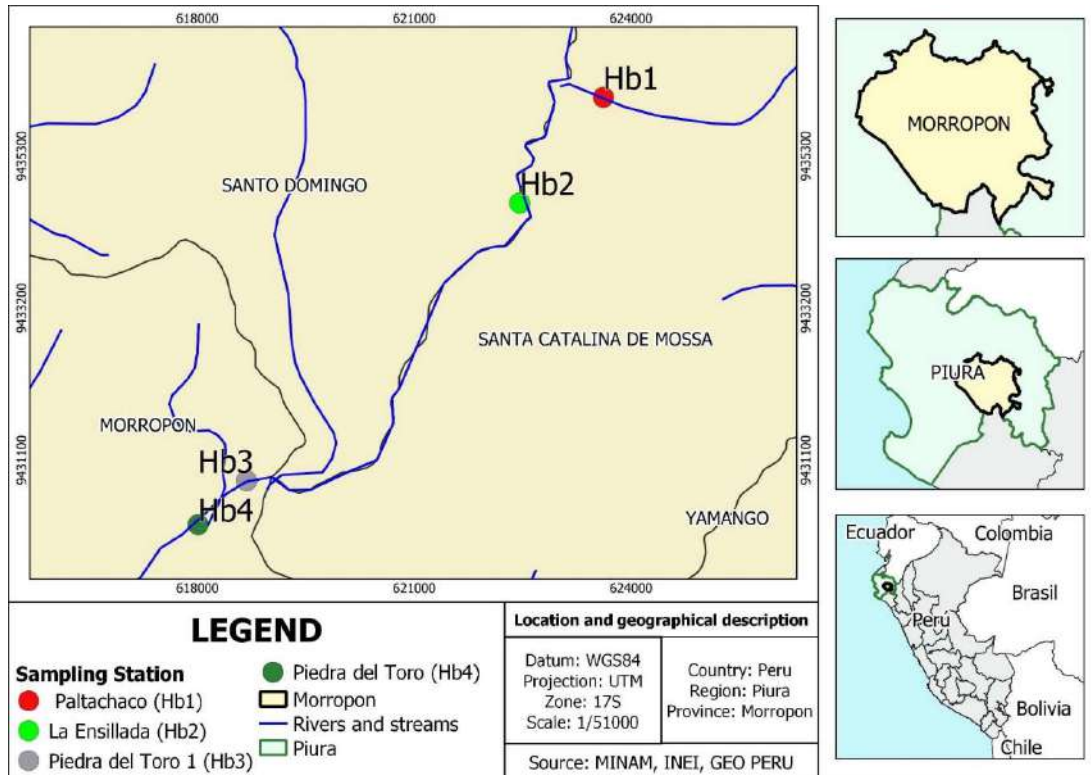


Fig. 1: Location of the study area, La Gallega-Morropón stream, Piura-Peru.

## MATERIALS AND METHODS

The La Gallega sub-basin, with 142 km<sup>2</sup>, includes the districts of Santo Domingo, Santa Catalina de Mossa, part of Chalaco and Morropón. The main course of the river begins at the confluence of the Santo Domingo and Ñoma streams; before flowing into the Piura River, it joins the Corral de Medio tributary. El Cerezo Creek has been integrated into this sub-basin. Its average annual discharge averages 1.68 m<sup>3</sup>/s, with the highest discharges occurring in March. In the February-May period, 79 % of the total annual volume is produced (average 53 million m<sup>3</sup>). The Corral del Medio River forms the Las Juntas River, which is very short until it joins the Piura River (Rojas & Ibáñez 2003).

Four sampling stations were established along the La Gallega stream (Fig. 1). For the collection of aquatic macroinvertebrates, two samplings were conducted during November 2018 and May 2019 (Fig.1), in the rainy and dry periods, respectively. For the collection, a Surber net of 30.5 × 30.5 × 8 cm, 500 μm mesh opening, with 3 replicates per substrate (leaf litter, rock and fine sediment) was used (MINAM 2017, Pinheiro et al. 2004). Samples were labeled with the sampling station preserved in 70% alcohol and

separated for later identification at the Zoology Research Laboratory, Faculty of Sciences, Universidad Nacional de Piura.

For the identification of the taxa, taxonomic keys of Domínguez & Fernández (2001), Domínguez et al. (2006), Domínguez & Fernández (2009), Posada & Roldán (2003), Roldán (1988) and Springer (2006) were used.

Simpson's dominance, Margalef diversity, and Shannon-Wiener equity indices were used to estimate diversity (MINAM 2017, Moreno 2001).

For each sampling station, the EPT (Ephemeroptera, Plecoptera, Trichoptera) (Carrera & Fierro 2001) and BMWP/Col (Biological Monitoring Working Party, modified for Colombia) indices were estimated (modified from Roldán 2003).

## RESULTS

A total of 1,772 macroinvertebrates were captured, distributed in 10 orders and 22 families. Psychodidae had the highest number of individuals with 670 individuals, followed by Chironomidae with 275 individuals, and Elmidae with 136 individuals. Fig. 2 shows the richness of the aquatic

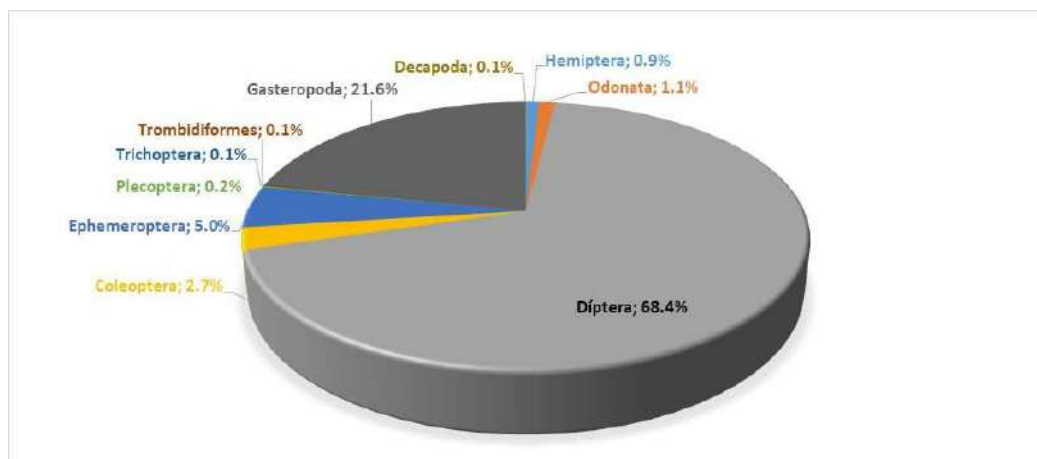


Fig. 2: Richness of aquatic macroinvertebrate taxa, La Gallega-Morropón stream, Piura-Peru.

Table 1: Alpha diversity indices of the sampling stations, La Gallega-Morropón stream, Piura-Peru.

Diversity indexes	Sampling stations			
	HB <sub>1</sub>	HB <sub>2</sub>	HB <sub>3</sub>	HB <sub>4</sub>
Simpson_1-D	0,526	0,549	0,132	0,695
Shannon_H	1,560	1,499	0,538	2,124
Margalef	1,864	1,573	1,165	1,669

macroinvertebrate taxa present in the La Gallega-Morropón stream, Piura-Peru.

As for the alpha diversity indexes, they show that there is no dominance of a specific group of taxa, due to the low diversity of species present in the sampling stations, the station that stands out with the highest value for Simpson's index is HB<sub>4</sub>, while in the Margalef index, the highest value was HB<sub>1</sub>, in terms of the value obtained from Shannon, HB<sub>4</sub> presented the highest value (Table 1).

Simultaneously for the water quality variable, the rating is varied for BMWP/Col in all stations, probably because this water quality index is calculated through the presence or absence of aquatic macroinvertebrate families, which may produce imprecision in the ratings (Table 2). In contrast, the EPT index calculates water quality based on the richness

of the Ephemeroptera, Plecoptera, and Trichoptera orders (Table 2), which makes this index useful in the detection of more sensitive disturbances, as well as evidenced (Álvarez & Pérez 2007). Finally, the water quality index method, such as BMWP/Col, presented one station with good (HB<sub>1</sub>), acceptable (HB<sub>2</sub>), and critical (HB<sub>3</sub> and HB<sub>4</sub>) quality; while EPT exhibited two stations with good quality (HB<sub>3</sub> and HB<sub>4</sub>), HB<sub>1</sub> regular quality and HB<sub>2</sub> poor quality.

For the physicochemical parameters, Figs. 3 and 4 evaluated in the development of the monitoring comply with the ECAs for natural body category, established in the Peruvian regulations (MINAM 2017).

## DISCUSSION

Rivera et al. (2008), state that contamination increases when there are low oxygen levels and the distribution of macroinvertebrates is related to water quality. It was possible to verify the presence of Chironomidae in the La Gallega stream, which was found in the sampling stations ranging from good, acceptable, and critical waters; where the oxygen level in HB<sub>1</sub> and HB<sub>2</sub> is high and low in HB<sub>3</sub> and HB<sub>4</sub>; in the case of Ephemeroptera, Custodio & Chaname (2016), comment that they live in sites with good oxygenation, in

Table 2: EPT and BMWP/Col indices for each sampling station, La Gallega-Morropón stream, Piura-Peru.

Sampling station	Station name	Water Quality Index			
		BMWP/Col		EPT	
HB <sub>1</sub>	Paltashaco	Good		Regular	
HB <sub>2</sub>	La Ensilada	Acceptable		Mala	
HB <sub>3</sub>	Piedra del toro	Critique		Good	
HB <sub>4</sub>	Piedra del toro 2	Critique		Good	

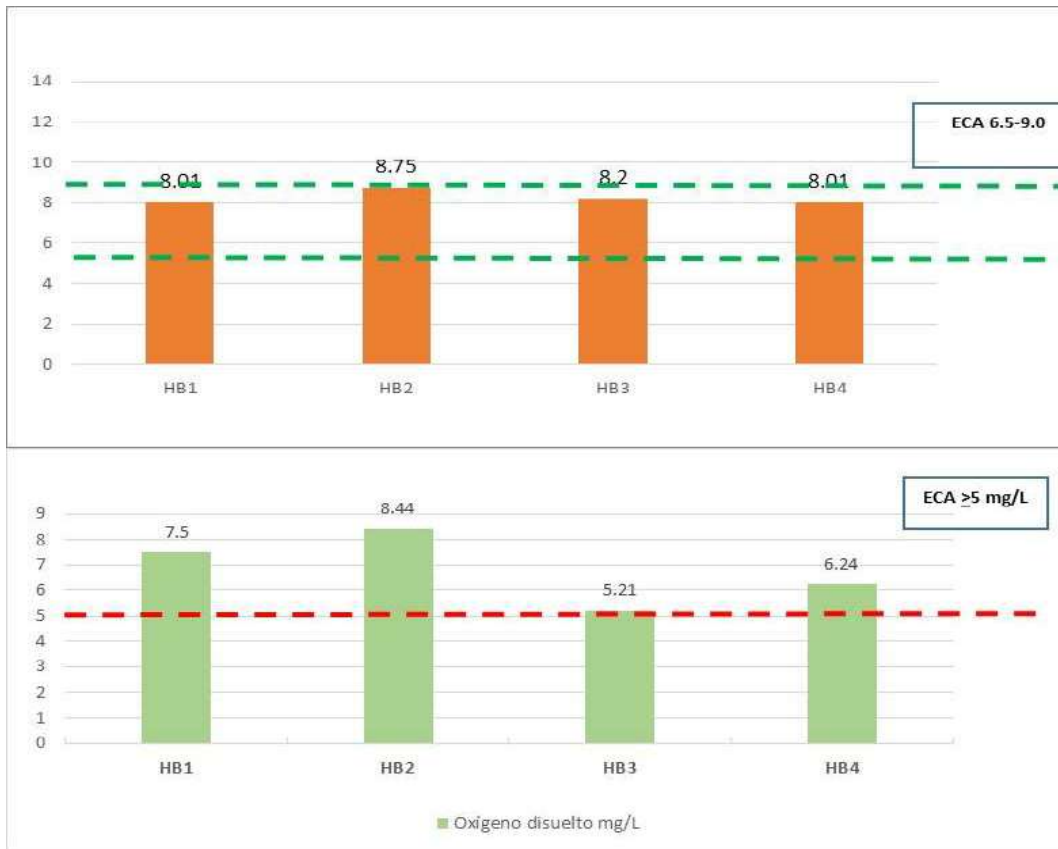


Fig. 3: Hydrogen potential (pH) and dissolved oxygen (mg/L) values of the sampling stations, La Gallega-Morropón stream, Piura-Peru.

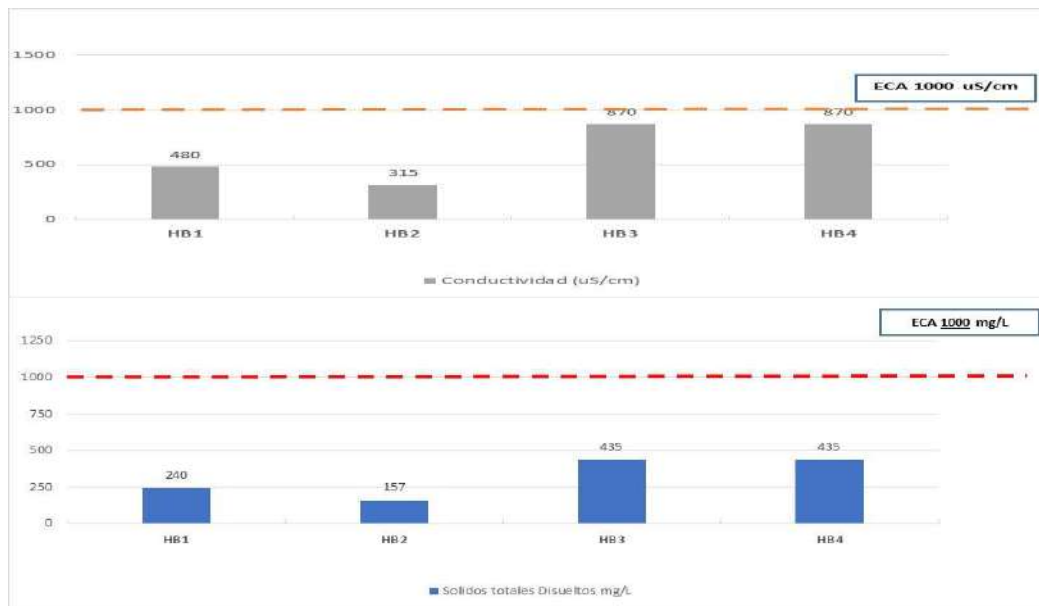


Fig. 4: Potential values of electrical conductivity (uS/cm) and Total Dissolved Solids (mg/L) of the sampling stations, La Gallega-Morropón stream, Piura-Peru.

substrates of sand, stone, that is, they live in water bodies with good quality, we can verify this in the HB<sub>1</sub> station, here the water quality gave us acceptable with 118 scores (BMWP/Col) the highest in all sampling stations.

Burdet & Watts (2009), argue that substrates dominated by leaf litter provide a greater availability of resources derived from biodegradation, so that in addition to presenting a high species richness, they allow sustaining a higher density of organisms. It was possible to identify that in the sampling stations in the La Gallega stream, all of them presented substrates with leaf litter, thus favoring some groups of macroinvertebrates such as Libellulidae, Zygoptera, Psychodidae, Chironomidae, Elmidae, Leptophlebiidae, Leptophlebiidae, and Leptophlebiidae.

Villamarín (2008), points out that, in rivers, the higher the altitude the water quality is good, but the availability of habitat is lower; the opposite happens when the altitude is lower and even the availability of water is higher; in the stations of La Gallega stream, the composition of the taxa was homogeneous, so there was no evidence of the influence of the altitudinal gradient. In addition, Giacometti & Bersosa (2006) comment that the diversity of macroinvertebrate species is influenced by the variables temperature and oxygen, while in La Gallega stream, dissolved oxygen obtained values >5mg/L in all sampling stations, complying with what is established in ECA (MINAM 2017) for natural water bodies.

Albuquerque (2018), details that the water quality of the confluence of Corrales, Medio, and Alto Piura sub-basins using the BMWP/Col index, reported 37 families belonging to 5 classes, with a predominance of Hemiptera, Diptera, Coleoptera, and Ephemeroptera, it was identified that the water quality is acceptable and regular in different sampling points; In La Gallega stream a total of 22 families were obtained, being Psychodidae the one with the highest number of individuals with 670, followed by Chironomidae with 306 and Elmidae with 228, this difference of decrease in the number of families is because the water body has been suffering alterations caused by anthropological effects (different livestock and agricultural activities). Domínguez & Fernández (2009), Quinn & Hickey (1990), and Roldán (1988) refer that physicochemical factors influence the aquatic macroinvertebrate community. They emphasize that water velocity, temperature, and oxygen availability are determining factors in the distribution of these organisms. In the results obtained, the physicochemical parameters (oxygen, temperature, pH, conductivity, turbidity) are within the range of values established in the ECA (MINAM 2017) for natural water bodies.

## CONCLUSIONS

The diversity of aquatic macroinvertebrates is low, due to the anthropogenic factor along the La Gallega-Morropón stream, Piura-Peru.

The water quality indexes, BMWP/Col, presented one station with good (HB<sub>1</sub>), acceptable (HB<sub>2</sub>), and critical (HB<sub>3</sub> and HB<sub>4</sub>) quality, while 2) EPT exhibited two stations with good quality (HB<sub>3</sub> and HB<sub>4</sub>), HB<sub>1</sub> regular quality and HB<sub>2</sub> poor quality.

The values of the physicochemical parameters evaluated all comply with the values established in the Peruvian regulations.

## REFERENCES

- Albuquerque, Z., 2017. *Water quality of the confluence of sub-basins: Corrales, medium and medium-high Piura using the BMWP index (adapted)*, Piura - Peru 2017.
- Álvarez, S. and Pérez, L., 2007. Water quality assessment using aquatic macroinvertebrates in the Yeguaré sub-basin, Honduras. Thesis, Pan-American Agricultural School, Zamorano, Honduras.
- Bailey, R., Norris, R. and Reynoldson, T., 2003. *Bioassessment of freshwater ecosystems using the reference condition approach*. Springer Press, USA.
- Bergkamp, G. and Orlando, B., 1999. Exploring collaboration between the Convention on Wetlands (Ramsar, Iran 1971) and the UN Framework Convention on Climate Change. *Climate Initiative*, IUCN, Washington, USA.
- Bonada, N., Prat, N., Resh, V.H. and Statzner, B., 2006. Developments in aquatic insect biomonitoring: a comparative analysis of recent approaches. *Annual Review of Entomology*, 51, pp. 495-523.
- Burdet, A. and Watts, R., 2009. Modifying living space: an experimental study of the influences of vegetation on aquatic invertebrate community structure. *Hydrobiologia*, 618, pp.161-173.
- Carrera, C. and Fierro, K., 2001. *Monitoring manual: Aquatic macroinvertebrates as indicators of water quality*. EcoCiencia, Quito.
- Coayla-Peñaloza, P., Chenux-Díaz, A.A., Moreno-Salazar, C.V., Cruz-Remache, C.E., Colque-Rondón, E.W. and Damborenea, C., 2023. Benthic macroinvertebrate communities and water quality assessment in high Andean wetlands Callali-Oscollo, Arequipa-Cusco, Peru. *Mexican Journal of Biodiversity*, 94, e944206. Available at: <https://doi.org/10.22201/ib.20078706e.2023.94.4206>
- Custodio, M. and Chanamé, F., 2016. Analysis of the biodiversity of benthic macroinvertebrates in the Cunas River using environmental indicators, Junín-Peru. *Scientia Agropecuaria*, 7(1), pp.33-44.
- Custodio, M. and Chávez, E., 2019. Quality of the aquatic environment of high Andean rivers evaluated through environmental indicators: A case of the Cunas River, Peru. *Ingeniare. Revista Chilena de Ingeniería*, 27(3), pp.396-409. Available at: <https://doi.org/10.4067/S0718-33052019000300396>
- De La Lanza, G., Hernández, S. and Carbajal, J., 2000. Water quality and pollution indicator organisms (bioindicators). First edition. Plaza y Valdez, S.A. de C.V., Mexico, pp.17-18.
- Domínguez, E. and Fernández, H., 2009. *Macroinvertebrados bentónicos sudamericanos: Sistemática y biología*. Fundación Miguel Lillo, Tucumán, Argentina, p.656. (In Spanish)
- Domínguez, E., Molineri, C., Fisherman, M., Hubbard, M. and Nieto, C., 2006. In: Adis, J., Arias, J.R., Thin-Wheel, G. and Wantzen, K.M. (eds.) *Aquatic biodiversity of Latin America*, Vol. 2, Pensoft, Moscow and Sofia, pp.646.

- Fernández, A., Fernández, L. and Di Risio, C., 2004. Water in Latin America. Water quality and management of aquatic ecosystems. *CYTEDXVII. Ibero-American Program of Science and Technology for Development*.
- Fernández, H. and Domínguez, E., 2001. *Guide for the determination of South American benthic arthropods*. National University of Tucumán, Tucumán, Argentina, pp.282.
- Giacometti, J. and Bersosa, F., 2006. Aquatic macroinvertebrates and their importance as bioindicators of water quality in the Alambi River. Thesis, Bachelor of Biology, Central University of Ecuador.
- Lara-Lara, J., Arreola, J., Calderón, L., Camacho, V., Espino, G., Escofet, A., Espejel, M., Guzmán, M., Ladah, L., López, M., Meling, E., Moreno, P., Reyes, H., Quebradas, E. and Zertuche, J.A., 2008. Coastal, island and epicontinental ecosystems. In: *Natural capital of Mexico*, vol. I: Current knowledge of biodiversity. Conabio, Mexico, pp.109-134.
- Ministry of the Environment [MINAM], 2017. Supreme Decree No. 004-2017-MINAM, of June 7, 2017. Approves Environmental Quality Standards (ECA) for Water and establishes Complementary Provisions.
- Martínez, F., Prieto, C., Martínez, P. and Ochoa Cueva, P., 2022. Ecological quality of water supply basins in the City of Loja – Ecuador. *Polytechnic Journal*, 52(2), pp.77-86. Available at: <https://doi.org/10.33333/rp.vol52n2.08>
- Medina, V. and Yasmy, K., 2011. Benthic macroinvertebrates as indicators of pollution in the Chili stream between June and August 2011, Arequipa – Peru. Thesis, Bachelor of Biology, National University of San Agustín.
- Moreno, C., 2001. Methods for measuring biodiversity. Volume 1. *Manuals and Theses: SEA*.
- Pinheiro, S., Ferraz De Queiroz, J. and Boeira, R., 2004. Protocol for collection and preparation of benthic macroinvertebrate samples in streams. *Technical Communication 19*, Ministry of Agriculture, Brazil.
- Posada, G. and Roldán, G., 2003. Illustrated key and diversity of Trichoptera larvae in northwestern Colombia. *Caldasia*, 25(1), pp.169-192.
- Quinn, M. and Hickey, C., 1990. Characterization and classification of benthic invertebrate communities in 88 New Zealand rivers in relation to environmental factors. *New Zealand Journal of Marine and Freshwater Research*, 24, pp.387-409.
- Rivera, U., Camacho, P. and Botero, B., 2008. Numerical structure of aquatic entomofauna in eight streams in the department of Quindío-Colombia. *Acta Biol. Colomb.*, pp.72-83.
- Rojas, G. and Ibáñez, O., 2003. Diagnosis of the Piura River basin with a risk management approach. *Piura*.
- Roldán, G., 1988. *Guide for the study of aquatic macroinvertebrates of the Department of Antioquia*. University of Antioquia, Bogotá, Colombia, p.216.
- Roldán, G., 2003. *Bioindication of water quality in Colombia*. First edition. Editorial Universidad de Antioquia, Medellín, p.170.
- Springer, M., 2006. Taxonomic key to larvae of the order Trichoptera (Insecta) from Costa Rica. *Rev. Biología Tropical*, 54, pp.273-286.
- Villamarín, C., 2008. Structure and composition of aquatic macroinvertebrate communities in high Andean rivers in Ecuador and Peru. Design of a water quality measurement system with multimetric indices. Thesis. PhD degree. University of Barcelona.

---

#### ORCID DETAILS OF THE AUTHORS

- Mónica Santa María Paredes-Agurto: <https://orcid.org/0009-0006-1227-6209>  
 Armando Fortunato Ugaz Cherre: <https://orcid.org/0000-0003-2808-1271>  
 José Manuel Marchena Dioses: <https://orcid.org/0000-0002-7321-8268>  
 Robert Barrionuevo Garcia: <https://orcid.org/0000-0001-6072-0235>





# Bisphenol A in Indian Take-Out Soups: Compliance, Implications and Sustainable Solutions

Sugata Datta<sup>1,2</sup>, Abhishek Chauhan<sup>2†</sup>, Anuj Ranjan<sup>2</sup>, Abul Hasan Sardar<sup>3</sup>, Hardeep Singh Tuli<sup>4</sup>, Ammar Abdulrahman Jairoun<sup>5,6</sup>, Moyad Shahwan<sup>7,8</sup>, Ujjawal Sharma<sup>9</sup> and Tanu Jindal<sup>2</sup>

<sup>1</sup>Amity Institute of Environmental Sciences, Amity University, Noida Campus, U.P., India

<sup>2</sup>Amity Institute of Environmental Toxicology Safety and Management, Amity University, Noida, U.P., India

<sup>3</sup>University of Calcutta, West Bengal, India

<sup>4</sup>Department of Bio-Sciences and Technology, Maharishi Markandeshwar Engineering College, Maharishi Markandeshwar (Deemed to Be University), Mullana, Ambala, 133207, India

<sup>5</sup>Health and Safety Department, Dubai Municipality, Dubai 67, Dubai, United Arab Emirates

<sup>6</sup>Discipline of Clinical Pharmacy, School of Pharmaceutical Sciences, Universiti Sains Malaysia (USM), Pulau Pinang, 11500, Malaysia

<sup>7</sup>Department of Clinical Sciences, College of Pharmacy and Health Sciences, Ajman University, Ajman 346, United Arab Emirates

<sup>8</sup>Centre of Medical and Bio-Allied Health Sciences Research, Ajman University, Ajman 346, United Arab Emirates

<sup>9</sup>Department of Human Genetics and Molecular Medicine, School of Health Sciences, Central University of Punjab, Bathinda, India

†Corresponding author: Abhishek Chauhan; akchauhan@amity.edu

Nat. Env. & Poll. Tech.  
Website: [www.neptjournal.com](http://www.neptjournal.com)

Received: 01-03-2024

Revised: 31-03-2024

Accepted: 05-04-2024

## Key Words:

Bisphenol A  
Food-contact materials  
Food safety  
Plastic packaging

## ABSTRACT

This research investigates the migration of Bisphenol A (BPA) from packaging containers into take-out vegetable soups and premixed tomato soups through three replicate studies. The samples underwent extraction using solid-phase extraction (SPE) cartridges, followed by separation on a C18 column. BPA concentrations in the soups were assessed at 15, 30, and 45-minute intervals, consistently revealing undetectable levels (<LOQ). Plastic packaging samples, known for BPA utilization in production, remained below the Specific Migration Limit (SML) set at 0.5 mg.kg<sup>-1</sup>, irrespective of material type or contact conditions. These results, conforming to EC regulations, suggest that food-contact materials (FCMs) in the Indian market pose no apparent health hazards during initial use. The absence of detectable BPA levels is attributed to the limited time-temperature relationship during the study. However, caution is warranted as BPA migration can occur with repeated use, emphasizing the importance of considering material quality and intended use of FCMs. The study underscores the significance of understanding BPA leaching under varied conditions, necessitating further research to explore long-term implications. Overall, the findings provide valuable insights for regulators, manufacturers, and consumers, contributing to the ongoing discourse on food safety and using plastic materials in food packaging.

## INTRODUCTION

Bisphenol A (BPA) is prominently featured among the most commonly utilized substances in contemporary industrial practices, serving as a fundamental constituent in the composition of epoxy resins and plastic containers. Its prevalence is attributable to its robust and transparent physical properties (Sharma et al. 2023). In 2020, the projected production of polycarbonate plastics (PC) in the United States amounted to roughly one million metric tons. PC boasts diverse applications, owing to its attributes such

as heat resistance, lightweight construction with exceptional durability, transparency, impact resistance, and inherent flame retardancy. These qualities are harmoniously balanced, contributing to the continuous growth of PCs and the exploration of novel, innovative applications. Consequently, its production has been experiencing an annual increase of approximately 4% (Koizumi et al. 2023). However, extensive investigations have identified BPA as a major environmental pollutant capable of permeating soil and water systems, with the potential to enter the food chain over an extended period. According to research findings, individuals' primary avenue

of bisphenol exposure is consuming food and beverages contaminated with BPA (Hahladakis et al. 2023). BPA can potentially permeate from plastic containers into the associated food or beverage, especially under conditions involving elevated temperatures or acidic substances (Dey et al. 2021, Kumar et al. 2023b). This phenomenon raises concerns about human exposure to BPA, which is associated with adverse health issues, including elevated anxiety levels, modified exploratory behavior, diminished social interaction, heightened aggression, and impairments in spatial or recognition learning and memory (Bakoyiannis et al. 2021). The BPA migration process encompasses both physical and chemical migration (Khalili et al. 2023). Physical migration results from the diffusion of residual BPA monomers after manufacturing. Conversely, chemical migration occurs due to BPA release from the polymer surface, predominantly due to hydrolysis. Hence, the presence of BPA in food items can be ascribed to either the migration of residual BPA or the hydrolysis of the polymers.

The European Chemical Agency (ECHA) has classified BPA as a highly toxic chemical, and therefore, many regulatory authorities have set specific limits on its usage and migration. However, in 2009, the World Health Organization (WHO) concluded that imposing public limits on BPA is unnecessary. In the United States, due to its potential hazards, the Food and Drug Administration (FDA) withdrew its approval for using BPA in packaging materials for baby formula and feeding bottles in 2014. Similar restrictions have been implemented by the European Union (EU) and Canada. The United States Environmental Protection Agency (USEPA) has determined that a toxic level of BPA is up to  $50 \mu\text{g}\cdot\text{kg}^{-1}$  of body weight per day but advises caution as lower amounts may not be entirely safe (EU - COM 2014/015, 2014).

Furthermore, the European Commission (EC) has established a Specific Migration Limit (SML) for BPA in foods at  $0.6 \mu\text{g}\cdot\text{g}^{-1}$  of the food substance. The Indian government banned manufacturing, importing, and selling PC baby bottles containing BPA in 2010, citing concerns about potential health effects on infants. However, there are currently no specific regulations or bans on using BPA in other food-contact materials (FCMs), such as epoxy resins and polystyrene containers.

In recent years, there has been much discussion regarding the use of BPA in food-grade plastic. Some studies suggest that low levels of exposure to BPA are unlikely to cause harm, while other research links BPA exposure to various health issues, including developmental and reproductive problems, cancer, obesity, and diabetes (Sharma et al. 2023). Additionally, its capacity to migrate

from FCMs into food matrices and the environment poses human and environmental health risks. FCMs, constructed from postconsumer materials, are particularly at high risk of containing these compounds. The assessment of post-consumer recycled feedstocks in FCMs is mandatory, and the careful selection of a suitable detection method is essential for compliance with relevant regulations, ensuring the comprehensive evaluation of human and environmental safety (Tumu et al. 2023). The amount of BPA released into food from FCMs depends on various factors such as material type, preparation time, environment, and nature of the food. According to recent studies by (Kumar et al. 2023a), the storage temperature and storage time of bottled water in polyethylene terephthalate (PET) bottles can have an impact on the release of BPA. The brand of the PET bottle can influence the degree of BPA release, possibly due to raw material contamination during the manufacturing or recycling process. Higher temperatures and longer storage durations have been observed to correlate with increased release of BPA (Khanniri et al. 2023). Additionally, the diffusivity of BPA is found to escalate with elevated storage temperatures (Ahmad et al. 2023). These findings suggest that factors such as temperature and storage duration play crucial roles in the release dynamics of BPA from packaging materials.

The significance of this study is underscored by several factors, given that BPA is a widely employed chemical found in various products, including plastic containers, food packaging, and epoxy resin. The potential for BPA to leach into the environment from these products raises concerns about its ability to pose health hazards. This has heightened apprehensions about the potential health consequences of BPA exposure, particularly in susceptible populations such as pregnant women and children. Considering that India is among the largest producers and consumers of plastic products globally, coupled with a swiftly expanding population and economy, BPA exposure levels in India are anticipated to increase.

## MATERIALS AND METHODS

### Sample Collection

A quantity of 200 mL of vegetable soup designated for take-out from local food establishments was distributed equally (30 mL) across six distinct types of containers. These containers were labeled as follows: BN1 for polycarbonate (PC) plastics, BN2 for polystyrene (PS) plastics, BN3 for polypropylene (PP) plastics, BN4 for polyethylene (PE) pouches, BN5 for aluminum foils, and BN6 for areca leaf containers (Fig. 1). The containers were procured from the local market. The investigation focused on examining the



Fig. 1: BPA leaching in take-out soups from various packaging containers, with material codes assigned as: BN1 for polycarbonate (PC) plastics, BN2 for polystyrene (PS) plastics, BN3 for polypropylene (PP) plastics, BN4 for polyethylene (PE) pouches, BN5 for aluminum foils, and BN6 for areca leaf containers.

potential migration of BPA from the packaging containers into the vegetable soup over durations of 15, 30, and 45 min. To facilitate comparison, 18.6 g of premix tomato soup sample was dissolved in 200 mL of hot water and distributed, with 30 mL allocated to each of the same six containers for parallel analysis of BPA leaching.

### Sample Temperature and pH

The soup samples, upon being packaged in the containers, were subjected to heating at a temperature of 70°C in an oven, in accordance with the temperatures commonly encountered in food establishments. Subsequently, the pH of the sample was measured using a calibrated pH meter (Systronics type 335). The pH of the vegetable soup was found to be 6.12, and the premix tomato soup was 6.91.

### Reagents and Chemicals

BPA (purity  $\geq 99\%$ ) was purchased from Sigma-Aldrich (Bengaluru, India). Acetonitrile (ACN) and methanol were procured from Merck (Mumbai, India). Water was supplied using a Milli-Q Ultrapure water purification system (Millipore, Bedford, MA, USA). Solid phase extraction (SPE) (Oasis MAX) cartridge (30 mg.mL<sup>-1</sup>) was purchased from Waters (MA, USA).

### Stock Solutions and Standard Solutions

The stock solution of BPA (100 mg.L<sup>-1</sup>) was prepared in methanol in dark amber bottles and stored at 4°C before use. Further dilution of the stock solution with water guides to all

standard working solutions of five different concentrations of 0.05, 0.2, 0.5, 1, and 5  $\mu\text{g.mL}^{-1}$ .

### Sample Preparation

The extraction methodology outlined by (Liao & Kannan 2013, Kaushik et al. 2009) was adhered to for this study. Each soup sample, amounting to 30 mL each, was precisely measured and subsequently transferred into the six distinct types of packaging containers, each with a capacity of 150 mL. Subsequently, they were spiked with 0.5 mg.L<sup>-1</sup> of the internal standard BPA. Extraction was done twice using ACN (5 mL each), employing a shaker for 60 minutes. The resulting sample mixture underwent centrifugation at 5000 g for 5 min, and the obtained extract was combined. This combined extract underwent evaporation to near dryness under a nitrogen stream at 50°C, and the resulting extraction residue was reconstituted in 1 mL of 100% ACN (v/v). The extract was purified using solid-phase extraction (SPE) through passage through an Oasis MAX cartridge.

### Migration Analysis

Agilent 1290 Infinity II HPLC System with Biosuite C18 column (500 Å, 7  $\mu\text{m}$ , 4.6 mm x 150 mm) fitted with a UV detector set at 217 nm. The mobile phase comprises 30% TFA in HPLC-grade water and 70% ACN. The injection volume was 50  $\mu\text{L}$  using a Hamilton syringe, the mobile phase flow rate was 1 mL.min<sup>-1</sup>, and the run time was set for 8 min. The conditions for HPLC are given in detail in Table 1.

Table 1: Analytical parameters and conditions for BPA determination by HPLC-UV.

Substance detected	Parameter	Conditions
BPA	Column	Biosuite C18 PA-A (500 Å, 7 µm, 4.6 mm × 150 mm)
	Detector	UV (217nm)
	Pump	Agilent 1290 Infinity II
	Mobile phase	30% TFA in HPLC grade water + 70% ACN
	Injection volume	50 µl using a Hamilton syringe
	Flow rate	1 mL min <sup>-1</sup>
	Run time	8 minutes

### Method Validation

Soup samples were spiked using the BPA with concentrations of 0.5 mg.L<sup>-1</sup> before the studies (Fig. 2). The results were repeated thrice after one week. The average recovery of BPA in spiked samples was in the range of 89-119%. Quantification of BPA was performed using regression equations (regression coefficient, R<sup>2</sup> > 0.99) generated from a 5-point calibration standard at concentrations ranging from 0.05 to 5 µg.mL<sup>-1</sup>. The limit of quantization (LOQ) detected for BPA was 0.3 ppm.

### Statistical Analysis

ANOVA statistical analysis was used to compare BPA leaching in different packaging containers at different time points using R statistical software. The p-values for both the containers factor and the time factor are very low (p < 0.05), indicating that both container type and time significantly affect BPA leaching. The interaction between containers and time also has a very low p-value, suggesting that the effect of time on BPA leaching differs among the packaging containers. Overall, these results suggest significant differences in BPA leaching among the packaging containers and across different time points, as well as significant interactions between container type and time.

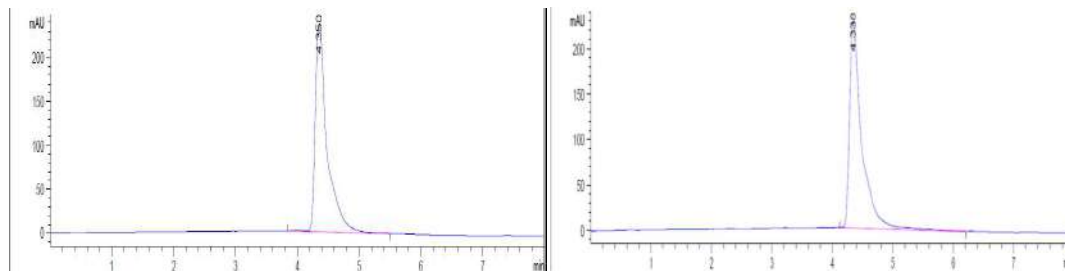
Table 2: Concentration (ppm) of BPA in take-out vegetable soup samples and premix tomato samples from packaging containers at different time intervals.

Packaging containers	Concentration of BPA					
	Take-out vegetable soup samples			Premix tomato soup samples		
	15 mins	30 mins	45 mins	15 mins	30 mins	45 mins
BN1	0.10	0.14	0.20	0.11	0.15	0.22
BN2	0.17	0.24	0.25	0.18	0.27	0.30
BN3	0.15	0.19	0.22	0.10	0.17	0.20
BN4	0.19	0.23	0.28	0.23	0.28	0.29
BN5	0.19	0.24	0.27	0.14	0.20	0.22
BN6	0.03	0.09	0.11	0.08	0.11	0.17

### RESULTS AND DISCUSSION

The investigation involved three replicate studies to determine how BPA migrates into take-out vegetable soup and premixed tomato soup from various packaging containers. Results from BPA concentration assessments in the vegetable soup samples and in premix tomato soup samples at time intervals of 15, 30, and 45 min consistently revealed concentrations below LOQ levels, as indicated in Table 2.

Although the levels of BPA found in both the take-out vegetable soup and premixed tomato samples were below LOQ, there was an observed increase in BPA concentration with extended packaging durations from 15 to 30 and 45 minutes. The vegetable soup packaged in PE pouches had the highest migration level of BPA, followed by those in aluminum foils and PS containers. On the other hand, minimal migration of BPA was observed in vegetable soup packaged in areca leaf containers. In the premixed tomato soup samples, the highest BPA migration was noted in PS containers, followed by PE pouches and aluminum foils. Similarly, the lowest migration of BPA, as observed in the vegetable soup, was noted for areca leaf containers, as indicated in Fig. 3.

Fig. 2: HPLC chromatograms for take-out soups with and without spiking with 0.5 mg.L<sup>-1</sup> BPA.

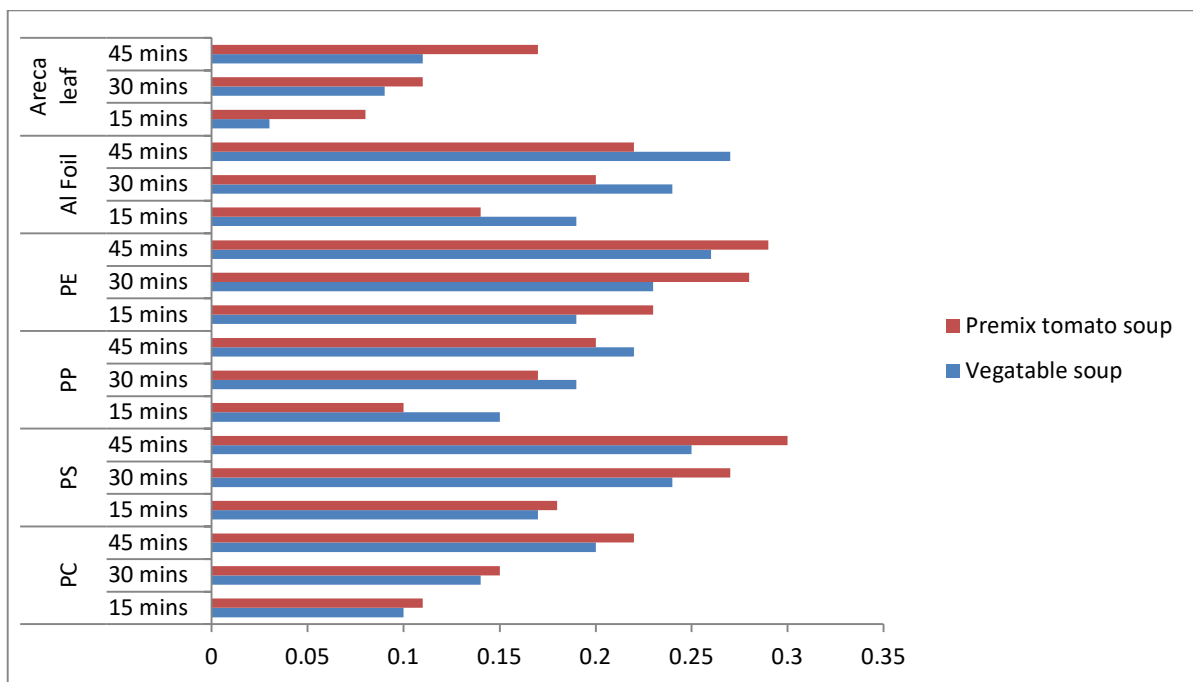


Fig. 3: Horizontal bar graphs showing the concentration of BPA leaching in take-out vegetable soup and premix tomato soup samples over time from different packaging containers.

The packaging container samples, tested and known for their utilization of BPA in production, exhibited BPA levels within the method's LOQ (0.3 ppm) for all tested soup samples. These levels were consistently below the SML for foodstuff, set at  $0.5 \text{ mg.kg}^{-1}$  by EC (Krivohlavek et al. 2023), irrespective of the packaging material type or the temperature and duration of contact with the food during migration tests. It is worth noting that our analysis was confined to BPA only, in adherence to the requirements of EU Directives. Upon initial examination, these findings suggest that packaging materials used in the Indian market conform to the permissible concentrations, posing no apparent health hazards regardless of the material composition. Consistent findings were reported by Baviera et al. (2023), indicating that the migration levels of BPA from the walls of PC bottles remained within acceptable limits. Even under extreme conditions, such as exposure to high temperatures in conjunction with washing scenarios involving detergents and the use of solid alkalis (which contribute to the degradation of PC material), the observed BPA contamination did not approach levels corresponding to the Tolerable Daily Intake (TDI) of  $4 \text{ } \mu\text{g.kg}^{-1}$  per body weight (bw) per day. These findings suggest that BPA migration does not occur during the initial use of FCMs. However, reports indicate that BPA migration into foods can occur with repeated use (Khalili et al. 2023). Therefore, how FCMs are utilized is crucial. Moreover, BPA migration is influenced by the

quality of plastic containers. Sturdy plastics tend to leach lower amounts of BPA than softer plastics like polystyrene. The findings from our study had similar observations. Softer plastics such as PE pouches and PS containers were found to leach maximum amounts of BPA as they exhibit temperature and size-dependent leaching and were limited by molecular diffusion throughout the bulk polymer (Gulizia et al. 2023). Similarly, Zhao et al. (2022) reported high concentrations of BPA and bisphenol S (BPS) in plastic products made from polystyrene, such as white foam take-out containers (WFTOCs) from China. Compared to other plastic containers, PS exhibited the highest BPA migration due to the stronger plasticity induced by the foaming process, resulting in higher levels of plasticizers being used. Similarly, PE pouches displayed elevated levels of BPA due to their thinness ( $25\text{-}50 \text{ } \mu\text{m}$ ), which necessitates high plasticity requirements and, consequently, a higher content of plasticizers compared to sturdier opaque PC and PP containers. Interestingly, aluminum foils also demonstrated increased BPA levels, which could be attributed to incomplete polymerization. According to Deshwal et al. (2019), unpolymerized monomers such as BPA can leach from the finished product.

Several studies have underscored the influence of storage temperature and duration on the release of BPA. Consequently, elevating the temperature and prolonging

storage time facilitates the release of BPA (Mârşolea et al. 2023). Ajaj et al. (2021) reported a 1.9-fold increase of styrene monomers between the inaugural and fourth day of storage, succeeded by a subsequent elevation of 3.1fold from the initial to the tenth day. However, the tested soup samples exhibited insignificant BPA leaching levels, and this observation can be attributed to the time-temperature relationship. As indicated by Nepalia et al. (2018), an increase in temperature has been linked to elevated BPA migration. Since most of the tested soup samples were packaged at 70°C for a maximum duration of 45 minutes, which may not be conducive to significant BPA leaching, it is noteworthy that if the time duration had been longer, a higher concentration of BPA might have been noted, as reported by Li et al. (2024). Therefore, it is crucial to acknowledge that an escalation in temperature and prolonged storage duration heightens the risk of BPA migration.

Areca catechu leaf containers were found to exhibit the lowest levels of leached BPA. These findings align with the assertions made by Kora (2019), which describe areca leaves as rigid, dense, and heat-tolerant, resulting in plates and cups that are leak-proof, water-resistant, and odorless. Furthermore, areca leaf products are deemed suitable for freezing, microwaving, and oven heating. They are naturally biodegradable and compostable, considered safe for single use with moist food, and reusable multiple times with dry food. Similarly, Umamakeswari (2023) utilized the Technique for Order Preference by Similarity to the Ideal Solution (TOPSIS) method to evaluate four types of leaf plates (Bamboo, Siali, Palm leaf, and Bagasse) based on criteria such as durability, biodegradability, and thermal resistance. The study concluded that Siali leaf plates emerged as the optimal choice. This research collectively underscores the importance of assessing and regulating packaging materials for potential chemical migration, advocating for sustainable alternatives such as natural leaf-based products like Areca catechu or Siali plates for their eco-friendly attributes and suitability for various food handling scenarios.

## CONCLUSION

The three replicate studies conducted to investigate the migration of BPA into take-out vegetable soups and premix tomato soups from various packaging containers yielded consistent and reassuring results. The BPA concentration assessments at time intervals of 15, 30, and 45 minutes consistently revealed undetectable concentrations (<LOQ), indicating that the tested soup samples complied with permissible concentrations, as outlined by the EC regulations. The levels of BPA in packaging containers were consistently below the SML set at 0.5 mg.kg<sup>-1</sup> for all tested samples,

regardless of material type or contact conditions. These findings suggest that, in the Indian market, packaging containers conform to permissible concentrations, posing no apparent health hazards under normal use conditions. Notably, the absence of detectable BPA levels in the tested samples can be attributed to the limited time-temperature relationship during the study period. While these results are promising for initial use, it is essential to consider the potential for BPA migration with repeated use, as reported in previous studies. The observed variation in BPA leaching among different plastic materials underscores the importance of considering the material composition and the quality and intended use of FCMs. Further research is warranted to explore the long-term implications and potential risks associated with BPA migration under varied conditions of use and storage. This study emphasizes the significance of evaluating and regulating packaging materials to mitigate potential chemical migration risks. It advocates for the use of sustainable alternatives, such as natural leaf-based products, due to their eco-friendly properties and suitability for diverse food handling applications.

## REFERENCES

- Ahmad, T., Manzar, M.S., Georjin, J., Franco, D.S.P., Khan, S., Meili, L. and Ullah, N., 2023. Development of a new hypercrosslinked resin based on polyamine-isocyanurate for the efficient removal of endocrine disruptor bisphenol-A from water. *Journal of Water Process Engineering*, 53, 103623. <https://doi.org/https://doi.org/10.1016/j.jwpe.2023.103623>
- Ajaj, A., J'bari, S., Ononogbo, A., Buonocore, F., Bear, J.C., Mayes, A.G. and Morgan, H., 2021. An insight into the growing concerns of styrene monomer and poly(styrene) fragment migration into food and drink simulants from poly(styrene) packaging. *Foods*, 10(5), p.5113. <https://doi.org/10.3390/foods10051136>
- Bakoyiannis, I., Kitraki, E. and Stamatakis, A., 2021. Endocrine-disrupting chemicals and behavior: A high risk to take? *Best Practice & Research. Clinical Endocrinology & Metabolism*, 35(5), p.101517. <https://doi.org/10.1016/j.beem.2021.101517>
- Baviera, M.B., Bolognesi, C., Chesson, A., Cocconcelli, P.S., Crebelli, R., Gott, D.M., Grob, K., Lampi, E., Mengelers, M., Mortensen, A., Rivi, G., Steffensen, I., Tlustos, C., Vernis, L., Zorn, H., Batke, M., Bignami, M., Corsini, E., Fitzgerald, R. and Loveren, H.V., 2023. Re-evaluation of the risks to public health related to the presence of bisphenol A ( BPA ) in foodstuffs. *Journal of European Food Safety Authority*, 21, p.685 <https://doi.org/10.2903/j.efsa.2023.6857>
- Deshwal, G. K., Panjagari, N.R. and Alam, T., 2019. An overview of paper and paper-based food packaging materials: health safety and environmental concerns. *Journal of Food Science and Technology*, 56(10), pp.4391–4403. <https://doi.org/10.1007/S13197-019-03950-Z>
- METRICS
- Dey, A., Dhumal, C.V., Sengupta, P., Kumar, A., Pramanik, N.K. and Alam, T., 2021. Challenges and possible solutions to mitigate the problems of single-use plastics used for packaging food items: a review. *Journal of Food Science and Technology*, 58(9), pp.3251–3269. <https://doi.org/10.1007/S13197-020-04885-6>
- EU - COM 2014/015 2014. *Official Journal of the European Communities*, Off. J. Eur. Union, 57( 20/01/2014), pp. 1–28.

Available at <http://eurlex.europa.eu/legal-content/EN/TXT/PDF/?uri=OJ:L:2014:015:FULL&from=EN>

- Gulizia, A.M., Patel, K., Philippa, B., Motti, C.A., van Herwerden, L. and Vamvounis, G., 2023. Understanding plasticizer leaching from polystyrene microplastics. *Science of The Total Environment*, 857, p.159099. <https://doi.org/https://doi.org/10.1016/j.scitotenv.2022.159099>
- Hahladakis, J.N., Iacovidou, E. and Gerassimidou, S., 2023. An overview of the occurrence, fate, and human risks of the bisphenol-A present in plastic materials, components, and products. *Integrated Environmental Assessment and Management*, 19(1), pp.45–62. <https://doi.org/10.1002/IEAM.4611>
- Khalili, E., Sayed, S., Hashemi, A., Nadjarzadeh, A., Askari, E., Akrami, F. and Fereshteh, M., 2023. Bisphenol A release from food and beverage containers: A review. *FSN*, 12, pp.3718–3728. <https://doi.org/10.1002/fsn3.3398>
- Khanniri, E., Bayanati, M., Koushki, M.R., Ferdosi, R., Sohrabvandi, S., Esmaili, S., Akbari, M. E. and Forouhar, P., 2023. Migration of bisphenol A and several phthalate acid contaminants into bottled drinking water: Influence of storage conditions and their health risks. *International Journal of Environmental Analytical Chemistry*, 22, p.869. <https://doi.org/10.1080/03067319.2023.2209869>
- Kaushik, P., Abhishek, C. and Pankaj, G., 2009. Screening of *Lyngbya majuscula* for potential antibacterial activity and HPTLC analysis of active methanolic extract. *Journal of Pure and Applied Microbiology*, 3(1), pp.169-174.
- Koizumi, K., Okabe, A., Kimukai, H., Sato, H., Taguchi, H., Nishimura, M., Kwon, B.G. and Saido, K., 2023. Novel decomposition of polycarbonate and effect on marine ecosystem. *RSC Advances*, 13(42), pp.29668–29674. <https://doi.org/10.1039/d3ra04127a>
- Kora, A.J., 2019. Leaves as dining plates, food wraps, and food packing material: Importance of renewable resources in Indian culture. *Bulletin of the National Research Centre*, 43(1), p.231. <https://doi.org/10.1186/s42269-019-0231-6>
- Krivohlavek, A., Mikulec, N., Budeč, M. and Baruši, L., 2023. Migration of BPA from food packaging and household products on the Croatian market. *International Journal of Environmental Research and Public Health*, 20(4), p.2877
- Kumar, A., Singh, D., Bhandari, R., Malik, A.K., Kaur, S. and Singh, B., 2023a. Bisphenol A in canned soft drinks, plastic-bottled water, and household water tank from Punjab, India. *Journal of Hazardous Materials Advances*, 9(11), p.100205. <https://doi.org/10.1016/j.hazadv.2022.100205>
- Kumar, P., Aruna Priyanka, R.S., Shalini Priya, P., Gunasree, B., Srivanth, S., Jayasakthi, S., Kapoor, A. and MuthuKumar, R., 2023b. Bisphenol A contamination in processed food samples: an overview. *International Journal of Environmental Science and Technology*, 20(12), pp.13975–13994. <https://doi.org/10.1007/s13762-023-04793-0>
- Li, Y., Liu, C., Yang, H., He, W., Li, B., Zhu, X., Liu, S., Jia, S., Li, R. and Tang, K. H. D., 2024. Leaching of chemicals from microplastics: A review of chemical types, leaching mechanisms and influencing factors. *Science of The Total Environment*, 906, p.167666. <https://doi.org/https://doi.org/10.1016/j.scitotenv.2023.167666>
- Liao, C. and Kannan, K., 2013. Concentrations and profiles of bisphenol A and other bisphenol analogs in foodstuffs from the United States and their implications for human exposure. *Journal of Agricultural and Food Chemistry*, 61(19), pp.4655–4662. <https://doi.org/10.1021/JF400445N>
- Mârşolea, A.C., Chiriac, F.L., Orbeci, C., Bobirić, L. and Bobirić, C., 2023. Migration and leaching behavior of Bisphenol A from polyethylene terephthalate water bottles under different storage conditions. *International Journal of Food Science & Technology*, 58(10), pp.5609–5615. <https://doi.org/10.1111/IJFS.16583>
- Nepalia, A., Singh, A., Mathur, N., Kamath, R. and Pareek, S., 2018. Assessment of mutagenicity caused by popular baby foods and baby plastic-ware products: An imperative study using microbial bioassays and migration analysis. *Ecotoxicology and Environmental Safety*, 162, pp.391–399. <https://doi.org/10.1016/J.ECOENV.2018.07.002>
- Sharma, V., Jain, D., Rai, A. R., Kumari, P., Nagar, V., Kaur, A., Singh, A., Verma, R.K., Pandey, H. and Sankhla, M. S., 2023. Toxicological assessment and concentration analysis of Bisphenol A in food grade plastics: A systematic review. *Materials Today: Proceedings*, 6, p.336. <https://doi.org/10.1016/J.MATPR.2023.06.336>
- Tumu, K., Vorst, K. and Curtzwiler, G., 2023. Endocrine modulating chemicals in food packaging: A review of phthalates and bisphenols. *Comprehensive Reviews in Food Science and Food Safety*, 22(2), pp.1337–1359. <https://doi.org/10.1111/1541-4337.13113>
- Umamakeswari, T., 2023. Evaluating the quality factors of leaf plates by fuzzy TOPSIS method. *Materials Today: Proceedings*, 80, 1562–1566. <https://doi.org/https://doi.org/10.1016/j.matpr.2023.01.390>
- Zhao, N., Zhu, J., Zhao, M. and Jin, H., 2022. Twenty bisphenol analogs in take-out polystyrene-made food containers: concentration levels, simulated migration, and risk evaluation. *Environmental Science and Pollution Research International*, 22, p.890. <https://doi.org/10.1007/S11356-022-22890-4>







# The Impact of Socio-Economic and Climate Change on Poverty in Indonesia

Watemin<sup>1,3†</sup> , Slamet Rosyadi<sup>2</sup> and Lilis Siti Badriah<sup>1</sup>

<sup>1</sup>Faculty of Economics and Business, Jenderal Soedirman University, Indonesia

<sup>2</sup>Faculty of Social and Political Sciences, Jenderal Soedirman University, Indonesia

<sup>3</sup>Faculty of Agriculture and Fisheries, Universitas Muhammadiyah Purwokerto, Indonesia

†Corresponding author: Watemin; watemyn@ump.ac.id

Nat. Env. & Poll. Tech.  
Website: [www.neptjournal.com](http://www.neptjournal.com)

Received: 29-02-2024

Revised: 30-03-2024

Accepted: 13-04-2024

## Key Words:

Farming  
Climate change  
Poverty  
Vulnerability

## ABSTRACT

Climate change can impact farmers' incomes as agricultural production still depends on the weather. Currently, the majority of the impoverished rely primarily on agriculture for their income. The connection between poverty and climate change has been extensively studied, but further research is needed in this area. This research was conducted to provide empirical evidence regarding the impact of climate change on poverty using time series data, which has never been done. This research wants to examine the impact of socio-economics (economic growth, agricultural sector growth, inequality, inflation) and climate change on poverty. This research uses time series data from 2007 to 2022. The Central Bureau of Statistics and Climate Change Performance Index (CCPI) reports are the sources of research data. The study results suggest that the government's performance index in combating inflation, agricultural sector growth, and climate change has a positive impact on poverty. Poverty is negatively affected by the Gini index and economic growth. Government efforts to adaptively address climate change are necessary to prevent worsening impacts on poverty rates. To reduce the risk of crop failure, farmers must also practice practical agricultural management.

## INTRODUCTION

One of the main goals of sustainable development (Sustainable Development Goals or SDGs) is to reduce poverty in all forms and everywhere. Poverty is still a major problem for developing countries. As a country that was still developing, poverty in Indonesia is still large. In 2022, the number of poor people in Indonesia will be 26.36 million (9.57%). This number has decreased compared to 2021, namely 26.50 million (9.71%). Most of the poverty in Indonesia is in rural areas, as much as 12.36%, while those living in urban are 7.53% (BPS 2023).

There are many factors related to poverty, but to recommend poverty alleviation measures, it is necessary to identify the predominant factors (Zebua et al. 2015). The definition of poverty is a condition in which society is still in a state of complete deprivation (World Bank 2005). Haughton & Khandker (2009) stated that there are key characteristics associated with poverty, namely regional, community, household, and individual characteristics. Regional characteristics include the geographical conditions of a region, such as susceptibility to floods or droughts, natural disasters, and the isolation of a region. Regional characteristics are also related to sustainable ecosystems and increasing the well-being of local communities (Shi et al.

2023). Community characteristics include the availability of infrastructure (roads, clean water, electricity), health and educational services, distance to markets, and social relationships. Social relationships in the form of community interactions can help households escape poverty if used appropriately (Onumah et al. 2023). Household and individual characteristics can now be identified from a demographic perspective (number of household members, age structure, dependency ratio). Human capital (migrant workers, labor, and education) has a positive moderating effect on the impact of poverty reduction, and education provides the most significant moderating effect (Cheng et al. 2021). The characteristics of poverty are considered from an economic perspective (employment status, number of hours worked, number of possessions). The economic aspect in the form of the financial sector can contribute to poverty reduction by providing capital to households (Erlando et al. 2020). The characteristics of poverty are considered from social aspects (health status, level of education, place of residence). The health status of the community depends heavily on the existing health facilities. Health facilities can reduce poverty by offering their patients cheap treatment costs (Qin et al. 2021), including health insurance (Alating & Williams 2019).

According to Isiwu et al. (2021), poverty is a multidimensional problem related to social, political, and

economic problems, asset ownership, and access to needed resources. The inability to obtain necessary access results in poor people being excluded from decision-making processes aimed at alleviating poverty, including access to economic growth through development aimed at reducing poverty. Poor people cannot enjoy economic growth due to limited access (Ebunoluwa & Yusuf 2018). Limitations on access to needed resources are exacerbated by limited access to information. In the long term, mastering access to information reduces households' vulnerability to poverty (Huang et al. 2023).

In addition to the problem of poverty, dealing with climate change is also a goal to be achieved in the SDGs. The connection between climate change and poverty is increasingly discussed, as poor people feel the effects most acutely (Schleicher et al. 2018). This is because poor people rely heavily on natural resources as their main source of livelihood (Miller et al. 2022).

In Africa, government performance in addressing climate change is measured using the African Climate Change Policy Performance Index (ACCPPI). The assessment is based on four main assessments, namely the greenhouse gas emissions assessment (30%), the renewable energy assessment (25%), the government climate policy assessment (25%), and the corruption perception assessment (20%) (Epule et al. 2021). Another measure to assess the government's performance in dealing with climate change is the Climate Change Performance Index (CCPI). The CCPI assessment is based on four categories, namely greenhouse gas emissions (40%), renewable energy (20%), energy consumption 20% and government policies dealing with climate change (20%) (Burnch et al. 2021).

Research on the impact of climate change on poverty was conducted (Azzarri & Signorelli 2020) using data from a household survey in South Africa. The research shows that small farmers are the group most affected by weather fluctuations due to both floods and droughts, compared to large farmers and non-agricultural households. This is because smallholder farmers have many limitations in accessing various resources that can be used to adapt to climate change. Society must adapt to avoid major losses. Adaptation to climate change can be carried out by society individually or through institutions (Gross et al. 2016). Individually, communities are adapting to climate change by adapting their activities. At the institutional level, adaptations are required in the use of natural resources and ecosystems to deal with climate change.

Climate change has an impact on macroeconomic stability. Management measures to combat climate change offer significant benefits for economic growth, although they entail both direct and indirect costs. However, the costs

incurred will increase if climate change is not addressed. Climate change influences economic growth, although this influence occurs through other variables such as savings and community capital accumulation (Fankhauser & Tol 2005, Kadanali & Yalcinkaya 2020). Economic growth also affects poverty and income distribution. Alrahman et al. (2022) analyzed inequality, economic growth, and unemployment on the island of Sumatra. The analysis results show that inequality and economic growth have a negative relationship.

It is hoped that the results of development, as measured by economic growth, can benefit all people, including those living in poverty. If development benefits the poor, economic growth should reduce inequality (Tan 2020). However, many factors influence inequality, both economic and social, including gaps in economic potential and activity, quality of human resources, investments, labor, and government spending (Walujadi et al. 2022). Economic growth, poverty, and inequality are targets in SDGs No. 1 and 10. Lin et al. (2022) conducted growth-poverty inequality modeling in the Nile Valley using data from 2000 to 2020. Research shows that economic growth reduces poverty, while high levels of inequality can worsen poverty. Therefore, high inequality can hinder economic growth and poverty reduction efforts. The results of this research strengthen previous research by (Adeleye et al. 2020). Likewise, research by (Capuno 2022) concluded that economic growth alone is not enough to reduce poverty.

Inflation affects people living in poverty. When the inflation rate is high, it means that prices are rising, which ultimately puts a strain on people's spending, especially those living in poverty. The increase in food prices in Turkey during 2016–2019 increased poverty (Kiroğlu & Sezgin 2021). The research conducted by (Susanto 2014) also came to the same conclusion. Rehman et al. (2022) found that inflation and poverty have a negative impact on economic growth. Meanwhile, Fitriady et al. (2022) found that inflation has no impact on poverty and economic growth. In addition, it is recommended that the government not only focus on economic growth but also strive to reduce regional disparities and invest in human resource development.

Human resource development plays an essential role in poverty alleviation. High-quality human resources are the capital for sustainable development. It can create a creative economy (Rosyadi et al. 2019). With sustainable economic development, human resources influence the effectiveness of poverty reduction efforts (Amaluddin et al. 2018). Therefore, personnel development is a measure of the success of the development. In addition, high-quality human resources can adapt more quickly to climate change, thereby reducing vulnerability to poverty (Zhou et al. 2022).

To this day, the agricultural sector plays an essential role in fighting poverty. Agricultural growth led by small farmers is more effective in reducing poverty than large farmers (Dorosh & Thurlow 2018). Meanwhile, non-agricultural growth in trade, transport services, and manufacturing, especially in the agricultural processing industry, is almost approaching the role of the agricultural sector. In Indonesia, agriculture is the leading sector in several regions, and most rural communities rely on the agricultural sector for their livelihoods. Based on 2014-2017 data from 33 provinces, it is known that the growth of the agricultural sector contributed to the economy and reduced the level of rural poverty in Indonesia (Arham et al. 2020). Meanwhile, the slowdown in agricultural growth in the 2000s could undermine poverty reduction and food security efforts in Mozambique (Pauw et al. 2012). Higher agricultural productivity may be associated with the availability of cheaper food for consumption by households and for use as input in the industrial sector. Increasing agricultural productivity results in an improvement in consumer welfare, which implies that it contributes to the reduction of poverty through the relationship between prices and input supply.

The problem of poverty concerns various dimensions that are interconnected. This means that progress or deterioration in one aspect can have an impact on other aspects (Prawoto & Basuki 2022). Another aspect related to poverty is the resources available in an area. Excessive use of resources in an area to accelerate poverty reduction can result in environmental damage that worsens or hinders poverty reduction programs. Based on this explanation, this research aims to examine the impact of socio-economic and climate change on poverty.

## MATERIALS AND METHODS

### Study Area

This research was conducted in Indonesia using secondary data on climate change and poverty. As a tropical country still dependent on agriculture, Indonesia is severely affected by climate change.

### Data Collection

This research uses secondary data collected through recording. Research data was obtained by institutions related to research, the Central Statistic Agency (BPS) and the Intergovernmental Panel on Climate Change (IPCC).

### Data Analysis

This research uses time series data from 2007 to 2022.

The data that has been collected will be tested with the Jarque-Bera test (JB test) to see whether the data used is normal. To determine the possibility of autocorrelation and multicollinearity, the data will be tested with the Breusch-Godfrey Serial Correlation LM test and Variance Inflation Factors (VIF). Meanwhile, to determine the presence of heteroscedasticity, the data will be tested using the Breusch-Pagan-Godfrey test. The research data was analyzed using a multiple linear regression model with natural logarithms. The relationship between economic growth, inequality, inflation, and HDI was studied by Lin et al. (2022), Walujadi et al. (2022), Tan (2020) and Alrahman et al. (2022) using a multiple linear regression model. This research uses the same model as previous studies, but the researchers added a climate change variable in the form of a climate change index, which was not available in previous research. The equation model in this research is as follows:

$$\text{Ln}P0 = \alpha + \beta_1 \text{Ln}GRO + \beta_2 \text{Ln}AGR + \beta_3 \text{Ln}INF + \beta_4 \text{Ln}GI + \beta_5 \text{Ln}HDI + \beta_6 \text{Ln}CCPI + \varepsilon \quad \dots(1)$$

where  $\alpha$  is a constant,  $P0$  is the percentage of poor people,  $GRO$  = economic growth expressed in percentage units,  $AGR$  = is the growth of the agricultural sector expressed in percentage units,  $INF$  = inflation,  $GI$  = Gini index,  $HDI$  = human development index,  $CCPI$  = Climate Change Performance Index, and  $\varepsilon$  is an error.

## RESULTS AND DISCUSSION

### Data Analysis Results

The number of poverty in Indonesia is still large, although it has decreased in recent years. The following Table 1 shows the number of poverty in Indonesia.

Poverty in Indonesia is experiencing a decreasing trend even though the number is still relatively large. Most of the poverty in Indonesia is in rural areas and relies on the agricultural sector as its main source of income. Until now, the agricultural sector is still dependent on climate conditions. The impact of climate change directly impacts agricultural sector production. The data obtained was analyzed using the EViews 12 application program. Table 2 shows the results of the data analysis carried out.

The results of the data analysis show that the adjusted R-squared value is 0.817691, which means that the independent variable of 81.76 percent can explain the dependent variable in the form of poverty. Data analyzed using multiple linear regression typically must have distributed residuals. To find out whether the residual normality of the data is normally distributed or not, the Jarque-Bera test (JB test) is performed. The analysis results show that the JB test value is 3.640249 (probably

Table 1: Poverty in Indonesia.

Year	Rural (%)	Urban (%)	Total (%)
2012	14.70	8.60	11.66
2013	14.42	8.52	11.47
2014	13.76	8.16	10.96
2015	14.09	8.22	11.13
2016	13.96	7.73	10.70
2017	13.47	7.26	10.12
2018	13.10	6.89	9.66
2019	12.60	6.56	9.22
2020	13.20	7.88	10.19
2021	12.53	7.60	9.71
2022	12.36	7.53	9.57

Source: BPS (2023)

Table 2: Data Analysis Results.

Variable	Coefficient	Std. Error	t-Statistic	Prob.
C	-6.604462	5.266950	-1.253944	0.2415
GRO	-0.025672	0.015257	-1.682686	0.1267
AGR	0.287896	0.073636	3.909708	0.0036
INF	0.102192	0.044928	2.274564	0.0490
GI	-3.389319	0.614185	-5.518400	0.0004
HDI	0.040900	1.076104	0.038007	0.9705
CCPI	1.299334	0.315867	4.113547	0.0026
R-squared	0.890615	Mean dependent var		2.439531
Adjusted R-squared	0.817691	S.D. dependent var		0.177745
S.E. of regression	0.075893	Akaike info criterion		-2.019355
Sum squared resid	0.051837	Schwarz criterion		-1.681347
Log-likelihood	23.15484	Hannan-Quinn criterion		-2.002046
F-statistic	12.21299	Durbin-Watson stat		2.110465
Prob(F-statistic)	0.000702			

Source: primary data analysis, 2023.

0.162006), which means that the residual data is normally distributed because the p-value is  $> 0.05$ . To test whether there is autocorrelation in the data used, the Breusch-Godfrey Serial Correlation LM test was performed. The test results show that the Breusch-Godfrey Serial Correlation LM test value is 0.5016 (probably Chi-square (2)  $0.2390 > 0.05$ ), which means there is no serial correlation problem. The multicollinearity in this research model is detected using the Variance Inflation Factors (VIF) value. The general values to indicate the limits of multicollinearity are  $VIF > 10$  and tolerance values  $< 0.10$  (Hamid & Anwar 2019). Based on

the results of multicollinearity analysis, it is known that the centered VIF value for all variables is  $< 10$ , so it can be determined that there is no multicollinearity problem in the model used. Next, the Breusch-Pagan-Godfrey test is used to determine heteroscedasticity. The results of the Breusch-Pagan-Godfrey test show that the probability value of Chi-square (6) in  $Obs * R\text{-square}$  is  $0.8130 > 0.05$ , which means that there is no problem with the assumption of non-heteroskedasticity. Based on the results of the F test analysis (overall test), it is known that the F-statistic value = 12.21299 (prob. = 0.000702). This shows that, overall, the independent variables in this study have a natural influence on poverty.

### Economic Growth

The economic growth analysis results show that the t-statistic value is -1.682686 (prob.=0.1267). This shows that economic growth does not have a significant direct effect on poverty reduction. The role of economic growth in poverty reduction has long been debated (Balasubramanian et al. 2023). This debate becomes important after the SDGs establish that reducing poverty in all its forms is the main goal, as well as promoting sustainable economic growth and providing decent work opportunities for all. Research by Seth & Alkire (2021) found a weak negative correlation between economic growth and the poverty index. Focusing on previous cross-country research (Alkire et al. 2017), there is no significant relationship between economic growth and changes in poverty in 27 sub-Saharan African countries. Meanwhile, studies by (Burchi et al. 2019) found a weak negative correlation between economic growth and poverty reduction in 51 low- and middle-income countries. In our research, we found that economic growth does not have a significant impact on changes in poverty. However, economic growth can reduce poverty through intermediate variables (Putro et al. 2017). Therefore, for economic growth to have a tangible impact on poverty reduction, economic development must be directed towards pro-poor activities, such as the provision of facilities and infrastructure needed by people experiencing poverty. Likewise, government spending is more focused on labor-intensive projects to reduce unemployment (Ebunoluwa & Yusuf 2018).

### Growth of the Agriculture Sector

The results of the analysis of the growth of the agriculture sector show that the agriculture sector has an impact on poverty. However, increasing growth in the agriculture sector has a positive impact on increasing poverty. Several research findings show that economic growth has a positive impact on poverty reduction (Ivanic & Martin 2018), although it is clear in which sector economic growth occurs. Poverty

is known to occur primarily in rural areas and is, therefore, very dependent on the agriculture sector. This is important, considering that the agriculture sector is a key factor in economic transformation and poverty reduction (Dorinet et al. 2021). However, as development progresses, there will be changes in the economic structure, reducing the role of agriculture and decreasing its productivity, making it less effective in poverty alleviation. The results of Fan & Cho (2021) say that smallholder agriculture growth in land-scarce countries has a significant impact on poverty alleviation. Furthermore, once agricultural productivity reaches a certain point, the availability of non-agricultural fields and migration from villages to cities will follow. In this phase, the role of the agriculture sector is significantly reduced. Likewise, the research by Urfels et al. (2023) found that the agriculture sector plays a minimal role in poverty reduction. Eichsteller et al. (2022) and Maqbool (2023) also noted that the role of the agriculture sector in poverty reduction in Kenya needs to be clarified as poor farmers find it very difficult to switch to more profitable agriculture strategies and climate change shocks exacerbate this condition. In this research, we found that the agriculture sector no longer plays a role in poverty reduction in Indonesia. This is because the agriculture sector in Indonesia is not the largest contributor to national income. The role of the agriculture sector in national income is third after the commercial and industrial sectors.

### **Inflation**

Inflation, poverty, and unemployment are the main problems for developing countries (Rehman et al. 2022). The problem of inflation, which increases prices, especially of food, affects household spending. The results of our analysis show that  $t$ -statistic = 2.274564 (prob.= 0.0490), which means that inflation has a significant impact on poverty. Inflation has a significant and positive impact on poverty, meaning that a 1% increase in inflation will cause an increase in poverty of 0.102%. The higher the inflation, the more poverty there will be. This happens because inflation causes people's purchasing power to decrease. The results of our research are supported by Ningsih & Andiny (2018) and (Mardiatillah et al. 2021), who concluded that inflation has a real impact on poverty. Meanwhile, research by Kiroğlu & Sezgin (2021) reports that food inflation may increase poverty in Turkey.

### **Inequality**

Poverty is closely linked to inequality. One measure of inequality is the Gini index. The results of the analysis show that  $t$ -statistic = -5.518400 (prob.= 0.0004), which means that inequality affects poverty. This means that poverty alleviation development has yet to be implemented in the

poorest communities. Many poor people cannot yet enjoy the results of the development carried out. These results are in line with the findings of (Etuk & Ayuk 2021) on agricultural commercialization projects in Nigeria, which concluded that although poverty alleviation projects have a positive impact on poverty reduction, those who are not poor have many benefits. It is necessary to pay attention to the poor people who are being targeted. Likewise, (Capuno 2022) said that poverty alleviation requires efforts to reduce inequality through redistribution of growth. Poverty alleviation strategies based on high growth apply only to high-income countries (Fosu 2017, Pasha 2022), while in low-income countries, poverty alleviation efforts should prioritize income distribution.

### **Human Development Index**

The Human Development Index measures the success of human quality development. The higher the human development index, the higher the qualifications of people. The human development index measurement is based on age, knowledge, and an adequate standard of living. The results of the analysis carried out show that the Human Development Index has no significant impact on poverty. Likewise, the research by (Nurlita et al. 2017) shows that the Human Development Index has neither a direct nor indirect impact on poverty reduction. The analysis results are also consistent with the results of (Alhudori 2017), which shows a positive relationship between the human development index and poverty. Increasing the Human Development Index does not guarantee that someone will survive poverty. Government support in the form of subsidies for education and health will increase the human development index. However, this does not automatically mean that the person concerned will escape poverty. Improved education and health, but not matched by higher skills and broader employment opportunities, will make it difficult for low-income families to leave the work they do (Kulyakwave et al. 2023). Increasing the number of workers with higher education while employment opportunities are limited will increase existing poverty. Therefore, it is important to improve the quality of education, not just the length of the training period, but must be accompanied by an increase in existing skills (Tubaka 2019). Increasing skills must also be accompanied by access to other resources so that poor people can use them. Increasing education for community groups will also improve their social status. Poor people with increasing social status will try to look for better jobs and leave their old jobs. However, the limited employment opportunities lead to a decrease in household income and, thus, an increase in the number of poor people.

## Climate Change

The results of the regression analysis show that the government's performance in dealing with climate change issues has a positive impact on poverty at a significant level of 0.05. The more attention the government devotes to addressing climate change, the more poverty will increase. The government's performance on climate change is related to the government's policies and spending. Government policy in dealing with climate change presents the government with a dilemma. The combination of government actions to address climate change and efforts to eradicate poverty places an increased financial burden on the government. Increasing spending on efforts to address climate change will cause spending on poverty alleviation efforts to decrease (Soergel et al. 2021). The result is increasing poverty (Bertram et al. 2018). Also found that there is a trade-off between the policies and costs of addressing climate change. Good climate protection measures require high costs, which increasingly burden people with low incomes.

To maximize government performance in addressing climate change, this can be done through the private sector. This is because several activities that the government cannot carry out can be carried out by the private sector in terms of dealing with climate change (Cao & Zheng 2016). Public awareness is needed to create a healthy living environment in addition to healthy living and consumption patterns. Awareness of healthy lifestyles needs to be raised in the community to facilitate government action to address environmental problems. For this reason, separate management is required to address poverty-related climate change. Of course, when dealing with climate change, changes in precipitation patterns, temperature, and existing humidity must also be considered. These changes affect agricultural production, health, and social problems in society.

Based on the results of the analysis and discussion, good adaptive management is required to deal with climate change. This is necessary so that government policy in dealing with climate change is consistent with poverty reduction policy (Abera & Tesema 2019). Information about the climate change taking place needs to be shared with the community so they can adapt. In the agricultural sector, adaptation to climate change occurs by adjusting planting plans. The information conveyed about climate change is, of course, locally specific (Chari & Ngcamu 2022). In addition, information about climate change is also needed so that society can regulate its activities. This is related to the emergence of several diseases in society due to climate change (Buizza et al. 2022). If the public can well understand information about climate change, they can adapt to the activities carried out.

## CONCLUSION

This research wants to examine the impact of socio-economics (economic growth, agricultural sector growth, inequality, inflation, human development index) and climate change on poverty. Based on the results of the analysis conducted, the government's performance in dealing with climate change has a positive impact on poverty. Agricultural sector growth and inflation also have a positive impact on poverty, while inequality has a negative impact on poverty. Other factors, namely economic growth and the human development index, have no significant impact on poverty.

To reduce the impact of socio-economic and climate change on poverty, the government can adopt policies by seeking economic growth that does not have a negative impact on the environment. Further research is needed to examine environmentally friendly economic growth.

## REFERENCES

- Abera, N. and Tesema, D., 2019. Perceptions and practices of climate change adaptation and mitigation strategies among farmers in the Konta Special District, Ethiopia. *Environmental and Socio-Economic Studies*, 7(4), pp.1–16. <https://doi.org/10.2478/environ-2019-0019>
- Adeleye, B.N., Gershon, O., Ogundipe, A., Owolabi, O., Ogunrinola, I. and Adediran, O., 2020. Comparative investigation of the growth-poverty-inequality trilemma in Sub-Saharan Africa and Latin American and Caribbean Countries. *Heliyon*, 6(12). <https://doi.org/10.1016/j.heliyon.2020.e05631>
- Alatinga, K.A. and Williams, J.J., 2019. Mixed Methods Research for Health Policy Development in Africa: The Case of Identifying Very Poor Households for Health Insurance Premium Exemptions in Ghana. *Journal of Mixed Methods Research*, 13(1), pp.69–84. <https://doi.org/10.1177/1558689816665056>
- Alhudori, M., 2017. The Influence of HDI, GRDP, and The Amount of Unemployment on The Poor Population in Jambi Province. *Ekonomis: Jurnal of Economics and Business*, 1(1), pp.113–124.
- Alkire, S., Jindra, C., Robles Aguilar, G. and Vaz, A., 2017. Multidimensional Poverty Reduction Among Countries in Sub-Saharan Africa. *Forum for Social Economics*, 46(2), pp.178–191. <https://doi.org/10.1080/07360932.2017.1310123>
- Alrakhman, D., Susetyo, D., Taufiq, and Azwardi, 2022. An Analysis On Inequality, Economic Growth, And Unemployment In Sumatera Island. *Quality - Access to Success*, 23(190), pp.302–314. <https://doi.org/10.47750/QAS/23.190.32>
- Amaluddin, A., Payapo, R.W., Laitupa, A.A. and Serang, M.R., 2018. A Modified Human Development Index and Poverty in the Villages of West Seram Regency, Maluku Province, Indonesia. *International Journal of Economics and Financial Issues*, 8(2), pp.325–330. Available at: <http://www.econjournals.com>
- Arham, M.A., Fadhli, A. and Dai, S.I., 2020. Does Agricultural Performance Contribute to Rural Poverty Reduction in Indonesia? *JEJAK*, 13(1), pp.69–83. <https://doi.org/10.15294/jejak.v13i1.20178>
- Nurlita, A.C., Haris Musa, A. and Budi Suharto, R., 2017. The Influence of Human Development Index (HDI) and Economic Growth on Unemployment and Poverty in Samarinda. *Jurnal Ilmu Ekonomi Mulawarman (JIEM)*, 2(1), p.16.
- Azzari, C. and Signorelli, S., 2020. Climate and poverty in Africa South of the Sahara. *World Development*, 125, p.691. <https://doi.org/10.1016/j.worlddev.2019.104691>

- Balasubramanian, P., Burchi, F. and Malerba, D., 2023. Does economic growth reduce multidimensional poverty? Evidence from low- and middle-income countries. *World Development*, 161, p.106119. <https://doi.org/10.1016/j.worlddev.2022.106119>
- Bertram, C., Luderer, G., Popp, A., Minx, J.C., Lamb, W.F., Stevanović, M., Humpenöder, F., Giannousakis, A. and Kriegler, E., 2018. Targeted policies can compensate for most of the increased sustainability risks in 1.5 °C mitigation scenarios. *Environmental Research Letters*, 13(6), p.1088. <https://doi.org/10.1088/1748-9326/aac3ec>
- BPS, 2023. *Profile of Poverty in Indonesia*. BPS
- Buizza, R., Carratore, R. Del, and Bongioanni, P., 2022. Evidence of climate change impact on Parkinson's disease. *Journal of Climate Change and Health*, 6. <https://doi.org/10.1016/j.joclim.2022.100130>
- Burchi, F., Malerba, D., Rippin, N. and Montenegro, C.E., 2019. Comparing Global Trends in Multidimensional and Income Poverty and Assessing Horizontal Inequalities. *Deutsche Gesellschaft für Internationale Zusammenarbeit GmbH*. <https://doi.org/10.23661/dp2.2019>
- Burnch, J., Uhlich, T., Bals, C., Höhne, N. and Nascimento, L., 2021. Climate Change Performance Index: Background and Methodology.
- Cao, S. and Zheng, H., 2016. Climate change adaptation to escape the poverty trap: role of the private sector. *Ecosystem Health and Sustainability*, 2(10). <https://doi.org/10.1002/ehs2.1244>
- Capuno, J.J., 2022. Growth with redistribution, finally: Regional poverty and inequality in the Philippines, 2000–2018. *Asia and the Global Economy*, 2(2), 100039. <https://doi.org/10.1016/j.aglobe.2022.100039>
- Chari, F. and Ngcamu, B.S., 2022. Climate change and its impact on urban agriculture in Sub-Saharan Africa: A literature review. *Environmental and Socio-Economic Studies*, 10(3), pp.22–32. <https://doi.org/10.2478/environ-2022-0014>
- Cheng, X., Chen, J., Jiang, S., Dai, Y., Shuai, C., Li, W., Liu, Y., Wang, C., Zhou, M., Zou, L., Zhang, P. and Kang, X., 2021. The impact of rural land consolidation on household poverty alleviation: The moderating effects of human capital endowment. *Land Use Policy*, 109. <https://doi.org/10.1016/j.landusepol.2021.105692>
- Dorinet, E., Jouvét, P.A. and Wolfersberger, J., 2021. Is the agricultural sector cursed too? Evidence from Sub-Saharan Africa. *World Development*, 140. <https://doi.org/10.1016/j.worlddev.2020.105250>
- Dorosh, P. and Thurlow, J., 2018. Beyond Agriculture Versus Non-Agriculture: Decomposing Sectoral Growth–Poverty Linkages in Five African Countries.
- Ebunoluwa, O.O. and Yusuf, W.A., 2018. Effects of Economic Growth on Poverty Reduction In Nigeria. *IOSR Journal of Economics and Finance*, 9(5), pp.25–29. <https://doi.org/10.9790/5933-0905012529>
- Eichsteller, M., Njagi, T. and Nyukuri, E., 2022. The role of agriculture in poverty escapes in Kenya – Developing a capabilities approach in the context of climate change. *World Development*, 149, p. 5705. <https://doi.org/10.1016/j.worlddev.2021.105705>
- Epule, T.E., Chehbouni, A., Dhiba, D., Moto, M.W. and Peng, C., 2021. African climate change policy performance index. *Environmental and Sustainability Indicators*, 12, p. 163. <https://doi.org/10.1016/j.indic.2021.100163>
- Erlando, A., Riyanto, F.D. and Masakazu, S., 2020. Financial inclusion, economic growth, and poverty alleviation: evidence from eastern Indonesia. *Heliyon*, 6(10). <https://doi.org/10.1016/j.heliyon.2020.e05235>
- Etuk, E.A. and Ayuk, J.O., 2021. Agricultural commercialisation, poverty reduction and pro-poor growth: evidence from commercial agricultural development project in Nigeria. *Heliyon*, 7(5). <https://doi.org/10.1016/j.heliyon.2021.e06818>
- Fan, S. and Cho, E.E.Y., 2021. Paths out of poverty: International experience. *Journal of Integrative Agriculture*, 20(4), pp.857–867. [https://doi.org/10.1016/S2095-3119\(20\)63295-6](https://doi.org/10.1016/S2095-3119(20)63295-6)
- Fankhauser, S. and Tol, R.S.J., 2005. On climate change and economic growth. *Resource and Energy Economics*, 27(1), pp.1–17. <https://doi.org/10.1016/j.reseneeco.2004.03.003>
- Fitriady, A., Silvia, V. and Suriani, S., 2022. Does Economic Growth Mediate Investment, Inflation, and Human Development Investment on Poverty in Indonesia? *Signifikan: Jurnal Ilmu Ekonomi*, 11(2), pp.437–456. <https://doi.org/10.15408/sjie.v11i2.26145>
- Fosu, A.K., 2017. Growth, inequality, and poverty reduction in developing countries: Recent global evidence. *Research in Economics*, 71(2), pp.306–336. <https://doi.org/10.1016/j.rie.2016.05.005>
- Gross, J., Woodley, S., Welling, L.A. and Watson, J.E.M., 2016. Adapting to climate change: Guidance for protected area managers and planners. *World Development*, 109, pp.440–451. <https://doi.org/10.1016/j.worlddev.2016.08.014>
- Hamid, R.S. and Anwar, S.M., 2019. *Variation-Based Structural Equation Modeling (SEM): Basic Concepts and Application with SmartPLS 3.2.8 Program in Business Research*. PT Inkubator Penulis Indonesia.
- Haughton, J. and Khandker, S.R., 2009. *Handbook on Poverty and Inequality*. Springer
- Huang, W., Ding, S., Song, X., Gao, S. and Liu, Y., 2023. A study on the long-term effects and mechanisms of internet information behavior on poverty alleviation among smallholder farmers: Evidence from China. *Heliyon*, 9(9). <https://doi.org/10.1016/j.heliyon.2023.e19174>
- Isiwu, G.D., Azike, L.C. and Ngwu, J.C., 2021. Poverty and economic growth nexus in Nigeria. *Journal of Social Science*, 6(2), pp.136–153.
- Ivanic, M. and Martin, W., 2018. Sectoral Productivity Growth and Poverty Reduction: National and Global Impacts. *World Development*, 109, pp.429–439. <https://doi.org/10.1016/j.worlddev.2017.07.004>
- Kadanal, E. and Yalcinkaya, O., 2020. Effects of climate change on economic growth: Evidence from 20 biggest economies of the world. *Romanian Journal of Economic Forecasting*, 23(3), pp.93–118.
- Kiroğlu, B.S. and Sezgin, Ş., 2021. The Impact of Food Inflation on Poverty in Turkey. *Journal of Economics, Business and Political Studies*, 8(2), pp.256–273. <https://doi.org/10.48064/equinnox.995580>
- Kulyakwave, P.D., Shiwei, X. and Wen, Y., 2023. Climate and Socio-economic Factors Affecting the Adoption of Irrigation Practices for Improved Rice Yield in Mbeya Region, Tanzania. *Journal of Environmental Science and Management*, 26(1), pp.1–11.
- Lin, Y., Zhang, T., Liu, X., Yu, J., Li, J. and Gao, K., 2022. Dynamic monitoring and modeling of the growth-poverty-inequality trilemma in the Nile River Basin with consistent night-time data (2000–2020). *International Journal of Applied Earth Observation and Geoinformation*, 112. <https://doi.org/10.1016/j.jag.2022.102903>
- Maqbool, N., 2023. Impact of Climate Change on Water in Pakistan. *The Pakistan Development Review*, 62(4), pp.605–616.
- Mardiattillah, R., Panorama, M. and Maftukhatusolikah, M., 2021. The Effect of Unemployment and Inflation on Poverty in South Sumatra 2015–2019. *Jurnal Intelektualita: Keislaman, Sosial Dan Sains*, 10(2), pp.365–370. <https://doi.org/10.19109/intelektualita.v10i2.8825>
- Miller, D.C., Cheek, J.Z., Mansourian, S. and Wildburger, C., 2022. Forest, trees and the eradication of poverty. *Forest Policy and Economics*, 140, p.1541.
- Ningsih, D. and Andiny, P., 2018. Analysis of the effect of inflation and economic growth on poverty in Indonesia. *Jurnal Samudra Ekonomika*, 2(1), pp.53–61.
- Onumah, J.A., Osei, R.D., Martey, E. and Asante, F.A., 2023. Welfare dynamics of innovations among agricultural households in Ghana: Implication for poverty reduction. *Heliyon*, 9(7). <https://doi.org/10.1016/j.heliyon.2023.e18066>
- Pasha, H.A., 2022. A new measure of inequality in Asian economies. *The Pakistan Development Review*, 61(4), pp.659–662.
- Pauw, K., Thurlow, J., Uaiene, R. and Mazunda, J., 2012. Agricultural growth and poverty in Mozambique: Technical analysis in support of the comprehensive Africa agriculture development program (CAADP).
- Prawoto, N. and Basuki, A.T., 2022. Factors affecting poverty in Indonesia: A panel data approach. *Quality - Access to Success*, 23(186), pp.156–161. <https://doi.org/10.47750/QAS/23.186.20>

- Putro, P.B.W., Mintarti, S. and Wijaya, A., 2017. Analysis of determination of economic growth and poverty. *Inovasi*, 13(2), pp.121-126.
- Qin, L., Chen, C., Li, Y., Sun, Y. and Chen, H., 2021. The impact of the new rural cooperative medical scheme on the “health poverty alleviation” of rural households in China. *Journal of Integrative Agriculture*, 20(4), pp.1068-1079. [https://doi.org/10.1016/S2095-3119\(20\)63372-X](https://doi.org/10.1016/S2095-3119(20)63372-X).
- Rehman, A., Cismas, L.M. and Milin, I.A., 2022. “The three evils”: Inflation, poverty and unemployment’s shadow on economic progress—A novel exploration from the asymmetric technique. *Sustainability (Switzerland)*, 14(14), p.642. <https://doi.org/10.3390/su14148642>.
- Rosyadi, S., Haryanto, A., Kusuma, A.S. and Fitrah, E., 2019. The role of creative economy in promoting sustainable rural development. *Advances in Social Science, Education and Humanities Research*, 389, pp.111-115.
- Schleicher, J., Schaafsma, M. and Vira, B., 2018. Will the sustainable development goals address the links between poverty and the natural environment? *Current Opinion in Environmental Sustainability*, 34, pp.43-47. <https://doi.org/10.1016/j.cosust.2018.09.004>.
- Seth, S. and Alkire, S., 2021. Multidimensional poverty and inclusive growth in India: An analysis using growth elasticities and semi-elasticities. *Working Papers 137*, Oxford Poverty and Human Development Initiative (OPHI), University of Oxford.
- Shi, C., He, Y. and Li, H., 2023. How does ecological poverty alleviation contribute to improving residents’ sustainable livelihoods? — Evidence from Zhejiang Province, China. *Sustainable Production and Consumption*, 41, pp.418-430. <https://doi.org/10.1016/j.spc.2023.09.002>.
- Soergel, B., Krieglner, E., Bodirsky, B.L., Bauer, N., Leimbach, M. and Popp, A., 2021. Combining ambitious climate policies with efforts to eradicate poverty. *Nature Communications*, 12(1), p.315. <https://doi.org/10.1038/s41467-021-22315-9>.
- Susanto, J., 2014. Impact of economic growth, inflation and minimum wage on poverty in Java. *Media Ekonomi & Teknologi Informasi*, 41, pp.418-430.
- Tan, R.P., 2020. Social capital and vulnerability to extreme climate in a semi-urban fishing community in Laguna de Bay, Philippines. *Journal of Environmental Science and Management*, 23(2), pp.89-101.
- Tubaka, S., 2019. Analysis of poverty in eastern Indonesia. *Cita Ekonomika*, 13(1), pp.113-130. <http://winardi-andalas-putro-blogspot.com>.
- Urfels, A., Mausch, K., Harris, D., McDonald, A.J., Kishore, A., Balwinder-Singh, van Halsema, G., Struik, P.C., Craufurd, P., Foster, T., Singh, V. and Krupnik, T.J., 2023. Farm size limits agriculture’s poverty reduction potential in eastern India, even with irrigation-led intensification. *Agricultural Systems*, 207, p.618. <https://doi.org/10.1016/j.agsy.2023.103618>.
- Walujadi, D., Indupurnahayu, I. and Endri, E., 2022. Determinants of income inequality among provinces: Panel data evidence from Indonesia. *Quality - Access to Success*, 23(190), pp.243-250. <https://doi.org/10.47750/QAS/23.190.26>.
- World Bank, 2005. *Introduction to poverty analysis*. World Bank. Available at: <https://documents1.worldbank.org/curated/en/775871468331250546/pdf/902880WP0Box380okPovertyAnalysisEng.pdf>
- Zebua, W.N., Bakke, D. and Hadi, S., 2015. Analysis of the dominant factors that influence poverty in Riau Province. *Indonesian Journal of Agricultural Economics (IJAE)*, 6(2), pp.158-167.
- Zhou, Y., Li, Y., Li, W., Li, F. and Xin, Q., 2022. Ecological responses to climate change and human activities in the arid and semi-arid regions of Xinjiang in China. *Remote Sensing*, 14(16), pp. 911. <https://doi.org/10.3390/rs14163911>.

---

#### ORCID DETAILS OF THE AUTHORS

Watemin: <https://orcid.org/0000-0002-4866-3415>  
 Slamet Rosyadi: <https://orcid.org/0000-0002-1173-0426>  
 Lilis Siti Badriah: <https://orcid.org/0000-0002-3376-0079>





# The Influence of Gibberellins and Smoke Water as a Stimulant for Germination and Vegetative Growth of *Syzygium aromaticum* (L.) Merr. & L. M. Perry

W. Muslihatin<sup>†</sup>, R. P. D. Wahyudi<sup>id</sup>, M. Iqbal<sup>id</sup>, T. B. Saputro<sup>id</sup> and T. Nurhidayati

Department of Biology, Faculty of Science and Data Analytics, Sepuluh Nopember Institute of Technology, Indonesia

<sup>†</sup>Corresponding author: Wirdhatul Muslihatin; [wirdhatul.muslihatin@its.ac.id](mailto:wirdhatul.muslihatin@its.ac.id)

Nat. Env. & Poll. Tech.  
Website: [www.neptjournal.com](http://www.neptjournal.com)

Received: 03-04-2024

Revised: 20-05-2024

Accepted: 29-05-2024

## Key Words:

Clove

Germination

Gibberellins

Smoke water

## ABSTRACT

Clove or cengkeh (*Syzygium aromaticum*) is one of Indonesia's commodities with high domestic and international potential, considering that this plant is used as raw material for the cigarette industry. Therefore, it is necessary to optimize the production of Indonesian cloves, one of which is by using growth stimulators such as plant growth regulators (PGR). This study uses gibberellic acid (GA<sub>3</sub>) and smoke water as exogenous growth triggers. The treatment given was soaking *S. aromaticum* seeds in gibberellic acid (GA<sub>3</sub>) and liquid smoke for 24 h. The GA<sub>3</sub> concentrations used were 100 ppm, 75 ppm, 50 ppm, and 25 ppm. Smoke water was obtained from the pyrolysis of coconut shells, and the concentrations used were 0.5%, 1%, 2%, and 3%. Observations were conducted for 11 weeks and divided into two phases, namely the germination phase and the vegetative growth phase. Parameters measured included germination percentage, radicle, and plumula length in the first phase, root length, plant height, and number and area of leaves in the second phase. The best results were achieved with the soaking treatment using 0.5% smoke water, which showed a significant increase in all observed growth parameters. This is due to the content of karrikin in smoke water, which acts like a growth hormone and triggers the performance of other growth hormones. In addition, karrikin plays an active role in the germination process by changing the morphology of the seeds.

## INTRODUCTION

*Syzygium aromaticum*, known as cloves or cengkeh, is a Dried Flower Bud that belongs to the family Myrtaceae and is native to the Maluku islands, Indonesia, and has spread and been cultivated around the world. The main part of the clove plant that is commercially valuable is its flowers, which are mostly used in the cigarette and food industry as spices or preservatives (Alfian et al. 2019, Batiha et al. 2020). In Indonesia, cloves are one of the superior commodities for plantations with high economic improvement potential (Zenti et al. 2021).

Based on data from the Ministry of Agriculture in 2020, Indonesia is the largest clove-producing country in the world. However, this does not make Indonesia the largest clove-exporting country in the world. Indonesia occupies the second position in clove exports after Madagascar, with an average export volume of 122.48 thousand tons (14.27%) (Zenti et al. 2021). This is because Indonesia uses most of its production to supply domestic industrial demand from the cigarette industry, which absorbs 85% of Indonesia's clove production (Hasibuan et al. 2022).

The increasing demand for cloves makes it necessary to optimize Indonesian clove production such as rehabilitation of non-producing or damaged plants and the introduction of technology that supports the plantation management process from pre-harvest to post-harvest. One of them is developing agricultural practices using growth stimulators such as plant growth regulators (PGRs) that can increase production. The use of PGRs can reduce the planting period and increase productivity in a shorter time (Matos et al. 2020).

Gibberellin (GA) is a phytohormone that regulates various aspects of plant growth and development through complex biosynthetic pathways. Specific roles of GA include seed germination, stem elongation, flower initiation, fruit, and seed development. Previous studies have shown that exogenous gibberellic acid (GA<sub>3</sub>) increases the percentage of seed germination and subsequent seedling growth in different crops (Hasibuan et al. 2022). The study of Winarso et al. (2021) found that soaking oil palm seeds in gibberellic acid solution affects the rate of seed germination, percentage of seed germination, seed height, root length, wet weight, and dry weight of sprouts. In addition to using exogenous phytohormones, increasing productivity can also be done

through innovative cultivation techniques, such as giving smoke water solutions to plants. Smoke water is produced from the pyrolysis and condensation of smoke from the burning process of coconut shells. The compounds contained in smoke water are karrikin, acetic acid, and methanol, which function to accelerate plant growth and production (Murniati et al. 2020). Smoke water as a growth stimulant has been used on many species, including rice, pepper, celery, and lettuce seeds (Gama et al. 2021, Gupta et al. 2020, Zhou et al. 2014). Research Amiroh et al. (2022) state that the concentration of 2% smoke water provides significant interactions on all parameters of rice plant growth and yield.

So far, research related to the effect of gibberellin and smoke water on the growth and development of clove vegetation is limited. This study aims to study the effect of gibberellin and smoke water on the growth and development of clove to improve clove production and quality.

## MATERIALS AND METHODS

### Plant Material

The clove seeds used were the Zanzibar variety obtained from a private field in Wonosalam, Jombang, East Java, Indonesia. The seeds were selected from clove fruits with physiologically ripe criteria (purple-black), at least 2.5 cm long, 1-2 cm in diameter, free of pests and diseases, and no black marks (Noya et al. 2018, Setiawan & Rosman 2015). The skin of the clove fruit is carefully peeled off so as not to injure the seeds. The seeds are washed to remove mucus until clean. Then, the seeds are stored for 6 days before treatment.

### Growth Stimulator Treatment

The treatments were soaking *S. aromaticum* seeds in gibberellic acid (GA<sub>3</sub>) and liquid smoke for 24 h. The concentrations of GA<sub>3</sub> used were 100 ppm, 75 ppm, 50 ppm, and 25 ppm, while liquid smoke was 0.5%, 1%, 2%, and 3%. As a control, the seeds were soaked in distilled water at the same time.

### Growing Media and Growth Parameters

Seeds that had been soaked in the growth stimulator were planted on cocopeat media to observe the germination phase for 4 weeks. In this phase, radicle length, plumula length, germination time, and germination percentage were measured with the following formula (Shah et al. 2021):

Germination rate (%) = (Number of normal sprouts/ Total number of sprouts) x 100%

In the second phase, seedlings of each treatment were taken and transplanted to a mixed medium of soil and organic fertilizer with a ratio of 2:1, and regular watering was done

in the morning. At the end of the phase, plant height, root length, number of leaves, and total leaf area were measured.

### Data Analysis

This study used an experimental method of complete randomized design with 9 treatments, namely control, gibberellin 25 ppm (G1), 50 ppm (G2), 75 ppm (G3), 100 ppm (G4), liquid smoke 0.5% (A1), 1% (A2), 2% (A3) and 3% (A4). Each treatment had 5 replicates. The research data were analyzed using SPSS software with a one-way ANOVA test and continued with the Duncan Multiple Range Test (DMRT) test with a 5% test level.

## RESULTS AND DISCUSSION

### Germination Percentage

Seed germination or dormancy breaking is considered the initiation of the first phase of development in the life cycle of higher plants and is followed by the vegetative growth of seedlings. Seed germination begins with water absorption or imbibition and finishes with the appearance of radicles from the cotyledons (Wolny et al. 2018). This process can be accelerated by reducing skin thickness, immersion in water, or immersion in a growth stimulator solution (Wahyuni et al. 2021). In this study, exogenous growth stimulators used in soaking clove seeds were phytohormones, gibberellic acid (GA<sub>3</sub>), and smoke water. The results showed differences in sprout morphology in each treatment that can be seen in Fig. 1. Normal sprouts of clove seeds in this study were determined based on the completeness of the essential structure of sprouts, namely roots, cotyledons, hypocots, epicots, and plumulae. The length of the sprout from the base of the root is at least 4 times the length of the seed. From all of the treatments, GA<sub>3</sub> 50 ppm and 75 ppm treatments and Smoked Water of 0.5%, 1%, and 2% showed the maximum germination percentage (Table 1). This is according to research by Abou El-Nour (2021), that low concentration of smoke water leads to an increase in the percentage and germination rate of seeds of pepper, celery, and lettuce.

The potential effect of smoke water in chemically breaking germination by the chemical interaction of smoke compounds with inhibitors in the seed coat, endosperm, or embryo, thereby enhancing seed germination. According to another study, the enhancing effect of smoke water may be related to changes in the synthesis/metabolism of endogenous hormones as a result of seed treatment with smoke. In addition, morphological factors where smoke particles can adhere, persist, and adsorb on the surface of plants and soil particles thus play an active role in the germination process by changing seed morphology and causing strong chemical

scarification on the seed surface, especially on seeds that have a hard shell. There is also the biological factor of the presence of a major active compound that has been identified as a butenolide recently named karrikin (KAR1); this compound is now recognized as initiating germination for many smoke-exposed and non-smoke-exposed species. KAR1 has effects similar to gibberellins and/or cytokinins, which can promote embryonic development and break seed dormancy in seeds so that seeds can germinate (Abou El-Nour 2021, Ghebrehiwot et al. 2008).

This study also shows a decrease in the percentage of germination of cloves with soaking  $GA_3$  and smoke water with increasing concentration. Mulik et al. (2021) explained that increased concentrations could cause toxicity in plants because of the phenolic content that can suppress the growth of radicles and increase free radical compounds in plants if given in high concentrations.

### Time of Germination

In this study, each treatment caused a difference in the germination time, as shown in Table 1. Time of germination is the length of time required for one seed to germinate (Al-

Ansari & Ksiksi 2016). Overall, soaking seeds with  $GA_3$  and smoke water had no significant effect ( $P>0.05$ ). The treatment with the fastest germination time is found in 0.5% smoke water treatment, 6 days, while the longest germination time is found in 3% smoke water treatment, 20 days. This is caused by acetic acid, methanol, and phenol compounds in smoke water, which help break down seed dormancy and stimulate embryonic growth (Gupta et al. 2020, Murniati et al. 2020, Sreekissoon et al. 2021, Wolny et al. 2018).

### Radicle and Plumula Length

Sprouts from seed soaking treatment in  $GA_3$  solution and smoke water for 24 hours can be seen in Fig. 2. Each treatment produces different radicles and plumules lengths (Table 1). Overall, both growth stimulators had a significant influence on radicle and lead length ( $p<0.05$ ). Compared to controls, 0.5% smoke water produced the highest radicle and plumula length. The results showed that the effect of smoke water on radicle length was very significant ( $p<0.05$ ). This is in line with research by Bhardwaj (2012), where low concentrations of smoked water (0.1% and 0.2%, V/V) applied to papaya seeds stimulate endosperm stretching, causing the seed coat

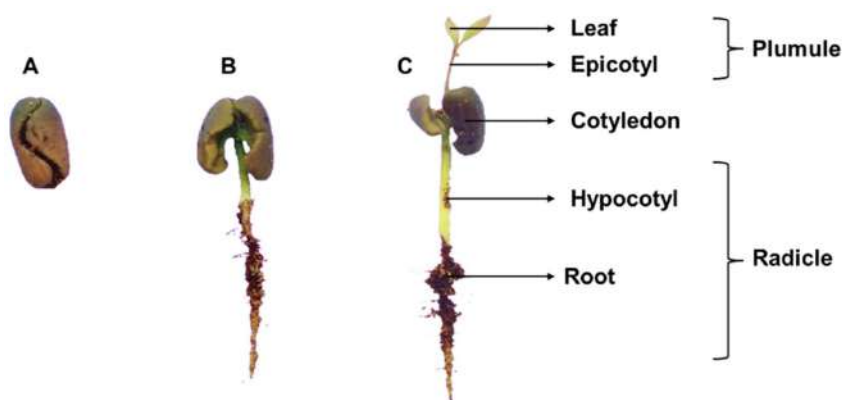


Fig. 1: Sprout type and morphology induced by soaking treatment of clove seeds in  $GA_3$  and smoke water solution. (A) non-germinated seeds, (B) abnormal sprouts, (C) normal sprouts.

Table 1: The effect of soaking seeds in  $GA_3$  solution and smoke water in the germination phase of cloves.

Treatment	Long Radicles [cm]	Plumule Length [cm]	Time of germination [day]	Rate of Germination [%]
Control	2.23 <sup>b</sup>	0.20 <sup>b</sup>	10.00 <sup>a</sup>	33%
$GA_3$ 25ppm	4.70 <sup>ab</sup>	0.85 <sup>ab</sup>	9.33 <sup>a</sup>	67%
$GA_3$ 50ppm	5.30 <sup>ab</sup>	0.60 <sup>ab</sup>	7.33 <sup>a</sup>	100%
$GA_3$ 75ppm	3.97 <sup>ab</sup>	0.33 <sup>ab</sup>	11.33 <sup>a</sup>	100%
$GA_3$ 100ppm	4.27 <sup>ab</sup>	0.20 <sup>b</sup>	11.33 <sup>a</sup>	67%
Smoke water 0.5%	6.03 <sup>a</sup>	1.30 <sup>a</sup>	6.00 <sup>a</sup>	100%
Smoke water 1%	5.37 <sup>ab</sup>	0.47 <sup>ab</sup>	9.67 <sup>a</sup>	100%
Smoke water 2%	4.73 <sup>ab</sup>	0.07 <sup>ab</sup>	11.33 <sup>a</sup>	100%
Smoke water 3 %	4.13 <sup>ab</sup>	0.17 <sup>b</sup>	20.33 <sup>a</sup>	67%

Note: Numbers were followed by different letters showing a significant difference based on the DMRT test ( $\alpha=0.05$ ).

to break and allow the radicle to elongate and emerge. The pyrolytic compound karrikin found in smoke water interacts directly or indirectly with important phytohormones, namely gibberellic acid, and auxin, in plants to trigger germination. Smoke-derived signaling molecules, known as karrikins, are composed of carbon, hydrogen, and oxygen. These low-molecular-weight compounds exhibit a characteristic bicyclic structure featuring a pyran and a butenolide-containing lactone ring. The first identified karrikin, 3-methyl-2H-furo[2,3-c] pyran-2-one (KAR1), demonstrates the highest abundance and efficacy in stimulating seed germination. Karrikins are to interact, either directly or indirectly, with key phytohormones such as abscisic acid, gibberellic acid, auxins, and ethylene. Remarkably, karrikins can induce germination in some plant species at exceptionally low concentrations, exhibiting potency comparable to established plant hormones (Chiwocha et al. 2009, Garrido et al. 2023, Waters & Nelson, 2023, Zhou et al. 2014). Germination begins with gibberellins that diffuse into the aleurone layer and stimulate the cell to synthesize amylase, which then hydrolyzes starch in the endosperm, producing maltose

molecules that are converted into glucose and transported to the embryo as the energy needed to grow and give rise to radicles (Lee et al. 2022). In addition, gibberellic acid and auxins also enhance the process of cell division and elongation, resulting in large seedlings compared to controls (AL-Hade & Alselawy 2019).

### Plant Height and Root Length

After germination, the plant will enter the vegetative growth phase, marked by the bud formation and the expansion of leaves, for initiating photosynthesis. Additionally, the roots and stems of the plant also grow and develop over time over time (Wei et al. 2023). The vegetative growth phase of the clove plant (*Syzygium aromaticum*) after 11 weeks is shown in Fig. 3.

In this study, data on root length and plant height taken at the end of the study were presented in Table 2. Overall, soaking seeds in GA<sub>3</sub> solution and smoke water had no significant effect on root length and clove plant height ( $P > 0.05$ ). However, soaking seeds in 25 ppm gibberellic acid

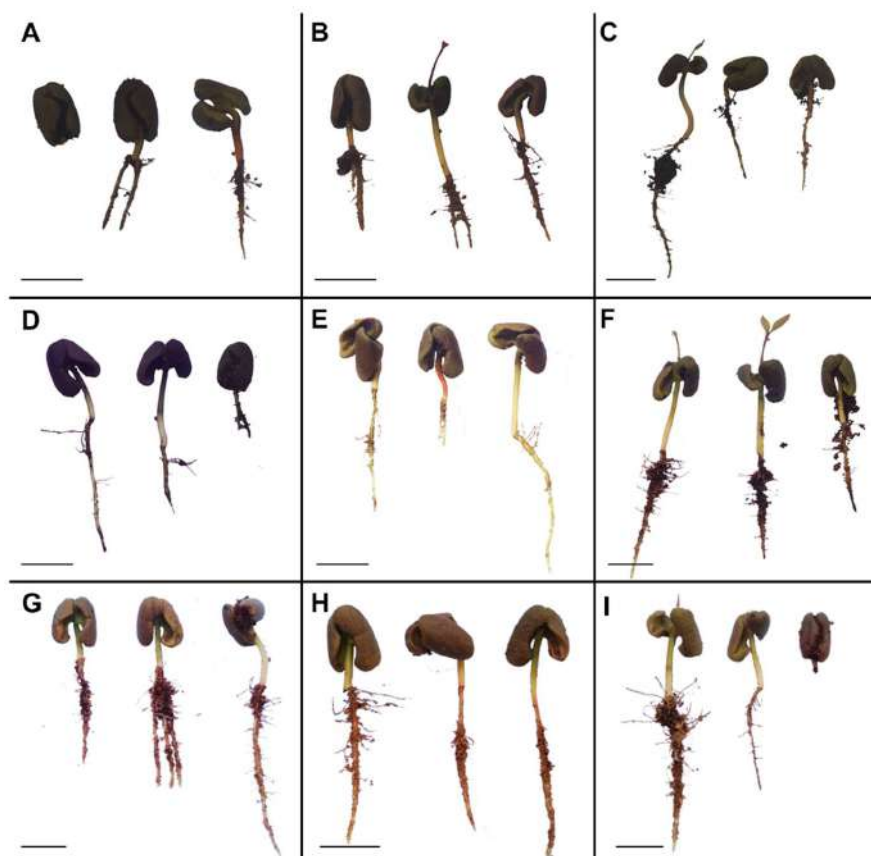


Fig. 2: Germination phase of cloves (*Syzygium aromaticum*) after soaking treatment of GA<sub>3</sub> and smoke water. Scale bar 2cm. (A) Control, (B) GA<sub>3</sub> 25ppm, (C) GA<sub>3</sub> 50ppm, (D) GA<sub>3</sub> 75ppm, (E) GA<sub>3</sub> 100ppm, (F) Smoke water 0.5% (G) Smoke water 1% (H) Smoke water 2% (I) Smoke water 3%.

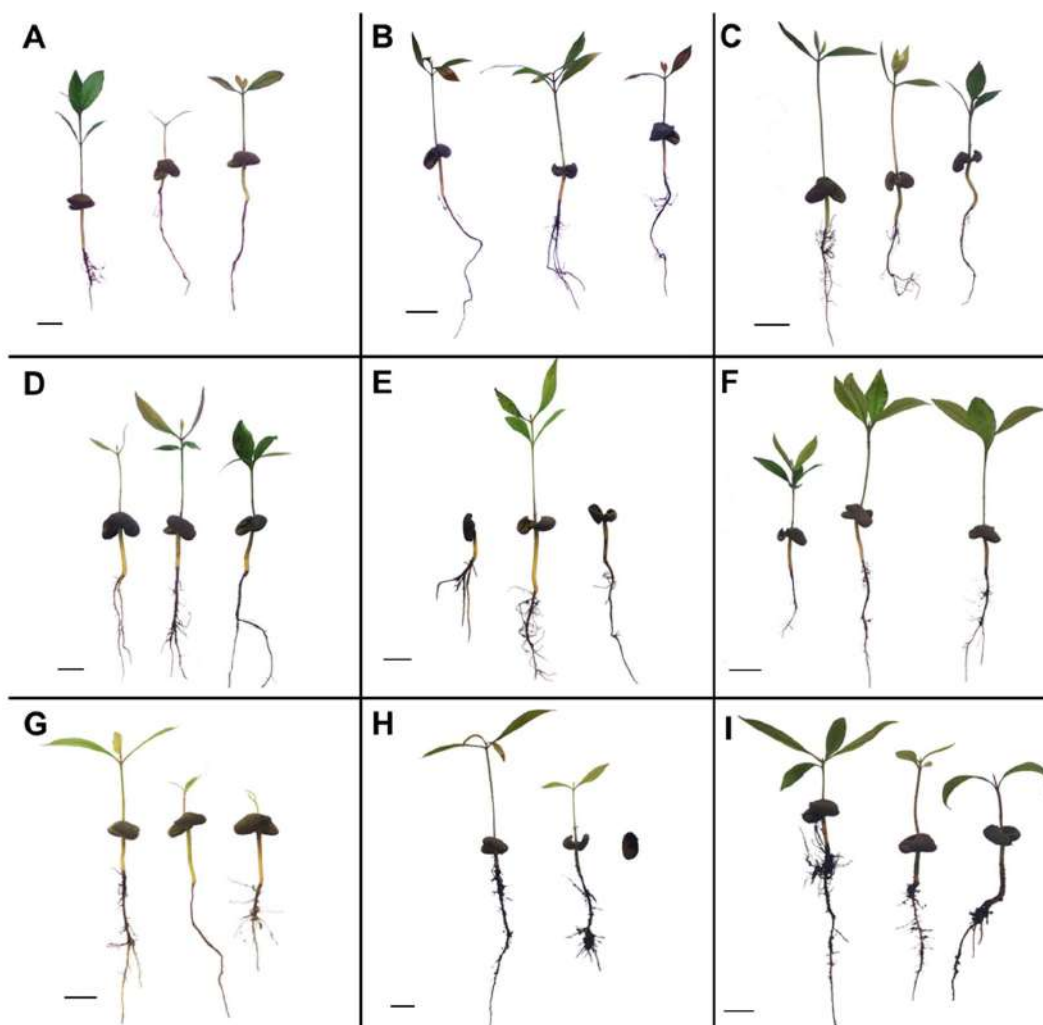


Fig. 3: Clove plant (*Syzygium aromaticum*) after soaking treatment of GA<sub>3</sub> and smoke water. Scale bar 2cm. (A) Control, (B) GA<sub>3</sub> 25ppm, (C) GA<sub>3</sub> 50ppm, (D) GA<sub>3</sub> 75ppm, (E) GA<sub>3</sub> 100ppm, (F) Smoke water 0.5% (G) Smoke water 1% (H) Smoke water 2% (I) Smoke water 3%.

had the greatest effect among other treatments and resulted in the greatest root length and plant height. Followed by Smoke water 3% for root length and gibberellic acid 50 ppm for plant height. Shtin et al. (2022) stated that gibberellin, or gibberellic acid, has an important role in the elongation of roots and stems. Gibberellin, together with auxins concentrated in the root elongation zone, will act as positive regulators of cell division. GA<sub>3</sub> also increases the activity of enzymes such as hydrolase enzymes that function to break down cell walls so that cells can develop and lengthen. Smoke water plays a role in cell elongation in the presence of karrikin, which triggers auxin synthesis and encourages cell elongation (Chumpookam et al. 2012). Some studies report statistically significant increases in both plant height and root length following Coconut shell smoke water application. Karrikin in smoke water might influence

the balance of key plant hormones like auxins, gibberellins, and cytokinins. These hormones play a crucial role in cell division, elongation, and root development. However, the specific hormonal interactions and their impact on height and root length remain unclear (Gama et al. 2021, Mulyawanti et al. 2019).

#### Number and Area of Leaves

Data related to the number and average leaf area of each treatment can be seen in Table 2. Overall, seed soaking treatment in GA<sub>3</sub> solution and smoke water had a significant effect on leaf count and leaf area ( $P < 0.005$ ). 0.5% smoke water treatment resulted in the highest number and area of leaves compared to the entire treatment. While the treatment with the lowest number of leaves and leaf area is GA<sub>3</sub>100ppm. This is in line with Chumpookam et al. (2012), where low

Table 2: Effect of soaking seeds in GA<sub>3</sub> solution and smoke water on the vegetative phase of clove plants.

Treatment	Root Length [cm]	Plant Height [cm]	Number of leaves	Leaf Area [cm <sup>2</sup> ]
Control	6.50 <sup>a</sup>	4.03 <sup>a</sup>	3.33 <sup>ab</sup>	144.33 <sup>ab</sup>
GA <sub>3</sub> 25ppm	12.97 <sup>a</sup>	5.67 <sup>a</sup>	5.33 <sup>ab</sup>	197.67 <sup>ab</sup>
GA <sub>3</sub> 50ppm	9.50 <sup>a</sup>	5.57 <sup>a</sup>	6.00 <sup>a</sup>	138.67 <sup>ab</sup>
GA <sub>3</sub> 75ppm	9.60 <sup>a</sup>	4.43 <sup>a</sup>	5.33 <sup>ab</sup>	134.67 <sup>ab</sup>
GA <sub>3</sub> 100ppm	5.37 <sup>a</sup>	2.03 <sup>a</sup>	2.00 <sup>b</sup>	43.67 <sup>b</sup>
Smoke water 0.5%	9.93 <sup>a</sup>	5.33 <sup>a</sup>	6.33 <sup>a</sup>	275.33 <sup>a</sup>
Smoke water 1%	10.20 <sup>a</sup>	2.83 <sup>a</sup>	3.00 <sup>ab</sup>	125.00 <sup>ab</sup>
Smoke water 2%	7.80 <sup>a</sup>	3.63 <sup>a</sup>	2.67 <sup>ab</sup>	148.67 <sup>ab</sup>
Smoke water 3 %	10.33 <sup>a</sup>	3.23 <sup>a</sup>	3.33 <sup>ab</sup>	212.33 <sup>ab</sup>

Note: Numbers were followed by different letters showing a significant difference based on the DMRT test ( $\alpha=0.05$ ).

concentrations help in the process of leaf formation in papaya seedlings by increasing the performance of IAA synthesis in the apical meristem of shoots containing leaf primordia can spur leaf formation. While gibberellins trigger leaf growth by stimulating cell division and elongation. An increase in the number of leaves also increases the amount of chlorophyll and photosynthesis so that more energy is obtained by the plant by maximizing its development. Leaf dilation is also triggered by plant hormones such as auxin (IAA) that stimulate leaf dilation by stimulating cell growth on the developing side of the leaf. Cytokinins can also stimulate cell division in growing leaves, which supports leaf dilation. The synthesis of these two hormones can be increased by the presence of Karrikin in smoke water (Chumpookam et al. 2012, Mulik et al. 2021, Ren et al. 2019).

## CONCLUSION

Based on the research conducted, soaking clove seeds in GA<sub>3</sub> solution and smoke water affects various aspects of early plant growth, especially germination percentage, radicle and plumula length, root length, plant height, and number and area of leaves. The best results were achieved by immersion treatment using 0.5% smoke water, which showed a significant improvement in all observed parameters. This is due to the karrikin content in smoke water, which can trigger the synthesis of growth hormones in plants. Despite this, it was found that an increase in the concentration of growth stimulators can reduce their effectiveness or even harm plant growth, as it increases phytotoxicity.

## REFERENCES

Abou El-Nour, H.H., 2021. Effects of smoke water on seed germination, seedling growth of some vegetables, and green yield productivity of *Phaseolus vulgaris*. *Al-Azhar Journal of Agricultural Research*, 46(1), pp.124-138. <https://doi.org/10.21608/ajar.2021.218211>

AL-Hade, M.Q.S. and Alselay, R.L.A., 2019. Effect of seed stimulation

and seed age of sorghum on the germination and traits of seedlings. *Plant Archives*, 19(2), pp.4477-4482.

- Alfian, A., Mahulette, A.S., Zainal, M., Hardin and Bahrin, A.H., 2019. The morphological character of raja clove (*Syzygium aromaticum* L. Merr & Perry.) native from Ambon Island. *IOP Conference Series: Earth and Environmental Science*, 343(1), p.12150. <https://doi.org/10.1088/1755-1315/343/1/012150>
- Amiroh, A., Prabowo, C., Istiqomah, I., Anam, C., Qibtiyah, M. and Kusumawati, D., 2022. Application of liquid smoke concentration to the growth and production of various rice varieties (*Oryza sativa* L.). *Paspalum: Jurnal Ilmiah Pertanian*, 10(1), p.86. <https://doi.org/10.35138/paspalum.v10i1.360>
- Batiha, G.E.S., Alkazmi, L.M., Wasef, L.G., Beshbishy, A.M., Nadwa, E.H. and Rashwan, E.K., 2020. *Syzygium aromaticum* L. (Myrtaceae): Traditional uses, bioactive chemical constituents, pharmacological and toxicological activities. *Biomolecules*, 10(2). <https://doi.org/10.3390/biom10020202>
- Bhardwaj, R.L., 2012. Effect of growing media on seed germination and seedling growth of papaya (*Carica papaya*) cv. 'Red Lady'. *Journal of Applied Horticulture*, 14(2), pp.118.
- Chiwocha, S.D.S., Dixon, K.W., Flematti, G.R., Ghisalberti, E.L., Merritt, D.J., Nelson, D.C., Riseborough, J.A.M., Smith, S.M. and Stevens, J.C., 2009. Karrikins: A new family of plant growth regulators in smoke. *Plant Science*, 177(4), pp.252-256. <https://doi.org/10.1016/j.plantsci.2009.06.007>
- Chumpookam, J., Lin, H.L. and Shiesh, C.-C., 2012. Effect of growing media on seed germination and seedling growth of papaya (*Carica papaya* cv. "Red Lady"). *Journal of Applied Horticulture*, 14(2), pp.118-123. <https://doi.org/10.24154/jhs.v8i1.332>
- Gama, Z.P., Purnama, R.M.A. and Melani, D., 2021. High potential of liquid smoke from coconut shell (*Cocos nucifera*) for biological control of rice bug (*Leptocoris oratorius* Fabricius). *Journal of Tropical Life Science*, 11(1), pp.85-91. <https://doi.org/10.11594/jtls.11.01.11>
- Garrido, R.M., Dayan, F.E. and Kolb, R.M., 2023. Herbicidal activity of smoke water. *Agronomy*, 13(4), pp.1-11. <https://doi.org/10.3390/agronomy13040975>
- Ghebrehiwot, H.M., Kulkarni, M.G., Kirkman, K.P. and Van Staden, J., 2008. Smoke water and a smoke-isolated butenolide improve germination and seedling vigor of *Eragrostis tef* (Zucc.) Trotter under high temperature and low osmotic potential. *Journal of Agronomy and Crop Science*, 194(4), pp.270-277. <https://doi.org/10.1111/j.1439-037X.2008.00321.x>
- Gupta, S., Hrdlička, J., Ngoroyemoto, N., Nemahunguni, N.K., Gucký, T., Novák, O., Kulkarni, M.G., Doležal, K. and Van Staden, J., 2020. Preparation and standardization of smoke water for seed germination

- and plant growth stimulation. *Journal of Plant Growth Regulation*, 39(1), pp.338-345. <https://doi.org/10.1007/s00344-019-09985-y>
- Hasibuan, A.I., Syaikat, Y. and Falatehan, A.F., 2022. Analysis of factors influencing Indonesian clove imports. *JRB-Jurnal Riset Bisnis*, 6(1), pp.144-160. <https://doi.org/10.35814/jrb.v6i1.4101>
- Lee, S.Y., Park, K., Jang, B.K., Ji, B., Lee, H., Baskin, C.C. and Cho, J.S., 2022. Exogenous gibberellin can effectively and rapidly break the intermediate physiological dormancy of *Amsonia elliptica* seeds. *Frontiers in Plant Science*, 13(October), pp.1-11. <https://doi.org/10.3389/fpls.2022.1043897>
- Matos, F.S., Freitas, I.A.S., Pereira, V.L.G. and Pires, W.K.L., 2020. Effect of gibberellin on growth and development of *Spondias tuberosa* seedlings. *Revista Caatinga*, 33(4), pp.1124-1130. <https://doi.org/10.1590/1983-21252020v33n427rc>
- Mulik, Y.M., Vertygo, S., Se'u, V.E. and Tang, B.Y., 2021. Germination capacity of *Indigofera zollingeriana* due to immersion using liquid smoke with different concentrations. *Journal of Tropical Animal Science and Technology*, 3(1), pp.36-44.
- Mulyawanti, I., Kailaku, S.I., Syah, A.N.A. and Risfaheri, 2019. Chemical identification of coconut shell liquid smoke. *IOP Conference Series: Earth and Environmental Science*, 309(1). <https://doi.org/10.1088/1755-1315/309/1/012020>
- Murniati, N., Sumini and Orlando, Y., 2020. Respon pertumbuhan dan produksi tanaman padi dengan pemberian konsentrasi dan asal bahan asap cair. *Jurnal Planta Simbiosis*, 2(1), pp.1-10.
- Noya, M., Riry, J. and Lesilolo, M., 2018. Pengaruh media dan periode simpan terhadap viabilitas benih cengkeh tuni (*Syzygium aromaticum* L.). *Jurnal Budidaya Pertanian*, 14(2), pp.97-104. <https://doi.org/10.30598/jbdp.2018.14.2.97>
- Ren, T., Weraduwege, S.M. and Sharkey, T.D., 2019. Prospects for enhancing leaf photosynthetic capacity by manipulating mesophyll cell morphology. *Journal of Experimental Botany*, 70(4), pp.1153-1165. <https://doi.org/10.1093/jxb/ery448>
- Setiawan, M. and Rosman, R., 2015. Status penelitian, penerapan teknologi dan strategi pengembangan tanaman cengkeh berbasis ekologi. *Perspektif*, 14(1), pp.27-36.
- Shah, S., Ullah, S., Ali, S., Khan, A., Ali, M. and Hassan, S., 2021. Using mathematical models to evaluate germination rate and seedlings length of chickpea seed (*Cicer arietinum* L.) to osmotic stress at cardinal temperatures. *PLoS ONE*, 16(12), pp.1-16. <https://doi.org/10.1371/journal.pone.0266990>
- Shtin, M., Dello Ioio, R. and Del Bianco, M., 2022. It's time for a change: The role of gibberellin in root meristem development. *Frontiers in Plant Science*, 13(5), pp.1-7. <https://doi.org/10.3389/fpls.2022.882517>
- Sreekissoon, A., Finnie, J.F. and Van Staden, J., 2021. Effects of smoke water on germination, seedling vigor, and growth of *Sceletium tortuosum*. *South African Journal of Botany*, 139, pp.427-431. <https://doi.org/10.1016/j.sajb.2021.01.025>
- Wahyuni, A.N., Saidah, Muchtar, Irmadamayanti, A., Syafruddin, A. and Padang, I.S., 2021. The effect of gibberellins soaking duration on germination frequency and growth of true shallot seed in the nursery. *IOP Conference Series: Earth and Environmental Science*, 762(1), pp.1-6. <https://doi.org/10.1088/1755-1315/762/1/012072>
- Waters, M.T. and Nelson, D.C., 2023. Karrikin perception and signaling. *New Phytologist*, 237(5), pp.1525-1541. <https://doi.org/10.1111/nph.18598>
- Wei, Y., Wang, S. and Yu, D., 2023. The role of light quality in regulating early seedling development. *Plants*, 12(14), pp.1-15. <https://doi.org/10.3390/plants12142746>
- Winarso, Y., Subardjo, B. and Sastrosayono, S., 2021. Shortening dormancy period of oil palm seeds (*Elaeis guineensis*) using sulfuric acid (H<sub>2</sub>SO<sub>4</sub>) and gibberellic acid (GA<sub>3</sub>) solutions. *Jurnal Lahan Suboptimal: Journal of Suboptimal Lands*, 10(2), pp.214-224. <https://doi.org/10.36706/jlso.10.2.2021.543>
- Wolny, E., Betekhtin, A., Rojek, M., Braszewska-Zalewska, A., Lusinska, J. and Hasterok, R., 2018. Germination and the early stages of seedling development in *Brachypodium distachyon*. *International Journal of Molecular Sciences*, 19(10), pp.2916. <https://doi.org/10.3390/ijms19102916>
- Zenti, A., Satriani, R. and Herry, A., 2021. Comparative advantage analysis of Indonesia's clove (*Syzygium aromaticum*) export in the international market. *Advances in Economics, Business and Management Research*, 199(Icsasard), pp.120-124.
- Zhou, J., Teixeira da Silva, J.A. and Ma, G., 2014. Effects of smoke water and karrikin on seed germination of 13 species growing in China. *Central European Journal of Biology*, 9(11), pp.1108-1116. <https://doi.org/10.2478/s11535-014-0338-6>

---

#### ORCID DETAILS OF THE AUTHORS

- W. Muslihatin: <https://orcid.org/0000-0001-7122-6785>  
 R. P. D. Wahyudi: <https://orcid.org/0009-0007-5635-1087>  
 M. Iqbal: <https://orcid.org/0009-0007-3043-8790>  
 T. B. Saputro: <https://orcid.org/0000-0002-8414-1438>







# Characterization of the Liquid Fuel Produced from Catalytic Depolymerization of Polymeric Waste Using Batch Reactor

O. L. Rominiyi<sup>1</sup>, M. A. Akintunde<sup>2</sup>, E. I Bello<sup>2</sup>, L. Lajide<sup>3</sup>, O. M. Ikumapayi<sup>4†</sup>, O. T. Laseinde<sup>4</sup>  
and B. A. Adaramola<sup>1</sup>

<sup>1</sup>Department of Mechanical and Mechatronics Engineering, Afe Babalola University Ado-Ekiti, (ABUAD), Nigeria

<sup>2</sup>Department of Mechanical Engineering, Federal University of Technology Akure (FUTA), Ondo State, Nigeria

<sup>3</sup>Department of Chemistry, Federal University of Technology, Akure (FUTA), Ondo State, Nigeria

<sup>4</sup>Department of Mechanical and Industrial Engineering Technology, University of Johannesburg, South Africa

†Corresponding author: O. M. Ikumapayi; ikumapayi.omolayo@gmail.com

Nat. Env. & Poll. Tech.  
Website: [www.neptjournal.com](http://www.neptjournal.com)

Received: 14-08-2023

Revised: 06-10-2023

Accepted: 12-10-2023

## Key Words:

Polymeric waste

Ultimate analysis

Catalyst depolymerization

Activated carbon

Calcium oxide

Liquid fuel characterization

## ABSTRACT

The high rate of generation of plastic waste in the country and the fact that all other means of Municipal Plastic Waste (MPW) management techniques had failed leading to the requirement of efficient and alternative disposal technique-depolymerization. The technique involves heating the polymeric waste at an elevated temperature in an inert environment to produce condensable, non-condensable, hydrocarbon and biochar. The plastic waste was collected at the Ilokun dumpsite in Ado-Ekiti, southwest Nigeria. Each component of the waste samples was depolymerized in a batch reactor without the use of a catalyst and with the addition of 10 g of activated carbon (AC) and calcium oxide (CaO) as catalysts. The liquid fuels which were produced between the temperature range of 219 and 232 were blended with standard fuel. Fuel samples with conventional diesel and depolymerized plastic diesel were characterized based on ASTM standards. The results of the proximate and ultimate analysis indicated that percentage moisture content ranges from 0.00-0.18%, volatile matter ranges between 96.66-99.75% and percentage ash content ranges from 0.13-3.03%. Fixed carbon ranges from 0.004-0.31% while the Gross Heating Value (GHV) ranges from 42.66-45.87 MJ/kg. The CHONS analyzer indicated the percentage of carbon, hydrogen, oxygen, nitrogen, and sulfur content range 81.64-85.51%, 12-31-18.04%, 0.00-1.51%, 0.00-0.73%, and 0.10- 0.97% respectively. The results of the physiochemical properties of the samples show that the density, API gravity, Kinematic viscosity and Flash point vary from 0.76-0.83 (g/cm<sup>3</sup>), 38.98-54.68, 17-2.80 (cm<sup>2</sup>/s) and 50.0-70.0 (°C) respectively while Cloud point, Pour point, Fire point and Cetane index range from -20-15.0 (°C), -23-7 (°C), 61.0-79.0 (°C) and 38.50-47.0. The pH values of the liquid fuel samples vary from 6.60-3.30. The overall results of the characterization indicated the fuel samples have proximity to the properties of the conventional diesel following the ASTM D975, ASTM D4737, ASTM D1298, ASTM D445, ASTM D2709, and ASTM D482 standards. The depolymerized polymeric waste is sustainable, with a low cost of production. Hence a good substitute as an alternative fuel and means of wealth creation from waste.

## INTRODUCTION

There is a gradual phasing out of ceramics and cans in the utilization cycle due to their nature and chemical composition. This has led to the replacement of polymeric materials and consequently the generation of municipal plastic waste in the metropolis. The rise in the usage of non-biodegradable plastic products has had negative repercussions, such as clogging drains, smothering some animals who mistakenly eat them, making ground surfaces impermeable to water, and posing a number of other risks. The challenge then becomes figuring out a secure way to transform these

plastic waste products into other beneficial and safe goods.

Plastic can be understood as polymeric, synthetic, or semi-synthetic materials that are made of big, organic molecules known as monomers. Polymers are the big molecules created during the polymerization process, according to Hazzan (2003). Polymers that are thermosetting and thermoplastic. Thermoplastics are a type of plastic that can be reshaped even after solidification since heat exposure does not cause chemical changes in its makeup. Thermosetting, on the other hand, refers to non-recycled polymers that, when heated, go

through an irreversible chemical transformation; they melt and adopt a shape only once before being immobile. It is impossible to overstate the importance of plastics in human life, which includes their use as furniture, toys, vehicle parts, household appliances, packaging materials, drinkable water and beverage containers, cooking utensils, and kitchenware (Abota 2012).

The reason plastic is used so frequently is because it is typically lightweight, affordable, and durable, which accounts for its favor over other materials (Hopewell et al. 2009). Every nook and cranny of the Nigerian terrain is littered with empty polythene plastic containers. Plastic is a non-biodegradable material that, when it gets into the soil, stops water from reaching the roots of plants and limits how far their roots may spread. Some of it prevents plants and animals from exchanging gases necessary for breathing (Rominiyi et al. 2017).

Unplanned garbage disposal by the side of the road, which creates an eyesore and hinders the free flow of run-off and cars, frequently leads to an accident during the busiest times of the day (Temitope et al. 2015). Some of the trash that is left on the streets makes its way into trenches, canals, and drains, where it clogs them and prevents water from flowing freely, which causes flooding. Municipal Plastic Wastes (MPW) have a severe influence on the environment, which is being exacerbated by the growing population and rising predilection for packaged goods (Kalilu 2013).

During the height of the rainy season, plastic waste is seen to accumulate on river banks after it has rained, seriously impeding the river's flow and ultimately causing the river bank to overflow (Kalilu 2013). As a result, a serious disaster occurs that results in the loss of many lives and extensive property damage. Recovering discarded or wasted plastics and processing them into useable items-sometimes products that are radically different from what they were in the first place is known as recycling plastic. Numerous academics have conducted various studies on the recycling of plastic garbage in the past. Trevor (2019), took into account the historical facets of plastics and the overdependence on polymeric materials for plastic waste. He emphasized the negative effects this material's use and disposal have on the ecosystem. A summary of the types and amounts of plastics in the trash stream is given by Vanessa (2007). Primary, secondary, tertiary, and quaternary recycling were the four categories of recycling outlined by Kalilu (2013). While a large portion of industrial wastes are not biodegradable, horticulture wastes are, and as a result, represent a hazard to health, drainage, and urban planning.

Temperature, reactor type, pressure, residence duration, fluidized bed type, and flow rate are a few variables that

affect how well plastic is pyrolyzed. Temperature is the most important of these variables because depolymerization involves the breaking or cracking of the chemical connection between the molecules. High temperatures facilitate the breakdown of chemical bonds (Sharaddin et al. 2018). Each type of plastic material has a different optimum temperature for pyrolysis. Low-Density Polyethylene (LDPE) ranges from 360 to 550 °C, while Polyethylene Terephthalate (PET) has an ideal temperature range of 350 to 520 °C. High-density polyethylene (HDPE) operates within a somewhat close range, operating between 378 and 539 °C (Anuar Sharaddin et al. 2016).

Due to the extremely slow rates of plastic waste decomposition, landfilling is not a viable alternative. The use of incinerators produces some air pollutants that have a negative impact on the environment. Therefore, techniques for recycling and recovering garbage have been utilized to lessen their negative effects on the environment and to lessen the harm that plastic waste causes. One of the most promising techniques for recovering used plastics is chemical recycling through the pyrolysis process, which involves the thermo-chemical breakdown of organic and synthetic materials at high temperatures without oxygen to produce fuels (Aguado et al. 2007) The procedure is typically carried out at temperatures ranging from 400°C to 800°C.

Aboulkas et al. (2010) looked into the behavior of polymers as they degraded thermally. For non-isothermal kinetic outcomes, the activation energy and the reaction model of the pyrolysis of polyethylene (PE) and polypropylene (PP) have been determined. The "contracting sphere" model can be used to explain the pyrolysis reactions of polyethylene, whereas the "contracting cylinder" model can be used to describe the reactions of polypropylene. The design of the cracking reactor has significant difficulties due to the high viscosity and limited thermal conductivity of plastics (Aboulkas et al. 2010).

PET boosted the production of new chlorinated hydrocarbons in liquid products and dramatically decreased the production of inorganic chlorine content when it was present in model mixed plastics and MPW. When MPW was converted, the contaminants were hazardous for acidic catalysts and caused easy catalyst deactivation (Wang & Wang 2011).

In 2009, Lee looked at upgrading pyrolytic oil made from municipal plastic waste (MPW) using FCC Fluid Cracking Catalyst. Due to greater cracking residue, the addition of FCC catalyst to the degrading process resulted in improved liquid and gas yields as well as a high fraction of heavy hydrocarbons in the oil output. Waste PE, PP, and PS have also been used to study non-catalytic pyrolysis. As

a result, waste PS created more liquid while waste PE and PP produced more gaseous products, according to the results (Demirbas 2004). While the gaseous product can be utilized as a heating source for the reactors or as a cooking gas stove application, the oil produced can be used in a pressured cooking stove. For co-firing with coal and biomass, which can be used as fuel for various purposes, the solid products will be utilized (Demirbas 2004).

Experimentally, HDPE, PP, and LDPE have calorific values that are all greater than 40 MJ/kg and are therefore regarded as having high energy usage. Due to the presence of an aromatic ring in its chemical structure, which has less combustion energy than an aliphatic hydrocarbon, PS typically has a lower calorific value than polyolefin plastic (PO) (Onwudili 2009). Due to the presence of benzoic acid in PET and chlorine compound in PVC, which reduced the fuel quality, these two materials had the lowest calorific values overall, falling below 30 MJ/kg. The low calorific value of PET was explained by the aromatic ring component of benzoic acid (Onwudili 2009). Both Cullis et al. (1981) and Panda et al. (2010) suggested a thorough investigation of the process of polymer heat degradation. The characterization and comparative analysis of conventional diesel and depolymerized plastic waste liquid fuel was done to suggest whether the latter can be used as an alternative to conventional diesel.

## MATERIALS AND METHODS

Materials used for this characterization including but not limited to the following: Raw HDPE liquid fuel sample; Activated carbon catalyzed HDPE liquid fuel sample; Calcium oxide catalyzed HDPE liquid fuel sample; Raw LDPE liquid fuel sample; Activated carbon catalyzed LDPE liquid fuel sample; Calcium oxide catalyzed LDPE liquid fuel sample; Raw HDPE/LDPE mixture 1:1; liquid fuel sample; HDPE/LDPE Activated carbon catalyzed mixture 1:1 liquid fuel sample; HDPE/LDPE Calcium oxide catalyzed mixture 1:1 liquid fuel sample; HDPE/ Conventional Diesel Blended 1:1 liquid fuel sample; HDPE/Conventional Diesel Blended 1:2 liquid fuel sample; HDPE/Conventional Diesel Blended 2:1 liquid fuel sample; LDPE/ Conventional Diesel Blended 1:1 liquid fuel sample; LDPE/ Conventional Diesel Blended 1:2 liquid fuel sample; LDPE/ Conventional Diesel Blended 2:1 liquid fuel sample; Conventional diesel; Kerosine; Petrol/ Gasoline; Silica crucible; Muffle furnace; Beaker; Two mouthed conical flask; Thermometer; Desicator; Bomb calorimeter; CHNS/O Elemental Analyzer; Pycnometer; Programmable Rheometer; Oakion ion-700 pH Meter.

The proximate analysis was conducted to ascertain the fuel sample's moisture content, volatile matter, ash content,

and calorific value. The mass of the silica crucible was determined by employing a digital weighing balance and denoted as W<sub>1</sub> (g). A mass of 1.00 g of the samples was introduced into the crucible. The contents contained within the silica crucible were quantified and documented as W<sub>2</sub> (g). The sample was thereafter subjected to thermal treatment within an oven, whereby it was exposed to a temperature of 105°C for one hour. The crucible is carefully removed from the experimental setup, allowed to cool in a desiccator to reach room temperature, and afterward weighed to determine its mass. The procedure of subjecting the sample to several cycles of heating, cooling, and weighing was iterated until a consistent mass of the anhydrous sample, denoted as W<sub>3</sub> (g), was achieved. Equation (1) was employed to ascertain the percentage moisture content of the specimen.

$$\% \text{ Moisture content} = \frac{W_2 - W_3}{W_2 - W_1} \times \frac{100}{1} \quad \dots(1)$$

The determination of the volatile matter content was conducted using the method of igniting the sample at a temperature of 950°C. The weight of the moisture-free sample in the silica crucible was measured using a digital weighing balance and recorded as W<sub>3</sub>(g). The provided sample was subjected to additional heating within a crucible that was equipped with a cover. This heating process took place in a muffle furnace, and the temperature was set to 950°C. The duration of this heating process was precisely 7 minutes, adhering to the guidelines outlined in ISO 1974/562. The sample was subjected to cooling within a desiccator and afterward measured using a digital weighing balance, yielding a weight of W<sub>4</sub> (g). The calculation of the volatile matter percentage in the sample was conducted using equation (2).

$$\% \text{ Volatile Matter} = \frac{W_3 - W_4}{W_3 - W_1} \times \frac{100}{1} \quad \dots(2)$$

Where:

W<sub>3</sub> – W<sub>4</sub> is the loss in weight of the moisture sample

W<sub>3</sub>– W<sub>1</sub> is the initial weight of the moisture-free sample

The crucible was measured using a computerized weighing balance and the recorded value was denoted as W<sub>1</sub>(g). A spatula was employed to transfer a mass of 1.00 g of the sample into the silica crucible. The weight was subsequently measured and documented as W<sub>6</sub>(g). The specimen contained within the exposed crucible was subsequently incinerated (in the presence of oxygen) at a temperature of 750 °C within a muffle furnace until a consistent mass was attained. The residual ash was quantified and documented as W<sub>7</sub> (g). Each of the combustible components of the fuel samples underwent three repetitions of the technique. The equation denoted as (3) was employed

to ascertain the proportion of ash content present in the given sample.

$$\% \text{ Ash content} = \frac{W_7 - W_1}{W_6 - W_1} \times \frac{100}{1} \quad \dots(3)$$

Where:

$W_7 - W_1$  is the weight of residual ash formed.

$W_6 - W_1$  is the weight of liquid fuel initially taken

The methods used in the determination of other parameters, such as ash content; calorific value; fixed carbon. Fixed carbon can be found in the work of Rominiyi (2017). The results are presented in Table 1.

The CHNS/O content in the sample was determined through the application of ultimate analysis utilizing a CHNS/O Elemental Analyzer. This analysis concurrently displays the weight percentages of carbon, hydrogen, oxygen, nitrogen, and sulfur in the sample, with the weight percentage of oxygen being obtained using a difference calculation.

The physical properties of liquid fuel, such as density, kinematic viscosity, specific gravity, pH value, pour point, flash point, cloud point, and cetane number of the prepared liquid fuel and the conventional diesel were analyzed with the standard equipment meant for that purpose and in accordance with ASTM standard and can be found in the work of Rominiyi (2017). The density was determined at 40. An empty density bottle (pycnometer) was weighed and recorded as  $W_1$ . Afterwards, the density bottle was filled with water and the weight was recorded as  $W_2$ . Furthermore, the bottle was emptied and properly cleaned the fuel sample was poured into the bottle and the weight was recorded as  $W_3$ . The density of the fuel was determined using equation (4). This was repeated for other samples, and their specific gravity and API gravity were calculated.

$$\text{Specific gravity } 60/60 \text{ } ^\circ\text{C} = \frac{W_o}{W_w} = \frac{W_3 - W_1}{W_2 - W_1} \quad \dots(4)$$

$$\text{Density of fuel at } 60 \text{ } ^\circ\text{C} = \text{Specific gravity} \times 1 \text{ g/cm}^3 \quad \dots(5)$$

The process of fractional distillation was quantified utilizing the ASTM D86 standard. The initial boiling point (IBP) refers to the temperature recorded by a thermometer when the first droplet of condensed vapor is observed emerging from the lower portion of the condenser tube. A lower initial boiling point (IBP) indicates the existence of lower hydrocarbon compounds within the sample. A continuous distillation method was employed to distill the pyrolyzed liquid fuel derived from polymeric waste into diesel-range fractions. The device has a notable degree of separation efficiency when it comes to the fractionation of gasoline and diesel cuts derived from pyrolysis hydrocarbon mixtures. The experimental setup comprises a 35 L round-bottomed flask made of stainless steel, which is affixed to

an aluminum support frame. The process of filling occurs through a 100 mm neck, which includes a viewing glass while draining is facilitated by a drain valve located at the bottom. The distillation column DN80, composed of borosilicate glass, is outfitted with a wire mesh packing to achieve a significant distillation rate accompanied by a notable separation efficiency. The fractions are systematically allocated to six individual receivers, each with a capacity of 20 liters, by an automated fraction collector. The software connected to the processor control unit DCD4001 regulates many distillation parameters, including temperature, vacuum, reflux ratio, and fraction collector.

The cetane index serves as a metric for assessing the igniting characteristics of diesel fuel within an internal combustion engine. This index can be derived by the analysis of density and distillation data. An alternative approach is the utilization of ASTM D976, in which the calculation of the cetane index (CI) is based on the outcome derived from the density measurement at a temperature of 15°C and the mid-boiling temperature of the specimen. ASTM D4737 might also be employed for its acquisition. The cetane index (CI) was determined using the “2” point method and density measurement in accordance with the ASTM-D976 specification at a temperature corresponding to 50% recovery. The cetane index (CI) was determined using equation (6) in accordance with the work of Joshua et al. (2009) and Dooley et al. (2012),

$$CI = 45.2 + 0.0892T_{10N} + (0.131 + 0.901B)T_{50N} + (0.0523 - 0.42B)T_{90N} + 0.00049(T_{10N}^2 - T_{90N}^2) + 107B + 60B^2 \quad \dots(6)$$

$$\text{where} \quad N_{10H} = N_{10} - 215 \quad \dots(7)$$

$$N_{50H} = N_{50} - 260 \quad \dots(8)$$

$$N_{90} = N_{90} - 310 \quad \dots(9)$$

$T_{10}$ ,  $T_{50}$ , and  $T_{90}$  are the distillation recovery temperatures at in degrees Celsius; at 10 %, 50%, and 90 % (WV) respectively.

$$B = \left( \text{Exp}^{-0.0035D_N} \right) - 1 \quad \dots(10)$$

$$D_H = D - 850 \quad \dots(11)$$

D is the density at 15

### Proximate and Ultimate Analysis

The proximate and ultimate analyses of different fuel samples and conventional diesel shown in Table 4.1 indicated that all the samples had negligible moisture content and varied between 0.00% and 0.18% with minimum for conventional diesel and maximum for HDPE/Diesel blended 2:1 sample. The percentage volatile matter (VM) of the samples tested

Table 1: Proximate, ultimate, and physical properties analysis of liquid fuel samples and conventional diesel.

Parameters	Standard (Conventional Diesel)	HDPE/ CaO	HDPE/ AC	HDPE (Raw)	LDPE/ CaO	LDPE/ AC	LDPE (Raw)	HDPE/Standard Diesel Blended		
								2:1	1:2	1:1
<b>Proximate Analysis (wt%)</b>										
Moisture Content (MC) (%)	0.00	0.12	0.11	0.08	0.14	0.14	0.14	0.18	0.14	0.16
Volatile matter (VM) (%)	96.66	99.73	99.75	99.61	99.70	99.68	99.63	96.68	98.15	97.94
Ash Content (AS) (%)	3.03	0.15	0.13	0.32	0.15	0.15	0.18	2.41	1.18	1.15
Fixed carbon (FC) (%)	0.31	0.01	0.01	0.004	0.04	0.03	0.05	0.09	0.02	0.01
Gross Heating Value GHV MJ kg <sup>-1</sup>	45.38	45.27	44.94	43.29	45.06	44.63	42.66	42.85	45.01	44.42
<b>Ultimate Analysis (wt%)</b>										
Carbon (%)	85.51,	82.25	82.49	81.64	84.37	84.62	84.62	82.81	82.82	82.61
Hydrogen (%)	12.34	17.44	17.2	18.05	15.45	15.16	15.16	13.97	13.44	14.29
Oxygen (%)	0.00	0.00	0.00	0.00	0.00	0.00	0.00	1.48	1.51	1.48
Nitrogen (%)	0.08	0.00	0.03	0.00	0.00	0.03	0.03	0.66	0.73	0.61
Sulfur (%)	0.40	0.3	0.31	0.3	0.18	0.15	0.15	0.10	0.14	0.97
<b>Physical Properties</b>										
Density (g/cm <sup>3</sup> )	0.83	0.78	0.76	0.79	0.79	0.78	0.81	0.77	0.76	0.77
API Gravity	38.98	49.91	54.68	47.61	47.61	40.91	43.91	52.27	54.68	52.27
Kinematic Viscosity (cm <sup>2</sup> /s)	2.54	2.69	2.70	2.68	2.77	2.80	2.75	2.22	2.17	2.20
Flash Point (°C)	68.0	55.0	53.50	52.0	68.0	70.0	65.0	53.0	55.0	50.0
Cloud Point (°C)	-20	8.0	8.0	6.0	13.0	10.0	15.0	10.0	10.0	11.0
Pour Point (°C)	-21	-8.0	-11.0	-8.0	-10	-14	7.0	-16.0	-20.0	-23.0
Fire Point (°C)	78.0	65.0	62.5	61.0	78.0	79.0	74.5	64.0	64.5	61.5
Cetane Number	47.0	40.0	38.50	40.0	42.0	42.0	45.0	47.0	46.0	44.0

ranged from 96.66% (for conventional diesel) to 99.75% in HDPE/AC. All the samples have the best rate of VM greater than 80% (Ndecky et al. 2022). The ash content of the sample tested ranges from 0.13% minimum for HDPE/AC and 3.03% maximum for conventional diesel. This suggested that all the samples tested should be considered as an alternative fuel since high ash content can result in an increment in combustion remnant resulting in a reduction in the heating effect of the fuel. Fixed carbon contents vary between samples with HDPE (Raw) having the minimum value and conventional diesel having the maximum value of 0.31%. All the samples tested had fixed carbon lower than 40%. The GHV MJ kg<sup>-1</sup> obtained ranged from 14.94 MJ kg<sup>-1</sup> minimum (for HDPE/AC) and 45.6 MJ kg<sup>-1</sup> maximum (for LDPE/CaO). The three (HDPE/CaO, HDPE/AC, HDPE (Raw)) have the lowest GHV (14.94 – 17.29 MJ kg<sup>-1</sup>) while the three (LDPE/ CaO, LDPE/AC, LDPE (Raw)) along with conventional diesel have higher GHV (42.66 – 45.38 MJ kg<sup>-1</sup>). LDPE and conventional diesel. All the samples indicated a proximity to the calorific value of conventional diesel. The ultimate analysis of the samples are results are summarized in Table 4.1.

### Physical Properties of the Liquid Fuel Samples

In terms of physical properties, the density of the samples

Table 2: The pH values of the liquid fuel samples.

S/N	Liquid Fuel Samples	pH Values
1.	HDPE Raw	3.62
2.	HDPE / AC	3.50
3.	HDPE/ CaO	6.60
4.	LDPE Raw	3.75
5.	LDPE/AC	3.60
6.	LDPE / CaO	3.80
7.	LDPE/ Diesel Blended 1:1	3.58
8.	LDPE/ Diesel Blended 1:2	3.52
9.	LDPE/ Diesel Blended 2:1	3.30
10.	HDPE/ Diesel Blended 1:1	3.90
11.	HDPE/ Diesel Blended 1:2	4.32
12.	HDPE/ Diesel Blended 2:1	4.10
13.	Diesel	4.70
14.	Petrol	5.06
15.	Kerosine	3.60

tested is less than  $1 \text{ g/cm}^3$  and varies between  $0.76 \text{ g/cm}^3$  minimum (for HDPE/AC and HDPE/Conventional Diesel blended) and  $0.83 \text{ g/cm}^3$  maximum (for conventional diesel). LDPE (Raw) of  $0.81 \text{ g/cm}^3$  has a close range to the conventional diesel density. The API gravity determined range from 38.98 – 54.68 for conventional diesel HDPE/AC and HDPE/Diesel blended 1:2. The Kinematic Viscosity of the samples varies from 2.17-2.80 with minimum value for HDPE/conventional diesel blended 1:2 and maximum value for LDPE/AC. The flash point of all other samples apart from LDPE/AC and LDPE/CaO is relatively lower than the flash point of conventional diesel. The cetane number of the sample product ranged from 3.50-47.0 with a minimum for HDPE/AC and a maximum for HDPE/conventional diesel blended 2:1 which is comparable to the cetane number of conventional diesel. The higher the cetane number of the fuel the higher the level of auto ignition in the internal combustion engine.

Table 4.2 shows that the pH values of all the liquid fuel samples tested indicated that they are all acidic with acidity strength range from 6.60-3.30 (HDPE/ CaO-LDPE/ Diesel Blended 2:1). This shows that HDPE/CaO is better when used in an engine because it has the least tendency of corroding the fuel tank since the acidity strength is less than that of the conventional diesel of 4.70 pH value.

## CONCLUSION AND RECOMMENDATIONS

The negligible moisture content, sulfur, nitrogen, ash, and high fixed carbon, cetane number volatile matter, and hydrogen content in all the samples is a good reason to justify that the liquid fuel produced through depolymerization of polymeric waste has the tendency to act as a good substitute to conventional diesel hence an alternative energy resource. The range of results obtained as physiochemical properties also vindicated that depolymerized liquid fuel samples have a good quality of a potential energy resource. pH test conducted revealed that all the liquid fuel samples are acidic and the lower the acidity level the better the fuel. The higher the degree of acidity level of the fuel the higher the tendency to cause rusting and corrosion in an internal combustion engine. That justifies the least acidity among the samples (HDPE/ CaO) as the best alternative to run the engine. The liquid fuel obtained through the depolymerization process can further be distilled to obtain purer samples that can be used directly to run the engine and its quality can be improved by blending.

## REFERENCES

Abota, C.A., 2012. *R<sup>n</sup>r<sup>\</sup>dg<sup>`</sup> h<sup>\_</sup>J<sup>z</sup>l<sup>r</sup>h<sup>W</sup>Z<sup>r</sup>l<sup>r</sup>l<sup>l</sup> l<sup>g</sup>G<sup>a</sup>Z<sup>g</sup>Z<sup>;</sup> ; W<sup>Z</sup>r<sup>h</sup> R<sup>n</sup>J<sup>n</sup>^<sup>^</sup>?g<sup>o</sup>l<sup>k</sup>h<sup>g</sup>f<sup>^</sup>g<sup>r</sup>n<sup>z</sup>e<sup>J</sup>k<sup>h</sup>l<sup>e</sup>f<sup>l</sup>/J<sup>h</sup>e<sup>n</sup>n<sup>h</sup>g<sup>l</sup>*. University of Ghana, Accra, Ghana.

- Aboulkas, A., Harfi, K.E. and Bouadili, A.E., 2010. Thermal degradation behaviors of polyethylene and polypropylene. Part I: pyrolysis kinetics and mechanisms. *Energy Conversion and Management*, 51, pp.1363-1369.
- Aguado, J., Serrano, D.P., Miguel, G.S., Castro, M.C. and Madrid, S., 2007. Feedstock recycling of polyethylene in a two-step thermo-catalytic reaction system. *Journal of Analytical and Applied Pyrolysis*, 79, pp.415-423.
- Anuar Sharuddin, S.D., Abnisa, F., Wan Daud, W.M.A. and Aroua, M.K., 2016. A review on pyrolysis of plastic wastes. *Energy Conversion and Management*. Available at: <https://doi.org/10.1016/j.enconman.2016.02.037>.
- ASTM D1298-12b, 2017. *Standard test methods for density, relative density, or API gravity of crude petroleum and liquid petroleum products by hydrometer method*. ASTM International. Available at: [www.astm.org/d1298-12br](http://www.astm.org/d1298-12br).
- ASTM D2709-22, 2022. *Standard Test Method for Water and Sediment in Middle Distilled Fuels by Centrifuge – eLearning Course*. Available at: <https://www.astm.org/astm-tpt-463.html>.
- ASTM D445-22, 2022. *Standard Test Method for Kinematic Viscosity of Transparent and Opaque Liquids (and Calculation of Dynamic Viscosity) -- eLearning Course*. Available at: <https://www.astm.org/astm-tpt-95.html>.
- ASTM D4737-09, 2009. *Standard Test Method for Calculated Cetane Index by Four Variable Equation*. ASTM International, West Conshohocken, PA. Available at: [www.astm.org](http://www.astm.org), DOI: 10.1520/D4737-09.
- ASTM D482-22, 2022. *Standard Test Method for Ash from Petroleum Products eLearning Course*. Available at: <https://www.astm.org/astm-tpt-96.html>.
- ASTM D5373, 2002. *Standard Test Methods for Instrumental Determination of Carbon, Hydrogen, and Nitrogen in Laboratory Samples of Coal and Coke*. ASTM International. Available at: [www.astm.org/d5373-93r02](http://www.astm.org/d5373-93r02).
- ASTM D86-20b, 2020. *Standard Test Methods for Distillation of Petroleum Products and Liquid Fuels at Atmospheric Pressure*. ASTM International. Available at: [www.astm.org/d0086-20b.h](http://www.astm.org/d0086-20b.h).
- ASTM D975-22, 2022. *Standard Specification for Diesel Fuel*. ASTM International. Available at: <https://www.astm.org/d0975-21.html>.
- ASTM D976-21, 2021. *Standard Test Methods for Calculated Cetane Index of Distillate Fuels*. ASTM International. Available at: [www.astm.org/d0976-21.htr](http://www.astm.org/d0976-21.htr).
- Cullis, C.F., Hirschler, M.M. and Rogers, R.L., 1981. The oxidation of decane in the liquid and gaseous phases. *Proceedings of the Royal Society of London. A. Mathematical and Physical Sciences*, 375(1763), pp.543-563.
- Demirbas, A., 2004. Pyrolysis of municipal plastic wastes for recovery of gasoline-range hydrocarbons. *Journal of Analytical and Applied Pyrolysis*, 72, pp.97-102.
- Hazzan, E.B., 2003. A study of plastic moulding techniques in Oyo state. Ladoke Akintola University of Technology, Ogbomosho, Oyo State.
- Hopewell, J., Dvorak, R. and Kosior, E., 2009. Plastics recycling: challenges and opportunities. *Philosophical Transactions of the Royal Society B: Biological Sciences*, 364(1526), pp.2115-2126.
- Kalilu, R.O., 2013. *Art from Art for Art: Conceptualising Existence in the Space of the Visual Arts*. Lautech Printing Press.
- Lee, K.H., 2009. Thermal and catalytic degradation of pyrolytic oil from pyrolysis of municipal plastic wastes. *Journal of Analytical and Applied Pyrolysis*, 85, pp.372-379.
- Ma, F. and Hanna, M.A., 1999. A review of bioresources technology. *Scientific Research Publishing*, 70, pp.1-15.
- Ndecky, A., Pierre, W.T., Aliou, S., Moustapha, K., Hawa, N. and Issiakha, Y., 2022. Proximate analysis of alternatives cooking solids fuels in sub saharan by using ASTM Standards. *International Journal of Clean Coal and Energy*, 11, 1. DOI: 10.4236/ijcce.2022.111001.

- Onwudili, J.A., Insura, N. and Williams, P.T., 2009. Composition of products from the pyrolysis of polyethylene and polystyrene in a closed batch reactor: Effects of temperature and residence time. *Journal of Analytical and Applied Pyrolysis*, 86, pp.293-303.
- Panda, A.K., 2011. *Mn]bl hg Jkh^lI I pntf tsZthg \_hk Jkh]n^nthg h\_ Lqnbj Fn^d\_khf WZnt JZntbI*. Ph.D. thesis, National Institute of Technology, Rourkela, India.
- Panda, A.K., Singha, R.K. and Mishra, D.K., 2010. Thermolysis of waste plastics to liquid fuel: a suitable method for plastic waste management and prospective. *R^g^wZte^ Zg] MlrvZgZte^ ?g^k^ r R^ob^wl*, 14(1), pp.233-248.
- Rominiyi, O.L., 2015. *?oZnZthg h\_ ^g^k^ r \hgrngmh\_f ngblpZe lhdj wZnt hg ; ]h-?kth MnkhphdI Hb^kZ*. M.Eng Thesis Department of Mechanical Engineering, The Federal University of Technology, Akure, Ondo State, Nigeria.
- Rominiyi, O.L., 2023. *D^o^dipf ^gmh\_ Z lZna k^Znhk \_hk \ZiZer nb\_ ]^phof ^kbsZthg h\_phof ^kb wZnt \_hk dqnj Zg] ^Z^hnl\_n^e pkh]n^nthg*. Ph.D. Thesis Department of Mechanical Engineering, The Federal University of Technology, Akure, Ondo State, Nigeria.
- Rominiyi, O.L., Fapetu, O.P., Owolabi, J.O. and Adaramola, B.A., 2017. Determination of energy content of municipal solid waste of Ado-Ekiti Metropolis, Southwest, Nigeria. *=nkk^gmJhngZeh\_ ; ppd^] Mlg^v Zg] N^aghd^ r*, 23(1), pp.1-11.
- Sharaddin, S.D.A., Abnisa, F., Daud, W.M.A.W. and Aroua, M.K., 2018. Pyrolysis of plastic waste for liquid fuel production as a prospective energy resource. In IOP Conference Series: Materials Science and Engineering. Available at: <https://doi.org/10.1088/1757-899X/334/1/012001>.
- Sharma, P.D., 2008. Plastic waste-reduce, reuse and recycle of plastic wastes are essential to make the environment greener and safer.
- Singh, R. and Sharma, P., 2008. Mechanistic publication of plastics degradation. *Jherf ^k D^ kZ] Zthg Zg] MZthm*, 93(3), pp.561-584.
- Singh, R.P., Tyagi, V.V. and Allen, T., 2011. An overview for exploring possibilities of energy generation from municipal solid waste (MSW) in Indian scenario. *R^g^wZte^ ?g^k^ r Zg] MlrvZgZte^ ?g^k^ r R^ob^wl*, 15(9), pp.4797-4808.
- Temitope, A.K., Abayomi, O.O., Ruth, O.A. and Adeola, P.A., 2015. A pilot recycling of plastic pure water sachets/bottles into composite floor tiles: a case study from selected dumping site in Ogbomoso. *JhngZe h\_ MZrkZe Mlg^v Zg] ?g^k^ r R^ob^wl*, 4, p.201. DOI: 10.4172/2169-0022.1000201.
- Trevor, M., 2019. Interview Conducted by Virginia Nicherson. Library of Congress Dublin.
- UNEP, 2009. Converting Waste Plastics into a Resource: Compendium of Technologies.
- Vannessa, G., 2007. Plastic Recycling. *Mlg^v Jkh^k^l*. Available at: [pubmed.gov](http://pubmed.gov).
- Wang, J.L. and Wang, L.L., 2011. Catalytic pyrolysis of municipal plastic waste to fuel with nickel-loaded silica-alumina catalysts. *?g^k^ r Mlnk^l, JZm ; R^h^o^kr, OnhsZthg, Zg] ?gokhg^ ^gnZe?\_ ^nh*, 33, pp.1940-1948.
- Yin, L.J., Chen, D.Z., Wang, H., Ma, X.B. and Zhou, G.M., 2014. Simulation of an innovative reactor for waste plastics pyrolysis. *=a^f bZe ?g^k^ r JhngZe*, 237, pp.229-235.

---

#### ORCID DETAILS OF THE AUTHORS

- Dr. Rominiyi, Oluwasina Lawan : <https://orcid.org/0000-0001-9358-3919>  
 Prof. MA Akintunde : <https://orcid.org/0000-0003-2780-9582>  
 Prof. Emmanuel Ibijola Bello : <https://orcid.org/0000-0002-8453-7539>  
 Professor Labunmi Lajide : <https://orcid.org/0000-0003-4911-5207>  
 Dr. Omolayo M. Ikumapayi : <https://orcid.org/0000-0002-9217-8476>  
 Prof. Opeyolu T. Laseinde : <https://orcid.org/0000-0001-7005-8951>  
 Dr. B. A. Adaramola : <https://orcid.org/0000-0001-9239-5676>







# Climate Change Effects on Crop Area Dynamics in the Cachar District of Assam, India: An Empirical Study

Mashud Ahmed<sup>1†</sup> , Md Kamrul Islam<sup>2</sup> and Samar Das<sup>2</sup>

<sup>1</sup>Department of Economics, Khairun Nessa Begum Women's College, Badarpur (Affiliated to Assam University, Silchar), Assam, India

<sup>2</sup>Department of Economics, Tripura University, Suryamaninagar, Tripura, India

†Corresponding author: Mashud Ahmed: hmashud786@gmail.com

Nat. Env. & Poll. Tech.  
Website: [www.neptjournal.com](http://www.neptjournal.com)

Received: 28-03-2024

Revised: 08-05-2024

Accepted: 18-05-2024

## Key Words:

Agriculture  
Climate change  
Crop area dynamics  
ARDL model

## ABSTRACT

Climate change is a worldwide phenomenon that significantly impacts the area, production, and yield of crops. Changes in climate conditions have diverse effects on farming globally. For instance, an increase in temperature can make specific crops more vulnerable to pests. Similarly, a decrease in rainfall reduces water availability, affecting both irrigated and rainfed farming practices. This study aims to investigate climate change effects on crop area dynamics in the Cachar district of Assam, India, for a period spanning from 1981 to 2017. The time series ARDL (Autoregressive Distributed Lag) model is employed to analyze the relationship between climate factors and areas under different crops. As a pre-requisite condition for ARDL, the Augmented Dickey-Fuller (ADF) test is employed to check the order of integration of area under selected crops. The research reveals that the annual average temperature negatively affects the area dedicated to chickpeas, while annual average rainfall negatively impacts the areas allocated to rice and chickpeas. Conversely, annual average relative humidity has a significant positive impact on the area of these crops in the study region. Policymakers may consider strategies and policies for agriculture by encouraging the cultivation of crop varieties that are more resilient to climate change.

## INTRODUCTION

Climate change encompasses any prolonged alteration in weather patterns stemming from either natural fluctuations or human actions (Lema & Majule 2009). According to the Intergovernmental Panel on Climate Change (IPCC) in their 2007 report, shifts in the average and/or variability of climate characteristics lasting multiple decades or beyond are key indicators of climate change. Top of Form Climate variability is the variation in weather mean states at each temporal and spatial scale, while climate change is the persistence of those variations, including their origin in natural physical processes and anthropogenic factors (Cardenas et al. 2006). There are two types of climate change variability: internal (caused by processes inside the climate system itself) and external (caused by natural and manmade external causes). Since the extratropical spatial structure of climate variability is highly reliant on the seasons, this variability is typically described in terms of "anomalies," where an anomaly is the difference between the instant state of the climate system and the climatology (Hurrell & Deser 2010).

Climate change can have a substantial impact on cropping patterns in different regions of the world. Changes in average temperature and pattern of rainfall can have a substantial impact on agricultural production and cropping patterns as agriculture depends on optimal temperature ranges and predictable rainfall patterns (Porter & Semenov 2005, Lobell et al. 2007, 2011). Relative humidity and wind speed may have detrimental effects on crops through dust concentration. Wind erosion is a severe land degradation process that can influence the agricultural production system (Santra et al. 2017, Csavina et al. 2014).

It is predicted by research that the amount of land that will be cultivated in Egypt's five agroclimatic zones will decrease due to increased water needs in 2030. The cultivated area in the current cropping pattern will also decrease by 13% in 2030 compared to its counterpart value in 2014-15 (Ouda & Zohry 2018). In the Satkhira district of Bangladesh, it is reported that crop production has significantly decreased due to the effects of climate change, and local farmers have modified their cropping patterns as a result (Islam et al. 2020). It has been revealed that climatic variables differently affect crop production in Assam's Cachar district (Ahmed & Saha 2021).

In the plains of Assam that have experienced flooding, it is observed that crop diversification significantly increases farm income (Mandal & Bezbaruah 2013). In China, climate change affects farmers' crop selections. Farmers favor maize and cotton over vegetables and potatoes when temperatures rise. Farmers choose wheat over rice, soybeans, oil crops, and vegetables when precipitation rises (Wang et al. 2010). It is revealed from farm-level survey data that farms with diversified cropping patterns were able to reap greater financial benefits from farming in Assam's plains (Mandal 2014). Farmers who use this strategy are found to be more successful when they have better irrigation and institutional credit facilities. A study based in the Jashore District of Bangladesh noted that climate change has a significant impact on cereal production and cultivation patterns. Farmers adjust their cropping practices over time in response (Shaibur et al. 2018). It is observed that rainfall significantly influences the cultivation area for maize, rapeseed, mustard, and potato in the Dima Hasao district of Assam (et al. 2022). The research found that, along with other driving forces, climate variability, and change are significant causes of changing agriculture and cropping patterns in Mizoram (Sati 2017).

The Cachar district of Assam falls under the Barak Valley agro-climatic zone of Assam. The crops grown in the region are essential for local food supply and the entire state. Therefore, it is imperative to acknowledge that agriculture serves not only as a driving force for economic prosperity but also holds a substantial position in the holistic advancement of the region.

This research examines the impact of climate variables on crop area dynamics under major crops in the Cachar district of Assam. Rice, wheat, maize, rapeseed and mustard, chickpea, pigeon pea, pulses, sesamum, safflower, castor, linseed, soybean, sugarcane, potatoes, onion, etc., are the principal crops of the district, according to statistics from the "International Crop Research Institute for Semi-Arid Tropics (ICRISAT)". For this study, rice, wheat, maize, rapeseed and mustard, chickpea, pigeon pea, pulses, and sesame are chosen which are the major crops in the district.

## MATERIALS AND METHODS

### Data Sources

Data on annual average temperature maximum ( $^{\circ}\text{C}$ ), temperature minimum ( $^{\circ}\text{C}$ ), relative humidity (%), wind speed (m/s), at 2 meters above the earth's surface, and total rainfall (mm), were collected from the freely accessible NASA's "Prediction of Worldwide Energy Resources (POWER) project (<https://power.larc.nasa.gov/data-access->

viewer/)" for the period 1981-2017 (Accessed on 10th December 2021). On the other hand, Data on the area (in 000 hectares) of rice, wheat, maize, rapeseed and mustard, sesame, chickpea, pigeon pea, and pulses at the district level were collected from the online portal of ICRISAT from 1981 to 2017 (As district level agricultural data are available up to 2017 only).

### Methodology

The relationship between climatic factors and area under different agricultural crops has been investigated using the time series ARDL (Autoregressive Distributed Lag) model. Charemza and Deadman (1992) introduced the ARDL test, which was then developed by Pesaran and Shin (1999) and Pesaran et al. (2001). In certain circumstances the strategy is more beneficial than other ways. First, the ARDL technique may be employed even when independent variables have distinct integration orders. Here according to the results of the unit root test, certain variables are stationary at level, while others are stationary at their first difference in this study (Table 1). This indicates that the integration order is mixed with both I (0) and I (1). ARDL model is hence appropriate for our investigation. Second, compared to other procedures, it provides more reliable findings for small samples. Third, since the ARDL test lacks residual correlation, it can handle potential endogeneity across variables (Marques et al. 2016). Fourth, short-run corrections may be merged with the long-run equilibrium by deriving the error correction mechanism (ECM) using a straightforward linear transformation without using the knowledge about long-run equilibrium in ARDL (Ali & Erenstein 2017). Through the automated lag selection option in Eviews12, the Akaike information criterion (AIC) is employed to establish the optimal lags for the variables.

To investigate the association of selected climate variables, i.e., average temperature, rainfall, relative humidity, and wind speed, with area under crops in the Cachar district of Assam throughout the period 1981-2017, the following model is specified:

$$CA_t = f(\text{Avgtemp}_t, \text{Rain}_t, \text{RH}_t, \text{WS}_t) \quad \dots(1)$$

Where  $CA_t$  indicates the area under a specific crop (in 000 hectares) over time.  $\text{Avgtemp}_t$  indicates average temperature ( $^{\circ}\text{C}$ ), which is measured as the gap between the annual average maximum and minimum temperature,  $\text{Rain}_t$  is the average annual rainfall (mm), which is calculated from the monthly total rainfall;  $\text{RH}_t$  represents the average annual Relative Humidity (%) and  $\text{WS}_t$  stands average annual Wind Speed (m/s) over time. Equation (1) can also be written as:

$$CA_t = \beta_0 + \beta_1 \text{Avgtemp}_t + \beta_2 \text{Rain}_t + \beta_3 \text{RH}_t + \beta_4 \text{WS}_t + \mu_t \quad \dots(2)$$

The research used all variables in their natural logarithmic forms to reduce multicollinearity and instability in the time series data. Equation (2) is transformed using the natural logarithm to get the log-linear model shown below:

$$\text{LnCA}_t = \beta_0 + \beta_1 \text{LnAvgtemp}_t + \beta_2 \text{LnRain}_t + \beta_3 \text{LnRH}_t + \beta_4 \text{LnWS}_t + \mu_t \quad \dots(3)$$

The ARDL approach consists of two phases. According to Pesaran et al. (2001), the first step is to determine the long-run cointegrating relationship using either the Wald-coefficient test or F-statistics. There are two different types of critical values: lower and upper bounds. Lower-level critical values are assigned to the I (0) variables, whereas higher-level critical values are assigned to the I (1) variables. If the estimated value of the F-Statistic exceeds the upper bounds, the null hypothesis of no co-integration among the variables is rejected, indicating the presence of a long-run cointegration relationship among the variables regardless of their integration order. We cannot reject the null hypothesis if the calculated F-statistic value is less than the lower limit of the critical value, indicating the absence of a long-run equilibrium connection. Without knowing the underlying regressors' order of integration, a clear conclusion cannot be drawn when the estimated F-statistic is between lower and upper-level bounds. The ARDL bounds-testing model for this work is represented mathematically as follows:

$$\begin{aligned} \Delta \text{LnCA}_t &= \beta_0 + \beta_1 \sum_{i=1}^n \Delta \text{LnCA}_{t-i} + \beta_2 \sum_{i=1}^n \Delta \text{LnAvgtemp}_{t-i} + \\ &\beta_3 \sum_{i=1}^n \Delta \text{LnRain}_{t-i} + \beta_4 \sum_{i=1}^n \Delta \text{LnRH}_{t-i} + \beta_5 \sum_{i=1}^n \Delta \text{LnWS}_{t-i} + \\ &+ \gamma_1 \text{LnCA}_{t-1} + \\ &\gamma_2 \text{LnAvgtemp}_{t-1} + \gamma_3 \text{LnRain}_{t-1} + \gamma_4 \text{LnRH}_{t-1} + \gamma_5 \text{LnWS}_{t-1} + \varepsilon_t \end{aligned} \quad \dots(4)$$

In this equation, Δ stands for change, β<sub>0</sub> For the intercept, n for the lag order. β<sub>i</sub>, i=1,...,5, represent the short-run effects on crop production of changes in lagged differences of crop area, average temperature, rainfall, relative humidity, and wind speed (all calculated at natural logarithmic values), respectively. Similarly, γ<sub>i</sub>, i=1,...,5, represents long-run effects of changes in lagged differences of the same explanatory variables on LnCA. ε<sub>t</sub> is an error term representing unobserved factors that affect crop production (LnCA) but are not included in the model. Pesaran et al. (2001) suggest testing the hypotheses as follows:

The null hypothesis H<sub>0</sub>: γ<sub>1</sub>=γ<sub>2</sub> = γ<sub>3</sub> = γ<sub>4</sub> = γ<sub>5</sub> = 0, means the absence of cointegration, which indicates no relationship between crop production with climate variables in the long run. Acceptance of H<sub>0</sub> implies we cannot reject the absence of cointegration against the alternative hypothesis H<sub>1</sub>: γ<sub>1</sub>≠γ<sub>2</sub> ≠ γ<sub>3</sub> ≠ γ<sub>4</sub> ≠ γ<sub>5</sub> ≠ 0, implying the existence of a long-run relationship between climate variables and

crop variables (output of selected crops). Rejection of the null hypothesis would indicate the existence of a long-run relationship.

The Error Correction Model (ECM), based on the ARDL approach, is used to examine the short-term connections between the variables, as shown in Equation (5).

$$\begin{aligned} \Delta \text{LnCA}_t &= \gamma_0 + \gamma_1 \sum_{i=1}^n \Delta \text{LnCA}_{t-i} + \gamma_2 \sum_{i=1}^n \Delta \text{LnAvgtemp}_{t-i} + \\ &\gamma_3 \sum_{i=1}^n \Delta \text{LnRain}_{t-i} + \gamma_4 \sum_{i=1}^n \Delta \text{LnRH}_{t-i} + \gamma_5 \sum_{i=1}^n \Delta \text{LnWS}_{t-i} + \\ &\gamma_6 \text{ECM}_{t-1} + \varepsilon_t \end{aligned} \quad \dots(5)$$

Where the ECM (-1) term is a lagged value of the residual of the model in which the long-term relationship is obtained, ECM (-1) is the speed of adjustment parameter, which is expected to be negative.

## RESULTS AND DISCUSSION

### Unit Root Test Results

A pre-requisite condition for the ARDL test is to check the stationarity and the integration order of the study variables. The Augmented Dickey-Fuller (ADF) test is employed to test the order of integration of climate variables, area, and yield of selected crops. As stated in Table 1, the stationarity test is applied by taking a natural log to each variable in

Table 1: Unit root test results for area under selected crops.

Variables	ADF Unit Root Test		Order of Integration
	Level	First Difference	
LnRA	-5.859167* (-3.540328)	-----	I (0)
LnWA	-3.402381 (-3.540328)	-4.685868* (-3.557759)	I (1)
LnMA	-3.824312* (-3.540328)	-----	I (0)
LnRMA	-4.231782* (-3.540328)	-----	I (0)
LnSA	-0.118247 (-3.557759)	-9.478349* (-3.544284)	I (1)
LnCPA	-4.477421* (-3.552973)	-----	I (0)
LnPPA	-2.803248 (-3.540328)	-7.685080* (-3.544284)	I (1)
LnPULSEA	-4.651485* (-3.540328)	-----	I (0)
LnAvgtemp	-4.503726* (-3.540328)	-	I (0)
LnRain	-4.227482* (-3.540328)	-	I (0)
LnRH	-4.492685* (-3.540328)	-	I (0)
LnWS	-6.493417* (-3.540328)	-	I (0)

**Note:** t-statistic of intercept and trend model, values in the parentheses are critical values. \*Indicates statistically significant at a 5 % level of significance.

level and first difference forms. The integration order is shown as a combination of I (0) and I (1) for crop area. Area under rice, maize, rapeseed and mustard, chickpea, and pulse are stationary at levels [I(0)] whereas area under wheat, sesame, and pigeon pea are stationary at their first order differences [I(1)] and climate variables are integrated at [I(0)].

LnRA, LnWA, LnMA, LnRMA, LnSA, LnCPA, LnPPA, and LnPULSEA denote the natural log value of area (000 hectares) under rice, wheat, maize, rapeseed and mustard, sesamum (sesame), chickpea, pigeon pea, and pulse production, respectively. LnAvgtemp, LnRain, LnRH, and LnWS are natural log values of average temperature ( $^{\circ}\text{C}$ ), rainfall (mm), relative humidity (%), and wind speed (m/s), respectively.

### Results of the Cointegration Test

The results of the ARDL bound test for crop area and averages of climate variables are presented in Table 2. It is observed that areas under three crops, namely rice, chickpea, and pulse, are showing long-run association with the averages of climate variables, i.e., average temperature, rainfall, relative humidity, and wind speed.

### Annual Averages of Climate Variables and Crop Area

**Long-run ARDL estimates:** Table 3 presents long-run ARDL coefficients of annual averages of climate variables, i.e., average temperature, rainfall, relative humidity, and wind speed with crop area as suggested by ARDL F-bound test results in Table 2. It is found that areas under three crops, namely rice, chickpea, and pulse, show long-run association with climate variables. Results indicate that area under rice is negatively and significantly affected by rainfall whereas it is positively and significantly impacted by relative humidity. The coefficient of rainfall implies that an increase of 1 percent in rainfall will reduce the area under rice production by 0.35 percent, whereas an increase of 1 percent in relative humidity will lead to a growth of 0.98 percent in the rice area. The area under chickpea production is negatively and significantly associated with average temperature and rainfall but positively and significantly influenced by relative humidity. A 1 percent increase in the average temperature and rainfall decreases chickpea production by 7.03 percent and 3.46 percent, respectively. However, an increase in relative humidity by 1 percent will enhance chickpea production by 10.09 percent. Though pulse area is showing long-run cointegration with climate variables as suggested by the

Table 2: Result of cointegration test for crop area with averages of climate variables.

F-Bound Test		Null Hypothesis: No long-term cointegration	
Model for Estimation		F-Statistics	
$F_{LNRA}$ ((LNRA/ LNAVGTEMP, LNRAIN, LNRH, LNWS)	ARDL (1, 0, 4, 1, 4)	<b>9.7047*</b>	
$F_{LNWA}$ ((LNWA/ LNAVGTEMP, LNRAIN, LNRH, LNWS)	ARDL (1, 1, 2, 3, 0)	3.2564	
$F_{LNMA}$ ((LNMA/ LNAVGTEMP, LNRAIN, LNRH, LNWS)	ARDL (4, 4, 4, 0, 4)	2.2400	
$F_{LNRMA}$ ((LNRMA/ LNAVGTEMP, LNRAIN, LNRH, LNWS)	ARDL (4, 4, 4, 3, 3)	0.8428	
$F_{LNLSA}$ ((LNLSA/ LNAVGTEMP, LNRAIN, LNRH, LNWS)	ARDL (4, 4, 3, 4, 0)	3.0739	
$F_{LNCPPA}$ ((LNCPPA/ LNAVGTEMP, LNRAIN, LNRH, LNWS)	ARDL (4, 1, 1, 1, 1)	<b>8.1688*</b>	
$F_{LNPPA}$ ((LNPPA/ LNAVGTEMP, LNRAIN, LNRH, LNWS)	ARDL (3, 3, 2, 3, 3)	1.6487	
$F_{LNPULSEA}$ ((LNPULSEA/ LNAVGTEMP, LNRAIN, LNRH, LNWS)	ARDL (1, 4, 0, 2, 4)	<b>4.2222*</b>	
Critical Value of Bounds			
Significance	Lower Bound (I0)	Upper Bound (I1)	
10%	2.20	3.09	
5%	2.56	3.49	
1%	3.29	4.37	

Note: \* signifies rejection of the null hypothesis at a 5% significance level.

Table 3: Crop area and averages of climate variables in the long run.

Crop Area	Average Temperature	Rainfall	Relative Humidity	Wind Speed
Rice	-0.2574 (0.1661)	-0.3552* (0.0120)	0.9825* (0.0331)	-0.0412 (0.8931)
Chickpea	-7.0319* (0.0048)	-3.4673* (0.0042)	10.0953* (0.0098)	0.9739 (0.5592)
Pulse	17.211 (0.2914)	-1.7236 (0.4960)	33.8279 (0.1151)	29.1303 (0.1799)

Source: Authors' own calculation using Eviews12. Note: \* denotes significance level at 5 percent. The values in the parentheses are p-values.

ARDL bound test, any statistically significant relationship is not detected between these variables.

**Short-run ARDL estimates:** The results of short-run ARDL coefficients of annual averages of climate variables with crop area and coefficients of error terms are presented in Table 4. The important outcome of the short-run dynamics is the calculation of the coefficient of ECM (-1), which is the speed of adjustment parameter in the long run, and it is likely to possess a negative value. ECM (-1) value of less than 1 implies monotonically convergence whereas ECM (-1) value of greater than 1 implies oscillatory convergence towards long-run equilibrium.

It is observed that short-run estimated results are different from the long-run estimates in terms of magnitudes and signs. However, the error correction coefficients of all the crops are negative and highly significant, indicating that any short-run disequilibrium is corrected back to the long-run equilibrium at certain rates through an error correction mechanism that works within the system. The coefficient of ECM (-1) is -1.1984 for rice area, which means the error correction process swings around the long-term value in a dampening manner (Narayan & Smyth 2006). After finishing the processes, the convergence to the equilibrium path will be at a rapid rate. This means an oscillatory convergence occurs for rice areas as producers adjust their cultivation and harvesting activities in response to changing climate variables in the long run.

The coefficient of error correction for areas under wheat, maize, rapeseed and mustard, sesame, chickpea, pigeon pea, and pulse are presented in the last column of Table 4,

implying around 53 percent, 72 percent, 2 percent, 43 percent, 65 percent, 7 percent and 61 percent any disequilibrium in the short run is corrected within one year.

It is noted from the results that the area under chickpeas is negatively affected by annual average temperature because chickpeas are generally cool-season crops and sensitive to high temperatures (Dixit 2022). High temperatures can lead to stress during critical growth stages, affecting the yield and cultivation areas of chickpeas. Average rainfall negatively affects the area under rice and chickpeas. Rice cultivation is often associated with flooded fields, especially in lowland rice systems. Excessive rainfall beyond what is suitable for rice cultivation can lead to waterlogging and flooding, negatively affecting rice areas (Ismail et al. 2012). Chickpea is generally cultivated as a rainfed crop, relying on natural rainfall rather than irrigation. However, too much rainfall can be detrimental to chickpea cultivation, as chickpea plants may not tolerate waterlogged conditions well. Average relative humidity positively affects rice and chickpea areas as higher humidity levels can create an environment less conducive to the development and spread of certain plant diseases, contributing to healthier crop areas. Therefore, areas of selected crops are affected by climate variables, depending upon the nature of the crops.

## CONCLUSIONS

The primary goal of this paper was to investigate the impact of climate change on crop area dynamics for selected crops in the Cachar district of Assam. For this purpose, the Autoregressive distributed lag (ARDL) bound test technique

Table 4: Crop Area and Averages of Climate Variables in the Short Run.

Crop Area	Average Temperature	Rainfall	Relative Humidity	Wind Speed	Coefficient of ECM (-1)
Rice	-----	-0.0192 (0.6839)	0.4179 (0.1379)	0.1964 (0.1245)	-1.1984* (0.0000)
Wheat	0.7210 (0.6143)	-2.2308* (0.0099)	5.2317 (0.1972)	-----	-0.5314* (0.0001)
Maize	-1.5882 (0.1920)	-0.6806* (0.0678)	-----	-3.1635* (0.0053)	-0.7277* (0.0009)
Rapeseed and Mustard	-3.0958* (0.0255)	-2.0030* (0.0012)	7.0495* (0.0056)	0.1635 (0.8455)	-0.0223* (0.0203)
Sesame	-0.5228 (0.1212)	-0.7624* (0.0005)	4.4278* (0.0001)	-----	-0.4369* (0.0002)
Chickpea	-1.2884* (0.0491)	-1.3397* (0.000)	1.5032 (0.3490)	-1.8644* (0.0058)	-0.6523* (0.0000)
Pigeon	-3.8973* (0.0000)	-0.7967* (0.0064)	1.6236 (0.2293)	-0.9545 (0.1334)	-0.0751* (0.0025)
Pulse	-0.8765 (0.6853)	-----	-0.3454 (0.9355)	2.8830 (0.2260)	-0.6197* (0.0000)

Source: Authors' own calculation using Eviews12. Note: \* indicates significance levels of 5%. The values in the parentheses are p-values.

was employed by taking the natural log of all variables. The results indicate that annual average temperature has statistically significant negative effects on the chickpea area. Annual average rainfall negatively affects areas under rice and chickpeas, while annual average relative humidity affects them positively. Wind speed has no significant effects on crop area under the selected crops. In the short run, coefficients of error correction for both area and yield of selected crops are negative and significant at a 5 percent level of significance, implying that any short-run disequilibrium is corrected back to the long-run value through an error correction mechanism.

Thus, it is concluded that the effects of climate variables on the area under different crops vary among the selected crops, i.e., for some crops, the impact of a specific climate variable is negative, whereas, for some other crops, the impact of the same climate variable may be positive depending upon the nature of the crops. Policymakers may consider strategies and policies for agriculture by encouraging the cultivation of crop varieties that are more resilient to climate change.

Based on available secondary data, the study is confined to examining the impacts of climate variables on crop area dynamics in the Cachar district of Assam using a time series ARDL approach. There are future scopes to study the effects of climate change in other districts of the region using different methods where data are available. Policymakers may develop policies for agriculture by encouraging the cultivation of crop varieties that are more resilient to climate change effects.

## REFERENCES

- Ahmed, M. and Saha, P., 2021. The relationships of climate variability and crop production: An analysis of the Cachar District of Assam, India. *Research Journal of Agricultural Sciences*, 12(6), pp.2007-2011.
- Ali, A. and Erenstein, O., 2017. Assessing farmer use of climate change adaptation practices and impacts on food security and poverty in Pakistan. *Climate Risk Management*, 16, pp.183-194.
- Cardenas, R., Sandoval, C.M., Rodriguez-Morales, A.J. and Franco-Paredes, C., 2006. Impact of climate variability in the occurrence of leishmaniasis in northeastern Colombia. *The American Journal of Tropical Medicine and Hygiene*, 75(2), pp.273-277.
- Charemza, W.W. and Deadman, D.F., 1992. *New Directions in Econometric Practice: General to Specific Modelling, Cointegration and Vector Autoregressions*. Edward Elgar Publication.
- Csavina, J., Field, J., Félix, O., Corral-Avitia, A.Y., Sáez, A.E. and Betterton, E.A., 2014. Effect of wind speed and relative humidity on atmospheric dust concentrations in semi-arid climates. *Science of the Total Environment*, 487, pp.82-90.
- Dixit, G., 2022. *Project Coordinator's Report 2021-22*. ICAR-Indian Institute of Pulses Research, Kanpur, pp.208-224.
- Hurrell, J.W. and Deser, C., 2010. North Atlantic climate variability: the role of the North Atlantic Oscillation. *Journal of Marine Systems*, 79(3-4), pp. 231-244.
- IPCC, 2007. *Climate Change 2007: Synthesis Report. Contribution of Working Groups I, II, and III to the Fourth Assessment Report of the Intergovernmental Panel on Climate*. IPCC.
- Islam, M.S., Roy, S., Afrin, R. and Mia, M.Y., 2020. Influence of climate-induced disasters and climatic variability on cropping pattern and crop production in Bangladesh. *Environment, Development and Sustainability*, 22(7), pp.6709-6726.
- Ismail, A.M., Johnson, D.E., Ella, E.S., Vergara, G.V. and Baltazar, A.M., 2012. Adaptation to flooding during emergence and seedling growth in rice and weeds, and implications for crop establishment. *AoB Plants*, 2, p.019.
- Lema, M.A. and Majule, A.E., 2009. Impacts of climate change, variability and adaptation strategies on agriculture in semi-arid areas of Tanzania: The case of Manyoni District in Singida Region, Tanzania. *African Journal of Environmental Science and Technology*, 3(8), pp.206-218.
- Lobell, D.B., Ortiz-Monasterio, J.I. and Falcon, W.P., 2007. Yield uncertainty at the field scale was evaluated with multi-year satellite data. *Agricultural Systems*, 92, pp. 76-90.
- Lobell, D.D., Schlenker, W. and Roberts, M.J., 2011. Climate trends and global crop production since 1980. *Science*, 333(6042), pp.616-620.
- Mandal, R. and Bezbaruah, M.P., 2013. Diversification of cropping pattern: its determinants and role in flood affected agriculture of Assam Plains. *Indian Journal of Agricultural Economics*, 68, pp.169-181.
- Mandal, R., 2014. *Cropping Pattern Choice and Risk Mitigation in Flood Affected Agriculture: A Study of Assam Plains, India*. SHSU, p.3.
- Marques, A.C., Fuinhas, J.A. and Menegaki, A.N., 2016. Renewable vs non-renewable electricity and the industrial production nexus: Evidence from an ARDL bounds test approach for Greece. *Renewable Energy*, 96, pp.645-655.
- Narayan, P.K. and Smyth, R., 2006. What determines migration flows from low-income to high-income countries? An empirical investigation of Fiji-US migration 1972-2001. *Contemporary Economic Policy*, 24(02), pp.332-342.
- Ouda, S.A. and Zohry, A.E.H., 2018. *Cropping Pattern Modification to Overcome Abiotic Stresses*. Springer, pp.89-102
- Pesaran, M.H. and Shin, Y., 1999. An autoregressive distributed-lag modeling approach to cointegration analysis. *Econometric Society Monographs*, 31, pp.371-413.
- Pesaran, M.H., Shin, Y. and Smith, R.J., 2001. Bounds testing approaches to the analysis of level relationships. *Journal of Applied Econometrics*, 16(03), pp. 289-326.
- Porter, J.R. and Semenov, M.A., 2005. Crop responses to climatic variation. *Philosophical Transactions of the Royal Society B: Biological Sciences*, 360(1463), pp. 2021-2035.
- Saha, P., Ahmed, M. and Baruah, M., 2022. Climate change and cropping pattern: An analysis of the Dima Hasao (North Cachar Hills) district of Assam. *Research Journal of Agricultural Sciences*, 13(1), pp. 187-191.
- Santra, P., Moharana, P.C., Kumar, M., Soni, M.L., Pandey, C.B., Chaudhari, S.K. and Sikka, A.K., 2017. Crop production and economic loss due to wind erosion in the hot, arid ecosystem of India. *Aeolian Research*, 28, pp. 71-82.
- Sati, V.P., 2017. Changing agriculture and cropping pattern in Mizoram, Northeast India. *SSRN*, 11, p.561
- Shaibur, M.R., Nahar, N. and Rahman, M.H., 2018. Probable relationship between climate change and cropping pattern in Jashore district, Bangladesh. *Journal of Jessore University of Science and Technology*, 3(1), pp. 7-13.
- Wang, J., Mendelsohn, R., Dinar, A. and Huang, J., 2010. How Chinese farmers change crop choice to adapt to climate change. *Climate Change Economics*, 1(03), pp. 167-185.

---

## ORCID DETAILS OF THE AUTHORS

Mashud Ahmed: <https://orcid.org/0000-0002-0092-7282>



# Laser Induced Spectroscopy (LIBS) Technology and Environmental Risk Index (RI) to Detect Microplastics in Drinking Water in Baghdad, Iraq

Estabraq Mohammed Ati<sup>1</sup>, Shahla Hussien Hano<sup>2</sup>, Rana Fadhil abbas<sup>1</sup>, Reyam Najji Ajmi<sup>1†</sup> and Abdalkader Saeed Latif<sup>3</sup>

<sup>1</sup>Department of Biology Science, Mustansiriyah University, POX 46079, Baghdad, Iraq

<sup>2</sup>Ibn Sina University of Medical and Pharmaceutical Sciences, Baghdad, Iraq

<sup>3</sup>National University of Science and Technology/College of Health and Medical Technology, Iraq

†Corresponding author: Reyam Najji Ajmi; reyam80a@yahoo.com

Nat. Env. & Poll. Tech.  
Website: [www.neptjournal.com](http://www.neptjournal.com)

Received: 18-02-2024

Revised: 27-03-2024

Accepted: 13-04-2024

## Key Words:

Microplastic detection  
Laser-induced spectroscopy  
Water treatment  
Ecological potential  
Ecological risk

## ABSTRACT

Drinking water contamination by microplastic particles is a global concern that is becoming increasingly common due to consumer abuse, and we use laser fractionation spectroscopy to examine what microplastic particles in water packaging can do. Several types of bottled water were sampled at several manufacturing facilities in Baghdad. The presence of the measured micropolymer species in water was immediately classified and detected using a laser production resolution spectrometer as well as signal and plasma scattering spectra, various MP polymers "polyethylene terephthalate, polystyrene, polypropylene, polyethylene, and polyvinyl chloride" are five polymers that were successfully detected in drinking water to validate the ability to identify health risk factors based on potential environmental risk index (RI) and potential environmental risk factors (Tin), the results are calculated to show that risk predicates have evolved over a decade depending on the risk factors. To do. The smallest particle was 20 microns and the largest particle was 63.4 microns. Microplastics were detected in 5 out of 10 samples, PET in 4 samples, PS and PP in 2 samples, and PVC in sample 1, the most common polymer in bottled water is polyethylene. The average C/H ratios of the five samples were PE (1.76), PET (1.21), PS (1.52), PP (1.23), and PVC (0.99), on average, the measured trends of C/H values were [PE greater than PS], [PP greater than PET], and [PVC greater than PET]. According to our results, the integration of LIBS technology provides a fast and efficient way to detect microplastics. It has a high resolution of fine particles, allowing the detection of very small particles associated with various adverse effects on human health. The feasibility study for water bottling was approved, and the WHO water quality criteria were confirmed. As a result, we will undertake a thorough analysis of the best water bottling quality. In this study, the initial LIBS signals of several samples were used to completely detect microplastics. Microplastics in bottled water samples have been detected and quantified using LIBS spectroscopy techniques with Ecological Potential Ecological Risk. Analytical technology is used to investigate sources, perform research, and collect relevant data, worldwide reports, and permitted statistics to deliver crucial insights and recommendations. Water samples were obtained from several locations throughout Baghdad. At the source, 2 liters of water were obtained in plastic bottles for each sample, for a total of 10 samples. Each sample is owned by the factories that supplied it.

## INTRODUCTION

Since 2018, an increasing number of scientists have examined the notion that tap water is precious with a huge impact on a human and a noun component of our everyday life. Most countries emphasize providing people need clean, safe water. However, in recent times, the usage of bottled drinking water has increased, with global consumption reaching 329.33 billion liters per year on average (Johnson et al. 2020, Almaiman et al. 2021, Dalmau-Soler et al. 2021,

Gomiero et al. 2021). Although bottled water is a popular option, it has considerable limitations because it is not as tightly regulated as municipal tap water (Mintenig et al. 2019, Lam et al. 2020, Kirstein et al. 2021). The majority of bottled water manufacturers favor plastic packaging, which is rarely recycled. As a result, plastic packaging winds up in landfills or as debris in seas and lakes, where it degrades into microplastic particles as a result of UV exposure, biofilm formation, mechanical shear, and wave action (Sultan et al. 2018). Microplastics can pollute drinking water and pose

major health risks such as cancer if consumed by people (Pivokonsky et al. 2018, Pivokonský et al. 2020, Sarkar et al. 2021).

Microplastics are categorized based on their size or origin. Their size determines whether they are considered as little or huge, the tiniest microplastics are 1m to 1mm in size. Based on their origin, microplastics are classed as secondary or primary. Secondary occurs when macroplastics break down as a result of continual exposure to poor environmental conditions. Microplastics have lately been found in a variety of environments, including soil and human feces; there have been a few researches on the prevalence of plastic materials in drinking water bottling. Several methods have been developed for detecting and measuring microplastics in seas, lakes, and groundwater. NIR, FTIR, SEM-EDS, and photoluminescence are among the techniques used (Kirstein et al. 2021). The FTIR method analyzes the molecular structure of a sample by evaluating its response to infrared light. This procedure is non-destructive, trustworthy, and simple (Pivokonsky et al. 2018). However, Because of particle faults in the reflection mode, the efficiency of this technique is significantly reduced. It is best suited for dry materials and particles larger than 10 m in diameter (Pivokonsk et al. 2020). NIR technology can also identify materials by analyzing the molecular vibrations caused by electromagnetic radiation. This method penetrates deeper and Compared to FTIR, it requires less sample preparation. It is, however, restricted to particles with a diameter greater than 1 mm (Domínguez & Luoma 2020, Kirstein et al. 2021). Photoelectroelectron spectroscopy, a new approach for identifying microplastics, is based on the idea that when optically stimulated materials return to their ground state, they release electromagnetic radiation. This approach has proven its worth by discriminating between plastic and non-plastic materials (Andrade & Rhodes 2012, Sarkar et al. 2021). However, this method is impeded by beam overlap, which makes discriminating between different plastics difficult. (Handbook of the Birds of the World 2018, Sarkar et al. 2021). Due to the drawbacks of present technologies, it is necessary to design a technique that is dependable and has the potential to be used in site investigations (Dudley 2008, Ati et al. 2022). There has been little investigation into the use of LIBs and spectroscopy to identify microplastics. A molecular analysis method based on the inelastic light scattering principle. This approach can assess the chemical material and identify constituent particles (Dudley et al. 2010, Domnguez & Luoma 2020). Because of its significant sensitivity to non-polar functional groups, precision in clarity of ultrafine particles, and little interaction with water, this technique has been widely employed in the level assessment of microplastics (Coetzee et al. 2014, Kirstein et al. 2021).

This element's characteristic electromagnetic radiation is emitted as a result of the cooling of the plasma containing the excited ions. Polymers were discovered by measuring the carbon and hydrogen line density ratios (Andrade & Rhodes 2012, Coetzer et al. 2014, WHO 2018). Polymers were discovered by studying molecular data. As a result, the study's purpose was to detect microplastics in bottled water samples while also closing a knowledge gap about them from multiple sources. The United States Environmental Protection Agency (USEPA 2006) defines the potential for adverse effects on ecosystems as a result of exposure to an environmental stressor or a combination of environmental factors, and an environmental potential factor is any physical, chemical, environmental stress factors that may have negative effects on certain natural resources, as well as the environment in which they interact with them. The term "risk assessment" refers to describing the nature, magnitude, or amount of health risks to the population as a result of microplastic or any other type of environmental stress that may be present in the environment (Chen 2020). Where it is calculated potential environmental risk index (RI) is calculated by the equation:

$$RI = T_{in} \times CRM / C_{io}$$

$T_{in}$  = the concentration of the metal in the sample

$C_{io}$  = level of pollution value of the metal

CRM= Certificate references materials

To assess concentration, the degree of contamination, pollution ( $C_{io} < 1$ ), low level of pollution ( $1 < C_{io} < 2$ ), moderate level of pollution ( $2 \leq C_{io} < 3$ ), strong level of pollution ( $3 < C_{io} < 5$ ) and very strong level of pollution ( $C_{io}$ ) (EC (2020).

## MATERIALS AND METHODS

The liters of water bottled in plastic were gathered from a local vendor for each sample, for a total of ten packaging source samples. LIBS measurements were performed using the method indicated in (Ruas et al. 2017), allowing for direct investigation of water samples for microplastic detection to take accurate volumetric measurements, a glass beaker

Table 1: Factors and degrees of the QA and QC of potential ecological risk factors (Kicińska & Wikar 2023).

Epr value	Grades of ecological risk of metals
$E_{pri} < 10$	Low risk
$10 \leq E_{pri} < 20$ R	Moderate risk
$20 \leq E_{pri} < 30$ R	Considerable risk
$30 \leq E_{pri} < 40$	High risk
$40 \leq E_{pri}$	Very high risk



deionized with water was employed. 100 cc of each collected water sample was placed in a glass holder and then the laser was focused directly to obtain the spectra. The components of the water samples were analyzed using laser-induced breakdown spectrometry to detect microplastics (LIBS). An Ocean Optics LIBS spectrometer was used in this study. Ocean Optics' LIBS2500plus spectrometer equipment was employed. Set the laser power to 300 mJ, pulse width to 10 ns, and PRF to 1-2 Hz. He reached a peak output of 32.25 MW in a second and a half. This device is capable of doing qualitative measurements in real time. Spectra were scanned with a resolution of 0.1 nm (FWHM) between wavelengths 200 and 980 nm. Seven spectral channels with wavelengths ranging from 198.16 to 971.11 nm were incorporated into the system. Ocean Optics provided LIB Splus version 4.5.0.7 for evaluating findings. The software enabled the LIBS 2500plus system to function by detecting different elements' emission lines, correlating background signals, showing emission spectra, collecting data, giving the spectrum, and firing the laser, also includes a spectrum library of 2,500 "National Institute of Standards and Technology" atomic emission lines. The LIBS2500Plus system was detected and calibrated using the emission lines. Each sample was randomly assigned 200 spectrums and evaluated independently, the method was done four times for each of the ten samples to ensure

Determination of the potential environmental risk index (RI) for samples: This was accomplished by determining the CRM (Certificate reference materials) and comparing the measurement results to the certified value reference materials.

CRM of water [ (0.91 ± 0.01), (0.01 ± 0.01), (0.81 ± 0.12)]

@Certified value ± 95% confidence interval of the mean value

c Mean ± standard deviation at 95% confidence limit with replicate

Then apply the equation below: depending the Table (1).

$$RI = T_{in} \times CRM / C_{io}$$

Various statistical coefficients of determination metrics, the correlation coefficient of concordance and the correlation coefficient of interclass were used in the analysis of variance, mean prediction of concentration is compared with data from their label and proposed guidelines published by WHO (2012) and USEPA (2009) under the Principal components with the test for significance between individual groups The smallest significant difference in probability at a 5% level (RI). Correlation analysis was also performed to determine the relationship between the heating value and each of the chemical components, as well as the final and proximal analysis, and by using the SAS statistical package to measure properties (Cox 2016).

## RESULTS AND DISCUSSION

The atomic spectra generated from the LIBS measurements were estimated based on the vibration spectra obtained from the tests to detect MP in the water samples used in the experiment, which have been identified as commonly used polymers in bottled water packaging. The bands are observed at 1163 cm<sup>-1</sup> and 1199 cm<sup>-1</sup>, which are related to C-C bond stretching, 1179 cm<sup>-1</sup>, which is related to CH<sub>2</sub> rocking vibration, and 1391 cm<sup>-1</sup>, which are related to CH<sub>2</sub> swing vibration and the CH<sub>2</sub> stretching in Fig 1. The atomic spectra of four distinct materials were calculated using LIBS. On average, The C/H ratio for the five samples was 1.49, the larger C/H value is related to it (WHO 2018, Ajmi et al. 2018), which also suggests the presence of polyethylene.

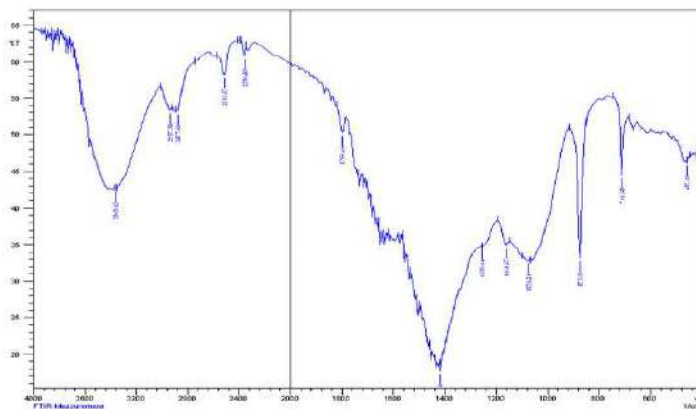


Fig. 1: LIBS spectra for samples containing polyethylene.

At  $898\text{ cm}^{-1}$ , It also showed asymmetric stretch vibrations for both C-C and C(O)-O bonds, while symmetric stretch vibrations were detected for C-O-C bonds, which bind to  $1138\text{ cm}^{-1}$  and  $1285\text{ cm}^{-1}$  of C-C bond stretching vibrations,  $1395\text{ cm}^{-1}$  of C(O)-O bond stretching vibrations,  $1430\text{ cm}^{-1}$  of O-CH, CH<sub>2</sub>, and C-CH bond bending vibrations, and  $1645\text{ cm}^{-1}$  of 8a Circular mode vibrations = 1730 in the Wilson extension (Fig. 2). The four samples' average C/H ratio was 1.11, which is comparable to been reported by (WHO 2013, Ruas et al. 2017), It provides evidence for the existence of polyethylene terephthalate in the sample.

The readings indicated two of the 10 samples had ranges of  $388\text{ cm}^{-1}$  due to CH bending and CH<sub>2</sub> bond shaking,  $899\text{ cm}^{-1}$  due to vibrations between CH, C-C and C-CH<sub>3</sub> bonds, and  $893\text{ cm}^{-1}$  due to vibrations between CH bonds (Fig. 3). And CH<sub>3</sub> and C, which leads to the curvature of the C-CH<sub>3</sub> and C-C bonds of  $1140\text{ cm}^{-1}$ . Torsion of CH<sub>2</sub> at  $1330$  and  $1488\text{ cm}^{-1}$  caused bending vibrations of CH, CH<sub>3</sub>, and CH<sub>2</sub>. The two samples' average C/H ratio was 1.27. The methyl and methylene groups in PP repeat units make them up. The

obtained ratio is significantly different from the measured by (WHO 2013, Kukkala & Moilanen 2013), which are polypropylene-based.

Ring deformation was identified in two more samples out of ten, including a notable peak at  $1001\text{ cm}^{-1}$  due to the aromatic carbon ring's circular breathing mode, a band of  $1031\text{ cm}^{-1}$  due to CH in-plane deformation, and  $1155\text{ cm}^{-1}$  due to  $1451\text{ C}_2$  stretching vibrations. Vibrations of structural rings are stretched and agreed with WHO (2013), Kukkala & Moilanen (2013), Coetzer et al. The visible bands are shown in Fig. 4.

PS bands of  $361\text{ cm}^{-1}$  were detected in one of the water samples due to the brief formation of a The C-Cl bond was in the PVC polymer,  $618\text{ cm}^{-1}$  concussions for the C-Cl stretch, and  $1485\text{ cm}^{-1}$  for the C-H homolog in the CM group. The band image is depicted in Fig. 4. These are PVC-specific peaks (WHO 2013). PVC has many additives which represents a sample mean C/H of 0.95. According to the value calculated by (Dudley 2008, WHO 2018, Fadhel 2019).

LIBS experiments detected atomic spectra lines at several characteristic wavelengths when the intensities of

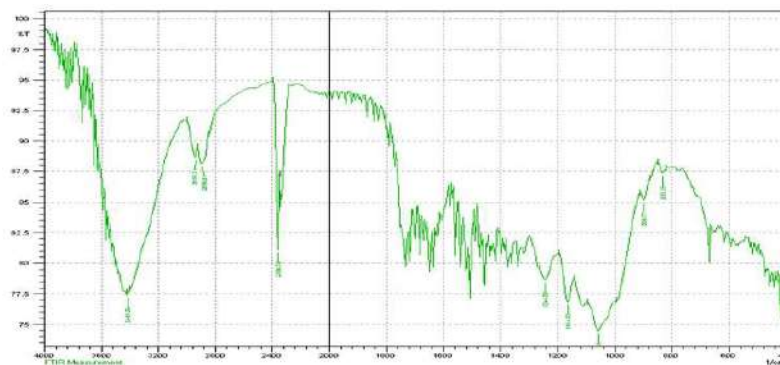


Fig. 2: PET-containing materials' LIBS spectrum.

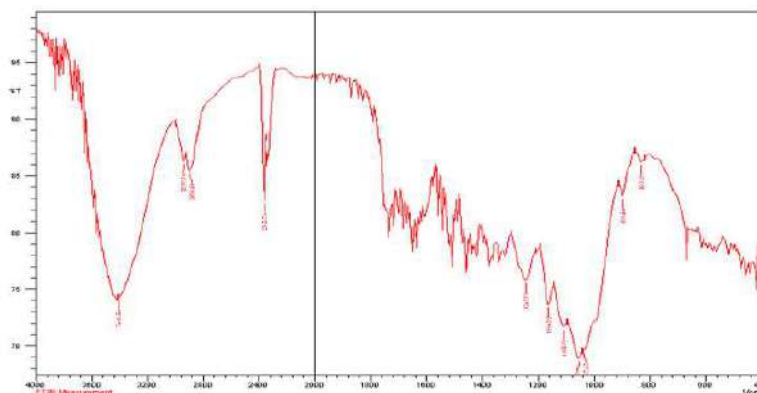


Fig. 3: LIBS spectra for samples containing PP.

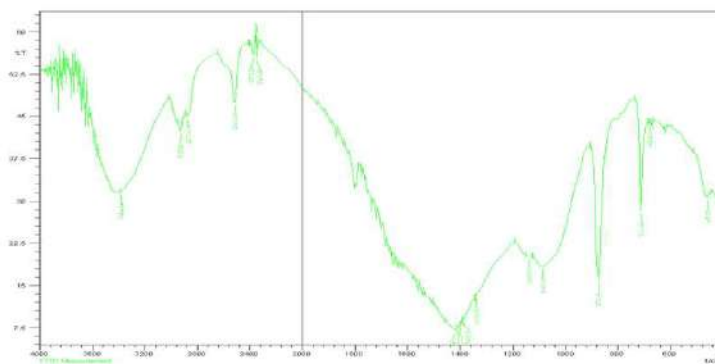


Fig. 4: LIBS spectra for samples containing PS.

specific spectral lines were drastically increased, when the interference from the emission lines is reduced, it leads to less absorption of particles. The transmission line at 257.81 corresponds to the electrical transition from the 2s22p2 to the 2s22p3s state in the LIBS observations. Hydrogen atoms make up emission line 398. The atomic of emission line 656.3 is the source of H atoms transitioning from energy levels in level 3 to lower energy levels in level 2. At 725.7 nm, PVC is the sole material having a noticeable Cl line (Dudley et al. 2010). An O(I) atom migrating from 2s22p3s to 2s22p3p triggers the 777.3 emission line, indicating LIBS's ability to detect trace elements.

To confirm the capacity to identify the elements in health risks according to the Potential Ecological Risk Index (RI) and potential ecological risk factor ( $T_{in}$ ) in dynamic modeling to predict changes in water concentration in environmental compartments exposure by calculating the concentration of microplastic and its concentration in the reference value

$$RI = T_{in} \times CRM / C_{io}$$

$T_{in}$  = Concentration of metals in the sample  $C_{io}$  = reference depending Table (1)

CRM Certificate Reference material in metal

The prediction for more than or less than ten years depends on Exposure Factors.

Results in water in five samples [1.00\*\*, 0.82\*\*, 0.02, 0.51\*, 0.05]

\* Average values to predicate risk for more than < ten years depending on Exposure Factors accumulated

\*\* Average high values to predicate risk less than > ten years depending on Exposure Factors accumulated

The results showed that the percentage of pollution as indicated is more vulnerable to pollution in the coming years. The results of the Potential Ecological Risk Index of

concentration that have been obtained from analyzed samples were reached of the bioindication environment and how to transition microplastic to water, according to Sultan et al. (2018) and Cristol et al. (2008).

## CONCLUSIONS AND RECOMMENDATIONS

This study was successful in identifying microplastics in plastic drinking water, with The tiniest particles measuring 20 m, while the largest measured 63.4 m. Microplastics were discovered in five of 10 samples, PET in four, PS and PP in two, and PVC in one. According to the study's findings, polyethylene is the most frequent polymer in bottled drinking water; the average C/H ratios of the five samples were PE (1.76), PET (1.21), PS (1.52), PP (1.23), and PVC (0.99). On average, the measured trend for C/H value was [PE more than PS], [PP greater than PET], and [PVC greater than PET]. Polymers were present in the water samples, based on the ratios. According to the findings, integrating LIBS technologies gives a quick and efficient technique for detecting microplastics. It has a high microscopic particle resolution and so can detect very minute particles. The approaches are also non-polar functional group sensitive and are unaffected by water samples. This study will help to direct future detection and classification research. Microplastics have also been linked to a variety of negative health impacts in humans. Identify and learn about critical actions for lowering their health consequences. As a result, the techniques investigated in this study can be utilized to detect and quantify in industrial environments. Its use will assure the availability of healthy drinking water that is free of health concerns.

## ACKNOWLEDGMENT

The authors would like to thank Mustansiriyah University (www.uomustansiriyah.edu.iq) Baghdad, Iraq for its support in the present work and extremely grateful to Ibn Sina

University of Medical and Pharmaceutical Sciences, and extremely grateful to the National University of Science and Technology/College of Health and Medical Technology for their cooperation and all the people help us to get our data.

## REFERENCES

- Ajmi, R.N., Lami, A., Ati, E.M., Ali, N.S.M. and Latif, A.S., 2018. Detection of isotope stable radioactive in soil and water marshes of Southern Iraq. *Journal of Global Pharma Technology*, 10(6), pp.160-171.
- Almaiman, A.A., Aljomah, M., Bineid, F.M., Aljeldah, F., Aldawsari, B., Liebmann, I., Lomako, K., Sexlinger, R. and Alarfaj, R., 2021. The occurrence and dietary intake related to the presence of microplastics in drinking water in Saudi Arabia. *Environmental Monitoring and Assessment*, 193, pp.1-13.
- Andrade, G.S. and Rhodes, J.R., 2012. Protected areas and local communities: An inevitable partnership toward successful conservation strategies. *Ecology and Society*, 17(14).
- Ati, E.M., Abbas, R.F., Ajmi, R.N. and Zeki, H.F., 2022. Water quality assessment in the Al-Musayyib river/Euphrates system using the River Pollution Index (RPI). *European Chemical Bulletin*, 11(5), pp.53-58.
- BirdLife International and Handbook of the Birds of the World, 2018. Bird species distribution maps of the world. Version 2018.1. Available at: <http://datazone.birdlife.org/species/requestdis>.
- Chen, S., Zhang, Q., Andrews-Speed, P. and McLellan, B., 2020. Quantitative assessment of the environmental risks of geothermal energy: A review. *Journal of Environmental Management*, 276, p.111287.
- Coetzee, B.W.T., Gaston, K.J. and Chown, S.L., 2014. Local scale comparisons of biodiversity as a test for global protected area ecological performance: A meta-analysis. *PLOS ONE*, 9, e105824. Available at: <https://doi.org/10.1371/journal.pone.0105824>.
- Coetzer, K.L., Witkowski, E.T.F. and Erasmus, B.F.N., 2014. Reviewing biosphere reserves globally: Effective conservation action or bureaucratic label? *Biological Reviews*, 89, pp.82-104. Available at: <https://doi.org/10.1111/brv.12044>.
- Cox, D.R., 2006. *Principles of Statistical Inference*. Cambridge: Cambridge University Press. ISBN 978-0-521-68567-2.
- Dalmou-Soler, R., Ballesteros Cano, J., Boleda, M.R., Paraira, M., Ferrer, N. and Lacorte, S., 2021. Microplastics from headwaters to tap water: Occurrence and removal in a drinking water treatment plant in Barcelona metropolitan. *Environmental Science and Pollution Control Series*, pp.1-11.
- Domínguez, L. and Luoma, C., 2020. Decolonising conservation policy: How colonial land and conservation ideologies persist and perpetuate indigenous injustices at the expense of the environment. *Land*, 9, p.65. Available at: <https://doi.org/10.3390/land9030065>.
- Dudley, N., Parrish, J.D., Redford, K.H. and Stolton, S., 2010. The revised IUCN protected area management categories: The debate and ways forward. *Oryx*, 44, pp.485-490. Available at: <https://doi.org/10.1017/S0030605310000566>.
- European Commission (EC), 2020. EU policy on cancer. Available at: [https://ec.europa.eu/health/non\\_communicable\\_diseases/](https://ec.europa.eu/health/non_communicable_diseases/). Accessed 02 Nov 2023.
- Fadhel, R., Zeki, H.F., Ati, E.M. and Ajmi, R.N., 2019. Estimation of free cyanide on the sites exposed to organism mortality in Sura river. *Journal of Global Pharma Technology*, 11(3), pp.100-105.
- Gomiero, K.B., Øysæd, L., Palmas, G. and Skogerbø, S., 2021. Application of GCMS-pyrolysis to estimate the levels of microplastics in a drinking water supply system. *Journal of Hazardous Materials*, 416, p.125708.
- Johnson, H.A.C., Ball, R., Cross, A.A., Horton, M.D., Jurgens, D.S., Read, J., Vollertsen, C. and Svendsen, M., 2020. Identification and quantification of microplastics in potable water and their sources within water treatment works in England and Wales. *Environmental Science and Technology*, 54, pp.12326-12334.
- Kicińska, A. and Wikar, J., 2023. Health risk associated with soil and plant contamination in industrial areas. *Plant and Soil Journal*. Available at: <https://doi.org/10.1007/s11104-023-06436-2>.
- Kirstein, F.I.V., Hensel, A., Gomiero, A., Iordachescu, L., Vianello, H.B., Wittgren, J. and Vollertsen, J., 2021. Drinking plastics? Quantification and quantification of microplastics in drinking water distribution systems by  $\mu$ FTIR and Py-GCMS. *Water Research*, 188, p.116519.
- Kukkala, A.S. and Moilanen, A., 2013. Core concepts of spatial prioritisation in systematic conservation planning: Concepts of systematic conservation planning. *Biological Reviews*, 88, pp.443-464. Available at: <https://doi.org/10.1111/brv.12008>.
- Lam, T.W.L., Ho, H.T., Ma, A.T. and Fok, L., 2020. Microplastic contamination of surface water-sourced tap water in Hong Kong—a preliminary study. *Applied Sciences*, 10, p.3463.
- Minténig, S.M., Löder, M., Primpke, S. and Gerdt, G., 2019. Low numbers of microplastics detected in drinking water from ground water sources. *Science of the Total Environment*, 648, pp.631-635.
- Pivokonsky, M., Cermakova, L., Novotna, K., Peer, P., Cajthaml, T. and Janda, V., 2018. Occurrence of microplastics in raw and treated drinking water. *Science of the Total Environment*, 643, pp.1644-1651.
- Pivokonský, M., Pivokonská, L., Novotná, K., Čermáková, L. and Klimtová, M., 2020. Occurrence and fate of microplastics at two different drinking water treatment plants within a river catchment. *Science of the Total Environment*, 741, p.140236.
- Ruas, A., Matsumoto, A., Ohba, H., Akaoka, K. and Wakaida, I., 2017. Application of laser induced breakdown spectroscopy to zirconium in aqueous solution. *Spectrochemistry Part B: Atomic Spectroscopy*, 131, pp.99-106.
- Sarkar, D.J., Sarkar, S.D., Das, B.K., Praharaj, J.K., Mahajan, D.K., Purokait, B., Mohanty, T.R., Mohanty, D., Gogoi, P. and Kumar, S., 2021. Microplastics removal efficiency of drinking water treatment plant with pulse clarifier. *Journal of Hazardous Materials*, 413, p.125347.
- Sultan, M., Ajmi, R.N. and Hanno, S.H., 2018. Bioabsorbent of chromium, cadmium and lead from industrial waste water by waste plant. *Journal of Pharmaceutical Sciences and Research*, 10(3), pp.672-674.
- USEPA (United States Environmental Protection Agency), 2009. Method No. 7473.
- World Health Organization, 2013. Ammonia in drinking water - background document for development of WHO guideline for drinking water quality, 4th Ed. WHO Series, Geneva.

---

## ORCID DETAILS OF THE AUTHORS

- Estabraq Mohammed Ati: <https://orcid.org/0000-0002-8411-1060>  
 Rana Fadhil Abbas: <https://orcid.org/0000-0001-7546-2320>  
 Reyam Naji Ajmi: <https://orcid.org/0000-0003-2623-6671>  
 Abdalkader Saeed Latif: <https://orcid.org/0000-0003-1901-9425>



# Technogenically Disturbed Lands of Coal Mines: Restoration Methods

S. Ivanova<sup>1,2†</sup> , A. Vesnina<sup>3</sup> , N. Fotina<sup>4</sup> and A. Prosekov<sup>5</sup>

<sup>1</sup>Department of the Comprehensive Scientific and Technical Program Implementation, Kemerovo State University, Krasnaya Street 6, Kemerovo, 650043, Russia

<sup>2</sup>Department of TNSMD Theory and Methods, Kemerovo State University, Krasnaya Street, 6, Kemerovo 650043, Russia

<sup>3</sup>Natural Nutraceutical Biotesting Laboratory, Kemerovo State University, Krasnaya Street, 6, Kemerovo 650043, Russia

<sup>4</sup>Laboratory of Phytoremediation of Technogenically Disturbed Ecosystems, Kemerovo State University, Krasnaya Street, 6, Kemerovo 650043, Russia

<sup>5</sup>Laboratory of Biocatalysis, Kemerovo State University, Krasnaya Street 6, Kemerovo, 650043, Russia

†Corresponding author: Svetlana Ivanova; pavvm2000@mail.ru

Nat. Env. & Poll. Tech.  
Website: [www.neptjournal.com](http://www.neptjournal.com)

Received: 18-04-2024  
Revised: 15-05-2024  
Accepted: 17-05-2024

## Key Words:

Carbon footprint  
Coal mining enterprises  
Land reclamation  
Biological remediation

## ABSTRACT

The issues of human impact on the environment are evident and pose a threat to the health and well-being of future generations. Technogenic disturbances in coal mining sites, such as open pits, excavations, and industrial waste, pose risks to both human health and the environment. Open-pit coal mines not only frequently cause the destruction of natural ecosystems, including landscapes, vegetation, and biodiversity, but they also significantly contribute to greenhouse gas emissions into the atmosphere. Addressing the carbon footprint necessitates not only the use of renewable energy but also the restoration of disturbed landscapes and vegetation, including trees and shrubs. All of this is achieved by implementing biological remediation within technogenically disturbed territories. This process fosters a return of biological balance and establishes favorable conditions for plant and animal life, while at the same time reducing carbon footprint indicators. The biological remediation of areas affected by the mining activities of coal mines can create new economic opportunities. The reclaimed land can be utilized for various purposes such as agriculture, forestry, park development, and tourism, thereby contributing to local economic growth and job creation. When planning measures for land bioremediation, it is essential to analyze all quality indicators of the land. In this case, the selection of technologies such as plants, fertilizers, and microorganisms can effectively restore territories.

## INTRODUCTION

Human activities in general, and those associated with mining in particular, have a negative impact on ecosystems. The activities of the coal mining industry give rise to a range of environmental concerns that harm the environment. These include the destruction of ecosystems, which can lead to the loss of animal and plant species, deforestation, and a reduction in biodiversity; additionally, there is a risk of soil degradation and the release of greenhouse gases, which contribute to global climate change and the gradual warming of the planet; health of people, especially those living localized near the mine; pollution of water resources; damage to the landscape with deformation of the land surface). All of these factors necessitate the search for and development of environmentally friendly, green, and long-term alternative technologies for obtaining energy, producing goods in an environmentally responsible manner, and reducing the negative impact of mining activities on

the environment. A targeted, comprehensive program is required to restore natural systems that have been damaged by human activities to preserve ecosystems for future generations. Measures to restore damaged landscapes and improve fertile soil quality hold a special place. In general, biological remediation of technogenically disturbed areas of coal mines contributes significantly to nature conservation, environmental rehabilitation, and the improvement of people's lives. Biological remediation can help to create a clean and healthy living environment, which benefits the overall health and well-being of the community.

We consider forestry and agricultural purposes of land reclamation to be the priority areas of land reclamation (Vesnina & Fotina 2023). The main stages of land remediation implementation are depicted in Fig. 1.

The choice of reclamation direction is primarily motivated by the need to organize efficient, cost-effective territory restoration. It is necessary to observe the following

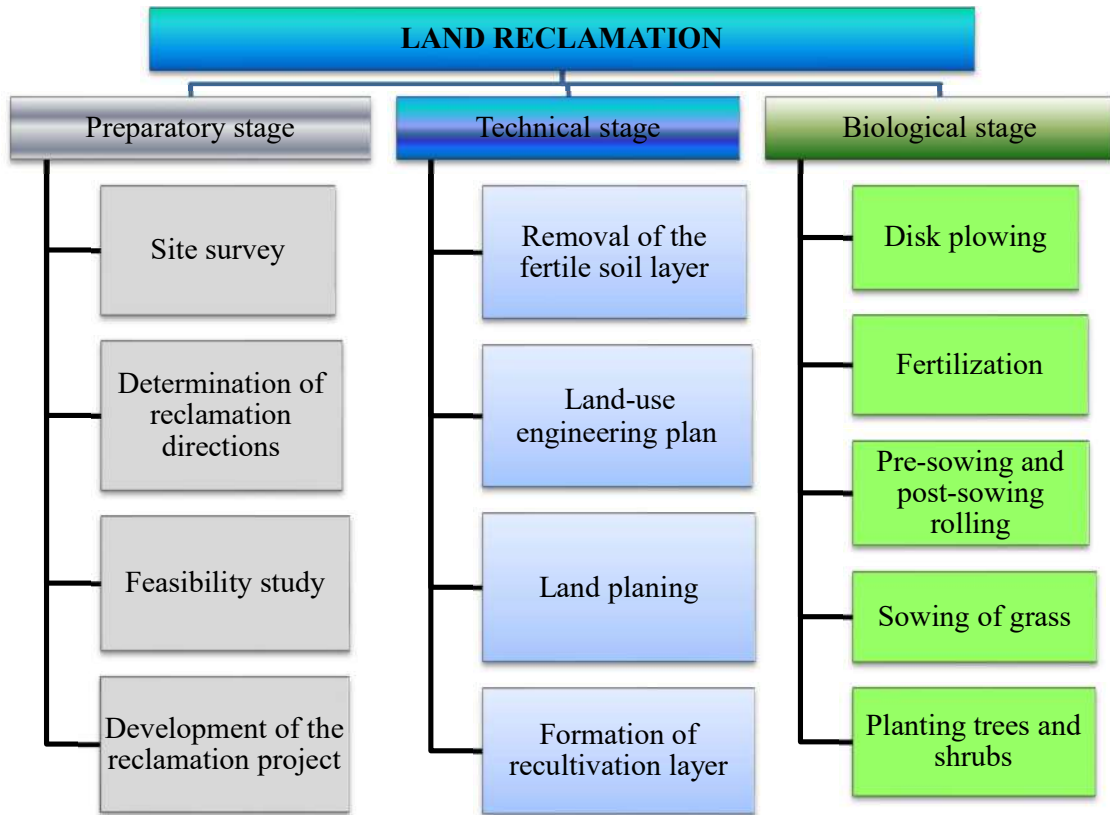


Fig. 1: Main stages of reclamation of technogenically disturbed lands.

conditions: Planning works to ensure soil stability in the process of realization of the technical stage of reclamation; the need to incorporate a comprehensive range of agro-technical and biological measures into the biological phase of biological reclamation of disturbed land to establish conditions for the restoration of biological productivity; production wastes of hazard class I-IV are not used in the reclamation process; to restore disturbed lands for forestry and/or agricultural use, all planned agrotechnical and phyto ameliorative measures will be carried out as part of the biological phase of reclamation (the application of mineral fertilizers, the sowing and planting of plants, and the maintenance of plants are carried out until the land is transferred to the owner; zonal biological rehabilitation of disturbed lands is carried out as part of the biological stage of land reclamation).

The study aimed to analyze existing foreign and domestic experience in the field of reclamation of technogenically disturbed lands.

## MATERIALS AND METHODS

### Objectives of the Study

The primary methods and technologies for reclaiming

technogenically disturbed lands, including coal mines, were the focus of the research. The was based on a bibliographic search and subsequent critical analysis of net resources and scientific manuscripts devoted to environmental problems and solutions to coal mining.

### Research Methods

The explorer was based on a bibliographic search and subsequent critical analysis of net resources and scientific manuscripts devoted to environmental problems and solutions of coal mining. Materials from open Internet sources and Scopus citation database were used. Considering the dynamism of reclamation technique development and the problem of technogenically disturbed lands, the depth of the search was limited primarily to the last five years, with the utility of citing some earlier works on specific issues of restoration of disturbed lands, phyto- and reclamation determined by the uniqueness and peculiarity of the results provided in them.

## RESULTS AND DISCUSSION

Plants stimulate the growth and activity of soil microbes, releasing organic and nutritive substances and oxygen

and enriching the microenvironment. It is also known that the synergistic interaction of microorganisms, plants, and the organic matter they excrete ensures the preservation of ecosystem integrity (Masciandaro et al. 2013). Phytoremediation is now recognized not only as the use of green plants to remove or neutralize environmental pollutants but also as a green biotechnology tool (Pilon-Smits 2005, Masciandaro et al. 2013). Plants create a rich micro-environment within the framework of this technology, providing microorganisms with activity and reproduction conditions via nutrients, oxygen, and organic materials. All of these together are necessary for the successful implementation of sustainable practices to restore environments such as air, water, and soil (Kurade et al. 2021, Wei et al. 2021). The soil structure restoration strategy is based on stimulating appropriate soil microbial communities and restoring nutrient flux function to disturbed soils. This flow of metabolites into the soil is ensured by plant-microbe interactions (Jansson & Hofmockel 2018).

This integration must take into account both the ability of microorganisms to utilize coal waste and/or carbon-containing pollutants to enrich soils during remediation and the ability of vegetation to capture both macro- and micronutrients by uptake through root cells. The main goal of reclamation remains the formation of necessary effective complexes in the soil to ensure the accumulation of humic compounds while ensuring the maintenance of plant and vegetation growth on the rehabilitated soil.

The mycophytoremediation strategy was developed for *Fungcoa* rehabilitation of surface waste and coal dumps (Sekhohola-Dlamini et al. 2022, Cowan et al. 2016). This strategy utilizes the fungal-plant symbiotic relationship to achieve the biodegradation of any carbon-based pollutant while promoting the activation of soil constituents and plant growth to support long-term restoration at South African mining sites. On this issue, several extensive reviews on this issue have been published (Stahl et al. 1988, Claassens et al. 2006). Bacteria-plant interactions (bioremediation) were proposed as a potential approach to the remediation of hydrocarbon-contaminated soils. (Claassens et al. 2006, Šourková et al. 2005). The paper (Wenzel 2009) provides a comprehensive report on rhizosphere control of microorganism-plant associations, bioavailability of organic and metalloid pollutants, effects on biodegradation, and the prospects of rhizosphere processing for management in soil phytoremediation. Multi-polluted soils are complex and varied, necessitating a holistic approach rhizosphere management process. This process employs a complex approach of the coal-derived and/or utilizing hydrocarbon microbes, and phytoextraction of contaminants to achieve desired soil and land management objectives.

Thus, the combination of plants *A. retroflexus* L., *Salix schwerinii* E.L. Wolf and microorganisms *Pleurotus ostreatus*, *Pseudomonas frederiksbergensi* for soils containing excessive amounts of nickel; *Solanum nigrum* L. and *Klebsiella pneumonia* for soils with arsenic; plants *Brassica juncea* (L.) Coss, *Pinus sylvestris* Lour., *Solanum nigrum* L. with microorganisms *Aspergillus fumigatus*, *Aspergillus niger*, *Azotobacter chroococcum*, *Cupriavidus taiwanensis*, *Enterobacter hormaechei*, *Klebsiella pneumonia*, *Pseudomonas putida*, *Rhizobium leguminosarum* bv. *Trifolii* and *Penicillium rubens* for soils with cadmium.

The use of biodegradable geotextile material (which includes natural fibers) is promising for improving soil fertility (Wu et al. 2020). Geotextiles can provide optimal conditions for seed germination and soil microflora development because they contain a variety of nutrients, can accumulate an optimal amount of moisture, and are an effective means of controlling soil erosion (Broda et al. 2020).

Thus, measures utilizing plants and microorganisms capable of accumulating these substances are effective in reducing heavy metal content. There are known papers (Hernandez-Rivera et al. 2011, Ibrahim et al. 2013, Obayori et al. 2017, Bechtaoui et al. 2019, Olawale et al. 2020, Smulek et al. 2020) that show that microorganism strains effective in coal bioconversion stimulate plant growth, most likely due to the production of organic acids (Borgi et al. 2020). Eventually, bacterial-plant interactions may lead to the development of candidate strains for a bioprocess to treat, stabilize, and even restore disturbed soils (Titilawo et al. 2020).

The use of biochar has the potential to help normalize pH levels and increase soil fertility. Biochar (charcoal) is a carbon and ash-containing product of oxygen-free pyrolysis of plant biomass (Ahmad et al. 2014). According to studies, biochar application helps to increase low soil pH values, affects nitrification and ammonification processes, increases the C/N ratio, is a phosphorus source, and increases soil cation exchange capacity, resulting in less leaching due to nutrient retention. This favors the development of microorganisms even in soil with low organic matter content (Nurhidayati & Mariati 2014, DeLuca et al. 2015, Rogovska et al. 2020).

Liming (using organic lime-sugar beet lime) and the application of composted solid organic matter into the fertile soil layer to reduce soil acidity, data on the reclamation of a copper mine (Poderosa deposit, Spain) (Fernández-Caliani et al. 2021).

Gypsumization and acidification of soils are used to reduce the alkaline pH of soils to a neutral value. Sodium is

replaced by calcium during gypsumization (the incorporation of gypsum and other industrial wastes into the soil, such as phosphogypsum—a waste product of mineral fertilizers, phosphoric acid, and phosphate fertilizers) (Bituh et al. 2021). During acidification, soils are acidified through the application of sulfur, sodium disulfate, etc. (Orlov et al. 1991).

One of the directions of phosphogypsum utilization considered in the paper (Chernysh et al. 2021) is the use of phosphogypsum as a mineral carrier for groups of useful microorganisms in bioprocesses of detoxification of environmental components, including technogenically disturbed lands of coal dumps.

Humic preparations have confirmed their effectiveness in heavy metal detoxification measures. Humic preparations for soil detoxification and remediation are natural solid, paste-like, or liquid substances produced by alkaline treatment of brown and oxidized hard coal (Gilmanova & Grekhova 2018, Stepanov et al. 2018). It has been found that humic preparations can bind metals, reducing their solubility, bioavailability, and mobility (Zhao et al. 2022).

Alternatively, specialized microorganisms can produce humic substances on-site from coal production waste. Under aerobic conditions, both abiotic and biotic processes oxidize coal to a weathered substance rich in humic substances (Romanowska et al. 2015). A group of bacterial enzymes,

both primary and secondary, depolymerize and metabolize carbon, producing a diverse range of alcohols and short-chain organic acids in anaerobic environments (Valero et al. 2014). These low-molecular-weight organic compounds, which include acetogens and methanogens, serve as substrates for a variety of microbial communities (Jones et al. 2008, Yin et al. 2009, Štrapoč et al. 2011, Huang et al. 2013). The study (van Breugel et al. 2019) used weathered coal from South African mines to produce fungi with specific characteristics to produce fungocoal, which was intended to be used to rehabilitate the lands of exhausted territories as a source of humic material as well as biofertilizers (Canellas et al. 2012, Sekhohola et al. 2013).

The recommendations for rehabilitating mine wastelands are presented in Table 1.

## CONCLUSION

The reclamation of technologically disturbed coal mine lands is essential for humanity's conscious transition to sustainable development and the use of natural resources while preserving the environment for future generations. In this situation, it is impossible to do without recultivation of land disturbed by anthropogenic impacts. Often, a compelling reason to restore disturbed lands is legal requirements that coal and/or mining companies restore disturbed lands and

Table 1: Remediation methods for disturbed lands of mines.

Indicators	Methods	References
Land rehabilitation	Bioremediation (phytoremediation + microorganisms)	(Stahl et al. 1988, Šourková et al. 2005, Claassens et al. 2006a, Claassens, et al. 2006b)
Soil fertility improvement	Biodegradable geotextile material	(Broda et al. 2020, Wu et al. 2020)
Normalization of pH, soil fertility improvement	Biochar	(Ahmad et al. 2014, Nurhidayati & Mariati 2014, Rogovska et al. 2014, DeLuca et al. 2015, Ghosh & Maiti 2020)
Soil acidity reduction	Liming (sugar beet lime)+ composted biosolids	(Fernández-Caliani et al. 2021)
Soil alkalinity reduction	Gypsification (application of gypsum, phosphogypsum, etc.) + acidification (application of sulphur, sodium disulphate, etc.) of soils	(Orlov et al. 1991, Bituh et al. 2021)
Heavy metal detoxification	Humic preparations	(Gilmanova & Grekhova 2018, Stepanov et al. 2018, Zhao et al. 2022)
Nickel detoxification	Plants ( <i>A. retroflexus</i> L., <i>Salix schwerinii</i> E. L. Wolf) + microorganisms ( <i>Pseudomonas frederiksbergensis</i> , <i>Pleurotus ostreatus</i> ).	(Stahl et al. 1988, Šourková et al. 2005, Claassens et al. 2006a, Claassens, et al. 2006b, Wenzel 2009)
Arsenic detoxification	<i>Solanum nigrum</i> L. + <i>Klebsiella pneumoniae</i> .	(Stahl et al. 1988, Šourková et al. 2005, Claassens et al. 2006a, Claassens, et al. 2006b, Wenzel 2009)
Cadmium detoxification	Plants ( <i>Brassica juncea</i> (L.) Coss, <i>Pinus sylvestris</i> Lour., <i>Solanum nigrum</i> L.) + microorganisms ( <i>Aspergillus fumigates</i> , <i>Aspergillus niger</i> , <i>Azotobacter chroococcum</i> , <i>Cupriavidus taiwanesis</i> , <i>Enterobacter hormaechei</i> , <i>Klebsiella pneumonia</i> , <i>Penicillium rubens</i> , <i>Rhizobium leguminosarum</i> bv. <i>trifolii</i> , <i>Pseudomonas putida</i> )	(Stahl et al. 1988, Šourková et al. 2005, Claassens et al. 2006a, Claassens, et al. 2006b, Wenzel 2009)



pay for environmental damages. Nonetheless, the benefits of restoring disturbed nature outweigh any moral concerns.

Restoration of such technogenically disturbed lands helps to restore the disturbed environment (vegetation, soil, water resources, landscape, fauna). Restored land is returned to agricultural use and/or reforestation, which is especially important in an era of global food security and hunger alleviation. In addition, the reclamation of anthropogenically disturbed land contributes to local quality improvement. Biological remediation is one of the existing technologies that can help restore ecosystems by reconstructing and rehabilitating areas using natural processes and mechanisms. Only limited data on the state of agrochemical characteristics, hygienic indicators, and soil pollutant content do not allow for the immediate organization of effective reclamation stages. Up-to-date data on soil quality is needed to compare “before” and “after” reclamation measures, which, together with modern scientific approaches, will allow the overall reclamation process to be intensified.

## ACKNOWLEDGEMENTS

This research was funded by the Russian Science Foundation and Ministry of Science, Higher Education and Youth Policy of Kuzbass, Grant number 22-14-20011.

## REFERENCES

- Ahmad, M., Rajapaksha, A.U., Lim, J.E., Zhang, M., Bolan, N., Mohan, D., Vithanage, M., Lee, S.S. and Ok, Y.S., 2014. Biochar as a sorbent for contaminant management in soil and water: A review. *Chemosphere*, 99, pp.19–33.
- Bechtaoui, N., Raklami, A., Tahiri, A.-I., Benidire, L., El Alaoui, A., Meddich, A., Gottfert, M. and Oufdou, K., 2019. Characterization of plant growth promoting rhizobacteria and their benefits on growth and phosphate nutrition of faba bean and wheat. *Biology Open*, 8, bio043968. Available at: <https://doi.org/10.1242/bio.043968>
- Bituh, T., Petrinc, B., Skoko, B., Babić, D. and Rašeta, D., 2021. Phosphogypsum and its potential use in Croatia: Challenges and opportunities. *Arhiv za Higijenu Rada i Toksikologiju*, 72(3), pp.93–100.
- Borgi, M.A., Saidi, I., Moula, A., Rhimi, S. and Rhimi, M., 2020. The attractive *Serratia plymuthica* BMA1 strain with high rock phosphate-solubilizing activity and its effect on the growth and phosphorus uptake by *Vicia faba* L. plants. *Geomicrobiology Journal*, 37, pp.437–445.
- Broda, J., Franitz, P., Herrmann, U., Helbig, R., Große, A., Grzybowska-Pietras, J. and Rom, M., 2020. Reclamation of abandoned open mines with innovative meandrically arranged geotextiles. *Geotextiles and Geomembranes*, 48(3), pp.236–242.
- Canellas, L.P., Dobbss, L.B., Oliveira, A.L., Chagas, J.G., Aguiar, N.O., Rumjanek, V.M., Novotny, E.H., Olivares, F.L., Spaccini, R. and Piccolo, A., 2012. Chemical properties of humic matter as related to induction of plant lateral roots. *European Journal of Soil Science*, 63, pp.315–324.
- Chernysh, Y., Yakhnenko, O., Chubur, V. and Roubík, H., 2021. Phosphogypsum recycling: a review of environmental issues, current trends, and prospects. *Applied Sciences*, 11, 1575. Available at: <https://doi.org/10.3390/app11041575>
- Claassens, S., Jansen Van Rensburg, P.J. and Van Rensburg, L., 2006a. Soil microbial community structure of coal mine discard under rehabilitation. *Water Air Soil Pollution*, 174, pp.355–366.
- Claassens, S., Riedel, K.J., Van Rensburg, L., Bezuidenhout, J.J. and Jansen van Rensburg, P.J., 2006b. Microbial community function and structure on coal mine discard under rehabilitation. *South African Journal of Plant and Soil*, 23, pp.105–112.
- Cowan, A.K., Lodewijks, H.M., Sekhohola, L.M. and Edeki, O.G., 2016. In situ bioremediation of South African coal discard dumps. In: Fourie, A.B., Tibbett, M. (eds) *Proceedings of the Mine Closure 2016. 11th International Conference on Mine Closure* (Perth, Australia, 15–17 March 2016), Australian Centre for Geomechanics: Perth, Australia, pp.501–509.
- DeLuca, T.H., Gundale, M.J., MacKenzie, M.D. and Jones, D.L., 2015. Biochar effects on soil nutrient transformations. In: Lehmann, J., Joseph, S. (eds) *Biochar for Environmental Management: Science, Technology and Implementation*, 2, pp.421–454.
- Fernández-Caliani, J.C., Giráldez, M.I., Waken, W.H., Del Río, Z.M. and Córdoba, F., 2021. Soil quality changes in an Iberian pyrite mine site 15 years after land reclamation. *Catena*, 206, 105538. Available at: <https://doi.org/10.1016/j.catena.2021.105538>
- Ghosh, D. and Maiti, S.K., 2020. Can biochar reclaim coal mine spoil? *Journal of Environmental Management*, 272, 111097. Available at: <https://doi.org/10.1016/j.jenvman.2020.111097>
- Gilmanova, M.V. and Grekhova, M.V., 2018. Evaluation of the use of humic preparations for biological reclamation. *The World of Innovation*, 1–2, pp.4–9. (In Russian).
- Hernandez-Rivera, M.A., Ojeda-Morales, M.E., Martinez-Vazquez, J.G., Villegas-Cornelio, V.M. and Cordova-Bautista, Y., 2011. Optimal parameters for in vitro development of the hydrocarbonoclastic microorganism *Proteus* sp. *Journal of Soil Science and Plant Nutrition*, 11, pp.29–43.
- Huang, Z., Urynowicz, M.A. and Colberg, P.J.S., 2013. Bioassay of chemically treated subbituminous coal derivatives using *Pseudomonas putida* F1. *International Journal of Coal Geology*, 115, pp.97–105.
- Ibrahim, M.L., Ijah, U.J.J., Manga, S.B., Bilbis, L.S. and Umar, S., 2013. Production and partial characterization of biosurfactant produced by crude oil degrading bacteria. *International Biodeterioration & Biodegradation*, 81, pp.28–34.
- Jansson, J.K. and Hofnackel, K.S., 2018. The soil microbiome - From metagenomics to metaproteomics. *Current Opinion in Microbiology*, 43, pp.162–168.
- Jones, E.J.P., Voytek, M.A., Warwick, P.D., Corum, M.D., Cohn, A., Bunnell, J.E., Clark, A.C. and Orem, W.H., 2008. Bioassay for estimating the biogenic methane generating potential of coal samples. *International Journal of Coal Geology*, 76, pp.138–150.
- Kurade, M.B., Ha, Y.-H., Xiong, J.-Q., Govindwar, S.P., Jang, M. and Jeon, B.-H., 2021. Phytoremediation as a green biotechnology tool for emerging environmental pollution: A step forward towards sustainable rehabilitation of the environment. *Chemical Engineering Journal*, 415, 129040. Available at: <https://doi.org/10.1016/j.cej.2021.129040>
- Masciandaro, G., Macci, C., Ceccanti, B. and Doni, S., 2013. Organic matter-microorganism-plant in soil bioremediation: A synergic approach. *Reviews in Environmental Science and Biotechnology*, 12, pp.399–419. Available at: <https://doi.org/10.1007/s11157-013-9313-3>
- Nurhidayati, N. and Mariati, M., 2014. Utilization of maize cob biochar and rice husk charcoal as soil amendment for improving acid soil fertility and productivity. *Journal of Degraded and Mining Lands Management*, 2, pp.223–230. Available at: <https://doi.org/10.15243/jdmlm.2014.021.223>
- Obayori, O.S., Salam, L.B., Oyetibo, G.O., Idowu, M. and Amund, O.O., 2017. Biodegradation potentials of polyaromatic hydrocarbon (pyrene and phenanthrene) by *Proteus mirabilis* isolated from an animal charcoal polluted site. *Biocatalysis and Agricultural Biotechnology*, 12, pp.78–84.

- Olawale, J.T., Edeki, O.G. and Cowan, A.K., 2020. Bacterial degradation of coal discard and geologically weathered coal. *International Journal of Coal Science & Technology*, 7, pp.405–416.
- Orlov, D.S., Malinina, M.S., Motuzova, G.V., Sadovnikova, L.K. and Sokolova, T.A., 1991. *Chemical pollution of soils and their protection: A dictionary-reference*. Agropromizdat, Moscow, pp.303. (In Russian).
- Pilon-Smits, E., 2005. Phytoremediation. *Annual Review of Plant Biology*, 56, pp.15–39.
- Rogovska, N., Laird, D.A., Rathke, S.J. and Karlen, D.L., 2014. Biochar impact on Midwestern Mollisols and maize nutrient availability. *Geoderma*, 230–231, pp.340–347. Available at: <https://doi.org/10.1016/j.geoderma.2014.04.009>
- Romanowska, I., Strzelecki, B. and Bielecki, S., 2015. Biosolubilization of Polish brown coal by *Gordonia alkanivorans* S7 and *Bacillus mycoides* NS1020. *Fuel Processing Technology*, 131, pp.430–436.
- Sekhohola, L.M., Igbinigie, E.E. and Cowan, A.K., 2013. Biological degradation and solubilisation of coal. *Biodegradation*, 24(3), pp.305–318.
- Sekhohola-Dlamini, L.M., Keshinro, O.M., Masudi, W.L. and Cowan, A.K., 2022. Elaboration of a phytoremediation strategy for successful and sustainable rehabilitation of disturbed and degraded land. *Minerals*, 12, 111. Available at: <https://doi.org/10.3390/min12020111>
- Smulek, W., Sydow, M., Zabielska-Matejuk, J. and Kaczorek, E., 2020. Bacteria involved in biodegradation of creosote PAH - A case study of long-term contaminated industrial area. *Ecotoxicology and Environmental Safety*, 187, 109843. Available at: <https://doi.org/10.1016/j.ecoenv.2019.109843>
- Šourková, M., Frouz, J., Fettweis, U., Bens, O., Hüttl, R. and Šantrůčková, H., 2005. Soil development and properties of microbial biomass succession in reclaimed post mining sites near Sokolov (Czech Republic) and near Cottbus (Germany). *Geoderma*, 129, pp.73–80.
- Stahl, P.D., Williams, S.E. and Christensen, M., 1988. Efficacy of native vesicular-arbuscular mycorrhizal fungi after severe soil disturbance. *New Phytologist*, 110, pp.347–354.
- Stepanov, A.A., Shulga, P.S., Gosse, D.D. and Smirnova, M.E., 2018. Application of natural humates for remediation of polluted urban soils and stimulation of plant growth. *Bulletin of the Moscow University. Series 17: Soil Science*, 2, pp.30–34. (In Russian).
- Strapoć, D., Mastalerz, M., Dawson, K., Macalady, J., Callaghan, A.V., Wawrik, B., Turich, C. and Ashby, M., 2011. Biogeochemistry of microbial coal-bed methane. *Annual Review of Earth and Planetary Sciences*, 39, pp.617–656.
- Titilawo, Y., Masudi, W.L., Olawale, J.T., Sekhohola-Dlamini, L.M. and Cowan, A.K., 2020. Coal-degrading bacteria display characteristics typical of plant growth promoting rhizobacteria. *Processes*, 8, 1111. Available at: <https://doi.org/10.3390/pr8091111>
- Valero, N., Gómez, L., Pantoja, M. and Ramírez, R., 2014. Production of humic substances through coal-solubilizing bacteria. *Brazilian Journal of Microbiology*, 45, pp.911–918.
- van Breugel, Y., Cowan, A.K. and Tsikos, H., 2019. Geochemical study of weathered coal, a co-substrate for bioremediation of south african coal discard dumps. *Minerals*, 9, 772. Available at: <https://doi.org/10.3390/min9120772>
- Vesnina, A.D. and Fotina, N.V., 2023. Principles of recultivation of coal mines of the Kemerovo region. In: *Scientific Research of Young Scientists. Proceedings of the XXIII International Scientific and Practical Conference* (Penza, 2023), Science and Education, Penza, Russia, pp.23–25. (In Russian).
- Wei, Z., Van Le, Q., Peng, W., Yang, Y., Yang, H., Gu, H., Lam, S.S. and Sonne, C., 2021. A review on phytoremediation of contaminants in air, water and soil. *Journal of Hazardous Materials*, 40(3), 123658. Available at: <https://doi.org/10.1016/j.jhazmat.2020.123658>
- Wenzel, W.W., 2009. Rhizosphere processes and management in plant-assist bioremediation (phytoremediation) of soils. *Plant and Soil*, 321, pp.385–408.
- Wu, H., Yao, C., Li, C., Miao, M., Zhong, Y., Lu, Y. and Liu, T., 2020. Review of application and innovation of geotextiles in geotechnical engineering. *Materials*, 13(7), 1774. Available at: <https://doi.org/10.3390/ma13071774>
- Yin, S., Tao, X., Shi, K. and Tan, Z., 2009. Biosolubilisation of Chinese lignite. *Energy*, 34, pp. 775–781.
- Zhao, K., Yang, Y., Peng, H., Zhang, L., Zhou, Y., Zhang, J., Du, C., Liu, J., Lin, X., Wang, N., Huang, H. and Luo, L., 2022. Silicon fertilizers, humic acid and their impact on physicochemical properties, availability and distribution of heavy metals in soil and soil aggregates. *Science of The Total Environment*, 822, 153483. Available at: <https://doi.org/10.1016/j.scitotenv.2022.153483>

---

#### ORCID DETAILS OF THE AUTHORS

- S. Ivanova: <https://orcid.org/0000-0002-1252-9572>  
 A. Vesnina: <https://orcid.org/0000-0002-4552-7418>  
 N. Fotina: <https://orcid.org/0000-0002-7655-0258>  
 A. Prosekov: <https://orcid.org/0000-0002-5630-3196>



# Fitting Probability Distributions and Statistical Trend Analysis of Rainfall of Agro-climatic Zone of West Bengal

Bhawishya Pradhan, Banjul Bhattacharyya, N. Elakkiya and T. Gowthaman†

Department of Agricultural Statistics, Bidhan Chandra Krishi Vishwavidyalaya, West Bengal, India

†Corresponding author: T. Gowthaman; agrigowtham77@gmail.com

Nat. Env. & Poll. Tech.  
Website: [www.neptjournal.com](http://www.neptjournal.com)

Received: 28-02-2024

Revised: 25-03-2024

Accepted: 05-04-2024

## Key Words:

Rainfall  
Probability distribution  
Mann-Kendall test  
Agro-climatic zones

## ABSTRACT

This research aimed to identify the most appropriate probability distribution for modeling average monthly rainfall in the agro-climatic zones of West Bengal and to detect any trends in this data. The study utilized historical rainfall data spanning 51 years (1970-2020) obtained from the IMD in Pune. To determine the best-fitting distribution and assess trends, 23 different probability distributions were employed, with the Mann-Kendall test and Sen's slope estimator used for trend analysis. Goodness-of-fit tests, including the Kolmogorov-Smirnov, Anderson-Darling, and Chi-square tests, were employed to determine the most suitable distribution. The findings indicated that the Generalized Extreme Value, Gamma, and Lognormal (3-parameter) distributions were the best fits for two specific districts. The monthly rainfall distributions can be effectively used for predicting future monthly rainfall events in the region. The Mann-Kendall test revealed an increasing trend in rainfall for Kalimpong and Nadia Districts and a decreasing trend for Malda District.

## INTRODUCTION

As climate change faces unprecedented changes, the stability of atmospheric conditions that administer rainfall is being disrupted, leading to a reflective influence on rainfall patterns, distribution, intensity, and frequency. The production and policy-induced abatement operations of the agricultural economy are highly affected by the impact of climate change (Mandal et al. 2013). One of the most obvious impacts of climate change on rainfall is the increase in extreme weather events and the effects of cropping systems and production. Intense and long-lasting periods of rainfall, often accompanied by harsh storms and flooding, have become frequent phenomena in many regions. Moreover, in India-like countries, the agriculture and allied sectors are highly dependent on the monsoon rains that occur between June to mid-October (Sathish et al. 2017). The active monsoon period rainfall is vital for irrigating crops, restocking water reservoirs, and sustaining groundwater levels. In many regions where irrigation infrastructure is limited, the timely arrival and distribution of monsoon rainfall is a vital source of agricultural productivity. Only adequate rainfall can ensure soil moisture balance which is essential for crop growth, development, and yield. Increasingly erratic, unpredictable monsoons coupled with extended dry spells disrupt agricultural planning, constrain crop growth, and increase the risk of pests and disease attacks. Thus, a climate change-induced hazard in rainfall

patterns is a significant challenge to agriculture (Dastidar et al. 2010).

The distinctive characteristics of West Bengal confine the sub-Himalayan in the north and coastal region in the south which makes the state disparate rainfall and cropping pattern in the agro-climatic zones. Hence, the state embraces the six agro-climatic zones namely Northern hilly, Terai-Teesta alluvial, Gangetic alluvial, Vindhyan alluvial, Undulating Red and Laterite and Coastal saline zone with their annual rainfall ranging from 1700 to 3550 mm (Mondal 2021). The state is at the forefront of inland fish, rice, and jute production and the second largest producer of potatoes owing to having expanded alluvial plains in Gangetic and Vindhyan alluvial zones and river basins namely the Ganga at the area of 81%, the Brahmaputra (12%) and Subarnarekha (Bandyopadhyay et al. 2014).

Studied probability analysis of daily maximum rainfall data for 37 years in six distinct locations of West Bengal to find out the best distribution model that could represent rainfall extremities, the sum of rank results revealed that Log Pearson type 3 distributions were best fit for three geographical places, namely Kharagpur, Bolpur, and Balurghat, Gumble distribution and Log logistic for Kolkata and Darjeeling, respectively (Basak et al. 2019). The distribution of Log-Logistic, Generalized Extreme Value, Pearson 5, Log-Pearson 3, 3-parameter Dagum, 4-parameter Generalized Gamma, and 3-parameter Generalized Gamma

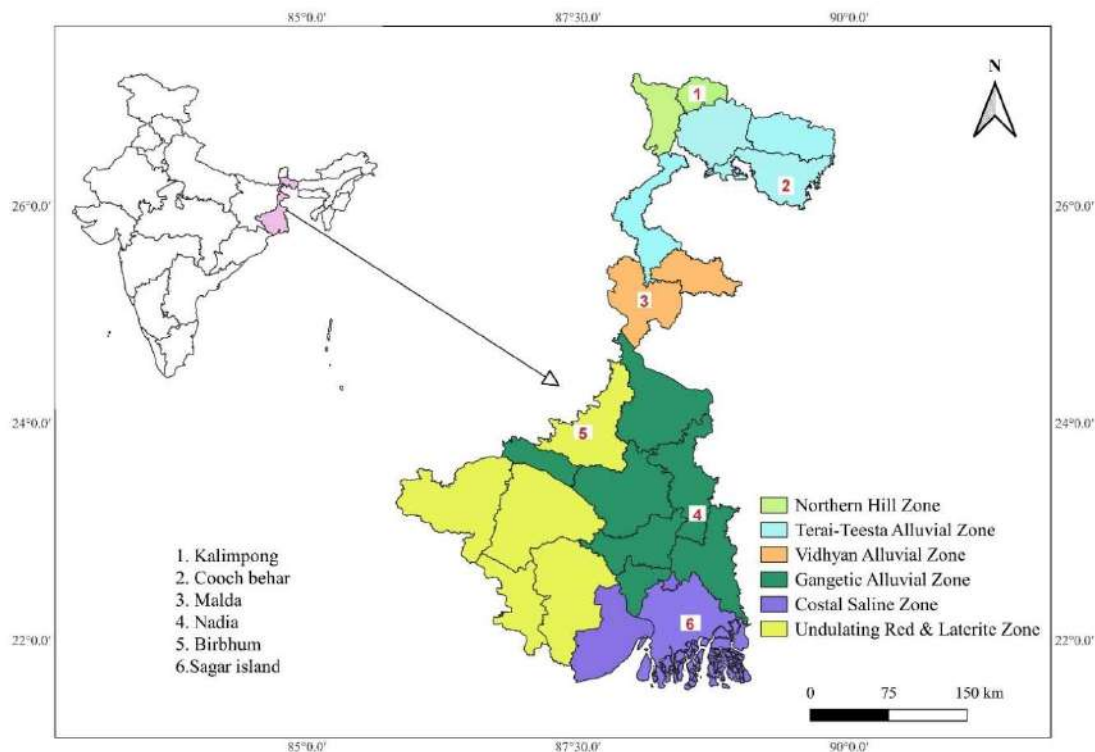


Fig. 1: Selected observatory in agro-climatic zones of West Bengal.

turned out to be best fit for monthly rainfall time series data from 1901 to 2013 in thirteen districts of Gangetic West Bengal (Pal & Majumdar 2015), Generalized Pareto distribution as best daily seasonal rainfall data from June to September in Nanded district (Alam et al. 2018), the best-fitted distribution for daily maximum rainfall in Karnataka is selected according to goodness of fit criteria mainly Kolmogorov-Smirnov, Anderson Darling and Chi-squared (Bhavyashree & Bhattacharyya 2018). Existing monotonically increasing and decreasing trends by Mann-Kendal Test and Sen's slope estimator test to assess their strength (Gowthaman et al. 2023). Due to climate change long-term upward and downward significant rainfall trends in West Kalimantan (Aditya et al. 2021) and rainfall trend analysis using Mann-Kendal and Sen's slope estimator test in Vamanapuram River basin, South Kerala (Brema 2018). Thus, the present study emphasizes the identification of the best-fitted probability distribution to model rainfall amounts by comparing different probability distributions for agro-climatic regions of West Bengal. Moreover, patterns or trends of climatic variables (Rainfall) have been examined.

## MATERIALS AND METHODS

Rainfall data for six districts, namely Kalimpong, Malda,

Coochbehar, Nadia, Birbhum, and Sagar Island, located in different agro-climatic zones, was collected from the Indian Meteorological Department (IMD) in Pune. The dataset covers a time frame of 51 years (1970 -2020). This data pertains to seasonal rainfall and specifically represents the average precipitation occurring during the active monsoon period, spanning from June to October. Fig. 1 provides a visual representation of the selected district within each corresponding agro-climatic zone.

## Fitting Probability Distributions

The study involved the use of 23 different continuous probability distribution models to assess their goodness of fit. Three statistical tests, namely the Kolmogorov-Smirnov, Anderson-darling, and Chi-Squared tests, were applied to evaluate the suitability of these selected distributions for seasonal rainfall data recorded during the monsoon period from June to October. Each GOF test generated a test statistic, which was then tested at a significance level of  $\alpha=0.05$ . Subsequently, for each of the three GOF tests, individual rankings were assigned to all the distributions based on their test statistic values. A ranking-based scoring technique was employed to identify the most appropriate distribution for monthly rainfall data, following the methodology outlined

Table 1: Description of continuous probability distributions.

S No.	Distribution	Probability density Function f(x)	Parameters
1	Beta	$f(x) = \frac{1}{B(m, n)} x^{m-1} (1-x)^{n-1}$	m, n = Shape
2	Chi-squared	$f(x) = \frac{1}{2^{k/2} \Gamma(k/2)} \exp\left(-\frac{x}{2}\right) \left(\frac{x}{2}\right)^{\frac{k}{2}-1}$	K= Degree of freedom
3	Chi-squared (2P)	$f(x) = \frac{(x-\gamma)^{\nu/(2-1)} \exp^{-(x-\gamma)/2}}{2^{\nu/2} \Gamma(\nu/2)}$	$\nu$ = Degrees of freedom $\gamma$ = Location
4	Exponential	$f(x) = \lambda e^{-\lambda x}$	$\lambda$ =constant rate
5	Exponential (2P)	$f(x) = \lambda e^{-\lambda(x-\gamma)}$	$\lambda$ =Rate $\gamma$ =Location
6	Gamma	$f(x) = \frac{(x)^{\alpha-1}}{\beta^\alpha \Gamma(\alpha)} e^{-\frac{x}{\beta}}$	$\alpha$ =Shape $\beta$ = Scale
7	Gamma (3P)	$f(x) = \frac{(x-\gamma)^{\alpha-1}}{\beta^\alpha \Gamma(\alpha)} e^{-(x-\delta)/\beta}$	$\alpha$ = Shape $\beta$ = Scale $\gamma$ = Location
8	Gen. Extreme value	$f(x) = \begin{cases} \frac{1}{\sigma} \exp\left(-\left(1+kz\right)^{-\frac{1}{k}}\left(1+kz\right)^{-1-\frac{1}{k}}\right) & k \neq 0 \\ \frac{1}{\sigma} \exp(-z - \exp(-z)) & k = 0 \end{cases}$	$\alpha$ = Shape $\beta$ = Scale $\gamma$ = Location
9	Gen.Pareto	$f(x) = \frac{1}{\sigma} (1 + \xi z)^{-\left(\frac{1}{\xi}+1\right)}$ Where, $z = \frac{x-\mu}{\sigma}$	$\sigma$ = Shape $\xi$ = Scale $\mu$ = Location
10	Gumbel Max	$f(x) = \frac{1}{\sigma} \exp(-z - \exp(-z))$ Where, $f(x) = \frac{x-\mu}{\sigma}$	$\sigma$ = Scale $\mu$ =Location
11	Laplace	$f(x) = \frac{1}{2} \lambda \exp^{-\lambda x-\mu }$	$\lambda$ = Scale $\mu$ = Location
12	Logistic	$f(x) = \frac{1}{1 + e^{-\frac{(x-\alpha)}{\beta}}}$	$\alpha$ = Location $\beta$ = Scale
13	Lognormal	$f(\log x) = \frac{1}{\sigma x \sqrt{2\pi}} \exp^{-\frac{1}{2} \left(\frac{\log x - \mu}{\sigma}\right)^2}$	$\mu$ = Scale $\sigma^2$ = Shape

Table cont...

S No.	Distribution	Probability density Function f(x)	Parameters
14	Lognormal (3P)	$\frac{\exp\left[-\frac{1}{2}\left[\frac{\ln(x-\gamma)-\mu}{\sigma}\right]^2\right]}{(x-\gamma)\sigma\sqrt{2\pi}}$	$\sigma$ = Shape $\mu$ = Scale $\gamma$ = Location
15	Normal	$f(x) = \frac{1}{\sigma\sqrt{2\pi}} \exp\left[-\frac{1}{2}\left(\frac{x-\mu}{\sigma}\right)^2\right]$	$\mu$ =Scale $\sigma$ =Shape
16	Pareto	$f(x) = \frac{\theta}{x_0} \left(\frac{x_0}{x}\right)^{\theta-1}$	$x_0$ =Scale $\theta$ = Shape
17	Rayleigh	$f(x) = \frac{1}{\sigma^2} x \exp\left(-\frac{x^2}{2\sigma^2}\right)$	$\sigma$ = Scale
18	Rayleigh(2P)	$f(x) = 2\lambda(x-\mu)\exp^{-\lambda(x-\mu)^2}$	$\lambda$ = Scale $\mu$ = Location
19	Student's t	$f(t_{n-1}) = \frac{1}{\sqrt{v}\beta\left(\frac{1}{2}, \frac{v}{2}\right)\left(1 + \frac{t^2}{v}\right)^{-(v-1)/2}}$ since $\beta\left(\frac{1}{2}, \frac{v}{2}\right) = \frac{\Gamma\left(\frac{v-1}{2}\right)}{\Gamma\frac{v}{2}\sqrt{\pi}}$ and $\Gamma\frac{1}{2} = \sqrt{\pi}$	$v$ = Degrees of freedom
20	Triangular	$f(x) = \begin{cases} \frac{2(x-a)}{(b-a)(c-a)} & , a < x \leq c \\ \frac{2(b-x)}{(b-a)(b-c)} & , c < x < b \end{cases}$	$a$ = Lower Limit $b$ =Upper Limit $c$ =Mode
21	Uniform	$f(x) = \frac{1}{b-a}$	$a$ = Minimum $b$ = Maximum
22	Weibull	$f(x) = \frac{\alpha}{\beta} \left(\frac{\alpha}{\beta}\right)^{\alpha-1} \exp\left(-\left(\frac{x}{\beta}\right)^\alpha\right)$	$\alpha$ = Shape $\beta$ = Scale
23	Weibull(3p)	$f(x) = \frac{\alpha}{\beta} \left(\frac{x-\gamma}{\beta}\right)^{\alpha-1} \exp\left(-\left(\frac{x-\gamma}{\beta}\right)^\alpha\right)$	$\alpha$ = Shape $\beta$ = Scale $\gamma$ =Location

by Sharma & Singh (2010). Detailed information on the 23 continuous probability density functions and their respective parameters can be found in Table 1.

### Kolmogorov-Smirnov Test

Let  $(x_1, x_2, \dots, x_n)$  be rainfall data with CDF  $F(x)$  from the continuous distribution. The difference between the theoretical and empirical cumulative distribution functions gives the test statistic ( $D_n$ ) as

$$D_n = \max_{1 \leq i \leq n} \left( F(x_i) - \frac{i-1}{n}, \frac{i}{n} - F(x_i) \right)$$

### Anderson-Darling Test

Comparing the fit of actual and expected actual Cumulative distribution function with giving weightage to tail characteristics of the distribution (Anderson & Darling 1954). It is defined as

$$A^2 = -n - \frac{1}{n} \sum_{i=1}^n (2i - 1) [\ln F(x_i) + \ln(1 - F(X_{n-i+1}))]$$

$$= \frac{n(n-1)(2n+5) - \sum_{i=1}^n t_i(t_i-1)(2t_i+5)}{18}$$

**Chi-Squared Test**

It is the non-parametric test that is used to test whether there is any difference between observed ( $O_i$ ) and expected ( $E_i$ ) frequency. The test statistic as:

$$\chi^2 = \sum_{i=1}^n \frac{(O_i - E_i)^2}{E_i}$$

**TREND ANALYSIS**

**Mann-Kendall Test**

The linear regression trend analysis needs the distribution-free (non-parametric) test when the estimated slope of linear regression is different from zero. Which can be accomplished by the Mann-Kendall (M-K) test (Mann 1945). Hence, it assesses statistically the monotonic upward (downward) trend in time series rainfall data. In addition, the M-K test is not influenced by the outliers since it depends on positive and negative signs. The strength of the trend depends upon the magnitude, sample size, and variations of data series. The M-K test statistic is equated as:

$$S = \sum_{i=1}^{n-1} \sum_{j=i+1}^n \text{sgn}(X_j - X_i)$$

The trend test is applied to  $X_i$  data values ( $i=1, 2, \dots, n$ ) and  $X_j$  ( $j=i+1, 2, \dots, n$ ). The data values of  $X_i$  are used as a reference point to compare with the data values of  $X_j$  which is given as:

$$\text{sgn}(X_j - X_i) = \begin{cases} -1 & \text{if } (X_j - X_i) < 0 \\ 0 & \text{if } (X_j - X_i) = 0 \\ 1 & \text{if } (X_j - X_i) > 0 \end{cases}$$

The above statistic represents the number of positive differences minus the number of negative differences for all the differences considered. The normal distribution with mean and variance ( $S=0$ ) test is conducted, when the sample is large ( $>10$ ) and the standard normal Z-statistic is given as

$$Z = \begin{cases} \frac{S-1}{\sqrt{\text{var}(S)}} & \text{if } S > 0 \\ 0 & \text{if } S = 0 \\ \frac{S+1}{\sqrt{\text{var}(S)}} & \text{if } S < 0 \end{cases} \text{ where, } \text{var}(S) :$$

Where  $n$  - number of tied groups and  $t_i$  - number of data points in the  $i^{\text{th}}$  tied groups. The upward and downward trend is interpreted based on the positive and negative values of Z statistic respectively.

**Sen's Slope Estimator Test**

Although the trend is identified by the M-K test, the magnitude of the trend is determined by a Theil-Sen slope or Sen's Slope Estimator (SSE), which is a robust method against outliers to estimate the slope of the trend (Sen 1968).

$$T_i = \frac{x_j - x_k}{j - k}$$

Where  $x_j$  and  $x_k$  are data values at the time  $j$  and  $k$  respectively. The median of these  $n$  values of  $T_i$  is represented as Sen's estimator of slope which is given as:

$$Q_i = \begin{cases} \frac{T_{\frac{n+1}{2}}}{2} & \text{for } n \text{ is odd} \\ \frac{T_{\frac{n}{2}} + T_{\frac{n+1}{2}}}{2} & \text{for } n \text{ is even} \end{cases}$$

A positive value of  $Q_i$  indicates an upward or increasing trend and *vice versa*.

**RESULTS AND DISCUSSION**

Table 2 provides a summary of statistics for a specific district within the agro-climatic zones of West Bengal. The results point out that the Kalimpong district in the Hill and Terai agro-climatic zones experiences the highest levels of rainfall throughout West Bengal. It receives significantly more rainfall compared to other zones, with Coochbehar coming next. Conversely, the Birbhum district has consistently received the lowest amount of rainfall over the years.

In terms of statistical characteristics, the Nadia district displays positive skewness and kurtosis values, suggesting that most of the rainfall events during this period have relatively lower intensity, with only occasional instances of heavy rainfall. For the Kalimpong district, both skewness and kurtosis values are negative, indicating a prevalence of rainfall events with lower intensity and infrequent heavy rainfall occurrences. In contrast, Birbhum exhibits the lowest kurtosis value, implying a flatter peak near the mean and a higher likelihood of a more even distribution with fewer extreme values. The skewness and kurtosis values collectively suggest that the data in these districts do not follow a normal distribution.

Table 2: Descriptive statistics for agro-climatic zones.

Districts	Minimum	Maximum	Mean	SD	CV	Skew	Kurtosis
Kalimpong	1329.45	4518.30	2914.34	797.37	27.36	-0.01	-0.73
Coochbehar	1709.61	4715.28	2670.08	587.87	22.02	0.89	1.36
Malda	401.00	2034.54	1108.09	305.42	27.56	0.14	1.16
Nadia	711.17	2370.07	1208.71	284.44	23.53	1.46	4.24
Birbhum	593.54	1820.34	1187.34	250.61	21.11	0.24	0.21
Sagar island	910.66	2794.20	1517.51	340.69	22.45	1.12	2.63

Table 3: Score-wise best fitted probability distribution with parameter estimates.

Districts	Name of Distribution	Total Score	Parameter estimates
Kalimpong	Gen Extreme value	65	$k=-0.30, \sigma=820.68, \mu=263.60$
Coochbehar	Gamma	59	$\beta=129.43, \alpha=20.62$
Malda	lognormal(3P)	68	$\gamma=5565.60, \sigma=0.04, \mu=8.80$
Nadia	Gen Extreme value	68	$k=-0.34, \mu=1011.71, \sigma=304.45$
Birbhum	Gamma	63	$\beta=52.89, \alpha=22.44$
Sagar island	Lognormal(3P)	63	$\gamma=422.51, \sigma=0.29, \mu=6.95$

Table 4: Results of M-K and Sen's slope estimator test on agro-climatic zones.

Locations	Kendall's Tau	S	Z	Sen's Slope	Trend	p-Value
Kalimpong	0.421	537.00	4.353	33.192	↑trend	<0.01
Coochbehar	0.055	71.14	-0.568	-2.264	no trend	0.56
Malda	-0.265	-339.37	-2.745	-9.399	↓trend	<0.01
Nadia	0.341	483.04	3.510	29.641	↑trend	<0.01
Birbhum	-0.047	-61.48	-0.487	-1.216	no trend	0.62
Sagar island	-0.179	-229.07	-1.851	-3.935	no trend	0.64

## Distribution Fitting

The study involved fitting average monthly rainfall data from six different districts in various agro-climatic zones of West Bengal to 23 different continuous probability distributions. For each district, three test statistics were computed using the Kolmogorov-Smirnov, Anderson-darling, and Chi-square goodness of fit tests. Each distribution was ranked separately for each test, and distributions that failed to fit the data received no rank. Since different distributions ranked differently in each goodness of fit test, it was challenging to determine a single best-fit distribution for each district. Consequently, a scoring method was employed as described in the methodology. Scores were assigned to each distribution for all three tests, and the final score was calculated by summing these three scores. The distribution with the highest total score was considered the best fit for the respective district.

The analysis of goodness-of-fit test results revealed that, in many cases, there was minimal difference between various distributions for each district. Furthermore, no single

distribution consistently ranked as the best fit across all locations. However, the Generalized Extreme Value, Gamma, and Lognormal (3-parameter) distributions emerged as the most suitable choices for the two districts. Specifically, the Generalized Extreme Value distribution was found to be the best fit for Kalimpong and Nadia districts, the Gamma Distribution for Coochbehar and Birbhum districts, and the Lognormal (3-Parameter) distribution for Malda and Sagar Island districts. Table 3 presents the best-fitted probability distribution for each district, along with the parameter estimates. In summary, the monthly rainfall distribution in West Bengal appears to be positively skewed, and the Gamma and Log-Normal distributions can be effectively used for predicting future monthly rainfall events in the region.

## Trend Analysis

The study examined the average monthly rainfall data for six districts within the agro-climatic zones of West Bengal using the Mann-Kendall test and Sen's slope estimator. Table 4 presents the M-K test statistics and associated p-values, and



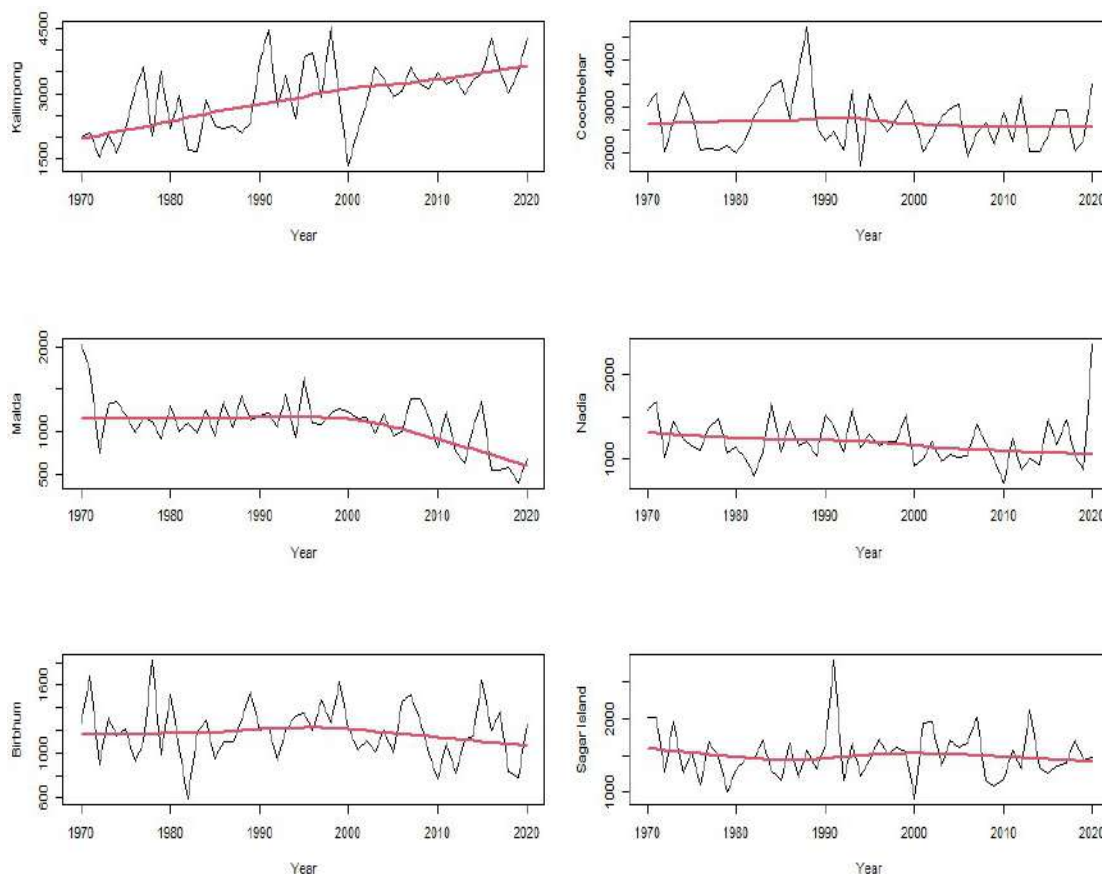


Fig. 2: Trend graph of rainfall for the period from 1970 to 2020.

Fig. 2 depicts the trend graph of rainfall for these districts. In this context, p-values less than 0.05 were considered significant, indicating a rejection of the null hypothesis, which assumes no trend in the data. The results revealed that the Kalimpong and Nadia districts had significant p-values of 0.42 and 0.34, respectively, with positive Kendall's Tau values, suggesting an increasing trend. In contrast, the p-value for Malda district was below the significance level at 0.26, accompanied by a negative Kendall's Tau value, indicating a decreasing trend.

Conversely, for Coochbehar, Birbhum, and Sagar Island districts, the p-values were 0.56, 0.62, and 0.64, respectively, exceeding the significance level of 0.05, indicating the absence of a significant trend in their data. The findings from the Sen's slope test supported those of the M-K test, and the Sen's slope values were provided in Table 4. It's worth noting that Sen's slope values were also calculated for districts with no discernible trend. This is because the M-K test considers the hypothesis above the 5% significance level, allowing for the possibility of a trend's existence beyond this threshold. The Sen's slope values for Kalimpong and Nadia

indicated positive slopes of 33.19 and 29.64, respectively, while the remaining districts exhibited negative slopes over the years. These results contributed to the assessment of the average monthly rainfall levels in the selected districts of West Bengal.

## CONCLUSIONS

A systematic evaluation approach was employed to determine the optimal probability distribution for modeling monthly rainfall data in six different districts of West Bengal. The study utilized the Mann-Kendall test and Sen's Slope estimation techniques to identify any monotonic trends in the data. Notably, the Generalized Extreme Value, Gamma, and Lognormal (3-parameter) distributions were found to be the most suitable choices for two of the districts each. According to the Mann-Kendall test results, Kalimpong and Nadia Districts exhibited an increasing trend in rainfall, while Malda District showed a decreasing trend. The ability to identify both the distribution and trend of rainfall has significant implications in various fields, including agriculture, hydrology, and climate research.

## ACKNOWLEDGEMENT

We would like to express our gratitude to IMD for providing data.

## REFERENCES

- Aditya, F., Gusmayanti, E. and Sudrajat, J., 2021. Rainfall trend analysis using Mann-Kendall and Sen's slope estimator test in West Kalimantan. In: *IOP Conference Series: Earth and Environmental Science*, 893(1), pp. 012006.
- Alam, M.A., Emura, K., Farnham, C. and Yuan, J., 2018. Best-fit probability distributions and return periods for maximum monthly rainfall in Bangladesh. *Climate*, 6(1), pp. 9.
- Anderson, T.W. and Darling, D.A., 1954. A test of goodness of fit. *Journal of the American Statistical Association*, pp.765-769.
- Bandyopadhyay, S., Kar, N.S., Das, S. and Sen, J., 2014. River systems and water resources of West Bengal: A review. *Geological Society Special Publication*, 3(2014), pp.63-84.
- Basak, J.S., Gupta, D., Saha, M. and Pan, S., 2019. Probability distribution of daily maximum rainfall data for six different geographical locations in West Bengal-A case study. *International Journal of Current Microbiology and Applied Sciences*, 8(11), pp.1437-1444.
- Bhavyashree, S. and Bhattacharyya, B., 2018. Fitting probability distributions for rainfall analysis of Karnataka, India. *International Journal of Current Microbiology and Applied Sciences*, 7, pp.1498-1506.
- Brema, J., 2018. Rainfall trend analysis by Mann-Kendall test for Vamanapuram river basin, Kerala. *International Journal of Civil Engineering and Technology*, 9(13), pp.1549-1556.
- Dastidar, A.G., Ghosh, S., De, U.K. and Ghosh, S.K., 2010. Statistical analysis of monsoon rainfall distribution over West Bengal, India. *Mausam*, 61(4), pp.487-498.
- Gowthaman, T., Kumar, S. and Bhattacharyya, B., 2023. Detecting air pollutants trends using Mann-Kendall tests and Sen's slope estimates. *Environmental Conservation Journal*, 24(3), pp.157-166.
- Mandal, S., Choudhury, B.U., Mondal, M. and Bej, S., 2013. Trend analysis of weather variables in Sagar Island, West Bengal, India: a long-term perspective (1982-2010). *Current Science*, pp.947-953.
- Mann, H.B., 1945. Nonparametric tests against trend. *Econometrica: Journal of the Econometric Society*, pp.245-259.
- Mondal, C., 2021. Inland fish production of West Bengal are declining – Its problems and protection. *International Journal of Scientific Research Multidisciplinary*, 7, pp.36-40.
- Pal, S. and Mazumdar, D., 2015. Stochastic modelling of monthly rainfall volume during monsoon season over Gangetic West Bengal, India. *Nature Environment and Pollution Technology*, 14(4), pp.951.
- Sathish, G., Banjul, B., Debashis, B. and Ramesh, D., 2017. Determination of onset and withdrawal of summer monsoon in different meteorological stations of West Bengal. *Trends in Biosciences*, 10(26), pp.5428-5433.
- Sen, P.K., 1968. Estimates of the regression coefficient based on Kendall's tau. *Journal of the American Statistical Association*, pp.1379-1389.
- Sharma, M.A. and Singh, J.B., 2010. Use of probability distribution in rainfall analysis. *N Y Sci. J.*, 3(9), pp. 40-49.

---

## ORCID DETAILS OF THE AUTHORS

T. Gowthaman: <https://orcid.org/0000-0002-9638-3995>



# Enhancing Driving Safety and Environmental Consciousness through Automated Road Sign Recognition Using Convolutional Neural Networks

M. H. F. Md Fauadi<sup>1†</sup>, M. F. H. Mohd Zan<sup>2</sup>, M. A. M Ali<sup>1</sup>, L. Abdullah<sup>1</sup>, S. N. Yaakop<sup>3</sup> and A. Z. M. Noor<sup>4</sup>

<sup>1</sup>Fakulti Teknologi dan Kejuruteraan Industri dan Pembuatan, Universiti Teknikal Malaysia Melaka, 76100 Melaka, Malaysia

<sup>2</sup>HSK Consult, Bandar Tasik Selatan, 57000, Kuala Lumpur, Malaysia

<sup>3</sup>Bahagian Governan dan Kecemerlangan, Jabatan Pendidikan Politeknik dan Kolej Komuniti, 62100 Putrajaya, Malaysia

<sup>4</sup>Universiti Kuala Lumpur Malaysian Spanish Institute, Kulim Hi-Tech Park, 09000 Kulim, Kedah, Malaysia

†Corresponding author: M.H.F. Md Fauadi; hafidz@utem.edu.my

Nat. Env. & Poll. Tech.  
Website: [www.neptjournal.com](http://www.neptjournal.com)

Received: 31-01-2024

Revised: 18-03-2024

Accepted: 05-04-2024

## Key Words:

Traffic sign recognition  
Convolutional Neural Network  
YOLOv3 network  
Environmental consciousness

## ABSTRACT

Traffic accidents remain a pressing public safety concern, with a substantial number of incidents resulting from drivers' lack of attentiveness to road signs. Automated road sign recognition has emerged as a promising technology for enhancing driving assistance systems. This study explores the application of Convolutional Neural Networks (CNNs) in automatically recognizing road signs. CNNs, as deep learning algorithms, possess the ability to process and classify visual data, making them well-suited for image-based tasks such as road sign recognition. The research focuses on the data collection process for training the CNN, incorporating a diverse dataset of road sign images to improve recognition accuracy across various scenarios. A mobile application was developed as the user interface, with the output of the system displayed on the app. The results show that the system is capable of recognizing signs in real time, with average accuracy for sign recognition from a distance of 10 meters: i) daytime = 89.8%, ii) nighttime = 75.6%, and iii) rainy conditions = 76.4%. In conclusion, the integration of CNNs in automated road sign recognition, as demonstrated in this study, presents a promising avenue for enhancing driving safety by addressing drivers' attentiveness to road signs in real-time scenarios.

## INTRODUCTION

With the growing demand for intelligent transport systems and the pursuit of safer road environments, automated road sign recognition has emerged as a promising technology. Convolutional Neural Networks (CNNs), a class of deep learning algorithms inspired by human visual processing, have revolutionized various fields, including image recognition tasks (Behera et al. 2022, Khan et al. 2023, Fredj et al. 2023, Kiliçarslan et al., 2023, Lee et al. 2021, Razi et al. 2023). Leveraging the power of CNNs, researchers, and engineers have made significant strides in developing automated road sign recognition systems that exhibit high accuracy and efficiency. This study aims to explore the application of CNNs in automatically recognizing road signs, and addressing challenges posed by diverse road sign designs, environmental conditions, and real-time processing requirements.

This research introduces a novel solution to tackle challenges in road sign recognition by presenting a robust and

efficient framework that surpasses existing methodologies in UAV inspection scenarios. The successful integration of CNN and You Only Look Once version 3 (YOLOv3) methodologies highlights the advantages of employing deep learning techniques to enhance road sign recognition algorithms. The framework's development involved extensive investigations into dataset generation techniques, picture classification methods, and network parameter determination, all aimed at optimizing the algorithm's performance.

Recognizing traffic signs is crucial for automated driving and driver assistance systems. However, various factors such as partial occlusion, diverse views, varying illuminations, and weather conditions pose significant challenges for computers in visually identifying traffic sign images. Researchers are actively addressing this complex task using established or specifically developed computer vision algorithms. Before the release of standardized benchmarks like the German Traffic Sign Benchmark (GTSRB) and German Traffic Sign Database (GTSDB), researchers lacked publicly accessible datasets

for comparison, hindering the evaluation and comparison of methods. Despite the availability of benchmarks, limitations persist, such as the focus on symbol-based traffic signs with regular shapes and colors, the reliance on static images, and the lack of comparability in identifying existing signs in a scene.

Researchers have made significant advancements in accurate road sign recognition by building a big dataset of road sign images and training CNNs on vast repositories of annotated data. Real-time implementation of CNN-based road sign recognition in cars is expected to enhance driving assistance systems by providing drivers with up-to-date information on speed limits, warnings, road signs, and directions (Luo et al. 2017, Chen et al. 2019, Dewi et al. 2022). The use of CNNs for road sign recognition has been shown to potentially reduce accidents caused by drivers misinterpreting or failing to observe road signs (Khan et al. 2023, Luo et al. 2017). This could help to improve the safety and dependability of driving. However, as stated there are still limitations to the technology which include processing of partially obstructed images or noisy images. This study aims to critically address the limitations and opportunities of CNN-based road sign recognition in modern driving environments. Apart from CNN, other methods have also been deployed to enable autonomous vehicles (Sudhakar & Priya 2023, Ramlan et al. 2022, Rosli et al. 2018, Noor et al. 2017, Bin Md Fauadi & Murata 2010).

This study integrates the CNN and YOLOv3 approaches to create a unique framework for an algorithm that recognizes traffic signs. The suggested method improves the quality of acquired road sign pictures by high-resolution restoration of blurry images using CNN. The enhanced clear images are processed with more training images to increase the dataset size and enhance the network's recognition performance. YOLOv3 is then utilized for precise road sign recognition in real-time situations. Extensive investigations were carried out on various aspects of the proposed framework. Furthermore, the dataset collection approach, picture classification methods, and network parameter determination were critically analyzed to optimize the algorithm's performance.

Traffic sign recognition is a critical factor for driver assistance systems and automated driving. Additionally, as the system needs to deal with a realistic environment, partial occlusion, varied angles, different illuminations, weather, and other factors make it challenging for the system to visually identify photographs of traffic signs. Most methods for recognizing traffic signals in an image involve two primary steps: detection and classification. Many academics are using well-established or specially created computer vision algorithms to tackle this difficult issue (Huang et al. 2020).

There was no publicly available dataset for comparison before the publication of the German Traffic Sign Benchmark (GTSDB) and German Traffic Sign Benchmark (GTSRB) (Stallkamp et al. 2012). As a result, researchers have a uniform dataset to assess and contrast their approaches with. Nevertheless, there are still issues with GTSRB and GTSDB:

- i. Both benchmarks encompass only three types of symbol-based traffic signs with regular shapes and colors, which are comparatively easier to detect and classify than text-based traffic signs.
- ii. GTSDB solely comprises static images, yet in practical scenarios, continuous video footage captured by an in-vehicle camera proves more beneficial for detection and classification (Luo et al. 2017).
- iii. The ultimate goal of traffic sign recognition is to identify existing signs in a scene, but the two benchmarks lack comparability in this aspect.

The unique contribution of this research lies in the innovative framework that integrated CNN and YOLOv3 methodologies, addressing challenges in road sign recognition and surpassing existing methodologies in UAV inspection scenarios. The innovative framework developed in this research offers a distinct advantage by compensating for the potential lack of state-of-the-art equipment in road sign recognition systems. While traditional approaches may rely heavily on advanced hardware or costly infrastructure to achieve accurate results, the integration of CNN and YOLOv3 methodologies provides an alternative solution. By leveraging deep learning techniques within the proposed framework, the system can achieve high levels of accuracy and efficiency without necessarily requiring the latest and most expensive hardware components. This means that the framework can be implemented in scenarios where access to state-of-the-art equipment may be limited or cost-prohibitive, making it a more accessible and practical solution for various applications.

The remainder of the paper is divided into the following sections: The method for recognizing the road signs is described in Section II, along with the function of each component of the framework. This section also provides a thorough introduction to the theoretical underpinnings of the proposed CNN algorithm and the proposed YOLOv3's detection principle. Section III discusses the dataset, experimental findings, assessment of our algorithms, and comparison to alternative approaches. The last section of this essay is Section IV.

## MATERIALS AND METHODS

### Proposed Model

Fig. 1 illustrates the main procedure of CNN for detecting

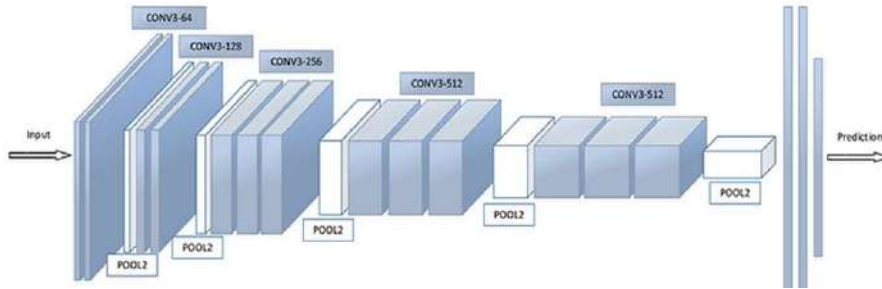


Fig. 1: CNN model.

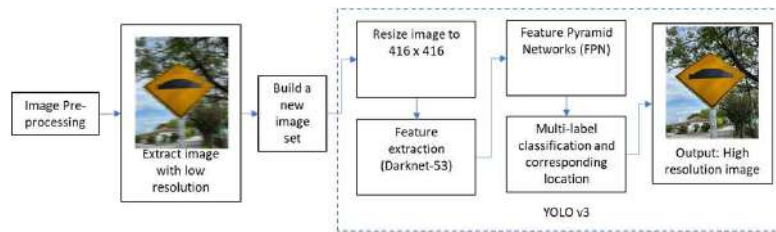


Fig. 2: Proposed flow.

the primary electrical components (Chen et al. 2019). In this research, preprocessing of the sign images involves the steps. Initially, the original image dataset is categorized into two groups. The first group comprises qualified images suitable for use as the training set, while the second group consists of blurred images with lower resolutions. Subsequently, the blurred image set undergoes super-resolution reconstruction using CNN, thereby enhancing its resolution to match that of the original images. The resulting processed images are then merged with the original images to form the appropriate inspection image sets.

Furthermore, based on Peng et al. (2021) and Qingyun et al. (2020), the original inspection image set is resized to a resolution of 416x416 within the YOLOv3 architecture. The resized images are subsequently input into Darknet53, enabling the extraction of relevant features associated with electrical components. The feature pyramid networks (FPN) are subsequently utilized to generate predictions across three distinct scales using the feature outputs from Darknet-53. The comprehensive predictions obtained from YOLOv3 encompass essential parameters, including bounding box information, objectness score, and class predictions. To refine the predictions, YOLOv3 employs a filtering process to remove anchors that exhibit substantial overlap with the ground truth object, subject to a selected threshold. Following this filtering step, the network proceeds to output the classification outcomes and corresponding positioning information for each bounding box. Ultimately, the YOLOv3 network yields comprehensive detection

results. The proposed flow for this study is depicted in Fig. 2.

### Experimental Setup

The dataset for this research project comprised a total of 450 images, consisting of 125 negative images and 325 positive images. The negative images encompassed road scenes containing objects like buildings, trees, cars, and roads devoid of road signs. These images were captured in Ayer Keroh, Melaka for several days. It is worth noting that all images used in the dataset were obtained directly from phone-captured photographs, and no images from external internet sources were utilized. The dataset exhibited diverse conditions, including variations in lighting and time of day, providing a comprehensive representation of real-world scenarios. Table 1 shows the summary of data collection.

The experiment was conducted on a personal computer equipped with an Intel(R) Core(TM) Pentium processor running at 3.7 GHz. It was configured with 8GB of RAM and operated on a 64-bit operating system. Data collection

Table 1: Data collection summary.

Setup for Data Collection	
Distance (Camera-to-sign)	3-7 meters
Time	9-11 am 9-11 pm
Weather Condition	Clear and rainy
Camera	12-megapixel iPhone 11 rear camera

employed an iPhone 11 camera featuring a high-definition (HD) 12-megapixel (MP) rear camera.

Moreover, the personal computer is equipped with Python 3.7.2 (64-bit), enabling clear and coherent programming with the added benefit of automatic memory management. The Python libraries used in this project include Opencv and Numpy, essential for image processing and numerical computations, respectively. Additionally, Google Colab serves as the software platform for model training, eliminating the need to install or configure additional software on the computer. This streamlined approach ensures a straightforward and efficient training process for road sign image recognition.

### Dataset Preparation

To construct the targeted dataset, five types of road signs as illustrated in Fig. 3 (a) Stop, (b) Bump Ahead, (c) Children Crossing, (d) Speed Limit and (e) No Entry - were meticulously collected as the primary data. The labels for these road signs are listed in Table 2. These five road sign types are commonly encountered on Malaysian roads. A total of 750 images were gathered, comprising 150 images for each road sign category. Subsequently, the dataset was automatically constructed using Google Colab, streamlining the data preparation process.



Fig. 3: Road signs.

Table 2: Labels used for the road sign.

Road Sign	Label (in Malay language)
Stop	Berhenti
Bump Ahead	Bonggol
Children Cross	Kanak-Kanak Melintas
Speed limit	Had laju 30km/j
Children Cross	Kanak-Kanak Melintas

### Network Structure of the Proposed CNN

The CNN network initially resizes the extracted blurred inspection image to the desired target size using the Bicubic interpolation algorithm, denoted as  $Y$ . The primary objective of super-resolution reconstruction is to recover  $Y$  to the high-resolution image  $H$ , resembling the original resolution image  $X$ . This is achieved through training to obtain the corresponding “end-to-end” mapping function  $F(Y)$ . The architectural representation of the CNN network is illustrated in Fig. 1, comprising a multi-layer CNN. The network is divided into three levels, corresponding to the three successive steps involved in image super-resolution reconstruction:

- The initial convolutional layer extracts image blocks from  $Y$  and represents these features at a lower resolution level.
- The subsequent convolutional layer performs non-linear mapping to generate high-resolution features.
- The final convolutional layer reconstructs high-resolution images, effectively producing images closely resembling the original high-resolution images.

### Training and Classification Using YOLOv3

YOLOv3, a real-time object identification technique utilizing neural networks, was employed for training and classification. Due to its remarkable combination of speed and accuracy, this algorithm has gained widespread adoption among users. Notably, it has successfully detected a diverse range of objects, including traffic lights, pedestrians, parking meters, and animals. Key advantages of YOLOv3 include its speed, high accuracy, and learning capabilities in object representation and detection.

The feature detector Darknet-53 in YOLOv3’s architectural design draws inspiration from established models such as ResNet and Feature Pyramid Network (FPN). With 52 convolutions featuring skip connections akin to ResNet and three integrated prediction heads similar to FPN, Darknet-53 exhibits the capacity to process images at various spatial compressions. This amalgamation of influential designs empowers Darknet-53 with the ability to effectively detect features in images across different spatial resolutions.

## RESULTS AND DISCUSSION

The assessment of the overall system performance primarily focuses on evaluating detection and classification accuracy across diverse conditions encompassing varying views, angles, distances, light intensities, and driving environments. Results are systematically organized into a tabular format,

incorporating values for True Positive, True Negative, False Positive, False Negative, error rates, and accuracy metrics. The comprehensive evaluation of the system involves employing computational theories through Google Colab, generating quantitative metrics crucial for assessing the system's efficacy and robustness. The evaluation metrics utilized in this study are defined as follows:

- True Positive: Video frames with road signs precisely detected and recognized as such by the experiment.
- True Negative: Video frames without road signs precisely detected and recognized as lacking road signs by the experiment.
- False Positive: Video frames without road signs incorrectly detected and recognized as having road signs by the experiment.
- False Negative: Video frames with road signs incorrectly detected and recognized as lacking road signs by the experiment.

### Detection and Recognition based at Varying Distances

The experiment involved detection and recognition procedures conducted at varied distances from the road sign, encompassing short and long ranges, captured during both day and night. Short-distance images were taken within 3 meters, while long-distance images were captured from 7 meters. Three distinct tests were performed, each involving fixed distances and road settings, accounting for daytime and nighttime conditions. Images, taken using an iPhone 11 with enhanced resolution, depict the detection and recognition outcomes of the five road sign types at a 3-meter distance in daylight. To ensure accuracy, each image was captured thrice, and average accuracy was computed.

Similarly, experiments were conducted at night between 8:00 pm to 10:00 pm, with illumination lower than 20 lux, aiming to evaluate system performance under varied lighting conditions. Fig. 4 illustrates the detection and recognition outcomes of the five road sign types at distances of 3 to 7 meters during nighttime conditions. Similar to daytime evaluation, images were captured thrice at the same distance, and average accuracies were determined. These comprehensive evaluations under different conditions aim to ensure robust and reliable system performance.

### Accuracy in Relation to Distance - Day and Night

The results demonstrate data collected from three repetitions for each road sign at distances of 3 to 10 meters. The experiment's highest accuracy of 95.00% was achieved for the Speed Limit label, while the lowest accuracy of 75.00% was observed for the Stop label.

Additionally, during nighttime recognition at a 3-meter distance with an illumination of 10 lux, the Speed Bump demonstrated the highest accuracy of 88%, whereas the Speed Limit label recorded the lowest accuracy of 62.00%. This revised version aims to improve the academic tone, clarity, and coherence of the content while ensuring the accurate presentation of experimental procedures and results. The results are shown in Figs. 5 and 6 respectively.

### Image Retraining

Fig. 7 illustrates the results, indicating that the accuracy of image detection for Stop and Children crossing signs obtained the lowest scores compared to image detection at a 3-meter distance. It was observed that both road signs did not undergo complete training in Google Colab due to

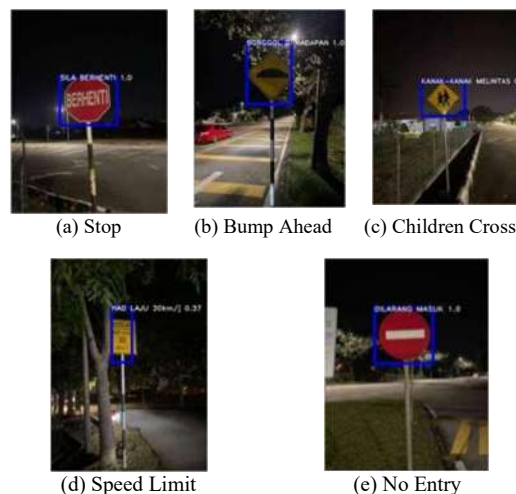


Fig. 4: Sample of images captured during night time.

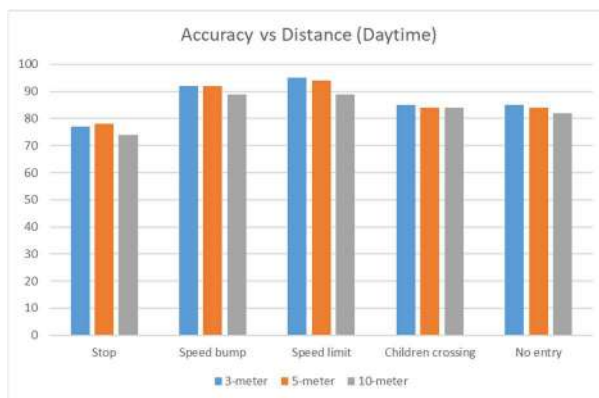


Fig. 5: Results accuracies (daytime).

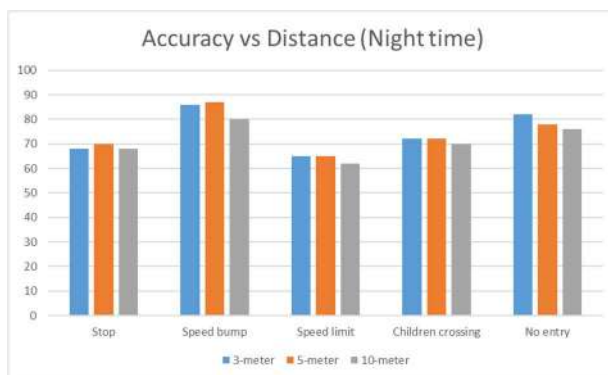


Fig. 6: Results accuracies (night time).

the platform's limited training time, capped at 60 hours. Consequently, retraining becomes imperative to enhance the accuracy score, allowing these road signs to achieve higher accuracy levels. However, achieving optimal accuracy for "Berhenti" and "Bonggol" signs might necessitate a lifetime purchase of training resources, given the insufficient training time available in Google Colab for comprehensive learning.

The study presents a comparative analysis of detection distances at 3-, 5- and 10-meters during daytime, both before and after retraining. Post retraining for image detection at a 10-meter distance, the accuracy for "Stop" and "Speed bump" signs exhibited significant improvement, increasing from 74% to 84% for "Stop"; and from 88% to 92% for "Speed bump." The enhancement is depicted in Figs. 7 and 8, illustrating notable accuracy rates for all signs during daytime and night time testing, respectively.

### Detection and Recognition Under Rainy Conditions

This experiment specifically aimed to evaluate the detection and recognition capabilities of the system in rainy weather conditions, assessing its ability to identify road signs

under adverse circumstances. The image captures were conducted around 9:00 a.m. during daylight hours. To ensure a comprehensive assessment, three separate tests were conducted, each utilizing distinct images to showcase the system's accuracy in detecting images under rainy conditions. All images were captured using an iPhone 11 with enhanced resolution. The results also shed light on the system's accuracy in detecting road signs consistently from a particular angle during rainy weather.

The data presented in Fig. 9 was obtained from three repetitions for each road sign under rainy conditions. The experiment's highest accuracy in detection and recognition remains at 0.96, equivalent to a percentage score of 96.00%, corresponding to the "No Entry" label. Conversely, the lowest accuracy was observed for the "Children Crossing" label, scoring 0.90. These findings highlight the system's varying performance in recognizing different road signs under challenging rainy conditions.

### CONCLUSIONS

In conclusion, the study successfully developed an automated



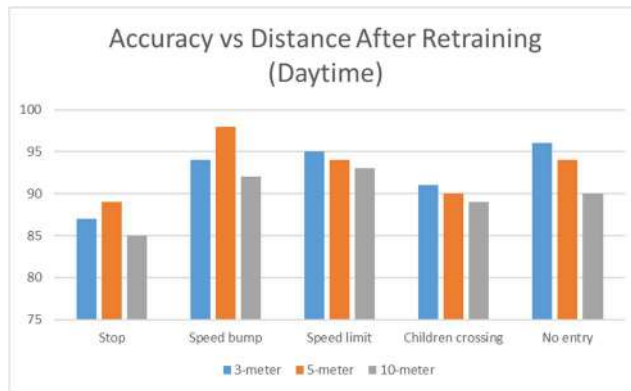


Fig. 7: Results accuracies after retraining (daytime).

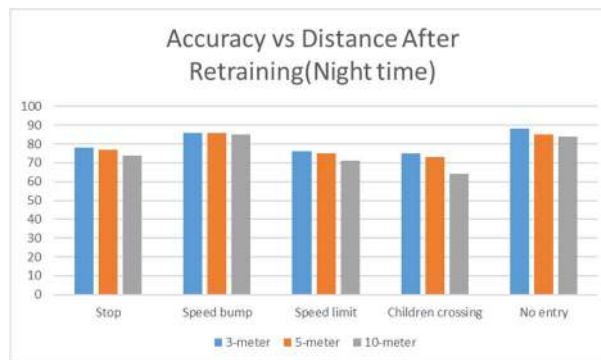


Fig. 8: Results accuracies after retraining (night time).

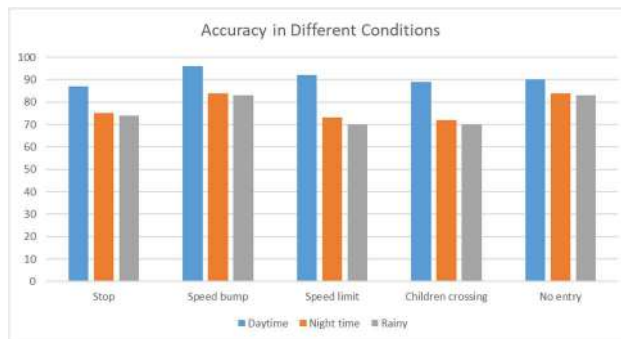


Fig. 9: Results accuracy during rainy conditions.

CNN-based system for traffic sign recognition. Following a thorough evaluation in a range of conditions, including varying illumination, distances, and weather, the system demonstrated respectable average accuracy levels: 89.8% in the daytime, 75.6% at night, and 76.4% in the rain. While these results are encouraging, there are significant drawbacks to using a phone camera as the input device. Most importantly, there was inadequate training time, which

resulted in reduced accuracy for some road sign labels (such as “Stop” and “Children Crossing”). Future research should focus on reducing these limitations by using high-speed cameras that can capture moving images at exposure lengths of less than 1/1000 seconds, potentially improving image quality and precision. Additionally, further exploration into optimizing training procedures and dataset augmentation techniques could contribute to improving overall system

performance. By addressing these challenges and exploring new avenues for refinement, future iterations of automated road sign recognition systems can aspire to achieve even higher levels of accuracy and reliability, ultimately enhancing driving safety and efficiency.

## ACKNOWLEDGEMENTS

The authors would like to thank Universiti Teknikal Malaysia Melaka for enabling the research to be carried out.

## REFERENCES

- Behera, S.A.S.M.I.T.A., Bhoi, S.S., Mishra, A.S.U.T.O.S.H., Nayak, S.S., Panda, S.K. and Patnaik, S.S., 2022. Comparative study of convolutional neural network and long short-term memory network for solar irradiance forecasting. *Journal of Engineering Science and Technology*, 17(3), pp.1845-1856.
- bin Md Fauadi, M.H.F. and Murata, T., 2010. Makespan minimization of machines and automated guided vehicles schedule using binary particle swarm optimization. *Lecture Notes in Engineering and Computer Science*, 2182, pp.1897–1902.
- Chen, H., He, Z., Shi, B. and Zhong, T., 2019. Research on recognition method of electrical components based on YOLO V3. *IEEE Access*, 7, pp.157818-157829.
- Dewi, C., Chen, R.C., Jiang, X. and Yu, H., 2022. Deep convolutional neural network for enhancing traffic sign recognition developed on Yolo V4. *Multimed Tools Appl*, 81(26), pp.37821-37845.
- Fredj, H.B., Chabbah, A., Baili, J., Faiedh, H. and Souani, C., 2023. An efficient implementation of traffic signs recognition system using CNN. *Microprocess Microsyst*, 98, p.104791.
- Huang, Y.Q., Zheng, J.C., Sun, S.D., Yang, C.F. and Liu, J., 2020. Optimized YOLOv3 algorithm and its application in traffic flow detections. *Applied Sciences*, 10(9), p.3079.
- Khan, M.A., Park, H. and Chae, J., 2023. A lightweight convolutional neural network (CNN) architecture for traffic sign recognition in urban road networks. *Electronics*, 12(8), p.1802.
- Kiliçarslan, S., Közkurt, C., Başı, S. and Elen, A., 2023. Detection and classification of pneumonia using novel Superior Exponential (SupEx) activation function in convolutional neural networks. *Expert Syst Appl*, 217, p.119503.
- Lee, W.K., Abdullah, M.D., Ong, P., Abdullah, H. and Teo, W.K., 2021. Prediction of flank wear and surface roughness by recurrent neural network in turning process. *Journal of Advanced Manufacturing Technology (JAMT)*, 15(1), pp.55-67.
- Li, H., Dong, Y., Liu, Y. and Ai, J., 2022. Design and implementation of uavs for bird's nest inspection on transmission lines based on Deep Learning. *Drones*, 6(9), p.252.
- Luo, H., Yang, Y., Tong, B., Wu, F. and Fan, B., 2017. Traffic sign recognition using a multi-task convolutional neural network. *IEEE Trans Intell Transp Syst*, 19(4), pp.1100-1111.
- Mittal, P., Singh, R. and Sharma, A., 2020. Deep learning-based object detection in low-altitude UAV datasets: A survey. *Image and Vision Computing*, 104, p.104046.
- Noor, A.M., Fauadi, M.M., Jafar, F.A., Nordin, M.H., Yahaya, S.H., Ramlan, S. and Aziz, M.S.A., 2017. Fuzzy Analytic Hierarchy Process (FAHP) Integrations for Decision Making Purposes: A Review. *Journal of Advanced Manufacturing Technology (JAMT)*, 11(2), pp.139-154.
- Peng, F., Miao, Z., Li, F. and Li, Z., 2021. S-FPN: A shortcut feature pyramid network for sea cucumber detection in underwater images. *Expert Syst Appl*, 182, p.115306.
- Qingyun, F., Lin, Z. and Zhaokui, W., 2020. An efficient feature pyramid network for object detection in remote sensing imagery. *IEEE Access*, 8, pp.93058-93068.
- Ramlan, S., Fauadi, M.H.F.M., Razali, N.H. and Hao, X., 2021. Agent-Based Chemical Mechanical Planarization Qualification for Semiconductor Wafer Fabrication. *Journal of Advanced Manufacturing Technology*, 15(3), pp.41-53.
- Razi, A., Chen, X., Li, H., Wang, H., Russo, B., Chen, Y. and Yu, H., 2023. Deep learning serves traffic safety analysis: A forward-looking review. *IET Intell Transp Syst*, 17(1), pp.22-71.
- Rosli, N.S., Fauadi, M.H.F.M., Awang, N.F. and Noor, A.Z.M., 2018. Vision-based defects detection for glass production based on improved image processing method. *Journal of Advanced Manufacturing Technology (JAMT)*, 12(1), pp.203-212.
- Stallkamp, J., Schlipsing, M., Salmen, J. and Igel, C., 2012. Man vs. computer: Benchmarking machine learning algorithms for traffic sign recognition. *Neural Networks*, 32, pp.323-332.
- Sudhakar, M. and Priya, R.M., 2023. Computer Vision Based Machine Learning and Deep Learning Approaches for Identification of Nutrient Deficiency in Crops: A Survey. *Nat. Environ. Pollut. Technol.*, 22(3).



# Evaluating Sustainability: A Comparison of Carbon Footprint Metrics Evaluation Criteria

Mahima Chaurasia, Sanjeev Kumar Srivastava<sup>†</sup> and Suraj Prakash Yadav

Department of Environmental Sciences, Dr. Rammanohar Lohia Avadh University, Ayodhya, U.P., India

<sup>†</sup>Corresponding author: Sanjeev Kumar Srivastava; sanjsri2001@gmail.com

Nat. Env. & Poll. Tech.  
Website: [www.neptjournal.com](http://www.neptjournal.com)

Received: 06-03-2024

Revised: 09-05-2024

Accepted: 18-05-2024

## Key Words:

Carbon footprint  
Climate change  
Carbon emission  
Global warming  
Greenhouse gas emission

## ABSTRACT

The two biggest environmental issues the world is currently dealing with are global warming and climate change. Minimizing energy consumption will help to cut down on greenhouse gas emissions, which is our responsibility. Companies choose 'Carbon Footprint' as a tool to calculate greenhouse gas emissions to show the impact of their activities on the environment. The techniques and procedures used in the analysis of carbon footprints are the primary focus of this study. Several criteria for evaluating carbon footprints were compared to one another to uncover parallels, variances, and deficiencies. Carbon footprints of companies and items were analyzed, and their objectives, ideas, topics of inquiry, calculation techniques, data choices, and additional elements were investigated. Standards for both organizations (ISO14064 and the GHG protocol) and products were compared and contrasted to arrive at accurate carbon footprint estimates. The most important aspects of a carbon footprint and assessment criterion are the research of GHG, system settings, measurement and carbon footprint, date, and treatment of individual emissions. Especially true for commercial enterprises and consumer goods. Guidelines have been produced for these challenges based on valuation criteria that have been used up to this point; nonetheless, they should be enhanced. This study highlights the need to formulate policies to reduce greenhouse gas emissions.

## INTRODUCTION

The problem of global warming indeed began as a scientific mystery; nevertheless, it has now expanded to encompass a wide variety of other topics, including politics, economics, society, technology, ecology, and the environment. It quickly becomes one of the most difficult problems that individuals in the modern world must deal with. The issue of global warming, in addition to a wide range of other problems, is a major source of concern for the international community. Programs for the reduction of carbon emissions will be implemented in most nations, according to the consensus. Any comprehensive strategy for global growth must, as a result, place a significant emphasis on the creation of a low-carbon economy, a low-carbon city, a low-carbon lifestyle, carbon trade, a carbon tax, and strategies for reducing carbon emissions. Many different groups want to see progress made toward low-carbon development, thus many different types of organizations, including governments, NGOs, and universities, have done studies on the economic, social, and other factors that are relevant to this topic. Recent years have seen significant advancement in the solution to the low-carbon challenge as a result of research into emission

accounting and reduction, carbon emission trading platforms, carbon taxes, and emission restrictions. One of the most important studies that have been done in the realm of low-carbon research is the carbon footprint and assessment standard. On the other hand, due to this problem, researchers have been unable to acquire reproducible results, which have had a significant impact on the industry. Recent months have seen a rise in the level of interest shown by governments as well as academic institutions in research about carbon footprint and evaluation criteria (Lenzen 2007, Letete et al. 2011, Klein-banai et al. 2013, Larsen et al. 2013). This article investigates the procedures and approaches used in investigations of various forms of carbon footprints.

## Carbon Footprint Theory

The influence that humanity has had on the ecosystems of the globe is sometimes referred to as their "ecological footprint," which is where the term "carbon footprint" originated from. It is a standardized measurement of the impact that human use of natural resources has on the surrounding ecosystem. It is the quantity of biologically productive land and waters that is necessary to satisfy the needs of a population as well as to

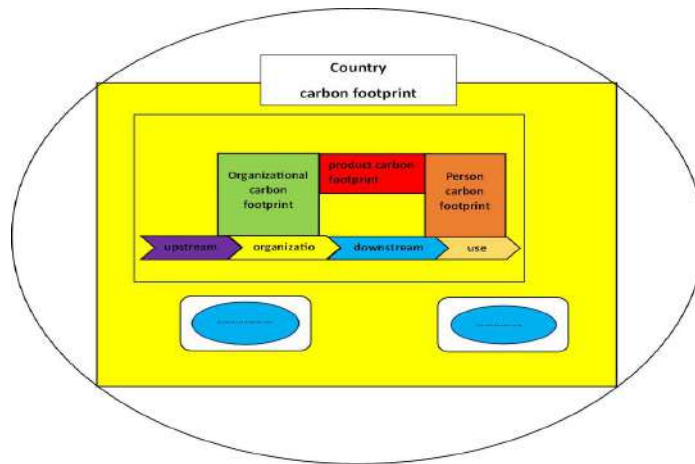


Fig. 1: Limits on carbon dioxide emissions vary by person, product, enterprise, and country.

digest the waste products that are produced by the activities of that population. Using this approach, it is feasible to calculate how much of Earth (or how many planet Earths) would be required to maintain a particular level of living for humanity.

However, a universally accepted or suitable definition of a carbon footprint has yet to be established. However, the term "footprint" denotes a certain action. Popularized the concept of a "carbon footprint," which is a way of calculating the entire amount of carbon dioxide emissions produced by an activity or accumulated throughout the lifetime of a product. The "footprint" of the product during its whole lifetime might be analyzed in this way. Conversely, carbon footprints may be thought of as numerical representations of carbon dioxide (CO<sub>2</sub>) emissions (Chaurasia et al. 2022a, Hertwich & Peters 2009, Larsen & Hertwich 2009, Robinson et al. 2015).

### Carbon Footprint Categories and Computation Approaches

The phrase "carbon footprint" is frequently used to refer to the influence that individuals, corporations, governments, and other entities have on the surrounding environment. A person's "carbon footprint" refers to the amount of carbon dioxide (CO<sub>2</sub>) that is created by the individual's day-to-day actions, such as getting dressed, eating, and driving. The total amount of energy that goes into the production of a product is what is referred to as its carbon footprint. This encompasses the whole life cycle of the product, from extraction of raw materials through final disposal, whether through reuse, recycling, or repurposing (Garg et al. 2001, Nagarajan et al. 2011, Wiedmann & Minx 2007, Weidemma et al. 2008). Greenhouse gas (GHG) emissions are produced as a result of a company's energy use in its buildings and cars, as well as

its manufacturing processes and transportation, and may be measured by calculating its "carbon footprint." The "carbon footprint" of a country is the sum of the greenhouse gases released into the atmosphere by that country due to its total consumption of materials and energy, its vegetation and other carbon sequestrations, and its direct and indirect import and export operations (Chaurasia et al. 2022b, Lenzen et al. 2010, Letete et al. 2011, Rippon 2008, Suwanmontri et al. 2013). The different limitations of personal, industrial, institutional, and national footprints are depicted in Fig. 1.

There is a degree of overlap between the characteristics of the four different groupings. The production stage, which is frequently linked to the PLC, would also be included in the organization's carbon footprint if it were to be calculated.

The carbon footprint definition should not contain the method used to calculate the footprint. The approach can be regarded as effective only if it meets the requirements specified in the definition. Consequently, a carbon footprint study may be performed for a wide range of functional units across sizes and using a variety of approaches. Estimating carbon emissions may be done with one of these three major methods: analysis of inputs and outputs (IO), life-cycle assessment (LCA), or a combination of the two.

In actual use, the methodology scales based on a functional unit. In national studies, the top-down IO analysis is utilized, but the bottom-up LCA approach is favored when analyzing consumer items. Hybrid methods, which combine the most beneficial aspects of LCA and IOA, are becoming an increasingly popular option among businesses (Battistini et al. 2022, Li et al. 2015, Addie et al. 2015, Chaurasia & Srivastava 2022).

**Criteria for Evaluating Carbon Footprints**

Numerous carbon footprint assessment standards have been introduced, primarily for businesses and consumer goods, by the likes of the “International Organization for Standardization (ISO)”, the “World Resources Institute (WRI)”, the “World Business Council for Sustainable Development (WBCSD)”, and the “British Standards Institution (BSI 2008)”. Some of these organizations are the “International Organization for Standardization (ISO)”, the “World Resources Institute (WRI)”, and the “World Business Council for Sustainable Development (WBCSD)”. In the long run, we were able to learn more about carbon footprint assessment standards including ISO14064, GHG Protocol, and PAS2050. These rules were a big help in the worldwide effort to cut carbon emissions.

Despite this, there are still a lot of problems with how these standards are being implemented. For instance, no method of accounting for carbon emissions is recognized by the majority of people. Insufficient scientific rigor has been applied to both the boundary definition and the carbon emission factors. It is necessary to do research and analysis, in particular about the organization and the product (Fig. 2).

**Standards for Measuring and Reducing the Carbon Footprint of Organizations**

**Carbon footprint of the organization:** A company’s “carbon footprint” is the sum of all of its CO<sub>2</sub> emissions, both direct and indirect, within the boundaries it sets for itself.

As a component of an organization’s carbon footprint, an inventory of sources and information on greenhouse gas emissions may be fully provided to the public as part of the findings of an assessment. This can be done as part of the results of an assessment.

The most common approach to measuring an organization’s carbon footprint at now is IO analysis-based terminal consumption analysis. Fig. 3 depicts the primary operations involved in determining an organization’s carbon footprint.

- (1) Limiting the scope of the carbon footprint to only those parts of the business that are truly necessary is crucial. Companies commonly integrate their greenhouse gas (GHG) emissions and removals at the organization level utilizing control and equity-sharing approaches even if they have several sites.
- (2) Establishing operational boundaries is necessary for deciding which emission sources will be monitored. Emissions from all preventable sources must be included. Emissions in Scopes 1 and 2 are mandated, but those in Scope 3 are discretionary. (Scopes 1, 2, and 3 are shown in Fig. 3) (GHG Protocol, 2004).
- (3) Gathering consumption data from all emission sources within the specified area is important for a precise carbon footprint to be calculated. If there were any assumptions or queries left unresolved during the footprint calculation, these should be clarified. A person’s carbon footprint is calculated by multiplying their activity data with standard emissions coefficients. However, there are other ways to calculate, such as through the use of models or by direct measurement.
- (4) A report should be generated by firms to help with inventory verification, and GHG program participation, or to alert external or internal users. Independent verification of carbon footprints was also recommended to boost confidence in publicly available carbon data.

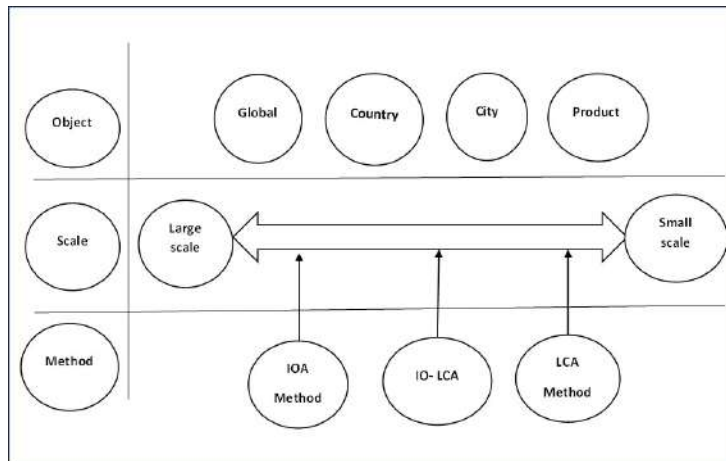


Fig. 2: Carbon footprint applications and associated methodologies.

**Criteria for evaluating a company's carbon footprint:** In 2004, the World Resources Institute and the World Business Council for Sustainable Development collaborated to create the GHG Protocol. It lays the groundwork for effective climate policy and strong, prosperous enterprises. Using a consensus-based multi-stakeholder approach, groups from all around the world, including businesses, government agencies, NGOs, and educational institutions, collaborated to create the standards. In 2004, the Greenhouse Gas Protocol (GHG Protocol) was created to provide a benchmark against which organizations and projects may measure and report on their greenhouse gas emissions. It addresses the challenge of quantifying the decrease in greenhouse gas emissions attributed to the implementation of mitigation strategies, and it does so by integrating industry-specific and general computation tools into the project protocol.

The International Organization for Standardization (ISO) released the ISO14064 standard in March 2006 to help governments and businesses better understand how to monitor and reduce their carbon footprints.

**A comparative study for the standards for evaluating an organization's carbon footprint:** During the process of developing these standards, efforts were made to harmonize all qualifying criteria; yet, there are still some minor differences between the two. Both the GHG Protocol and ISO 14064 provide guidelines for determining how to evaluate an organization's contribution to the emission of greenhouse gases (GHG). Table 1 contains information on the methodologies, including the primary distinctions between them as well as an estimation of the effects that these changes would have on the overall result.

(1) Comparison of the criteria used by the two organizations to evaluate carbon footprints allows for the identification of any differences. The Greenhouse Gas Protocol is the

first worldwide benchmark that is used to evaluate a company's contribution to the emission of greenhouse gases. The Greenhouse Gas Protocol is an initiative that is entirely voluntary but which sets a premium not just on the process of analysis but also on the outcomes of that process. These outcomes are then utilized in the process of reducing emissions and engaging in carbon trading. The certification process, rules, and framework are all aspects that are addressed by ISO14064, an international standard that is based on the GHG Protocol. As a consequence of this, it is most commonly used in the process of certifying firms' compliance with GHG accounting standards to demonstrate their dedication to social responsibility.

(2) The six greenhouse gases included in the Kyoto Protocol serve as the foundation for both of the criteria. The configurations of the two standards' organizational boundaries are the same, yet the configurations of their operational boundaries are completely different. There are a few different ways that the two standards are quantified in terms of their carbon impact. To get at a quantization, one popular and highly suggested method is to multiply the data on GHG activity by the components that represent emissions or removal. Guidelines for Quantifying GHG Reductions from Grid-Connected Electricity Projects (2007), the GHG Protocol for Project Accounting (2005), which was published in 2005, Land Use, Land-Use Change and Forestry Guidance for GHG Project Accounting (2006), and Corporate Scope 3 (value chain) (2008), which was published in 2008, were all published at roughly the same time as one another and serve as supplementary standards. Accounting and Reporting (2011), the Greenhouse Gas Protocol makes it simpler to recognize

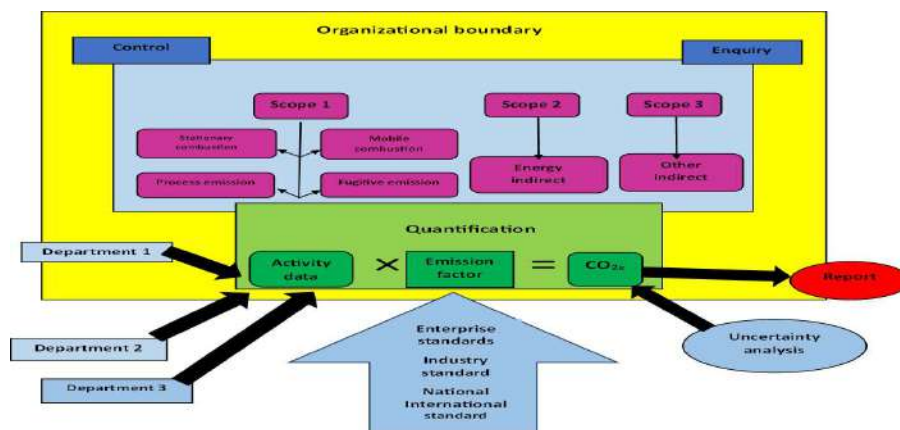


Fig. 3: Methods for evaluating an organization's carbon footprint.

Table 1: Contrastive analysis of the GHG Protocol and ISO14064.

	ISO14064	GHG protocol
Essential Information		
Publisher	ISO	WBCSD&WRI
Date	2006	2004,2011 (revise)
Type Version	Official	Official
Operating	Instructional	Operability
Properties	International standard	Voluntary initiatives Standard
Objects	Organizations	Organizations
Application	Mainly used in industry enterprises	Various industries, governments, (NGOs), carbon trading platform
Goal, Scope and principle	Specifies principles and requirements for the design, development, management, reporting and verification of an organization’s GHG inventory.	
Goal		
Principle	Essentially the same drawing on ISO14044, including relevance, completeness, consistency, accuracy and transparency.	
GHG		
GWP	Six GHGs in the Kyoto Protocol. The second report of IPCC (1996).	
System boundary	Same methods to consolidate organization facility-level GHG emissions and removals: by control or by quite share	
Organizational Boundary	Both divide the whole emissions to three parts: direct emission, energy indirect emission and other indirect emission	
Operation boundary		
Qualification	Calculation, detection, combination of detection and calculation	
Quantization method	Energy indirect emission was denoted as indirect emissions from the generation of imported electricity, heat or steam consumed by the organization	Energy indirect emission was denoted as indirect emissions only from the generation of imported electricity consumed by the organization.
Double counting	Not expected	Refer to emission factors and direct monitoring, as well as cross-industry tools and industry-specific tools. The method was proposed to Avoid double counting.

and collect data about GHG-related activities as well as emission standards. These additional criteria might be used by the energy industry, for instance, to quantify its carbon footprint and gain a better understanding of how to lower the amount of greenhouse gas emissions it produces.

**Carbon Footprint and Rating Criteria for Products**

**Product carbon footprint:** Carbon footprints measure the entire quantity of greenhouse gases produced as a result of a product’s manufacturing and use during its lifetime. A life cycle assessment (LCA) method is

Necessary to fulfill the requirements for increased precision and accessibility in carbon footprint estimates. In 1996, ISO announced the publication of the ISO14040/44 standards, which included assessment frameworks and methods for environmental management that were based on the LCA method.

Life cycle assessment (also known as LCA) is the method that is now considered to be the industry standard for evaluating the carbon footprint of a project. Fig. 4 depicts the main procedures involved in determining a product’s carbon footprint:

- (1) Identification of all materials, activities, and processes that go into the life cycle of the product of interest is a crucial step in doing a product life cycle analysis. First, you must disassemble the functional unit of the product you’ve chosen so that you may analyze its lifecycle. Prioritize the most important ones and write down what goes into making them, how they are made, where they need to be stored, and how they need to be transported.
- (2) Once a product’s life cycle has been analyzed, reasonable boundaries may be set for the carbon footprint study. This is important since it will determine which individual operations to include in the analysis of the product’s carbon footprint.

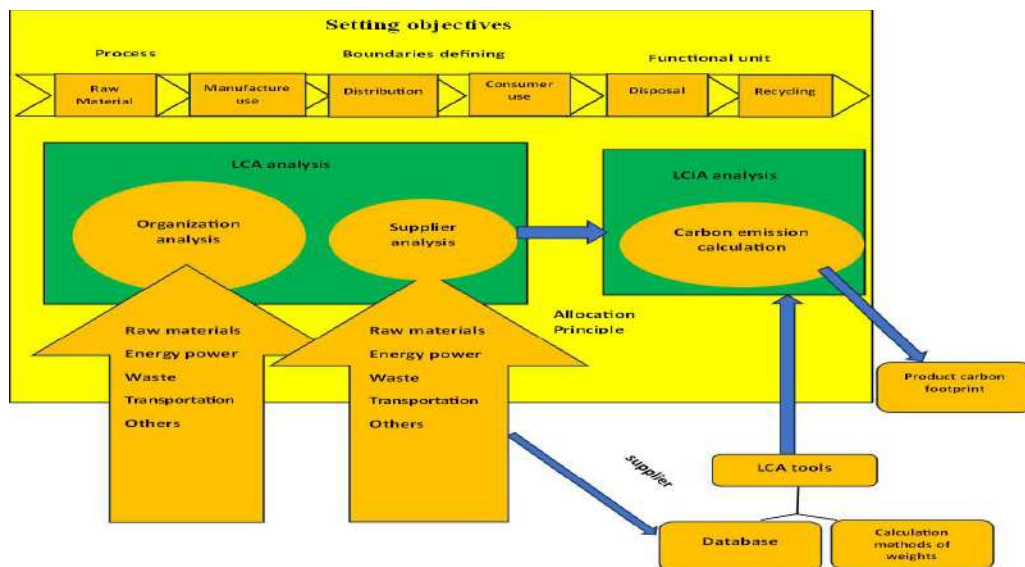


Fig. 4: Methodologies for evaluating product's carbon footprints.

- (3) Consumption data for all emission sources inside the system boundary of the whole product life cycle must be compiled for an exact carbon footprint to be calculated. Throughout the many stages of a product's lifecycle, data on material amounts, activities, and emission factors should be gathered. A complete carbon footprint estimate takes into account all inputs, outputs, and waste products.
- (4) To demonstrate compliance with this standard, businesses must compile a report detailing their product carbon footprint measurement results, outlining their goals, and detailing the steps they took to reach those goals. Meanwhile, declarations, labels, claims, reports, and performance tracking reports based on carbon footprint standards can be used to facilitate information exchange.

#### Methods for assessing one's carbon footprint:

- The British Standards Institution, the Carbon Trust, and the Department of Environment, Food, and Rural Affairs (DEFRA) have revised the Publicly Available Specification (PAS) twice since its first release in 2008. The goal of this document is to establish guidelines for utilizing Life Cycle Assessment (LCA) and Product Category Rules (PCR) to determine a product's total lifecycle greenhouse gas emissions.
- The Japanese Ministry of Economy, Trade, and Industry published the "General Principles for the Assessment and Labelling of Carbon Footprint of Products" as part of the Technical Specification TSQ0010 in April 2009 in response to a carbon footprint trial project and the

creation of CF PCRs. Therefore, in April 2009, the TSQ0010 Technical Specification was released.

- A Product Life Cycle Accounting and Reporting Standard for the GHG Protocol's Product/Supply Chain Initiative is complemented by the Specifications for the Third Tier of Supply Chain Accounting and Reporting. World Resources Institute and the World Business Council for Sustainable Development released it as a joint publication.
- ISO has been working on a standard for measuring and communicating a product's carbon footprint since 2007, and it has also proposed a standard for measuring and communicating an organization's carbon footprint. Using this criterion, companies may track the "carbon footprint" of their products to see how they fare throughout their whole life cycle. In addition to public reporting and trade, this information may also be used for internal research. Publication of the international benchmark is planned for 2013.

#### A comparative study of the standards for evaluating the carbon footprint of products:

- Even though the four standards methodologies and methods are comparable to one another, there are still important differences between them. The evaluation of a product's impact on greenhouse gas emissions may be conceptualized and directed by the four criteria.
- We can see from a comparison of the four different standards that greenhouse gas selection, system



settings, measurement, and carbon footprint, managing specific emissions and removals, and other difficulties remain crucial to both the research and implementation of product carbon footprint assessment standards.

- The four criteria for the Kyoto Protocol were reduced to six GHGs after being narrowed down. Assessments of carbon footprints made between businesses and consumers can make use of GHG and ISO, whereas assessments made between consumers and consumers can only make use of TS-Q0010. The PCR method described in ISO 14025 has been singled out as the approach that should be used for determining the system boundaries.
- A company's carbon footprint can be determined using one of four distinct approaches, each of which is based on a somewhat different set of criteria. However, the most popular and credible approach is to multiply GHG activity data by GHG emission or removal factors. Data on activities and variables measuring emissions collected from either primary or secondary sources can be used interchangeably in either context. By definition, "secondary data" is information that has been gathered from sources that are in no way connected to the firm or the product in question. The objective of these metrics is to provide a standard, aggregate evaluation of similar processes or resources. Multi-sector life cycle databases, industry-specific databases, and country-specific data sources are all examples of databases that serve as secondary data repositories. Secondary data are measurements or averages of processes or materials that are conceptually equivalent to one another but are not taken directly from the product itself. Actual measurements taken at various points throughout the product's lifespan make up the bulk of the data set.
- To obtain a more comprehensive understanding of the carbon effect of a product, researchers and other organizations focused on a variety of aspects, including changes in land use, delays in emissions, renewable energy sources, and carbon storage. The four different standards each have their approach to dealing with the many different types of emissions and removals.
- All of the iterations of the Product Life Cycle Accounting and Reporting Standard (PAS2050) and the Technical Specification for Quality Assurance (TSQ0010) are now authoritative. The PAS2050 assessment standard is currently employed in the vast majority of carbon footprint.

- Assessment scenarios, whereas the TSQ0010 standards are only used in Japan and the applications of the Product Life Cycle Accounting and Reporting Standard are only being begun. However, only the Japanese market recognizes the TSQ0010 standards. All sorts of products, from food and drink to apparel and hygiene items, are made with these three things in mind. In 2013, ISO will produce ISO14047, which will bridge the gap between the current set of assessment standards and the forthcoming ones.

## CONCLUSION

In recent years, the phrase "carbon footprint" has come to be linked with an all-encompassing accounting of greenhouse gas emissions (GHG) across the life cycle of a product or activity. The first step in researching ways to reduce one's carbon footprint is to investigate one's carbon footprint. Organizations are now counting their carbon output as well as the carbon output of their goods and adopting efforts to minimize emissions to fulfill the green consumer expectations of customers or the request of government agencies. The commercial use of the term "carbon footprint" comes about as a result of this trend. The commercialization of the carbon footprint presents a substantial potential to inspire businesses to increase production efficiency, decrease resource consumption and waste, and promote the expansion of innovation and technology; all of these factors may lead to the establishment of new business opportunities. These opportunities can be found in the commercialization of the carbon footprint. However, due to the growing reporting of carbon footprints in response to the needs of commercial and regulatory entities, the vast majority of calculations are now done by the GHG protocol and PAS worldwide. Now since it involves the natural world as well, it's crucial to address the inevitable emissions. The kind of greenhouse gas (GHG), the settings of the system, the quantification and the carbon footprint, the choice of date, and the management of individual emissions should all be given special consideration in the study on carbon footprints and assessment standards. Although these issues were amenable to the existing evaluation criteria, more work was required. It is crucial to establish legislative guidelines that will direct and monitor these estimates, and it is also crucial to ensure that these estimates are accounted for when choosing between businesses and products now that carbon emissions are a tradable commodity. To handle problems such as carbon leakage and border-tax adjustments brought on by the development of reliable procedures and instruments for the worldwide issue of climate heating, research on carbon footprints and assessment standards that have a global scope is required.

## ACKNOWLEDGMENTS

The authors are grateful to the authorities of Dr. Rammanohar Lohia Avadh University, Ayodhya, and the Higher Education Department of U.P., India were highly thankful for rendering their support and help for the completion of this work.

## REFERENCES

- Addie, J.D., Keil, R. and Olds, K., 2015. Beyond town and gown: Universities, territoriality and the mobilization of new urban structures in Canada. *Territory, Politics, Governance*, 3, pp. 27–50.
- Battistini, R., Passarini, F., Marrollo, R., Lantieri, C., Simone, A. and Vignali, V., 2023. How to assess the carbon footprint of a large university? The case study of University of Bologna's multi-campus organization. *Energies*, 16, pp.166-170.
- BSI, 2008. PAS 2050-Specification for the assessment of the Geneva, Switzerland, life cycle greenhouse gas emissions of goods and services. *British Standards Institution*, London, UK.
- Chaurasia, M. and Srivastava, S.K., 2022. Environmental carbon footprint: As an environmental sustainability indicator. *International Journal for Modern Trends in Science and Technology*, 8(04), pp.185-189.
- Chaurasia, M., Prasad, N. and Srivastava, S.K., 2022. Carbon footprint as climate change disclosure: A step towards regulating climate changes. *International Journal of Multidisciplinary Research in Science, Engineering and Technology*, 5(3), pp.390-394.
- Chaurasia, M., Prasad, N., Srivastava, S.K. and Shukla, S., 2022. Role of plant canopy in reducing carbon footprint of an institutional area. *International Journal of Innovative Research in Science, Engineering and Technology*, 11(3), pp.2456-2471.
- Garg, A., Bhattacharya, S., Shukla, P.R. and Dadhwal, V.K., 2001. Regional and sectorial assessment of greenhouse gas emission in India. *Atmospheric Environment*, 35(15), pp.2679-2695.
- GHG Protocol, 2004. The greenhouse gas protocol: A corporate accounting and reporting standard. *World Resources Institute / World Business Council for Sustainable Development*.
- Hertwich, E.G. and Peters, G.P., 2009. Carbon footprint of nations: A global, trade-linked analysis. *Environmental Science & Technology*, 43, pp.6414–6420.
- ISO, 2010. Carbon footprint of products (ISO/CD 14067-1, Under development). *International Organization for Standardization*, Geneva, Switzerland.
- ISOI, 14064-1, 2006. Greenhouse gases-Part 1: Specification with guidance at the organization level for quantification and reporting of greenhouse gas emissions and removals. *International Organization for Standardization*.
- Klein-Banai, C., Theis, T.L., Brecheisen, T.A. and Banai, A.A., 2013. Greenhouse gas inventory as a measure of sustainability for an urban public research university. *Environmental Practice*, 12(1), pp.35-47.
- Kyoto Protocol, 2008. Kyoto Protocol. Reference manual. On accounting of emissions and assigned amount.
- Larsen, H.N. and Hertwich, E.G., 2009. The case for consumption-based accounting of greenhouse gas emissions to promote local climate action. *Environmental Science & Policy*, 12, pp.791–798.
- Larsen, H.N., Pettersen, J., Solli, C. and Hertwich, E.G., 2013. Investigating the carbon footprint of a university - The case of NTNU. *Journal of Cleaner Production*, 48, pp.39-47.
- Lenzen, M., 2007. Shared producer and consumer responsibility: Theory and practice. *Ecological Economics*, 61, pp.27–42.
- Lenzen, M., Wood, R. and Wiedmann, T., 2010. Uncertainty analysis for multiregional input-output models-a case study of the UK's carbon footprint. *Economic Systems Research*, 22, pp.43–63.
- Letete, T.C.M., Mungwe, N.W., Guma, M. and Marquard, A., 2011. Carbon footprint of the University of Cape Town. *Journal of Energy in Southern Africa*, 22(2), pp.514-520.
- Li, X., Tan, H. and Rackes, A., 2015. Carbon footprint analysis of student behavior for a sustainable university campus in China. *Journal of Cleaner Production*, 106, pp.97-108.
- Nagarajan, C., Adithya, P.S. and Jayalakshmi, R., 2011. Corporate ecological footprint (CEF) of SRM University towards sustainability. *International Conference on Environmental Science and Development, IPCBEE 4*, pp.53-55.
- Rippon, S., 2008. Green campus action plan. *University of Cape Town, Cape Town*.
- Robinson, O., Kemp, S. and Williams, I., 2015. Carbon management at universities: A reality check. *Journal of Cleaner Production*, 106, pp.109–118.
- Suwanmontri, C., Kositanont, C. and Panich, N., 2013. Carbon dioxide absorption of common trees in Chulalongkorn University. *Modern Applied Science*, 7(3), pp.1-7.
- The United Nations Intergovernmental Panel on Climate Change, 2007. Climate change. Synthesis report. *IPCC*, Geneva, Switzerland, 10.
- Weidemma, B.P., Thrane, M. and Christensen, P., 2008. Carbon footprint. *Industrial Ecology*, 12, pp.3-6.
- Weidemma, T. and Minx, J., 2007. A definition of carbon footprint. *ISA Research Report*, 7, pp.1–7.
- WRI, 2011. The greenhouse gas protocol: A corporate accounting and reporting standard (Revised Edition). *World Business Council for Sustainable Development*, Geneva, Switzerland.
- WRI, 2011. Product life cycle accounting and reporting standard. *World Business Council for Sustainable Development*, Geneva, Switzerland.

---

## ORCID DETAILS OF THE AUTHORS

Sanjeev Kumar Srivastava: <https://orcid.org/0000-0002-8640-0712>



# A New Approach to Assessing the Accuracy of Forecasting of Emergencies with Environmental Consequences Based on the Theory of Fuzzy Logic

Eduard Tshovrebov<sup>1</sup> , Vladimir Moshkov<sup>1</sup>, Irina Oltyan<sup>1</sup> and Filyuz Niyazgulov<sup>2†</sup>

<sup>1</sup>All-Russian Scientific Research Institute for Civil Defence and Emergencies of the EMERCOM of Russia (Federal Science and High Technology Center), Moscow, 121352, Russia

<sup>2</sup>Russian University of Transport (RUT MIIT), Moscow, 127994, Russia

†Corresponding author: Filyuz Niyazgulov; flyuz1989@yandex.ru

Nat. Env. & Poll. Tech.  
Website: [www.neptjournal.com](http://www.neptjournal.com)

Received: 14-02-2024  
Revised: 22-03-2024  
Accepted: 10-04-2024

## Key Words:

Forecasting of emergencies  
Environmental safety  
Justifiability of the forecast  
Fuzzy logic

## ABSTRACT

Prevention of the occurrence and development of emergencies of a natural and man-made nature is one of the basic fundamental foundations of ensuring the national security of any state. The most important mechanism for preventing emergencies is an effective system of monitoring and forecasting emergencies established at the state level. In the process of functioning such a system, one of the main urgent problems requiring constant attention, continuous research, system analysis, and the search for solutions by scientific methods and methods is to increase the reliability of emergency forecasts. In this format, special attention is currently being paid worldwide to a comprehensive assessment of the adverse consequences of emergency situations, primarily related to the safety of the population, environmental conservation, and environmental safety. From the standpoint of solving this significant scientific and practical problem, the purpose of this work was to develop and justify a more advanced method for calculating the feasibility of forecasts of emergencies with environmental consequences as a tool for a reasonable detailed assessment of the quality, optimality of emergency forecasting processes and the reliability of the forecasts themselves.

## INTRODUCTION

Forecasting of possible emergencies and related risks is aimed at ensuring the safety of life and protecting the population, the environment, and territories from natural and man-made emergencies, and their wide range of adverse consequences. In this regard, it seems to be the most important and relevant to ensure the effectiveness, quality, accuracy, and validity of emergency forecasting, the results of which are currently evaluated by the analytical indicator “justifiability of emergency forecasts”.

The calculation of the feasibility of emergency forecasts is carried out following the Methodology for calculating the indicator “The proportion of justified emergency forecasts prepared by the emergency monitoring and forecasting system in the total number of emergency forecasts”. In this Methodology, the proportion of justifiability of emergency forecasts ( $P_i$ ) prepared by the emergency monitoring and forecasting system (reliability of the forecast) is calculated using the formula:

$$P_i = \frac{n(T)}{N(t)} * 100 \%, \quad \dots(1)$$

$n(T)$  - the number of emergencies and incidents during the time period  $T$  provided for by the forecast;

$N(t)$  - the actual number of emergencies and incidents over a period of time  $T$ ;

$T$  - the forecast time period (year, season, month, decade, day).

The share of justified emergency forecasts in their total number ( $K_o$ , %) is determined by dependence:

$$K_o = \frac{\sum_1^i P_i}{i} \quad \dots(2)$$

$P_i$  – the indicator of the justifiability of the  $i$ -th forecast,  
 $i$  - the number of forecasts.

A high expected result for this indicator can be achieved provided that effective information support is provided, and a high degree of intersubjective, interdepartmental interaction of participants in the unified state emergency prevention and response system is achieved.

However, the practice of predicting emergencies of a mixed natural and man-made nature shows that this approach reduces the accuracy and validity of forecasting due to the underestimation of some factors:

1. The full range of possible upcoming adverse events;
2. A reasonable assessment of the final results of forecasting;
3. The mutual influence of the resulting dangerous events among themselves.

A decrease in the degree of accuracy and validity of emergency forecasting occurs in the absence or incompleteness of objective reliable data for monitoring dangerous events, sources of negative impact on the environment and public health, accounting for such information in state information systems (registers, cadastres, etc.). In addition, when predicting a large number of emergencies, or consistently transforming among themselves, it appears the use of statistical, heuristic methods is ineffective.

Problems and contradictions in the field of emergency forecasting, analyzed based on the results of evaluating the application of methods for calculating the reliability of forecasts, are classified from the positions:

1. Unclear identification of emergencies themselves and their adverse consequences; incompleteness, unreliability of initial forecast data.
2. Incompleteness, unreliability of the initial forecasting data.
3. Underestimation of all conditions, external and internal factors in the process of emergency forecasting, cause-and-effect relationships between dangerous events and phenomena, and their resulting consequences.
4. The unreasonableness or inaccuracy of choosing a predictive method for a specific event, situation, phenomenon, or incident.
5. Imperfections of one or another predictive method that does not provide the necessary level of forecast accuracy.

There is an insufficient number of scientifically based emergency forecasting methods for all types of emerging emergencies, both single and sequentially occurring with a domino effect, assessing their adverse environmental and other consequences within the framework of an integrated approach.

In this regard, there is a need to find new methods and ways to evaluate the results of forecasting in conditions of incomplete data. The present work of the team of authors presented to readers is devoted to the methods of solving the raised scientific and practical problem.

## MATERIALS AND METHODS

The materials for this study were the results of research by

domestic and foreign authors in the field of application of modern technologies for forecasting natural emergencies (Akimov et al. 2023, Arefyeva et al. 2022), safety in construction (Lomakin et al. 2021, Arefeva et al. 2019, Telichenko et al. 2016, Slesarev et al. 2020, Zelinskaya et al. 2019), environmental and economic risks in waste management (Hart et al. 2019, Hertwich et al. 2020, Kirchherr et al. 2017, Murray 2002, Domenech et al. 2019), environmental safety of life support facilities and forecasting man-made hazards of sources of negative impact on the environment (Tskhovrebov et al. 2018, Tshovrebov et al. 2021, Tskhovrebov et al. 2018, Zelinskaya et al. 2021), forecasting emergency risks (Anisimov et al. 2016, Oltyan et al. 2020, Plyuschikov et al/ 2021, Prus et al. 2022), mathematical methods for analyzing various systems (Buryi et al. 2020, Vahdani et al. 2013), modeling of safety processes in natural and man-made systems (Sereda et al. 2019, Sereda et al. 2021, Sereda et al. 2022).

Research methods include collection, generalization, systematization, grouping, composition of initial information and research results, classification, comparative and comparative analysis, and numerical methods of processing the data obtained. The method proposed by the authors for assessing the feasibility of emergency forecasts and their environmental consequences is based on the application of fuzzy logic theory and soft computing methods.

## RESULTS AND DISCUSSION

As part of the implementation of the task, the use of the apparatus of mathematical logic in proving the truth of the statements of the hypothesis put forward was chosen from the position that the analysis carried out using records in the language of predicate logic essentially implements the function of transition from the “organizational and technical” formulation of the problem to its mathematical formalization. In this process, the possibilities of effective use of the method are revealed in conditions of incompleteness, insufficient accuracy, and reliability of the initial data for predicting emergencies.

A similar approach has already been used by Perm scientists S.N. Kostarev and T.G. Sereda in assessing the safety of technical means and has received an effective practical application in the adaptation process in predicting the safety of technical and technological systems.

Let's formulate a logical statement in the language of predicates.

**Statement:** An unjustified forecast is either a statement about a future event that did not come true (did not actually occur) or the absence of a statement about an event that

subsequently actually occurred (within the forecasting period).

**Proof:** Let's say: F – forecast (a statement about the occurrence of a possible dangerous event in a certain period of time); E – event forecast; J – justifiability of the event forecast.

Let's form a logical formula for expressing the justifiability of the forecast:

$$J = (\forall F \rightarrow \exists \neg E) \vee (\forall E \rightarrow \exists \neg F)$$

Let's build truth tables of a given formula using definitions of logical operations:

Since the last column consists only of units, the formula presented above is logically consistent.

Based on the results of the logical and mathematical justification, it is proposed to improve the calculation of the indicator of the validity of emergency forecasts and to assess the accuracy of predicted man-made emergencies according to the formula:

$$D = (1 - P_J) * 100, \quad \dots(3)$$

D – accuracy of the forecast;

P<sub>J</sub> – the probability of an incorrect (erroneous) forecast.

F	E	F®E
0	0	1
0	1	1
1	0	0
1	1	1

E	F	E®F
0	0	1
1	0	0
0	1	1
1	1	1

F®E	E®F	∨ (J)
1	1	1
1	0	1
0	1	1
1	1	1

$$P_J = P_1 + P_2, \quad \dots(4)$$

P<sub>1</sub> – the proportion of unjustified forecasts equal to the ratio of the number of predicted but not occurred events to the total number of predicted events within the framework of this forecast;

Table 1: Threshold impact of technospheric emergencies on natural components.

Technosphere emergencies	Threshold effect on natural components		
	Water	Soil quality	Atmospheric air
Accidents of freight and passenger trains with the release, spillage, scattering, and dumping of hazardous chemicals	1	1	1
Accidents of cargo and passenger ships	1	1	0
Aviation disasters	1	1	1
Major car accidents	0	1	0
Accidents on oil pipelines	1	1	1
Accidents on main gas pipelines	0	0	1
Accidents on electric power systems	0	1	0
Accidents on utility systems	1	1	1
Accidents on heating networks	0	0	1
Hydrodynamic accidents	1	1	0
Accidents with the release (threat of release) of chemically hazardous substances	1	1	1
Accidents at agricultural facilities	1	1	0
Explosions in buildings in populated areas	0	1	1
Explosions at industrial facilities	0	1	1
Explosions on communications	1	1	1
Sudden collapse of buildings	0	1	1
Sudden collapse of rocks, dumps, embankments	0	1	1
Poisoning and pollution of water bodies	1	0	0
Forest fires and forest arson	0	0	1
Fires in landfills	0	0	1
Infiltration, the translocation of toxicants from the body of landfills and landfills into the environment	1	1	1

$P_2$  – the proportion of unfounded forecasts equal to the ratio of the number of events that actually occurred, but were not predicted, to the total number of predicted events within the framework of this forecast.

We note the limitations, scope, and conditions of application of the proposed method for assessing the feasibility of forecasts. According to experts and specialists, the derived formula will be most applicable in calculating short-term forecasts as part of the implementation of the forecasting process at the federal, interregional, and regional levels.

It is proposed to assess the environmental consequences of an emergency using the soft computing method in conditions of incomplete data in a matrix way: according to the types of emergency situations classified according to established criteria in the format of effects on the components of the natural environment: atmospheric air, water, soil (Table 1).

The presented method, according to the authors, will contribute to increasing the degree of validity and accuracy of predicted emergencies due to the systematic analysis of both justified events and predicted factors and forecasting conditions.

## CONCLUSIONS

The conducted research has a high level of practical significance in solving the issues of system analysis of the processes of forecasting man-made emergencies. The approbation and implementation of the method proposed by the authors for calculating the feasibility of emergency forecasts, on the one hand, will contribute to increasing the degree of responsibility of bodies and officials involved in the preparation of such forecasts, and, on the other, will give impetus to the development of a scientific and methodological basis for forecasting, the search for optimal, effective methods, tools and algorithms that provide a complex increase in the level of reliability, the validity, accuracy and quality of the emergency forecasting process.

Taking into account the fact that science has no state borders, the authors of the work invite readers to discuss the urgent scientific problem of emergency prevention and their dangerous environmental consequences, concerning the safety of the entire world community, the life and health of future generations in order to develop optimal, effective ways and measures to resolve it.

## REFERENCES

- Akimov, V., Bedilo, M. and Derendiaeva, O., 2023. Statistical models for forecasting natural emergencies. *Reliability: Theory & Applications*, 18(4), pp.1067-1072.
- Anisimov, V.G., Zegzhda, P.D., Anisimov, E.G. and Bazhin, D.A., 2016. A Risk Oriented Approach to the Control Arrangement of Security Protection Subsystems of Information Systems. *Automatic Control and Computer Sciences*, 50(8), pp.717–721.
- Arefyeva, E.V., Muraveva, E.V. and Frose, T.Y., 2019. Considering emergency hazards in construction and operation of infrastructures. *IOP Conference Series: Materials Science and Engineering*, International Conference on Construction, Architecture and Technosphere Safety - 6. Analysis, Assessment and Technologies of Natural and Man-Made Disasters Reduction, p.066023.
- Arefyeva, E., Alekseeva, E. and Gorina, L., 2022. Assessment of the vulnerability of architectural monuments to dangerous natural processes. *Technological Advancements in Construction*, Cham, pp.159-170.
- Buryi, A.S., Lomakin, M.I. and Sukhov, A.V., 2020. Quality assessment of “stress-strength” models in the conditions of big data. *International Journal of Innovative Technology and Exploring Engineering*, 9(3), pp.3276-3280.
- Domenech, T. and Bahn-Walkowiak, B., 2019. Transition Towards a Resource Efficient Circular Economy in Europe: Policy Lessons from the EU and the Member States. *Ecological Economics*, 155, pp.7-19.
- Hart, J. and Adam, K. et al., 2019. Barriers and drivers in a circular economy: the case of the built environment. *Procedia CIRP*, 80, pp.619–624.
- Hertwich, E., Lifset, R., Pauliuk, S. and Heeren, N., 2020. Resource Efficiency and Climate Change: Material Efficiency Strategies for a Low-Carbon Future. A Report of the Int. Resource Panel. United Nations Environment Programme, Kenya. Available at: <https://www.unep.org/resources/report/resource-efficiency-and-climate-change-material-efficiency-strategies-low-carbon>.
- Kirchherr, J., Reike, D. and Hekkert, M., 2017. Conceptualizing the circular economy: An analysis of 114 definitions. *Resources, Conservation & Recycling*, 127, p.9.
- Lomakin, M.I., Dokukin, A.V., Moshkov, V.B. and Oltyan, I.Yu., 2021. Technologies of civil. *Security*, 18(3), p.15.
- Murray, R., 2002. Zero waste. Greenpeace Environmental Trust, 211 p.
- Oltyan, I.Y., Arefyeva, E.V. and Kotosonov, A.S., 2020. Remote assessment of an integrated emergency risk index. *IOP Conference Series: Materials Science and Engineering*, International Conference on Construction, Architecture and Technosphere Safety, ICCATS 2020, Sochi, 1, p.042053.
- Plyuschnikov, V.G., Avdotin, V.P., Gurina, R.R., Arefyeva, E.V. and Bolgov, M.V., 2021. Hydrological risk management of urbanized areas in framework of the smart city concept. *IOP Conference Series: Earth and Environmental Science*, 5th International Conference on Environmental Engineering and Sustainable Development, CEESD 2020, p.012019.
- Prus, Y.V., Tatarinov, V.V. and Prus, M.Y., 2022. Matrix representation of emergency risks. *AIP Conference Proceedings: Modeling in Engineering 2020*, p.020005.
- Sereda, T.G. and Kostarev, S.N., 2019. Development of automated control system for waste sorting. *IOP Conference Series: Materials Science and Engineering*, 537(6), p.062012.
- Sereda, T.G. and Kostarev, S.N., 2021. Development of the automated workstation for the operator of the solid municipal wastes landfill. *IOP Conference Series: Earth and Environmental Science*, 677(4), p.042107.
- Sereda, T.G., Kostarev, S.N., Novikova (Kochetova, O.V.) and Ivanova, I.E., 2022. Study of solid municipal waste accumulation rates in penitentiary facilities in Perm Krai during the pandemic of 2020. *IOP Conference Series: Earth and Environmental Science*, 1043(1), p.012005.
- Slesarev, M. and Makarova, A., 2020. Environmental safety of construction as a factor of graphoanalytical modeling of product parameters. *Revista Inclusiones*, 7, pp.477-488.
- Telichenko, V. and Benuzh, A., 2016. Development green standards for construction in Russia. XXV Polish - Russian - Slovak Seminar

- “Theoretical Foundation of Civil Engineering”. *Procedia Engineering*, 153, pp.726–730.
- Tshovrebov, E., Velichko, E. and Shevchenko, A., 2018. Methodological approaches to a substantiation resource- and energetically effective economic model of object of placing of a waste. *Advances in Intelligent Systems and Computing*, 692, pp.1296-1305.
- Tshovrebov, E.S., Velichko, E.G., Kostarev, S.N. and Niyazgulov, U.D., 2021. Mathematical model of environmentally friendly management of construction waste and waste of urban economy. *IOP Conference Series: Earth and Environmental Science*, 937(4), p.042062.
- Tskhovrebov, E., Velichko, E. and Niyazgulov, U., 2018. Planning measures for environmentally safe handling with extremely and highly hazardous wastes in industrial, building and transport complex. *Materials Science Forum*, 945, pp.988-994.
- Vahdani, B., 2013. A new fuzzy mathematical model in recycling collection networks: a possibilistic approach. *World Academy of Science, Engineering and Technology*, 78, pp.45-49.
- Zelinskaya, E., Tolmacheva, N., Pronin, S., Garashchenko, A. and Kurina, A., 2021. Theoretical aspects of disposal of liquid mineral waste. *Procedia Environmental Science, Engineering and Management*, 8(1), pp.125-135.
- Zelinskaya, E.V., Tolmacheva, N.A., Barakhtenko, V.V., Burdonov, A.E., Garashchenko, N.E. and Garashchenko, A.A., 2019. Waste-based construction materials. *International Journal of Engineering Research in Africa*, 41, pp.88-102.

---

**ORCID DETAILS OF THE AUTHORS**

Eduard S. Tshovrebov: <https://orcid.org/0000-0002-9481-3832>

Irina Yu. Oltyan: <https://orcid.org/0000-0002-2178-5033>

Filyuz Kh. Niyazgulov: <https://orcid.org/0000-0001-6901-3318>







# Sustainability and Environmental Impact of Mining and Maintaining Cryptocurrencies: A Review

D. Srinivasa Rao<sup>1†</sup>, Ch. Rajasekhar<sup>2</sup>, P. M. K. Prasad<sup>3</sup> and G. B. S. R. Naidu<sup>1</sup>

<sup>1</sup>Department of ECE, GMRIT, Rajam, India

<sup>2</sup>Department of EECE, GITAM School of Technology, GITAM (Deemed to be University), Visakhapatnam, India

<sup>3</sup>Department of ECE, GVP College of Engineering for Women, Visakhapatnam, India

†Corresponding author: D. Srinivasa Rao; [srinivasa.dasari@gmail.com](mailto:srinivasa.dasari@gmail.com)

Nat. Env. & Poll. Tech.  
Website: [www.neptjournal.com](http://www.neptjournal.com)

Received: 31-01-2024

Revised: 20-03-2024

Accepted: 27-03-2024

## Key Words:

Bitcoin mining  
Carbon footprint  
Electronic waste  
Energy usage  
Blockchain

## ABSTRACT

Cryptocurrency has seen an increased popularity with the introduction of Bitcoins. It has been adapted in several countries and has become an alternate solution to conventional currency. Despite its benefits, some controversies surround the manufacturing of bitcoins. While all the countries are moving to sustainability development and global warming control, Bitcoin production has raised several concerns about environmental pollution and sustainability. The increased carbon emissions and high electrical consumption have accompanied the popularity of cryptocurrency. Hence, there is an immediate need to reduce the carbon footprint and electricity consumption caused by human cryptocurrency for a sustainable future. This study presents the current scenario and trends of worldwide cryptocurrency growth and discusses the environmental impact of cryptocurrency mining. It explores crypto mining worldwide and provides a qualitative review. Further, this article highlights the need to take necessary measures to control cryptocurrency circulation.

## INTRODUCTION

In the past few years, a wide variety of electronic or digital currencies called cryptocurrencies that serve as means for commerce have grown firmly. Many countries are showing interest in using or generating cryptocurrency to gain the benefits early. The sustainability aspect of cryptocurrency has become a major concern as it contributes to the environmental effects (Corbet et al. 2020); an increase in global crypto mining activities increases greenhouse gas emissions and requires a large water footprint (Siddik et al. 2023). The cryptocurrency mining process is highly complicated, and it involves the use of specialized machines that store the transaction information in decentralized digital blockchains. The increase in computational power requires large electricity in the generation of cryptocurrency. However, the growing energy consumption produces huge carbon emissions and poses harm to the environment. Electronic waste (E-waste) generation is another major factor in cryptocurrency mining. E-waste increases the risk to the environment by releasing harmful substances into the soil and making the air polluted. Further, the inadequate recycling process will contribute to water pollution. This report aims to discuss the environmental impact of cryptocurrency mining

and compare it to the benefits it will provide to society and the economy.

## KEY FINDINGS AND ANALYSIS

Cryptocurrency represents an alternate form to traditional currency by identifying its qualities and advantages of using and considering the impact on the environment. The sustainability of Cryptocurrency has become a challenge owing to its rising environmental consequences regarding energy usage and increasing carbon footprint. Cryptocurrency mining generates vast amounts of electronic waste, carbon dioxide, and fossil fuels (Wendl et al. 2023). It states that with the increase in the power consumption for the mining process, the carbon emissions linked with this technology pose a significant concern.

Further, the pollution produced by cryptocurrency mining, the use of renewable energy, and the knowledge of environmental damage produced by cryptocurrency mining will all help to solve the sustainability issue (Alonso et al. 2021). As mentioned by (Badea & Mungiu 2021), the study suggests that Bitcoin is still widely used in the economy for several reasons despite its considerable use of energy and adverse impact on the environment. Therefore, the benefits

that the cryptocurrency offers and its sustainability depend on energy consumption during the mining process and various aspects that impact the environment during its production and usage.

### ENERGY CONSUMPTION

The growing use of cryptocurrency and increased crypto mining activities require more electric energy for the generation. As per the energy consumption report of (Raynor 2023a), the bitcoin energy consumption recorded an estimated maximum value of up to 204.5 Terawatt-hour (Twh) during early 2022. According to the estimates for the year 2018, bitcoin consumed at least 40.0 TWh and as much as 62.3 TWh of electricity. In May 2023, bitcoin mining had an estimated electrical energy consumption of 95.58 Twh. It recorded its greatest annual electricity consumption in 2022, reaching at 204.5 terawatt-hours, exceeding the Finnish power usage. The global energy consumption of bitcoin has significantly increased from the year 2017 to

2023 (see Fig. 1) (Raynor 2023a). Hence, it can be realized that energy consumption also increases with the increase in crypto mining.

Furthermore, according to (Raynor 2023b), in the visualization of percentage share by several countries towards the bitcoin energy consumption; it can be noticed that the Czech Republic contributes about 136.7% of energy share powered by bitcoin (see Fig. 2). It can be observed that some of the big nations, such as the USA, UK, Australia, Russia, and Canada account for the bitcoin power in the total energy consumption. For example, The United States is projected to house over one-third of the global crypto mining activities, which now consume 0.9% to 1.7% of total U.S. power consumption.

The trends from the Bitcoin power share indicate there is a potential growth in the electricity demand for crypto-asset operations. Many big countries are involved in crypto-mining activities and contributing electrical energy share to bitcoin generation (see Fig. 2) (Raynor 2023b). From

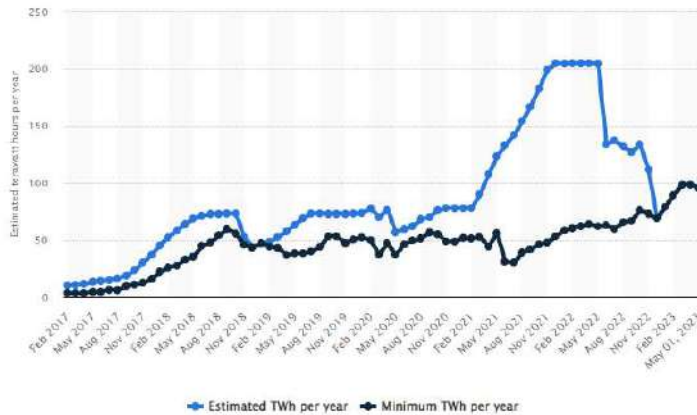


Fig. 1: Bitcoin energy consumption worldwide (Raynor 2023a).

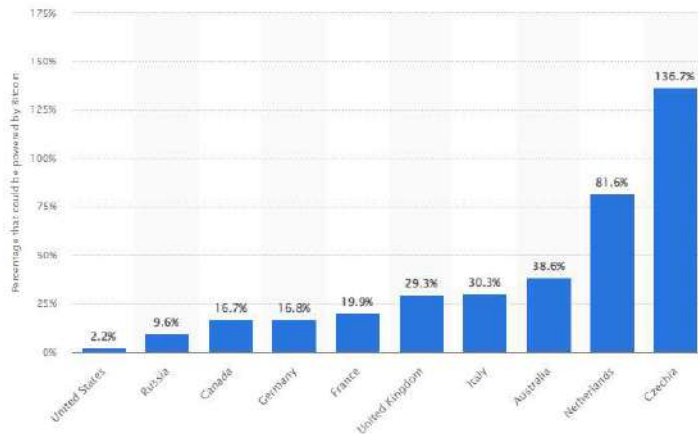


Fig. 2: Global bitcoin energy consumption share by countries (Raynor 2023b).

this perspective, it is worth noting that the electrical energy requirements across several nations vary significantly due to the increase in the share of Bitcoin energy consumption.

In this regard, the University of Cambridge deployed an online tool to assess the global Bitcoin energy consumption across various countries and measures the Bitcoin Electricity Consumption Index (University of Cambridge 2023). According to the online tool, Bitcoin consumes more power than Norway (122.20 TWh), the Netherlands (108.8 TWh), the United Arab Emirates (113.20 TWh), and Argentina (121 TWh). It claimed that the energy it consumes could run every microwave in the United Kingdom for 27 years. It also implies that the total amount of electricity used annually on household appliances in the US could run the whole Bitcoin system for an entire year. According to a Cambridge

University estimate, Bitcoin uses more power per year than the entire country of Argentina (see Fig. 3) (University of Cambridge 2023). Therefore, the online tool from the University of Cambridge suggests that Bitcoin consumes more power annually than The Netherlands, Argentina, and the United Arab Emirates combined.

**ENVIRONMENTAL IMPACT**

Bitcoin can significantly impact the environment with carbon emissions and may lead to global climate change. A visualization by (Bruna 2023) (see Fig. 4) shows that carbon dioxide emissions from bitcoin mining reached over 17.29 million metric tonnes, with the Inner Mongolia area of China accounting for about 26.2% of those emissions. This country was responsible for over half of the carbon

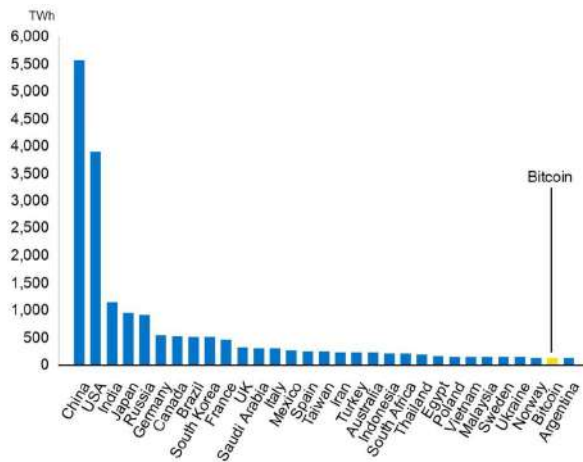


Fig. 3: Global bitcoin energy consumption by countries per year (University of Cambridge 2023).

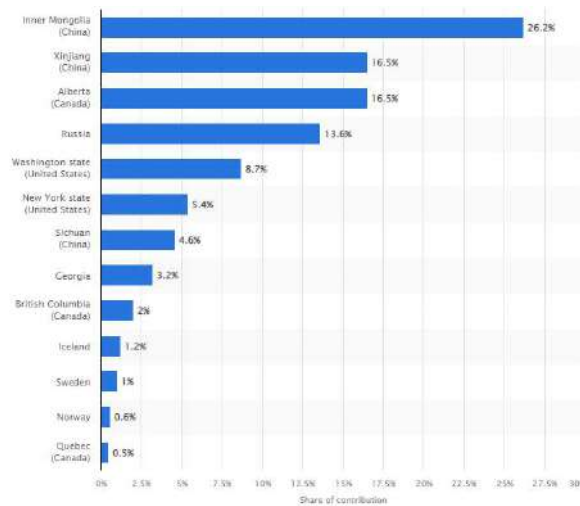


Fig. 4: Bitcoin mining carbon footprint worldwide (Bruna 2023).

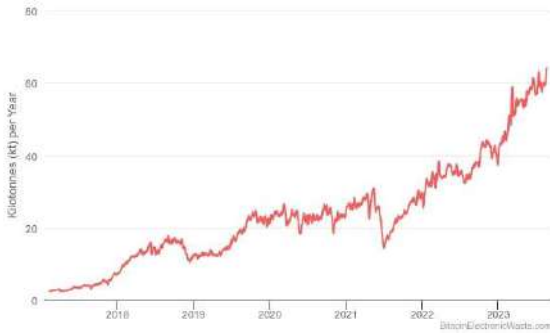


Fig. 5: Bitcoin electronic waste generation 2017–2023 (Alexander 2023).

footprint of Bitcoin mining worldwide. The calculations are based on the presumption that carbon emissions from power production remain constant across China; a nation that continues to dominate worldwide bitcoin mining. However, when the mining environment in China is broken down by area to account; it leads to a substantially lower projected global footprint for Bitcoin in 2018 of 17.29 megatons of CO<sub>2</sub>. The fact that Inner Mongolia, which relies heavily on coal, produces 12.3% of all Bitcoins mined, or an enormous 25% of all emissions, reflects these variations. Therefore, with the increase in global Bitcoin energy consumption, CO<sub>2</sub> emissions have risen significantly.

The growing electronic waste from bitcoin generation poses a threat to the environment; including issues like pollution due to harmful substances and metals. According to (Digiconomist 2023), the generation of electronic waste related to Bitcoin for 2017–2023 is illustrated. It is found that a predicted 2.9 million active devices, which together weigh 39.75 metric kilotons, produce 30.7 metric kilotons of e-waste per year (see Fig. 5). E-waste as a whole constitutes an increasing risk to the environment, from harmful substances and metals that are leaking into soils caused by inadequate recycling; according to the environmental protection agency. A further statement is made to the effect that at peak Bitcoin price levels expected at the beginning of 2021, the yearly quantity of e-waste could go beyond 64.4 metric kilotons in the future. The quantity of electronic waste production currently amounts to 272 grams of e-waste

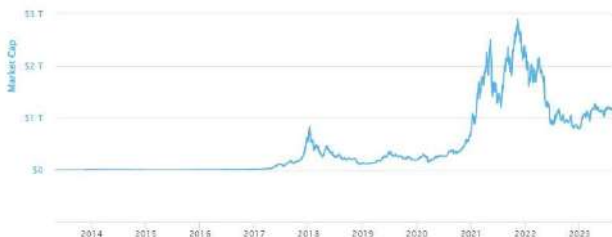


Fig. 6: Global cryptocurrency chart (Coinmarketcap 2023).

for each blockchain transaction. It claims that replacing the mining system entirely would be the best way to address this e-waste production. In this context, the electronic waste produced due to Bitcoin mining has dramatically increased, posing environmental concerns.

## CRYPTOCURRENCY MARKET TRENDS

The global cryptocurrency market is evolving, and the bitcoin circulation has significantly increased. The total consists of steady currencies and coins, and the market capitalization peaked in early 2022 (see Fig. 6) (Coinmarketcap 2023). Many cryptocurrency enthusiasts consider this a critical Bitcoin chart for comprehending the whole space. In addition, to demonstrate the existence of cryptocurrency, the graph depicts the historical quantity of bitcoin in circulation (see Fig. 7) (Statista 2024). It does not take into account lost bitcoins. Currently, there are 19,465,818.75 bitcoins in circulation. This value fluctuates every 10 minutes as fresh blocks are mined. At the moment, each new block contributes 6.25 bitcoins to the system. In this context, the bitcoin currency market capital and circulation have widely increased despite its environmental impact.

## EFFECTIVE MANAGEMENT

### Block Chain Technology

The growth in harmful greenhouse gas emissions across various regions worldwide raises questions about partnership and reliability. In this case, blockchain solutions show the potential way for nations to take necessary steps to ensure the impact on climate is low (Kamusalic et al. 2021).

### Low Energy Solutions

Blockchain also accelerates the use of renewable energy sources such as wind and solar, helping to create these

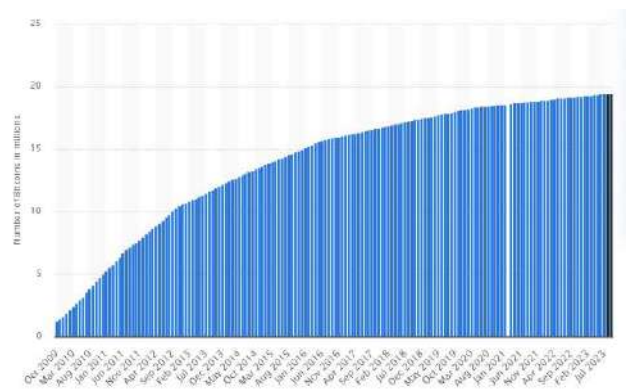


Fig. 7: Global Bitcoin Circulation (Statista 2024).

markets and further eliminate our dependency on fossil fuels (Sedlmeir et al. 2021).

### Investment on Climate

More financial investments are needed to slow down the rate of climate change. These investments could be further boosted if the global carbon markets rise.

### Monitoring Guidelines

Strong guidelines must be framed by national authorities; this setting is required to monitor crypto-assets continuously and may require timely changes. The authorities must possess the appropriate capabilities and resources to monitor the changing crypto asset ecosystem.

### CONCLUSIONS

Cryptocurrency, while accounting for a small fraction of economic transactions, is rapidly gaining acceptance as legal tender by significant businesses and governments. However, this exponential growth has raised serious concerns about its environmental impact. Our research reveals that the energy consumption, ecological footprint, and electronic waste generated by Bitcoin mining pose significant sustainability challenges. Using quantitative analysis, represented in graphs and charts, has allowed us to draw implications from large data sets, highlighting the alarming trend of increased electricity consumption for cryptocurrency mining between 2021 and 2022. This trend is global and varies significantly among countries, underscoring the urgent need for more sustainable practices in this sector.

Bitcoin mining, unfortunately, contributes to the expansion of the global carbon footprint and generates significant electronic waste. However, it is important to note that the circulation of Bitcoin currency has also drastically increased, with market capitalization reaching new heights in recent years. The environmental impact of the mining process is a clear challenge to sustainability, but it is not insurmountable. Like many commercially exploited factors, the perception of cryptocurrency extends beyond its environmental implications. Focusing on sustainable practices can pave the way for a more environmentally responsible future in the cryptocurrency industry.

### REFERENCES

- Alonso, S.L., Vazquez, J., Fernandez, M.A. and Forradellas, R.F., 2021. Cryptocurrency mining from an economic and environmental perspective: Analysis of the most and least sustainable countries. *Energies*, 14(14), p.4254.
- Alexander, N., 2023. University of Cambridge. Cambridge Bitcoin Energy Consumption Index. Retrieved September 30, 2023, from <https://www.jbs.cam.ac.uk/2023/bitcoin-electricity-consumption/>
- Badea, L. and Mungiu, M.C., 2021. The economic and environmental impact of Bitcoin. *IEEE Access*, 9, pp.48091-48104.
- Bruna, A., 2023. Distribution of Bitcoin mining's carbon footprint worldwide as of 2018, by region. Retrieved September 25, 2023, from <https://www.statista.com/statistics/1087192/bitcoin-mining-contribution-carbon-footprint-distribution-globally-by-region/>
- Coinmarketcap, 2023. Global cryptocurrency charts. Retrieved August 20, 2023, from <https://coinmarketcap.com/>
- Corbet, S., Urquhart, A. and Larisa, Y. (eds.), 2020. *Cryptocurrency and blockchain technology*. Walter de Gruyter GmbH & Co KG, pp.151.
- Digiconomist, 2023. Bitcoin electronic waste monitor. Retrieved September 19, 2023, from <https://digiconomist.net/bitcoin-electronic-waste-monitor/>
- Kamisalic, A., Kramberger, R. and Fister, I. Jr., 2021. Synergy of blockchain technology and data mining techniques for anomaly detection. *Applied Sciences*, 11(17), p.7987.
- Raynor, B., 2023a. Bitcoin energy consumption worldwide from February 2017 to May 1, 2023. Retrieved August 25, 2023, from <https://www.statista.com/statistics/881472/worldwide-bitcoin-energy-consumption/>
- Raynor, B., 2023b. Energy consumption from Bitcoin compared to the total energy consumption in selected countries worldwide as of May 1, 2023. Retrieved September 20, 2023, from <https://www.statista.com/statistics/881522/bitcoin-energy-consumption-relative-to-selected-countries/>
- Sedlmeir, J., Buhl, H.U. and Fridgen, G., 2021. The energy consumption of blockchain technology: Beyond myth. *Business & Information Systems Engineering*, 62, pp.599-608.
- Siddik, M.B., Amaya, M. and Landon, T.M., 2023. The water and carbon footprint of cryptocurrencies and conventional currencies. *Journal of Cleaner Production*, 411, p.137268.
- Statista, 2024. Number of Bitcoin tokens in circulation from October 2009 to August 2, 2023. Retrieved September 30, 2023, from <https://www.statista.com/statistics/247280/number-of-bitcoins-in-circulation/>
- Wendl, M., Doan, H. and Sassen, R., 2023. The environmental impact of cryptocurrencies using proof of work and proof of stake consensus algorithms: A systematic review. *Journal of Environmental Management*, 326, p.116530.

### ORCID DETAILS OF THE AUTHORS

- D. Srinivasa Rao: <https://orcid.org/0000-0002-3651-6303>  
 Ch. Rajasekhar: <https://orcid.org/0000-0002-6976-256X>  
 P. M. K. Prasad: <https://orcid.org/0000-0003-2121-0800>





# Community-Based Plastic Waste Management Model in Bangun Village, Mojokerto Regency, Indonesia

A. S. Ulum<sup>1†</sup>, M. S. Djati<sup>2</sup>, Susilo<sup>3</sup> and A. I. Rozuli<sup>4</sup>

<sup>1</sup>Department of Environmental Science, Brawijaya University, Malang, Indonesia

<sup>2</sup>Department of Biology, Brawijaya University, Malang, Indonesia

<sup>3</sup>Department of Economics, Brawijaya University, Malang, Indonesia

<sup>4</sup>Department of Sociology, Brawijaya University, Malang, Indonesia

†Corresponding author: A.S. Ulum; akhdiyati@student.ub.ac.id; syabril@gmail.com

**Nat. Env. & Poll. Tech.**  
Website: [www.neptjournal.com](http://www.neptjournal.com)

Received: 18-03-2024

Revised: 17-04-2024

Accepted: 28-04-2024

## Key Words:

Plastic waste management

Waste segregation

Recycling facilities

Community awareness

Sustainable practices

Public health improvement

## ABSTRACT

This study aims to design a community-based plastic waste management model specifically for Bangun Village, Mojokerto. Using a qualitative approach through a detailed case study, we gathered rich data from observations, interviews, and document reviews. Our findings reveal that the plastic waste management situation in Bangun Village is fraught with significant social, economic, and environmental challenges. These include inadequate waste segregation, limited recycling facilities, and a general lack of community awareness and participation. The proposed model seeks to address these issues by implementing several key components: community-based plastic waste collection and processing, educational programs to raise awareness and promote sustainable practices, partnerships with external stakeholders such as local government bodies, NGOs, and private sector entities, and institutional restructuring to support and sustain these initiatives. Central to this model is the belief that community education and awareness are crucial foundations for fostering sustainable behavior. By actively involving the community in the waste management process, the model not only aims to mitigate the plastic waste problem but also seeks to provide economic and social benefits to the residents of Bangun Village. This includes creating job opportunities, improving public health, and enhancing the overall quality of life. The strength of this model lies in its ability to integrate community participation, policy support, and external partnerships, making it a robust and effective solution for sustainable plastic waste management. By fostering a collaborative and inclusive approach, the model aims to create a sustainable and resilient community that can effectively tackle the plastic waste challenge while reaping economic and social benefits. In conclusion, the community-based plastic waste management model proposed for Bangun Village has the potential to bring about significant positive changes in the way plastic waste is managed. Through this model, we hope to empower the community to contribute to solving the plastic waste problem while also benefiting economically and socially.

## INTRODUCTION

Plastic, as an integral part of modern life, has provided significant benefits to various industries and everyday needs. However, awareness of its negative impacts on the environment and human health is increasing alongside the rise in plastic production and usage. One of the most striking impacts is the escalating problem of plastic waste accumulating in various locations, including villages worldwide (Saputra & Noormansyah 2024). Due to the increasing production of municipal solid waste (MSW), the environment and non-renewable resources suffer losses. Urban governments face various challenges, including land limitations, environmental damage due to waste disposal, and the loss of recyclable resources due to ineffective

waste management (Regassa et al. 2011, Kurniawan et al. 2024).

Data from 2021 by the Directorate General of Waste Management, Hazardous Waste, and B3 (Ditjen PSLB3) of the Ministry of Environment and Forestry (KLHK) reported that Indonesia's waste amounted to 68.5 million tons and increased to 70 million tons in 2022 (dpr.go.id). According to the Ministry of Environment and Forestry, throughout 2021, East Java Province generated about 1.28 million tons of waste. Based on this data, Mojokerto regency does not rank as the largest waste producer in various cities and regencies in East Java Province because the Ministry of Environment and Forestry data for 2022 reported a total waste amount of 24,168.48 kg, making Mojokerto regency the area with the

lowest waste volume in East Java Province. However, this data contrasts with the fact of waste processing activities in Mojokerto regency, which have drawn national attention due to the discovery of various plastic waste types originating from various countries, suspected to be originating from Bangun Village, Mojokerto regency (Purwanto & Aryani 2022).

Such conditions are indeed alarming, considering that in 2018, data from the Central Statistics Agency reported that imported waste entering Indonesia reached 738,665 tons from various exporting countries, including the United States, Italy, the United Kingdom, South Korea, Australia, Singapore, Greece, Spain, the Netherlands, and New Zealand. Then, in July 2019, the Tanjung Perak Customs Office in Surabaya reportedly detained at least 38 containers of waste from the United States and 8 containers from Australia (CNN Indonesia). It is suspected that these wastes contain waste paper with hazardous and toxic waste materials and are disposed of in Bangun Village, Mojokerto Regency.

Bangun Village, like many other local communities, is not exempt from waste issues. The increased production of plastic waste in this village has posed various challenges, including environmental pollution, waterway blockages, and threats to the sustainability of natural resources. In this context, a coordinated and sustainable approach is needed to manage plastic waste at the local level. Environmental pollution levels in Bangun Village are quite high due to it being used as a final disposal site for raw paper waste mixed with foreign waste and hazardous toxic materials. As a result, environmental crises continue to occur and affect the quality of life in the community (Novaradila et al. 2020).

A community-based plastic waste management model is one promising solution to address the challenges of plastic waste (Ferdoush et al. 2024). By directly involving the community in the collection, sorting, and processing of plastic waste, this model aims not only to reduce its negative impacts on the environment (Barros & Gupta 2024) but also to strengthen active participation and shared responsibility in maintaining cleanliness and environmental sustainability (Johannes et al. 2021). Through this approach, the community becomes not only consumers but also key stakeholders in managing plastic waste, which ultimately can contribute to creating a cleaner and more sustainable environment for future generations (Opusunju et al. 2024).

This approach is not only focused on technical steps alone but also considers the social, economic, and cultural aspects of the local community (Suthar & Singh 2015). By taking into account these various dimensions, the community-based plastic waste management model in Bangun Village is aimed not only at reducing the amount of plastic waste ending up in the environment but also at improving the overall quality of

life and economic self-reliance of the community. Through this approach, communities are empowered to engage in various waste management activities, which in turn can increase awareness of the importance of a clean and healthy environment and provide new economic opportunities for the community (de Oliveira et al. 2023, Chakim et al. 2023). Thus, this model not only creates direct positive impacts on the environment but also brings about positive changes in the social and economic structure of the local community.

This research aims to design a model for plastic waste management, focusing on the participation of the local community in Bangun Village. The study discusses concrete steps that can be taken to implement this model, as well as its potential positive impacts on the environment, economy, and society at the local level. It is hoped that this model can serve as a guide for other villages facing similar issues in managing plastic waste sustainably.

## MATERIALS AND METHODS

### Research Method

This research adopts a qualitative approach, specifically through a case study approach. By using this design, the research can conduct an in-depth exploration of the plastic waste management model in the context of Bangun Village, Mojokerto Regency. The case study approach allows researchers to comprehensively investigate various aspects related to the implementation and effectiveness of the model in the local environment. Through this approach, the research can explore the complex nuances and contextual factors that influence the success or failure of the community-based plastic waste management model in Bangun Village. Thus, this research is expected to provide a deeper understanding and richer insights into the practices of plastic waste management at the village level.

### Data Sources

Data collection in this research is conducted through several sources, including direct observation, interviews, and document reviews. Each of these data sources contributes valuable insights into the practices of plastic waste management in Bangun Village. Here are the details:

#### 1) Observation

Direct observation of practices and challenges related to plastic waste management in Bangun Village will provide valuable insights into the existing situation.

#### 2) Interviews

Structured and semi-structured interviews will be conducted with key stakeholders, including representatives from the



Mojokerto Regency Environmental Agency, members of the local community, and relevant non-governmental organizations (NGOs). These interviews will focus on gathering perspectives, experiences, and suggestions to improve plastic waste management practices.

### 3) Documents

Relevant documents such as government policies, reports, and community initiatives related to plastic waste management in Bangun Village and Mojokerto Regency will be reviewed to provide contextual background and additional information.

### Sample Selection

In the process of sample selection, various stakeholders who play crucial roles in the context of plastic waste management in Bangun Village, Mojokerto Regency, are involved. The sample size in this study consists of 11 respondents. Participants include officials from the Mojokerto Regency Environmental Agency, members of the local community such as village leaders, waste collectors, and residents, as well as representatives from local NGOs actively involved in environmental conservation efforts. Sampling is done purposefully, considering the expertise, involvement, and relevance of informants to the research topic. The aim of this technique is to ensure that selected informants can provide significant contributions to understanding the practices of plastic waste management in Bangun Village.

### Data Collection Procedures

Below are the details of the data collection procedures we applied to gain a comprehensive understanding of plastic waste management in Bangun Village:

#### 1) Observation

Researchers directly observe waste management practices, infrastructure, and environmental conditions in Bangun Village, documenting their findings through field notes and photographs.

#### 2) Interviews

Interviews are conducted face-to-face or via virtual platforms based on participant availability and preferences. Audio recordings and detailed notes are made during interviews to ensure accurate data recording.

#### 3) Document Review

Relevant documents are collected and systematically reviewed to extract relevant information regarding

plastic waste management initiatives and policies.

### Data Analysis

Thematic analysis is utilized to analyze the qualitative data collected from observations, interviews, and document reviews. The data will be coded, categorized, and interpreted to identify recurring themes, patterns, and key findings.

### Validity and Reliability

The following strategies are implemented to ensure the validity and reliability of the collected data:

- a. The triangulation of data sources (observations, interviews, document reviews) will enhance the validity and reliability of the findings.
- b. Peer debriefing and member checking will be used to validate the interpretations and conclusions drawn from the data.

By employing a qualitative case study approach and utilizing various data collection methods, this research aims to provide a comprehensive understanding of the plastic waste management model in Bangun Village, Mojokerto Regency, and offer valuable insights into sustainable waste management practices at the local level.

## RESULTS AND DISCUSSION

### Objective Conditions of Local Community-Based Plastic Waste Management in Bangun Village

Community-based plastic waste management in Bangun Village is an approach that involves the active participation of the community in managing plastic waste in their area. However, challenges in community-based waste management are identified in three main aspects: social, economic, and environmental as shown in Table 1.

Bangun Village should adopt appropriate strategies to address the issue of plastic waste management, which has been a concern for some time. Through community participation, it will promote awareness of sustainable waste management. Therefore, efforts are needed in the form of socialization, as indicated by the interview with the Environmental Agency of Mojokerto Regency:

“It is crucial to increase public awareness about proper waste management, and thus, socialization is necessary. The goal of socialization is to educate the community about the importance of waste management. The community also wants to engage in proper waste management practices to avoid negative publicity that would ostracize the Bangun Village community and disrupt the local economy.”

Table 1: Issues in community-based waste management.

No.	Issues	Community-Based Waste Management	Sources
1	Social	The lack of awareness among the community regarding waste management, coupled with the cessation of waste management activities by the government.	Interview with the Environmental Agency of Mojokerto Regency
2	Economic	The cessation of income sources for communities is dependent on waste management.	The community of Bangun Village
3	Environment	Environmental pollution is due to the uncontrolled accumulation of waste.	Interviews with the Environmental Agency of Mojokerto Regency, the community, and NGOs.

(Source: Primary data, processed by researchers)

The waste management conducted by the community is very simple, where waste is sorted based on its type, especially plastic, aluminum, and metal. These wastes are then collected and sold to collectors. Based on interviews with waste collectors, it is revealed that:

“waste is sorted by type, including plastic waste, metal waste, and so on. Most of the waste managed by residents does not come from food materials and cannot be composted, such as plastic, rubber, and cans.”

Speaking about the waste management model, the community obtains waste from several paper companies in East Java, especially PT Parkerin, located in Bangun Village. Where the waste is bought by residents and then dumped on their empty lands, then the waste is sorted by type. Almost all types of waste can be used or utilized for resale. Simply put, the actors involved here are the waste provider producers (PT in East Java), the community (sorters and collectors), and consumers (tofu factories and others).

“As for the waste obtained from several companies in East Java, we do not know the exact names of the PTs; perhaps what is clear is that PT Parkerin used to be a waste supplier, but now it is prohibited. In terms of sorted waste types, especially plastic waste, some are bought by tofu factories to be used as fuel”.

The waste management model in Bangun Village consists of the community, waste-providing industries, and waste-utilizing industries, where waste management is still very simple, collected in residential yards or empty land without adequate infrastructure to support these activities. This indicates the absence of an integrated waste management system and institutional system and the lack of waste management infrastructure and facilities, as well as insufficient awareness among the community about the importance of sustainable waste management.

In terms of infrastructure support, it seems that the government is less serious about it, as the promised landfill construction program is currently stalled (Fig. 1). The community feels disadvantaged by the promises or hopes given by the government, but the reality is that the community can no

longer continue waste management activities. The community sincerely hopes that this program can continue.

“Our hope is that this program can continue waste management in Bangun Village so that it can meet the requirements of proper plastic waste management. We expect the support and involvement of all components, both government and private, regarding waste management in Bangun Village.”

If the waste management model in Bangun Village is inadequate, it should not be closed but rather improved with various supports, especially in terms of infrastructure. With such development activities, community awareness of the importance of waste management and an integrated and sustainable waste management system can be achieved in Bangun Village. Moreover, Bangun Village has great potential to develop a model of plastic waste management that involves the local community. Key findings include the involvement of village governments, cooperation with non-governmental organizations, the utilization of plastic waste, and changes in the attitudes and behaviors of the local community.

Therefore, the community-based plastic waste management model in Bangun Village should encompass various initiatives and policies involving active community participation in plastic waste management. Some components included in this model are plastic waste collection and processing, community education and awareness, partnerships with external parties, and institutional restructuring. With the integration of these three components, it is hoped to create a clean and healthy environment while also economically empowering the local community.

### Development of a Community-Based Plastic Waste Management Model

The community-based plastic waste management model is an approach to plastic waste management that involves the active participation of the local community. This model emphasizes the importance of community involvement in the entire cycle of plastic waste management, from collection,



(Source: Primary data, processed by researchers)

Fig. 1: Land area prepared for the construction of the landfill in Bangun Village.

sorting, processing, and recycling (Andini et al. 2023). Its goal is to create a sustainable system, reduce environmental pollution, and improve community well-being. Through this approach, it is hoped that the local community can be part of the solution to addressing the plastic waste problem while also benefiting economically and socially from waste management activities.

The community-based plastic waste management model in Bangun Village (Fig. 2) includes various initiatives and policies involving active community participation in plastic waste management. Some components included in this model are:

### 1) Plastic Waste Collection and Processing

Involving community participation in sorting and collecting plastic waste at the household and community levels is an important initial step (Sunari & Nurhayati 2023). Additionally, Bangun Village can develop plastic waste processing systems, such as recycling, composting, or using other environmentally friendly technologies, to increase the value of waste. Thus, community participation in processing activities can also significantly increase.

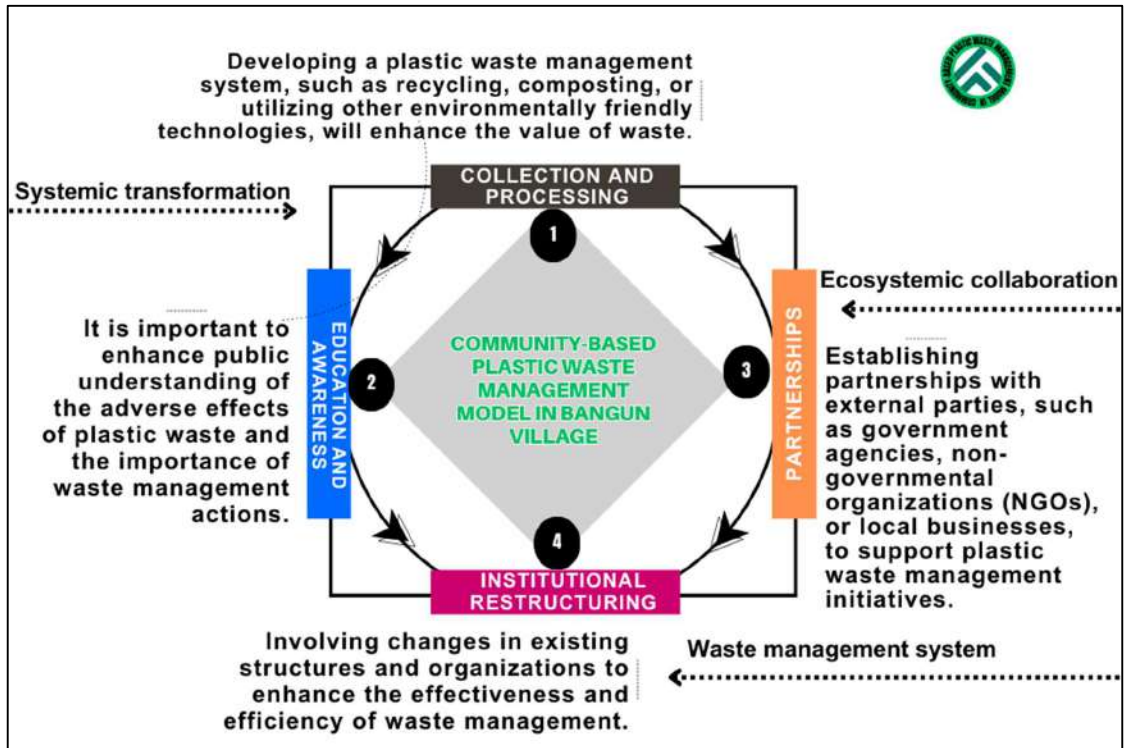
By implementing these measures, Bangun Village can increase the value of plastic waste, reduce the amount of

waste polluting the environment, and create economic opportunities through recycling and processing plastic waste. Community participation in processing activities will also increase as they see the benefits of better waste management for the environment and the daily lives of the local community.

### 2) Education and Community Awareness

It is important to increase community understanding of the negative impacts of plastic waste and the importance of waste management actions. Education programs, campaigns, and training can be part of this model (Hondroyiannis et al. 2024). By conducting education and training, the community's awareness of how to manage waste in Bangun village can be sustainable in terms of social, economic, and environmental aspects.

Education programs can be implemented through various means, such as seminars, workshops, or public campaigns (Giurea et al. 2024). In this program, communities are provided with information about plastic waste issues, including its impacts on the environment, health, and social life (Mihai et al. 2021). Communities are also given knowledge about environmentally friendly waste management practices, such as reducing plastic usage, waste sorting, and recycling.



(Source: Primary data, processed by researchers)

Fig. 2: Community-based plastic waste management model.

With increasing community awareness of the importance of proper waste management, significant behavior changes are expected to occur. Communities will be more inclined to reduce the use of single-use plastics, sort waste, and take steps to recycle or process waste in an environmentally friendly manner. In the community-based waste management model, education and community awareness are crucial pillars supporting the success of waste management. By enhancing understanding and community involvement, Bangun village can create positive changes in sustainable waste management.

### 3) Partnership with External Parties

Bangun Village can establish partnerships with external parties, such as the government, non-governmental organizations, or local businesses, to support plastic waste management initiatives. As a community-based waste management model, Bangun Village can form partnerships with external parties as a strategic step in supporting plastic waste management initiatives. Partnerships with the government, NGOs, or local businesses can provide various benefits for more effective and sustainable waste management.

Through partnerships with external parties, Bangun Village can leverage the expertise, resources, and networks held by the government, NGOs, and local businesses. With strong collaboration, Bangun Village can develop innovative and sustainable solutions for plastic waste management and increase community participation in these efforts. In the community-based waste management model, partnerships with external parties become one of the crucial pillars supporting the success of plastic waste management in Bangun Village.

### 4) Institutional restructuring within the community

Restructuring the institutions in local community-based waste management in Bangun village involves changes in existing structures and organizations to improve the effectiveness and efficiency of waste management. The goal of this restructuring is to develop a more integrated, sustainable, and community-participatory system (Suyanto et al. 2022).

With the restructuring of institutions in the local community-based waste management system in Bangun village, it is hoped that a more effective, well-coordinated, and sustainable waste management system will be created. This will have a positive impact on the

environment, the quality of life of the community, and the sustainable development of Bangun village.

Thus, the community-based waste management model in Bangun village is grounded in several key aspects of plastic waste management. First, systemic transformation refers to fundamental changes in waste management approaches. Second, ecosystemic collaboration involves the active participation of the community, education, and partnerships with external stakeholders. Third, institutional restructuring aims to improve existing waste management systems. Waste management in Bangun village is based on the needs and demands of the community. This means that waste management activities are planned, implemented, monitored, and evaluated together with the local community. In this regard, the government and other supporting organizations in waste reduction act as motivators and facilitators.

The waste handling activities include waste sorting, collection, transportation, waste management, and final waste processing. Every piece of waste entering the landfill site is always recorded to determine the measured waste handling burden. This waste recording can be done mechanically using weighbridge scales. With the implementation of this community-based waste management model, it is hoped that Bangun Village can create positive changes in sustainable waste management.

### **Community-Based Plastic Waste Management Model: Empowering Local Agencies for Sustainable Change**

From the four components (Collection and Processing of Plastic Waste, Education and Community Awareness, Partnership with External Parties, Institutional Restructuring) of the community-based plastic waste management model in Bangun village, the primary priority should be given to education and community awareness. This is due to several reasons:

- 1) **Important Foundations for Sustainable Behavior:** Education and community awareness are important foundations for building sustainable waste management behavior. When communities understand the negative impacts of plastic waste and the importance of good management, they will be more motivated to change their behavior (Pottinger-Glass et al. 2024, Ledda et al. 2024).
- 2) **Increasing Community Participation:** Increased awareness will encourage active community participation in various waste management activities, such as sorting, collection, recycling, and reducing plastic usage. Active community participation is a key factor in achieving the success of waste management models (Ayad & Omayer 2024).

- 3) **Positive Domino Effect:** Education and awareness have a positive domino effect on other components. When communities are aware, they will be more supportive of waste collection and processing efforts, as well as encourage partnerships with external parties. Awareness will also drive more effective and participatory institutional restructuring (Akpuokwe et al. 2024).
- 4) **Long-term investment:** Education and awareness are not only short-term solutions but also long-term investments in building a culture of good waste management in Bangun village. The knowledge and awareness instilled in the younger generation will continue to have a positive impact on the future (Mirzayeva & Abulova 2023).

While education and awareness are given top priority, it doesn't mean that other components are neglected. All four components are interconnected and mutually supportive. To achieve effective and sustainable plastic waste management in Bangun village, integrated implementation of all four components is necessary. Here are some strategic steps to implement education and awareness:

- a. **Diverse education programs:** Utilize various educational methods, such as lectures, workshops, seminars, public campaigns, and social media, to reach all segments of society.
- b. **Engage stakeholders:** Involve government, schools, community organizations, and religious leaders in educational programs to enhance effectiveness and reach.
- c. **Use understandable language:** Ensure education is conveyed in language that is easily understood by the general public.
- d. **Provide real-life examples:** Demonstrate real-life examples of the negative impacts of plastic waste and the benefits of good waste management.
- e. **Involve the community in the education process:** Provide opportunities for the community to actively participate in education programs and provide feedback.

With optimal education and awareness, Bangun Village can build an effective, sustainable, and participatory model of community-based plastic waste management. This model aims to create a clean and healthy environment while also empowering the local community economically. By involving active participation from the community, it is hoped that this model can be sustainable in the long run. Moreover, Bangun Village has great potential to develop a model of plastic waste management that involves the local community. Various key findings, including the involvement of village government, cooperation with non-governmental organizations, utilization

of plastic waste, and changes in the attitudes and behaviors of the local community, are strong factors in driving sustainable community-based plastic waste management models.

The community-based plastic waste management model in Bangun Village has several advantages that make it effective and efficient in managing plastic waste. Some of these advantages include:

- a) This model involves active participation of the community in the collection, sorting, and processing of plastic waste. By engaging the community, this model can cover a wider area and efficiently collect more plastic waste.
- b) This model includes various initiatives and policies that support better plastic waste management. With this support, Bangun Village can create a conducive environment for effective plastic waste management.
- c) The model also emphasizes the importance of education and awareness among the community about the harmful effects of plastic waste. By increasing public understanding, Bangun Village can change community behavior in managing plastic waste.
- d) The model enables Bangun Village to establish partnerships with the government, non-governmental organizations, or local businesses. These partnerships can assist Bangun Village in developing innovative solutions and gaining support in plastic waste management.
- e) The model also involves restructuring institutions in community-based plastic waste management in Bangun Village. This restructuring aims to improve the effectiveness and efficiency of waste management through changes in existing structures and organizations.

The community-based model of plastic waste management in Bangun Village has the potential to be effective and efficient in achieving sustainable plastic waste management. By engaging the active participation of the community, this model can cover a larger area and efficiently collect more plastic waste. Additionally, the support of initiatives and policies that promote better plastic waste management is also an advantage of this model. Education and awareness of the community are also emphasized in this model, which can change community behavior in managing plastic waste. Partnerships with external parties can also assist Bangun Village in developing innovative solutions and gaining support for plastic waste management. Finally, with the restructuring of institutions, this model can improve the effectiveness and efficiency of waste management. All of these advantages make the community-based model of plastic waste management in Bangun Village an effective

and efficient solution for achieving sustainable plastic waste management.

The study by Chotimah et al. (2021), titled “Collaborative Governance Model in Managing Marine Plastic Waste to Realize Maritime Environmental Resilience in Thousand Islands,” found that despite collaboration through various program initiatives, monitoring, project financing for waste management, and the provision of waste management technology and infrastructure, this model has some weaknesses as a community-based waste management model.

The study by Marlina (2020), titled “Household Waste Management through Community and Village Empowerment in Indonesia,” also shows several weaknesses of a community-based waste management model, namely: (1) Empowerment, starting from generating ethics, morals, awareness, mindset, and responsibility towards the environment in society, has not been fully effective in addressing waste issues. (2) Community empowerment in effective household waste management is carried out starting from the level of neighborhood units (RT/RW), but there are still obstacles to its implementation. (3) Strengthening villages with the delegation of waste management responsibilities from districts or cities to villages is not yet fully optimal. (4) Innovative and comprehensive waste management designs are needed in accordance with relevant village regulations.

Thus, both studies indicate that, despite having advantages, community-based waste management models also have weaknesses that need to be addressed and improved in efforts to achieve better environmental sustainability. Based on the comparison between studies on the community-based model of plastic waste management in Bangun Village, the study by Chotimah et al. (2021) on the collaborative governance model in managing marine plastic waste in the Thousand Islands, and the study by Marlina (2020) on household waste management through community and village empowerment in Indonesia, Overall, the community-based model of plastic waste management in Bangun Village has advantages in engaging active community participation, supporting initiatives and policies, educating and raising awareness among the community, partnering with external parties, and institutional restructuring. This makes this model an effective and efficient solution for achieving sustainable plastic waste management.

The perspective of social change theory explains how communities adapt and change their behaviors in response to environmental changes (Indrayaningtias 2021). In this context, the community-based model of plastic waste management in Bangun Village reflects the social change that

occurs in how communities manage plastic waste. Through active community participation, support for initiatives and policies, as well as community education and awareness, this model encourages more sustainable behavioral changes in addressing plastic waste issues (Vitaloka et al. 2023).

Furthermore, agency theory emphasizes the role of individuals and groups in creating social change (Ardini 2023). In the community-based model of plastic waste management in Bangun Village, the community plays an active role in managing plastic waste and participates in decision-making related to waste management. The community becomes change agents involved in implementing initiatives, creating partnerships with external parties, and restructuring institutions to achieve more effective and efficient plastic waste management (Kruljac 2012).

Individuals and groups in the local community of Bangun Village can act as agents of change in various ways. For example, they can initiate plastic waste management programs, organize community awareness campaigns, or forge partnerships with external parties to gain the support and resources needed. Through this active role, individuals and groups in the local community can influence broader social changes in perspectives and behaviors related to plastic waste management.

Moreover, the community-based model of plastic waste management also provides space for active community participation in decision-making related to waste management. The community has the opportunity to contribute to policy formulation, plan initiatives, and engage in decision-making processes involving plastic waste management governance. Thus, the local community of Bangun Village is not only a recipient of established policies but also influences shaping and directing these policies.

With the active role of individuals and groups in the community-based model of plastic waste management in Bangun Village, more sustainable and effective changes in plastic waste management can be achieved. This underscores the importance of agency in creating social changes directed toward environmental sustainability.

## CONCLUSIONS

The community-based model of plastic waste management in Bangun Village is an approach to plastic waste management that involves the active participation of the local community. This model emphasizes the importance of community involvement in the entire cycle of plastic waste management, from collection, sorting, and processing to recycling. Its goal is to create a sustainable system, reduce environmental pollution, and improve community welfare.

Through this approach, it is hoped that the local community can be part of the solution to address the issue of plastic waste while also benefiting economically and socially from waste management activities. The model includes various initiatives and policies that involve active participation of the community in plastic waste management, such as plastic waste collection and processing, community education and awareness, and partnerships with external parties as well as institutional restructuring. By engaging in active community participation, it is hoped that this model can be sustainable in the long term.

Future research should delve into various aspects to advance community-based plastic waste management practices. This includes evaluating the effectiveness of community engagement strategies such as educational programs and participatory decision-making processes, understanding the drivers of behavioral change towards waste management, exploring the role of policy frameworks and governance structures in supporting initiatives, investigating technological innovations to enhance efficiency, and assessing the social and economic impacts of these models on local communities. Such research endeavors are essential for informing policy and practice towards sustainable waste management solutions.

## ACKNOWLEDGMENT

We would like to express our gratitude to all parties who have contributed to and supported this research on the Community-Based Model of Plastic Waste Management in Bangun Village, Mojokerto Regency. We extend our thanks to the Mojokerto Regency Environmental Agency for their permission and assistance provided during the data collection process. We also thank the village leaders, community members, and representatives of local NGOs who willingly participated as informants in this study. Without their cooperation and participation, this research would not have been possible. We also extend our gratitude to all those who have provided moral and material support throughout the implementation of this research. Your contributions and support have been invaluable to the success of this study.

## REFERENCES

- Akpuokwe, C.U., Adeniyi, A.O., Bakare, S.S. and Eneh, N.E., 2024. The impact of judicial reforms on legal systems: A review in African countries. *International Journal of Applied Research in Social Sciences*, 6(3), pp.198-211.
- Andini, D.R., Olivia, D. and Ratnasari, A., 2023. Penerapan konsep arsitektur berbasis komunitas pada pusat edukasi daur ulang sampah. *IKRA-ITH Teknologi Jurnal Sains dan Teknologi*, 7(3), pp.1-12.
- Ardini, L., 2023. Budget from an agency theory perspective. *Scientific Journal of Accounting and Finance*, 1(1), pp.48-58.

- Ayad, H.E. and Omayr, H.M., 2024. Proposal model for a community-friendly wetland park in Egypt: A social approach. In *IOP Conference Series: Earth and Environmental Science*, 1283(1), p.012005.
- Barros, R. and Gupta, R., 2024. From bean to textiles: Sustainable production from coffee and plastic waste. *Migration Letters*, 21(S7), pp.581-592.
- Chakim, M.H.R., Sunarya, P.A., Agarwal, V. and Hikam, I.N., 2023. Village tourism empowerment against innovation, creative economy, and social environment. *Aptisi Transactions on Technopreneurship (ATT)*, 5(2), pp.162-174.
- Chotimah, H.C., Iswardhana, M.R. and Rizky, L., 2021. Model collaborative governance dalam pengelolaan sampah plastik laut guna mewujudkan ketahanan maritim di Indonesia. *Jurnal Ketahanan Nasional*, 27(3), pp.348-376.
- CNN Indonesia, 2019. Protesting imported waste, mobs in East Java attack the American consul general. *CNN Indonesia*. Available at <https://www.cnnindonesia.com/nasional/20190712174254-20-411673/protes-sampah-impor-massa-di-jatim-geruduk-konjen-amerika>.
- de Oliveira, R.T., Ghobakhloo, M. and Figueira, S., 2023. Industry 4.0 towards social and environmental sustainability in multinationals: Enabling circular economy, organizational social practices, and corporate purpose. *Journal of Cleaner Production*, 603, p.139712.
- DITJEN 2022. Directorate General of Waste, Waste and B3 Management (Ditjen PSLB3). Available at <https://www.dpr.go.id/berita/detail/id/40924/t/Ditjen+PSLB3+KLHK+Didesak+Miliki+Langkah+Terukur+r+Tangani+Volume+Sampah>. Accessed on 24 Dec 2023.
- Ferdoush, M.R., Al Aziz, R., Karmaker, C.L., Debnath, B., Limon, M.H. and Bari, A.M., 2024. Unraveling the challenges of waste-to-energy transition in emerging economies: Implications for sustainability. *Innovation and Green Development*, 3(2), p.100121.
- Giurea, R., Carnevale Miino, M., Torretta, V. and Rada, E.C., 2024. Approaching sustainability and circularity along waste management systems in universities: An overview and proposal of good practices. *Frontiers in Environmental Science*, 12, p.1363024.
- Hondroyiannis, G., Sardianou, E., Nikou, V., Evangelinos, K. and Nikolaou, I., 2024. Waste generation and macroeconomic drivers: A panel study for European countries and regions. *Management of Environmental Quality: An International Journal*, 16, p.411.
- Indrayaningtias, R., 2021. Community adaptation strategies after ecotourism development in Sendi Village, Mojokerto Regency. *Paradigma*, 10(1), pp.64-70.
- Johannes, H.P., Kojima, M., Iwasaki, F. and Edita, E.P., 2021. Applying the extended producer responsibility towards plastic waste in Asian developing countries for reducing marine plastic debris. *Waste Management & Research*, 39(5), pp.690-702.
- Kruljac, S., 2012. Public-private partnerships in solid waste management: Sustainable development strategies for Brazil. *Bulletin of Latin American Research*, 31(2), pp.222-236.
- Kurniawan, T.A., Meidiana, C., Goh, H.H., Zhang, D., Othman, M.H.D., Aziz, F. and Ali, I., 2024. Unlocking synergies between waste management and climate change mitigation to accelerate decarbonization through circular-economy digitalization in Indonesia. *Sustainable Production and Consumption*, 46, pp.522-542.
- Ledda, V., George, C., Glasbey, J., Labib, P., Li, E., Lu, A. and Bhangu, A., 2024. Uncertainties and opportunities in delivering environmentally sustainable surgery: The surgeons' view. *Anaesthesia*, 79(3), pp.293-300.
- Malihah, L., Rahmah, M. and Nawiyah, L., 2023. Opportunities and challenges for managing circular economic activities at the Cahaya Kencana Martapura Final Processing Site (TPA). *e-Jurnal Ekonomi Sumberdaya dan Lingkungan*, 12(1), pp.1-20.
- Marlina, A., 2020. Household waste management through community and village empowerment in Indonesia. *Jurnal Ilmu Pendidikan (JIP) STKIP Kusuma Negara*, 11(2), pp.125-144.
- Mihai, F.C., Gündoğdu, S., Markley, L.A., Olivelli, A., Khan, F.R., Gwinnett, C. and Molinos-Senante, M., 2021. Plastic pollution, waste management issues, and circular economy opportunities in rural communities. *Sustainability*, 14(1), p.20.
- Mirzayeva, F.O. and Abulova, M.K., 2023. Preparing future teachers for educational activities based on innovative technologies. *Galaxy International Interdisciplinary Research Journal*, 11(12), pp.548-552.
- Novaradila, G., Ali, Y.I., Astin, L.A., Aryani, M.I. and Purwanto, A.M.D.C., 2020. The threat of imported waste to human security: A case study of Bangun and Tropodo Villages 2018-2019. *Global and Policy Journal of International Relations*, 8(02), pp. 12-20.
- Opusunju, O.C., Azubuike, E.J. and Nwabude, I., 2024. Study assessing Port Harcourt superstores' contributions to Sustainable Development Goals via consumer waste management behaviors. *Journal of Economics, Innovative Management and Entrepreneurship*, 2(1), p.7781.
- Pottinger-Glass, C., Vanhuysse, F., Asvanon, R. and Archer, D., 2024. Bangkok's waste metabolism: Barriers and opportunities for inclusive circularity. *Journal of Material Cycles and Waste Management*, 26, pp.946-960.
- Purwanto, A.M.D.C. and Aryani, M.I., 2022. Urgency of waste import regulations for communities in East Java. *Veteran Justice Journal*, 4(1), pp.01-11.
- Regassa, N., Sundaraa, R.D. and Seboka, B.B., 2011. Challenges and opportunities in municipal solid waste management: The case of Addis Ababa city, central Ethiopia. *Journal of Human Ecology*, 33(3), pp.179-190.
- Saputra, H.L. and Noormansyah, R., 2024. Scavengers as an alternative waste management project: A study on the civil society of Kiringan Village in Sustainable Development Goals 15 through 3R waste management. *POPULIKA*, 12(1), pp.110-124.
- Sunari, R. and Nurhayati, S., 2023. Community environmental education through a local knowledge-based learning program on plastic waste management. *Journal on Education*, 5(4), pp.13093-13099.
- Suthar, S. and Singh, P., 2015. Household solid waste generation and composition in different family size and socio-economic groups: A case study. *Sustainable Cities and Society*, 14, pp.56-63.
- Suyanto, E., Lestari, S., Windiasih, R., Widyastuti, T.R., Wuryaningsih, T. and Kusumanegara, S., 2022. Government policy revitalization model in the zero waste concept of community participation-based urban waste management in Purwokerto-Central Java-Indonesia. *Baltic Journal of Law & Politics*, 15(7), pp.602-616.
- Vitaloka, M., Kuswardani, D.C. and Utaminingsih, A., 2023. Implementation of policies to control the use of plastic bags in Semarang City. *JiIP-Jurnal Ilmiah Ilmu Pendidikan*, 6(12), pp.10484-10490.
- Wibiksana, I.G., 2020. Community empowerment through the Reduce, Separate, and Utilize (Kang Pisman) program in Bandung City. Doctoral dissertation. Indonesian Computer University.



... Continued from inner front cover

- The text of the manuscript should run into Abstract, Introduction, Materials & Methods, Results, Discussion, Acknowledgement (if any) and References or other suitable headings in case of reviews and theoretically oriented papers. However, short communication can be submitted in running with Abstract and References. The references should be in full with the title of the paper and mentioning names of all the authors.
- The figures should preferably be made on a computer with high resolution and should be capable of withstanding a reasonable reduction with the legends provided separately outside the figures. Photographs may be black and white or colour.
- Tables should be typed separately bearing a short title, preferably in vertical form. They should be of a size, which could easily be accommodated in the page of the Journal.
- References in the text should be cited by the authors' surname and year. In case of more than one reference of the same author in the same year, add suffix a,b,c,... to the year. For example: (Thomas 1969, Mass 1973a, 1973b, Madony et al. 1990, Abasi & Soni 1991).

### List of References

The references cited in the text should be arranged alphabetically by authors' surname in the following manner: (Note: The titles of the papers should be in running 'sentence case', while the titles of the books, reports, theses, journals, etc. should be in 'title case' with all words starting with CAPITAL letter). The references should be given in the "Harvard Pattern" as exemplified below.

- Dutta, A. and Chaudhury, M., 1991. Removal of arsenic from groundwater by lime softening with powdered coal additive. *Journal of Water Supply: Research and Technology—Aqua*, 40(1), pp.25-29. **(For Papers Published in Journals)**
- Goel, P.K., 2006. *Water pollution: Causes, Effects and Control*. New age international, New Delhi. **(For Authored Books)**
- Environmental Protection Agency (EPA), 2023. Air Quality and Pollution Data. Retrieved June 25, 2024, from <https://www.epa.gov/air-quality-and-pollution-data> **(For Data Retrieved from a Website)**
- Hammer, D.A. (ed.), 1989. *Constructed Wetlands for Wastewater Treatment-Municipal, Industrial and Agricultural*. Lewis Publishers Inc., pp.831. **(For Edited Book)**
- Haynes, R.J., 1986. Surface mining and wetland reclamation. In: J. Harper and B. Plass (eds.) *New Horizons for Mined Land Reclamation*. Proceedings of a National Meeting of the American Society for Surface Reclamation, Princeton, W.V. **(For Papers published in Edited Books)**

### Submission of Papers

- The paper has to be submitted online in a single WORD file through the online submission portal of journal's website: [www.neptjournal.com](http://www.neptjournal.com)

### Attention

1. Any change in the authors' affiliation may please be notified at the earliest.
2. Please make all the correspondence by e-mail, and authors should always quote the manuscript number.

**Note:** In order to speed up the publication, authors are requested to correct the galley proof immediately after receipt. The galley proof must be checked with utmost care, as publishers owe no responsibility for mistakes. The papers will be put on priority for publication only after receiving the processing and publication charges.

# Nature Environment and Pollution Technology

**(Abbreviation: Nat. Env. Poll. Tech.)**  
**(An International Quarterly Scientific Journal)**

Published by



**Technoscience Publications**  
A-504, Bliss Avenue, Opp. SKP Campus  
Balewadi, Pune-411 045, Maharashtra, India

In association with  
**Technoscience Knowledge Communications**  
Mira Road, Mumbai, India

For further details of the Journal, please visit the website. All the papers published on a particular subject/topic or by any particular author in the journal can be searched and accessed by typing a keyword or name of the author in the 'Search' option on the Home page of the website. All the papers containing that keyword or author will be shown on the home page from where they can be directly downloaded.

**[www.neptjournal.com](http://www.neptjournal.com)**

**©Technoscience Publications:** The consent is hereby given that the copies of the articles published in this Journal can be made only for purely personal or internal use. The consent does not include copying for general distribution or sale of reprints.

Published for Proprietor, Printer and Publisher: Ms T. P. Goel, A-504, Bliss Avenue, Balewadi, Pune, Maharashtra, India; Editors: Dr. P. K. Goel (Chief Editor), Prof. K. P. Sharma (Honorary Editor) and Ms Apurva P. Goel (Executive Editor)